Proceedings of the
Thirty-Ninth

IWCS

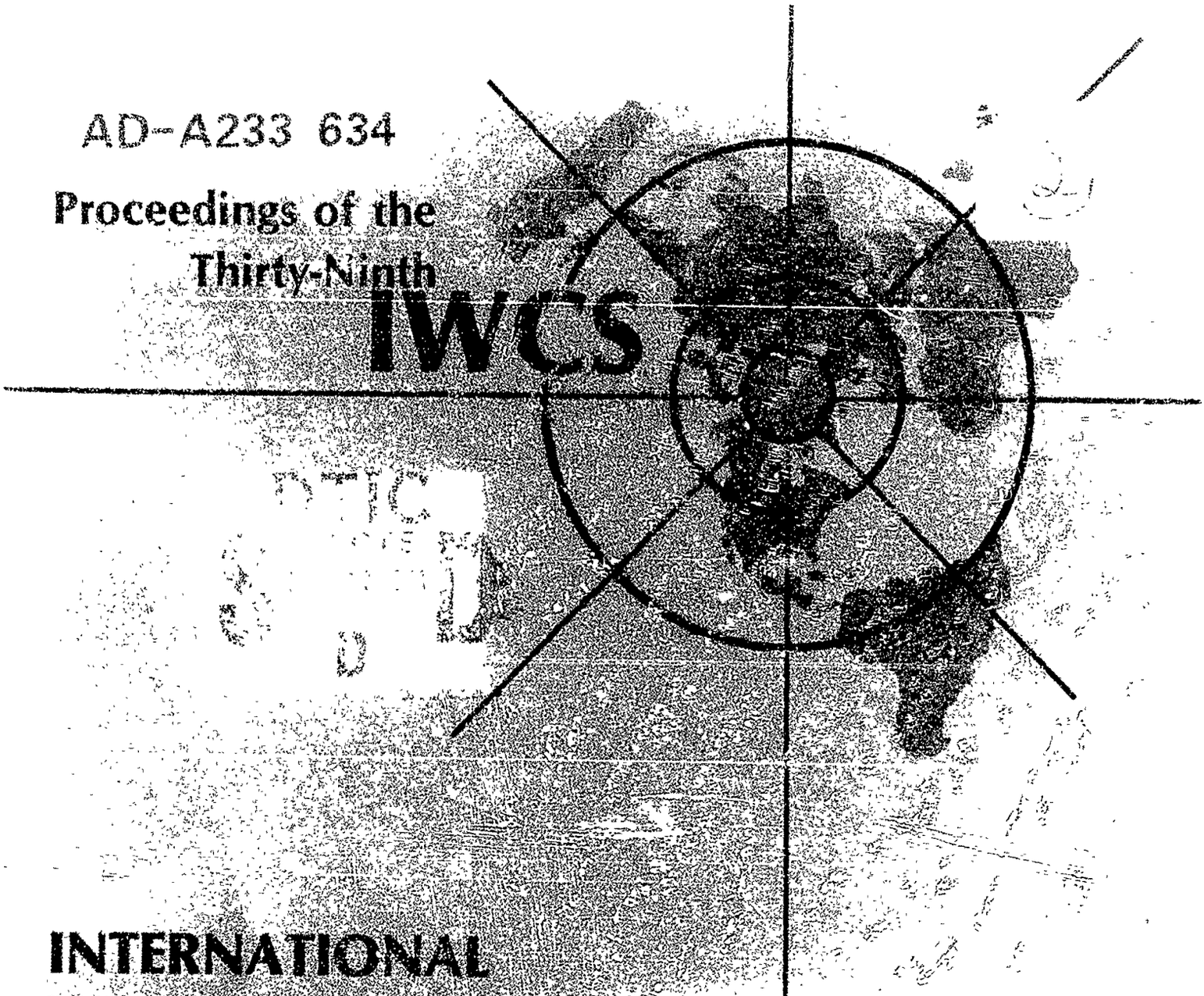

INTERNATIONAL WIRE AND CABLE SYMPOSIUM

November 13 thru 15, 1990

Sponsored by
International Wire and Cable Symposium (IWCS)

With Participation by
US Army Communications-Electronics Command
(CECOM)
Fort Monmouth, New Jersey

PROCEEDINGS OF 39TH INTERNATIONAL WIRE AND CABLE SYMPOSIUM

Sponsored by
International Wire and Cable Symposium (IWCS)

With Participation by
US Army Communications-Electronics Command (CECOM)

Fort Monmouth, New Jersey

BALLY'S RENO HOTEL
RENO, NEVADA
NOVEMBER 13, 14 and 15, 1990

APPROVED FOR PUBLIC RELEASE: DISTRIBUTION UNLIMITED

39TH INTERNATIONAL WIRE AND CABLE SYMPOSIUM

SYMPOSIUM COMMITTEE

ELMER F. GODWIN (President/Director)
GEF Associates
3A Buttonwood Drive
Shrewsbury, NJ 07702
(201) 741-8864 (Home)
(201) 544-4615 (Office)
Fax: 201-544-4084

DR. C.RONALD SIMPKINS (Chairman)
E.I. DuPont de Nemours & Co., Inc.
WCEO-Room 4062
P.O. Box 6097
Newark, DE 19714-6097
(302) 451-4732
Fax: 302-451-0654

Dr. Ken-ichi Aihara
NTT America, Inc.
One Landmark Square Rm 700
Stamford, CT 06901
(203) 967-9379
Fax: 203-325-2316

Dr. Robert Baboian
Texas Instruments, Inc.
34 Forest Street
MS 10-13
Attleboro, MA 02703
(508) 699-1350
Fax: 508-699-1819

David Fallowfield
(Secretary)
Alberta Government Telephones
Room 142B
10025 Jasper Ave.
Edmonton, Alberta T5J-1S6
Canada
(403) 493-6907
Fax: 403-493-6918

Rene G. Freeman
Union Carbide Chemicals and Plastic Company, Inc.
2970 Clairmont Road
Suite 500
Atlanta, GA 30329
(404) 320-3527
Fax: 404-320-3520

Dave Fischer
Superior Cable Corp.
150 Interstate North Parkway
Suite 300
Atlanta, GA 30339
(404) 953-8338

Hans A. Mayer
Olex Cables Division of Pacific Dunlop Ltd.
207 Sunshine Road
Tottenham, 3012
Melbourne, Australia
61-3-316-2222
Fax: 61-3-3140383

James J. Pickering
(Vice Chairman)
Neste Chemicals, Inc.
303 George Street
Suite 103
New Brunswick, NJ 08901
(201) 249-3900
Fax: 201-249-4884

Frank Short
B.I.C.C. Cables Limited
Helsby, Warrington, Cheshire
WA6 ODJ
England
011-44-9282-2727 or 4363
Fax: 09282-3005
Telex: 628811 (BECLH)

Homer Vela
AT&T Network Systems
505 North 51st Avenue
P.O. Box 13369
Phoenix, AZ 85002
(602) 233-5552
Fax 602-233-5069

Manual R. Santana
AT&T Bell Laboratories
2000 NE Expressway
Norcross, GA 30071
(404) 447-2574

ADVISORY

Dr. Peter R. Bark
Siercor Corporation
P.O. Box 489
489 Siecor Park
Hickory, NC 28603
(704) 323-6205
Fax: 704-323-6264

Leo Chattler
DCM Industries, Inc.
2930 Faber Street
Union City, CA 94587
(415) 429-9500
Fax: 415-429-1250

Michael A. DeLucia
David Taylor Research Center
Energy R&D Office, Code 2759
Annapolis, MD 21402-5067
(301) 267-3825
Autovon 281-3825
Fax: 301-267-2875

Marta Farago
Northern Telecom Canada Ltd.
P.O. Box 6122, Station A
Montreal, Quebec H3C-3J4
Canada
(514) 634-3511 X2262
Fax: 514-634-9684

Irving Kolodny
Consultant
80-56 230th Street
Bellerose Manor, NY 11427
(718) 464-9197

CONSULTANTS

Dr. Reiner J. Gerdes
Contel Laboratories
270 Scientific Drive
Suite 10
Technology Park/Atlanta
Norcross, GA 30092
(404) 551-4901 or 448-2206
Fax: 404-448-2945

Dr. Raymond E. Jaeger
SpecTran Corporation
50 Hall Road
Sturbridge, MA 01566
(508) 347-2261
Fax: 508-347-2747

MISSION

The International Wire and Cable Symposium provides a forum for the exchange of technical information amongst suppliers, manufacturers, and users on technological advancements in materials, processes, and products used for voice, data and video signal transmission systems.

TECHNICAL SESSIONS

Tuesday November 13, 1990

9:00 a.m.	SESSION I	Global Markets for Communication Cables
1:30 p.m.	SESSION II	Optical Fiber and Cable Design I
1:30 p.m.	SESSION III	Copper Telecommunication Cables and Networks
1:30 p.m.	SESSION IV	Military Applications

Wednesday, November 14, 1990

8:30 a.m.	SESSION V	Optical Fiber and Cable Design II
8:30 a.m.	SESSION VI	Environmental Effects on Cables and Systems
8:30 a.m.	SESSION VII	Splicing and Connectorization Technology
2:00 p.m.	SESSION VIII	Fiber Optic Cable Installation
2:00 p.m.	SESSION IX	Thermal Aging of Plastic Insulated Conductors
2:00 p.m.	SESSION X	Technology Advancements in Copper Telephone Cable Production
3:30 p.m.	SESSION XI	Poster Session

Thursday, November 15, 1990

8:30 a.m.	SESSION XII	Fiber Optic and Superconductor Cable Applications
8:30 a.m.	SESSION XIII	Telecommunication Networks in the European Community
8:30 a.m.	SESSION XIV	Testing of Cables, Components and Materials I
1:00 p.m.	SESSION XV	Fire Hazard Considerations
1:00 p.m.	SESSION XVI	Impact of Coating Properties on Fiber Performance
1:00 p.m.	SESSION XVII	Testing of Cables, Components and Materials II

PAPERS

The papers in this volume were printed directly from unedited reproducible copies prepared by the authors. Responsibility for contents rests upon the authors and not the symposium committee or its members. After the symposium, all the publication rights of each paper are reserved by their authors, and requests for republication of paper should be addressed to the appropriate author. Abstracting is permitted, and it would be appreciated if the symposium is credited when abstracts or papers are republished. Requests for individual copies of papers should be addressed to the authors.

PROCEEDINGS
INTERNATIONAL WIRE AND CABLE SYMPOSIUM

Bound—Available at Fort Monmouth

30th International Wire & Cable Symposium Proceedings—1981—$8.00
31st International Wire & Cable Symposium Proceedings—1982—$8.00
32nd International Wire & Cable Symposium Proceedings—1983—$8.00
33rd International Wire & Cable Symposium Proceedings—1984—$10.00
34th International Wire & Cable Symposium Proceedings—1985—$15.00
35th International Wire & Cable Symposium Proceedings—1986—NOT AVAILABLE
36th International Wire & Cable Symposium Proceedings—1987—NOT AVAILABLE
37th International Wire & Cable Symposium Proceedings—1988—NOT AVAILABLE
38th International Wire & Cable Symposium Proceedings—1989—$30.00
39th International Wire & Cable Symposium Proceedings—1990—$35.00

Extra Copies: 1-3, $35.00 per copy; 4-10, $30.00 per copy; 11 and above $25.00 per copy.

Make a check or bank draft payable in US dollars to the INTERNATIONAL WIRE & CABLE SYMPOSIUM and forward request to:

International Wire and Cable Symposium
P.O. Box 7597
Shrewsbury, NJ 07702

Telephone inquiries may be directed to Pat Hudak (201) 544-3163.

NOTE: Proceedings shipped by surface mail can not be traced in the event they are not delivered. Overseas air mail will be an additional $35.00 per copy for Europe and $40.00 per copy for Asia.

Photocopies are available for complete sets of papers for 1964 thru 1989. Information on prices and shipping charges should be requested from the:

US Department of Commerce
National Technical Information Service (NTIS)
Springfield, Virginia 22151
USA
Telephone: (703) 487-4650
Include Title, Year and "AD" Number

13th Annual Wire & Cable Symposium (1964)	– AD 787164
15th Annual Wire & Cable Symposium (1966)	– AD A006601
16th International Wire & Cable Symposium (1967)	– AD 787165
17th International Wire & Cable Symposium (1968)	– AD 787166
18th International Wire & Cable Symposium (1969)	– AD 787167
19th International Wire & Cable Symposium Proceedings 1970	– AD 714985
20th International Wire & Cable Symposium Proceedings 1971	– AD 733399
21st International Wire & Cable Symposium Proceedings 1972	– AD 752908
22nd International Wire & Cable Symposium Proceedings 1973	– AD 772914
23rd International Wire & Cable Symposium Proceedings 1974	– AD A003251
24th International Wire & Cable Symposium Proceedings 1975	– AD 7017787
25th International Wire & Cable Symposium Proceedings 1976	– AD A032801
26th International Wire & Cable Symposium Proceedings 1977	– AD A047609
27th International Wire & Cable Symposium Proceedings 1978	– AD A062322
28th International Wire & Cable Symposium Proceedings 1979	– AD A081428
29th International Wire & Cable Symposium Proceedings 1980	– AD A096308
30th International Wire & Cable Symposium Proceedings 1981	– AD A110859
31st International Wire & Cable Symposium Proceedings 1982	– AD A125662
32nd International Wire & Cable Symposium Proceedings 1983	– AD A136749
33rd International Wire & Cable Symposium Proceedings 1984	– AD A152119
34th International Wire & Cable Symposium Proceedings 1985	– AD A164384
35th International Wire & Cable Symposium Proceedings 1986	– AD A180828
36th International Wire & Cable Symposium Proceedings 1987	– AD A189610
37th International Wire & Cable Symposium Proceedings 1988	– AD A200903
38th International Wire & Cable Symposium Proceedings 1989	– AD A216023
Kwic Index of Technical Papers, International Wire & Cable Symposium (1952-1975)	– AD A027588

MESSAGE FROM THE PRESIDENT/DIRECTOR

This year's exciting program should provide the assurance for another successful symposium. It is with this assurance that I welcome each one, on behalf of the International Wire and Cable Symposium (IWCS) Committee and CECOM, Fort Monmouth, New Jersey to this year's major technical event on wire/cable technology. The technical program, as always, is considered unique, since with the large worldwide response to the call-for-paper, the program includes information on the latest developments/advancements on wires, cables, materials and cable systems from more than sixteen different countries.

The overall objective of the committee is for the symposium to remain a reflection of the needs and interest of its attendees and contributors, therefore, it is hoped that the technical program will always include topics of pertinent interest to all wire, cable, materials and connector manufacturers/users. The program will at all times be a reflection of the current interests as indicated by the response to the call-for-papers. In addition, this year's opening tutorial session entitled "Global Markets for Communication Cables" and the special or invited sessions are intended to provide information on a technology that is constantly changing and should again provide the interest for an exciting symposium.

Committee member Dr. C. Ronald Simpkins of the E.I. DuPont de Nemours & Co., Inc. and Mr. George Webster of AT&T Bell Laboratories are retiring from the committee. Ron and George, by their efforts and specialized knowledge, contributed significantly to the success of the symposium. On behalf of the IWCS Committee, I extend to each a very special thanks for their sincere dedication, cooperation and support of the symposium objectives. The committee was saddened by the untimely death this year of committee member Robert Streich of AT&T Network Systems, Pheonix, AZ. Bob will be long remembered by his committee members and business associates for his many valuable contributions to the IWCS Committee and the wire/cable industry.

The committee continues to explore new ideas for improving the technical level of the symposium activities. Therefore, the committee solicits and need the continued support of all members of the wire and cable industry. Your comments and suggestions for improving the symposium are welcomed.

The 1991 Symposium (40th) will be in St. Louis, Missouri at the Adam's Mark Hotel. The 1992 (41st) Symposium will return to Bally's Reno Hotel, Reno, Nevada.

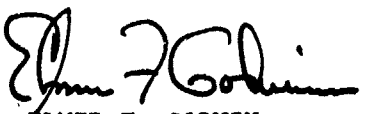

ELMER F. GODWIN
Director, IWCS

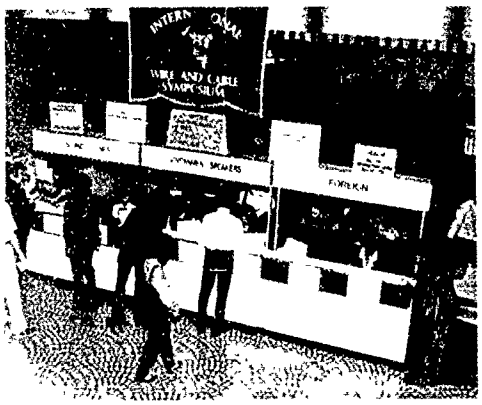

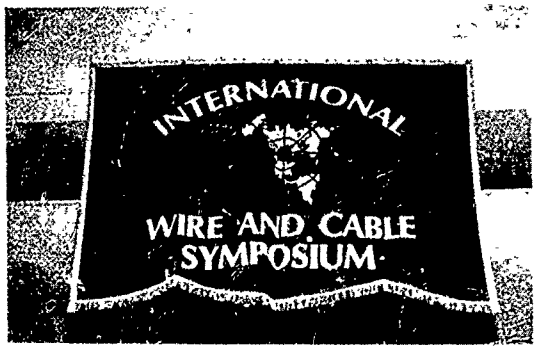

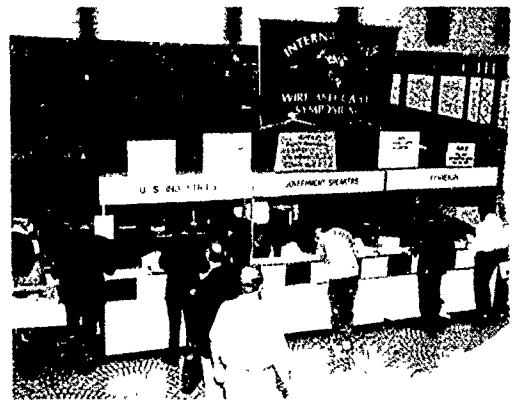

REGISTRATION IWCS

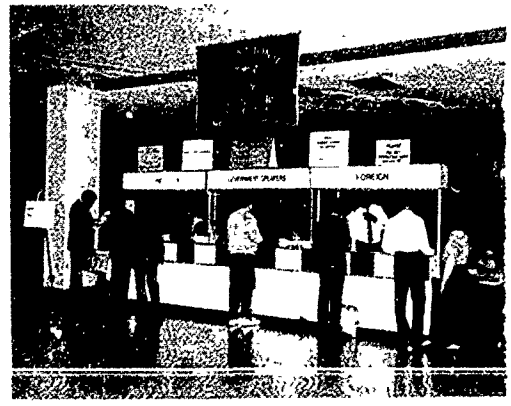

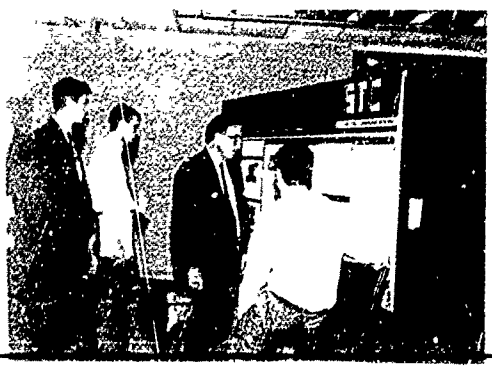

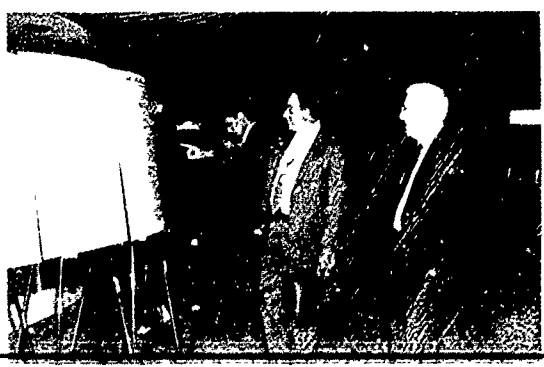

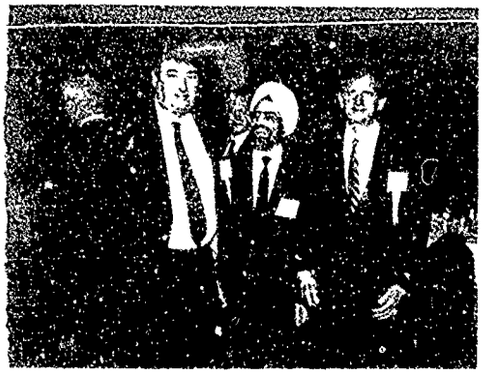


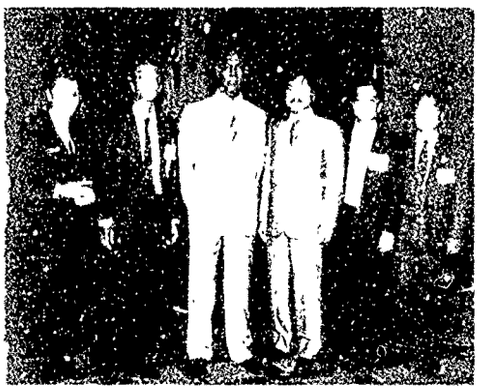


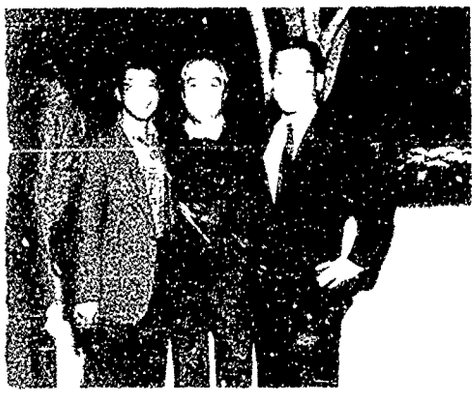






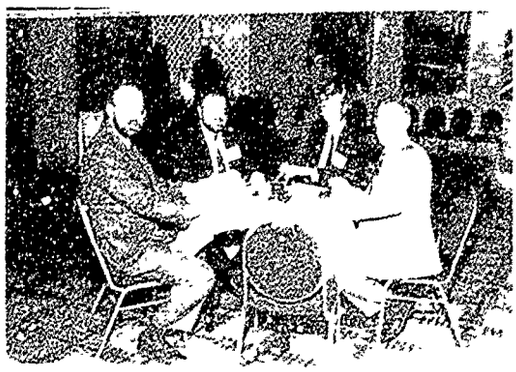


GETTING ACQUAINTED

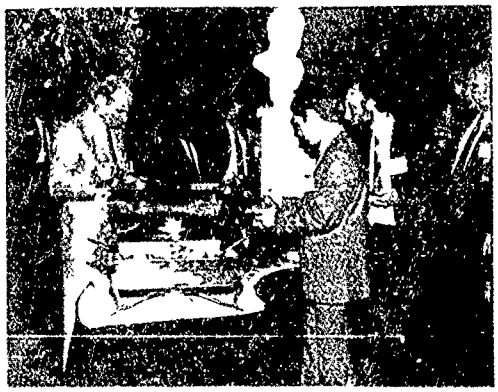




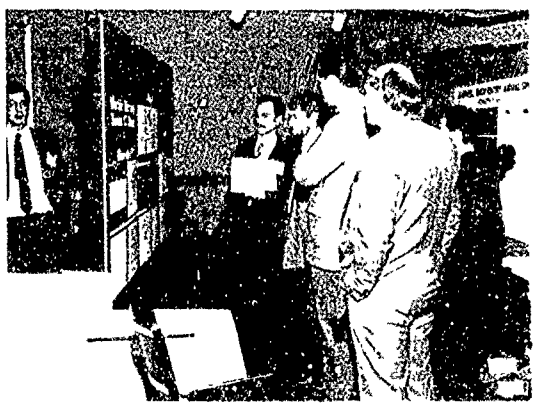
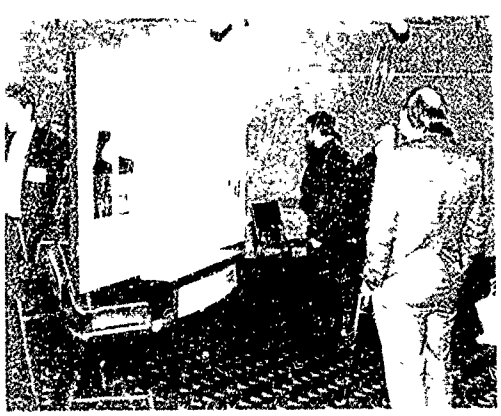
COCKTAIL
PARTY
POSTER
PAPERS
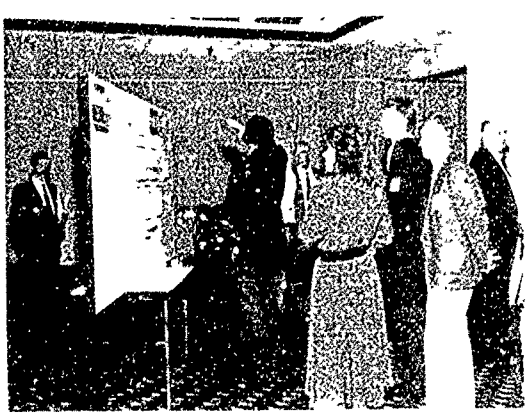
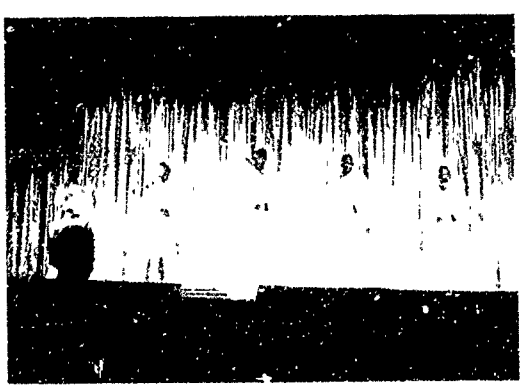
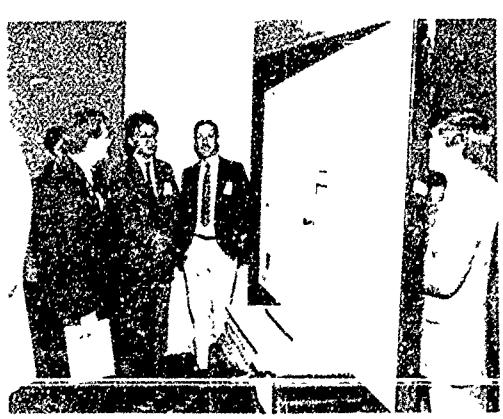

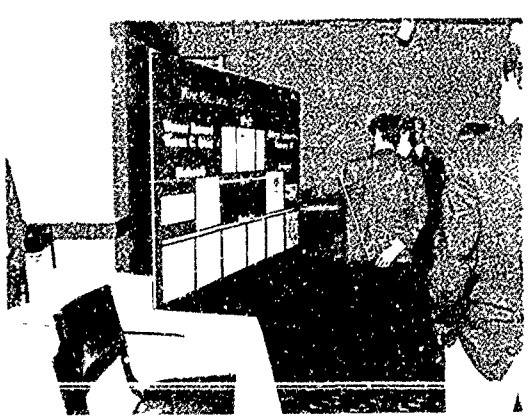




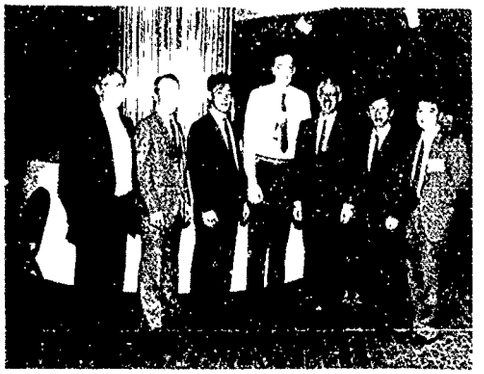




TWCS SESSION SPEAKERS TWCS

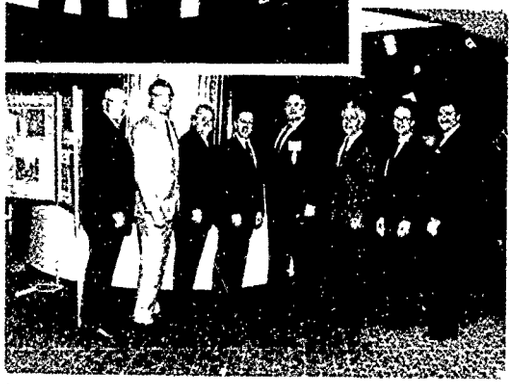
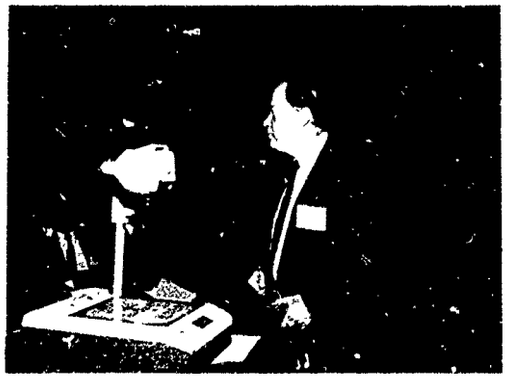

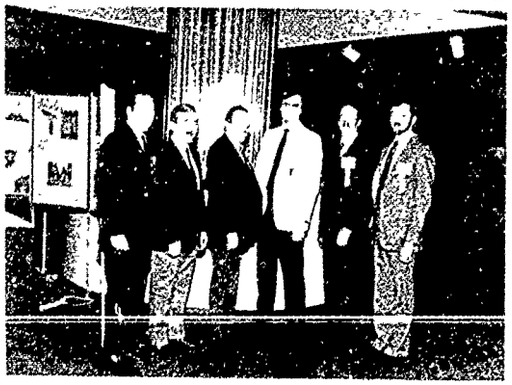



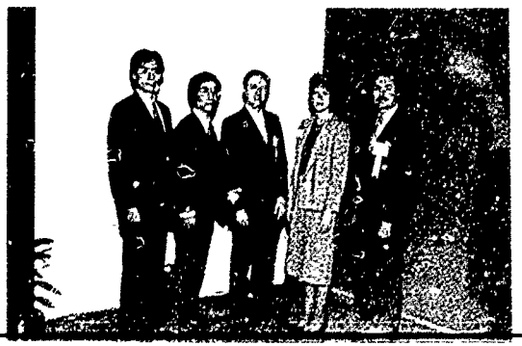


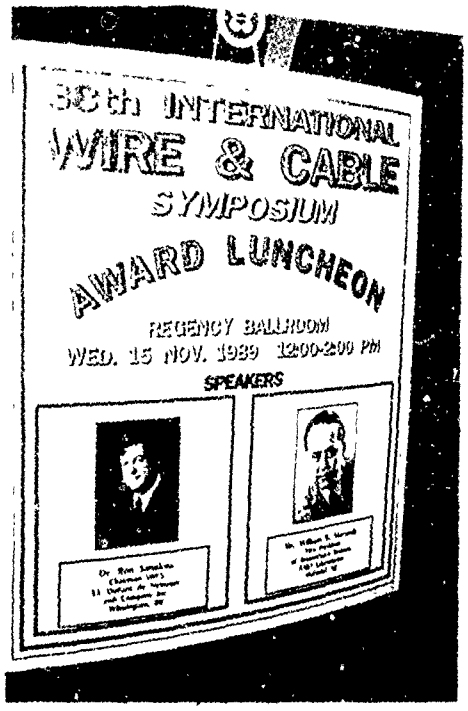
38th INTERNATIONAL
WIRE & CABLE
SYMPOSIUM
AWARD LUNCHEON
REGENCY BALLROOM
WED. 15 NOV. 1989 12:00-2:00 PM
SPEAKERS

AWARDS

Outstanding Technical Paper

H. Lubars and J. A. Olszewski, General Cable Corp. – "Analysis of Structural Return loss in CATV Coaxial Cable"

J. P. McCann, R. Sabia and B. Wargotz, Bell Laboratories—"Characterization of Filler and Insulation in Waterproof Cable"

D. E. Setzer and A. S. Windeler, Bell Laboratories—"A Low Capacitance Cable for the T2 Digital Transmission line"

R. Lyenger, R. McClean and T. McManus, Bell Northern Research—"An Advanced Multi-Unit Coaxial Cable for Toll PCM Systems"

J. B. Howard, Bell Laboratories—"Stabilization Problems with Low Density Polyethylene Insulations"

Dr.H. Margin, Kabelmetal—"High Power Radio Frequency Coaxial Cables, Their Design and Rating"

D. Doty, AMP Inc. – "Mass Wire Insulation Displacing Termination of Flat Cable"

T. S Choo, Dow Chemical U.S.A. – "Corrosion Studies on Shielding Materials for Underground Telephone Cables"

N. J. Cogelia, Bell Telephone Laboratories and G. K. Lavoie and J. F. Glahn, US Department of Interior – "Rodent Biting Pressure and Chemical Action and Their Effects on Wire and Cable Sheath"

T K. McManus, Northern Telecom Canada Ltd. and R. Beveridge, Saskatchewan Telecommunications, Canada—"A New Generation of Filled Core Cable"

F. Suzuki, S. Sato, A. Mori and Y. Suzuki; Sumitomo Electric Industries, Ltd. Japan—"Microcoaxial Cables Insulated with Highly Expanded Polyethylene By Chemical Blowing Method"

S. Masaki, Y. Yamazaki and T. Ideguchi, Nippon Telegraph and Telephone Public Corporation, Japan—"New Aluminum Sheath Cable Used for Electromagnetic Shielding"

P Kish and Y. BeBorgne, Northern Telecom Canada Limited,Motreal, Canada—"General Crosstalk Model For Paired Communication Cables"

C. J. Arroyo, N. J.Cogelia, Bell Laboratories, and B. J. Darsey, Western Electric—"Thermal Behavior of Experimental Plenum Cable Sheaths Determined in a Radiant Heat Chamber"

R. H. Whiteley, Raychem Ltd.—"A Comprehensive Small Scale Smoke Test"

V A. Fentress, Raychem Corp. and D. V. Nelson, Stanford University—"Fracture Mechanics Evaluation of the Static Fatigue Life of Optical Fibers in Bending"

M. Fujise and Y. Iwamoto, KDD Research & Development Laboratories, Tokyo, Japan—"Self-Core-Alignment Arc-Fusion Splicer Based on a Simple Local Monitoring Method"

James A. Krabec and John W. Kincaid, Jr., Belden Technical Research Center—"Advances in the Optimization of Multi-Layer Shield Design"

Simon D. Dadakarides and Bruce B. Lusignam, Stanford University—"Magnetically Loaded Cables"

Best Presentation

1968 N. Dean, B.I.C.C. – "The Development of Fully Filled Cables for Distribution Network"

1969 J. D. Kirk, Alberta Government Telephones—"Progress and pitfalls of Rural Buried Cable"

1970 Dr. O. Leuchs, Kable and Metalwerke—"A New Self-Extinguishing Hydrogen Chloride Binding PVC Jacketing Compound for Cables"

1971 S. Nordblad, Telefonaktiebolaget L. M. Ericsson—"Multi-Paired Cable of Nonlayer Design for Low Capacitance Unbalance Telecommunications Network"

N. Kojima Nippon Telegraph and Telephone – "New Type Paired Cable for High Speed PCM Transmission"

1972 S. Kaufman, Bell Laboratories—"Reclamation of Water-Logged Buried PIC Telephone Cable"

1973 R. J. Oakley, Northern Electric Co., Ltd.—"A Study Into Paired Cable Crosstalk"

1974 G. H. Webster, Bell Laboratories—"Material Savings by Design in Exchange and Trunk Telephone Cable"

1975 J. E. Wimsey, United States Air Force—"The Bare Base Electrical Systems"

1976 Michael DeLucia, Naval Ship Research and Development – "Highly Fire-Retardant Navy Shipboard Cable"

1977 William L. Schmacher, AMP Inc.—"Design Considerations for Single Fiber Connector"

1978 Richard C. Mondello, Bell Labs.—"Design and Manufacture of an Experimental Lightguide Cable For Undersea Transmission Systems"

1979 I. Wadehra, IBM Corporation—"Performance of Polyvinyl Chloride Communication Cables in Modified Steiner Tunnel Test"

1980 J. J. Refi, Bell Laboratories—"Mean Power Sum Far-End Crosstalk of PIC Cables as a Function of Average Twist Helix Angle"

1981 G. S. Anderson, Belden Corporation—"Installation of Fiber Optic Cable on 457 Meter Tower"

1982 A. Yoshizawa, The Furukawa Electric Co., Ltd.—"Structure and Characteristics of Cables for Robots"

1983 J. R. Bury, Standard Telecommunication Laboratories, Ltd., Hailow, England—"Development of Flame Retardant, Low Aggressivity Cables"

1984 William E. Dennis, Dow Corning Corporation, Midland, Michigan—"Hydrogen Evolving Tendencies of Cable Fillers and Optical Fiber Coatings"

1985 Stephen Hornung, British Telecom Research Laboratories—"Manufacture and Performance of Fibre Units for Installation by The Viscous Drag of Air"

1986 Dave Fischer, Superior Cable Corp.—"Progress Towards the Development of Lighting Test for Telecommunication Cables"

John C. Chamberlain, Siecor Corp.—"Zero Halogen Fire Retardant Fiber Optic Shipboard Cable"

Outstanding Technical Paper	*Outstanding Poster Paper*	*Best Presentation*
1987 Stephen B. Pierce—Conel Laboratories—"Digital Transmission on Customer Premises Wiring"	William Wood—Bell Communication Research "Performance Analysis of Optic Fiber Cleavers"	Richard Rossi—General Cable Company "Cable Sheathing Design and Performance Criteria"
1988 Martin C. Light Jr., James A. Moses, Mark A. Sigmon and Christopher A. Story – Siecor Corp. – "Design and Performance of Telecommunication Cable Optimized for low Fiber Count"	Dr. R. Raman - Contel Laboratories —"Loss at Dissimilar Fiber Splices"	Janice B. Haber - AT&T Laboratories "Single-Mode Media and Apparatus for Fiber to the Home"
1989		
Outstanding Technical Paper Michel Plasse, Lise Desroches and Paul-Andre Guilbert - Northern Telecom Canada Limited - "High Performance Twisted-Pair Cable for LAN Systems"	*Outstanding Poster Paper* Werner Bernard and Susan C. Grant - Siecor Corporation - "Fiber Optic Drop Cables in the Subscriber Loop"	*Best Presentation* Michel de Vecchis - Les Cables de Lyon - "Results on a Large Scale Installation of a Fibre Optic Distribution Network"

CONTRIBUTORS

AEG KABEL Aktiengesellschaft
Monchengladbach, Germany

Alberta Government Telephones
Calgary, Alberta Canada

Ant Machrichtentechnik GmbH
Backnang, Germany

AT Plastics, Inc.
Brampton, Ontario, Canada

Barcel Wire and Cable Corp.
Irvine, CA

Belden Engineering Center
Richmond, IN

Building Industry Consulting Service International (BICSI)
Tampa, FL

Canada Wire and Cable Limited
Winnipeg, Manitoba Canada

Carlew Inc.
Quebec, Canada

Ciba-Geigy Corporation
Hawthorne, NY

Contel Laboratories
Norcross, GA

DuPont Canada Inc.
Mississauga, Ontario, Canada

Dussek Campbell Limited
Belleville, Ontario, Canada

Dussek Campbell Ltd.
Crayford, Kent, U.K.

Dussex Campbell Pty. Ltd.
Regents Part, N.S.W. Australia

EMS-Chemie AG
Domat/Ems. Switzerland

Ericsson Cables AB
Hudiksvall, Sweden

Essex Group, Inc.
Decatur, IL

Furukawa Electric Co., Ltd.
New York, NY

General Cable Company
South Plainfield, NJ

Hong Kong Telephone Co Ltd
Hong Kong

Huls AG
Marl, West Germany

Kabelmetal Electro North America, Inc.
Larchmont, NY

Kroschu-Kabelwerke Krombert & Schubert GmbH u. Co.
Wuppertal, West Germany

MM Cables-Telecommunications
Clayton VIC, Australia

Philips Kommunikations IND. AG.
Koeln, West Germany

RXS Schrumpftechnik-Garnituren GmbH
Hagen, West Germany

Showa Electric Wire & Cable Co., Ltd.
Sagamihara, Kanagawa, Japan

Siemens AG
Munich 70, West Germany

Sumitomo Electric Industries, Ltd.
Sakae-ku, Yokohama, Japan

Superior TeleTec Inc.
Atlanta, GA

Swedish Telecom
Farsta, Sweden

Tensolite Company
St. Augustine, FL

Toray Plastics (America) Inc.
North Kingstown, RI

CONTRIBUTORS

AFA Industries
20 Jewell Street
Garfield, NJ

Akzo Fibers
801-F Blacklawn Road
Conyers, GA

Allied Apical Company
Columbia Road & Park Avenue
Morristown, NJ

AT&T Bell Labs
2000 Northeast Expressway
Norcross, GA

AT&T Network Cable Systems
P.O. Box 13369
Phoenix, AZ

ATOCHEM North America, Inc.
Three Parkway
Philadelphia, PA

Ausimont, Inc.
44 Whippany Road
Morristown, NJ

Belding Corticelli Thread Co.
Special Engineered Yarns Div.
4421 Stuart Andrew Blvd.
Charlotte, NC

Bell Canada
700 La Gauchetiere W. RM 18E2
Montreal, Quebec, Canada

The BFGoodrich Company
Geon Vinyl Division
6100 Oak Tree Boulevard
Cleveland, OH

Breen Color Concentrates, Inc.
306 Route 179
Lambertville, NJ

Camden Wire Co., Inc.
12 Masonic Avenue
Camden, NY

Cary Chemicals Inc.
R.R. #2, Box 255.5
Farmingdale, NJ

Chase & Sons
19 Highland Avenue
Randolph, Ma

Chromatics, Inc.
19 Francis J. Clarke Circle
Bethel, CT

Corning Incorporated
Main Plant RO-03-2
Corning, NY

DCM International Corporation
2930 Faber Street
Union City, CA

The Dow Chemical Co.
2020 WHDC
Midland, MI

DSM/Desotech, Inc.
1700 South Mt. Prospect Rd.
Des Plaines, IL

E.I. du Pont de Nemours & Co.
Little Falls Center II
P.O. Box 80810
Wilmington, DE

Facile Technologies
165 Sixth Avenue
Paterson, NJ

Fitel General, Inc.
201 Industrial Blvd.
P.O. Box 486
Carrollton, GA

Gary Chemical Corp.
Pioneer Industrial Park, Gitto Dr.
Leominster, MA

GE Plastics
One Plastics Avenue
Pittsfield, MA

Gem Grauvure Company, Inc.
112 School Street
W. Hanover, MA

GTE Test Mark Laboratories
3050 Harrodsburg Rd.
Lexington, KY

Hargro Industrial Packaging
20 Sand Park Road
Cedar Grove, NJ

ICI Advanced Materials
475 Creamery Way
Exton, PA

KT Industries Ltd.
1130 Wall Street
Winnipeg, Manitoba R3E 2R9 Canada

Lantor BV
P.O. Box 45, 3900 AA Veenendaal
The Netherlands

CONTRIBUTORS

Lindsay & Williams Limited
Ogden Lane Works
Columbine St.
Manchester, England

Mobay Corporation
Mobay Road
Plastics & Rubber Div., Bldg. 8
Pittsburgh, PA

Mohawk Wire and Cable Corporation
9 Mohawk Drive
Leominster, MA

NEPTCO, Inc.
Box 2323, 30 Hamlet Street
Pawtucket, RI

Nokia-Maillefer, Inc.
749 New Ludlow Road
South Hadley, MA

Northern Telecom Canada Ltd.
150 Montreal-Toronto Blvd.
Lachine, Quebec H8S 1B6 Canada

Northern Telecom Canada Ltd.
1370 Fletcher Road
Saskatoon, Saskatchewan, Canada

NTT America, Inc.
One Landmark Square, Room 700
Stamford, CT

Olex Cables
A Division of Pacific Dunlop Ltd.
207 Sunshine Road, Tottenham, 3012
Melbourne, Victoria, Australia

Optical Fibres
Second Ave., Deeside Industrial Park
Deeside, CLWYD, CH5 2NX, UK

Owens-Corning Fiberglas Corp.
Fiberglas Tower, T/8
Toledo, OH

PENRECO
106 South Main Street
Butler, PA

Photomatrix
[illegible] Road
[illegible]
Beaverton, [illegible]

Pirelli Cable Corp.
700 Industrial Drive
Lexington, SC

Quantum Chemical Corp., USI Division
11500 Northlake Drive
Cincinnati, OH

Siecor Corporation
489 Siecor Park
Hickory, NC

SpecTran Corporation
50 Hall Road
Sturbridge, MA

STC Cables
Wednesbury St.
Newport, Gwent, UK

The Stewart Group Ltd.
259 Steelcase Road W.
Markham, Ontario, Canada

Sumitoma Electric U.S.A. Inc.
21221 S. Western Ave., Suite 200
Torrance, CA

Teknor Apex Company
505 Central Avenue
Pawtucket, RI

Texas Instruments, Inc.
34 Forest Street
Attleboro, MA

3M TelComm Products Division
P.O. Box 2963
Austin, TX

UBE Industries (America), Inc.
666 5th Avenue
New York, NY

Union Carbide Corporation
Weston Canal Center, CN 450
Somerset, NJ

Vista Chemical Company
900 Threadneedle
Houston, TX

Water Guard Cable Products, Inc.
P.O. Box 1079
Channelview, TX

Weber & Scher Mfg. Co., Inc.
263 Sussex Avenue
Newark, NJ

Witco Corporation
520 Madison Avenue
New York, NY

TABLE OF CONTENTS

TUESDAY EVENING—6:30 PM-8:00 PM
HOSPITALITY HOUR
Broadway Room

Admission by tickets issued to all registrants

WEDNESDAY MORNING—8:30 AM-12:00 PM
Capital Rooms

SESSION V: OPTICAL FIBER AND CABLE DESIGN II

Chairperson: Mr. Manuel R. Santana, AT&T Bell Laboratories, Norcross, GA

WEDNESDAY MORNING—8:30 AM-12:00 PM
Bijou Complex

SESSION VI: ENVIRONMENTAL EFFECTS ON CABLES AND SYSTEMS

Chairperson: Dr. Robert Baboian, Texas Instruments, Inc , Attleboro, MA

WEDNESDAY MORNING—8:30 AM-12:00 PM
Adelphi Room

SESSION VII: SPLICING AND CONNECTORIZATION TECHNOLOGY

Chairperson: Mr. David Fallowfield, Alberta Government Telephones, Edmonton, Alberta, Canada

AWARDS LUNCHEON
12:00 Noon-2:00 PM
Ziegfield Theatre

Admission by tickets issued to all registrants

WEDNESDAY AFTERNOON—2:00 PM-4:00 PM
Capital Rooms

SESSION VIII: FIBER OPTIC CABLE INSTALLATION

Chairperson. Dr. C. Ronald Simpkins, E.I. DuPont de Nemours and Company, Inc., Wilmington, DE

WEDNESDAY AFTERNOON—2:00 PM-4:00 PM
Bijou Complex

SESSION IX: THERMAL AGING OF PLASTIC INSULATED CONDUCTORS

Chairperson: Mr. Homer Vela, AT&T Network Systems, Phoenix, AZ

WEDNESDAY AFTERNOON—2:00 PM-4:00 PM
Adelphi Room

SESSION X: TECHNOLOGY ADVANCEMENTS IN COPPER TELEPHONE CABLE PRODUCTION

Chairperson: Mr. Leo M. Chattler, DCM International Corporation, Union City, CA

WEDNESDAY AFTERNOON—3:30 PM-6:00 PM
Broadway Room

SESSION XI: POSTER SESSION

Chairperson: Dr. Peter R. Bark, Siecor Corp., Hickory, NC and Dr. Ken-ichi Aihara, NTT America Inc.

THURSDAY MORNING—8:30 AM-12:00 Noon
Capital Rooms

THURSDAY MORNING—8:30 AM-12:00 Noon
Bijou Complex

THURSDAY MORNING—8:30 AM-12:00 Noon
Adelphi Room

THURSDAY AFTERNOON—1:00 PM-4:30 PM
Capital Rooms

THURSDAY AFTERNOON—1:00 PM-4:30 PM
Bijou Complex

SESSION XVI. IMPACT OF COATING PROPERTIES ON FIBER PERFORMANCE

Chairperson: Dr. Raymond E. Jaeger, SpecTran Corp., Sturbridge, MA

THURSDAY AFTERNOON—1:00 PM-4:30 PM
Adelphi Room

SESSION XVII. TESTING OF CABLES, COMPONENTS & MATERIALS II

Chairperson: Mr. Irving Kolodny, Consultant, Bellerose Manor, NY

Dr. Raymond E. Jaeger
President & CEO
SpecTran Corporation
Sturbridge, MA

Dr. Jaeger is one of the founders of SpecTran Corporation. He has served as President and Chief Executive Officer since the company's inception in April 1981 and was named Chairman of the Board of Directors in 1986. Previously, he had been employed for five years as Director of Research and Development and then Vice President, Corporate Research and Development of Galileo Electro-Optics Corporation. Before that, Dr. Jaeger worked for Bell Telephone Laboratories where, for more than fifteen years, he was engaged in research on fiber optic and related materials and processes.

Dr. Jaeger is named as the inventor or co-inventor on numerous patents assigned to AT&T and SpecTran, and has written over thirty technical publications. A graduate of Rutgers, he holds a Ph.D. in Ceramics. In 1980, Dr. Jaeger was granted the Rutgers University Award for Outstanding Achievement in the field of engineering.

Russell Bodoff
Vice President
External Affairs
American National Standards Institute
New York, NY

Mr. Bodoff has been associated with the American National Standards Institute (ANSI) since 1981. He currently is Vice President of External Affairs, a position which he assumed in 1983. In this capacity, he is responsible for all membership, marketing and public relations activities. His prior assignments were as Director of Development from 1983 to 1988 and Sr. Program Administrator from 1981 to 1983.

Mr. Bodoff has a BS degree from Temple University and a MA degree from New York University. He holds memberships in the Standards Engineering Society, American Society of Association Executives and the Council of Engineering and Scientific Society of Executives.

John N. Kessler
President
KMI
Newport, RI

Mr. Kessler, President of KMI, heads an international consulting firm that specializes in fiberoptics market research. Mr. Kessler has prepared or directed more than 100 reports in this field, authored many articles on fiberoptics, and presented papers on fiberoptics markets and the techniques for forecasting such markets at universities and at professional society conferences in the U.S. and overseas. He wrote the first engineering article on fiberoptic communications for Electronics magazine in July, 1971.

Before co-founding KMI Corporation, Mr. Kessler directed market research in the area of optoelectronics for International Resource Development and for Frost & Sullivan. Prior to his work in fiberoptics, Mr. Kessler was a Member of the Administrative Staff at Bell Telephone Laboratories. He graduated with honors from the University of Pennsylvania and is a member of the IEEE and the Optical Society of America.

Lee J. Liebler
Vice President
Electrical/Electronics Products Markets
Copper Development Association Inc.
Greenwich, CN

Mr. Liebler is Vice President - Electrical/Electronics Products Markets for the Copper Development Association Inc. He joined CDA early in 1989 following nineteen years of progressive experience at AMP Inc. in market research, new product development and business development. He led AMP's efforts which resulted in the development and acceptance of the connector and tool to reterminate, with copper "pigtails," dangerous aluminum building wiring systems installed in the 1970's.

Prior to his employment at AMP, Mr. Liebler held engineering positions at ALCOA and U.S. Steel. At ALCOA he was involved in the development of electrical connectors for underground distribution systems. He has a bachelor's degree in electrical engineering from the University of Dayton and an M.B.A. from Northern University.

O.J. Gusella, Jr.
Executive Director
Exchange Carriers Standard Association
Bethesda, MD

Mr. Gusella is Executive Director of the Exchange Carriers Standards Association. In this position he is responsible for all administrative activities for the technical committees and disciplines of the Association. These include: the Exchange Telephone Group Committee, accredited Committee T1-Telecommunications, and the International Relations group.

Mr. Gusella started with ECSA in January 1984 after retiring from GTE. He is active in CCITT, where he is head of the U.S. Delegation to study Group XI; ANSI; IFAC-2; and the USTR where he has recently been a member of two U.S. Trade Missions.

He and his wife, Marlene, reside in Germantown, Maryland.

Joseph J. Pucilowski, Jr.
Director, CECOM Center for Command, Control and Communications Systems
U.S. Army Communications-Electronics Command, Fort Monmouth, NJ

Mr. Joseph J. Pucilowski, Jr. was appointed as Director of the CECOM Center for Command, Control and Communications (C3) Systems, U.S. Army Communications-Electronics Command (CECOM), August 1990. He has command responsibility for planning, coordinating, managing and implementing internal and external research, development and engineering programs to fill the Army's tactical C3 needs, while also providing full technical support to U.S. Army Program Executive Officers and Project Managers in C3. He leads and manages 300 engineers and scientists in the execution of these tasks. In his 27 years of government experience, he has been involved in many aspects of Research and Development for Command, Control and Communications Systems.

He received a Bachelor of Arts in Physics, with a minor in Mathematics from Rutgers University, and a Master of Science in Electrical Engineering from Fairleigh Dickinson University. He was appointed by the Secretary of the Army to the Senior Executive Service in November 1986.

In his previous assignment as Director of the Product Assurance and Test Directorate, (CECOM), he had command responsibility for the development and execution of Reliability, Maintainability, Quality Assurance and Testing for all CECOM R&D and production programs.

Mr. Pucilowski's assignments have included: Associate Director for Research and Technology and Associate Technical Director for Automation, for the CECOM Research, Development and Engineering Center, Associate Director for Information Processing Technology, in the Center for Communications/ Automatic Data Processing, and Deputy Director and Acting Director of the Center for Tactical Computer Systems, U.S. Army CECOM, Fort Monmouth

Mr. Pucilowski serves on the Executive Committee and is also a Director for the Fort Monmouth Chapter of the Armed Forces Communications and Electronics Association (AFCEA). He is a past President and was the Chairman of the 14th Annual AFCEA Symposium. He also serves as an Honorary Advisor Member of the Board of AUSA.

Mr. Pucilowski served as the United States representative to NATO SubGroup IX, Defense Equipment Reliability and Maintainability (RAM) Assurance and as a member of the American British Canadian Australian (ABCA) Committee on RAM. He has been Chairman of the DoD Technology of Distributed C3 Systems subpanel while a member of the DoD C3 Technology Assessment Steering Group. He has been a member of the N.J. Department of Higher Education's Panel on Faculty Development in Telecommunications and Army Member of the Joint Logistic Commanders (JLC)/Joint Directors of Laboratories (JDL) Subcommittee on Computer Sciences, as well as, an ad-hoc member of the JLC/JDL subcommittee on C3. He has published or presented thirty-three technical papers.

He is married to the former Maryann Giambalvo. They have six children--Adam, Joseph, Linda Ann, Mary, Kristin and Francine.

Arthur W. Brothers
President
The Beehive Telephone Company
Lakepoint, UT

Art celebrates his 60th birthday next month.

Many of us are regular readers of his stories in Telephone Engineering and Management magazine. Art has been writing those stories for ten years. Many of us turn to the back page of TE&M - and if "The Party Line" is not there, the magazine goes to file 13.

Art's column permits us to get "down in the trenches" of daily problems of a tiny telco serving the left-overs. Art's service areas are those tiny pockets of people whom, as the Wall Street Journal says "were passed over by the larger companies as not being profitable to serve."

The Beehive Telephone Company is known throughout Utah as an aggressive David, battling the Goliath of U.S. West, AT&T, Government, States, Counties, and Cities. He has been featured on numerous TV broadcasts and in local and national newspaper articles.

The University of Wyoming has set aside a special section in its Western History Department as a repository of information about Art and his efforts to provide telephone to rural areas. Many isolated areas, from the islands off Maine, to the islands off California - got their phones from individuals who received their encouragement by the example of Art's "leading the way" - or from the larger companies that "got off their duff" just to "keep him out."

Art was born in Salt Lake City. His parents died at an early age, and he was raised as a ward of the State until he left high school at age 17 and joined the U.S. Air Force. Five years later he was discharged with five bronze stars from Korea, and a solid background in all phases of tube and mechanical electronics.

Things have changed.

During his four years at the University of Utah, Art distinguished himself by:

(1) Getting more (unpaid) traffic tickets than any other student.

(2) Making it through his major in Business Management.

(3) Working a lot - repairing TV sets and buying/selling war surplus radios.

(4) And occasionally, going out on dates.

(5) Going to law school for 5 months.

(6) Turning down a job with Bank of America "to help them computerize their bank." (Art says they did not offer him enough money - and he didn't know you could bargain for more - they didn't teach that in business management.)

So he went to New York City as an assistant Editor for the Amateur Radio magazine "CQ." Art says it was like paying him to play. Amateur Radio has always been his hobby.

From New York, Art went to California and Edited a small regional Amateur Radio publication on the side. He worked in a variety of electronics industry positions and eventually started his own company as a manufactures representative.

In 1963 Art filed for and received authority from the State of Utah to provide telephone service to northwest Utah. His first system was turned up in January of 1966. From then on, Art has literally plowed the money back into the ground as he upgraded from surplus cable on fences, to fiber today.

Beehive has nine digital Central Offices and over 450 route miles of toll serving a total of 600 customers in Utah and Nevada.

Art has appeared as expert witness before the Federal Communications Commission, and Public Utilities Commissions in several States.

LOW LOSS HEAT RESISTANT PLASTIC CLADDING FIBER WITH POLYORGANOSILSESQUIOXANE CLADDIGNG

M.Honjo , Y.Matsuda and T.Yamanishi

Sumitomo Electric Industies, Ltd.

1,Taya-cho, Sakae-ku, Yokohama, Japan

Abstract

A plastic cladding optical fiber(PCF) with a polysilsesquioxane (a ladder polysiloxane) cladding was developed. This ladder polysiloxane cladding fiber has higher optical and mechanical properties than that of a linear polysiloxanecladding fiber or a fluoroacrylate cladding fiber. The attenuation at 0.81 μm wavelength and the numerical aperture for the LS-PCF are 4.2dB/km and 0.4 respectively. The primary advantage of the LS-PCF is superior thermal stability than that of the conventional plastic cladding fibers. The LS-PCF also has the capability to the crimp and cleave optical connector system, because the ladder polysiloxane cladding layer is enough hard to be connectorized mechanically.

1.Introduction

Recently PCF has been used for various purposes such as an optical short link system, a medical application and an optical fiber sensor.

A ladder siloxane polymer has been investigated as a coating material for the optical fiber, because of its coating capability and excellent physical properties including abrasion resistance and thermal stability.

However the successful application of the ladder siloxane polymer to the PCF utilizing its optical purity and appropriate refractive index as a cladding material have not been reported.

We developed the LS-PCF which has higher optical and mechanical properties than that of the conventional PCF such as a linear polysiloxane cladding fiber or a floroacrylate cladding fiber.

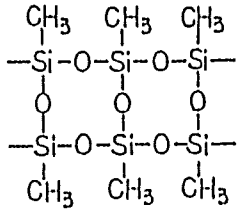

Fig 1 Structure for a ladder polysiloxane.

2.Characteristics of Ladder Polysiloxane

The ladder polysiloxane has an intermediate molecular structure between the organic polysiloxane and the inorganic polysiloxane. The idealized molecular structure of a ladder polysiloxane is shown in Fig.1. The specific ladder polysiloxane which has methyl pendant groups was selected as the cladding material in consideration with refractive index. The methyl ladder siloxane polymer has lower refractive index than that of the silica glass and sufficient rigidity, enough thermal stability.

In order to make a film of ladder polysiloxane,the solution of ladder siloxane is prepared by dissolving ladder siloxane oligomer in a solvent. The ladder siloxane oligomer has hydroxy and ethoxy functional groups as the terminal groups and polymerizes by dehydration and condensation reactions of the terminal functional groups. The selection of the solvent was carefully considered in view of the solubility and reactivity with the ladder siloxane polymer.

Table 1 Properties of the ladder polysiloxane

hardness(Shore D)	50
Young's modulus	100kg/mm^2
elongation	8%
refractive index n^{25}_D	1.42
coefficient of linear expansion	5×10^{-5}°C^{-1}

Finally we found that the solvents containing -ROH groups had good solubility and reactivity with the ladder polysiloxane. The polymer solution cures by vaporization of the solvent and polymerization of the ladder siloxane oligomer by the dehydration and the condensation reactions with H_2O and C_2H_5OH as byproducts. During cure, the solvent is also taken into the ladder polysiloxane, because -ROH groups of the solvent also react with the functional groups of the ladder siloxane oligomer.

A film of 200 μm in thickness of the ladder polysiloxane was prepared by two steps of heat treatment at 60 ℃ for 24 hours and at 120 ℃ for 24 hours. The evaluation results of the film sample were shown in Table 1. The ladder polysiloxane has higher hardness and lower coefficient of linear expansion than that of the ordinary organic polymers because of its intermediate molecular stracture between the organic materials and the inorganic materials.

Simultaneously the ladder polysiloxene has good stability in high temperture. The weight change of the ladder polysiloxane films measured by thermogravimetry at elevated temperatures is shown in Fig.2

The weight loss below 200 ℃ are due to the evaporation of some part of the solvent. The uncured oligomer and the byproducts of curing reaction vaporize in the temperature range of 200 ℃ to 400 ℃. Above 400 ℃, the methyl pendant groups of the ladder polysiloxane main chain decomposed. The amount of the weight loss of the ladder polysiloxane is very little compared with that of the linear polysiloxane and the other organic polymers.

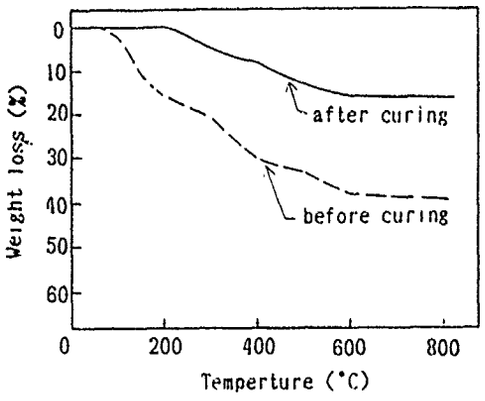

Fig. 2 Weight loss of ladder polysiloxane at high temperature.

3.Fiber Fabrication

The polymer solution of ladder siloxane was prepared in the same manner with the above mentioned film preparation. The viscosity was adjusted to about 3000cps by adding the appropriate amount of the solvent. The LS-PCF was manufactured by drawing a pure silica fiber to a diameter of 200 μm and coating the polymer solution onto the pure silica fiber to a diameter of 240 μm as shown in Fig.3.

The coating layer was dried and cured by passing the curing furnace located just below the coating applicater. The curing temperature of the ladder siloxane cladding was about 250 ℃.

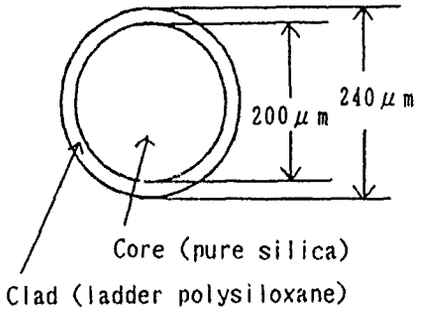

Fig. 3 Cross section of LS-PCF.

4.Proprerties of LS-PCF

4-1.Transmission properties

Typical spectral attenuation for the LS-PCF is shown in Fig.4. The attenuation loss at 0.81 μ m wavelength and the numerical aperture are 4.2 dB/km and 0.4 respectively.

The polts of α vs. $1/\lambda^4$ indicated that the attenuation loss corresponding to the structural irregularity is less than 1dB/km as shown in Fi.5. Fig.6 shows the attenuation loss at low temperatures for 1km length fiber. The loss increase at -20 ℃ is 0.93dB/km. This value is nearly equal to that of fluoroacrylate cladding fiber and much lower than that of linear polysiloxane cladding fiber. This is due to sufficient low linear expansion coefficient of the ladder polysiloxane. The transmission loss change in high humidity condition of 60 ℃ 95%RH is less than 0.5dB/km.

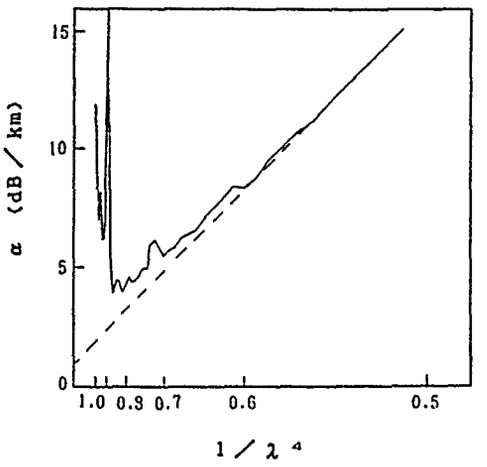

Fig. 5 Plots of α vs. $1/\lambda^4$ for LS-PCF.

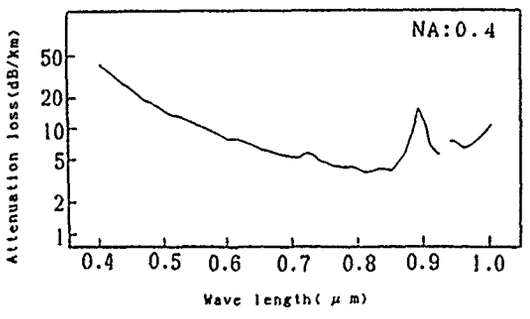

Fig. 4 Spectral attenuation for LS-PCF.

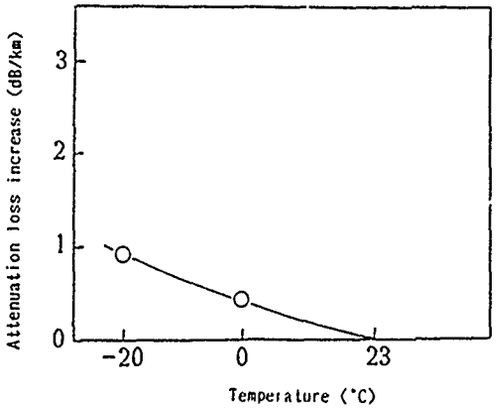

Fig. 6 Attenuation loss increase for LS-PCF at low temperature.

4-2.Mechanical properties.

Fig.7 shows the Weibull plots of tensile strength for the LS-PCF measured on 300mm gage length with 100mm/min tensile speed. The LS-PCF has the sufficient strength and no low strength region, because the glass fiber surface is protected from an external attack by the hard cladding layer. The repeated bending test was conducted with 2 seconds repetition period at 23 ℃ in air as shown in Fig.8. The fibers were bent 90 degrees around the mandrel of 5mm diameter for both side with 5g tension. The repetition number to failure was 30000 times. The LS-PCF has excellent flexibility than the conventional PCF.

The crimp and cleave optical connector system was applicable, because the ladder polysiloxane

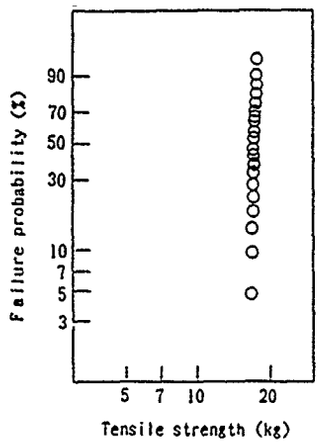

Fig. 7 Weibull plots of tensile strength for LS-PCF.

cladding layer is hard enough to be connecterized mechnically. The static fatigue of the LS-PCF was evaluated using the mandrel winding method. The gage length of specimens was 1m and 10 specimens were tested at each condition. The static fatigue data were plotted as median time to failure vs. applied strain (Fig.9). Both of the fatigue parameter n in air at 23 ℃ and in water at 23 ℃ were 29. This value is superior to the ordinary glass fibers. It is thought that the ladder polysiloxane cladding layer acts as a good water and moisture barrier.

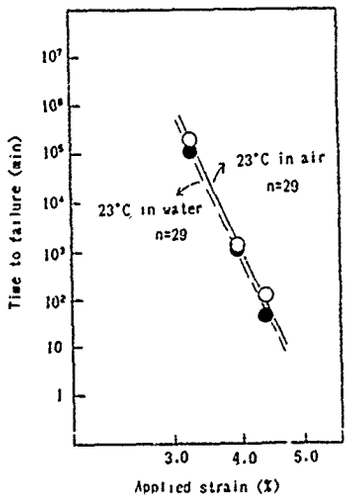

Fig. 9 Static fatigue properties for LS-PCF.

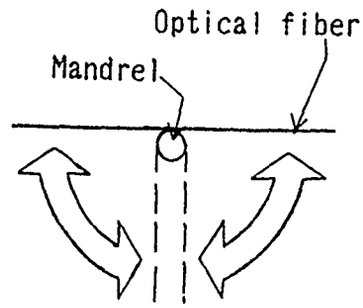

Fig. 8 Method of repeated bending test.

4-3.Thermal stability

The LS-PCF has stable optical properties in high temperature compared with the conventional PCF. The conventional PCF showed attenuation loss increase after 125 ℃ aging as shown in Fig.10. In a case of the LS-PCF, no loss increase for the aged fibers at 125 ℃ for 60 days was observed.

We monitered the attenuation loss increase for the LS-PCF aged at 180 ℃, 200 ℃ and 230 ℃. The time when the attenuation loss increase was observed was ploted against the temperature in Fig.11. Arrhenius plots of Fig.11 indicate that estimated time when the loss increase occur in the fiber operated at 150 ℃ is 1 year.

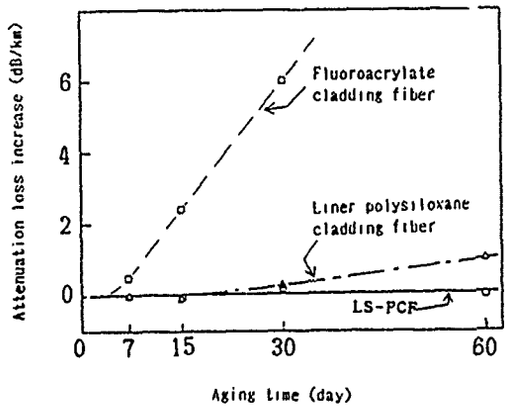

Fig. 10 Attenuation loss increase for LS-PCF after aging at 125℃.

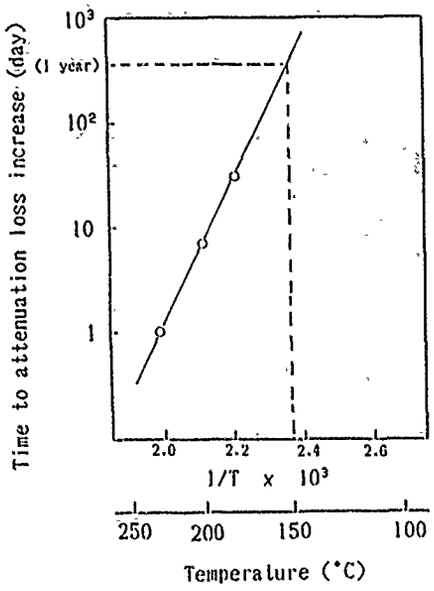

Fig. 11 Arrhenius plots of time to attenuation loss increase for LS-PCF.

5.Conclusion:

The first application of the ladder polysiloxane to the plastic cladding fiber was successfully conducted. Newly developed LS-PCF has higher optical and mechanical properties than that of the conventional PCF.

The properties of the LS-PCF in comparison with the conventional PCF are shown in Table 2.

The remarkable properties of the LS-PCF are as follows;

1) The LS-PCF has the low attenuation loss and the high numerical aperture.
2) The LS-PCF is superior in the thermal stability to the conventional PCF.
3) The LS-PCF has the sufficient tensile strength, flexibility, and high static fatigue parameters.
4) The crimp and cleave optical connector system is applicable.

Table 2 The transmission characteristics and mechanical properties of LS-PCF

	LS-PCF	Linear polysiloxane cladding fiber	Fluoroacylate cladding fiber
Transmission characteristics			
Attenuation loss λ=0.81 μm (dB/km)	4	4	4
NA L=2m	0.4	0.4	0.5
Attenuation loss increase at -20℃ (dB/km)	0.9	2.3	1.0
Attenuation loss increase after aging at 125℃ for 30days (dB/km)	<0.1	0.3	6.0
Mechanical properties			
Tensile strength L=300mm (kg)	16	16	16
Repeated bending test 5mmϕ mandrel repetition number to failure	30,000	5,000	30,000
Static fatigue n value at 23℃ in air	29	24	29
Application of crimp & cleave connector	○	×	○

Reference

1) H.Nishimoto, M.Sugai, Y.Okuda, et al, "Development of Hard Clad PCS Fiber" Sumitomo Electric Technical Review 28, 95 (1989)

2) B.G.Bagley, C.R.Kurkjian and W.E.Quinn, "The Use of an Organosilsesquioxane for the Coating / Cladding of Silica Fibers", Material Research Society Symposium Proceeding, 88, 35 (1987).

3) B.G.Bagley and W.E.Quinn, "The Processing and Use of Organosilicon Polymers for Photonic Application", Polymer Engineering and Science, 29, 17, 1197 (1989).

4) S.Araki, T.Shimomichi and H.Suzuki, "A New Heat Resistant Optical Fiber with Special Coating", 37th International Wire and Cable Symposium Proceeding, 745 (1988).

Yasuo Matsuda
Sumitomo Electric Industries,Ltd.
1,Taya-cho
Sakae-ku
Yokohama 244
Japan

Yasuo Matsuda received the M.S. degree in industrial chemistry from Tokyo University in 1978. He joined Sumitomo Electric Industries, Ltd. in 1978, and has been engaged in research and development of optical fiber and cables.

Mr. Matsuda is a senior engineer of Transmission Media R & D Department, Yokohama Research Laboratories.

Makoto Honjo
Sumitomo Electric Industries,Ltd.
1,Taya-cho
Sakae-ku
Yokohama 244
Japan

Makoto Honjo received the B.S. and M.S. degrees in applied chemistry from Osaka University in 1982 and 1984, respectively. He joined Sumitomo Electric Industries Ltd. in 1984, and has been engaged in research and development of optical fibers and cable. Mr.Honjo is a member of Chemical Society of Japan.

Toru Yamanishi
Sumitomo Electric Industries,Ltd.
1,Taya-cho
Sakae-ku
Yokohama 244,Japan

Toru Yamanishi received a B.S. degree of Chemical Engineering from Hokkaido University in 1972. He joined Sumitomo Electric Industries, Ltd. and worked on the research and development of optical fiber fabrication, especially fiber drawing and coating. Mr.Yamanishi is now a chief research associate of Transmission Media R & D Department.

High-NA Large-Bandwidth Hard Plastic Clad GI Silica Optical Fiber for Front-End LAN Applications

Hiroaki NISHIMOTO*, Takayuki MISHIMA*, Hiroki NAGASE** and Toshihiro AKIE*

*Sumitomo Electric Industries, Ltd.
Osaka, Japan

**Sumitomo Electric Industries, Ltd.
Yokohama, Japan

Abstract --- A development of 200μm core / 230μm cladding Graded Index type Hard Plastic Clad Silica (H-PCS) optical fiber which employs germanium doped silica glass for the core and a integrated hard protective polymer for the cladding is presented. Particular emphasis is placed on maximizing bandwidth performance with inexpensive short wavelength LED, with maintaining unique characteristics of H-PCS such as high numerical aperture (NA=0.4), high reliability and easy termination with crimp&cleave type optical connectors which can be assembled in 3minutes per end. Measurements with a surface emitting LED of 850nm exhibit the bandwidth and optical loss of more than 80 MHz.km and less than 7 dB/km respectively, and maximum coupled optical power of 10dB larger than that of a typical 50μm / 125μm GI silica fiber. These results demonstrate the possibility to realize quite economical, easy-handling fiber optic high speed data-link systems for Front-end LAN applications.

I. Introduction

Recent rapid spreadding of Engineering Work Stations (EWSs) and personal computers with high performance has been accelerating the use of fiberoptic high speed Local Area Networks (LANs) for the effective sharing of increasing information resources. Particularly, the standardization of the FDDI (Fiber Distributed Data Interface) by ANSI (American National Standard Institute), an international standard for 100 Mbps tokenring fiber optic LAN which employs long wavelength (λ=1,300 nm) LED for the E/O device and 62.5/125 μm silica fiber for the transmission media has contributed to the rapid market growth of the fiberoptic LAN equipments especially in the field of Backbone LAN applications. [6] On the other hand, because of the practically shorter distance between nodes and larger number of node equipments, the Front-end LAN market is much more sensitive to the cost of node equipments than the Backbone LAN market. Therefore, it is no exaggeration to say that the growth of the fiberoptic Front-end LAN market depends on the cost of the optical data-link (E/O, O/E) devices and connector assembling works, and the necessity for considering the new derivative standards has begun to be proposed to realize more inexpensive physical layers by using for example low cost fiberoptic data-link devices which employ short wavelength LEDs. [4]

Recently, as a key component to meet such demands as realizing economical data-link devices and easy connector assembling works, Hard Plastic Clad Silica (H-PCS) Optical Fiber, [5] which employs silica glass for the core and a hard protective polymer for the cladding, has become to receive much attention. H-PCS is a unique and attractive optical fiber which has such special features as;

- high Numerical Aperture (NA=0.4) and large core diameter (200 μm) accomplish extremely high coupling efficiency with LED and allow to design economical data-link devices and connectors
- dramatically easier field connector assembly works by using economical "crimp & cleave" type [7] new departure optical connectors (less than 3 minutes / end)
- high tensile strength and reliability during rough handling and extreme temperatures.
- low transmission loss at the wavelength range of various LEDs (4 to 6 dB/km at 700 to 870 nm), (7 to 10 dB/km at 650 to 900 nm), (7 to 10 dB/km at 1300 nm)

which have resulted in the rapid expansion of the market share for the H-PCS, particularly in the area of low speed (up to 10 Mbps) short distance industrial data-links and Factory Automation LAN systems for CIM applications. The H-PCS has recently also been utilized in the area of higher-speed Front-end LAN and RGB image transmission applications in the office which requires minimum data speed of 100 to 250 Mbps at the node to node length of 100 to 500 meters. These new applications require a H-PCS type new fiber with an even larger bandwidth than the previous H-PCS, because the bandwidth characteristics of the previous H-PCS is not always large enough to realize the maximum demands for high speed data transmission in this application field. Hence, In order to extend the application field of H-PCS, bandwidth enlargement technology is strongly required.

As a upper-compatible line-up of 200 μm core, 230 μm cladding PCS products which have authorized as a standard fiber by JIS (Japanese Industrial Standard) and are under consideration for standardization by IEC, the authors developed a high NA, broad bandwidth new H-PCS fiber with Graded Index (GI) core, by optimizing the index profile and designing new cladding materials. Maintaining the attractive features of the conventional Step Index (SI) H-PCS, the developed fiber exhibited much higher NA and almost the same bandwidth properties (more than 80 MHz.km) as the 50 μm / 125 μm GI silica fiber with inexpensive short wavelength LED light sources,

throughout the practical operational temperature range. The examination of the various basic performance parameters which include the applicability to the crimp & cleave type optical connectors confirmed that this new fiber accomplished the requirements for practical use in this field of applications. In this paper, we report the results of evaluations we made on the various characteristics of the GI H-PCS fiber.

II. Target Specifications

It is generally known that most of the transmission cable lengths between nodes for intra-office front-end LAN are no more than 100 meters. In this transmission length, conventional 200 / 230 µm Step Index (SI) type H-PCS fiber can realize the high-speed data transmission of up to 125 Mbps, which meets the data-rate specification of FDDI. But when planning a fiberoptic data transmission system with high universality, system designer has to employ the optical fiber which meets the demand of the greatest common measure. Therefore it was unavoidable that the demand for higher data-rate and longer transmission distance which occupies less than a few percentages of the total demands in the application field, prevented the system designer from employing the H-PCS fiber which has such unique properties as indicated above.

The purpose of the fiber development in this paper was to eliminate the technical limitation of the application market for H-PCS fibers, and to provide the attractive features of H-PCS fibers for LAN system customers. The primary design target was to achieve the bandwidth properties as broad as that of the standard 50 /125 µm GI silica fiber with using economical short-wavelength Surface emitting LED (S-LED) as E/O device. Because of the effect of the material dispersion of the fiber, [3] as shown in Figure 1, the bandwidth of the standard 50 /125 mm GI silica fiber, which exhibits broad bandwidth of more than 500 MHz.km with a 1,300 nm LD as the light source, was measured to be approximately 80 MHz.km with a 850 nm S-LED which has larger spectrum width. Therefore the target value for the bandwidth of new fiber were selected to be 80 MHz.km (typical) and 50 MHz.km (minimum). The secondary design target were to keep structural compatibility with the conventional H-PCS fiber and to preserve such advantages of H-PCS as high coupling efficiency with LED, small bending loss, high tensile / bending strength, large operating temperature and the applicability to the crimp & cleave type optical connectors.

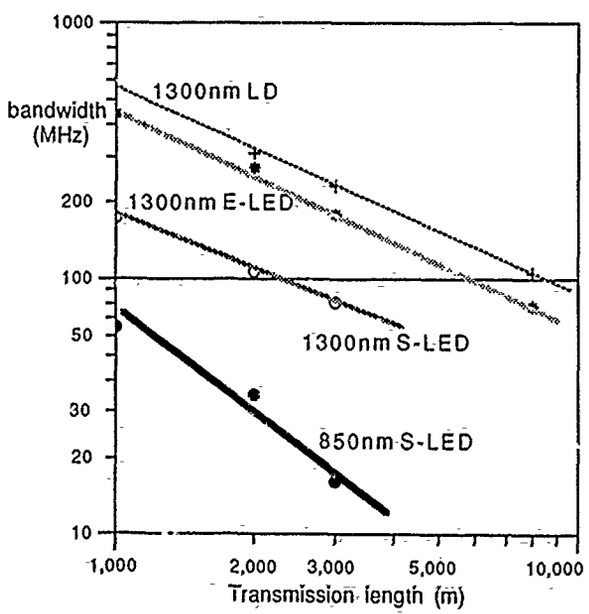

Figure 1. Typical transmission bandwidth characteristics for 50 / 125 µm GI silica fiber with various types of semiconductor light source

To solve the trade-off relationships between the bandwidth property and the bending loss / coupling efficiency properties of the fiber, [2] the optimization of the index profile which include the design of the refractive index characteristics of the cladding material was essential.

The following lists the target specifications for the GI H-PCS optical fiber.

*	Maximum NA	: 0.4 or larger
*	Storage temperature	: -40 to 70 °C
*	Operating temperature	: -20 to 70 °C
*	Bandwidth	: 80 MHz.km (typical)
	with 850 nm S-LED	: 50 MHz.km (Minimum)
	[Insertion NA=0.25, 1 km]	
*	Optical loss	: 5 dB/km (Typical)
	with 850 nm S-LED	: 6 dB/km (Maximum)
	[Insertion NA=0.25, 25 °C, 1 km]	
*	Optical loss increase at	: no more than 2 dB/1 km
	low temperature (-20 °C)	: no more than 1.5 dB/100 m
	[Insertion NA=0.25, compared with 25 °C]	
*	Bending Loss	: no more than 0.3 dB
	by 10 turns×5 mm radius	
	[Insertion NA=0.25]	
*	Optical loss increase by	: no more than 0.5 dB / end
	crimp & cleave type	[with CF-1011,-2011 series
	connector assembly	JIS F05,07 based
	[Insertion NA=0.25, 1 m]	connectors]

III. Constructions and Index Profiles

Table 1 and Figure 2, 3 show the index profile and the construction of the newly developed GI type H-PCS and the conventional SI type H-PCS. Both fibers have a core diameter of 200 µm, a cladding diameter of 230 µm and a simple construction with a protective coating of 0.5 mm diameter, and have the mechanical compatibility for connection each other.

As functions of the core diameter (a), the maximum refractive index of the core (n_1), refractive index of the cladding (n_2), index profile multiplier coefficient of the core (α) and a coefficient to determine the uncontinuity of the refractive index on the boundary between core and cladding (ρ), the index profiles of Figure 2 are given by the following equations:

$$n(r) = \begin{cases} n_1 [1-2\rho\Delta(r/a)^{\alpha}]^{1/2} & (0 \ll r \ll a) \\ n_2 = n_1 [1-2\rho\Delta]^{1/2} & (a<r) \end{cases} \quad \cdots\cdots (1)$$

where $\Delta = (n_1^2-n_2^2)/2n_1^2$ ..... (2)

The fiber we have developed this time is what is called a "Truncated" type GI fiber which has a special index profile featured by $\rho < 1$.

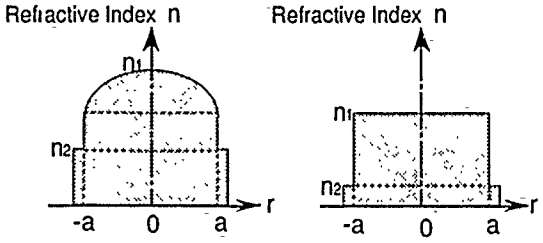

Figure 2. Index profile of GI and SI H-PCS fiber

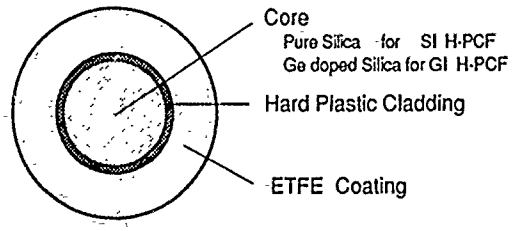

Figure 3. Construction of H-PCS fiber

Table 1. Construction of GI and SI H-PCS fiber

Item	Unit	Specification	
		GI H-PCS	SI H-PCS
Core Diameter	μm	200±5	200±5
Cladding Diameter	μm	230^{+0}_{-10}	230^{+0}_{-10}
Core/Clad Offset	μm	≦6	≦6
Coating Diameter	μm	500±50	500±50
Maximum NA	–	0.4	0.4
Δ	%	3.6	3.8
α	–	2	∞
ρ	–	0.36	0

Figure 4 shows the cross sections of typical cords and cable that use the GI H-PCS fiber. Both the cord and cable have the same construction as the conventional H-PCS products. Therefore various types of crimp & cleave connectors for H-PCS are directly applicable for the new fiber.

IV. Characteristics of GI H-PCS

The following sections provide measured characteristics of the GI H-PCS fiber we developed. Unless otherwise stated, a short-wavelength S-LED which has the properties listed in Table 2 was used as the light source for the measurements under the excitation conditions listed in the same table.

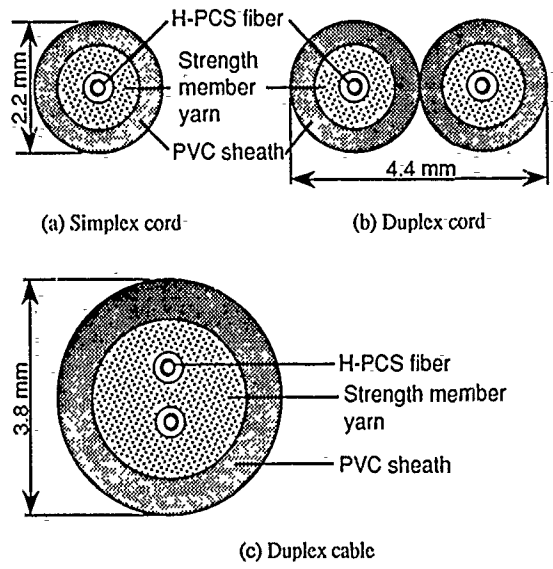

Figure 4. Typical cord/cable construction for GI and SI H-PCS fiber

Table 2. Specifications of LED light source used for the measurement of the characteristics of fibers

Item		Unit	Specification
Type			GaAlAs S-LED
Peak wavelength		nm	850
Spectrum width		nm	45
NA	50 % FFP	---	0.17
	90 % FFP	---	0.25
	Cut off	---	0.28
Spot size diameter		mm	> 0.2

A. Optical Coupling Efficiency with LED

The fiber which has the index profile featured by $\rho=1$ of equation (1) is so called the matched clad type optical fiber. It is known that the maximum number of the transmission modes N of the light propagating through the matched clad fiber is obtained by the following equation: [1)]

$$N = \{\alpha/(\alpha+2)\}a^2k^2n_1^2\Delta \quad \text{..... (3)}$$

where $k = 2\pi / \lambda$

In case of $\rho \neq 1$, equation (3) is extended to the following:

$$N = \{\alpha/(\alpha+2)\}a^2k^2n_1^2\rho^{-2/\alpha}\Delta \quad \text{..... (4)}$$

When all the transmission modes are assumed to be uniformly excited by a LED light source, the maximum coupling efficiency between light source and fiber is in proportion to the N of equation (4).

Optical coupled powers with LED of Table 2 for the GI and SI 200/230 µm H-PCS fibers were compared with that for a typical 50/125 µm GI silica fiber of $\Delta = 0.1$. The results of measurement are shown in Table 3.

B. Spectral Loss Characteristics

Figure 5 contains typical spectral loss characteristics for simplex fiber cords shown in Figure 4 (a) that use the GI and SI H-PCS fibers shown in Table 1. Both the fibers exhibited the primary and secondary low loss bands at the wavelength range of 730 to 890 nm and 1,270 to 1,320 nm respectively. Typical values of measured optical attenuation for GI H-PCS cord under the excitation condition of NA=0.25 (90% FFP) were approx. 4 to 5 dB/km at 850 nm and approx. 7 to 10 dB/km at 1,300 nm.

C. Bandwidth Characteristics (with short-wavelength LED)

We measured the dependence of baseband bandwidth characteristics on transmission distance for the 200 / 230 µm GI and SI H-PCS simplex fiber cords by using the light source in Table 2. The characteristic for a typical 50 / 125 µm GI silica fiber which exhibits the bandwidth of more than 700 MHz·km with 1,300 nm LD light source was also evaluated for reference. Figure 6 shows the result of measurement for each fiber.

When we describe the transmission bandwidth, $f(L)$, for each fiber as a function of fiber length, L (km), by equation (5), the bandwidth at $L = 1$ km, f_0, and gradient, γ, for each fiber are calculated from the measured data as shown in Table 4.

$$f(L) = f_0 L^{-\gamma} \text{ (MHz)} \quad \text{..... (5)}$$

As indicated, bandwidth characteristic of the developed GI H-PCS fiber is a significant improvement from that of conventional H-PCS fiber. It is clear that, despite large core and truncated index profile, the modal dispersion of the developed H-PCS fiber is reduced to almost same level of that of typical GI silica fiber.

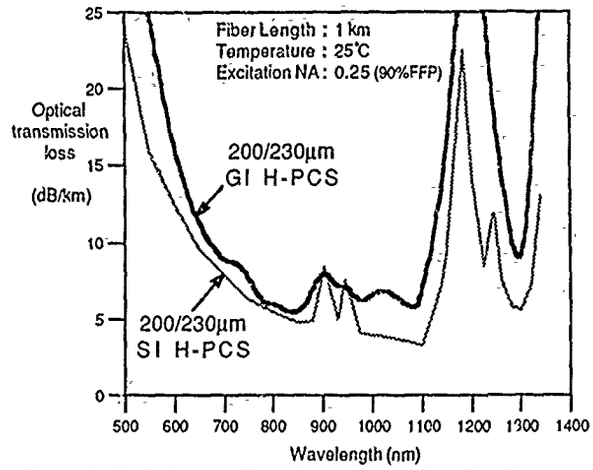

Figure 5. Typical spectral loss characteristics for 200 / 230 µm GI and SI H-PCS simplex fiber cords

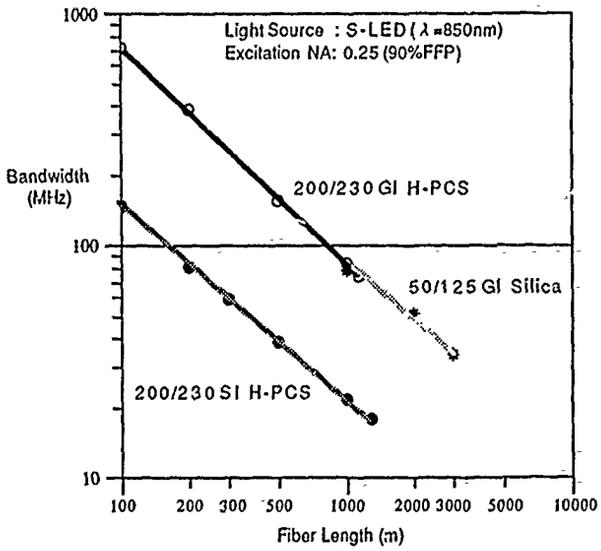

Figure 6. Baseband bandwidth characteristics with short-wavelength S-LED light source for the 200 / 230 µm GI and SI H-PCS fibers and a typical 50 / 125 µm GI silica fiber (850 nm LED, Excitation NA=0.25)

Table 3. Comparison of optical coupling efficiency for the 200 / 230 µm GI and SI H-PCS fibers with that for a typical 50 / 125 µm GI silica fiber (850 nm LED, Excitation NA=0.25)

Type of fiber sample	unit	Relative optical coupled power
200/230µm GI H-PCS	dB	+11.4
200/230µm SI H-PCS	dB	+11.6
50/125µm GI silica	dB	0.0 (reference)

Table 4. Baseband bandwidth parameters for the 200 / 230 µm GI and SI H-PCS fibers and a typical 50 / 125 µm GI silica fiber (850 nm LED, Excitation NA=0.25)

Type of fiber sample	f_0 (MHz)	γ
200 / 230 µm GI H-PCS fiber	85	0.91
200 / 230 µm SI H-PCS fiber	22	0.83
50 / 125 µm GI silica fiber	81	0.78

D. Loss Dependence on Distance

The dependence of optical unit loss on transmission distance for the 200 / 230 μm GI H-PCS simplex fiber cord was measured by using the LED light source of Table 2 with different excitation NAs (0.25 and 0.4). The results are shown in Figure 7. The figure shows that the transmission loss, α (dB/km), with excitation NA of 0.25, satisfies the following specification.

$$\alpha_{\text{at } \lambda=850\text{nm, Ins.NA:0.25, Ta=25℃}} \leqq 6 \text{ (dB/km)} \quad \ldots\ldots\ (6)$$

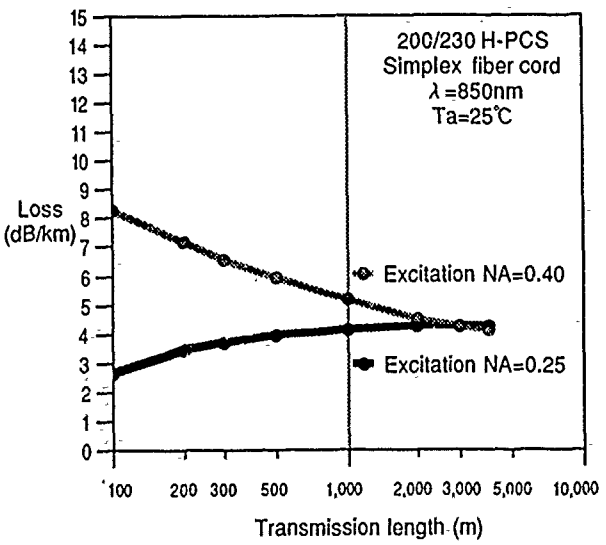

Figure 7. Typical transmission length dependence of optical loss for 200 / 230 μm GI H-PCS fiber with different excitation conditions

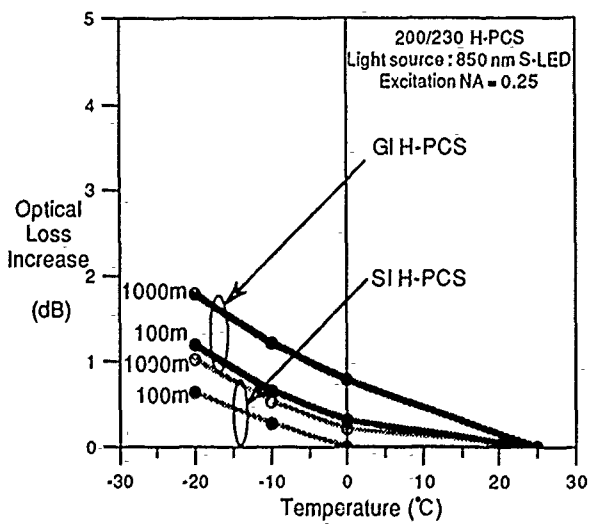

Figure 8. Typical temperature dependence of optical loss for 200 / 230 μm GI and SI H-PCS fibers of different fiber lengths (850 nm LED, Excitation NA=0.25)

E. Temperature dependence of Loss & Bandwidth

One of the important basic characteristics for PCS fiber is the temperature dependence of fiber NA caused by the temperature dependence of the refractive index of cladding material. It is thus important for us to improve and investigate both the increase in loss at low temperature caused by the decrease of transmission mode and the decrease in bandwidth at high temperature caused by the increase of transmission mode. These reversible temperature dependence characteristics are primarily determined by the cladding's coefficient of temperature expansion. [5] Therefore, in addition to the design of index profile, the development of integrated cladding polymer with small coefficient of temperature expansion was one of the key elements to solve in this development.

We measured the temperature dependence of the frequency response of output optical power transmitted through loosely coiled GI and SI H-PCS simplex fiber cords of different length in a heat chamber. The results of measurement are shown in Figures 8 and 9. It was confirmed by this examination that the typical increase in transmission loss at the lower end of the operational temperature range (-20 ℃) is approx. 1.8 dB and the typical decrease in transmission bandwidth at the higher end of the operational temperature range (70 ℃) is approx. 10 Mbps for 1 km of GI H-PCS simplex fiber cord.

F. Bending Loss Characteristics

Figure 10 shows the increase in transmission loss for the 200 / 230 μm GI H-PCS fiber as it is wound up to ten (10) turns on mandrels with different diameters. The characteristic for a typical 50 / 125 μm GI silica fiber is

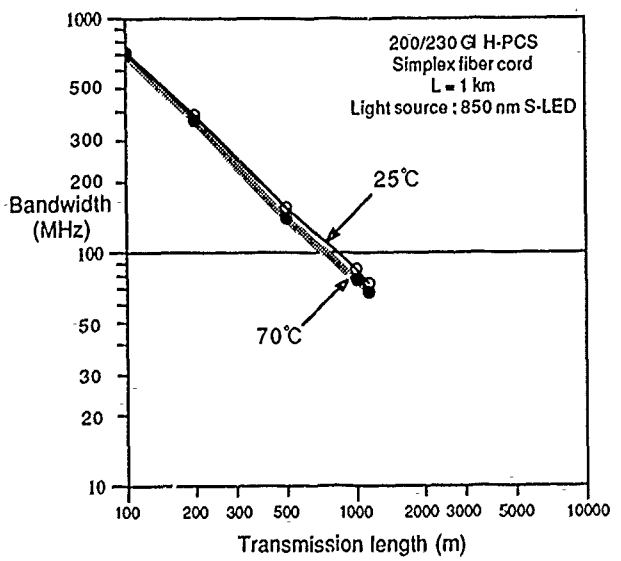

Figure 9. Typical temperature dependence of bandwidth for 200 / 230 μm GI H-PCS fiber (850 nm LED, Excitation NA=0.25)

also indicated for reference. The increase in loss in this measurement tends to stabilize when the fiber is wound several turns. In Figure 11, plotted are the measured increase in loss, in relation to bend diameters, measured for GI H-PCS fiber after it was wound 10 turns on each mandrel, in comparison with that of conventional 200 / 230 µm SI H-PCS fiber and 50 / 125 µm GI silica fiber. As indicated in the 2 figures, the increase in loss of the GI H-PCS is significantly smaller than that of conventional GI silica fiber.

G. Mechanical Strength

Figure 12 shows a typical Weibull plot for tensile strength of the GI H-PCS fiber. The Weibull plot line in the figure, which is standing almost vertically at the tensile strength of more than 17 kgf/core (770 K PSI), indicates that the developed GI H-PCS fiber exhibits quite high tensile strength and uniformity. The on-line proof test level for this fiber, 1.61 kgf/core (0.7 % strain), is the same as the conventional SI H-PCS fiber's.

H. Adoptability of Crimp & Cleave Connectors

The primary advantage of the H-PCS fibers is that it can be used with new departure, the crimp & cleave optical connectors which allow operators without skill to assemble optical connectors on fiber in a few minutes. [5),7)] To evaluate practical applicability, we compared the increase in loss, for the GI H-PCS fiber, caused by the crimping stress, with that of conventional SI H-PCS fiber. We carried on the measurement by using a JIS F05 based crimp & cleave optical connector (Sumitomo Electric's model CF-1011) with 850nm LED light sources of different excitation NA. The test results are shown in Table 5.

As indicated in Table 5, although the increase in loss of GI H-PCS fiber is larger than that of SI H-PCS fiber, the value measured under the practical excitation NA of 0.25 is adequate to design short distance data-links for front-end LAN applications.

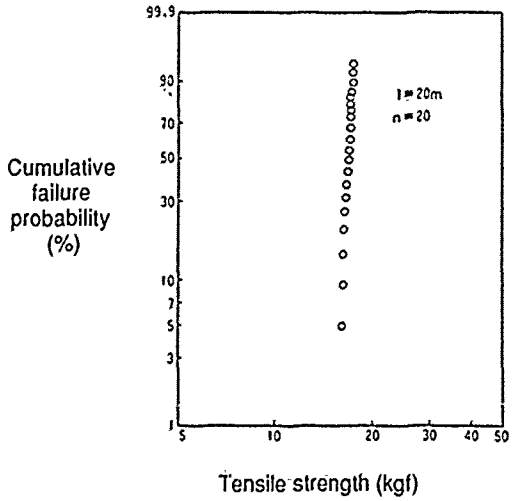

Figure 12. Typical tensile strength Weibull plot for 200 / 230 µm GI H-PCS fiber

Table 5. Typical optical loss increase for 200 / 230 µm GI and SI H-PCS fibers caused by crimp connector assembly (n ≧ 5 / condition)

Type of fiber sample	unit		Excitation NA 0.1	0.25	0.4
200/230µm GI H-PCS	dB/end	Mean	0.006	0.22	0.86
		Max	0.01	0.26	0.95
200/230µm SI H-PCS	dB/end	Mean	0.002	0.01	0.39
		Max	0.01	0.02	0.49

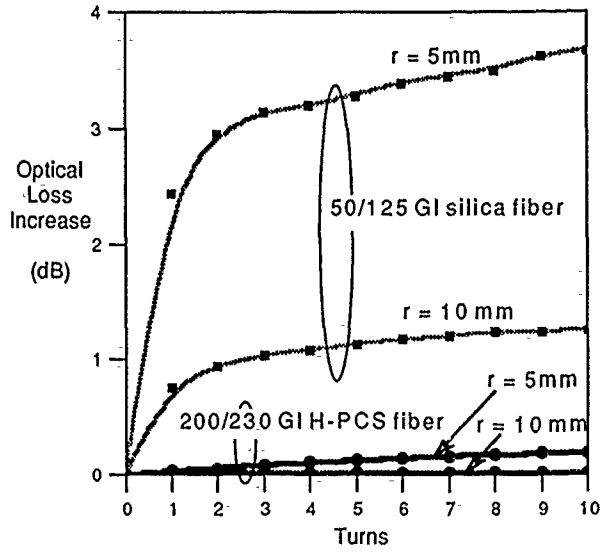

Figure 10. Typical bending loss characteristics for 200 / 230 µm GI H-PCS fiber and conventional 50 / 125 µm GI silica fiber (850 nm LED, Excitation NA=0.25)

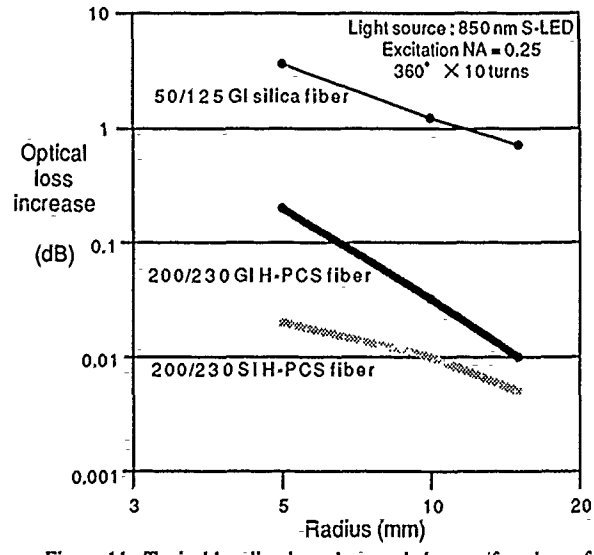

Figure 11. Typical bending loss characteristics as a function of bend radius for 200 / 230 µm GI and SI H-PCS fibers and a typical conventional 50 / 125 µm GI silica fiber (850 nm LED, Excitation NA=0.25)

V. Conclusion

A 200/230 μm truncated type Graded Index Hard-Plastic Clad Silica fiber has been developed and its major characteristics have been evaluated. It was confirmed that the developed fiber exhibits superior bandwidth characteristic of more than 80 MHz.km with 850 nm S-LED to typical 50/125 μm GI silica fibers, preserving attractive features of conventional H-PCS such as high NA that realizes coupling efficiency with LED of more than 10 dB superior to ordinary 50/125 μm GI silica fibers, low loss, high tensile strength, small bending loss and easy assembling work with crimp & cleave optical connectors. These measured characteristics are sufficient to realize 100 Mbps data transmission for intra-office Front-end LAN applications at the maximum applicable fiber length of up to 500 meters with using economical short wavelength S-LED and crimp & cleave connector which dramatically reduces cable termination cost.

When compared with the metal-wired (coaxial cable or twisted wire) LANs, the FDDI based fiberoptic LAN, that use 62.5/125 μm or 50/125 μm GI silica fiber, has had drawbacks in the cost of opto-electronic devices, ease of cable connections and flexibility of system expansion or relocation. The GI H-PCS fiber, that was developed as a upper-compatible line-up of 200/230 μm conventional SI H-PCS fiber, has overcome all these problems, and expected to allow the LAN users to take the full advantages of the fiberoptic LAN such as high speed and high noise immunity. The H-PCS fibers with core/cladding diameters of 200/230 μm is already authorized as a standard PCS fiber by JIS (Japanese Industrial Standard) to ensure universality and versatility as an optical cable for various applications.

Acknowledgment

The authors wish to extend their appreciation to T.Kuwabara for his encouragement and helpful discussions, The authors also wish to acknowledge the expert technical support of Y. Tejika, E. Abo, H. Konda, M. Uchino and S.Okumi.

References

[1] D. Gloge and E. Marcatili, "Multimode Theory of Graded-Core Fibers", B.S.T.J. vol.52, No.9, pp.1563-1578 (1973)
[2] K. Yoshimura, T. Nakahara, A. Tsukamoto and A. Isomura, "Low-Loss Plastic-Cladding Fiber", Electronic Letters, vol.10, pp.534-535 (1974)
[3] R. Olshansky and D. Keck, "Pulse Broading in Graded-Index Optical Fibers", Appl.Opt., vol.15, No.2, pp.483-491 (1976)
[4] B. Williams, "The Push for Fiberoptic Computer Interconnections", Newport Conference on Fiberoptics Markets, Oct.25&26, 1988
[5] H. Nishimoto, et.al., "Development of Hard Clad PCS Fiber", Sumitomo Electric Technical Review, No.28, pp.94-102 (1989)
[6] Y. Kida, et.al., "FDDI Based 100Mbps Fiber-Optic LAN", Sumitomo Electric Technical Review,No.29, pp.109-116(1990)
[7] H. Nishimoto, et.al., "Crimp & Cleave Optical Connector System for SUMINET-3200® Fiber Optic LAN", Sumitomo Electric Technical Review, No.29, pp.131-136 (1990)

Hiroaki Nishimoto was born in Okayama, Japan on December 27, 1958. He received the B.S. and M.S. degrees in electrical engineering from the Okayama University in 1981 and 1983 respectively. Since joining the Sumitomo Electric Industries, Ltd., Osaka, Japan, in 1983, he has been engaged in the development work on the optical fibers and passive components for short distance data-comm. applications. Mr. Nishimoto is a member of the Institute of Electronics, Information and Communication Engineers of Japan. His mailing address is: Industrial Fiberoptics & Systems Section, Industrial Wire & Cable Division, Sumitomo Electric Industries, Ltd., 1-1-3 Shimaya, Konohana-ku, Osaka 554, Japan.

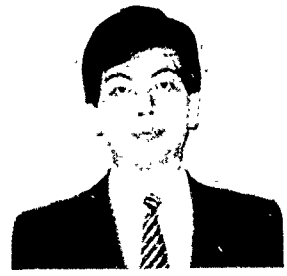

Takayuki Mishima was born in Osaka, Japan on April 21, 1961. He received the B.S. and M.S. degrees in applied chemistry from the Osaka University in 1985 and 1987 respectively. Since 1987, he has been engaged in the research & development work on conductive polymers and fiberoptic polymers in Sumitomo Electric Industries, Ltd., Osaka, Japan. Mr. Mishima is a member of the Chemical Society of Japan.

Hiroki Nagase was born in Ibaraki prefecture, Japan on May 5, 1961. He received the B.S. and M.S. degrees in applied physics from the Science University of Tokyo in 1985 and 1987. Since joining the Fiberoptics Division of the Sumitomo Electric Industries, Ltd., Yokohama, Japan, in 1987, he has been engaged in the production engineering work mainly on the VAD (Vapor Axial Deposition) processes.

Toshihiro Akie, photograph and biography not available at the time of publication.

ATTENUATION AND BENDING LOSS OF VAD DUAL SHAPE CORE DISPERSION-SHIFTED FIBER

Y.TAKAHASHI, N.YOSHIOKA, S.ENDO, H.KANAMORI, Y.KUBO

SUMITOMO ELECTRIC INDUSTRIES, LTD.

1 TAYA-CHO, SAKAE-KU, YOKOHAMA, 244 JAPAN

Abstract

We investigated the influence of refractive index profile and fiber parameters (MFD, λc) on attenuation and bending loss for three types of dispersion-shifted fiber with dual shape core. A comparison between experimental fabrication and theoretical calculation by FEM (Finite Element Method) gave the following results.

(i) The lower attenuation can be achieved by decreasing refractive index difference due to possible reduction of Rayleigh scattering loss.

(ii) Among many parameters, the ratio of MFD to λc is well correlated with bending loss, as was already reported in the study of conventional 1.3 μm single mode fiber.

1 Introduction

The dual shape core dispersion-shifted fiber has been proposed as one of the candidates for under sea and trunk line systems because of its low attenuation and better bending performance (1) ~ (4). In actual production, the requirement to adjust zero dispersion wavelength at 1.55 μm limits the allowable ranges of parameters such as refractive index profile, λc and MFD. There has been no detailed report on the relation between fiber parameters and optical performance in large-scale trial production.

However, recent trend to long repeater spacing and high bit rate system requires the investigation on this relation. We have been investigating characteristics of VAD dispersion-shifted fibers with dual shape core and pure silica cladding. In this paper, the influence of refractive index profile and fiber parameters (MFD, λc) on the attenuation and bending loss is experimentally studied through 1130km trial production in comparison with theoretical calculation by FEM.

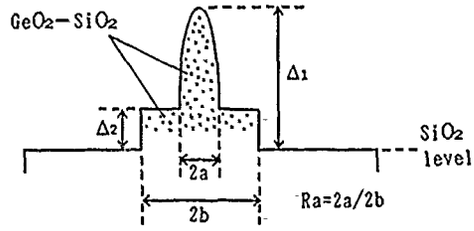

Fig.1 Refractive Index Profile

2. Refractive index design and fiber parameters.

A typical refractive index profile and parameters for 1130km fibers are shown in Figure 1 and Table 1. The fibers have dual shape core of GeO_2-SiO_2 and pure silica cladding. Refractive index profile of this fiber is characterized by four parameters Δ_1, Δ_2 , Ra and 2b. For this study, we selected three types (I, II and III) with the various combinations of Δ_1 and Ra. Since Δ_2 and 2b are not dominant factors to influence transmission characteristics, we chose Δ_2 and 2b arbitrarily so as to adjust λo at 1.55 μm. Trial production fiber length and fiber parameter medians are shown in Table 2 for three types, respectively.

Table 1 Typical Parameters

Type	Δ_1 [%]	Δ_2 [%]	Ra	2b[μm]
I	0.97	0.17	0.30	12.5
II	0.84	0.09	0.30	14.5
III	0.84	0.08	0.23	17.0

Table 2 Fiber Parameter Medians

Type	Median			Fiber length
	λo [μm]	MFD [μm]	λc [μm]	[km]
I	1.550	8.2	1.2	500
II	1.545	8.2	1.1	500
III	1.570	7.8	1.1	130

3. Controllability of λo, MFD and bending loss

We developed FEM simulation program to predict various fiber characteristics theoretically. In actual production, controllability of λo, MFD and bending loss must be considered. We calculated allowable range of Δ_1 and 2b when λo, MFD and bending loss are required to be within the following tentative tolerance.

$1.535\mu m \leqq \lambda o \leqq 1.565\ \mu m$
$7.4\ \mu m \leqq MFD \leqq 8.6\ \mu m$

Bending loss (diameter $20mm^{\phi}$) ≦ 1.0dB/m

Figure 2 shows an example of the calculation. The result from type I, II and III is shown in Figure 3. From the comparison between type I and type II, it is clearly shown that the higher Δ_1 of type I leads to the wider range of Δ_1 and 2b in the case of constant Ra. And from the comparison between type II and III, it is also shown the smaller Ra leads to the wider range of Δ_1 and 2b in the case of constant Δ_1.

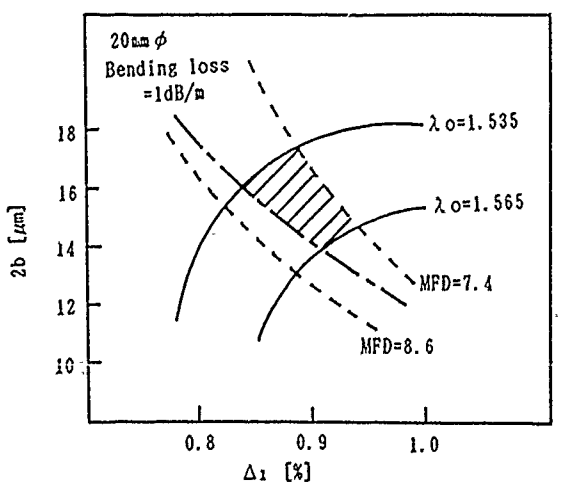

Fig.2 A example of calculated allowable range

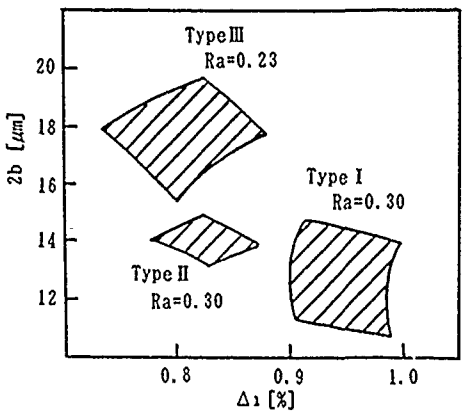

Fig.3 Calcuated result from type I, II and III

4. Attenuation

We statistically analyzed the influence of Δ_1 and Ra on 1.55 μm attenuation of 1130km fibers and compared it with FEM calculation. Figure 4 shows dependence of measured attenuation at 1.55 μm on Δ_1 which is derived from the fibers of type I and II. We obtained the following regression equation from the dependence with constant Ra.

$$\alpha_{1.55} = 0.046 \times \Delta_1 + \text{const.}$$

And Figure 5 shows dependence of measured attenuation at 1.55 μm on Ra for the fibers of type II and type III. We didn't clearly find strong correlation in this dependence. However, we obtained the following regression equation from the dependence with constant Δ_1

$$\alpha_{1.55} = -0.029 \times Ra + \text{const.}$$

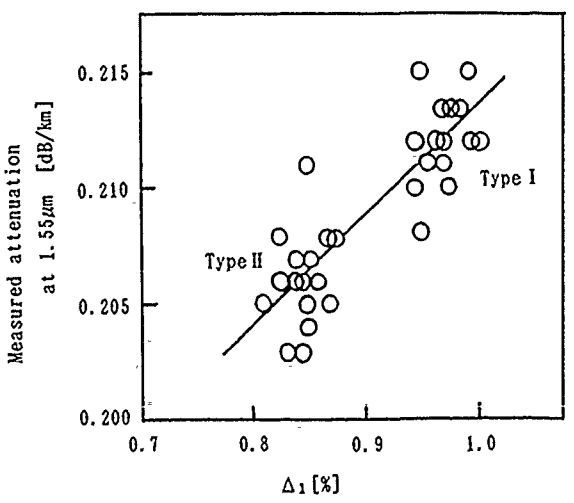

Fig.4 Dependence of measured attenuation at 1.55μm on Δ_1

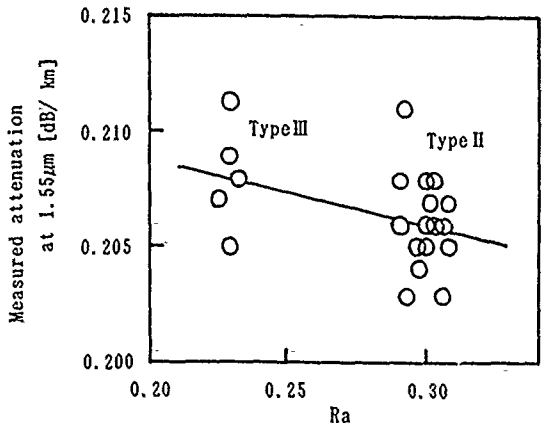

Fig. 5 Dependence of measured attenuation at 1.55μm on Ra

Total attenuation of dispersion-shifted fiber is well described as follows.

$$\alpha(\text{Total}) = \alpha(\text{Rayleigh}) + \alpha(\text{OH}) + \alpha(\text{IR}) + \alpha(\text{UV})$$

α(Rayleigh): Rayleigh scattering loss.

α(OH): OH absorption loss

α(IR): IR absorption loss

α(UV): UV absorption loss

Assuming α(Rayleigh) depends on Δ_1 and Ra, and other absorption losses don't depend on profile parameters, we calculated α(Rayleigh) values for various Δ_1 and Ra around the condition of type I, II, III by FEM, and obtained the following linear approximation.

$$\alpha_{1.55}(\text{Rayleigh}) = 0.036 \times \Delta_1 - 0.019 \times \text{Ra} + 0.124$$

Therefore,

$$\alpha_{1.55} = 0.036 \times \Delta_1 - 0.019 \times \text{Ra} + 0.124 + \text{const.}$$

By comparing this calculation with the experiment, we concluded the attenuation difference between type I and type II was mainly attributed to Rayleigh scattering effect.

Table 3 Calculated 25mmφ bending loss

(λ_o= 1.550μm, MFD= 8.0μm)

Type	I	II	III
Calculated 25mmφ bending loss [dB/m]	0.02	0.35	0.20

Table 4 Average of measured 25mmφ bending loss

Type	I	II	III
Average of measured 25mmφ bending loss [dB/m]	0.01	0.15	0.06

5. Bending loss

We investigated the influence of fiber parameters on bending loss by measuring 1.55μm bending loss of 1130km fibers with 25mmφ and 30mmφ diameter. First, we calculated bending loss at diameter 25mmφ in the case of λ_o=1.55μm and MFD=8.0μm by FEM. Comparison between type I, II and III is shown in Table 3. The higher Δ_1 of type I leads to the lower bending loss and the smaller Ra of type III leads to the slightly lower bending loss with constant λ_o and MFD. In the experimental result shown in Table 4, we could observe general tendency predicted by FEM. However, there was no exact agreement between calculation and experiment. We investigated other parameters correlating well with bending loss and found that the ratio of MFD to λ_c (MFD/λ_c) correlates well among many parameters, as was already reported in the study of conventional 1.3μm single mode fiber.

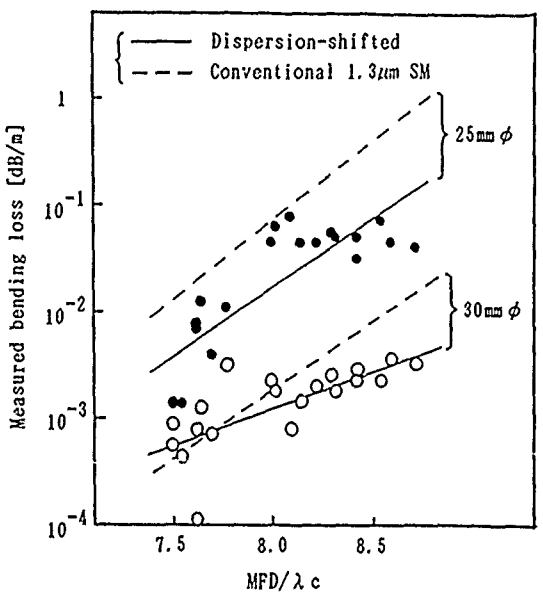

Fig. 6 Relationship between 1.55μm bending loss and (MFD/λ_c)

Relationships between 1.55 μm bending loss and (MFD/λc) for type II are shown in Fig 6. Solid lines and broken lines indicate the regression line of trial production dispersion-shifted fibers, MFD values of dispersion-shifted fibers were measured at 1.55 μm and conventional 1.3 μm SM fibers measured at 1.3 μm , respectively. Furthermore, less bending sensitivity of dispersion-shifted fiber becomes more significant with small bending diameter and large MFD/λc.

6.Conclusion

1130km dispersion-shifted fibers with dual shape core and pure silica cladding were fabricated as a trial.

FEM theoretical study showed parameter controllability of λo and MFD in actual production was influenced by the choice of Δ_1 and Ra properly.

It was confirmed the low attenuation can be achieved by decreasing Δ_1 due to possible reduction of Rayleigh scattering loss.

It was found the ratio of MFD to λc (MFD/ λc) correlates with bending loss as was for the conventional 1.3 μm SM fiber.

7. Reference

(1) N.KUWAKI et al., "Dispersion-shifted convex index single-mode fibers", Electron Lett., Vol.21, No.25/26, pp.1186~1187, (1987)

(2) M.OHASHI et al., "Bend Optimized dispersion-shifted step-shaped-index (SSI) fibers", Electron. Lett., Vol. 22, No.24, pp. 1285～1286 (1986)

(3) N.KUWAKI et al., "Characteristics of dispersion-shifted dual shape core single-mode fibers", J. Lightwave Tech., Vol. LT-5, No.6, pp. 792～797, (1987)

(4) M.SHIGEMATSU et all., "Transmission characteristics of dispersion-shifted single-mode fibers with dual shape core and fluorine added cladding by VAD method" in Proc. 13th European Conference on Optical communication,pp.163~165,(Helsinki, 1987)

YUJI TAKAHASHI

Yuji Takahashi was born in 1958 and received a M.S. degree from Tokyo University in 1984. He joined Sumitomo Electric Industries, Ltd. in 1984,and has been engaged in development of manufacturing optical fiber.

NAOKI YOSHIOKA

Naoki Yoshioka was born in 1950 and received a M.S. degree from Osaka University in 1975. He joined Sumitomo Electric Industries, Ltd. in 1975, and has been engaged in research and development of optical fiber fabrication. He is a manager of fiber optics production engineering section.

SHIGEKI ENDO

Shigeki Endo received the B.S. degree for Electrical Engineering from Waseda University in 1976. He joined Sumitomo Electric Industries, Ltd. and worked on the production engineering of 9.5 and 4.4 coaxial cable. Thereafter he was engaged in the development of mother preform for optical fiber for more than 10 years. He is senior engineer of fiber optics production engineering section of fiber optics division.

HIROO KANAMORI

Hiroo Kanamori was born in Nara,Japan,on August 21, 1956. He received the B.S. and M.S. degrees in physics from Tokyo Institute of Technology, Tokyo, Japan, in 1979 and 1981, respectively.

He joined Sumitomo Electric Industries, Ltd. in 1981 and has been engaged in the research and development of optical fiber and component as a senior engineer of Transmission Media R & D.

He is a member of the Institute of Electronics and Communication Engineers of Japan, the Japan Society of Applied Physics and the Physical Society of Japan.

YUJI KUBO

Yuji Kubo was born in 1963 and received the B.S. and the M.S. degrees from Hokkaido University in 1987. He joined the Sumitomo Electric Industries, Ltd. in 1987, and has been engaged in research and development of optical fibers. He is a member of Institute of Electronics and Communication Engineers of Japan.

PERFORMANCE OF LOW-LOSS SUBMARINE CABLES

Niels H. Skovgaard A. Baungaard K. Bundgaard Jensen

NKT Telecom Cables
13, Sognevej, 2605 Broendby, Denmark

ABSTRACT

Since 1985 a number of submarine, unrepeatered cables have been installed in the Baltic Sea and the connecting Scandinavian waters leading to the North Sea. The construction of these cables is briefly described, emphasizing the precautions taken against internal and external influences that could threaten the low-loss performance of the fibers. The problems concerning hydrogen sources are discussed, based on experience and upon theoretical evaluations as well. In particular hydrogen entrapment in the sea bed around buried cables is analysed.

1. INTRODUCTION

As it appears from fig. 1, the Baltic Sea extends into a number of straits and smaller seas to the North Sea, thus containing a number of islands and separating the Scandinavian Peninsula from Denmark and the central part of Europe.

It can also be seen from fig. 1, that a network, comprising many submarine cables, has developed and is still developing to cross all these waters and connect the surrounding countries.

The first submarine cable was laid in 1985 soon followed by similar, relatively short links.

The longest cable, laid in 1989, has a length of 156 km and connects Bornholm, a Danish island in the Baltic Sea with the island of Zealand.

A new cable laid this summer now connects Bornholm to Poland.

A link between Norway and Denmark is planned for the future.

All of the cable links mentioned are unrepeatered, and most of the cables are buried in the sea bed.

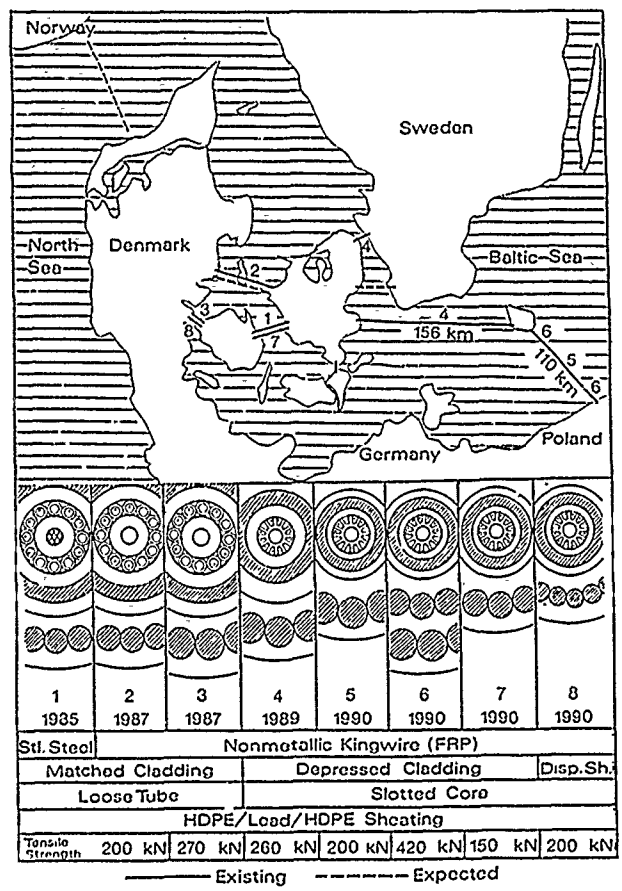

Fig.1 Submarine optical links in southern Scandinavian waters.

2. CABLE DESIGNS

A common feature for all the cables, installed so far, is the outer protection, made up of a lead sheath between two polyethylene jackets, and reinforced by layers of 3-5 mm galvanized steel wires, protected by layers of asphalt and polypropylene yarns.

While this is an old and traditional way to protect submarine cables, it has proved very efficient and is also suited for optical fiber submarine cables.

The need for strong cables with heavy armour has been questioned, and lightweight types have been proposed, in particular for burial in the sea bed. However, we have recently experienced, that even a buried cable can be caught by a trawl, if the sea bed is soft. A visual examination of the cable showed that it had been exposed to very strong forces, the optical performance of some of the fibers was affected, however the service was never interrupted. We regard this as a compelling argument for holding on to strong, well-armoured cables with tensile strengths not less than 200 kN. This robustness also allows for high recovery speeds, repair operations at high sea swells and reduces the risk of accidental overload.

The lead sheath provides the cables with good handling properties, such as easy coiling and no tendency to kinking, which has been proven by the laying of around 500 km of cable. (Only half of this amount is seen in fig. 1, the remaining part has been laid in overseas waters). Our experiences and studies have shown that the lead sheath also offers effective protection against outer hydrogen sources.

The most recently manufactured and also the longest cables are of the slotted core type with depressed clad fibers. To preserve the very low losses, no metallic elements are present under the lead sheath, and the materials have been carefully chosen with regard to very low hydrogen emission. As a further precaution 1 km samples of the internal core portion including the lead sheath have been heated 3 months at 95°C and tested for hydrogen induced loss. No added loss from dissolved hydrogen has been found.

In order to obtain very low losses a moderate degree of selection took place to exclude those fibers expected to be most sensitive to bending losses.

3. HYDROGEN EFFECTS

3.1 Recently reported results.

In the last few years considerable attention has been paid to the occurrence of hydrogen in optical submarine cables. It has been found [1], [2] that corrosion of galvanized steel wires is the most important source of hydrogen. Further it has been found that the partial pressure of hydrogen is correlated with the water depth and shows a slowing rate of increase with time. [2] shows that a lead sheath separating the armour from the fibers is a very efficient barrier against externally generated hydrogen.

In [3] it is argued that high rates of corrosion can cause generation of bubbles of hydrogen entrapped in the cable structure resulting in hydrogen pressures ultimately limited by the hydrostatic pressure of the surrounding water.

[4] presents measurements of hydrogen pressures within 2 years after the installation of cables without a metallic barrier where the armour is protected by a high density polyethylene sheath. The measured hydrogen pressures are 1 or 2 sizes of order lower than the maximum pressures found in [1] and [2]. The most important reason for the lower partial pressure is probably that the polyethylene sheath offers a diffusion resistance against water thus resulting in primarily a delayed but possibly also in a reduced corrosion. Another part of the explanation might be that the cables are laid directly on the sea bottom resulting in a free escape of the outward diffusing hydrogen to the sea water.

3.2 Buried submarine cables.

For a buried submarine cable the resistance to hydrogen diffusion from the sea bottom materials has to be taken into account. For buried submarine cables where corrosion takes place at high rates an entrapment of hydrogen bubbles can take place in the sea bottom materials resulting in hydrogen pressures ultimately limited by the hydrostatic pressure of the water. Also, at the lower rates of hydrogen generation e.g. in situations of better protected and more corrosion resistant armour materials, the sea bottom materials represent a certain resistance to the outward diffusion. This will result in an increase of the hydrogen partial pressure at the position of the cable.

Fig. 2 shows the result of the calculation of the hydrogen partial pressure at the position of a buried submarine cable due to corrosion of galvanized steel armouring. The detailed conditions of the calculations are given in the Appendix.

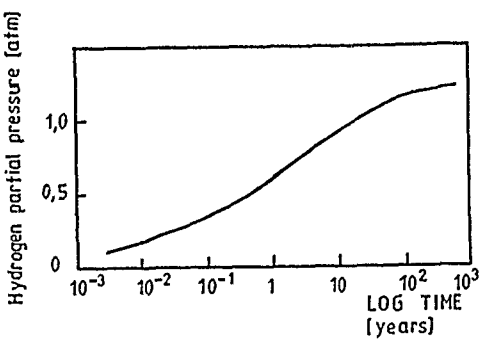

Fig.2 Calculated hydrogen partial pressure at the position of a buried Submarine Cable at constant rate of hydrogen generation from corrosion.

It can be seen from fig. 2 that within a short time a considerable hydrogen pressure builds up due to the presence of the sea bottom materials. This is followed by a slowing rate of increase with time (in accordance with the measurements in [1] and [2]) until a steady state is attained after several years. Despite the uncertainty on the exact values of corrosion rate, hydrogen solubility and permeability in the material on the sea bottom, the calculated example illustrates the necessity of a hermetic barrier separating the fibers from hydrogen due to corrosion of the outer armouring.

4. HYDROGEN PRESSURE MEASUREMENTS IN THE OLDEST BURIED SUBMARINE CABLE.

Just before the installation of our first manufactured optical fiber submarine cable in June 1985, careful measurements of the attenuation vs. wavelength were carried out. Repeated measurements using the insertion loss method were carried out in June 1990 by Telecom Denmark, the owner of the cable.

Using the method of [1] of separating the 1240 nm peak from the Rayleigh scattering baseline, a comparison was made between the 1240 nm peaks from 1985 and 1990. Taken into account small wavelength shifts and differences in spectral resolution due to the use of 2 different measurement set-ups it was concluded that no added loss at 1240 nm was found. (Detection limit 0.01 dB/km).

5. CONCLUSION

Our calculations have indicated that armour corrosion of buried submarine cables will create high hydrogen partial pressure. Consequently the fibers must be shielded against hydrogen. Because of the high amounts of hydrogen a hydrogen absorber will not have a sufficient long term effect.

Five years of experience from inspection of installed submarine cables has shown, that the traditional asphalt embedded galvanized steel armour in combination with a lead sheath does not cause any hydrogen problems. The only additional precaution needed is a careful selection of the materials inside the lead sheath in order to exclude the most severe hydrogen emitting sources.

6. ACKNOWLEDGEMENT

Henrik Kristiansen from Telecom Denmark is cordially thanked for carrying out the attenuation measurements on the submarine cable.

REFERENCES

1. W.T. Anderson, A.J. Johnson, J.P. Kilmer and R.M. Kanen, "Hydrogen Gas Effects on Installed Submarine Single-Mode Fiber Cables", 37th International Wire and Cable Symposium, Reno, Nevada, November, 1988.

2. W.T. Anderson, A.J.Johnson and A. DeVito, "Field Measurements of the Effects of Hydrogen Gas on Installed Submarine Single-Mode Fiber Cables", 38th International Wire and Cable Symposium, Atlanta, Georgia, November 1989.

3. N.E. Hardwick, L.C. Hotchkiss, J.J. Blee and D.L. Philen, "Corrosion Resistant Armour to prevent H_2 induced Loss in Underwater (Wire - Armoured) Fiber Optic Cable, 38th International Wire and Cable Symposium, Atlanta, Georgia, November 1989.

4. S. Hopland, "Investigation of Total an Distributed Hydrogen Levels in Installed Fiber Optic Submarine Cables", 38th International Wire and Cable Symposium, Atlanta, Georgia, November 1989.

5. P.C. Novelli, M.I. Scranton, and R.H. Michener, "Hydrogen distributions in marine sediments", Limnol. Oceanogr, 32 (3), 1987, 565 - 576.

6. H.S. Carslaw and J.C. Jaeger, "Conduction of Heat in Solids" 2.ed., Oxford at the Clarendon Press, 1959, 338 - 339.

7. J. Kiil and A. Baungaard, "Unrepeatered Submarine Links in Denmark". International Conference on Optical Submarine Telecommunication Systems "SUBOPTIC", Paris 1986, page 84 - 88.

APPENDIX

CALCULATION OF HYDROGEN PARTIAL PRESSURE DUE TO ARMOUR CORROSION IN A BURIED SUBMARINE CABLE.

1. Steady state pressure.

Consider the situation shown below:

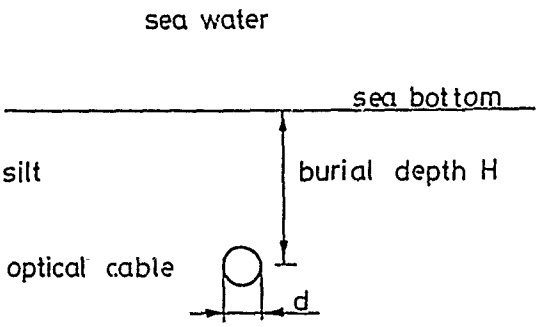

The steady state hydrogen partial pressure P at the surface of the cable can be calculated based on analogous electrostatic problems (wire/plane capacitor)

$$P = s_1 \times \frac{\ln \frac{4H-d}{d}}{2 \pi K} \qquad (1)$$

where

s_1 is the constant rate of hydrogen generation per unit length of the cable.

H is the burial depth.

d is the diameter of the cable at the position of the armour.

K is the permeability of hydrogen in silt.

K is found from :

$$K = D \times c \qquad (2)$$

where

c is the solubility of hydrogen in silt i.e. the amount of dissolved hydrogen per unit volume in silt per unit partial pressure.

D is the diffusion coefficient of hydrogen in silt.

According to [5]:

$$D = 1.3 \times 10^{-5} \frac{cm^2}{s}$$

$$c \approx 7 \times 10^{-7} \frac{mole}{cm^3\ atm}$$

(2) gives

$$K = 9.1 \times 10^{-12} \frac{mole}{cm\ s\ atm}$$

s_1 is related to the corrosion rate of the galvanized steel wires. In neutral and acidic environments self corrosion of Zn takes place following the net reaction scheme:

$$Zn + 2H^+ \rightarrow Zn^{++} + H_2$$

Well protected galvanized steel corrodes at a rate ranging from of 0.1 - 1.0 μm Zn per year. Poorly protected galvanized steel in sea water corrodes at an even higher rate. Let us chose 1 μm Zn per year as an example of the corrosion rate. Referring now to the surface area of the galvanized steel wires in a typical submarine cable, this corrosion results in a rate of hydrogen generation of

$$s_1 = 1.4 \times 10^{-11} \frac{mole}{cm\ s}$$

With d = 4 cm
H = 0.8 m

(1) gives a steady state hydrogen partial pressure

P = 1.07 atm

2. Transient hydrogen pressure.

The short term pressure around a buried cable is independent of the burial depth. An analytical solution exists for a cable surrounded by a medium with infinite radial extension from the cable. [6]

1) Small values of time, i.e.

$$\frac{Dt}{\left(\frac{d}{2}\right)^2} \leq 10$$

Numerical calculations have been carried out. [6] The result with our numerical examples is shown as curve 1) in fig. 3.

2) Larger values of time.

The approximate solution with the terminology used here is

$$P \approx \frac{s_1}{4\pi K} \times \ln \frac{4\ Dt}{b \times \left(\frac{d}{2}\right)^2}$$

Where b = 1.7811. [6]

The result with our numerical examples is shown as curve 2) in fig. 3.

Further curve 3) gives the steady state pressure for a cable buried at a specific depth (0.8 m). The actual pressure at the position of the cable will follow curve 1) and 2) for small values of time and finally reach curve 3) asymptotic.

Asger Baungaard

NKT Telecom Cables
13, Sognevej
DK-2605 Broendby
Denmark

Asger Baungaard was born in East Jutland, Denmark in 1926. He received his M. Sc. degree in Electrical Engineering in 1952. Since 1953 he has been with NKT working in different research areas such as HV-cables, Electronics, Telecommunication and optical fiber cables.

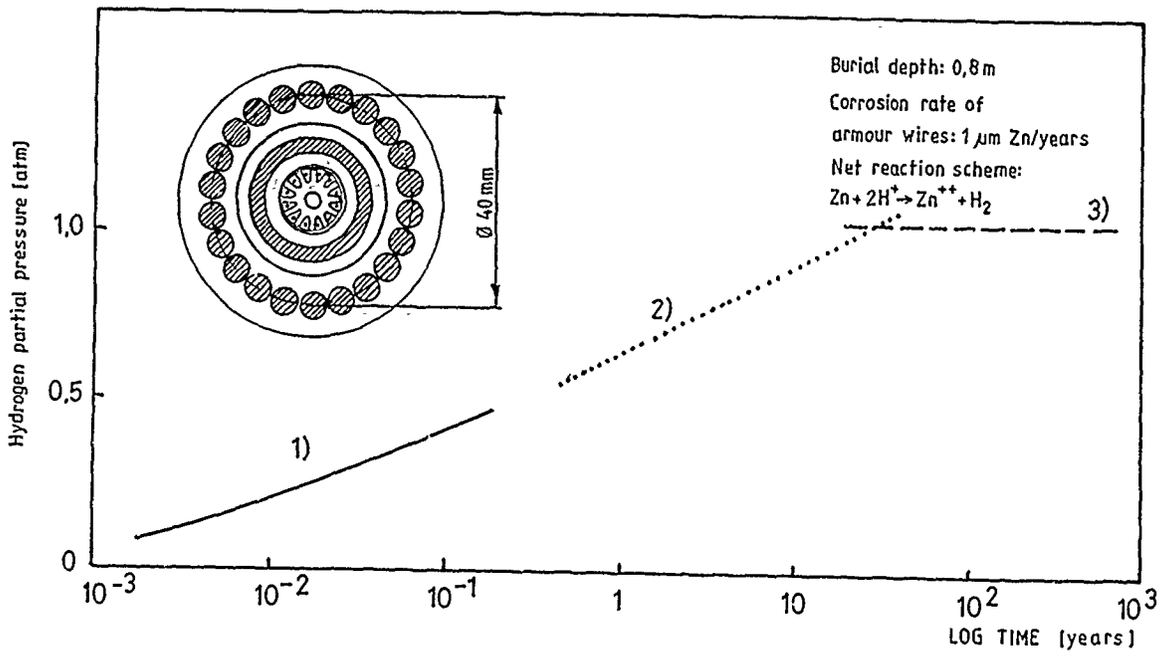

Fig.3 Calculated hydrogen partial pressure at the position of a buried Submarine Cable at constant rate of hydrogen generation from corrosion.

1) Small values of time
2) Larger values of time
3) Steady state pressure

Niels H. Skovgaard

NKT Telecom Cables
13, Sognevej
DK-2605 Broendby
Denmark

Niels H. Skovgaard was born in Copenhagen, Denmark in 1952. He received his M.Sc. degree in Mechanical Engineering in 1981. From 1981 he worked as researcher at The Technical University of Denmark. In 1984 he joined NKT working with research and development of optical fiber cables. Since 1986 he has been manager of the design and development department of NKT Telecom Cables.

Knud Bundgaard Jensen

NKT Telecom Cables
13, Sognevej
DK-2605 Broendby
Denmark

Knud Bundgaard Jensen was born in Copenhagen, Denmark in 1944. He received his M.Sc. degree in Electrical Engineering in 1968. The same year he joined NKT's electrotechnical laboratory. From 1975 he worked with research and development of optical fibers. Since 1986 he has been working with development of optical fiber cables.

CABLE DESIGN FOR UNREPEATERED SINGLE SPAN SYSTEMS

C.J. Rochester * S.R. Barnes * P. Worthington * A.J. MacLeod * B.A. Eales **

* STC Submarine Systems, Southampton. U.K.

** STC Technology Ltd., Harlow. U.K.

Abstract

Due to the recent advances in fibre optic technology, unrepeatered communication cable systems can now operate at distances of over 200 km. Traditionally the submarine cable has been designed for long haul repeatered systems between the continents across deep oceans. A design study has therefore been completed for a cable to specifically meet the performance requirements for unrepeatered systems. The main design criteria have been to produce a high quality, high reliability product for unrepeatered systems consistent with traditional submarine cable standards and practices.

Introduction

For over 100 years STC has been involved in the design, manufacture and installation of submarine telecommunication systems. During this period STC has manufactured over 200,000 km of coaxial and 20,000 km of optical submarine cable. The traditional market has been long haul submarine cable systems with submerged underwater repeaters to regenerate the electrical or optical signal. Recent advances in fibre optic technology have enabled cable communication systems to operate at distances of up to 200 km. Due to the increase in unrepeatered transmission distances many regions that could previously have only been linked with a repeatered system can now be traversed by a single unrepeatered length of cable. To span these distances the systems have to operate at 1550 nm and it is the current availability of low loss fibre, very stable high power lasers and extremely sensitive stable detectors that have made these distances achievable.

The categories of applications identified for these unrepeatered systems are:-

- Mainland to Island Links: Systems where the island is on the continental shelf of the mainland in the shallower waters. These systems encompass most of the North European and Mediterranean islands.

- Island to Island Links: Systems which connect islands together that may be situated on the shallower Continental Shelf or subsea mountain ranges containing deeper depressions. These systems are typically in the Pacific, Caribbean and the Far East.

- Coastal Festoons: Systems that are used as part of the national network to link cities on the coast when the terrain is rugged or the path too difficult to negotiate.

- Point to Point Links: Systems that join two locations across a strait or large bay. These have been common to date in Northern Europe where the geography and traffic density is most suitable.

- Inland Lake Links: Systems where the system is a direct extension of the national land cable system.

A survey of the world market has shown that the relative distribution of the above applications in terms of total system lengths expressed as a percentage of the total market is as shown in Figure 1.

FIGURE 1

PERCENTAGE OF CABLE REQUIRED BY APPLICATION

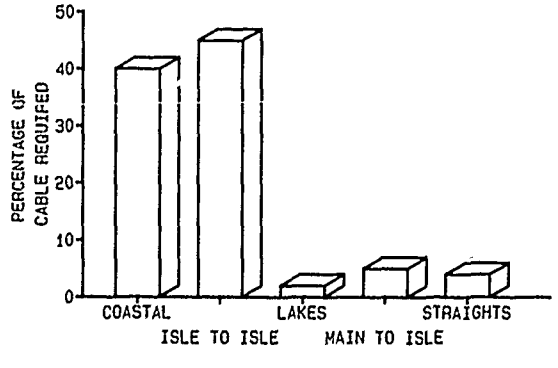

As can be seen, most of the systems are either coastal or island to island. The survey has also revealed that most of the systems are required in water depths of less than 4 km, as shown in Figure 2.

FIGURE 2

PERCENTAGE OF CABLE REQUIRED BY DEPTH CLASS

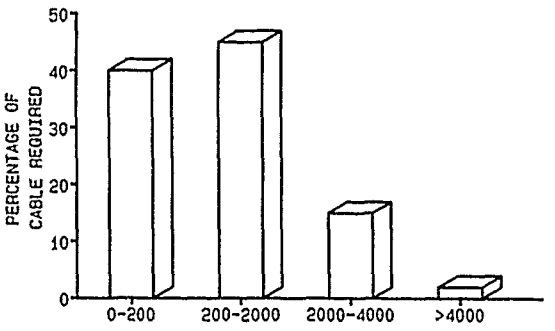

Submarine cables are traditionally laid from specialist cable ships designed specifically for deploying deep water, trans-oceanic cable systems with many repeaters. This means that for the majority of single span systems, the facilities and carrying capacity of these vessels will be vastly under-utilised.

This leads to a high cost of installation for the system when laid in this way. However, this situation can be avoided if the cable is designed to enable the maximum flexibility in transportation and laying methods and equipment. These savings created by matching the cable and equipment can be further enhanced if the plant can be utilised on a wide range of marine platforms, allowing the system provider the freedom to select the most cost effective and appropriate technical solution for each particular project.

Cable Design Considerations

The current STC submarine cable product NL Ref. (1) has been successfully used for unrepeatered cable systems such as UK-Netherlands and UK-Channel Islands using conventional cable ships, but these cable have traditional design features that are not germain to unrepeatered systems.

These are:-

- Very high cable strength
- Power feed
- Hydrostatic pressure resistance
- High Voltage insulation

For unrepeatered systems a more economic cable design is possible with performance matched to the service requirements.

For minimum transportation and deployment costs a small, light cable is required. Strength must be adequate for laying and recovery to the maximum depth of 4 km, so that high strength to weight in water is required.

In shallower water, where primary protection can be most effectively provided by burial, a high density is required to ensure that ploughed cable remains buried in service. To meet these design requirements, four key target parameters were identified as follows:-

- Maximum weight in air
- Maximum diameter
- Minimum UTS
- Minimum density

These design constraints can be plotted against two common axes of cable diameter and cable weight/km as shown in Figure 3. The key parameters can then be defined on these axes by lines defining complaince with the specified targets. This enables a map to be constructed which results in the definition of a 'design window' in which compliant designs must sit.

FIGURE 3

S^3 CABLE DESIGN WINDOW

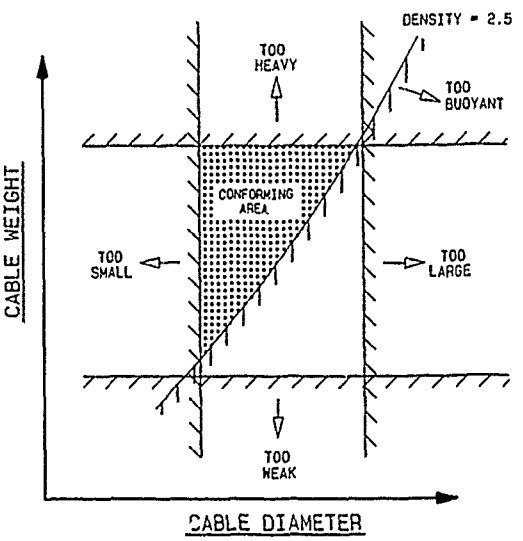

Design Procedures

Starting with these baseline design targets, the relative merits of different design approaches can be evaluated. The assumption used for all designs was to place the fibre package at the centre of the cable where it is afforded maximum protection and minimum strains in service.

Protection of the fibre package from hydrostatic pressure may be provided by a pressure tube placed directly around the fibres, or by using a bridged structure provided by the strength member. Fibres must also be protected from hydrogen, which can be achieved in several ways:-

- Provision of a hydrogen barrier in the cable.
- Use of hermetic fibre.
- Introduction of a hydrogen getter in the cable.

Designs of cable with and without a hydrogen barrier were therefore considered.

In all the designs evaluated, the cable strength is provided by high tensile steel as this is by far the most economic solution and well proven for submarine cable applications.

The cable strength member can be positioned close to the centre of the cable directly around the fibre package or the pressure tube containing the package. Alternatively an external strength member may be used with an intervening extruded insulation layer between the fibres (or fibres and pressure tube) and the strength member. This approach has advantages in providing good abrasion resistance and fishbite protection to the cable insulation. However, the increased pitch diameter of the strength member means that a torsionally balanced (or torsion free) design must be used to avoid torsional instability in service.

With an internal strength member close to the centre of the cable, unilay (unbalanced) strand designs may be considered, providing that the overall torsional stiffness of the cable is sufficiently high to limit twist induced by tension in deployment. A welded copper tube around a unilay strength member is an effective and proven method of providing a hydrogen barrier and a high degree of torsional rigidity.

Figure 4 shows generic designs which have been evaluated based on the various design options which have been described.

The study has built on the experience STC has with its existing cable products. The designs were looked at in terms of the overall cable performance and the individual performance of each of the elements.

The emphasis of the study was to design a high quality, reliable product.

Attenuation

Low loss is essential for such systems, particularly coastal festoons where total cost can be reduced considerably through reduction of land based repeater stations. The current NL cable product has used a tight buffered package, as shown in Figure 5, and this has given exceptional loss performance and stability.

FIGURE 4

GENERIC CABLE DESIGNS

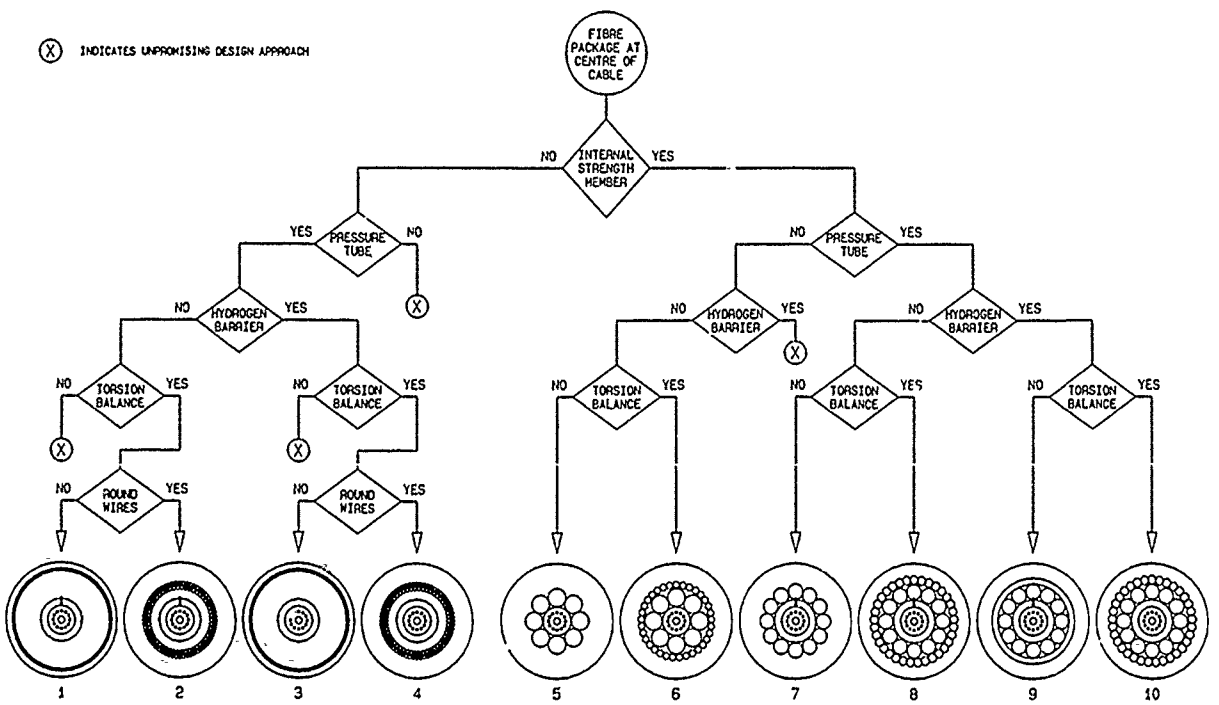

FIGURE 5

STC OPTICAL FIBRE PACKAGE

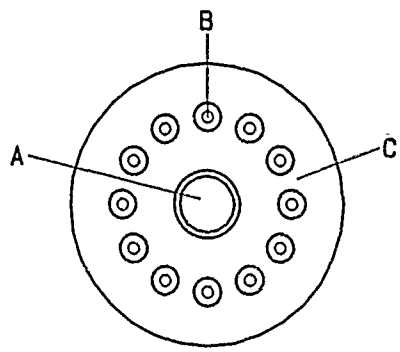

A - COPPER PLATED STEEL WIRE 0.71 mm DIA.
B - ACRYLIC COATED FIBRE 0.28 mm DIA.
C - HYTREL ELASTOMER 3.10 mm DIA.

By this method the fibres are firmly and reliably held in the configuration shown providing a low optical loss. Table 1 shows the losses achieved in our recent UK-Channel Islands and UK-Netherlands systems. STC has to date manufactured many thousands of kilometres of this type of package.

Using this configuration there is no measurable loss difference between fibre bought in and manufactured cable, other than for splices. This package design will therefore be used in the unrepeatered cable.

TABLE 1

NL UNREPEATERED CABLED FIBRE LOSSES

Fibre	Loss dB/km at 1550 nm UK-Channel Isles 1988	UK-Netherlands 1989
Red	0.214	0.194
Yellow	0.217	0.196
Magenta	0.223	0.191
Brown	0.212	0.194
White	0.215	0.194
Violet	0.218	0.195
Green	0.215	0.194
Pink	0.215	0.194
Grey	0.211	0.194
Blue	0.214	0.195
Orange	0.227	0.195
Natural	0.225	0.194
Mean	0.217	0.194

Residual Strain

Cable strains during laying to the maximum design depth of 4 km will be relatively low for the unrepeatered cables and are expected to be typically 0.2% or less. Cable deployed in deep water (greater than 1 km) is laid on to the sea bed with slack, so that in service there is no residual strain in the fibre other than the small residual strain from manufacture.

Additional strain may be introduced in regions where the cables are buried by ploughing during laying. Data obtained from larger cables shows that tension increases with cable weight and diameter, and is also higher for armoured cables than for smoother and more flexible lightweight cables. Hence for these small, light and flexible designs the expected residual strains for burial are small, and of the order of 0.1% or less.

The maximum tension in service will occur in recovery in deep water when peak tensions of 2.5 - 3 wD may be expected (w = weight in water, D = depth). However as the cables have a high strength to weight ratio and maximum design depth is 4 km, the maximum expected strain in recovery is less than 0.5%.

The fibre proof test is determined from the required high survival probability in service and the measured strength distribution of the fibre. The strength distribution is obtained from dynamic tests to break on representative samples of fibre. The measured stength distribution can be approximated to a Weibull characteristic:-

$$\psi_D = \exp - \left(\frac{\varepsilon_o}{a}\right)^b$$

ψ_D = Sample survival probability

ψ_D = Measured breaking strain of sample length Ls tested at strain rate

a, b = Experimentally determined constants

The survival probability when subjected to a proof test ε_p (%) for time tp is given by:-

$$p = \exp - \left\{ \frac{((N+1)\dot{\varepsilon}\,\varepsilon_p^{\,N}\,t_p)^{\frac{1}{N+1}}}{a} \right\}^b$$

Where: N = Fatigue constant

The subsequent survival probability of this proof tested fibre when subjected to strain in service of a (%) applied for time ta is:-

$$\psi_a = \frac{\exp - \left\{ \frac{((N+1)\dot{\varepsilon}(\varepsilon_p^N t_p + \varepsilon_a^N t_a))^{\frac{1}{N+1}}}{a} \right\}^b}{\exp - \left\{ \frac{((N+1)\,\dot{\varepsilon}\,\varepsilon_p^{\,N}\,t_p)^{\frac{1}{N+1}}}{a} \right\}^b}$$

This is the survival probability of a length of fibre equal to the sample test length Ls.

For longer length (L) the survival probability is

$$L = (\psi a)^{L/Ls}$$

Using this, the proof test level can be determined which will ensure a high survival probability under all service conditions.

The unrepeatered cables use a tight buffered fibre package which is closely coupled to the rest of the cable by a viscous waterblocking material.

This close coupling subjects the fibres to controlled and predictable strains equal to the cable strain during deployment and recovery operations. However, the viscous nature of the coupling enables localised high strains to dissipate with time, thus reducing the possibility of long term high residual strain in the fibre caused by local high strains in the cable.

Hydrostatic Pressure Resistance

In order to prevent microbending loss resulting from hydrostatic pressure when the cable is on the seabed, the Hytrel package is encased in a pressure tube. The internal dimension of the pressure tube, together with the method of waterblocking the tube bore, will be identical to that used in NL cable. This will maintain the fibre package in a similar environment to the extremely reliable NL cable.

The pressure tube may be a fully closed 'C' section but can be welded along the seam to double up as a hydrogen barrier. The pressure resistance of the tubes are limited by yielding of the material at the bore and the thickness of tube required can be calculated using the Von Mises equation:-

$$P = \frac{\sigma (K^2 - 1)}{3\sqrt{K^2}}$$

Where: P = External tube pressure
σ = Yield strength
K = Diameter ratio OD/ID

A variety of materials can be used in the pressure tube construction but when it is also required to act as the hydrogen barrier, copper is chosen as it is more ductile and can be easily drawn down after the welded tube has been formed.

Hydrogen

The potential problems with hydrogen in contact with optical fibres was identified in 1983, Ref. (2). It will cause an increase in attenuation and must therefore be considered carefully when designing a cable. It can be generated within the cable structure as a biproduct of chemical corrosion of the metallic elements, and externally due to organic degradation or magneto hydrodynamic effect. The polymeric materials may also outgas dissolved hydrogen or degrade, leading to its formation.

In order to minimise the attenuation increase an effective hydrogen barrier must be used to minimise the attenuation increase. Hermetic coating of the fibres can achieve this but the technology is very new and is still being proved for underwater systems. The proven alternative is to use a metallic tube such as copper to ensure system reliability.

The increase in optical loss due to hydrogen can be calculated, Ref. (3), using:-

$$= 1.4 \times 10^{-2} P(H_2).S_\lambda \exp \frac{1550}{RT} \text{ dB/km} \quad .. (1)$$

Where: P = Pressure of hydrogen (atm)

T = Temperature (k)

R = Gas constant (1.987 $cal.mol^{-1}\ {}^{\circ}K^{-1}$)

S_λ = Scaling factor for a given wavelength (at 1.55 microns S = 2.7)

The acrylic fibre and Hytrel package with viscous waterblocking inside a hydrogen barrier will outgas up to $8cc(H_2)/km$. This gives an increase in optical loss for a 200 km unrepeatered system of 0.1 dB after 25 years.

Hydrogen will diffuse, albeit very slowly, through the hydrogen barrier. The amount of hydrogen that can pass through can be calculated assuming the internal concentration within the tube is negligible, Ref. (4), using:-

$$Q = \frac{2\ R\ P^{1/2}\ t}{\ln (b/a)}$$

Where: Q = The amount of hydrogen passing through the barrier per unit length.

R = Penetration rate of hydrogen through copper

t = Time

P = Hydrogen pressure difference across barrier

a = Internal diameter of barrier

b = Outer diameter

Assuming a very worst case where hydrogen surrounds the tube at the maximum sea bed pressure of 40 MPa:-

$$R = 2 \times 10^{-18}\ cc(H_2)\ cm^{-1}\ S^{-1}\ Pa^{-1/2}$$

The quantity of hydrogen that will pass through, for example, a copper tube 0.4 mm thick will be 5 cm^3 per kilometre of cable. Using Equation 1 this will given an increase in loss for a 200 km unrepeatered system of 0.06 dB after 25 years.

Fibres contained within this type of environment will therefore be adequately protected from an increase in attenuation due to hydrogen.

Electrical Requirements

For unrepeatered systems there is no requirement for a high voltage insulated power feed conductor. However, an insulated conductor with low attenuation at low frequencies is still required to enable a 25 Hz toning signal to be transmitted for fault location in the event that the cable is damaged in service.

In the design with a central strength member a combination of the strand and pressure tube will act as the signal conductor. For the outer strength member design the pressure tube alone will conduct the signal.

Sheath

The sheath must adequately protect the cable during the laying/burial operations and for the lifetime of the system. It must be capable of withstanding potential abrasion, impact, tearing and stripping forces that may be encountered during normal handling operations. It must also be able to withstand any abrasion on the sea bed caused by cable movement. Cable movement is in fact minimised by burial and having a cable density higher than the sea bed material.

A reasonably high torsional stiffness for the cable is important as it will reduce the amount of cable twist under tension. A material with a high rigidity is therefore needed.

HDPE has been chosen as it has the required mechanical properties and is easily processed. It has a good abrasion performance and has a high rigidity.

As an additional protection from more severe damage a steel tape may be wrapped longitudinally around the sheath and a second layer of HDPE applied. Any damage will therefore only penetrate the outer sheath down to the tape.

Bottom feeding sharks have been known in rare circumstances to bite submarine cables. The additional steel tape will also protect the cable from this potential hazard.

Additional Protection

In the shallower waters of the Continental Shelf in water depths of less than 1000 metres the cables can become damaged by external hazards. Fishing is the most common cause of submarine cable damage although there are other hazards such as ships anchors or rocky seabeds. The fishing activity can penetrate the seabed to a maximum of 60 cm.

One of the ways of overcoming these hazards is to apply large amounts of additional armour. It has been found that the thicker the armour and thus larger cable diameter, the lower is the probability of it becoming damaged. This type of cable does not though have a small enough minimum bend radius to creel into a container.

An alternative way of protecting the cable is to bury it into the seabed below the depth disturbed by fishing activity. A plough can be used during the laying operation to insert the cable as it is laid. This approach will minimise the risk of in-service damage. The cable will have a high enough density to ensure that the cable remains buried.

Conclusion

This paper describes the design process for a cable that must meet the very high performance and reliability targets for unrepeatered submarine telecommunication systems. This approach has enabled us to evolve two cable designs that are currently undergoing qualification with confidence that they will meet all the service requirements. The cables will be manufactured using our high standard manufacturing equipment and procedures to produce a high total quality product.

Acknowledgements

Many thanks to the STC Submarine Systems directors for their kind permission to publish this work.

References

(1) Worthington P.

"Cable Design for Optical Submarine Systems"

IEEE Journal on Selected Area in Communications - Vol. SAC-2, No. 6, Nov 1984

(2) Machizaki K., Narrihira Y., Yamamoto H.

"Transmission Loss Increase in Optical Fibres Due to Hydrogen Permeation"

Electronics Letters, 1983, 19, pp 743 - 745.

(3) Barnes S.R., Pitt N.J., Hornung S.

"A Model for Predicting Hydrogen Degradation in Optical Cables"

IOOC - ECOC 1985, pp 897 - 899.

(4) Jerkins W.E., Bogeal D.R.

"Permeation and Diffusion of Hydrogen in Ceramuar, Copper and Ceramuar-Copper Laminates"

Sandia Labs, Albuquerque New Mexico 1972.

Biography

Dr. C.J. Rochester
STC Submarine Systems
West Bay Road
Western Docks
Southampton, U.K.
SO9 4YZ

Dr. Christopher Rochester was born in Greenwich, England. He obtained a BSc in Chemistry and a PhD in Materials Science at the University of Sheffield.

He started work at TSL Glass in Tyne & Wear, where he worked in the research and development department as the Project Chemist on producing very high purity doped silica glass for fibre manufacture.

He then became the Technical Manager of a moulding company in Northampton, with responsibility for all technical aspects of the company and the quality assurance department.

In 1988 he joined STC Submarine Systems as a senior engineer in the cable R.& D. department. He is responsible for high strength fibre splicing, unrepeatered and DOD cables.

Mr. B.A. Eales
STC Technology Ltd
London Road
Harlow
Essex, U.K.
CM17 9NA

Brian A. Eales obtained a High National Certificate in Applied Physics from the North London Polytechnic in 1966. Since that time he has been mainly involved in the development of semi-conductor lasers and associated packing technology for military and telecommunications use. In particular he was responsible for the development of the first high reliability 1.3 um single mode laser package for both landline and submarine systems use. He is currently a Senior Principal Research Engineer working in the Optical Cable Technology Laboratory.

Dr. S.R. Barnes
STC Submarine Systems
West Bay Road
Western Docks
Southampton, U.K.
SO9 4YZ

Dr. Stuart Barnes was born in Worksop, England, in 1953 and educated at King Edward VI Grammar School, Retford, and Queen Mary College, University of London, where he obtained a BSc (Eng) and PhD.

After Post Doctorate work on Fracture Mechanics he joined the Polymer Technology Group at STC Technology Ltd. in Harlow. During his years at STC Technology he worked on a whole range of cable types and was the design authority for the current submarine optical cable.

In 1986 Dr. Barnes joined the Cable Products Division at STC where he became Technical Manager for Optical Cables. In 1988 he joined STC Submarine Systems as Technical Manager, Cable.

Over the years he has published many papers on cable design and cable related topics and has been invited speaker at a number of overseas conferences.

Mr. P. Worthington
STC Submarine Systems
West Bay Road
Western Docks
Southampton, U.K.
SO9 4YZ

Peter Worthington is a development engineer with STC Submarine Systems which he joined in 1974.

He received a BSc. in Electronics and Electrical Engineering from the University of Birmingham in 1971. Since 1977 he has been involved in the development of optical cables for submarine systems.

Mr. A.J. MacLeod
STC Submarine Systems
Wes[illegible]ay Road
West[illegible] Docks
So[illegible]apton, U.K.
SO9 4YZ

Andrew MacLeod was born in 1957 in Loughborough, England, and gained his MA in Materials Science from Keble College, Oxford University, in 1980.

He joined the Research & Development Department of Pirelli General Cables, Southampton, working on high voltage insulation materials, fine performance polymer compounds and progressed to manage a group responsible for the formulation of high performance polymer compounds and cable products.

In 1986 he moved to a Product Management position with Pirelli Special Cables with responsibility for the development and marketing of high performance military and fibre optic cable products.

In 1988 he assumed his current position in STC Submarine Systems, Southampton, as Product Manager, Unrepeatered Systems, with specific responsibility for the definition, development and management of system products for this application area.

He is a Chartered Engineer and a Corporate Member of the Institute of Metals and the Plastics and Rubber Institute.

DEVELOPMENT OF OPTICAL UNIT FOR OPTICAL / ELECTRIC POWER COMPOSITE UNDER SEA CABLE

N. Okada, A. Mogi, M. Miyamoto, H. Suzuki

Fujikura Ltd. Chiba, Japan

Abstract

A newly designed optical / electric power composite under sea cable has been investigated. To combine optical fibers with a stiff electric power cable, it is very important to design the optical unit structure. Especially, in the case of the under sea cable, the unit should be superior in mechanical strength and optical fiber protection from sea water. The jelly filled stainless steel pipe(SUS) buffered optical units are adopted to combine with an electric power cable.

Moreover, the best combining method is studied to manufacture the composite cable without degradation of the good characteristics of the optical fiber and the electric power cable.

We manufactured the short composite cable experimentally, and subjected it to severe tensile test. As a result, it was verified that the cable has excellent performance to be applied to practical use.

1. Introduction

Many optical composite power cables has been developed and are used in various fields because of the advantages of optical fibers such as immunity from electromagnetic interference, long repeater spacing, wide band-width, small size and light weight. Especially, the cost to construct an under sea transmission system is so high that it is very profitable to combine the optical fibers with an under sea electric power cable.

In the case of under sea cable, the optical fibers must be shielded from sea water by metallic materials. Several types of metallic pipe buffered optical units shown in Fig.1 have been suggested and used.[1),2),3),4)] (A) is single fiber type, (B) is fiber stranding type, (C) is slotted core type, and (D) is tape-fiber type.

To manufacture the composite cable, 2 types of composite cable structure are considered as shown in Fig.2. The composite cable type (A) has optical units in the gap of the standing three power cables, and type (B) has optical units around the electric power cable by stranding method. Type (A) has been well known in general [3),5)], while type (B) is not. However, type (A) is not suitable to composite so many optical units with an electric power cable, so we studied type (B) structure.

The optical fiber is inserted into the SUS pipe together with jelly compound. The SUS pipe buffered optical units enable to strand around the stiff power cable because of its high resistance to the lateral pressure and to the humidity.

Moreover, from the view point of long term reliability, the composite cable should be designed to protect the optical fibers from the stress under severe installation and environmental conditions. Usually, the under sea cable is armored by the steel wires to protect the cable from the mechanical damages and to suppress the elongation of the cable under the installation. The key point is how to strand the optical units and the steel armors around an electric power cable. The stranding directions, stranding lay length, and pitch diameters are very important.

The optical fiber / electric power composite cable was manufactured experimentally and was subjected to severe tensile test assuming the installation of an under sea power cable. As results, this composite cable showed sufficient performance.

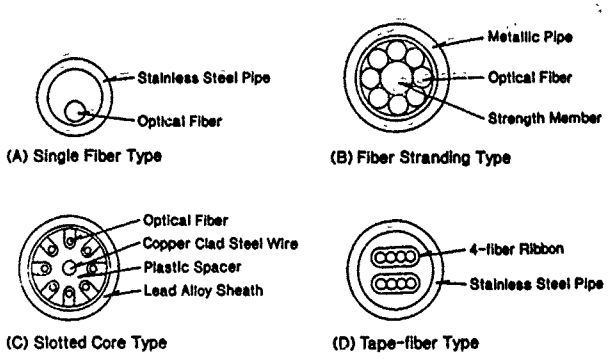

Fig.1 Cross Sections of Metallic Pipe Buffered Optical Units

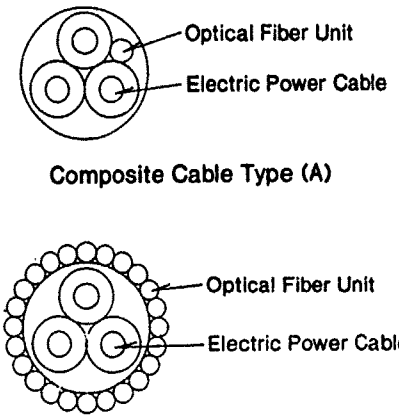

Fig.2 Cross Sections of Composite Cables

2. Cable design

To manufacture the optical / electric power composite under sea cable without degradation of the excellent cable characteristics, the important points are how to design the optical unit and how to combine it with an electric power cable.

2-1. Optical fiber unit structure

The requirements for the optical fiber unit are the followings.

a) Small diameter
The optical unit should have small diameter to combine with an electric power cable in small diameter.

b) High resistance to the lateral pressure
The optical units should have high resistance to the lateral pressure to combine them with a stiff electric power cable.

c) Optical fiber protection from the sea water
The optical fiber worsen its mechanical property in water. So the unit structure should protect the fibers from the sea water.

d) Long length unit with long term reliability
The optical fiber should be given high proof test considering severe installation and environmental conditions. Moreover, to manufacture so long optical units, the optical fibers must be spliced with high strength in small diameter.

Based on these criteria, the optical fiber unit structure is designed.

The 400um UV curable resin coated fiber is adopted to manufacture so long optical unit with high reliability. This fiber has good resistance to 2% proof test. The fibers can be spliced each other by arc-fusion method and the splicing point can be re-coated by UV curable resin with high mechanical strength.

The optical fiber unit should be designed to have high resistance to the lateral pressure because the optical units are combined with an heavy, large, and stiff electric power cable. Moreover, in the case of the under sea cable, the unit structure should protect the optical fibers from the sea water. Therefore the optical fibers are inserted into the SUS pipe together with jelly compound. This unit structure satisfies the condition concerning small diameter unit. And the pipe is jacketed with poly-ethylene to protect the SUS pipe from the sea water.

In the case that the optical fibers are placed in the SUS pipe loosely, the points to which special attention should be paid are the excess fiber length in the SUS pipe and the shrinkage of the SUS pipe by bending.

2-1-1. Excess fiber length in the SUS pipe

The characteristics of the SUS pipe buffered fiber are influenced significantly by the excess fiber length in the SUS pipe. If the length of the SUS pipe is longer than the optical fiber, the critical strain may appear on the optical fiber. But, the loss increase results from so much excess fiber length. So the

region of the excess fiber length tolerance exists.

It is assumed that the excess fiber length is put in the SUS pipe as shown in Fig.3. The curvature of the optical fiber is given by

$$y = A\sin\left(\frac{2\pi x}{P} - \frac{\pi}{2}\right) + A \qquad (1)$$

Here, A and P are the amplitude and the pitch of the sin-curving optical fiber in the SUS pipe. The radius of the curvature R is evaluated from the definition and the minimum radius Rmin is obtained at x=0,P,2P,....

$$R = \frac{(1 + y'^2)^{\frac{3}{2}}}{y''} \qquad (2)$$

$$Rmin = \frac{P^2}{4A\pi^2} \qquad (3)$$

Fiber length L is obtained by

$$L = \int \sqrt{1 + y'^2}\, dx = x\left(1 + \left(\frac{\pi A}{P}\right)^2\right) \qquad (4)$$

The ratio of the excess fiber length K is defined by

$$K = \frac{l - x}{x} \qquad (5)$$

From (3),(4),(5), the ratio of the excess fiber length K as a function of the amplitude A and the minimum radius Rmin of the optical fiber curvature is given by

$$K = \frac{A}{4Rmin} = \frac{Dsi-Df}{8Rmin} \qquad (6)$$

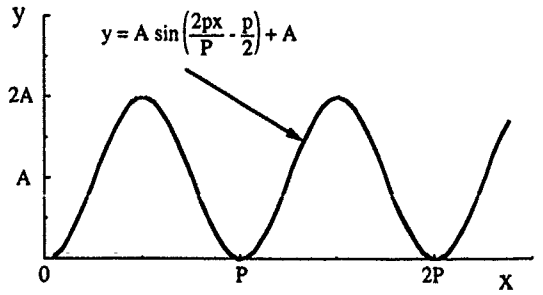

Fig. 3 Curve of Optical Fiber in SUS Pipe

The amplitude of the optical fiber curvature A is determined by the inside diameter of the SUS pipe Dsi and the outside diameter of the optical fiber Df.

For the case that the 400um UV fiber is inserted into the SUS pipe, the relationship between the ratio of excess fiber length K and the minimum radius of optical fiber in the SUS pipe Rmin is shown in Fig.4. From the view point of the loss increase, the minimum bending radius of the optical fiber is considered 20mm. And it is desired that the allowable excess fiber length is larger than 0.2%, because the large allowable region of the excess fiber length gives easier control of the manufacturing process.

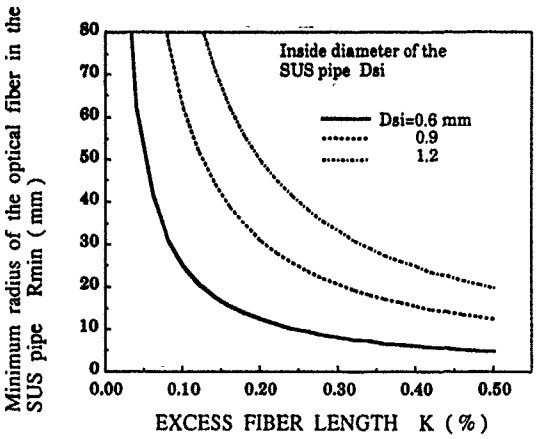

Fig. 4 Relationship between Ratio of Excess Fiber Length K and Minimum Radius of Optical Fiber in SUS Pipe

2-1-2. Shrinkage of the SUS pipe

The SUS pipe is fabricated by SUS tape forming, welding, and drawing process. At the same time, the fiber and jelly compound are inserted into the SUS pipe. The SUS pipe shrinks due to the residual strain releasing when the SUS pipe is bent. The shrinkage causes the increase of the excess fiber length in the SUS pipe and then loss increase may be observed. This phenomenon occurs when the bending stress is larger than the elastic limit. Fig.5 shows the bending stress of the several SUS pipe. So the allowable bending radius should be decided considering the elastic limit. From the experimental results, the elastic limit of the used SUS pipe was found about 0.4%.

As mentioned above, the diameter of the SUS pipe should be larger from the

view point of the excess fiber length tolerance. But the large diameter SUS pipe should not be bent into small diameter. So we designed the dimensions of the SUS pipe as shown in Fig.6. The outside and inside diameter of the SUS pipe are 1.1mm and 0.9mm.

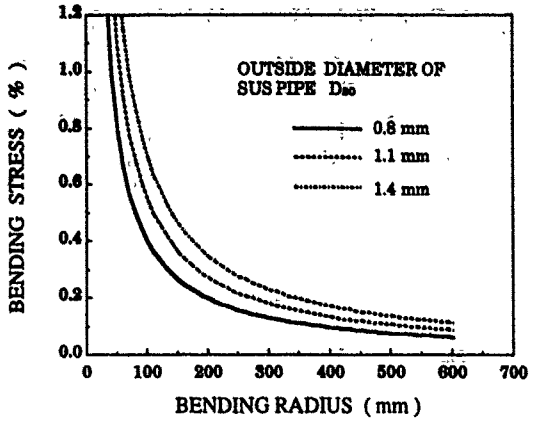

Fig. 5 Bending Stress dependence on Outside Diameter of SUS Pipe

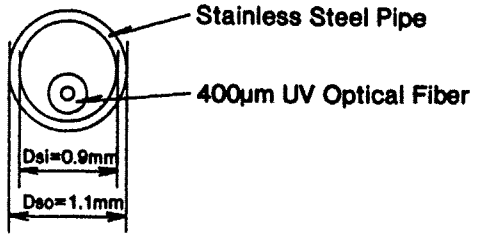

Fig.6 Cross Section of Stainless Steel Buffered Optical Unit

2-2. Composite cable structure

The SUS pipe buffered fibers can be stranded around an electric power cable because of its excellent lateral pressure resistance. This method is superior to composite so many optical units with an electric power cable.

Generally, the under sea cable is armored by the steel wires to protect the cable from the mechanical damages and to suppress the cable elongation during the installation. So the steel armors are stranded over the cable that the SUS pipe buffered fibers are stranded around the electric power cable. In this case, the cable may be twisted easily in the direction that the steel armors are loosened. The cable elongation is mainly due to the excess steel armors loosening, and at the same time, the critical strain may appear on the optical fibers. To solve this problem, when the cable is twisted, the optical fiber should be loosened, too. Therefore the stranding direction of the optical units should be designed the same as that of the steel armors. Moreover, it is desired that the optical units are not stressed under the twisted cable condition. The key points are how to strand the optical units and how to strand the steel armors around the electric power cable. The pitch diameter and stranding lay length are very important parameters.

The composite cable which has L0 m in length is lengthened to L1 m by twisting through S degrees. Then the length of the optical units may be changed as shown in Fig.7. Here, Ps and Ds are the lay length and the pitch diameter of the steel armors, and Pf and Df are those of the optical units. The strain of the optical units are influenced by the ratio of the lay length to the pitch diameter of the steel armors Pf/Df and that of the optical units Ps/Ds. The best ratio is found that (Pf/Df)/(Ps/Ds) is equal to Df/Ds. For example, when Df=100mm, Ds=120mm, Ps=1560mm, the best lay length of fiber Pf is calculated 1090mm. Fig.8 shows that the strain of the optical fiber when the composite cable is twisted. The optical units are not stressed under several twisting conditions.

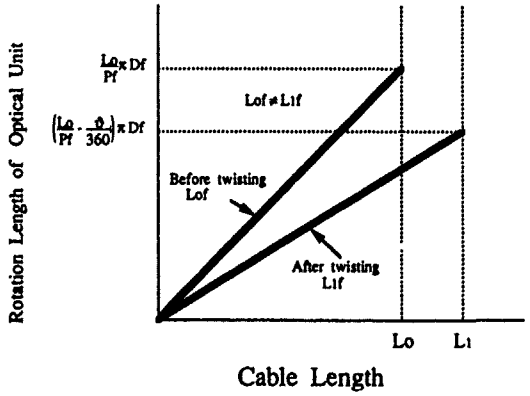

Fig. 7 Change of Optical Unit Length by Cable Twisting

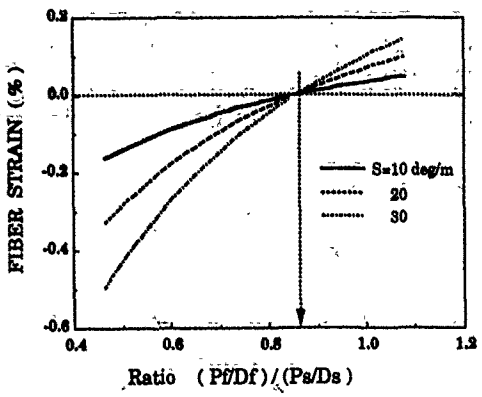

Fig. 8 Dependence of Fiber Strain in Twisted Cable on Ratio (Pf/Df)/(Ps/Ds)

3. Characteristics

3-1. SUS pipe buffered optical unit

The SUS pipe unit shown in Fig.6 was manufactured experimentally and investigated the several characteristics. The 400um UV coated optical fiber which has 9.5um of mode field diameter and 1.24um of cut off wavelength was inserted into the SUS pipe.

3-1-1. Resistance to the lateral pressure

The SUS pipe buffered optical unit shows excellent resistance to the lateral pressure shown in Fig.9. The loss increase is not observed at 2.5kg/mm.

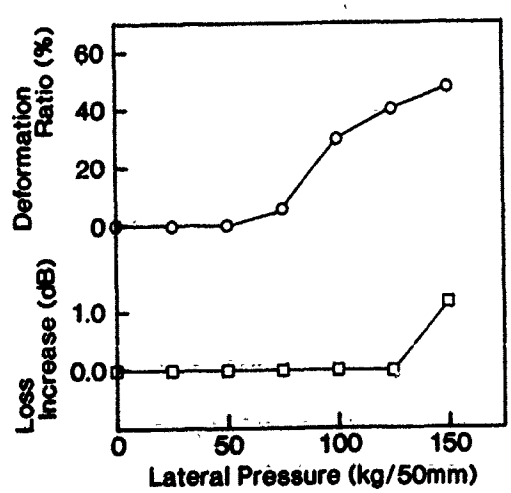

Fig.9 Result of Lateral Pressure Test

3-1-2. Excess fiber length in the SUS pipe

The excess fiber length in the SUS pipe is very important factor. So the excess fiber length is investigated in detail. As a result, it is verified that around 0.05% of the excess fiber is arranged in the SUS pipe.

3-1-3. Shrinkage of the SUS pipe

The shrinkage of the SUS pipe by bending is investigated. The SUS pipe is passed through the testing line several times shown in Fig.10. As a result, it is verified that the shrinkage is related to the bending radius. From Fig.11, it is noted that the shrinkage is very large as bending radius is less than 100mm.

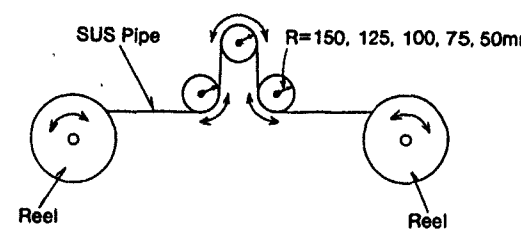

Fig.10 Test Line of SUS Pipe Shrinkage by Bending Radius R

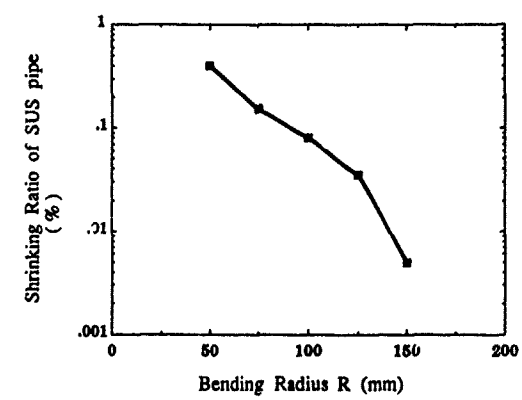

Fig. 11 Result of Shrinking Ratio by Bending Radius R

3-2. Experimental composite cable

The short composite cable was manufactured experimentally, and was

subjected to several tests to examine optical performance under mechanical environments. The SUS pipe buffered units are jacketed with poly-ethylene to protect it from sea water. The jacketed unit diameter is about 3.0mm. These optical units and steel armors are stranded around an electric power cable as mentioned in chapter 2-2.

3-2-1. Tensile test

We subjected the composite cable to the tensile test while monitoring attenuation loss changes and the strain of the optical fibers. The result is shown in Fig.12. The cable was lengthened as twisting, however the loss changes and the strain of the optical fibers were not observed. The result verified the validity of the design based on theoretical P/D relations.

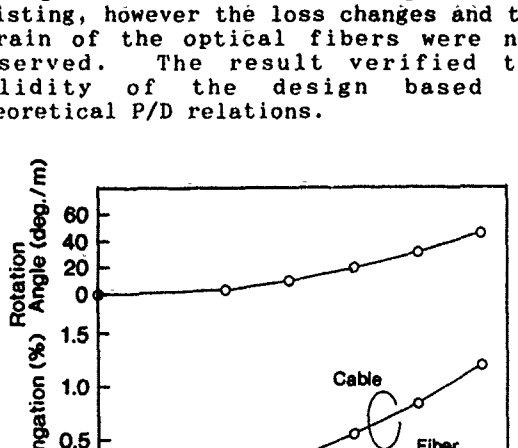

Fig.12 Result of Tensile Test

Conclusion

The newly optical fiber / electric power composite under sea cable was designed. The optical fibers are inserted into the stainless pipe together with jelly compound and the poly-ethylene covers the pipe to increase the reliability. These optical units are stranded around an electric power cable in the same stranding direction as that of the steel armors.

The experimental composite cable was subjected to the tensile test on assumption of the installation of an under sea electric power cable. As a result, it was verified that the composite cable showed sufficient properties for practical application.

References

1) M. Niijima, S. Sentsui, and K. Komiyama, "Development of the optical fiber cable installed in the sewer pipe network", Proceedings of the 38th IWCS, 1989, pp.591-596

2) Y. Hiramoto, S. Toya, H. Maeda, and M. Hirasawa, "Study on multi optical fibers of metallic encapsulation", IEEE Trans., B-403, 1989

3) M. Iizumi, Y. Asada, A. Takase, H. Inoue, H. Ishikura, M. Iwana, K. Suzuki, and Y. Miyajima, "Long length optical fiber composite power submarine cable", Proceedings of the 37th IWCS, 1988, pp.321-326

4) F. Shibasaki, T. Saegusa, A. Mogi, H. Suzuki, T. Maruoka, and R. Tonegawa, "Development of thin size optical fiber cable", IEEE Trans., B-829, 1990

5) T. Yahata, T. Iwabuchi, M. Sakamoto, M. Nemoto, T. Shouji, N. Ohmori, and S. Ishi, "Development and installation of long-length optical fiber / power complex cable", IEEE Trans., B-832, 1990

Naoki Okada

Fujikura Ltd.

1440 Mutsuzaki, Sakura, Chiba, 285, Japan

Mr. Okada was born in 1964. He joined Fujikura Ltd. after his graduation from Chiba University with the B.E. degree in 1986 and has been engaged in research and development of optical cables. He is now an engineer of optical cable section and a member of the Electronics, Information and Communication Engineers of Japan.

Akio Mogi

Fujikura Ltd.

1440 Mutsuzaki,
Sakura, Chiba, 285,
Japan

Mr. Mogi was born in 1946. He joined Fujikura Ltd. after his graduation from Haneda Institute High School in 1967 and has been engaged in research and development of the metallic cables and optical cables. He is now the senior engineer of telecommunication cable section and a member of the Institute of Electronics, Information and Communication Engineers of Japan.

Matsuhiro Miyamoto

Fujikura Ltd.

1440 Mutsuzaki,
Sakura, Chiba, 285,
Japan

Mr. Miyamoto was born in 1953. He received the B.S. degree from Nagoya Institute of Technology in 1976 and the M.S. degree from the Tokyo Institute of Technology in 1978. In 1978 he joined Fujikura Ltd. and has been engaged in research and development of optical fibers and cables. He is now the senior engineer of telecommunication cable section and a member of the Institute of Electronics Information, and Communication Engineers of Japan.

Hideo Suzuki

Fujikura Ltd.

1440 Mutsuzaki,
Sakura, Chiba, 285,
Japan

Mr. Suzuki was born in 1946. He joined Fujikura Ltd. after his graduation from Gunma University with the B.E. degree in 1971 and has been engaged in materials, polymer processing and development of optical cables. He is now the manager of telecommunication cable section and a member of the Institute of Electronics, Information, and Communication Engineers of Japan.

DEVELOPMENT OF FRP ARMORED NON-METALLIC OPTICAL CABLE AND THE ARMORING PROCESS

Y. Kuwata*, K. Niikura*, H. Horima*, K. Kozuka**, S. Matsuno**, M. Okada**

* Sumitomo Electric Industries, Ltd. 1, Taya-cho, Sakae-ku, Yokohama 244, Japan
** UBE-NITTO KASEI Co.,Ltd. 579-1, Yabuta, Gifu 500, Japan

ABSTRACT

With the expanded application of optical cable, a movement to introduce the optical cable in various field is intensified. Particularly needs of a non-metallic type optical cable utilizing largely the characteristics of optical fiber has been increased remarkably. Under such a background and on assumption to increase introducing of a non-metallic cable to very severe environment, we have developed a FRP outer sheath type non-metallic optical cable excellent to the transmission and the mechanical characteristics and have developed an economical manufacturing process to its outer sheath process for a direct burying of optical cable in an area of frequent occurrence of earthquake, landslide or upheaval at the permanent frozen cold district.

1. Introduction

With the expanded application of optical cable, introduction of an optical cable comes in a positive investigation even in an severe environment that a copper communication cable has not been considered so far. The stable transmission characteristics with a low loss and a wide band of non-metallic optical cable and the wide temperature range which is the striking characteristics of optical cable are a large factor to the expanded application of it. For a communication network in a district where lightning damage occurs frequently, which is one of severe environment, optical cables frequently are directly buried into the land at these districts, as well as a non-metallic cable is very effective in these cases. Accordingly the cable is armored to give a mechanical protection and it is generally used with a metallic material such as iron or steel. These metals are needed to take a measure against lightning damage. Although the measures with combination of some metallic materials of different conductivities have been tried, they are not always effective.① Therefore, a necessity of the optical cable with an outer sheath using non-metallic materials is intensified and an more expanding application of this type cable will be expected with an installation in the region where earthquakes and landslides frequently occur as well as upheaval of lands in a cold district. The author et al have developed a FRP armored non-metallic optical cable possible for direct burial installation, which is arranged densely with FRP rod (of an excellent tension resistance and an excellent pressure fracture strength) as outer sheath on the internal core cable. This paper is described about the structure, manufacturing process and evaluated results of this FRP armored non-metallic optical cable.

2. Optical Cable Design

The sectional view of the developed FRP armored non-metallic optical cable is shown in Figure 1. 24 cores jelly-filled grooved spacer type non-metallic optical cable used with a single mode 4-fiber-ribbon was used to the internal core cable. This core cable is stranded closely with a polyethylene covered several millimeter diameter FRP rod in about 500mm pitch, filled with jelly and then mounted with a polyethylene sheath. The diameter and number of FRP rod are possible to set to suit a laying tension, but in this case two types cables of FRP rod diameter 3.5mm A type and 5.5mm B type were designed and manufactured. The structural item of the 2 types of cables is shown in the table 1.

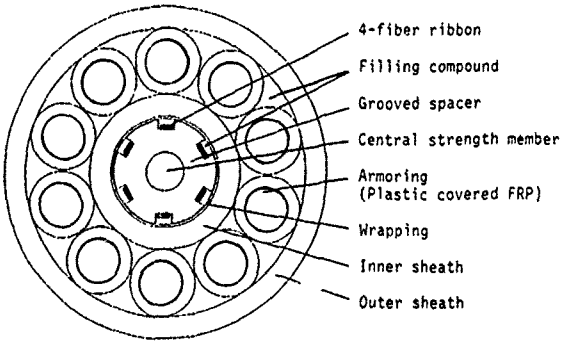

Fig.1 The structure of FRP Armored non-metallic optical cable

Table 1. Structural item of FRP armored non-metallic optical cable

Item	Type A	Type B
FRP rod diameter	3.5mm	5.5mm
Primary coating diameter	4.5mm	6.5mm
Number of FRP rod	12	10
Cable diameter	25mm	31mm
Cable Weight	600kg/km	1000kg/km

3. FRP Armoring Process

In the FRP armored non-metallic optical cable arranged densely with the several millimeter FRP rod designed in the previous section, stranding a cured FRP rod as it is on an optical cable core may cause some trouble in the following points. The stranding is difficult due to the repulsion force of FRP rod, and the handling properties as cable and the stability of stranding are no good. Although it is wound with tape, the stranding may return around the breaking point of cable and fall into disorder by repeated bending. Also the process is complicated together with a high cost. The author et al reported the manufacturing process of the FRP strand cured in tandem through stranding a uncured rod-like FRP product.[2] Recently, with a more development of this process, we have developed the manufacturing process of FRP armored non-metallic cable to settle the above problems. Its outline is shown in Figure 2 and Photo 1. The optical cable core is fed in a constant tension with turning in a constant rotary speed and a uncured rod-like FRP product coated thinly with a flexible thermoplastic resin such as polyethylene is stranded on the outer periphery of the core under a constant tension. Then, it is covered with a polyethylene sheath and is set by a curing of the uncured FRP in a hot water chamber about 100°C. The rotated taking-up machine and the rotated winding machine are controlled in interlocking with the rotated supply machine for cable core. The taking-up speed is 2m/min, the length of curing chamber is 16m and the retention time is 8 minutes. A longer length of curing chamber is possible to speed up.

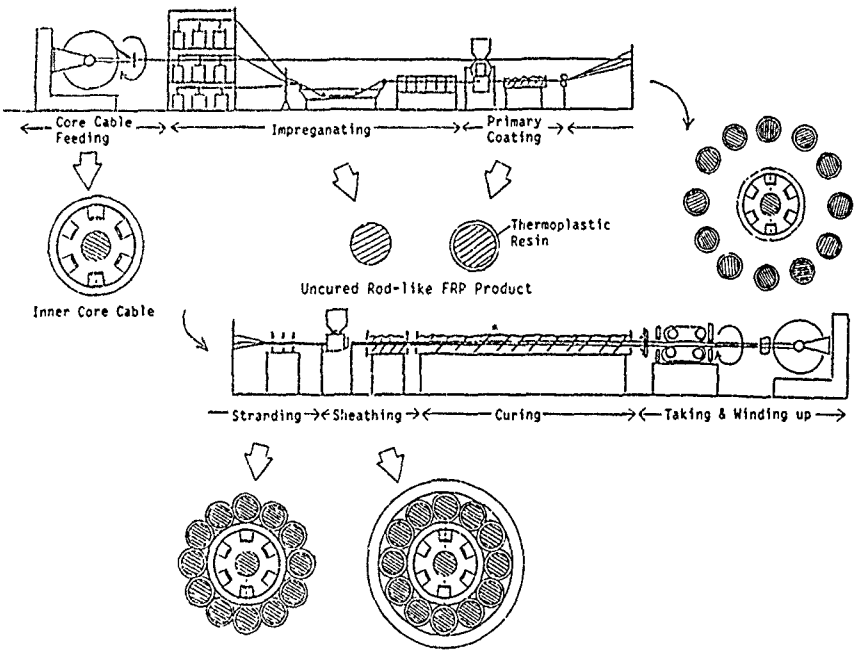

Fig.2 Outline of manufacturing process & products of FRP Armored non-metallic optical cable

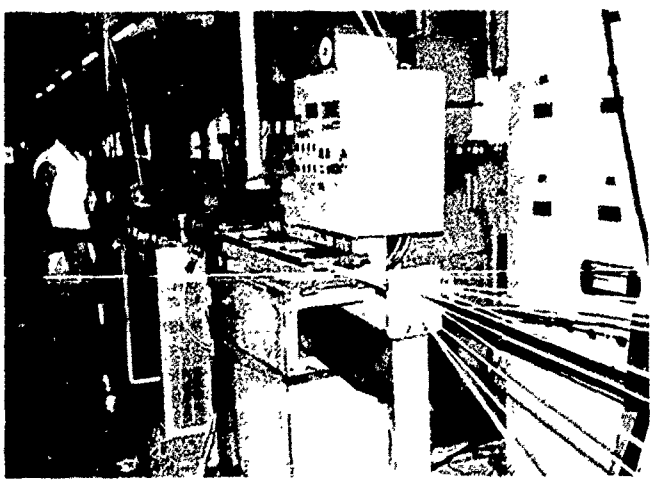

Photo 1

View of manufacturing process of FRP Armored non-metallic optical cable (especially for stranding and sheathing process)

4. Characteristics of FRP Armored Non-metallic Optical Cable

This section is described about the evaluated results of the FRP armored non-metallic optical cable.

4-1. Optical Characteristics

4-1-1. Attenuation Changes After Cabling

This cable is used with a UV-resin coated single mode fiber having the characteristics shown in Table 2, on condition of use in 1.3μm band. The evaluated results of the attenuation fluctuation between the processes across the FRP armoring process for 1000 meter cable are shown in Figure 3. The attenuation fluctuation for the 24-core single mode fiber shows the very stable characteristics within the maximum 0.01 dB/km.

Table 2. Characteristics of fiber

Item	Characteristics
Fiber type	Single mode
Operating wavelength	1.3μm
Number of fibers	24
Attenuation (1.3μm)	< 0.4 dB/km
Cutoff wavelength	1.10 ∿ 1.28μm
Dispersion (1.285 ∿ 1.33μm)	< 3.5 ps/nm·km
Coating diameter	250μm

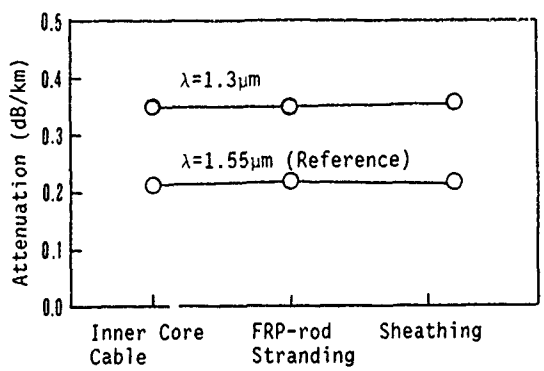

Fig.3 Attenuation of optical fibers in cable manufacturing

4-1-2. Temperature Characteristics

The attenuation fluctuation in 1.3μm due to temperature change within the temperature range of -40 to +70°C was evaluated in a condition of loop connection to the 24-core fiber. The results are shown in Figure 4. The loss fluctuation in this temperature range was within 0.05 dB/km and any deterioration of the characteristics due to the FRP armoring process was not recognized. The stable characteristics were shown even in the low temperature of -40°C. The cable was proved to be enough possible for application even in a cold region.

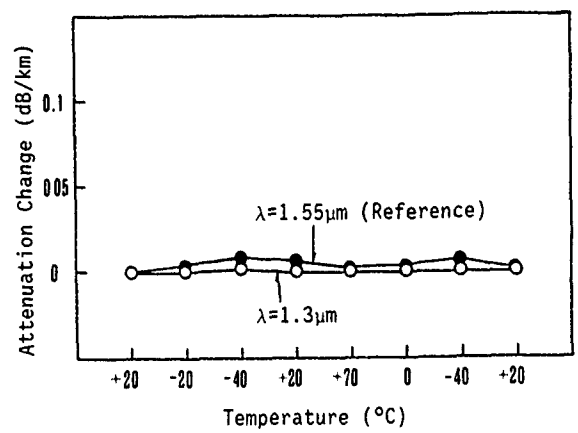

Fig.4 Temperature test

4.2 Mechanical Characteristics

4-2-1. FRP Rod's Mechanical Characteristics After Cabling

The mechanical or physical characteristics of the FRP rod after cabling and the FRP rod cured in a usual linear line condition were compared by the following test. The results and test methods of the 3-point bend test, the compression test, the repeated bend test and the 3-point bend test in -30°C are shown in Table 3. The physical characteristics of the FRP rods in a room temperature, -30°C and after cabling are little changed, though they are cured in a linear line condition. The cable stranded in 250mm pitch with FRP rods cured in a linear line condition and the cable cured after stranding in the same pitch with uncured FRP product were evaluated with the tensile characteristics and its results are shown in Table 3 with test apparatus. The initial Young's modulus among them was almost the same value of about 4400 kg/mm².

4-2-2. Mechanical Characteristics of FRP Armored Non-metallic Optical Cable

The mechanical characteristics of the recently developed FRP armored non-metallic optical cable are summarized in Table 4. The detail test results of the tensile and pressure breaking

Table 3. Comparison Data for physical properties between FRP rod after cabling and FRP rod cured in a usual linear line condition

ITEM	TEST METHOD		FRP rod after cabling	FRP rod cured in a usual linear line condition
3-Point Bend	JIS K 7005 FRP rod diameter: 5.5mm 	at 23°C	Breaking Load 62kg	Breaking Load 64kg
		at -30°C	Breaking Load 71kg	Breaking Load 75kg
Compression	JIS K 7220 FRP rod diameter: 5.5mm 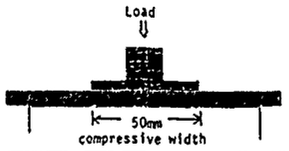	at 23°C	Breaking Load 483kg/50mm	Breaking Load 452kg/50mm
Young's Modulus	ORIGINAL TEST METHOD FRP rod diameter: 3.5mm 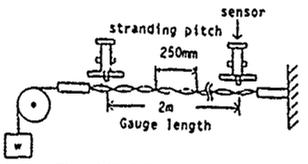	at 23°C	4450 kg/mm²	4430 kg/mm²

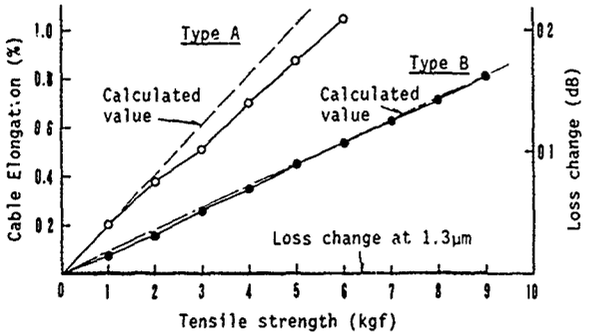

Fig.5 Tensile test results

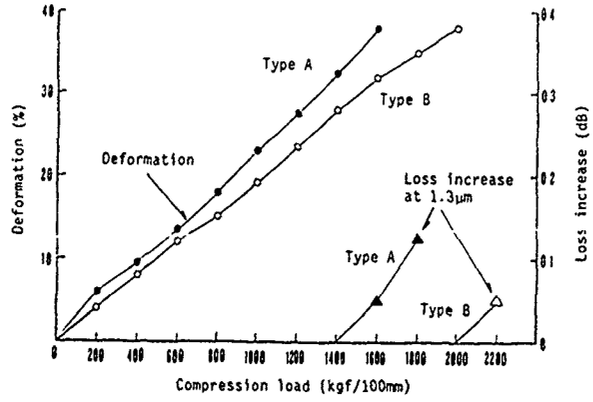

Fig.6 Compression test result

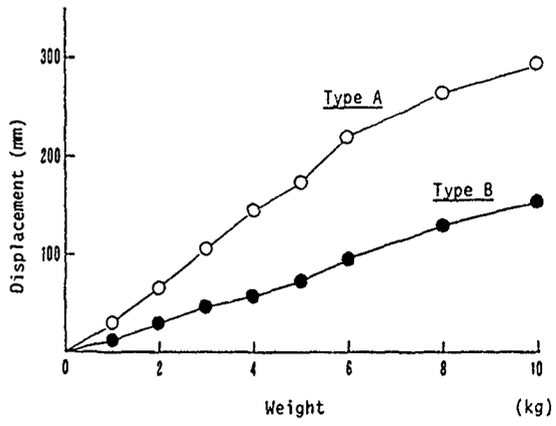

Fig.7 Flexibility test results

characteristics and the flexibility are shown in Figure 5 to Figure 7, but particularly the tensile characteristics was calculated on the basis of the initial tensile modulus of FRP rod indicated in the previous section. It is found that the tensile load-elongation characteristics agrees almost with the experimental value. It is indicated that each FRP rod has been uniformly arranged on the internal core cable. From the results of Table 4 and Figure 7, it is proved that the FRP armored non-metallic optical cable is practically no problem in the flexibility.

Table 4. Mechanical Characteristics of FRP Armored Non-Metallic Optical Cable

ITEM	TEST METHOD	RESULTS	
		TYPE A	TYPE B
Tensile strength	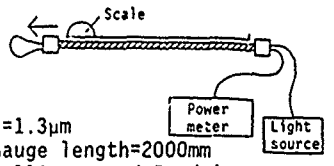 λ=1.3μm Gauge length=2000mm Pulling speed=5mm/min	No loss increase to 6.5 tons. Load at 0.2% elongation: 1.0 ton Tensile breaking load : 16.9 tons	No loss increase to 9.0 tons. Load at 0.2% elongation: 2.4 tons Tensile breaking load : 32.1 tons
Compressive strength	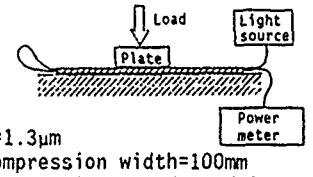 λ=1.3μm Compression width=100mm Compression speed=1mm/min	No loss change to 2.2 tons/100mm. Load at 20% flattening: 1050kg	No loss change to 1.4 tons/100mm. Load at 20% flattening: 900kg
Bend	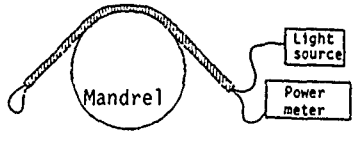	No loss change to 300mm. Min. bend dia.: 300mm	No loss change to 400mm. Min. bend dia.: 400mm
Tortion	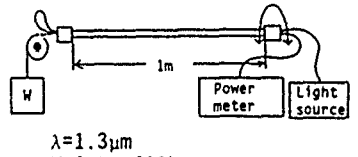 λ=1.3μm Weight=200kg	No loss change to ± 360°	No loss change to ± 360°
Flexibility	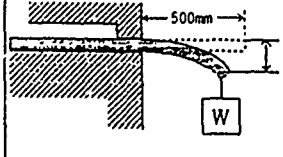	Deflection at load 10kg: 260mm	Deflection at load 10kg: 150mm
Thermal resistive bend	 [condition] 80°C X 48 hour	No breaking of FRP to 500mmφ.	No breaking of FRP to 700mmφ.

5. Conclusion

We designed a non-metallic optical cable with FRP armor possible for a direct burial installation even to a very severe environment such as thunder frequent occurrences, cold regions and frequent upheavals of lands, furthermore improved the reliability and handling properties as an optical cable and developed an economical manufacturing method. The recent developed optical cable is expected to show the excellent performance of the transmission and mechanical characteristics and to expand much more the application range of optical cable.

ACKNOWLEDGMENTS

We would like to thank all these in and outside the company who participated in this development for their guidance and cooperation.

REFERENCE

① M.R.Reynold and C.J.Arroyo, "Primacy Rodent and Lighting Protective Sheath for Lightguide Cable, International Wire & Cable Symposium Proceedings 1986, pp455-pp463.

② S. Matsuno et al, "DEVELOPMENT OF THE STRANDED FRP AND ITS APPLICATION TO OPTICAL CABLE" International Wire & Cable Symposium Proceedings 1989, pp331-pp337.

Yuji Kuwata
Sumitomo Electric
Industries, Ltd.
1, Taya-cho,
Sakae-ku,
Yokohama 244, Japan

Yuji Kuwata received the B.E. degree in engineering from Waseda University in 1984 and joined Sumitomo Electric Industries, Ltd. He has been engaged in design and development of optical fiber cables. He is now an engineer of Fiber Optics Division.

Koji Niikura
Sumitomo Electric
Industries, Ltd.
1, Taya-cho,
Sakae-ku,
Yokohama 244, Japan

Koji Niikura received the B.E. degree in engineering from Waseda University in 1984 and joined Sumitomo Electric Industries, Ltd. He has been engaged in the development and design of optical fiber cables in the Fiber Optics Division.

Hiroaki Horima
Sumitomo Electric
Industries, Ltd.
1, Taya-cho,
Sakae-ku,
Yokohama 244, Japan

Hiroaki Horima received the M.S. degree in engineering from Osaka University in 1972. He then joined Sumitomo Electric Industries, Ltd. and worked on the development of CATV coaxial cable, multipair PEF-insulated junction cables and low loss unbalanced type cables. Thereafter, he concentrated on the development of optical fiber cables. He is now Section Manager of the Fiber Optics Division at Sumitomo Electric Industries, Ltd. He is a member of the Institute of Electronics and Communication Engineers of Japan.

Kenji Kozuka
UBE-NITTO KASEI Co.,Ltd.
579-1, Yabuta
Gifu 500, Japan

Kenji Kozuka received the B.E. degree in engineering from Nagoya Institute of Technology in 1979 and joined UBE-NITTO KASEI Co.,Ltd. He has been engaged in research and development of fiber reinforced plastics in the optical fiber cables, and so on. He is now a group leader of Gifu Research Laboratory.

Shigehiro Matsuno
UBE-NITTO KASEI Co.,Ltd.
579-1, Yabuta
Gifu 500, Japan

Shigehiro Matsuno received the B.E. degree in engineering from Kyoto University in 1974 and joined UBE-NITTO KASEI Co.,Ltd. He has been engaged in research and development of fiber reinforced plastics in the optical fiber cables, and so on. He is now a chief engineer of Gifu Research Laboratory.

Masao Okada
UBE-NITTO KASEI Co.,Ltd.
579-1, Yabuta
Gifu 500, Japan

Masao Okada received the B.E. degree in engineering from Kyoto University in 1963 and then joined Nitto Boseki Co.,Ltd. Since 1966 he joined UBE-NITTO KASEI Co.,Ltd. and has worked on the development of fiber reinforced plastics of pultrusion, advanced composite materials and glasses by Sol-gel method and so on. He is now the head of Gifu Factory. He is a member of the Society of Polymer Science of Japan.

DEVELOPMENT OF COMMUNICATIONS CABLES IN THE USSR

I. B. Peshkov

All-Union Scientific Research Institute of the Cable Industry
111112 Shosse Entusiastov 5, Moscow USSR

Abstract.

Communications in the USSR are based on the Central Automatic Communications Network of the USSR, which unites all electrical means of communications into a common state system. Taking into account the enormous dimensions of our country, long-distance cable lines are a necessary means for providing reliable and high-quality electrical communications, as well as radio and TV broadcasting. Therefore, the broadening of the network of cable lines continues to be a primary object on today's agenda and it is closely tied into a corresponding increase in the production of long-distance cables. The development of these transmission cables is associated with the broadening of the frequency range and an increase in the number of communication channels as well as an increase of communication distance and maximum automation of cable channels. Optical cables find their most effective application in long-distance cable connections. Nevertheless, coaxial lines still make up the majority of long-distance cable lines in the USSR.

Communication Cable Types.

Conventional Transmission Cables.

Trunk cables with four standard type 2.6/9.5 mm coaxial units and five star quads are produced in quantity in the USSR. Cables are multiplexed with K-1920, K-3600 and, in the future, with K-5400 systems in the frequency range up to 60 MHz. Transition to digital transmission with systems numbering 1,920 channels is in preparation.

Cables with metal sheaths of different types (lead and aluminum) are produced. Copper wires and polyethylene spacers are used, respectively, as inner conductors and as insulation in coaxial cables.

Production methods for coaxial cables, in wide use in the USSR, consist of separate fabrication of the polyethylene spacers, combined calibration and cleaning of the inner conductor in single-die drawing units. The spacers are then placed around the inner conductor, followed by the application of the outer conductor copper tape and a screen made from two steel tapes and a protective jacket.

The cable core consists of four stranded coaxial units and five star quads of polyethylene-insulated conductors. The core is covered with paper tapes or other insulating material. It has a metal sheath with a protective polyethylene jacket.

In areas subject to electro-magnetic radiation or where difficult laying conditions may be encountered, armored cables with different types of protective coverings are used.

The electrical properties of the 2.6/9.5 mm coaxial units are in accordance with CCITT recommendations, that is:

Characteristic impedance
(@ 2.5 MHz): 75 ohms±0.4 ohms

Reflection coefficient at any point of the factory length of the coax unit: 3% max.

Nominal attenuation (@ 1.0 MHz): 2.4 dB/km

In addition to this type coaxial cable, miniature cables with 1.2/4.6 mm units and five symmetrical pairs are produced in the USSR.

The cable cores are enclosed by metal sheaths (lead or aluminum) and they are multiplexed with K-1020 in a frequency range up to 10 MHz for analog systems and PCM-480 up to 40 MHz for digital systems. The inner conductors of coaxial units consist of copper wires with solid polyethylene insulation.

The manufacturing process of coaxial units includes the following stages: extrusion of the polyethylene insulation on the inner conductor of the coaxial unit, placing the outer conductor in the form of a tube made from copper strip, applying the screen which consists of two helically-laid steel tapes and a layer of plastic tapes.

The conductors in the symmetrical pair are polyethylene-insulated. The cable consists of four stranded coaxial units, five symmetrical pairs and a control single. The core is protected with a layer of belted paper tape, a metal sheath and a protective polyethylene jacket.

Fiber optic transmission cables.

No increase is planned in the production of traditional transmission cables in the USSR over the next five years. Further development in this field calls for the use of fiber optic cables in long-distance communication lines. For example, the 1,100 km Leningrad - Minsk line is presently under construction. Some design variations are being considered, such as various types of single-mode optical fiber cables with from 4 to 16 fibers for manual and mechanized laying in soil and in water for river crossings, and single-fiber cables for unattended repeater stations.

Cables may or may not contain metallic components. However, cables intended for laying in rivers and marshes more than 2 m deep must contain metallic protective layers.

First-generation cables have the following optical characteristics:

Attenuation (@ 1.3 μm):	0.5 to 0.7 dB/km
Max. dispersion	
1.285 to 1.330 μm:	3.5 ps/nm km
1.270 to 1.340 μm:	6 ps/nm km
Cutoff wavelength:	1.00 to 1.280 μm

The cable has a solid hydrophobic filler and is protected against rodents. It is resistant to the following environmental conditions:

-40°C to +50°C (steady-state and cyclical)

Relative humidity: up to 100% (@35° C)

Second-generation long-distance single-mode cables are designed for use at the 1.55 μm wavelength. They are characterized by attenuation up to 0.3 dB/km, dispersion value of 2.7 ps/nm km for cables with 560 Mbit/s capacity and 3.5 ps/nm km for cables with 144 Mbit/s capacity. The first cables of this type are being manufactured this year.

Figs. 1 and 2 show the designs of a 4-fiber optical cable with glass-reinforced plastic members and steel wire reinforcement and that of an 8- fiber optical cable with glass-reinforced plastic and glass-plastic reinforcements, respectively.

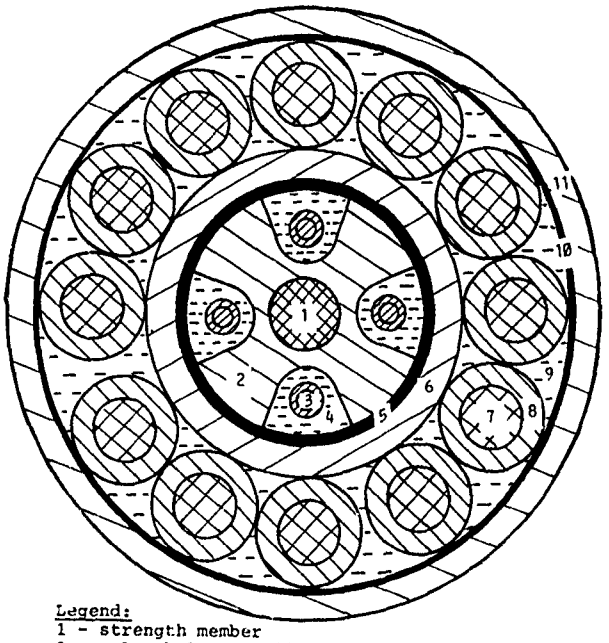

Legend:
1 - strength member
2 - polyethylene profile
3 - fiber with cladding
4 - petrojelly
5 - polyester tape
6 - polyethylene covering
7 - steel
8 - polymer
9 - filler
10- polymer tape
11- polyethylene jacket

Fig. 1 Design of a fiber optic cable with glass-reinforced plastic strength member and steel wire reinforcement.

The change-over to optical cables for inter-city communication lines is planned but at the present time these lines are still, for the most part, equipped with traditional cables.

A few high-frequency cable types are produced for regional communication lines not exceeding 200 km. These cables traditionally consist of quads with polystyrene helixes. Cables of this type are intended for use in analog transmission systems in the frequency range up to 552 kHz. Transmission of 1,380 telephone channels is ensured by multiplexing of one of the quads of the four-quad cable with the K-1020 system and the other quads with K-60. The use of ternary PCM-480 digital transmission systems allows for the use of 3,840 telephone channels.

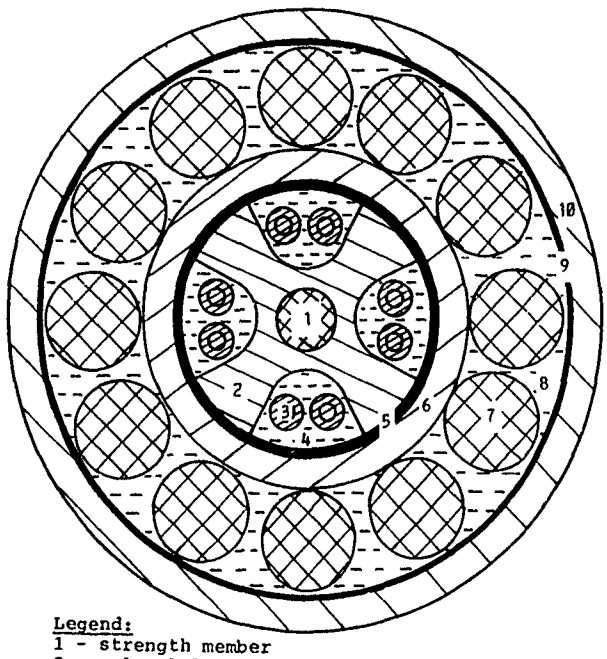

Legend:
1 - strength member
2 - polyethylene profile
3 - fiber with cladding
4 - petrojelly
5 - polyester tape
6 - polyethylene covering
7 - glass-reinforced, plastic strength member
8 - filler
9 - polymer tape
10- polyethylene jacket

Fig. 2 Design of an 8-fiber optical cable with glass-reinforced plastic strength member and glass-plastic reinforcement.

The number of quads in the cables is 4 or 7. The core is of traditional design: 1.2 mm dia. (No.17 AWG) copper conductors and helical polystyrene spacers. The insulated conductors are stranded in quads, four or seven quads stranded into a core and covered with paper tape.

Depending on the application, the cables are provided with protective lead, or corrugated aluminum or steel sheaths. The sheaths are covered by polyethylene jackets.

The use of a special laminated polyester-polyethylene insulating tape enabled us to double the electrical breakdown strength without changing the frequency-dependence of the attenuation. Furthermore, by substituting the traditional steel strip armor (in protective covers) by corrugated armor, we increased the cable's resistance to lightning, while improving its resistance to external mechanical loads, especially the compression strength.

Finally, the placing of two polyethylene jackets (over the aluminum and over the corrugated, welded sheath, respectively) provides reliable protection of the cable against corrosion and electrical and mechanical stresses.

The use of high-frequency symmetrical cables with foam skin polyethylene insulation is planned during the transition period for increased use of fiber optic cables for regional communications.

Alongside with regional communication cables, plastic-jacketed polyethylene-insulated single-quad cables and four-quad cables with polyethylene insulation in aluminum sheaths are used. The latter are intended for regions with high lightning activity. The cables described above are designed for multiplexing with K-60 analog systems in the 252 kHz frequency range. PCM-480 is used in digital systems.

Regional fiber optic communication cables.

The main properties of multi-mode optical cables for 34 Mbit/s first-generation regional communication lines are:

Number of fibers:	4 and 8
Attenuation (@ 1.3 μm):	0.7, 1.0 and 1.5 db/km
Bandwidth:	not less than 500 and 800 MHz/km
Operating temperature range:	-40 to +50°C
Factory length:	not less than 2,000 m

Exchange cables (e.g.: for communications between central office and distant offices) are used in trunk networks. Traditional copper telephone cables with up to 2,400 pairs wherein a number of pairs is PCM-80 multiplexed to increase the number of channels, are used in subscriber communication lines. Coaxial cables and high-frequency symmetrical cables with multi-channel multiplexing systems are used in exchange links. The use of fiber optic cables in subscriber lines may well be considered in the future.

Taking into consideration that production of telephone cables with copper conductors and polyethylene insulation will be around for a long time to come, efforts to improve existing cable designs and the creation of modern production facilities for telephone cables will continue.

Fiber optic cable designs for links between central offices and communication centers are designed for distances between 5 and 10 km and they are, naturally, run without repeaters.

Fiber optic cable designs developed for urban communication systems use loose-tube (polymer) construction modules of 4 or 8 fibers. The 4- or 8- module members, along with strength members, are stranded into a core over which a polyethylene jacket is applied. The core has a hydrophobic filler to protect the cable from water penetration. These cables are designed for laying in ducts.

In accordance with the requirements of our specifications, first-generation fiber optic cables for urban communication lines have the following characteristics:

Attenuation (@ 0.85 μm): 3 to 5 dB/km

Minimum bandwidth: 500 or 250 to 500 MHz/km

Operating temperature: -40 to +50°C

Factory length: not less than 2 km

Second-generation multi-mode cables for the 1.3 μm wavelength have a maximum attenuation of 0.7 dB/km for 1 GHz bandwidth. Single-mode cables which we developed exhibit maximum attenuation of 0.7 dB/km.

Fiber optic cables in subscriber loops.

The application of fiber optic cables in subscriber communication loops deserves special attention. Subscriber lines with conventional electrical cables, in general, cannot be used with multiplexing, i.e.: a wire pair is needed for one conversation. The transmission of different media (data, television, radio) on subscriber lines needs also to be considered. Also, subscriber lines are very short (from 30 - 50 m to 3 - 5 km). These features point out the difficulties which arise when using optical fiber cables in subscriber networks. It is evident that transition to fiber optic systems in the described networks will become economically expedient only when it is possible to transmit all types of data over a single circuit to a single receiving apparatus.

In the development of optical fiber subscriber lines in the USSR the main attention was paid to the creation of inexpensive multiplexing equipment and other optoelectronic devices. The high cost of optoelectronic equipment is the main obstacle on the way to implementation of fiber optic systems in subscriber loops.

Calculations show that previously developed single-mode cables for the 1.3 μm wavelength and optimized for operation at 1.55 μm can already now be used in subscriber loops. This trend finds support in the USSR but it still remains at the stage of development and technical-economical evaluation. Practical application of fiber optic systems in subscriber lines is expected to become a reality in about five years.

CATV Cables.

Large-scale development of cable TV systems in the USSR began in the early 1980s. Production of a series of cables for cable TV systems, including transmission, distribution and subscriber cables with solid and foam polyethylene insulation and corrugated copper tape outer conductors began in the same years. Table 1 presents the construction and characteristics of cables produced at the present time.

The main difference among the referenced series of cables lies in the construction of their outer conductors and in the production process which combines the application of the outer conductor with the protective jacket. The copper tape is first corrugated (longitudinally and transversely), wrapped around the cable core, whereupon the protective jacket is applied. The shape of the corrugation and the forming method of the outer conductor provide the cable with high immunity to noise, negligible reflection and excellent flexibility, while making possible, at the same time, a highly efficient production process. The only disadvantage of this type of cable is the lack of imperviousness to water in the longitudinal direction. Mechanical damage to the protective jacket and flooding of the cables with water can lead to cable damage over the whole length between repeaters. However, this applies only to transmission cables laid in ducts.

Operational experience with CATV systems has shown that damages of this kind are infrequent and that replacement expenses are compensated by lower cable costs.

Average cable requirements per TV subscriber are: 3 to 4 m of transmission, distribution and in-house cable and 20 m of lead-in cable. While the overall need for cables in the USSR is about 250,000 km (annually 20,000 to 30,000 km), the need for lead-in cables has already reached 150,000 to 200,000 km per year.

Cable type:	Inner conductor dia.. (mm)	Insulation material:	Insulation dia.: (mm)	Outer dia. of jacket: (mm)	Attenuation (@ 200 MHz): (dB/100 m, nominal/max.)	SWR: (aver./max.)
Transmission						
RK 75-17-13S	2.73	PE	16.3±0.2	22.3±1.0	3.4/4.6	1.15/1.35
RK 75-17-33S	4.15	FPE	17.3±0.3	22.3±0.5	2.2/3.2	1.15/1.35
RK 75-11-11S	1.88	PE	11.5±0.15	15.4±0.6	4.7/6.2	1.15/1.35
RK 75-11-32S	2.57	FPE	11.5±0.25	15.4±0.6	3.1/4.1	1.15/1.35
Distribution						
RK 75-7-110	1.20	PE	7.25±0.2	10.2±0.4	7.3/8.5	1.15/1.35
RK 75-7-313	1.63	FPE	7.25±0.15	10.2±0.4	5.2/6.2	1.15/1.35
Subscriber						
RK 75-4-113	0.80	PE	4.6±0.2	7.0±0.4	10.3/15	--
RK 75-3,7-31	0.90	FPE	3.7±0.15	5.8±0.3	10.3/15	--

Table 1 Principal characteristics of CATV coaxial cables in the USSR

In the near future, coaxial transmission cables will gradually be replaced by fiber optic cables. However, the distribution and subscriber loops will probably continue to use coaxial cables.

Some aspects of fiber optic cable design.

A great deal of theoretical and experimental effort has been devoted in our country to the investigation of the optical and mechanical characteristics of fiber optic cables. A major subject has been the analysis of the effects of microbending. It may be of interest therefore to summarize briefly a theoretical approach developed by our scientists.

The main design principle of a fiber optic cable is to provide stability of its transmission characteristics while the cable is under the influence of environmental factors (tensile stress, pressure, cooling, etc.) and the prevention of corrosive effects caused by mechanical stresses.

In modern fiber optic cable construction these principles are realized by providing excess length of fiber in the cable. A relative excess length (E_ℓ) of fiber in a fiber optic cable can be defined as:

$$E_\ell = \frac{\ell_f - \ell}{\ell} \qquad (1)$$

wherein ℓ_f and ℓ are the corresponding lengths of the fiber and the axis of the loose tube or slot into which the fiber is inserted.

In this case the main problem is the optimization of the design to improve resistance to the adverse effect of external factors.

For example, to improve the fiber resistance to tensile stress, the excess fiber length in a cable must be increased. The effect of lower temperatures or ambient (e.g.: hydrostatic) pressure in the case of non-metallic cable constructions will possibly require a smaller value.

Thus, the initial relationship for an optimum design under specified operating conditions is given by Eq. (2) [1].

$$\varepsilon_s(\alpha_p) < \varepsilon_\ell < \varepsilon_p(\Delta\alpha_p) = \sqrt{\frac{\rho_p}{\rho_p - \frac{w}{2}}} - 1 \qquad (2)$$

wherein:

$\Delta\alpha_p$ = allowed increase in attenuation (or of any other transmission parameter);

$\varepsilon_\ell(\Delta\alpha_p)$ = allowed fiber excess length corresponding to the possible radius of curvature ρ_p at which the increase in attenuation is $\Delta\alpha_p$ or at which the fiber tension values are less than is permitted;

$\varepsilon_s(\Delta\alpha_p)$ = allowed longitudinal displacement of the protective tube axis (shaped core, loose tube or slot) into which the fiber is placed;

W = distance between the fiber and the inner wall of the tube.

In practice we use methods that allow us to calculate the design parameters ε_p and W in such a way that the excess length of the fiber in a cable is optimal.

Relationships for the determination of radial displacements in optimal designs of fiber optic cables, including multilayer and shaped members, tube assembly, etc. under the effect of ambient pressure and tensile stresses have been derived.

Complications resulting from political problems forced the USSR industry to develop its own technological equipment. In particular, this refers to the fiber drawing tower and to the production of fibers with different types of coatings. Special attention was paid to a number of problems. Thus, an arrangement consisting of four mercury vapor lamps of average pressure and 1 kW power, are placed around the central channel containing the fiber, as a UV-radiation source. This source is provided with a UV reflector so as to concentrate the radiation on the fiber. UV-radiation sources using spherical ultra-high pressure mercury vapor lamps are now in use as well.

Epoxy acrylates and similar materials are among the coating materials which are presently being developed in the USSR. Taking into account the relative transparency of acrylates in the UV region of the spectrum, the possibility of GeO_2-P_2O_5, UV-radiation-induced colored centers in the fiber core material was investigated. Spectral attenuation measurements disclosed the absence of the colored centers, starting with a 20 m/min drawing rate. This feature allows us to recommend this kind of UV-radiation source for all fiber types, including low-loss fibers.

Additional studies were undertaken with the aim of determining the optimal relationship between the diameters of the primary and secondary coatings of the fiber from the point of view of microbending, on the one hand, and development of the required low temperature resistance (down to -60°C), on the other hand. Naturally, the sensitivity to microbending decreases as the primary coating diameter D_1 increases and the modulus of elasticity E_1 decreases. In this case it is advisable to increase simultaneously the modulus of elasticity of the secondary coating E_2.

However, with decreasing temperature, polymer coatings give rise to longitudinal compression stress which is due to the difference between the temperature coefficients of linear expansion of silica glass (5×10^{-7}) and polymers (about 2×10^{-4}). It is evident that, as the compression stress increases with E_2, there appears to be instability which leads to bending of the optical fiber and, as a result, to additional optical losses. Loss calculation methods for the specified bending geometry are well-known. Therefore, only conditions of the mentioned bending phenomenon are analyzed below[2].

Let us assign the following parameter designations (Fig. 3):

- R_k, R_1, R_2: radii of silica glass, primary and secondary coatings respectively;
- E_k, E_1, E_2: moduli of elasticity of silica glass, primary and secondary coatings, respectively;
- ΔT: temperature difference with respect to ambient temperature;
- W : strain energy;
- r : radius of silica glass fiber helix;
- φ : angle between the axis and the tangent helix;
- ε : relative elongation of the glass fiber;
- ρ : radius of curvature of the silica glass fiber;
- α_T : temperature coefficient of linear expansion of the secondary coating material.

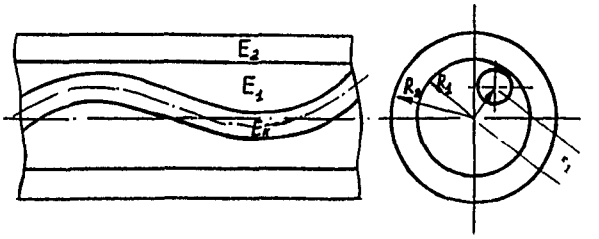

Fig. 3 Low temperature bending characteristics of a dual-coated optical fiber

Heat shrinkage of the primary coating is not taken into account provided that $E_2 >> E_1$. For the same reason it is assumed that the secondary coating retains its cylindrical form and that the silica fiber bending causes radial strain of the primary coating. In accordance with the assumption of small strains ($\varepsilon << 1$, $\varphi << 1$, $\varphi^2 = \varepsilon$) the strain energy of the optical fiber per unit length can be written in the following form:

$$W = \frac{\pi}{8} E_k \frac{R_k^4}{2} \varphi^4 + \frac{Br^2}{2} \frac{R_k^2}{(R_2 - R_1)^2} + \frac{\pi}{2} (R_2^2 - R_1^2) E_2 (\varepsilon - \alpha_T \Delta T)^2 \quad (3)$$

wherein the first term is the strain energy of the helical silica fiber, the second term is the strain energy of the primary coating, the third is the strain energy of the secondary coating undergoing shrinkage and B is a geometrical factor on the order of 1.

$$\gamma = \frac{\pi}{4} E_k R_k^4 , \quad \beta = \frac{BR_k^2}{(R_2 - R_1)^2} ,$$

$$\delta = \pi E_k (R_2^2 - R_1^2) , \quad \varepsilon_T = \alpha_T \Delta T$$

As a result we get:

$$W = \frac{\gamma \varepsilon^2}{2r^2} + \frac{\beta}{2} r^2 + \delta (\varepsilon - \varepsilon_T)^2 \quad (4)$$

The helix parameters are determined by calculating the minimum values:

$$\frac{\partial W}{\partial r} = 0 \quad ; \quad \frac{\partial W}{\partial \varepsilon} = 0 \quad (5), (6)$$

which leads to the following equations:

$$\left(\frac{\gamma}{r^4} + \delta \right) \varepsilon = \delta \varepsilon_T \quad (7)$$

$$\beta_r = \frac{\gamma \varepsilon^2}{r^3} \quad (8)$$

As a result of a number of transformations we get:

$$r^2 = \frac{1}{2} \sqrt{\frac{\pi E_k}{B}} \alpha_2 \Delta T R_k^2 - \frac{E_k}{E_2} \cdot \frac{R_k^2}{4(R_2^2 - R_1^2)} \quad (9)$$

Here the radius (of the helix) becomes a real value, provided that:

$$\Delta T \geq \frac{\sqrt{BE_k E_1}}{2\sqrt{\pi} E_2 \alpha_2} \cdot \frac{R_k^3}{(R_2^2 - R_1^2)(R_2 - R_1)} \quad (10)$$

The derived formula determines the critical temperature T_k below which bending of the optical fiber occurs in a two-layer coating, causing additional optical losses.

The dependency of the fiber curvature on temperature is shown in Fig. 4.

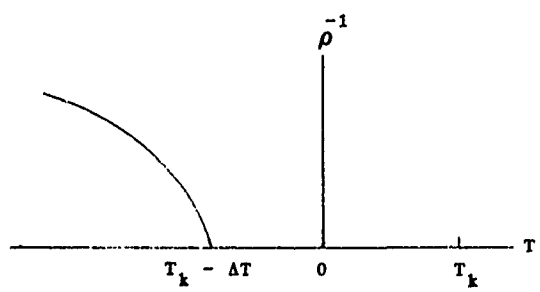

Fig. 4 Relationship between fiber bending and temperature.

The data transmission capacity of optical cables for communications systems is determined by the parameters of the optical fiber used. Therefore, there exists a constant tendency to improve their parameters and to standardize them according to the field of application.

Four classes of optical fibers are produced today in the USSR:

- fibers of the "silica-polymer" type;
- multimode graded index fibers;
- single-mode fibers for the 1.3 μm wavelength;
- single-mode fibers for the 1.55 μm wavelength;

Typical fiber type:	Category, per IEC 793-1:	Compliance of sizes to Standard*:	Operating wavelength: (μm)	Attenuation: (dB/km)	Bandwidth coefficient: MHz/km (Dispersion, ps/nm km)	Operating temp. range: (°C)	Application:
Silica with polymer light-reflecting cladding	A3	200/300	0.83 - 0.85	4.0 - 20.0	10 - 50	-60 to +200	LANs
Multimode, graded-index	A1	50/125	0.85 1.30	2.2 - 5.0 0.6 - 1.5	250 - 2,000 500 - 2,000	-60 to +55	Urban/regional communications
Single-mode	B1.1	(10)/125	1.30	0.35 - 0.7	< 3.5	-60 to +55	Long-distance communications
Single-mode	B1.2	(8.5)/125	1.55	0.20 - 0.30	< 2.0 < 3.5	-40 to +55	Long-distance communications

*Core diameter (mode field)/cladding diameter

Table 2 Optical fibers for communications cables produced in the USSR

The first type listed is used in local and building communication systems. The second type is employed for trunk communications and regional systems. The latter types are used in long-distance systems. The main parameters of the mentioned fiber classes are specified by CCITT Recommendation G653 and IEC 793-1 and 793-2. Table 2 lists data on the produced optical fibers.

A comprehensive development program for optical cables and their applications in different fields of industry has been prepared for 1991 and for the years to follow.

Acknowledgments.

The author wishes to express his appreciation to Mr. Dimitri R. Stein for suggesting and organizing the presentation of this paper. Particular thanks are due to Mr. Henry Hofheimer for his meticulous editing of the manuscript and preparing it for printing. Mr. Stein is President and Mr. Hofheimer is Vice President of Cable Consultants Corp., Larchmont NY 10538.

References.

1. Proceedings of 7th International Conf. ELIZOT-88, Varna, Bulgaria, Ref. 4-16.

2. Proceedings of 7th International Conf. ELIZOT-88, Varna, Bulgaria, Ref. 4-18.

Izyaslav Peshkov
All-Union Scientific Research Institute of the Cable Industry, 111112 Shosse Entusiastov 5, Moscow, USSR

Izyaslav Peshkov graduated in 1960 from the Moscow Power Engineering Institute with a degree in Electrical Engineering. He then joined the All-Union Cable Research Institute (VNIIKP) as a development engineer and, in 1970, became its director. He received a Doctor of Science degree for research in cable engineering and was appointed a Professor at the Moscow Power Engineering Institute. Dr. Peshkov is the author and co-author of numerous books and articles dealing with cable design and technology. He is presently director-general of VNIIKP, chairman of the board of the USSR Cablemakers Association and Member of the Council of the International Cablemakers Federation.

THE EVALUATION OF HIGH SPEED EXTRUSION OF HDPE AND PP INSULATING MATERIALS FOR TELEPHONE CABLE

Zhang Yi Xi

Chengdu Cable Plant, P. R. China

Abstract

It is known that PE and PP are good insulating materials for telephone cable.However, their processibilities are found different in production, even if they have similar basic physical properties, such as melting index and density, some of them are perfect in extrusion but the others are not.Usually people consider that the processibilities of polyloefin depend on molecular weight (MW), especially molecular weight distribution (MWD). But further development shows that MWD is one of effective factor. By measuring the characteristics of GPC (gel permeation chromatography) curve for several polyolefin resin, the results indicate that MWDI is not the only thing involved, symmetry of GPC curve must also be considered.

At the same time, I also determined the non-Newton Index(NNI) -- the ratio of shear rate, γ_2/γ_1 , at two different shear stress and flow ratio.

In general, the value of NNI and flow ratio should be higher. But there are no strict corresponding relation among NNI, flow ratio, MWDI and the symmetry of GPC curve, V_l/V_h.

Introduction

HDPE and PP have been used in producing telephone cable successfully. Today, people in Europe and America use these materials very widely. Japanese people who used to utilize LDPE in manufacturing telephone cable also turned to the developement and application of HDPE and PP for this purpose.

In developing and using HDPE and PP to produce telephone cable,there is an unresolved problem so far. That is, how to evaluate the extrusion of those materials in the Lab.. People have to spend a lot of HDPE or PP to make tests in the production line in order to assess if the processibility of theirs is good or not.

In the past, people used to take MI as the criterion, but today, the line speed is up to 2000^m/min or more, the value of MI can no longer be taken as the criterion for the good or poor processibility of HDPE or PP.

In order to approach the extrudability of polyolefin and evaluation of the methods in the Lab.. The author measured several commercial brands of HDPE and PP for MW, MWDI, V_l/V_h, NNI as well as flow ratio and analyzed the results compared with the practical extrusion tests. Finally, I found out the relationship between the results from Lab. and those from extrusion.

1. Experiment

1.1 Material

The sample materials used in various experiments include 8 commercial of HDPE and 4 grades of PP. HDPE are all ethylene-butene (1) copolymer and PP, propylene-ethylene copolymer produced with Zeiglar catalyst.

1.2 Instruments

1.2.1 MW and MWDI

G.P.C 150C - ALC/GPC
Column: μ-styrogel 10^5,10^4, 10^3 500Å
Solvent: 1,2,4 trichlorobenzene
Temperature: 135°C

1.2.2 NNI Value

Model 3210 Instron Capillary Rheometer
Nozzle L/D = 40
Die: 90°angle inlet
Temp. 230°C

1.2.3 Flow Ratio

Melting Indexer
Temperature 190°C for HDPE
230°C for PP
Load: 2.16kg, 10kg, 21.6kg

1.2.4 Surface Roughness

Microscope X40

1.3 Characteristics of Materials

Table I and Fig. 1 - Fig. 10 show the charactoristics of sample materials. For HDPE, $\bar{M}n$ is from 1.31×10^4 to 2.15×10^4 and $\bar{M}w$ is about 12.60×10^4-15.74×10^4, MWDI is 6.17-9.84. For PP $\bar{M}n$ is 2.01×10^4-2.41×10^4, $\bar{M}w$ is $(12.75\text{-}16.04) \times 10^4$, MWDI is 5.59-7.95. Both HDPE and PP have Median-width molecular weight distribution.

Fig. 1 to Fig. 6 show the GPC curve of HDPE. Sample A.B.C.D.F have different MI, but their GPC distribution is symmetric. Sample E with middle MI value of 0.42 g/10min has slight asymetric MWD. In lower molecular weight side, the curve is to rise. (see the dotted line in Fig. 5)

For PP, there are more differences among the GPC curves of sample L.M.N.O. The distribution of sample N and O is very symmetric. The GPC curve of sample M is nearly symmetric and raised in high molecular weight side (see the arrow in Fig.8). Comparing with sample N, sample L with the wider MWDI of 7.95 has serious asymmetric MWD, seemingly in two peaks - a main peak and a sub-peak. shown by the dotted line in Fig. 7)

1.4 Extrusion Test

Extrusion Tests were conducted on production line. The extrusion line consists of a wire-drawing machine, annealer, preheater, extruder, water trough and auto- matic take up. This line was supplied by Niehoff Co. and Maillefer Co..The extruder can monitor and/or control the extrusion temperature, line speed, extrusion pressure, diameter of insulated conductor, coaxial capacitance and spark failure, furthermore, record extrusion temperature, crosshead pressure and coaxial capacitance.

The extrusion test parameters, such as the fluctuation range of coaxial capacitance, spark failure are shown in Table 2 and Table 3.

The photoes show the surface appearance of insulated conductors.

2. Results and Discussion

2.1 MW, MWDI and the symmetry of MWD

Average molecular weight is a basic structural property. In my experiment, there is favourable $\bar{M}n$ and $\bar{M}w$ for all HDPE and PP.

MWDI is also an important factor that has effect on the properties and processibility of polymer. Usually, people consider that the wider the MWD is, the better the extrusion. But the above thinking is found not correct. For example, sample E with MWD value of 9.86 has wider MWD than other samples, and its extrusion is the worst. The surface of insulated wire is smooth at the rate of 600m/min, but when line speed goes up to 800m/min the surface is very rough like shark skin as shown in photo 3. PP also behaves similarly, the processibility of sample L with MWDI value of 7.95 is bad and the surface is so rough that the fluctuation of coaxial capacitance & spark test can not meet the requirements.

Why do the above phenomena occur? It is known that higher MW fractionation mainly contributes to $\bar{M}w$ and lower MW fractionation contributes to $\bar{M}n$. Obviously, MWD can not clearly describe the situation of higher MW end and lower MW end, especially that of MWDI obtained by GPC method.

Above test results indicate that the extrusion do not only relate to MWDI, but also depends the symmetry of GPC curve basically.

I measured the asymmetry by means of M.R. Amber's method as illustrated in the following scheme:

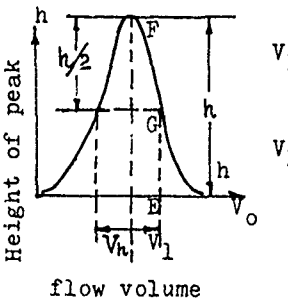

V_l: The flow volume of lower MW fractionation.

V_h: The flow volume of higher MW fractionation.

Fig. 11 symmetry of GPC

When $V_l/V_h = 1$, the distribution of molecular weight is symmetric. So V_l/V_h indicates the symmetry of MWD. V_l/V_h values of all samples are listed in Table 4.

Table 4 V_l/V_h Value of HDPE and PP

Sample HDPE	A	B	C	D	E	F
V_l/V_h	0.937	0.946	0.944	0.942	1.222	0.897
Sample PP	L	M	N	O		
V_l/V_h	0.681	0.791	0.813	1.147		

Thus it is important to research the symmetry of MWD. As MWDI can not present this characteristics of polymer entirely. The data in Table 4 show that V_l/V_h value of sample E is far away from 1, so the

symetry is bad and extrusion is poor.

In fact, according to the theory of molecular movement, we can explain that the molecular movement of much higher MW is so difficult that the molecular rearrange ment is not consistent so as to lead to unstable melt flow and rough surface.

For sample E, the wider MWD isdistributed to by lower MW, low MW molecules are broken easily at high speed to cause the melt fracture and poor surface appearance.

As a result, we should evaluate the extrusion and extablish the optimum design of HDPE and PP by measuring MW, MWDI and V_l/V_h.

2.2 NNI Value

Some people described MWD using non-Newton Index which is the ratio of shear rate at different shear slress as follows

$$NNI = \dot{\gamma}_2/\dot{\gamma}_1$$

Where $\dot{\gamma}_1$ and $\dot{\gamma}_2$ are shear rate (S^{-1}) at shear stress $\tau_1 = 4\times10^{5}dyn/cm^2$ and $\tau_2 = 2.4\times10^{6}dyn/cm^2$ separately. All HDPE sample except sample B and E have higher NNI value. Sample E has lower NNI value of 28 and higher MWDI value of 9.84. For sample B, though its NNI value of 43 is lower than that of sample A, its extrusion is the same as latter.

The above results show a fact that there is no strict corresponding relation among the NNI value, MWDI, V_l/V_h and the processibility. Nevertheless there is a trend to show that NNI value should be higher.

2.3 Flow Ratio

In a common Lab., there is no GPC apparatus, some people measure the flow ratio in order to assess the extrusion of the polymer. Flow ratio can be calculated with MI at the same temperature but at different load as follows:

$$\text{Flow Ratio} = \frac{MI_{21.6}}{MI_{2.16}} \text{ or } \frac{MI_{10}}{MI_{2.16}}$$

$MI_{21.6}$, MI_{10}, $MI_{2.16}$ are melting index at the load value of 21.6kg, 10kg and 2.16 kg separately. Usually, people consider that the higher the flow ratio is, the better the processibility. But neither the data in Table I nor the extrusion tests proved this idea. Such as sample A and B with flow ratio $MI_{21.6}/MI_{2.16}$ values of 167 and 99 are similar extrusion at high speed. For sample C and D. $MI_{21.6}/MI_{2.16}$ are 73 and 127 separately, according to above idea, the extrusion of sample C should be worse than that of sample D. On the contrary, sample C has lower crosshead pressure of 700 Bar at 2305m/min and sample D has higher crosshead pressure value of 750 Bar at the speed of 1600m/min.

For sample E, it has too low flow ratio and it can not be extruded at above speed of 800m/min.

Similar to NNI, there is a trend to show that Flow Ratio can not be so low either. And there is no strict corresponding relationship among the Flow Ratio, MWDI and V_l/V_h.

3. Conclusion

3.1 MWDI is an important parameter of MWD and processibility. But it can not describe the distribution characteristics comprehensively.

3.2 Middle MW and median width MWD is necessary for extrusion of HDPE and PP at high speed.

3.3 The symmetric distribution of GPC curve is more important for the processibility at high speed. V_l/V_h of GPC can be used to describe the symmetry of MWD. when $V_l/V_h = 1$, GPC curve is symmetrical.

3.4 There is no strict corresponding relation amony NNI, MWDI and V_l/V_h, but NNI value can not be too low.

3.5 Flow Ratio is a parameter similar to NNI.

3.6 Both NNI and Flow Ratio can only be used in assessing the extrusion roughly.

References

1) Y. Morita, T. Takai, S. Yamaguchi, K. Nishida 33th IWCS Proceedings, PP287-289

2) Gudzinowicz, B.J., Alden, K.J. Chromatography Sci., 9,65 (1071)

3) Yin Wi Chong "Polymer Review", PP 17-23 Vol 1 (1978)

Table 1 Characteristics of HDPE and PP

Sample	MI	Density	Flow Ratio		$\bar{M}w$	$\bar{M}n$	MWDI	NNI	V_l/V_h
Unit	9/10min	$9/cm^3$	MI_{10}/MI	$MI_{21.6}/MI$	$X10^4$	$X10^4$	$\bar{M}w/\bar{M}n$		
HDPE A	0.30	0.949	28.4	167	13.28	2.07	6.42	59	0.937
B	0.82	0.945	32.5	99	15.19	1.89	8.04	43	0.946
C	0.80	0.944	14.9	73	12.60	1.80	7.01	59	0.944
D	0.22	0.948		127	12.65	2.05	6.17	60	0.902
E	0.42	0.943	11.2	46	12.91	1.31	9.84	28	1.222
F	0.46	0.945	21.2	124	15.74	2.15	7.32	58	0.897
PP L	1.90	0.913	20.8		16.04	2.01	7.95		0.681
M	3.36	0.910			13.27	2.35	5.65		0.791
N	1.95	0.905	27.7		14.58	2.41	6.05		0.813
O	2.90	0.903			12.75	2.28	5.95		1.147

Table 2 The Extrusion Test Parameters and Results of HDPE

	Unit	A	B	C	D	E	F
Conductor dia.	mm	0.5	0.5	0.4	0.5	0.5	0.5
Extrusion Temp.	°C	225 - 255	220 - 250	220 - 230	200 - 230	240 - 285	230 - 260
Crosshead Pressure	Bar	680	680	700	750	650	
Line speed	m/min	2000	2000	2035	1600	800	1800
Cooling Water	°C	15	15	15	15	15	15
Coaxial Capacitance	PF/m	233 ± 1.8	233 ± 1.8	233 ± 2.3	233 ± 2.4	233 ± 5.0	233 ± 2.4
spark Voltage	V	6000	6000	4500	6000	6000	6000
Spark Failure	No./Drum	0	0	0	0	> 50	3
Surface Appearance		smooth	smooth	smooth	smooth	rough	smooth

Table 3 The Extrusion Test for PP

	Unit	L	M	N	O
Conductor Dia.	mm	0.5	0.5	0.5	0.5
Extrusion Temp.	°C	220 - 270	210 - 260	210 - 260	210 - 255
Crosshead Pressure	Bar	700		600	680
Line Speed	m/min	2000	2000	2000	1510
Cooling Water	°C	15	15	15	15
Coaxial Capacitance	PF/m	233 ± 3.0	233 ± 2.3	233 ± 2.3	233 ± 2.6
Spark Voltage	V	2000	6000	6000	3000
Spark Failure	No./drum	20	0 - 2	0 - 3	50
Surface Appearance		slight rough	smooth	smooth	smooth

GPC Curve of All Samples

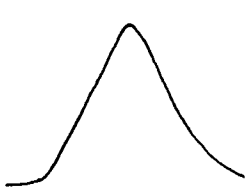

Fig. Sample A

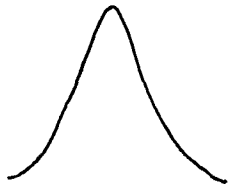

Fig. 2 Sample B

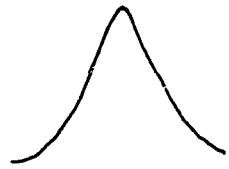

Fig. Sample C

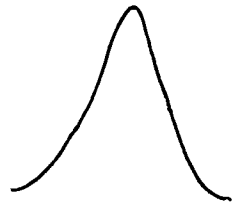

Fig. 4 Sample D

Flow Volume ——→

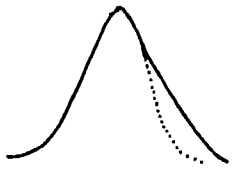

Fig. 5 Sample E

Fig. 6 Sample F

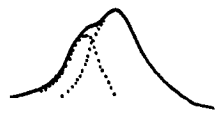

Fig. 7 Sample L

Fig. 8 Sample M

Fig. 9 Sample N

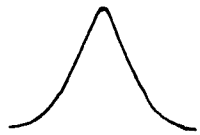

Fig. 10 Sample O

The Surface Appearance of Insulating Conductor
(Photo 1 - Photo 6)

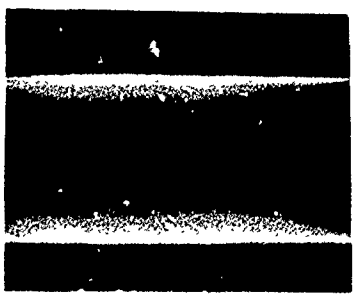

1

2

3

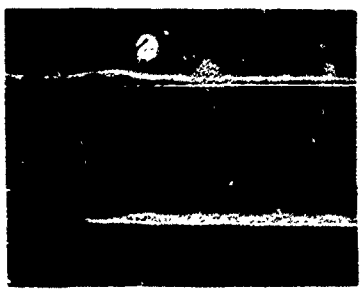

4

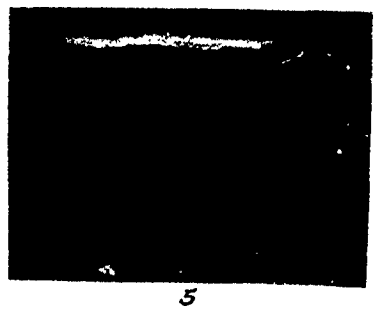

5

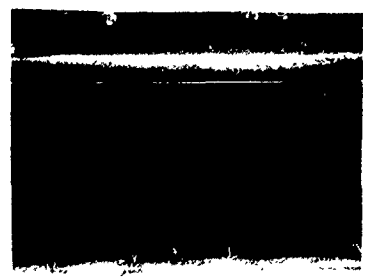

6

Zhang Yi Xi

Research Lab.
Chengdu Cable Plant of PTIC

Madam Zhang Yi Xi graduated Chengdu University of Science and Technology majoring in Polymer Chemical Engineering in 1967.

Then she joined Chengdu Cable Plant and has been engaged in the research and development of raw materials for communication cable. Now Madam Zhang Yi Xi is senior engineer of Research Laboratory at Chengdu Cable Plant.

A FAULT LOCATION EXPERT SYSTEM USING PULSE ECHO TESTS FOR PAIRED SUBSCRIBER CABLES

K. Takeda T. Abe Y. Mitsunaga H. Koga

NTT Transmission Systems Laboratories
Take, Yokosuka-shi, Kanagawa-ken, 238-03, Japan

ABSTRACT

A new effective fault location system is proposed for subscriber paired cables that are composed of different gauge cables and/or branch cables. The system is mainly composed of a new pulse echo test system for approximating fault location, and an expert system. This new pulse echo test system estimates the fault distance by matching the pattern of the measured waveform with the theoretical waveform. The expert system improves the accuracy of the pulse test in location the fault. Its knowledge is based on the investigation of fault records at cable maintenance offices. A field test was carried out, using a prototype system with knowledge based on about 1000 fault records. Error distances of less than 100 m were obtained for subscriber cables of about 3000 m with a branch cable and an open fault.

1. Introduction

Nowadays, huge-scale subscriber paired cables are being constructed in Japan. However, maintenance work is difficult because cable faults are rapidly increasing due to cable plant deterioration. Therefore, to support cable maintenance, an efficient fault location system is required.

In developing the fault location system, the main problem was that, at NTT, the subscriber cables are constructed with different gauge cables and/or branch cables, and the current fault location methods are not applicable for these cables.

A new fault location system is proposed for the subscriber cables. The system mainly consists of a new pulse echo test system, which estimates approximate fault distance, using pulse echo waveform pattern matching, and a new expert system, which improves fault location accuracy of the pulse test based on fault records at cable maintenance offices.

This paper presents the configuration of the new fault location system, the main features of the new pulse echo test and expert system, and the results of the field test.

2. Requirements and Outline of New System

2.1 Requirements

Several fault location methods are used in communication cables. Some of these are (a) dc resistance measurement methods (b) capacitance measurement methods (c) pulse echo methods[1][2] and so on. However, (a) requires maintenance people to work in the field; (b) and (c) can not be applied to a subscriber cable with different gauge cables and/or branch cables. Therefore, the following requirements for a new fault location system were developed.

(1) The fault location system can be applied to any configuration of subscriber cables; whether it be different gauge cables and/or branch cables.
(2) The fault location accuracy is less than 100 m for typical subscriber cables.
(3) All types of faults such as, open faults, close faults, and insulation faults can be located.
(4) The fault location system is equipped only at the central office, and does not require any auxiliary equipment in the field.

2.2 New System's Outline

The new fault location system is composed of several subsystems. An outline of the system is shown in Fig. 1.

Locating a fault is carried out in accordance with the following sequence.

(1) The Switch selects and connects the fault pair to the Subscriber Cable Test System and Pulse Echo Test System.
(2) The Subscriber Cable Test System measures loop resistances, capacitances, leakage dc voltages and so on. These numerical values are sent to the Fault Type Analysis System.

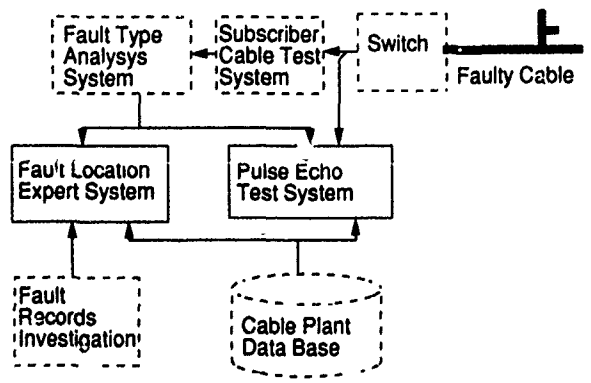

Fig.1 Fault Location Expert System

(3) The Fault Type Analysis System decides the type of fault and transfers the type to the Fault Location Expert System and the Pulse Echo Test System.
(4) The Pulse Echo Test System estimates the approximate fault distance based on the type of fault and the Cable Plant Data Base, and transfers the fault distance to the Fault Location Expert System.
(5) The Fault Location Expert System improves location accuracy of the pulse test using data from the Cable Plant Data Base (Cable Plant DB) and data from the Fault Record Investigation, and displays the results on the CRT. Here, the Cable Plant DB stores subscriber cable structure data. The Fault Records Investigation prepares the knowledge required for the Fault Location Expert System.

The newly developed Pulse Echo Test System and Fault Location Expert System are mainly described in this paper.

3. Pulse Echo Test System

3.1 Principle

A block diagram of the Pulse Echo Test System is shown in Fig. 2. The principle is as follows.
(1) The Pulse generator sends a pulse wave to the faulty cable.
(2) The Echo wave raised at the fault is measured and memorized (called measured waveform).
(3) A waveform is calculated theoretically for the same cable structure as the faulty cable, using the calculation model based on the Cable Plant DB and fault type from the Fault Type Analysis System. This waveform is called the reference waveform. Here, the fault distance is assumed, because the actual fault distance is unknown.
(4) The reference waveform is compared with the measured waveform. When the reference waveform coincides with the measured waveform, the fault distance for the reference waveform is the estimated fault distance.
(5) But if the waveform does not coincide, the reference waveform calculation is carried out again for another fault distance, and waveform comparison of (4) is repeated.

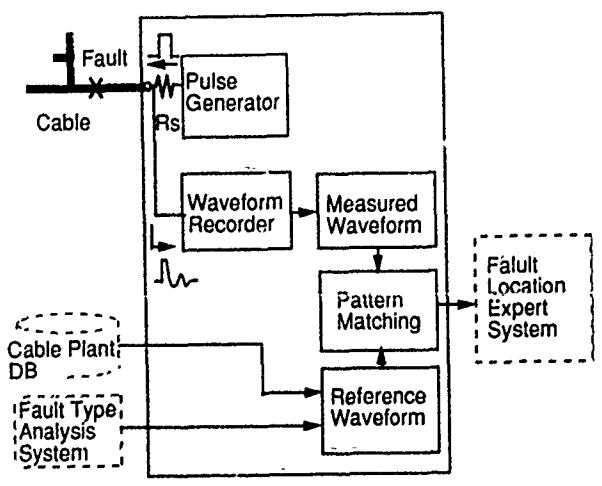

Fig.2 Pulse Echo Test System

3.2 Fault Location Method

Reference waveform vc(t,x) in paragraph 3.1 is calculated using the following equation[3][4].

$$v_c(t,x) = F^{-1}\{ V_s(\omega)\, Z(\omega,x) / (R_s + Z(\omega,x)) \} \quad (1)$$

Where, t, x, $V_s(\omega)$, Rs, and $Z(\omega,x)$ denote time, assumed fault distance, source pulse of the pulse generator, internal resistance, and cable input impedance, respectively. F^{-1} denotes inverse Fourier transform.

The fault distance evaluation function is defined as follows.

$$E(x) = \int_0^T | v_m(t,x_f) - v_c(t,x) |^2 \, dt \quad (2)$$

Where, $v_m(t,x_f)$ is the measured waveform, and x_f is the actual fault distance and T is the source pulse period.

x is varied to minimize E(x) and when this condition is satisfied, x is the estimated fault distance.

3.3 Experiment

The subscriber cable structure for the experiment is shown in Fig. 3 (a). It has one branch cable. The fault is an open fault, and the fault distance is 780 m from the branch point. All cables are plastic insulated cables with a conductor diameter (dn) of 0.5 mm. The cable constants shown in Table 1 are for several cables.

There are 1024 sampling points for the waveform. The source pulse waveform is rectangular with

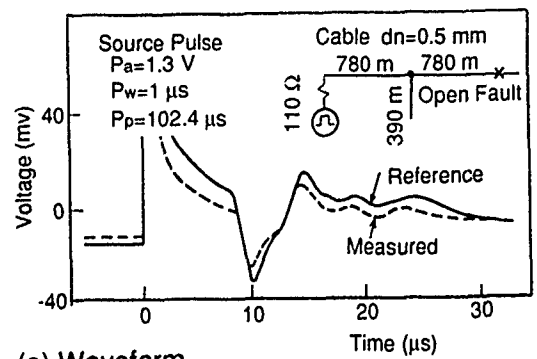

(a) Waveform

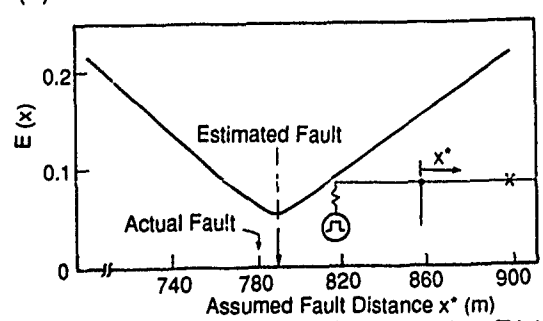

(b) Fault Distance Evaluation Function E(x)

Fig. 3 Fault Location Experiment Result

amplitude Pa=1.3 v, period Pp=102.4 μs, and pulse width Pw=1 μs. Internal resistance Rs is 110 ohms.

The measured waveform and reference waveform are calculated and shown in Fig. 3(a). The reference waveform is obtained from the same model as the experiment. We can see that both waveforms coincide well with each other.

Figure 3(b) shows the fault distance evaluation function E(x). The minimum value of E(x) is at 790 m from the branch point, and the fault location error is about 10 m.

We obtained a good estimation in the above experiment. However, it is expected that the farther the fault distance, the greater the location error. Also, variations of cable constants will cause location error.

3.4 Location Error and Location Limit

In this system, if the calculation model coincides completely with the actual cable; there is no location error. However, in actuality, cables have a considerable variation in their constants (i.e. transmission characteristics).

When a cable constant in the calculation model is represented by p, and the same constant in the actual cable by p+Δp, location error x' is obtained using the below approximation.

$$x' = \{ \int_0^T \frac{\partial v}{\partial p} \frac{\partial v}{\partial x} dt \Big/ \int_0^T \left(\frac{\partial v}{\partial p} \right)^2 dt \} \Delta p \qquad (3)$$

Where, v is the pulse echo waveform.

We assume a no-branched cable with an open fault. Also, we assume that d (conductor diameter), D(distance between conductor centers), εr(relative permittivity) of the actual cable are larger than the calculation model by 1%. These cable constants are shown in Table 1.

Figure 4(a) shows the relationship between fault distance and location error. In Fig.4(a), we notice that there are fault distances where the location error increases rapidly. For example when dn=0.5 mm, this distance is about 5200-5400 m. Therefore, we can assume that these fault distances show the fault location limits of the Pulse Echo Test System.

Figure 4(b) shows the relationship between fault distance and location error due to cable constant difference of εr for several source pulse periods. The longer the source period, the farther the fault location limit.

3.5 Location Error Reduction

The cable constants are different between the actual cable and the calculation model. However, we can

Table 1 Cable Constants

Noninal Conductor diameter dn (mm)	0.4	0.5	0.65
Conductor diameter d (mm)	0.40	0.49	0.64
Distance between Conductors D (mm)	0.96	1.06	1.26
Insulator Thickness th (mm)	0.09	0.15	0.20
Relative Permittivity εr	1.73	1.92	1.76

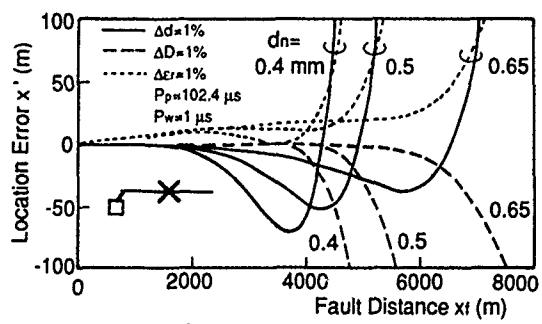

(a) Parameter : Conductor Diameter dn (mm)

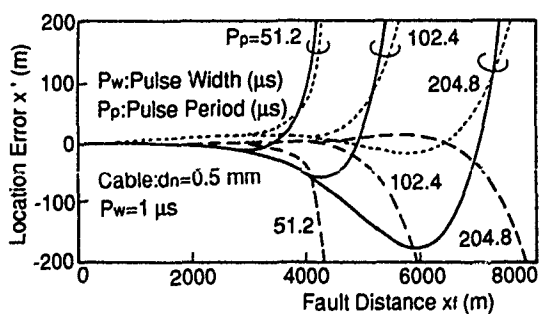

(b) Parameter : Pulse Period T (μs)

Fig.4 Location Errors due to Cable Constant Difference

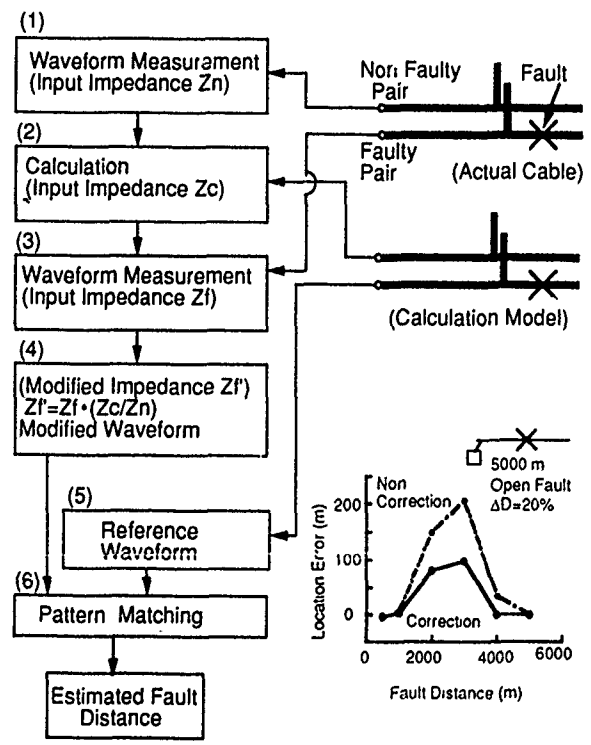

Fig. 5 Location Error Reduction

estimate actual faulty pair characteristics based on its neighboring no faulty pair's waveform.

A location error reduction method is described in Fig. 5.

In Fig. 5, the faulty pair's waveform is modified, then a pattern matching with the calculation waveform is carried out.

The modified waveform is obtained using the modified input impedance Zf', which is represented by the following equation.

$$Z_f' = Z_f \cdot (Z_c / Z_n) \quad (4)$$

Where, Zf is the actual faulty pair's input impedance, Zn is the neighboring pair's impedance, and Zc is the impedance of the calculation model for the neighboring pair.

The effect of this method is shown in Fig. 5, which is calculated, assuming a no-branched cable (dn=0.5mm) with an open fault, and ΔD = 20 %. The location error distance is decreased by 1/2 using this method.

4. Fault Location Expert System

Maintenance offices have numerous data about various past cable faults. The Fault Location Expert System improves location accuracy using those data as knowledge[5].

4.1 Principle

The principle of the Fault Location Expert System is described in Fig. 6. The fault location procedure is as follows.

(1) Maintenance offices' fault records are collected and analyzed. This result is stored in the Fault Knowledge Base (Fault KB) .

(2) The fault cable's structure data are extracted from the Cable Plant DB. This data is stored in the Cable Structure Knowledge Base (Cable Structure KB).

(3) The Reasoning Engine estimates fault distance based on the Cable Structure KB ,Fault KB and pulse echo test.

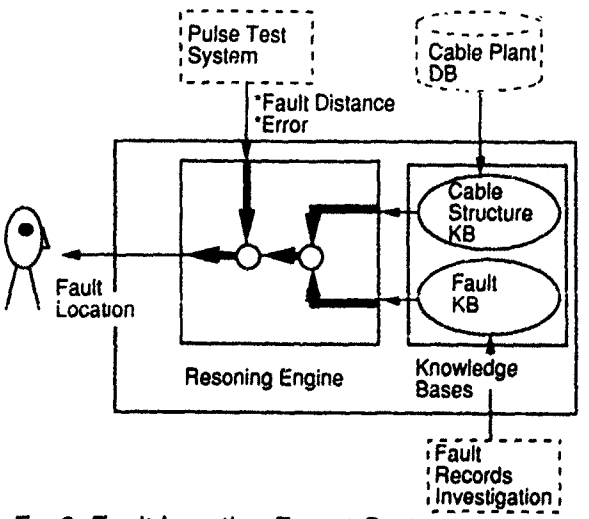

Fig.6 Fault Location Expert System

4.2 Knowledge Representation

We have two sources of knowledge. Two knowledge bases are made using this knowledge.

4.2.1 Cable Structure KB

The Cable Plant DB has data on cable types, joint types, manhole distances, telephone pole distances, joint distances, construction years, etc.. The Cable Structure KB is made by extracting data on the faulty cable from the Cable Plant DB. The Cable Structure KB is made for each cable section of the faulty cable. Here, the cable section is composed of several cable components between two telephone poles, or two manholes or between a manhole and a telephone pole, as is shown in Fig. 7.

The Cable Structure KB is represented by frame[6], and has slots for route name, section's name, fault type, components' name, construction year, environment and fault rate. An example of the Cable Structure KB is shown in Fig. 8.

4.2.2 Fault KB

Cable faults are recorded at maintenance offices. These records contain the type of fault, component name, construction name, environment, fault date. These are shown in Fig. 9(a). The Fault KB is made based on these records.

The Fault KB is represented using the same frame as the Cable Structure KB, as shown in Fig. 9(b). Here, the fault rate λ is defined by the following equation.

$$\lambda(t,t+\Delta t) = n_f(t,t+\Delta t) / n(t)\Delta t \quad (5)$$

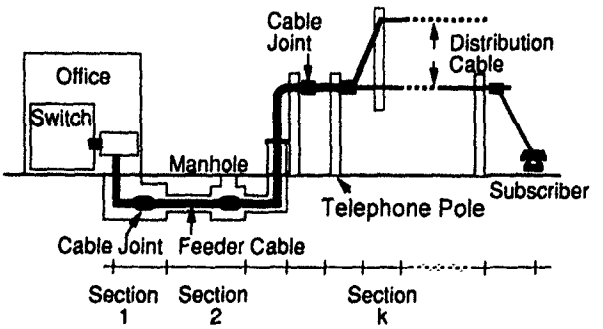

Fig.7 Subscriber Cable Structure

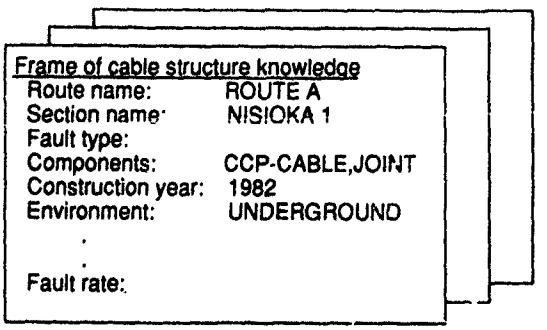

Fig.8 Cable Structure Knowledge Base

Where, n(t) is the number of components which includes no fault at time t, and nr(t,t+Δt) is the component's number that faults occur between time t and t+Δt.

4.3 Reasoning Engine

The Reasoning Engine decides the order of cable sections when we search the fault in the field. The order is based on the fault existing probability for each cable section, which is derived from the result of the pulse test and the fault rates in the Fault KB (Fig. 10).

The approximate fault distance and its error can be determined from the pulse test. Here, we assume that the fault existing probability Pmij for each cable section is represented as the following equation.

$$P_{mij} = c \cdot \exp\{-(x_j - x_i)^2 / 2\sigma^2\} \quad (6)$$

Where, Pmij is the probability that a fault occurs at section i, and the pulse test indicates the fault at section j. xi and xj are the distances of section i and j, respectively, and σ is the standard deviation of the pulse test location error and c is the normalizing constant.

The fault existing probability Pfi for each cable section is also defined by the following equation, based on the Fault KB and Cable Structure KB.

$$P_{fi} = \lambda_i \Big/ \sum_{j=1}^{n_s} \lambda_j \quad (7)$$

Where, λ, i, j and ns are fault rate, section numbers, and the last section number, respectively.

The probability Peij that section i is indicated by the pulse test and the fault exists at section j is written by the following equation, using the above two probabilities.

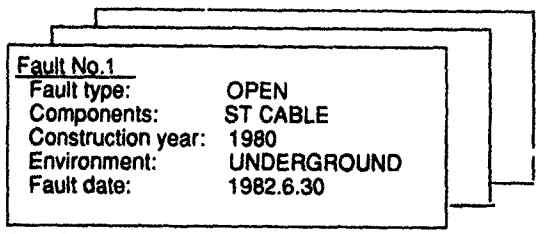

(a) Fault Records

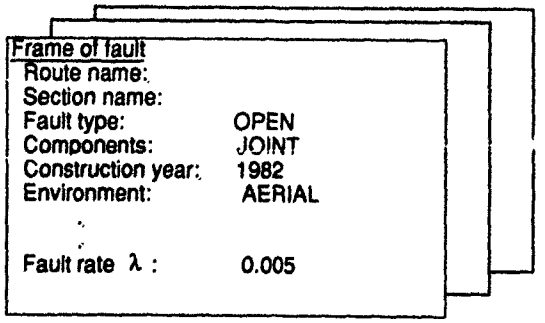

(b) Fault KB

Fig.9 Fault Records and Fault KB

$$P_{eij} = P_{fj} P_{mji} \Big/ \sum_{k=1}^{n_s} P_{fk} P_{mki} \quad (8)$$

The fault section searching order is decided in order from the largest Peij.

The output example of the Reasoning Engine is described in Fig. 10. Where, lines and circles represent cable sections and telephone poles or manholes, respectively. The thickest line shows the largest fault existing probability section. The second thickest line shows the second fault existing section.

5. Field Test

A field test was conducted for 3 faulty cables. Each cable had about 30 sections, about 10 joints, and one branch cable, and the total length of each cable was about 3000 m. We collected about 1000 fault records, and obtained about 50 frames of Fault KB, for this field test.

The results are shown in Table 2. Two types of results are described. One is by the Fault Location Expert System, and the other is by only the pulse test. Two routes by the Expert System coincide with the actual faults. However, only one route with the pulse test coincides.

The results show that the fault section searching order is effectively improved using the Fault Location Expert System.

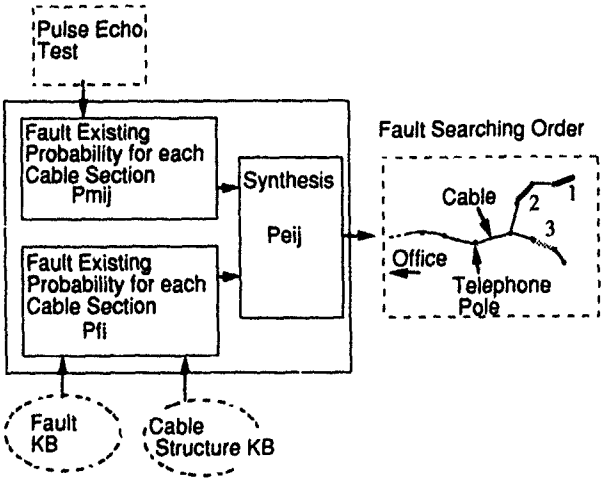

Fig.10 Reasoning Engine

Table 2 Field Test Results

Route No.	Fault Type	Fault Distance (Error) m	Order	Estimated Fault Section: Expert sys.	Estimated Fault Section: Only Pulse Test
M17-8	Open	1662 (42)	1	E-main43(70.2%)*	E-main43 *
			2	E-main45(26.2%)	E-main44
			3	E-main41(19.4%)	E-main42
M17-13	Open	1806 (45)	1	E-main46(30.5%)*	E-main47
			2	E-main45(29.9%)	E-branch1
			3	E-main48(25.3%)	E-main46 *
M17-48	Open	1702 (43)	1	E-main45(49.4%)	E-main44
			2	E-main43(33.1%)*	E-main45
			3	E-main46(14.5%)	E-main43 *

* Actual Fault

6. Conclusion

A new precise fault locating technique was investigated for subscriber paired cables with different gauge cables and/or branch cables. The following techniques were clarified:
(1) Using waveform pattern matching, a new pulse echo test system is applicable for the subscriber cable fault location.
(2) An expert system can improve fault location accuracy of the pulse test, which is composed of two knowledge bases and a reasoning engine.
(3) Field test was carried out, using a prototype system with knowledge based on about 1000 fault records, and error distances of less than 100 m were obtained.

Acknowledgements

The authors would like to thank Toshiyuki Saeki, and Tetsuya Nakagawa for their fruitful discussions and Akira Sakamoto for his encouragement.

References

1. W. Kleinke. 'Impulsechomeβverfahren an Nachrichtenkabeln der DB, Teil 1', Signal+Draht 80 No.7/8 pp.190-194 , 1988
2. L. P. V. Biesen, J. Renneboog and Alain R. F. Barel,'High Accuracy Location of Fault on Electrical Lines Using Digital Processing of Sampled Data Records from a Reflectogram', Comf Proc IEEE Instrum Meas Technol Conf pp.462-466,1989
3. R. Croze, and L. Simon 'Transmission Telephonique', Editions Eyrolles, Paris, 1964
4. N. Kojima, S. Fujita, S. Shimano and K. Osada,'Crosstalk Characteristics and Transmission Properties of Existing Intercity Cables', Review of the ECL, NTT, Jpn., 20, 7, 1971
5. T. Abe, Y. Akiyama, Y. Mitsunaga,'A Fault Location Expert System for Telephone Subscriber Loops',Tenth International Workshop, Expert Systems & their Applications, 1990,pp.13-22
6 S. Ishigaki, I. Morihara and K. Kushima, 'KBMS - An Expert System Building Tool', Review of the ECL, NTT, Jpn.,37,1,1989

KAZUTOKI TAKEDA
NTT Transmission System Laboratories
Kanagawa-ken, Japan

Kazutoki Takeda is a Senior Research Engineer in the Transmission Line System Laboratory of NTT Transmission System Laboratories, located in Kanagawa-ken, Japan. He received his B.E. degree in Electronics engineering from Osaka Electro-Communication University in 1971. He joined NTT in 1971, was engaged in research work for cable pressurization and splice closures. Since 1988, he has been engaged in research on subscriber cable fault location systems.

TETSUJI ABE
NTT Transmission System Laboratories
Kanagawa-ken, Japan

Tetsuji Abe is a Senior Research Engineer in the Transmission Line System Laboratory of NTT Transmission System Laboratories, located in Kanagawa-ken, Japan. He received a B.S. degree in physics and an M.S. degree in electrical engineering from Kyoto University, Kyoto, Japan, in 1980 and 1982, respectively. He joined NTT in 1982, and has been engaged in research work on reliability of optical fiber cables and subscriber loops maintenance systems.

YUTAKA MITSUNAGA
NTT Transmission System Laboratories
Kanagawa-ken, Japan

Yutaka Mitsunaga is a Senior Research Engineer, Supervisor in the Transmission Line Systems Laboratory of NTT Transmission Systems Laboratories. He received his B.S., M.S. and ph.D. degrees from Tokyo Institute of Technology in 1975, 1977 and 1985, respectively. Since he joined NTT in 1977, he has been engaged in research works on design and reliability of optical fiber cables and maintenance expert systems for subscriber cable networks.

HIROAKI KOGA
NTT Transmission System Laboratories
Kanagawa-ken, Japan

Hiroaki Koga is a Senior Research Engineer, Supervisor in the Transmission Line Systems Laboratory of NTT Transmission Systems Laboratories. He received his B.S. and M.S. degrees in electrical engineering from Kagoshima University, Japan, in 1968 and 1970, respectively. He received his ph.D. from Tohoku University, Japan, in 1988. He joined the NTT Transmission System Laboratories in 1970. He has been engaged in research work for subscriber cables maintenance systems. His early work dealt with the design of water-blocking optical fiber cables and the overvoltage protection in paired cables against lightning surges.

Leaky Coaxial Cable Systems for High Speed Trains in Tunnels and other Enviromental Conditions - Theory and Experience

Helmut G. Haag, Klaus Lehan, Karl Schulze-Buxloh and Wolfgang Stremme

AEG KABEL Aktiengesellschaft

Mönchengladbach, Federal Republic of Germany

Abstract

Extended requirements for modern telecommunications systems need new transmission techniques. In the field of mobile communication even in those areas where radio links can hardly be provided caused by environmental conditions communication systems are being installed. The use of leaky coaxial cables seems to be an efficient solution to achieve this purpose. This contribution describes a tunnel radio system and the development, the construction and the installation of radiating coaxial cables.

1. Introduction

Today the demand for mobile communication increases all over the world. The final aim is a world-wide mobile communication system which is able to maintain the connection to mobile subscribers at any point, even in road - or railway tunnels. One possibility supplying radio waves inside tunnels is the installation of leaky coaxial cables. These cables are connected to fixed transmitter/receiver stations and form the antenna feeder cable and the antenna itself. The difference between a conventional antenna and the leaky coaxial cable is the mechanism of radiation.

For the increase of the attractivity of railway travelling the German Railways want to offer new services to the passengers of the new high speed trains ICE.

Therefore on the newly built high speed routes Hannover-Würzburg and Mannheim-Stuttgart with large sections in tunnels or valleys a tunnel radio system is being installed in these days. The following interactive and distributive public services shall be supplied:

- mobile telephone (C-net)
- FM broadcasting
- european radio locator service (Eurosignal)

These services shall be transmitted inside tunnels and other areas with poor propagation properties using their original frequency positions /1/. Tunnels usually are not supplied by public installations.

2. Project Description

For the communication between fixed and mobile subscribers usually radio links are used. The increasing demand for communication requires the availability of mobile subscribers at any place - even inside trains passing tunnels. At this stage the public services which are to be offered are only supplied on the new high speed routes Hannover-Würzburg and Mannheim-Stuttgart. The layout of these lines avoids ascending gradients. Therefore the location of the lines is partly in areas which inhibit the propagation of radio waves. For example 160 km of the new lines are running in up to 11 km long tunnels. In order to guarantee a continuous radio supply the tunnel radio system TFS91 was necessary /2/. In the free space supplementary antennas are installed which are able to supply even those sections running in cuttings. Caused by the great length of the tunnels and by the different frequency ranges to be transmitted a solution with additional antennas inside the tunnels seemed to be impossible to realize. In those sections where the lines are shadowed by big overhead crossings or tunnels radiating broad-band cables are used.

Fig. 2.1 High Speed Express Train ICE

Experiences from other fields, - e.g. road tunnels - have shown that radiating cables because of their broad-band capacities and their little need of space keep big advantages compared with directional antennas.

The leaky coaxial cables used for TFS 91 are also designed for the future european mobile telephone net (D-net) which will operate in the frequency range between 890 MHz and 960 MHz.

The German Railways intend in the long run to provide all main-lines with such a radio system.

3. System Configuration

3.1 Frequency Ranges and Radio Supply

As already mentioned the three public services mobile telephone, FM broadcasting and Eurosignal shall be offered to the railway passengers. These services are using different frequency ranges.

The radio locator service - the so-called Eurosignal - needs two channels. Its frequencies are 87,365 MHz and 87,460 MHz. The frequency range of the FM broadcast service expands from 87,5 MHz to 108 MHz.

The mobile telephone uses two ranges inside the UHF-band. The fixed stations transmit between 461 MHz and 465,74 MHz and the mobile subscribers answer between 451 MHz and 455,74 MHz. The required minimum field intensity is 30 dBµV/m for the mobile telephone, 40 dBµV/m for FM broadcasting and 26 dBµV/m for the Eurosignal.

The tunnel radio system is designed for a speed of up to 250 km/h.

The supply of mobile telephone in the areas of the greater towns and inside two tunnels of the line Mannheim-Stuttgart is done by German PTT itself. The sections between tunnels are supplied by free-radiating antennas.

If these sections are not supplied sufficiently by FM broadcasting and Eurosignal also free-radiating antennas will be installed. But for these applications gaps up to 100 m are tolerated.

The tunnel sections after all are equipped with a radiating cable which meets the requirements mentioned above.

Inside the tunnels the leaky coaxial cables are fed by the so-called tunnel radio stations. These stations are spaced at a maximum distance of 1500 m. The stations itself are fed by an optical fiber cable which runs along the railway line and leads to the so-called tunnel radio head station.

3.2 Tunnel Radio Head Station

The tunnel radio head station forms the interface between the services transmitted in the free space and the tunnel radio system.

Three radio programs and the Eurosignal are picked up. The frequencies are transformed and transmitted via an analogue broadband optical transmission system to the tunnel radio stations, where the signals are retransformed into their original frequency positions and fed to the leaky coaxial cables (System Bosch Telecom /1/, Fig. 3.1).

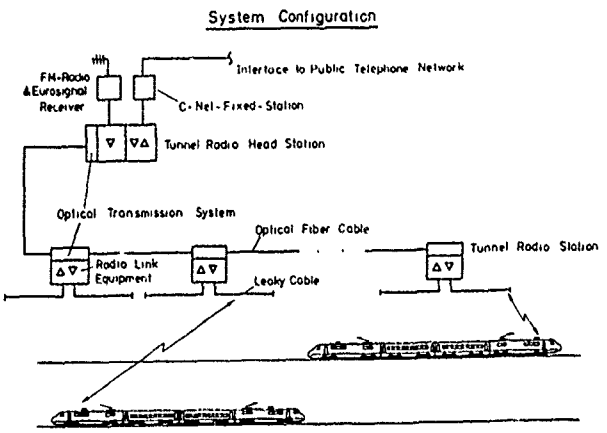

Fig. 3.1 System configuration

The signals of the mobile telephone are picked up at the radio frequency interface of the C-net fixed station of the PTT which is situated near by the tunnel radio head station. The signals are transformed in a similar way as the other ones, transmitted optically to the tunnel radio stations and retransformed and fed to the cables. Seven voice channels and one organisation channel are transmitted, so that in the area of one tunnel radio head station seven telephone calls can be done at the same time.
In the tunnel radio station the returning telephone channels received by the leaky coaxial cable are filtered by an frequency diplexer, transformed to another frequency range and fed back to the tunnel radio head station by the optical transmission system.

The location of the head stations is chosen in such a way, that on one hand a faultless reception of the distributive services and a trouble free radio link to the nearest public C-net fixed station are possible.

Another criterion for the choice of location of the head stations is the so-called overlap-area. In this area telephone calls are handled over from one C-net radio cell to another. For this purpose an overlap-zone of about 5 km is provided. Usually these overlap-zones are located in the free space between two tunnel sections. They are supplied from both sides by free-radiating antennas.

From topographic reasons overlap-zones can be located inside tunnels or even mixed configurations are possible. In this cases the zones can be shorter than 5 km.

3.3 Tunnel Radio Stations

Inside the tunnel radio stations the signals transmitted from the head stations via the optical transmission system are reconverted to electrical signals and retransformed into their original frequency position. They are fed to the leaky coaxial cables and emitted according to the requirements concerning the minimum field intensity described in chapter 3.1.

A broad-band receiver picks up the whole lower C-net band, which is transmitted to the head station after frequency transformation and electro-optical conversion.

Inside the overlap-zones the broad-band receiver feeds an radiolocation receiver. Its task is the early identification of trains coming from adjoining radio cells, so that the telephone calls can be handled over in time.

Besides this each tunnel radio station is equipped with an error detection system. Detected errors are transmitted to the head stations. After being brushed up they are transmitted to a central fault detection processor of the German Railways. For each tunnel radio station two error messages are provided - one for the distributive services and one for the mobile telephone.

3.4 Optical Transmission System

The optical transmission equipment consists of a linear analogue broad-band transmission system - as it is used e.g. for the wide-area distribution of broadcast and TV channels /1/,/3/ - and an optical fiber cable plant with single mode fibers. Depending on the direction of transmission the tunnel radio stations are connected radially or linearly to the tunnel radio head station. Usually one head station supplies a route of 15 km at each side and additionally 5 km overlap zone - if necessary.

The connection from the head station to the tunnel stations is performed radially. Three optical fibers are used for this direction. The first fiber supplies an area up to 7 km from the head station by coupling optical energy to the tunnel stations with passive means. The second one supplies the following area up to 12 km, and the third one supplies the remaining 3 km up to 15 km. In the first area a maximum of 7, in the second one 5, and in the third one 3 tunnel stations can be provided because of the distribution of the optical signals is purely passive via optical splitters, no opto-electrical conversion is necessary at these points.

The connection of the other direction is linear. The fiber of the return channel is looped through all tunnel stations belonging to one side of a head station. After opto-electrical conversion this signal and the return signal of the tunnel station itself are multiplexed in the frequency range. Then the electrical multiplex signal is converted to an optical one and is transmitted to the next tunnel station or finally to the head station.

4. Leaky Coaxial Cable

4.1 Construction

Radiating cables have a coaxial design. They consist of a central conductor, a concentric insulation dielectric, an outer conductor covering the dielectric, and an outer thermoplastic sheath. The inner conductor is made of massive copper or for cables with larger dimensions it is made of copper cladded aluminium wire or a copper tube filled with polyethylene for reduction of weight and for economic reasons. For the dielectric a low relative dielectric constant is necessary to get low longitudinal attenuation and broad-band radiation characteristics. Both is achieved by using a dielectric in bamboo construction: on the inner conductor polyethylene discs are placed in a constant distance of a few centimeters. Over these discs a polyethylene tube of anout 2 millimeters is extruded. This system of air chambers resembles bamboo tubes /4/.

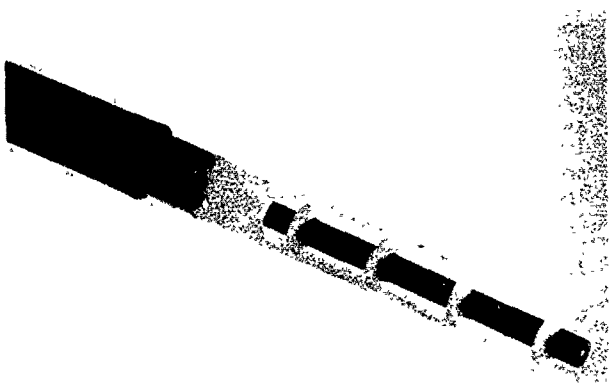

Fig. 4.1 Bamboo Dielectric

Because of the air portion the resulting dielectric constant is in the range of 1.2 to 1.3. The bamboo is longitudinally and laterally watertight. Radiating cables have relatively large dimensions, so the bending characteristics are an important topic. The bamboo dielectric fulfils the tough requirements and has high lateral stability. For the outer conductor of radiating cables prepunched copper tapes are used which are longitudinally applied by forming a tube. The slot configuration is periodically repeated along the cable length. Over the copper outer conductor a sheath consisting of flame-retardent non-halogenuous thermoplastic material is extruded. In an open flame the material shows only low smoke emission.

4.2 Operating Function of Leaky Coaxial Cables

Openings in the outer conductor cause electromagnetic coupling of the inner wave through the outer space of the coaxial cable to an antenna and vice versa. The most important characteristic

for energy transport along the cable is the longitudinal loss, i.e. the loss of energy per unit of length. The longitudinal attenuation is mainly determined by the dimensions and the material properties of the cable. In addition coupling loss affects longitudinal attenuation. The coupling of energy from the leaky coaxial cable to the outside is described by the coupling loss. This is defined as the ratio of energy received at the antenna to the transmitted energy on the leaky coaxial cable opposite to the place of the antenna. This is also valid for the transmission from the antenna to the leaky coaxial cable (reciprocity). The radiation increases the longitudinal loss. Radiation is caused by a regular stimulation by the periodic aperture configuration. The intensity of radiation is mainly determined by the number of openings per periodicity length. The arrangement of the openings within the configuration produces a nearly homogeneous radiation all over the chosen frequency bands. Also shape and area of the single opening play an important part in the design process.
The slot configuration of the leaky coaxial cable LK37 has the following properties:
32 openings shaped as slots of 3x20 mm^2 perpendicular to the cable axis are arranged in non regular density within the periodicity length of about 1050 mm. So all the normally used frequency bands at 4 meters, 2 meters, 0.7 meters and 0.3 meters for the frequencies around 80 MHz, 150 MHz, 450 MHz and 900 MHz are covered. The seemingly chaotic configuration of the slots is the result of a complicated mathematical model computation. A description would by far exceed the scope of this paper and has been described before /5/.

4.3 Specification of the Leaky Coaxial Cable LK37

The mechanical and electrical properties for the Lk37 with flame-retardent non-halogenuous sheath are listed below:

diameter of inner conductor	9,45	mm
diameter of outer conductor	23,60	mm
thickness of outer conductor (with slot configuration)	0,25	mm
diameter of leaky coaxial cable	28,10	mm
impedance	50	Ω

longitudinal attenuation in open area, 1.5 m distance from unarmoured concrete floor

80 MHz	≤ 1.4	dB/km
450 MHz	≤ 3.4	dB/km
960 MHz	≤ 6.8	dB/km

longitudinal attenuation near a "wall", 0.12 m distance from unarmoured concrete floor

80 MHz	≤ 1.6	dB/km
450 MHz	≤ 3.5	dB/km
960 MHz	≤ 6.1	dB/km

coupling loss (average), measured in open area with vertically polarized " /2 " - dipole in 2 m distance, longitudinal attenuation not taken into account

80 MHz	≤ 65	dB
450 MHz	≤ 70	dB
960 MHz	≤ 70	dB

structural return loss (measured cable length approximately 70 m)

80 - 108 MHz	≤ 25	dB
147 - 170 MHz	≤ 20	dB
450 - 465 MHz	≤ 18	dB
890 - 960 MHz	≤ 16	dB

relative propagation velocity	87	%
max. **tensile strength**	1000	N
min. **bending radius** (with model)	950	mm
weight (guiding value)	810	g/m

4.4 Laying of Leaky Coaxial Cable

Normally, leaky coaxial cables are mounted at the side wall about 5 metres above railway track. Obstacles like hanging weights for stretching the aerial contact line, signalling posts etc. are passed by. The leaky coaxial cable is mounted on stand-off clamps providing a distance of 12 cm between cable and wall. This distance has shown as an optimum for a variety of leaky coaxial cable parameters. The ends of the leaky coaxial cable are led into the tunnel radio station using isolators which can bear a test voltage of 2.000 V (direct current). In addition, high voltage protection deductors with an ignition voltage of approximately 200 V are installed. The outer sheaths of the leaky coaxial cables are connected to the tunnel-ground.

5. Measurement Technique

If the most important characteristics of leaky coaxial cables are to be recorded, the standard measurement equipment has to be modified according to these special requirements. The important transfer properties are longitudinal attenuation, structural return loss and coupling loss. These parameters cannot be measured at a cable on a drum. Because of the mutual influences of the radiating slots of neighbouring lays, those leaky coaxial cables are tested only under mounting conditions. For this a test route has been erected (Fig. 5.1).

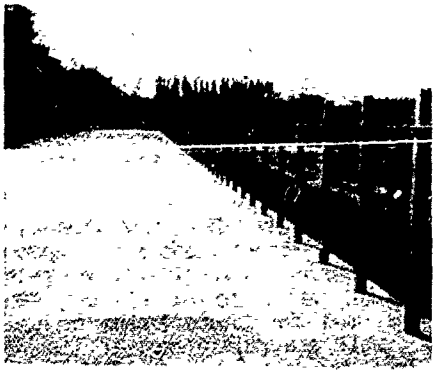

Fig. 5.1 Test route

These parameters describe the characteristics under operating conditions. This measurement equipment was built to registrate all these properties in the important frequency range with only a small number of measuring devices (Fig. 5.2).

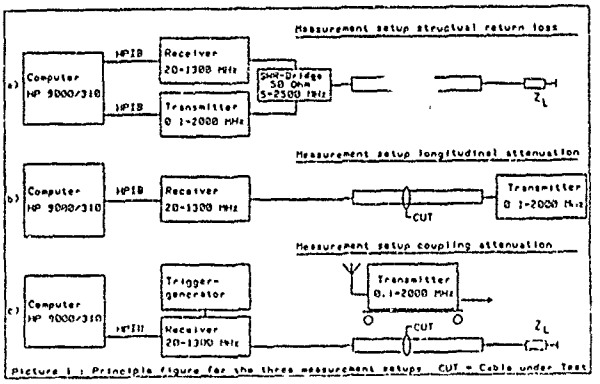

Fig. 5.2 Principal Figure for the three measurement setups

In fig. 5.2 a) the setup for the measurement of the structural return loss is shown. In this case the measurement steps are f = 200 KHz in the whole operation range of the leaky coaxial cable. Periodical disturbations due to wrong mounting conditions are to be seen directly.

$$a_R = 20 * \log (1/ r) \quad (dB)$$

r = reflection coefficient

Fig. 5.3 shows the graph of such a measurement.

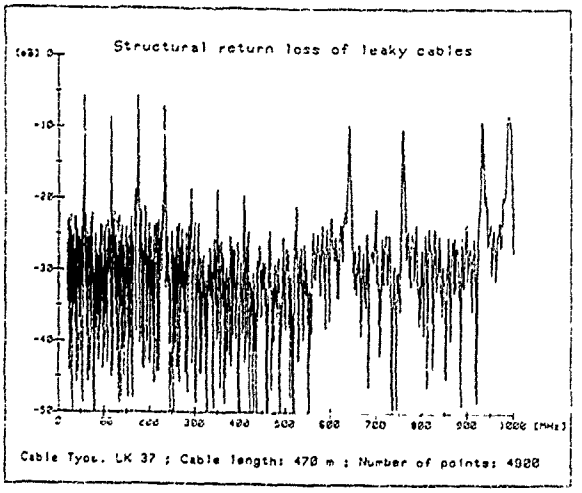

Fig. 5.3 Structural Return Loss; Cable Type LK37

The peaks over the frequency range are produced by the mismatching of the cable at these special frequencies. If the peaks in the working range are less than - 15 dB the longitudinal wave will not be disturbed.

By the mounting of the cable near the wall both cable ends are not available at the same place for the measurement of the longitudinal attenuation. Leaky coaxial cables are used in a wide frequency range, so it makes no sense to take a classical measurement equipment to measure longitudinal attenuation at one frequency. In this method receiver and transmitter are "tele-synchronized" (Fig. 5.2 b). If the measuring time of the receiver is much smaller than the switching time of the transmitter from one frequency to the next frequency, so it is possible to measure in a similar way like the classical procedure and get quasi-continuous plot of the attenuation.

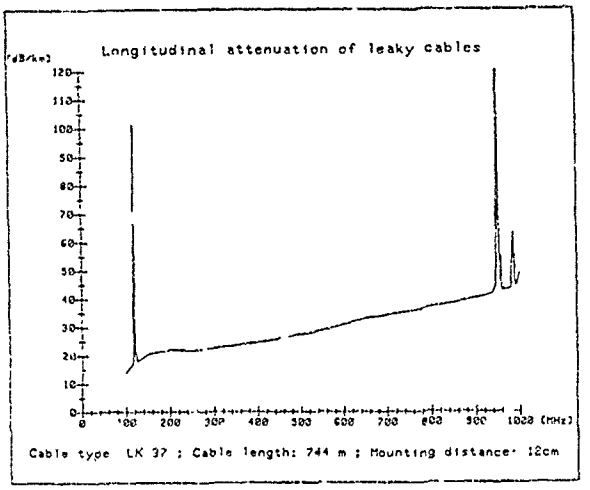

Fig. 5.4 Longitudinal Attenuation; Cable Type LK37

The frequency range from 20 to 1000 MHz in steps of 1 MHz is measurable in a few minutes and a nearly continuous graph of the attenuation is achieved (Fig. 5.4). Coupling loss and longitudinal attenuation depend on the environment, that means the specifications are not the same for open area and the working condition in a tunnel. The actual longitudinal attenuation is used to correct the result of the coupling loss in the setup Fig. 5.2 c). The local measured field intensity is compensated by the longitudinal attenuation after measuring.

In this procedure the field intensity is measured in up to 300 times per second in maximum along the leaky coaxial cable. The field intensity at the receiver's antenna is the transmitter output power reduced by the sum of coupling loss and longitudinal attenuation. This sum is the so-called "system value". After a statistical evaluation the mean-value and the 95 %-value describe the quality of the coupling loss.

These evaluations are important to give a statement on the quality of the leaky coaxial cable. All measured data are saved on hard discs and so it is possible to perform mathematical data processing later.

This automatical measuring equipment gives the possibility to find out a system value for a special tunnel profile for each leaky coaxial cable type.

6. Results

In this chapter the investigations on environmental effects affecting the various leaky coaxial cable parameters will be presented. Fig. 6.1 shows the result of a open area coupling loss measurement in our test facility.
The upper diagram shows precisely the behaviour of the receiver input level, below the statistical evaluation of the coupling loss is presented. The most important result is the average of the coupling loss d(50 %) as well as the d(95 %) - value which is used for planning of tunnel radio systems.

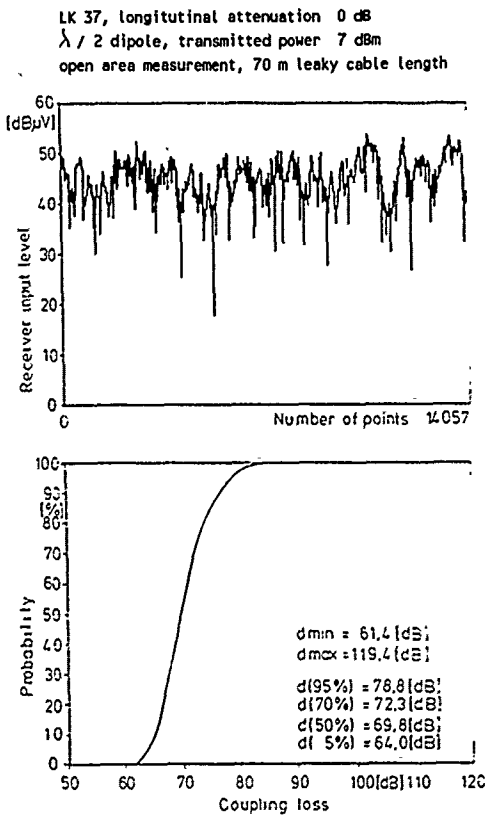

Fig. 6.1 Measuring Record of Coupling Loss

For tunnel radio system planning the sum of longitudinal attenuation and coupling loss is used. Both parameters depend on the operating frequencies and on the length of the leaky coaxial cable. Long term experiences have shown that leaky coaxial cables in tunnels often behave different from leaky coaxial cables in open area installations. The reasons are the mounting material and fixing method as well as the tunnel profile and tunnel installations, for example the aerial contact line or signal posts. Those effects are due to the environment of the leaky coaxial cable and cannot be predicted precisely. The adjacent problems can be minimized by mounting with 12 cm-clamps to keep a sufficient stand-off from wall and ceiling, respectively. Free space results may not be used for system planning purposes without careful investigations. But they allow to some extent the comparison of different leaky coaxial cable types. A security margin has to be taken into account for tunnel installations based on the experiences of the system engineers. The influence of the distance between mobile antenna and leaky coaxial cable in open area is shown in tables 6.1 and 6.2:

Table 6.1

Coupling loss/dB for different distances between leaky coaxial cable and mobile antenna

frequency MHz	2 m 50%/95%	4 m 50%/95%	6 m 50%/95%
70	60,9/75,3	66,1/79,1	70,0/82,4
87	61,3/71,6	67,7/77,7	70,5/80,6
100	59,2/72,1	64,7/75,3	68,2/77,5
160	63,8/74,4	68,1/77,7	70,0/82,5
460	64,6/77,9	68,6/80,0	70,1/81,1
920	66,5/78,1	68,2/79,7	69,8/80,1
950	66,9/79,1	68,8/79,4	71,6/83,0

Table 6.2

Coupling loss/dB for different distances between leaky coaxial cable and mobile antenna

frequency MHz	2 m 50%/95%	4 m 50%/95%	6 m 50%/95%
70	58,0/68,0	64,7/76,5	69,6/80,8
87	63,8/74,1	70,0/82,2	73,1/84,0
100	63,4/76,1	70,8/82,7	75,1/87,3
160	68,8/78,6	75,8/86,2	76,5/88,3
460	60,9/71,8	64,9/74,3	67,0/76,9
920	58,7/68,5	62,9/74,1	64,5/76,0
950	63,0/109,7	63,4/75,0	65,0/75,7

Theoretically the receiver input signal level is predicted to be just half the value when the distance is doubled. This can be seen by an increase of the coupling loss of 6 dB per doubling the distance or about 10 dB per tripling the distance. This is most obvious in the 4 m- band and also to be seen in the 2m-band. At frequencies around 460 MHz the effect is reduced and nearly vanishes at 900 MHz. But the general trend remains in both tables.

Table 6.1 shows the measured open area values of a leaky coaxial cable with a polycthylene sheath and a non-metallic supporting rope, the periodicity length of the slot configuration is about 1050 mm the number of slots is 32. Having used the same measuring procedure the results of the same measuring procedure of a leaky coaxial cable of the same diameter and impedance, but with a mica-tape on the dielectric and a

flame-retardant non-halogenuous sheath are shown in table 6.2. The number of slots is 64, distributed in a periodicity length of 2200 mm. It is remarkable that the results are similar but influenced by the construction details.

It is to be taken into account, that the ratios of distance and wavelength approach more and more the far field conditions when the operation frequency rises. In addition to that the reflection properties of the concrete floor change for different frequencies. In open area measurements no other reflections than those on the ground do occur normally as long as there are no additional obstacles. Contrarily to the open area results there is no systematical behaviour for changes in distance between leaky coaxial cable and mobile antenna within a tunnel.

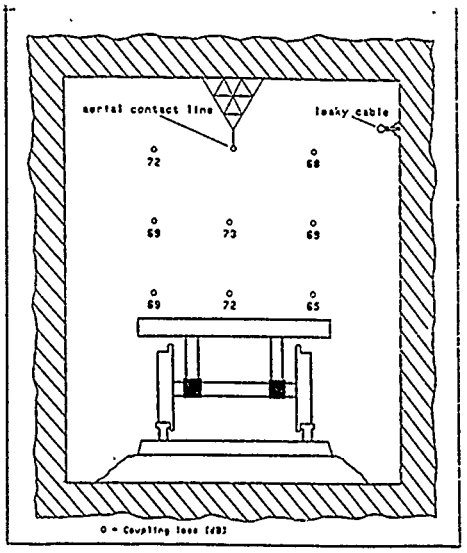

Fig. 6.2 Distribution of coupling loss within the tunnel profile

Measurements at 450 MHz with eight different antenna positions (Fig. 6.2) have shown a field intensity amplitude distribution within the tunnel profile for three distances and three heights. The measured mean values of the coupling loss vary unsystematically around the mean value of 70 dB in a range of ±4dB. The values near the leaky coaxial cable are not the best results, the values far from the leaky coaxial cable are not the worst results. This behaviour has been described as a sort of "filling effect" which means that the superposition of many direct signals (i.e. air line distance between radiation aperture and mobile antenna) plus indirect signals (i.e. single and multiple reflections) always delivers similar results.The longitudinal attenuation as a function of the distance between leaky coaxial cable and wall or ceiling, respectively, has been determined in a series of tests. As a first test a leaky coaxial cable was laid directly on the surface of the mentioned above unarmoured concrete floor mentioned above in form of a loop. The result was as bad as anticipated. Then wooden blocks of 4 cm height were placed under the cable of 70 m length. The longitudinal attenuation decreased. Then the height of the blocks simulating a non-metallic mounting clamp was augmented by steps of 2 cm. The results are shown in figure 6.3. This figure shows clearly, that 12 cm is an optimum, because higher mounting does not improve the longitudinal loss significantly but reduces the free profile space of the tunnel. It has also shown that the orientation of the slots is uncritical. Coupling loss measurements for this kind of mounting could not be done because the electro-vehicle simulating the mobile subscriber would always have "collected" the radiation of the two branches of the leaky coaxial cable loop at the same time. So the result would not be comparable to other measurements before.

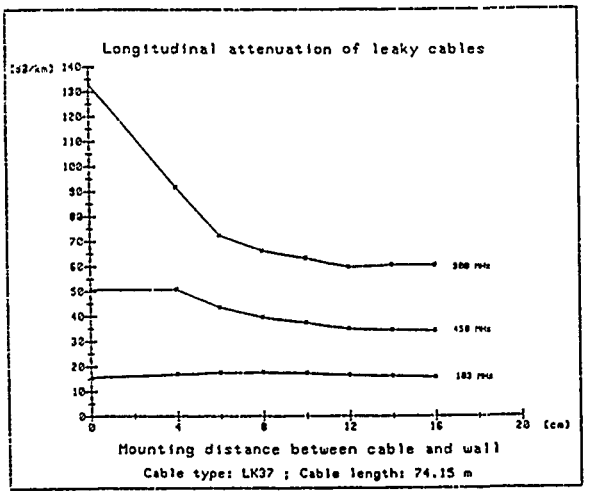

Fig. 6.3 Longitudinal Attenuation Depending on Mounting Distance between Cable and Wall

The influence of the distance between leaky coaxial cable and wall or ceiling, respectively, on the radiation performance has been tested in a typical tunnel for the high speed trains. Two leaky coaxial cables of the same type were mounted, one on stand-off clamps of 6.5 cm, the other one on clamps of 12 cm distance.

6.4 Test Installation with 6.5 and 12 cm Distance between Cable and Wall

The results of the measurement of the longitudinal loss of 750 m leaky coaxial cable were very similar to those of the open area measurements with a 70 m leaky coaxial cable of the same type. The measurement of the coupling loss under nearly perfect indentical environmental conditions except the clamp heights is documented in Fig. 6.5. The decrease of the coupling loss with rising distance from the wall is to be seen clearly, as well as the much less erratic behaviour of the curve of the system value. So the 12 cm-clamp has proven to be the optimal mounting material.

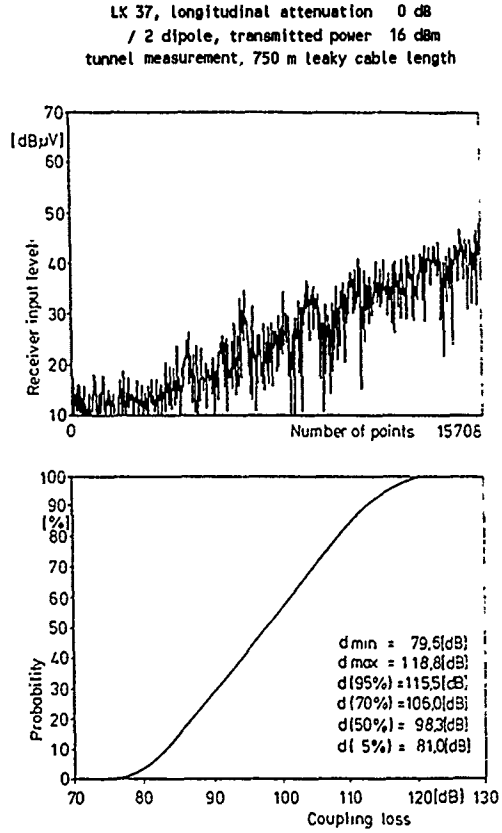

Fig. 6.5 a Coupling Loss at 6,5 cm Mounting Distance

7. Conclusion

Experiences with radiating coaxial cables for use in tunnel radio systems have shown that because of the broad-band characterictics and little need of mounting space there are many advantages compared with single directional antennas. Important is also the possibility of operation in the 900 MHz frequency band in the future. So the application of radiating coaxial cables for all the often used frequency bands for mobile communication in tunnels, buildings and valleys is the most promising method to meet the requirements of modern communication systems.

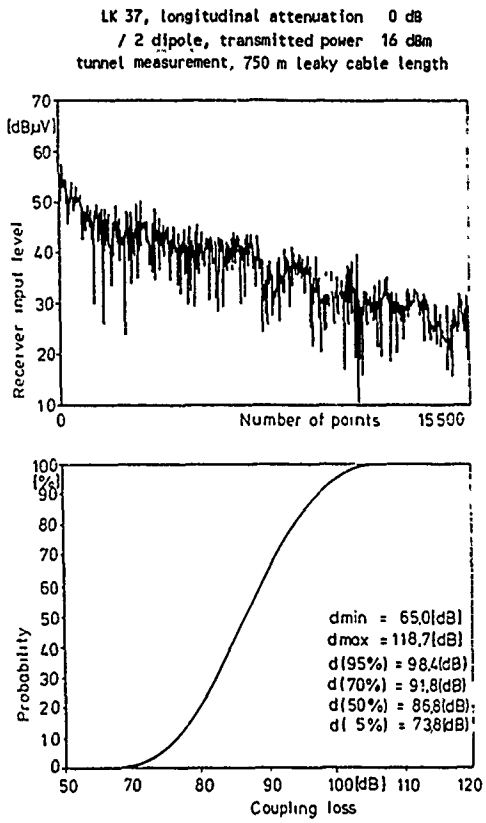

Fig. 6.5 b Coupling Loos at 12 cm Mounting Distance

Literature

/1/ System Bosch Telecom (Mobile Kommunikation)

/2/ Leinweber, J., NBS-Tunnelfunk für Kundendienste, Signal + Draht 82 (1990) 6, pp. 117

/3/ Haag, H. G., Der Einsatz der LWL-Technik bei der Deutschen Bundespost im Zug, im Stellwerk und auf der Strecke, Der Eisenbahn Ingenieur, August 1988

/4/ Thönneßen, G., Zamzow P. E., Dämpfungsarme Koaxialkabel für Kabel-TV-Netze in Europa, 15th International T.V. Symposium, Montreux '87 (Proceedings)

/5/ Haag, H. G., Thönneßen, G., Schulze-Buxloh, K., Leaky Coaxial Cables for Mobile Communication, IWCS 1989 (Proceedings), pp. 286

Helmut G. Haag
AEG KABEL AG
Sales Division for Telecommunications
Mönchengladbach, West Germany

Helmut G. Haag (42) is Manager of Sales Division for Telecommunications. After reaching his Dipl.-Physiker-degree from the University of Stuttgart he joined AEG KABEL in 1975 for the development of coaxial cables. Later he has been also responsible for the development of optical fiber cables. From 1980 to 1983 he built up the production plant for these cables. In autumn 1983 he took over the Technical Sales Division and in Jan. 1990 the Sales Division as a whole.

Klaus Lehan
Telecommunication Development
Mönchengladbach, West Germany

Klaus Lehan (27) is an engineer in the Development Department for Telecommunication Cables. He finished his studies at the Fachhochschule Düsseldorf in 1987 as Dipl.-Ing. In 1988 he joined AEG KABEL. Since this time he is engaged in the development of symmetrical cables and special measurement techniques.

Karl Schulze-Buxloh
AEG KABEL AG.
Telecommunication Development
Mönchengladbach, West Germany

Karl Schulze-Buxloh (34) is an engineer in the Development Department for Telecommunication Cables. He finished his studies at Ruhr-Universität Bochum in 1986 as Dipl.-Ing. In 1986 he joined AEG KABEL. Since this time he is engaged in the development of leaky coaxial cables.

Wolfgang Stremme
AEG KABEL AG
Technical Sales
Mönchengladbach, West Germany

Wolfgang Stremme (40) is an engineer in the Technical Sales Division for Telecommunications. He finished his studies in communication engineering at Technische Hochschule Aachen in 1978. Afterwards he was engaged in the research of traffic control. He graduated as a Dr.-Ing. in 1984. In 1985 he joined AEG KABEL.

Ultrafine Miniature Coaxial Cable with Highly Expanded Microcell Insulation

T.KAKUTA, T.YAMANISHI and A.MORI

Sumitomo Electric Industries Ltd.

Abstract

The low dielectric constant in the ultra thin insulation layer for miniature coaxial cables was perfomed utilizing the newly developed insulation technology. The novel insulation method using UV-curable resin containing heat expansive microspheres was developed.

In the thin insulation layer of 0.07mm thickness, the low dielectric constant about 1.5 was achieved. The muniature coaxial cable with 198 conductors was realized with small diameter of 7.9mm and low capacitance of 85pF/m.

The other application of the new insulation method for high speed data transmission cable was also successfully conducted.The velocity of the propagation delay of 88.6% speed of light and dielectric constant of 1.27 in the 0.175mm thickness insulation layer was performed.

1. Introduction

Recently, multi coaxial cables with more than 100 conductors and small diameter less than 10mm are strongly required for the application to medical instruments such as ultrasonic diagnostic equipments. And high speed coaxial cables with the velocity of propagation delay time (Td) less than 3.78 nsec/m (88% speed of light) are also expected to be developed.

In order to realize the above requirements, the coaxial cable with a thin insulating layer and a low dielectric constant is essential.

As the conventional methods for making the thin insulating layer with a low dielectric constant, the spiral wrapping method using the expended polytetrafluoroethylene (PTFE) [1] tape over conductor and the forming extrusion method of thermoplastics such as a polyethylene and a polyfluoroalchoxy-ethylene (PFA) are well known [2][3]. However, the ultra-thin insulation layer less than 0.1mm with a low dielectric constant has not been performed by those conventional methods.

This paper describes a newly developed thin insulation coating method with a low dielectric constant utilizing UV-curable resin composition containing heat expansive microspheres as well as properties of the produced coaxial cables.

2. Insulation material and coating process

The newly developed insulation layer consisted of the UV-curable resin composition containing heat expanded microspheres. The mean diameter of the expanded microspheres was about 40μm, and the shell thickness was below 0.1μm. The dielectric constant and tan δ value of the UV-curable acrylate were about 2.9 and 1.8×10^{-3} (@1MHz, 23 ℃), respectively.

The heat expansive microspheres consisted of the shell of poly (vinylidene chloride-acrylonitrile) copolymer and iso-butane enclosed inside of the shell.The expansive microspheres had the mean diameter about 10μm. The microspheres had the volume expansion ability about 50 times by the appropriate heat treatment around 100 ℃ to 150 ℃.

The UV curable resin composite containing the heat expensive microspheres was coated onto a conductor. The thin insulation layer with independent cells was produced by the controled heat treatment and UV-radiation. High porosity more than 74% to 90 % was achieved.

3. Application for multi-coaxial cables

3.1 Multi-coaxial wires

Two types of the coaxial wire with different porosity and thickness of the insulation layer were prepared to evaluate the electrical properties. Fig.1 shows the cross sectional structure of the coaxial wire .

The stranded seven copper wires (AWG40) was used as the center conductor. The insulated stranded wire with expanded microspheres was wrapped by polyester tape as the covering insulation. The details of the cable stractures and the electrical properties of the two types of the cables are shown in Table 1 and Table 2.

In the type A coaxial wire, the ultra thin insulation layer of 0.07mm thickness was achieved with a low dielectric constant value of 1.53. In consequence, a miniature coaxial wire with small diameter of 0.34mm and low capacitance of 85pF/m was realized. In type B, the lower dielectric constant value of 1.3 in the inner insulating layer of 0.13mm thickness was achieved, and the lower capacitance of 50pF/m was performed in the coaxial wire with diamter of 0.47mm.

In order to evaluate the durability of the new insulation layer, the stability of the capacitance of the coaxial wire was investigated nuder the various environmental conditions such as high temperature aging at 80 ℃, high humidity condition of 60 ℃ 95%RH and temperature cycles from -40 ℃ to 60 ℃. The changes of the capacitance under the three conditions for 100days were only less than ±1% of the initial value. No change of the capacitance was also confirmed after vacuum treatment of 100mmHg at 65 ℃ for 2days.

3.2 Properties of the multicoaxial cable

The multi coaxial cable with 198 coaxial wires was manufactured using the coaxial wires of Type A. The multi coaxial cable consisted of 12 stranded units of 16 coaxial wires and 3 units of 2 coaxial wires, as shown in Fig.2. The miniature multicoaxial cable with small diameter of 7.9mm was realized. The change of capacitance during the manufacturing processes of the cable was only less than ±5pF/m. Table 3 shows the electrical properties of the minuature multi coaxial cable.

The resistance to repetitious bending tortion of the cable was also evaluated at 1KVDC. Fig.3 and Fig.4 show the method for bending and tortion test, respectively. A dielectric breakdown or a snapping of a conductor were not obserbed during 300,000 cycles.

4. Application for high speed coaxial cables

4.1 High speed coaxial cable

Two types of coaxial wires cables with different thickness of the insulation layer were prepared. The porosity of the insulation layer was about 90% for both cables. Fig.5 and Table 4 show the costruction of the coaxial cable. The silver plated copper wire (AWG33, 1/0.18mmϕ) was used as the conductor. The insulated conductor with the microcells was wrapped by polyester

tape and the shielding of copper alumininzed polyester tape was applied on the polyester tape.

The coaxial cables of square shape with a drain wire (AWG30 1/0.254mmϕ) were produced by extrusion of PVC.

4.2 Electrical properties

Table 5 shows electrical properties of two types of the high speed coaxial cables. Low impedance was achieved for both coaxial cables as shown in table 5.

The velocity of the propagation delay was 88.6% speed of light in type X. The effective dielectric constant value of 1.27 in the insulation thickness of 0.175mm was calculated from the velocity of the propagation delay time of 3.76 nsec/m. Fig.6 to Fig 8 show the characteristic impedance, attenuation and velocity of propagation against the change of frequency for type X coaxial cable, respectively.

5. Conclusion

The low dielectric constant in the ultra thin insulation layer for miniature coaxial cables was perfomed utilizing the newly developed insulation technology. The novel insulation method using the UV-curable resin containing the heat expansive microspheres was demonstrated. The low dielectric constant about 1.5 was achieved in the ultra thin insulation layer of 0.07mm. It conrtributed to realize the miniature multi-coaxial cable of 7.9mm diameter with 198 conductors. And the low capacitance of 85pF/m was performed in the multi-coaxial cable for medical application.

The developed coaxial wires and cables had good stability under the voriaus environmental conditions.

The coaxial cable with high velocity of propergation of 88.6% speed of light was also realized with 0.175mm thickness insulation layer.

The novel insulation technology utilizing the UV-curable resin with the expansive microspheres will contribute to the progress of high speed data transmission and highly efficient measuring instruments for medical application.

6. References

[1] "Expanded PTFE Cables" edited from publications of G. Hansell and D. Slothour and printed for a meeting of the Boston Chapter, May 1979.

[2] F.Suzuki and A.Mori et al., "Microcoaxial Cable Insulated with Highly Expanded Polyethytene by Chemical Blowing Method" in Proc. 27th International Wire and Cable Symposium, 1978.

[3] F.Suzuki, T.Komura and A.Mori, "High Speed Coaxial Cable Insulation with Highly Expanded Irradiated Polyolefin" in Proc. 34th International Wire and Cable Symposium, pp.300-307,1984.

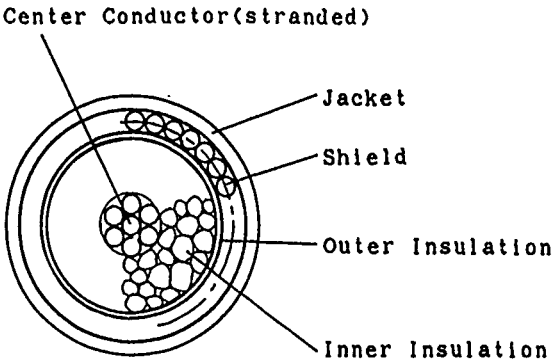

Fig.1 Cross sectional structure of a coaxial wire

Table 1 Construction of miniature coaxial wires

Unit[mm]

Item \ Type		A	B
Conductor	Material	Tinned copper alloy wire	
	Composition	7/0.03(AWG40)	
	Outer Diameter	0.09	
Inner Insulation	Material	UV cured acrylate resin with expanded microspheres	
	Thickness	0.07	0.13
	Porosity(%)	74	86
Outer Insulation	Material	Polyester tape(wrapping)	
	Outer Diameter	0.25	0.37
Shield	Material	Tinned high strength copper wire	
	Composition	Spiral shield of 0.03	
Jacket	Material	Polyester tape(wrapping)	
	Outer Diameter	0.34	0.47

Table 2 Electrical properties of miniature coaxial wires

Item \ Type	A	B
Characteristic Impedance (Ω)	60	75
Capacitance (pF/m)@1kHz	85	50
Attenuation (dB/km)@10MHz	470	330
Dielectic Constant ε @1kHz		
Inner Insulation	1.53	1.30
Total Insulation	1.61	1.33

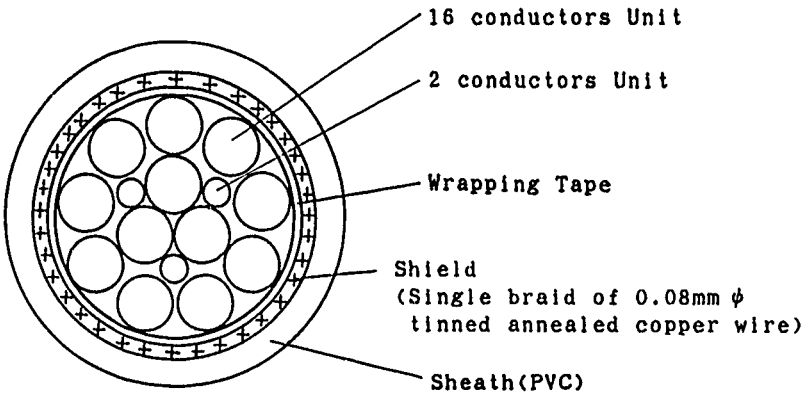

Fig.2 Cross section of a multi coaxial cable (198 conductors)

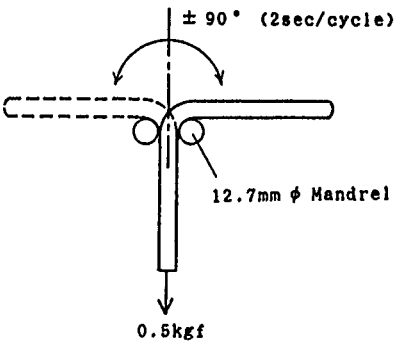

Fig.3 Test method for bending

Table 3 Electrical Properties of the multi coaxial cable

(at;20℃)

Item	Unit	Details
Conductor Resistance	Ω /km	Max. 5000
Insulation Resistance	MΩ -km	Min. 1000
Dielectric Strength	ACV/1min.	300
Capacitance @1kHz	pF/m	85

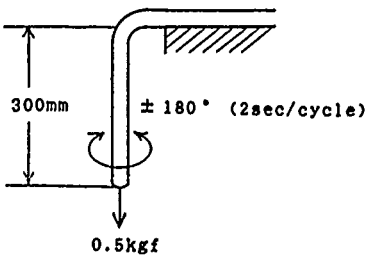

Fig.4 Test method for tortion

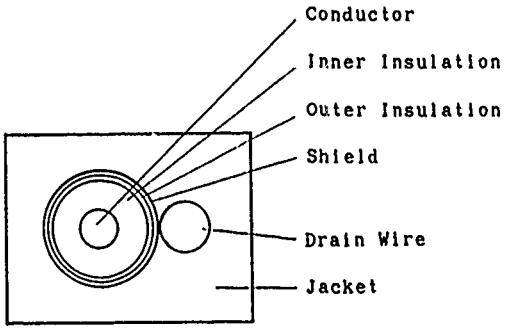

Fig.5 Cross section of a high speed coaxial cable

Table 4 Construction of high speed miniature coaxial cables

Unit[mm]

Item \ Type		X	Y
Conductor	Material	Silver plated copper alloy	
	Composition	1/0.18(AWG33)	
	Outer Diameter	0.18	
Inner Insulation	Material	UV cured acrylate resin with expanded microspheres	
	Thickness	0.175	0.11
Outer Insulation	Material	Polyester tape(wrapping)	
	Outer Diameter	0.535	0.430
Shield	Material	Copper coated aluminized polyester tape	
	Thickness	0.015	
Drain Wire	Material	Silver plated copper wire	
	Composition	1/0.254(AWG30)	
Jacket	Material	PVC	
	Thickness	0.22	0.25
	Size	1.27 × 1.0	

Table 5 Electrical properties of high speed miniature coaxial cables

Item \ Type	X	Y
Characteristic Impedance (Ω) @10MHz	64.5	53.6
Attenuation (dB/km) @100MHz	550	680
Velocity of Propagation (%)	88.6	86.5
Td(nsec/m)	3.76	3.85
Effective Dielectric Constant ε_{eff}	1.27	1.34
Capacitance(pF/m) @1kHz	61.1	75.9

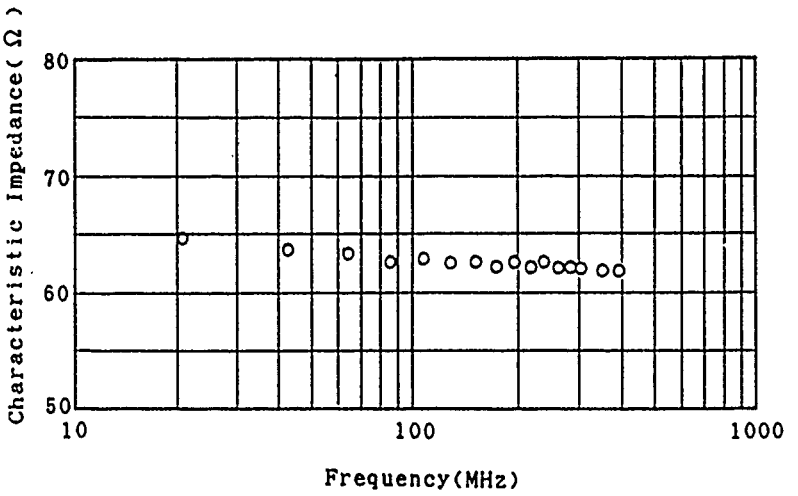

Fig.6

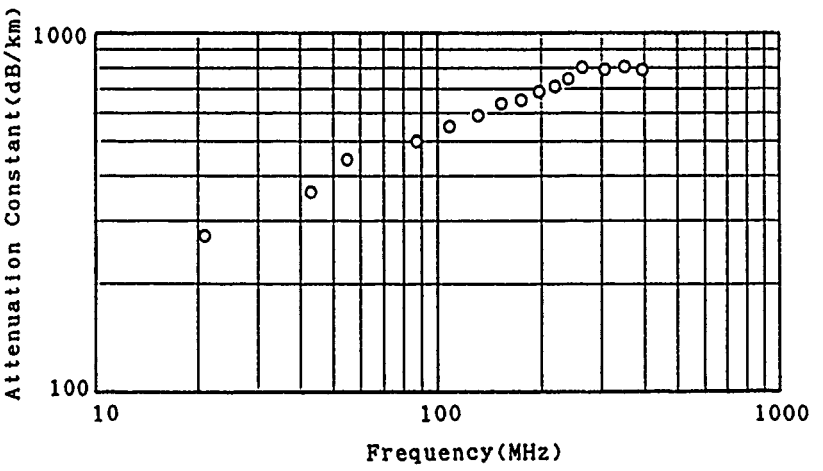

Fig.7

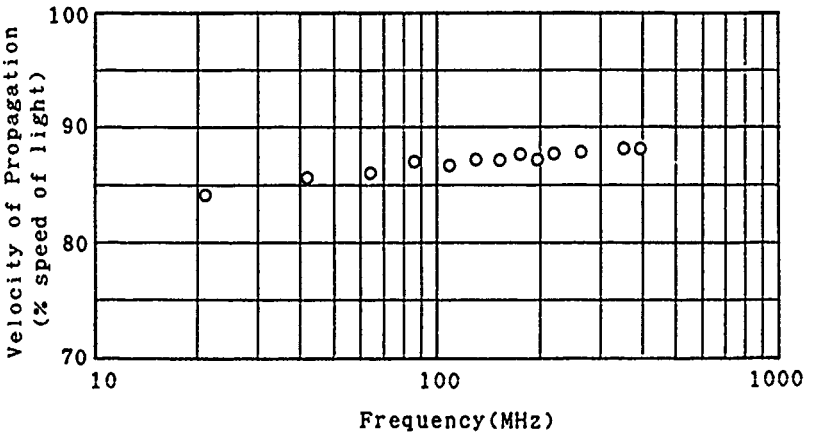

Fig.8

Tatsuya Kakuta

Sumitomo Electric
Industries,Ltd.
1,Taya-cho
Sakae-ku
Yokohama 244
Japan

Toru Yamanishi

Sumitomo Electric
Industries,Ltd.
1,Taya-cho
Sakae-ku
Yokohama 244,
Japan

Tatsuya Kakuta received the B.S.and M.S. degrees in applied chemistry from Osaka University in 1983 and 1985, respectively. He joined Sumitomo Electric Industries, Ltd. in 1985, and has been engaged in research and deveropment of optical fiber and cables.

Mr. Kakuta is a member of Transmission Media R & D Department in Yokohama Research Laboratories.

Toru Yamanishi received a B.S. degree of Chemical Engineering from Hokkaido University in 1972. He joined Sumitomo Electric Industries, Ltd. and worked on the research and development of optical fiber fabrication, especially fiber drawing and coating. Mr.Yamanishi is now a chief research associate of Transmission Media R & D Department.

Akinori Mori

Sumitomo Electric
Industries, Ltd.
3-3, Satsuki-cho
Kanuma-city
Tochigi
Japan

Akinori Mori received the B.S. degree in mechamical enginearing from Kyushu University in 1970. He then joined Sumitomo Electric Industries, Ltd. and has been engaged in development and design of plastic cables.

Mr.Mori is now a manager of Data Transmission Engineering Section in Electronics Wire Division.

LIGHT WEIGHT CABLES FOR COMMUNICATION SATELLITES

Eiichi SAKITA and Jun'ichi SEKI

NTT Technical Assistance and Support Center
Musashino, Tokyo, 180 JAPAN

ABSTRACT

Light weight semirigid coaxial cables and insulated power cables are developed. The cables are designed to reduce the lift-off costs of communication satellites through a reduced wire harness weight. For this purpose, a new clad aluminum alloy pipe is invented to replace the copper outer conductor of a semirigid coaxial cable. This pipe has a silver inner layer and a copper outer layer and is produced by the warm hydrostatic extrusion method. The light weight insulated power cable is created through the concept that aluminum is a more effective conductor than copper of the same weight. A silver clad aluminum wire is newly developed to replace the nickel plated copper wire used for the cable's conductors and braid shield. This clad aluminum wire has a copper middle layer to suppress detrimental diffusion of aluminum into the silver. The light weight cables are attached to connectors and tested. It is confirmed that the electrical characteristics are equal to those of conventional cables, and that the mechanical properties and reliability are sufficient for them to be used as a satellite wire harness. The development of these cables could result in a one-third reduction in weight thereby making them efficient for use in satellites.

1. INTRODUCTION

Recently, there has been a move to increase the number of transponders in telecommunication satellites due to the increasing amount of calls[1]. However, satellite lift-off costs are significant[2]; therefore, it is very important to make the equipment as light as possible.

In a two-ton class communication satellite about 100 kg of wire harness is used; consequently, reducing the weight of the wire harness can result in significant savings. Up to now, no one has succeeded in reducing the cable weight, thus the same heavy cables that are used on earth have been adopted by communication satellites. Therefore, the authors decided to develop light weight cables suitable for communication satellites, and chose semirigid coaxial cables and insulated power cables as targets because they are widely used for wire harnesses of communication satellites.

The outer conductor of semirigid coaxial cables has been primarily made of copper for its good electrical and mechanical properties. This outer conductor occupies a large amount of the cable weight, so reducing the weight of this part is effective in reducing the cable weight. Aluminum outer conductor cables have been developed due to their light weight, but they do not have adequate electrical characteristics for communication satellites. Therefore, the authors moved on and noticed that the outer conductor of a semirigid coaxial cable is made of a thick wall pipe, even though electrical signals only flow through a very thin inner layer (the skin depth is only 0.002 mm). Based on this point of view, the development of a silver inner clad aluminum pipe was agreed upon to replace copper as the outer conductor.

As a spin-off, the authors noticed that an aluminum conductor allows a greater electric current than a copper conductor of the same weight. However, the technology to produce a silver coated aluminum wire was not developed. Therefore, the development of a silver clad aluminum wire was started for application to an insulated power cable for communication satellites.

2. CABLE DESIGN

2.1 Semirigid Coaxial Cable

In this development, a 3.6 mmø (0.141 inch) semirigid coaxial cable was investigated considering its generality. In a copper cable of this size the outer conductor occupies 59 % the weight of the entire cable.

Fig. 1 shows a construction of an experimental light weight semirigid coaxial cable. The outer conductor is a newly developed pipe which has three layers: a silver inner layer for excellent electrical characteristics, an aluminum middle layer for strength and a copper outer layer for good solderability to mount connecters. The inner conductor and insulator are same as those of a conventional cable. The calculated weight of this cable is 28 g/m, which is about less than 40 % that of a conventional cable of 47 g/m weight. Fig. 2 shows a photograph of a cable.

2.2 Insulated Power Cable

In this development, a cable similar to the AWG #28 four-conductor cable was investigated.

Fig. 3 shows a construction of an experimental light weight insulated power cable. A new clad aluminum wire was developed to replace the conventional nickel plated copper wire that is used for conductors and braid shield. This new wire consists of three part: an aluminum core for efficient electrical conduction, a silver outer layer for good solderability and a copper layer between them. The copper layer is inserted to suppress aluminum diffusion into silver during the production process. The designs of the conductor strand and braid shield are same as those of the conventional cable, but the diameters of the aluminum clad wire are larger than those of a copper cable due to electrical con-

ductivity compensation. A conductor wire diameter is 0.24 mm corresponding to 0.20 mm of the copper conductor wire. A shield wire diameter of 0.15 mm was determined from the restriction in braid production.

Materials of the outer jacket and sheath were selected taking reliability in space, heat and radiation resistance, into account. The calculated weight of this cable is 29 g/m, which is less than 30 % that of a conventional cable of 41 g/m weight. Fig. 4 shows a photograph of a cable.

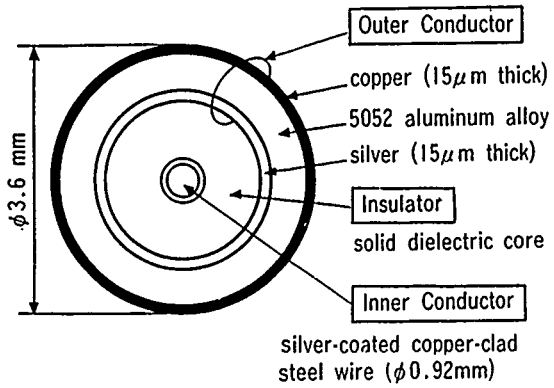

Figure 1 Cross section of the light weight semirigid coaxial cable

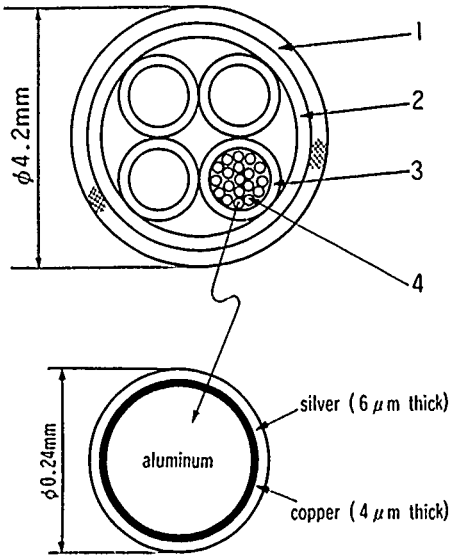

1 Outer Jacket (FEP/Polyimide/FEP)
2 Silver Clad Aluminum Braid Shield (φ0.15mm, 6×16)
3 Sheath (FEP/Polyimide/FEP)
4 Silver Clad Aluminum Conductor (φ0.24mm, 19)

Figure 3. Cross section of the light weight insulated power cable.

Figure 2 Photograph of the light weight semirigid coaxial cable

Figure 4 Photograph of the light weight insulated power cable

3. MANUFACTURING PROCESS

3.1 Semirigid Coaxial Cable

It is necessary to create a Cu/Al/Ag three layered complex pipe to obtain the light weight cable. Plating is one method to produce a multi layer pipe, but the silver plating technique over aluminum is not an established method and uniform tight inner plating for a long thin pipe is quite difficult. Moreover, neither the direct extrusion nor the drawing method is available for such a complex pipe. Therefore, *warm hydrostatic extrusion* was considered as the only possible method to obtain a sound three layer clad pipe[3].

Concerning the Cu/Al/Ag clad pipe, the inner silver layer and the outer copper layer must be clad as thinly as possible from the standpoint of weight reduction. In addition, each layer must have uniform thickness and all layers must combine together tightly to obtain good characteristics. For production of this pipe type with these severe requirements, billet conditions (shape and size), machine conditions (mandrel and die) and process conditions[4] (operation temperature and lubricant) must be carefully considered. Therefore, trial productions were carried out to find the appropriate conditions. The authors succeeded in determining the manufacturing conditions for a sufficient Cu/Al/Ag clad pipe. For this pipe, 5052 aluminum alloy was employed as the middle layer to ensure even deformability to the other two layers.

The extruded Cu/Al/Ag clad pipe was drawn and annealed before a sinking process. The annealed pipe was inserted the inner part and sunken to complete the light weight semirigid coaxial cable. Fig. 5 shows the manufacturing procedure for the cable.

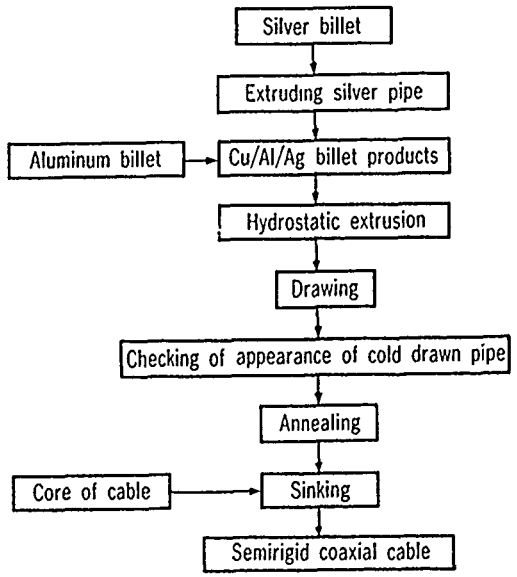

Figure 5 Manufacturing process for the light weight semirigid coaxial cable

3.2 Insulated Power Cable

The warm hydrostatic method was also employed to produce the clad wire for conductors and shield braid.

At first, an attempt was made to develop a silver clad aluminum wire, but it was found that aluminum diffuses into silver by heating during the sheathing process. Al-Ag compound formation caused by aluminum diffusion is known to be detrimental to the adherence and electrical properties of a silver layer. It is difficult to prevent aluminum diffusion because of the large diffusion coefficient of aluminum in silver[5]; therefore, the copper middle layer was introduced as a barrier.

Fig. 6 shows a relation between heating temperature and compound layer thickness. In the Ag/Cu/Al wire, Cu-Al compound is formed slightly but no Ag-Cu compound appears. On the other hand, an Ag-Al compound thick layer is formed in the Ag/Al wire. It is obvious that the copper middle layer is quite effective to suppress aluminum diffusion into silver.

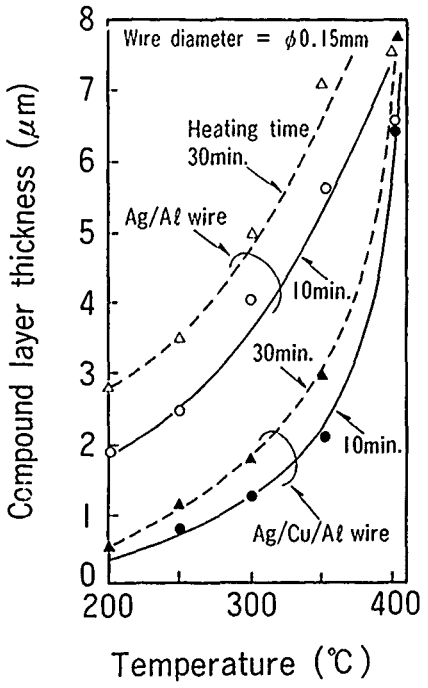

Figure 6 Temperature effect on the Compound layer thickness

The extruded wire rod is cold drawn to obtain an Ag/Cu/Al clad wire. Fig. 7 shows a manufacturing procedure for the clad wire. The clad wire is stranded, wrapped with FEP/Polyimide/FEP three layer film and heated to make a sheathed conductor. Four conductors are combined, shielded with clad wire braid, wrapped with FEP/Polyimide/FEP film and heated to complete the light weight insulated power cable.

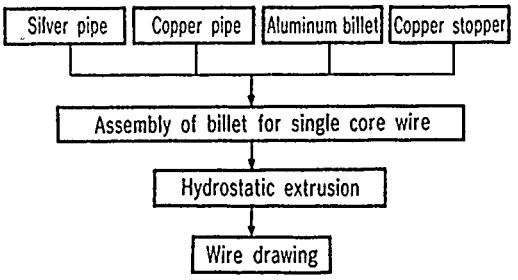

Figure 7 Manufacturing process for silver and copper clad aluminum wire.

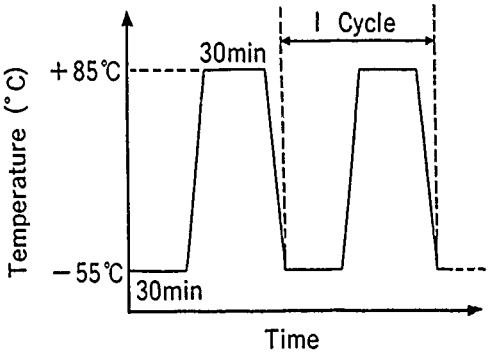

Figure 9 Schematic view of heat shock test for evaluating the effect of Satellite exposure in space

4. RESULT AND DISCUSSION

4.1 Experimental Method

It is impossible to repair communication satellites; therefore, extremely high reliability is required of their parts. Furthermore, communication satellites are influenced by particular effects, e.g., vibrations during lift-off and heat shocks caused by eclipses on static orbit. Therefore, reliability was examined by comparing the values before and after tests simulating a satellite's entire life time. Fig. 8 and Fig. 9 show conditions of vibration and heat shock tests, respectively.

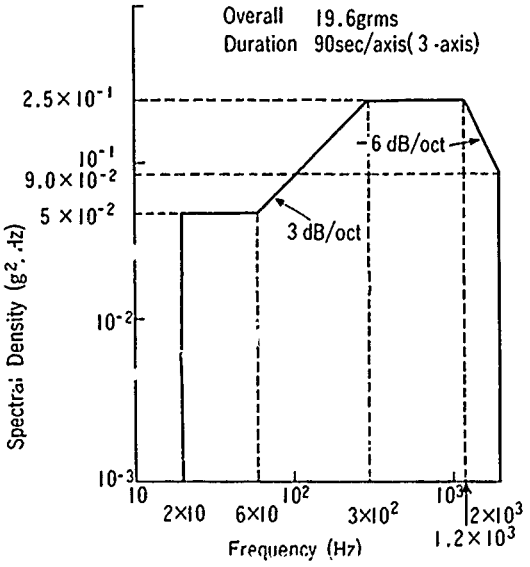

Figure 8 Condition for vibration test for evaluating the effect of satellite lift-off (random wave vibration test)

4.2 Semirigid Coaxial Cable

4.2.1 Electrical Characteristics

Characteristic impedance, measured as 51 Ω, agrees with the designed range. Attenuation and V.S.W.R. were measured after the simulation tests, and compared with initial values. The specimen was a cable 1 m long, on which there were attached connecters on both ends. It is shown in Fig. 10.

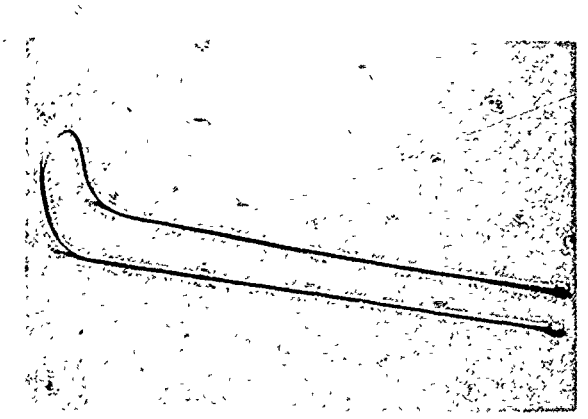

Figure 10 Photograph of a semirigid coaxial cable specimen for vibration and heat shock tests

As shown in Table 1, the absolute electrical characteristics of the Cu/Al/Ag cable were recognized to be of the same level as the copper cable both before and after the simulation tests. The connecting stability was judged to be sufficient, because the characteristic changes in the Cu/Al/Ag cable during the simulation tests were same as those in the copper cable.

4.2.2 Connecter Attaching Strength

Table 2 shows joining strength of the light weight cable (Cu/Al/Ag cable) and SMA connecter. The results in the table are compared with results from a conventional copper cable and a light weight cable with no copper outer layer (Al/Ag cable).

The Cu/Al/Ag cable has good solderability due to its copper surface, and its joining strength is stable and equal to that of the copper cable. By contrast, the Al/Ag cable has difficulties in soldering because of its aluminum surface, so the joining strength is not sufficient. Moreover, a long time is required to solder connecters. Consequently, heat effect to the insulator is not negligible.

Corrosion resistance of the Cu/Al/Ag cable is equal to that of the copper cable. The creep deformation of soldering part caused by cable's dead weight is smaller than that of the copper cable because of the light weight.

Table 1 Electrical characteristics changes of semirigid coaxial cables during simulation test

with connecters on both sides n=3

Cable \ Item		Attenuation (dB)			V.S.W.R.			Characteristic impedance
		1GHz	6GHz	10GHz	1GHz	6GHz	10GHz	
Cu/Al/Ag	Initial value	0.43	1.07	1.47	1.02	1.12	1.24	51.0
	After simulation test value	0.69	1.35	1.74	1.00	1.08	1.13	—
Cu	Initial value	0.42	1.06	1.43	1.03	1.08	1.23	51.7
	After simulation test value	0.69	1.35	1.73	1.00	1.08	1.09	—

Table 2 Connecter joining strength of semirigid coaxial cables

n=5 unit : kgf

Item \ Cable	Cu/Al/Ag clad cable		Al/Ag clad cable		Cu cable	
	Average	Standard deviation	Average	Standard deviation	Average	Standard deviation
Initial value	79.5	0.48	69.2	1.94	85.7	0.91
After vibration test value	79.0	0.63	68.6	1.15	86.4	0.63
After heat shock test value	80.6	1.07	70.1	1.84	85.6	1.18

4.2.3 Bending Characteristics

Semirigid coaxial cables are used after bending to suit the equipment arrangements; therefore, the bending radius limitation must be examined. The bending characteristics were estimated by appearance and V.S.W.R., which is the most sensitive against excessive bend. Table 3 shows the results of a Cu/Al/Ag cable bent 180 degrees around a 12~40 n m diameter (6~20 mm radius) mandrel. The results are :ompared with those of the copper cable. The examination results indicate that the Cu/Al/Ag cable can be bent over a 15 mm radius. Cables of this size are usually handled over a 18 mm (5 times the cable diameter) radius; as a result, the Cu/Al/Ag cable can be used as a wire harness.

4.3 Insulated Power Cable

4.3] :ectrical Characteristics

The electrical resistance, measured as 30 mΩ/m, agrees with the planned value. Surface transfer impedance was measured to be at the same level as that of the conventional cables, therefore, the shield effect of this cable was judged to be sufficient.

Contact resistance between the conductor and connecter was examined before and after the simulation tests to estimate the connecter attaching reliability. A 110 mm long conductor was attached to a pin contact or a socket contact of a D-Sub connecter by crimping, and the electrical resistance was measured.

As shown in Table 4, the values changed during neither the vibration test nor the heat shock test. This indicates that the contact resistance between the conductor and the connecter is recognized to be stable.

Table 3 Minimum bending radius of semirigid coaxial cables

Cable	Item	Minimum bending radius (mmR)			
		20	15	10	6
Cu/Al/Ag Cable	Outside appearance	◎	◎	○	×
	V.S.W.R	◎	◎	○	×
Cu cable	Outside appearance	◎	◎	◎	◎
	V.S.W.R.	◎	◎	◎	○

Degrees of deterioration ◎ Nil ○ Little × Much

Table 4 Connecter contact resistance of siiver and copper clad aluminum conductor

n=5

Contact type	Item		Resistance(mΩ/110mm)	
			Average	Standard deviation
Pin contact	Vibration test	Before	2.81	0.11
		After	2.82	0.10
	Heat shock test	Before	2.82	0.04
		After	2.82	0.03
Socket contact	Vibration test	Before	2.75	0.08
		After	2.75	0.06
	Heat shock tdst	Before	2.79	0.06
		After	2.79	0.06

Table 5 Connecter joining strength of silver and copper clad aluminum couductor

n=5

Contact type	Item	Connecter joining strength (kgf)	
		Average	Standerd deviation
Pin contact	Initial value	9.9	0.74
	After vibration test value	10.1	0.37
	After heat shock test value	9.8	0.46
Socket contact	Initial value	9.1	0.35
	After vibration test value	8.9	0.30
	After heat shock test value	9.2	0.64

4.3.2 Connecter Attaching Strength

Attaching strength between the conductor and the connecter was also measured before and after the simulation tests. The sheathed conductor was attached to a contact by crimping and then examined.

As shown in Table 5, the attaching strength did not change during each simulation test. This indicates that the attaching stability is recognized to be good.

4.3.3 Bending Test of Connecter Attached Part

Durability against repeated bending was examined to estimate the reliability of the connecter attached part of the conductor. The insulated conductor attached to the pin contact was repeatedly bent right and left at the attached part. The conditions were: that bending radius of 1 mm and bending angles of 90 degrees.

The time that it took to fracture was measured before and after the simulation tests, and recognized to be stable.

5. CONCLUSIONS

Light weight cables for communication satellites were newly developed. These cables employed a new construction design and utilized a warm hydrostatic extrusion method for manufacturing. Their features and characteristics are as follows.

Light Weight Semirigid Coaxial Cable

(1) A light weight 3.6 mmø semirigid coaxial cable has been created through the development of a silver and copper clad aluminum alloy pipe as an outer conductor. The silver inner layer is quite efficient because of its electrical properties and the copper outer layer is effective because of its solderability.

(2) The new cable is equal to a copper cable with regard to characteristic impedance, return loss, and the connection strength between the cable and a connector.

(3) The new cable's reliability was determined to be sufficient for use as a satellite wire harness from test results involving vibration and heat shock, which simulate satellite lift-off and exposure in space, respectively.

(4) The cable weight is 28 g/m, which is about 60 % that of a conventional copper outer conductor cable.

Light Weight Insulated Power Cable

(1) A light weight shielded and insulated power cable has been created by using a newly developed silver clad aluminum wire. The copper middle layer between the silver surface layer and the aluminum core is effective to suppress detrimental aluminum diffusion into the silver layer.

(2) The new cable is equal to copper cables with regard to electric resistance.

(3) Contact resistance at the connection between the conductor and a crimped connector remained unchanged during vibration and heat shock tests.

(4) The cable weight is only two-thirds that of a normal copper outer conductor cable for satellites.

These light weight cables are effective for reducing the weight of equipment in not only communication satellites but also other spacecraft and aircraft.

ACKNOWLEDGEMENTS

The authors would like to thank Dr. M. Seido, Mr. R. Kaizu and Mr. H. Kikuchi for the cable production and measurement, and Mr. K. Okada for the electrical measurement. We also thanks Dr. G. Yamauchi and Mr. K. Arita for their helpful suggestions and encouragement.

REFERENCES

(1) S. Saito and K. Miyauchi: "State of the Art Technology and Trends of Satellite Communications Systems", IECE Trans., **J69-B**, p.1171, (1986)
(2) A. Tsukamoto: "New Materials for Aerospace and Automotive Industries", Chemistry and Chemical Industry, **40**, p.202, (1987)
(3) M. Seido and S. Mitsugi: "Industrial Use of Hydrostatic Extrusion", J. Jpn. Inst. Light Metals, **32**, p.104, (1982)
(4) N. Inoue and M. Nishihara: "Hydrostatic Extrusion - Theory and Applications", Elsevier Applied Science Publishers, London and New York, (1985)
(5) C. J. Smithells: "Metals Reference Book", Butterworths Scientific Publications, New York, (1949)

Eiichi SAKITA

NTT Technical Assistance and Support Center

Midori-cho, Musashino-shi, Tokyo, 180 JAPAN

Eiichi Sakita graduated from junior colleges of technology of the University of Electro-communications in 1980. He joined NTT in 1968, and has been engaged in the research of evaluation for the mechanical properties. He is now a engineer of the Outside Plant Engineering Group.

Jun'ichi SEKI

NTT Technical Assistance and Support Center

Midori-cho, Musashino-shi, Tokyo, 180 JAPAN

Jun'ichi Seki received his M.E. degree in Material Science from Tokyo Institute of Technology in 1976, and then joined NTT. He has been engaged in the development of metallic parts. He is now a senior engineer of the Outside Plant Engineering Group.

THE ESTABLISHMENT OF A MODERN TELEPHONE CABLE PRODUCTION FACILITY IN A DEVELOPING COUNTRY - A CASE STUDY

Madam Zhang You Kun
Chengdu Cable Plant, Chengdu, Sichuan, China

Dr. James S. Tyler
Essex Group, Inc., Decatur, Illinois 62525

I. ABSTRACT

This paper summarizes the key elements required for the design, construction, equipping, start-up, and operation of a telephone cable manufacturing facility in a developing country based on the supply of technology from a more advanced country. The transfer of technology from Essex Group, Inc. of the United States to the Posts and Telecommunications Industry Corporation of the People's Republic of China is used as a case study to describe a systematic approach for accomplishing each key element. While the paper focuses primarily on the technical details of such a project, consideration of such nontechnical aspects as cultural and philosophical differences, governmental policies and regulations, commercial practices, and language barriers are also discussed and methods described for minimizing difficulties.

II. INTRODUCTION

It is the desire of many third world and developing countries to upgrade and expand their industrial infrastructure, especially in the area of telecommunications. Most of these countries do not have sufficient cable manufacturing capacity to meet their internal demands nor the available technology and expertise to raise the quality of their production to world standards. In such cases, they must rely on the import of cable. This is undesirable since it requires significant expenditures of limited foreign exchange. In order to increase their indigenous manufacturing capacity and, at the same time, upgrade the quality standards of their cable, many of these countries have entered into agreements, e.g., technology transfers or licenses, with more advanced countries for the establishment of modern cable production facilities within their borders.

For a technology transfer to be successful, the following key elements must be considered:

1. Organization and Administration
2. Definition of Project Scope
3. Civil Works
4. Equipment and Processes
5. Raw Materials
6. Training
7. Trial Production
8. Production Management
9. Quality
10. Technical Exchange
11. Market Support
12. Human Factors

All of these elements are interrelated, and, in the final analysis, no one factor is more important than the others. To be successful, the implementation of each element must be based on an atmosphere of confidence and mutual trust and a spirit of cooperation and mutual benefit. In the remainder of this paper, each element is broken down into its various facets and the methodology used in transferring the technology from Essex Group, Inc. to the China National Post and Telecommunications Industry Corporation is described.

III. BACKGROUND OF THE PROJECT

In December, 1978, at the request of the China National Posts and Telecommunications Industry Corporation (CNPTIC), a delegation of technical experts from the Telecommunication Products Division of Essex Group, Inc. presented a series of technical seminars on PIC telephone cable to approximately sixty of their Chinese counterparts in Beijing, China. The topics covered included modern cable design and performance characteristics, materials of construction, manufacturing techniques, equipment

design and installation and splicing methods. From this initial meeting, further technical exchanges took place between the two parties, with Essex personnel visiting Chinese manufacturing facilities and Chinese personnel visiting the plants of Essex. These technical interchanges led to commercial discussions which ultimately resulted in a signing of a Technology Transfer Agreement between CNPTIC and Essex. The Agreement, which became effective on August 15, 1982, had as its objective the construction and initial operation of a modern production facility for polyolefin insulated and integral sheathed telephone cables at the Chengdu Cable Plant located in Chengdu, Sichuan, China (hereafter referred to as the PROJECT). The new facility was to have an annual production capability of 1.2 million pair - km.

The Chengdu Cable Plant (CDC) is one of many manufacturing facilities under CNPTIC which is the manufacturing arm of The Ministry of Posts and Telecommunications (MPT) of China. Begun in 1958, CDC is the primary plant specializing in telecommunications cable. The relationship between CDC, CNPTIC, and MPT is similar to that existing prior to divestiture between the Atlanta Works, Western Electric, and AT&T. Located on a site of approximately 300,000 square meters and employing nearly 3,000 workers, CDC's main products in 1982 were paper insulated and lead sheathed telephone cable, switchboard cable, mining cable, radio frequency cable, and CATV cable.

IV. PROJECT ORGANIZATION AND ADMINISTRATION

It is critical for the successful completion of such a project that a formal project team be established, an implementation plan developed, and procedures for communication and reporting defined. Approximately one week after finalization of the Agreement between the two parties, an organizational meeting, lasting two weeks, was held at the Chengdu Cable Plant. At this meeting, the basic project plan and implementation procedures were developed. While minor modifications were subsequently made to reflect the actual situations as the PROJECT progressed, the discussions made at this meeting formed the basis of all future activities.

In anticipation of reaching an agreement, both parties had formed their own project team. Each team consisted of an overall Project Manager supported by various areas of expertise. The initial team from Essex was comprised of the Director of Engineering (the Project Manager) and two technical experts, one in equipment and process engineering, and one in plant and facilities engineering. Similarly, the team from CDC consisted of the Chief Engineer (the Project Manager) and personnel from process and equipment engineering as well as the purchasing, planning, and administrative functions. While the members of each project team varied depending on the current phase of the PROJECT, both Project Managers remained unchanged.

At this initial planning meeting, the members of each project team were brought together. Also in attendance were representatives from CNPTIC and the China National Machinery Import and Export Corporation (MACHIMPEX). While most of the individuals had already met one another, this was the first time that the entire Project Team had been assembled at one time. The areas of responsibility of each team member and the limits of their authority were defined and reviewed in detail so that each member of the team understood their individual role and that of the other members comprising the joint Project Team. Specific counterparts from each team were identified and their functional areas of cooperation defined. MACHIMPEX was identified as the organization responsible for the commercial activities and importation of equipment, raw materials, and other items not available within China. All major technical decisions were to be agreed to by both Project Managers prior to implementation.

Lines of communication were established and procedures generated to control the preparation and dissemination of information. It was agreed that all information and correspondence would be provided in triplicate. All communications and documents would be sequentially numbered and a logging procedure established. All correspondence would be addressed to each team's Project Manager. A document center was established at CDC which was staffed by an individual who organized, filed, and controlled the access to and the withdrawal of information. Similarly, office facilities were provided for Essex personnel on-site and a complete file was retained there as well.

When two parties do not share a common language, communications and a true understanding of what is being discussed becomes a critical concern. It was agreed that all correspondence and information, documentation, drawings and prints transmitted between the two parties would be in the English language. Such information already in use by Essex could use the Imperial System of weights and measures. Information prepared specifically in support of the PROJECT would, however, be provided in the Metric System. It was also agreed that drawings and prints generated in support of the PROJECT by both parties would utilize a common drafting format called True Dimensions. Formal meetings and discussions were held in China with CDC supplying interpreters and translators. Initially, Essex also provided their own interpreters, but this soon became unnecessary as confidence in the abilities of the CDC personnel and mutual trust and respect between the two parties grew.

An overall project schedule was jointly developed which was based on the experiences of Essex in constructing new facilities within the U.S. However, during the discussion it became apparent that the timing for such an activity in China would vary significantly from that expected in the United States. Using the CDC and MACHIMPEX knowledge of the governmental regulations and logistical constraints, the proposed schedule of Essex was modified to reflect the conditions prevailing in China at the time. The PROJECT was divided into phases. Phase I was for six months. During this phase, the design of the production and support facilities, quantification of utility requirements, and the specifying and ordering of equipment was to be completed. In Phase II, which was for eighteen months, the construction of all production and auxiliary facilities, the provision of all utilities, the installation and trial operation of all equipment, and trial production would be completed. In the third phase, beginning two years after the beginning of the PROJECT, the plant would go into commercial production with a ramping-up of production output occurring at a planned rate until full production capacity was achieved. GANT charts were used to define the overall PROJECT and PERT charts were generated for the major activities.

A method for project review and status reporting was developed. It was agreed that weekly review meetings would be scheduled between the Project Team members on-site. Essex personnel on-site also provided written project reports back to the U.S. In addition, the progress of the PROJECT would be reviewed by both participating Project Managers. Initially these meetings, which usually took place in Chengdu, were scheduled for every four to six weeks. As the PROJECT progressed, these meetings took place approximately every two months. Project meetings addressed the following subjects: 1) schedules reviewed and adjusted to reflect the current situations, 2) identification of new objectives, 3) responsibilities distributed, 4) overall general discussions to better understand goals and requirements.

Documentation of project status, action plans, and decisions made were an important part of these review meetings. For this purpose, two types of records were utilized. The first called a Work Protocol contained the record of major activities and agreements. Work Protocols were used to more specifically define and supplement the requirements contained in the original Agreement. As such, they needed to be signed by both Project Managers, were written in both the Chinese and English language, and became amendments to the Agreement. Work Memorandums were used to document specific project activities or technical decisions which were not addressed by the Agreement. Such Work Memorandums could be signed by the team member from each party assigned responsibility for the specific technical activity covered.

V. DEFINITION OF PROJECT SCOPE

While the Agreement described in general terms the sizes and types of products to be produced, it was necessary to specifically define the governing product specifications, pair count ranges, conductor diameters, sheath types, and product mix to be manufactured. Such details must be known in order to properly 1) identify the numbers, types, and technical requirements of the production and support equipment, 2) provide for efficient material handling, process flow, and storage, 3) determine the necessary types and quantities of raw material, and 4) identify, size, and locate the various types of utilities required.

It was agreed during the initial planning that the cable plant would have the capability of producing cables in accordance with Essex internal specifications, the cable specifications of REA and IEC SC 46C, and the national cable standards of China. Standard conductor diameters would be 0.32, 0.4, 0.5, 0.6, 0.63, 0.7, and 0.9 mm. The maximum pair count would be 3600 pair for the 0.32 and 0.4 mm conductor sizes with lower maximum pair counts established for the larger conductor sizes. Cable types would be solid insulated air core and solid and cellular (both foam and foam/skin) insulated filled cables. Figure-8 and PCM cables were also included as well as shielding configurations consisting of flat and corrugated coated aluminum and a dual shielding system of coated aluminum and coated steel. Based on historical data and market research, CDC provided product mix information showing the percentage of each product to be manufactured as a function of conductor size, pair count range, insulation type, and sheath design. It was also agreed that the factory would be equipped to produce quads (of a limited amount) as well as pairs and that the equipment would be designed to produce cable cores based on either 10 or 25 pair unit constructions.

It was further agreed that the Essex specifications would be modified as appropriate to reflect the national standards of China. Such modifications included, for example, the use of mm conductor diameters and their corresponding resistances in lieu of AWG conductor sizes, and requirements of attenuation and near end crosstalk based on the European 30 channel carrier system which operates at the Nyquist frequency of 1.024 MHz instead of the American system of 24 channels operating at 772 kHz. Essex product design engineers prepared such product specifications for CDC and these product specifications became the governing specifications for all future type approval and quality assurance activities.

All these decisions were documented using Work Protocols, and they became the basis for all future project activities relating to plant design and layout, equipment design and selection, and raw material and utility requirements.

VI. CIVIL WORKS

The initial plan for the new manufacturing facility called for the refurbishment of two existing structures, their interconnection, and the construction of various ancillary facilities. Three parties were involved in these activities - Essex, CDC and an outside company which was responsible for the civil design and physical construction of the facilities. This third party was the prime contractor for the civil works and was directly responsible to CDC. The use of an experienced construction unit was necessary since neither CDC nor Essex had sufficient expertise in the areas of civil engineering and construction. In addition, the civil construction unit had knowledge of the Chinese laws and regulations governing such construction activities. This soon became an important consideration during the design phase of the PROJECT.

As in all facets of the PROJECT, planning and review meetings were held on a regular basis with all parties involved. Essex supplied on-site facilities experts who were responsible for the sizing of the facilities; general plant layout; identification, sizing, and distribution of utilities such as electricity, water, steam, and compressed air; and the design of support facilities such as raw material storage, wire drawing solution systems, and process water cooling system. CDC assigned plant engineering and drafting personnel to work with the Essex engineers in this phase of the PROJECT. CDC also provided direct liaison with the civil construction unit. Weekly planning and review meetings were held between all three parties while more frequent meetings were held between CDC and the civil construction unit.

Such meetings were most important in the early stages of the PROJECT because of the need to identify and comply with Chinese regulations concerning the construction of the buildings and environmental considerations as well as to adopt methods and techniques consistent with the specific conditions and constraints common in China. For example, it was learned that Chinese law governing the refurbishment of an existing facility required that such a building be earthquake proof. This necessitated the demolition of one of the two structures to be renovated and its complete rebuilding. Similarly, China had regulations concerning the disposal of waste materials, which for the PROJECT was the waste wire drawing solution. Since China did not have available disposal capabilities similar to those found in the U.S., this meant that a means of treating and handling the waste drawing solution needed to be included in the design of the facility. CDC developed a three stage treatment system which incorporated de-emulsifiers, flocculating agents, and filtration media.

The most cost effective means for performing a function often differed in China from that in the U.S. Such alternative approaches were discussed among the parties and the ultimate decision included in the overall plant design. An example of this was the use of coaling towers at CDC to treat the process water whereas Essex uses a cooling pond. While the result obtained was the same, the use of the towers was more practical due to space constraints and overall cost.

Within six months of the beginning of the PROJECT, Essex provided CDC with a general plant layout, estimated utility requirements, and other basic information required for the civil design work. This information was general in nature since specific and detailed requirements could not be completely identified until decisions were made regarding the selection of the actual manufacturing and support equipment. As equipment was selected and information obtained from the equipment suppliers, this general information was revised to reflect actual requirements. In this manner, detailed plant layouts evolved showing the position of each piece of manufacturing and support equipment; storage and office areas; piping and drain locations; power steam, and compressed air supply points; lighting requirements; load requirements for overhead hoists and cranes; and specific foundation and flooring requirements.

VII. EQUIPMENT AND PROCESSES

Concurrent with the initial civil design phase of the PROJECT, the process of equipment selection and ordering was undertaken. According to the Agreement, ordering of all imported equipment was to be completed within six months. The following steps were found to be most effective in meeting this time frame.

As described in Section V, one of the first objectives of the Project Team was to define the cable types, pair count ranges, and product mix to be produced by the new factory. Based on this information, Essex prepared various scenarios of equipment and processes which could be used to meet the production requirements. Quantities of equipment required by each scenario were determined based on Essex experiences of productivity and production rates with similar processes and equipment. These experiences were an important element since the maximum machine rates and speeds quoted by various equipment suppliers are not always practical in a continuous operating mode.

The various options were jointly reviewed by the Project Team and evaluated based on productivity and quality considerations as well as overall costs. Once a decision was made as to which option to use, Essex provided CDC with a list of the quantities and types of all equipment required along with basic performance specifications and the names and addresses of at least two manufacturers of each piece of equipment. This information was used by CDC to make initial contact with potential suppliers outside China and to locate acceptable sources within China. These activities were completed in one month.

CDC then provided Essex with the technical performance characteristics of equipment already existing at CDC or available from suppliers within China. Essex reviewed this information and determined the suitability of such equipment and, where appropriate, offered proposals of how such equipment could be modified to become acceptable. These activities were completed within three months.

Concurrent with these activities, Essex prepared detailed purchasing specifications. These specifications contained not only the technical specifications and performance requirements of the equipment but also warranty terms and acceptance testing procedures. They also defined the obligations of the suppliers relative to installation, debugging, and training. This information was incorporated into Requests For Quotations (RFQ) by MACHIMPEX and CDC. A response time of one month was required. Once the quotations were received and evaluated, a delegation from MACHIMPEX and CDC together with an Essex expert visited the major vendors to resolve any technical questions and to work out the commercial issues. Essex did not participate in the commercial discussions but acted only as a technical expert and consultant.

A critical element of all the equipment specifications and RFQ procedures was the identification of types and quantities of spare parts. Here again, a knowledge of the existing situation within China was vital for determining these requirements. Unlike the U.S., for example, it was not always possible to find readily available spare parts - one could not drive down to the local hardware or electrical supply store to obtain a replacement component or call a supplier and have a part shipped in overnight. Therefore, each RFQ contained requirements for the types and quantities of spare parts to be provided based on Essex experiences, the manufacturer's recommendations, and the constraints within China.

Essex also provided CDC detailed drawings and prints of equipment, parts, and tooling of its own design. These items ranged from tooling to filling and flooding tanks. In some cases, CDC had local suppliers produce the items while, in other cases, CDC manufactured the equipment in its own workshops.

In this manner, all the major production equipment and most of the ancillary and support equipment was ordered within the first six months of the Agreement. The result was a production facility containing the most advanced equipment available at the time with the imported equipment being supplied by fourteen different companies representing seven different countries.

CDC was responsible for clearing all the imported equipment through customs and for transporting the equipment from the Chinese port to the factory site. CDC engineers installed the equipment supported by on-site Essex experts and supplier's engineers. These three parties worked together to complete the debugging, trial operation, and acceptance testing of all equipment as defined in the purchasing documents.

VIII. RAW MATERIALS

It was the desire of CDC to source, as much as practical, the raw materials used in the manufacture of the cables from suppliers within China. Based on the agreed to product mix and cable specifications, Essex provided CDC with raw material specifications for the required materials, a listing of approved sources for each material, and projected material usage figures. Usage calculations took into account project scrap rates during the term of the Agreement, being highest during the initial start-up phase of the PROJECT and decreasing as the factory reached full production.

Based on the raw material specifications, CDC contacted various raw material suppliers within China and supplied Essex with laboratory samples and their corresponding specifications. Essex material engineers evaluated these materials and either approved or rejected the materials based on their analysis. Such evaluations not only considered the characteristics of the material but its packaging as well. For example, binders must be supplied on cops compatible with the manufacturing equipment. Similarly, the packaging of bulk materials influenced the design of the material handling, transport, and storage systems within the plant. In some instances, the materials were deemed to be acceptable with modification. CDC worked with the local supplier to achieve the suggested modifications.

With some materials, it was not sufficient to judge their suitability based only on laboratory evaluations. Such considerations as processibility and their interaction with other components of the cable required the actual production of a finished product. In these cases, CDC supplied quantities of raw material sufficient to produce trial cables at Essex' own

facilities in the U.S. Jacketing compounds and metal tapes, for example, were evaluated in this manner.

For materials which could not be sourced within China, the Essex material specifications were used as the basis for importing the required materials. As was the case for the equipment, MACHIMPEX and CDC performed the actual commercial activities.

In order to limit its dependency on the importation of raw materials for which there was no acceptable Chinese source, CDC investigated methods for producing their own raw materials. This was not a new concept. For example, CDC already produced their own shipping reels, having a saw mill and metal working shop already in operation. In some cases, CDC was able to develop their own raw material production operation. An example of this was the manufacture of plastic tapes used as color and unit binders. In other cases, CDC licensed technology from foreign suppliers. For example, based on an agreement with a major U.S. producer of coated tapes, CDC constructed a facility to coat and slit metal tapes used as cable shields.

IX. TRAINING

The manufacture of any product can be likened to a 3-legged stool. One leg represents the production equipment, one leg represents the raw materials, and one leg represents the people who manage, operate, and use the materials and equipment. No matter how good the raw materials or how sophisticated the equipment, it is the people who ultimately determine the results. To a large extent, the competency of the people is determined by adequacy of the training they receive. From beginning of the PROJECT, both CDC and Essex recognized the importance of training.

At the initial joint planning meeting, a comprehensive training program and schedule was established. More than ten man-years of training were provided to CDC management, technical, and operation personnel at the various Essex locations in the U.S. The trainees were divided into three groups, each group consisting of ten people. The training period of each group was four months. The areas of training were scheduled to support the events occurring at CDC. For example, the training of maintenance personnel was scheduled to be completed prior to the installation and debugging of the equipment so that these individuals could participate in these activities. Similarly, the training of equipment operators and process engineers was timed so that they would return to CDC just prior to the equipment being placed into trial production. Hence, there was not an extended period between training and actual operation of the equipment and the trainees were better prepared to assimilate the on-site training on each specific piece of equipment provided by the equipment supplier's personnel.

Selection of the specific individuals to be trained was the responsibility of CDC with Essex acting in an advisory capacity. For each area of training, Essex provided CDC with a description of desired experience and capabilities. Written tests were provided by Essex to CDC for completion by the potential trainees. The results of these tests and the background of each trainee were reviewed by both parties and the final selection made by CDC. Essex used this information to develop specific training programs for each individual based on their level of expertise. In order to overcome the language barrier, CDC provided each trainee with classes in the English language although each group was accompanied by an experienced interpreter.

Each trainee was assigned an experienced Essex counterpart who was responsible for the trainee's education. Training consisted of lectures and demonstrations followed by actual "hands-on" experience. Training manuals were prepared for each trainee and forwarded to CDC prior to their departure to the U.S. Weekly tests and progress evaluations were prepared for each trainee to evaluate the effectiveness of the training program. In certain areas, the training at the Essex locations was augmented by additional sessions provided by equipment suppliers.

In this manner, all aspects of production management, manufacturing, and test were covered. Once these trainees returned to CDC they were able to immediately apply the knowledge they had received and to train the remaining CDC personnel. In many cases, the people who were trained in a particular function became the managers and supervisors of that function in the new facility.

Essex also provided experts to participate in the on-site training of the additional personnel at CDC. The Essex personnel provided assistance and training during the installation, trial production, acceptance testing, and commercial production phases of the PROJECT. Almost ten man-years of Essex experts were spent at CDC in these activities.

The success of the PROJECT resulted in no small measure from the dedication and competency of both the trainees and trainers.

X. TRIAL PRODUCTION

A methodology of trial production was used to verify the performance of the equipment supplied and the effectiveness of the technology transferred. Trial production involved two stages. In the first stage, major components and

complete process lines were operated by CDC personnel in conjunction with the technical staff of the equipment supplier. The performance of the equipment was compared to the quality and productivity standards specified in the purchasing documents. Once the equipment demonstrated the required performance, it was deemed to have been commissioned and was accepted by CDC.

After the equipment had been commissioned, stage two of the trial production process began. To verify the technology transferred, CDC and Essex jointly selected various cable types and sizes to be evaluated. Various conductor sizes, pair counts, and cable designs were identified. Both air core and filled cables were included with the filled cables having either solid or cellular insulation. A minimum of three reels of each cable were produced and the quality of the finished product evaluated by comparing the test results to the product specification requirements previously prepared and agreed to.

The cables were produced by CDC under the supervision of Essex engineers. As each cable type was produced and found to be in compliance with the applicable product specification, a Certificate of Acceptance was prepared for that particular design and that design was placed into commercial production.

XI. PRODUCTION MANAGEMENT

The transfer of technology to CDC did not only include the technical and manufacturing aspects of the production facility but management methods and practices as well. Management personnel from CDC were included in the groups which were trained by Essex in the U.S.

Training consisted of general introductions to U.S. management techniques which were then applied to the specific management of the Essex manufacturing and support activities. Production management concentrated on such aspects as plant organization and staffing, plant loading, manning and manufacturing standards, scrap control, quality improvement processes, training, and budgets. The Essex Commitment to Quality program was explained and the various elements of the program defined and discussed. Support functions including accounting, personnel, and purchasing were also described.

Reporting methods and procedures were explained with emphasis on the key performance indicators and their interpretation. This education in the U.S. was supplemented by Essex management staff on-site at CDC who worked directly with their counterparts during the start-up and initial production phases of the PROJECT. Both parties realized, however, that the direct application of American or Essex management practices was not always practical nor desirable due to cultural, philosophical, and political differences. Thus, the information and instructions provided by Essex was often modified by CDC to be compatible with the conditions existing in China. In some cases the techniques were directly applicable, for example, scrap control and production reporting, while in others the methods could not be applied at all and served only as background information for future reference.

XII. QUALITY

A common commitment to quality was shared by both CDC and Essex throughout the implementation of the PROJECT. People, equipment, raw materials, manufacturing processes, and finished product were all expected to "Conform to Requirements". Product specifications defined the finished product. Material specifications defined the raw materials. Performance specifications defined the equipment. Job descriptions, production standards, and operating procedures defined the requirements of the personnel and the processes. Training, both at the Essex facilities, and the on-going training program established at CDC insured that everyone knew what the governing requirements were and what was expected.

Specific training of CDC personnel in the areas of quality control and quality assurance was included in the training programs conducted by Essex in the U.S. Raw material and in-process quality control and inspection procedures were provided by Essex. Qualification and acceptance plans for raw materials and the first production of finished products were prepared. Sampling plans and test frequencies were developed based on statistical analysis of resulting data, and methods for continued quality improvement activities were documented and their applications explained. These activities were further supported by Essex quality engineers at CDC, and a detailed quality system manual was jointly prepared at CDC.

Necessary test and measurement equipment was identified and technical specifications generated in the same manner as was done for the production equipment. Calibration techniques were developed, and controls concerning the disposition of non-conforming materials, components, and finished products were established. A record keeping and reporting system was established to insure that senior management was involved in the overall quality process.

The emphasis on quality by both parties was immediately recognized. One year after the beginning of commercial production, the new production facility at CDC was awarded the Gold Medal Quality Award by the State Economic Commission. Since that time, the CDC facility has also been recognized as an Advanced

Five Year Plan by the State Economic Commission, the First Place Quality Management Award presented by the City of Chengdu, the first Quality Management Award presented by CNPTIC, an Advanced Enterprise of Quality Control by the Sichuan Province Inspection Bureau as well as many other city, provincial, and national quality and technology awards.

XIII. TECHNICAL EXCHANGE

As an adjunct to the technical activities relating directly to the implementation of the PROJECT, yearly technical exchange meetings were held between the two parties. The site of these meetings alternated between the U.S. and China. The primary purpose of these meetings was to discuss advances and trends in materials, products, processes, and equipment which were occurring within the industry. In addition, any new technology which was developed by one of the parties was shared with the other. These meetings also had a very important side benefit in that they enhanced the business and personal relationships between the two parties.

XIV. MARKET SUPPORT

Since the Chinese had limited experience with the advanced types of cables CDC would be producing in the new facility, it was most important to introduce the properties and characteristics of these cables to the end users. Besides requiring an understanding of the products themselves, information on the handling, installation and splicing was also needed.

Such information was provided CDC by Essex during the training of CDC product engineers in the U.S. In addition, Essex arranged meetings with various cable accessory suppliers in the U.S. who worked directly with CDC in these areas. Based on this information, CDC prepared catalogs and application guidelines and instructions for the end users. Technical seminars were arranged by CDC with the main end users at which Essex product and application engineers provided information on the cable designs and characteristics, installation practices and splicing techniques and demonstrated the use of splicing and terminating hardware. To further support the use of the new cable designs, CDC developed and began production of such accessories as discrete connectors and heat shrinkable sleeves for splicing.

XV. HUMAN FACTORS

The importance of the people, the human factor, in the success of the PROJECT cannot be over emphasized. Here were two companies separated not only by geography and language, but by cultural, economic, political, and historical differences. Yet both parties were able to overcome these differences because of their dedication and commitment to a common goal. The interaction of the Essex experts at CDC and of the CDC trainees in the U.S. formed bonds of mutual respect, trust, and friendship which transcended any technical differences which arose. In such an atmosphere, disagreements could be openly discussed and effectively resolved. By visiting each others families, experiencing the history and culture of the host country, celebrating national holidays, or simply relaxing together after a long day on the job, the spirit of personal and technical respect and understanding flourished.

XVI. SUMMARY

Exactly two years after the signing of the Technology Transfer Agreement between Essex and CDC, the new production facility produced its first commercial cable. Since that time, the factory has reached its goal of producing 1.2 million pair-km per year of advanced telephone cable. The quality of its products, the efficiency of its management, and the productivity of its manufacturing operations have been recognized throughout China. The technology transferred by Essex has placed CDC in the leadership position in China for telecommunications cable and technology. For both parties, the PROJECT was 大成エ力 (A GREAT SUCCESS).

XVII. ACKNOWLEDGEMENTS

The authors would like to acknowledge the contributions of Mr. Wang Nai Da of CNPTIC (retired), Mr. Zhu Ming Jiu of MACHIMPEX (deceased), and Mr. Lei Tian Xu formerly of CNPTIC whose perseverance and belief in this project made it a reality and all the staff and workers of the Chengdu Cable Plant and the Telecommunication Products Division of Essex Group, Inc. whose dedication, commitment, and technical competency made it a success.

Zhang You Kun
Chengdu Cable Plant
Chengdu, Sichuan, China

Madam Zhang You Kun graduated from Xian Jiao Tong University majoring in electrical insulation and cable technology. After graduation, she joined the Chengdu Cable Plant and has been engaged in cable design and manufacturing technology. In 1981 she was promoted to Chief Engineer and is responsible for the technical development of new products. She is a senior engineering member of the Telecom Line Committee of the China Telecommunications Society. In 1986, she was awarded the title of National Expert for her outstanding contributions in China.

James S. Tyler
Essex Group, Inc.
800 E. Garfield Ave.
Decatur,Illinois 62525

Dr. James S. Tyler graduated from the University of Dayton in 1966 with a Bachelors of Science Degree in Chemical Engineering. He received his M.S. and Ph.D. degrees in Chemical Engineering from the University of Notre Dame in 1968 and 1971 respectively. In 1973, he joined the Telecommunication Products Division of Essex Group, Inc. where he is currently Director of Engineering.

Optical Fibers for Tethered Vehicle Applications: Fiber Design and System Analyses

Marcus W. Shute, Sr.
Mickey R. Reynolds

AT&T Bell Laboratories
Norcross, Georgia 30071

ABSTRACT

The performance of various fiber designs proposed for tethered vehicle applications was evaluated. The fibers were evaluated for resistance to bend-induced loss generated at the peel point during high speed deployment using a peel point bend simulation test. Also, a non-contact method of evaluating the bend loss over the entire length of the fiber is presented. System analyses were performed to compare the system capabilities of a fiber optic guided vehicle (FOG-V) system using the different fiber designs. Also, the radiation response of the fibers was characterized at -32°C, 26°C, and 63°C.

1. INTRODUCTION

Several characteristics that optical fibers proposed for tethered vehicle applications should exhibit are resistance to bend-induced attenuation generated at the peel point, resistance to radiation-induced loss, and the potential for extended range data links. In this paper, several fibers were evaluated for resistance to bend-induced attenuation generated at the peel point during high speed deployment using a peel point bend simulation test; system analyses were conducted to compare the system capabilities of a fiber optic guided vehicle (FOG-V) system using the different fibers, and the radiation response was measured at -32°C, 26°C, and 63°C.

2. FIBER DESIGNS

Three fiber designs were considered in the scope of this work. The first design was the AT&T AccuTether 100 Fiber which is based on the depressed-clad, triangular profile, dispersion-shifted single mode fiber[1]. The second design, the AT&T AccuTether 200 Fiber, is a depressed-clad, step index, single mode fiber[2]. A third design that has been proposed for tethered vehicle applications is also considered, Fiber X, which is a matched-clad, step-index single mode fiber. Table I summarizes some of the fiber parameters for the fiber designs considered in this paper. The AccuTether 100 and AccuTether 200 have been optimized for one of the standard operating wavelengths of FOG-V data link systems, i. e. the zero dispersion wavelength coincides with one of the transmission wavelengths, while Fiber X has not been optimized for operation at either of the standard operating wavelengths.

3. PEEL POINT BEND SIMULATION TEST

A peel point bend simulation test was conducted on these fiber designs as well as a matched-clad, dispersion-shifted fiber (DSF-B) for comparison. The added loss from the insertion of a 90° bend with a bend radius ranging from 1.2 to 6.35 mm was measured at 1310 nm and 1550 nm. Table II summarizes the test results. The added loss for a 1.6 mm radius bend at 1550 nm is about 2 dB for the AccuTether 100 compared to 22 dB for DSF-B. The bend loss for Fiber X at 1550 nm with a 90°, 1.6 mm bend is 0.25 dB while the AccuTether 200 has a bend loss of only 0.06 dB at 1550 nm, under the same test conditions.

A non-contact method of evaluating the bend loss over the entire length of fiber has been developed. A bi-directional OTDR analysis is used, along with discrete measurements of the bend loss at the ends of each spool using the peel point bend simulation test, to evaluate the bend loss over the entire length of fiber. For small diameter bends, such as the bend induced in the fiber at the peel point, any macrobending loss variation along the length of a fiber is related primarily to variation in the mode field diameter (mfd). The relative variation of the mode field diameter can be observed by using a bidirectional OTDR analysis.[3] [4]

The power of the backscattered signal from the OTDR measurement is given by

$$P(z) \propto P_o\, \alpha_s(z) B(z) \exp\left[-2\int_0^z \alpha_T(x)dx\right] \qquad (1)$$

where

P_o = Launched power
$\alpha_s(z)$ = Rayleigh scattering coeeficient
$B(z)$ = Backscatter capture fraction $\propto \left[\frac{\lambda}{\omega}\right]^2$
where ω = Mode field diameter
and λ = Wavelength
$\alpha_T(z)$ = Attenuation (total).

The measured OTDR loss of the fiber is determined from equation (2).

$$\text{OTDR loss} = \frac{d}{dz}\left\{5\log_{10}[P(z)]\right\} \qquad (2)$$

The change in (2) due to a change in the total attenuation has the same sign, i.e. positive or negative, regardless of the propagation direction of the OTDR light pulse. Therefore, the

TABLE I. FOG-V FIBER DESIGNS

FIBER PARAMETERS	FIBER DESIGN		
	AccuTether 100	AccuTether 200	Fiber X
Intrinsic Loss (dB/km)			
1310 nm	0.45	0.55	0.55
1550 nm	0.25	0.30	0.30
Mode Field Diameter (μm)			
1550 nm	7.0	6.0	~6.0
λ_0 (nm)	1550	~1320	~1450
Maximum Dispersion (ps/nm-km)			
1310 nm	18	3.5	10
1550 nm	2.7	17	7

TABLE II.

PEEL POINT SIMULATION TEST RESULTS (θ=90°)					
Fiber Type	λ (μm)	Bend Radius (mm)			
		6.35	3.2	1.6	1.2
DSF-B	1.3	0.0	0.60	8.46	12
	1.55	0.23	6.20	22.2	27
AccuTether 100	1.3	0.0	0.0	0.16	0.41
	1.55	0.0	0.14	1.85	2.95
Fiber X	1.3	0.0	0.0	0.01	0.04
	1.55	0.0	0.0	0.25	0.52
AccuTether 200	1.3	0.0	0.0	0.0	0.02
	1.55	0.0	0.0	0.06	0.14

exponential decay term in (1), due to scattering and absorption, is insensitive to the fiber end from which the input pulse is launched. The backscatter capture fraction, B(z), is sensitive to local imperfections which cause changes in the mode field diameter, and depends on the OTDR launch end, i.e. the sign of the change in (2) due to changes in the $\alpha_s(z)B(z)$ term depends on the propagation direction of the light. The addition of the two semi-log OTDR signals obtained from each direction gives the imperfection line for a fiber of length L. Equation (3) describes the imperfection line where $S_F(z)$ and $S_R(z)$ are the OTDR signals in the forward and reverse directions, respectively.

$$I(z) = S_F(z) + S_R(L-z) = 10\log_{10}[\alpha_s(z)B(z)] + const. \quad (3)$$

Variations in the fiber profile imperfection line reflect changes in the mode field diameter and α_s; it has been shown that the contribution of the variation of α_s to the imperfection line can usually be neglected when compared to the contribution due to variation of the mode field diameter.[3] Since the peel point bend loss is also related to the mode field diameter (fiber profile), the fiber profile imperfection line can also be used to determine the relative variation in the peel point bend loss. Also, since α_T is related to α_s, variations in α_s would result in variations in α_T which would cause variations in the "true" loss (as determined from the slope of S_F - S_R); therefore, it is possible to separate contributions from variations in α_s and mfd. However, attributing all observed variation in I(z) to the B(z) term in (3), i.e. mfd variations, leads to a conservative estimate of the bend loss variation. The imperfection line from the bidirectional OTDR analysis along with end sample measurements of the peel point bend loss can be used to estimate the maximum bend loss over the entire length of fiber. Figure 1 shows the correlation of bend loss measurements as a function of length with profile variations along the length. The measurement error is somewhat higher at 1550 nm (≈ 0.4 dB) than at 1310 nm (≈ 0.1 dB). The data shows, within experimental error, that as the intensity of the profile imperfection line decreases, the bend loss increases. Therefore, the imperfection line coupled with discrete bend loss measurements can be used to determine the uniformity of the bend loss as a function of fiber length in addition to estimating the maximum bend loss over the entire length. This technique allows the bend loss to be evaluated over the entire fiber length without increasing the risk of damaging the fiber because of increased handling.

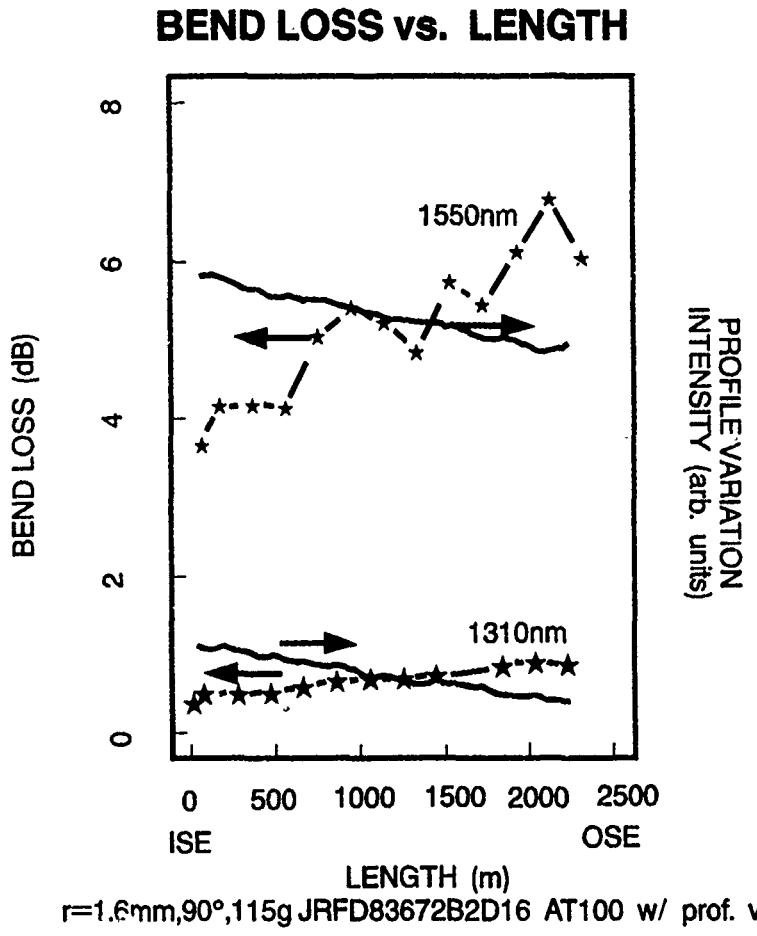

FIGURE 1.

4. FOG-V SYSTEM ANALYSES

Systems analyses were performed to determine the maximum deployment range for single and dual bobbin systems[5]. Table III shows the fiber parameters used to develop the analyses. The -32°C wound bobbin loss (intrinsic + added) and the induced loss from a single peel point was used in the single bobbin analyses; the -46°C wound bobbin loss and twice the peel point induced loss was used in the dual bobbin analyses. Digital video transmission from the vehicle was assumed to occur at 180 Mb/s and digital control signals were assumed to occur at 1-2 Mb/s. The spectral width of MLL laser sources was assumed to be 3 nm; frequency "chirp" of SLL laser sources was neglected. The mean distance between splices was 10 km. The receiver sensitivities (200 Mb/s, 10^{-9} bit error rate) used were -37 dBm and -47 dBm; -5 dBm and 1 dBm was used for the transmitter power. A 3 dB system margin was used in all cases. Tables IV and V show the maximum deployment range for various system configurations of single and dual bobbin systems. The dispersion-limited (shaded regions) and attenuation-limited region were determined. The AccuTether 100 design was optimized for lower intrinsic loss and has a higher bend loss sensitivity. This tradeoff results in higher added loss on the bobbin(s) at low temperature which dominates other loss mechanisms and is responsible for the reduced deployment range of the dual bobbin system relative to the single bobbin system. However, the AccuTether 100 design will easily support applications such as the NLOS FOG-V program. The AccuTether 200 design has the greatest possible range with conventional MLL sources and will support the 50 km range goal of aerial dual bobbin systems. It also has the greatest potential for a 100 km range using a ~1550 nm SLL WDM scheme. Fiber X requires a SLL laser source for video in order to achieve a 50 km range because of its dispersion characteristics.

TABLE III. Fiber Parameters Used in Systems Analysis				
Fiber Parameters		Fiber Type		
		AccuTether 100	AccuTether 200	Fiber X
Intrinsic Loss (typical)	1310 nm 1550 nm	0.45 dB/km 0.25 dB/km	0.55 dB/km 0.30 dB/km	0.55 dB/km 0.30 dB/km
-32°C Added Loss (single bobbin)	1310 nm 1550 nm	0.03 dB/km 0.25 dB/km	0.0 dB/km 0.0 dB/km	0.0 dB/km 0.0 dB/km
-46°C Added Loss (dual bobbin)	1310 nm 1550 nm	0.05 dB/km 0.40 dB/km	0.0 dB/km 0.0 dB/km	0.0 dB/km 0.0 dB/km
Mode Field Diameter	1550 nm	7.0 μm	6.0 μm	~6.0 μm
Dispersion (maximum)	1310 nm 1550 nm	18 ps/(nm-km) 2.7 ps/(nm-km)	3.5 ps/(nm-km) 17 ps/(nm-km)	10 ps/(nm-km) 7 ps/(nm-km)
Dispersion Slope (maximum)	1310 nm 1550 nm	0.1 ps/(nm²-km) 0.05 ps/(nm²-km)	0.1 ps/(nm²-km) 0.06 ps/(nm²-km)	0.1 ps/(nm²-km) 0.06 ps/(nm²-km)
Peel Point Loss (typical)	1310 nm 1550 nm	0.6 dB 3.0 dB	0.1 dB 0.5 dB	0.4 dB 1.0 dB
Splice Loss (typical)	1310 nm 1550 nm	0.30 dB 0.25 dB	0.35 dB 0.30 dB	0.35 dB 0.30 dB
Connectors and WDMs		3.2 dB	3.2 dB	3.2 dB

TABLE IV. Fiber/System Comparisons — Single-Bobbin Range Limitations (km)									
Fiber Design	AccuTether 100			AccuTether 200			Fiber X		
Optical Power Budget (dB)	26	32	38	26	32	38	26	32	38
1310 nm Video/1550 nm Control	18	18	18	44	55	65	33	33	33
1310 nm Control/1550 nm Video	44	55	67	19	19	19	43	47	47
1310 nm Control/1550 nm SLL Video	44	55	67	44	55	65	43	54	64
~1550 nm SLL WDM Video/Control	44	55	67	77	95	113	76	94	112

TABLE V. Fiber/System Comparisons — Dual-Bobbin Range Limitations (km)									
Fiber Design	AccuTether 100			AccuTether 200			Fiber X		
Optical Power Budget (dB)	26	32	38	26	32	38	26	32	38
1310 nm Video/1550 nm Control	18	18	18	43	54	61	33	33	33
1310 nm Control/1550 nm Video	29	38	47	19	19	19	42	47	47
1310 nm Control/1550 nm SLL Video	29	38	47	43	54	64	42	53	63
~1550 nm SLL WDM Video/Control	29	38	47	76	94	112	71	90	108

5. RADIATION-INDUCED LOSS

In tactical applications, such as FOG-V, the survivability of the system after exposure to nuclear radiation is extremely important. Usually, the fiber is the most susceptible component of the system to nuclear radiation. The radiation response of the AccuTether 100 and AccuTether 200 was measured at 1310 nm and 1550 nm using EIA/TIA-FOTP-49A, "Procedure for Measuring Gamma Irradiation Effects in Optical Fibers and Cables" at -32°C, 26°C, and 63°C. A ^{60}Co source was used to deliver 3000-6000 rads of gamma radiation at a dose rate of 50 rads/s. The radiation-induced loss generally increases as the irradiation temperature is decreased; therefore, the radiation response of the fibers at -32°C represents the worst case. Figure 2 shows the radiation response at 1310 nm and 1550 nm of the (a)AccuTether 100 and (b)AccuTether 200 after a 3000 rad exposure at -32°C. Both fiber designs exhibited excellent resistance to radiation-induced loss. Table VI lists the radiation sensitivities at 1310 nm and 1550 nm for the AccuTether 100 and AccuTether 200 at -32°C, 26°C, and 63°C. The radiation sensitivity is defined as the peak radiation-induced loss divided by the total radiation dose, and may be used to estimate the expected radiation-induced loss for doses between 0-10 krads since the relationship between the radiation-induced loss and the total radiation dose is approximately linear in that region.[6] [7]

The AccuTether 100 design was also exposed to a transient radiation environment. Figure 3 shows the radiation-induced loss at 1310 nm and 1550 nm of the AccuTether 100 design during and after exposure to a radiation dose of about 1.4×10^{10} rads(Si)/s at -32°C. The maximum radiation-induced loss was about 140 dB/km at 1310 nm and 75 dB/km at 1550 nm; after a 10s recovery period the radiation-induced loss approached zero.

6. CONCLUSIONS

Three fiber designs were evaluated for resistance to peel point bend-induced loss. A non-contact method for evaluating the peel point bend-induced loss over the entire fiber length was presented. This method will increase the overall reliability of the FOG-V system because the bend loss can be evaluated over the entire fiber length without increasing the opportunity for damage by additional handling. System analyses were performed for the fiber designs considered in this work. The AccuTether 200 offers the greatest ranges (> 60 km) using MLL laser sources and has the greatest potential of achieving a 100 km range. The radiation performance was evaluated for the AccuTether 100 and 200 designs in steady state and transient radiation environments. Both designs exhibited significant recovery after removal from the radiation field at all temperatures and radiation environments.

7. ACKNOWLEDGEMENTS

The authors would like to thank R. B. Kummer for helpful suggestions, discussions and assistance in developing the non-contact method to evaluate the bend loss over the entire fiber length. The authors would also like to acknowledge the efforts of C. L. Bice, D. F. Marcille, and H. T. Shang in support of this work.

TABLE VI. RADIATION SENSITIVITIES (mdB/(km-rad))

Fiber Design	Temperature (°C)	1310 nm	1550 nm
AccuTether 100	-32	2.0	1.4
	26	0.43	0.32
	63	0.30	--
AccuTether 200	-32	1.1	0.60
	26	0.32	0.10
	63	0.25	--

REFERENCES

1. H. T. Shang, T. A. Lenahan, P. F. Glodis, and D. Kalish, "Design and Fabrication of Dispersion-Shifted Depressed-Clad Triangular-Profile Single-Mode Fiber," *Electron. Lett.*, **21**, 201, (1985).

2. M. W. Shute, Sr., and H. T. Shang, "Optical Fibers for Tethered Vehicle Applications," *Proceedings of Department of Defense Fiber Optics Conference '90*, McLean VA, March 1990.

3. P. Di Vita and U. Rossi, "Backscattering Measurements in Optical Fibers: Separation of Power Decay from Imperfection Contribution," *Electron. Lett.*, **15**, 467, (1979).

4. M. S. O'Sullivan and R. S. Lowe, "Interpretation of SM Fiber OTDR Signatures," *SPIE Optical Testing and Metrology*, **661**, 171, (1986).

5. M. W. Shute, Sr. and M. R. Reynolds, "System Design Considerations for Tethered Vehicle Applications," *Proceedings of the Department of Defense Fiber Optics Conference '90*, McLean, VA, March 1990.

6. K. Kathiresan, M. W. Shute, Sr., M. R. Gotthardt, C. J. Arroyo, B. A. Khorramian, J. W. Shea, J. B. Fluevog, and J. W. Baumgart, "Fiber-Optic Cable for Shipboard Systems," *Proc. of 37th International Wire and Cable Symposium*, 303, (1988).

7. M. W. Shute, Sr., M. M. Michie, J. R. Duncan, and J. A. Krinsky, "The Performance of Optical Fibers in Nuclear Radiation Environments," *Proceedings of 39th International Wire and Cable Symposium*, Reno, NV, November 1990.

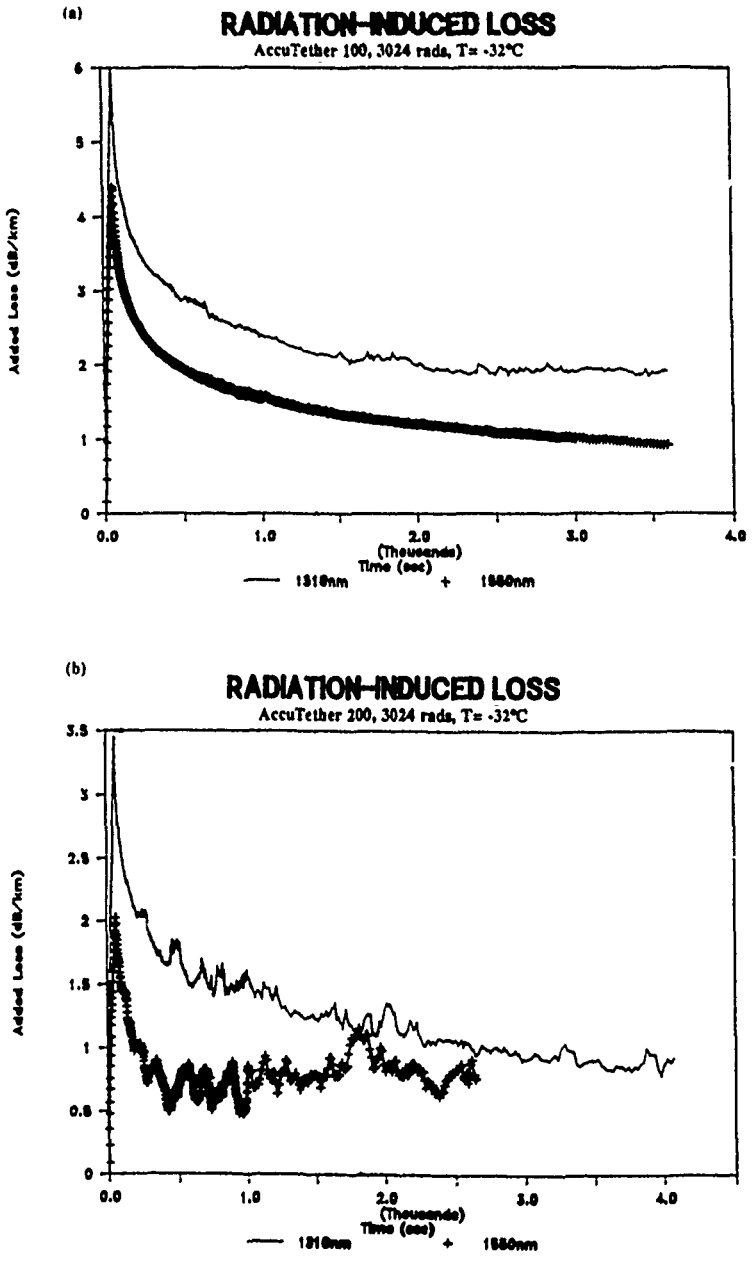
(a)
RADIATION-INDUCED LOSS
AccuTether 100, 3024 rads, T= -32°C
Added Loss (dB/km)
0
1
2
3
4
5
6
0.0
1.0
2.0
3.0
4.0
(Thousands)
Time (sec)
1310nm
+
1550nm
(b)
RADIATION-INDUCED LOSS
AccuTether 200, 3024 rads, T= -32°C
Added Loss (dB/km)
0
0.5
1
1.5
2
2.5
3
3.5
0.0
1.0
2.0
3.0
4.0
(Thousands)
Time (sec)
1310nm
+
1550nm

FIGURE 2.

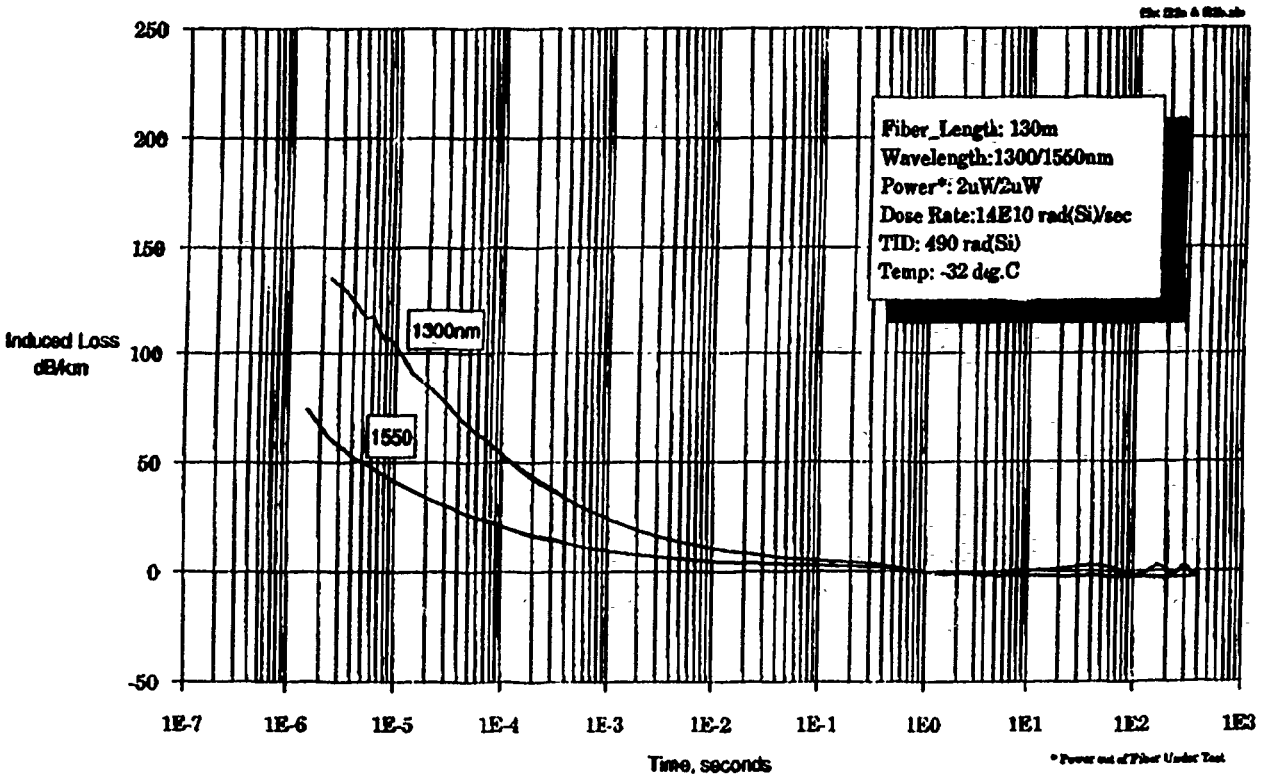

FIGURE 3.

Marcus W. Shute, Sr. was born in Sioux City, IA, on October 3, 1962. He received the B. S. degree in Mechanical Engineering from Tennessee State University, Nashville, TN, in 1984; the S. M. degree in Materials Science and Engineering from the Massachusetts Institute of Technology, Cambridge, MA, in 1986, and is currently pursuing the Ph. D. degree in Mechanical Engineering at the Georgia Institute of Technology, Atlanta, GA.

He joined the Lightguide Fiber Department of AT&T Bell Laboratories, Norcross, GA, as a Member of Technical Staff in 1986. Initially, he was involved in the evaluation of fiber properties and characterization of various optical fiber designs, including specialty fibers such as polarization-maintaining fibers. Presently, his interests are radiation effects in optical fibers, fiber optic guided vehicles, and fiber optic sensors.

He is a registered Professional Engineer in the state of Georgia and is currently, or formerly, a member of the Optical Society of America, Society of Photo-Optical Instrumentation Engineers, National Society of Black Engineers, American Society of Mechanical Engineers, Tau Beta Pi, and Omega Psi Phi Fraternity, Inc.

(photo not available)

Mickey R. Reynolds is Technical Supervisor of the Fiber Winding/ProofTesting Technology Group at AT&T Bell Laboratories, Norcross, Georgia. He joined AT&T Bell Laboratories in 1978 after receiving BS and MS degrees in Engineering Mechanics from the Georgia Institute of Technology in 1978 and 1979, respectively. His responsibilities include Fiber Optic Guided Vehicle (FOG-V) program management and product development. He earlier worked in commercial and military fiber optic cable design, single mode fiber splicing, and copper cable mechanical characterization.

ADVANCED ADHESIVE SYSTEM FOR FIBER-OPTIC-GUIDED-VEHICLE FIBER PACKAGING

B. J. Overton, C. R. Taylor, J. W. Shea, R. J. Darsey,

AT&T Bell Laboratories, Norcross, Georgia

ABSTRACT

An optical fiber product pre-coated with a polymeric adhesive material has been developed for Fiber Optic Guided Vehicle applications. The product allows the continuous, uninterrupted winding of bobbin packages. Stabilization of the package is accomplished by a post-winding thermal treatment to develop a prescribed bond strength between fibers on the bobbin. Wound bobbins stabilized with the preapplied adhesive have performed well in payout at -50, -18 and 25°C. The properties of the adhesive are stable through a lifetime storage under the Hot Climatic Type storage conditions of MIS 40921 and through the humidity aging prescribed by MIL-STD 810D.

INTRODUCTION

Fiber Optic Guided Vehicle (FOG-V) applications utilize optical fiber precision wound on a pay-out bobbin to provide communication between the vehicle and the control station. The optical fiber package must be stabilized to maintain the precision wind configuration during shipment and storage prior to use and to provide stable high-speed payout. Current FOG-V technologies in most of the industry utilize silicone adhesives for stabilizing the fiber on a bobbin. In one procedure, a solution of the silicone adhesive is sprayed over the surface of each layer of fiber as the layer is completed during the bobbin winding process. These processes result in excess adhesive in the package, which can affect fiber loss and the reliability of the payout, and expose the fiber coating to the effects of solvents for relatively extended periods. The spray-on process in particular yields a variable distribution of coating and requires a drying interval after each layer is put on to allow the solvent to evaporate from the adhesive. Winding mistakes are difficult to correct. Finally, with these systems the reliability of bobbin payout throughout the deployment temperature range has not been demonstrated to date.

Preapplication of a stabilizing adhesive to the fiber prior to winding a bobbin was proposed to address the problems inherent in other packaging techniques. In this technology, an adhesive material with appropriate properties is concentrically coated on fiber through a solution process. The solvent is immediately flashed off, leaving the adhesive in a uniform, thin layer on the fiber, Figure 1. The adhesive-coated fiber is taken up on a spool and stored until needed for bobbin winding. After precision winding, the bobbin package is stabilized by developing a controlled level of adhesion through a thermal treatment. The winding step itself is simplified and speeded up with a preapplied adhesive on the fiber, as shown schematically in Figure 2.

FIGURE 1. CONCEPT FOR ADHESIVE COATED FIBER FOR FOG–V

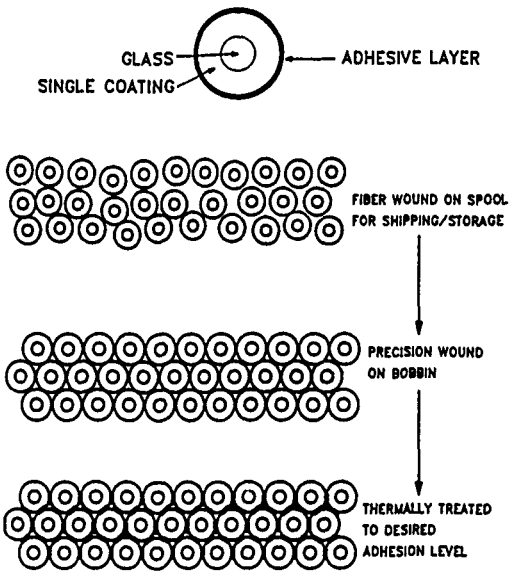

A preapplied adhesive fiber product has been developed which meets the requirements for FOG-V applications, Figure 3, and which has been successful in bobbin payout experiments at -50, -18 and 25°C as summarized in Table I. This paper focuses on the study of material properties which has led to the introduction of the preapplied adhesive product for FOG-V designs.

FIGURE 2. COMPARISON OF SPRAY-ON AND PREAPPLIED PROCESSES FOR FOG-V BOBBINS

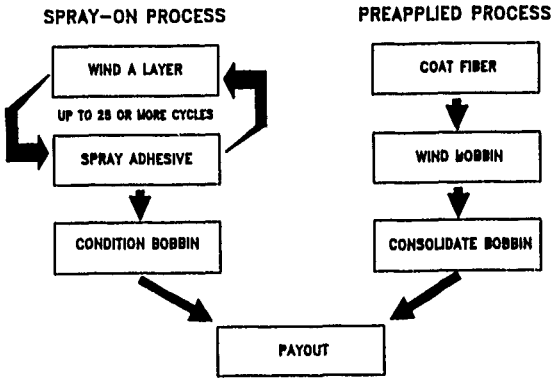

DEVELOPMENT

Materials

Several promising polymers for the preapplied adhesive concept were evaluated against the requirements listed in Figure 3. The material chosen to develop the product is referred to as "the adhesive" through the remainder of the paper.

FIGURE 3. FOG-V PREAPPLIED ADHESIVE FEATURES

FEATURE	REQUIREMENT MET
HIGH Tg	SMOOTH, RELIABLE HIGH SPEED PAYOFF -50 TO 60C
UNIFORM, THIN COATING	ECONOMY OF ADHESIVE FOR A STABLE, RELIABLE PACKAGE WITH MINIMAL EFFECT ON FIBER LOSS
SLICK SURFACE	EASE OF BOBBIN WINDING, SMOOTH PAYOFF IN BOTH "EASY" AND "HARD" DIRECTIONS
WINDING MISTAKES CORRECTABLE	EASE OF BOBBIN WINDING
NO SOLVENTS	EASE OF BOBBIN WINDING, NO SOLVENTS IN CONTACT WITH FIBER COATING
PEEL PROPERTIES INDEPENDENT OF TEMPERATURE THROUGHOUT THE DEPLOYMENT ENVIRONMENTAL RANGE	SMOOTH, RELIABLE HIGH SPEED PAYOFF -50 TO 60C
THERMALLY AND HYDROLITICALLY STABLE	STABLE PROPERTIES THROUGH STORAGE AND USE CONDITIONS

The dynamic mechanical properties of the adhesive were determined in shear with a Rheometrics™ RDS-2 instrument, measuring the elastic and viscous components of the dynamic shear modulus at frequencies from 0.1 to 100 radians/second and temperatures from 27 to 103°C. Time-temperature superposition techniques[1] [2] were applied to generate a master curve of modulus versus reduced frequency for the adhesive, Figure 4.

Processing

The adhesive is applied to the fiber in a continuous process comprising a preapplication fiber diameter monitor, an adhesive applicator, a concentricity monitor, a solvent removal system and a post-application diameter monitor. The process accomplishes the application of a consistent, thin, concentric layer of adhesive, keeping the volumetric contribution to the wound bobbin to a minimum.

FIGURE 4. MASTER CURVE AND SHIFT FACTORS FOR THE PREAPPLIED ADHESIVE

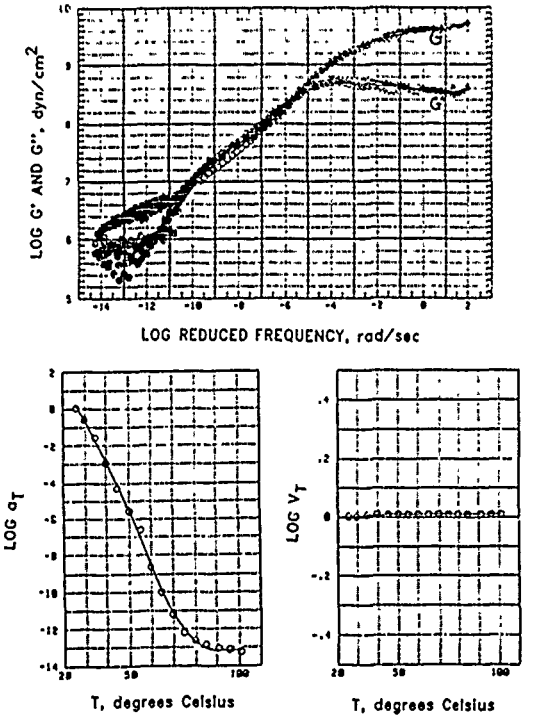

Bobbin Model

A model of the FOG-V bobbin, Figure 5, was designed in order to study effectively the relevant parameters for producing a stable FOG-V package without having to wind large numbers of actual bobbins. These mandrel packages, usually comprising 6 layers, can be precision wound rapidly with a small amount of fiber. Following the

FIGURE 5. MANDREL MODELING OF FOG-V BOBBIN

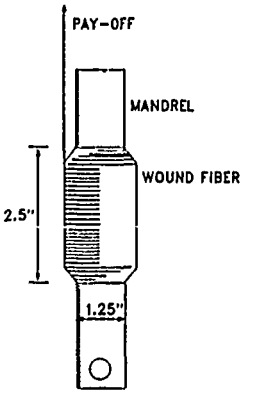

ADVANTAGES

- SMALL AMOUNT OF FIBER
- RAPID PRODUCTION
- RAPID EXPLORATION OF PRODUCTION AND ENVIRONMENTAL PARAMETERS

conditioning step, the force to peel the fiber from the package is determined with an Instron tensile tester at a peel speed of 100 inches/minute.

Package Consolidation With Preapplied Adhesive

Mandrels wound with adhesive coated fiber were consolidated (heat treated to develop adhesion between the fibers, stabilizing the package) at 70 and 80°C for various times, after which the fiber peel force was determined at 25°C. The results are shown in Figure 6, where the peel force for each layer on the mandrels is given as a function of the consolidation time. Overall, the level of adhesion developed at 80°C is virtually constant from 30 to 3000 minutes of treatment. To insure a uniform level of adhesion throughout packages while keeping thermal exposure low, a consolidation treatment of 100 minutes at 80°C is preferred.

FIGURE 6. MANDREL PEEL FORCE WITH CONSOLIDATION TIME AT 70 AND 80 DEGREES CELSIUS FOR PREAPPLIED ADHESIVE FIBER

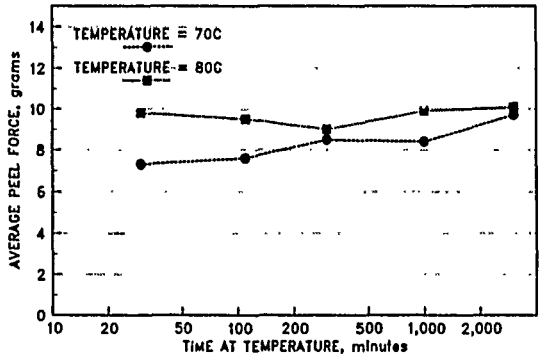

RELIABILITY

Adhesive Long-Term Mechanical Properties

MIS 40921 gives environmental criteria for Non-Line-of-Sight Fiber Optic Guided Missile reliability evaluations. The requirement for temperature extremes is 10 years storage under the Hot Climatic Type given in section 3.3.4.1 of the specification. These conditions are equivalent to 8 days at 85°C in their effects on the mechanical properties of the adhesive, as discussed below. Adhesive coated fiber was wound on a set of mandrels, which were then consolidated at 80°C for 100 minutes. These mandrels were then aged at 85°C and ambient humidity. At 8 days and 16 days, sets of mandrels were removed and peel tested at 25 and -70°C at 100 inches/minute. The peel results are shown in Figure 7.

Aging

Films of the adhesive approximately 0.2 mm thick were cast from solution. Specimens cut from the films were aged 5 days at 125°C and ambient RH, 7 days at 95°C and ambient RH, or 7 days at 95°C and 95 percent RH. The

FIGURE 7. ADHESIVE PRE-COATED FIBER ACCELERATED MECHANICAL PROPERTIES AGING MANDREL PEEL FORCE versus TIME AT 85C

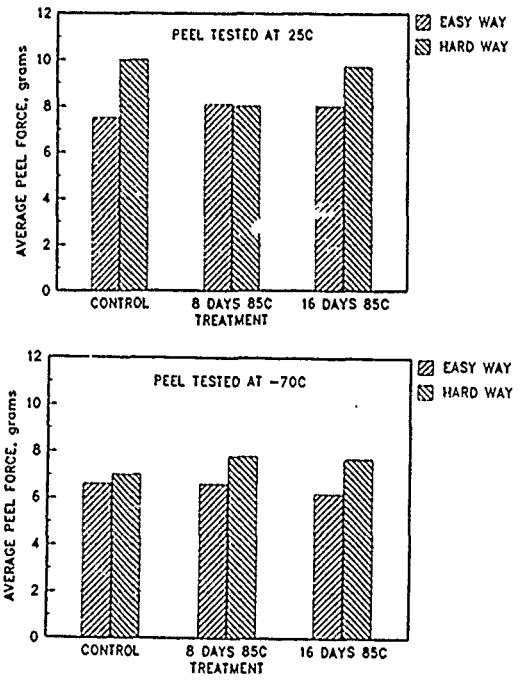

dynamic mechanical properties were measured in shear at 1 radian/second from 25 to 120°C with the Rheometrics™ RDS-2 spectrometer, Figures 8 - 10.

FIGURE 8. MECHANICAL PROPERTIES OF THE ADHESIVE AGED 7 DAYS AT 95C AND 95% RH

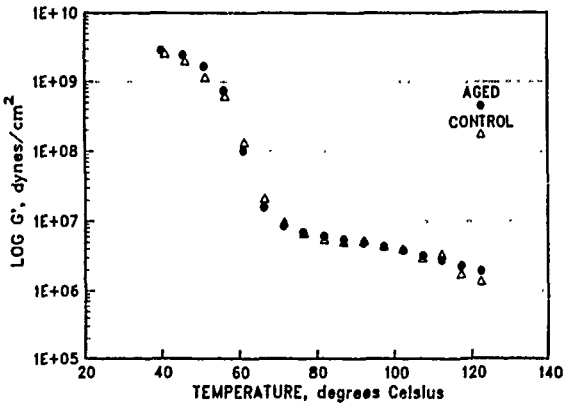

FIGURE 9. MECHANICAL PROPERTIES OF THE ADHESIVE AGED 7 DAYS AT 95C

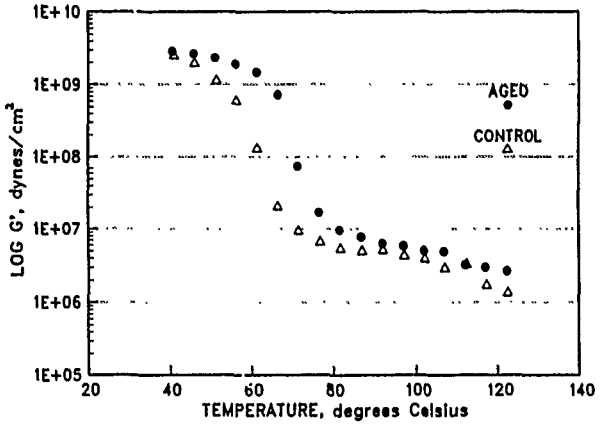

FIGURE 10. MECHANICAL PROPERTIES OF THE ADHESIVE AGED 5 DAYS AT 125C

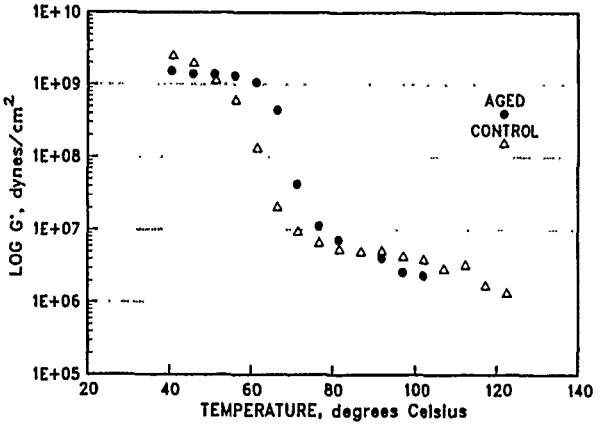

FIGURE 11. SCHEMATIC OF MIL-STD 810D TEMPERATURE/HUMIDITY CYCLE

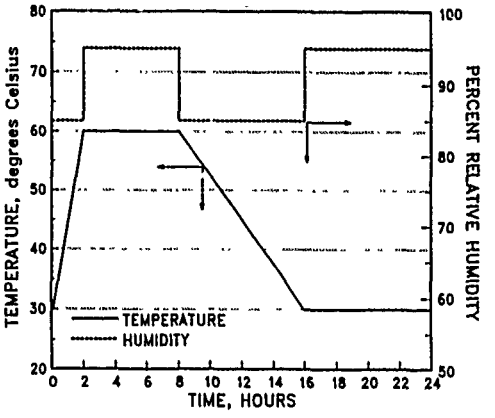

FIGURE 12. MANDREL PEEL TEST FOR THE ADHESIVE PRECOATED FIBER AFTER MIL-STD 810D TEMPERATURE-HUMIDITY CYCLING

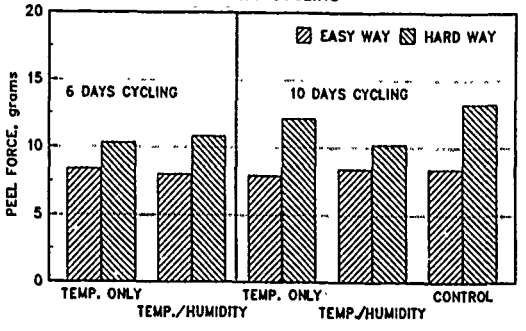

Humidity Effects on Peel

MIL-STD 810D prescribes a conditioning procedure for military materiel to test the effects of deployment in a humid environment. Figure 11 shows a schematic of the cycle. After ten cycles, appropriate properties of the test subject are to be examined. Mandrels were wound with pre-applied adhesive fiber, consolidated for 100 minutes at 80°C and placed in an environmental chamber programmed to conform to the MIL-STD 810D temperature and humidity cycling requirement. Specimens were removed and peel tested at 25°C after 6 days and after 10 days. Other consolidated mandrels were conditioned with the temperature cycle only, and also tested at 6 and 10 days. The results are in Figure 12.

Films of the adhesive were conditioned for 10 days per MIL-STD 810D to examine the effects on the mechanical properties. Microtensile specimens from these films were pulled on an Instron tensile tester at 10 mm/minute to obtain the tensile modulus and yield stress for the films before and after the conditioning (Table II).

DISCUSSION

The glass transition temperature of the adhesive is approximately 70°C, so that at room temperature the adhesive provides a slick surface to the pre-coated fiber, aiding in bobbin winding. Bobbin winding proceeds uninterrupted with no exposure of the fiber to solvents. Winding mistakes are easily correctable, in contrast to the spray-on process which stabilizes each layer as the bobbin is wound.

The stabilization of the pre-applied adhesive fiber package on a FOG-V bobbin depends on the migration of adhesive molecular segments across the boundary between adjacent, adhesive-coated-fiber turns. The rate of migration depends in turn on the molecular mobility within the polymer. Figure 13 shows how the time dependent mechanical properties of the adhesive control the process. The time scales at 25°C and 80°C are used. The material in the glassy zone of behavior exhibits very low molecular mobility and has a slick, tack-free surface, hence the pre-

coated fiber may be spooled and stored at 25°C until needed for bobbin winding. In a time scale in which the material enters the transition zone of mechanical response, molecular motion begins to increase. In the rubbery zone, polymer segments are mobile enough to cross the boundaries between adjacent fibers to a significant degree, inter-penetrating to form an adhesive bond. In the terminal zone (not shown in Figure 13) the inter-layer penetration erases the boundaries, and the adhesive coating becomes a uniform continuum between fiber segments.

FIGURE 13. MECHANICAL MODEL FOR THE DEVELOPMENT OF BONDING BETWEEN ADHESIVE PRE-COATED FIBER

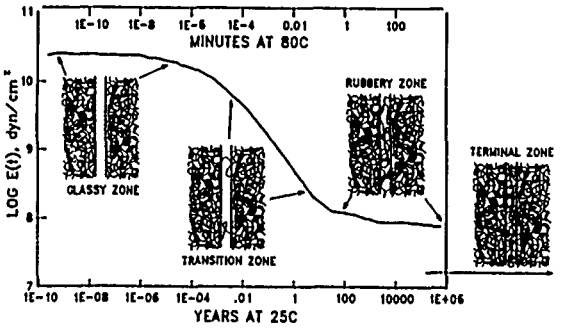

The payout properties of the adhesive are also controlled by the mechanical properties. Figure 14 gives master curves of the mechanical properties of the adhesive referenced to 25°C and to 60°C, the latter being the highest ambient temperature at which payout of a FOG-V bobbin would be required. Bobbin payout speeds of 750 - 900 feet/second induce strain rates in the adhesive layer on the fiber of 2 to 4 X 10^7 sec-1. (These strain rates correspond to frequencies of the order of 10^7 rad/second in the master curves in Figure 14.) At such rates the mechanical response of the adhesive remains glass-like from -50 to 60°C, hence the payout characteristics of bobbins stabilized with the preapplied adhesive are similar in all deployment environments.

The intent of the preferred consolidation treatment of 100 minutes at 80°C is to provide an adhesion level that is stable for very long times at environmental temperatures. The Hot Climatic Type storage environment from MIS 40921, shown schematically in Figure 15, represents the extreme thermal exposure for FOG-V bobbins. The effects of this environment may be examined through accelerated aging by applying the shift factors obtained in the treatment of the mechanical data.

Table III breaks the temperature profile of Figure 15 into the average ambient and induced temperature for each of the 24 hours in the day.[3] The sum of the times at the various induced temperatures may be converted to an equivalent time at a single constant temperature for the purpose of evaluating the effect on the mechanical properties of the adhesive. To do this the shift factors or

FIGURE 14. PREAPPLIED ADHESIVE MASTER CURVES E' versus REDUCED FREQUENCY, REFERENCED 25C AND 60C.

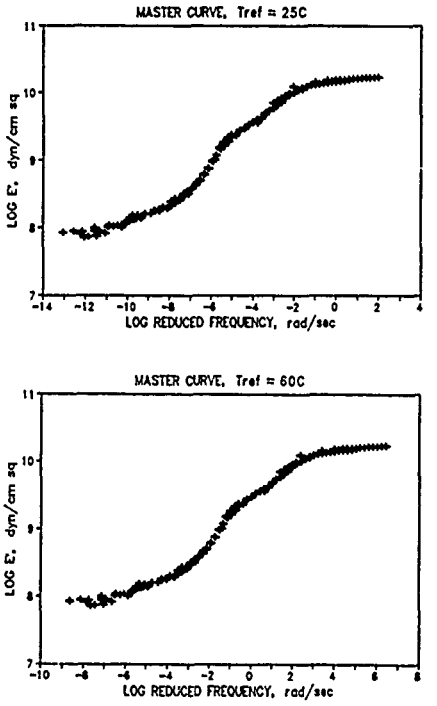

FIGURE 15. HOT CLIMATIC TYPE STORAGE ENVIRONMENT, MIS 40921, SECTION 3.3.4.1 INDUCED CONDITIONS

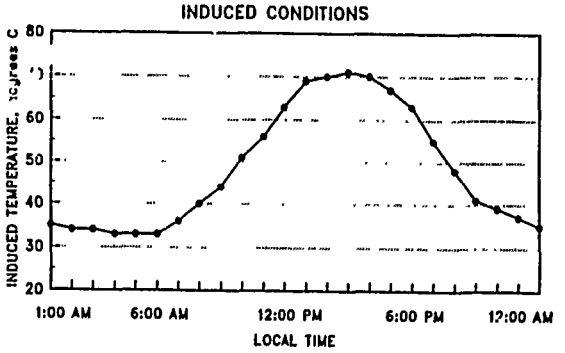

acceleration factors obtained from the dynamic mechanical properties, Figure 4, are applied as follows:

$$t(T_{ref}) = \int_T t(T) a_T dT \qquad (1)$$

where T_{ref} is the constant temperature of choice, t(T) is the time as a function of temperature describing the 24 hour temperature profile, and a_T is the shift factor at temperature T relative to T_{ref}. In this work, instead of a continuous time-temperature function the induced temperatures in Table III were used to approximate $t(T_{ref})$ by

$$t(T_{ref}) = \sum_i [t(T_i) a_{T_{ref}} / a_{T_i}] \qquad (2)$$

A treatment of eight days at 85°C is, by equation (2), equivalent to 10 years under the Hot Climatic Type storage conditions in terms of the effects on the mechanical properties of the adhesive. Mandrels wound with adhesive coated fiber consolidated at 80°C were given heat treatments of 8 and 16 days at 85°C, by equation (2) equivalent in the effect on the mechanical properties of the adhesive to 10 and 20 years, respectively, in the hot storage environment. The peel properties at room temperature and -70°C were unchanged after the treatment, Figure 7, demonstrating the mechanical stability of the adhesive in this use.

Figures 8 - 10 show the adhesive to be stable against thermal and hydrolytic chemical aging as well. These conditioning parameters are severe, but minimal impact on the mechanical properties is evident. In the 95°C/95% RH aging, Figure 8, moisture is taken up by the material, evidenced by opacity in the films, but the aged samples behave identically with the control. The effects of 95 and 125°C dry aging are similar, Figures 9 and 10. (The increase of 8 - 10 degrees in the glass transition temperature relative to the control may be due to loss of residual solvent acting as a plasticizer. This effect is under further study.)

The adhesive is also stable under the conditions prescribed by MIL-STD 810D for high temperature-high humidity environments. The bond developed between pre-coated fiber turns is found to be unaffected by the conditioning regimen, Figure 12. Likewise, the tensile properties of films treated per MIL-STD 810D show no significant change after the aging period, Table III.

CONCLUSIONS

An optical fiber pre-coated with a preferred adhesive material has been developed as a product for use in Fiber Optic Guided Vehicle bobbin packages. The product exhibits advantages in facilitating FOG-V bobbin winding, in economy of material used, in the long-term reliability of the stabilized fiber optic package, and in the reliability of the bobbin payout. The adhesive material is mechanically and chemically stable for lifetime storage and deployment in the environments specified by MIS 40921 and MIL-STD 810D.

FUTURE WORK

Second generation adhesive resins are under study for pre-coated fiber. These resins have higher T_g's than the current preferred material, which suggests the potential that the level of adhesion between fiber segments could be tailored, and that this adhesion level would be stable through the storage and use conditions required for FOG-V bobbins.

ACKNOWLEDGMENTS

The authors are indebted to other members of AT&T Bell Laboratories for help in this work; D. F. Marcille for providing optical fiber, D. J. Harper for adhesive solutions, J. A. Rennell for coating the fiber, K. W. Womack for precision winding mandrels and bobbins, and B. D. Dritschler for the peel tests on the mandrel sets. All made significant contributions to the success of this project.

REFERENCES

1. J. D. Ferry, Viscoelastic Properties of Polymers, 3rd edition, (1980, Wiley & Sons, New York).
2. I. M. Ward, Mechanical Properties of Solid Polymers, 2nd edition, (1983, Wiley & Sons, New York).
3. MIS 40921

TABLE I. PRELIMINARY BOBBIN PAYOUT RESULTS WITH USE OF PREAPPLIED ADHESIVE

	NUMBER OF LAYERS	PAYOUT SPEED, fps	PAYOUT TEMP. deg C	PERFORMANCE
1	7	750	(50)	EXCELLENT
2	9	600	(50)	EXCELLENT
3	12	600	25	FAIL (UNKNOWN)
4	25	600	25	EXCELLENT
5	21	600	25	EXCELLENT
6	31	600	25	EXCELLENT
7	25	600	25	EXCELLENT
8	21	600	25	EXCELLENT
9	21	750	25	EXCELLENT
10	15	750	(18)	EXCELLENT
11	7	750	25	EXCELLENT
12	15	750	(18)	EXCELLENT
13	19	750	25	EXCELLENT

TABLE II. ADHESIVE TREATED PER MIL-STD 810D TENSILE MODULUS AND YIELD STRESS

TREATMENT	TEST TEMPERATURE	TENSILE MODULUS	YIELD STRESS
CONTROL	25 C	172,000 psi	6100 psi
CONTROL	80 C	250 psi	110 psi
MIL-STD 810D	25 C	149,000 psi	5590 psi
MIL-STD 810D	80 C	230 psi	224 psi

TABLE III
HOURLY AVERAGE TEMPERATURES IN HOT CLIMATIC TYPE
STORAGE CONDITIONS FOR FOG–V CANISTERS

	AMBIENT TEMPERATURE	INDUCED TEMPERATURE
LOCAL TIME	degrees Celsius	degrees Celsius
0100	35	35
0200	34	34
0300	34	34
0400	33	33
0500	33	33
0600	32	33
0700	33	36
0800	35	40
0900	38	44
1000	41	51
1100	43	56
1200	44	63
1300	47	69
1400	48	70
1500	48	71
1600	49	70
1700	48	67
1800	48	63
1900	46	55
2000	42	48
2100	41	41
2200	39	39
2300	38	37
2400	37	35

DESIGN AND DEVELOPMENT OF AN IMPROVED FIELD DEPLOYABLE OPTICAL CABLE

C. S. Pegge, K. G. Hodge, M P. Knott, B. J. Elliott

BICC Cables Limited, Helsby, England

ABSTRACT

The subject of this paper is a smaller diameter, lighter weight, all dielectric optical cable with superior performance to current field deployable optical cables. This innovative development produced a cost competitive, high performance cable assembly offering a degree of mechanical integrity and user friendliness not previously achieved in field deployable cable systems.

A prototype of an improved cable system has been manufactured. Of particular note, this product offers superior crush, bend and kink resistance whilst minimising weight and diameter.

MARKET ASSESSMENT

The criteria identified as boundary conditions for the improved design were as follows;

- Four high performance 50/125 dual window multimode fibres.
- Target cable diameter of 5.2mm
- Target cable weight of 25 kg/km
- Cable assembly optical performance operating temperature range -45°C to +70°C.
- Cable sheath material qualities; flame retardant, low-toxicity, abrasion resistant and flexible over wide temperature range.
- Improved optical connector performance; facilitating fast and easy in the field repair.
- Rugged light weight cable deployment reel.

MODEL OF CABLE

BICC's current field deployable cable design employs conventional fibre strain margin to protect the optical fibres from mechanical and environmentally induced strain. In recognition of the superior behaviour of modern fibres the basis for the improved design allows the fibres to see strain. This facilitates a smaller optical unit which can be positioned in the centre of the cable structure placing the fibres closer to the neutral axis of the construction. The benefits offered by this are reduction of the fibre strain induced by cable bending and torsion and reduction of the overall size of the cable. The size and weight of the cable thus reduced enabled the strength bearing component to be incorporated without prejudicing the strength to weight ratio, a key parameter for deployable cables.

To counter the effects of compressive load it is normal practice to add a relatively high radial thickness of sheath material. Since the sheath is a major contributor to cable weight in products of this type, considerable reduction in weight can be achieved by relatively small changes in sheath thickness. Previous work[1] has shown that to increase the load carrying capacity of helically stranded elements one must interstitially fill the components so that they support and share the load when the whole structure is under lateral pressure.

Analysis of the resistance of multi-layer cylindrical structures to lateral pressure has given a method of optimising the thickness of the sheath material. The method involves balancing the pressure supported by the optical element such that no attenuation increment is observed at the total pressure specified for the cable. This balance can be achieved by varying the relative thicknesses of each of the layers. The equation used is a formula relating lateral pressure and deformation for cylindrical tubes which has been adapted to multi-layer structures as follows.

Deformation of cylindrical tube under lateral pressure:

$$\partial = 12 \left(\frac{\pi}{4} - \frac{2}{\pi}\right) \frac{(1-\gamma^2)}{E} \frac{R^3}{t^3} \frac{P}{L} \qquad \text{.....(eq.1)}$$

Where;

∂ = Total tube deformation

γ = Poissons ratio

E = Young's modulus of tube

R = Outer radius of tube

t = Thickness of tube wall

P = Lateral load

L = Length of tube under pressure

Solution for multi-layer tube:

Deformations in each layer $\partial_1, \partial_2, \partial_3, \partial_4$ to.....∂_n can be defined by equation 1 in terms of the lateral pressures supported by each layer P_i (for i = 1 to n), and the individual layer dimensions and moduli. The deformations each layer would have shown were they carrying the total load P can be calculated by putting P in the equations for ∂_i (for i = 1 to n). The resulting values of ∂ are defined as ∂_i' , these are related to the total deformation of the structure Δ by the following equation;

$$\frac{1}{\Delta} = \frac{1}{\partial_1'} + \frac{1}{\partial_2'} + \frac{1}{\partial_3'} + \ldots\ldots\ldots + \frac{1}{\partial_n'} \qquad \text{.....(eq.2)}$$

Once the overall deformation Δ has been found values of P_i can be calculated by assuming that for low lateral deformation $\Delta = \partial_1 = \partial_2 = \partial_3 \ldots = \partial_n$. This gives a method of rating the performance of different cable structures such that the pressure generated in the optical elements is at a level which will not give rise to attenuation.

CABLE DESIGN

The final design was a four fibre, rugged cable providing excellent mechanical protection within the minimum sheath dimensions, see figure 1. The prototype cable diameter is nominally 5.5mm and has a weight of approximately 27Kg/km compared with the existing BICC field deployable cable design which is 10mm in diameter and weighs 75 kg/km. Based on the experience with the prototype there is scope to reduce the size and weight of this cable further.

Fibre

The fibre type selected was a high proof tested (>1.5%) 50/125 µm fibre with a multi-buffered secondary coating up to 850µm, offering good mechanical protection and wide temperature performance. The optical and geometrical parameters for the fibre are as follows;

Attenuation	:	0.8dB/km maximum at 1290nm±30nm
Bandwidth	:	500MHz.km (measured on 1km length) at 1290nm ±30nm
Chromatic dispersion	:	6ps/nm.km maximum
Numerical aperture	:	0.22±0.02
Core diameter	:	50µm ± 6%
Cladding diameter	:	125µm ± 2.4%
Primary coating diameter	:	250µm ± 6%
Proof test level	:	1.5 %

Inner Sheath

An inner sheath is incorporated in the cable design to increase protection of the fibres from compressive forces. The inner sheath achieves this in two ways, firstly it locks the quad structure together such that the tight buffer units share the load imposed. Secondly, the inner sheath material is cellular, the inclusion of 60µm diameter air bubbles (40% by volume) in the material has the additional effect of cushioning the fibres from lateral pressure. The use of a cellular material also has the benefit of being low in density.

The circular section provided by the inner layer has the benefit of providing a surface around which to distribute the strength member evenly. It is essential to have a uniform formation of strength member because it gives the cable a good tensile performance and permits the loading of the cable whilst in torsion or bending.

Strength Member

The requirement was for a non-metallic, high specific modulus material which is easily terminated. An aramid-polymer yarn was an obvious choice for the strength member for a cable of this type. The optical fibres were placed as close to the centre of the cable as possible in order to minimise strains induced by bending so the use of a central strength member was therefore precluded. Serving the aramid yarn around the inner sheath provides a good tensile strength whilst maintaining cable flexibility.

The cable tensile strength is designed to limit fibre strain to 0.50% at 1,300 Kg. The 0.50% level equates to $\frac{\sigma}{3}$, where σ is the fibre proof stress level chosen to ensure satisfactory fibre lifetime.

Outer Sheath

The harsh environment in which this cable will have to operate demands a superior sheath material. Features identified in which the sheath material must excel were, flexibility (especially at low temperatures), flame resistance, low density, high tear resistance and good water resistance. It was also essential that the sheath material was suitable for internal and external applications.

A matrix was drawn up, evaluating several commercially available materials against the requirements identified. From this evaluation a flame retardant polyurethane material was selected.

SELECTION OF TERMINATION SYSTEM

Field Deployable Cable Connector Requirements

- Maximum number of channels 4
- Maximum insertion loss 2dB with 50/125 fibre
- Hermaphroditic construction
- Expanded beam optics
- Ruggedised to military specifications
- Field terminable

Features of Chosen Connector System

The Stratos 900 series connector (figure 2) was chosen following a thorough evaluation of suitable connectors. No other military connector fully satisfied all the requirements. The ease of termination compared to other connectors was also an important factor [2].

The Stratos 900 series uses ferrules from standard 430 series single fibre connectors which use the well established 3-ball alignment technique. The 430 series connector is one of the standard multimode connectors which has been used by British Telecom in the junction network.

These alignment ferrules or inserts fit into the rear of a precision machined body which houses up to four expanded beam lenses. The geometry of this body is optimised with the optical properties of the graded index rod lenses during manufacture.

This approach of using standard alignment ferrules and a factory optimised lens body means that the connector can be terminated with the minimum of special tooling and skills. It is merely a matter of terminating the fibres onto four standard ferrules, mounting these into the lens body, and assembling the connector rear end.

DESIGN OF CABLE DEPLOYMENT REEL

Key parameters for the cable stowage and deployment reel were low weight, ease of access to each cable end, safe stowage of the connectors and good ergonomics for user handling.

The eventual design (see figure 3) was a pressed metal construction which offered high mechanical strength with a surprisingly low net weight (<10kg for a capacity of 500m of cable).

CABLE MANUFACTURING TRIAL

The production of a cable of this type lends itself to some tandemisation of processes. However, for the purpose of the prototype manufacturing trial each operation was carried out individually in order to evaluate the effect on fibre performance. A summary of the attenuation results compared before and after manufacture is included, see figure 4.

The inner sheath compound was selected by looking for a cellular material of a significantly lower processing temperature than the melt temperature of the fibre secondary coating. This was done in an effort to ensure no effect on fibre attenuation and easy separation of the fibres from the inner sheath. In order to minimise cable diameter a target thickness for the inner sheath was 0.2mm. The extrusion conditions for this process were critical because dimensional control and degree of 'blow' of the cellular material were competing requirements.

During the laying up of the aramid-polymer yarn the tension control on the centre element and the strength members was adjusted to give the required load bearing characteristics in the finished cable. The tension settings were checked and adjusted throughout the operation because of the decision to run each process of the cable manufacture separately for the trial.

A special precaution must be made at final sheathing to dry the cable before extrusion. It was thought necessary to run the cable through a heater tube on line to drive off any additional moisture but this proved unnecessary. The extrusion conditions were controlled to keep sheath retraction to a minimum. It is known that retraction can have an adverse effect on cable low temperature performance.

CONNECTOR SYSTEM TRIAL

Termination Trial

The cable design was well suited to the chosen connector system. No difficulties were encountered with the termination trials. The termination of the optics uses a standard ferrule type, because of this failures at this stage are rare. Consequently the projected yield figures for this connector are very high.

Connector Qualification

The connector has been subjected to a comprehensive programme of mechanical and environmental tests. These tests include temperature and humidity exposure for prolonged periods, 2500 matings without degradation of optical performance, vibration and water immersion to 1m. Considerable numbers of connectors are in service and feedback to the connector supplier has so far been very favourable.

CABLE TESTING

The full cable test programme consists of five groups, optical, cable physical, materiai, cable environmental and material environmental. The tests have been selected from the British MoD's Defence Standard 60-1. This MoD standard is a generic document from which suppliers can select a relevant subset of cable test methods. The test programme for this product is detailed below;

DEFSTAN 60-1 clause	Parameter to be measured	Relevant Specification
Optical Tests		
A1	Spectral attenuation (fibres & Cables)	BS 6558 Part 1 App D
A2	Radiation angle NA	BS 6558 Part 1 App D4
A3	Bandwidth	BS 6558 Part 1 App D3
A4	Refractive Index Profile	BS 6558 Part 1 App D5
Cable Physical Tests		
B2	Cable Tensile Strength	BS 6558 Part 1 App E3
B3	Cable Torque Test	BS 6558 Part 1 App E7
B4	Cable Flexing Test	BS 6558 Part 1 App E6
B5	Cable Bend Test	BS 6558 Part 1 App E4
B6	Cable Crush Test	BS 6558 Part 1 App E9
B7	Cable Cyclic Bend	BS 6558 Part 1 App E5
B8	Cable Impact Test	BS 6558 Part 1 App E8
B9	Strain Member Security	
B12	Cable Sheath Creep	
B13	Cable Abrasion Test	BS 6558 Part 1 App E2
B14	Dynamic Cut Through	BS G212 2.14.4
B18	Flammability	BS G230 test no. 28a)b)
B21	Cable Snatch Test	BS 6558 Part 1 App E10
N/A	Knot Test	E1A RS-455, FOTP 87
Materials Tests		
B15	Notch Propogation Test	BS G230 test no. 27
B16	Thermal Ageing	BS5691:Part 1
B17	Ageing in Air	BS G212:2.6
B20	Tear Resistance	B6469

DEFSTAN 60-1 clause	Parameter to be measured	Relevant Specification
Cable Environmental		
C.1.1	A. Cold	BS 2011:2.1
C.1.1	B. Dry Heat	BS 2011:2.1
C.1.1	Ca. Damp Heat	BS 2011:2.1
C.1.1	Db. Damp Heat	BS 2011:2.1
C.1.1	N. Change of Temperature	BS 2011:2.1
N/A	Ice Crush Test	DOD STD 1678 Method 4050
Material Environmental		
C.2.5 & C.1.1	R. Resistance to Fluids	BS 2011:2.1
C.1.1	J. Mould Growth	BS 2011:2.1
C.1.1	Sr. Radiation	BS 2011:2.1
C.2.1	Smoke Index	NES 711
C.2.2	Toxicity Index	NES 713
C.2.3	Oxygen Index	BS 2782 part 1 method 141
C.2.4	Temperature Index	NES 715

CABLE TEST RESULTS

There follows a selection of test results from the comprehensive range detailed above.

Impact Test

Severity	20 impacts of 2.5Nm impact energy at -45°C, ambient and +70°C.
Pass/fail criteria	Maximum attenuation change ±0.05dB after testing.
	No permanent damage to cable or components

The major challenge encountered in this test was to sample the optical data fast enough to pick up the transient effect of the hammer impact on the cable. Computer aided data acquisition was used to store the data, a sampling interval of 100ms was the limit of the output of the optical power meter that was used. Typical results were as figure 5.

No significant difference in results was observed at either -45°C or +70°C. Cable samples examined after testing showed no visible permanent damage.

Cyclic Bend

Severity	3500 cycles, 10kg load, rate 1 cycle/second
Pass/fail criteria	Maximum attenuation change ±0.05dB
	No permanent damage to cable or components

Figure 6 shows the typical attenuation change monitored during a cyclic bend test.

Compression Resistance

Severity	1000N on a cable sample length of 50mm. Hold load for 10 minutes
Pass/fail criteria	Maximum attenuation change ±0.05dB
	No permanent damage to cable or components

The mean attenuation results from five compression tests is shown in figure 7, the maximum recorded attenuation change in any one of the tests was 0.05dB. The results are statistical in nature because of the effect of geometrical positioning of the fibre being monitored relative to the compression plates.

CONCLUSIONS

An improved field deployable optical cable assembly has been successfully developed. The cable performance is superior to previous designs and through exhaustive testing a thorough understanding of the limits of the new product has been established. With this knowledge of margin on the performance the cable design has been optimised to the minimum required size and weight. By virtue of this optimization this product represents a cost competitive solution to the user.

The targeted market for this product is in the military sphere. However, many commercial opportunities now exist. The rugged construction and high reliability of this light weight optical link lend it for use in areas such as building construction, security, and geophysical applications. Rapidly deployable optical cables could also provide reusable temporary repair links for fixed terrestrial optical installations of all types.

The future for field deployable cables lies in the use of even more strain tolerant fibres and smaller cabling packages. One could envisage the ultimate system of a fibre or fibres, embedded in a single matrix which performs all the functions of the current cable components and lends itself to full flexible restoration for field repairs. Development in new materials is already providing potential composities and compounds to fulfil such a role.

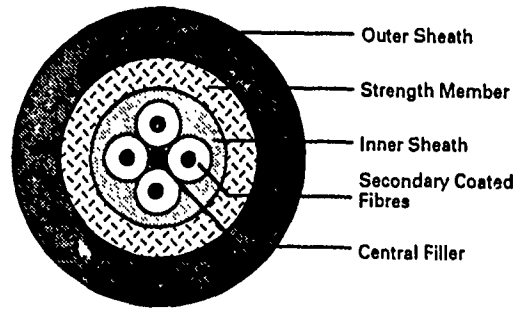

Figure 1: Cable design

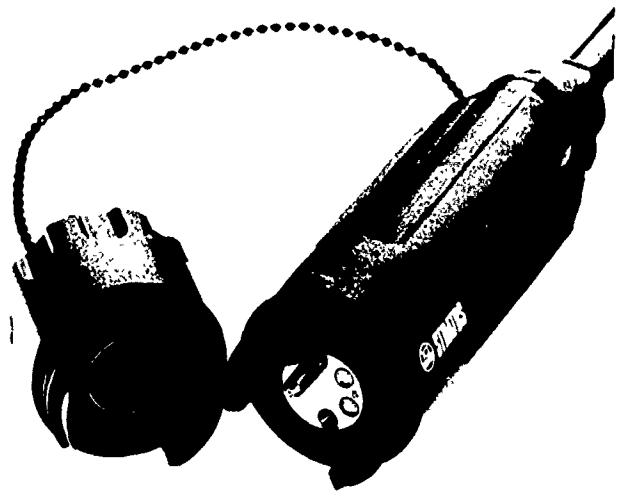

Figure 2: Stratos Hermaphroditic Expanded Beam Connector

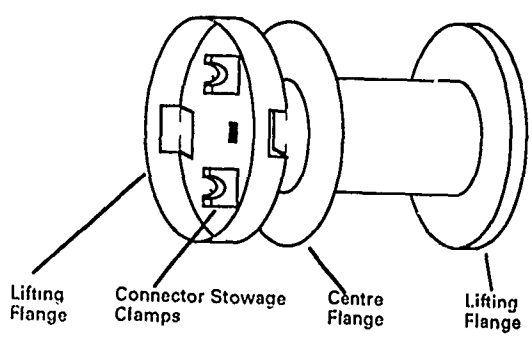

Figure 3: Cable Deployment Reel

Attenuation @ 1300nm (dB/km)				
	Fibre Colour			
Stage	Orange	Blue	White	Red
As delivered	0.43	0.68	0.68	0.51
After Manufacture	0.54	0.78	0.74	0.58

Figure 4: Attenuation Summary For Development Cable

Figure 5: Typical Impact Test Results

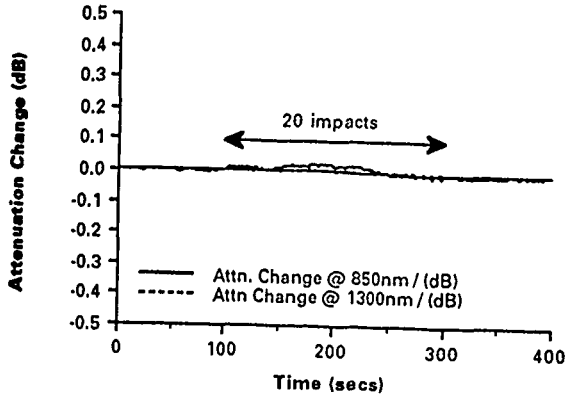

Figure 6: Typical Cyclic Bend Test Results

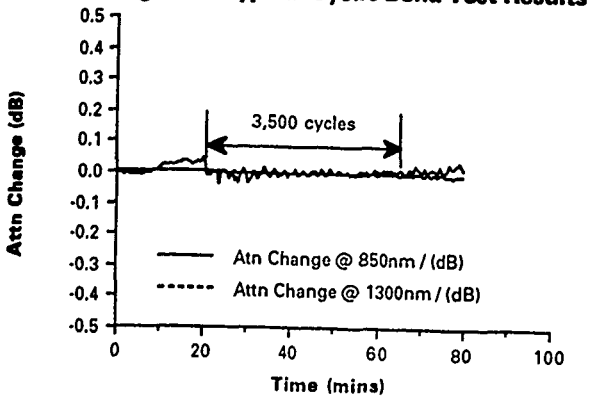

Figure 7: Average Compression Test Results From 5 Measurements

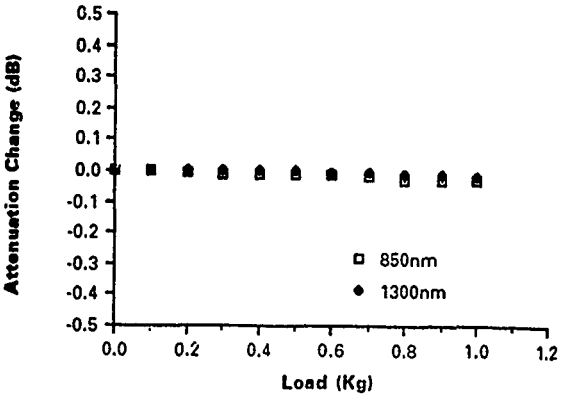

Acknowledgements

The authors would like to thank Ian Knight for co-ordinating the many hours of testing carried out on this product and Martin Davies for performing and evaluating the termination work on the prototype assemblies. Finally the assistance of Andy McKeown of the Optical Cable Manufacturing unit is greatly appreciated for his effort in getting the many process trials succesfully completed.

References

1."Designing Compression Resistance in Loose Tube Cables", P. E. Neveux, W. H. Hatton, IWCS Proceedings 1987.

2."Development of a Ruggedised, High Performance, Field Terminable, Expanded Beam Connector". SPIE O-E/Fibre '87 Symposium on Fibre Optics and Integrated Optoelectronics, San Diego, August 1987.

3. "Optical Cable Deformation Characteristics Under Lateral Load". N. Mitsun ıga, U. Katsuyama, Y. Ishida, IEEE J. J64-B No.2, February 1981.

C. S. Pegge

Chris Pegge has worked in the field of optical cable and connector technology since graduating from Bristol University with an honours degree in Mechanical Engineering in 1985. He joined BICC in 1988 and currently holds the title of Group Leader, Optical Cable Design within the Helsby Technology Centre. This centre provides a central research and development facility in optical and advanced material technology for the BICC Group worldwide.

K. G. Hodge

Ken Hodge graduated from Liverpool University in 1981 with a B.Eng in Mechanical Engineering. After two years spent on BICC's graduate trainee scheme he joined the company as a development engineer in short haul cabling. He has been involved in optical fibres since 1983 and is now Senior Optical Cable Design Engineer in the Helsby Technology Centre.

M. P. Knott

Mike Knott is Senior Interconnect Engineer, Helsby Technology Centre, BICC Cables. He received his B.Sc. in Mechanical Engineering in 1985 at UMIST, and has been involved in fibre optics since 1987. He is currently involved with the development of optical interconnect components.

B. J. Elliott

Barry Elliott graduated from Kent University with a degree in Communication Engineering in 1982. He is a Chartered Electrical Engineer and a member of the Institution of Electrical Engineering. He is currently Product Marketing Manager in the DataComms and Defence Unit of BICC Cables' Communications and Electronics Division.

A FOUR-FIBER TACTICAL CABLE

W. S. Liu and K. Kathiresan
AT&T Bell Laboratories
Norcross, Georgia 30071

J. B. Fluevog
AT&T Network Systems
Norcross, Georgia 30071

ABSTRACT

The design and development of a four optical-fiber cable for use in tactical applications have been completed. Development effort was guided by the detailed performance criteria given in the military specification DoD-C-85045C, "General Specification for Fiber Optics Cables (Metric)". The cable employs a 50/125 μm radiation-hardened multimode fiber. The cable outer diameter is 5.85 mm. It has a tensile rating of 1780 N, and it has an operational temperature range of -46 ° C to 71 ° C. The cable design is similar and a complement to the single- and two-fiber single-mode and multimode tactical cables previously developed for the U.S. Army. The four-fiber tactical cable was tested to the specification requirements and the results of optical, environmental and mechanical performance tests are presented in this paper.

INTRODUCTION

The design and development of a four optical-fiber cable for use in tactical fiber-optic applications have been completed. The military specification DoD-C-85045C, "General Specification for Fiber Optics Cables (Metric)", provided the performance requirement guidelines for the design and development of the cable. The cable was developed for use in radar remoting, robotic vehicle control/communication, and other general tactical communication system applications. The cable uses a 50/125 μm core/cladding radiation-hardened multimode fiber. Prior to cabling, the fibers are prooftested to 690 MPa (100 ksi). This multimode cable can be operated at both the 850 nm and 1300 nm wavelengths.

The operating temperature range for this cable is -46 ° C to 71 ° C. The design criteria for the four-fiber cable are similar to those used for the single- and two-fiber single-mode and multimode tactical cables previously developed for the U.S. Army CECOM.[1] [2] [3] The design, development and performance test results for the four-optical-fiber tactical cable described above are presented.

CABLE DESIGN

The cross-sectional view of the four-fiber tactical cable design is given in Figure 1. The cable design is all-dielectric and uses the 50/125 μm radiation-hardened multimode fiber. The fiber is coated with a dual acrylate coating which is mechanically strippable. The fiber is then tight-buffered to a 0.9 mm (.035 inch) diameter. The buffered fibers are color-coded with blue, orange, green, and brown colors for identification purposes. These buffered fibers, which comprise the cable core, are placed in the cable in the same color sequence given above. The buffering material is also mechanically strippable in order to facilitate repair and connector termination in the field. The buffering material was chosen to minimize microbending losses induced by exposure of the cable to temperature extremes of -46 ° C and 71 ° C and to meet the stringent mechanical performance requirements. Aramid yarns, which are the main tensile-load-carrying members, are stranded over the buffered fibers. Appropriate amount of aramid yarns is used to attain the 1780 N tensile rating. A flame-retardant polyurethane outer jacket is then extruded over the aramid yarns.

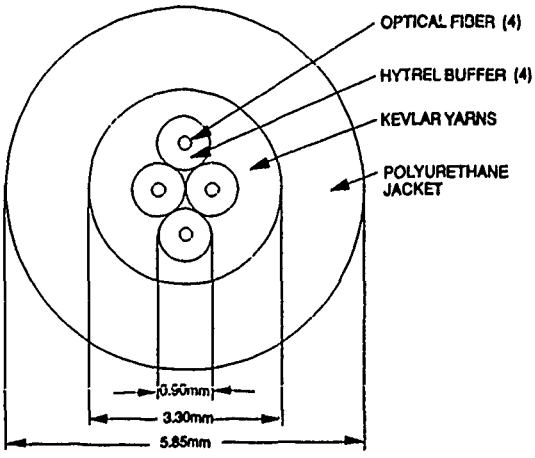

FIGURE 1. Cross Section of Four-Fiber Tactical Cable

PERFORMANCE

The cable was subjected to all the required optical, environmental and mechanical performance tests. The fiber was also subjected to a battery of optical, mechanical and dimensional requirements before it was used in the cable. Typical results of fiber performance tests can be found in Reference 4. This reference contains temperature cycling and accelerated aging test results for coated fibers as well as buffered fibers. Thus, performance was evaluated both for the finished cable and the individual components. In the cable performance evaluation, three cable samples were used for each environmental and mechanical test.

First an attenuation test was conducted for the finished cables. Typically the cables were manufactured in 1-km lengths. The attenuation rate results for multimode cables at 850 nm and 1300 nm are given in Figure 2. The requirements are 3.75 dB/km at 850 nm and 1.5 dB/km at 1300 nm. The cable was then subjected to a battery of environmental and mechanical tests. These tests are enumerated in Table I.

TABLE I. BATTERY OF ENVIRONMENTAL AND MECHANICAL TESTS

ENVIRONMENTAL	
1. TEMPERATURE CYCLING	3. LONG-TERM AGING
2. HUMIDITY CYCLING	
MECHANICAL	
1. TWIST BEND	6. KNOT
2. CYCLIC FLEXING	7. RADIAL COMPRESSION
3. IMPACT	8. TENSILE STRENGTH
4. COLD BEND	9. OPERATING TENSILE LOAD
5. FREEZING WATER IMMERSION	10. FLAMMABILITY

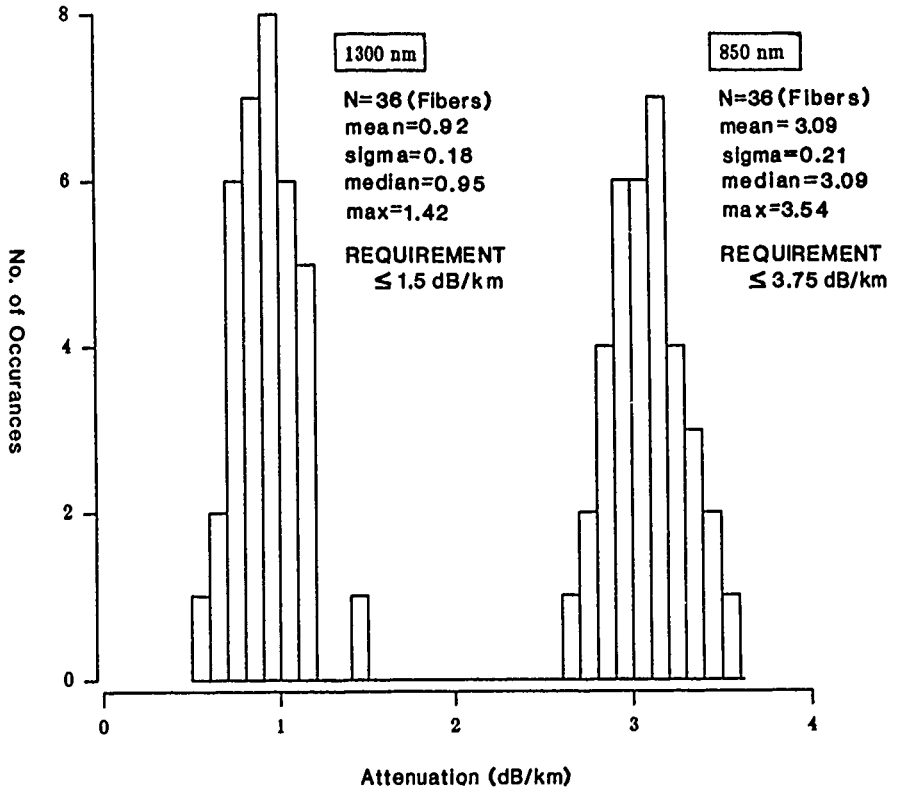

FIGURE 2. Four-Fiber Tactical Cable Attenuation

The three primary environmental tests are temperature cycling, humidity cycling, and accelerated aging. The temperature cycle used for the cable evaluation is presented in Figure 3. The temperature range requirement for tactical cables is from -46 ° C to 71 ° C. The results of temperature cycling for the four-fiber tactical cables are presented in Figures 4 and 5 for 850 nm and 1300 nm wavelengths, respectively. The maximum allowed increase in attenuation rate for multimode cables is 0.5 dB/km at both 850 nm and 1300 nm wavelengths. The results are given for five temperature cycles. The cable meets the requirement showing excellent performance.

The humidity cycling used for the cable evaluation is presented in Figure 6. In the humidity cycling, the cable is subjected to a constant relative humidity of 94±4% and cycled between the temperatures of 20 ° C and 65 ° C. The maximum increase in attenuation rate requirement for the humidity cycling is also 0.5 dB/km at both wavelengths. The results for five humidity cycles are presented in Figures 7 and 8 for 850 nm and 1300 nm wavelengths, respectively. There is practically no increase in attenuation rate at either wavelength.

The accelerated aging test consists of subjecting the cables to a temperature of 110 ° C for 10 days. This test temperature and duration simulates the mechanical response of the cable materials to an exposure of 85 ° C for the design life of 20 years. This simulation criterion was arrived at using the viscoelastic mechanical properties equivalence principle described in Reference 5. The results of the accelerated aging tests are presented in Figures 9 and 10 for 850 nm and 1300 nm, respectively. The added loss requirement for accelerated aging tests is the same as those for the temperature cycling and humidity cycling tests. These results show excellent performance of the cable in the accelerated aging test.

The cable was also subjected to the required mechanical tests listed in Table I. Table II presents the results and the requirements of mechanical tests for the cable at the primary wavelength of 1300 nm. As can be seen from the table, the cable either meets or surpasses all the mechanical requirements.

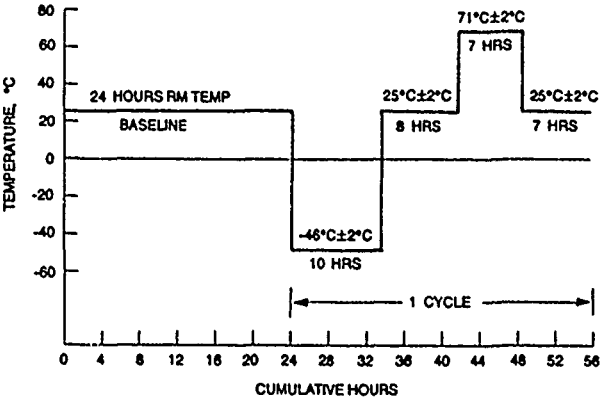

FIGURE 3. Temperature Cycle

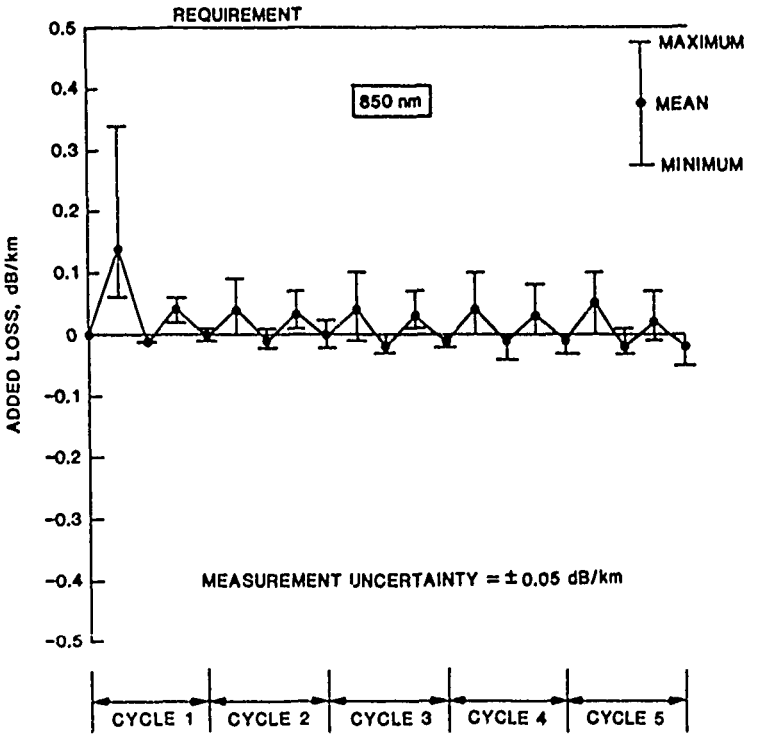

FIGURE 4. Temperature Cycling Results for Four-Fiber Tactical Cable at 850 nm

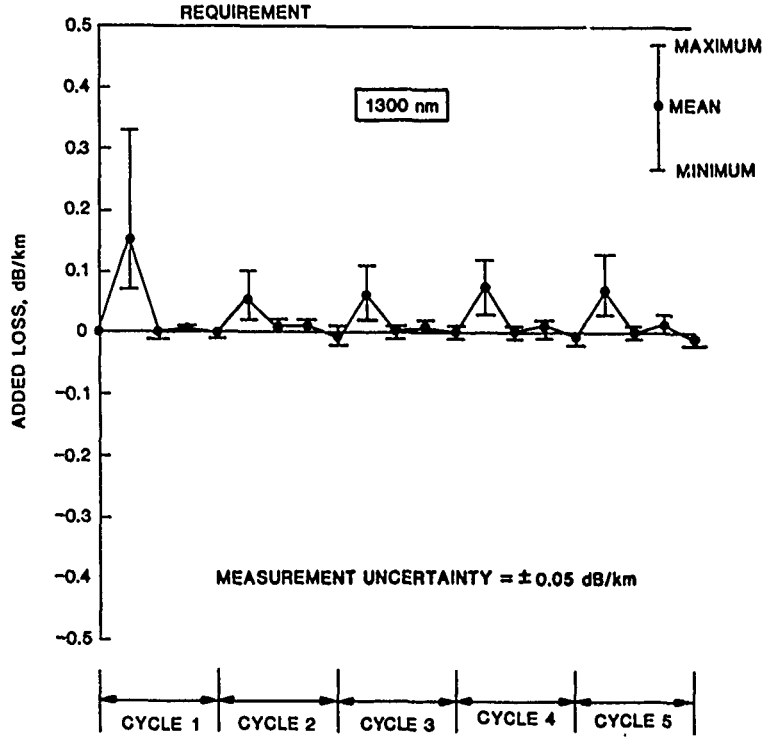

FIGURE 5. Temperature Cycling Results for Four-Fiber Tactical Cable at 1300 nm

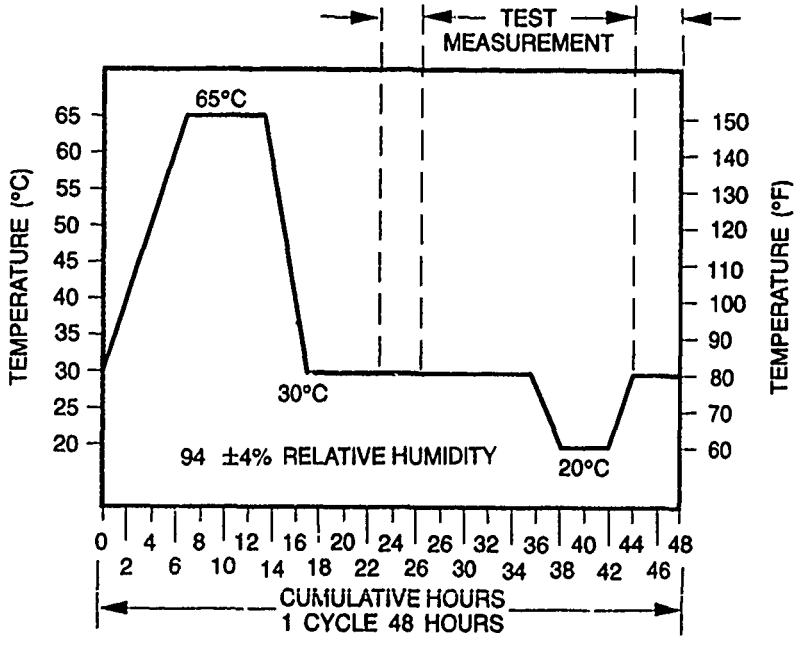

FIGURE 6. Humidity Cycle

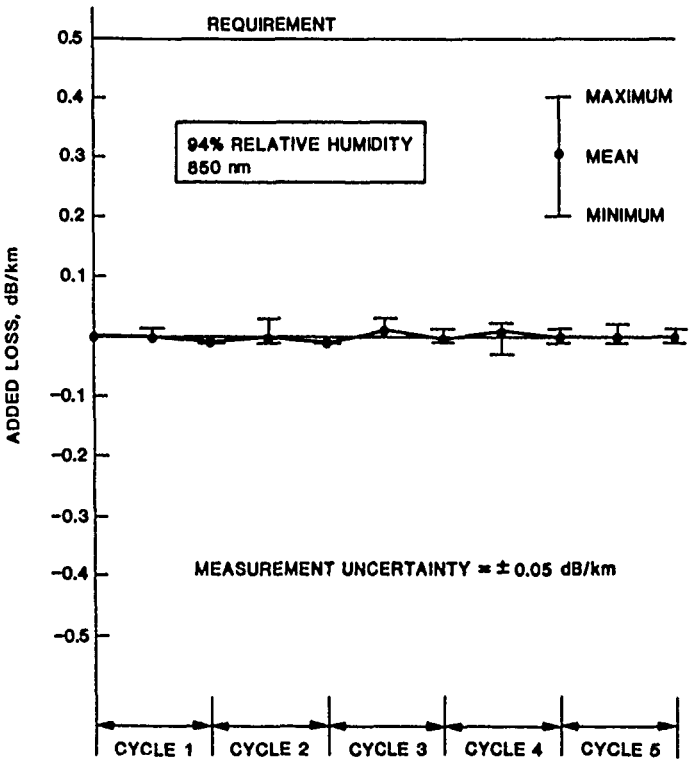

FIGURE 7. Humidity Cycling Results for Four-Fiber Tactical Cable at 850 nm

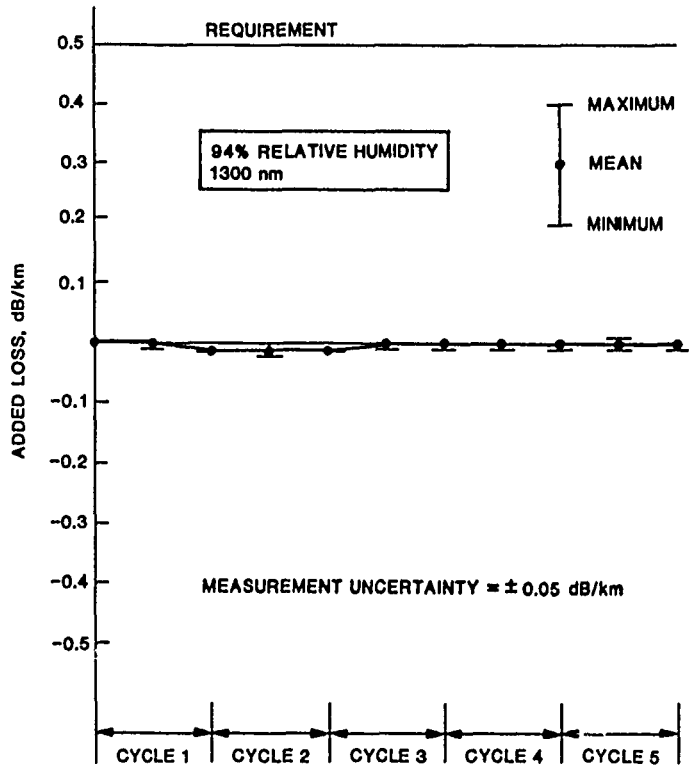

FIGURE 8. Humidity Cycling Results for Four-Fiber Tactical Cable at 1300 nm

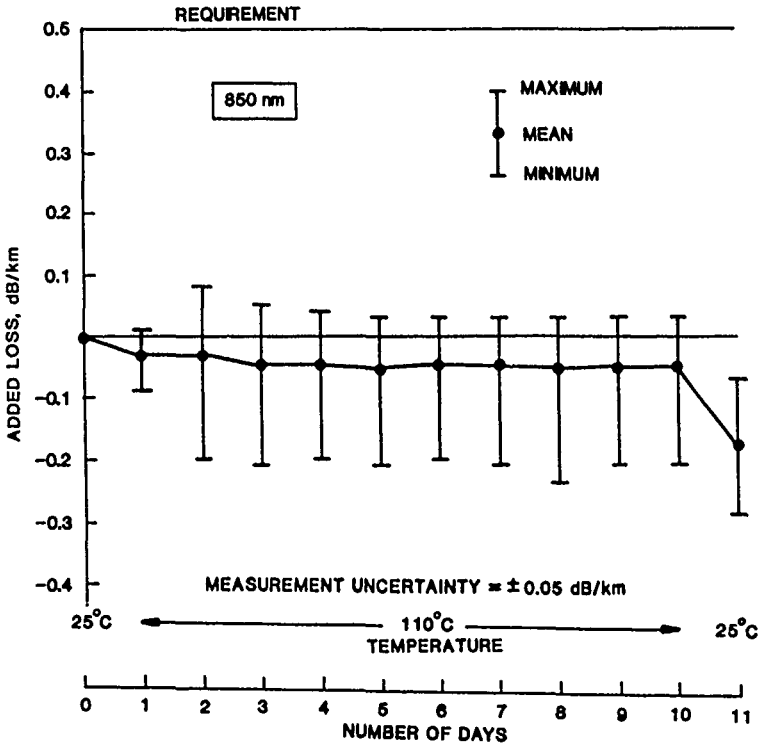

FIGURE 9. Accelerated Aging Results for Four-Fiber Tactical Cable at 850 nm

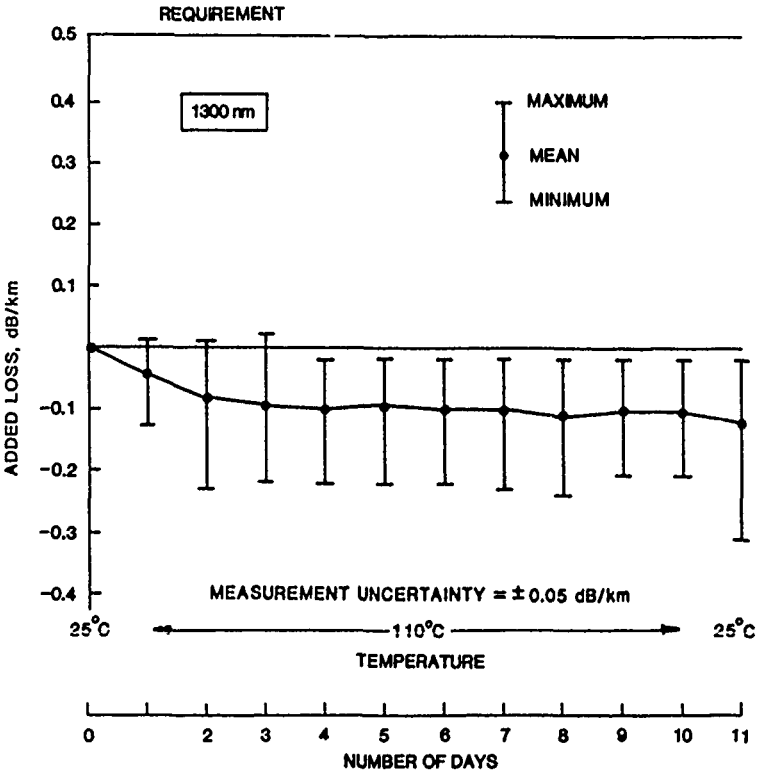

FIGURE 10. Accelerated Aging Results for Four-Fiber Tactical Cable at 1300 nm

TABLE II. RESULTS OF MECHANICAL TESTS FOR FOUR-FIBER TACTICAL CABLE

NO	TEST DESCRIPTION	REQUIREMENTS	RESULTS mean/max
1	Twist Bend	DOD-STD-1678, 2060 Mandrel Dia. = 30mm 10 kg, 2000 cycles Added Loss, $\Delta \leq 0.5$ dB	0.11/0.45 dB
2	Cyclic Flexing	DOD-STD-1678, 2010 Mandrel Dia. = 30 mm 10 kg, 2000 cycles $\Delta \leq 0.5$ dB	0.06/0.29 dB
3	Impact	DOD-STD-1678, 2030 1.0 kg, 100 cycles, 15 cm $\Delta \leq 0.5$ dB	0.01/0.08 dB
4	Cold Bend	DOD-STD-1678, 2020 Mandrel Dia. = 30mm, −46°C, 10kg, 3 Turn $\Delta \leq 0.5$ dB	0.01/0.07 dB
5	Freezing Water Immersion	DOD-STD-1678,4050 −10°C, 24 Hrs; −2°C, 1 Hrs $\Delta \leq 0.5$ dB	0.02/0.14 dB
6	Knot	DOD-C-85045, 300N (66lbf), Mandrel Dia. = 30mm $\Delta \leq 0.5$ dB	0.02/0.06 dB
7	Radial Compression	DOD-STD-1678, 2040 10.1 cm Dia., 1500N (337lbf) $\Delta \leq 0.5$ dB	0.20/0.40 dB
8	Tensile Strength	EIA-455-33A, 1780N(400lbs) Elongation $\leq 2.0\%$ $\Delta \leq 0.5$ dB	$\leq 0.5\%$ 0.13/0.20 dB
9	Operating Tensile Loading	EIA-455-33A 300N(66 lbf), 24 Hrs. $\Delta \leq 0.5$ dB	0.03/0.24 dB
10	Flammability	DOD-STD-1678, 5010 60 Angle Test, Flame travel distance $\leq$ 10 cm Extinguish $\leq$ 30 sec.	4.5/5.5 cm 4.5/5.5 sec.

The diameter and mass requirements for the cable are 5.85±0.15 mm and ≤32 kg/km, respectively. The diameter and mass results for the cable are given in Table III.

TABLE III. DIAMETER AND MASS RESULTS FOR FOUR-FIBER TACTICAL CABLE

PARAMETER	REQUIREMENT	RESULT (Average)
DIAMETER (mm)	5.85	5.81
MASS (kg/km) (Max)	32	29.4

CONCLUSIONS

The four-fiber tactical cable described herein meets or surpasses all the optical, environmental and mechanical requirements given in the military specification DoD-C-85045C. The technology utilized in the design and development of this cable is similar to that of its single- and two-fiber predecessors, enhancing field serviceability, compatibility and maintainability.

ACKNOWLEDGEMENT

The authors gratefully acknowledge the extensive contributions of several members of AT&T Bell Laboratories and AT&T Network Systems.

REFERENCES

1. "Single-Fiber Optical Cable Assemblies (SFOCA)", U. S. Army CECOM Contract No. DAAB07-85-C-K556.
2. "Single-Mode Fiber Optic Communication Systems (SIMFOCS)", U. S. Army CECOM Contract No. DAAB07-85-C-K565.
3. "Tactical Fiber-Optic Cable Assemblies (TFOCA)", U. S. Army CECOM Contract No. DAAB07-84-C-K551.
4. "Final Engineering Design Model (FEDM) Test Report for Tactical Fiber Optic Cable Assemblies (TFOCA)", Report submitted to U. S. Army CECOM for Contract No. DAAB07-84-C-K551.
5. K. Kathiresan, et al., "Selection and Test Criteria for Polymeric Materials for Tactical Fiber-Optic Cables", Proceedings of the 1988 Annual Technical Conference (ANTEC) of the Society of Plastic Engineers, Atlanta, Georgia, April, 1988.

Wing S. Liu joined AT&T Bell Laboratories in Norcross, Georgia in 1986 as a Member of Technical Staff in the Lightguide Media Department. He is responsible for the design and development of specialty fiber optic cables, including those for military applications. Prior to his current assignment, he was working on analytical modeling and design of lightguide splicing. He received his BSME degree from Polytechnic Institute of New York in 1984, and MSME degree from Massachusetts Institute of Technology in 1986 specializing in robotics.

Kris Kathiresan is a Member of Technical Staff in the Lightguide Technology Department at AT&T Bell Laboratories in Norcross, Georgia. He is responsible for the design and development of specialty fiber optic-cables, including those for military applications.

Dr. Kathiresan joined AT&T Bell Laboratories in 1985. He has a B. E. Hons degree in Mechanical Engineering from University of Madras, India, an M. E. in Aerospace Engineering from Indian Institute of Science, India, and a Ph. D. in Engineering Science and Mechanics from Georgia Institute of Technology, Atlanta, Georgia.

Dr. Kathiresan is a Senior Member of American Institute of Aeronautics and Astronautics and a Member of American Society of Mechanical Engineers. He is a registered Professional Engineer (Mechanical) in the States of Georgia and Florida.

Jill B. Fluevog is a Development Engineer in the Lightguide Cable Engineering Department at AT&T Network Systems, Norcross, Georgia. She joined AT&T in 1985 after receiving a Bachelors Degree in Chemical Engineering from Georgia Institute of Technology. She is responsible for the development of lightguide cable products and processes for military applications. Ms. Fluevog is a member of American Institute of Chemical Engineers, Institute of Electrical and Electronics Engineers and Society of Plastic Engineers.

TACTICAL FIBRE OPTIC CABLE ASSEMBLIES

JP. BONICEL* P. GAILLARD* M. DE VECCHIS**

* LES CABLES DE LYON - 170 Avenue Jean JAURES - 69344 LYON - FRANCE
** LES CABLES DE LYON - 30 Rue des CHASSES - 92111 CLICHY - FRANCE

ABSTRACT

The design and development of tactical fibre optic cable assemblies have been completed.
For the cable aspect, a slotted core structure (loose type) has been selected as it offers advantages on fibre selection and reliability with an O.D. similar to that of a tight tube structure. For the connector aspect a careful analysis based on ergonomics has led to an easy to handle tactical product.

This paper describes the qualification procedure and gives an example of operational application.

INTRODUCTION

A tactical fibre system must survive extreme temperatures, very high strength, excessive vibration/shock, rough handling, severe bending, etc...

One possible approach is to develop a fiber with sufficient strength to provide a reliable signal transmission over the entire system life (1). This is used in particular with cable structures containing tightly buffered fibers where a part of external strength can be applied to fibres. In that case a combination of microbending resistance and high proof test level is needed (2).

An other possibility is to use a loose structure designed to avoid transmission to fibres of external strengths and to minimize microbending effects. In that case any standard fibre can be used to meet the same specification as in the first case. If a microbending resistant high proof test fibre is used, the level of the safety margin is consequently increased. From the point of view of long term reliability, loose structure have been proved to be very safe as, in such a structure, the fibers are free from permanent microbending in the normal conditions of operation, providing that the design of the cable structure has been conveniently done.

On the other hand, loose structures are generally less attractive considering cable size and bending radius.

To verify the quality of the design, it is necessary to perform sophisticated temperature cycling tests taking precautions for avoiding any parasitic effect on the test results due to the measurement conditions. The tests that we have used are fully compliant with the new text of the IEC Method 794 - 1 - F.1. Temperature cycling (3) that lists the risks of errors due to measurement conditions and recommends some possible ways to obtain good results.

CABLE

We have selected the second option (loose structure) as the reliability under severe environmental conditions has been considered very important for the tactical application. In that case, the matching between the cable and the connector is more critical in order to maintain at the vicinity of the interface, the freedom of the fibre and the accuracy of the excess length control which are important parameters for a good design of a loose structure. This problem has been solved during the design of the connector described below ; consequently the best conditions for the optimum lifetime are provided for the complete cable assembly.

The cable uses a four groove slotted core structure with a FRP central strength member.

Aramide yarns are used as sheath reinforcements.

The outer sheath is fire resistant.

Main characteristics are given below and figure 1 shows a cross section of the cable.

Nominal outer diameter	7 mm
Nominal weight	38 kg/km
Nominal thickness of sheath	0.8 mm
Maximum tensile load (corresponding to an elongation $\leq 1,5°/_{oo}$)	220 daN

Several samples have been tested without damage up to 5000 N

Crush resistance	40 daN/cm
Minimum bending radius	
Static	100 mm
Dynamic	150 mm

Temperature range - 40 to + 70°C
with less than 0.2 dB attenuation increase for 850 and 1300 nm multimode fibres.

These characteristics have been optimized considering the practical requirements of the tactical application in order to provide the most cost effective solution

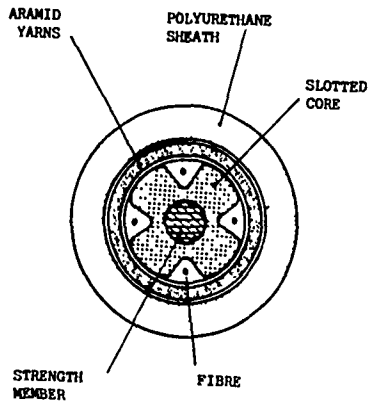

Figure 1

The design offers the advantage of being usable with the same characteristics with one to four fibres. If necessary, different types of fibres can be used in the same cable.

Furthermore, this structure allows the use of any type of standard fibre which is an advantage compared to the other designs where specific requirements are needed for example related to the primary coating.

Compared to other designs, previously reported, using tight buffered fibres the O.D. and weight per km values are similar.

CONNECTORS

The tactical connector is constructed around an hermaphroditic expanded beam interface, that has been used for a complete set of products (plug, shunt plug, attenuating shunt plug) which are necessary to operate the tactical transmission system.

Details on the interface design have been given in a previous paper (4). Cable retention on the connector has been optimized for use with the mechanical requirements of the cable (see figure 2).

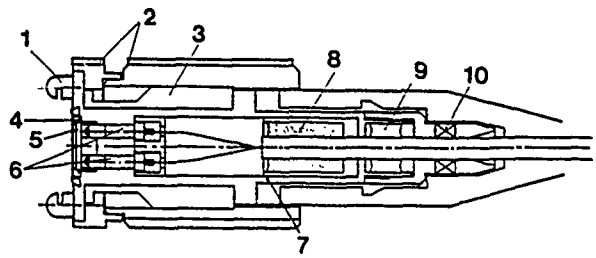

1 Guiding pin
2 Tactile indexes
3 Locking ring
4 O seal
5 Glass window
6 Optical points
7 Plug body
8 Cable retention
9 Ring
10 Strain relief

Figure 2

Lenses used for beam expansion allow optimized operation at both wavelength (850 nm and 1300 nm) for multimode fibres. The design of the optical system allows for field termination of the fibre ends, with an available tool kit. So, reparation and maintenance can be performed in the field.

A glass window protects the lenses, making the interface almost totally flat, and therefore allowing an easy, quick and efficient cleaning of optical face. O rings make the connector water-tight.

The ergonomics of the connector has been carefully studied to provide optimum tactical operating conditions.

For example, in order to make night-and-day termination easier, the interfaces are equipped with alignment pins of different sizes, with a guiding groove and a tactile peripheral indexing. The connexion can be achieved by aligning the tactile indexes, then bringing both interfaces into contact, and finally locking by symetrical rotation of the plugs through an angle of 30°.

As the ergonomics is a very important point, it has been verified in practice by field deployment : operation by the French Army under extreme environmental conditions (low temperature, mechanical agressions, poor climatic conditions, nightly operation....) has revealed the advantages of the selected solutions.

Each connector is supplied with a rubber protective cap. The inside of this cap is reinforced with a metallic sheathing, which improves the mechanical protection and thus ensures an electrical continuity for the electro-magnetic protection. The caps can be locked together when not in use, avoiding internal pollution when the plugs and receptacles are connected.

The figure 3 shows the dimensions of the plug.

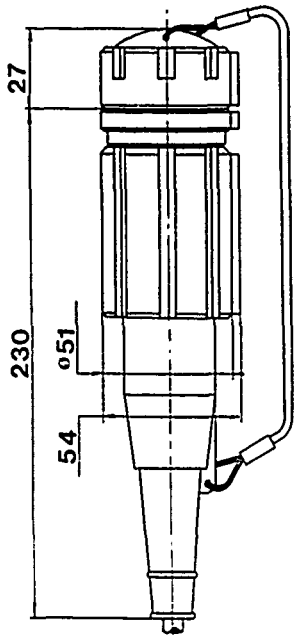

Figure 3

The shunt plug is available as a test unit which may be used during installation to loop the line. Then it is possible to check that the former cable section (s) is (are) not cut off.

The attenuating shunt plug is used in the same way with 9 dB extra attenuation when connected to the active receptacle to avoid receiver saturation.

Active and passive receptacles are available in bulkhead versions (i.e for wall crossing).

The four channel - type active receptacle can be equipped with two LED and two PINS diodes.

The table below summarizes the characteristics of the connector for multimode fibres.

TESTS	RESULTS
Connections	2 or 4 channels (upon request)
Insertion loss (0.85 and 1.3 μm)	<3 dB in the whole operating temperature range
Uniformity	+ - 0.2 dB
Operating temperature range	- 40°C < T < + 70°C
Storage temperare range	- 40°C < T < + 85°C
Mechanical endurance	1500 matings/unmatings
Vibrations	5-300 Hz-amplitude 1.25 mm p-p
Mechanical shocks	30 g - 11 ms - 2.06 m/s
Shakes	1000 - 25 g - 6 ms
Water immersion	1 m depth (0.1 bar)
Tensile strength	220 daN

The figure 4 shows the optical interface with alignment pins.

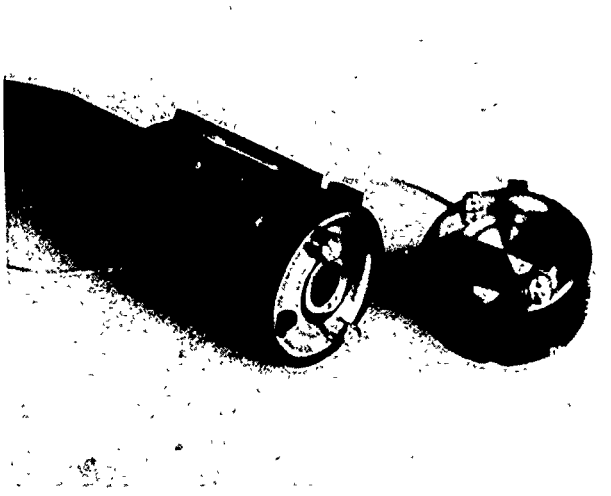

Figure 4

CABLE ASSEMBLY

The cable is delivered equipped at both ends by the connectors and wound on an adapted drum. The length of cable changes according to the application and lengths up to 3 km have already been realized.

For a first practical application in the French Army, this cable was used to replace a copper quad and the size of the drum was fixed.

Delivery length has been fixed to 600 m and in order to reduce the total weight, a special low weight drum has been developed with the following characteristics :

Overall diameter : 488 mm

Overall width : 460 mm

Weight : 6 kg

This drum is made with reinforced plastic and can handle up to 800 meters of cable with a protective flange for connectors (see figure 5).

Figure 5

QUALIFICATION TESTS

These tests are performed on the cable alone, on the optical plug alone and on the cable assembly wounded on the drum. The lists of tests are given below.

Cable

Geometrical parameters of fibre

Transmission parameters

Tensile performance

Cable bend

Crush

Abrasion

Impacts

Sheath cut

Repeated bend

Repeated torsion

Repeated flexing

Temperature cycling

Dry heat

Wet heat

Dry cold

Cold bend

Composite climatic test

Fire resistance

Chemical fluids resistance

Solar radiation resistance.

Connectors

Insertion loss

Stability of insertion loss

Operating temperature

Storage temperature

Vibrations

Impacts

Shakes

Immersion (water)

Electromagnetic characteristics :

- Earth continuity
- Electromagnetic pertubations
- Electromagnetic susceptibility

Tensile test on connectors.

Cable assembly on drum

Vibrations

Impacts

Shakes

Fall

Environmental tests.

- Storage - Dry heat
- Storage - Dry cold
- Storage - Wet heat

PRACTICAL APPLICATION

This equipment is now used by the French Army for practical transmission Systems in place of copper quads.

Therefore a junction box has been developed for an easy connexion to the existing transmission equipments : on one side there are standard electrical interfaces and on the other side optical hermaphroditic junctions.

Two types of junctions boxes are used : a single junction box for radio link terminations and a six junction box for inter shelter links.

CONCLUSION

A tactical fibre optic cable assembly has been developed based on an analysis of reliability and ergonomics.

It passed laboratory and field tests for qualification and is now operationally used in place of copper quads. For that purpose, junction boxes are available that allow an easy connection to existing transmission equipments.

ACKNOWLEDGEMENTS

CABLES de LYON (ALCATEL CABLES) thanks very much the French Army for sponsoring this development.

References :

(1) H. P HSU - V.E. KALOMIRIS "Optical Fiber Design challenges for Tactical System Applications" I.W.C.S. 1989 Proceedings pp172 - 178.

(2) B.V. DARDEN - K. KATHIRESAN - B.G. LE FEVRE - J.B. FLUEVROG - V.E. KALOMIRIS. "Single and Multimode Tactical Cable Assemblies". I.W.C.S 1989 Proceedings pp 648 - 657.

(3) IEC Publication 794 - 1 Optical Fiber Cables - Generic Specification 2nd edition. Amendment n° 2.

(4) P. POUYEZ. Ph. KAYOUN SMTique/CONNECTique PARIS 12 April 1988.

BIOGRAPHY

JP. BONICEL - LES CABLES de LYON
170 Av. Jean Jaurès - 69344 LYON - FRANCE

Jean-Pierre BONICEL was born in 1952. He received his engineer degree from the Institut des Sciences de l'Ingénieur de MONTPELLIER (ISIM) in 1976. He joined Les CABLES de LYON in 1977 where he was in charge of material and mechanical problems for telecommunication cables. Now he is the head of telecommunication cables laboratory.

P. GAILLARD - LES CABLES de LYON
170 Av. Jean Jaurès - 69344 LYON - FRANCE

Pierre GAILLARD was born in 1956. He received his engineer degree from the Ecole Catholique des Arts et Métiers in 1980. He joined LES CABLES de LYON in 1983 where he is in charge of cables definition and transmission characterisation.

M. de VECCHIS - LES CABLES de LYON
30 Rue des Chasses - 92111 CLICHY - FRANCE

Michel de VECCHIS was born in 1946. He is graduated from Ecole Nationale Supérieure des Télécommunications (1969)He joined LTT in 1970 where he worked on microwave components. He started to work on fiber optics in 1974 and he has been Technical Director of the cable Division until the merging of LTT cable activities with les CABLES de LYON in 1986. He is now Director of Technical International Marketing at the CABLES de LYON Telecommunication Branch.
He is involved in International Standardization of optical fibers and Cables (Chairman of CECC WG 28 and Secretary of IEC SC 86 A).

FIELD REPAIRABLE TACTICAL OPTIC FIBER CABLE

H. Troendle, V. Koelschbach, D. Lohmueller

Philips Kommunikation Industrie AG
Nachrichtenkabel und -anlagen
Piccoloministr. 2
D-5000 Koeln 80
Federal Republic of Germany

ABSTRACT

The described Repairable Tactical Fiber Optic Cable (RTFOC) has been designed all-dielectric with up to 4 tightly-buffered fibers. FRP-rods and aramid-yarns are used as strength members. The cable is jacketed by a flame retardant polyurethane sheath.
Various types of connectors can be fitted tc the cable. In the field, cables are connected by an approved hermaphroditic connector.
Tests concerning humidity and water immersion will be discussed. Additional mechanical tests for long-term tensile load and the transmission characteristic during a back-blast firing test will be presented.

An optimized fiber coating eliminates humidity and water influence. In addition simple field repair is guaranteed by the special fiber coating.

For RTFOCs two different repair techniques are avaible. First, restoration of optical transmission in the field needs to be guaranteed within a few minutes by simple means. As a result of our development no tools for fiber stripping or endface preparation are necessary for mechanical splicing. Second, in order to restore all mechanical and optical properties a workshop repair technique has been developed including a special set up for restoring strength members and cable sheaths.

The reliability of our RTFOC-system has been proven in field trials.

INTRODUCTION

The demand for tactical fiber optic assemblies has increased continuously worldwide in last few years. The complete multimode cable assemblies consist of a cable, containing two or four tightly-buffered graded index fibers terminated with duplex, hermaphroditic expanded beam connectors.

The RTFOC uses a 50/125 µm multimode fiber and offers a good combination of low loss, low microbending-and macrobending sensitivity and high bandwidth. The cable assemblies can be operated at 850 nm and 1300 nm. Both cable designs are identical except for the fiber number and the number of FRP-rods. All cables have a 2000 N tensile rating and a 6 mm outer diameter. The total weight of the cable assembly, consisting of a 1 km cable, two connectors and a robust reel is less than 42 kg. The complete cable assembly has been tested for operating temperature between -40°C to 70°C and a storage temperature range from -55°C to 85°C.

Besides the stringent requirements laid down by the relevant standards /1//2/, it was recognized during long-term testing, that water immersion may have considerable influence on attenuation.

Moreover, there is a strong demand for quick field repair and complete workshop overhaul.

ASSEMBLY SPECIFICATION

The development of these multimode cable assemblies for use in tactical field environments and for indoor applications has been completed. RTFOCs will be utilised for long distance use. The indoor assembly has been developed for short Fiber Optic Trunk Cables (FOTCs).
These cable assemblies have been designed to meet stringent specifications imposed by the contract agency.
The environmental, mechanical and chemical test requirements are given in Table 1.

RTFOCs and FOTCs use a 50/125 µm multimode fiber. A completed long distance RTFOC assembly terminated at both ends with herma-phroditic expanded beam connectors is illustrated in Figure 1.

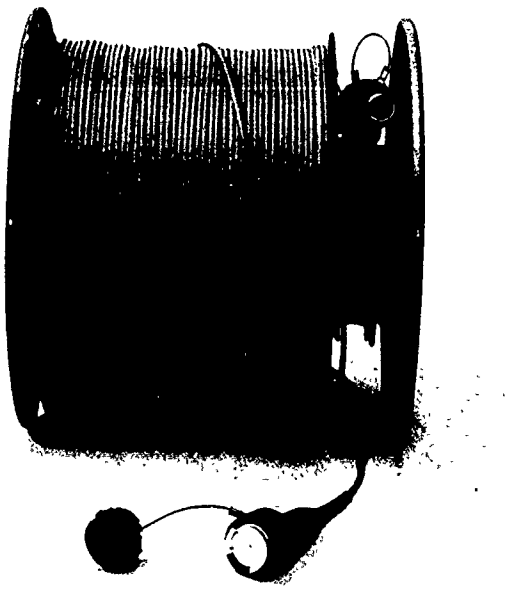

Figure 1 Repairable Fiber Optic Cable (RTFOC) assembly

An illustration of a FOTC with terminated indoor expanded beam connectors is shown in Figure 2.

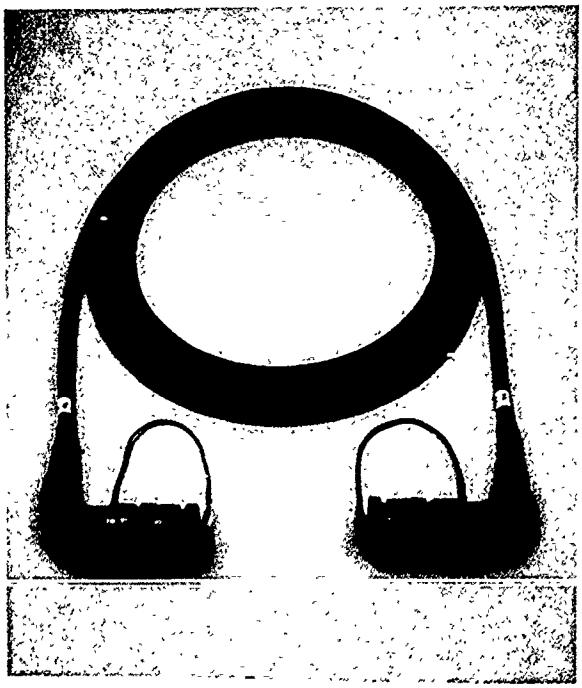

Figure 2 Fiber Optic Trunk cable (FOTC)

CABLE DESIGN

The cable construction consists of two or four multimode, tightly-buffered fibers. The fibers lay parallel to each other and are not stranded. Fibers, FRP-rods and aramid-yarns form the center core of the cable. All elements are loosely sheathed with a polyurethane inner tube. Additional aramid-yarns are stranded around them and the outer flame-retardant polyurethane sheath is extruded directly around the strength members. The cable has a weight of 34 kg/km, a 2000 N tensile load rating, and a compressive strength loading of 1000 N.
The cable- and fiber elongation under 2000 N tensile loading is 0.37 % respectively 0.21 % as shown in Figure 3. Every fiber used in RTFOCs has been proof tested to 690 MPa.
A cross-sectional view of the cable is illustrated in Figure 4.

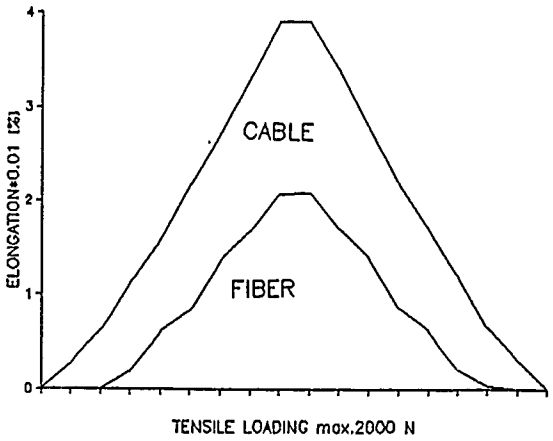

Figure 3 Elongation, Fiber, Cable

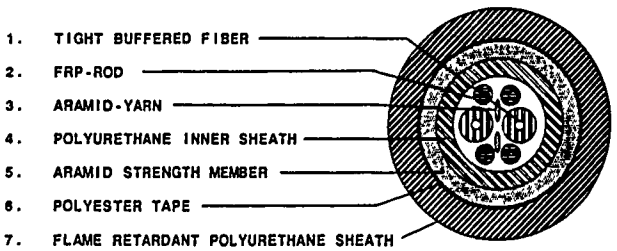

Figure 4 Cross-sectional view of RTFOC, FOTC

TABLE 1. Environmental properties of the cable

TEST	REQUIREMENT FOR RTFOC/FOTC	CABEL PERFORMANCE RTFOC/FOTC
ENVIRONMENTAL TESTS		
Humidity and water immersion	PKI-test, Water, 150 d, (60 d), 20°C, (50°C) length 500 m, $d\alpha \leq 0.3$ dB/km	$d\alpha = 0.2$ dB/km
Freezing water immersion - Ice crush	DOD-STD-1678, Method 4050, T = -10°C length 380 mm, da ≤ 0.1 dB	da = 0.03 dB undamaged sheath
Temperature cycling on reel	temp. range -40°C to 85°C, length 500 m on steel reel, 5 cycles, $d\alpha \leq 0.5$ dB/km	$d\alpha = 0.32$ dB/km
Temperature cycling without reel	temp. range -40°C to 85°C, length 500 m lose ring, 5 cycles, $d\alpha \leq 0.5$ dB/km	$d\alpha = 0.34$ dB/km
Cold impact	VG 95218 part 2 No.5.3.1.3, T = -40°C 9 impacts, h = 100 mm, m = 200 g	no fiber breakage undamaged sheath
Cold bend	VG 95218 part 2 No.5.3.1.2, T = -40°C ϕ = 25 mm, 6 windings	no fiber breakage undamaged sheath
Accelerated aging	T = 80°C, t = 50 d, $d\alpha \leq 0.1$ dB/km length = 500 m	$d\alpha = 0.05$ dB/km
MECHANICAL TESTS		
Tensile strength	DOD-STD-1678 Method 3010, before impact test, F = 2000 N, da ≤ 0.5 dB	da = 0.15 dB
Long-term tensile strength	PKI-test, length = 180 m, F = 200 N t = 90 d, da ≤ 0.2 dB, reversible	da = 0.08 dB lengthening 0.02 %
Compressive strength	F = 1000 N, loading 100 N/2min pressure cylinder ϕ 50 mm, da = 0.5 dB	da = 0.06 dB
Cycling flexing	DOD-STD-1678 Method 2010 Procedure I cycles 1000, m = 10 kg, bendradius = 7.5 mm	no fiber breakage
Cable twist bend	DOD-STD-1678 Method 2060 Procedure I cycles 1000, m = 10 kg, vert.motion ± 90°	no fiber breakage
Impact	DOD-STD-1678 Method 2030, m = 2 kg 50 impacts, 30 impacts/min	no fiber breakage undamaged sheath
Knot	DOD-C-85045 C, F = 500 N, da ≤ 0.1 dB	da = 0.04 dB, no fiber breakage
Fiber strippability	PKI-test, fingernail strippable, after accelerated aging	easily removable
Flammability	VG 95218 part 2, No.5.3.4.2, t = 60 sec	self-extinguishing
Cable abrasion	VG 95218 part 2, No. 5.2.5.2, cycles 2000, m = 0.5 kg, wire ϕ = 0.6 mm	undamaged sheath
CHEMICAL TESTS		
Aviation gasoline Benzine Lubricating oil Hydraulic fluid Deicing	examination time = 6 h, length 1 m, T = 50°C	maged sheath

wavelength 1300 nm, $d\alpha$ - increase in attenuation coefficient, da - increase in attenuation

BUFFERED FIBER DESIGN

The optimized cable contains tightly-buffered fibers with dual acrylate coatings and a low modular 0.9 mm diameter secondary-coating. All coating layers can be stripped mechanically in order to facilitate termination and repair in the field. The buffer material has been chosen to minimize microbending loss induced by exposure to extreme temperature and long-term humidity and water immersion.

HUMIDITY AND WATER IMMERSION TEST

In practice, the coils may be wet during their storage periods. Also it has to be recognized that coils may be exposed to humidity for some weeks. Special tests have to be developed in order to examine optical performance under such conditions. Due to the permeability of sheaths and coating materials water will reach the fiber surface after a certain time.
Coating materials with a high modulus of elasticity and a high water absorption rate, cause tensions between fiber and coating layers. During water absorption, an increase in attenuation may be observed as a consequence of micro-bending. The optimized coating layers minimize the humidity and water influence and show an excellent temperature behavior pattern.
An uninterrupted sequence of temperature and water immersion tests is given in Table 2.

TABLE 2. Temperature- and water immersion test
5 temperature cycles from -40°C to 70°C Figure 5a
water laying at T = 50°C, for 12 days Figure 5b
drying at T = 50°C, 4 days
5 temperature cycles from -40°C to 70°C Figure 5c

The results on a loosely wounded 500 m cable length are shown in Figure 5a-5c.

The long-term test consisted of the immersion of the cable under water for 150 days, followed by the freezing of the cable for a period of 4 days.
Result of this test show an excellent behavior pattern.

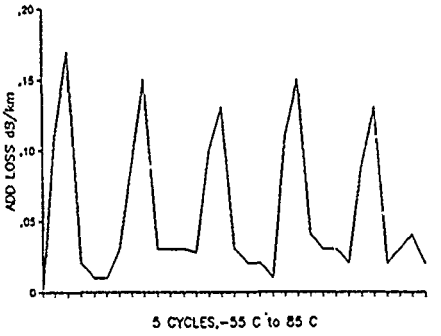

Figure 5a Temperature cycling

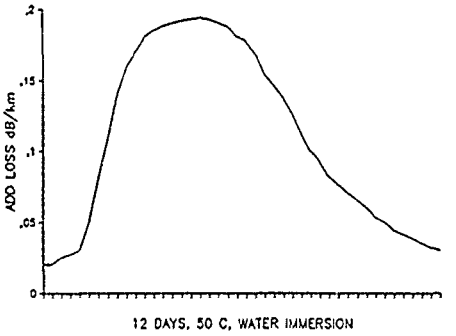

Figure 5b Water immersion

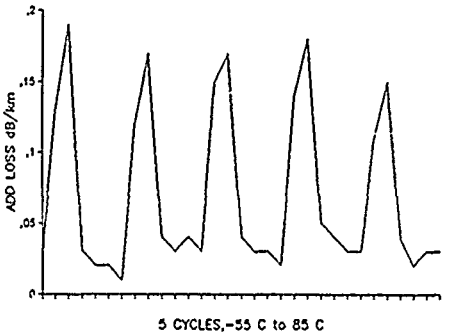

Figure 5c Temperature cycling

LONG-TERM TENSILE STRENGTH

The tensile strength test was performed using a 180 m length cable, loaded with a traction of 200 N, installed in a pulley system. The distance between two pulley units was 20 m. The test took place in winter and had a duration of 90 days. The elongation, the attenuation variation and the wind velocity were checked on-line. After the test, the cable was stretched by 0.02 %, the level of attenuation variation was less than the accuracy of measurement. The recorded maximum wind velocity was 90 kph.

BACK-BLAST FIRING TEST

The influence of missile back-blast on RTFOCs was also tested.
The experiment was designed to give more information about

- increased bit error rate on digital data link on RTFOCs during and after missile launch
- increased optical attenuation on RTFOC during and after missile launch
- physical damage to fiber and cable jacket.

Two cables under test were laid on the ground. The cable length was approximately 1 km in both cases and the fibers were connected with a splice at the far end. The shortest distance between cables and missile was 1.8 m. The test was carried out at 1300 nm. The optical source was modulated with NRZ data at 8 Mbit/sec. Monitoring equipment was installed for data error detection purposes. The attenuation variation was less than the accuracy of measurement. During and after missile launch no data errors appeared. Aside from the two parallel cables melted together and a burnt sand inside the cable jacket were no damage observed.

Figure 6a-6b illustrates the tested cable.

Figure 6a RTFOC after back-blast firing test, direct influence

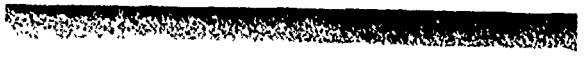

Figure 6b RTFOC after back-blast firing test, distance 5 m

CONNECTOR PERFORMANCE

Two different expanded beam connectors (EBC) have been developed for use in indoor and outdoor cabling. Both types exist as a feed-through panel connection. A four channel contact is available for the connectors.

EBC 6210/6220, INDOOR CONNECTOR

At the front of the indoor EBC 6210/6220 there are two or four lenses positioned in circular pattern. The lens and the optical fiber are mounted in a cartridge. Using a special adjusting device, errors in angle are minimized. The assembled cartridges are mounted into a shell fitted with spring-suspension. During connecting, a pilot pin and a precision bore allow a proper alignment.

The SJT shell houses the precision-part assembly. The cable clamp can withstand a tensile load of 140 N and has a total weight of 100 g. All metal connector components including the receptacle and dust cover are wrought aluminium with an olive-drab cadmium surface.

The dust cover prevents water or dust entry into an uncoupled connector. When two connectors are coupled, their respective dust covers can be joined in order to prevent contamination.

The connector EBC 6210 has a SJT shell and is used as a receptacle. It has the same interior assembly as the EBC 6220. The advantage of this expanded beam connector is the possibility of easy cleaning. In Figure 7 the typical insertion loss, measured in accordance to the IEC 874-1 Method 7, is given.

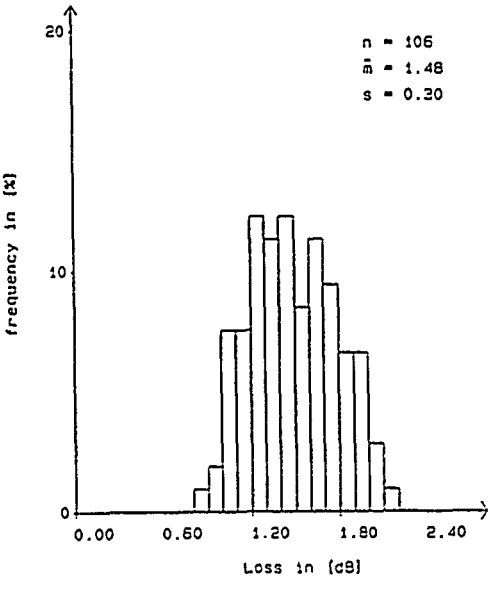

Figure 7 Insertion loss for EBC 6210/6220

EBC 7220, OUTDOOR CONNECTOR

The EBC 7220 is a hermaphroditic outdoor expanded beam connector with a length of 280 mm, an outer diameter of 58 mm and has a weight of 440 g. It has a plastic shell with a cable clamp and withstands a 1800 N tensile load rating.

A pane protects the coated lenses. Inside the coupling head an elastomeric seal blocks water and dust entry in a coupled condition. Therefore easiest cleaning methods are possible.

Figure 8 shows the typical insertion loss, measured in accordance to IEC 874-1, Method 7.

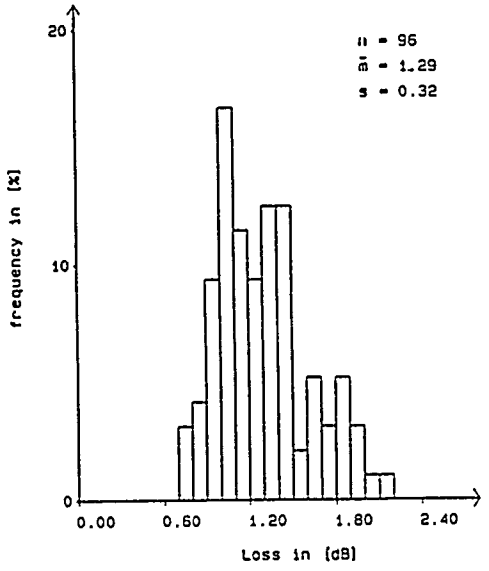

Figure 8 Insertion Loss for EBC 7220

In Table 3 test procedures for EBC 6220 and EBC 7220 are summarized.

TABLE 3. Connector requirements for EBC 7220/6220

TESTS	EBC 6220	EBC 7220
Optical requirements		
insert. 850 nm loss 1300 nm	≤ 2.0 dB ≤ 2.0 dB	≤ 2.5 dB ≤ 2.0 dB
Enviromental requirements		
operation temp. range	-40°C to 70°C	-40°C to 70°
storage temp. range	-55°C to 85°C	-55°C to 85°C
water immersion	0.2 bar, 24 h	0.2 bar, 24 h
dust	DIN 40050 IP 55	VG 95319, part 5.35
Mechanical requirements		
mating durability	500 Cycles	1000 Cycles
vibration	10 Hz-20 kHz 0.5 G²/Hz 15 min	10 Hz-20 kHz 0.5 G²/Hz 15 min
shock drop	40 G, 6 msec 4000 Cycles	40 G, 6 msec 4000 Cycles
shock	100 G, 6 msec	100 G, 6 msec
cable retension	140 N	1800 N
twist life	±180°, 100 N	±180°, 100 N

CABLE REPAIR TECHNIQUES

The widespread distribution of the tactical fiber optic cables demands repair techniques in field and workshop overhaul. Field repair must be performed in a short time.

The following requirements are imposed on a field repair technique:

- splice loss ≤ 1.5 dB

- minimum of tools.

Numerous tests have been carried out to verify the performance features such as temperature cycling, tensile load retention, insertion loss, water immersion and flexibility.

FIELD CABLE REPAIR TECHNIQUE

The proposed field repair may be quickly carried out.

A durable mechanical compact splice is used for the fiber joint. An inserted index-matching gel allows easily made, low loss joints even with bad end-faces. After stripping all coating layers, easily done by fingernail, the fiber ends are threaded into the connector. During this process the fiber may be observed through the transparent cover and is fixed into the correct position. The dimensions of the compact splice allow it to be stored in a confined space.
The strength member is connected with a coupling link. The cable inlet and a special lock mechanism guarantee a water-proof connection box.
The total length is 300 mm including the protective rubber sleeve. The diameter is 50 mm.
All requirements are listed in Table 4.

TABLE 4. Requirements of field cable splice

TESTS	REQUIREMENTS
repair time after fault location	< 10 minutes
low loss connection without endface prep.	< 1.5 dB
waterproofed	> 24 h, 0.1 bar
number of mountable splices	up to 6
tensile load	< 100 N
reusable	max. 4 times
charging time	< 8 days
windable	$\phi \geq 200$ mm
operation temperature range	-40°C to 70°C
storage temperature range	-55°C to 85°C
inconspicuous	
producable without special tools	

Figure 9 illustrates a complete field repair.

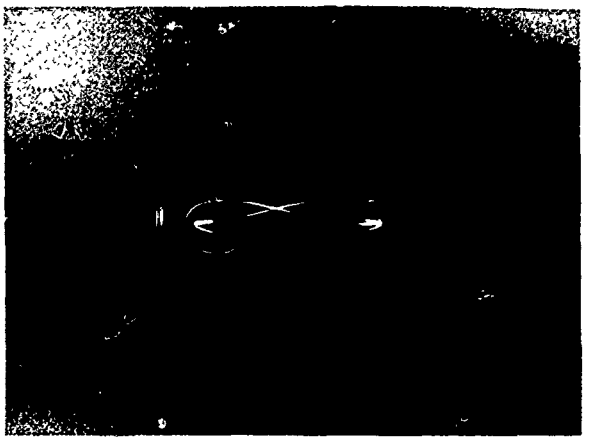

Figure 9 RTFOC field repair

CABLE WORKSHOP OVERHAUL

A workshop repair technique to restore all cable properties has also been developed. The stricter requirements, as compared with the field repair technique are listed in Table 5.

TABLE 5. Requirements of workshop overhaul

TESTS	REQUIREMENTS
Tensile load	2000 N, @ 50°C
splice loss	≤ 0.3 dB @ 1300 nm
windable	ϕ > 150 mm
useful life	lifetime of cable
flexing test	1000 Cyc. ϕ >200 mm
repair time after fault location	< 2 hrs
diameter of splice	$\phi \leq 12$ mm
operation temperature range	-40°C to 70°C
storage temperature range	-55°C to 85°C
inconspicuous	

Special equipment is necessary to overhaul a cable under these strict requirements. The first step is to locate the damaged section with an optical time domain reflectometer (OTDR).

After the damaged cable length has been cut out, all necessary shrinkable sleeves have to be put over the cable ends. During removal of the sheath and the inner jacket the aramid-yarns have to be split up into individual cords.
All fibers have to be cut to the same length in a special cable mounting. The fiber splice is made with a commercial fusion fiber splice device. A special splice protector is mounted onto each fiber. The strength members are connected with an adhesive.

The significantly longer length of the fibers in comparison to the strength members is adjusted using the cable mounting. The cable sheath has to be restored with a flexible tube and a water-tight shrinking sleeve.
Both ends of the splice are protected with a high flexible coating. The cable splice, with an outer diameter of approximately 12 mm and a length of 1200 mm has been tested in field trials and fulfills all requirements.

Figure 10 illustrates a complete cable overhaul.

Figure 10 RTFOC overhaul repair

CONCLUSION

Cable assemblies which show an optimized behavior pattern in long-term humidity and water immersion tests, long-term tensile tests and missile back-blast firing immersion have been developed.
The maximum insertion loss for a 1 km RTFOC assembly is 3.5 dB @ 1300 nm and 5.5 dB @ 850 nm.

Two cable repair techniques have been developed. One can be performed in a few minutes in order to restore optical transmission. The second technique even restores mechanical properties of the cable.

ACKNOWLEDGEMENT

The authors gratefully acknowledge the support and contributions of H. P. Dann, W. Eutin, J. Grunst and W. Hoffmann.

REFERENCES

/1/ Technical terms of delivery, Bundesamt für Wehrtechnik und Beschaffung TL 6020-0001

/2/ Technical terms of delivery, Bundesamt für Wehrtechnik und Beschaffung TL 6020-0002

Hubert Troendle was born in 1952. He received the degree of Dipl.-Ing. in electrical engineering in 1981 from the Rheinisch-Westfaelische Technische Hochschule Aachen. In 1981 he joined the Philips Kommunikations Industrie AG where he was engaged in the development of cable measurement equipment and is now as Senior engineer responsible for the development of fiber optic cables.

Veit Koelschbach was born in 1959. He received the diploma degree in experimental physics from the university of Bonn.
He joined Philips Kommunikations Industrie AG in 1986. Since 1990 he is head of the product development section for optical fiber cables.

Detlev Lohmueller is a development engineer in the optical connectors engineering department. He joined Philips Kommunikations Industrie AG in 1985 after he received a Dipl.-Ing. degree in mechanical engineering from the Fachhochschule Dortmund.
He is responsible for the design of optical connectors. Detlev Lohmueller is member of Verein Deutscher Ingenieure VDI.

A STUDY ON AERIAL OPTICAL CABLE WITH OPTICAL CONNECTORS ON BOTH ENDS FOR OPTICAL TRANSMISSION LINE

Y. Ushizaka *, Y. Komaki *, K. Niikura **, H. Horima **,
M. Sato*** and Y. Yamada***

*Tohoku Electric Power Co., Inc. 3-7-1, Ichibancho, Aoba-ku, Sendai 980, Japan
**Sumitomo Electric Industries, Ltd. 1, Taya-cho, Sakae-ku, Yokohama 244, Japan
***Kitanihon Electric Cable Co., Ltd. 1-2-1, Koriyama, Taihaku-ku, Sendai 982, Japan

ABSTRACT

With the increasingly highly information-oriented nature of modern society, the installation of transmission line incorporating optical fiber has been increasing in recent years.

In such optical fiber transmission line, one of the most important considerations is how splicing operations can be simplified and how the man-hours for such splicing can be shortened to reduce installation construction costs.

With these considerations in mind, we designed various types of aerial optical cable having optical connectors at both ends and studied the application of such aerial optical cable under severe natural conditions. As a result, a small-sized optical connector, an optical connector protector and an accommodation box for excess length of optical cable have been produced on a trial basis. A simulated experimental line was installed using these components and devices.

Results have demonstrated that the installation of aerial transmission line employing optical connector splicing is very effective in shortening the required splicing time.

1. Introduction

With the increasingly highly information-oriented nature of modern society, more and more transmission lines using optical fiber cable have been installed in recent years.

Tohoku Electric Power Company has so far introduced about 3000 km of self-supporting type optical fiber cable for aerial use installed on power transmission lines under severe natural environmental conditions such as snow accretion, strong wind and low temperature.

In such installation, the connection between aerial optical cables has been performed by fusion splicing on the poles. Although the technique of fusion splicing has been extensively improved since the initial stage of development, higher skill and long man-hours are still required.

On the other hand, technicians capable of such splicing are in short supply because of the increase in demand for optical transmission line installation, and it has become very difficult to install such transmission line efficiently. In addition, multi-core optical cable is expected to be introduced in the near future, and thus it is very important to find ways to shorten the man-hours needed for such connection.

In this respect, simplification of the current connecting technique and reduction of the man-hours needed for such connection are the most important problems faced in efforts to reduce construction costs and to overcome the shortage of technicians who can perform such work.

Under such circumstances, connection of optical fibers by optical connectors seems to hold promise for simplifying the connecting technique, and construction of optical transmission line using aerial optical cable with optical connectors at both ends has been studied.

Also, a small-sized, light-weight box for accommodating excess length of optical cable, mountable on poles, has been produced on a trial basis to realize flexible control of small-sized single-core optical connector for single mode (SM); Furthermore, a low-cost, durable protector for the protection of the optical connector during cable pulling and for flexible control of cable piece length has been developed. All of these components have been shown to have high workability and long-term reliability under severe aerial conditions.

The applicability of these devices to the small-sized optical closure now in use has been evaluated with regards to optical cable connect. As a result, it has been demonstrated that optical connector splicing is very useful to shortning the splicing time compare with the conventional fusion splicing.

2. Outline of optical transmission line

The arrangement of the optical transmission line using aerial optical cable with optical connectors at both ends is given in Fig. 1.

3. Design and characteristics of small-sized single-core optical connector for SM fiber use

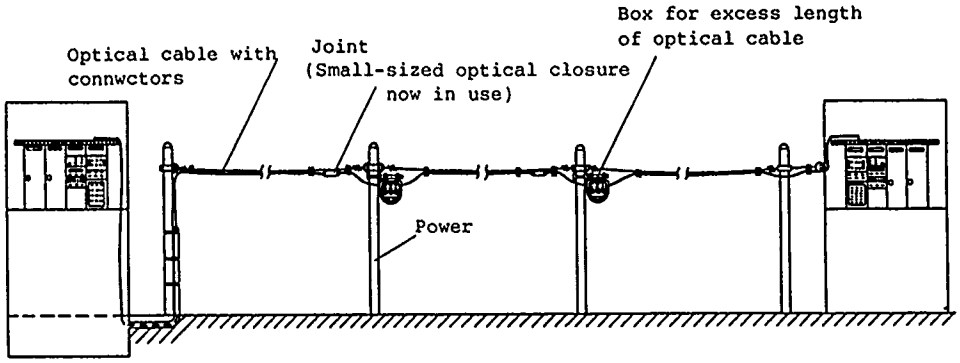

Fig. 1 Outline of optical transmission line

3.1 Design study

The essential conditions for the development of the optical connectors to be used at both ends of aerial optical cable are excellent maneuverability and workability even under severe field conditions, and long-term reliability of stable transmission characteristics, requiring no special technique for connection.

The FC type optical fiber connector conventionally in use is too large for our connection purposes. If the same optical closure is used, the number of core conductors should be extensively decreased compared with that in fusion splicing.

Also, the protector at the cable tip where the optical connector is mounted has a larger outer diameter due to the increase of number of optical fibers, and this means more difficulties when cable is pulled over sheaves. In this connection, we have attempted to study the application of optical connector to optical closure and to produce an optical connector protector of smaller diameter. thus, optical connectors of smaller size and diameter than the conventional type fusion spliced cable have been studied.

3.2 Structure and features

Figure 2 shows the structure of the newly developed small-sized single-core optical connector for SM use. This small-sized single-core optical connector for use with nylon coated SM fiber is designed so that the ferrules of the conventional FC type optical connector are connected with each other by a cylinder type adaptor and clip. Low-cost zirconia with excellent workability is used for these ferrules.

A compact design has been attained with the adoption of a structure of small diameter connecting the ferrules with the cylinder type adaptor and clip.

Compared with the method of connecting FC type optical connectors which are screwed into the adaptor, this small-sized optical connector provides a low loss, stable and connectable structure because the ferrules are inserted into the cylinder type adaptor and squeezed by clip, and the ferrules are kept in contact with each other by constant pressure. Axial adjustment is attainable at every 90 degrees (4 directions), and the ferrules are connected by aligning the markers, which are specified at the time of factory inspection as having the lowest connection loss.

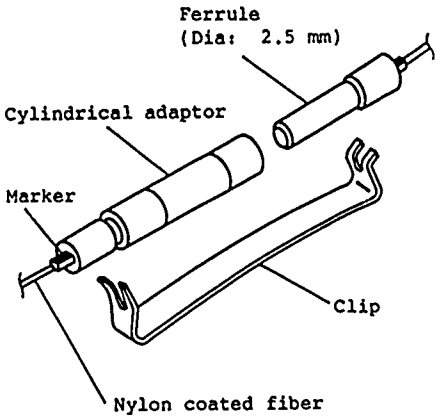

Fig. 2 Structure of small-sized single-core optical connector for SM fiber

3.3 Characteristics

The characteristics of newly developed optical connector were evaluated in tests. The results of the tests are summarized in Table 1.

As a result, it was found that the transmission characteristics are the same as these of conventional FC type optical connector, showing that there is substantially no problem in the practical application of this newly developed connector.

4. Design and characteristics of optical connector protector

4.1 Design study

Table 1 Test results of the single-core optical connectors

measurement at a wavelength of 1.3 μm.

	Test item	Item of measurement	Test condition	No. of specimens	Test results
Optical properties	Connection loss	Connection loss	• Connection with master plug • Average value from 3 insertions and removals	10	0.7 dB or less
	Reflection attenuation	Reflection attenuation	• Connection with master plug	10	25 dB or more
Mechanical properties	Plug removal	Loss increase End surface condition	• 500 removals and insertions • End surface cleaned after every 10 times	2	0.4 dB or less No abnormal signs
	Vibration	Loss increase	• 10-55 Hz • 1.5 mm p-p • 3 directions; 2 hours each	2	0.1 dB or less
	Impact	Loss increase	• 100G, 6 ms 3 directional 3 times	2	0.1 dB or less
	Tension	Loss increase	• 0-0.6 kgf	2	0.1 dB or less
Resistance to environmental conditions	Temperature change	Loss increase End surface condition	• -20- +60°C • 4-6 hours/cycle • 10 cycles	2	0.3 dB or less No abnormal signs
	Temperature and high humidity	Loss increase End surface condition	• +60°C • 90% RH • 100h	2	0.2 dB or less No abnormal signs
	High temperature	Loss increase End surface condition	• +80°C • 100h	2	0.2 dB or less No abnormal signs
	Low temperature	Loss increase End surface condition	• -20°C • 100h	2	0.3 dB or less No abnormal signs

To install aerial optical fiber cable with optical connectors at both ends, it is necessary to protect the cable tip having optical connectors from external force.

Special care was taken with regard to installation efficiency, such as in passing the cable over sheaves in aerial pulling, and the optical cable protector has been designed so as to have a small diameter and high flexibility to endure lateral pressure when it is passed over sheaves by pulling tension.

4.2 Structure and features

Figure 3 shows the structure of the self-supporting optical cable[1][2] which was used for the development of the optical connector protector. The structure of as optical connector protector is given in Fig. 4.

The tip of the optical cable mounted with small-sized single-core optical connector for SM fiber is protected by a durable corrugated PE tube with high flexibility. The tip of the corrugated PE tube is provided with a conical guide, and the connector protector is fixed on the cable suspension wire with a high-strength band to facilitate passage over the sheaves.

Excess length of core for connection is accommodated in the grooves of the PE spacer in the

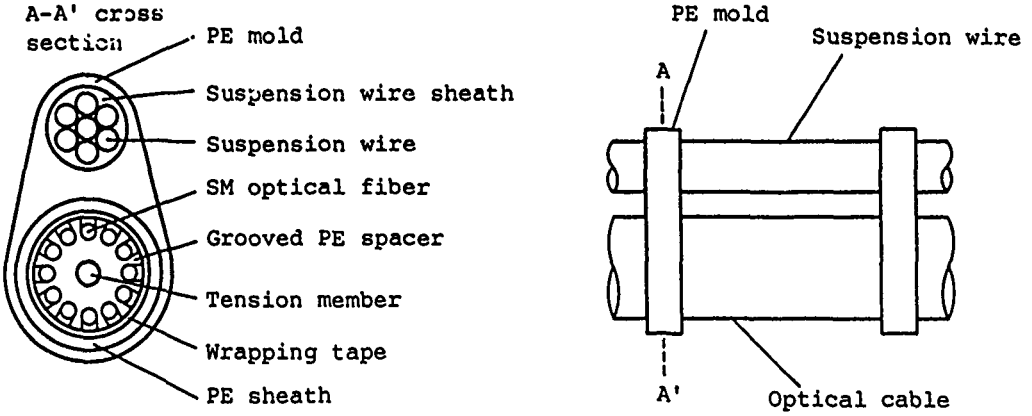

Fig. 3 Structure of self-supporting optical cable

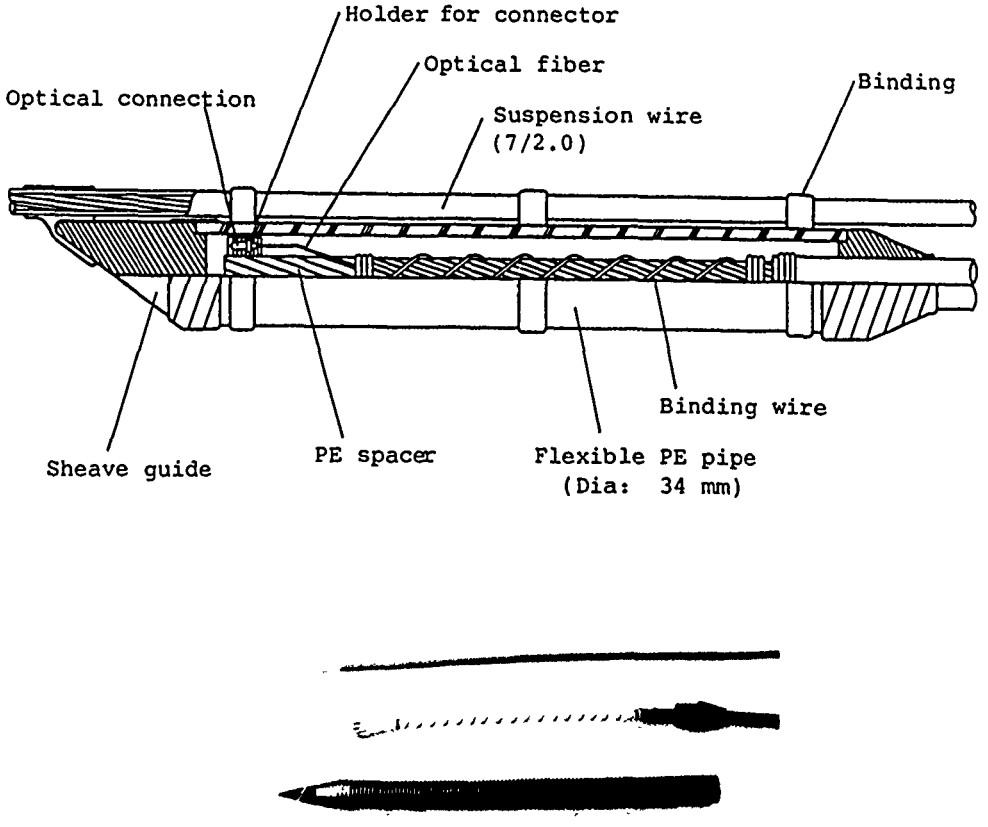

Fig. 4 Optical connector protector

longitudfinal direction of the cable, and binding wire is used for lashing.

To fix the optical connector, there are PE connector holders at the mounting position of the optical connector and on the PE spacer at the same position, and the connector is accommodated in the holder. Thus, a dual protection structure to which can endure external force such as lateral pressure has been designed.

By utilizing cable spacer and by accommodating excess length of core in spiral grooves, it is possible for the optical connector protector to bend with bending of the cable. A compact structure is attained through use of a small-sized optical connector.

4.3 Characteristics

In view of mechanical external force applied to the optical connector protector during installation, the characteristics of this protector were evaluated by tests.

The results of mechanical tests are summarized in Table 2.

The characteristics were evaluated by visual inspection of external appearance and by measurement of the change in transmission loss. Damage to the protector was found in none of the tests and transmission characteristics were also satisfactory. Thus, it was confirmed that there is substantially no problem in the practical application of this protector.

5. Accommodation box for excess length of cable structure and features

5.1 Design study

For aerial optical cable with optical connectors at both ends, it is necessary to strictly control the distance between joints and cable piece length.

It is desirable that cable piece length be the same as the distance between joints and that there be no excess length of cable after installation. However, it is very difficult to perform strict control on cable piece length in actual installation of aerial cable, and excess length should be included in the design length of the cable.

In this respect, it is necessary to accommodate excess length of cable, if any, on aerial line at cable joints after installation. Availability of accommodation space, cable protection external appearance, etc., must be considered.

After careful study of these factors, it was concluded that the best solution was to have a special box to accommodate excess length of cable, so as not to interfere with other devices and components.

For this purpose, a small-sized, lightweight box has been designed which can be installed on poles and which has minimum wind pressure load. It can accommodate 30 m or more of cable at an outer diameter of 15 mm.

5.2 Structure and features

Figure 5 shows the structure of this box for accommodating excess length of optical cable, and Table 3 summarizes the technical data.

Stainless steel is adopted as the material for this box because of its corrosion-resistant property. The surface of the box is painted the same color as that of the concrete pole.

A lightweight, compact design is adopted to facilitate its installion on poles. Punching plates perforated at fixed spacings are used on all sides of the box, and the box is semi-circular in shape. In order not to interfere with the other devices and components, this accommodation box must be fixed to a pole with a support arm; the box is mounted on the fixing arm at one point about 250 mm from the pole.

To accommodate the cable, the cable is pulled into

Table 2 Results of mechanical tests of optical connectors protector

Test item	Test conditions	Test results	
		Transmission (λ = 1.3 μm)	External appearance of protector
Jerking	• Tension: 150 kgf • Sheave passing angle (θ): 90° • Sheave type: No.4 sheave	Loss increase: 0.2 dB or less	No sign of damage or breakage
Repeated bending	• Mandrel radius: 300 mm • 90° bending: 15 times of reciprocal bendings	Loss increase: 0.2 dB or less	No sign of damage or breakage
Impact	• Impact body: 25 mmø cylinder • Impact load: 3 kgf • Falling height: 0.3 m	Loss increase: 0.2 dB or less	No sign of damage or breakage

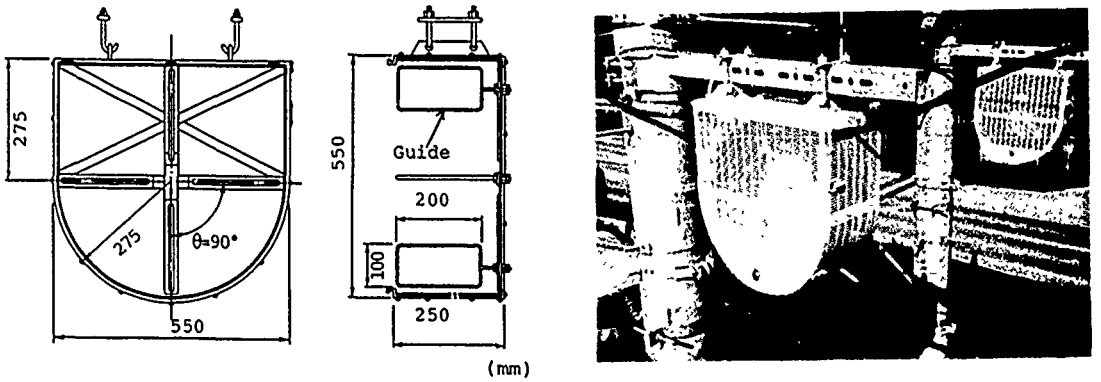

Fig. 5 Structure of accommodation box for excess length of optical cable

Table 3 Technical data of accommodation box for excess length of optical cable

Item		Technical data
Size	Longitudinal dimension	550 mm
	Lateral dimension	550 mm
	Width	250 mm
Plate type		Punching plate
Plate material		Stainless steel
Accommodatinng procedure		Wound on guide
Minimum cable accommodating diameter		300 mm
Weight		11 kg (incl. supporting fixture)

the cable inlets on both sides of the accommodation box and is wound on the guide in the box.

5.3 Characteristics

(1) Accommodation characteristics

Full-scale aerial tests were performed and the characteristics of accommodation of excess length of cable were tested. The results are given in Table 4.

The time required for accommodating excess length of cable was as short as about 15 minutes.

(2) Wind noise test

a. Test method

Wind was applied to the accommodation box at a wind velocity of from 10 m/sec. to 30 m/sec. The wind induced noise was recorded by microphone, and frequency analysis was performed on the values indicated by the sound level meter with a 1/3 octave band analyzer.

b. Test results

Figure 6 shows the results of the measurement of wind induced noise. For comparison purposes, the results of measurements of wind noise of a conventional pole-top outdoor joint box (550 mm x 500 mm x 300 mm; long. x lateral x width) used in the past are also given.

The wind noise level of the accommodation box for excess length of optical cable was the same as that of the conventional type pole-top outdoor joint box, and no abnormal noise was heard during the test. Thus, there is no problem with wind noise.

6. Evaluation of applicability of the small-sized optical closure now in use

To evaluate the applicability of the small-sized optical closure[3] now in use (Fig. 7) for optical connector splicing, assembly test and verification test were carried out.

The results of the tests are given in Table 5.

The transmission characteristics were satisfactory, and the applicability has thus been verified.

7. Evaluation of splicing workability

Splicing workability was compared between fusion splicing as used in the past and the splicing of the newly developed small-sized optical connector using the small-sized optical closure now in use.

The results of the comparison of needed man-hours are shown in Table 6.

Table 4 Results of tests on characteristics of acommodation excess of length of optical cable

Test item	Conditions	Test results
Accommodation workability	Full-scale performance on experiment line (work on pole) Number of workers: 2 Scope of work: Accommodation of 45 m of excess length of cable from cable mainline and suspension wire	Working time: About 15 min.
Accommodation length	Design accommodation length: 30 m; Cable outer diameter; 15 mmø	40 - 45 m
Loss change in accommodation	When 45 m of cable is accommodated (λ = 1.3 μm)	No increase in loss

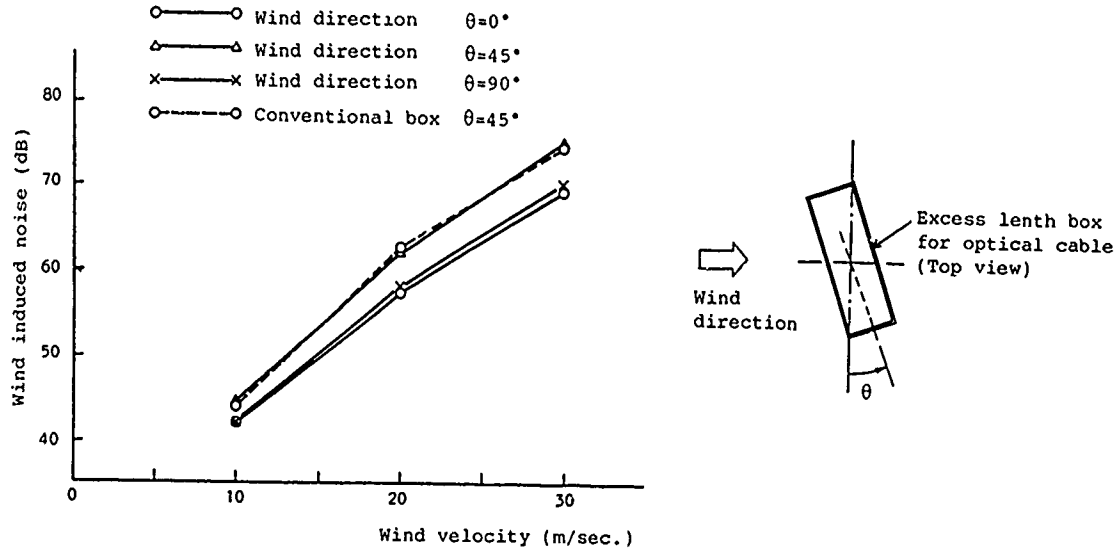

Fig. 6 Results of wind noise measurement

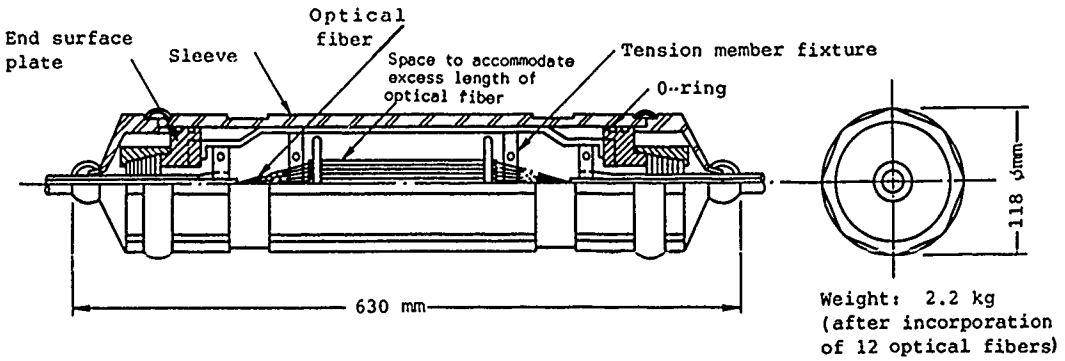

Fig. 7 Structure of small-sized optic1 closure now in use

By the comparison of workability, it was found that the man-hours needed time for splicing of 12 optical fibers cable using optical connector splicing is about 1/3 of the man-hours needed for fusion splicing.

8. Conclusion

In order to simplify the fusion splicing technique, aerial self-supporting optical cable with optical connectors at both ends was evaluated.

Table 5 Test results of applicability of the small-sized optical closure now in use

(connector splicing number 18)

Item	Test conditions	Test results
Connection loss	No matching oil	0.7 dB or less
Excess fiber length accommodation	Sheet accommodation system; 60 mmø in dia., 18 fibers	0.4 dB or less
Vibration	10 Hz; ±5 mm; 10^6 times	0.1 dB or less
Temperature change	-20 to +60°C; 10 cycles	0.3 dB or less

Table 6 Comparison of needed man-hours between fusion splicing and connector splicing (converted to 12 optical fibers)

Operations	Fusion splicing		Connector splicing	
Pre-treatment	Parts insertion; Sheath stripping	9 min.	Disassembling of protector; Parts insertion	8 min.
	Total	9 min.	Total	8 min.
Tension member fixing	Stripping of wrapping tape	5 min.	Cutting of grooved PE spacer	1 min.
	Cutting of grooved PE spacer; Fixing of grooved PE spacer	5 min.	Fixing of grooved PE spacer	5 min.
	Total	10 min.	Total	6 min.
Excess fiber length accommodation	Accommodation	24 min./ 12 fibers	Accommodation	24 min./ 12 fibers
	Total	24 min.	Total	24 min.
Sheath connection	End surface plate, cap nut;	3 min.	End surface plate, cap nut;	3 min.
	Taping	6 min.	Taping	6 min.
	Total	9 min.	Total	9 min.
Suspension		20 min.		20 min.
	Total	20 min.	Total	20 min.
Subtotal		72 min./ 12 fibers		67 min./ 12 fibers
Fibers connection	15 min./fiber × 12 fibers = 180 min.		0.5 min./fiber × 12 fibers = 6 min.	
Total	252 min. (4 h 12 min.)		73 min. (1 h 13 min.)	

For this purpose, the following products have been developed: a small-sized single-core optical connector for SM fiber use with high workability and small-diameter; a durable optical connector protector; and a lightweight box to accommodate excess cable length of 30 m.

Optical fiber splicing by optical connector, using the small-sized optical closure now in use, is effective for decreasing the cost of transmission line installation and the man-hour needed for such installation.

The newly developed accommodation box for excess length can be flexibly used for future installation if, installed on transmission line in advance. Also, this box is useful for determining splicing points and for standardization of cable piece length.

The results of the present study will be utilized when these new products are introduced into practical use.

References

(1) T. Konno et al., "Fire-resistant characteristics of aerial optical cables," Proceedings of International Wire & Cable Symposium, 1985, p.223-240.

(2) M. Suzuki et al., "Snow accretion resistant self-supporting optical fiber cables" 5th International Workshop on Atmospheric Icing of Structures, Tokyo 1990; B7-3.

(3) Y. Usizaka, S. Hasegawa, K. Niikura, Y. Yamasita, M. Sato and Y. Yamada: "Development of mechanical closures for optical fiber cables," IEICE Spring 1988; B-603.

Yoshihiro Ushizaka
Tohoku Electric
Power Co., Inc.
3-7-1, Ichibancho,
Aoba-ku, Sendai
980, Japan

Yoshihiro Ushizaka graduated from Gakuhou Fukushima Technical School in 1974. He then joined Tohoku Electric Power Co. Inc., and has been engaged in engineering of telecommunication. He is now an engineer in development of optical fiber communication system.

Hiroaki Horima
Sumitomo Electric
Industries, Ltd.
1, Taya-cho,
Sakae-ku, Yokohama
244, Japan

Hiroaki Horima received his M.S. degree in engineering from Osaka University in 1972. He then joined Sumitomo Electric Industries, Ltd. and worked on the development of CATV coaxial cable, multipair PEF-insulated junction cables and low loss unbalanced type cables. Thereafter, he concentrated on the development of optical fiber cables. He is now Section Manager of the Fiber Optics Division at Sumitomo Electric Industries, Ltd. He is a member of the Institute of Electronics and Communication Engineers of Japan.

Yoichi Komaki
Tohoku Electric
Power Co., Inc.
3-7-1, Ichibancho,
Aoba-ku, Sendai
980, Japan

Yoichi Komaki graduated from Kamaishi Technical School in 1960. He then joined Tohoku Electric Power Co. Inc., and has been engaged in engineering of electric distributions. He is now a supervisor of telecommunications engineering section, and engaged in engineering of optical fiber communications system.

Masafumi Sato
Kitanihon Electric
Cable Co., Ltd.
1-2-1, Koriyama,
Taihaku-ku,
Sendai 982, Japan

Masafumi Sato was born in 1962. He joined Kitanihon Electric Cable Co., Ltd. and has been engaged in the design and development of communication cables, power cables and accessories for these cables.

Koji Niikura
Sumitomo Electric
Industries, Ltd.
1, Taya-cho,
Sakae-ku, Yokohama
244, Japan

Koji Niikura received his B.E. degree in engineering from Waseda University in 1984 and joined Sumitomo Electric Industries, Ltd. He has been engaged in the development and design of optical fiber cables in the Fiber Optics Division.

Yuichi Yamada
Kitanihon Electric
Cable Co., Ltd.
1-2-1, Koriyama,
Taihaku-ku,
Sendai 982, Japan

Yuichi Yamada was born 1952. He joined Kitanihon Electric Cable Co., Ltd. and has been engaged in the design and development of communication cables, power cables and accessories for these cables. He is a member of the Institute of Electronics and Communication Engineers of Japan.

LIGHTWEIGHT FIBER OPTIC CABLE

P. D. Patel

AT&T Bell Laboratories
Norcross, Georgia 30071

A. J. Panuska

AT&T Network Systems
Norcross, Georgia 30071

1. ABSTRACT

A proven loose fiber bundle and linear strength member philosophy was applied to develop an optimized low fiber count cable that is economical and lightweight. This challenge was met by exploiting the excess fiber length while retaining excellent optical and mechanical performance. The resulting 10 mm diameter, armor-free cable accommodates as many as 24 fibers and weighs only 90 kg/km which makes it one of the lightest cable with the highest fiber density in the industry. Although intended primarily for aerial applications, this cable is also suited for buried and underground installations. The lightweight cable is an ideal choice for the CATV market, which has about 85% of cables in the aerial plant, as well as loop and campus applications.

2. INTRODUCTION

To date, attention has been given to fiber optic cables with high fiber counts used in point-to-point telephony applications. A high percentage of fiber optic cable sales, however, have historically consisted of low fiber counts ($\leq$ 24 fibers). Therefore, a great need exists both in telephony and specialty markets for an economical design optimized for low fiber counts. A number of low fiber count cables are presently offered, but the designs are based on high fiber count usage. These designs fall into two major classes: a loose tube design and a loose fiber bundle design.

In the loose-tube design, a maximum of 12 fibers are packaged in an individual buffer tube, and several tubes are stranded together over a central member to form a core. This construction is inherently space inefficient and results in large and heavy cables. On the other hand, the loose-fiber-bundle design consists of several 12 fiber bundles in a single core tube which is positioned straight along the center line of the cable without stranding[1]. This design is better suited for low-fiber-count optimization. A metallic armor cable, based on this loose fiber bundle approach, has been reported[2]; however, it is limited to a single bundle with 12 fibers.

Based on customer input and requests, we have developed a 24 fiber cable to fill the low fiber count cable needs for telephony and specialty markets. This lightweight armor-free design utilizes proven fiber bundle core and linear strength member sheath technologies. In this paper, a cable design philosophy will be described first and then cable testing results, including qualification and supplementary tests, will be presented.

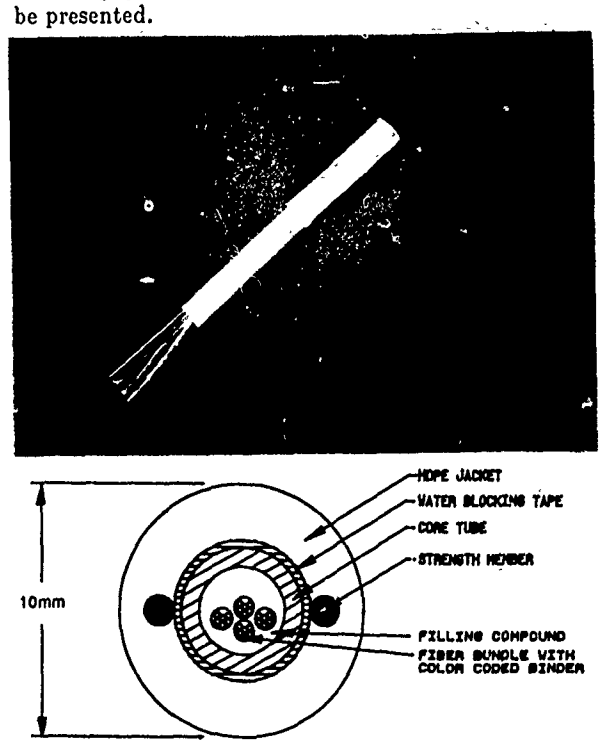

FIGURE 1. LIGHTWEIGHT CABLE

3. CABLE DESIGN PHILOSOPHY

Customer input and requests indicated that an economical, lightweight cable optimized for a maximum of 24 fibers is needed for predominantly aerial applications. The key design challenge was to provide an economical cable that is small in size and weight yet retains excellent optical performance along with the 600 lb tensile load rating. This is accomplished by adopting the loose fiber bundle approach for the core design[1] and linear strength member technology for the sheath design[3]. A photograph in Fig. 1 shows the lightweight fiber optic cable that is designed based on following core and sheath design philosophy.

3.1 Core Design

A cable core consists of a filled core tube made from a durable material to provide enhanced mechanical protection and up to four loose fiber bundles as shown in Fig. 1. Each loose fiber bundle contains six fibers held together by a color coded binder yarn as shown Fig. 2. The fibers may be singlemode, pure silica, multimode (62.5/125 μm), or a combination of them. The fibers must be protected from the service and installation environment. Specifically, they must be guarded from high tensile strains and from excessive bending that results in attenuation increases. To understand these effects, some of the critical parameters that are considered in the design process are described next.

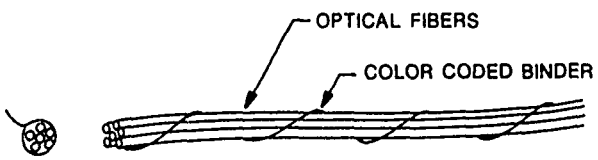

FIGURE 2. LOOSE FIBER BUNDLE

3.1.1 Packing Density: The most effective way to define packing density is based on the inside diameter of the core tube rather than the outside diameter of the cable since there are numerous options available for the sheath. Packing density (PD) is defined as a ratio of total fiber area to core area in percent.

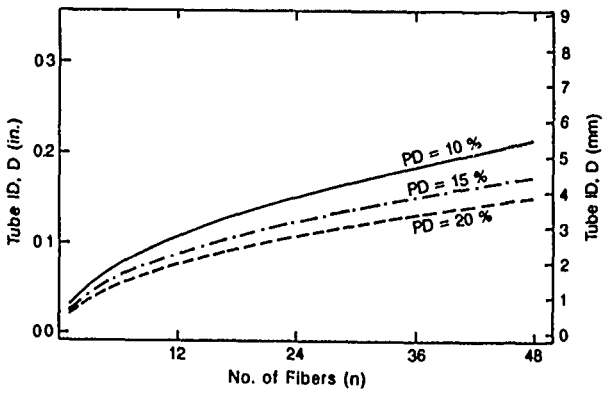

FIGURE 3. PACKING DENSITY CURVES

$$PD = 100\, n \left(\frac{d_f}{D}\right)^2 \qquad (3.1.1.1)$$

Where
n = Number of fibers
d_f = Fiber diameter (250 μm)
D = Inside diameter of core tube

Based on this result, three packing density curves as a function of D and n are shown in Fig. 3. For a given packing density, a core tube may be sized from these design curves for any number of fibers. Cables with a high packing density result in compact and lightweight designs. However, the design challenge increases with increase in packing density because the fibers are more confined. The loose fiber bundle design offers higher packing density than the multiple individual buffer tube design since the fiber bundles share a common free space in a single core tube.

3.1.2 Excess Fiber Length: The excess fiber length (ϵ_c) in a cable is defined as a ratio of the difference between the fiber length (L_f) and the cable length (L_c) to the cable length expressed in percent as follows:

$$\epsilon_c = 100\left(\frac{L_f - L_c}{L_c}\right) \qquad (3.1.2.1)$$

Traditionally, a small amount of excess fiber length, on the order of 0.1%, is provided in the loose fiber bundle design to insure that fiber does not exceed short-term safe design strain limits (typically 0.33% for 50kpsi proof-tested fibers). By increasing and precisely controlling this excess length, one could

exploit it to offer an advantage. For example, a 0.1% increase in excess length would allow a corresponding 30% reduction in tensile stiffness (for 50kpsi proof-tested fibers). However, an increase in excess length generally means smaller fiber bend radius and more demanding design requirements. The fibers in the loose fiber bundle design assume a path of least resistance to accommodate the excess length. For analysis purpose, this path may be mathematically treated as having a shape of either a helix or a sinusoid.

Schematics of the helix and sinusoidal models with corresponding geometric parameters are shown in Figs. 4 and 5, respectively. Let us first consider the helix (subscript h) model to derive the excess fiber length as a function of core tube inside diameter (D), fiber bundle diameter (d), pitch or lay length (P), and radius of curvature of fiber bundle (R). The fiber length (L_f), the excess fiber length (ϵ_{eh}), and the radius of curvature (R_h) for this model is given by:

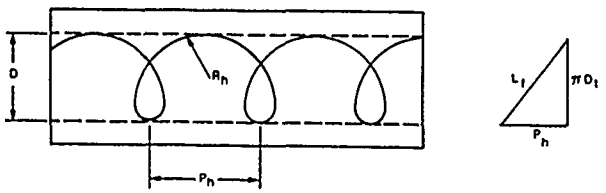

FIGURE 4. HELIX MODEL

$$L_f = \left(P_h^2+(\pi D_t)^2\right)^{1/2} \tag{3.1.2.2}$$

$$\epsilon_{eh} = 100\left[\left(1+\left\{\frac{\pi D_t}{P_h}\right\}^2\right)^{1/2}-1\right] \tag{3.1.2.3}$$

$$R_h = \frac{D_t}{2}\left[\left\{\frac{P_h}{\pi D_t}\right\}^2+1\right] \tag{3.1.2.4}$$

Where the helix diameter D_t and radius R_t is given by:

$$D_t = 2R_t = D-d \tag{3.1.2.5}$$

Combining Equations (3.1.2.3) and (3.1.2.4), we get:

$$\frac{R_h}{R_t} = \frac{a}{a-1} \tag{3.1.2.6}$$

$$\frac{P_h}{R_t} = 2\pi\left[\frac{1}{a-1}\right]^{1/2} \tag{3.1.2.7}$$

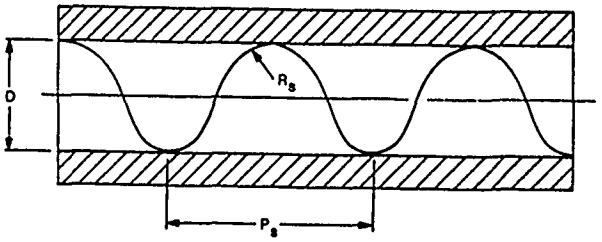

FIGURE 5. SINUSOIDAL MODEL

Where

$$a = \left(1+\frac{\epsilon_{eh}}{100}\right)^2 \tag{3.1.2.8}$$

Figure 6 shows two design curves of ϵ_{eh} and $\frac{P_h}{R_t}$ as a function of bend radii for the helix model.

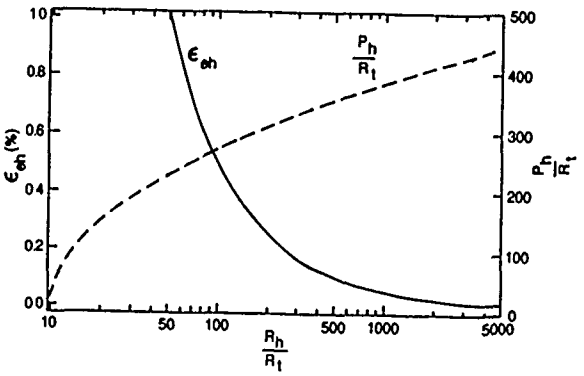

FIGURE 6. HELIX MODEL

Similarly, let us consider the sinusoid (subscript s) model. The length of fiber, L_f, along the sinusoidal curve is given by:

$$L_f = \frac{2P_s}{\pi}\int_0^{\frac{\pi}{2}}\left(1+k^2\cos^2\phi\right)^{1/2}d\phi \tag{3.1.2.9}$$

Where

$$k = \frac{\pi D_t}{P_s} \qquad (3.1.2.10)$$

The integral in Equation (3.1.2.9) is an elliptical integral of second kind and it can be represented by an infinite series. The excess fiber length (ϵ_{es}) and the minimum radius of curvature (R_s) for the sinusoidal model is given by:

$$\epsilon_{es} = 100\left[(1+k^2)^{1/2}\left(1-p\right)-1\right] \qquad (3.1.2.11)$$

Where

$$p = \frac{1}{4}q^2+\frac{3}{64}q^4+\frac{1}{256}q^6+\cdots \qquad (3.1.2.12)$$

$$q = \frac{k}{\left(1+k^2\right)^{1/2}} \qquad (3.1.2.13)$$

$$R_s = \frac{D_t}{2}\left(\frac{P_s}{\pi D_t}\right)^2 \qquad (3.1.2.14)$$

We observe from Equation (3.1.2.11) that the first term is the same as the excess fiber length for the helix model and that the sinusoidal model always gives a lower value for excess length. Furthermore, the radius of curvature for the helix model is constant along the curve in contrast with a variable radius of curvature for the sinusoidal model. For a given excess fiber length, the sinusoidal model is conservative and gives a lower minimum radius than the helix model.

Combining Equations (3.1.2.11) and (3.1.2.14), we get:

$$\frac{R_s}{R_t} = \frac{1-q^2}{q^2} \qquad (3.1.2.15)$$

$$\frac{P_s}{R_t} = 2\pi\left[\frac{1-q^2}{q^2}\right]^{1/2} \qquad (3.1.2.16)$$

Figure 7 shows two design curves for ϵ_{es} and $\frac{P_s}{R_t}$ as a function of minimum bend radii for sinusoid.

3.1.3 Static Fatigue: The strength of optical fibers degrades (or flaw size grows) under the influence of time, stress and humidity. For a constant stress, this phenomenon is commonly known as static fatigue. A relationship between minimum time to failure and applied uniform tensile stress for a given proof-tested fiber is given in Fig. 5.4 of Reference[4]. Based on static fatigue considerations for a 40 year life, the minimum allowable bend radius is about 45 mm for a 50 kpsi proof-tested fiber. Again, this value is conservative since the probability of failure in bending is significantly less than in uniform tension. This provides one constraint on the minimum bend radius for the fiber. The other constraint is the increase in attenuation due to bending.

3.1.4 Bending Losses: As we have shown above, the fibers are bent to a certain radius depending on the amount of excess fiber length and the core tube diameter. Minimum bend radius for given number of fibers is obtained by using the sinusoidal model. Environmental effects must be considered since the worst case occurs at lowest operating temperature. This minimum bend radius can be used in conjunction with the fiber parameters to estimate the increase in attenuation. One such model for computation of attenuation is given by Marcuse[5]. In general attenuation increases at 1300 nm and 1550 nm are insignificant at bend radii greater than 30 mm in the presently available commercial single mode fibers.

3.1.5 Filling Compound: A single filling compound is used in this design which prevents the migration of water or other liquids along the cable core. The material is chosen such that its rheological properties in the operating temperature range, allow easy fiber movement when they are strained. This is accomplished by carefully selecting the critical shear stress behavior of the filling material. This property is also critical in terms of controlling excess fiber length during processing. Furthermore, at high temperatures, the compound should remain in the cable and pass the Bellcore's compound flow test at 65 °C [6]. The compound should be non-volatile, non-toxic, and chemically compatible with the optical fibers and other cable components. The compound also should be stable over the service life of the product.

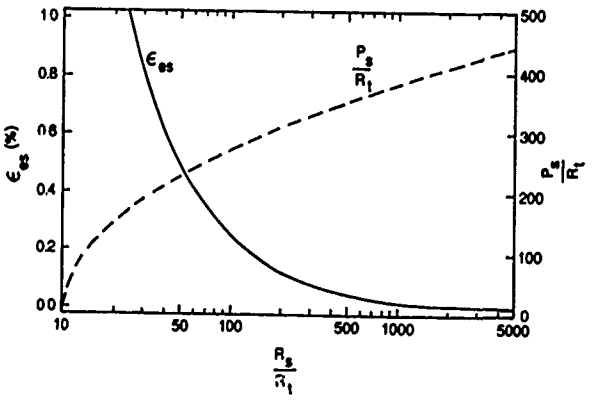

FIGURE 7. SINUSOID MODEL

3.1.6 Optimum Core Size: Based on the above considerations, one could optimize the core size for a given number of fibers and excess length. For example, using Fig. 3, a tentative core tube diameter can be obtained by assuming a packing density between 10% and 20% for a given number of fibers. Then a minimum bend radius can be obtained from Figs. 6 and 7 for a given excess fiber length. Finally, bending losses are estimated to check if the attenuation increase is in the tolerable limit. This process can be repeated until a satisfactory design is obtained. Of course, the design is completed only after a cable sample is manufactured and tested satisfactorily.

3.2 Sheath Design

The sheath design must be such that it protects fibers from the rigors of processing, installation, and service environments. Specifically, fibers must be guarded against excessive tensile and compressive strains caused by these environments. The lightweight cable sheath consists of two linear wire strength members in the outer jacket to form a composite structure. Although rip cords are not shown in Fig. 1, they are provided as needed.

3.2.1 Cable Shrinkage: All polymeric materials used in cables shrink due to thermal contraction during processing. If this shrinkage is excessive, it induces high compressive strains on the fibers and the attenuation increases as the fibers are constrained to small bend radii. Various materials and techniques are used to overcome this problem. For example, strength members (e.g. metallic wires, glass rods) having both tensile and compressive stiffness, metallic armor, and lightly-impregnated fiber glass rovings are used to limit the excessive shrinkage with varying degree of success.

3.2.2 Tensile Response: A linear tensile response (load vs. strain curve) of the cable is desirable so that a predictable amount of excess fiber length can be obtained. Sheaths with linear steel members do provide the desired linear response. However, the use of semi-rigid or lightly impregnated strength members *alone* do not offer enough compressive resistance and therefore result in a non-linear behavior with a "knee" in the response curve. A large knee in the curve means the cable sees higher strains at the rated load of 2,700 N (600 lbs). Fig. 8 shows a tensile characteristics of a lightweight cable sheath as compared to a sheath having stranded lightly impregnated fiber glass roving strength members. Note that the lightweight design with steel wires provides a linear response whereas the lightly impregnated roving design shows a large knee. This knee effect must be compensated by providing higher excess fiber length to limit installation strains on the fibers.

3.2.3 Environmental Effects: All cable components, including the core and the sheath, must be stable over the operating temperature range of -40°C to 85°C for the life of cable. All distribution cables are required to pass the Bellcore's component aging test. [7]. This test insures high reliability of the cable over its service life particularly at a service access point. For example, tests have shown that some polymers when aged under high temperature and humidity degrade very rapidly and their elongation at break drops from 400% to near zero[8] [9]. For this reason a hydrolytically stable materials must be chosen for all cable components.

4. CABLE TESTING

All new cable designs are subjected to customer specified qualification testing as well as supplementary testing to evaluate their design capability.

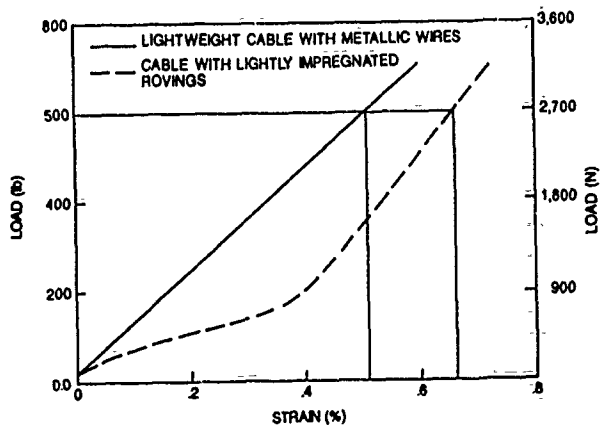

FIGURE 8. TENSILE RESPONSE OF CABLE

4.1 Qualification Tests

4.1.1 Mechanical Performance: The lightweight cable was subjected to a series of mechanical endurance tests to assure superior performance in the field. Table I summarizes the major standard tests performed on this cable. They are conducted according to the Bell Communications Research (Bellcore)[6] and the Electronic Industries Association (EIA)[10] test Procedure. The lightweight cable meets or exceeds all of the requirements.

Table I. MECHANICAL TESTS		
Test	Specification	Requirement
Low and High Temperature Bend	EIA-455-37 §5.1.1	Mandrel Diameter = 20x Cable OD 4 Wraps each at -30 °C and 60 °C
Impact Resistance	EIA-455-25A §5.1.2	4 kg from 150 mm Height, 25 Impact Cycles
Compressive Strength	EIA-455-41 §5.1.3	220 N/cm
Tensile Strength	EIA-455-33A §5.1.4	2,700 N Mandrel Diameter = 30x Cable OD
Cable Twist	EIA-455-85 §5.1.5	±180 ° Twist, 10 Cycles
Cyclic Flex	EIA-455-104 §5.1.6	Sheave Diameter = 20x Cable OD 30 Cycles/min, For 25 Cycles
External Freezing	EIA-455-98A §5.1.7	1 hr. min freeze at -2 °C

§ *Section numbers from Bellcore TR-TSY-000020, Issue 4.*

4.1.2 Optical Performance: The lightweight cable is designed to give the same optical performance as comparable armored designs. Figure 9 shows the optical loss distribution for a prototype lightweight cable with 24 singlemode fibers. This cable was manufactured to meet a maximum individual fiber loss of 0.40 and 0.26 dB/km at 1310 and 1550 nm, respectively. The results show virtually zero added loss in cabling.

In addition to the room temperature optical loss, the cable was subjected to standard Bellcore environmental test. Figure 10 shows the results of this test over the temperature range of -40 °C to 85 °C. This design shows excellent thermal stability over the entire temperature range.

4.2 Supplementary Tests

In addition to required qualification tests, several other tests were performed to insure high reliability of new designs. Several of these tests are described below; and they include aerial lightning simulation, field simulation, and field trial.

4.2.1 Aerial Lightning Simulation: The armor-free lightweight design is primarily intended for aerial applications. In this application, the cable is lashed to a metallic support strand with a metallic lashing wire. A standard sand box lightning test used for buried cables is not representative of lightning conditions in the aerial plant. Therefore, a modified sand box test, without the sand, was devised to test the lightning susceptibility of this cable in aerial plant;

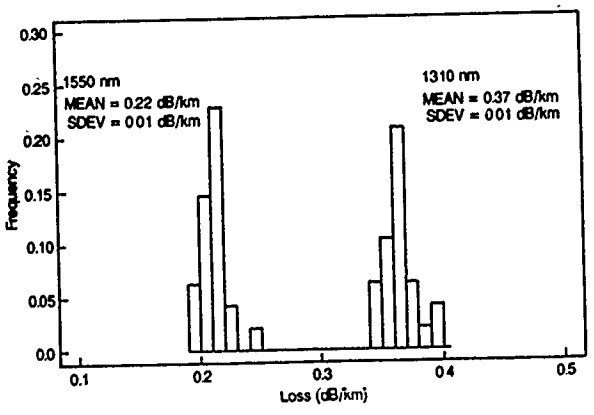

FIGURE 9. LIGHTWEIGHT CABLE OPTICAL LOSS

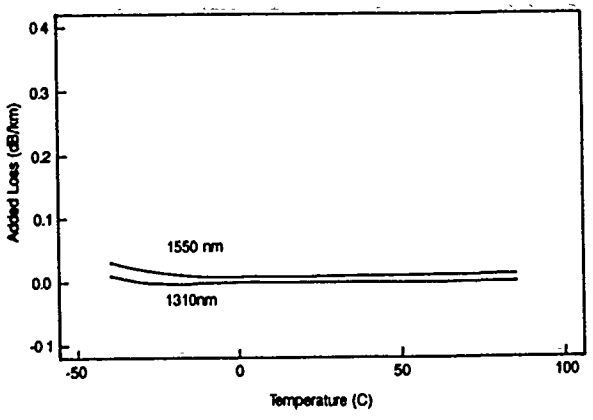

FIGURE 10. LIGHTWEIGHT CABLE ENVIRONMENTAL PERFORMANCE

Numerous tests were performed on armored, dielectric, and armor-free designs. Tests have confirmed that all designs performed equally well when lashed to a metallic strand. There was no damage to the core or fibers.

4.2.2 Field Simulation: As a standard practice, all new cable designs under go numerous field simulations to guarantee highest reliability. For example, the lightweight design was tested for underground cable handling, aerial cable handling, sheave test under tension, figure-8 crushing test, and various plowing tests. These tests were performed at the AT&T Bell Laboratories Chester Field Testing Laboratory. The cable behaved exceptionally good under all test conditions without a permanent change in attenuation or a sheath damage. These tests show that the cable design is rugged and craft friendly for both aerial and buried applications. Although, the design is primarily intended for aerial application, it is equally suitable for plowing in a buried installation.

4.2.3 Field Trial: The final step in the design process is to test the cable in the field. A customer is selected based on typical installation and environmental conditions to provide early feedback on the new design. A 20 kilometer length of this cable was field trialed in May of 1990 in California. This experience indicates that the cable performed as intended and the handling performance was excellent.

5. SUMMARY

A lightweight cable having 10 mm (0.4 inch) diameter and weighing 90 kg/km (60 lb/kft) has been designed and optimized for 24 fibers. This armor-free design takes advantage of loose fiber bundle core and linear strength member sheath technologies. Furthermore, by exploiting the excess fiber length, the cable retains a 2,700-N (600-lb) tensile load rating. This design offers the same excellent optical performance as comparable armored designs; and it meets or exceeds common industry standards. The cable is compatible with universal fiber optic closures, splices, connectors, and other hardware. Although intended primarily for aerial applications, the cable is also suited for buried and underground installations. The lightweight cable is an ideal choice for the CATV market, which has about 85% of cables in the aerial plant, as well as loop and campus applications.

6. ACKNOWLEDGEMENTS

The authors would like to thank R. J. Brown, Terry Coffman, W. H. Ficke, and R. L. Porter for their invaluable help in developing this cable. Our special thanks to D. L. Pope and his group for carrying out the field simulation tests.

REFERENCES

1. P. D. Patel and C. H. Gartside, III, "Compact Lightguide Cable Design," 34th International Wire and Cable Symposium Proceedings, 1985, pp. 21-27.
2. Martin C. Light, James A. Moses, Mark A. Sigmon, Christopher A. Story, "Design and Performance of Telecommunication Cables Optimized for Low Fiber Counts," 37th International Wire and Cable Symposium Proceedings, 1988, pp. 63-71.
3. P. D. Patel, M. R. Reynolds, M. D. Kinard, A. J. Panuska, "LXE- A Fiber-Optic Cable Sheath Family with Enhanced Fiber Access," 37th International Wire and Cable Symposium Proceedings, 1988, pp. 72-78.
4. Optical Fiber Telecommunications II, Edited by Stewart E. Miller and Ivan P. Kaminow, Academic Press, Inc., pp. 226.
5. D. Marcuse, "Influence of Curvature on the Losses of Doubly Clad Fibers," Applied Optics, Vol. 21, page 4208, December 1, 1982.
6. Bell communications Research Inc., "Generic Requirements for Optical Fiber and Optical Fiber Cable," Technical Reference TR-TSY- 000020, Issue 4, March 1989.
7. Bell communications Research Inc., "Generic Requirements for Optical Distribution Cable," Technical Advisory TA-TSY- 000944, Issue 1, July 1989.
8. Donald R. Parris, "A Lifetime Prediction Method for Thermoplastic Polymers," 38th International Wire and Cable Symposium Proceedings, 1989, pp. 105-110.
9. Jürgen Eickholt and Dr. Ralf Schuler, "Polybuthylene Terephthalate (PBT) with Improved Hydrolysis Resistance and Low Post Shrinkage for Loose Buffer Tubes," 38th International Wire and Cable Symposium Proceedings, 1989, pp. 120-122.
10. EIA Standard RS-455 and Addenda, Standard Test Procedures for Fiber Optic Fibers, Cables, Transducers, Connecting and Terminating Devices, Electronic Industries Association.

P. D. PATEL
AT&T Bell Laboratories
Norcross, GA 30071

P. D. Patel is a Distinguished Member of Technical Staff at AT&T Bell Laboratories, Norcross, Georgia. He joined Bell Laboratories in North Andover, Massachusetts in 1969 after receiving degrees in Mechanical Engineering, including a B. E. from Maharaja Sayajirao University, India, and Engr. Sc. D. degrees from Columbia University. Since 1979 he has worked in the Lightguide Media Department at Norcross and is currently working in the Exploratory & Military Lightguide Cables & Measurements Group. He is a member of the American Society of Mechanical Engineers.

A. J. PANUSKA
AT&T Network Systems
Norcross, GA 30071

Andrew J. Panuska is a Senior Development Engineer with AT&T Network System in Norcross, Georgia. He received B. S. degree in Mechanical Engineering and Civil Engineering, both from Johns Hopkins University. He joined AT&T in 1963 at Baltimore Works and worked on Ocean Cables. Then, he was assigned in 1969 to Atlanta Works on Copper Cable sheathing and jacketing. Since 1979, he has worked in the development of lightguide cable products and processes.

DESIGN AND TEST CONSIDERATIONS FOR FIBER OPTIC AERIAL CABLES

Andrew S. Dodd Harvey R. McDowell III Richard S. Wagman

Siecor Corporation
489 Siecor Park
Hickory, NC 28603

Abstract

Fiber optic cables are well suited for aerial applications. This paper will discuss the design and test considerations for three cable designs that are used aerially. The first design is a self-supporting "Figure 8" cable. This cable is composed of a steel messenger and fiber optic cable core both with a common plastic jacket. The next cable discussed is an all-dielectric low fiber count cable designed to meet the requirements of a lashed and/or overlashed environment. The third design is a self-supporting, all-dielectric pre-stranded optical system. This cable is comprised of an optical cable stranded around an aramid messenger. These designs comprise a cable family that meets the requirements of many aerial applications.

Introduction

Cables placed aerially are exposed to ultraviolet radiation, temperature extremes, ice loading and wind loading to name a few. All aerial cables should have certain common qualities. They must withstand these environmental forces for many years. The optical fiber must be protected so that it is never at risk to attenuation increases due to bending or catastrophic breaks due to fatigue.

The environment of the cable should be considered so that the right cable is selected. This is so that the cable will be strong enough to withstand the storm loading conditions of that particular area and yet be cost effective. To this end the National Electric Safety Code ANSI C2-1990 (NESC) gives guidance for the selection of the storm loading conditions. Given this information and then knowing the span length, sag restrictions, and the geographical region, a computer model may be used to aid in the selection of the correct messenger and/or cable design.

Installation costs are also a prime consideration when a cable system is being chosen. As a general rule, lashed cables are costlier to install than self-supporting cables due to the need to string up a messenger and then lash the cable. These cables do offer advantages to customers who wish to have the ability to expand at some future date with minimal costs. The self-supporting cables cost less to install but are not as easily expanded.

The main thrust of the paper is to discuss the important design aspects of these three cables as well as how they may be tested to ensure that the design is suitable for the prescribed environment.

Design and Test Considerations

Figure 8 Cable

Figure 8 cable, also known as Integrated Messenger (IM) cable, is a self- supporting aerial cable where a jacket is extruded over both an aerial messenger and a cable core. The cable and messenger are connected by a "web" (see Figures 1 and 2) which provides coupling that spreads the loading over the entire length of the cable.

Figure 8 cables typically use the same type of stranded steel messengers used in lashed cable installations except, they have an asphaltic flooding compound in their interstices. This helps prevent corrosion of the messenger.[1] With a steel messenger, care must be taken to ensure the messenger is well grounded for the lifetime of the cable.

Figure 8 cables have been used with copper cable cores for many years. The use of a Figure 8 design

with fiber optic cable cores is just beginning with most of the major fiber optic cable producers introducing designs over the last couple of years. A Figure 8 typically costs approximately 35% less to install than a lashed cable. Figure 8 cable uses standard deadend grips, but with tangent clamps modified for Figure 8 designs. To install a deadend grip, the messenger is split from the cable portion by cutting the web. The plastic over the messenger is removed, and the deadend grip is applied. Attaching the cable to a tangent clamp is very simple. The messenger portion of the cable fits in the tangent clamp with the web and optical portion hanging below.

The shape of Figure 8 cable has advantages and disadvantages. Its shape allows easy installation and permits the fiber optic cable to be easily separated from the messenger, by simply cutting the web. Currently, it is difficult to over-lash Figure 8 cable because of the separation between the messenger and the cable and because the cable is twisted during installation. Because of the Figure 8 cable's shape it has a tendency to move in the wind. With the right tensions and wind conditions the cable can gallop. [For information on galloping, consult "Transmission Line Vibration Due to Sleet" by J. P. Harog in AIEE Transactions, Volume 51, 1932.] There are now procedures to avoid galloping. During installation the cable is twisted several times in each span length. These twists present different airfoil shapes to the wind which dampens the galloping tendency.

Design: The design of a Figure 8 fiber optic cable is simplified by the Figure 8's successful use with copper cable cores. The basis for making a fiber optic Figure 8 cable is to understand the forces and environmental conditions imposed by the aerial cable plant upon the fiber optic portion of the cable. The cable should then be designed to meet those forces and conditions.

Many of the requirements of the optical portion of a Figure 8 cable are also requirements of a standard fiber optic cable that is lashed. These requirements include sunlight and lightning resistance, cyclic flexing, hot and cold bending, temperature cycling and aging, etc. These requirements are currently met by the standard loose tube cable designs. Many of the requirements for hardware compatibility and installation are met by using standard messenger and jacketing techniques. In designing a Figure 8 optical cable it was recognized that the steel messenger provides the tensile strength to the Figure 8 cable. The optical cable does contain yarn strength members to allow them to be tied to splice enclosures and to give the optical portion some tensile strength.

A special consideration for the design of Figure 8 cable is the tear resistance of the jacketing material. Starting at a split in the web, the optical cable portion can tear away from the messenger. To avoid such zippering a relatively tear resistant jacketing material is required. The standard material for Figure 8 jackets is black polyethylene, used for its sunlight and weather resistance. To choose a jacket material, various polyethylenes were tested for tear resistance.

The most important difference between lashed cable and Figure 8 cable is cable strain. In a lashed cable, the messenger is tensioned before the fiber optic cable is attached to it. For Figure 8 cable, the fiber optic portion is tensioned along with the messenger. The Figure 8 cable core will see more strain than a comparable lashed cable.

The tensile design approach for the fiber optic Figure 8 cable was to ensure that the optical fibers do not experience strain during the normal lifetime of the cable. The factors involved with this design procedure were steel messenger elongation, tensile window of the fiber optic cable core and excess cable length with respect to the steel messenger. Tensile window refers to the elongation of a fiber optic core where fiber strain begins.

Very early in the design procedure it was recognized that a large tensile window would be needed for the loose tube cable. Testing confirmed this. To achieve a larger tensile window, standard large size buffer tubes were used with a slightly decreased lay length. This allowed the tensile window to be large enough to meet the design requirements.

Testing and Performance: In choosing a jacketing material for the Figure 8 optical cable, various polyethylenes were tested for tear resistance. The materials were evaluated at room temperature and at -40°C using two test methods. The -40°C testing was performed because materials tend to become brittle at lower temperatures. Tearing is a property usually measured on rubber materials; plastics have higher tear resistance. To ensure tearing, the samples were notched in the desired tear direction. The results are summarized in Table 1 for a low density polyethylene (LDPE), a linear low density

polyethylene (LLDPE) and a medium density polyethylene (MDPE). These materials were all jacketing grades of polyethylene. The results are not necessarily indicative of all varieties and types of these materials. Based on the results, the MDPE was chosen as the jacketing material for Figure 8 cables.

TABLE 1

TEAR TESTING ON PLASTIC STRIPS

	METHOD 1		METHOD 2	
	Peak Load Newtons/ mm thickness	Toughness Newtons	Peak Load Newtons/ mm thickness	Average Load Newtons/ mm thickness
ROOM TEMPERATURE				
LDPE	121 (3)	506 (58)	12 (2)	11 (0)
LLDPE	132 (3)	846 (65)	21 (3)	19 (4)
MDPE	178 (3)	1439 (361)	31 (3)	30 (3)
MINUS 40° C				
LDPE	176 (36)	58 (12)	21(2)	20 (2)
LLDPE	325 (9)	963 (462)	54(1)	51 (3)
MDPE	314 (22)	1731(205)	49(4)	47 (4)

Standard Deviations In Parenthesis
LDPE (Low Density Polyethylene)
LLDPE (Linear Low Density Polyethylene)
MDPE (Medium Density Polyethylene)

METHOD 1 - Sample D 62C Die

METHOD 2 - Pants Leg Sample

20mm/minute Pull Rate

Figure 8 optical cables were tested for the mechanical and environmental performance typically required for standard fiber optic cable. The results showed that the Figure 8 cable design met the current customer specification. In addition, evaluations were performed to ensure proper performance in the aerial environment. These evaluations included galloping, lightning, tangent clamp pullout tests, cable handing, messenger gripping with a "come along", and a test installation. These results are summarized in Table 2. No problems were found with the performance of the fiber optic Figure 8 cables.

The most critical performance issue is the potential for fiber strain during the life of the fiber optic Figure 8 cable. To determine whether the optical fibers will see strain in the aerial environment, Figure 8 cable elongation under worst case load was compared to the elongation where fiber strain begins. The maximum elongation under load should exceed the minimum elongation where fiber strain begins.

Using the strength properties of the messenger to determine the elongation under load is a conservative approach. To address this, the steel messenger was evaluated. The steel messenger when installed will see varying amounts of strain over its lifetime. While under load, the stranded messenger will tend

TABLE 2

FIGURE 8 APPLICATION TESTING

TEST	DESCRIPTION	RESULT
Galloping	150' Span 36" Amplitude, 2 Hertz Deadend and 3 Bolt Tangent Clamp	Test Stopped > 100,000 Cycles No Fiber Breaks
Tangent Clamp Pullout Strength	3 Bolt Tangent Clamp	No Slipping 2,000 lbs.
Grip Strength	Strand Puller on Messenger Jacket	No Slipping 2,000 lbs.
Test Installation	Independent Contractor 11 poles ~ 1,800 ft.	No Problems Fibers Under Long Term Monitoring
Handling & Stripping	Ease of Stripping, Handling & Attachment to Hardware & Enclosures	No Difficulties
Lightning	Bellcore TR-20	No Fiber Breaks

to increase in elongation with time. This change in the steel messenger's elongation will tend to exponentially decay with time, which can be attributed to construction stretch. To understand this phenomena, various manufacturers and experts were contacted for input and 6 reels of steel messenger were tensile tested to the requirements of the NESC. The testing involved cycling the messenger between 0 and 60% of its minimum rated breaking strength (MRBS), holding the cable at 60% MRBS for a week, and a final cycling. The results of this testing show a 1 week elongation average of 0.486% when subjected to 3,900 pounds of tension. The 1 week elongation is used as the maximum elongation under load. Only insignificant amounts of construction stretch would be seen with further testing time.

A combination of testing was performed to address where fiber strain may begin. Combined were tests on the optical core with the messenger removed, and tests to determine the length of the optical core with respect to the length of the messenger. These two results determine the cable elongation where fiber strain occurs. With the messenger removed, the optical core did have the designed tensile window from testing per EIA 455 FOTP 33A. The length of the optical core was found to be nearly the same as the messenger from in process testing and from testing according to Bellcore TR-TSY-000102.

To compare the results generated from the messenger and cable tensile testing, additional factors were considered, including the effects of process variations on the tensile window, and the potential for long term creep of the messenger. The combination of the test results show that the optical fibers in this design of Figure 8 cable will not see strain in its intended application.

Low Fiber Count, All-Dielectric Cable

Fiber optic cables have been lashed and overlashed to messengers from the beginning of their development, following the use of lashed and overlashed copper cables. Lashing is accomplished by pulling the cable parallel and up to an already in-place dedicated messenger (stranded steel), and stranding one or two steel wires over the cable and messenger. This couples the cable to the messenger. Other cables can subsequently be overlashed to the previously lashed cable/messenger combination using the same procedure.

The advantage of attaching cables in this manner is that the system can be easily upgraded in the future by overlashing. The disadvantage is in the high initial cost of installing first a messenger and then the fiber optic cable.

Lashed cables are subject to a wide array of environmental forces such as sunlight, extreme temperature fluctuations, tensile loading, and repetitive cycling due to wind loading. The lashed cable must be able to "stand on its own" in any environment because there is not complete coupling to the messenger as in a Figure 8 cable. For example, the cable may contract more than the messenger at low temperatures. The cable must also be rugged so as not to be damaged during installation in even the most severe conditions.

Design: A fiber optic cable that functions well in a lashed or overlashed environment should meet all customer requirements as to environmental and mechanical concerns; and because of the cyclic movement, the cable should be reliable in a repetitive motion environment. The cable must be strong to withstand potential installation abuse. This implies a tensile strength and flexibility to protect the fiber even under high tension installations. Two additional characteristics that the cable should have are light weight (to allow the smallest messenger possible) and non metallic for lightning considerations.

A cable design that meets the above criteria is one that uses a central loose tube (Figures 1 and 3). This negates the use of a central support element, thus making the cable smaller in size and lighter. Excess fiber length is introduced to minimize the tensile strain placed on the fiber for long life and high reliability even in the worst case condition of high wind loading. The basic tube design technology already exists and has been deployed for several years.[2]

The cabling of the central tube is key to the desired characteristics. The tensile strength and cable shrink resistance of the cable can be met by using one flexible material - impregnated fiberglass. This material offers the tensile strength of fiberglass yarns but has improved handling properties that resists abrasion. This is due to the complete flooding of a matrix material that keeps the fiberglass from abrading itself and protects it from abrasion by other materials, process, installation, and handling equipment. The matrix material also keeps "fuzzing" to a minimum during processing. The key property that the matrix material gives the yarn is the stiffness that resists the shrinkage of the cable polymers at low temperature. These yarns, however, must be processed such that they exhibit little or no movement in the cable. This prevents the yarns from buckling.

The impregnated yarns offer a number of advantages over conventional epoxied fiberglass rod material. The yarns are highly flexible so they are easily stranded. Stiff tensile elements tend to hold their shape so that if they are stranded, the members will try to unwind during handling and/or processing if care is not taken. If the epoxied fiberglass rods are processed longitudinally (parallel with the cable) they will tend to have high strain on the outer section of the bend. The impregnated yarns may be processed just like aramid yarns so that they do not have to be incorporated into the jacket.

The techniques used in processing impregnated yarns are crucial for proper tensile and low temperature performance. Too much yarn slack will contribute to a high amount of cable elongation at the rated tensile load. Conversely, if the cable is stretched too much some excess fiber length may be pulled out. The process variables that determine these two properties have to be controlled.

A statistically designed experiment was useful to determine the important processing variables that

govern the above mentioned tensile properties of the cable as well as the low temperature shrinkage. In this case two responses were monitored: cable strain at 600 lbs and low temperature shrinkage (-40 C). Temperature cycling with attenuation measuring was not effective in this experiment because of the long lengths and amount of test time required. Therefore a method of determining the amount of shrinkage in a cable has been developed,[2] using conductive strain gages to measure the shrinkage of a cable at low temperatures. This allows the use of short cable lengths (30 meters).

A matrix like the one in Table 3 was used to find the key process parameters. The example shows the tensile response for a 5 variable experiment. The numbers on the bottom row indicate the relative importance of each variable - in this case, the construction stretch of the cables. Once these have been determined, it is important to be able to control them consistently. By controlling the important process variables proper cable shrinkage resistance and tensile properties may be optimized.

TABLE 3

Designed Experiment Response Example

Response: Construction stretch of cable in % strain

	X1	X2	X3	X4	X5	X6	RESPONSE
CABLE 1	–	–	–	–	+	–	.14
CABLE 2	+	–	–	+	–	–	.08
CABLE 3	–	+	–	+	–	+	.06
CABLE 4	+	+	–	–	+	–	.16
CABLE 5	–	–	+	+	+	–	.03
CABLE 6	+	–	+	–	–	+	.18
CABLE 7	–	+	+	–	–	–	.14
CABLE 8	+	+	+	+	+	+	.09
	+.032	+.008	0	-.09	-.008	+.015	

Testing and Performance: The tests performed on this cable design, including all standard mechanical and environmental tests must first conform to present customer specifications. Results show that a cable of this design can meet all customer requirements. One key test is temperature cycling and aging. Results from this test show that the impregnated yarns work extremely well in limiting the cable shrinkage. Fungus tests were also performed on the strength members to confirm their suitability in an aerial environment.

Mechanical reliability is important not only because of installation stresses but also because the cable will be in motion due to wind loading. Mechanical tests such as cyclic flex, impact, and cable twist bend (DOD test for tight buffer products) were performed to many cycles to determine the relative reliability of the cable and specifically the tensile members. A summary of these tests can be seen in Table 4.

TABLE 4

LOW FIBER COUNT ALL-DIELECTRIC:

MECHANICAL RELIABILITY TESTING

TEST	DESCRIPTION	RESULT
		# Cycles to Initial Wear
Impact	FOTP-25	6,000 (7,000 to 50% Reduction)
Cycle Flex	FOTP-104	25,000 (Test Stopped)
Twist Bend	DOD-STD-1678 Method 2060	500 (5,000 to 50% Reduction)

One important aspect of the lashed environment concerns how the lashed cable is coupled to the messenger. A study was undertaken to determine the degree of coupling between a messenger and lashed and overlashed cable. Here a 300 foot section of stranded steel messenger was strung between two fixed posts, and both ends were terminated using steel grips with one end tied to a load cell. The messenger was tensioned using an electric wench. A multi-tube cable was then lashed onto the messenger and then a single tube cable was overlashed. The messenger was then tension cycled. The relative motion between the cables and the messenger were monitored. Although crude, this test showed that there is significant but incomplete coupling between the lashed and overlashed cables and the messenger. Cables to be lashed or overlashed will be considered completely coupled to the messenger during wind and ice loading as a conservative estimate. The cable is considered uncoupled for low temperature situations also as a conservative estimate.

Pre-Stranded Optical System

The requirements for self-supporting aerial fiber optic cables are as varied as the applications that dictate their use. Span distances vary and worst case ice and wind loading conditions change from one geographic area to another. These changing requirements limit the use of most self-supporting aerial cables (such as Figure 8) to installations limited by a tightly defined specification.

A dielectric pre-stranded optical system (Figure 1) has been designed as a means to meet the different aerial requirements with one basic design. The pre-stranded optical system consists of a standard loose tube cable and a separate messenger. Various messengers can be substituted for a specific application. The messengers are manufactured in variety of standard sizes ranging from Types A - E, with each messenger yielding a larger rated breaking strength.

Many cables are designed as "one size fits all". This results in an overkill product for short spans in Light NESC regions and not enough strength member for more severe applications unless lashed to a dedicated messenger. The pre-stranded optical system enables the customer to use smaller, less expensive messengers for shorter spans and larger messengers for the more extreme applications. Also, fiber count is not a limiting factor for the pre-stranded optical system . The use of variable messengers, with variable tensile ratings, allows the cable to be tailored to the customer's requirements and still accommodate fiber counts up to 192 fibers in both single-mode and multimode.

Another advantage the pre-stranded optical system offers is the ability to combine aerial installations with a duct application. The two component design makes it possible to strand only a portion of the fiber optic cable around the messenger, thus leaving a length of fiber optic cable un-messengered and available to be pulled directly into a duct. This offers the customer the ability to avoid splice points and the extra cost of unneeded messenger strength as in the case of Figure-8 and concentric cables.[3]

Typically, a major concern when using aramid yarns is the ability to control the construction stretch. As will be discussed below, numerous tests have been performed to better understand construction stretch and how it pertains to the pre-stranded optical system . The messengers are manufactured to keep the construction stretch at the lowest possible level for all messengers. Computer models allow us to predict the construction stretch for each messenger and application.

The material cost of the pre-stranded optical system will usually be greater than the cost of a steel messenger, a fiber optic cable, and the lashing wire. This is driven by the higher cost of aramid yarn versus steel. However, the advantages of the pre-stranded optical system more than compensate for this higher cost. The use of aramid yarn as the strength element insures that 1) the pre-stranded optical system cable will be light and easy to handle and 2) that the system is lightning resistant, requiring no grounding. Because of the high strength to weight ratio of Kevlar®, installations of up to 4 kms can be made in a single pull without exceeding the maximum recommended installation tension. The labor cost of installing the pre-stranded optical system is less than lashing a cable to a dedicated messenger. It takes approximately the same amount of time to completely install the pre-stranded optical system as it does to install the messenger in a lashing process. As a result, actual installation cost estimates for the pre-stranded optical system typically have been 35-45% less than lashing.

Design: In order to meet requirements for long span lengths and all-dielectric cables, aramid yarn messengers have been incorporated so the fiber optic component may be isolated from the high tensions that can be placed on the messenger during installation and worse case environmental loading. Thus, the fibers remain in a virtually strain-free state throughout operation.

The pre-stranded optical system cable is comprised of two separate and distinct components: 1) a standard all-dielectric loose tube cable and 2) a polyurethane jacketed impregnated aramid yarn messenger. The fiber optic cable is helically wrapped around the messenger; however there is no physical bond between the two, as in a Figure 8 cable. The aramid yarns within the messenger are chemically bonded to a UV and fungus resistant polyurethane jacket. The messenger is also constructed such that the pre-stranded optical system cable is torque balanced. The stranded product enables the complete system to be pulled in at once, both the messenger cable and fiber optic cable. The messenger is easily assessable, which allows the tangent hardware to couple directly to the messenger, as opposed to the concentric design where the fiber optic cable core is also in contact with the compressive forces of the hardware and subject to bending stresses.

The use of aramid yarns as the strength member allows the cable to be all-dielectric. To achieve rated breaking strength (RBS) performance in the order of 8,000 lbs to 10,000 lbs, hundreds of ends of yarn are required. When working with so many yarns, it is critical to achieve equal tensioning as well as minimal construction stretch. This becomes even more critical when the rope / messenger cable is combined with a fiber optic cable and 0% tensile

fiber strain is required. In conjunction with the messenger supplier, the messenger cable construction has been maximized.

Early on in the tests it became apparent that significant increases in messenger performance could be realized if the amount of slack yarn in the messengers were minimized. By minimizing the slack / construction stretch, the messenger would reach a greater load without going beyond the fiber optic cable's tensile window. The goal was to determine to what values the tension and strain would drift or creep over time. The following test method allowed the messenger cables to be analyzed: A 100 meter messenger cable sample was pulled to a specific strain value equivalent to the tensile window of the fiber optic cable. The tensile load was recorded at 0.05% intervals. The messenger was then held at this constant strain while the tensile load was monitored. The final tensile load value, after the messenger relaxed, was equivalent to maximum load the messenger could withstand before inducing fiber strain. The tensile load of the messenger was then reduced, again recording load values at 0.05% intervals. The residual strain on the messenger after load removal at zero load was determined to be the the amount of construction stretch of the messenger. A key to the project; therefore was to minimize the construction stretch which then increases the maximum load at the fiber optic cable's tensile window.

To complete the design, hardware must be selected. For convenience and familiarity, it was decided to select and test hardware common to both telephony and utility markets. A mechanical deadend and a 3-bolt tangent clamp were desired. Because the pre-stranded optical system has two separate components, the fiber optic cable is never directly involved in the termination or tangent attachment, which made hardware selection easier. Only the messenger is attached to the poles and subjected to high tension. The pre-stranded optical system was designed to incorporate a three-bolt tangent attachment which could handle up to a 20° running angle. Typical deadends for Kevlar cables are the standard socket with a polyester resin. The biggest negative is the preparation and curing time required to install a resin socket deadend. With this in mind a mechanical deadend was sought which would reduce the installation time. After evaluating various terminations, the internal plug termination was determined to be the best. This deadend couples directly onto the aramid yarn. It does not rely upon the outer jacket for support and can be attached to standard pole attachments. This deadend provides excellent environmental stability over the operating range.

Testing and Performance: Once each separate component was tested and their performance was well understood, the next area was to explore the complete system performance. Because of the standard profile, the cable is aerodynamically stable, creating a self-dampening effect during windy periods. This in turn will reduce the cable's tendency to gallop or experience aeolian vibrations. However to insure the stability and ability of the pre-stranded optical system to endure the most severe environments, the hardware and cable system was subjected to the following tests.

- Galloping
- Aeolian Vibration
- Static Fatigue
- Load Unbalance

The tests listed are above and beyond the typical customer requirements. The fiber optic cable is a standard dielectric loose tube design and meets all of the customer requirement. The messenger, where applicable, meets all the customer requirements, such as mechanical tests, water penetration and material properties.

The static fatigue testing was the first test to determine the stability of the mechanical deadend. The intent of this test was to determine the threshold of the deadend when exposed to a constant load at constant high temperature. Various deadends were tested and eliminated by this test. The test criteria was for the deadend and messenger cable to endure +65°C for a minimum of 24 hours. +65°C is the normal temperature range a cable is tested to using Bellcore standards and the 24 hours would be twice the exposure time of the hardware. The internal plug deadend yielded consistent performance and was unaffected by temperature.

For aerial cables, the tangent clamp is the critical link of the aerial plant aside from the cable. The tangent should be able to support the product even if an adjacent span is broken thereby holding just as a deadend. The unbalanced load test determines the maximum load the tangent assembly can support when the cable is tensioned just on one side. This test is similar to the static fatigue test with the tangent assembly acting as a deadend. The data gathered would indicate the stability of the tangent and also determine the maximum span difference

(delta) on each side of the tangent that could be supported. The tangent was not expected to give the same performance as a deadend; however a 20% efficiency with the larger messengers and 25% efficiency on the smaller messengers was achieved. These tension values equate to a span delta ranging from 345 to 450 feet. The performance of this tangent assembly verifies its ability to support the pre-stranded optical system in the worst of conditions even if the tangent clamp is exposed to tremendous unbalanced loads.

The galloping test subjects the cable and hardware to a minimum of 100,000 galloping cycles at the single loop resonant frequency. The peak-to-peak antinode amplitude/loop length ratio was maintained at 0.04. The cable sample was 75 ft between deadend abutments with a tangent clamp located at the midway point. The pre-stranded optical system cable was tensioned up to a typical span installation tension of 400 lbs and driven by an electronically-controlled shaker in the vertical plane. Hardware and cable inspections were made every 5,000 cycles. The test was repeated with the tangent assembly turned to an offset angle of 20° in order to determine the limitations of the hardware. The test continued for 100,000 galloping cycles. No damage was recorded on the messenger, fiber optic cable, deadend or tangent assembly at either 0° or 20° offset.

Aeolian vibration is typically a concern with concentric cables. Yet to insure the stability of the pre-stranded optical system, aeolian vibration tests were conducted. Perhaps the most important area of concern with this system is the ability of the hardware to withstand material fatigue or yarn breakage, when subjected to such high frequencies as what would be experienced with aeolian vibration. The setup was similar to that used in the galloping tests. During this test the cable samples were tensioned to 500 lbs. The shaker was located in the span close to the deadend, to allow a minimum of six vibration loops between the suspension / tangent assembly and the shaker. The frequency of the test span was maintained at the frequency produced by a 10 mph wind, 60.1 Hz. The loop peak-to-peak antinode amplitude was maintained at one-third the diameter of the cable. The cable samples were subjected to a minimum of 100 million vibration cycles. Inspections were make twice a day, with the sample and test captured on video. There was no damage to the complete system. Neither the hardware or cable showed any damage.

After both the galloping and vibration tests, the samples, with the deadends still in place, were pulled to break to evaluate any static fatigue. All samples achieved the same strength efficiency as with previous samples tested. This indicated that the cable system would remain secure even after being exposed to significant galloping and aeolian vibrations.

Conclusion

Three cable designs have been presented which meet various fiber optic aerial application requirements: 1) A self-supporting, steel messenger cable known as a figure 8 cable. 2) A low fiber count all-dielectric cable well suited for lashed and overlashed environments. 3) A pre-stranded optical system that consists of a dielectric messenger with a helically wrapped loose tube optical fiber cable. All three cable types have certain common design requirements, with tensile performance identified as the most critical. The three methods of assuring proper tensile characteristics and unique design challenges were discussed in the respective section.

Test results for specific key areas were presented for each cable, showing that each cable meets all customer-published requirements for cable performance.

Acknowledgements

The authors would like to thank the many people at Siecor who have helped in the design and testing of these three cables. The authors would also like to thank M. Genovese for his help with this paper.

References

[1] AIEE Paper #62-229, "Figure 8 Thermoplastic Insulated and Jacketed Telephone Cables", 2/16/62.

[2] "Design and Performance of Telecommunication Cables Optimized for Low Fiber Counts", Proceedings of the 37th International Wire and Cable Symposium, November 1988, pp. 63 - 71.

[3] James Scott, "PSOS: A Unique All-Dielectric Self-Supporting Aerial Fiber Optic Cable Design", NFOC 1989.

Figure 1

Lashed Fiber Optic Cable

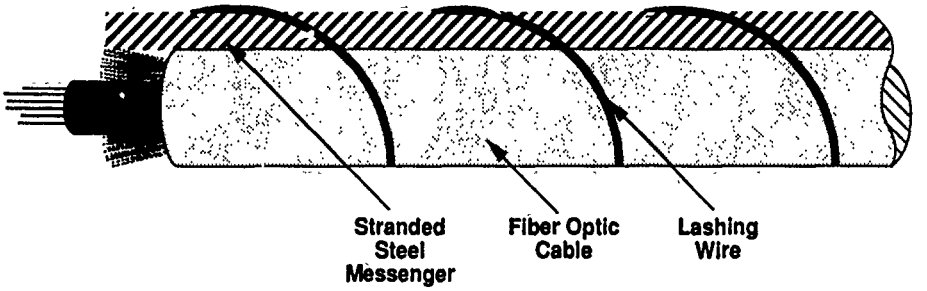

Figure 8 Fiber Optic Cable

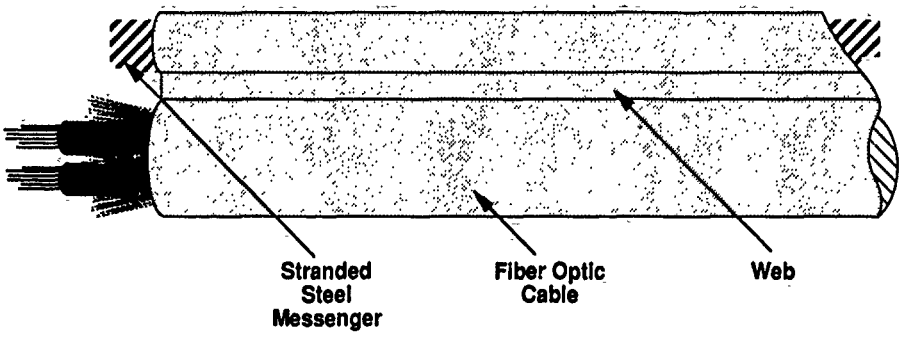

Prestranded Optic Cable System

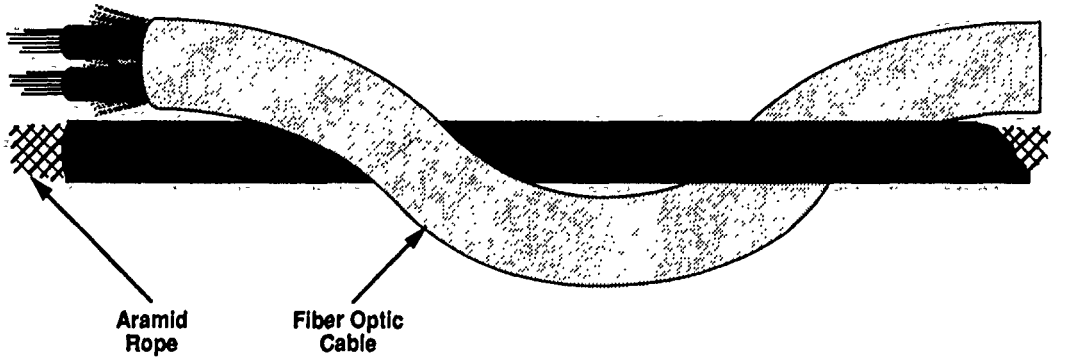

Note: This Illustration is Not to Scale

AD69-14

FIGURE 2

Armored Self Support Figure 8 Optical Cable

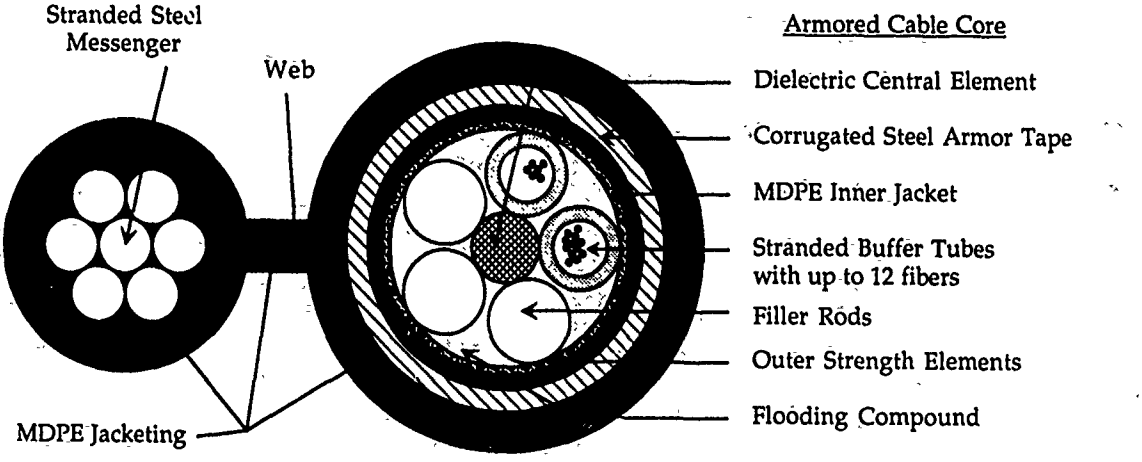

FIGURE 3

ALL-DIELECTRIC LOW FIBER COUNT CABLE

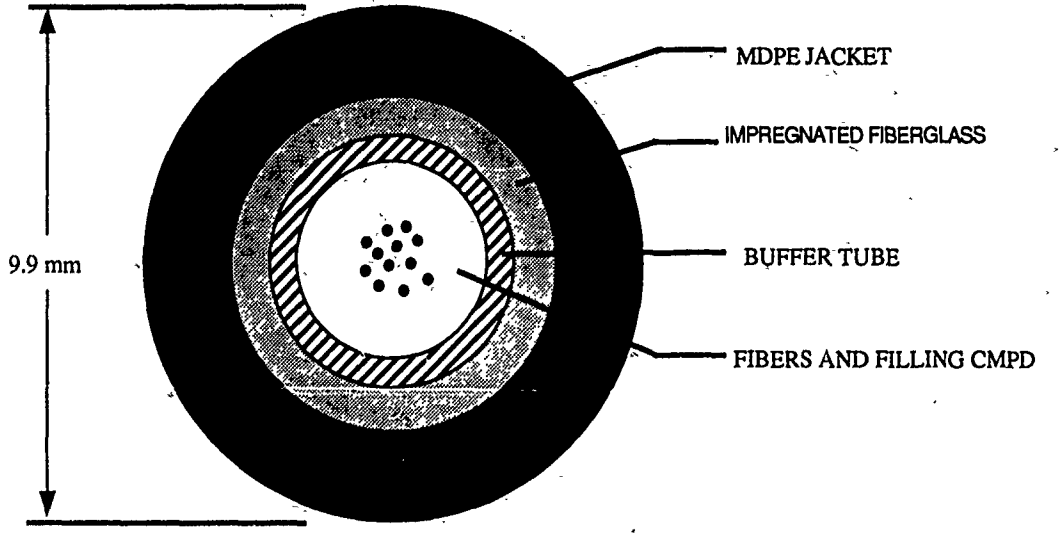

Andrew S. Dodd

Siecor Corporation
489 Siecor Park
Hickory, NC 28603

Andrew S. Dodd was born in West Orange, New Jersey in 1956. He graduated from Clemson University in 1984 with a B.S. degree in Mechanical Engineering. He has been employed at Siecor since January 1985 and is currently the Supervisor of the Telco Cable Development group in the Research, Development and Engineering department.

Richard S. Wagman

Siecor Corporation
489 Siecor Park
Hickory, NC 28603

Richard S. Wagman was born in Dallastown, Pennsylvania in 1956. He received his Bachelor of Science Degree in Engineering Science from The Pennsylvania State University in 1978, and his Bachelor of Science Degree in Electrical Engineering from The John Hopkins University in 1984. He worked for 7 years as a Product Engineer at Continental Wire & Cable before joining Siecor Corporation in 1985. At Siecor, he has worked in the product development area. He is currently employed as a Senior Product Development Engineer in the Research, Development and Engineering department.

Harvey R. McDowell III

Siecor Corporation
489 Siecor Park
Hickory, NC 28603

Harvey R. McDowell III was born in Hickory, North Carolina in 1963. He received his B.S. degree in Electrical Engineering from North Carolina State University in 1985. Since then he has worked as a Product Development Engineer for Siecor Corporation in Research, Development and Engineering and is currently Supervisor, CPC Cable Development.

DEVELOPMENT OF STRESS-FREE 24-CORE OPGW

K.Ishida*1, K.Kawabata*1, M.Kazumori*1, M.Matsuo*1, H.Ishii*2
H.Suzuki*2, K.Yokoyama*3, H.Shiga*4, Y.Aida*5, Y.Kimura*6

*1 The Kansai Electric Power Co., Ltd. Osaka, Japan
*2 Fujikura Ltd. Chiba, Japan
*3 Fujikura Ltd. Tokyo, Japan
*4 Hitachi Cable, Ltd. Ibaraki, Japan
*5 The Furukawa Electric Co., Ltd. Tochigi, Japan
*6 Sumitomo Electric Industries, Ltd. Osaka, Japan

Abstract

A loose multi-core OPGW has been developed, and as a result of the development of a 24-core optical cable with a small diameter, and of the development of a strand conductor section with a large diameter. This OPGW can accommodate twice as many fibers as the existing loose OPGW without losing its strain relief effect. We will describe in this paper the specifications and construction of the newly developed OPGW, as well as report on the results of various evaluation tests and a field test.

1.Introduction

Since the use of OPGW began in 1982, The Kansai Electric Power Co., Ltd. has been using it in a wide range of applications, including power transmission systems and data communication systems, and has carried out the development of multi-core OPGW to promote lager communications capacity.

Generally, OPGW is divided into two types : fixed and loose. The fixed OPGW is available as a layer type and as an spacer type, both having the advantage of being easy to make in multi-cores. On the one hand, the loose OPGW, which has a space between the aluminum pipe and the optical cable, has the advantage of relieving strains imposed on fibers when the cable is wired. On the other hand, the loose OPGW is difficult to make in multi-cores because it requires a space between the aluminum pipe and the optical fiber cable, thus limiting to 12 cores. Under such conditions, we have developed a loose 24 -core OPGW, or twice as many cores as allowed by the conventional loose OPGW.

2.Cable design

2-1.Design criteria

The design criteria are as follows :

(1) Capable of accommodating SM fibers in more than 24 cores.

Because OPGW is often laid in trunk lines, we will use single-mode(SM) fiber. As the maximum number of cores in the conventional loose OPGW was 12, we set a development target to double that figure.

(2) The cable should have strain relief effect.

The multi-core construction should not impair the cable's strain relief effect.

(3) The cable should have mechanical and electrical characteristics such that it can be installed on existing towers.

Installing an OPGW includes replacing the existing overhead ground wire and mounting on the tower, but in either case the design of the tower is identical. Therefore, the new OPGW should have mechanical and electrical characteristics such that it can be installed on existing towers.

(4) The cable should have better or equal transmission characteristics than the existing OPGW.

This OPGW is used for transmission in the normal SM band of 1.3 μm. Therefore, we set a target to improve the transmission characteristics of the existing SM 12 core OPGW.

(5) The cable should be capable of installing without any special processes or tools.

To minimize an increase in construction costs associated with the new OPGW, the cable should be capable of installing without any special processes or tools.

To meet these requirements, we focused development on the following four points :

(1) Develop a 24-core optical cable with a small diameter.

(2) The aluminum pipe should be of such dimensions that ensure sufficient space between the aluminum pipe and the optical cable.

(3) Develop such a stranded conductor section that can be installed on existing towers.

(4) The optical cable must be composed of metal-free and heat-resistant materials.

2-2.Specifications

Table 1 compares the specifications of the newly developed 24-core OPGW with the conventional 12-core OPGW. The table shows 55 mm^2 as an example of the stranded conductor in a single layer, and 120 mm^2 as an example of a double layer. We used the SM fiber of 1.3 μm band that has an MFD of 10 $\pm$ 1 μm, a clad diameter of 125 μm, and a cut-off wavelength of 1.10 to 1.28 μm.

2-3.Small diameter 24-core optical cable

The structure of the 24-core optical cable with small diameter is shown in Fig. 1, and that of the conventional 12-core optical cable in Fig. 2. Both cable are non-metallic and structured with materials having a heat resistance greater than 300 °c. The optical fiber with silicone resin coating is used in order to provide for heat resistance. The small diameter 24-core optical cable comprises four small diameter 6-core units assembled with plastic string fillers, and is jacketed with a Teflon sheath. The small diameter 6-core units are assembled with six optical fiber, and with silicone resin filled around an FRP tension member. Then thin polyimide tape is wound around the unit. The polyimide tape allows the diameter to be smaller, and makes cable easier to manufacture. The silicone resin prevents the transmission and mechanical characteristics from degradation if the unit sheath should be removed.

Fig. 3 shows the result of a lateral pressure test performed on two kinds of 24-core optical cables, one filled with silicone resin, and the other not. In this test, a loss increase was measured when a 24-core SM fiber was connected in a loop and compressed using a flat plate that is 50 mm wide. The figure indicates an apparent improvement in its lateral pressure characteristics as a result of the filling with silicone resin.

The plastic string filler serves to form a circular cross-section, thus making the cable easier to manufacture. The outer Teflon sheath protects the unit and produces a strain reduction effect as a result of its small frictional coefficient.

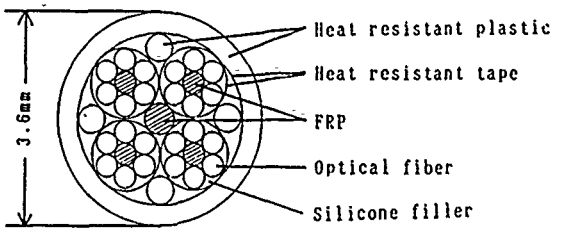

Fig.1. Cross section of 24 core optical cable

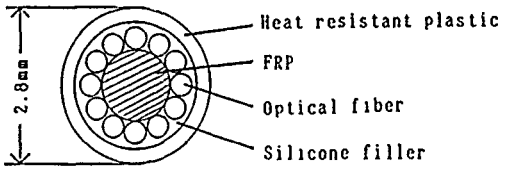

Fig.2. Cross section of 12 core optical cable

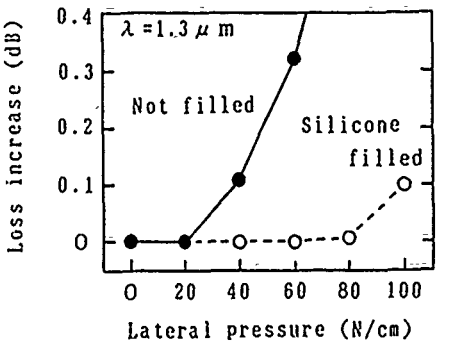

Fig.3. Loss increase versus lateral pressure

Table 1. Specifications

Item		Unit	New OPGW		Conventional OPGW	
			55mm^2	120mm^2	55mm^2	120mm^2
OPGW	Outer diameter	mm	10.6	18.5	9.6	17.5
	Weight per unit length	kg/km	385	821	344	736
	Ultimate tensile strength	kN	64.0	108	54.0	96.6
	Elastic modulous	kN/mm^2	149	94.4	149	93.7
	Expantion coefficient	1/°C	12.9×10^{-6}	17.3×10^{-6}	12.9×10^{-6}	17.4×10^{-6}
	Electrical resistant(20°C)	Ω/km	1.36	0.207	1.54	0 225
Aluminum Pipe	Outer diameter	mm	6.0		5.0	
	Inner diameter	mm	4.6		3.8	
	Thickness	mm	0.7		0.6	
Optical Cable	Outer diameter	mm	3.6		2.8	
	Weight per unit length	kg/km	15		10	
	Gap between Aluminum pipe	mm	1.0		1.0	
	Number of optical fiber	–	24		12	

2-4.Aluminum pipe

An aluminum pipe with an outer diameter of 6 mm and inner diameter of 4.6 mm, as shown in Table 1 was used. The space between the inside of the aluminum pipe and the optical cable was set at 1 mm, identical to the conventional cable in order to achieve a strain relief effect equivalent to that of the existing loose OPGW. This 1 mm clearance includes a crushing margin for the bolt-tightening clamp, and for the size of the welding beads on the inside of the aluminum pipe. The pipe thickness, which was 0.6 mm in conventional cables, was increased by 0.1 mm to 0.7 mm in order to prevent degradation that would result from the increase d outer diameter.

2-5.Stranded conductor

(1)Single-layer structure (55 mm^2)

Fig. 4 shows the structure of the newly developed 55 mm^2 OPGW. In determining the structure of the stranded conductor, we examined the following three models using a 6 mm aluminum pipe :

Type I : The outer diameter of the OPGW is identical to that of conventional wires (outer diameter equivalence).

Type II : The cross-sectional area of the stranded conductor is identical to that of conventional wires (cross-sectional area equivalence).

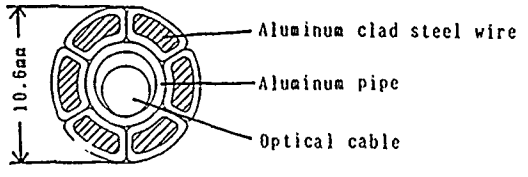

Fig.4. Cross section of 24 core OPGW 55mm^2

Type III : The thickness of an aluminum-clad steel wire is identical to that of conventional wires (thickness equivalence).

The specifications for existing overhead ground-wire and conventional OPGW are shown collectively in Table 2, in addition to the specifications for the above three models. Maximum working tension was examined when mounting these cables in a manner such that the lowest temperature and the sag at no wind are 80% of the power cable mounted under conditions shown in Table 3. Fig. 5 shows the results. The figure indicates that cases in which the maximum working tension of the GSW 55 mm^2 is exceeded are limited to cases in which the span length was long in the thickness equivalence. However, we discovered as a result of examining the tower strength in this case, that the strength margin for tower members is decreased by only 1% to 2%. Hence, there are no problem with its practical use.

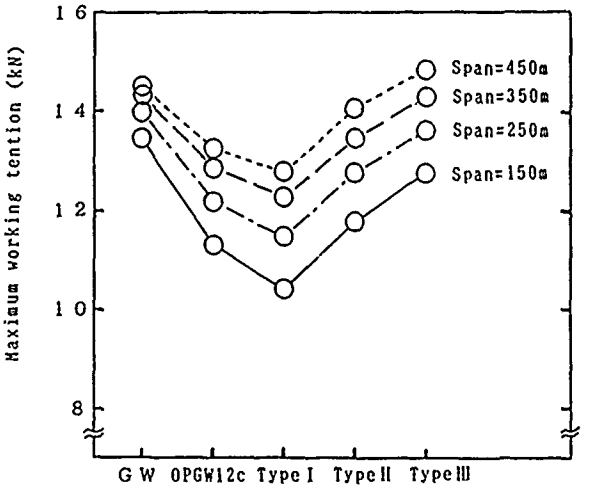

Fig.5. Maximum working tention of OPGW 55mm^2

Table 2. Data of ground wire and OPGW

Item \ Name & Number of fibers	CONVENTIONAL GW(GSW) 55mm^2 No fiber	CONVENTIONAL OPGW 55mm^2 12 fibers	NEWLY DESIGNED OPGW 55mm^2 24 fibers Type I	Type II	Type III
Strand construction (1/mm)	7/3.2	6/(3.24)	6/(2.95)	6/(3.25)	6/(3.44)
Outer diameter (mm) Whole	9.6	9.6	9.6	10.2	10.6
Outer diameter (mm) Aluminum pipe	—	5.0	6.0	6.0	6.0
Weight per unit length (kg/km)	446	344	302	357	395
Section area (mm^2)	56.3	49.2	41.0	50.0	55.8
Ultimate tensile strength (kN)	63.4	56.7	47.1	57.2	64.0
Elastic modulous (kN/mm^2)	206	149	149	149	149
Expantion coefficient (1/°C)	11.5×10^{-6}	12.9×10^{-6}	12.9×10^{-6}	12.9×10^{-6}	12.9×10^{-6}

Table 3. Stringing condition of overhead transmission line

Tower span length	from 150m to 450m
Hight difference	0m
Conductor	ACSR 330mm^2
Load condition (Worse case)	Temp. 15°C Wind pressure 981N/m^2 or Temp.-15°C Wind pressure 490N/m^2 Icing 0mm
Maximum working tension	32.4kN

Fig. 6 shows the results of comparing the safety ratio of the cables mounted under the same conditions as in Fig. 5, where the safety ratio is represented by formula [1] below. The calculations showed that the span length was long in the outer diameter equivalence. However, in this case, as well, the safety ratio is ensured to be more than 3, a value that presents no problems for the cable mounting design.

$$\text{Safety ratio} = \left(\frac{\text{UTS}}{\text{MWT}}\right) \times 100 \quad \text{--- [1]}$$

where UTS = Ultimate tensile strength
MWT = Maximum working tension

The results of the above examination show that the outer diameter equivalence, the cross sectional area equivalence and the thickness equivalence are applicable. However, the stranded conductor structure design was determined according to the thickness equivalence, after taking into account the improved lightening resistant characteristic of the strand and its larger tensile strength, exceeding that in conventional OPGWs.

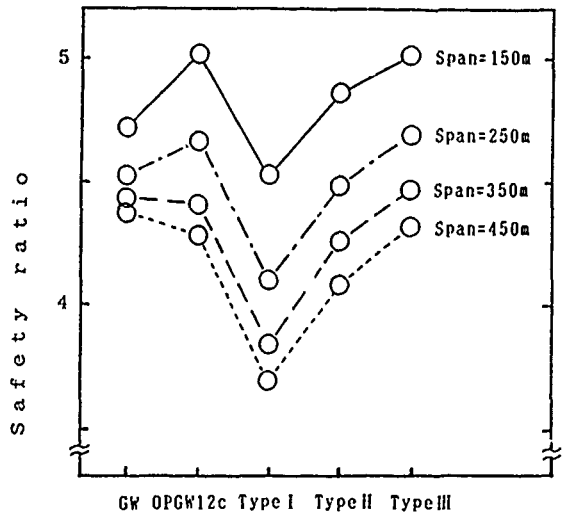

Fig.6. Safety ratio of OPGW 55mm²

(2)Double layer structure (120 mm²)

Fig. 7 shows the structure of the newly developed OPGW 120 mm². Regarding the OPGW with double-layered stranded conductors, while the first layer structures is assumed to be designed according to the thickness equivalence of conventional OPGWs as in the case of single-layered structure, the following two models were examined with respect to their diameter and the number of strands in an aluminum wire in the second layer :

Type IV : The number of aluminum wires equals 12 as with conventional OPGW.

Type V : The outer diameter of aluminum wire is the same as that of the conventional OPGW.

The specifications for the existing overhead ground-wire and conventional OPGW are shown collectively in Table 4, as are those for the above two models. The maximum working tension was examined in cases mounting these cables in a manner such that the lowest temperature and the sag at no wind are 80% of the power cable mounted under the conditions described by Table 5. Fig. 8 shows the results. The figure indicates that the cases in which the maximum working tension of GSW 120 mm² is exceeded are limited to cases in which the number of aluminum conductor is the same. However, examining the tower strength in this case, revealed that it was within the allowable strength margin for the tower, and that hence there were no problems in the practical use.

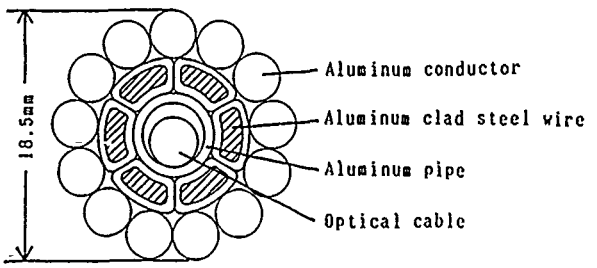

Fig.7. Cross section of 24 core OPGW 120mm²

Table 4. Data of ground wire and OPGW

Item	Name & Number of fibers	CONVENTIONAL GW 120mm² No fiber	CONVENTIONAL OPGW 120mm² 12 fibers	NEWLY DESIGNED OPGW 120mm² 24fibers Type IV	NEWLY DESIGNED OPGW 120mm² 24fibers Type V
Strand construction	Aluminum conductor	12/3.5	12/3.5	12/3.9	13/3.5
	Al clad steel wire	7/3.5	6/(3.86)	6/(3.86)	6/(3.86)
Outer diameter (mm)	Whole	17.5	17.5	19.3	18.5
	Inner layer	10.5	10.5	11.5	11.5
	Aluminum pipe	—	5.0	6.0	6.0
Weight per unit length (kg/km)		846	736	882	821
Section area (mm²)		183	178	214	195
Ultimate tensile strength (kN)		109	96.6	111	108
Elastic modulous (kN/mm²)		116	93.7	91.8	94.4
Expantion coefficient (1/°C)		15.5x10⁻⁶	17.4x10⁻⁶	17.6x10⁻⁶	17.3x10⁻⁶

Table 5. Stringing condition of overhead transmission line

Tower span length	350m
Hight difference	0m
Conductor	ACSR 410mm² × 2
Load condition (Worse case)	Temp. 15℃ Wind pressure 883N/m² or Temp.-20℃ Wind pressure 442N/m² Icing 9mm
Maximum working tension	44.1kN

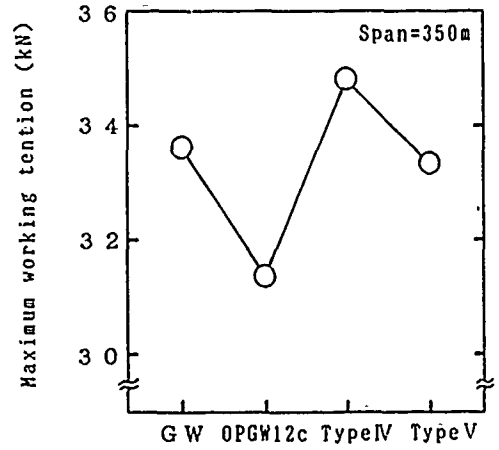

Fig.8. Maximum working tention of OPGW 120mm²

Fig. 9 shows the result of comparing the safety ratio of the cables mounted under the same conditions as in Fig. 8. Fig. 9 confirms that the safety ratio changes very little, or is assured at more than 3, hence there are no problems in the cable mounting design. Furthermore, the shared stress on the aluminum conductors of the outer layer was investigated and was found to be approximately equivalent to that in the conventional OPGW. Thus, we confirmed that there were no problems in the vibration preventive design.

While the above examination proves that the two models have no particular problems, a design plan using the same strand diameter as that used for the conventional product was adopted by taking into account that it has a small outer diameter and is light weight.

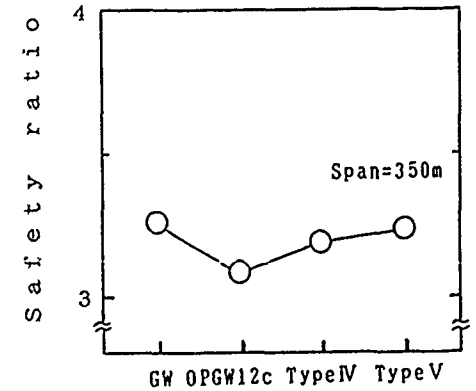

Fig.9. Safety ratio of OPGW 120mm²

3.Evaluation test

The newly developed OPGW must be sufficiently reliable as it is used mainly for trunk line routes. Therefore, we have conducted various tests to evaluates characteristics.

(1)Loss variation in manufacturing

The OPGW was measured to check its loss during each manufacturing process using OTDR with 1.3 μm and 1.55 μm. Fig. 10 shows the loss variation in 24 core OPGW of approximately 1 km, which proved to be as stable in terms of loss variation as 0.02 dB/km or less.

(2) Loss temperature characteristic

The 24 core optical cable was submitted to heat cycle test. The results are shown in Fig. 11, indicating that the loss variation is as small as 0.03 dB/km.

(3) Frictional coefficient

A strain relief effect, which is one of the features of a loose OPGW, is produced from the slippage occurring between the aluminum pipe and the optical cable. Therefore, we measured the frictional coefficient. The OPGW was bent to a radius of 500 mm to measure the pull-out tensile strength of the optical cable, and the frictional coefficient was calculated by using formula [2].

$$\mu = \ln\left(\frac{T}{Tb}\right) \Big/ \theta \qquad \text{---[2]}$$

where μ = Frictional coefficient
T = Pull-out tension
Tb = Back tension
θ = Bending angle (radius)

As a result, the static friction coefficient (frictional coefficient when the optical cable begins to move) was 0.31, and the dynamic friction coefficient (frictional coefficient while the optical cable was moving) was 0.26.

(4) Other characteristics

The newly developed OPGW was subjected a number of evaluation tests such as heat resistant test, vibration test, sheave wheel test, tensile test, compression test, short circuit test, arc test and so on. Test results confirmed that the OPGW has the excellent characteristics.

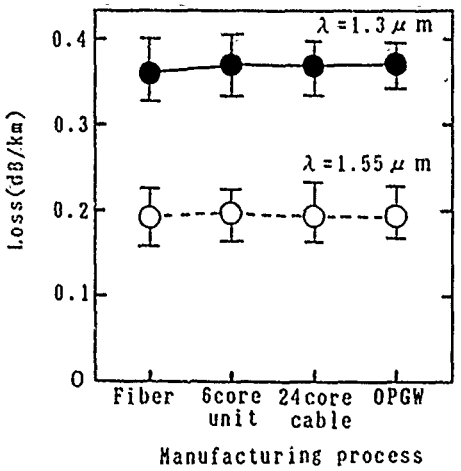

Fig.10. Transmission loss in cable manufacturing

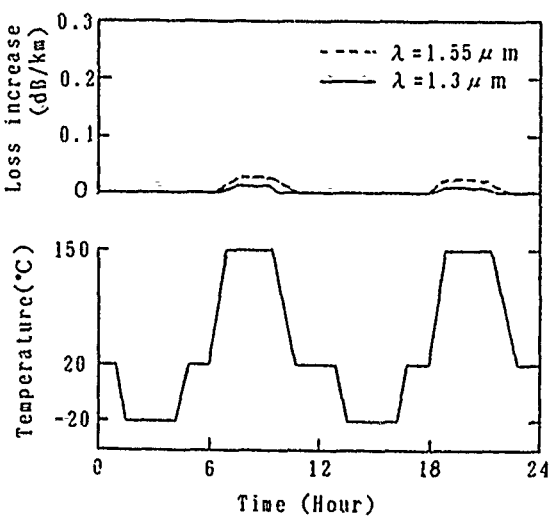

Fig.11. Heat cycle test for 24 core optical cable

4.Field test

To verify its practical usability, a field test was carried out, during which time notes were taken on the three points, namely, the applicability of the conventional processes, the strain relief effect and the loss stability.

4-1.Stringing method with small pulleys

Using stringing method with small pulleys, which is a standard process of the conventional OPGW, a 12-core OPGW 55 mm^2 of the conventional type was replaced by the newly developed 24-core OPGW 55 mm^2. All the tools used during the installation were standard, except for the clamp and come-along which differed from the usual ones to account for the difference in the outer diameter. Fig. 12 (a) through (c) provide a summary of the stringing process.

(a)Evolving suspending pulleys and extending the new OPGW.

Suspending small pulleys, each comprising two pulleys coupled on a short rope are evolved on the existing OPGW at intervals of approximately 15 m. The suspending small pulleys are tied on a pilot rope for evolution and collection. The new OPGW is connected to a messenger rope (towing rope) which has been passed through the lower pulleys, and is pulled at a low tension.

(b)Reversal

The tension on the existing OPGW is increased so that the sag on the new OPGW is smaller than that on the existing OPGW. Thereafter, the tension on the new OPGW is provisionally secured.

(c)Withdrawing the existing OPGW, and collecting the suspending pulleys.

After releasing the clamp on the existing OPGW, the OPGW is wound on a drum. Thereafter, the suspending small pulleys are collected.

(d)Securing the tension.

The tension on the new OPGW is decreased, the sag is adjusted, and the OPGW is finally tensed.

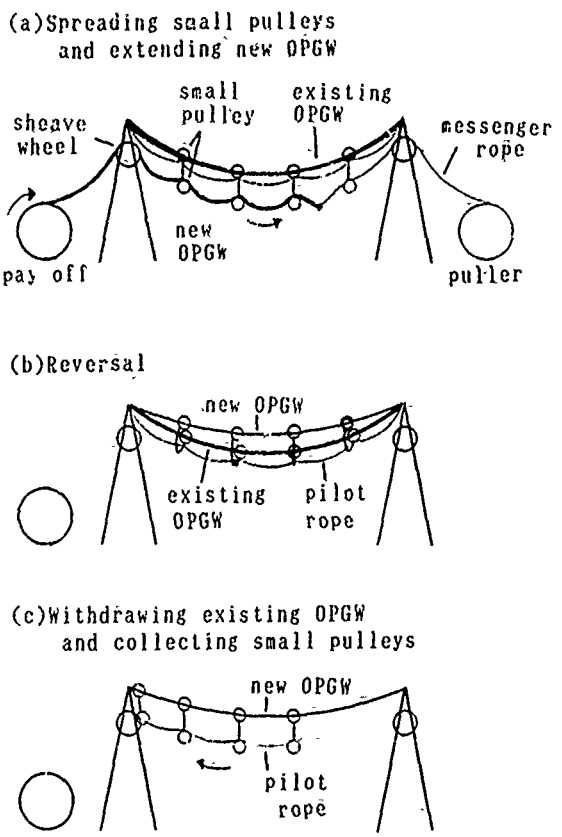

Fig.12. Stringing method with small pulleys

4-2.Strain variation during the cable installation

Fig. 13 shows the results of the measurement taken on the variation of the elongation strain imposed on the OPGW and the fibers during the installation using the stringing process mentioned above. The fiber strain was measured through the phase shift method, with the modulation frequency set at 100 MHz. The OPGW elongation was checked by calculation based on the tensile strength. The pull-in amount of the optical cable is the sum of the amount of cable moved at both ends, and divided by the cable length. In the figure, the OPGW elongation strain at the reversal, during which the largest tension is applied, was 0.2%, but the fiber elongation strain was suppressed to 0.05% because the optical cable was moving inward. The fact that the elongation strain after the cable has been tensed as small as 0.02% explains the high reliability regarding the life of optical fibers.

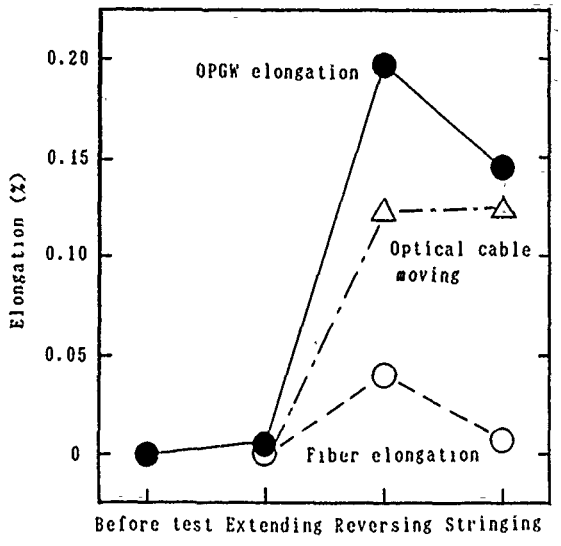

Fig.13. Variation of elongtion during the installation

4-3.Loss variation

With the 24-core OPGW 55 mm^2 completed with wiring kept under the conditions shown in Fig. 14, the loss over an extended time period was monitored. Assuming practical cable mounting, the #1 and #3 towers used tension clamps, and the #2 tower used suspension clamps. Further disposed in the vicinity of the joint boxes of the #1 and #3 towers were jumper turns with a 1 m diameter x 2 turns. Under these conditions, the loss was measured by using an OTDR from just before the wiring to a period of six months after the wiring. As a result, the loss variation was observed to be stable at 0.03 dB·km or lower for both the 1.3 μm and the 1.55 μm wavelength.

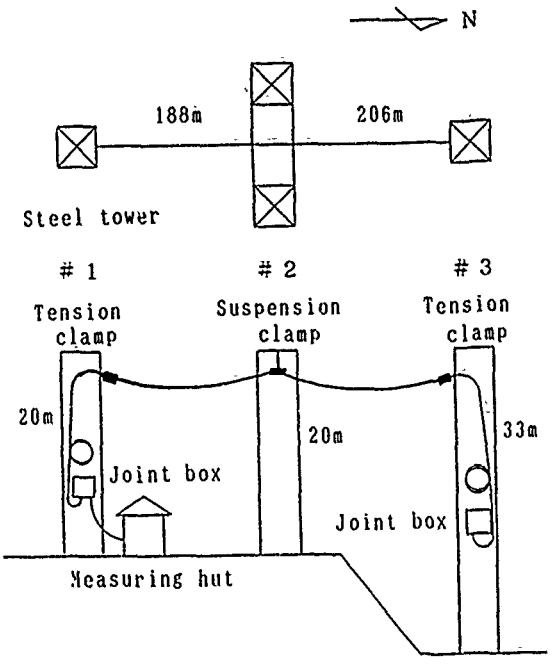

Fig.14. Outline of testing field

5.Conclusion

The newly developed 24-core OPGW was submitted to various evaluation tests and a field test. As a result, the cable was confirmed as having sufficiently reliable characteristics regarding the stress reduction effect, the mechanical performance, the thermal performance, and the loss stability. The Kansai Electric Power has started using this loose type 24-core OPGW since October, 1989, and has already covered approximately 500 km of routes with it.

6.Reference

H.Nabeshima,et.al, in Proc.IWCS'82,45,1982

Hiroshi Ishii

Fujikura Ltd.

1440, Mutsuzaki, Sakura-shi, Chiba-ken, 285, Japan

Mr. Ishii was born in 1961. He joined Fujikura Ltd. after his graduation from Hirosaki University with a B.S. degree in 1983 and had been engaged in research and development of optical cables. He is now an engineer of optical fiber cable manufacturing engineering section and a member of IEICE of Japan.

Hideo Suzuki

Fujikura Ltd.

1440, Mutsuzaki,
Sakura-shi, Chiba-ken,
285, Japan

Mr. Suzuki was born in 1948. He joined Fujikura Ltd. after his graduation from Gunma University with a B.E. degree in 1971 and has been engaged in materials, polymer processing and development of optical cables. He is now the manager of optical cable section and a member of IEICE of Japan.

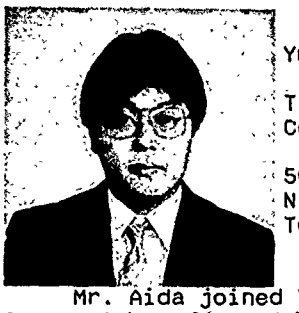

Yukikatsu Aida

The Furukawa Electric Co., Ltd.

500, Kiyotaki-cho,
Nikko-shi,
Tochigi-ken, Japan

Mr. Aida joined The Furukawa Electric Co., Ltd. after his graduation from Yokohama National University in 1986. He now belongs to development section of research and development department of bare wire and cable division.

Kazuo Yokoyama

Fujikura Ltd.

1-5-1, kiba,
Koto-ku, Tokyo,
135, Japan

Mr. Yokoyama was born in 1947. He joined Fujikura Ltd. after his graduation from Hachinohe National College of Technology in 1968 and has been engaged in transmission line engineering.

Hirokazu Shiga

Hitachi Cable, Ltd.

1500, Kawajiri-cho,
Hitachi-shi,
Ibaraki-ken, Japan

Mr. Shiga was born in 1950. He joined Hitachi Cable, Ltd. after his graduation from Shizuoka University with a B.E. degree in 1974 and had engaged in overhead transmission line construction. He now belongs to engineering section of design and development of aluminum conductor for overhead transmission line.

Yuji kimura

Sumitomo Electric Industries, Ltd.

1-1-3, Shimaya,
Konohana-ku, Osaka,
554, Japan

Mr. Kimura was born in Kyoto in 1952. He received his M.E. degree in Electrical Engineering from Kyoto University in 1978. He joined Sumitomo Electric Industries, Ltd., and has been engaged in research and development of overhead transmission lines. He is a senior engineer of Transmission Line Engineering Section, and a member of Electric Engineers of Japan.

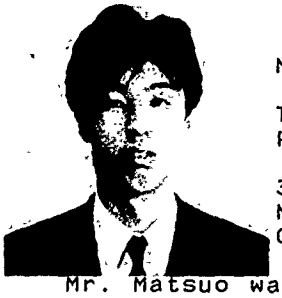

Mitsuhisa Matsuo

The Kansai Electric Power Co., Inc.

3-22, 3-chome,
Nakanoshima, Kita-ku,
Osaka, 530, Japan

Mr. Matsuo was born in 1963. He received the B.S. degree in electrical engineering from Kyoto University in 1987. He then joined The Kansai Electric Power Co., Inc., and has been engaged in planning and management of optical communication network. He is now an engineer of communications section.

Masaharu Kazumori

The Kansai Electric
Power Co., Inc.

3-22, 3-chome,
Nakanoshima, Kita-ku,
Osaka, 530, Japan

Mr. Kazumori was born in 1953. He received the B.S. degree in electrical engineering from Osaka Prefectural University in 1977. He then joined The Kansai Electrical Power Co., Inc., and has been engaged in planning and management of telecommunication systems. He is now an assistant manager of communications section.

Kinya Kawabata

The Kansai Electric
Power Co., Inc.

3-22, 3-chome,
Nakanoshima, Kita-ku,
Osaka, 530, Japan

Mr. Kawabata was born in 1951. He received the M.S. degree in electrical engineering from Kanazawa University in 1975. He then joined The Kansai Electric Power Co., Inc., and has been engaged in planning and construction of overhead transmission line. He is now a deputy manager of construction section, and a member of Electrical Engineers of Japan.

Kazuhisa Ishida

The Kansai Electric
Power Co., Inc.

3-22, 3-chome,
Nakanoshima, Kita-ku,
Osaka, 530, Japan

Mr. Ishida was born in 1946. He joined The Kansai Electric Power Co., Inc. after his graduation from Doshisha University in 1969. He has been engaged in planning and construction of overhead transmission line. He is now a section manager of power system engineering department, and a member of Electric Engineers of Japan.

DESIGN OF BURIED SERVICE LIGHTGUIDE (BSL) CABLES

Don Mathis and Jim Holman

AT&T Bell Laboratories, AT&T Technologies
2000 Northeast Expressway, Norcross, Georgia 30071

Abstract

Fiber-to-the-Customer (FTTC) installations require robust but also flexible optical fiber cables. The cables should be patterned in many ways after copper service cables used for POTS. These optical fiber cables should be rugged, small, light weight, and easy to enter. The objective here is to minimize installation costs. This paper describes a dielectric service cable and a metallic service cable which contain from 1 to 4 buffered singlemode fibers. The designs meet Bellcore's TA-TSY-000843 requirements. A grease filled, nylon, inner tube contains the 1 to 4 buffered fibers. Strength members are placed on each side of the nylon tube and a PVC sheath is extruded around the inner tube. Water blocking yarn and tape are used to stop water penetration. A new proprietary fiber buffering method is used which is robust yet can be stripped with standard copper wire strippers. The cable can be easily and quickly entered by pulling the rip cord, removing the sheath, scoring the nylon tube and removing it, thus exposing the buffered fibers.

I. Introduction

Certain economies and cross-over points still need to be realized in order to create a strong demand for deployment of fiber all the way to the home. Present FTTC (Fiber to the Customer) systems deploy fiber to a pedestal. Twisted copper-pair or co-axial cable is then used to connect the pedestal to the customer's home.

Some optical fiber service cable is presently being used for system tests and field applications. Mass deployment of fiber all the way to the customer's home will depend on technology, band-width demand, and economics.[1] Some predictions say that this demand will occur in 1992-1995. As part of continuing development work,[2] a family of buried service lightguide cables has been developed to fill this application.

II. Environmental Constraints

A. Premise Environment

The buried service cable environment is one of the most severe in the telecommunications' network. The cable is buried at shallow depths on the customers' property thus exposing it to gardeners' shovels, sprinkler system installation crews, and post hole diggers. The cables need to be flexible for ease of installation and low-cost to decrease installation costs. This implies a small diameter cable with little armoring. This is incompatible with the above requirement of protection from shovels and digging tools.

The cables must be installed on customers' houses and thus are exposed to temperature and weather extremes. Also since the cable is attached to the house it must be fire retardant.

Many service cables are installed before houses are constructed. Consequently the cable must be bent and coiled into a package to fit inside of a pedestal or buried water meter box. For storage these bends can easily be as small as 4 inches in diameter.

Finally the cables are sometimes installed by contractors and by craftspeople who have minimal training for outside plant splicing. Yet the application of this cable requires short lengths and many splices. This requires a cable which is easy to enter yet protects the fibers from handling accidents.

In summary the buried service cables are required to meet outside plant environmental specifications, flame retardant specifications, cost objectives and the human factor engineering requirements of cable entry and connectorization.

III. Requirements

A. Bellcore

Bellcore has defined general requirements for an optical fiber service cable. These are contained in their Technical Reference, TR-TSY-000843.[3] These requirements define the following:

1. Cable Materials
2. Continuity of Materials
3. Operation of the Cable Components (rip cords, shields, water blocking materials, binders, etc.)
4. Color Coding
5. Marking, Packaging, and Shipping

Original equipment manufacturers (OEM) sometimes add or subtract from these requirements for their specific application but generally, the Bellcore standards are sufficient for most applications. In some instances manufacturers add their own requirements to the Bellcore requirements to further enhance the over-all cable quality.

IV. Cable Types

The buried service lightguide cables comprise a family of cables; metallic and dielectric. Both the metallic and dielectric cable designs contain from 1 to 4 single mode buffered fibers.

Multiple fiber service cables are needed to supply service to multi-family dwellings such as duplexes and apartment houses and serve the current architecture of fiber to the pedestal.

Some applications require dielectric cables because of the high incidence of lightning strikes in certain parts of the country. Other applications require a metallic shield for somewhat better protection during trenching and plowing operations. The metallic shield also provides a means of carrying an electrical signal for cable location. These are the reasons for having both metallic and dielectric cable designs.

V. Design

The product was designed based on performance requirements and systems cost. The design incorporates human factors engineering because of the end use of this product; that is, field applications require short lengths and many splices. Therefore ease of entering and splicing the cable are very important cost saving items for the customer. The cable layers have different colors chosen to aid in this operation.

A. Metallic Cable

The metallic cable design (Figure 1) uses a nylon tube containing water-resistant compound and one to four buffered fibers. Water blocking tape is placed around the nylon tube. Corrugated bronze is then placed around the tape and a stainless steel wire is placed on either side of the bronze wrapped tube for strength members. Water blocking thread is wrapped around each strength member. A black PVC containing UV inhibitors is then extruded over this assembly. The outside diameter for the metallic cable is 0.40 inches for one through four fibers.

B. Dielectric Cable

The dielectric cable design (Figure 2) uses the same nylon tube containing grease and one to four buffered fibers. Dielectric strength members are placed diametrically on either side of the tube. Water blocking threads are placed around the rip cord and the tube. PVC is then extruded over this structure. The outside diameter for the dielectric cable is 0.36 inches for one through four fibers.

C. Material Rationale

The fibers are buffered in a manner to ease strippability. The coated fibers are run through a solution containing a solvent mixture. After coating the fibers with this mixture the solvent is removed from the fiber leaving an angstrom thick coating of a special material. The fibers are then buffered with PVC. The pre-coating applied before the buffering reduces the adhesion of the buffer. The buffer can be very easily stripped using standard electrical wire strippers.

The grease, used inside of the tube, is water resistant and provides excellent environmental loss performance over the life of the cable.

Nylon was chosen for the tube for a variety of reasons. It is not affected by micro-organisms living in the soil in some parts of the world. It also has a high resistance to cut-through. A craftsperson entering the cable can feel the difference in cutting through the PVC sheath and the inner nylon tube. Also, the bright yellow color of the nylon tube contrasts with the black color of PVC. After the yellow nylon tube is exposed it is simple to score the tube with a knife and break it without cutting or damaging the buffered fibers. It can then be slipped off the buffered fibers.

The dielectric design requires a dielectric strength member. The dielectric cables use a resin impregnated fiber-glass roving. These have been tested using the EIA FOTP tests and found to be more than adequate for Bellcore's 150 pound tensile-strength rating.

It is important that service cables be protected from water penetration. One solution to this problem is to flood the cables at all layers with grease. However, this makes the cable more difficult to strip and handle. We chose instead to use water-resistant grease only in the inner tube and water blocking materials at the other layers.[4] These are dry to the touch and yet swell upon being wet and prevent water from entering the cable. A water blocking string was wound around the strength members on the metallic design and the rip cord on the dielectric design thus blocking water seeping down these members. A tape was applied around the nylon tube under the bronze tape on the metallic design. These designs have passed all of the Bellcore water penetration tests.

The corrugated 0.004 inch thick bronze was used as added protection for applications requiring trenching or plowing. This cable design using this bronze has been tested in the field and has proven more than adequate for this hostile environment.

VI. Testing and Evaluation

In order to qualify a cable a large number of tests must be passed. These may be categorized as:

1. Environmental Tests
2. Mechanical Tests
3. Optical Tests
4. Specialized Tests

Additionally, there are a large number of specifications for the optical fiber which must be satisfied before the cable is made.

The tests contained in the four categories listed above are:

ENVIRONMENTAL	MECHANICAL
Water penetration	Longitudinal shield fatigue
Water resistance test	Low/high temperature bend
Filling compound flow	Impact tests
Temperature cycling	Compressive strength
Aging	Tensile strength
Flammability	Twist
Color permanence	Cyclic flex
Hydrogen in cables	Jacket elongation
Freezing	Plasticizer compatibility
Jacket shrinkage	Buffer strippability
OPTICAL	**SPECIALIZED TESTS**
Attenuation	Ease of entering
Added attenuation	Appearance
Cutoff wavelength	Printing legibility
	Printing permanence

Details of the tests are given in Technical Reference, TY-TSY-000843.[3] The Buried Service Lightguide Cables passed all of these tests. Results of these tests requiring a minimum loss increase (dB/km) are shown in Figure 3.

The environmental temperature cycle is shown in Figure 4. The test chamber temperature is changed and allowed to stabilize over 24 hours. At this point loss is measured. The cable is cycled from -40°F to 65°C and then the cable is held at a temperature of 85°C for five days. This aging is to simulate long term environmental effects on optical transmission performance. The requirement from the Bellcore specification is that the loss increase after aging should be ≤ 0.6 dB/km. The test results showed a maximum loss increase of 0.06 dB/km which occurred at -40°C after the aging cycle.

VII. Design Highlights

A. Flammability

The Bellcore Flammability test is a difficult test to pass with a dielectric cable. It requires passing the Underwriters Lab test UL 444, Section 25. This involves holding a 1500°F - 2000°F flame at the surface of a vertically mounted 18 inch length of cable. The flame is held there for 15 seconds and then removed for one minute. Then the flame is re-applied and the cycle is continued. The test sample passes the test if during each of five cycles the burning cable sample:

1. is extinguished within 60 seconds
2. does not ignite paper flags on the sample ends
3. does not drop burning material on cotton below the sample.

The UL requirement is 5 cycles of the flame. The present dielectric cable will survive 15 cycles.

The metallic design easily passed the VW-1 flammability test because the bronze tape acted as a heat sink to distribute the heat over a greater surface.

B. Bronze Sheath

Copper service cables have traditionally used a corrugated bronze armor underneath the outer sheath. It had several purposes. It was grounded and served as an electromagnetic shield. It also was used to carry a signal such that the cable could be found after being buried. This shield is typically on the order of 0.004 inches thick.

There is a similar purpose for this corrugated bronze in an optical fiber service cable. An electronic signal can be placed on the bronze and used to locate the buried cable. The bronze also provides protection during trenching and plowing operations.

The bronze is placed around the inner nylon tube with a diameter of 0.20 inches. This small inside tube diameter, in addition to the backing with the somewhat rigid nylon, protects the bronze from high bending stresses.

One of the most destructive installation operations occurs if the cable is being trenched-in and the trenching machine is stopped but the vibratory plow is allowed to continue to vibrate for 5 minutes to 10 minutes. This usually cracks metal cable shields. The new family of buried service cables all pass this test with no cracking.

VII. Manufacturability

The cable designs are not complicated and consequently are easy to manufacture at a high rate of speed on the cable line. This is a corporate goal and it is also a benefit to the customer. Because of the ease of manufacture the cable quality can be held to very high standards.

VIII. Summary

The buried service lightguide cable designs provide the final link for an all fiber network. The cables are available from one to four buffered fibers in either a dielectric or metallic sheath. The cables employ the latest technology in materials as well as the proven copper service cable principles of ruggedness, simplicity and easy usage. These cables meet very stringent product specifications which are required for service cable applications. These cables maintain the same quality transmission performance when connected to the main distribution cables.

Human factors engineering was one of the major objectives used in the design of these cables. This was important so that the cables can be opened and spliced easily without damage. Consequently, lower installation costs can be achieved.

IX. Acknowledgement

The authors gratefully wish to acknowledge the assistance of the many talented people who helped in the successful completion of this family of cable designs

BRONZE
BURIED SERVICE LIGHTGUIDE (BSL)
TWO FIBER CABLE DESIGN

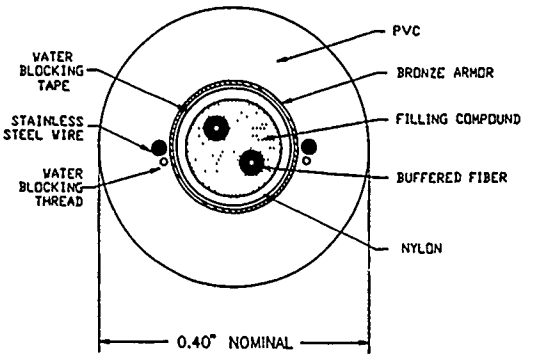

FIGURE 1

DIELECTRIC
BURIED SERVICE LIGHTGUIDE (BSL)
TWO FIBER CABLE DESIGN

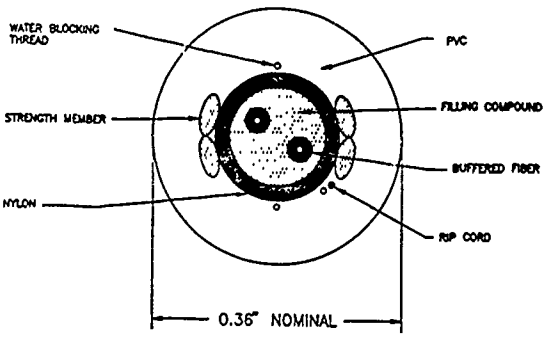

FIGURE 2

MECHANICAL AND ENVIRONMENTAL PROPERTIES
BURIED SERVICE LIGHTGUIDE
(ADDED LOSS - dB/km)

TEST DESCRIPTION	REQUIREMENT (dB/km)	METALLIC 1310 NM (dB/km)	METALLIC 1550 NM (dB/km)	DIELECTRIC 1310 NM (dB/km)	DIELECTRIC 1550 NM (dB/km)
TENSILE STRENGTH EIA-455-33	$\Delta \leq 0.2$	0.0	0.0	0.03	0.02
COLD BEND EIA-455-65	$\Delta \leq 0.2$	0.02	0.03	0.01	0.0
IMPACT EIA-455-25	$\Delta \leq 0.2$	0.0	0.02	0.01	0.01
COMPRESSION EIA-455-41	$\Delta \leq 0.2$	0 0	0.03	0.0	0.0
CYCLIC FLEXING EIA-455-104	$\Delta \leq 0.2$	0.0	0.02	0.01	0.01
FREEZING EIA-455-98A	$\Delta \leq 0.2$	0.07	0.05	0.01	0.01
TWIST EIA-455-81	$\Delta \leq 0.2$	0.01	0.01	0.01	0.01
HOT BEND EIA-455-37	$\Delta \leq 0.2$	0 01	0.0	0.0	0.01
COLD BEND EIA-455-37	$\Delta \leq 0.2$	0.02	0.03	0.01	0.01

Figure 3

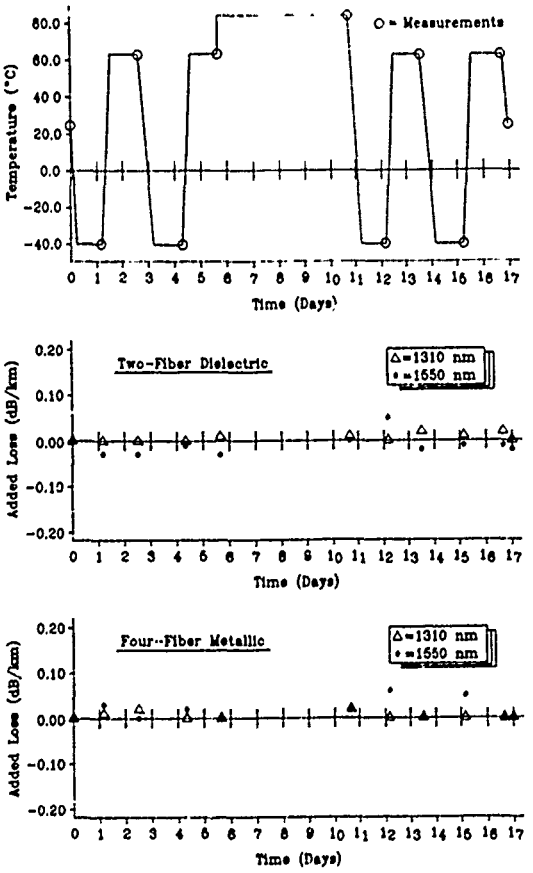

Figure 4 BSL Cable Thermal Cycle and Aging Performance

X. References

1. J. B. Haber, D. Kalish, and J. J. Refi, "Single-mode Media and Apparatus for Fiber-to-the-Home," International Wire and Cable Symposium Proceedings, Reno, 1988.
2. E. R. Campbell, F. J. Mullin, and W. C. Reed, "Fiber/Metallic Service and Distribution Media," International Wire and Cable Symposium Proceedings, Arlington, 1987.
3. Bellcore Technical Reference, TR-TSY-00843, Generic Requirements for Optical and Optical/Metallic Buried Service Cable, Issue 1, 1989.
4. C. J. Arroyo, P. Debban, Jr., and W. J. Paucke, "Water Resistant Communications Cable," Patent 4,815,813, 1989.

Don Mathis is a Member of Technical Staff in the Lightguide Technology Department at AT&T Bell Laboratories in Norcross, Georgia. He is responsible for design of optical fiber service cables and premise cables.

Dr. Mathis joined AT&T Bell Laboratories in 1972. He has B.S. and M.S. degrees from Oklahoma State University, and a Ph.D degree in Mechanical Engineering from the University of Houston.

He has been granted five patents with three more pending.

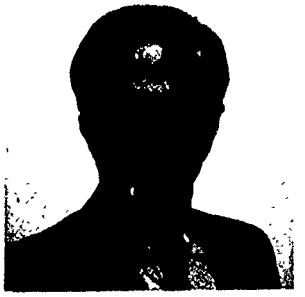

Jim Holman is a Senior Development Engineer in the Lightguide Cable Process Development Group at AT&T Technologies in Norcross, Georgia. He is responsible for the development of manufacturing processes for optical fiber service cables and premise cable products.

Mr. Holman began his career with AT&T Bell Laboratories in 1966 and later transferred to Network Cable Systems. He has a B.S. degree in Electrical Engineering from the Georgia Institute of Technology.

He has been granted three patents with one more pending.

CHARACTERISTICS OF JELLY-FILLED NON-METALLIC RIBBON-FIBER SLOTTED-CORE CABLES

Y. Yamazaki, H. Horima, H. Igarashi, K. Niikura

Sumitomo Electric Industries, Ltd.
1, Taya-cho, Sakae-ku, Yokohama, 244 Japan

ABSTRACT

Various kinds of non-metallic multi-fiber optical cables which employ 4-fiber-ribbon and are filled with jelly were designed, manufactured and evaluated. The multi-slot core optical cable can be manufactured easily and the obtained characteristics were as stable as those of the single slot core optical cable. A SZ polyethylene-slotted core was applied to 4-fiber-ribbon for mid-span branching of optical fiber and was successfully manufactured and evaluated.

1. Introduction

A non-metallic type optical cable which optimizes the dielectric property of glass fiber is an innovative communication cable, which is required to be small-diameter and light weight. Jelly compound is usually filled in the non-metallic cable for ease of maintenance and for waterproof. The needs for this jelly-filled non-metallic optical cable will increase in a variety of fields because of its excellent characteristics.
Optical cable will be used not only for trunk lines but also for subscriber lines and the demand is increasing for a high-fiber-count optical cable. To meet such demand, a ribbon-fiber slotted-core cable was manufactured to produce a 1000-fiber cable on commercial basis in Japan.① But most of the constructions consist of metallic type air core. As a corollary, it was apparent that the development of the existent constructions was essentially required to meet the needs for the jelly-filled non-metallic optical cable.
To this aim, various jelly-filled non-metallic ribbon slotted-core cables based on the 4-fiber-ribbon have been newly designed, manufactured, and evaluated. The results gained have proved a prominent practicality of these cables, and their details are reported as follows.

2. Construction of jelly-filled non-metallic ribbon slotted-core cable

2.1 Coated SM fiber

The SM type optical fiber used in this cable is manufactured in the wholly synthesized VAD method to make its transmission loss and core eccentricity error extremely low. Table 1 shows the typical value of the geometrical parameters of the optical fiber applied in this evaluation. The glass fiber of 125μm in diameter is coated with two-layer UV resin, with its diameter of 250μm.

Table 1. Geometrical parameters of SM VAD fiber

Item	Typical value
Mode field diameter	9.46 μm
Cladding diameter	124.8 μm
Eccentricity error	0.13 μm
Cladding non-circularity	0.3 %
Primary coating diameter	250 μm

Sample number: 100

2.2 4-fiber-ribbon

The cable lately manufactured is constructed with 4-fiber-ribbon as its basic unit. The marker method that the color of one of the fibers in a ribbon should be taken to make the identification among the ribbons has been so far widely adopted. However, to make the ribbon-identification further easier, a new method different from the above, making not only the fibers identified but also the ribbons themselves colored, was introduced. The colored ribbons have been available which are manufactured by mixing the UV resin for ribbon with various coloring agents to adjust the curing condition of the resin and to have a characteristics similar to that of the non-color ribbon.

2.3 Jelly compound

As the jelly compound in slots for the ribbon fiber, the one with the physical properties shown in Table 2 is used. This jelly is selected to have a large cone penetration at the wide range of temperature just shown in Fig.1 and assure stable transmission characteristics especially at the range of low temperature. Moreover, owing to this high dripping point, the jelly will never become liquid in the cable even under the high temperature circumstances. It has been confirmed that there is no problem on the compatibility of this jelly with the coatings of the ribbon and fiber.

Table 2. Physical properties of jelly compound for fiber-ribbon

Item	Unit	Value
Specific gravity		0.85
Oil separation*	%	Less than 0.01
Evaporation loss*	%	Less than 0.01
Dripping point	°C	220

* Measured after 24 hours at 100°C

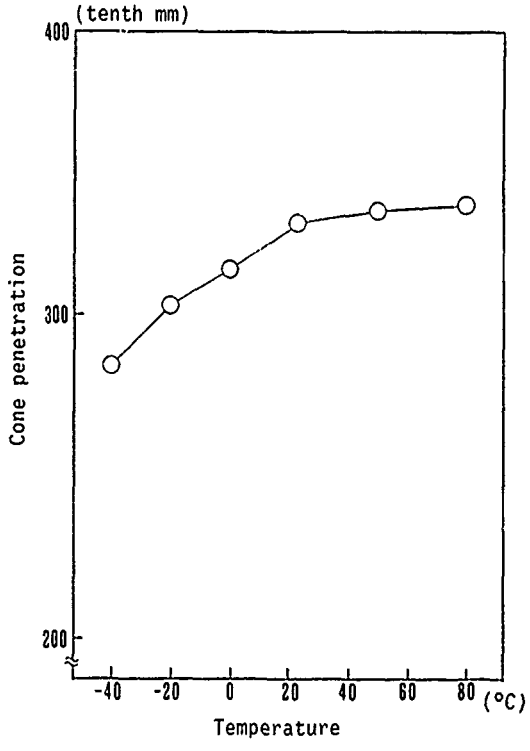

Fig.1 Temperature dependence of cone penetration of jelly compound for fiber-ribbon

2.4 Ribbon slotted-core cable

Initially, Fig.2 shows the cross-sectional view of the single slot cable to deal with the number of fibers from 4 to 96 fibers, as the development of the design of the existing metallic air core type cable. While Fig.3 indicates that of the multi-slot type cable capable to deal with the high-fiber-count optical cable from 100 to 576 fibers. Fig.2 shows a cable in which 4-fiber-ribbons are arranged in one slot, i.e., 16 fibers are inserted and up to 96 fibers can be constructed using polyethylene slotted-core with six slots. Fig.3 shows a cable with built-in 576 fibers by stranding six slotted-cores in Fig.2 around the FRP central strength member. In the cables shown in Figures 2 and 3, 4-fiber-ribbons are accumulated in the slot and are stranded either in S or Z direction. The hollow space inside of the cable is filled up with the jelly for waterproof. The more the number of fiber ribbons in a slot becomes, the more difficult the complete filling up of the jelly gets with the less efficiency of waterproofing. Therefore, the number of the fiber-ribbons in a slot is limited to 4 at the most, and the number of slots in a polyethylene slotted core is also limited to 6 for the same reason. This structure has allowed the multiple-ribbon jelly-filled cable to be available. The outer sheath both of the cables shown in Fig.2 and Fig.3 consists of polyethylene. Photo.1 depicts the appearance of 36-fiber ribbon optical cable which is constructed with the slotted-core just shown in Fig.2, with two 4-fiber-ribbons into each of the three slots of the six ones and one ribbon into each of the remaining three slots, namely, nine 4-fiber ribbons in total built in the cable. The two cables abovementioned have been manufactured in the uni-direction stranding method. On the other hand, a cable in the SZ stranding method to enable the mid-span branching after being laid down has been manufactured. The side condition and the cross-sectional view of the SZ stranding 4-fiber-ribbon slotted-core cable made on the experimental basis are shown in Photo.2 and Fig.4, respectively. The reversing lay length of the slot shown in Photo.2 is designated to be 500mm.

Photo 1. Appearance of jelly-filled non-metallic 36-fiber ribbon slotted-core cable

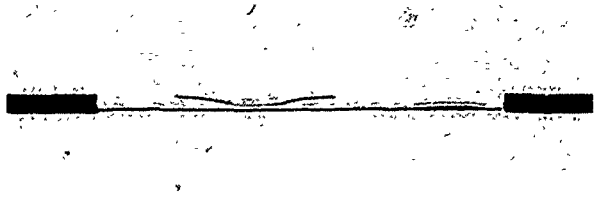

Photo 2. Side view of prototype 4-fiber ribbon SZ slotted-core cable

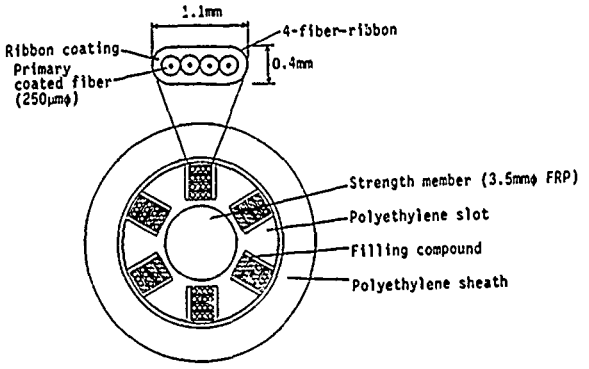

Fig.2 96-fiber single slot cable

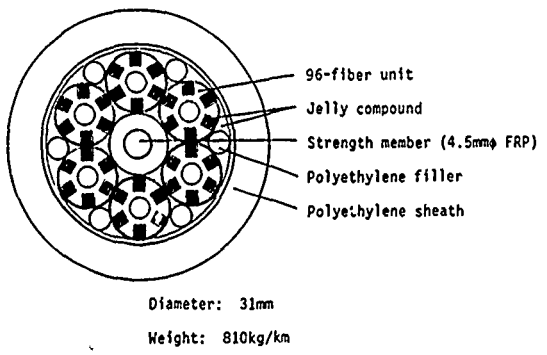

Fig.3 576-fiber multi-slot cable

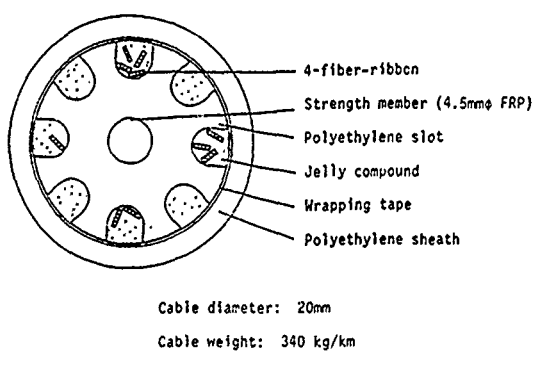

Fig.4 Cross section of prototype 4-fiber-ribbon SZ slotted-core cable

3. Transmission characteristics

3.1 Transmission loss

The optical fiber used in this cable is a standard SM type, and its transmission characteristics have been evaluated as for both the uses in the optical transmission system of normal 1300nm band (wavelength from 1285 to 1330nm) and that of 1550nm band (wavelength from 1530 to 1570nm). The variations of the transmission loss in the three kinds of the cables aforementioned at their manufacturing process are shown in Fig.5. Incidentally, the transmission loss histograms for 36-fiber ribbon slotted-core cable shown in Fig.6 (a) and (b).

3.2 Chromatic dispersion

Not only the transmission loss but the chromatic dispersion may be weighty factors in optical signals being transmitted at high speed. The dispersion value itself has been so far taken as a means to evaluate the chromatic dispersion, however, recently the zero-dispersion wavelength and the zero-dispersion slope have also used as the means. Table 3 shows the chromatic dispersion characteristics of the fibers in ribbons.

3.3 Temperature characteristics

The fluctuations of the transmission loss have been evaluated at the wavelengths of 1310nm and 1550nm in the temperature range from -40°C to +70°C. The results gained are shown in Fig.7 displaying stable characteristics with the fluctuation of the loss under 0.03dB/km in both the wavelengths, which ensures that they will be able to stand up to the wide use ranging from the hottest districts to the coldest ones.

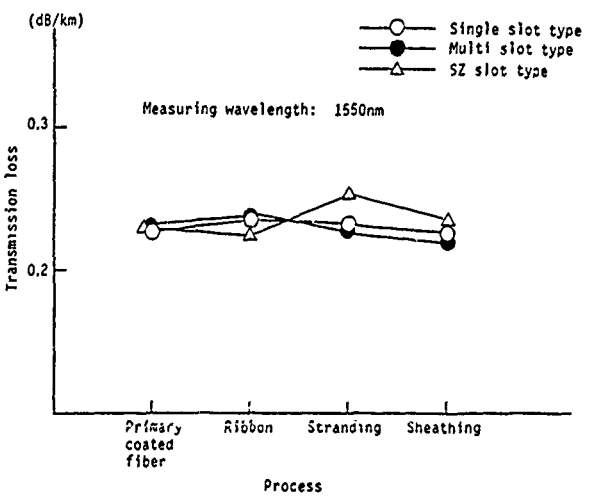

Fig.5 Transmission loss change in manufacturing process

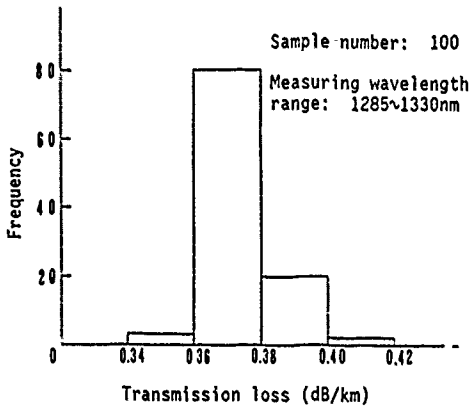

(a) Transmission loss in the wavelength range of 1285∿1330nm

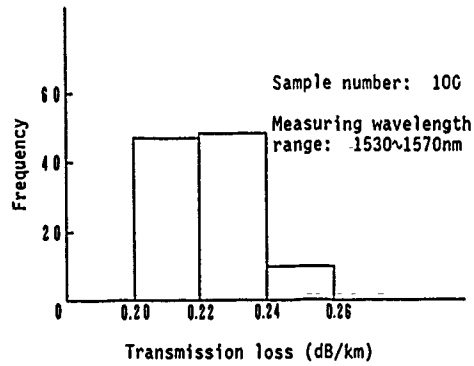

(b) Transmission loss in the wavelength range of 1530∿1570nm

Fig.6 Histrogram of transmission loss for single slot type 36-fiber ribbon cable

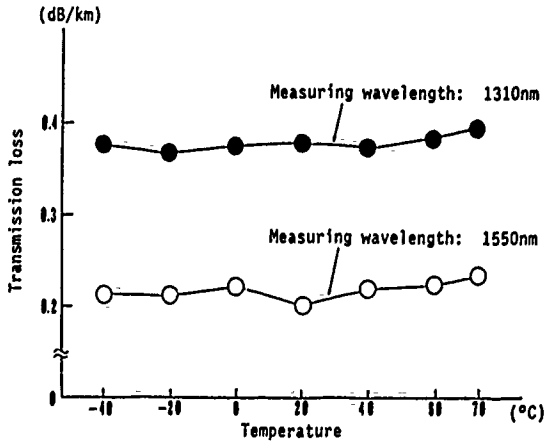

Fig.7 Temperature characteristics for single slot type 36-fiber ribbon cable

Table 3. Chromatic dispersion for SM VAD 4-fiber-ribbon slotted-core cable

Item	Typical value
Zero dispersion wavelength	1318 nm
Zero dispersion slope	0.088 ps/nm²/km
Chromatic dispersion at 1550 nm	16.18 ps/nm/km

Sample number: 100

4. Physical Properties

4.1 Mechanical Properties

As for the 36-fiber cable shown in Photo.1, the mechanical properties listed in Table 4 have been evaluated. Most of the test methods are based on the IEC standard. The cables have demonstrated their steadfast properties and ensured that there would be no problem in their transmission characteristics even if under the external force assumed in their being laid down.

Table 4. Mechanical properties for single slot type 36-fiber cable

Test item	Test method	Result
Tension	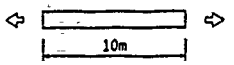	No loss increase up to 800kgf tension
Compression (Plate)	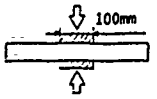	No loss increase up to 700kgf/100mm compression
Compression (Mandrel)	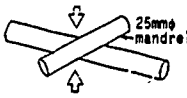	Δα<0.1dB at 225kgf/25mmφ
Bend	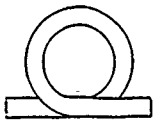	No loss increase at 400mmφ (room temperature)
Cold bend		No loss increase at 600mmφ (-10°C)
Impact	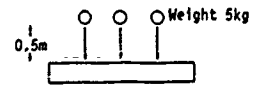	No fiber break at 5kg×0.5m×3 impacts
Torsion	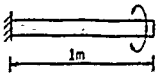	No loss increase at ±360° × 5 cycles

Measuring wavelength: 1550nm

4.1.1 Tension test

Three loops were made by splicing every 12 fibers out of 36 fibers in the cable. The two loops of them were used to monitor the fluctuations of the transmission loss at the wavelengths of 1310nm and 1550nm, while the another loop was used to measure the strain of the optical fiber by the modulation phase method.② Fig.8 shows the results obtained in this tension test. The tension at the moment the rate of increase of the fiber reached 0.2% was 125kgf.

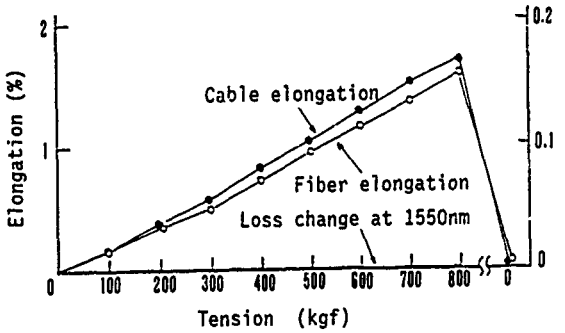

Fig.8 Tension test result for 36-fiber ribbon slotted-core cable

4.1.2 Compression test

The relation between the loss increase and the load in the case that the cable was compressed with a board 100mm wide is shown in Fig.9. There is no loss increase even at the load 700kgf/100mm, showing a favorable characteristics against compression. Furthermore, assuming the case that the several cables laid down simultaneously being pressed, two mandrels of 25mm in diameter were laid one on the other at the right angles to be pressed, resulting the loss increase below 0.1dB in the 1550nm wavelength at the load 225kgf/25mmφ.

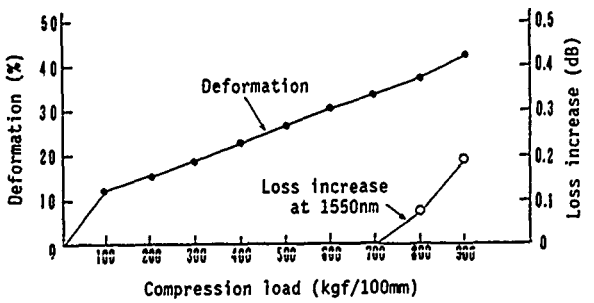

Fig.9 Compression test result for 36-fiber ribbon slotted-core cable

4.1.3 Flexibility

Since FRP is used as the strength member in the cable, it was anticipated that the cables, especially of the multi-slot type assembling slot-rods, might be hard to flex. Fig.10 shows the test method and the results of the comparison of the flexibility of the single slot type and that of the multi slot type. There is no conspicuous difference in flexibility among the two types in the case a cable 30cm long was bent by the weight of 10kg. It appears from the above that the flexibility would not cause any serious problem practically.

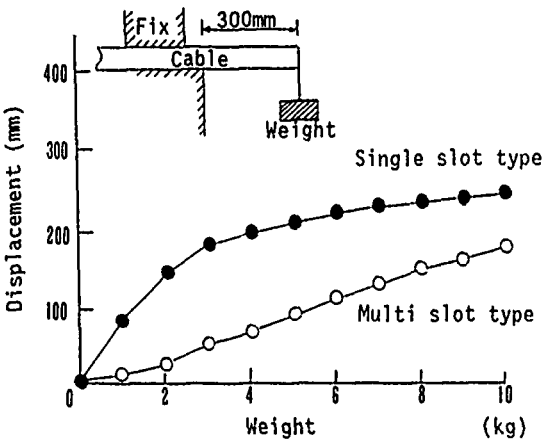

Fig.10 Flexibility test

Table 5. Compound flow and waterproof test results

Test method	Result
Compound flow test 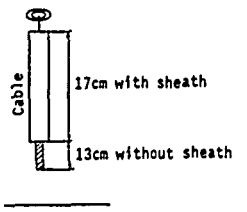	Single slot type: 70°C x 24 hours Multi slot type: 60°C x 24 hours No jelly drop
Waterproof test 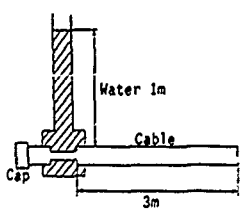	No water leakage after 24 hours

4.2 Compound flow and waterproof

As was noted previously, the hollow space inside of the cable is filled up with the jelly for waterproof. An improper selection of the compound for the jelly or insufficient filling may cause the jelly to flow from the cable and water to get in it after the cable laid down. As such, not only the transmission characteristics but also this waterproof should be evaluated with keen interest. Table 5 shows the test method and the results obtained ensuring the excellent waterproof property as well as no fear of the jelly flowing out from the cable even under the high-temperature circumstances.

5. Conclusion

In conclusion, there follows a brief explanation. For the aim of the further development of the ribbon slotted-core cables that are now spreading-widely, various jelly-filled non-metallic ribbon slotted-core cables based on the 4-fiber-ribbon have been newly designed, manufactured, and evaluated. The results gained have proved the promising possibility of designing the high-fiber-count optical cable having both the sufficient waterproof property and the excellent transmission characteristics equal to those of the air-core cables. Since the structure of this type of cable is the one to take full advantage of the superb characteristics of optical fiber, it is greatly expected that its application will cover the wide range not only in the public communication lines including the optical subscriber lines but also in the optical LAN lines and the optical cable to be installed in special environment.

ACKNOWLEDGMENTS

We would like to thank all those in and outside the company who participated in this development for their guidance and cooperation.

REFERENCES

① T. Uenoya, "The Optical Fiber Loop 21 Plan", OEC '90 (Makuhari Messe, Japan), 1990.

② S. Tanaka et al., " Lifetime Design of Optical Fiber Cable for Long Term Use", Sumitomo Electric Technical Review, Number 21, Jan. 1982.

Yosuke Yamazaki
Sumitomo Electric
Industries, Ltd.
1, Taya-cho,
Sakae-ku,
Yokohama 244, Japan

Yosuke Yamazaki graduated from Tokyo Institute of Technology in 1983 with a B.S. in mechanical engineering. He then joined Sumitomo Electric Industries, Ltd., where he is an cable design engineer in the Fiber Optics Division.

Hiroaki Horima
Sumitomo Electric
Industries, Ltd.
1, Taya-cho,
Sakae-ku,
Yokohama 244, Japan

Hiroaki Horima received the M.S. degree in engineering from Osaka University in 1972. He then joined Sumitomo Electric Industries, Ltd. and worked on the development of CATV coaxial cables, multipair PEF-insulated junction cables and low loss unbalanced type cables. Thereafter, he concentrated on the development of optical fiber cables. He is now Section Manager of the Fiber Optics Division at Sumitomo Electric Industries, Ltd. He is a member of the Institute of Electronics and Communication Engineers of Japan.

Hajime Igarashi
Sumitomo Electric
Industries, Ltd.
1, Taya-cho,
Sakae-ku,
Yokohama 244, Japan

Hajime Igarashi received the B.S. degree in engineering from Waseda University in 1988 and joined Sumitomo Electric Industries, Ltd. He has been engaged in the development and design of optical fiber cables in the Fiber Optics Division.

Koji Niikura
Sumitomo Electric
Industries, Ltd.
1, Taya-cho,
Sakae-ku,
Yokohama 244, Japan

Koji Niikura received the B.E. degree in engineering from Waseda University in 1984 and joined Sumitomo Electric Industries, Ltd. He has been engaged in the development and design of optical fiber cables in the Fiber Optics Division.

CHARACTERISTICS OF ONE-THOUSAND-FIBER WATER PROOF CABLE

Y. KIKUCHI, H. SAWANO, Y. SATO, K. KOBAYASHI,
K.OKAMURA, H.SUZUKI and N. SATO

FUJIKURA LTD.

ABSTRACT

A water proof optical fiber cable with one thousand fibers has been developed.

New cable is using water swellable materials as wrapping tapes and filled yarns, and other fundamental structures are similar to conventional cables which have been used for gas pressurized system.

In this paper, a design criteria for accommodating the water swellable materials and experimental results concerning water blocking properties, thermal properties, mechanical properties and long term reliability tests are described.

1.Introduction

The use of optical fiber cables has quickly broadened into subscriber network. High-density, high-count optical fiber cables are required to shorten the construction period and save the maintenance cost. To realize such requirement, high fiber count cables using multi fiber ribbons and cable joining technologies such as mass fusion splice machine and multi fiber connector have been developed[1-4]. This high fiber count cable is generally maintained by gas pressurized method, so the maintenance cost is expensive compared with water proof cable.

Water proof cables such as jelly filled cable and dry type water proof cable are widely used as maintenance free cable[5]. Jelly filled cable has a disadvantage in cable connection and cable weight, because jelly compound should be completely wiped out to join the fibers. On the other hand, dry type which uses water swellable materials, is applied to one or a few hundreds fiber cable in commercial use, and has been investigated to be applied to one thousand fiber cable[6].

In this paper, we present a newly designed one thousand water proof cable. The fundamentals of this cable are based on conventional cabling technology and cable joining technology.

2.Design criteria

For cables used in subscriber network, following requirements should be taken into account.

1) High fiber count and compact cable.
2) Rapid cable joining capability.
3) Mid span access capability.

As the reply to above requirements, the following technologies have been already developed and in commercial use : dividable eight fiber ribbons, high fiber density one thousand fiber cable, mass fusion splice machine and multi fiber connectors.

Water blocking function should be added to the conventional one thousand fiber cable without missing above technologies.

In designing the water proof cable with water swellable materials, the following reliabilities should be insured.

a) Water blocking properties should be stable against thermal effect or interaction between water swellable materials and other cable composition.
b) Transmission loss should be stable, even after the water penetration into the cable. In other words, no hydrogen generation or no effect by frozen water will come to problem on the transmission system.
c) Fiber life time should be insured for practically use period.

These criteria will be realized the following experimental examinations.

3. Cable design

(1)Structural design

The cross sectional structure of newly developed water proof cable is shown in Fig. 1.

This cable has an unfilled structure, so its weight is equal to conventional gas maintained cable and no special treatment will be required for cable joining.

Five 8-fiber-ribbons are stacked in each of the five rectangular slots grooved on a polyethylene rod to make a two hundred fiber unit and each unit is wrapped with a water swellable tape. Five units are stranded on a central strength member to make a one thousand fiber cable. This cable core is covered with a laminated aluminum sheath. A plastic film is adhered to the inner side of aluminum tape to suppress the hydrogen generation. Open space inside the cable is filled with water swellable yarns. This cable is 40mm in diameter and 1.2kg/m in weight.

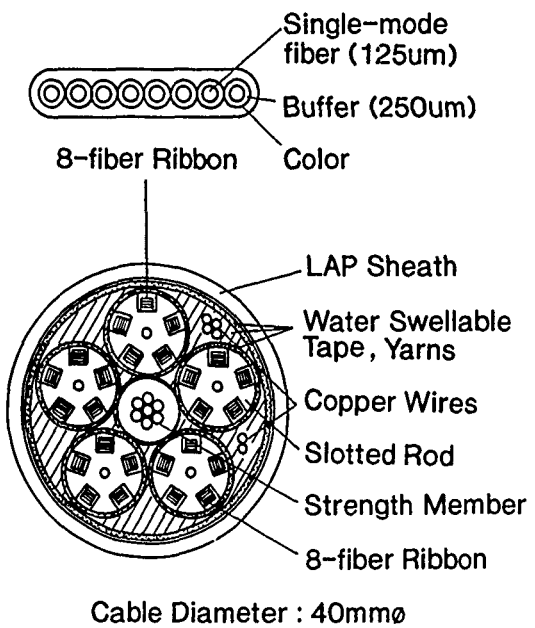

Fig.1 Cable Structure.

(2)Water swellable materials

Two kinds of water swellable materials are used in this cable. One is a water swellable tape, the other is a water swellable yarn.

The water swellable materials should have proper structures and stability in chemical nature.

The water blocking properties of three kinds of water swellable tapes were investigated. Tape A has sandwich structure. This tape was composed of water swellable powder between two unwoven cloths. Tape B was composed of an unwoven cloth which was made of water swellable fiber. In tape C, water swellable powder was adhered to an unwoven cloth. The water blocking properties were examined by the water penetration length through 3.0X3.0mm square slot. Table 1 shows that tape C has the best water blocking performance, because the water swellable powder disconnect itself from the substrate unwoven cloth and fill the vacancy, when water contact it. Fig.2 shows the relation between the amount of adhered water swellable powder and water blocking ability. The proper amount of adhered water swellable powder was determined according to this result.

Table 1 Water blocking properties of water swellable tapes.

	Structure	Penetration Length	Method
A	Sandwitch	>10m	3X3mm slot 1m height 24Hour
B	Fibric Type	>10m	
C	Water Swellable Powder Adhered	5m	

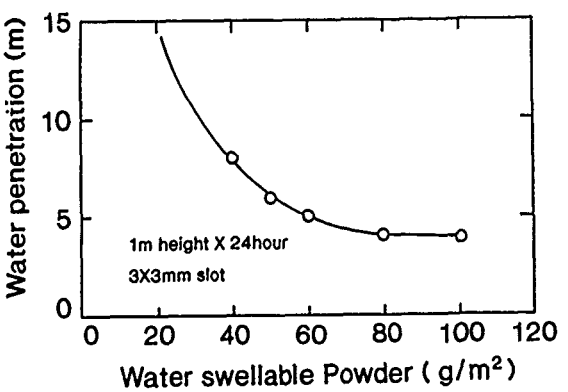

Fig.2 Relation between the amount of water swellable powder and water penetration.

The water swellable powder should be chosen to be accommodated to the ocean water as well as fresh water. Conventional water swellable powder, used in water proof cable, was made from acrylic acid salt. So the water absorption ability is reduced as the metallic ion content increase. To overcome this weak point, other organic derivatives were introduced to conventional acrylic acid salt. The reduction of water absorption ability in ocean water can be kept within 1/20 of that of conventional one. Thermal stability of water swellable material is shown in Fig. 3. The degradation in air shows the Arrehnius relation. The degradation of water absorption at 30C for ten years is predicted less than 30% of original condition. Taking into account for above results, new water swellable tape was determined. In addition, the hydrogen generations in muddy water and at high temperature were checked by means of Ref.5 . The results are shown in Fig. 4 and Fig. 5. No hydrogen generation was observed in these tests.

The water swellable yarn was also designed in the same manner of water swellable tape.

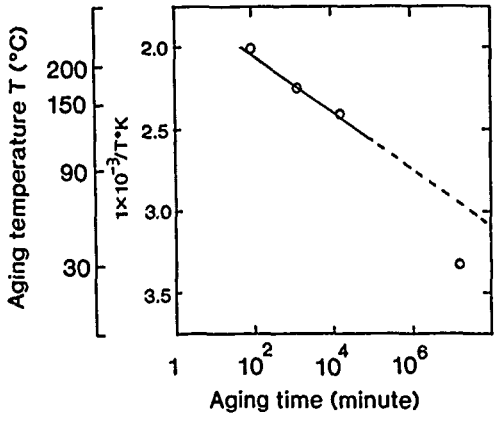

Fig.3 Relation between temperature and period until 30% degradation of water absorption ability.

(3)Sheath composition

Laminated aluminum sheath was adopted to protect the cable core. But as well known, aluminum generates hydrogen when it contact with water, so laminated aluminum tape is entirely covered with plastic material. Fig. 6 shows the hydrogen generation characteristics at 80C. Hydrogen generation from newly adopted laminated aluminum sheath was so small as 1/1000 than from conventional one.

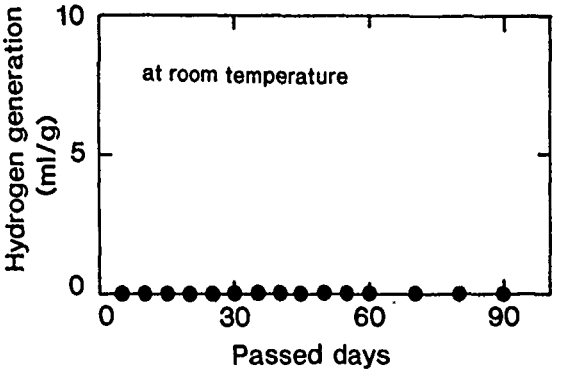

Fig.4 Hydrogen generation in muddy water.

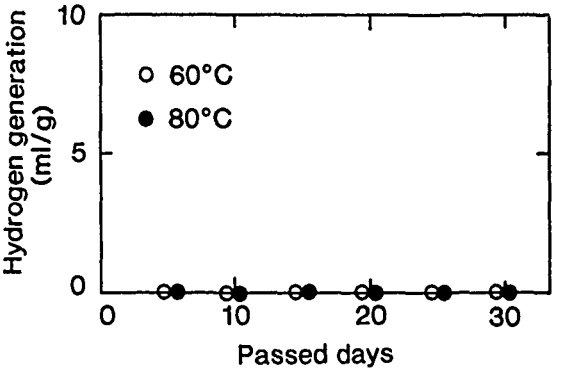

Fig.5 Hydorogen generation at high temperature.

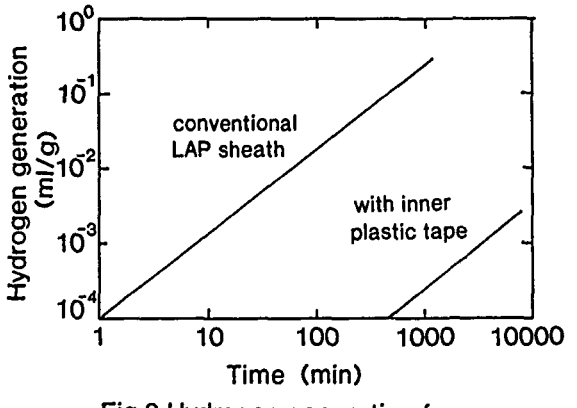

Fig.6 Hydrogen generation from sheath material.

4.Cable properties

(1) Loss change and residual strain in cable manufacturing process

The losses and strains through cable manufacturing is shown in Fig.7 and Fig.8. The loss change and standard deviation were 0.01dB/km and less than 0.01dB/km at 1.55um wavelength. Strains were measured by phase shift method. Maximum strain at manufacturing process and residual one were 0.015% and 0.01%, respectively. This means that the strain on fibers is negligibly small from the view point of life time.

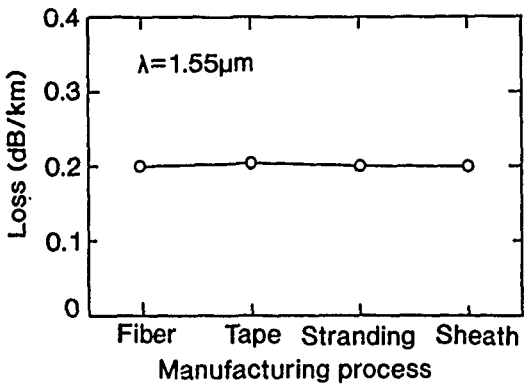

Fig.7 Optical losses in manufacturing process.

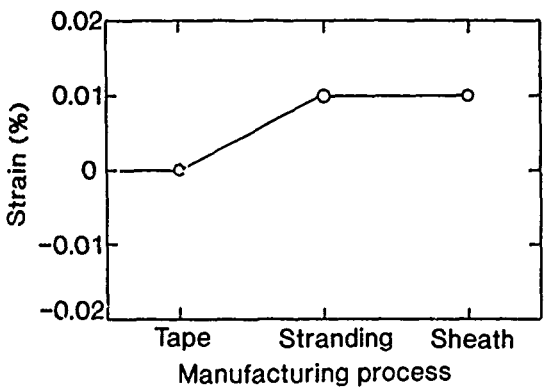

Fig.8 Strains in manufacturing process.

(2) Mechanical properties of newly developed cable

Table 2 shows the mechanical properties of newly developed cable. This cable was designed that the allowable tensile load and minimum bending radius were 800kgf and 240mm, respectively. The 800kgf of tensile load is corespondent to 0.2% of fiber elongation. This value insure that the 10 Fits/fiber*100km of fiber failure rate.

Table 2. Mechnical properties of 1000-fiber water proof cable.

Item	Condition	Result
Crush	Up to 250kgf/50mm of lateral force	<0.01dB
Bending	R=400mm,180deg. 10 times	<0.01dB
Tensile	Up to 800kgf,l=100m	<0.01dB
Squeezing	R=600mm,T=800kgf l=100m	<0.01dB
Impact	1kgf,1m height	<0.01dB
Torsion	360deg./m	<0.01dB

(3) Temperature characteristics

Three kinds of temperature tests were performed. They were cyclic test, frozen test and high temperature test of water penetrated cable. Added loss due to cyclic temperature change from -40C to 70C per day was measured. Fig. 9 shows the result. Added loss was so small as 0.02dB/km at -40C and 0.05dB/km at 60C in 1.55um wavelength. Low temperature test was performed to investigate the effect of frozen water in the cable. Test cable was 10m long and filled with water. Added loss due to the temperature change from -20C to 20C was 0.03dB/10m. This result shows that the transmission characteristics will not be disturbed by frozen water, because the transmission line is generally more than several km and the water penetration into the cable is less than 10m. To investigate the effect of the generated hydrogen in the cable at the water penetrated into the cable, spectral loss changes in the 1000m long cable were measured. Fig.10 shows the result. No added loss due to hydrogen generation was observed for six months at 60C.

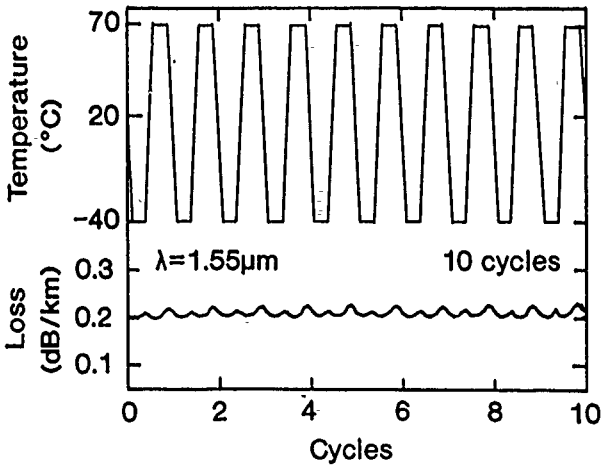

Fig.9 Cyclic temperature test.

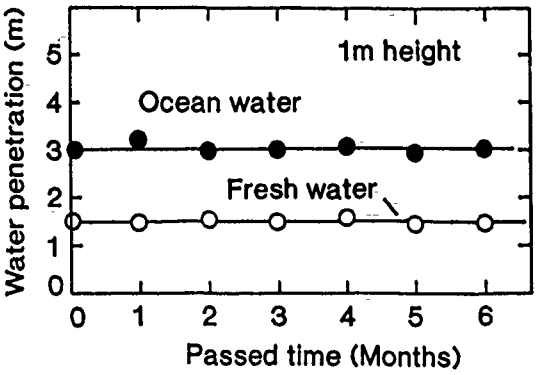

Fig.11 Water penetration length.

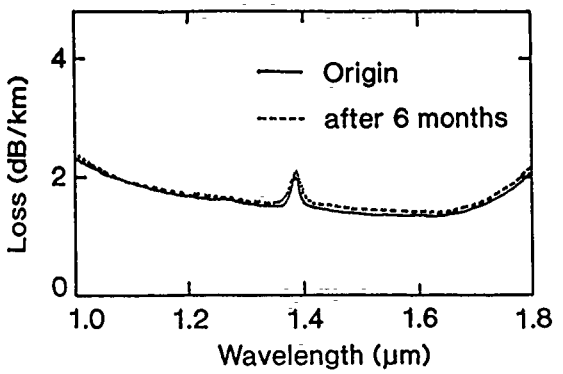

Fig.10 Effect of Hydrogen generated in cable.

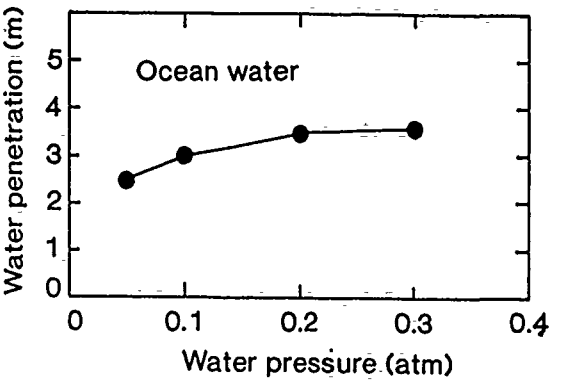

Fig.12 Pressure dependence of penetration length.

(4) Water blocking properties

Water blocking properties of dry type cable are affected by water nature, water pressure and temperature, because the water swellable powder activities depend on the above conditions. Fig.11 shows the water penetration length. Water penetration length of fresh water and ocean water were 1.5m and 3.0m, respectively. The penetration length did not elongate after six months. The relation between water penetration length and the water pressure is shown in Fig.12. Under 0.3 atm of water pressure, the water penetration length was 3.4m. The pressure dependence of water penetration length was very small. Temperature dependence of water penetration length is shown in Fig. 13. At 60C, the penetration length was 3.2m, temperature dependence of water penetration length was scarcely observed.

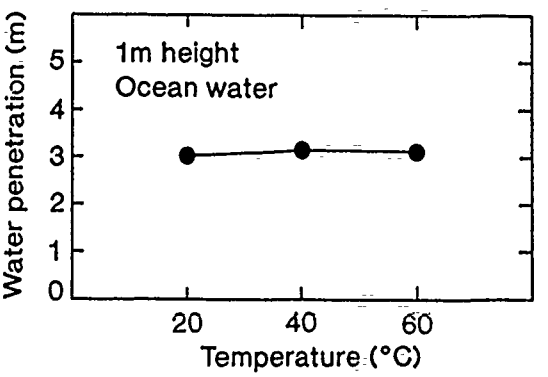

Fig.13 Temperature dependence of water penetration length.

(5) Field test

A newly developed water proof cable was installed in 300m long duct to investigate the long term reliability. Fig.14 shows the loss histogram of installed cable. Average and maximum losses were 0.21dB/km and 0.25dB/km at 1.55um wavelength respectively. This results shows that the cable has sufficient strength to protect fibers from the force caused in installation. Optical loss change of the installed cable has been measured for eight months. Result is shown in Fig.15. The evaluated fiber length was 12km long and loss change was less than 0.05dB/km. This loss change is acceptable for practical transmission system.

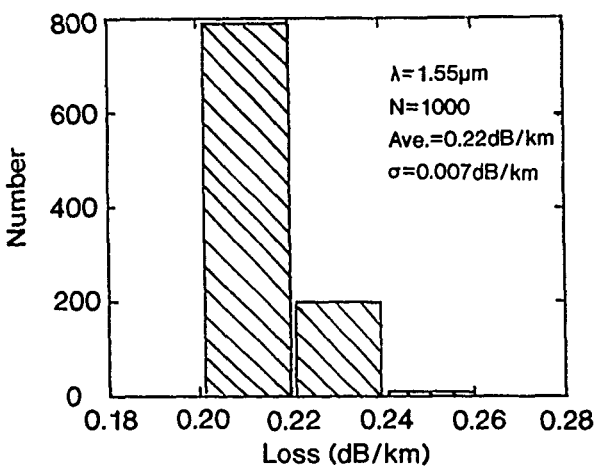

Fig.14 Loss histogram of installed cable.

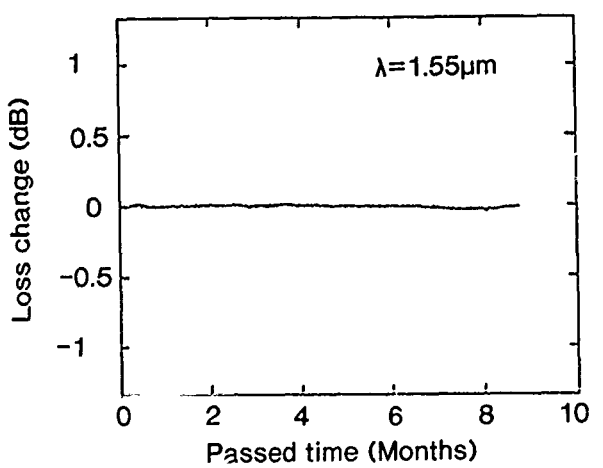

Fig.15 Loss change of 12 km long installed cable.

5. Conclusion

One thousand fiber water proof cable with slotted cores has been successfully developed by using water swellable materials such as water swellable tape and yarn. The water swellable materials were designed to be accommodated to not only fresh water but also ocean water, and the cable using them was composed of eight fiber ribbons assembled with eight fiber connectors to shear splicing time at system construction. This cable and water swellable materials were subjected to several mechanical and long term reliability tests and it was verified that the newly developed water proof cable has enough performance for practical use.

Acknowledgment

Authors express their sincere appreciation to Dr. Inada for his helpful discussions and suggestions.

References

[1] M.Kawase, T.Fuchigami, T.Haibara, S.Nagasawa and S.Takashima, "Loop-Network configuration for subscriber loops and single-mode optical fiber cable technologies suitable for mid-span access", 37th IWCS 1988.

[2] H.Sawano, Y.Kikuchi, k.Kobayashi, N.Okada, N.Misono, H.Suzuki and N.Sato, "One-thousand-fiber cable composed of eight fiber ribbons", 38th IWCS 1989.

[3] Y.Kato, A.Ishikura, T.Sano and S.Takashima, "Single-mode optical fiber ribbon splicer", 36th IWCS 1987.

[4] T.Haibara, S.Nagasawa, M.Matsumoto and M.Kawase, "Single-mode multi fiber jointing techniques for high-density high-count subscriber cables", 37th IWCS 1988.

[5] S.Kukita, T.Nakai, A.Hayashi and H.Koga, "A new nonmetallic and waterproof optical fiber cable with absorbent polymer ribbon", 36th IWCS 1987.

[6] S.Tomita, M.Iwasaki and F.Ashiya, "Water blocking cable includes 1000 fiber-cores", Spring national convention record, IEICEJ 1990

Yoshio KIKUCHI

Fujikura Ltd.

1440 Mutsuzaki
Sakura, Chiba, 285,
Japan

Mr. KIKUCHI was born in 1950. He joined Fujikura Ltd. after his graduation from Tohoku University with a M.E. degree in 1980 and has been engaged in research and development of optical fibers and optical cables. He is now a chief of Telecommunication Cable Section and a member of IEICE of Japan.

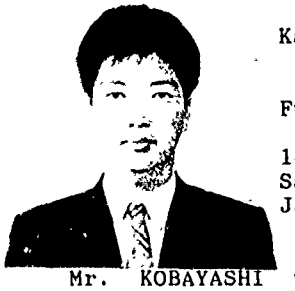

Kazunaga KOBAYASHI

Fujikura Ltd.

1440 Mutsuzaki
Sakura, Chiba, 285
Japan

Mr. KOBAYASHI was born in 1961. He joined Fujikura Ltd. after graduation from Gumma University with a M.E. in 1985 and engaged in research and development of optical fiber coatings. He is now an engineer of Telecommunication Cable Material Section and a member of IEICE of Japan.

Hiroyuki SAWANO

Fujikura Ltd.

1440 Mutsuzaki
Sakura, Chiba, 285
Japan

Mr. SAWANO was born in 1955. He joined Fujikura Ltd. after his graduation from Hokkaido University with a M.S. degree in 1983 and has been engaged in research and development of optical cables. He is now an engineer of Telecommunication Cable Section and a member of IEICE of Japan.

Keisuke OKAMURA

Fujikura Ltd.

1-5-1 Kiba,
Koto-ku, Tokyo, 135,
Japan

Mr. OKAMURA was born in 1958. He joined Fujikura Ltd. after graduation from Tokyo Metropolitan University with a B.E. degree in 1983 and has been in the development and design of optical fiber cables and these systems. He is now an engineer of Network Engineering Section in Telecommunication Division.

Yoshiyuki SATO

Fujikura Ltd.

1440 Mutsuzaki
Sakura, Chiba, 285
Japan

Mr. SATO was born in 1963. He joined Fujikura Ltd. after his graduation from Tohoku University with a M.E. in 1987 and has been engaged in research and development of optical cables. He is now an engineer of Telecommunication Cable Section and a member of IEICE of Japan.

Hideo SUZUKI

Fujikura Ltd.

1440 Mutsuzaki
Sakura, Chiba, 285
Japan

Mr. SUZUKI was born in 1948. He joined Fujikura Ltd. after graduation from Gumma University with a B.E. in 1971 and has been engaged in research and development of telecommunication materials. He is now the manager of Telecommunication Cable Section and a member of IEICE of Japan.

Nobuyasu SATO

Fujikura Ltd.

1440 Mutsuzaki
Sakura, Chiba, 285
Japan

Mr. SATO was born in 1943. He joined Fujikura Ltd. after graduation from Tohoku University with a B.E. in 1966 and has been engaged in research and development of transmission cables. He is now the manager of Transmission Line Department and a member of IEICE of Japan.

ACIDITY AND CORROSIVITY MEASUREMENTS OF FIRE EFFLUENT

by

M.-F. Bottin

Northern Telecom Canada Limited
Communication Cable Division

ABSTRACT

The intent of this paper is to compare data from a conventional pH and conductivity test, similar to the IEC procedure, with data obtained from the CNET designed equipment, which uses the resistance of model printed circuit boards to evaluate the corrosivity of fire effluents.

We used an acid gas evolution test in which the combustion parameters, i.e., time and temperature were varied. In the CNET chamber the relative humidity was varied. The change of resistance has also been measured after the printed circuit board was removed from the fire gases in order to assess longer time corrosive impact. The surfaces of corroded printed circuit boards are illustrated with SEM pictures.

It is demonstrated that a direct measure, such as the CNET, is an appropriate method to present corrosivity data and its impact on electronic equipment exposed to fire effluents, for a broad range of materials.

INTRODUCTION

There are many recorded incidents where the smoke generated during a fire have caused severe damage in locations away from the actual fire source. The damage has been particularly catastrophic for sensitive electronic equipment.

The fire gases are usually acidic and, for this reason, the majority of the work within the cable industry has been to develop test methods to determine the acidity of gases from burning polymers. In these tests a sample of the material is burned and the gaseous effluent is trapped in water. The aqueous solution is then analyzed for pH, conductivity or percent halogen.

More recently, a test method has been developed by Centre National d'Etudes et de Telecommunications (CNET) in France to more directly compare the impact of fire gases on electrical equipment. The polymer is burned under controlled humidity in a closed chamber. A printed circuit board, mounted in the chamber and maintained at a temperature lower than the chamber, is used as the corrosion target. The change of resistance of the copper tracks is used as the corrosion measure.

For any test to be of practical value to both manufacturers and users, it would be preferable that it be capable of ranking materials.

The results of a comparative study between the acidity method and the CNET method using materials typical from the cable industry are presented in this paper. The use of the CNET method has been extended to include the effect of continued corrosion of the printed circuit board after it has been removed from the test chamber and stored under atmospheric conditions. Visual observations are also included.

MATERIAL SELECTED

So that the two test methods could be evaluated, eight typical cables materials were selected as follows:

* NH : a typical flame retarded non-halogenated compound.
* BR : a flame retarded compound, containing decabromodiphenyloxide
* C1 : a low Hydrogen Chloride content Polyvinylchloride (PVC) compound
* C2 : a typical "CMP" type chlorinated compound
* C3 : a medium filled "CMR" type PVC compound
* C4 : a highly filled "CMR" type PVC compound
* F1 : a Fluoroethylenepropylene (FEP) compound
* F2 : a Polyvinyldifluoride (PVDF) compound

Throughout this article, this coding will be used when referring to materials.

Note: CMR and CMP denote categories of flame retardancy tested to UL 1666 and UL 910 respectively.

ACID GAS ANALYSIS

PRINCIPLE

It is known that the acid gases evolved when cable insulating and jacketing polymeric materials are burned, have been a cause of extensive damage to electrical and electronic equipment. As a result, methods were developed to measure the amount of acid gas evolved when these materials are burned.

Several tests exist based on the same principle using the equipment shown schematically in figure 1. A precisely weighed mass of sample is burned under controlled conditions. The temperature of the furnace and the burning time are chosen to be representative of a real fire scenario. The smoke from the decomposition is swept away and trapped in wash bottles. The resulting aqueous solution is then either analyzed chemically by titration or measured for pH and conductivity.

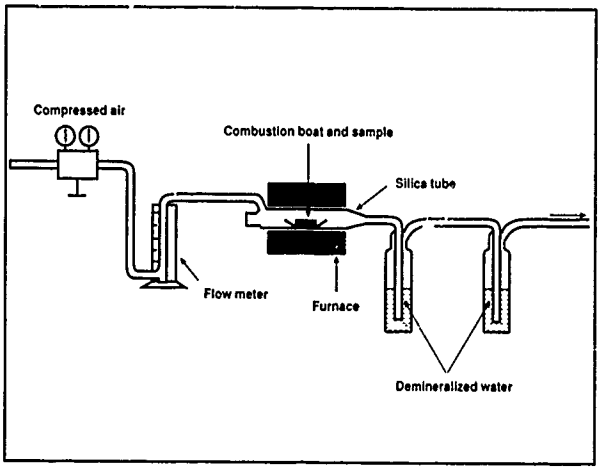

Fig. 1: Acid Gas Test Apparatus

OPERATING CONDITIONS

For the purpose of this study, two methods were reviewed: these are the International Electrotechnical Commission test "Test on Gases Evolved during Combustion of Electronic Cable Components"[1] and the Canadian Standards Association test "Test to Determine Acid Gases Evolution Test".[2] The basic differences of the two methods are illustrated in table 1:

	IEC	CSA
tube diameter	32-45 mm	approx. 25 mm
ventilation	15-30 l/h	6 l/h
sample weight	1000 mg	500 mg
combustion time	30 min	10 min
temperature	950 °C	800 °C
measurement	pH/ conductivity	titration

Table 1 : Comparison of IEC and CS A Test Parameters

The IEC test is aimed at differentiating halogenated materials from non-halogenated materials. Through experimentation, we observed that most chlorinated compounds had pH values in the 2 to 3 range which made it difficult to distinguish between these materials.

In the CSA test, the titration process is suitable for chlorinated materials, but the test is still being evaluated for other halogenated materials.

These constraints limited our attempts to rank a broader range of halogenated materials. Consequently, we needed to modify the test procedures so the test would be more sensitive to materials' differences.

After experimentation, we selected the IEC test as the basic test but reduced the weight from 1000 mg to 200 mg. Even then, we found that the pH value did not give a sufficient range of values to segregate medium and high levels of halogen. For this reason, we used conductivity as the preferred critical unit of measure. Conductivity will vary with the degree of the materials' decomposition because it is dependent on the amount of acidic species liberated during the combustion.

We did however verify that the concentration of acidic ions [H+] obtained by titration, provided the same ranking order as the order obtained from conductivity values, wherever it was possible to do the testing.

Additionally, the testing was done at three temperatures 600, 800 and 950 °C, with two combustion times 10 and 30 min. All of these have previously been proposed as test conditions. This test is referred to as the "acidity test" for the rest of the article.

RESULTS

REPRODUCIBILITY

All the materials tested had good reproducibility, in the range of 10 %, except for fluoropolymers where the results were found not reproducible. In some of these cases, an accumulation of a fine white aggregate was noticed at the end of the bubbling tubes. It was analyzed and found to be a fluorosilicate. This suggests that the equipment is not adequate for all types of fluoropolymers, because the evolved fluorine attacks the glass surfaces of the apparatus. Therefore we do not show any results for fluoropolymers from the acidity test in this article .

THE ROLE OF TEMPERATURE AND COMBUSTION TIME

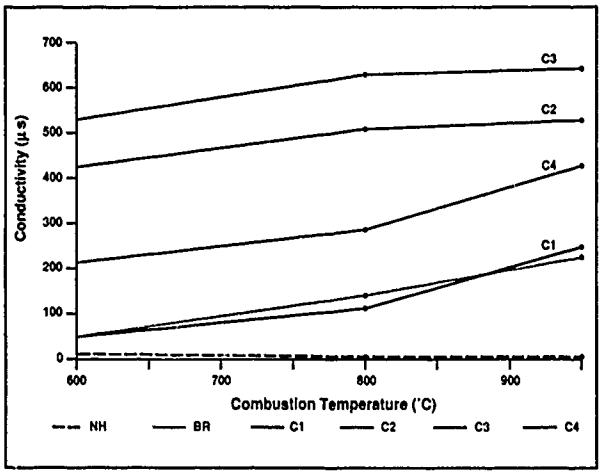

Fig. 2: Conductivity as a Function of Temperature

	conductivity (μS)	
	10 min	30 min
NH	7	5
BR	175	160
C1	105	111
C3	570	625
C4	300	280
C2	432	510

Table 2: Conductivity as a Function of Combustion Time

Figure 2 shows the variation of conductivity as a function of furnace temperature, the combustion time being 30 min. Table 2 shows the effect of combustion time on conductivity, the furnace temperature being 800 °C. Data are given in micro Siemens (μ S). These data demonstrate that the degradation of materials is not complete at 600 °C and that, in some cases, even further degradation takes place when going from 800 °C to 950 °C. In most cases increasing the time of combustion does not lead to further degradation of the materials.

In summary, we have shown:

1) the test is capable of ranking materials by amount of acid gas liberated in the selected conditions, independent of the type of halogen . Nevertheless, in its present form, it cannot be used for fluoropolymers; therefore it is not suitable for a complete materials' ranking.

2) the combustion conditions are extremely important: 800 °C does not always guarantee a complete decomposition, although the ranking stays the same for the three temperature conditions.

CORROSIVITY MEASUREMENT

PRINCIPLE

The basic principle of the method was developed at Centre National d'Etudes de Telecommunications (CNET). The test method is now a standard of France Telecom[3] and a round-robin is being organised by ISO/TC 61/SC4/WG2 to evaluate the test's suitability as an international standard.

It reproduces the natural phenomenon in a fire in which condensation of hot humid smoke occurs on surfaces whose temperature is equal or less than the dew point of the smoke.

The test consists of burning a predetermined quantity of the material in a leak tight test chamber, at a constant temperature and defined relative humidity. The combustion products condense out on the corrosion target which is a small printed circuit board kept at a constant temperature lower than the dew point of smoke. The change of its resistance is used as the measure of corrosion.

TEST APPARATUS

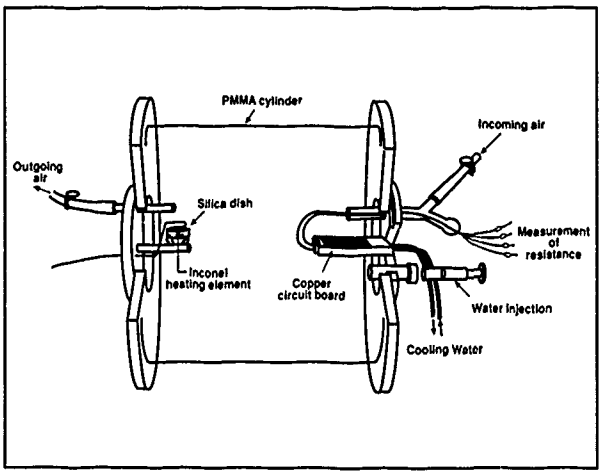

Fig. 3: CNET Corrosivity Test Apparatus

The CNET equipment (see fig. 3) consist of a PMMA (polymethylmethacrylate) cylinder approximately 20 dm^3. Flanges at each end of the cylinder seal the chamber against both heat and gas loss. Inside the chamber, which is regulated at 50 °C, is a corrosion resistant heating element used to burn the test sample. This heating element is capable of temperatures greater than 800 °C. The corrosion target is a 3 x 6 cm printed circuit board with

copper tracks 130 000 Å thick and a resistance of approximately 8 ohms. During the experiment, the printed circuit board is maintained at 40 °C by a water bath circulating underneath.

At the start of the test, the sample to be evaluated is placed on the heating element, the printed circuit board is mounted in the chamber and the flanges sealed. The chamber is conditioned and dried by air flow. The air flow is stopped and a quantity of water is injected in the chamber to give the desired humidity. After the chamber has been allowed to stabilise, the material sample is burned for 2 min 30 at a combustion temperature of 800 °C. The corrosion is allowed to take place for an hour after the combustion and the resistance of the printed circuit board is monitored during the hour. The time taken for each test is 3 to 4 hours depending on the relative humidity selected. It includes the cleaning of the chamber after each test.

CALCULATIONS OF THE CORROSIVITY FACTOR "COR"

The resistance values used are R_i, the initial value measured immediately after the 2 min 30 sec sample ignition and R_f the final value measured one hour after the ignition. The corrosivity can be expressed as the following ratio:

$$\frac{R_f - R_i}{R_i}$$

So that data can be compared, the corrosion is referred back to a "standard board" of 8 ohms resistance at 40 °C using the expression:

$$COR = \frac{1}{\frac{R_i \cdot R_f}{8[R_f - R_i]} - 1}$$

The derivation of COR is detailed in appendix 1.

The COR value will be given in percentage throughout the text.

REPRODUCIBILITY

The measured values of COR, the average values and the standard deviation are shown in table 3:

materials	COR (%)	average and standard deviation (%)
material 1	0.98 0.84 1.34 0.6 1.08	0.97 ± 0.25
material 2	12.23 10.04 10.12	10.79 ± 1.24
material 3	19.33 28.86 25.75 25.58	24.88 ± 3.46

Table 3: The Reproducibility of Corrosivity Factors

These values illustrate the typical standard deviation obtained. The very low values of COR, around 1 %, would indicate that the corrosion attack is small enough to be negligible. At high corrosion levels of COR greater than 30 % (not shown in table 3), the standard deviation was generally found greater. At this level, the copper is already badly damaged and it is difficult to quantify a corrosion percentage with the same precision. This severe attack is depicted in the SEM pictures in a later section.

THE ROLE OF HUMIDITY

The CNET procedure calls for test conditions which produce condensation on the target probe. Because of the chemical nature of the corrosivity, the initial humidity plays an important role in the copper attack. To study this impact we selected three relative humidity (RH) conditions by injecting different quantities of water into the chamber. The relative humidities were measured with a humidity gauge. The corresponding dew point for each of the three conditions was calculated from the Clausius-Clapeyron Equation applied to pure water.

The selected conditions are the following:

condition 1:
one injection, which developed 33 % RH in the chamber. From the Clausius-Clapeyron Equation, the dew point is 29 °C; because the surface of the printed circuit board is at 40 °C, no condensation is expected.

condition 2:
two injections separated each by a period of 20 min to allow complete water evaporation. The resulting RH was 52% and the dew point 37 °C; again no condensation is expected.

condition 3:
three injections separated each by a period of 20 min. The resulting RH was 70 % and the dew point 43°C; for this condition, condensation is expected.

The results for NH, BR, C1, C2, C3, F1, F2 are shown in figure 4:

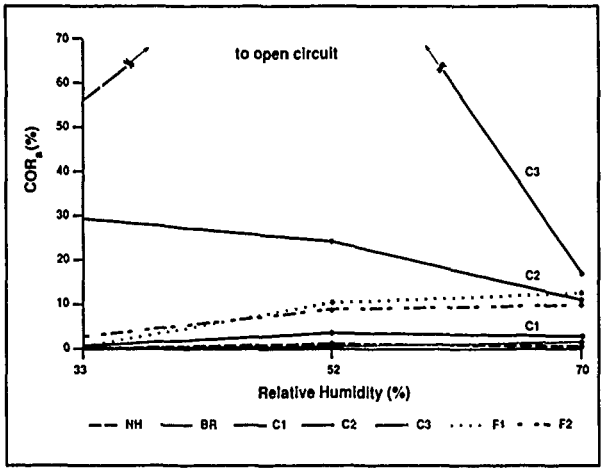

Fig. 4: Corrosivity as a Function of Humidity

For all cases where the corrosivity factor is not negligible it has been influenced by the relative humidity: in most cases, the corrosion is increased by the humidity at the surface of the printed circuit board. It is also noticeable that even in a relatively dry environment (33 % RH), corrosion takes place and for some compounds, it is significantly high .

All the materials do not show the same behaviour, the chlorinated compounds in particular being distinctive. For C3, we observed an open circuit at the medium relative humidity (52%). In this case, we have noticed condensation although it was not expected. One explanation of this could be that the combustion of chlorinated materials liberates hydrogen chloride whose affinity to water is great; it is extremly soluble in water where it ionizes to give acid solutions. Therefore, the presence of HCl in the humid air inside the test chamber provokes the condensation of acid solutions on the printed circuit board, earlier than in pure water vapor. However, condition 3 (70%) also produces condensation but the quantity of water is in large amount at the printed circuit board surface, and a dilution of the corrosive acid species may decrease their damaging effect.

In this test, as in the acidity test, the role of combustion temperature may also be of importance and this parameter is planned to be studied in a future set of experiments.

In summary, we have demonstrated that the test can be used to differentiate the corrosivness of many types of materials. Different PVC compounds were found to have corrosion factors varying from very high to very low values. Fluoropolymers can be handled without the hardware constraints encountered in the acidity test. Also, we know that some other types of corrosive materials such as polysulfones have been evaluated in the CNET labs.

In a real fire situation, humidity is present and we have determined with this test, that the humidity conditions have a critical impact on the damage to the electronic equipment. Therefore it is necessary to control the relative humidity in any kind of materials selection test.

VISUAL OBSERVATIONS

Fig. 5: SEM Pictures

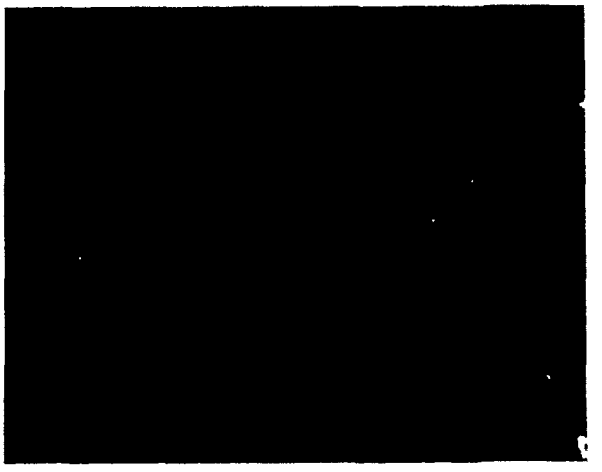

NH

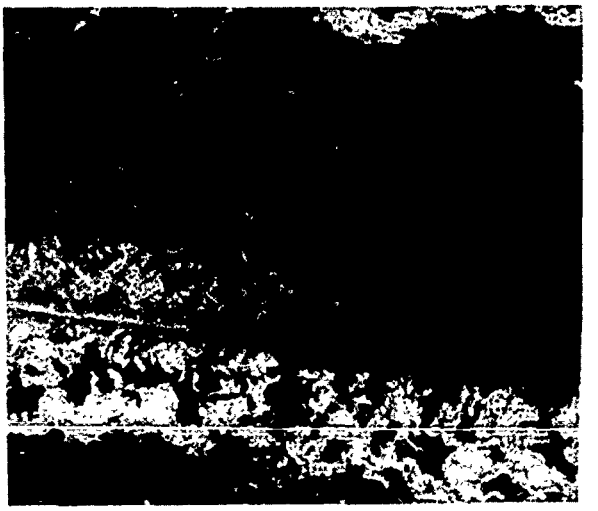

BR

C3

F1

These pictures (fig. 5) represent the surface of copper tracks, taken with a Scanning Electron Microscope, at a magnification in the range of 100. They illustrate different aspects of structural alteration at the copper surface of printed circuit boards as a result of their exposure to corrosive smoke. It appears that the copper tracks have been less affected by non-halogenated and brominated materials.

LONG TERM AGING

If a fire occurs, parts of the electrotechnical equipment may remain affected by deposited fire effluent, after the fire has been extinguished but before any corrective action can take place. For this reason, a study of the dependency of the corrosivity factor with time was undertaken.

After the one hour corrosivity measurement, the samples were removed from the chamber, allowed to cool down in a desiccator and then kept for up to 28 days at room temperature either in a desiccator or at 50% RH. The resistance was periodically measured and a corrosivity factor due to aging (COR_a) was calculated using as a final resistance each of the "aged" resistance measured and as the initial resistance the value of Rf, previously measured. This corrosivity factor (COR_a) expresses the degree of further corrosion of the sample after its removal from the fire effluent.

The results are shown in figures 6 and 7 .

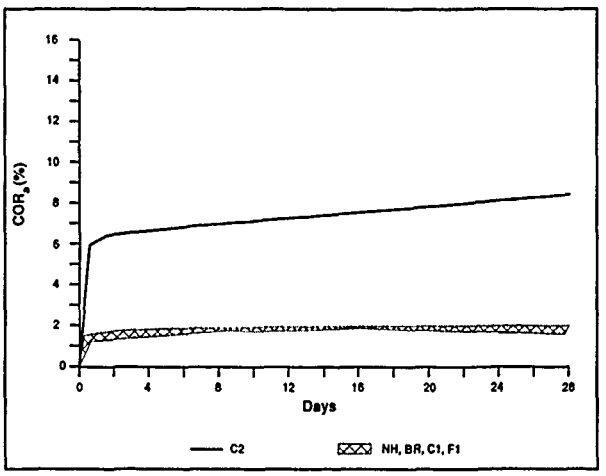

Fig. 6: Corrosivity after Aging - at low Humidity

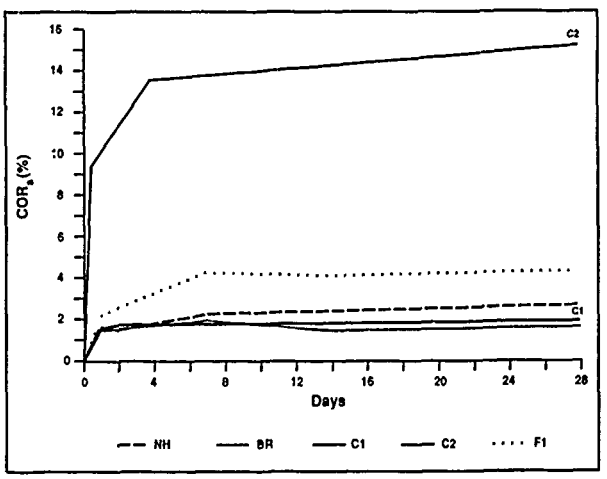

Fig. 7: Corrosivity after Aging - At High Humidity

The measurements reported herein are those taken from printed circuit boards tested in condition 2. From these two graphs, we observe:

1) The major part of aging occurs in the first hours following the combustion. In reality it implies that in order to stop further damage due to corrosion, it is necessary to react fast.

2) The degree of sensitivity to aging either in a dry or humid atmosphere varies with materials. The worst cases are some PVC compounds where medium to high levels of chlorinated effluents are released. Copper printed circuit boards will generally degrade on aging to a greater extent after their exposure to chlorinated fire effluents than to other types of halogenated effluents.

3) Except for the non-halogenated sample and the brominated one, the aging is more pronounced in the humid atmosphere. It indicates that keeping the exposed electrical and electronic parts in a very dry atmosphere may inhibit further copper degradation.

COMPARISON OF DATA FROM THE TEST METHODS

So that a comparison of the two tests methods could be made, we have included in table 4 data from the acidity test and data from the CNET test taken at 800 °C. For the acidity test, the data selected are at 10 min so they correspond closer to the CNET conditions. The values for the CNET test correspond to 50% RH.

material	conductivity(μS)	COR (%)
NH	15	1.2
BR	175	0.9
C1	105	3.6
C2	420	24.5
C3	570	70
F1	*	10.8
F2	*	9.02

Table 4: Comparison of Conductivity with Corrosivity

In both methods, the ranking is the same within the group of chlorinated compounds. Nevertheless, the ranking is dependent on the method used when comparing two different types of halogenated materials. The brominated compound BR was shown more acid than the C1 in the acidity test but it is actually no more corrosive than a non-halogenated sample in the CNET test. Indeed the acidity measurement does not take into account the nature of the acid species produced during the combustion. It is therefore suggested that it is more correct to call for "non-corrosive cables" rather than "non-halogenated cables" when specifying cables to be used in sensitive locations.

CONCLUSION

The CNET test has the ability to measure corrosivity factors for all halogenated materials. In addition, some other pertinent information can be obtained such as the effect of ambient humidity, visual observations of the damage and continued aging of the corroded printed circuit boards. Furthermore, experiments can be planned with metals other than copper as targets, and by using techniques of surface analysis which would provide a better materials understanding. In comparison, the acidity test has limitations because it is unsuitable for fluoropolymers and, in the case of other polymers, the acidity has not been found sufficient to predict the corrosiveness of materials in a real fire situation. Therefore, a tool such as the CNET corrosivity test is required to satisfy the industry's need for selecting materials based on a realistic estimation of their corrosivity when they burn and for predicting the damaging effect to electronic parts of equipment.

It has also been shown that chlorinated compounds can have corrosivity from extremely severe to almost benign depending on their formulation. The most corrosive chlorinated compounds are the typical PVC formulations used presently for CMR application; however, by selective formulation, it seems that the level of their corrosivness can be reduced to levels closer to non-halogenated compounds. Finally the corrosive damage caused by materials whose flame retardant is decabromodiphenyloxide is expected to be negligible.

ACKNOWLEDGEMENTS

The author would like to thank the Centre National d'Etudes et de Telecommunications in Lannion for loaning one of their corrosivity chambers to Northern Telecom and for agreeing to this publication. We thank, in particular, Mr Pierre Rio from CNET for supplying various technical information. Sincere appreciation is expressed to Mr Eric Gouldson who gave numerous advice throughout this work. Thanks are also extended to Mr. Claude Talbot and Mr. Michel Lussier for their assistance with the experiments and to Dr. J. Cornibert and Dr. Ph.Guerin who participated in our discussions.

REFERENCES

1) IEC publication 754-2, "Test on gases evolved during combustion of electronic cable components".

2) CSA No 22.2 No. 0.3-M1985-sec 4.31, "Test to Determine Acid Gases Evolution Test".

3) Recommandation et directive d'emploi des matieres plastiques par rapport a leur comportement au feu ou a la chaleur, dec 26-0611, Ed 3, France Telecom.

APPENDIX 1

CORROSIVITY MEASURE REFERRED BACK TO A STANDARD BOARD OF 8 ohms AT 40°C
(Calculation originally supplied by CNET)

Each copper track on the printed circuit board can be represented by:

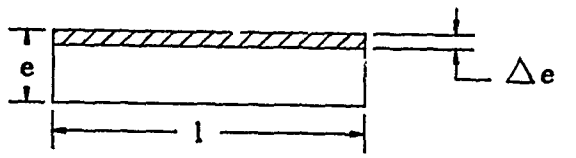

with l = copper width
e = copper thickness
Δe = copper thickness lost by corrosion
L = total length of tracks on the printed circuit board.

The printed circuit board resistance is

$$R = \rho \frac{L}{l \times e}$$

for all tracks, $\rho \frac{L}{e}$ is the same: K

$$R = \frac{K}{e}$$

Consider two circuits whose initial values at 40°C are R_{1i} and R_{2i} and final values R_{1f} and R_{2f}.

For our purpose, R_{2i} and R_{2f} will be experimental values and R_{1i} and R_{1f} referred back to the standard 8Ω board.

$$R_{1i} = \frac{K}{e_1}; \quad R_{2i} = \frac{K}{e_2}$$

The two circuits are affected by the same corrosion, therefore, the thickness variation is the same Δe.

Values for the final resistances are:

$$R_{1f} = \frac{K}{e_1 - \Delta e}; \quad R_{2f} = \frac{K}{e_2 - \Delta e}$$

We thus obtain:

$$e_1 = \frac{K}{R_{1i}}; \quad e_2 = \frac{K}{R_{2i}}$$

$$e_1 - \Delta e = \frac{K}{R_{1f}}; \quad e_2 - \Delta e = \frac{K}{R_{2f}}$$

$$\Delta e = e_1 - \frac{K}{R_{1f}} = e_2 - \frac{K}{R_{2f}}$$

$$\frac{1}{R_{1i}} - \frac{1}{R_{1f}} = \frac{1}{R_{2i}} - \frac{1}{R_{2f}}$$

Given $R_{1i} = 8\Omega$, we obtain:

$$R_{1f} = \frac{8 R_{2i} R_{2f}}{R_{2i} R_{2f} - 8(R_{2f} - R_{2i})}$$

The value of COR for a printed circuit board of 8Ω resistance affected by a thickness variation Δe is:

$$COR = \frac{R_{1f} - 8}{8}$$

Using equation (1) we obtain:

$$COR = \frac{R_{2i} R_{2f}}{R_{2i} R_{2f} - 8(R_{2f} - R_{2i})} - 1$$

$$= \frac{R_{2i} R_{2f} - R_{2i} R_{2f} + 8 (R_{2f} - R_{2i})}{R_{2i} R_{2f} - 8 (R_{2f} - R_{2i})}$$

$$COR = \frac{1}{\frac{R_{2i} R_{2f}}{8 (R_{2f} - R_{2i})} - 1}$$

We will use this value multiplied by 100 to obtain a percentage.

Marie-Francoise Bottin received her Engineering Degree from the Institut National des Sciences Appliquées in 1977 and her Docteur-Ingénieur Diploma from the Université Claude Bernard in 1979 in Lyon, France. She joined Northern Telecom Canada Limited Communication Cable Division's Research and Development department in 1981, where she is responsible for materials development and corrosivity analysis.

The Performance of Optical Fibers in Nuclear Radiation Environments

Marcus W. Shute, Sr.

AT&T Bell Laboratories
Norcross, Georgia 30071

Michael M. Michie

AT&T Network Systems
Norcross, Georgia 30071

John R. Duncan

CDI Corporation
Atlanta, Georgia 30346

Jeffrey A. Krinsky

Boeing Aerospace and Electronics
Seattle, Washington 98124

ABSTRACT

The radiation performance of several fiber designs including single mode, dispersion-shifted, tethered vehicle fiber designs, radiation-hardened multimode, and standard multimode fiber designs was evaluated over a temperature range from -46°C to 71°C in a steady state radiation environment. The performance of a dispersion-shifted, single node fiber design and a 50 μm radiation-hardended multimode fiber was also evaluated during and after exposure to a transient (high dose rate) radiation pulse at temperatures from -46°C to 71°C. The radiation response of the 50 μm radiation-hardened fiber was evaluated during and after exposure to a neutron radiation pulse at -46°C, 25°C, and 71°C. All fiber designs considered in this work, with the exception of the standard multimode fiber designs, exhibited significant recovery after exposure to these nuclear radiation environments.

1. INTRODUCTION

As tactical applications of fiber optic systems increase, the nuclear survivability of these systems becomes increasingly important. Usually, the optical fiber is the most susceptible component of the system to nuclear radiation; therefore, the radiation response of the fiber is critical to the reliability and the ultimate performance of the system.

The radiation performance of several Ge-doped silica core fiber designs including single mode, dispersion-shifted, a tethered vehicle fiber design, radiation-hardened multimode, and standard multimode fiber designs is evaluated over a temperature range from -46°C to 71°C in a steady state radiation environment. The performance of a dispersion-shifted fiber design and a 50 μm radiation-hardened multimode fiber is also evaluated during and after exposure to a transient (high dose rate) radiation pulse at temperatures from -46°C to 71°C. The radiation response of the 50 μm radiation-hardened fiber is evaluated during and after exposure to a neutron radiation pulse at -46°C, 25°C, and 71°C. Also, preliminary results on the effect of draw speed and germanium concentration are presented.

2. FIBER DESIGNS EVALUATED

The radiation performance of several optical fiber designs was evaluated. Both standard and radiation-hardened (RH) 50 μm, 62.5 μm, and 100/140 μm Ge-doped silica core, graded index, multimode fibers were tested. Table I summarizes some of the fiber parameters for the multimode fiber designs evaluated in this work. Several Ge-doped silica core, single mode fibers were also evaluated. The depressed-clad, step index, single mode fiber, the AccuTether 100 fiber (a fiber used in tethered vehicle applications derived from the standard depressed-clad, triangular index profile, dispersion-shifted fiber), and the AccuTether 200 fiber (a fiber used in tethered vehicle applications) were used in this study.[1] Some of the fiber parameters for the single mode fiber designs evaluated in this work are shown in Table II.

3. NUCLEAR RADIATION ENVIRONMENT

The nuclear radiation environment considered in this work is composed of delayed gamma radiation, prompt gamma radiation, and neutron radiation. Other effects that may be present in a nuclear radiation environment such as the shock wave, thermal radiation, and the electromagnetic pulse generated by the detonation of a nuclear device, were not considered in this work.[2]

3.1 Delayed Gamma Radiation

The delayed gamma radiation is primarily a result of weapon debris and neutron reactions with weapon materials and its surroundings. It is considered a steady state type of radiation. The dose rate depends on the yield of the weapon, ambient conditions, distance from the detonation point, etc., and can range from a few rads(Si)/s to hundreds of rads(Si)/s. The primary effect of steady state (delayed) gamma radiation in optical fibers is ionization.

Table I. Multimode Fiber Designs

Core/Cladding Dia. (μm)	50/125		62.5/125		100/140	
Type	STD	RH	STD	RH	STD	RH
Intrinsic Loss (dB/km)						
850 nm	2.52	2.60	2.99	2.94	4.41	3.47
1300 nm	0.75	0.58	0.71	0.89	1.22	0.82
Numerical Aperature	0.21	0.23	0.27	0.27	0.28	0.28
Bandwidth (MHz-km)						
850 nm	466	219	179	144	364	308
1300 nm	1177	649	472	522	266	439

Table II. Single Mode Fiber Designs

FIBER	SM	AT 100	AT 200
Intrinsic Loss (dB/km)			
1310 nm	0.36	0.42	0.48
1550 nm	0.23	0.22	0.29
Mode Field Diameter (μm)			
1310 nm	8.7	~ 6	~ 5
1550 nm	~ 10	6.7	5.8
Index of Refraction Diff., Δ (%)	0.34	0.8	1.1
λ_0 (nm)	1306	1545	~ 1325

3.2 Prompt Gamma Radiation

The prompt gamma radiation is mainly produced from the weapon and results from electronic transitions caused by high energy photons and fast neutrons. The prompt gamma radiation has a pulsed or transient nature and is referred to as transient radiation. The dose rate is much higher than the delayed gamma radiation; typically it is about 10^9 rads(Si)/s. The pulse width of the radiation is on the order of a microsecond. The primary effect of transient radiation in optical fibers is ionization.

3.3 Neutron Radiation

The neutron radiation is produced by the weapon. The effect of neutron radiation on materials is dependent on the energy and fluence of the neutrons. Neutron radiation produces ionization effects similar to gamma radiation. High energy neutrons can cause displacement effects (vacancy and interstitial defects) in the material. High neutron fluences (> 10^{19} n/cm^2) can produce radioactive materials. In tactical radiation environments, a typical neutron fluence is about 10^{12} n/cm^2 and 1 MeV equivalent energy; therefore, the primary effect is ionization.[3]

4. EXPERIMENTAL PROCEDURE AND APPARATUS

4.1 Steady State Gamma Radiation

The steady state gamma radiation response of the optical fibers was measured using the "Adverse Nuclear Environments Test Procedure" outlined in FOTP - 49 (EIA/TIA-455-49), entitled "Procedure for Measuring Gamma Irradiation Effects in Optical Fibers and Optical Cables," with some modifications. A ^{60}Co source was used as the gamma radiation source. The optical fibers were exposed to a total radiation dose of 3000 ± 100 rads (Si) and the dose rate was ~ 50 rads/s. An NIST traceable electrometer was used to measure the radiation dose rate. The total dose was obtained from the dose rate and the exposure time which was measured with a clock/timer directly calibrated from the NIST atomic clock by NIST transmitted calibration frequencies. This yields a more accurate measurement of the total radiation dose; thermoluminescent detectors (TLDs) are subject to as much as a 15% variation in thermoluminescent sensitivity which can result in a significant error in the measured radiation dose. Appropriate light launch conditions were used consistent with the type of fiber tested. The launched power was maintained below 1 μW. The radiation-induced loss in the optical fibers at 850 nm and 1300 nm for the multimode fiber designs, and 1310 nm and 1550 nm for the single mode fiber designs was monitored during exposure to the gamma radiation and recovery for at least 2000 seconds, or until there was no apparent change in the radiation-induced loss, after the radiation source was removed. The tests were performed at -46°C, 25°C, and 71°C for the multimode fiber designs, and -32 °C, 25 °C, and 63 °C for the single mode fiber designs. The length of the test sample ranged from 50m to 1 km depending on the test temperature and the degree to which the fiber was radiation-hardened. Data was collected by a Si/InGaAs photodetector, lock-in amplifier, and computer. A reference path was used via an optical splitter to monitor source stability. A schematic of the experimental apparatus is shown in Figure 1.

4.2 Transient Radiation

The 50 μm RH, multimode fiber and the AT 100 fiber were exposed to transient radiation of ~ 500 rads in a 35 ns pulse (dose rate ~ 1.4×10^{10} rads(Si)/s) using the FX-75 Flash X-ray Machine at Boeing Aerospace & Electronics, Seattle, WA. The multimode fibers were irradiated at -46°C, 25°C, and 71°C and the radiation-induced attenuation was measured at 1300 nm. The AT 100 fiber was irradiated at -32°C and the radiation-induced attenuation was measured at 1310 and 1550 nm. The

sample length was 20m. Appropriate light launch conditions were used and a reference path was used to monitor the stability of the light source. The launched power was < 4 μW. The signal was monitored using digital storage oscilloscopes from 10^{-7}s to 10^{2}s. The total integrated dose (TID) was measured using thermoluminescent diodes (TLDs). Figure 2 is a schematic of the experimental apparatus used in the transient radiation tests.

4.3 Neutron Radiation

The 50 μm RH, multimode fiber was exposed to a neutron fluence of 1×10^{12} n/cm^2, 1 MeV equivalent energy, in a pulse of < 175 μs using the Sandia National Laboratory SPR-III Pulse Reactor, Albuquerque, NM. The 60m fiber samples were irradiated at -46°C, 25°C, and 71°C and the radiation-induced loss was measured at 1300 nm. The signal was monitored using transient digitizers from 10^{-4}s to 10^{4}s. Sulfur activation and TLDs were used for dosimetry. A reference path was used to monitor the stability of the light source. The launched power was < 10 μW. The test configuration is shown in Figure 3.

5. RADIATION RESPONSE OF OPTICAL FIBERS

5.1 Mechanisms for Radiation-Induced Loss

The radiation response of optical fibers is composed of two components: darkening and recovery. Optical fibers experience darkening, or transmittance loss, after exposure to nuclear radiation. The primary mechanism for radiation-induced loss in optical fibers is absorption at the common operating wavelengths for optical fiber transmission systems, 0.85 μm, 1.3 μm, and 1.55 μm. This absorption is caused by trapped carriers, which are created by ionization from the nuclear radiation, at defect sites in the glass matrix.[4] The recovery of the fiber depends on the recombination rate of the carriers; the fiber composition, particularly the type and concentration of the dopants, has a significant impact on the radiation sensitvity of the fiber. Many other factors are also important to the radiation response of the fiber such as the dose rate, total ionizing dose, temperature, processing conditions, operating wavelength, power level of transmitted light (photobleaching effects), etc.[1] In general, the radiation response of optical fibers worsens as the ambient temperature is decreased or as the operating wavelength is decreased.

5.2 Steady State Radiation Response

5.2.1 Multimode Fiber Designs

Figures 4, 5, and 6 show the radiation response at 850 nm and 1300 nm for the standard and radiation-hardened multimode 50 μm, 62.5 μm, and 100/140 μm fiber designs, respectively, at -46°C for a 3000 rad exposure. Similar data was obtained at 25°C and 71°C. In all cases, the RH fiber designs show significant recovery after removal from the radiation field as compared to the standard multimode fiber designs. The RH fiber designs typically recovered to < 5 dB/km after 3600s at 1300 nm after a 3000 rad exposure at -46°C. The standard multimode fibers did not recover after removal from the radiation field. Figure 7 shows the effect of thermal annealing on the radiation-induced loss. The ambient temperature was increased to 25°C after it appeared that recovery of the 50 μm RH fiber from a 3000 rad, -46°C exposure ceased. The radiation-induced loss decreased dramatically during the period that the temperature was increased. This phenomena was observed for all types of fibers evaluated although the degree of recovery varied. At 1300 nm, the maximum radiation-induced loss is usually much lower for the RH fiber designs compared to the standard multimode fiber designs. However, at 850 nm, the maximum radiation-induced loss is lower for the standard fiber designs compared to the RH fiber designs. Table III shows the radiation sensitivities, which is defined as the peak radiation-induced loss divided by the total radiation dose, for the multimode fiber designs at -46°C, 25°C, and 71°C. The radiation sensitivity can be used to estimate the peak radiation-induced loss for the RH fiber designs or fiber designs that exhibit recovery after removal from the radiation field for total integrated doses < 10 krads.

5.2.2 Single Mode Fiber Designs

Figures 8, 9(a), and 9(b) are the radiation response curves for the SM, AT 100, and AT 200 fibers, respectively, at 1310 nm and 1550 nm after a -32°C, 3000 rad exposure. Similar data was obtained at 25°C and 63°C. All fibers show good recovery at both wavelengths after removal from the radiation field. Figure 8 also shows the effect of thermal annealing on the single mode fibers. The ambient temperature was increased to 25°C after it appeared that recovery stopped. The AT 100 and AT 200 fibers exhibited similar behavior. Table IV shows the radiation sensitivities for the three single mode fiber designs at -32°C, 25°C, and 63°C. Figure 10 shows the correlation between the relative index of refraction difference between the core and cladding (Δ), and the maximum radiation-induced loss and the induced loss after recovery. The AT 200 fiber exhibited the lowest radiation sensitivity at -32°C relative to the other single mode fibers evaluated, but had the highest Δ (1.1%). This contradicts the correlation between intrinsic loss and Δ. This data shows the trend, particularly at 1310 nm, that fibers with higher Δ (higher Ge concentration) have a lower sensitivity to radiation at low temperature possibly because it is more difficult to ionize carriers trapped at Ge defect sites compared to other defect sites present in the glass matrix. Also, the effect of draw conditions on the radiation response of single mode fiber designs was considered. Several single mode fibers drawn at constant temperature but diffferent draw speeds were irradiated using steady state gamma radiation to a total dose of 3000 rads(Si) at -32°C and the response was monitored at 1310 nm. Figure 11 shows the radiation-induced loss as a function of draw speed. There was not a significant effect of the draw speed on the maximum radiation-induced loss or induced loss after 4700s recovery for the range of draw speeds considered. It has been reported that other fabrication and processing conditions, such as hydrogen treatment[5] and oxygen stoichiometry,[6] may impact the radiation response and should be investigated for the fiber designs considered in this work.

Table III. RADIATION SENSITIVITIES (mdB/(km-rad)) Multimode Fiber Designs

Fiber Type	λ (μm)	Temperature (°C) -46	25	71
50 μm RH	0.85	46.3	5.3	--
	1.3	6.9	0.63	0.13
50 μm STD	0.85	≥29.8	51.2	--
	1.3	≥17.8	15.5	12.6
62.5 μm RH	0.85	35.0	3.6	--
	1.3	4.0	0.56	0.16
62.5 μm STD	0.85	≥20.5	44.0	--
	1.3	≥8.9	13.9	11.2
100/140 μm RH	0.85	47.7	5.4	--
	1.3	5.3	0.43	0.22
100/140 μm STD	0.85	≥11.6	13.8	--
	1.3	≥6.2	6.1	5.9

Table IV. RADIATION SENSITIVITIES (mdB/(km-rad)) Single Mode Fiber Designs

Fiber Type	λ (μm)	Temperature (°C) -32	25	63
SM	1.31	2.5	0.57	0.29
	1.55	1.4	0.42	--
AccuTether 100 (DSF)	1.31	2.0	0.43	0.30
	1.55	1.4	0.32	--
AccuTether 200	1.31	1.1	0.32	0.25
	1.55	0.60	0.10	--

5.3 Transient Radiation Response

The response of the 50 μm RH multimode fiber after exposure to a transient radiation pulse of about 500 rads (dose rate ~ 1.4×10^{10} rads(Si)/s) at -46°C, 25°C, and 71°C is shown in Figures 12, 13, and 14, respectively. The maximum radiation-induced loss at 1300 nm and -46°C was about 225 dB/km and recovered to < 3 dB/km 40s after removal from the field. At 25°C, the maximum radiation-induced loss at 1300 nm was about 170 dB/km and recovered to < 1 dB/km after 40s. At 71°C, the maximum radiation-induced loss at 1300 nm was about 140 dB/km and recovered to < 1 dB/km after 10s. Similar performance is expected from the other RH multimode fiber designs.

The response of the AT 100 fiber at 1310 nm and 1550 nm after exposure to transient radiation at -32°C is shown in Figure 15. The maximum radiation-induced loss was about 140 dB/km at 1310 nm and 70 dB/km at 1550 nm. After 10s recovery, the radiation-induced loss was < 1 dB/km at both wavelengths. Similar performance is expected from the other single mode fibers.

5.4 Neutron Radiation Response

The response of the 50 μm RH multimode fiber to a neutron radiation environment (1×10^{12} n/cm^2 neutron fluence in 150 μs) at -46°C, 25°C, and 71°C is shown in Figures 16, 17, and 18. The maximum radiation-induced loss at 1300 nm was about 35 dB/km, 10 dB/km, and 6 dB/km at -46°C, 25°C, and 71°C, respectively. After 600s recovery, the induced loss was < 2 dB/km at -46°C, and < 1.5 dB/km at 25°C and 71°C. Similar or better performance is expected from the other RH multimode and single mode fiber designs. Some noise and drift were present in the data because short sample lengths were necessary to measure the maximum induced loss and it was not practical to use lock-in amplifiers to monitor the signals in the 10^{-4}s range.

For the neutron fluence and neutron energy considered, the mechanism for the radiation-induced loss is ionization, as previously mentioned. Therefore, it should be possible to simulate the effects of the neutron radiation environment with an equivalent dose of gamma radiation. About 420 rads(Si) was produced from the neutron fluence used in these tests as measured by the TLDs; the relationship between the neutron fluence and gamma radiation dose is 1 rad(Si) ≈ 3×10^9 n/cm^2. The maximum induced loss from a 418 rad, steady state gamma radiation exposure is much less than the maximum induced loss produced by the neutron radiation exposure. The maximum radiation-induced loss is primarily determined by the dose rate for pulsed radiation exposures while the radiation-induced loss after recovery is related to the total absorbed radiation dose. The "permanent" radiation-induced loss after recovery, or no significant change in the radiation-induced loss, is similar for both radiation environments. The "permanent" radiation-induced loss at 1300 nm for a steady state gamma radiation exposure of 418 rads(Si) is calculated to be about 0.4 dB/km at -46°C. The "permanent" radiation-induced loss at 1300 nm due to the neutron radiation exposure at -46°C was about 0.5 dB/km. Additional work is needed to further develop the relationship between neutron fluence and gamma radiation total dose for this type of neutron radiation environment.

6. CONCLUSIONS

Several Ge-doped silica core multimode and single mode fiber designs were evaluated in different nuclear radiation environments. The radiation-hardened multimode fiber designs and all of the single mode fiber designs exhibited excellent resistance to radiation-induced loss after exposure to steady state gamma radiation over a wide temperature range, as evidenced by the recovery of the induced loss after removal from the radiation field. Data was presented that suggested a correlation between Δ and radiation response; as Δ increased, the radiation sensitivity decreased. Also, the effect of the draw speed on the radiation response was considered. The draw conditions did not have a significant effect on the radiation response for the draw conditions considered. The 50 μm RH multimode fiber and the AT 100 single mode fiber were exposed to transient radiation. Both designs showed significant recovery within seconds after low temperarture, transient radiation exposures. The 50 μm RH multimode fiber was also

evaluated in a neutron radiation environment over a wide temperature range, and performed well during and after exposure to this environment. Also, the relationship between neutron fluence and absorbed gamma radiation dose was investigated. Further work is needed to establish equivalency between neutron radiation and gamma radiation for the neutron fluences and total doses of importance in most tactical applications.

7. ACKNOWLEDGEMENTS

The authors wish to thank K. H. Chang, AT&T Bell Laboratories, D. F. Marcille, and J. W. Baumgart, both of AT&T Network Systems, for the fiber samples; D. Parker, Georgia Institute of Technology Neely Nuclear Research Center, for assistance in the steady state gamma radiation tests; J. L. Wert and J. R. Beymer, Boeing Aerospace and Electronics, for assistance in the transient radiation tests and data reduction; D. Berry, Sandia National Laboratory, for arranging the neutron radiation tests, and S. T. Davies, AT&T Bell Laboratories, for assistance in connectorizing the samples.

REFERENCES

1. M. W. Shute, Sr. and H. T. Shang, "Optical Fibers for Tethered Vehicle Applications," *Proc. of DoD Fiber Optics Conf. '90,* McLean, VA, March 1990.

2. S. Glasstone and P. J. Dolan, **The Effects of Nuclear Weapons,** U. S. Dept. of Defense and Energy Res. and Dev. Admin.: Washington, D.C. (1977), 324-460.

3. E. J. Friebele and D. L. Griscom, "Radiation Effects in Glass," *Treatise on Material Science and Technology,* **17: Glass II,** M. Tomozawa and R. H. Doremus, ed. (1979), 261-263.

4. K. Kathiresan, M. W. Shute, Sr., M. R. Gotthardt, et al., "Fiber Optic Cable for Shipboard Systems," *Proc. of 37th International Wire and Cable Symposium,* Reno, NV, November 1988.

5. J. R. Simpson, "Radiation Effects in Optical Fibers," **TUG3,** *Tech. Digest of OFC '88,* New Orleans, LA. January 1988.

6. E. J. Friebele, et al., "Systematic Investigation of Matched Clad Single-Mode Fiber Radiation Response," **TUG4,** *Tech. Digest of OFC '88,* New Orleans, LA, January 1988.

STEADY STATE RADIATION TEST SCHEMATIC

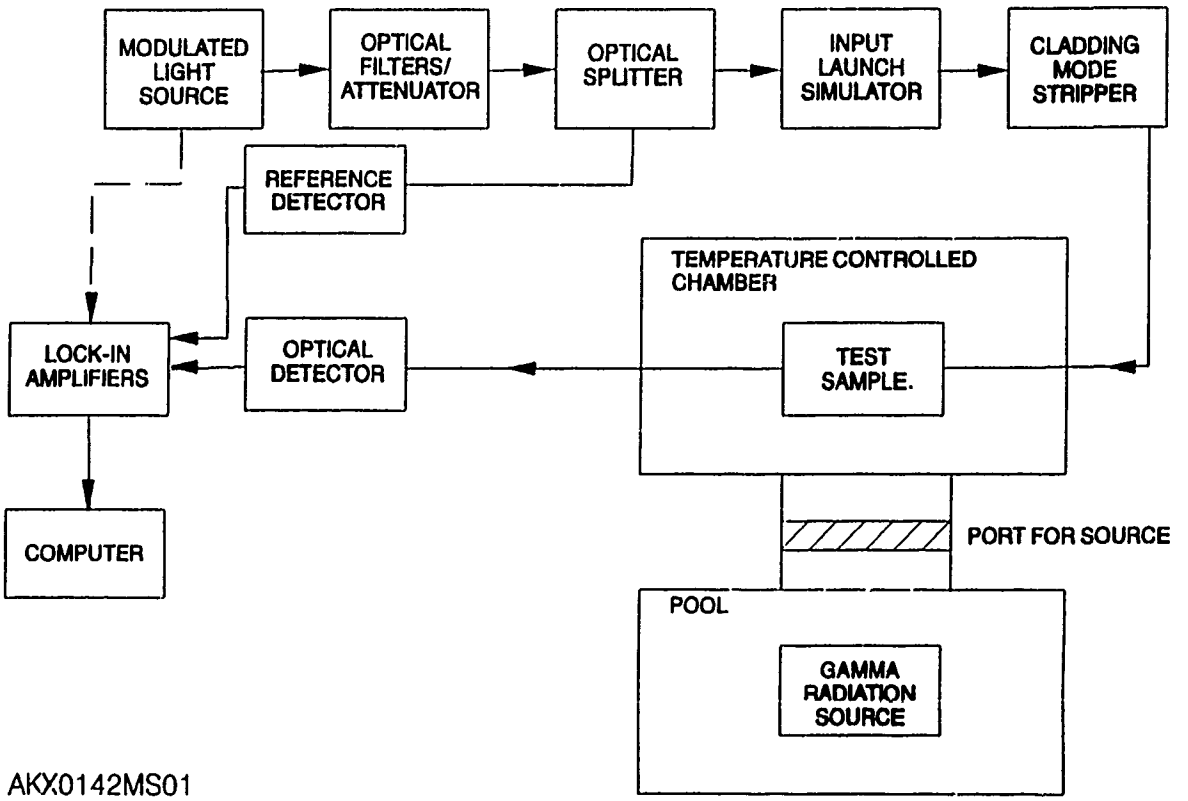

FIGURE 1.

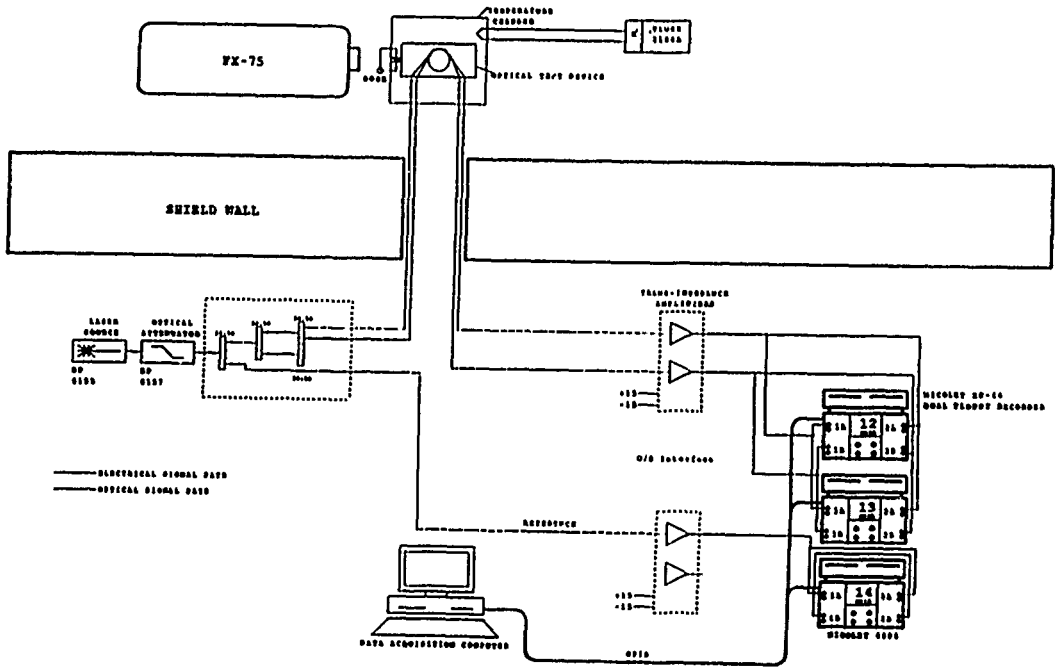

Figure 2. Schematic of Transient Radiation Test Apparatus

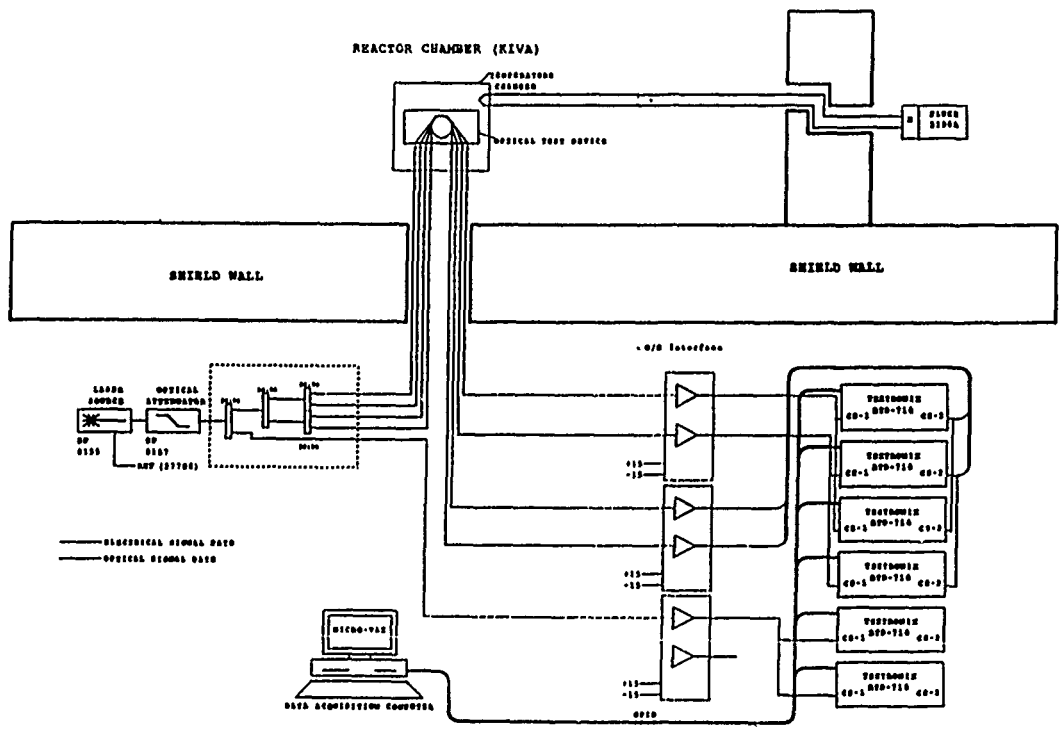

Figure 3. Schematic of Neutron Radiation Test Apparatus

Radiation-Induced Loss - 50 µm

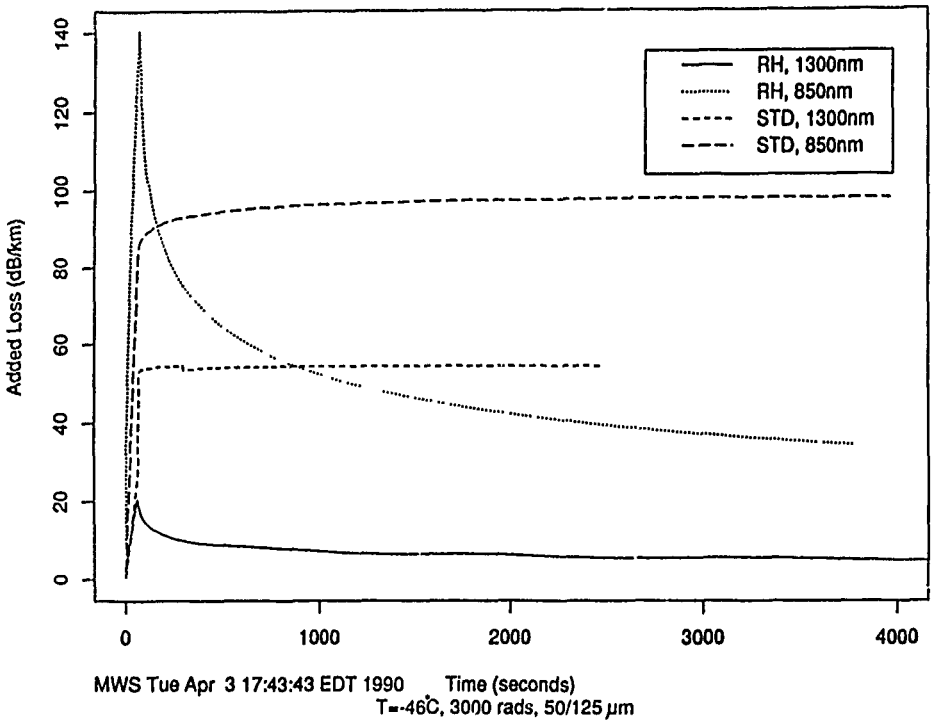

FIGURE 4.

Radiation-Induced Loss - 62.5 µm

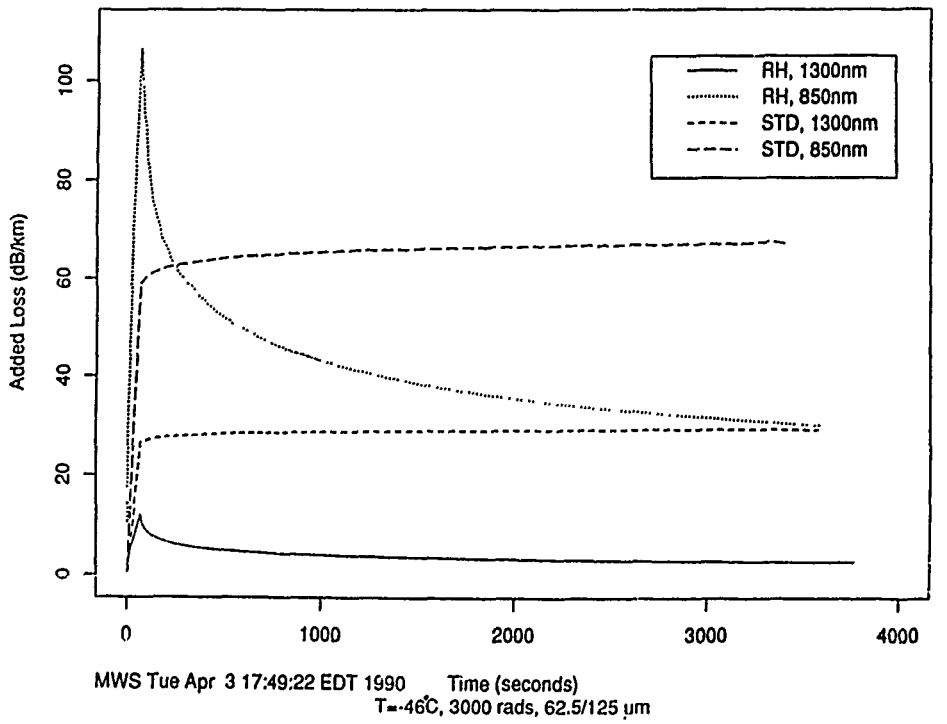

FIGURE 5.

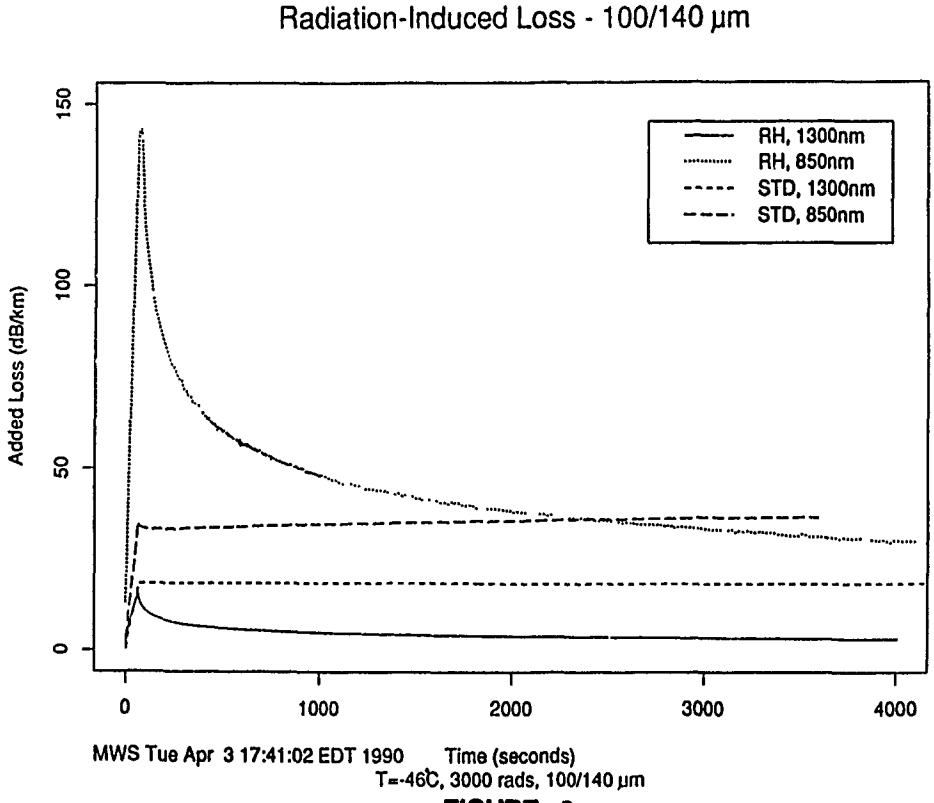

FIGURE 6.

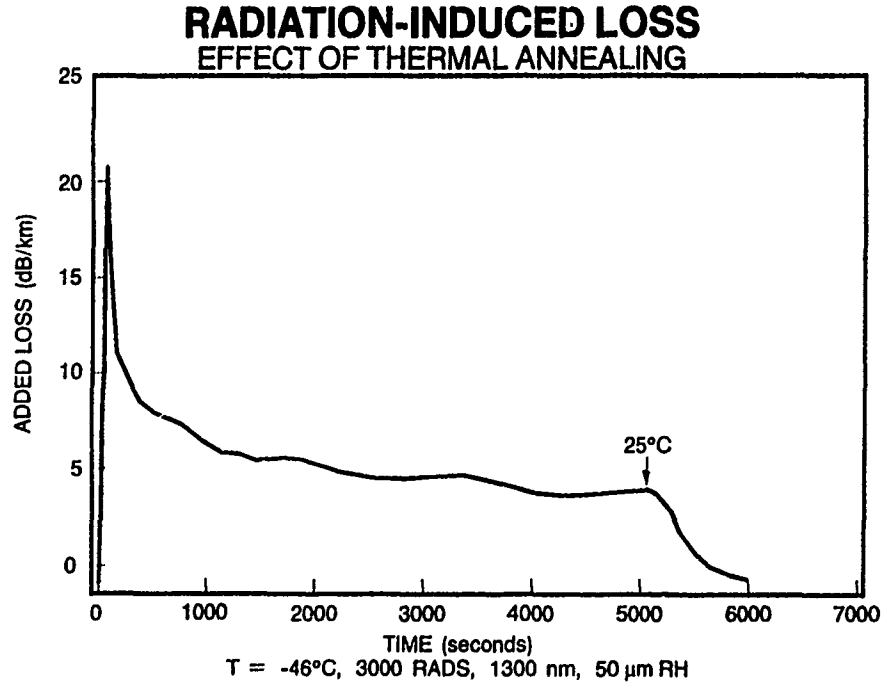

FIGURE 7.

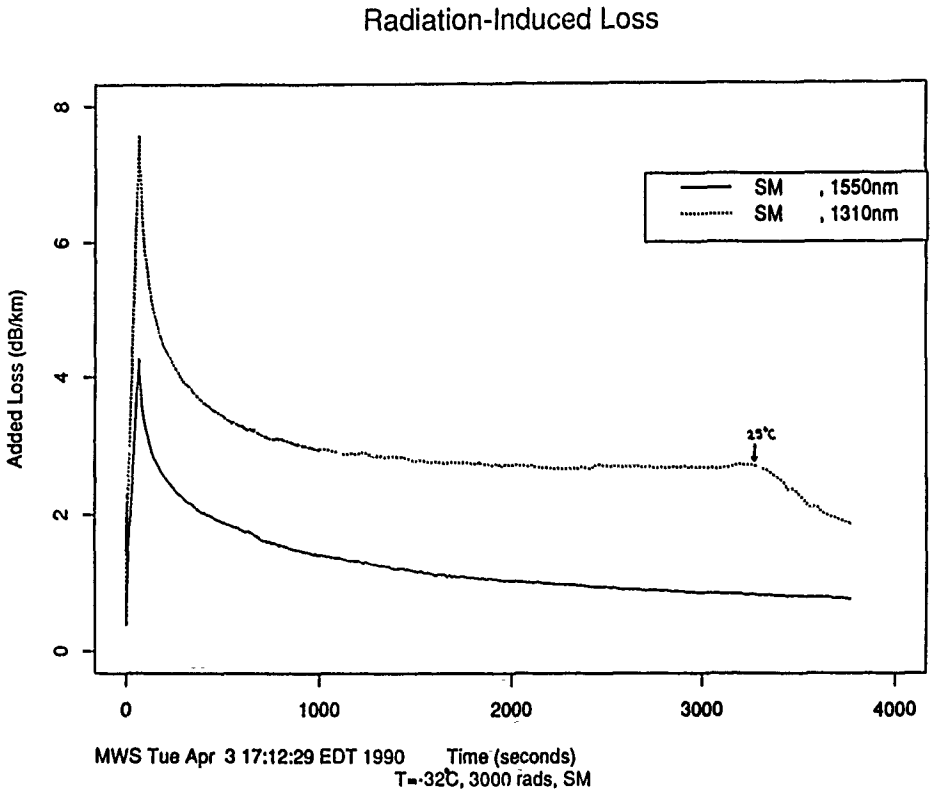

FIGURE 8.

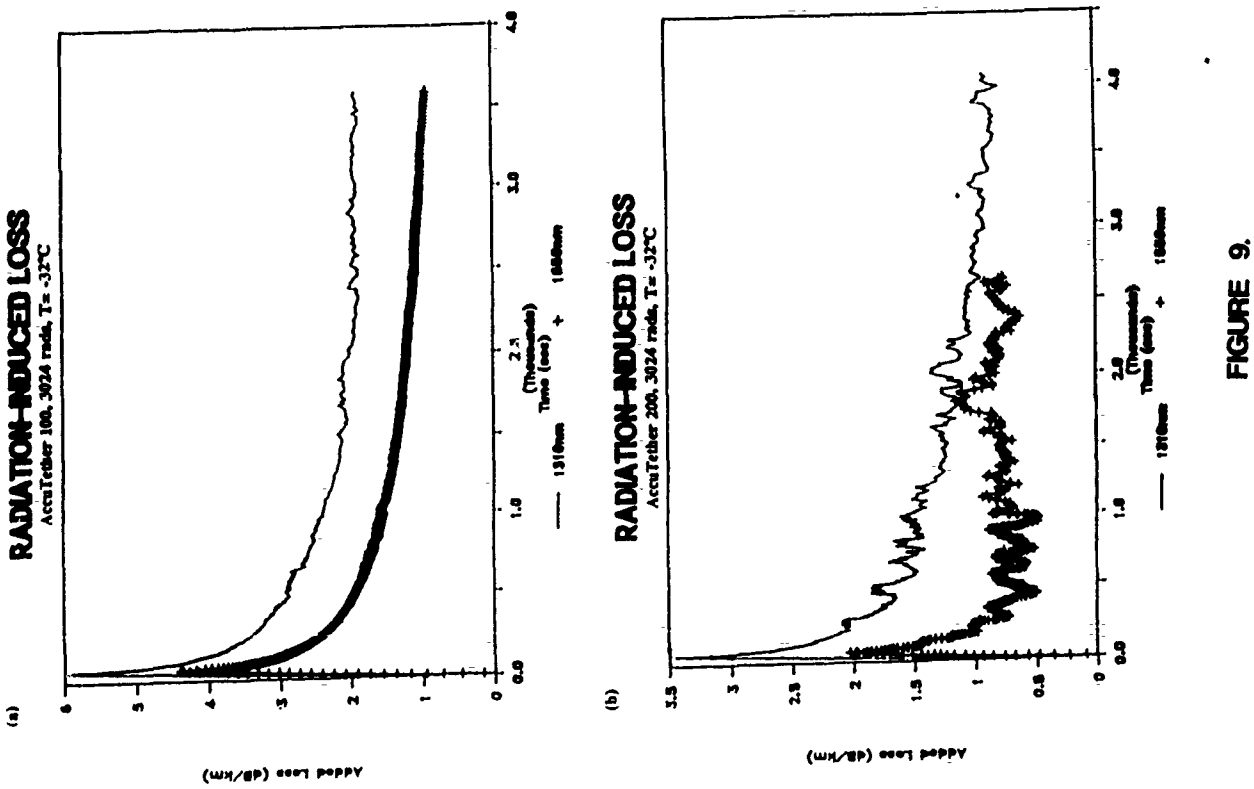

FIGURE 9.

Radiation-Induced Loss vs. Delta

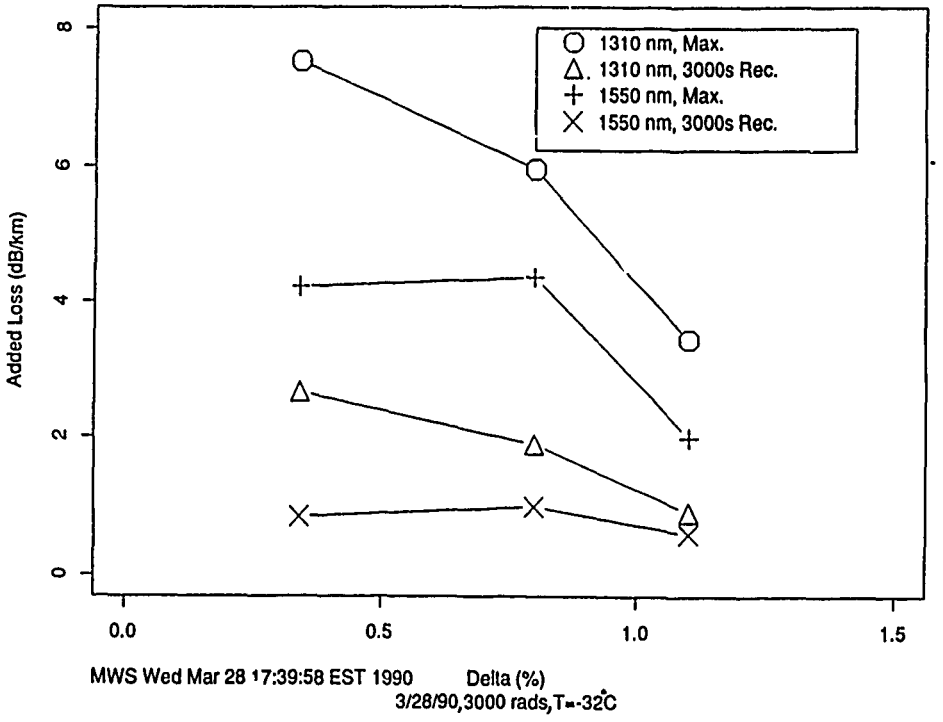

FIGURE 10.

Radiation-Induced Loss vs. Draw Speed

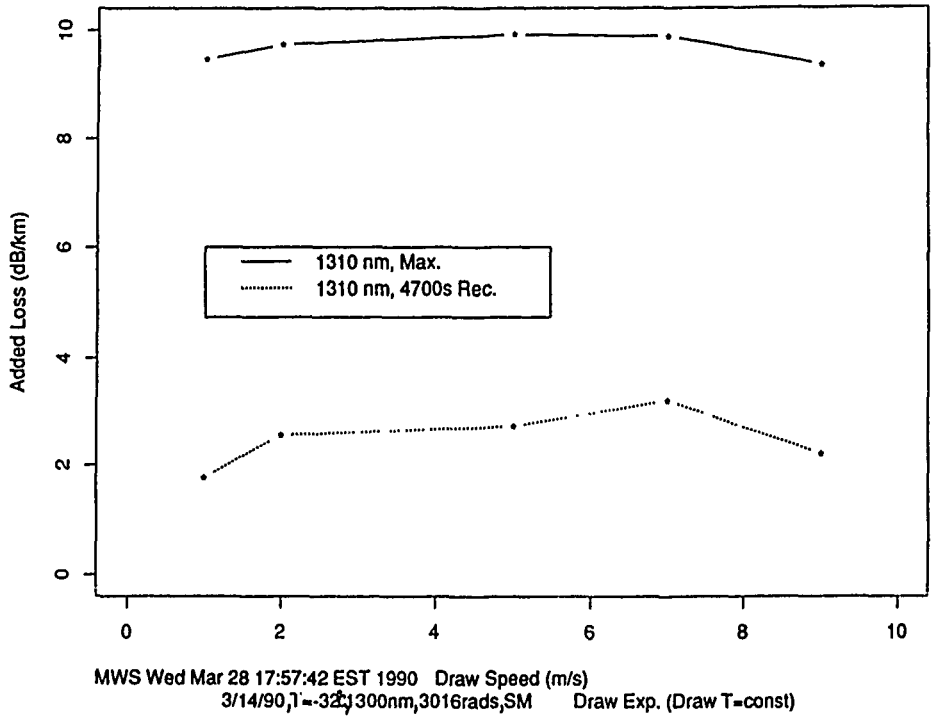

FIGURE 11.

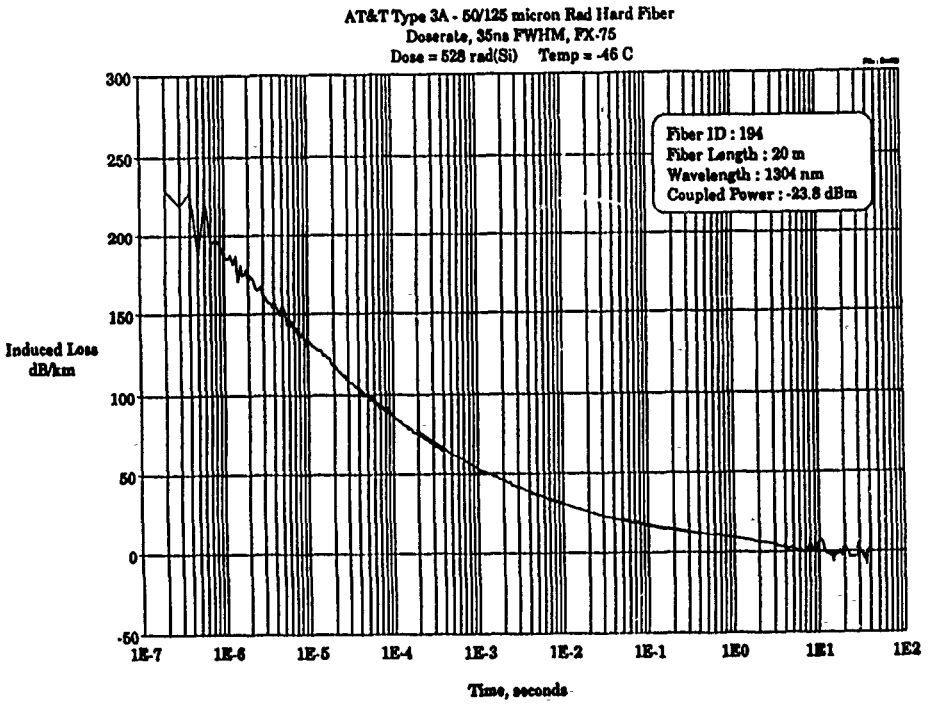

Figure 12. Transient Radiation Response of the Radiation-Hardened 50 µm Multimode Fiber at -46°C

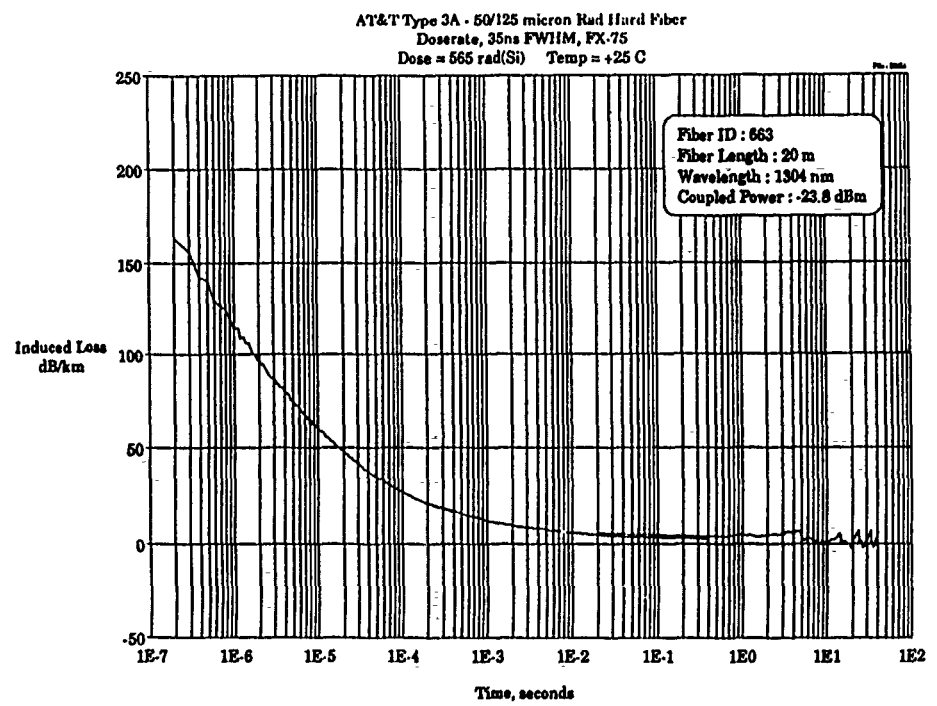

Figure 13. Transient Radiation Response of the Radiation-Hardened 50 µm Multimode Fiber at 25°C

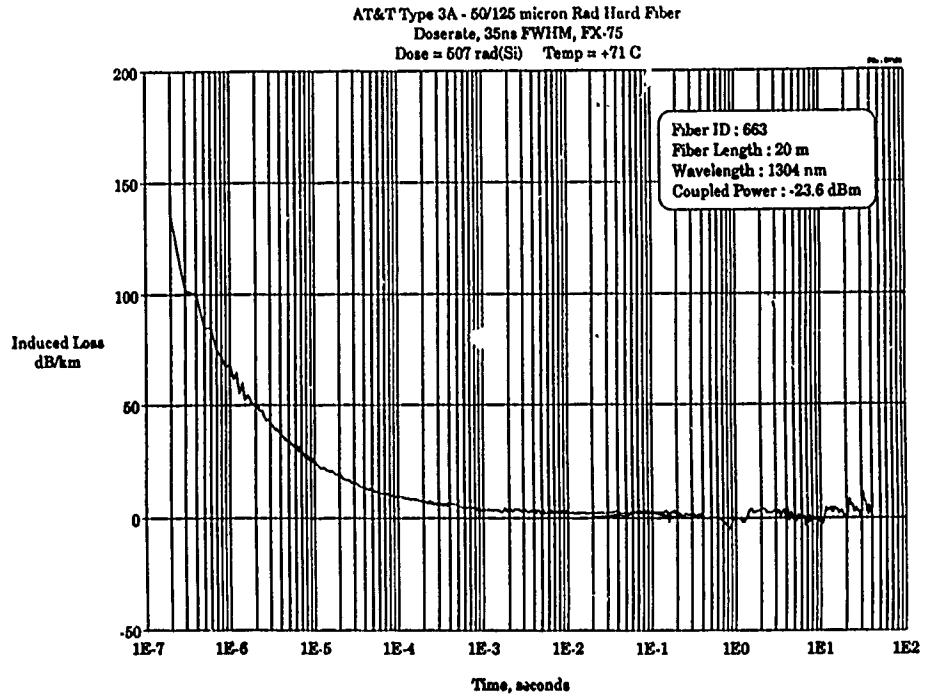

Figure 14. Transient Radiation Response of the Radiation-Hardened 50 µm Multimode Fiber at 71°C

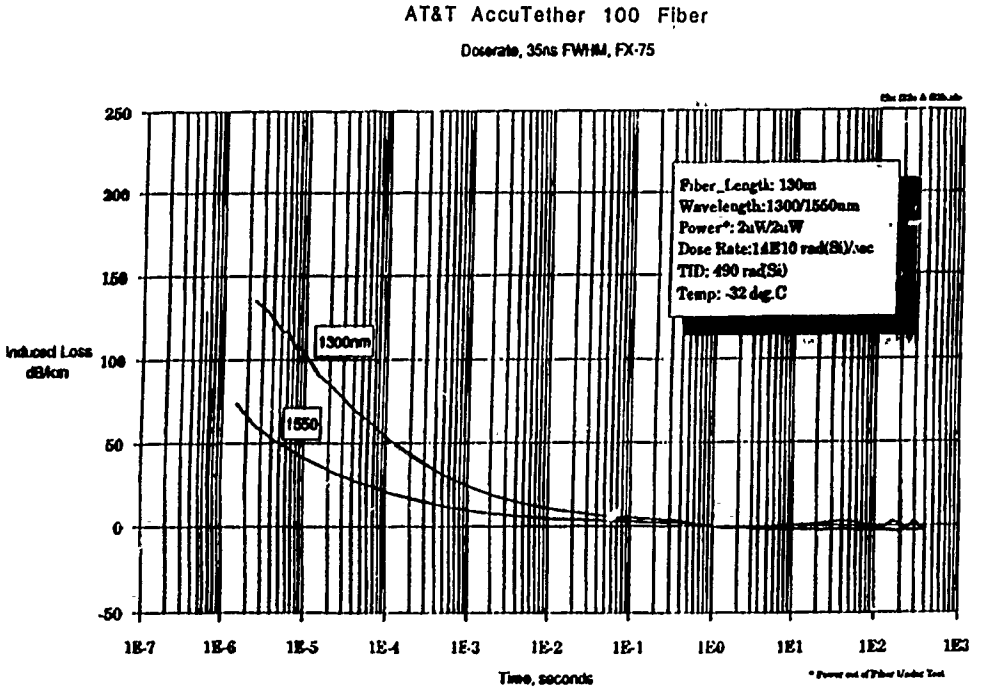

Figure 15. Transient Radiation Response of the AccuTether 100 Fiber at -32°C

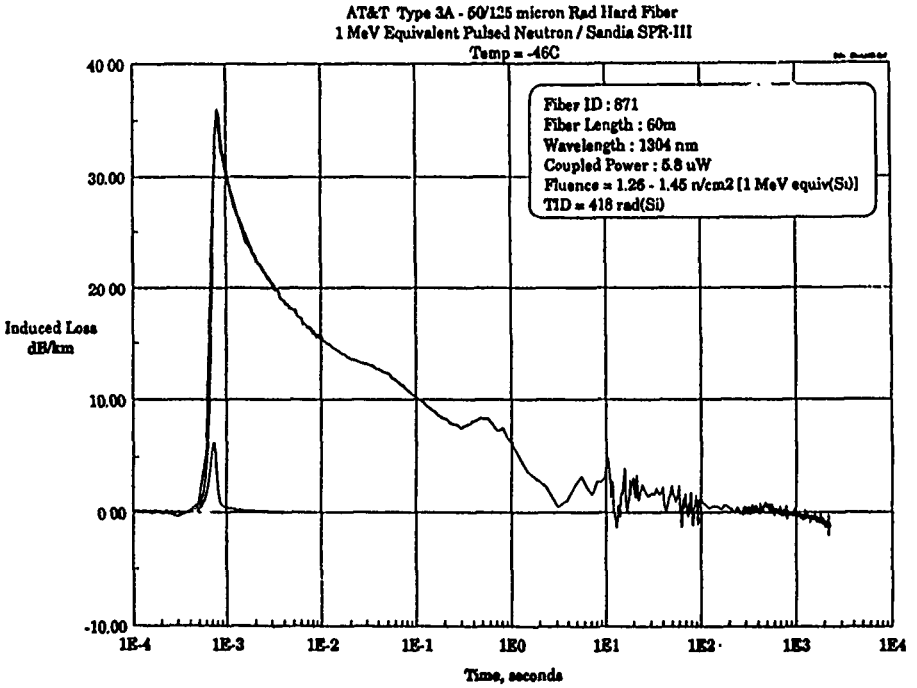

Figure 16. Neutron Radiation Response of the Radiation-Hardened 50 µm Multimode Fiber at -46°C

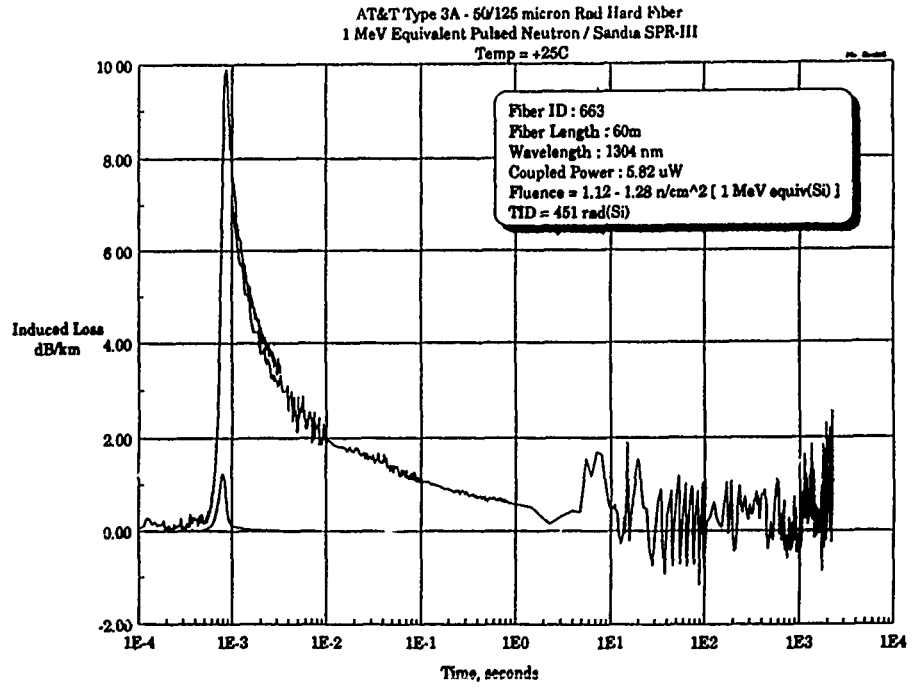

Figure 17. Neutron Radiation Response of the Radiation-Hardened 50 µm Multimode Fiber at 25°C

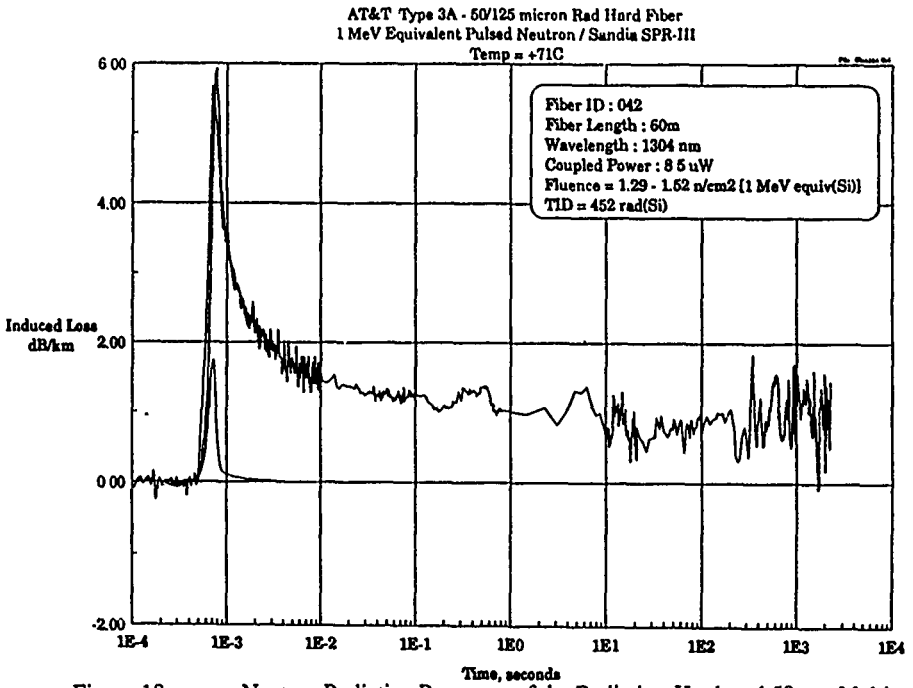

Figure 18. Neutron Radiation Response of the Radiation-Hardened 50 μm Multimode Fiber at 71°C

Marcus W. Shute, Sr. was born in Sioux City, IA, on October 3, 1962. He received the B. S. degree in Mechanical Engineering from Tennessee State University, Nashville, TN, in 1984; the S. M. degree in Materials Science and Engineering from the Massachusetts Institute of Technology, Cambridge, MA, in 1986, and is currently pursuing the Ph. D. degree in Mechanical Engineering at the Georgia Institute of Technology, Atlanta, GA.

He joined the Lightguide Fiber Department of AT&T Bell Laboratories, Norcross, GA, as a Member of Technical Staff in 1986. Initially, he was involved in the evaluation of fiber properties and characterization of various optical fiber designs, including specialty fibers such as polarization-maintaining fibers. Presently, his interests are radiation effects in optical fibers, fiber optic guided vehicles, and fiber optic sensors.

He is a registered Professional Engineer in the state of Georgia and is currently, or formerly, a member of the Optical Society of America, Society of Photo-Optical Instrumentation Engineers, National Society of Black Engineers, American Society of Mechanical Engineers, Tau Beta Pi, and Omega Psi Phi Fraternity, Inc.

Michael M. Michie received the BSEE degree from Christian Brothers College in 1984. He joined AT&T Network Systems, Norcross, GA, in 1984 as a Development Engineer in the Optical Fiber Measurements group. Since then he has worked primarily in test equipment development for optical fiber characterization, specifically related to transmission and environmental performance. He is a member of Tau Beta Pi.

(photo not available)

John R. Duncan received the BS degree in Applied Physics from the Georgia Institute of Technology, Atlanta, GA, in 1988. He joined CDI Corporation and began working at AT&T Bell Laboratories, Norcross, GA, as a contract employee in 1988. His responsibilities have included hydrogen testing and radiation testing of optical fibers. He is a member of the American Physical Society and his currently pursuing the MS degree in Applied Physics at the Georgia Institute of Technology.

(photo not available)

Jeffrey A. Krinsky received the M.A. degree in physics and applied math from the Florida Institute of Technology, Melbourne, FL, in 1979 and 1986, respectively.

He is the principal investigator for photonics and radiation effects for the Boeing Aerospace and Electronics Physics Department, Seattle, WA. His current work involves the effects of ionizing radiation on optical fibers, optical fiber sensors, and optical fiber communication systems and components. His previous employment includes Harris Semiconductor and Government Systems (1980-1985), Martin Marietta (1979, 1980), and Telephonics (1977). In addition, he was an adjunct faculty member of the Florida Institute of Technology departments of physics, math, mechanical engineering, and computer science.

Effect of Alternating Current on Corrosion of Mechanical Splice Closures in Underground Cable Plant

J.H.Wang, Y.T.Horng,

Telecommunication Laboratories
P.O.Box 71, Chung-Li, Taiwan, 32099, R.O.C.

ABSTRACT

The present experimental work is to evaluate the 60 Hz AC effects on the pitting corrosion of metallic components (AISI 304 and 316 SS) of mechanical splice closure in chloride containing solutions. The results show that AC shifts the corrosion potential toward the negative direction and slightly promotes the corrosion resistance of 304 and 316 SS in 3% NaCl. While,in 0.1 M HCl, the 304 and 316 SS suffer more severe pitting attack if AC is present. Measurements of the anodic polarization curve of the artificial pit suggest that AC effect on accelerating the pitting growth is more significant for 304 SS than for 316 SS.

INTRODUCTION

Corrosion by Alternating Current (AC) has received interests in recent years. An AC originated from electrical transmission system usually travels through the environment and enters the underground telephone plant. AC has been found to depolarize the anodic or cathodic reaction of metals and accelerate their corrosion rates [1-6]. Therefore, it is much concerned whether the AC would damage the metallic components of underground cable plant or not,especially in an aggressive environment.

Mechanical splice closure is not popular in Taiwan and its long term reliability is still under further studies before wide-spread deployment. Most types of mechanical closures are made of AISI 304 and 316 stainless steels (SS) or plastic materials. AC effects on the localized corrosion of stainless steel are not well understood and ,therefore, introduce additional uncertainty in the long term reliability of mechanical splice closures in an aggressive environment.

Since the pitting corrosion is one of the most important corrosion behaviors for austenitic stainless steel in an aggressive environment, the purpose of this paper is to evaluate the effect of 60-Hz sinusoidal AC (1 V rms) on the pitting corrosion of metallic components (304 and 316 SS) of mechanical splice closure in very aggressive environments, namely,3% NaCl and 0.1 M HCl solutions. In this work, electrochemical laboratory measurements and Scanning Electronic Microscopy (SEM) examinations are taken to investigate the influences of AC on the pitting corrosion of stainless steel. For studying the growth rate of an existing pit, the artificial pit [7] technique is also used.

EXPERIMENTAL

Preparation of Test Specimens

Commercial AISI 304 and 316 SS are prepared as cylindrical specimens, 20 mm in length and 8 mm in diameter. The top surface of each specimen is provided with a shallow screw hole, 3 mm in diameter. Electrical connection to the specimen is made by an AISI 304 SS lead, which is screwed into the hole in the specimen.

All specimens are polished with 600 grit SiC paper,rinsed with distilled water,and immediately introduced into the test cell.

For studying the growth of an existing pit, an artificial pit is made as following:
First, the surface of a cylindrical specimen is coated with epoxy and a small hole (0.5 mm) left in it. Then, this specimen is activated at 500 mV (SCE) for 6 hours in 3% NaCl solution to form an artificial pit. By electrically coupling an artificial pit (anode electrode) through a zero resistance ammeter (Z.R.A) with an unpitted cylindrical specimen (cathode electrode) in solution, as shown in Fig.1, the current flowing between the galvanic couple can therefore be regarded as the pit growth current of the artificial pit. Thus, the pit growth rate can be estimated by the galvanic couple cell.

Test Procedures

In this work, electrochemical measurements are carried out in 3% NaCl and 0.1 M HCl solutions at room temperature. The 60-Hz sinusoidal AC with a constant voltage, 1 V rms, are applied to the test specimens by a function generator. The DC voltage output is offset by the function generator itself and only AC is applied to the test specimens.

The following experiments are conducted:(1) measurements of the corrosion potentials (Ecorr) during the immersion period of 140 hours ;(2) measurements of the electrochemical impedances and pitting potential (Enp) immediately after immersion time of 140 hours; (3) examination of the pit morphology by SEM immediately after immersion time of 140 hours;(4) measurements of galvanic current of the artificial pit under different conditions; and (5) measurements of the anodic polarization curve of the artificial pit and cathodic polarization curve of the specimen.

Measurements of (2), (4) and (5) are performed under nature condition without superimposing AC onto the test specimens.

All potential reported in this paper are converted to the SCE scale.

Electrochemical impedance measurements are taken at open circuit potential. A minimum perturbation potential of 10 mV is applied over the frequency range from 100 kHz to 5 mHz.

RESULTS and DISCUSSION

The changes in corrosion potential (Ecorr) vs time under various testing conditions are shown in Fig.2-5. In order to investigate the AC effect on the Ecorr of 304 and 316 SS,the Ecorr with and without AC application is put in the same figure for comparison. As seen, the AC effect on Ecorr is dependent on the corrosion environment. In 3% NaCl (Fig.2 and 3), the Ecorr is shifted toward the negative direction and a significant fluctuation in Ecorr is observed during the initial time because of the presence of AC. After nearly 80 hours, the Ecorr is settled at a nearly same potential either with or without AC. While, AC results in a different change of Ecorr when in the 0.1 M HCl. From Fig.4 and 5, a more positive Ecorr is induced with the presence of AC . The Ecorr is shifted toward the noble direction nearly 25 mV for 316 SS and 65 mV for 304 SS as AC applied in 0.1 M HCl.

The electrochemical impedance data for 304 and 316 SS is presented in Fig.6-9. The presence of AC is found to slightly increase the electrochemical impedance for both 304 and 316 SS in 3% NaCl (Fig.6 and 7) whereas slightly decrease the impedance in 0.1 M HCl (Fig.8 and 9). This results indicate that corrosion resistance of stainless steel is slightly suppressed in 0.1 M HCl but slightly enhanced in 3% NaCl if AC is present. In addition, the lower impedance in 0.1 M HCl than in 3% NaCl suggests that the former is a more aggressive environment for the stainless steel.

Another than the electrochemical impedance, the pitting potential (Enp) ,i.e. potential above which pits nucleate and develop, is also taken into this study to investigate the influence of AC on the corrosion behavior of stainless steel. Usually, the Enp is considered as a measure of the susceptibility of different metals to pitting in various aggressive environments. The more positive Enp, the more resistant is the metal to pitting. Table 1 gives the Enp, evaluated from the shape of

the anodic polarization curve, under various testing conditions. It is seen that if AC is present, the Enp is slightly more positive in 3% NaCl but slightly more negative in 0.1 M HCl. Meanwhile, the Enp is much more negative when in the latter solution. The results from the Enp and electrochemical impedance measurements are consistent and suggest that AC effect on the corrosion behavior of 304 and 316 SS is dependent on the corrosion environment. It demonstrates that AC is harmful to stainless steel when in 0.1 M HCl but not in 3% NaCl during 140 hours' immersion.

SEM examination on 304 and 316 SS specimens after immersion time of 140 hours shows that there is no pitting corrosion for 304 and 316 SS in 3% NaCl neither with nor without AC. On the other hand, more or less pitting is found with SS in 0.1 M HCl. Figure 10 shows a set of pit morphology of 304 and 316 SS after the 140 hours' immersion in 0.1 M HCl. No AC is applied to the specimen in Fig.10(a) and 10(c). The effect of AC on pitting corrosion of specimen is shown in Fig.10(b) and 10(d) in comparison with Fig. 10(a) and 10(c). According to the large pits in Fig.10(b) and many small pits in Fig. 10(d),it demonstrates that pitting corrosion of 304 and 316 SS have been markedly accelerated because of the presence of AC.

All the above results indicate that the presence of AC can shift Ecorr of 304 and 316 SS toward the positive direction and simultaneously accelerate the pitting corrosion. The reason for why a shift in Ecorr toward the positive direction will also promote the pitting growth rate can be understood by the kinetics of pit growth. It is known that pitting growth process is caused by the corrosion cell current, which is a function of the potential difference between the anode and the cathode as well as the IR voltage in the corrosion environment. The potential difference depends on the polarization behavior of the metals in the cell; the IR voltage is determined by the geometric shape and the conductivity of the current's conducting path. Any factor that promotes the potential difference between the anode and cathode will increase the driving force for the corrosion cell current and accelerate the pitting growth. Since there is a large IR voltage drop inside the pit, it is reasonably supposed that AC will affect the polarization behavior of cathode outside the pit but not the anodic polarization behavior inside the pit. In the presence of AC, the most possible explanation of the increase in pitting corrosion rate accompanied with a positive shift in Ecorr is that depolarization of the cathodic reaction and an increase in potential difference of the pitting corrosion cell are caused by AC.

The pitting corrosion cell can be simulated by a galvanic cell consisting of an artificial pit and an electrically separated specimen, as shown in Fig.1. The pitting growth rate(current) is determined by the anodic polarization curve of the artificial pit and the cathodic polarization curve of the specimen. Fig.11 and 12 give the polarization curves of the galvanic cell in 0.1 M HCl. The Icoupled in these figures is the pitting growth current with no AC application. As AC applied, the corrosion potential of 304 SS would be shifted toward positive direction by 65 mV(from Fig.4),and therefore the cathodic polarization changed, (shown as the dashed line in Fig.11). As a result, the pitting growth current of 304 SS increased from Icoupled (about 1 uA)to I'coupled (about 2.2 uA) by AC, which depolarized the cathodic reduction. In the case of 316 SS in 0.1 M HCl(Fig.12), a more significant polarization of anodic oxidation,i.e. a more slowly increasing in current with potential, is found with the artificial pit. The pitting growth current of 316 SS is about 0.35 uA and is less than that of 304 SS. This result is consistent with the fact that 316 SS is more resistant to pitting corrosion than 304 SS. Besides, Ecorr of 316 SS is shifted only about 25 mV by AC,as shown in Fig.5. Consequently, only little increase in pitting growth current, from Icoupled(about 0.35 uA) to I'coupled (about 0.41 uA), is caused by passing AC to 316 SS, as shown in Fig.12. These results suggest that AC effect on accelerating the pitting

growth rate should be more significant for 304 SS than for 316 SS.

The above discussion has described that the pitting corrosion of 304 and 316 SS is accelerated by AC in 0.1 M HCl. In 3% NaCl, although no harmful effect of AC on the susceptibility to pitting corrosion is observed during the short testing period, prolonged measurements should be performed furthermore to clarify the influence of the AC on pitting corrosion of SS in a less aggressive environment.

CONCLUSIONS

1. No harmful effect of AC on the pitting corrosion of 304 and 316 SS is observed in 3% NaCl. While in 0.1 M HCl, the presence of AC is found to markedly promote the pitting corrosion.

2. The increase in Ecorr toward the positive direction caused by AC, which therefore increasing the potential difference between the galvanic couple of pitting corrosion cell, plays an important role in accelerating the pitting corrosion.

3. AC effect on promoting the pitting growth is more significant for 304 SS than for 316 SS because of the different anodic polarization characters of pit and Ecorr shift between them.

Table 1. Enp under various conditions

Enp,mV	304 SS		316 SS	
	NaCl	HCl	NaCl	HCl
AC	360	215	450	285
Non AC	325	235	430	310

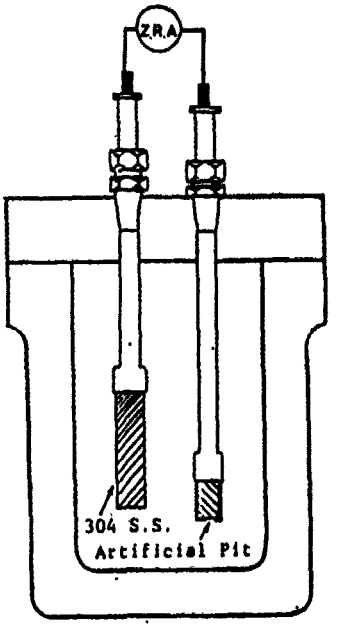

Figure 1. Schematic of galvanic couple cell for measurement of pitting growth.

REFERENCES

1.A.W.Hamlin, Materials Performance, Vol.1, No.1, p.55 (1986)
2.D.A.Jones and B.E.Wilde, Corrosion, Vol.43 ,No.2, p.66 (1987)
3.Kenneth G.Compton, P.E. Corrosion/81, paper number 145
4.T.C.Tan and D-T Chin, Corrosion, Vol. 45,No.12, p.984 (1989)
5.Der-Tau Chin and S.Venkatesh, J.Electrochem.Soc. 126, p.1908 (1979)
6.D-T Chin and P.Sachdev,J.Electrochem. Soc.Vol.130, No.8. p.1714 (1983)
7.T.R.Beck and S.G.Chan, Corrosion,Vol. 37,No.11, p.665 (1981)

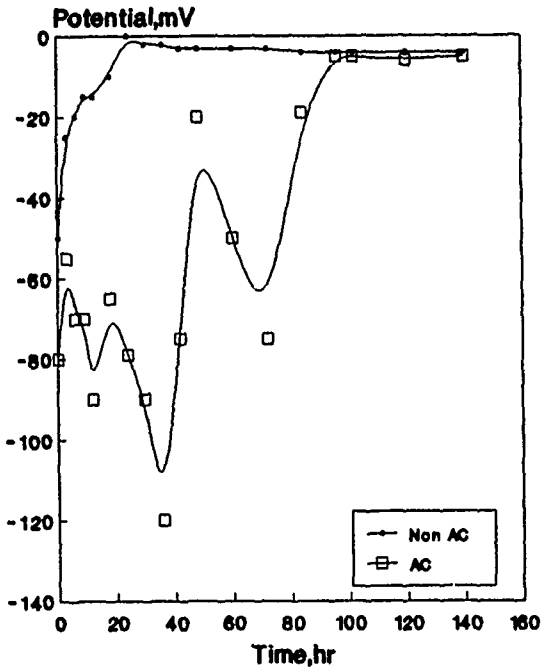

Figure 2. Changes in Ecorr vs time of 304 SS in 3% NaCl.

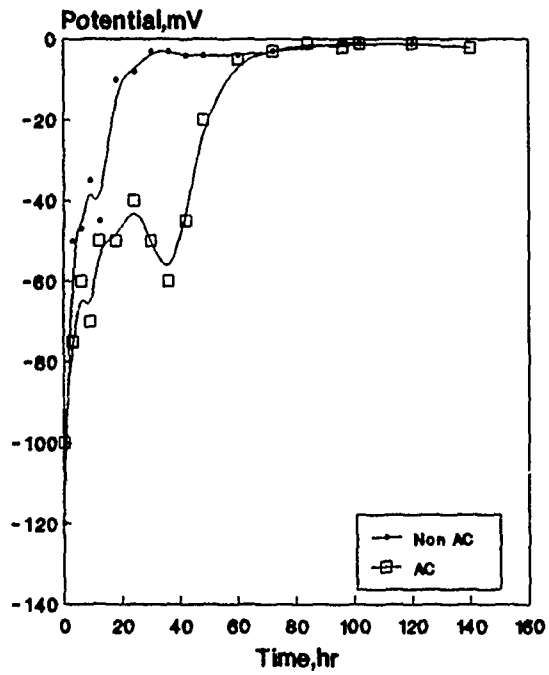

Figure 3. Changes in Ecorr vs time of 316 SS in 3% NaCl.

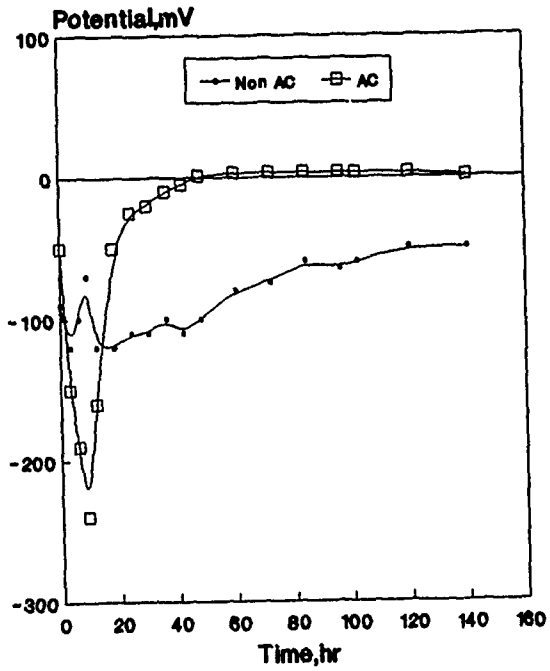

Figure 4. Changes in Ecorr vs time of 304 SS in 0.1 M HCl.

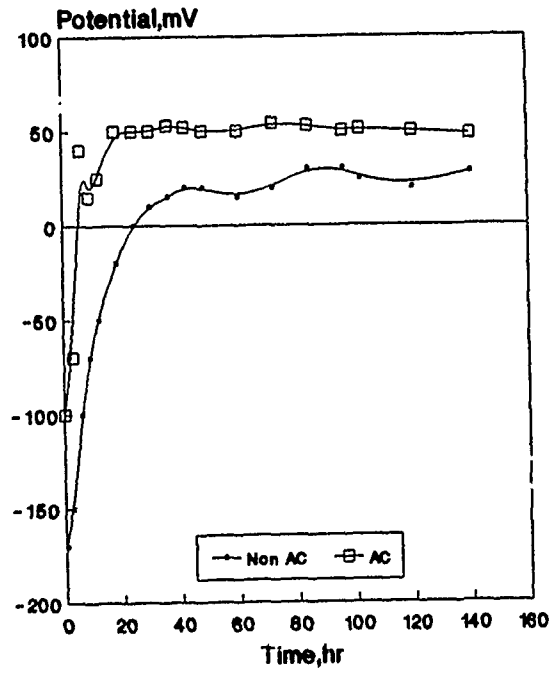

Figure 5. Changes in Ecorr vs time of 316 SS in 0.1 M HCl.

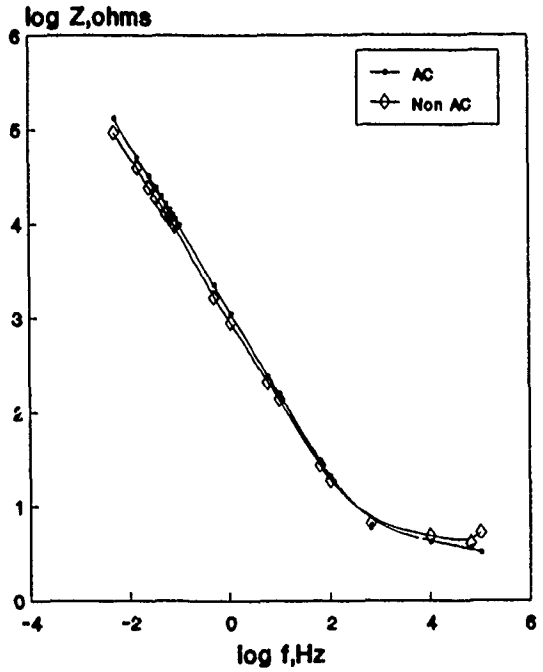

Figure 6. Bode plot of 304 SS in 3% NaCl.

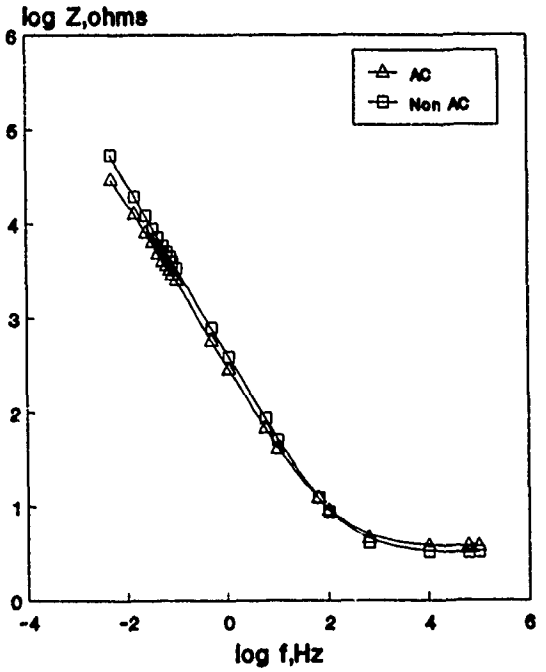

Figure 8. Bode plot of 304 SS in 0.1 M HCl.

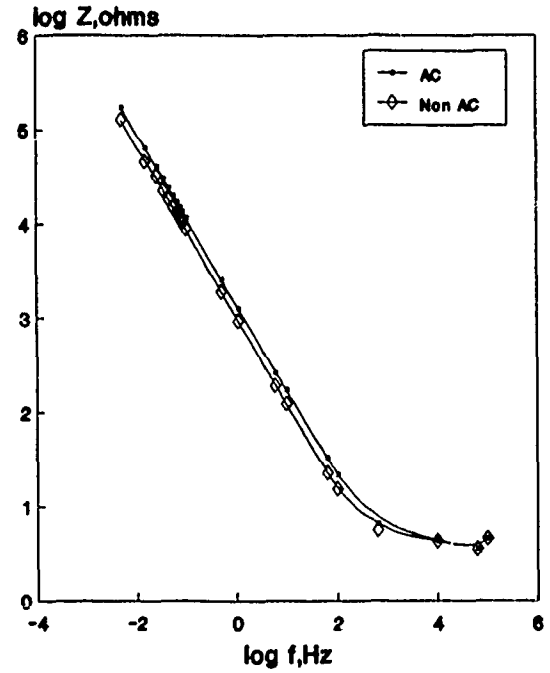

Figure 7. Bode plot of 316 SS in 3% NaCl.

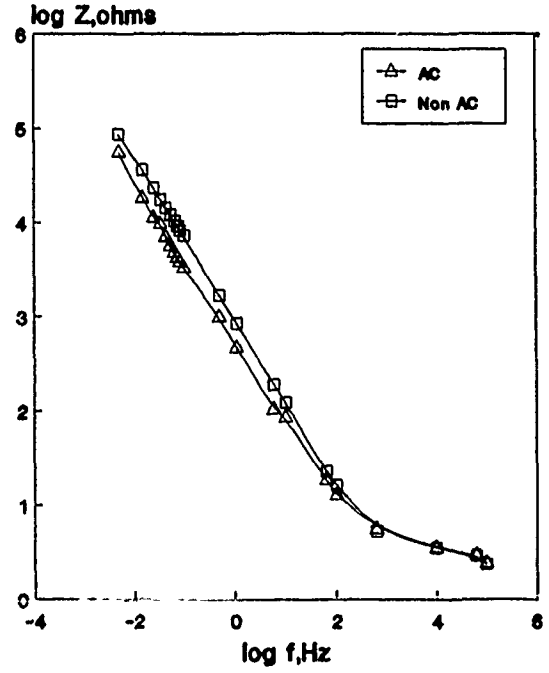

Figure 9. Bode plot of 304 SS in 0.1 M HCl.

a

b

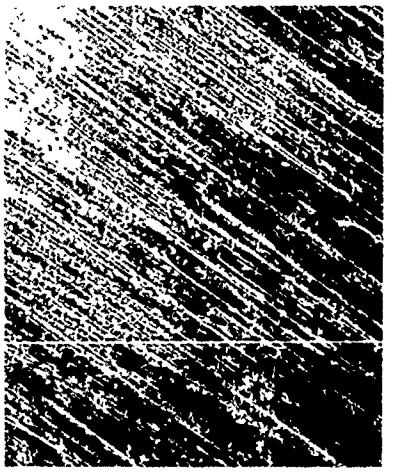

c

d

Figure 10. Pit morphology after immersion time of 140 hours in 0.1 M HCl (a) 304 SS without AC (b) 304 SS with AC (c) 316 SS without AC (d) 316 SS without AC, (X100).

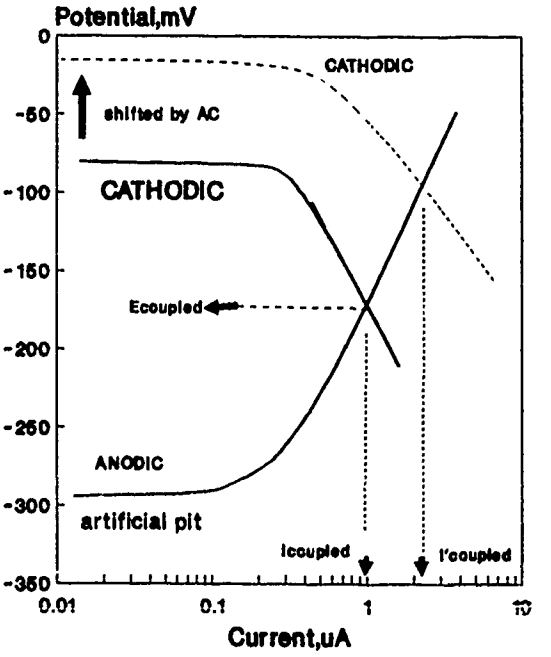

Figure 11. Polarization curves of galvanic couple; Full line - experimental; Dashed line - speculative; 304 SS in 0.1 M HCl.

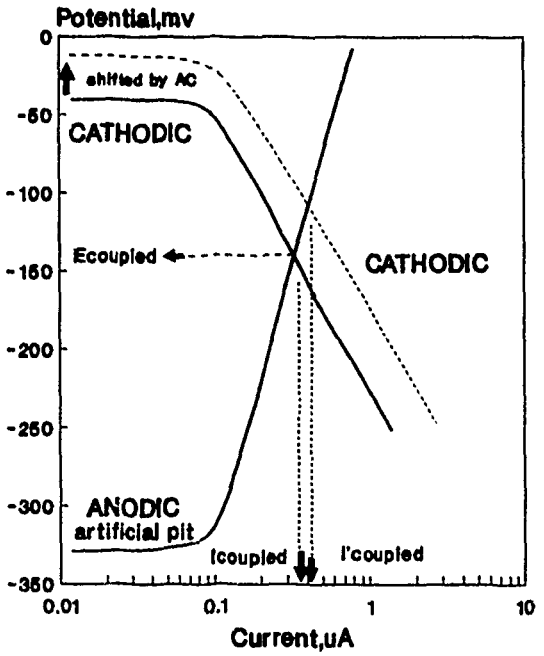

Figure 12. Polarization curves of galvanic couple; Full line - experimental; Dashed line - speculative; 316 SS in 0.1 M HCl.

Jyh-Hwa Wang
Outside Plant Lab.
Telecommunication Labs.
P.O.Box 71, Chung-Li
Taiwan, R.O.C.

Mr. Jyh-Hwa Wang received his M.S. degree in Materials Science from National Cherng-Kung University in 1981. From 1983 to 1988 he worked in Materials Research Labs. In 1988, he joined T.L. and has been engaged in Outside Plant technology.

Yaw-Tzong Horng
Outside Plant Lab.
Telecommunication Labs.
P.O.Box 71, Chung-Li
Taiwan, R.O.C.

Mr. Yaw-Tzong Horng received his M.S. degree in Electrochemistry in 1983 from National Taiwan Normal University. He joined T.L. in 1983 and has been engaged in Outside Plant technology. He is also a member of the Corrosion Engineering Association of the Republic of China.

TESTING OF FIBER OPTIC CABLE CORE MATERIALS AFTER ACCELERATED HEAT AND HUMIDITY AGING

Donald R. Parris
Bradley A. Warner

Siecor Corporation
489 Siecor Park
Hickory, NC 28603

Abstract

The inside of a pedestal can have extreme temperatures and humidities which will affect rates of cable core material degradation. The objective of this work was to develop test methods and procedures specific to fiber optic cable core components which more accurately reflect real-life situations. This allows the long term performance of the finished product to be more accurately evaluated in a short period of time.

Introduction

Polymeric cable materials typically are laboratory tested under various conditions to assess their suitability in various applications. To date, the majority of this testing has been conducted on polymer samples that have been compression molded, injection molded, or extruded. These samples are measured for their relevant, initial property values and then may be aged at some elevated temperature in appropriate environments to accelerate any potential degradation reactions. The performance is then evaluated by monitoring these relevant properties as a function of aging time. In the case of mechanical properties, the widely accepted and standardized practice is to test materials in a uniaxial tension test[1].

As fiber optic cables spread further into the network toward the home or curb, the cable core itself will be exposed to a wide variety of environmental conditions. It is, therefore, important that the testing used to measure and evaluate the performance of the core materials accurately describes the real (application) environment. A test program was developed to meet this objective. This program consists of three steps: sample preparation, aging, and test performance. This paper discusses each of these steps individually.

Procedure

Sample Preparation

Cable core materials must have certain physical characteristics to be suitable for processing, provide the necessary protection for the optical fibers, and allow for installation and handling in real life environments. Additionally, these materials are expected to maintain this performance for 20 to 40 years.

Materials are commonly tested according to established procedures. The most widely accepted materials standards organization in the United States is the American Society for Testing and Materials (ASTM). These standards specify test sample preparation and conditioning, aging environments and times, test procedures, and interpretation of results.

Fiber optic cable materials are typically made from a thermoplastic and serve the primary purpose of providing mechanical and environmental protection for the optical fibers. The most common shape of the materials is to form a tube in which to hold the fibers. Secondly, these tubes may serve to group and identify fibers. Mechanical properties such as tensile strength, crush resistance, kink performance, and fatigue resistance are of great interest. Standard materials test methods, however, may not be able to completely or correctly predict the performance of a finished product. Their is no ASTM test procedure to evaluate the crush resistance or the kink performance of small diameter thermoplastic tubes. Additionally the tensile properties of these tubes may not be the same as the tensile properties of ASTM specified samples. Differences in tensile behavior between tubes and ASTM samples may arise as a result of processing methods used to prepare the samples and/or the use of multiple layers of different polymers to form composite tubes.

A generic thermoplastic stress-strain curve is shown in Figure 1. In this figure it can be seen that the material has an elastic and a plastic region which are separated by the yield point. A stress-strain curve for a composite tube is shown in Figure 2. In this figure it is notable that even though the individual materials in this tube had stress-strain curves that were similar to the generic material in Figure 1, the composite tube's performance is distinctly different.

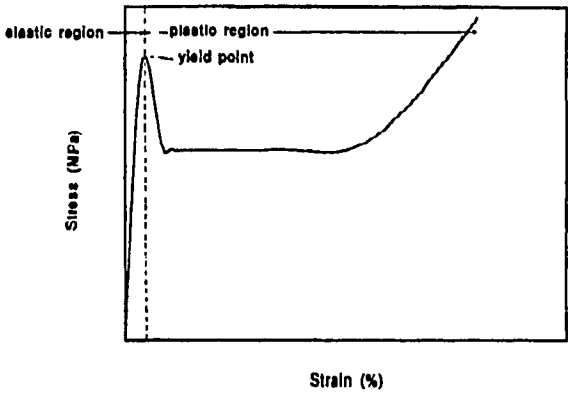

Figure 1

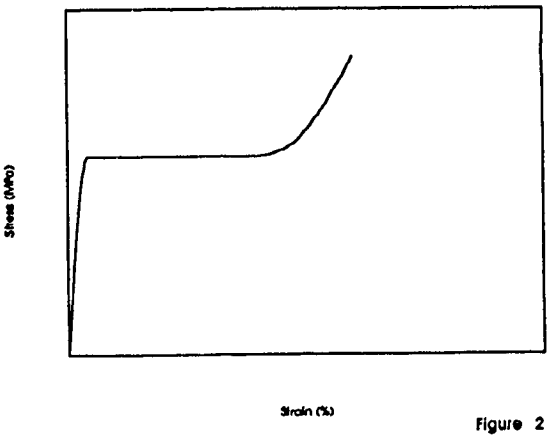

Figure 2

Evaluation of materials for long-term performance also involves testing for compatibility of the materials with other chemicals that they will be exposed to during their service life, including air, water, and any flooding and/or filling compound inside the cable. A standard ASTM materials test method may involve coating a material sample with, or submerging it in, such chemicals, aging the system at a specified temperature and then removing samples and monitoring their mechanical properties as a function of aging time. The pass/fail criteria are typically based on either minimum (or maximum) absolute property requirements or some maximum allowable property change.

These methods, however, fail to recognize some effects that will occur in the finished product; a cable core tube in this case. In the case of fiber optic cables, core tubes typically employ a filling compound which serves as a "cushion" for the optical fiber and as a water block for the tube. This filling compound, if it interacts with the core tube material, only has access to the tube at the inner surface. Conversely, any chemicals (i.e. flooding compound) that may be outside of the core tube can only access the tube through the outer surface. Any interactions of the tube materials with air (oxidation) or water (hydrolysis) could also be affected by the presence of the filling and flooding compounds. Additionally, differences in the processes used to make the ASTM sample and the tube may result in differences in polymeric morphology (crystallinity)[2] which could cause the mechanical and aging characteristics to differ.

Based on the considerations listed above, it is clear that the best test specimen to accurately reproduce real-life cable material-environment interactions would be the actual finished product, with any filling compounds inside the tube and the appropriate reactants outside the tube.

Aging Conditions

The pedestal environment is very severe in terms of heat, humidity and other outdoor conditions. The objective of this section was to create specific aging conditions which simulate the thermal and physical characteristics of the pedestal environment. Inside the pedestal, the cable jacket will be stripped away leaving the cable core exposed. Pedestals may have an interior width as small as 100 to 150 mm (4" to 6") and may be used to store extra lengths of coiled core tubes. The stresses applied to the these materials by being coiled could cause accelerated "stress cracking" or material degradation. Based on this scenario, all accelerated aging tests in this study were performed on cable core tubes that were stressed by wrapping them around a 100 mm (~4") mandrel.

A temperature of 85°C (185°F) and a duration of 30 days were chosen for this testing. Additionally it was decided to perform all aging at 94% relative humidity. This humidity level was the highest at-

tainable based on existing test equipment limitations. The core tube will have some specific performance lifetime in this accelerated test environment. The equivalent performance lifetime in real life will depend on the actual aging conditions and on the particular materials being tested. Temperature and humidity can often work together to degrade materials, but in a real pedestal environment, the humidity will most likely decrease as the temperature increases. The effect of increasing temperature has been observed to increase degradation rates in an exponential fashion. The effect of increasing relative humidity has been observed to increase degradation rates in a more linear fashion. It is felt that the degradation resulting from these aging conditions is equivalent to the degradation that will occur during the service life of cable materials in a typical pedestal environment.

Test Performance

Standard Tests: Standard tensile test methods consist of measuring the mechanical performance of standardized test samples. The performance is evaluated by measuring certain mechanical properties in a uniaxial tensile test. Mechanical properties such as stress and strain at break, stress and strain at yield and tensile modulus are commonly of interest. The long term performance of a material is then evaluated by monitoring the important mechanical properties as a function of aging time. In the first phase of this work, an attempt was made to perform standard test methods and procedures on cable core tubes.

Three different core tube types were tested, the major differences being the types of materials from which the tubes were made. Sample type A was a single layer polyester tube. Sample type B was a dual layer tube with polycarbonate as the inner layer and a polyester as the outer layer. Sample type C was a dual layer tube with a nylon as the inner layer and a polyester as the outer layer. These materials and material combinations represent the majority of those used in the fiber optic industry for cable core tubes. Samples were wrapped around a 100 mm diameter mandrel and aged at 85°C and 94% relative humidity for 30 days. Samples were tested before and after aging according to ASTM specification D638 (Standard Test Method for Tensile Properties of Plastics).

A typical ASTM standardized test sample is prepared such that the center section of the sample has a smaller cross section than the ends where the sample is gripped. This practice induces a localized stress region in the center of the sample so that during testing, elongation will occur in the center. Since core tubes have a constant cross-section there is no localized stress region in the cente sample. Altering the sample by thinning the center cross section is difficult to do without creating surface flaws and this also violates the intent of using finished product samples as discussed in the sample preparation section. During the initial phases of testing, the core tubes were deformed so severely in the grips of the tensile test machine that they would often fail at one of the grips, thus, invalidating the test. It was possible to avoid the extreme tube damage in the grips by inserting a plastic or metal rod into the tube to prevent its total collapse when gripped. This method greatly reduced the tube damage during gripping and allowed for complete testing of the tubes.

Table 1 summarizes the results from the testing of sample types A, B & C. The table reports the change in yield stress and strain as a consequence of aging. Core tubes are designed to perform mechanically within their elastic region. That is, no permanent (plastic) tube deformation is desired during normal use and handling. Thermoplastic cable core tube materials will have yield strains significantly greater than allowable optical fiber strain levels. Therefore, yield point properties are important because they define the upper limits of interest. Ideally the yield point is where the stress-strain relationship is no longer linear. For most plastics this occurs at very small strain levels, if at all. Therefore, a more practical definition of the yield point has been adopted to better approximate this value. The yield point is defined in this testing (as in ASTM D638) as the point where an increase in strain occurs with no associated increase in stress. This is the point where the slope of the stress-strain curve goes to zero. Samples were considered brittle if they broke before the yield point was reached.

Table 1

Sample Type		Initial	Final	Δ (%)
A	yield strain	11.8	14.4	+ 22.0
	yield stress (MPa)	40.9	43.6	+ 6.6
B	yield strain	6.3	6.7	+ 6.3
	yield stress (MPa)	49.3	54.7	+ 11.0
C	yield strain	10.7	11.9	+ 15.0
	yield stress (MPa)	38.6	44.4	+ 11.2

Several inadequacies have been observed using this test procedure. In actual field use, cable core tubes will be bent during handling. The standard uniaxial tensile test does not account for the compressive and shear loads encountered in bending. The data from the uniaxial tensile test is also difficult to interpret. Figure 3 is a plot of the after aging stress-strain curve for sample type A. In this figure, according to ASTM D638, the point of zero slope is marked as point B. It is obvious that this point lies well within the region of plastic deformation and cannot be considered as the approximate yield point. Point A on the graph is a better approximation of the yield point, however, its selection is somewhat arbitrary.

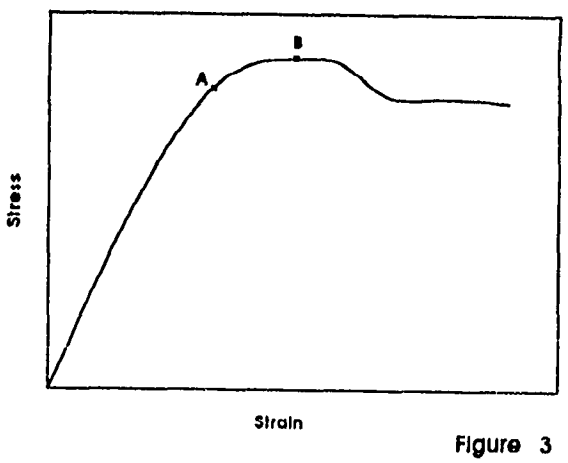

Figure 3

Additionally, once the data is acquired it is difficult to equate changes in mechanical properties to changes in handling characteristics. One can observe in Table 1 that the tensile performances as measured according to ASTM D638 for all of the core tube types were similar. The changes in yield stress ranged from +6.6% for sample type A to +15% for sample type C. The changes is yield strain ranged from + 6.3% for sample type B to + 22% for sample type A. All samples exhibited a yield point after aging that was within 25% of the original yield point. Sample types B and C were easily handled after the aging process, but sample type A was observed to break quite easily when handled.

Similar inadequacies are encountered when other mechanical properties such as secant modulus are monitored. Thus, more realistic tests are required to approximate actual field handling conditions so that unacceptable long term performance can be evaluated.

Functional Tests: A set of tests were needed that more accurately represented the field use mechanical loads that the core tube would be subjected to. The objective in establishing these tests was that they had to be relatively simple to perform while accurately simulating actual field handling conditions. Also, the fewer the number of tests, the better. Two tests were developed to test the aged and unaged core tubes. These tests evaluate a tube's durability and kink performance.

Durability - Cyclic Flex Test

The first test is a variation of the cyclic flex test performed on cables. It was fashioned after FOTP (Fiber Optic Test Procedure) 104, entitled Fiber Optic Cable Cyclic Flexing Test. The same equipment and setup was used as prescribed in FOTP 104. A one meter core tube sample was placed in the test apparatus with a 1.5 kg (3.3 lbs) weight attached to the end. This weight insured that the core tube would stay flush with the sheave during testing. The sheave diameter around which the core tube was flexed was 20 times the core tube diameter. This formula for the sheave diameter is typical for flex testing of finished cables and means a bend diameter of about 50 mm (2") for a 2.5 mm (0.1") core tube. Such a sheave diameter will create a strain level of 5% at the outer surface of the core tube. This strain level is within the elastic region for typical core tube materials and is also a

realistic strain level that the core tube might encounter during handling in the field.

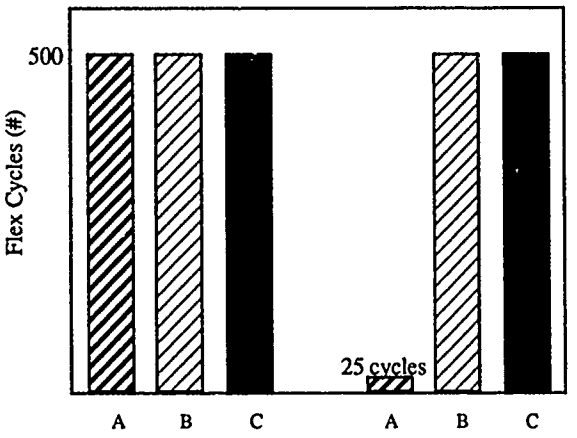

Figure 4

Figure 4 shows the results of the cyclic flex testing of sample types A, B & C before and after aging. All samples types were flexed for 500 cycles. Before aging, all three sample types were cycled the 500 cycles without splitting, cracking or breaking. After aging, samples B and C again withstood the 500 flex cycles; sample type A broke after an average of 24 cycles. This test simulates the simultaneous tensile, compressive and shear forces that the core tubes will be subjected to during the cable installation and subsequent pedestal or cable re-entry procedures.

Kink Performance - Loop Test

The second test was devised to evaluate the minimum bend radius of a core tube and the point at which kinking occurs. It is necessary in any cable installation, restoration or mid-span access that the core tubes be removed from the cable in order to access the optical fibers. This typically means bending the core tube at the point of connection or splicing to properly locate it for long term placement. It is important for the core tube to withstand relatively high, short term strains without kinking. Core tube kinking can cause extreme optical fiber attenuation increases and in the worst case, can cause the optical fibers to break. A simple test was devised in which the core tube is formed into a loop and the ends are pulled apart until kinking occurs. The stress and strain values at kinking can be monitored. Comparisons of these values before and after the aging process can indicate how the core tube will perform over the long term.

A 0.75 meter (2.5 ft) length of core tube was marked 10 cm (4") from each end. The tube was bent to form a loop and a metal ring was placed at the crossover point of the loop to prevent the loop from twisting out during testing. The tensile test machine grips were set 10 cm (4") apart. The looped core tube was placed in the grips such that the marks on each end of the tube were at the entrance to the grips. This configuration resulted in a loop which did not form a perfect circle. The shape of the loop was elliptical on the half nearest the metal ring and grips, but the outer half was approximately circular. The outer diameter of this outside half of the loop was about 80 mm (3") (see Figure 5). The test crosshead speed was 250 mm/min. (10 in/min.) and a plot of load versus crosshead extension was recorded for each measurement. A typical test plot is shown in Figure 6 . Here it can be seen that the load increases with crosshead extension in a linear fashion until a peak is reached at which point the tube collapses (or kinks) and the load decreases. This peak in the load versus extension curve is defined as the "kinking point". The outer diameter at kinking is calculated based on the assumption that all crosshead movement reduces the the diameter of the loop according to the formula:

Loop O.D. = initial loop O.D. - (crosshead displacement / π)

This assumption was found to be accurate when compared with direct measurements.

This testing was performed on unaged and aged (85°C / 94 % relative humidity / 30 days around a 100 mm mandrel) core tube sample types.

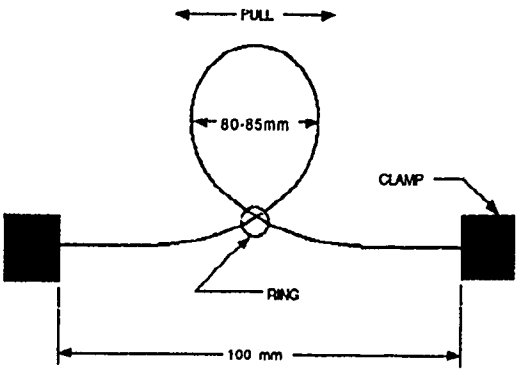

Figure 5

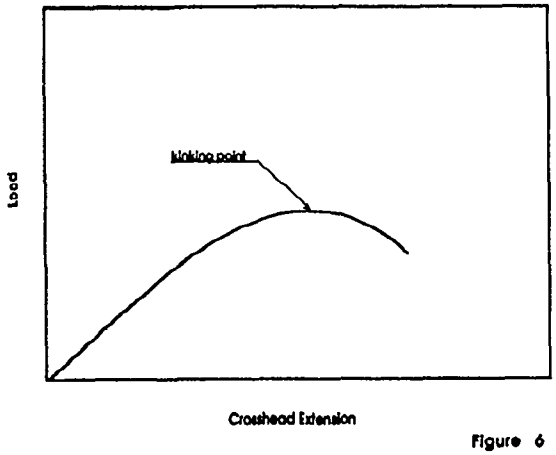

Figure 6

The loop test results for the unaged and aged core tubes sample types are shown in Figure 7 . Here it can be seen that the core tubes typically kinked initially at relatively small O.D.s and then kinked after aging at some larger O.D. . Additionally some core tube types after aging would snap break instead of kink. As kinking involves very high localized strains, a sample that exhibits no plastic deformation will break. Such a failure is known as a brittle instead of a ductile failure. The crosshead extension versus load curve for a brittle core tube differs from that of a ductile tube in that instead of a curved peak, the load increases steadily until it drops suddenly to zero.

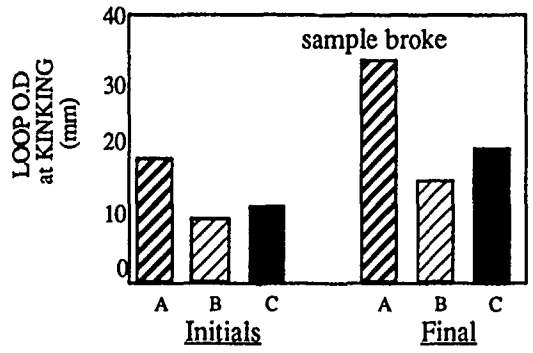

Figure 7

Sample types A, B and C had outer diameters of 2.5 mm (0.1"). Sample types B and C kinked initially at similar outer diameters. Sample A kinked at a larger outer diameter. After aging, sample type A broke at a diameter twice that of its original kinking diameter. The kinking diameters of samples B and C both increased but remained below 20 mm (0.8").

From the functional testing, sample types B and C (the composite core tubes) had better performance characteristics than sample type A (the single material tube). This performance difference was not observable with the uniaxial tensile test. This indicates that such functional tests can be valuable tools to assess long term cable core material performance.

Conclusion

It is logical to assume that the best test sample to evaluate long term product performance is the product itself. The best aging conditions are those which simulate the actual product environment and the best tests simulate the actual mechanical loading scenarios that the product will be exposed to in field use. Selection of relevant aging conditions and development of appropriate tests are critical to obtaining meaningful long term product performance information.

It is the purpose of this paper to demonstrate that it is possible to develop and obtain meaningful results from functional tests and that such functional testing gives a more realistic indication of product performance for defined applications and environments.

References

[1] ASTM D638

[2] S. Turner, Mechanical Testing of Plastics, George Godwin, 1983.

Bradley A. Warner

Siecor Corporation
489 Siecor Park
Hickory, NC 28603

Bradley A. Warner received his B.S. degree in Geophysical Engineering from the Colorado School of Mines in 1984. He then served 5 years in the U.S. Navy as nuclear trained submarine officer. He joined Siecor in 1989 where he is an applications engineer in the Engineering Services Department.

Donald R. Parris

Siecor Corporation
489 Siecor Park
Hickory, NC 28603

Donald R. Parris received his B.S and M.S. degrees in Materials Engineering from Virginia Tech in 1984 and 1986. He joined Siecor in 1986, and worked in the Siemens Fiber Optic Materials Labs in Munich, West Germany for 18 months in 1987 and 1988. He is currently supervisor of the Materials Lab in Research, Development and Engineering.

HYDROGEN SOURCES FOR SIGNAL ATTENUATION IN OPTICAL FIBERS

George Schick, Karen A. Tellefsen, Aaron J. Johnson and Casey J. Wieczorek

Bell Communications Research
Morristown, NJ

ABSTRACT

Laboratory studies established that corroding galvanized steel and hydrogen-producing bacteria can generate enough hydrogen to cause appreciable signal attenuation in optical fibers. Simulations of these two effects in the laboratory caused hydrogen indicators to increase up to 7.2 dB/km.

The effect of hydrogen-producing bacteria can be suppressed by sulfate-reducing bacteria (SRB) in the absence or limited presence of fermentable hydrocarbons. In the abundant presence of these hydrocarbons the optical fibers will attenuate, and even high concentrations of SRB can not counteract this effect. During the fermentation process, acetic and butyric acids are produced. If these acids lower the pH of the environment below 5, the hydrogen is consumed by the formation of n-butanol and acetone.

Data from fiber attenuation experiments in H_2/N_2 gas mixtures show that the attenuation at saturation increases approximately linearly with increasing $p(H_2)$ and decreases with increasing temperature.

1. Introduction

Hydrogen diffusion into optical fibers can cause signal attenuation in optical fiber cables.[1-3] Although signal attenuation can be related to chemical reactions which involve -OH formation with P- and Ge-doping agents in multimode fibers, our interest is centered around the attenuating effect of molecular hydrogen in single-mode fibers. The effect is important because single mode fiber cables are the dominant technology in the telecommunications plant.

Our main concern is the attenuation that may take place at wavelengths in the transmission window used for communications (about 1255 to 1360 nm). However, for investigative purposes, the absorption peak at 1240 nm is monitored, because this peak is the "fingerprint" of molecular hydrogen in the fiber. Field and laboratory experiences indicate that the tail of the 1240 nm peak can cause significant signal attenuation at the shorter wavelengths within this window.[4]

Experiments in H_2/N_2 gas mixtures were done in order to compare the hydrogen-caused attenuation results obtained in our laboratory to those previously reported in the literature for similar conditions [1-3], and to serve as a reference for optical fibers exposed to the more complex environments of our other experiments.

The work described in this paper established the signal-attenuating effects of hydrogen generated by corrosion and by a species of hydrogen-producing bacteria. It also showed the effect of sulfate-reducing bacteria (SRB) on hydrogen production by these sources. Galvanized steel armor wires corrode, and conditions for the proliferation of SRB and hydrogen-producing bacteria can exist at water crossings where considerable attenuation in fiber cables has been measured.

2. Experimental Method

This section is divided into six parts: (1) equipment used to expose the fibers to various environmental conditions, (2) equipment used to expose a fiber to different H_2/N_2 gas mixtures, (3) signal attenuation monitoring equipment, (4) test environments, (5) testing procedure and (6) hydrogen analysis.

2.1 Equipment and preparations for optical fiber exposure to test environments

The test specimens were 240 m long, 0.9 mm OD, nylon-jacketed, single mode fibers. These fiber sections were wound on 40.6 cm long, 26.0 cm OD, 1.6 cm wall thickness, rigid (unplasticized) PVC cylinders. The middle section, 39.4 cm, of the cylinders was machined to provide 1 mm wide and 3 mm deep helical grooves. 0.48 cm diameter holes were drilled on 2.5 cm centers along the circumference and the length (Figure 1). The fiber was wound three layers deep in the grooves of the cylinder. After winding a layer of the fiber, the fiber was transferred from the outer (grooved) surface to the inner (smooth) surface. Then it was spiraled to the opposite end of the cylinder along the inner wall and brought to the outer surface for the next layer. In order to prevent small radius bends, the fiber was transferred between the inner and outer surfaces of the cylinder in three gently curving grooves, on the top and bottom surfaces of the cylinder. These transfer grooves were machined 120° apart. The fiber was attached to the inner surface at three points: at the middle and at the two ends. These attachments ensured large bending radii for the fiber on the inner surface of the cylinder. The fiber was attached to the inner surface at three points: at the middle and at the two ends. The attaching fixtures were made of 2.5 cm × 0.95 cm × 0.64 cm nylon pieces with a 0.9 mm wide and 0.9 mm deep groove along the 0.95 cm width and a threaded hole through the 0.64 cm dimension, 0.64 cm away from the groove (Figure 1). Nylon screws were used to hold the fiber in place with these fixtures.

The PVC cylinders with the fiber were placed in 30 liter capacity glass cells that were described in a previous paper.[5] The fibers exiting the rigid PVC cell covers were sealed in 7.6 cm, 9 mm O. D. glass tubes with epoxy resin.

In two of the cells, the PVC cylinders were surrounded by 40.6 cm long, 30 cm I.D., galvanized steel cylinders with a wall thickness of 0.8 mm. In one of the cells, the PVC cylinder was surrounded by a mild steel cylinder of similar size and shape, and a helically wound zinc ribbon anode was installed in the center of the cell, coiled around the heater tube. The metal cylinders and zinc ribbon anode had conductive leads attached and the contact areas were masked with a bituminous compound. The leads were sealed into 7.6 cm, 9 mm O. D. glass tubes with epoxy resin. The fourth test chamber contained no metal, only the fiber wound on the rigid PVC cylinder.

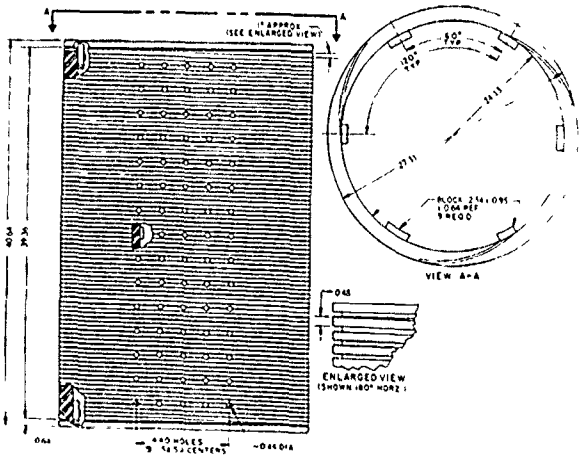

Figure 1. Rigid, grooved, PVC cylinder support for 240 meters of optical fiber.

2.2 Equipment and preparation procedures for optical fiber exposure to H_2/N_2 gas mixtures

A 180 m buffered optical fiber was exposed to different partial pressures of hydrogen at three different temperatures. The apparatus, shown in Figure 2, and procedures used in these measurements are described in the following paragraphs.

A two-piece hydrogen/nitrogen gas mixture exposure vessel was custom made of Pyrex and is shown in Figure 2. The vessel was 30 cm in diameter; the bottom part of the vessel was 35 cm high and the top part 10 cm high. The bottom part was connected to the top part by a flange joint with a Viton rubber gasket, coated with high-vacuum stopcock grease, placed between the two halves of the flange joint. This joint was secured with four flange clamps. The bottom half of the vessel was equipped with a 15 cm diameter, 30 cm high inner cavity for a resistance heater and with a gas inlet port with a vacuum stopcock. The top part had a gas exhaust port with a vacuum stopcock and three 12/5 ball-joint ports. The exposure vessel was wrapped in a fiberglass insulation blanket to minimize temperature gradients within the vessel.

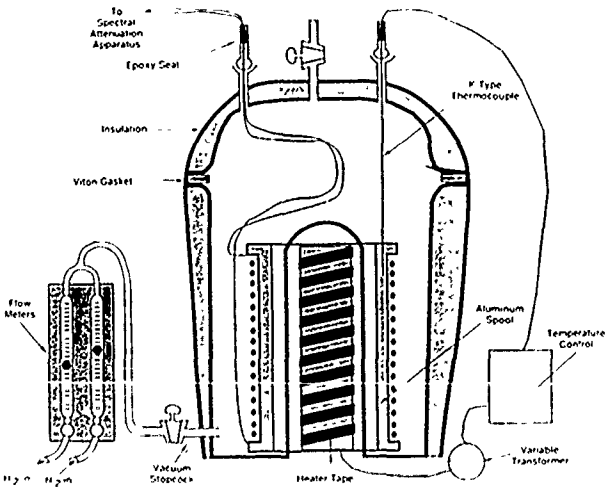

Figure 2. Apparatus for attenuation experiments in H_2/N_2 mixtures.

The 180 m optical fiber was wound on a 20 cm diameter, 30 cm high aluminum bobbin with 1 cm thick walls. The bobbin was equipped with a 5 cm deep thermocouple well and a 5 mm diameter, 31 cm high fiber-restraining rod. The two ends of the optical fiber were fed through one of the ball joint ports and sealed into the upper, male part of the joint with epoxy. A K-type (chromel-alumel) thermocouple was fed through another of the ball-joint ports in a similar way and the male port was sealed with epoxy.

Several different partial pressures of hydrogen were prepared by mixing 99.9% hydrogen and 99.985% nitrogen with a gas proportionator. The proportionator was equipped with valves and ball-in-tube-type flowmeters for both gases. The concentration of hydrogen in the gas mixture was analyzed by gas chromatography; gas samples were taken from the exposure vessel's gas exhaust port.

The exposure vessel was heated with an 832 watt, 2.5 m by 2.5 cm wide, tape-style resistance heater that was wrapped around a 14 cm diameter, 30 cm high, cardboard cylinder covered in aluminum foil. The heater assembly was placed in the inner cavity of the exposure vessel. The heater was connected to a variable transformer set at 25 V; the transformer was connected to a temperature controller and the thermocouple probe was also attached to the temperature controller. The temperature control system was able to maintain a constant temperature in the exposure vessel to ± 1.5°C.

2.3 Signal attenuation monitoring equipment

The signal attenuation was monitored with equipment similar to that described in the Electronic Industries Association Standard EIA-455-78.

2.4 Test environments

The experiments were conducted in several different environments, some of them simulating the environment in which the fiber cables are found: (a) 3.5 percent (by weight) NaCl solution, (b) a culturing solution (Table I) inoculated with sulfate-reducing bacteria (Desulfovibrio desulfuricans, ATCC*7757), (c) a culturing solution (Table II) inoculated with hydrogen-producing bacteria (Clostridium acetobutylicum, ATCC*824), (d) a mixture of the hydrogen-producing (c) and sulfate-reducing (b) bacteria in their mixed culturing solutions, and (e) various mixtures of H_2 and N_2 gases.

(a) The 3.5 percent NaCl solution was used to investigate whether corrosion of galvanized steel (material of the armor wire on cables that cross a body of water) can generate enough hydrogen eventually to cause signal attenuation in the fibers.

(b) The sulfate-reducing bacteria (SRB) medium was used to establish whether the increased rate of corrosion[5] in this medium will generate more hydrogen than in the 3.5 percent NaCl solution, and whether sulfides formed on the surface of galvanized steel or mild steel can keep the cathodically generated hydrogen in the atomic state, thus facilitating its entry into the fiber.

(c) The hydrogen-producing bacteria medium was used to establish the effect of environmentally generated hydrogen with and without the presence of corroding metals, that is whether the bacteria-and corrosion-generated hydrogen effects are additive.

The above test environments were selected because: (a) optical fiber cables are often placed at salt water crossings; (b) SRB are commonly found in the bottom mud of seas, rivers, ponds and in soils, which are places where optical fiber cables have been installed; (c) hydrogen-producing bacteria can be found in some soils, human and animal feces, sewage sludges, and food processing plants.[6, 7, 8] Effluents from these sources can find their way into the anaerobic bottom muck of the bodies of water where optical fiber cables are placed. It is less likely, but not impossible, that these bacteria can be found in the

* ATCC = American Type Culture Collection
12301 Parklawn Drive, Rockville, MD 20852

underground plant, e.g., due to sewer pipe failures. However, the underground plant can be cleaned and aerated, while the water crossings can not. We have found both SRB and hydrogen-producing bacteria in a mud sample collected at a cable crossing during a field investigation.[9]

TABLE I

Composition of the SRB Test Medium

Component	Concentration gram/liter
KH_2PO_4	0.5
NA_2SO_4	2.7
$MgSO_4 \cdot 7H_2O$	2.0
$FeSO_4 \cdot 7H_2O$	0.15
NH_4 Cl	1.0
$CaCl_2$	0.18
Sodium Lactate (60% solution)	4.0 ml/l

The pH of the solution is adjusted to 7.5 ± 0.3 with 5% (by weight) NaOH solution.

TABLE II

Culturing Solution for Clostridium Acetobutylicum

5 gram	Bacto-peptone
5 gram	Bacto-tryptone
5 gram	Yeast extract
10 gram	Glucose
0.005 gram	Hemin
0.2 ml	0.5% solution of vitamin K, in 95% ethanol
20 ml	Salts solution*
1000 ml	Deionized water

The solution pH was adjusted to 7.3 ± 0.2 and degassed with N_2.

After transferring the culturing solution into the test chambers and further purging with N_2, 1 milli-mole of Na_2S was added as reducing agent.

* Salts Solution contains per 1 liter of deionized water

0.23 gram	$CaCl_2 \cdot 2H_2O$
0.48 gram	$MgSO_4 \cdot 7H_2O$
1.0 gram	K_2HPO_4
1.0 gram	KH_2PO_4
10.0 gram	$NaHCO_3$
2.0 gram	NaCl

2.5 Testing procedure

The heater units in the test chambers were adjusted so that the outer surface temperatures of the liquid containing test chambers were 32 ± 2°C. These temperatures were monitored throughout the experiment. Previously, it was established that the solution temperature at the location of the fiber is about 2.4°C warmer than on the outer surface of the test chamber.[5] Thus, the experiments in the liquid environments were conducted at 34.4 ± 2°C. In all test environments, the mild steel cylinder (cathode) that surrounded the fiber in one test cell was connected to the zinc ribbon (anode) by a one ohm resistor. The hydrogen generated on the cathode surface is generally proportional to the current between the anode and cathode of the steel-zinc galvanic couple. The current produced by the steel-zinc couple was monitored by measuring the millivolt drop across the one ohm resistor. The physically separate, but electrically connected, anode and cathode materials imitate partially corroded armor wire, where some zinc is left on the surface, but some of the underlying steel is exposed. In two test cells, the fibers were surrounded by galvanized steel cylinders, imitating the effect of galvanized steel armor wire where the underlying steel is not exposed. The fiber in one test cell was not surrounded by metal, imitating a cable without armor wire.

When the fibers were exposed to the 3.5 percent NaCl solution, one of the test cells, where the fiber was surrounded with galvanized steel, was deaerated with N_2 for 24 hours at the start of the experiment; the others were not. For both the SRB and the hydrogen-producing bacteria culturing solutions, all test chambers were purged with N_2 for 24 hours before inoculation and for 6 hours after inoculation, because the bacteria needed anaerobic conditions.

The signal attenuation was measured against one or two unexposed reference fibers for all the test fibers at 54 different wavelengths between 1,100 and 1,600 nanometers. A typical spectral attenuation plot is illustrated in Figure 3. From these data the hydrogen indicator, H_{ind} may be calculated. The hydrogen indicator was defined by Anderson et al.[4] as signal attenuation at 1240 nm, the wavelength of an absorption peak characteristic of hydrogen-caused darkening, less that at 1310 nm.

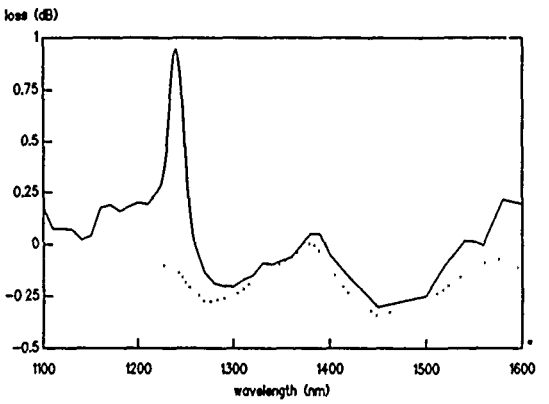

Figure 3. Typical spectral attenuation of optical fiber with (solid line) and without (dotted line) hydrogen.

2.6 Hydrogen analysis

The partial pressures of H_2 gas in the head spaces above the liquids and in the flowing gas phase in the H_2/N_2 mixtures were monitored frequently by analyzing samples for their H_2 content by gas chromatography. A Gow-Mac isothermal 580-type gas chromatograph with a 2.5 m, 3 mm diameter molecular sieve 5A column and a thermal conductivity detector was used. The carrier gas was 99.998% argon and its flowrate was 30 cc/min. The column, detector and injector temperatures were set at 50, 135 and 135°C, respectively, and the detector current was 40 mA. The detector signal was recorded and processed on a Spectra Physics integrator.

The chromatograph was calibrated with duplicate samples of 0.250 ml of 99.9% hydrogen and 0.500 ml of room air (about 21% oxygen and 78% nitrogen). Gases were sampled with a 0.5 ml gas-tight syringe with a valve.

3. Results

The most significant result of the experiments in this study is the signal attenuation, reported as H_{ind}, attained for the various test environments studied. Another significant result is the partial pressure of hydrogen [$p(H_2)$] measured in the test environments. In all the test environments, the attenuation (hydrogen indicator) follows $p(H_2)$. The

results obtained in the various test environments indicate the contribution of corrosion-generated and microbiologically-generated or -consumed hydrogen to the signal attenuation.

3.1 3.5 percent NaCl solution

In the three cells where the fibers were surrounded by metallic cylinders, the levels of corrosion-generated H_2, and, correspondingly, the hydrogen indicators, H_{ind}, of these fibers are high. In Figure 4A and B, the attenuation as a function of time at 1240 nm is compared to that of the 1300 nm window, and 1580 nm wave length for an optical fiber surrounded by a galvanized steel cylinder.

The experiments were conducted under four different conditions.

A. The fiber was surrounded by a galvanized steel cylinder, and the NaCl solution contained air. Figure 5 shows that up to 0.29 atm. $p(H_2)$ caused up to 4.6 dB/km H_{ind}.

B. The fiber was surrounded by a galvanized steel cylinder and the NaCl solution was deaerated with N_2. The corrosion of the galvanized steel generated up to 0.26 atm $p(H_2)$, and the maximum H_{ind} was 2.9 dB/km (Figure 6).

C. The fiber was surrounded by a mild steel cylinder that was connected to a helically wound zinc ribbon through a one ohm resistor. The galvanic corrosion reaction generated up to 0.4 atm. $p(H_2)$, and the H_{ind} rose to 3.2 dB/km (Figure 7).

D. In the cell without metal, corrosion did not take place, thus, there was no measurable H_2 in the head space, and the H_{ind} remained zero throughout the experiment.

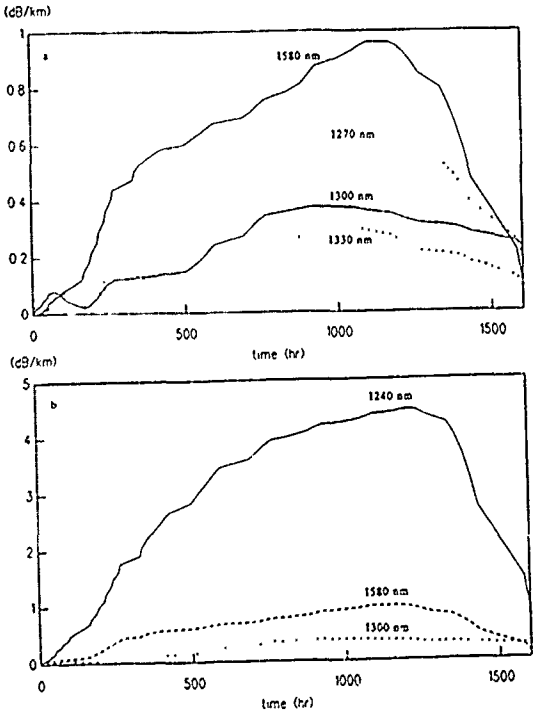

Figure 4. Change in attenuation at various wavelengths vs. time for an optical fiber in 3.5% NaCl and galvanized steel.

A. 1580, 1270, 1300, and 1330 nm
B. 1240, 1580 and 1300 nm

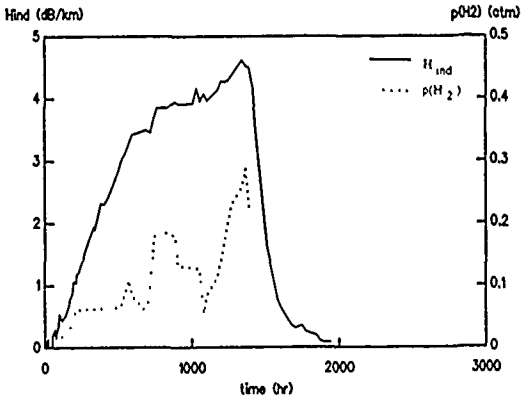

Figure 5. Optical fiber H_{ind} (solid line) and $p(H_2)$ (dotted line) vs. time for a cell containing non-deaerated 3.5% NaCl solution and galvanized steel.

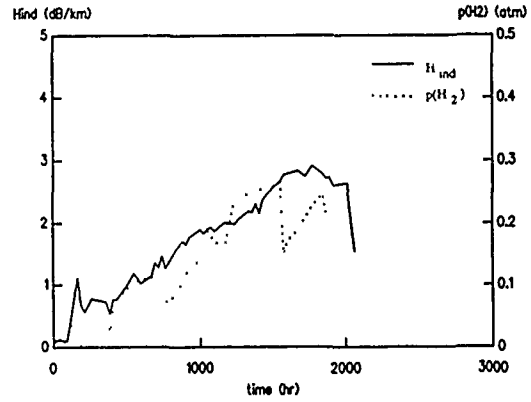

Figure 6. Optical fiber H_{ind} (solid line) and $p(H_2)$ (dotted line) vs. time for a cell containing deaerated 3.5% NaCl solution and galvanized steel.

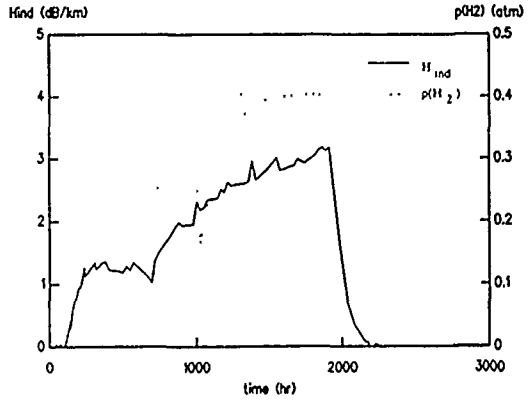

Figure 7. Optical fiber H_{ind} (solid line) and $p(H_2)$ (dotted line) for a cell containing non-deaerated 3.5% NaCl and a zinc/steel galvanic couple.

3.2 Sulfate-reducing bacteria (SRB) environment

At the start of these experiments, the culturing solution (Table I) without SRB corroded the metal cylinders and generated hydrogen, which caused signal-attenuation in the fibers. In the various test cells, described below, the following changes were observed:

A. In one cell, the fiber was surrounded by a mild steel cylinder that was connected to a helically wound zinc ribbon through a one ohm resistor. Here, besides $H_{ind.}$ and $p(H_2)$, the galvanic current (I) between zinc and steel was also measured (Figure 8). Because of the corrosiveness of the deaerated, non-inoculated SRB culturing solution[5], the $p(H_2)$ reached 0.3 atm. in less than 500 hours, and the corresponding $H_{ind.}$ had risen to over 3 dB/km. After inoculation with SRB, the $p(H_2)$ became too low to measure in less than 100 hours. The corresponding $H_{ind.}$ also abated to negligible values. Between 1150 and 1630 hours of exposure, $p(H_2)$ gradually increased to 0.12 atm. and the corresponding $H_{ind.}$ had risen to 1.1 dB/km. The galvanic current (I) first gradually decreased, then significantly increased, for a short time, as a result of SRB inoculation. As the SRB took control at 670 hours of exposure, I increased for about 200 hours, then slowly abated to a low level. At 4150 hours, when 14 liters of the solution was replaced, the current again showed a sudden increase, followed by gradual decrease.

B. In one cell, the fiber was surrounded by a galvanized steel cylinder (Figure 9). The limited corrosion of the galvanized steel cylinder by non-inoculated SRB culturing solution generated only up to $p(H_2)$ = 0.006 atm. of hydrogen, and the corresponding $H_{ind.}$ reached only 0.83 dB/km. After inoculation with SRB, the $p(H_2)$ and $H_{ind.}$ both became negligibly low. After 500 hours of exposure, a limited amount of hydrogen was generated for short time periods, producing relatively low $H_{ind.}$ (0.1-0.2 dB/km). After about 900 hours of exposure, only a trace amount of hydrogen was found in the head space, and $H_{ind.}$ became non-measurable.

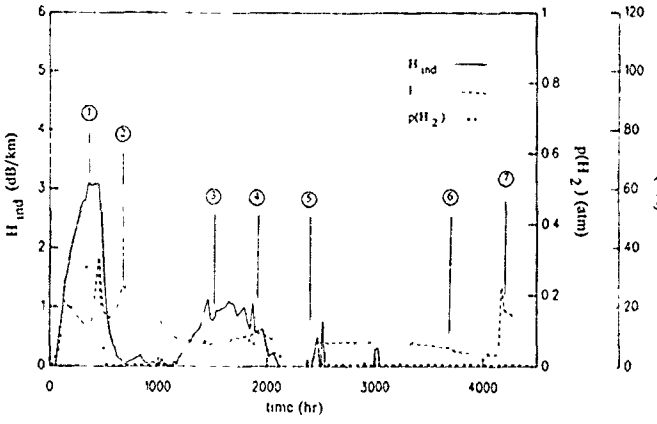

Legend

(1) SRB inoculated into the culturing solution

(2) SRB proliferated, estimated bacteria count 10^8 – 10^9/ml

(3) Estimated SRB count 10^7 – 10^8/ml

(4) Estimated SRB count 10^6 – 10^7/ml

(5) Estimated SRB count 10^5 – 10^6/ml

(6) Estimated SRB count 10^4 – 10^5/ml

(7) Under N_2 atmosphere, 14 liters of the solution was replaced with fresh SRB culturing solution
Estimated SRB count 10^6 – 10^7/ml

Figure 8. Optical fiber $H_{ind.}$ (solid line), $p(H_2)$ (dotted line) and I (dashed line) vs. time for a cell containing a steel/zinc couple and sulfate-reducing bacteria culture.

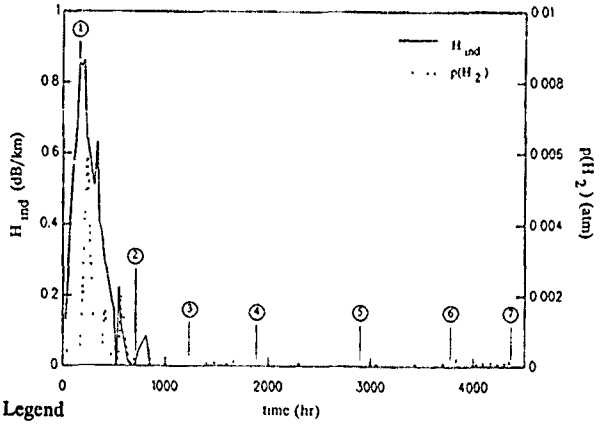

Legend

(1) SRB inoculated into the culturing solution

(2) Estimated SRB count 10^9 – 10^{10}/ml

(3) Estimated SRB count 10^{10} – 10^{11}/ml

(4) Estimated SRB count 10^6 – 10^7/ml

(5) Estimated SRB count 10^6 – 10^7/ml

(6) Estimated SRB count 10^6 – 10^7/ml

(7) Under N_2 atmosphere, 14 liters of the solution replaced with fresh SRB culturing solution.

Figure 9. Optical fiber $H_{ind.}$ (solid line) and $p(H_2)$ (dotted line) vs. time for a cell containing sulfate-reducing bacteria culture and galvanized steel.

3.3 Hydrogen-producing bacteria environment

The hydrogen-producing bacteria (Clostridium acetobutylicum) was propagated from a freeze-dried pellet in cooked meat with glucose medium (ATCC 593), that was placed in an incubator at 37±2°C. When the bacteria revived, indicated by turbidity of the solution (gas evolution), the revitalization medium with the bacteria was transferred into culturing solutions (Table II). The hydrogen-producing bacteria experiments were carried out in test cells without metal present and with a galvanized steel cylinder surrounding the fiber.

A. One cell had no metal and contained only fiber (Figure 10). The formation of hydrogen was very fast after inoculation of the solution,

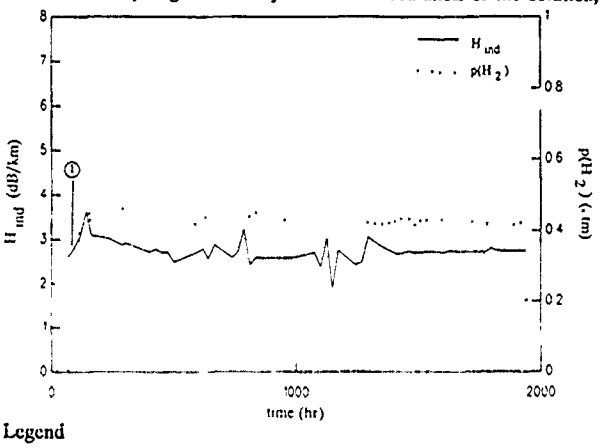

Legend

(1) Clostridium acetobutylicum inoculated into the culturing solution.

Figure 10. Optical fiber $H_{ind.}$ (solid line) and $p(H_2)$ (dotted line) for a cell containing a hydrogen-producing bacteria culture with no metal.

and $p(H_2)$ became 0.47 atm. within two days. The corresponding $H_{ind.}$ rose up to 3.7 dB/km. During the experiment, $p(H_2)$ settled around 0.42 atm. and the $H_{ind.}$ around 2.7 dB/km.

B. One cell had the fiber surrounded by a galvanized steel cylinder (Figure 11). The corrosion of galvanized steel produced some hydrogen even before inoculation with hydrogen producing bacteria. Within a few days, $p(H_2)$ reached 0.52 atm. and eventually climbed up to 0.63 atm. Correspondingly, the $H_{ind.}$ reached 3.2 dB/km within 144 hours and at the highest $p(H_2)$ it was 4.4 dB/km.

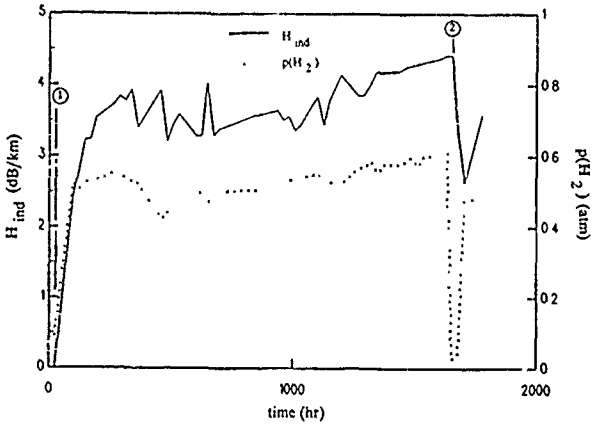

Legend

(1) Clostridium acetobutylicum inoculated into the culturing solution

(2) Under N_2 atmosphere, 12 liters of the solution removed and replaced with non-inoculated SRB culturing solution + 120 grams of glucose

Figure 11. Optical fiber $H_{ind.}$ (solid line) and $p(H_2)$ (dotted line) vs time for a cell containing hydrogen producing bacteria culture and galvanized steel.

3.4 Mixed hydrogen-producing and sulfate-reducing bacteria environment

These experiments were carried out by gradual replacement of inoculated SRB-culturing solutions with inoculated hydrogen-producing bacteria cultures and vice-versa, until all cells contained 50-50 percent mixture of the two bacteria-culturing solutions.

A. In one cell, the original solution contained only hydrogen-producing bacteria and the test cell did not contain any metal (Figure 12). The test started with $p(H_2)$ = 0.42 atm, and the $H_{ind.}$ was 2.7 dB/km. After 1960 hours of exposure time, 12 liters of the hydrogen-producing bacteria culture was replaced with non-inoculated SRB culturing solution and 120 grams of glucose. Inoculation with 750 cc SRB culture resulted in 50 percent reduction of the $p(H_2)$ and 58 percent reduction of the $H_{ind.}$. Further replacement of 7 liters of the solution with SRB culture reduced the $p(H_2)$ to between 0.02 and 0.035 atm and the $H_{ind.}$ became negligible. The SRB suppressed hydrogen production between 2700 and 3230 hours of exposure, but after 3230 hours, both $p(H_2)$ and $H_{ind.}$ started to increase. Adding dextrose to the solution further increased hydrogen production. The $p(H_2)$ went up to 0.58 atm., and the $H_{ind.}$ reached 7.2 dB/km. At this point, the SRB content of the solution was relatively low (10^3 – 10^4/ml). However, after these high $p(H_2)$ and $H_{ind.}$ levels, in spite of adding dextrose and SRB nutrients, both of these parameters went down to non-measurably low levels. At the end of this experiment, the pH of the solution was found to be between 3.5 and 4.0.

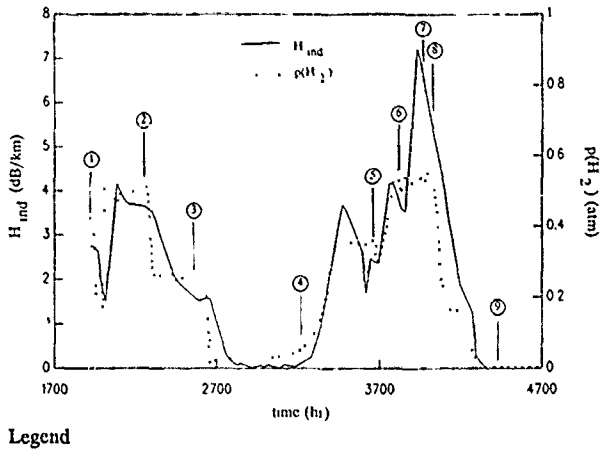

Legend

(1) Under N_2 atmosphere, 12 liters of the solution were removed and replaced with SRB culturing solution (without SRB) + 120 grams of glucose

(2) The solution was inoculated with 750 ml of SRB culturing solution that had an estimated SRB count of 10^7 – 10^8/ml

(3) Under N_2 atmosphere, ¼ of the solution (7 liters) was taken out and replaced with SRB culturing solution that had an estimated SRB count of 10^6 – 10^7/ml

(4) Estimated SRB count 10^6 – 10^7/ml. Test for hydrogen-producing bacteria was positive

(5) 60 grams of dextrose added to the solution

(6) 200 grams of dextrose added to the solution

(7) Estimated SRB count 10^3 – 10^4/ml

(8) 27g Na_2SO_4 + 20g $MgSO_4 \cdot 7H_2O$ + 16ml Na-lactate + 50 g dextrose added to the solution.
Under N_2 atmosphere, the solution was changed to 50 percent SRB and 50 percent hydrogen-producing bacteria

(9) Estimated SRB count 0
Test for hydrogen producing bacteria was positive and pH of test solution was 3.5-4.0.

Figure 12. Optical fiber H_{ind} (solid line) and $p(H_2)$ (dotted line) vs. time for a cell containing a hydrogen-producing bacteria culture with no metal with additions of sulfate-reducing bacteria culture.

B. In another cell, the fiber was surrounded by a galvanized steel cylinder, and the original solution contained only hydrogen producing bacteria (Figure 13). The low $p(H_2)$ and sharp dip in the $H_{ind.}$ curve at 1680 hours of exposure coincides with the replacement of 12 liters of the hydrogen-producing bacteria culture with non-inoculated SRB culturing solution. Inoculation of the test cell with 750 cc of SRB culture caused a temporary 37 percent reduction of $p(H_2)$ that was almost completely recovered in less than 340 hours. The corresponding $H_{ind.}$ gradually decreased from 4.2 to 3.6 dB/km. Further replacement of 7 liters of the solution with SRB culture caused a drop in $p(H_2)$ from 0.5 to 0.05 atm. The corresponding $H_{ind.}$ changed from 3.6 to 1.9 dB/km. Both $p(H_2)$ and $H_{ind.}$ immediately started to recover and at 3200 hours exposure time reached 0.47 atm. and 3.3 dB/km, respectively. The SRB concentration at this point was low (10^2 – 10^3/ml). The change of the culturing solution to 50-50 percent SRB and hydrogen-producing bacteria reduced the $p(H_2)$ and $H_{ind.}$ to low levels. Addition of first 60 grams, then 200 grams of dextrose raised the $p(H_2)$ to 0.52 atm and the $H_{ind.}$ 3.7 dB/km. These $p(H_2)$ and $H_{ind.}$ levels were maintained for the rest of the experiment. Addition of SRB nutrients increased the SRB population from an estimated 10^5 – 10^6/ml to 10^8 – 10^9/ml. At the end of the experiment, the pH of the solution was 6.5 - 7.0.

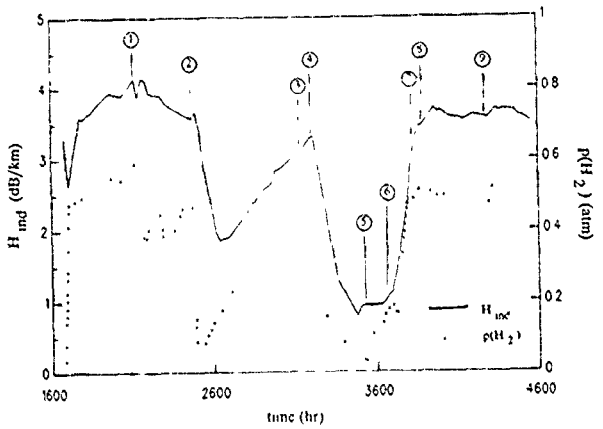

Legend

(1) The solution was inoculated with 750 ml of SRB culturing solution that had an estimated SRB count of $10^7 - 10^8$/ml

(2) Under N_2 atmosphere, ¼ of the solution (7 liters) was taken out and replaced with SRB culturing solution that had an estimated SRB count of $10^7 - 10^8$/ml

(3) Estimated SRB count $10^2 - 10^3$/ml. Test for hydrogen producing bacteria was positive

(4) Under N_2 atmosphere, the solution was changed to 50 percent SRB and 50 percent hydrogen-producing bacteria

(5) 60 grams of Dextrose added

(6) 200 grams of Dextrose added

(7) Estimated SRB count $10^5 - 10^6$/ml

(8) 27g Na_2SO_4 + 20g $MgSO_4 \cdot 7H_2O$ + 16 ml Na-lactate + 50g Dextrose added

(9) Estimated SRB count $10^8 - 10^9$/ml
Test for hydrogen producing bacteria was positive and pH of test solution was 6.5-7.0

Figure 13. Optical fiber $H_{ind.}$ (solid line) and $p(H_2)$ (dotted line) vs. time for a cell containing hydrogen-producing bacteria culture and galvanized steel with additions of sulfate-reducing bacteria culture.

C. In a third cell, the fiber was surrounded by a mild steel cylinder that was connected to a helically wound zinc ribbon through a one ohm resistor. The original solution contained only SRB. The estimated SRB concentration was $10^6 - 10^7$/ml (Figure 14). Seven liters of the solution were replaced with hydrogen-producing bacteria culture at 4370 hours of exposure, causing a temporary rise in the galvanic current between zinc and steel but leading to no measurable hydrogen production or $H_{ind.}$. Addition of first 60 grams, then 200 grams of dextrose to the solution at 5395 and 5570 hours, respectively, made $p(H_2)$ rise from trace amount to 0.80 atm, and the corresponding $H_{ind.}$ increased from non-measurable to 5.5 dB/km. The galvanic cell current also increased 20 times in magnitude before the addition of hydrogen-producing bacteria. During the steep $p(H_2)$ and $H_{ind.}$ increase, the approximate SRB count was very high ($10^9 - 10^{10}$/ml). Addition of SRB nutrients at 5760 hours did not stop the increase of hydrogen evolution. Changing the solution to 50-50 percent SRB and hydrogen-producing bacteria cultures at 5760 hours gave a boost to the hydrogen production and helped to increase the $H_{ind.}$. With the drastic increase of $p(H_2)$ and I, the steel cylinder turned light gray and about 90 percent of the black deposit was removed from its surface. As the galvanic current passed its peak, the steel cylinder became gradually darker shades of grey. The estimated SRB count toward the end of the experiment was $10^6 - 10^7$/ml. The pH of the solution was between 6.0 and 6.5.

D. In a fourth cell, the fiber was surrounded by a galvanized steel cylinder, and the original solution contained only SRB (Figure 15). Replacement of 7 liters of the solution with hydrogen-producing bacteria culture did not produce hydrogen evolution beyond a trace amount. The estimated SRB concentration was $10^7 - 10^8$/ml. Changing the solution to 50-50 percent SRB and hydrogen-producing bacteria cultures did not increase the level of hydrogen production. First 60 gram, then 200 gram additions of dextrose, at 5590 and 5775 hours of exposure, respectively, started to increase hydrogen production, and $p(H_2)$ rose to 0.32 atm. The $H_{ind.}$ increased to 3.7 dB/km. Addition of SRB nutrients helped to increase their concentration from $10^5 - 10^6$/ml to $10^6 - 10^7$/ml. At the end of the experiment, the solution pH was between 7.0 and 7.5.

At the end of the experiments, the solutions of SRB and hydrogen-producing bacteria mixtures were analyzed by gas chromatography for fermentation waste products. These test results, together with the pH data, are listed in Table III.

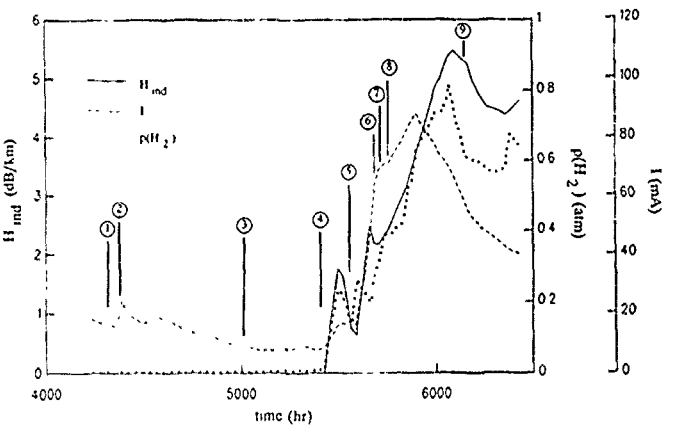

Legend

(1) Estimated SRB count $10^6 - 10^7$/ml

(2) Under N_2 atmosphere, ¼ of the solution (7 liters) was taken out and replaced with inoculated Clostridium acetobutylicum culturing solution

(3) Estimated SRB count $10^7 - 10^8$/ml
Test for hydrogen producing bacteria was positive

(4) 60 grams of Dextrose added to the culturing solution

(5) 200 grams of Dextrose added to the culturing solution

(6) Black deposit removed from the surface of the steel cylinder

(7) Estimated SRB count $10^9 - 10^{10}$/ml

(8) Under N_2 atmosphere, the solution was changed to 50 percent SRB and 50 percent hydrogen-producing bacteria
27g Na_2SO_4 + 20g $MgSO_4 \cdot 7H_2O$ + 16 ml Na-lactate + 50g Dextrose added to the culturing solution

(9) Estimated SRB count $10^6 - 10^7$/ml
Test for hydrogen producing bacteria was positive and pH of test solution was 6 0-6.5

Figure 14. Optical fiber $H_{ind.}$ (solid line) $p(H_2)$ (dotted line) and I (dashed line) vs. time for a cell containing a steel/zinc couple and sulfate-reducing bacteria culture with additions of hydrogen-producing bacteria culture.

3.5 H_2/N_2 gas mixtures

Figure 16 shows the $H_{ind.}$ as a function of hydrogen exposure time at 1 atm. H_2 and 21°C. $H_{ind.}$ follows an exponential decay, as described in the literature [1-3], and has a relaxation time, τ, of about 200 hrs. Our values for saturation $H_{ind.}$ and τ agree well with previously published work [1-3].

Figure 17 shows the saturation $H_{ind.}$ vs. $p(H_2)$ at three different temperatures, 21, 31, and 41°C. The saturation $H_{ind.}$ increases approximately linearly with increasing $p(H_2)$ and decreases with increasing temperature. The slopes of the three lines are 9.0, 7.8 and 7.0 dB/(km atm) for 21, 31, and 41°C, respectively. The relaxation time for $H_{ind.}$ decreases with increasing temperature, as expected. Again, these results agree well with previously published work[1-3].

TABLE III

Results of the Dextrose Fermentation Waste Products Analysis

Metal in test cell	Original solution	Additive solution	Figure #	Waste product component (percent)					Solution pH
				Acetone	n-Butanol	Acetic acid	Butyric acid	iso-Pentanoic acid	
None	Hydrogen-producing bacteria	SRB	12	0.050	0.081	0.065	0.580	—	3.5-4.0
Galvanized steel	Hydrogen-producing bacteria	SRB	13	—	—	—	—	0.125	6.5-7.0
Steel/zinc couple	SRB	Hydrogen-producing bacteria	14	0.051	0.037	0.109	0.116	—	6.0-6.5
Galvanized steel	SRB	Hydrogen-producing bacteria	15	0.040	0.011	0.004	0.140	—	7.0-7.5

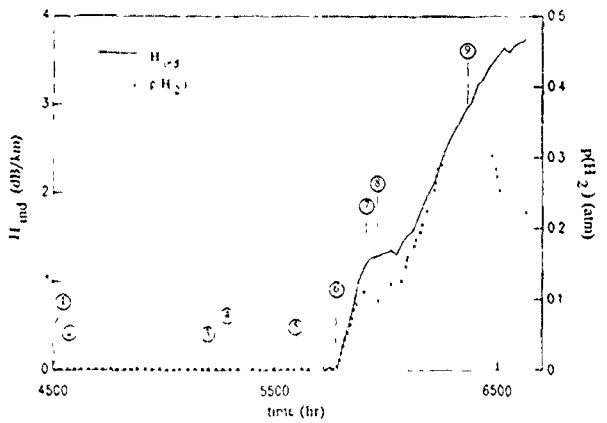

Legend

(1) Estimated SRB count 10^7 – 10^8/ml

(2) Under N_2 atmosphere, ¼ of the solution (7 liters) was taken out and replaced with inoculated Clostridium acetobutylicum solution

(3) Estimated SRB count, 10^8 – 10^9/ml
Test for hydrogen producing bacteria was positive

(4) Under N_2 atmosphere the solution was changed to 50 percent SRB and 50 percent hydrogen-producing bacteria

(5) 60 grams of Dextrose added to the solution

(6) 200 grams of Dextrose added to the solution

(7) Estimated SRB count 10^5 – 10^6/ml

(8) 27g Na_2SO_4 + 20g $MgSO_4 \cdot 7H_2O$ + 16ml Na-lactate + 50g Dextrose added to the solution

(9) Estimated SRB count 10^6 – 10^7/ml
Test for hydrogen producing bacteria was positive and pH of test solution was 7.0-7.5

Figure 15. Optical fiber $H_{ind.}$ (solid line) and $p(H_2)$ (dotted line) vs. time for a cell containing sulfate-reducing bacteria culture and galvanized steel with additions of hydrogen-producing bacteria culture.

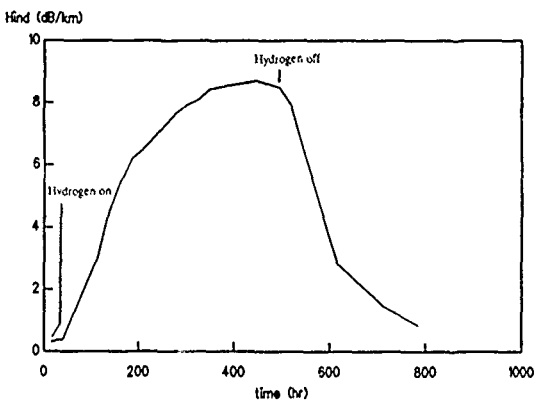

Figure 16. Optical fiber $H_{ind.}$ vs. time for 1 atm H_2 at 21°C.

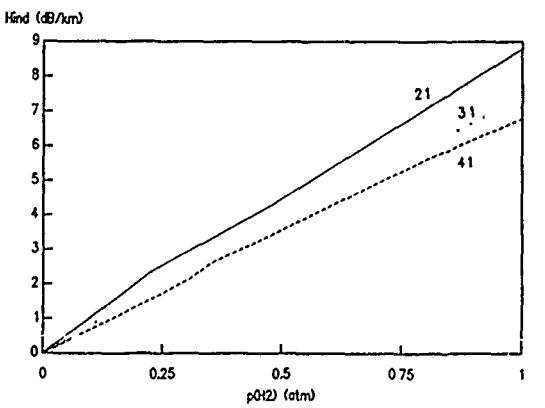

Figure 17. Saturation $H_{ind.}$ vs. $p(H_2)$ for H_2/N_2 gas mixtures at 21°C, 31°C, and 41°C

4. Discussion of the Results

4.1 Contribution by the corrosion process

The experiments conducted in 3.5 percent NaCl solution (Figures 5, 6, 7) and in non-inoculated SRB culturing solutions (Figures 8, 9), show that hydrogen, generated at the cathode of a corrosion cell, can enter the fiber and cause signal attenuation. The $H_{ind.}$ changes with $p(H_2)$. At the time the experiments in 3.5 percent NaCl solution were conducted, it was necessary to take duplicate gas samples from the head space of all the four cells in 125 ml glass containers equipped with two stopcocks at their two ends. These containers were then sent from Morristown to Navesink (about 60 miles) for analysis by gas chromatography. During the elapsed time of 5-7 hours between sampling and analysis, an appreciable amount of hydrogen was lost from the gas sample containers by diffusion. This fact renders the $p(H_2)$ data from the 3.5 percent NaCl solution tests quantitatively unreliable. Therefore, the $H_{ind.}$ data from these tests are compared to those obtained with H_2/N_2 gas mixtures to obtain the approximate $p(H_2)$. This comparison indicates that the hydrogen indices of 4.6 dB/km, 3.0 dB/km, and 2.9 dB/km correspond with hydrogen partial pressures of 0.6 atm., 0.4 atm., and 0.4 atm., respectively. For the ensuing experiments with bacteria culturing media, the test cells were equipped with gas sampling ports (glass-tube - vacuum stopcock - teflon septum), and a gas chromatograph was installed in the laboratory. This arrangement allowed us to analyze the hydrogen gas content of the head space within a few seconds after sampling.

4.2 Sulfate-reducing bacteria environment

Sulfate-reducing bacteria consumed the corrosion-generated hydrogen in less than 100 hours to a non-measurable level. This observation supports the theory that SRB increases the rate of corrosion by consuming the cathodic hydrogen, thereby depolarizing the cathode.[10-13] The sudden increase of the galvanic current between steel and zinc after inoculation also supports the cathodic depolarization theory (Figure 8).

The gradual increase of $p(H_2)$ to 0.12 atm. and the accompanying augmentation of $H_{ind.}$ to 1.1 dB/km between 1150 and 1630 hours can be explained by a temporary take over of hydrogen-producing SRB (Figure 8).[14] A further support of this statement is that the galvanic current decreased during the same time period; thus, the increased hydrogen could not be generated by corrosion. The SRB are primarily hydrogen-consuming bacteria; this characteristic is illustrated by the gradual abatement between 1630 and 2400 hours of both $p(H_2)$ and $H_{ind.}$ values to trace and non-measurable levels, respectively. Again, the re-establishment of the depolarization effect by the SRB was accompanied by an increase of the galvanic current. The general tendency of gradual decrease of the galvanic current was most likely caused by the build-up of corrosion products on the anode surface and the thickening of the sulfide film formed on the cathode. The sudden increase of galvanic currents at 4150 hours was most likely caused by the physical action of solution removal and addition (Figure 8).

The corrosion of galvanized steel (Figure 9), in non-inoculated SRB culturing solution generated far less hydrogen $[p(H_2) = 0.006$ atm.$]$ than the zinc-steel galvanic couple (Figure 8). Correspondingly, the highest $H_{ind.} = 0.85$ dB/km was also low. It seems that after the hydrogen was consumed by the SRB (330 hours exposure), the hydrogen formation reoccurred at low levels for short times ($p(H_2)$ between 0.0004 and 0.002 atm.) with accompanying small increases of signal attenuation ($H_{ind.}$ between 0.09 and 0.2 dB/km). These anomalies were probably caused by temporary take-over of hydrogen-producing SRB.[14]

4.3 Hydrogen-producing bacteria environment

The hydrogen formation in the Clostridium acetobutylicum culturing solution was caused by the bacterial fermentation of glucose and does not require the presence of metal for this process. The hydrogen formation is fast both in the presence and absence of corroding metal. Comparing Figures 10 and 11 indicates that, although the electrochemical and microbiological contributions to hydrogen formation are additive, the microbiological contribution is more substantial. It is possible that the abundant amount of hydrogen produced by the bacteria represses the electrochemical hydrogen formation $H^+ + e^- \rightarrow H$. The strong loss and fast recovery of $p(H_2)$ and the accompanying dip of $H_{ind.}$ in Figure 11 were caused by partial solution replacement under N_2 pressure.

4.4 Mixed sulfate-reducing and hydrogen-producing bacteria environment

The studies in mixed sulfate-reducing and hydrogen-producing bacteria environments were approached from two different directions: (A) hydrogen-producing bacteria environment inoculated gradually with SRB, and (B) SRB environment inoculated gradually with hydrogen-producing bacteria.

(A) In the cell without corroding metal (Figure 12), inoculation with 750 cc SRB caused appreciable reduction of $p(H_2)$ and $H_{ind.}$, and further inoculation with 7 liters of SRB reduced both of these parameters to trace levels. Both of the above inoculations took place under N_2 atmosphere, and the more or less instantaneous drops of $p(H_2)$ were most likely caused by physical removal of hydrogen. The hydrogen consumption by SRB, estimated SRB count of $10^6 - 10^7$/ml, kept the $p(H_2)$ at the levels created by the N_2 pressure. As the sharp drop and recovery at 1980 hours indicate, physical removal of H_2 alone allows fast recovery of $p(H_2)$. It is important to note that the hydrogen-producing bacteria were able to overcome the hydrogen-consuming effect of a relatively high concentration of SRB. Addition of dextrose provided the fermentable hydrocarbons needed to reach high levels of $p(H_2)$ and $H_{ind.}$. The steep decline of the $H_{ind.}$ and $p(H_2)$ started at a relatively low SRB concentration ($10^3 - 10^4$/ml). Despite adding SRB nutrients and glucose, $p(H_2)$, $H_{ind.}$ and the SRB concentration went down to non-measurably low levels and zero, respectively. The sudden decrease of both $p(H_2)$ and $H_{ind.}$ after reaching their highest peak is attributed to the decrease of the pH. The solution became acidic because the dextrose fermentation process produces acetic and butyric acids. Below pH 5, these acids are no longer produced; however, n-butanol and acetone are formed with a net consumption of hydrogen. This result is in agreement with the findings of Ford and Mitchell.[6] Our results also show that the SRB can not live in such acidic environment. The high concentration of butyric acid and moderate concentration of acetic acid are most likely responsible for the high acidity (Table III). The combined high level of reduced components, acetone and n-butanol, is responsible for the total consumption of hydrogen (Figure 12).

In the cell where the galvanized steel cylinder surrounded the fiber (Figure 13), inoculation with 750 cc SRB culture caused little change in the $H_{ind.}$ The sudden drop in $p(H_2)$ can be attributed to the application of N_2 pressure, and the presence of SRB slowed down the partial $p(H_2)$ recovery. Further inoculations first with 7 liters of SRB solution, then by a change to a 50-50 percent mixture of SRB and hydrogen-producing bacteria cultures, had more appreciable effects. At both times, the $p(H_2)$ dropped suddenly because of the N_2 pressure, and the $H_{ind.}$ also decreased appreciably. The slow recovery of $p(H_2)$ and $H_{ind.}$ are attributed to the presence of SRB. The final $p(H_2)$ and $H_{ind.}$ recovery, that started at 3700 hours exposure time, was aided by the addition of dextrose. It seems that the biological hydrogen formation is primarily dependent on the quantity of available fermentable hydrocarbons. This statement is supported by the fact that, although addition of SRB nutrients increased the estimated SRB count from $10^5 - 10^6$/ml to $10^8 - 10^9$/ml, the added dextrose maintained the $p(H_2)$ and $H_{ind.}$ at high levels to the end of the experiment. The solution pH of 6.5 - 7.0 at the end of the experiment assured the survival of SRB. The finding of iso-pentanoic acid instead of acetic and butyric acid is a surprise (Table III). The absence of reduced components, acetone and n-butanol, the production of which consume hydrogen, can explain the consistently high level of $p(H_2)$ at the end of the experiment (Fig. 13).

(B) Figure 14 indicates that in the cell where the fiber is surrounded with a steel cylinder, connected to a zinc ribbon, and the solution contained only SRB, inoculation with 7 liters of hydrogen-producing bacteria did not generate a measurable quantity of hydrogen. The small increase of I at 4390 hours of exposure is probably caused by disturbing the black deposit on the steel cylinder with the exchange of the 7 liter of solution. The $p(H_2)$ and $H_{ind.}$ started to increase only after the addition of dextrose to the solution, illustrating that the biological hydrogen formation depends on the availability of fermentable hydrocarbons, even in the presence of highly concentrated SRB ($10^7 - 10^8$/ml to $10^9 - 10^{10}$/ml). The hydrogen evolution became so intense that it removed approximately 90 percent of the black deposit from the steel cylinder. The clean steel cathode allowed the galvanic current (I) to increase about 20 times, and, in turn, contributed to the hydrogen production. The $p(H_2)$ and $H_{ind.}$ values continued to increase even after the addition of SRB nutrients. This process was also most likely helped by changing the solution to a 50-50 percent mixture of SRB and hydrogen-producing bacteria cultures. Toward the end of the experiment, the $p(H_2)$ and $H_{ind.}$ settled at high values. This is most likely due to the bacterial contribution to hydrogen formation, because I continuously decreased after about 5900 hours of exposure time, thereby decreasing the electrochemical contribution of H_2. At the end of the solution, pH was slightly acidic (6.0 - 6.5), and the SRB concentration remained quite high ($10^6 - 10^7$/ml). The moderate levels of acetic and butyric acids can explain the slightly acidic nature of this solution (Table III). The moderate concentration of the reduction products, acetone and n-butanol, that are formed by hydrogen consumption, are probably responsible for the moderate dip in $p(H_2)$ after 5900 hours of exposure (Figure 14).

In the cell where the fiber was surrounded by galvanized steel and the solution contained only SRB (Figure 15), inoculation with 7 liters of hydrogen-producing bacteria solution did not start hydrogen formation. The estimated SRB count was high ($10^8 - 10^9$/ml). Changing the solution to a 50-50 percent mixture of SRB and hydrogen-producing bacteria cultures did not cause any changes either. The $p(H_2)$ and $H_{ind.}$ started to increase rapidly after adding dextrose to the solution. This observation further underlines the statement that the biological hydrogen production is dependent on the available fermentable hydrocarbon. The addition of SRB nutrient helped to increase the SRB count from an estimated $10^5 - 10^6$/ml to $10^6 - 10^7$/ml but did not initiate any effective hydrogen consumption. At the end of the experiment, the solution pH was between 7.0 and 7.5. This condition helps to maintain the high concentration of SRB. The very low level of acetic acid is most likely responsible for the neutral pH (Table III). The moderate to small degree of acetone and n-butanol formation (that consumes hydrogen) is the probable cause of the dip in $p(H_2)$ towards the end of the experiment (Figure 15).

5. Summary

Laboratory studies of the signal-attenuating effect of hydrogen in optical fibers indicate the following:

(a) Corrosion of galvanized steel, the material of armor wires, can generate enough hydrogen to cause appreciable attenuation in optical fibers. This effect can take place only where the galvanized steel is exposed to the corrosive environment.

(b) Sulfate-reducing bacteria (SRB), if present in the environment as the only microbiological species, can consume the corrosion-generated hydrogen and eliminate the signal attenuation in the fiber. The SRB are sessile bacteria, they deposit on solid surfaces, and they are most effective at the surface where the corrosion-generated hydrogen evolves.

(c) Hydrogen-producing bacteria are spore-forming and generate hydrogen from fermentable hydrocarbons (in this experiment from dextrose). The hydrogen-producing process can take place both at a solid surface and in the bulk of the solution. Hydrogen produced by such bacteria can attenuate the signal in optical fibers both in the presence and absence of a corroding metal. In the presence of a corroding metal, the hydrogen production from the two sources is additive.

(d) In mixed SRB and hydrogen-producing bacteria culturing solutions, the hydrogen-producing process is dependent on the availability of fermentable hydrocarbons. In the absence or limited presence of such a hydrogen source, the fibers did not attenuate. In the abundant presence of fermentable hydrocarbons, a high degree of signal attenuation occurs even where the SRB count is very high.

(e) The waste products of the fermentation process by the hydrogen-producing bacteria used in these experiments are acetic and butyric acids When these acids lower the solution pH below 5.0, n-butanol and acetone formation (reduction processes) consume the hydrogen, and the fibers don't attenuate. In such an acidic environment the SRB do not survive. In one of the cells, the waste product was iso-pentanoic acid (Figure 13).

(f) Fiber attenuation experiments in H_2/N_2 gas mixtures show that the $H_{ind.}$ follows an exponential decay and has a relaxation time of 200 hrs at 21°C and 1 atm as was previously shown[1-3]. The saturation $H_{ind.}$ increases with increasing $p(H_2)$ and decreases with increasing temperature. The relaxation time for $H_{ind.}$ decreases with increasing temperature.

6. Conclusions

Based on the results of these experiments and the presence of hydrogen-producing bacteria found at one water crossing by a fiber cable, the authors conclude that in time many of the currently used cables at water crossings, constructed with an overlapped metal shield and jute-and-tar-covered galvanized steel armor wires, will be attenuated by hydrogen. The cause of the attenuation will be H_2 produced by corrosion, bacteria, or both.

Acknowledgments

We thank Messrs. W. T. Anderson, and R. M. Kanen for providing, installing, and explaining, the attenuation measuring equipment, Mr. E. Thomas for splicing optical fibers, Mrs. Irene Plitz for the initial hydrogen analyses, and Mr. D. M. Heffernan for designing, assembling, and installing the heater monitoring devices.

References

(1) S. R. Nagel, "Reliability Issues in Optical Fibers," in Reliability Considerations in Fiber Optic Applications, D. K. Paul ed., Proc. SPIE 717, 8 (1987).

(2) B. Wiltshire and M. H. Reeve, J. Lightwave Technology., 6 (2), 179 (1988).

(3) J. Stone, Lightwave Technology, LT-5 (5), 712 (1987).

(4) W. T. Anderson, A. J. Johnson, J. P. Kilmer, and R. M. Kanen, "Hydrogen Gas Effects on Installed Submarine Single-Mode Fiber Cables", Proc. 37th Int. Wire and Cable Symp., Nov. 1988.

(5) G. Schick, "Corrosion in the Presence of Sulfate-Reducing Bacteria", Paper #121 Corrosion/90, April 23-27, 1990, Bally's Hotel, Las Vegas, Nevada

(6) T. E. Ford and R. Mitchell, "Hydrogen Embrittlement: A Microbiological Perspective" Preprint of Paper #189 presented at CORROSION/89 April 17-21, 1989 in New Orleans, LA.

(7) V. Holdeman, E. P. Cato, and W. E. C. Moore, "Anaerobe Laboratory Manual" Fourth Edition, Virginia Polytechnic Institute and State University, Anaerobe Laboratory, Blacksburg, VA, 24060, November 1977.

(8) American Type Culture Collection (ATCC), "Catalogue of Bacteria and Bacteriophages", 17th edition, 1989, Editors: R. Gherna and P. Pienta, ATCC, 12301 Parklawn Drive, Rockville, MD, 20852.

(9) G. Schick and K. A. Tellefsen, Unpublished results.

(10) C. A. H. Von Wolzogen Kühr and L. S. Van der Vlugt, "The Graphitization of Cast Iron as an Electrobiochemical Process in Anaerobic Soils". Water (The Hague), Vol. 18, No. 16, 1934.

(11) J. Horvath, and M. Solti, "Beitrag Zum Mechanisms des Anaeroben Mikrobiologischen Korrosion der Metalle in Boden", Werkstoffe und Korosion, Vol. 10, No. 624, 1959.

(12) A. K. Tiller and G. H. Booth, "Polarization Studies of Mild Steel in Cultures of Sulfate-Reducing Bacteria, Part 2: Thermophilic Organisms", Trans. Faraday Soc. Vol. 58, No. 1, 1962.

(13) G. H. Booth and A. K. Tiller, "Polarization Studies of Mild Steel in Cultures of Sulfate-Reducing Bacteria. Part 3: Halophilic Organisms", Trans. Faraday Soc. Vol. 58, No. 2, 1962.

(14) I. P. Pankhania, "Hydrogen Metabolism in Sulfate-Reducing Bacteria and its Role in Anaerobic Corrosion" Biofouling, Vol. 1, pp 27-47, 1988.

AUTHORS

George Schick was born in Budapest, Hungary, in 1929. He received a Dipl. Eng. degree in Electrochemistry and Electrometallurgy from the Ecole Nationale Superieure d'Electrochimie et d'Electrometallurgie de Grenoble, France in 1958, the MS degree in Metallurgy from Massachusetts Institute of Technology in 1961, and the Ph.D. in Metallurgy and Materials Science from New York University in 1972. He worked at Bell Telephone Laboratories from 1961 to 1983 in the area of corrosion. In 1984 he joined Bell Communications Research where he is working on corrosion control and on the effects of the environment on optical fibers. Dr. Schick is a member of the National Association of Corrosion Engineers and the American Society for Testing and Materials.

Karen A. Tellefsen was born in Hackensack, NJ, in 1955. She received the B.S. degree in Chemistry from Stevens Institute of Technology in 1977 and the Ph.D. degree in Physical Chemistry from the University of Ottawa, Ontario in 1988. She worked for Energetics Science, Inc. between completing her B.S. degree and beginning her Ph.D. program, where she worked on the development of an electrochemical hydrazine vapor detector. She joined Bell Communications Research in 1988, where she is working on corrosion control and on the effects of the environment on optical fibers.

Aaron J. Johnson was born in Washington, DC, in 1958. He received the B.S. degree in Electrical Engineering and Economics from Carnegie-Mellon University in 1980 and the M.S. degree in Electrical Engineering from Georgia Institute of Technology in 1981. He worked for IIT Research Institute from 1982 to 1984, where he was engaged in electromagnetic compatibility analysis. Since 1984, he has been with Bell Communications Research where he has been developing novel optical fiber measurements and writing generic requirements for optical fibers and optical fiber cables. Mr. Johnson is a member of the Optical Society of America.

Casey J. Wieczorek is a member of the Optical Cable Group in Bellcore, Morristown, NJ. He joined Western Electric in 1967 and worked on various cable designs and manufacturing processes. He is currently responsible for the development of generic requirements and test procedures for optical cables. He holds a B.S. degree in Mechanical Engineering from Fairleigh Dickinson University and did graduate work at Stevens Institute of Technology.

CONDITIONS AND MECHANISMS FOR THE FORMATION OF DAMAGING HYDROGEN IN FIBER OPTIC CABLE

Gardner Haynes and Robert Baboian

Texas Instruments Incorporated
Attleboro, MA 02703

This paper addresses the conditions for and mechanisms of hydrogen production in fiber optic cable. Previous publications have demonstrated that damage to optical fibers in telephone cable can occur due to reaction with hydrogen.[1-4] In order to design cable systems that are not subjected to damaging hydrogen, it is important to understand the mechanisms and conditions under which hydrogen is formed. In cables, one of the most important hydrogen producing reactions can occur during the corrosion process of the metallic shield. This work was conducted to determine what conditions are required for metallic shielding materials to cause damaging hydrogen to be formed.

The results show that zinc and magnesium are highly susceptible to corrosion and the accompanying hydrogen production reactions dominate during that process. The hydrogen producing reaction on corroding steel depends on the nature of the environment. Increasing acidity, such as acid rain, causes increasing corrosion and hydrogen production on steel. The corrosion of copper and stainless steels is generally accompanied by the oxygen reduction reaction in these environments.

The results of this study show what conditions are required for damaging hydrogen to be produced in the presence of metallic shielding in fiber optic cable. The knowledge of mechanisms of hydrogen formation and conditions for that formation are important for designing cables to avoid this type of damage. The techniques used in this study can be utilized to evaluate new materials or other environments for their tendency to produce the hydrogen reaction.

Introduction:

Previous work has demonstrated that hydrogen gas increases attenuation of optical fibers.[1-4] While factors such as cable depth, type of jacket, damage to the jacket, diffusion of hydrogen out of the cable and exposure time have been shown to influence the degree of damage, there has been general consensus that the damaging hydrogen is produced by corrosion of galvanized steel armour wires. Hardwick, et. al., have proposed the use of stainless steel armour wires to eliminate the source of hydrogen.[3]

In designs incorporating metallic tapes as armours, corrosion of this shield can result in the production of hydrogen. Extensive literature has been published on the corrosion of cable shielding tapes for telecommunications cable.[5-8] The relationship between corrosion of the shields and the production of hydrogen was not evaluated in these studies.

Metallic corrosion (anodic reactions) is accompanied by cathodic reactions such as hydrogen ion reduction, oxygen reduction, and reduction of metal ions. It is the hydrogen ion reduction reaction which produces damaging hydrogen in fiber optic cables. Therefore, if this reaction can be avoided, damaging hydrogen will not be available for reaction with the optical fibers.

Electrochemical techniques have been used to determine what conditions are required for hydrogen ion reduction. The study includes the effect of metal and alloy type and the environment. Polarization curves have been measured for various metals and alloys including zinc, aluminum, steel, copper, nickel, and stainless steels. Environments were chosen to simulate the soil environment electrolyte including groundwater contamination from road deicing salts and acid rain.

Theory:

Corrosion of metals can be treated by application of the mixed potential theory first described by Wagner and Traud.[9] The theory is based on two simple hypotheses. First, any electrochemical reaction can be divided into two or more oxidation or reduction reactions, and second, there can be no net accumulation of electrical charge during an electrochemical reaction. That the various partial reactions can be treated separately, as stated in the first hypothesis, can be demonstrated experimentally. The second hypothesis is only satisfied when the total rate of oxidation (corrosion) equals the total rate of reduction.

The anodic (oxidation) reaction occurs when electrons are removed from an area on the metal surface and positively charged ions go into solution. It can be represented by the equation:

(1) $M \text{ ---> } M^+ + e^-$

The electrons flow to other areas on the metal surface where they are consumed by the cathodic reaction. There are several different cathodic (reduction) reactions which occur. The most common ones are:

(2) $2H^+ + 2e^- \text{ ---> } H_2$
(Hydrogen Evolution)
(3) $O_2 + 4H^+ + 4e^- \text{ ---> } 2H_2O$
(Oxygen reduction: acidic solutions)
(4) $O_2 + 2H_2O + 4e^- \text{ ---> } 4OH^-$
(Oxygen reduction: neutral solutions)
(5) $M^{+n} + e^- \text{ ---> } M^{+(n-1)}$
(Metal ion reduction)

A combination of these reactions can occur providing that the net total reduction rate equals the net total oxidation rate. A number of factors including solution composition, pH, aeration, diffusion, and catalytic properties of the metal surface determine which reactions predominate.

Electrochemical techniques are most commonly used to study these reactions.[10] Use of the mixed potential theory is demonstrated by the activation polarization curves for a reversible electrode in Figure 1. When an electrochemical reaction is forced away from equilibrium, it is termed polarization and one reaction (either oxidation or reduction) proceeds faster than the other. The potential change due to polarization is η, defined as overvoltage and the current applied to polarize the potential away from equilibrium is the net rate of reaction. The expression relating reaction rate and overvoltage for activation polarization is:

(6) $\eta = \pm\beta \log i/i_o$

Equation 6 is called the Tafel equation where i_o is the exchange current density and β is the Tafel constant (or Tafel slope). This equation is valid when the applied current is a linear function of overvoltage on a logarithmic scale such that i is a measure of the oxidation (for example, corrosion) or reduction (for example, hydrogen reduction) current.

The Tafel equation is valid when reactions are under activation control. In many cases, diffusion control plays an important part in the system, i.e. the rate of reaction is limited by diffusion. Polarization curves demonstrating both activation and diffusion control are shown in Figure 2.

In Figure 2, the anodic polarization curve for the corrosion reaction (equation 1) is characterized by the Tafel equation (equation 6). The corrosion rate, i_c, is calculated by use of the Tafel equation (i.e. extrapolating the Tafel region back to E_1, the equilibrium potential).

The cathodic polarization curve in Figure 2 is complex in that activation and diffusion controlled reactions occur. Close to the equilibrium potential, E_1, oxygen reduction occurs (equations 3 or 4) and the current is diffusion limited at i_d. At higher polarization potentials, hydrogen reduction under activation control occurs according to equation 2, in addition to oxygen reduction. The rate of hydrogen reduction, i_H, is calculated from the Tafel equation (equation 6) i.e. extrapolation of the Tafel slope to E_1. The total reduction rate is the sum of i_H and i_d and this sum is equal to the total oxidation rate (i_c) at the equilibrium potential, E_1.

Experimental Procedure:

Potentiodynamic Polarization Measurements

The metals and alloys included in this study are listed in Table I. Disk-shaped specimens for polarization measurements were punched from sheet material in the mill-annealed condition. The specimen surface was polished with 600-grit silicon carbide paper, followed by ultrasonic cleaning in detergent solution, and finally rinsed with distilled water. The specimen was mounted in the type of holder described previously by Myers et.al. [11]. In use, the specimen holder exposed 1 cm^2 of specimen to the electrolyte. This design avoids solution contamination and crevice effects, while allowing the use of flat metal specimens.

The 5 neck 2 liter polarization cell for this study was similar to the one described in ASTM Designation G5-87.[12] The 5 necks allowed introduction of the specimen holder, a salt bridge for the SCE reference electrode, a platinum counter electrode, a thermometer, and a gas purging frit. For oxygenated measurements, air was bubbled through the electrolyte at a rate of 150cc/minute while argon was bubbled at the same rate for de-aerated measurements. Purging began when the specimen was immersed one hour before initiation of polarization and continued throughout the experiment. The electrolyte was ASTM (D2570) corrosive water which contained 100 parts per million of chloride, sulfate, and bicarbonate ions. The effects of acid deposition on soil water chemistry were simulated by adjusting the pH of the corrosive water to values of 2, 4, 6, or 8 with a mixture of 3 parts sulfuric acid and 1 part nitric acid. Reagent grade chemicals and distilled water were used to prepare all solutions. The temperature was maintained at 30 ± 1^oC by immersion of the cell in a water bath.

Potentiodynamic polarization measurements were made with a Princeton Applied Research Model 342 corrosion measurement system. All scans were made at a rate of 0.6 volts per hour. Three curves were measured for each metal-electrolyte combination. The first scan was begun 30 millivolts positive to the open circuit potential and the specimen was polarized in the active direction to a potential of -2 volts versus the saturated calomel electrode (SCE). The second scan was from a potential of 30 millivolts negative to a potential 300 millivolts positive to the open circuit potential. The final scan was started at -2 volts versus the SCE and continued

in the anodic direction to a potential 300 millivolts positive to the open circuit potential. In addition to recording and plotting the log of the current density versus the specimen potential, the computer based instrument automatically calculated the anodic Tafel constant, the cathodic Tafel constant, the corrosion rate based on Tafel extrapolation, the polarization resistance and the corrosion rate based on the linear polarization technique from each test.[13]

Constant Potential Tests

Constant potential tests were conducted to confirm the hydrogen evolution data from the potentiodynamic polarization measurements on some of the metals. The experimental apparatus (Figure 3) consisted of a one liter beaker filled with ASTM corrosive water at various pH's, a luggin probe to contain the SCE and minimize IR drop, a platinum clad niobium counter electrode, and a 25 milliliter glass jar which was inverted over the S shaped specimen to collect hydrogen. A low cost potentiostat[14] was used to control the potential of the 20 cm^2 specimen at various potentials and the current was monitored for 72 hours. If no hydrogen was produced as indicated by the current and presence of gas in the jar, the specimen potential was changed to a value 100 millivolts more cathodic (negative). This procedure was repeated until hydrogen was collected above the specimen. A mass spectrometer was used to confirm that the gas collected was hydrogen.

Results and Discussion

The average corrosion potential after one hour of specimen immersion (3 runs) under aerated and deaerated conditions is listed in Table II. Removal of oxygen from the electrolyte, in general, caused the corrosion potential to shift in the active direction. This was either due to the modification of a (passive) film on the metal surface or due to a shift toward the hydrogen reduction reaction since diffusion limited reduction of oxygen is substantially less under deaerated conditions. At pH's of 4, 6, and 8, the shift in potential of tin, nickel, aluminum, 430 stainless steel, and 304 stainless steel is due to the former while the shift in potential for steel, lead, and copper are due to the latter. Zinc exhibited mixed behavior while little change occurred in the potential of magnesium, suggesting that hydrogen reduction is the principal cathodic reaction. At a pH of 2 steel, zinc, magnesium, tin, lead, and nickel had very little change in potential due to the removal of oxygen indicating that hydrogen reduction was the more important cathodic reaction. Copper, aluminum, 430 stainless steel, and 304 stainless steel had a more active potential when deaerated at a pH of 2 indicating either passive behavior or an increased hydrogen reduction reaction.

The cathodic potentiodynamic polarization curves for copper, 430 stainless steel, steel and aluminum at a pH of 6 in aerated solution are shown in Figure 4. The shape of the curves agreed with the theoretical model (Figure 2). Copper, 430 stainless steel, and steel had a diffusion limited oxygen reduction (equation 3 or 4) current density of 50 $\mu a/cm^2$ and the Tafel slope for hydrogen reduction began at -1.1 volts versus the SCE. The initial reduction reaction on copper above -0.4 volts is probably associated with reduction of a surface film (equation 5) formed at open circuit conditions. The oxygen reduction rate on aluminum was one fifth that of the other alloys although the Tafel slope began at the same potential.

The diffusion limited current density for oxygen reduction for all of the alloys in this study as a function of pH is listed in Table III. At pH's of 4, 6, and 8, the current density was the same for all alloys except aluminum which had a much lower value and magnesium where oxygen reduction was not observed. At a pH of 2 steel, aluminum, zinc, and magnesium showed no evidence of oxygen reduction while those alloys which normally form protective (copper, tin, and lead) or passive (nickel, 304 stainless steel, and 430 stainless steel) films did have a reduction reaction other than hydrogen reduction.

Since the oxygen reduction reaction is diffusion limited, the current density was influenced by the degree of aeration. This is demonstrated in Figure 5 for steel at a pH of 8. As shown, the diffusion limit is 50$\mu a/cm^2$ for the degree of aeration in this study while essentially, there was no oxygen reduction when the solution was deaerated. The effect of pH on oxygen reduction on steel is shown in Figure 6. At pH's of 4, 6, and 8, the limiting current density was nearly identical while at a pH of 2 oxygen reduction was not observed. These trends were the same for all of the alloys tested.

The current densities for hydrogen reduction (I_H) at the corrosion potential obtained from extrapolation of Tafel slopes are listed in Table IV for both aerated and deaerated solutions at all pH's. Since aeration (or deaeration) alters the corrosion potential as well as the corrosion rate for most alloys, the values for erated and deaerated conditions were different. Magnesium, where oxygen reduction was minimal, showed good agreement at all pH's between aerated and deaerated hydrogen reduction rates while film forming or passive alloys (copper, 430 stainless steel, and 304 stainless steel) had a large variation. Excluding copper, 304 stainless steel, and 430 stainless steel, the rate of hydrogen reduction was greatest at a pH of 2. There was little difference in the rates at pH's of 4, 6, and 8. Based on Tafel extrapolation, the overall tendency for the alloys in this study to produce hydrogen at the corrosion potential was:

Cu<304SS<430SS<Sn<Pb<Ni<Al<St<Zn<Mg

The average corrosion current density (Table V) was an important result since the total rate of reduction must equal the corrosion current density. An indicator of the relative importance of the hydrogen reaction can be obtained by comparing the values for aerated and deaerated

results for alloys which do not form a passive film. For example, the average corrosion current density for steel at pH's of 4, 6, and 8 is substantially higher when aerated indicating that the oxygen reduction reaction predominates. At a pH of 2 aeration has little effect on the corrosion current density indicating that the hydrogen reduction reaction is dominant. The magnitude of the current density is also important since, assuming only hydrogen reduction, a current density of 1 μa/cm^2 produces 3.5 cm^3 of hydrogen per year. Copper produced no hydrogen, since it had a comparatively low corrosion current and oxygen reduction predominated under all conditions. Steel had a comparatively high corrosion rate, but oxygen reduction predominated at pH's of 4, 6, and 8. Hydrogen reduction was the main cathodic reaction on steel at a pH of 2. Magnesium was the most efficient metal for producing hydrogen, since hydrogen reduction was significant under all conditions and its current density was high. Based on corrosion current density measurements for alloys which do not form a passive film, the overall tendency to produce hydrogen was:

Cu<<Steel<Pb<Zn<<Mg.

The relationship between the corrosion current density and the tendency to produce hydrogen for alloys which form a passive film is more complicated. Generally, these alloys have a limiting anodic current density on the order of 1 μa/cm^2, which is necessary to maintain their film. Under conditions of pH and aeration where the film cannot be maintained, the corrosion current density increases dramatically and the principal reduction reaction is hydrogen reduction. Thus, nickel and aluminum (Table III) at pH's of 2 and 4 produced hydrogen while the stainless steels produced none under all conditions. Based on corrosion current density measurements, the relative tendency for passive alloys to produce hydrogen was:

304SS<430SS<Sn<Al<Ni

The results from the constant potential tests in which the potential of the metals was controlled in the hydrogen producing Tafel slope are in Table VI. In all cases, the mass spectrometer confirmed that the gas collected was hydrogen. Comparison of the data at a pH of 6 with the polarization curves in Figure 4 shows that the specimens were polarized well into the Tafel region before hydrogen was collected. This was also true at all of the other pH's. Diffusion of atomic hydrogen into or away from the specimen before forming molecular hydrogen may be one reason for the lack of sensitivity of this technique. Although the technique was unable to differentiate the tendency of the alloys to produce hydrogen, it did confirm that the Tafel slopes on the polarization curves were the hydrogen reduction reaction. The use of longer periods between potential steps might improve the sensitivity of the technique, but is probably not practical.

Conclusions

Electrochemical techniques can be used to determine the conditions necessary for hydrogen ion reduction. Open circuit potential and potentiodynamic polarization measurements show the reduction reactions which accompany metallic corrosion. Extrapolation of the anodic Tafel slope to the corrosion potential gives the corrosion current and extrapolation of the Tafel slope for hydrogen reduction to open circuit conditions can be used to determine the amount of the corrosion current associated with the hydrogen reduction reaction. Constant potential tests coupled with mass spectrometer analysis can be used to confirm the Tafel slope for hydrogen reduction.

The amount of oxygen and the pH in the cable environment affect corrosion of shielding materials as well as the rate of hydrogen production. The effects of pH and aeration depend upon the alloy. Types 430 and 304 stainless steels were corrosion resistant under all conditions of pH and aeration and the oxygen reduction reaction predominated. Although the corrosion rate of copper increased slightly with decreasing pH, it was very highly corrosion resistant and oxygen reduction was the principal cathodic reaction. The rate of corrosion of aluminum increased with decreasing aeration and pH and hydrogen reduction was the main cathodic reaction. Steel had a comparatively high corrosion rate, but oxygen reduction predominated at pH's of 4, 6, and 8. Hydrogen reduction was the main cathodic reaction on steel at a pH of 2. Magnesium and zinc had the highest corrosion rates and the largest rates of hydrogen reduction. The performance of other alloys was mixed. Overall, the relative amount of hydrogen produced by corrosion of the alloys in this study decreased in the order:

Mg>Zn>Steel>Al>Ni>Pb>Sn>430SS>304SS>Cu

The impact of acid deposition on cable shielding materials is significant since it can produce acidic ranges where hydrogen reduction can occur. This is important for metals like steel, aluminum, and nickel where the dominant cathodic reaction can change from oxygen reduction to hydrogen reduction.

The techniques used in this study can be utilized to evaluate new materials or other environments for their tendency to produce the hydrogen reaction. Although beyond the scope of this study, these techniques can also be used to determine galvanic effects and the resulting effect on hydrogen reduction.[10]

References

1. W.T. Anderson, A.J. Johnson, J.P. Kilmer, and R.M. Kanen, "Hydrogen Gas Effects on Installed Submarine Single-Mode Fiber Cables", Proceedings of the 37th International Wire and Cable Symposium, Reno, Nevada, November 15-17, 1988, pp.188-199.

2. W.T. Anderson, A.J. Johnson, and A. DeVito, "Field Measurements of the Effects of Hydrogen Gas on Installed Submarine Single-Mode Fiber Cables", Proceedings of the 38th International Wire and Cable Symposium, Atlanta, Georgia, November 14-16, 1989, pp. 675-683.

3. N.E. Hardwick, III, L.C. Hotchkiss, J.J. Blee, and D.L. Philen, "Corrosion-Resistant Armor to Prevent H_2-Induced Loss in Underwater (wire-armored) Fiber Optic Cable", Proceedings of the 38th International Wire and Cable Symposium, Atlanta, Georgia, November 14-16, 1989, pp.689-695.

4. S. Hopland, "Investigation of Total and Distributed Hydrogen Levels in Installed Fiberoptic Submarine Cables", Proceedings of the 38th International Wire and Cable Symposium, Atlanta, Georgia, November 14-16, 1989, pp. 684-688.

5. R. Baboian, G. Hessler, K. Bow, and G. Haynes, "The Effect of Alternating Current on Corrosion of Cable Shielding Materials in Soils", Proceedings of the 37th International Wire and Cable Symposium, Reno, Nevada, November 15-17, 1988.

6. R. Baboian, S.R. Hartley, and E.D. Hyman, "High Strength, Corrosion Resistant Clad Metal Shielding for Telephone Wire and Cable", paper presented at the 23rd International Wire and Cable Symposium, Atlantic City, NJ, 1974

7. J.L. Fink and E. Escalante, Corrosion Evaluation of Underground Telephone Cable Shielding Materials, NBSIR83-2702, prepared for the Rural Electrification Administration; National Bureau of Standards, May 1983.

8. J.L. Fink, D. Matthews, G. Hessler, and E. Speed, "Corrosion Evaluation of Underground Telephone Cable Shielding Materials", NBSIR87-3546. Prepared for the Rural Electrification Administration; National Bureau of Standards, January, 1988.

9. C. Wagner, and W. Traud, Zeitschrift fur Electrochemie, Vol. 44, 1938, p.391.

10. Electrochemical Techniques for Corrosion Engineering, R. Baboian, Ed., NACE, Houston, TX, 1987.

11. J.R. Myers, F.G. Gruewler, and L.A. Smulczenski, Corrosion, Vol. 24, 1968, P.352.

12. ASTM Designation G5-87, Standard Reference Test Method for Making Potentiostatic and Potentiodynamic Anodic Polarization Measurements, ASTM Annual Book of Standards, Volume 03.02, American Society for Testing and Materials, Philadelphia, PA, 1990

13. Model 342 Softcore Corrosion Measurement Software Operating Manual, EG+G Princeton Applied Research, Princeton, NJ, 1989

14. R. Baboian, L. McBride, R. Langlais, and G. Haynes, "Effect of Modern Electronics on Corrosion Technology", Materials Performance, Vol. 18, No. 12, pp. 40-44, December, 1979.

BIOGRAPHIES

Robert Baboian is a TI Principal Fellow and Head of the Electrochemical and Corrosion Laboratory of Texas Instruments Inc. He received his Ph.D. degree from Rensselaer Polytechnic Institute in 1964 and his B.S. degree from Suffolk University in 1959. He has edited 6 books and authored 110 technical publications in the field of electrochemistry and corrosion. Dr. Baboian served as Chairman of the Board of ASTM in 1987 and received the Frank Newman Speller award for outstanding contributions to Corrosion Engineering from the National Association of Corrosion Engineers in 1988.

Gardner Haynes is currently a Member Group Technical Staff of the Electrochemical and Corrosion Laboratory of Texas Instruments Inc. He received his Bachelor's Degree in Mechanical Engineering Technology from Northeastern University in 1974. He has been active in the field of corrosion for 20 years and has published many papers, edited one book, and holds 7 patents. His professional activities include chairmanship of numerous groups in both the American Society for Testing and Materials and the National Association of Corrosion Engineers.

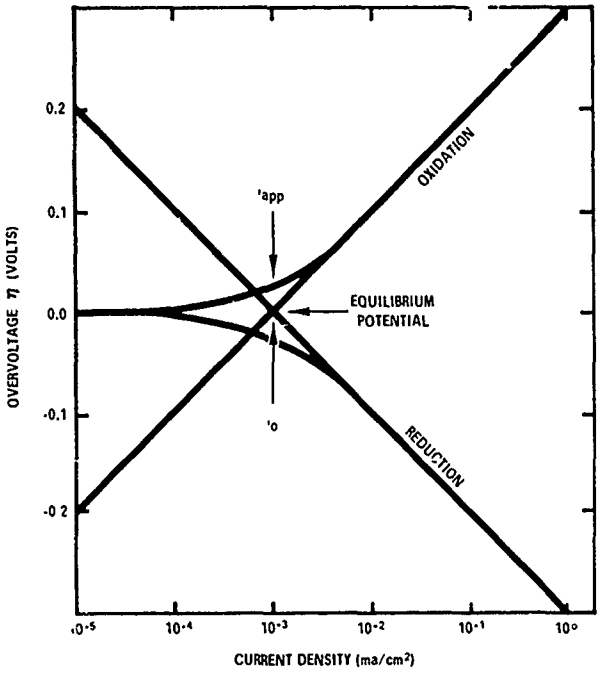

Figure 1 - Activation Polarization Curves for a Reversible Electrode

Figure 3 - Experimental Apparatus for Constant Potential Tests

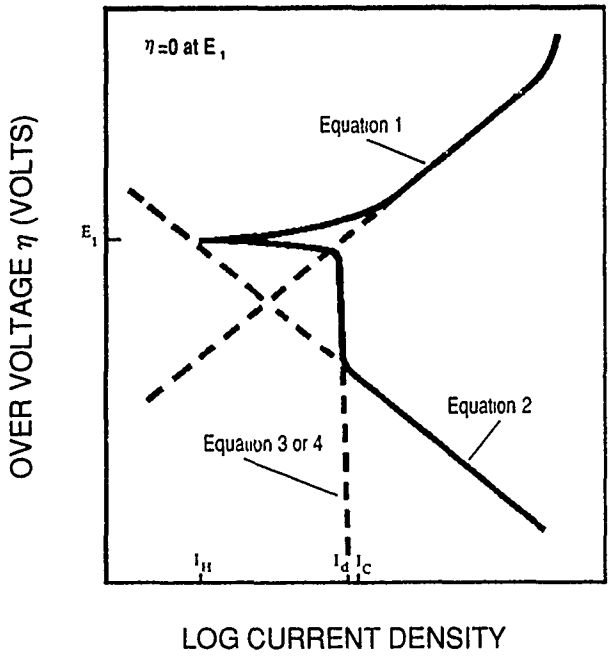

Figure 2 - Polarization Curve Demonstrating Both Activation and Diffusion Control

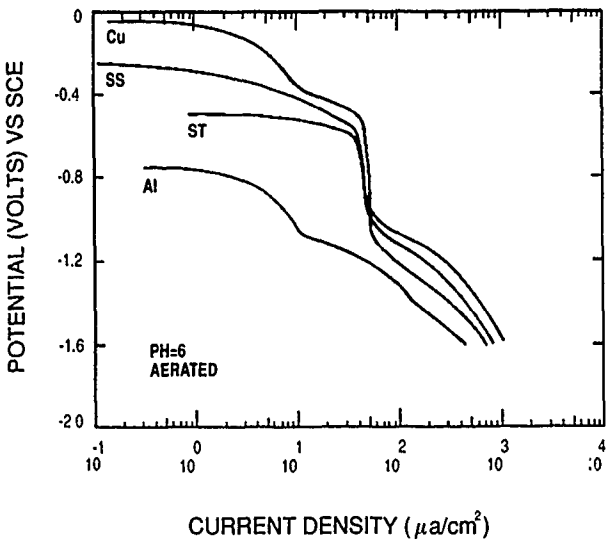

Figure 4 - Cathodic Potentiodynamic Polarization Curves for Copper, 430 Stainless Steel, Aluminum and Steel (pH=6, Aerated)

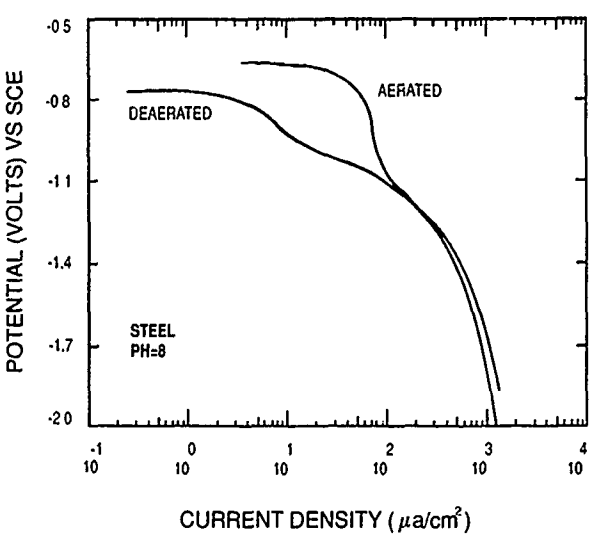

Figure 5 - Cathodic Potentiodynamic Polarization Curves for Steel (ph=8) showing the Effect of Aeration

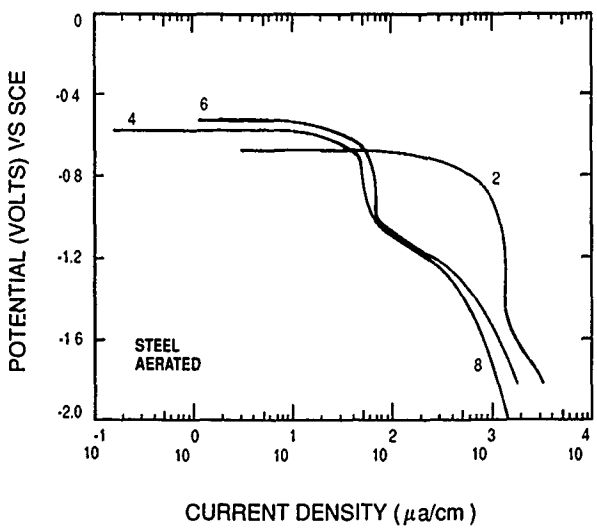

Figure 6 - Cathodic Potentiodynamic Polarization Curves for Steel (Aerated) Showing the Effect of pH

Table I

List of Materials

Metal or Alloy	UNS Number
Aluminum	A91100
Copper	C38600
Magnesium	M10000
Nickel	N02200
Lead	L50000
Type 430 Stainless Steel	S43000
Type 304 Stainless Steel	S30400
Carbon Steel	G10060
Zinc	Z13001

Table II

Average Potential in ASTM Water
(Volts vs. SCE)

Alloy	pH							
	2		4		6		8	
	Aerated	Deaerated	Aerated	Deaerated	Aerated	Deaerated	Aerated	Deaerated
Steel	-0.634	-0.613	-0.607	-0.735	-0.613	-0.783	-0.658	-0.792
Al	-0.683	-0.775	-0.573	-0.849	-0.648	-1.002	-0.585	-0.989
Cu	-0.040	-0.118	-0.045	-0.158	-0.092	-0.291	-0.104	-0.250
Zn	-1.048	-1.051	-1.016	-1.116	-1.045	-1.180	-1.096	-1.197
Mg	-1.742	-1.745	-1.559	-1.565	-1.539	-1.592	-1.614	-1.636
Sn	-0.481	-0.493	-0.427	-0.563	-0.517	-0.820	-0.604	-0.883
Pb	-0.513	-0.550	-0.514	-0.607	-0.551	-0.728	-0.536	-0.635
430SS	-0.314	-0.411	-0.421	-0.544	-0.265	-0.500	-0.148	-0.523
304SS	-0.126	-0.323	-0.234	-0.355	-0.176	-0.373	-0.283	-0.533
Ni	-0.257	-0.289	-0.196	-0.475	-0.259	-0.494	-0.258	-0.452

Table III

Diffusion Limited Current Density for Oxygen Reduction
(μ a/cm^2)

Alloy	pH			
	2	4	6	8
Steel	0	50	50	50
Al	0	10	10	10
Cu	5	50	50	50
Zn	0	50	50	50
Mg	0	0	0	0
Sn	5	50	50	50
Pb	5	30	50	50
430SS	1	50	50	50
304SS	2	50	50	50
Ni	20	50	50	50

Table IV

Hydrogen Reduction Current Density from Tafel Extrapolation
(μa/cm^2)

Alloy	pH							
	2		4		6		8	
	Aerated	Deaerated	Aerated	Deaerated	Aerated	Deaerated	Aerated	Deaerated
Steel	100	70	1	0.7	1	1	7	0.8
Al	50	100	0.5	3.5	0.45	10	0.2	1.8
Cu	1	0.001	0.2	1	0.1	0.4	0.5	0.001
Zn	400	250	9.5	3.5	7.5	4.5	9.5	6.5
Mg	250	400	55	35	60	12	30	15
Sn	0.3	0.1	0.09	0.005	0.25	0.03	0.35	1.2
Pb	44	1	0.9	0.05	10	0.5	2.5	0.5
430SS	0.02	5	0.8	0.08	0.3	0.002	0.4	0.01
304SS	0.6	0.1	0.4	0.08	0.4	0.01	1	0.03
Ni	10	20	1.5	5	2.5	0.01	2.5	0.1

Table V

Average Corrosion Current Density
(μa/cm^2)

Alloy	pH							
	2		4		6		8	
	Aerated	Deaerated	Aerated	Deaerated	Aerated	Deaerated	Aerated	Deaerated
Steel	95	85	10.5	3.2	14.4	1.2	28.9	2.73
Al	17.5	18.4	2.8	1.05	0.97	1.8	0.98	2.06
Cu	26.3	0.5	7.8	1.2	4.8	0.21	2.2	0.46
Zn	120	202	17.2	4.3	17	3.1	23.4	2.1
Mg	109	140	18.9	16.1	22.9	11.5	17.7	14.4
Sn	98	135	0.28	0.7	0.22	0.26	0.67	0.94
Pb	82	15.5	9.1	12	7.9	1.77	9.5	3.4
430SS	1.7	5.4	1.5	1.8	0.5	0.87	0.19	0.93
304SS	0.67	2.6	0.36	0.87	0.16	0.35	0.52	0.89
Ni	24.5	10.6	3.6	3.0	0.58	0.43	0.4	0.17

Table VI

Potential at Which Hydrogen Was
Collected in Constant Potential Tests
(Volts vs. SCE)

Alloy	pH			
	2	4	6	8
Al	-0.65	-1.30	-1.30	-1.30
Steel	-0.70	-1.20	-1.20	-1.20
Cu	-0.70	-1.30	-1.30	-1.30

APPLICATION-SPECIFIC, END-OF-LIFE CONTACT CURRENT RATING METHODS

James H. Wise, P.E.
AMP Incorporated

ABSTRACT

The rating of electrical contacts for current-carrying capacity has taken on increased importance as the packaging density of the interconnection systems used in modern electronic systems has increased. Even with increased density requirements, there have been additional requirements not only to maintain the existing current-carrying capacity on individual contacts, but also to increase the capacity of the contact pairs. The combination of higher density and increased current levels creates an environment hazardous to the ability of the contacts to provide a reliable interconnection not only initially, but also over the life of the product.

As the density requirements increase, the physical space available for electrical contacts decreases even though the current levels to be conducted may increase substantially. Density considerations require that the contact system be optimized for smallest size. Any requirements to maintain or increase the required current-carrying capacity generate additional design constraints to insure that excessive temperature rises or other current-related phenomena do not decrease the reliability of the contact system. Consequently, it is important that the contact current carrying rating assigned to the contact system reflect its abilities not only initially, but also at the end of its useful life in the presence of all manner of waveforms.

A methodology will be presented to determine a basic contact current rating for a specified set of application-specific conditions, to verify that rating after end-of-life conditioning, and then to present it in the product specification in a unique presentation format. The format will be suitable for allowing an interconnection system designer to determine the actual current rating for an individual contact pair in a housing in a specific application based on bulk temperature rise considerations. The application-specific conditions considered are allowable bulk temperature rise, attached wire AWG, and bundling (contact loading density in a given housing). The methodology presented works effectively for well-behaved, continuous waveforms such as sinusoidal AC waveforms and DC currents that can be accurately characterized solely through their RMS value.

The paper will also extend the methodology into the environment of less well-behaved waveforms that introduce additional considerations based on supertemperatures due to the presence of high peak values of varying durations. Severe duty cycle applications, high crest factor waveform applications, and applications involving peak anomalies such as transients and temporary overloads will be incorporated into the methodology.

In summary, a novel methodology will be presented whereby a contact pair is assigned a basic current-carrying capacity based on a defined set of conditions. These conditions include a single contact pair being contained in a specified housing and attached to wire of a specified AWG. The designer is then allowed to determine the basic current rating of the contact from a current versus temperature rise graph in the product specification for the bulk temperature rise appropriate to the application. The basic current rating is then converted into an application-specific current rating by using a table in the product specification. A tabular approach allows the design to adjust the current rating to reflect the actual wire AWG and bundling present in his unique application. A final adjustment is made through additional tables and specification elements to incorporate the peak value supertemperature considerations into the current rating that the application-specific waveforms present.

INTRODUCTION

The determination of the current ratings for electrical and electronic contacts in specific applications has long been considered "black magic." Many designers await the arrival a Merlin-like figure who will sprinkle magic dust over his design, mumble a few secret incantations, and magically allow his one ampere contact pair to carry five amperes for eternity. While this approach sometimes works, truly a magical event, the approach more often results in a witch's caldron of fire and smoke. Since the supply of Merlins is very limited, a better approach would seem in order.

The rating of electrical contacts for current-carrying capacity has taken on increased importance as the density of the interconnection systems used in modern electronic

systems has increased. Along with the increased density, many applications require concomitant increases in the current levels present in the connectors used in these same interconnection systems. The brutal combination of higher densities and increased current levels oft times taxes the ability of the contacts to transfer power and data signals across the interconnection without excessive losses for the life of the product.

As interconnection density requirements increase, it is an unavoidable fact that the physical space available for each contact concurrently decreases, re -dless of the current levels to be conducted. This creat a paradox in that it requires that the contact pairs be optimized for smallest size; all the while conducting required currents that are generally rising in a manner that does not generate excessive temperature rises or other untoward behaviors that threaten the reliability of the contact pair. Consequently, it is important that the contact current rating assigned to the contact system reflects its ability to efficiently transport energy not only initially, but also at the end of its useful life.

Electrical contacts in general, and power contacts in particular, need to exhibit low initial termination resistances that are stable over the life of the product. Since any contact being operated near full capacity is, in reality, a power contact, it is incumbent on interconnection systems designers to provide stable, low resistance current paths for the life of the product for each and every signal. This requires a disciplined determination of the true application-specific current rating for each contact pair. This determination is a joint effort of the connector manufacturer and the interconnection system designer.

The connector manufacturer, through the product specifications associated with given connectors, can provide the designer with data indicating the performance of a contact pair under a defined set of test conditions. This performance is typically indicated by a "Base Rated Current" curve that shows the ampacity of the contact pair in a specified housing. The product specification or application notes supporting a connector can be used to convey additional information to the designer that will allow this base current to be derated to a magnitude more appropriate of an application's specific combination of attached conductor size, local ambient temperature excursions, and housing loading densities.

The ability to scientifically determine a valid application-specific contact current rating is dependent on accurate characterization of the termination resistance of the contact pairs initially, when a contact pair is first put into service, and also at the end of the design life for the contact pair. To be truly accurate, the contact pair should have been conditioned to reflect the combinations of environmental conditions and physical abuses given in the product specification.

A methodology has been developed, and will be presented here whereby the principle failure mechanisms of electronic contacts are sequentially exercised in a standardized test sequence. This sequence, although initially developed for power contacts, is suitable for all electronic contacts. The test sequence serves to accelerate the activation of any potential performance degrading mechanisms in the contact pair, and to reflect the contact pair's performance at the end of its design life.

Next a standardized graphical presentation format, suitable for inclusion in all product specifications, will be presented. The format allows the user to quickly determine the true continuous current-carrying capacity of a single contact pair in a housing. This capacity, or continuous current rating, is based on the current versus bulk temperature rise characteristics and termination resistance stability of the contact at the end of life.

The methodology presented works effectively for well-behaved, continuous waveforms such as sinusoidal AC waveforms and DC currents that can be accurately characterized solely through their RMS value. Unfortunately, electronic contacts function in a world more accurately characterized by nice, well-behaved waveforms that are bruised and abused by transients, overloads, and Merlins.

Consequently, the methodology will reach into the environment of less well-behaved waveforms generally viewed as non- sinusoidal and periodic. These waveforms are typified by the presence of high peak values which threaten the contact interface. The methodology will encompass peak anomalies such as transients and temporary overloads, high crest factor waveform applications, and duty cycle applications

CURRENT RATING TENETS

Several fundamental tenets determine the final current rating for any electronic contact pair. The first tenet is that every current rating is application specific. Since the number of combinations of contacts, housings, environments, and signal waveforms possible for an application generates an extremely large number of permutations, it is impossible for a connector manufacturer to give one, or even a few, current ratings for a contact pair. Since the designer controls these combinations, it falls to the designer to determine the proper final current rating required for his application.

The second tenet is that the application-specific current rating should be based on end-of-life performance, and not on straight, out-of-the-box performance. By necessity, dense interconnection systems, and power distribution systems, run near their maximum rated capability. For contact pairs rated solely on their new performance

capabilities, any degradation of performance capability over the life of the product will result in field failures. Rather than incurring the cost penalties associated with over-specifying initially, and hoping that they do not degrade substantially, the wise designer will use contact pairs that are performance rated on end-of-life performance.

The last tenet of interest here is that the current rating is very dependent on the type of waveform being conducted. A contact pair is rated differently for DC waveforms than for high crest factor or pulsed waveforms. As will be seen in this paper, the type of waveform dramatically alters the final current rating of a given contact pair in specific applications.

END OF LIFE CHARACTERIZATION

The key to superior contact performance is to provide a low- resistance path between source and load, effectively allowing the contact pair to be invisible to the waveforms being conducted. For circuits used for power distribution, and for circuit designed for minimum power consumption, the primary design consideration is the minimization of millivolt drop (MVD). Since MVD is the direct result of the contact resistance, a critical contact parameter is initial resistance. It is equally important to maintain this low resistance path throughout the life of the product. Controlled, stable resistance over the lifetime of a product is critical to the maintenance of low MVD and low power consumption.

More importantly, stable resistance is a precursor of reliable contact performance. The resistance of a contact pair directly determines its response to various applied waveforms. The combination of applied energy and resistance generates heat. The response of the contact pair is temperature rise, the basis for establishing a contact's current rating. An intimate relationship exists between resistance stability, temperature rise, and current rating, initially and at end-of-life.

CURRENT RATING METHODOLOGY

Continuous Current, DC and Sinusoidal AC

In order to effectively determine the application-specific contact current rating for a contact pair in a given application, the methodology requires the identification of two fundamental characteristics of the waveform to be conducted, regardless of its complexity. The first essential element involves characterizing the waveform present in a given application in terms of the RMS value of the continuous or periodic component of the waveform. A direct correlation between this RMS value and the bulk temperature rise of the contact system can then be made. The information contained in the product specification will then allow the designer to modify the basic contact current rating into an application- specific current rating to suit his particular application. Graphs and tables contained in the product specification will be used to change the basic current rating to reflect the combination of allowable temperature rise, wire AWG, and bundling present in the application.

The second essential element involves characterizing the waveform in terms of the peak values present, their duration, and their frequency. A direct correlation can then be established between these peak values and the supertemperature rise of the contact pair. The paper will discuss the additional considerations necessary to incorporate the effects of this supertemperature rise into determining the application-specific current-carrying capacity of the contact pair.

Once a contact pair has been designed to carry a specified current at a given bulk temperature use, it is subjected to a current rating verification testing program. The program is intended to condition the contacts to an "end of life" state with respect to durability, normal force and corrosion. In effect, the contact pair has been subjected to a worst case scenario based on the combinations of physical and environmental abuse allowed by the product specification. The contact pair is monitored during verification testing for the initial and final values of current versus temperature rise, resistance and millivolt drop. The allowed change in contact resistance after conditioning is based on supertemperature rise. The final current rating is then determined by evaluation of the temperature rise characteristics of the contact pair after the end-of-life conditioning is completed.

The verification test has as its goal the verification of contact stability under specified test conditions simulating a pre-determined operating environment. The procedure used in the verification testing has been standardized in AMP Test Specification 109-151. The sequence of tests used to exercise the major failure mechanisms of contact pairs, and condition the contact to the pre-determined end-of-life equivalency is shown in Figure 1.

The test sequence has been designed to verify that the contact pair is stable and that its resistance to current flow remains within acceptable limits for the operating life of the product. The objective of this testing is to verify the current-carrying capacity of the contact pair as a function of operating temperature for the stated life of the contact pair. The procedure sequentially introduces wear, corrosion, stress relaxation and mechanical disturbance into the contact system. Measurements of the performance characteristics of the contact system are taken before and after this conditioning sequence. Depending on the intended application for a contact pair, this sequence may be altered and/or additional tests, such as thermal shock, temperature cycling and current cycling included. It is also important to emphasize that end-of-life conditions are

simulated using accelerated aging techniques which have been successfully correlated (that is, shown to be equivalent) with real-time aging effects.

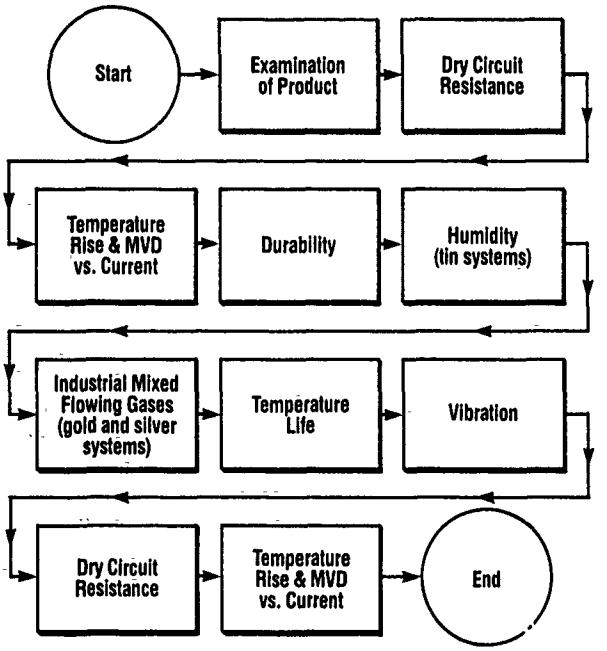

Figure 1. EOL Simulation Test Sequence

Once the contact pair has been conditioned to reflect end-of- life performance, the final readings from the temperature rise and MVD versus current measurements are used to construct a base current rating curve or current carrying capability curve. An example of this curve is shown in Figure 2 for the Ampliwidget Connector.

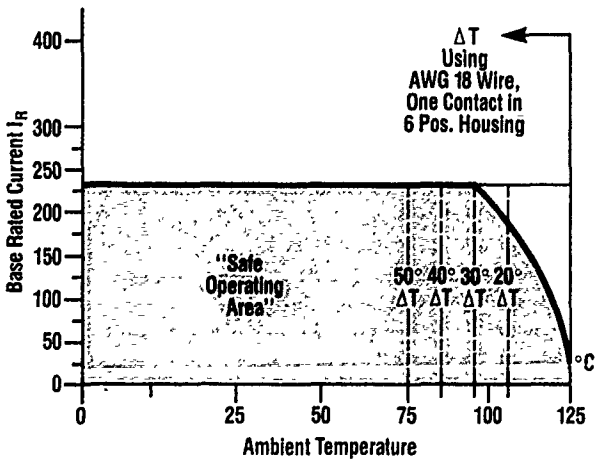

Figure 2. Ampliwidget Connector Current-Rating Curve

Inclusion of curves such as this in the product specification allow the designer to determine directly the base current rating for a given contact pair at end-of-life in his application. The ultimate goal for this verification test program and presentation format is to allow the full use of the area under the curve, called the Safe Operating Area (SOA).

Each curve will be supplied with a definition of the specified conditions under which it was produced. The standard conditions used will be a single contact in a housing terminated on an appropriate, stated wire gauge. The designer is now free to determine a base current rating for the given contact based on the temperature conditions present in the application. For example, a designer may determine that his application is constrained by a maximum 20 degree centigrade temperature rise requirement. Examination of Figure 2 reveals that the Ampliwidget Connector could carry as much as 180 amperes as long as the maximum localized ambient temperature (that is, the contact bulk temperature) did not exceed 105 degrees centigrade.

The designer is free to choose any combination of temperature rise, maximum bulk temperature and continuous current that result in an interaction in the Safe Operating Area. For example, if the maximum localized ambient temperature were 95 degrees centigrade, and the application specifications allowed a contact temperature rise of 30 degrees centigrade, a base continuous current of 227 amperes could be allowed.

In addition to determining the end-of-life continuous current rating for the contact pair based on bulk temperature rise considerations, the designer must also be able to vary one or two other principle determinants of final current rating- the number of contacts, or density of the contact pattern, in the connector, and the size of the attached conductors. The standard conditions used to generate Figure 2 were a single contact in a six position housing with 18 AWG wire terminated to the contact pair.

Although the designer may use the contact pair at the base current rating determined from Figure 2, he may find it necessary to change the conductors he will use in his application. The Base Current Modifier Chart shown in Figure 3, is provided for this purpose. For example, if the contact pair were configured using 22 AWG conductors rather than 18 AWG conductors, the previously determined base current rating should be reduced by 25%. Additionally, if the designer added two more contacts to the housing for his unique application, the base current would have to be reduced further. He would now have to reduce the original base rated current by 50% for this application.

The conversion of the connector manufacturer's base current curve into an application-specific continuous rating can be determined by the designer directly from the

product specification through the use of Figure 3. Referring to the Figure, we find the intersection of the column representing the conductor AWG used in his application, and the row representing the number of contacts placed in the housing. The number located at the intersection of this row and column is called the Base Current Modifier factor, F. The application-specific continuous current rating for the given contact pair is then determined relationship shown in Equation (1).

$$I = I_B \cdot F \qquad (1)$$

where

I = Continuous Current Rating (Amperes)
I_B = Base Rated Current (Amperes, RMS)
F = Base Current Modifier

Loading Density \ Wire Gauge	22	18	14
1	.75	1.00	1.25
3	.50	.75	1.00
6	.25	.50	.75

F

Figure 3. Ampliwidget Base Current Modifier Chart

Non-Sinusoidal Waveforms

The methodology just detailed, although conservative, works very effectively for well-behaved, continuous waveforms such as sinusoidal AC waveforms and DC currents. Fundamentally, the effectiveness of the methodology to this point is based on the fact that these waveforms can be accurately characterized with respect to their contact heating characteristics solely through their RMS value. Lacking any unusual or excessive peak values that would create untoward supertemperature rises, these waveforms exhibit very stable heating characteristics. This stability is the basis of the aforementioned contact current rating methodology.

Since the majority of applications subject contact pairs to one or more other types of waveforms, we must extend the methodology into the environment of less well-behaved non- sinusoidal waveforms that are typified by the presence of high peak values. The waveforms to be addressed will be divided into classifications involving single peak anomalies such as transients, temporary overloads, high crest factor waveform applications, and duty cycle applications.

The resulting contact current rating methodology involves identifying two fundamental characteristics of the waveform to be conducted, regardless of its complexity. The first essential element involves characterizing the waveform in terms of the RMS value of the continuous or periodic component of the waveform. A direct correlation between this RMS value and the bulk temperature rise of the contact system can then be made to determine the continuous current portion of the final current rating.

The second essential element involves characterizing the waveform in terms of the peak values present, their duration, and their frequency. A direct correlation can then be established between these peak values and the supertemperature rise of the contact system. This action will allow us to extend the earlier methodology to incorporate the effects of this supertemperature rise into the rating of the contact's current-carrying capacity initially and at end-of- life.

Once the impact of a waveform on the bulk temperature rise and on the supertemperature rise has been determined, the final contact current rating for a given contact in a given application can be readily assessed. Before assessing these impacts, it is necessary to understand the temperature related contact failure mechanisms that determine these same impacts.

TEMPERATURE RELATED FAILURE MECHANISMS

The determination of the appropriate current rating for an electrical contact revolves around isolating the current-related failure mechanisms present in an application. The principle effect, of interest here, of electrical current passing through a contact here is the internal generation of heat in the contact through Joule Heating. Depending on the amount of heat generated, one of several failure mechanisms can be actuated. These failure mechanisms can be broadly categorized as being either bulk temperature related, or supertemperature related.

Earlier we saw that the contact continuous current rating for well-behaved waveforms (DC and sinusoidal AC) is based on defining the wire AWG of the attached conductors, the maximum environmental operating temperature, and density of the contact pattern in the housing selected for this specific application. With these factors in hand, we can predict the bulk temperature rise that will result from the passage of a various current levels (always measured in continuous RMS amperes) through the contacts that can be used in the selected housing.

All the factors involved in determining the contact current rating for continuous waveforms can be directly related to heat. While the failure mechanisms related to wear and corrosion are certainly important, the principle mechanism that we are to be concerned with here is that of stress relaxation. Wear-and corrosion-related failure mechanisms are incorporated into the contact current rating methodology through the use of end-of-life contact characteristics, which are determined by the verification test sequence that exercises these failure mechanisms, as the basis for establishing the base current curve. By selecting combinations of factors that maintain the contact system within its Safe Operating Area, the maximum immunity to heat- related failures due to bulk temperature excursions is achieved throughout the lifetime of the product.

These considerations focus on the bulk temperature rise since it is directly related to the continuous RMS current flowing in the contact pair. Whenever less well-behaved waveforms are present, a second set of considerations must also be included in the determination of the contact current rating. These factors are of result of the failure mechanisms associated with excessive supertemperature rise. Here the principle effect is not the initiation or acceleration of stress relaxation, but the degrading or destruction of the contact interface. Any degrading of the interface obviously leads to an exacerbation of the wear- and corrosion-related failure mechanisms and a shortened life for the product. Just as obviously, the destruction of the interface dramatically indicates that we have selected an inappropriate contact for a given application.

The reason for this differentiation can begin to be understood by examining Figure (4). The constriction resistance of an interface, which is a function of current being forced to flow through a limited number of asperities rather than the bulk of the contact, generates localized heating when current flows through it. This localized heating is referred to as supertemperature. Since the mass of the asperities is very small, their thermal time constant is very, very short. Consequently, the temperature in these asperities follows the peak values of the conducted waveforms, and not the RMS magnitudes. The brutal combination of a short thermal time constant, and limited cross-sectional area in the asperities through which the current can flow, makes the interface prone to overheating (due to supertemperature rise) and failure.

The true danger in these types of waveforms in terms of their impact on current rating, is illustrated by the analogy of the engineer who drowned at a pool party. The engineer, being one who ran his life according to statistics and averages, decided that he could jump into the pool even though he could not swim. He based his decision on the fact that someone said that the average depth of the pool was only two feet. Unfortunately, he chose to jump into the deep end of the pool.

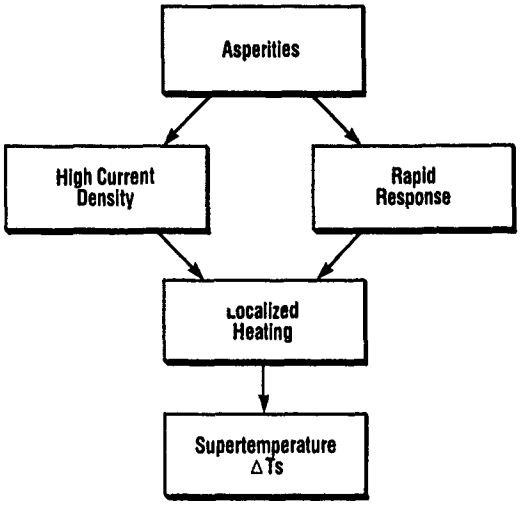

Figure 4. Effect of Peak Currents

The RMS value of a waveform characterizes the average heating effect of a waveform, but it does nothing to tell us about the "deep end" of the waveform represented by transients, overloads, and high peak anomalies. A current rating based solely on RMS current magnitudes works well to prevent failures due to bulk-temperature related failure mechanisms. In order to accommodate these other types of waveforms, we must also incorporate supertemperature related effects. The additional steps included in the methodology will focus on also controlling the maximum supertemperature produced by the waveforms present in a given application.

CONTACT SYSTEM THERMAL TIME CONSTANTS

Various organizations publish ampacity charts for wire. Generally speaking, these ampacity ratings are based on the relationship between the internal heating of the wire (due to the resistance of the wire and the Joule heating phenomenon) and the ability of the wire either to store that heat, causing a bulk temperature rise of the wire, or to remove that heat by some combination of conduction, convection, and radiation cooling. Broadly speaking, in the case of the wire itself, the convection and radiation cooling mechanisms are inhibited by the presence of the insulation around the conductors. Therefore, the final bulk temperature rise of the wire, and hence its ampacity or current rating in a given application, is predominantly based on the interaction of the heat storage capability of the thermal capacitance of the copper wire, and the heat sinking ability of the conductor terminations to conductively cool the wire.

In an analogous manner, a contact system in a housing exhibits a bulk temperature rise that is related to the interaction of the applied waveform, the thermal

capacitance of the contacts, and the conduction cooling supplied by the conductors attached to the contact system.

If we were to apply a continuous waveform to a contact system and monitor the bulk temperature near the contact interface, we could observe a behavior such as that shown in Figure 5. Initially the contact is stabilized at the ambient temperature. As time passes, the bulk temperature begins to rise until such time as a thermal equilibrium is reached. At this point, a balance is reached between the internal generation of heat in the contact, the internal storage of that heat in the contact's thermal capacitance, and the cooling provided to the contact by the conductor terminations. In a manner directly analogous to that of the charging of the capacitor in a series RC electrical circuit, the time required to reach this state of thermal equilibrium is a function of the thermal capacitance and resulting thermal time constant of the contact system and attached terminations.

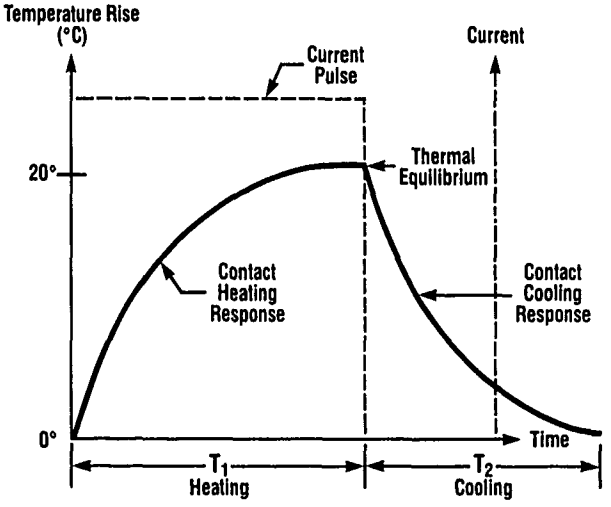

Figure 5. Contact System Thermal Response

A continuous waveform, whether AC or DC, will remain by definition for a period of time exceeding four or five thermal time constants. Thus, the contact system reaches a point of thermal equilibrium at whatever bulk temperature rise was selected after a finite period of time. The equation describing the Contact Temperature Response in the heating mode is given in Equation (2) below.

$$\Delta T = I^2 A(1 - e^{-t/\tau}) \qquad (2)$$

where

I = Electrical Current (Amperes)
T = Temperature Rise (°C)
A = Contact Constant
t = Time (Seconds)
τ = Thermal Time Constant (Seconds)

Upon examination of this equation, we can determine that the principle factors affecting the temperature rise of the contact are the current magnitude (I), and the relationship between the thermal time constant of the contact system (τ) and the amount of time the waveform is present (t). When the relationship shown in Equation (3) holds true, we can consider the waveform continuous waveform and apply the methodology described earlier. In situations where the equation is not true, such as when transients are present, then we must modify the procedure.

$$T_1 > 5\tau \qquad (3)$$

where

T_1 = Heating Time (Seconds)
τ = Thermal Time Constant (Seconds)

Before leaving Figure 5, it is useful to examine the behavior of the contact system when the current is removed. Assuming that the local ambient has not increased significantly, the contact begins to cool since there is no longer any internal heat generation. Equation (4) describes the Contact Temperature Response in the cooling mode.

$$\Delta T = Ce^{-t/\tau} \qquad (4)$$

where

ΔT = Temperature Rise (°C)
C = Constant (InitialConditions)
t = Time (Seconds)
τ = Thermal Time Constant (Seconds)

It is important to note that the ratio of the time (t) to thermal time constant (τ) again plays a significant role in the contact system's response. For periodic waveforms, and even for transients and overloads, the ability of the contact system to cool before the next application of the driving waveform can have a significant bearing on the resulting contact current rating.

In the case of both heating and cooling, we have seen that the thermal time constant of the contact system is a key constituent in the determination of the rate of bulk temperature rise. It is important to recognize that the thermal time constant of interest here is not that of the contact system alone. The thermal performance of the contact is very dependent on the heat sinking effect of the attached conductors. Consequently, the thermal time constant of the interest is the one that results when we combine a contact system with the wire or printed circuit boards that will be attached to it in a specific application. Just as we determine the current rating for a contact system by including the thermally relevant variables of attached wire AWG, loading density, and ambient temperatures, we must include the wire in the determination of the thermal time constant. A contact

manufacturer cannot supply this data as it is a function of each unique application.

Several methods are available to allow the determination of a system's thermal time constant. The most straight forward method is experimental measurement. A contact pair can be terminated with the appropriate wire to be used in an application and loaded into the housing selected for the application. Temperature measurements can be made near the contact interface and a table constructed showing time versus temperature. Once thermal equilibrium has been achieved, an appropriate data point can be used to solve equation (4) for the thermal time constant of the system.

A second method may also prove to be useful in some applications. Since many designers are already familiar with simulating the electrical performance of circuits using SPICE, a thermal simulation can also be run using SPICE. The thermal-electric analogy allows electrical resistance and capacitance to be related to thermal resistance and capacitance, voltage to temperature, and current to heat flow.

As an example, let us consider the Pluggable Bus Bar Connector illustrated in the Figure 6. The electrical and thermal macromodels of the contact are shown in Figures 7 and 8. When terminated with macromodels for the bus bars, the thermal equivalent circuit shown in Figure 8 can be exercised by SPICE in order to show the thermal response of a terminated contact. The output will be a table of time and temperatures from which the thermal time constant can be calculated just as in the direct measurement technique.

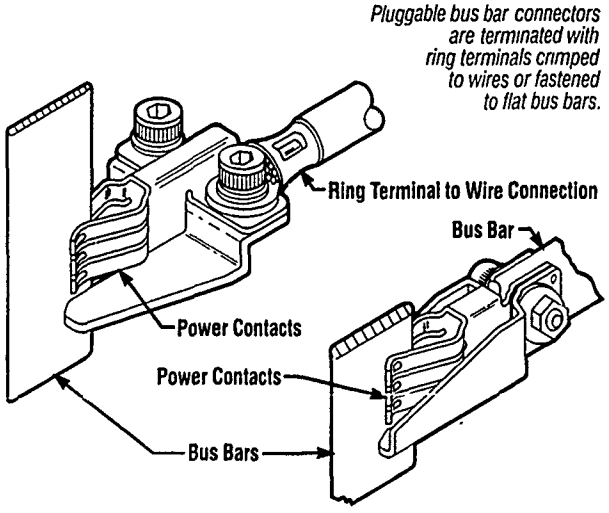

Figure 6. Pluggable Bus Bar Connectors

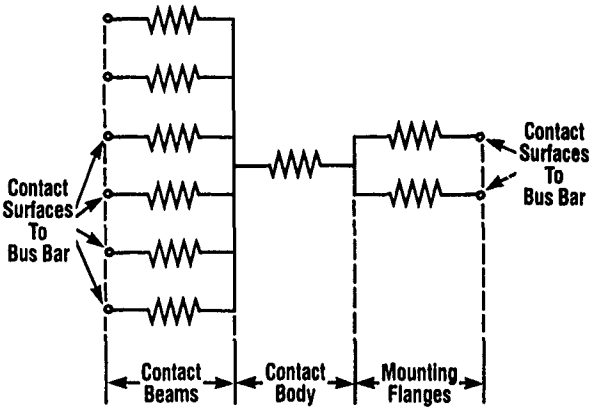

Figure 7. Contact Electrical Macromodel

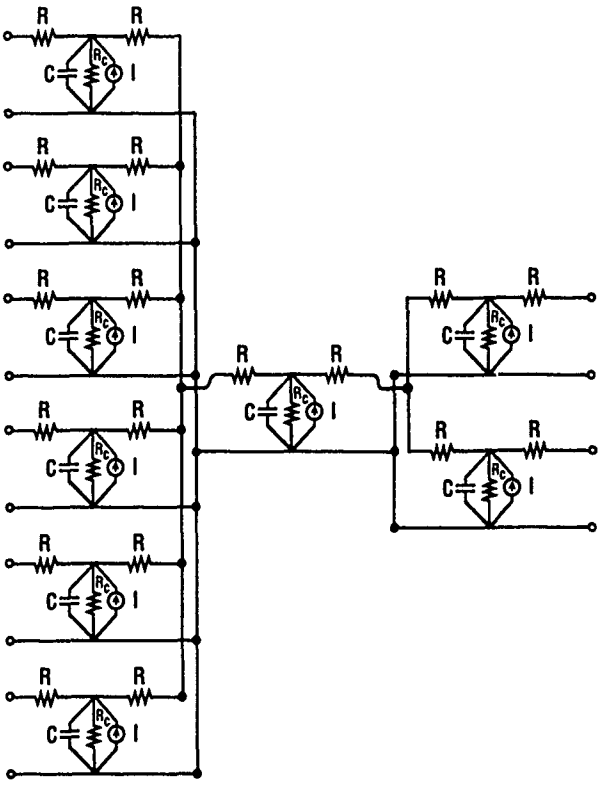

Figure 8. Contact Thermal Macromodel

WAVEFORM CLASSIFICATIONS

The thermal time constant of a system is important due to the role it plays in determining what classification to which a waveform belongs. A continuous waveform is one which is present for any period of time longer than which is required for the contact system to reach thermal equilibrium. Additionally a "well-behaved" waveform is one

which obeys the rule given in Equation (5), the classical relationship between the RMS and peak values for AC currents.

$$Pk=(1.414)(rms) \quad (5)$$

where

Pk = Peak Current (Amperes)
rms = RMS Current (Amperes)

Transients and some forms of overload currents violate the continuous definition. High crest factor currents, some periodic currents, and SMPS (switched-mode power supply) input currents violate Equation (5).

Consequently, each type of waveform must be considered separately when determining a contact's current rating for these types of load currents. The methodology presented here will focus on establishing the current rating for transients which do not meet the continuous definition; for surges and overloads which, although they are finite in their duration, are present for time intervals sufficient to produce significant bulk heating; for high crest factor waveforms that violate Equation (5); and for periodic or duty cycle rated waveforms.

TRANSIENTS

Transients are defined as waveforms resulting from state changes in electrical circuits. By definition, they occur only once. Realistically, they may occur more than once, but they must be separated by sufficient elapsed time to allow the contact system to cool back to ambient. Obviously, the determination of the required time is a function of the thermal time constant of the contact system in a specific application. Figure 9 illustrates one very common transient, an Exponential Double Decay Pulse resulting from inductive load switching. Since it is common for these types of transients to generate voltage amplitudes of several thousand volts, the resulting currents must be factored into the required contact current rating.

A very common use of signal contacts in a computer environment would find the contacts comprising part of a 50-ohm circuit. The designer, following the procedure given earlier, determined that a continuous current rating of one ampere was required. An additional consideration involves the impact of this transient in the circuit. If it is assumed that a peak transient pulse amplitude of 2000 volts is feasible, a quick calculation will show a peak transient current of 8 amperes. The astute designer will quickly recognize that in addition of this application requiring a contact system capable of continuously carrying one ampere, a contact system is required that will also tolerate an 8-ampere transient.

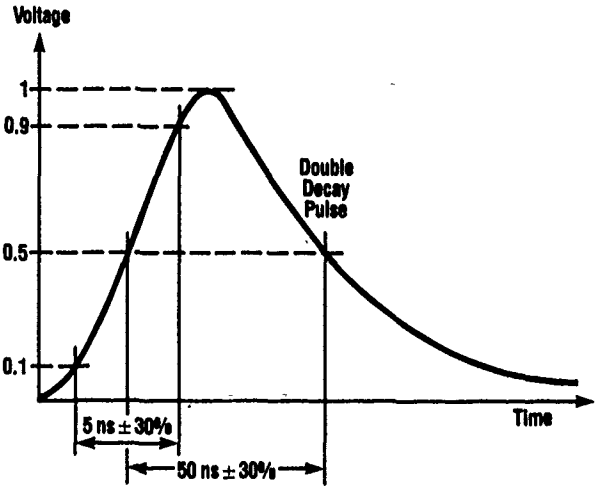

Figure 9. Voltage Template for a Fast-Switching Transient Pulse Under Inductive Load Switching

The procedure for establishing the transient current rating for a contact system is twofold. The designer must consult the section of the product specification addressing "Absolute Maximum" or "Transient" ratings. These ratings, when available, are provided in an effort to prevent failures due to excessive supertemperatures. The "Peak Transient Current" rating establishes the maximum peak current that is acceptable for a given contact system. In this example, the designer requires a contact system that has a continuous current rating of one ampere, and a transient current rating of eight or more amperes.

The second part of this procedure is to insure that the transient waveform is in fact a transient in terms of its impact on the contact system. One possibility is that the "Transient" rating section of the product specification may include information defining the maximum length of time elevated peak currents may be tolerated. In the absence of this information, the designer may construct a graph similar to that shown in Figure 10. The graph is based on the earlier work completed to determine the thermal time constant of the contact system. Using that data, Equation (2) may be solved for time (t) at several current levels. The current and time data can then be plotted as shown. The assumption inherent in this process is that the contact system can tolerate the maximum peak transient current for the time period required to raise the bulk temperature of the contact to whatever temperature rise was selected for the continuous current rating. In the example shown, a design value of 20°C was chosen. The time required for the contact system to reach this value, T_1 in Figure 10 is the maximum allowable time for the transient to be present. If the waveform being rated is present for longer than this time period, then the waveform must be rated as another classification such as an overload, et cetera.

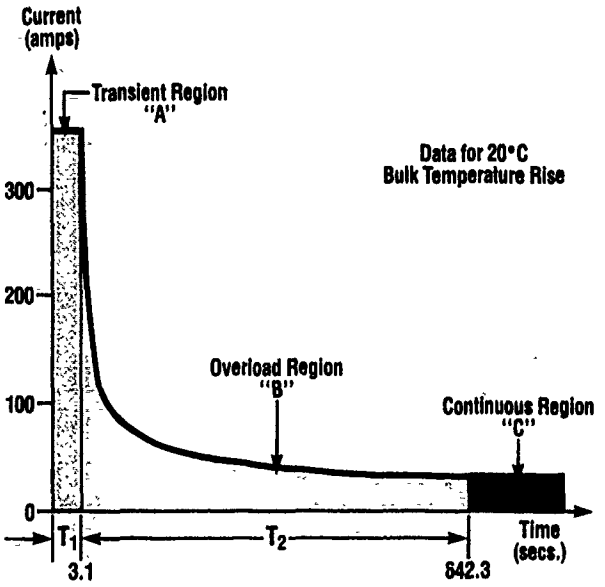

Figure 10. Contact System Transient/Overload Thermal Response

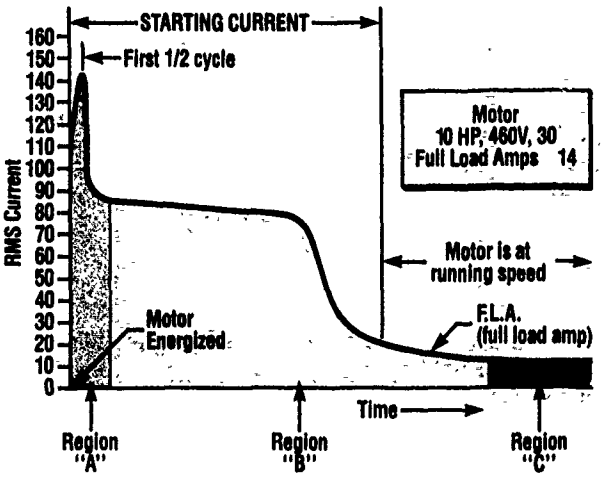

Figure 11. Composite Waveform: Motor Starting

In summary, for transients, the designer must rate the contact system for continuous current through the RMS value of the waveform; for peak transient current through the use of the peak current value of the waveform; and for duration of the transient.

SURGES AND OVERLOADS

The words surge and overload are often times interchangeable. The essential definition of each is that a temporary increase in the current levels being carried through a contact system is being experienced. While a transient is generally not a sinusoidal or other well-behaved waveform, an overload generally is. It is defined, in terms of the contact current rating methodology, as a sinusoidal current in excess of the intended application-specific continuous current rating determined earlier. Figure 11 illustrates an example of a composite waveform containing an overload.

Figure 11 illustrates a typical induction motor starting. The resulting composite current waveform consists of three distinct regions that must all be considered in determining the proper contact current rating. Region A is the inrush current that occurs when the locked rotor is initially energized. It is considered a transient since it generally lasts no longer than one cycle. Generally speaking, the peak current present here is ten times the full load continuous current. This portion of the waveform would be rated as a transient.

Region B of the figure represents an overload condition. As the motor begins to accelerate under load, it draws more load current than when running at full speed. The time occupied by this region is determined by the designer of the motor control system, and varies with each application. Although the current in this region is generally a well-behaved sinusoidal waveform, it should be treated differently than a continuous current. The reasoning behind this decision is one of cost. Since the currents in this region generally run 4 to 6 times the full load continuous currents, using this magnitude of current to rate the contact system would result in selection of a contact much larger than that required to carry the true full load continuous running current.

To determine the suitability of a contact system to function in this application, after determining the transient current rating, consideration is given to the overload current. The factors of interest are RMS current magnitude and duration. Similar to the section on transient current rating, we again can consult the product specification to determine if data is included on the allowable combinations of RMS magnitude versus time. In its absence, the designer can consult Figure 10 again.

Referring to the Figure 10, region A was defined earlier as the safe operating area for transient currents. Region B is the safe operating area for overloads. The graph gives the combinations of current levels and the maximum times that they are allowable before the bulk temperature of the contact system exceeds the selected maximum allowable bulk temperature rise.

The designer, in this application must now insure that he has selected a contact system that can meet his continuous current requirement, his transient current requirement, and also his overload current requirement. Failure to address the transient current requirements creates the

potential for catastrophic contact failure due to interface damage. Failure to address the overload current requirements may damage the interface due to excessive supertemperatures, or it may damage the contact system through the various bulk temperature related failure mechanisms.

In summary, for overloads, the designer must rate the contact system for continuous current through the RMS value of the waveform; and for duration of the overload.

Before leaving Figure 11, it is of interest to note that Region C represents the full load running current of the motor. This region represents a continuous current, and would be rated through the use of the earlier methodology.

HIGH CREST FACTOR LOADS

The crest factor of a waveform is the ratio of the peak voltage or current to the RMS voltage or current. We earlier defined a well-behaved waveform as one where this ratio is 1.414, the normal relationship of peak value to the RMS value in a sinusoid. In situations where the crest factor exceeds 1.414, the designer is cautioned to include an additional check in his contact current rating procedure.

Figure 12 illustrates a common situation found in modern electronic systems. The two principle examples of this situation that we must consider are the neutrals in three phase power distribution systems that may carry significant third harmonic currents, and input currents to switched-mode power supplies (SMPS).

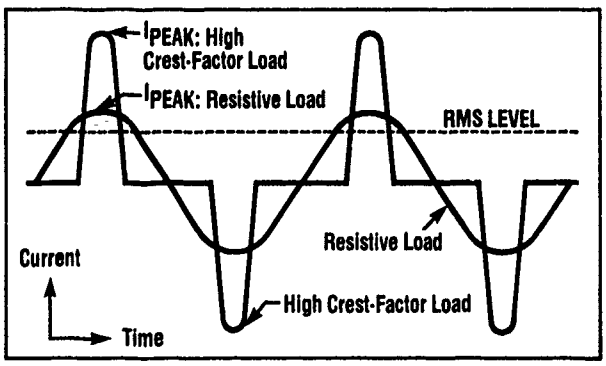

Figure 12. High Crest-Factor Waveform

Third Harmonic Waveforms. In many multiphase power distribution systems in office environments, designers will often find a plethora of personal computers. Many of these computers use SMPS. As we will see later, SMPS draw unique current loads. Where we would expect to find no neutral current in a balanced network, we actually find a high crest factor waveform like that shown in a worst case condition in Figure 12. It is important to note that there are varying degrees of this phenomenon. The figure illustrates a worst case scenario where the waveform has actually been distorted into a series of Haversine current pulses. The correct current rating procedure for this worst case condition will be addressed under the next section.

For a less severe condition, where portions of the resistive load sine-wave still exist but are distorted by a Haversine-like spike near the waveform apexes, a different procedure can be used. For example, a designer recently found that he was confronted with a waveform of this type that exhibited a true 15 ampere RMS value. He also found that the waveform registered a 2.7 crest factor. For a well-behaved continuous current, one would expect a 21 ampere peak load, rather than the 40.5 ampere peak he found. A very conservative, and costly, approach to this application would have the designer select a contact system capable of continuously carrying the 40 ampere load. A less conservative, but more economical, solution was found when the designer consulted AMP engineering. With the waveform well characterized, engineering was able to determine that the peak energy was not sufficient in this application to significantly change the bulk temperature of the contact system, nor to raise the supertemperature of the interface beyond the maximum allowable value.

In the case of high crest factor waveforms, we cannot use the RMS value alone to current rate the contact system. The designer must first determine the continuous current rating required for the application using the RMS level indicated by the continuous, repetitive nature of the waveform. Then the designer must verify that the peak values present in the waveform do not violate the contact specifications for maximum transient peak current. Upon fully characterizing the waveform, engineering should then be contacted to insure that the abnormally high peak value associated does not damage the contact interface. In very severe applications, such as that shown in Figure 12, the waveform should be classified as a Duty Cycle Waveform and current rated accordingly.

Switched-Mode Power Supply Waveforms. Figure 13 illustrates the waveform typically generated at the input to a SMPS. The figure depicts the voltage across the input capacitors and its relationship to the input current and voltage waveforms. Current is drawn only during the time period when the capacitors are recharging. Consequently, the input current appears as a repetitive series of Haversine pulses. The significance of this waveform is that although we have a continuous waveform, it is no longer sinusoidal, nor is the relationship of Equation (5) valid. As we have seen earlier, when this equation is not valid, we must modify our procedure to insure that the peak currents present do not damage the contact system through excessive supertemperatures.

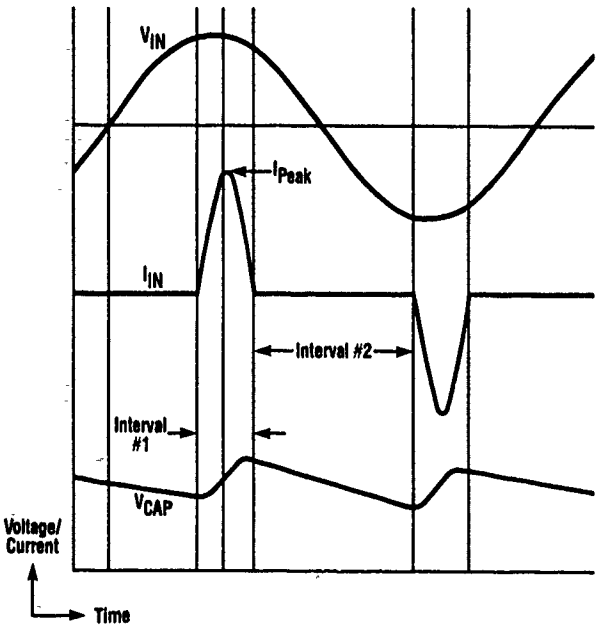

Figure 13. SMPS Waveforms:
Top - Input Voltage
Middle - Input Current
Bottom - Capacitor Voltage

In a typical SMPS, we can expect to find a power factor on the order of .65 or so. With this magnitude of power factor, we can expect to find peak currents that are approximately 3 times the RMS magnitude. Due to the absence of any current flow between these current pulses, the designer should consider this type of application to be a Duty Cycle classification, and current rate his contact system accordingly.

In summary, for high crest factor waveforms possessing a valid continuous current content, the designer must rate the contact system for continuous current through the RMS value of the waveform; and for peak transient current through the use of the peak current value of the waveform.

DUTY CYCLE RATED WAVEFORMS

In many applications, the current drawn by a load occurs in finite length pulses. We refer to these waveforms as being "Duty Cycle Rated" due to the discontinuous nature of the current flow. Figure 14 illustrates 10% and 50% duty cycle waveforms. When the period for the duty cycle waveform is less than the thermal response time (based on the thermal time constant determined earlier) of the contact system, the bulk temperature of the contact will never reach its normal 100% duty cycle (continuous) current magnitude. With a lower bulk temperature, the supertemperature will not reach its normal 100% duty cycle (continuous) current value. This condition allows the contact designer to generate a rerated continuous current rating of a higher magnitude for duty cycle applications for this particular application.

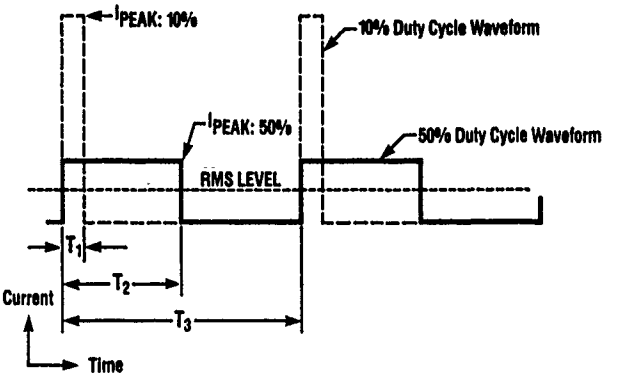

Figure 14. Duty Cycle Rated Waveforms

The designer confronting a duty cycle application should not simply current rate his contact system based on the effective or RMS magnitude present in his application. The two waveforms shown in the figure have the same RMS value even though they exhibit drastically different peak values. Many designers use very short duration, high amplitude pulses to position motors. The 10% duty cycle waveform is representative of this condition. If this waveform were present only once, or sporadically, then the use of the transient classification for current rating would be appropriate. These types of waveforms activate the failure mechanisms associated with supertemperature. Consequently, the use of the RMS magnitude to current rate is inappropriate.

For duty cycle applications, the designer must consult a modifier chart similar to that shown in Figure 15. The rerating procedure mentioned above allows the contact manufacturer to generate a graph that details the amount that the continuous current can be increased for various duty cycles. This modifier can be used in a manner analogous to the Base Current Modifier (F) in our original current rating procedure to increase the application-specific continuous current rating (I) of an contact system in a given application. This relationship is given in Equation (1). The final application-specific continuous current rating becomes the one given in Equation (6).

$$I = I_B \cdot F \cdot G \qquad (6)$$

where

I = Continuous Current Rating (Amperes)
I_B = Base Rated Current (Amperes)
F = Base Current Modifier
G = Duty Cycle Modifier

Wire Gauge

Duty Cycle	22	18	14
90%	.8	1.0	1.2
50%	1.2	1.4	1.6
10%	1.8	2.0	2.2

G

Figure 15. Ampliwidget Duty Cycle Modifier Chart

SUMMARY

In summary, a methodology has been given that allows a designer to determine the current rating for a given contact system in a specific application. The procedure allows a continuous current rating to be derived from a base current curve characteristic of the contact pair. This current is modified to reflect the size of the conductor terminated to the contacts, the maximum ambient temperature, the desired bulk temperature rise, and the loading density of the contacts in a housing.

The methodology also allows the contact to be rated for transients and overloads by inclusion of considerations focused on the peak current, and their durations. The quantities that must be characterized in order to successfully current rate a contact system are given in Table 1.

Consideration has also been given to periodic waveforms with high crest factors and to the pulse widths typically used in duty cycle applications. The methodology includes a second modifier chart for use in rerating the contact system for duty cycle applications.

- **Continuous Current Rating**
  - —DC
  - —AC, RMS
  - —Periodic, Effective
- **Transient Current Rating**
  - —Peak
  - —Duration
- **Overload Current Rating**
  - —Peak
  - —Duration
  - —Waveform
- **Composite Current Rating**
  - —all of the above

TABLE I

BIOGRAPHY
JAMES H. WISE, P.E.

Jim holds a Bachelor of Science degree in Electrical Engineering and a Master of Business Administration degree from Pennsylvania State University. He is a registered Professional Engineer in Pennsylvania. At his alma mater, he is a member of the Electrical Engineering Program Advisory Committee, and has been an instructor at the Capitol Campus of PSU teaching analog circuit design, digital circuit design, and microprocessor-based data-acquisition systems design. He is currently a Development Engineering Manager in the Business Development unit of Capital Goods Business Sector at AMP Incorporated. Jim came to AMP in 1974, and has worked in product and development engineering for several divisions. He holds over thirteen patents for his work there, and has a number of publications to his credit.

A New Generation of Fiber Splices and Installation Results

G. F. DeVeau, J. A. Aberson, and J. K. Lo

AT&T Bell Laboratories, Norcross, Georgia 30071

Abstract

Using the combined resources of customer input, laboratory design and field testing, a fiber splice has evolved that provides for the first time a totally applicable product for the future.

As optical fibers become widely spread throughout all areas of telecommunications and electro-optic manufacturing applications, there will be increasing pressure for low cost and high productivity. In trying to anticipate this trend during the past two years, AT&T Network Cable Systems determined through surveys of all the major market customers that mechanical splice hardware that emphasizes user friendliness and direct simple feedback is needed. Thus far, although a myriad of mechanical splices are available, none meets all desired requirements. Using these surveys, however, and continued customer reactions, a customer-driven fiber splice has been developed, tested and introduced. As a result, this fiber splice and its assembly tools also embody all of the features dictated by current users for the future fiber-to-the-premise revolution.

Splice Development

Early during the development of AT&T's Next Generation Splice, interaction with selected customers provided the feature and performance criteria that would be necessary for a mechanical splice to meet the needs of a changing splicing environment. Fiber splicing is now most often done by well trained crews who regularly join outside-plant cables in controlled environments, ie., air-conditioned vans, trucks or trailers. Future splicing scenarios, particularly for fiber-to-the-home, include more numerous splicing crews and individual splicers with less formal training and little experience. These splicers will often gain experience on the job from associates and from instructional video tapes or manuals and the splicing environment will frequently be curbside with minimum protection from the elements.

From frequent informative discussions with our customers, the required performance/features for a mechanical splice that satisfy the needs of a changing environment are:

Low Cost - Often the first customer consideration is splicing costs. Not only the first cost of the splice itself but the total installation cost taking into account splicing time, splice yield and tool costs.

Splice Loss - Meeting the transmission requirements for present and future systems, splice losses averaging 0.20 dB or less for passive splicing are required. All passive splice designs are dependent on fiber quality to achieve this splice loss, and the rising trend to tighter fiber specs will ultimately lower these average splice losses.

Reflectance - Reflections averaging less than -50 dB, with worst case less than -32 dB (fiber backscatter), are required.

Operating Temperature Range - Since splices will be deployed in all of outside-plant environments, from manholes to pedestals splices must be stable from -40° F to 185° F.

Storage Temperature Range - Splices must be capable of long-term storage in warehouses, trucks and vans without any degradation to the performance of the device.

Splice Assembly - The splice must be a cleaved fiber design not requiring polishing or adhesives for assembly. Index matching material must be an integral part of the splice and should not require any curing operation. All splice components should be in place with no loose parts requiring any field pre-assembly.

Universal Size - Great importance is placed on being able to use one universal splice to join coated (250 μm) and buffered (900 μm) fibers or a mix of the two. This eliminates the necessity, cost and complexity of ordering and stocking several sizes of splices.

Craft Feedback - There was desire expressed for a unique splice design feature that gives the splicer confidence that he or she has made an acceptable, low-loss splice without test equipment or remote monitoring.

Reusability - To be able to quickly and reliably reuse a splice that is unacceptable because of bad fiber cleaves or improper splicing procedures is important for lowest cost to be achieved.

Training and Support - Clear instructions and training aids such as video tapes are of utmost importance. The splice should be easy to use whether the splicer is engaged in day-to-day splicing or, as with restoration crews, it is used infrequently for emergency restoration.

Shelf Life - Unlimited shelf life is absolutely required. Having to keep dated material checked, reordered and replaced is costly and cumbersome.

Initially three different splice designs that met these requirements (other than reusability) were presented to customers for their reactions. The design chosen by them is the AT&T CSL LightSplice™ System, which can be reused and tests are underway to validate this feature and will be reported at a later.

Design Features

Especially designed to meet emerging customer requirements for minimal training, low-cost and high productivity, this universally applicable mechanical splice uses cleaving for fiber end preparation, a one-part factory-installed index-match material for the splice interface, a precision slotted capillary to align the mating fibers and a metal spring clip with compliant tape to press and hold the spliced fibers. It introduces a unique technology that provides strong visual feedback, which is a universally understood means, for informing the splice user about the physical positioning of fiber coatings/bufferings and about the all-important fiber-to-fiber contact. To achieve this, transparent materials (glass and plastic) are used for the splice. Furthermore to enhance viewing, the clear-plastic splice housing is purposely designed and assembled to magnify the fiber juncture. Field results show that this high visibility gives both better splice quality and higher productivity than all the other currently available mechanical splices.

Another unique feature is that its universal size accepts all combinations of 250 µm and 900 µm coatings/bufferings, and it accepts all 125 µm OD single-mode and multimode fibers. Consequently, designers, distributors and splicers need have only one splice for all permanent and restoration installations.

Splice Design

Figure 1 shows an exploded view of the splice components. The injection-molded clear-plastic housing has a lens incorporated to magnify the view of the fibers during insertion. Pre-filled with an index-matching grease, the glass capillary is funneled at both ends to coordinate with a series of funnels molded into the housing. Altogether, these enable quick and easy insertion, guidance and positioning of fibers, coatings and bufferings into the splice. Contact between the cleaved ends in the slotted splicing area, where the spring will capture and permanently hold the mated fibers, is verified by viewing through the housing lens. Field use has enthusiastically endorsed this unique characteristic and installation results show enhanced productivity because of it.

SPLICE - EXPLODED VIEW

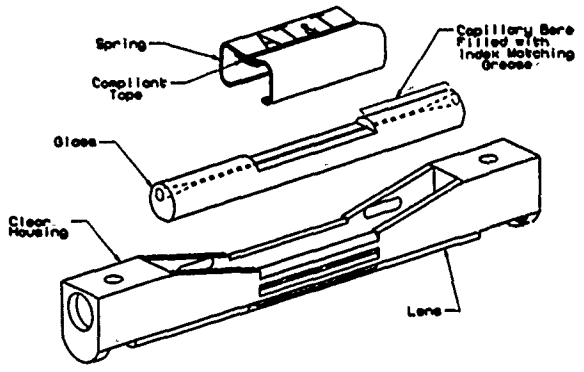

Figure 1

Housing

The plastic material used to make the housing must be optically clear to permit a visual indication of fiber contact. This material also must be rugged enough to withstand temperature and humidity extremes without any significant dimensional changes. Polysulfone is chosen as the ideal plastic to meet these requirements. Since the retention spring when closed relies on the dimensionally stability of the housing to maintain a near constant force on the fibers, the plastic must be resistant to creep over the life of the splice. Finite element analyses and accelerated testing simulating a 20-year exposure in a fully loaded outdoor cabinet in Yuma, AZ shows negligible creep that is well within the allowable deflection range of the closed spring.

Spring

Any alloy used for the retention spring must have high strength, ready formability and superior stress-relaxation performance. It should also have good dimensional stability during post-forming heat-treatment. A Spinodal alloy, developed by AT&T Bell Laboratories and selected for the spring design, has properties which exceed those exhibited by traditional beryllium-copper alloys.

Glass Capillary

A slotted glass capillary tube is the heart of the splice. As for the housing, optical clarity of this component is necessary for fiber visibility and the thermal expansion characteristics of this glass, being very similar to the glass fiber, give this design excellent environmental performance. End entrances of the capillary bore are funneled to allow easy fiber entry, and the bore is smooth and free of irregularities which could result in fiber misalignment. The slotted area is precision ground to expose the top halves of fibers for uniform contact and retention by the closed spring.

Index-Match Material

One of the most critical components of any mechanical splice, insuring long-term reliability, is the fiber index-matching material. The one selected for this splice has a refractive index that is very closely matched to the fiber core and is transparent at all operating wavelengths. Its viscosity remains gel-like over the entire operating and storage temperature ranges without stratification and splice components and fiber coatings are completely compatible with this matching material.

Compliant Tape

A compliant tape applied to the longitudinal fiber-contact length of the spring provides three major functions. It acts as a buffer between the spring and the fiber, accommodates fiber OD differences, and seals the area between the spring and glass capillary from water or other contaminate ingress. While achieving these important features, the tape, in contact with the fiber joint, does not degrade the environmental performance of the splice.

Splice Operation

How the component parts are used to affect a low-loss, permanent fiber optic splice can best be explained by examining a detailed cross sectional view of the splice's slotted region shown in Figure 2. Here the metal spring is in the open position, and the fibers are freely longitudinally movable. The unslotted capillary sections at each end keep the fiber ends coarsely transversely positioned so that they do not miss each other during insertion. The compliant tape is shown bonded to the spring with a layer of index matching material on it's surface to reduntantly seal the fiber joint from environmental intrusions. Index-matching material fills the unslotted capillary sections to provide wells of grease that the fibers pick up to match out the splice interface and it fills the interstice between the glass capillary and the housing to aid fiber visibility. Note that the curvature on the housing is precisely radiused to produce a fiber magnification of about 5x.

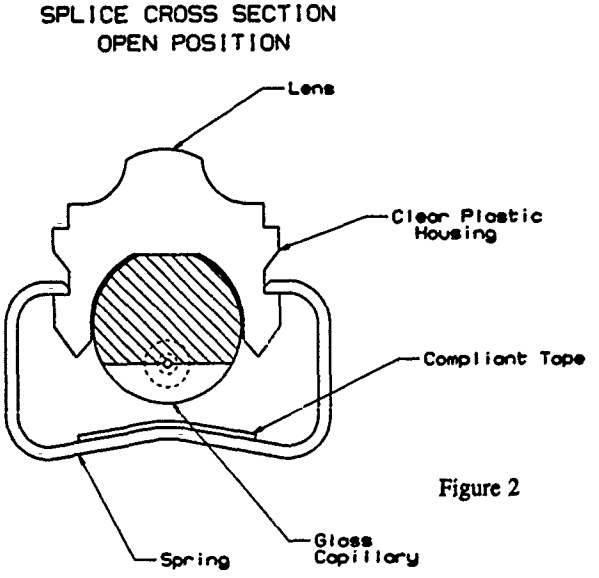

Figure 2

Figure 3 illustrates the same cross section for the completed (closed) splice. The spring is closed on the second set of detents molded into the housing to press both index-matched fibers into the groove of the slotted capillary. In this final position, the fiber ends are precisely aligned to achieve low insertion-losses, low return-losses and fiber retention in a permanent mechanical splice.

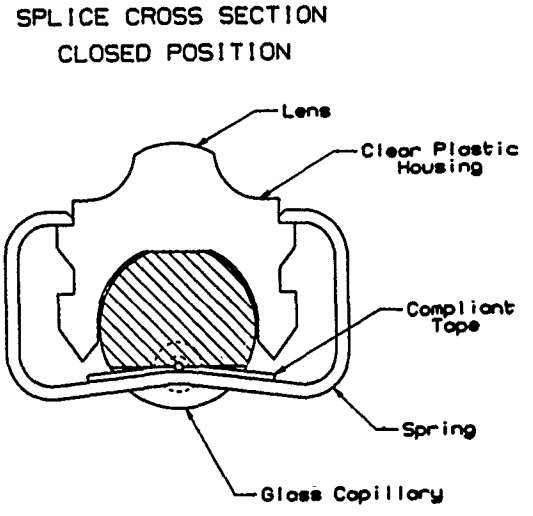

Figure 3

Workstation

As with the design of the splice, the workstation is a result of ongoing, direct interactions with our customers. Figure 4 shows the layout of the workstation. Mounted on a strong base to provide stability during splicing, the splice-holder pedestal is tilted toward the splicer at 25° for optimum viewing. Fiber-gripping pedestals on each side of the splice holder have foam inserts which hold the fibers in place even during windy conditions but which allow the fibers to be easily slid into the splice entry funnels. Spring closure is accomplished with the closing-lever arm. Integral to this arm is a force-limiting spring which eliminates overloading while ensuring sufficient force on the splice. A light mounting bracket and battery-powered lamp enhance viewing when splicing under poorly illuminated conditions. A cleaver-mounting captive screw and tripod mount are added features to make splicing more convenient. Affixing the cleaver prevents wasted motions and makes a "system" of the splicing set-up. Very high productivity is possible with this system approach.

A hand-held tool is also available without the lamp and cleaver mount. The workstation may be obtained with a tool kit which includes basic fiber preparation tools necessary to make a fiber splice and a video tape with step-by-step splicing instructions.

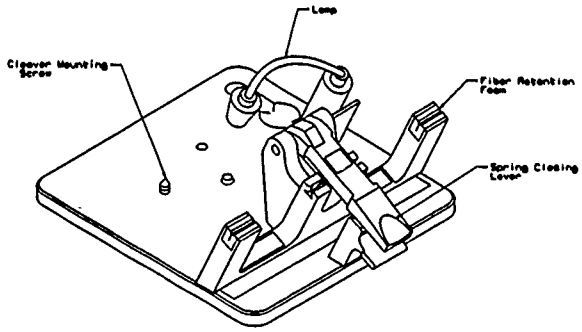

WORKSTATION

Figure 4

Laboratory Testing

Thermal Cycling

Laboratory thermal cycling tests have been completed which simulate an extended outside plant environment. The thermal cycle, plotted in Figure 5, ranges from -40° F to 185° F. During cycling tests, splice insertion-loss and return-loss measurements are made bidirectionally with an OTDR at the temperature extremes and at room temperature. In Figure 6 the average splice loss of 12 splices is plotted. The splices were cycled 100 times, however, for clarity only cycles 1-25 and 75-100 are shown. Average changes are cyclic, are less than 0.05 dB and show no residual added loss.

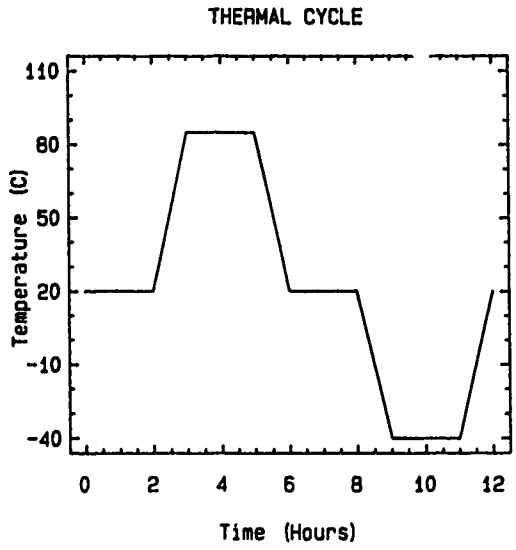

Figure 5

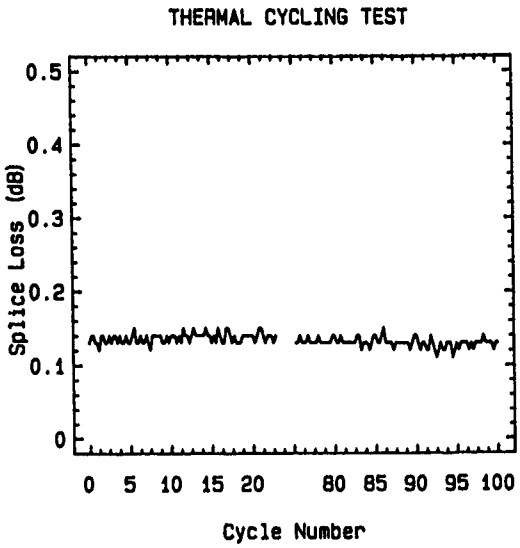

Figure 6

Water Immersion

Twelve splices were immersed in 110° F tap water for 7 days while monitoring splice loss. Figure 7 shows the loss variations from the initial measurements through day 7. The maximum change seen was less than 0.05 dB. All changes were completely recovered within 2 hours of removal from the water. These same 12 splices were then subjected to another 100 thermal cycles (Figure 5) with behavior the same as shown by Figure 6.

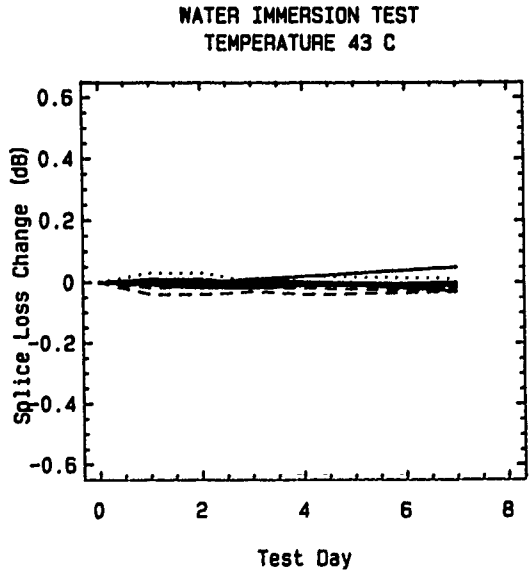

Figure 7

Vibration Testing

In order to verify the integrity of the splices when subjected to vibrations, 12 splices were tested according to EIA Standard FOTP 11. The splices were inserted into a splicing tray which was mounted onto a vibration platform, first with the splices in a horizontal direction, and finally with the splices rotated 90° from horizontal. The table was cycled from 10 Hz to 55 Hz to 10 Hz every minute with a total excursion of 0.06". This cycle was run for two hours in each plane. No change in the average splice loss was observed from vibrations in either plane and individual splice losses varied a maximum of 0.01 dB, which is within OTDR measurement error.

Fiber Pullout Tests

Fiber pullout tests were done on an Instron tensile testing machine with a crosshead speed of 5 inches per minute. Thirty splices were tested and the results show that the splice is capable of withstanding a minimum strength of 0.60 pounds. The average tensile force of the splice is 1.15 pounds with 90% of the splices having a strength of over 0.75 pounds and 80% over 1.00 pound.

Return Loss

Return loss was measured at -40°C, 9°C, 21°C and 85°C. Figure 8 shows the average return loss of 12 splices measured at 1310 nm.

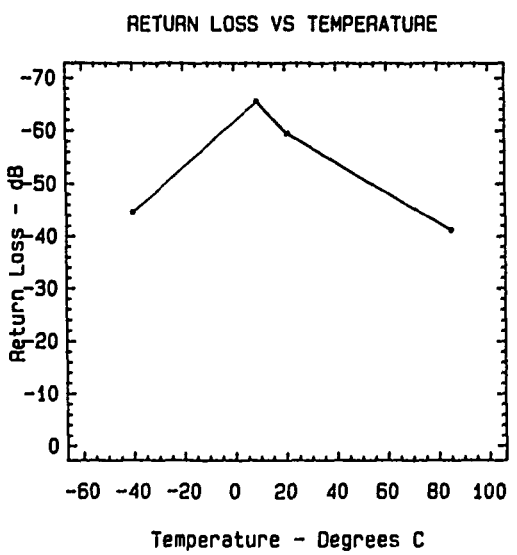

Figure 8

Field Results

A customer field trial was completed in early, 1990 to gain field experience, and to obtain "real world" splice loss and yield data on this new splice. The crew selected for this trial had previous although limited fiber joining experience; they only splice fiber sporadically three or four times a year. A two-hour training session was held in the work center wherein the craft viewed a short video tape, were given a demonstration and then made some practice splices with two fiber spools and an OTDR.

Field splicing began immediately on two 144-fiber ribbon cables. Only 120 of the 144 fibers were joined leaving the remaining 24 fibers unspliced to be used at a later date. Splicing was done in a van and two OTDR's were set up in the two offices to record splice loss. The splicing was to be accomplished passively, that is without test equipment, so the splicers were not given any indication of splice quality until after the splices were made. Figure 9 is a histogram of the splice losses of the 120 passively aligned splices. The average splice loss was 0.18 dB with a standard deviation of 0.13 dB. Out of 120 splices 5 splices were remade because of insertion losses greater than 1.0 dB for a yield of 96%. This performance is consistent with the advertised average loss of less than 0.20 dB.

Feedback from the splicers was very positive and the unique ability to see the fibers butt together and being able to observe the position of the fiber coating gave them added confidence in the splicing operation.

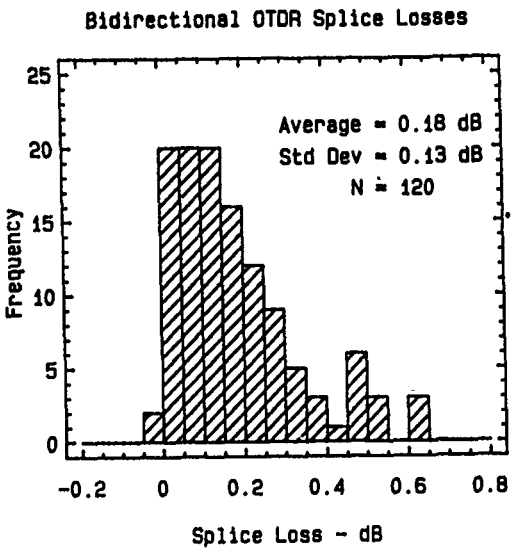

Figure 9

Conclusion

As defined by extensive customer surveys, a new generation optical splice has been designed, tested and field trialed. This splice meets all the performance characteristics on insertion loss, reflection, environmental testing, universal size, minimal training, low cost and high productivity required by current and future users. Importantly, it also introduces a vital new dimension: universally understandable visual verification. In the future, this last feature may be its most unique contribution.

George F. DeVeau is a Member of Technical Staff at AT&T Bell Laboratories, Norcross, Georgia. After joining Bell Laboratories in 1967 he was involved with multipair cable design and development. Since 1980 Mr. DeVeau has been engaged in the design and development of fiber optic splicing systems.

James A. Aberson has been at AT&T Bell Laboratories since 1980, where he has worked principally on analysis and design of fiber splicing methods and devices. Since 1986, he has been Supervisor of the Lightguide Joining Group which is responsible fo all fiber splicing methods for AT&T and its customers. He holds BS, MS, and PH.D degrees in Structures and Mechanics from North Carolina State University.

Joseph K. Lo is a Member of Technical Staff at AT&T Bell Laboratories, Norcross, Georgia. Joseph joined Bell Laboratories in 1986 and he has been instrumental in the desigr. and development of lightguide splicing products and associated test apparatus. He recieved his BS in Mechanical Engineering from the Massachusetts Institute of Technology in 1986 and his MSME from Stanford University in 1987.

FACTORY SPLICED FIBERS: TECHNOLOGY, PERFORMANCE AND FIELD EXPERIENCE

Hans Damsgaard and Ole Hansen

LYCOM A/S
NKT Alle 75, DK-2605 Brøndby, Denmark

ABSTRACT

To provide long continuous fiber length for cable operations a method for splicing fibers, re-establishing the coating around the splice point, and finally prooftesting the splice point has been developed and implemented in standard production environment. The technology has proven to be a consistent cost efficient way to achieve up to 50 km continuous lengths of primary coated optical fiber. Average splice strength is > 2 % and average splice loss is 0.07 dB at 1300 nm and 1550 nm.

Life time test based on dynamic fatigue measurements indicates the same minimum life time of the splices as of the fiber and this conclusion is supported by more than 5000 splices being cabled and installed in the field during the last 3 years with no observed failures.

INTRODUCTION

For many optical fiber cablers it is important to have longest possible standard length of fiber as raw material, for example 30-60 km. This increases production efficiency because of less upstart time and also it allows efficient production planning with high yield since the long cable lengths can be cut to customer desired lengths yielding good flexibility. Finally, for certain types of submarine cables long fiber length is a key factor.

To address these requirements a method for factory splicing including re-establishing of coating and prooftesting at the splice point was developed.

In this paper the technology is discussed and loss and strength results are reported. Also life time considerations for the splices based on stress corrosion measurements are included, and finally the field experience obtained during the last 3 years is reported.

TECHNOLOGY

A commercial fusion splice system FSU850 from Ericsson is utilized for splicing the fibers. Local injection is applied for positioning of the two fiber cores. Before splicing a few mm of coating is removed and the fiber is cut with a commercial FK 11 fiber cleaver from York.

After the splice process the coating is re-established around the splice point by positioning of the spliced fiber in a precision made tube, which is then filled with the same UV-curable acrylate as is used as the secondary coating on the D-LUX 100 P/S dual layer coated fiber. Finally, the coating is cured by UV light and the splice point is prooftested for 1 sec at a level of 1.5 times the prooftest level of the fiber, typically 1.5 percent.

The outer diameter of the re-established coating is nominally 400 µm and it extends in length to cover also part of the 250 µm fiber coating, see figure below. Thereby the glass surface becomes well protected. The length of the re-established coating is approximately 2 cm.

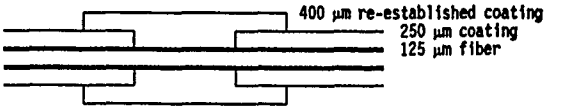

The coating stripping and re-establishing processes ensure good adhesion to the original coating so that even hard bending of the fiber at the splice point will not allow e.g. water to penetrate to the fiber.

As expected for most cable constructions, specifically for slotted core and loose tube cables, the quality of the re-established coating has been observed to imply the same smooth cabling operation as for non-spliced fibers.

LOSS AND STRENGTH RESULTS

Fig. 1 shows a typical loss distribution at 1300 nm and 1550 nm. The average splice loss is approximately 0.07 dB at both wavelengths as measured by 2 way OTDR. Loss is defined as the average of the OTDR readings. These figures represent values from production, where a typical specification is 0.15 dB or for tighter specified products 0.10 dB splice loss.

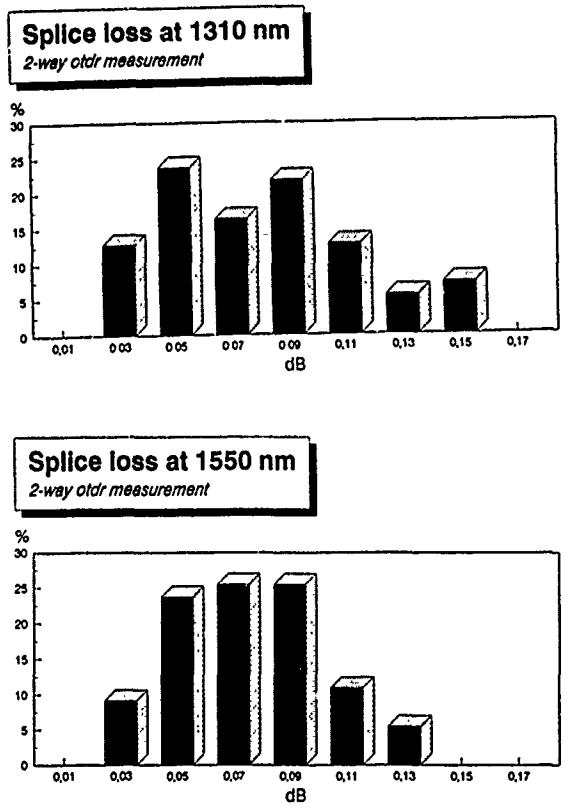

Fig. 1 Splice loss distributions at 1300 nm and 1550 nm as measured by two way OTDR (production results)

The splice machine settings (fusing current and fusing time) are optimized to achieve maximum strength. If loss was to be minimized a slight strength reduction may be observed.

Fig. 2 shows the strength of the splices as measured at different loading rates in a tensile strength test machine from Instron. Average strength is in excess of 2 percent.

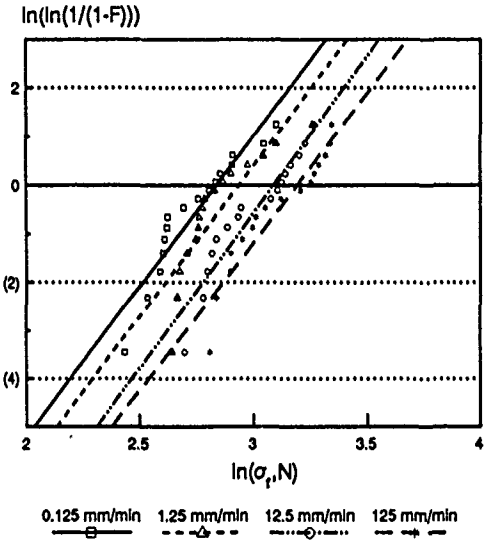

Fig. 2 Weibull distributions for the splices as obtained at different strain rates: N x 0.125 mm/min, N = 1, 10, 100, 1000

LIFE TIME OF SPLICES

When calculating life time or time to failure for optical fibers a stress corrosion model is often used, 1-3). Based on the actual prooftest level of the fiber the fiber life time can be calculated either on a statistical basis 1) or as a guaranteed minimum life time based on the prooftest of the fiber, 2-3). For both approaches the key factor in the calculation is

$$(Sp/Ss)^{n}$$

Ss: static appled stress in the field
Sp: prooftest level
n : stress corrosion exponent

Since n typically is in the range of 18-25 for commercial fibers the life time is very sensitive to the static load applied to the fiber. Normally a 30 years life time is expected if Ss is kept below 25-30 % of the original prooftest level for fibers with an n value of e.g. 23, which is a typical value today.

For the splices a stress corrosion exponent n = 18 ± 2.5 was obtained by measuring the strength as function of loading rate and using fitting to Weibull curves to minimize the effect of the somewhat high standard deviation of the results, see fig. 2,3.

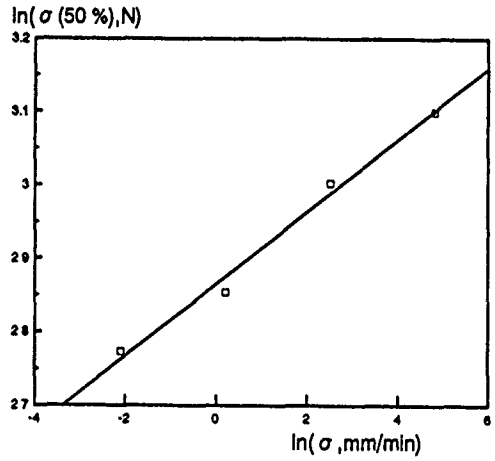

Fig. 3 Determination of stress corrosion exponent by plotting ln (loading rate) versus ln (F = 50%) and making a least squares fit.

The reason for the lower n value of the splice point than the n = 25 for the D-LUX 100 P/S dual coated fiber may be caused by different glass history or that the splice is recoated using a hard single coating, namely the same coating as is used as the secondary coating on the fiber. To compensate for the slightly lower n value than the n = 23 used in most life time calculations it was decided to prooftest the splices at 1.5 times the prooftest level of the fiber. According to above for a 1 % prooftested fiber the same life time of 30 years will then result when loading the fiber or the splice to the extreme of 0.3 % static load.

The impact of the single layer of coating at the splice point on the temperature window of the fiber is considered to be negligible because of 1) the very short length of fiber coated with single coating and 2) our experience with long length of single coated fibers with good temperature performance. The same arguments apply regarding microbending sensitivity.

FIELD EXPERIENCE

During the last 3 years LYCOM A/S factory spliced fibers have been cabled and delivered to different markets. About 5000 factory splices are in cables in operation in Denmark. Also a significant amount of our factory splices have been installed internationally. So far no failures or problems have been reported.

In addition our factory splices have also been widely utilized for manufacturing of long continuous length of submarine cables.

CONCLUSION

Factory spliced optical fibers have been successfully implemented and introduced on the marketplace for primary coated optical fibers with the positive impact on cable cost, flexibility, yield and possible continuous cable length > 50 km.

Average splice loss is 0.07 dB at both 1300 nm and 1550 nm and average strength is in excess of 2 %

The stress corrosion exponent n = 18 for the splices has been measured by dynamic fatigue. This figure is within the range of expected values. To compensate for the difference of n between the splice and the fiber the splice prooftest level was set at 1.5 times the prooftest of the fiber. This ensures that the same minimum life time of 30 years will result for a 1 % prooftested fiber and a 1.5 % prooftested splice, when being exposed to the extreme of 0.3 % static load.

An extensive field experience with more than 5000 factory splices being cabled and installed during the last 3 years with no observed failures during installation or operations heavily supports that factory spliced fibers are as reliable and as easy to cable as non-spliced fibers.

ACKNOWLEDGEMENT

The authors wish to thank Mr. John Krause, AT&T Bell Laboratories, Murray Hill, New Jersey for helpful discussions.

REFERENCES

1. Y. Mitsunaga et. al., Electr. Lett. Vol. 17, no. 16, p. 567 (1981)

2. A.G. Evans and S.M Wiederhorn, Int. Journ. Fract. 10, p. 379 (1974)

3. K. Jakus et. al., Journ. Mat. Science, 13, p. 2071 (1978)

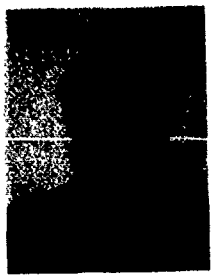

Hans Damsgaard
LYCOM A/S
NKT Allé 75
DK-2605 Brøndby
Denmark

Hans Damsgaard was born in Denmark in 1956 and is a graduate of the University of Aarhus in Physics. Upon graduation he got a PhD-degree from the Technical University of Denmark and NKT. Since 1981 he has been working in the optical fibers Development and Engineering department of NKT and from 1987 in LYCOM A/S and is now Manager of D&E.

Ole Hansen
LYCOM A/S
NKT Allé 75
DK-2605 Brøndby
Denmark

Ole Hansen was born in Denmark in 1958. In 1982 he became a Measurement Technologist and since 1983 he has been working as a Technical Specialist in the fiber optic Development and Engineering department of NKT and from 1987 in LYCOM A/S.

Field Mountable Two-Fiber Ribbon Mechanical splice

H. Tsukiyama* H. Yokosuka** H. Hirao** Y. Nomura** H. Furukawa**

* Chubu Electric Power Company, Inc.(Nagoya, Japan)

** FUJIKURA LTD. (Chiba, Japan)

Abstract

We developed a novel and simple mechanical splice for single mode 2-fiber ribbon in preparation for a higher diffusion of optical fiber subscriber networks in future. The novel mechanical splice has a mean splice loss of 0.54 dB and the average assembly time for splicing including the time necessary for UV adhesive curing is less than 3 minutes. By using an assembly tool provided for the purpose, the mechanical splice can be mounted at site without any special skills and can achieve a uniform quality.

1. Introduction

When optical fiber subscriber networks reach all the households in Japan in the near future, information unprecedented in quality and volume will become easily accessible. Such optical fiber networks, however, is difficult to build unless the technology to connect optical fibers as easily as those used currently for copper cables is established. Anticipating such needs, we developed a mechanical splice which can be attached easily and quickly at site and a method of assembling the splice.

2. Structure

Fig. 1 shows the appearance of a connector.

Fig.1 Connector

The main body has two thin ferrules molded with rubber. The outer diameter of a ceramic ferrule is 1.0 mm which is 40 % of the currently prevailing FC type ferrule of 2.5 mm outer diameter. Successful reduction of the ferrule diameter enabled us to develop a connector which is smaller in size, lighter in weight and easier in handling. (Size: 10 x 15 x 5)

The ferrules are manufactured at a higher precision in order to achieve low splice losses. The eccentricity between the center of the ferrule outer diameter and the center of the hole remained at 0.7 um or less, which is comparable to the FC type. The main body is molded of rubber in order to permit slight independent movements of ferrules when they are being connected. As the ferrules are allowed to move independently, they can be precisely and smoothly inserted respectively into a sleeve in alignment.

The rubber body also contracts in ferrules axis in order to compensate a gap between the mating surfaces of two ferrules.(Fig.2)

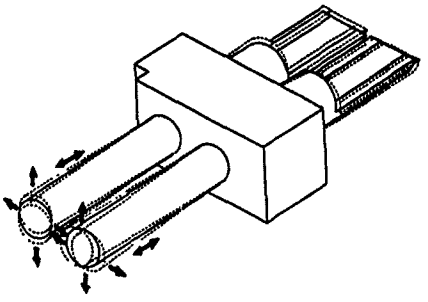

Fig.2 Mechanism of movement

Fig. 3 shows the structure of a mechanical splice. A mechanical splice comprises two pairs of connectors, a plastic adaptor and a clamp spring.

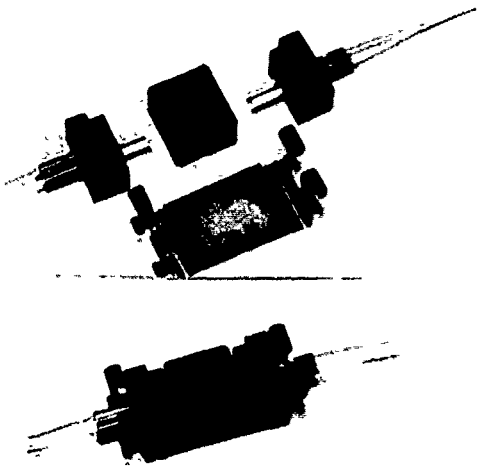

Fig. 3 Mechanical splice

The plastic adaptor houses two ceramic sleeves for engagement. The ceramic sleeves are reduced in size correspondingly to the ferrules having 1.0 mm diameter. The sleeve has a thickness of 0.2 mm, has a slit in the axial direction, and can securely fix ferrules. As they are made of ceramics, they have a higher wear resistance than the conventional metal sleeves.

3. Connector Assembly Method and Its Unique Feature

We succeeded in developing a compact jigs which can assemble connectors in a short time. Fig. 4 shows the jigs.
It is consist of six parts.

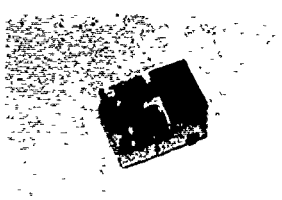

Fig. 4-a Separation cutter

Fig. 4-b Remover

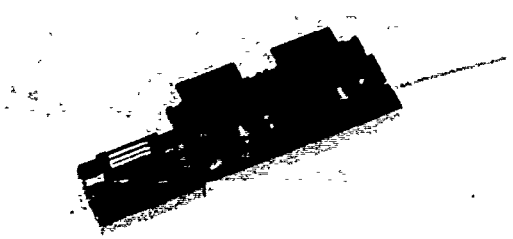

Fig. 4-c Fiber holder

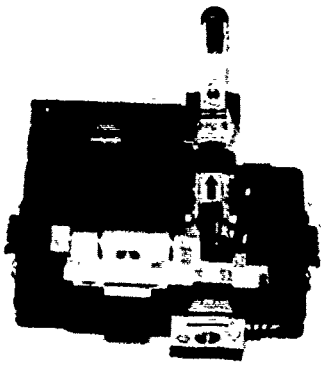

Fig. 4-d Fiber cutter

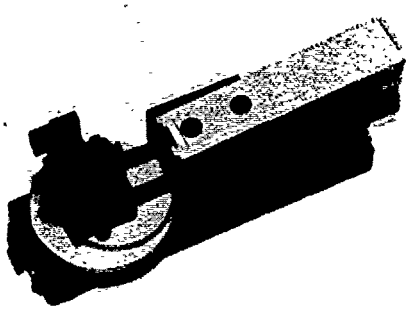

Fig. 4-e Assembly jig

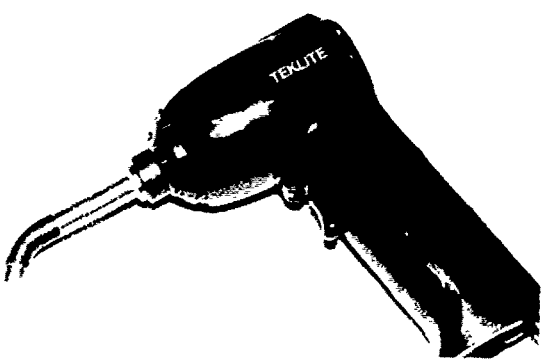

Fig. 4-f UV light-source

Fig. 5 shows the assembly process and typical time required for each step.

Fig. 5

No	Operation	Assembly time
1	Fiber splitting	50 seconds
2	Fiber cutting	20 seconds
3	Fiber insertion	25 seconds
4	Curing/fixing	1 minute 20 seconds
	Total time	2 minutes 55 seconds

3-1 Separation of fibers

A 2-fiber tape is splitted into single fibers at the connector attachment section. (Fig. 6-a)

Fig. 6-a

3-2 Cutting of fibers

As the connectors are not polished, fibers are cut by a high precision cutter to make the fiber end face vertical. (Fig. 6-b)

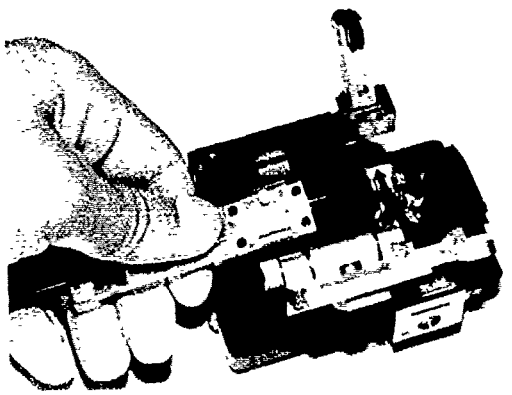

Fig. 6-b

3-3 Insertion of fibers

Fibers are set together with a fixing jig on an assembly jig and inserted by rotating a cam and advancing a slider. The jig is quite effective for insertion although the fiber insertion work usually requires certain skills and experiences. the fiber end face and the connector end face are aligned by butting them on the glass surface on the jig. (Fig. 6-c)

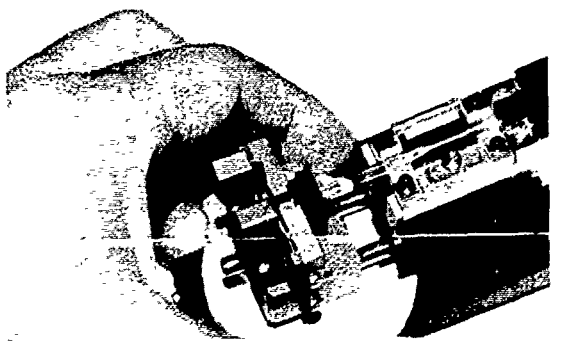

Fig. 6-c

3-4 Attachment, fixation

As fibers fixed with a UV adhesive, the time required for curing is as short as 1 minute. (Fig. 6-d)

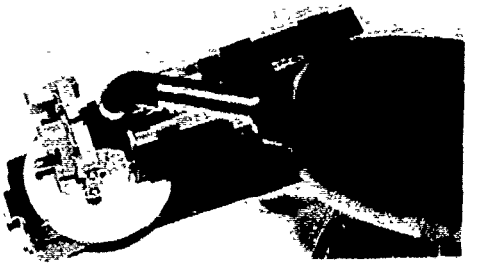

Fig. 6-d

4. Positional Precision on Fiber End Face

The mating surface of a ferrule and the cut face of a fiber are positioned on the same plane on the glass surface of the assembly jig and are adhered together with a UV adhesive. We succeeded in maintaining the positional precision of the fiber end face against the ferrule mating face within the range of +10 um to -30 um. Fig. 7 shows the data obtained by the measurement of the fiber positions on the ferrule mating face.

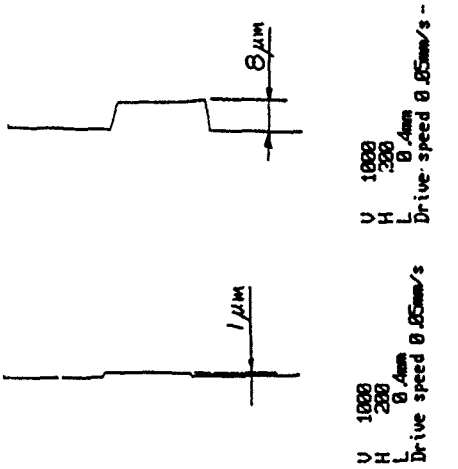

Fig. 7 The fiber position on the ferrule mating face

5. Evaluation Test

In order to verify the reliability of the splice, we conducted various evaluation tests and confirmed that the splice was satisfactory for practical purposes.

5-1. Connection test

We used a ferrule of 126-0 um inner diameter, and fibers of 124.5 um outer diameter. We designed connectors for outdoor use which allows insertion of 125±1um fibers for this trial manufacture. If a lower splice loss is required, ferrules of several different diameters should be prepared and an adequate size should be selected from them. As there are fluctuations in the interval distance between fiber end faces, we used matching oil of a low viscosity. The mean splice loss obtained was 0.54 dB and the maximum loss was 1.1 dB. A lower splice loss is expected if the movement allowance is increased for two pairs of ferrules in a rubber mold.

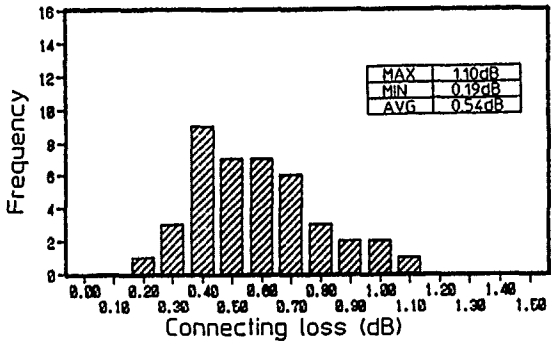

Fig. 8 Connection test

5-2. Attachment / detachment test

Attachment/detachment test was conducted continuously for 100 times to verify the ferrule strength and attachment face strength. (Fig. 9)

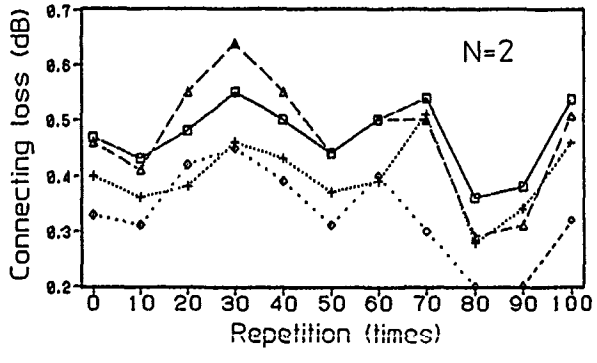

Fig. 9 Attachment / detachment test

In the tests, end faces were cleaned once every 10 tests, and splice losses were measured. Even if a fiber end face projected by ca. 10 um, the fiber end face did not crack or break in normal operations.

5-3. Impact test

Splices in the connected state were dropped from the height of 1 meter to the concrete floor for 10 times in order to study changes in splice losses. As the weight of a connector itself was light, it did not break. (Fig. 10)

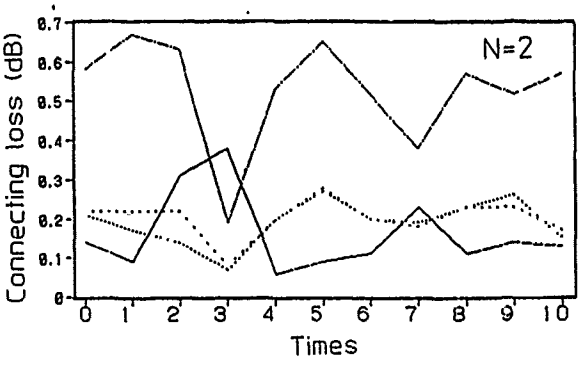

Fig. 10 Impact test

5-4. Tensile test

We used a UV adhesive in order to shorten the curing time. The fiber fixing force of adhesives was measured and an appropriate UV adhesive was selected. Among UV adhesives, we selected one having the maximum tensile strength. If the adhesive has the minimum of 0.7kg tensile strength, the fibers would not slip out during normal connection works. (Fig. 11)

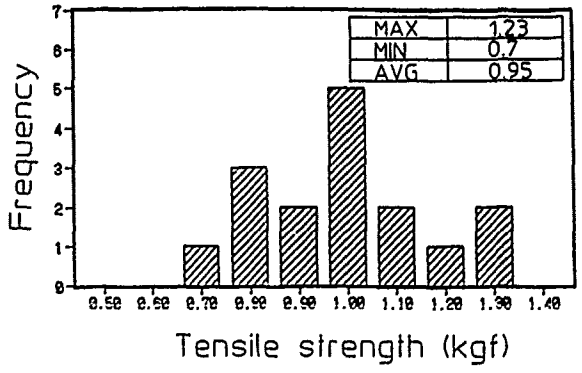

Fig. 11 Tensile test

5-5. Vibration test

A vibration test was conducted in 3 directions for 2 hours each by sweeping at amplitude of 1.5 mm and the frequency of from 10 to 55 Hz., and changes in losses were measured. No optical degradation was observed for vibration. (Fig. 12)

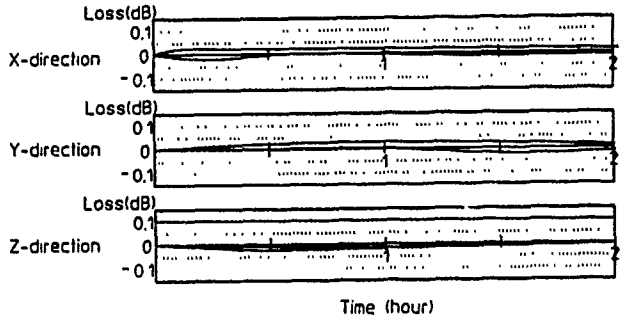

Fig. 12 Vibration test

5-6. Temperature cycle test

Under the temperature of from -30°C to +60°C and 6 hours/cycles, samples were subjected to 10 cycles of temperature changes, and changes in losses were measured. A loss increase of 0.28 dB at maximum was occurred at low temperatures.(Fig. 13)

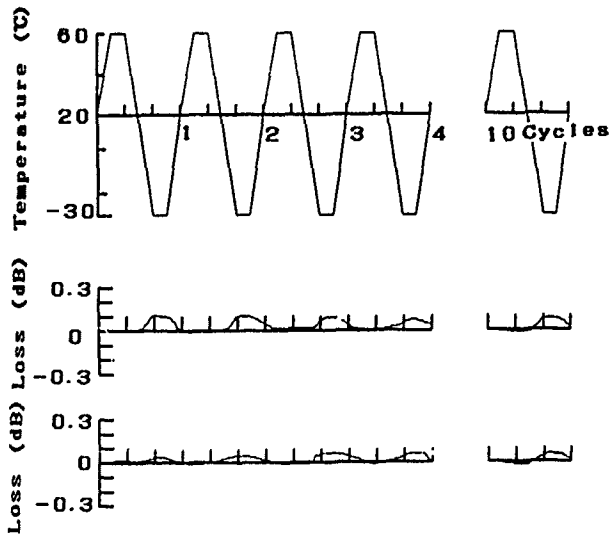

Fig.13 Temperature cycle test

5-7. High-temperature and high-humidity test

Under the conditions of 60°C and 90% RH, samples were left standing for 100 hours and changes in losses were measured. Loss change was as low as 0.2 dB or less.
(Fig. 14)

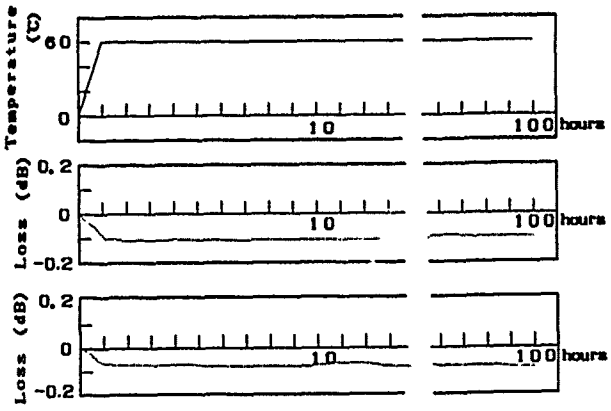

Fig. 14 High-temperature and high-humidity test

6. Conclusion

(1) We developed a single mode 2-fiber mechanical splice for easier splicing.

(2) We succeeded in obtaining satisfactory properties of the splice such as the mean splice loss of 0.54 dB and the mean assembly time of 3 minutes.

Hisanori Tsukiyama

Electric Power Research & Development Center
Computer and Communication Research Section
Chubu Electric Power Company,Inc.

20-1,Kitasekiyama,Odaka-cho,Midori-ku,
Nagoya-shi,Aichi,459,Japan

Hisanori Tsukiyama was born in 1964. He graduated from Hekinann Technical High School in 1982. He joined Chubu Electric Power Company,Inc in 1982 and has been engaged in research and development of telecommunication.

Hiroshi Furukawa

Opt-Electronics
Laboratory
FUJIKURA LTD.

1440, Mutsuzaki,
Sakura-shi, Chiba, 285

Hiroshi Furukawa was born in 1959. He graduated from Chiba University in 1984.

He joined Fujikura, Ltd., and has been engaged in research and development in the Fiber and Cable Accessory Section

Mr. Furukawa is a member of the Institute of Electronics and Communication Engineers of Japan.

Yoshikazu Nomura

Opt-Electronics
Laboratory
FUJIKURA LTD.

1440, Mutsuzaki,
Sakura-shi, Chiba, 285

Yosikazu Nomura was in 1951. He graduated in mechanical engineering from Shinsyu University.

He has been engaged in research and development of telecommunication cables and accessories.

He is now an assistant chief of the fiber and cable Accessory Depertment.

Hideo Hirao

Opt-Electronics
Laboratory
FUJIKURA LTD.

1440, Mutsuzaki,
Sakura-shi, Chiba, 285

Hideo Hirao was born in 1951. He received the B.E.M. degree agricultural mechanical engineering in 1974 from Mie University.

He joined Fujkura Ltd. in 1974 and has been engaged in research and development of telecommunication cables and accessories.

He is now an chief of the Fiber and Cable Accessory Department.

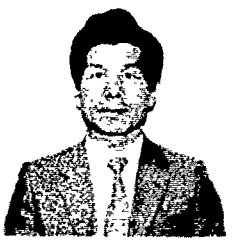

Hiroshi Yokosuka

Opt-Electronics
Laboratory
FUJIKURA LTD.

1440, Mutsuzaki,
Sakura-shi, Chiba, 285

Hiroshi Yokosuka graduated in mechanical engineering from Tokyo Metropolitan Technical Junior College in 1967.

He has been engaged in development of telecommunication cables and accessories. He is now a Manager of the Fiber and Cable Accessory Department of Fujikura Ltd.

Mr. Yokosuka is a member of the Institute of electronics and Communication Engineers of Japan.

MASS-FUSION SPLICING OF HERMETICALLY COATED OPTICAL FIBER RIBBON

Tsutomu Watanabe Keiji Osaka Toru Yanagi Yoichi Ishiguro Yasuo Asano

Communication R&D Department, Yokohama Research Labolatries,
Sumitomo Electric Industries, Ltd.

Abstract

This paper reports the characteristics of mass fusion splicing of carbon coated optical fiber (CCF) ribbon . It was reported[1] that when a pair of CCF was fusion-spliced using a direct-core-monitoring fusion splicer, the carbon layer removing process was necessary in order to monitor the cores. However in mass fusion splicing the cores are not monitored. Hence the effects of carbon layer removing process to the mass fusion splicing properties were investigated. According to the experimental results, it was found that the CCF ribbon was able to be spliced with as low splice loss as the standard fiber ribbon, whether or not its carbon layer was removed before fusion splicing process.

1. Introduction

Recently the optical fiber properties have been improved by coating a certain kind of materials on the fiber surface. It has been reported that a hermetically carbon coated fiber has an excellent characteristics against hydrogen induced loss increase and mechanical fatigue[2]. The original failure strength of the CCF has increased to the level of the standard fiber. An application of the cable composed of CCFs was proposed to submarine cables to take advantage of these properties. Also a structure of high fiber count density cable composed of CCF ribbons was proposed[3].

The splicing technologies should be developed for these newly developed cables. Recently the mass-fusion splicing technique is getting popular because of its economy dut to the short splice time and the small reinforcement size as well as its low splice losses. The CCF ribbons and the standard fiber ribbons were mass fusion spliced respectively and the characteristics about the splice loss and the failure strength were compared.

2. Sample fiber ribbon

Fig. 1 shows the cross section of 4-CCF ribbon. The dimension of 4-standard fiber ribbon was the same as that of the CCF ribbon. The geometrical parameters of the fiber are shown in Table 1. The original failure strength of CCF was about 6 Kgf on the average. This value was equal to that of standard fibers. In the following experiments, both the CCF ribbons and the standard fiber ribbons were spliced using a commercially standard mass fusion splicer.

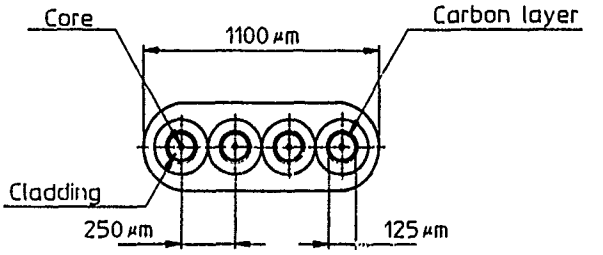

Fig.1 The structure of CCF ribbon

Table 1 The parameters of the fiber

Parameters	Value
Cladding diameter	125 μm
M.F.D	10 μm
Core eccentricity	<1.0 μm

3. Procedure of splicing

Fig. 2 denotes the procedure of mass fusion splicing.

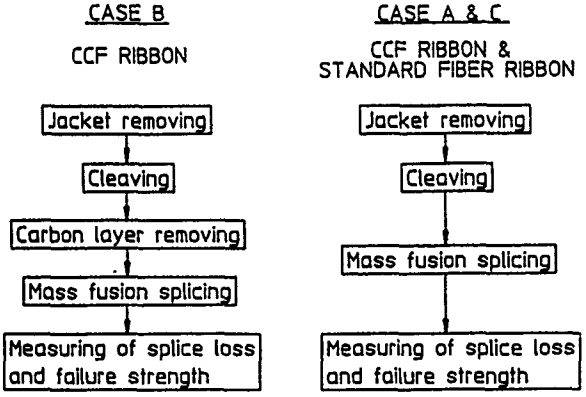

Fig.2 Procedure of splicing

(i)Jacket removing and cleaving

Initially the jacket of UV curable resin was removed using a standard jacket remover with hot iron. Then the fibers were wiped with gauzes soaked with ethyle alcohol, and cleaved using a standard mass cleaver. Special adjustments for the CCF cleaving were not necessary.

(ii)Carbon layer removing (CASE B in Fig. 2)

About 3 mm length of carbon layer from the cleaved end were removed by burning off with electrical discharge. The removing process of carbon layer was performed by a newly developed equipment.

The discharge power for removing was kept lower than that for normal splicing because high power discharge melted a fiber end faces too much and increased a splice loss when they were spliced. Fig. 3 shows an appearance of the fiber before/after the carbon layer removing process. Any carbon residual could not be observed or detected by Energy Dispersive X-ray analyzer (Fig. 4) at all. From these results, it was clear the carbon layer was removed completely.

(iii)Mass fusion splicing

Fiber ribbons were mass fusion spliced using mass fusion splicer.

(iv)Measuring

After the CCF ribbon was spliced, the splice loss and the failure strength were measured. The splice losses were measured at 1.3 micron region. The failure strength is defined as the tensile load that the first breakage among the 4 fiber occured. The strain rate was 2.5 %/min and the gauge length was 200 mm.

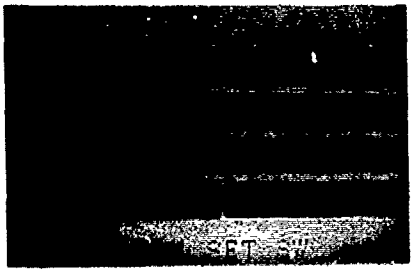

(a) Before removing

(b) After removing

Fig.3 The pictures of CCF ribbon through a microscope

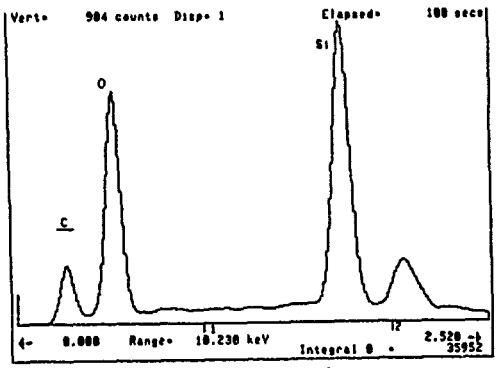

(a) Before removing

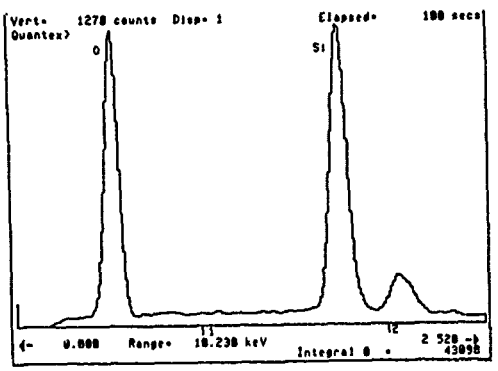

(b) After removing

Fig.4 The results of EDX analysis

4. Experimental results

(i)Splice loss

Fig. 5 shows the distribution of splice loss. The avarage splice losses ($\bar{\alpha}_1$) and the standard deviations (σ_1) are listed in Table 2.

Table 2. A list of splice loss

	$\bar{\alpha}_1$(dB)	σ_1(dB)
CASE A	0.04	0.03
CASE B	0.04	0.03
CASE C	0.04	0.03

CASE A: Standard fiber ribbon
CASE B:CCF ribbon with removing process of carbon layer
CASE C:CCF ribbon without removing process of carbon layer

Comparing the results of CASE B and CASE C with the result of CASE A, it could be said that the former were almost equal to the latter. Even in CASE C, exactly the carbon layer was removed just before splicing; that is , the CCFs were exposed in the electric discharge during very short time of 0.2 seconds before the mating fibers make a contact.

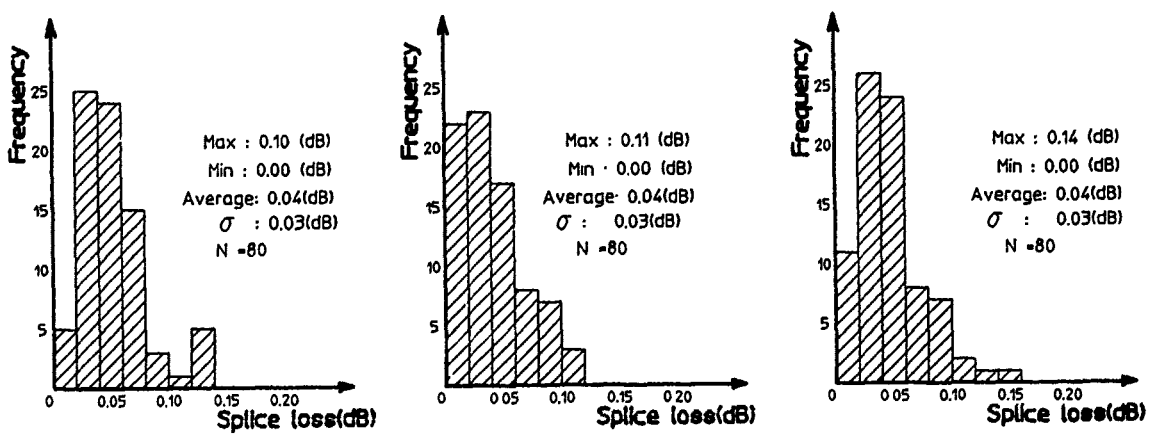

(a) Standard fiber ribbon (b) CCF ribbon (with removing) (c) CCF ribbon (without removing)

Fig.5 Distributions of splice loss

(ii)Failure strength

Fig. 6 shows the distribution of failure stength at the spliced points on a Weibull chart. The average failure strengths ($\bar{x}_f$) and the standard deviations (σ_f) are listed in Table 3.

Table 3. A list of failure strength

	$\bar{x}_f$(Kgf)	σ_f(Kgf)
CASE A	2.26	0.39
CASE B	2.73	0.60
CASE C	3.50	0.73

CASE A: Standard fiber ribbon
CASE B: CCF ribbon with removing process of carbon layer
CASE C:CCF ribbon without removing process of carbon layer

The $\bar{X}_f$ of each CASES (A,B and C) was arranged in order of strength as following inequality.

CASE A < CASE B < CASE C

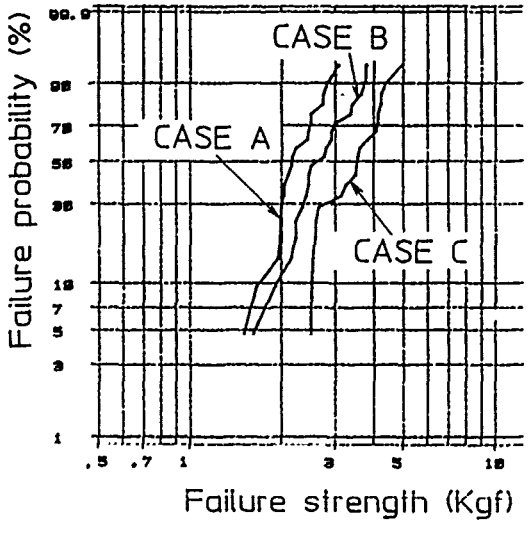

Fig 6 Weibull plots of failure strength

These differences can be attributed as follows.

The longer the bare fiber region is exposed, the higher the probability of fibers' physical contact with the ambient articles becomes. Namely, the failure probability depend upon the bare fiber length. From this view point, the extra step for removing the carbon layer is not necessary for the CCFs.

5. Conclusion

(1)The CCF ribbons could be mass fusion spliced using a commercially standard mass fusion splicer with as low splice loss as the standard fiber ribbon.

(2)The spliced CFF fiber ribbons without the removing process of carbon layer was stronger than that with the process. However there was not a significant difference of failure strength between the standard fiber ribbon and the CCF ribbon with the removing process.

(3)From the view of mass fusion splicing technique the CCF ribbon could be spliced with the same procedure as the standard fiber ribbons, and the extra step for removing the carbon layer is not necessary.

References:

(1)K. Osaka et. al., "Fusion splicing characteristics of hermetically carbon coated fiber", ECOC 90.

(2)H. Aikawa et. al., "Characteristics of Carbon Coated Optical of Carbon Coated Optical Fiber", OEC'90

(3)N. Yoshizawa et. al., "A one-hundred-fiber submarine cable composed of hermetically coated fiber ribbons inserted into slots." , Proc. of 38th IWCS, 1989

Tsutomu Watanabe

Sumitomo Electric Industries, Ltd.

1, Taya-cho, Sakae-ku Yokohama, Japan

Tsutomu Watanabe was born in 1964 and received his B.S. degree in mechanical engineering form Tokyo University in 1987. He joined sumitomo Electric the same year and has been enagaged in research and development of fusion splice technology. He is a member of Japan Society of Mechanical Engineers.

Keiji Osaka

Sumitomo Electric Industries, Ltd.

1, Taya-cho, Sakae-ku Yokohama, Japan

Keiji Osaka was born in 1955 and received his M.S. degree in precision mechnical engineering from Kyoto University in 1981. He joined Sumitomo Electric Industries the same year and has been engaged in research and development of automated fusion splicing technology. He is now a staff member of Communications R&D Dept. Yokohama Research Labs. and a member of the Institute of Electronics, Information and Communication Engineers of Japan.

Toru Yanagi

Sumitomo Electric Industries, Ltd.

1, Taya-cho, Sakae-ku Yokohama, Japan

Toru Yanagi was born in 1939. He joined Sumitomo Electric Industries in 1964 and has been engaged in research and development of fusion splice technology. He is a member of the Institute of Electronics, Information and Communication Engineers of Japan.

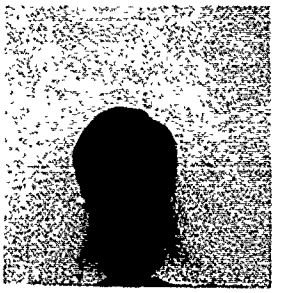

Yoichi Ishiguro

Sumitomo Electric Industries, Ltd.

1, Taya-cho, Sakae-ku Yokohama, Japan

Yoichi Ishiguro was born in 1957. He received the B.S. degree in applied physics from University of Tokyo in 1981 and the M.S. degree in applied physics from Tsukuba University in 1983. He joined Sumitomo Electric in the same year and has been engaged in research and development of fiber fabrication. He is a member of the Japan Society of Applied Physics.

Yasuo Asano

Sumitomo Electric Inudstries, Ltd.

1, Taya-cho, Sakae-ku Yokohama, Japan

Yasuo Asano received his B.S. degree in mechnical engineering from Waseda University in 1968. He joined Sumitomo Electric Industries in 1971 and has been engaged in development of communication cable jointing technologies. He is now a Chief research associate of Communication R&D Dept Yokohama Research Laboratories and a member of Japan Society of Mechnical Engineers and the Institute of Electronics, Information and Communication Engineers of Japan.

PREDICTION OF BLOWING VELOCITY AND DISTANCE IN AIR BLOWN FIBER CABLING SYSTEM

Y. Terasawa H. Sano S. Tanaka

Sumitomo Electric Industries, Ltd.
Yokohama, Japan

1. Introduction

The Air Blown Fiber (ABF) Cabling System is a new optical fiber cable installation technique which blows a fiber bundle into a previously installed tube by compressed air. This technique was proposed by British Telecom Research Laboratories (BTRL) in 1983. Fig.1 and Fig.2 show the equipments of ABF Cabling System and the fiber bundle cross section structure, respectively. The fiber bundle diameter is 2mm and tube inner/outer diameters are 6/8mm. The fiber bundle is blown into the tube by the blowing head, together with compressed air fed from the compressor, and is drawn through the tube by the viscous drag of the air. The ABF Cabling System has the following characteristics;

① Fibers are splice-free at the point of cable junction by jointing the tubes at the necessary length in advance. This dramatically reduces the number of optical fiber splices.

② Since the blowing force is distributed over the entire length, almost no tensile stress causes to the fiber bundle during installation.

③ An fiber bundle can be blown into an existing tube has been installed in the section where the need for an optical fiber line is expected. This allows the user to avoid over-installation of optical fibers and reduces the initial cost.

Therefore the ABF Cabling System has drawn the attention for wiring in a building.

Though the blowing characteristics of ABF are very important element to design the blowing route, there have been no report on the quantitative relations that predicts the blowing performance by calculation. Therefore the blowing route was designed on experience base.

In this paper we report the theoretical prediction of the blowing performance of horizontal and vertical routes by analyzing the blowing force on a fiber bundle. The change of blowing velosity can be calculated under the given conditions of air pressure and tube lengths.

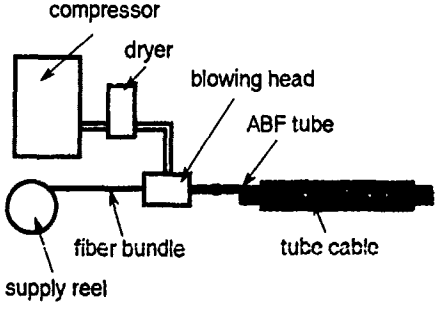

fig.1 Equipments of ABF Cabling System

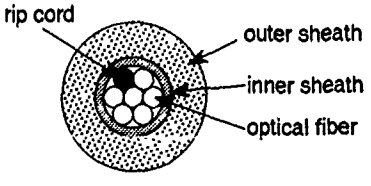

Fig.2 Cross Section Structure of Fiber Bundle

The accuracy of results are within ±20%. As a result of this study it has become possible that the blowing route is designed with calculation. Chapter 2 describes the theoretical investigation of blowing force on a fiber bundle. Chapter 3 and 4 describe the derivation of expression of a blowing performance on a horizontal route, and that on a vertical route, respectively.

2. Aerodynamic Analysis in ABF Tube

2-1 Blowing Force on Fiber Bundle

Before analyzing blowing characteristics, we describe the blowing force on a fiber bundle in this section.

When a fiber bundle exists at the center in the tube, blowing force per unit length (f) is given by the following equation:

$$f = -\frac{\pi d_1 d_2}{4}\frac{dp}{dl} \quad \cdots (1)$$

where d_1 and d_2, as shown in Fig.3, indicate the tube inner diameter and the fiber bundle outer diameter, respectively.

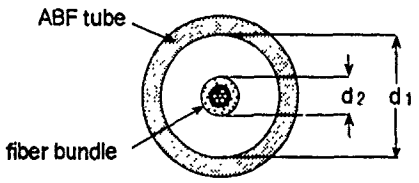

Fig.3 Tube and Fiber Bundle Sizes

dp/dl indicates the pressure gradient in the tube. Because all terms except dp/dl in equation (1) are constant, blowing force (f) is in proportion to only dp/dl. Pressure gradient (dp/dl) is not uniform over the entire length of the tube, because air is compressible fluid. Since the insertion length of the fiber bundle is gradually growing, the tube effective clearance changes by each position. Therefore the blowing force vary in relation to the insertion length. There has been no report on the theoretical analysis of blowing force change as a function of pressure gradient which described in the above context. In the next section, the theoretical equation, expressing the pressure gradient in the tube, is derivated.

2-2 Pressure Gradient in a Tube

It is well known that pressure drop of compressible fluid in the tube is described as:

$$\frac{P_1 - P_2}{\rho_0} = \lambda \frac{l}{d} \frac{V_0}{g} \quad \cdots (2)$$

where P_1 is the absolute pressure at any position in the tube, P_2 is the absolute pressure at the position at distance l drownstream from P_1, ρ_0 is the mean density of the fluid, λ is coefficient of friction between the fluid and the tube inner surface, d is the tube inner diameter, g is the gravitational acceleration and V_0 is the mean fluid velocity. From equation (2), pressure drop of a fiber bundle inserted tube can be calculated. Pressure P(l) at the l from the tube inlet is given by

$$p(l') = \left(\frac{p(l')^2 - P_{in}^2}{l'} l + P_{in}^2 \right)^{\frac{1}{2}} \quad \cdots (3)$$

and p(l'), the pressure at the tip of optical fiber bundle, is given as:

$$p(l') = \left\{ \frac{P_{in}^2 \, d_1'^{\frac{19}{4}} (L - l') + P_{out}^2 \, d_1^{\frac{19}{4}} l'}{d_1^{\frac{19}{4}} l' + d_1'^{\frac{19}{4}} (L - l')} \right\}^{\frac{1}{2}} \quad \cdots (4)$$

where P_{in} is the absolute pressure at the tube inlet, P_{out} is the absolute pressure at the tube outlet (atmospheric pressure), l' is the insertion length of a fiber bundle, d_1' is the effective tube diameter of a fiber bundle inserted tube. d_1' equal 5.1mm, under the standard combination of d_1 and d_2 of 6.0mm and 2.0mm, respectively. In this case, supposed equivalent cross section ($=\pi d_1'^2/4$) is 81% of the crealance between the fiber bundle outer diameter and the tube inner diameter. Symbols are shown in Fig.4.

Fig.5 plots the theoretical and measured pressure drop distributions when a 500m of fiber bundle is inserted into a 1060m tube. The theoretical pressure drop distribution shows good agreement with the measured one, which means that (4) is good model of the actual pressure drop distribution. As the result of theoretical calculation, the pressure gradient | dp/dl | takes the minimum value at the tube inlet, and with increasing the length from the tube inlet (l), the pressure gradient increases. Since the

blowing force (f(l)) is proportional to dp/dl, f(l) takes the minimum value at the tube inlet.

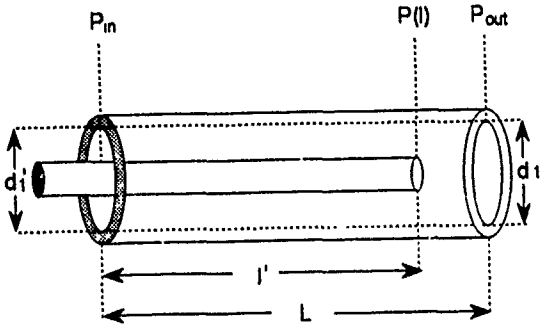

Fig.4 Notation

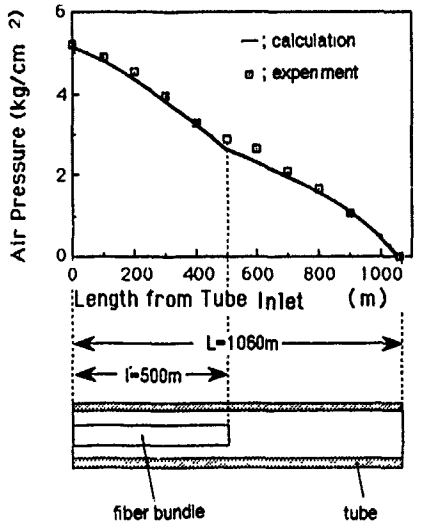

Fig.5 Pressure Drop in ABF Tube

2-3 Derivation of Blowing Force Equation

From equation (1)(3)(4), when fiber bundle insertion length is l', blowing force (f(l)) per unit length at the length l from the tube inlet is expressed as:

$$f(l)=\frac{\pi d_1 d_2}{8}\left(\frac{p(l')^2-P_{in}^2}{l'}l+P_{in}^2\right)^{-\frac{1}{2}}\frac{P_{in}^2-p(l')^2}{l'} \quad \cdots (5)$$

Fig.6 shows the calculation of the blowing force distribution at P_{in}=8kg/cm² when insertion length (l') is 250m, 500m and 1000m. At the fixed point of distance l, blowing force (f(l)) becomes smaller with increasing the insertion length of the fiber bundle.

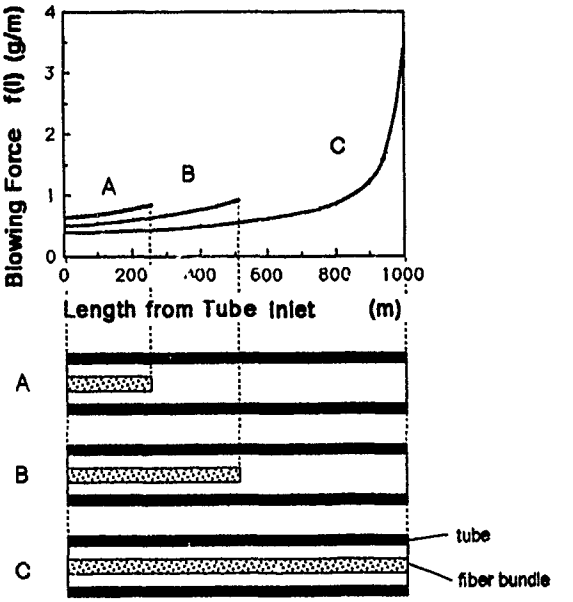

Fig.6 Calculation of Blowing Force

3. Prediction of Blowing Velocity on Horizontal Route

3-1 Modeling of Blowing Condition

Blowing behavior is decided by the relation between blowing force and resistant force consisting of friction. It is presumed that the resistant force is uniform at each part of a fiber bundle because each part of a fiber bundle moves at the same velocity. On the other hand, a blowing force takes the minimum value at the tube inlet. Fig.7 shows the schematic model of the blowing force (f(l)) and the resistant force (f(V)) per unit length in the tube. Since the resistant force is presumed to depend on blowing velocity, it is symbolized by F(V). The blowing force at the tube inlet (l=0) is given from equation (5) by the following expression:

$$f(0)=\frac{\pi d_1 d_2}{8}\frac{P_{in}^2-p(l')^2}{l'}P_{in}^{-1} \quad \cdots (6)$$

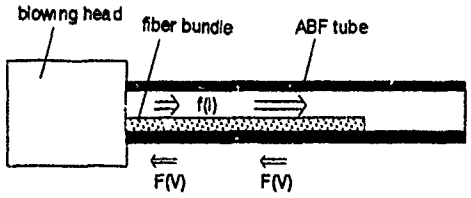

Fig.7 Force Balance in ABF Tube

Thus the equation of dynamic balance between blowing and resistant forces is given by:

$$f(0) = F(V) \qquad \cdots (7)$$

If the resistant force F(V) becomes clear, the blowing velocity will be predicted. In the next section, F(V) will be formulated by experimental data.

3-2 Prediction of Blowing Velocity

Fig.8 shows the measured blowing velocities for more than 20 combinations of various blowing conditions; tube length of 200~1000m and blowing pressure of 3.5~9.0kg/cm². From this figure, F(V) is calculated as a function of the blowing velocity (V) by substituting the measured results into equation (7). Fig.9 summarizes the calculated relationship between F(V) and V. There exists a unique relation between F(V) and V independent of the tube length and the blowing pressure, as follows;

$$F(V) = 1.25 \times 10^{-2} V + 3.4 \times 10^{-1} \qquad \cdots (8)$$

where dimensions of F(V) and V are g/m and m/min, respectively. From equation (6)(7)(8), the blowing velocity V is predicted by the following equation, when pressure P_{in}, tube length L and insertion length l' are given;

$$V = 80 \left\{ \frac{\pi d_1 d_2}{8} \frac{(P_{in}^2 - P_{out}^2) d_1^{\frac{19}{4}}}{d_1^{\frac{19}{4}} l' + d_1^{\frac{19}{4}} (L - l')} P_{in}^{-1} - 3.4 \times 10^{-1} \right\} \qquad \cdots (9)$$

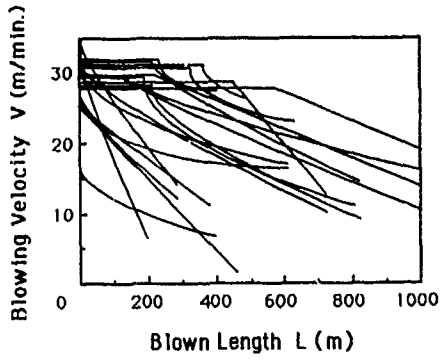

Fig.8 Change of Blowing Velocity

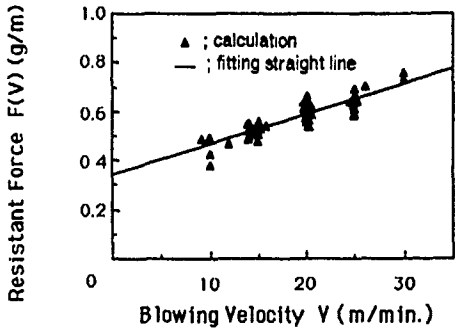

Fig.9 Dependence on Blowing Velocity of Resistant Force

3-3 Verification of Calculation

The calculation and experimental blowing velocity are shown in Fig.10 for the case of tube length L=400m and blowing pressure of 4kg/cm². Both values are in good agreement. Generally, discrepancy between calculation and experimental is found within 20%, for the various combinations of blowing conditions. Therefore validity of derivated equation in confirmed.

In addition, the maximum blowable length for the given pressure can be calculated by substituting blowing pressure and final blowing velocity in (9). Fig.11 represents the maximum blowable length as a function of blowing pressure. The calculation indicates that the blowing a more than a 1000m fiber bundle is possible. Many installation works, blowing more than 1000m fiber bundle, are already practiced in the field.

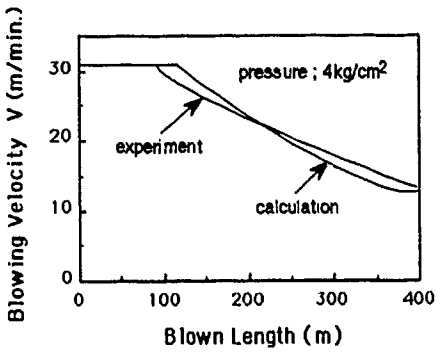

Fig.10 Calculation and Experiment of Blowing Velocity Change

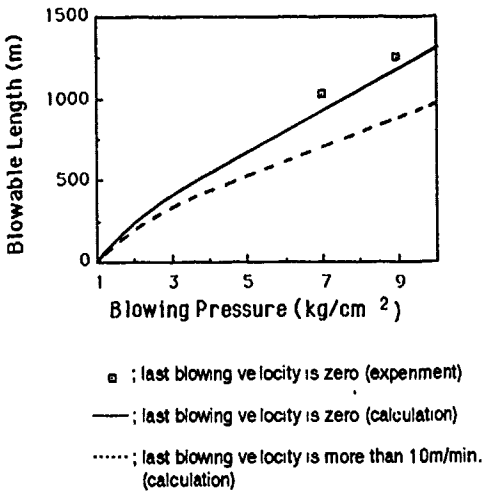

Fig.11 Blowable Lengths

4. Calculation of Blowing Performance for a Route Including Vertical Part at Tube Inlet

4-1 Modeling of Blowing Condition

In this section we discuss the blowing route shown in Fig.12, consisting a vertical part and a succeeding horizontal part. Since the weight of a fiber bundle adds the resistant force at the vertical part, the blowable length for a route which includes a vertical part becomes shorter than that for a horizontal case. The relation between the blowing force and the fiber bundle weight under the condition of pressure 7kg/cm² and tube length of 260m is shown in Fig.12. In this case, however blowing force (f(l)) is larger than

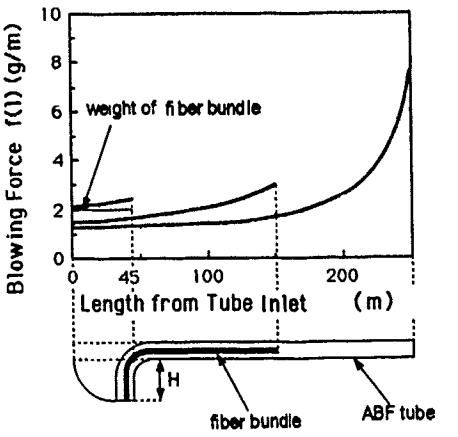

Fig.12 Blowing Force and Optical Fiber Unit Weight

the fiber bundle weight (m) when the tip of fiber bundle exists in the vertical part, the relation becomes reversed as the tip of fiber bundle is in the horizontal part. Therefore the force only in the vertical part can not explained the blowing phenomenon.

The fiber bundle in the vertical part is dragged by the tension from horizontal part. Assuming this effect, the force balance is expressed as follows;

$$\int_0^{L'} f(l)\, dl = mH + L'F(V) \quad \cdots (10)$$

where m is the fiber bundle weight per unit length (=2g/m), H is the vertical part length and L' is the "effective dragging length" which affect the dragging force to the fiber bundle of the vertical part. Derivation of L' is described in the next section.

4-2 Derivation of Effective Dragging Length

We extracted the experimental relationship, as shown in Fig.13, among the blowing force affecting to the vertical part (f_H), the vertical part length (H) and the blowing velocity V by measuring under various conditions, H=10~45m and L=80~400m. Independent of the tube length and the blowing pressure, this relationship exist universally. The following equation is given by Fig.13:

$$f_H = \int_0^{L'} f(l)\, dl = (0.034H - 0.15)V + (2.3H + 10) \quad \cdots (11)$$

where dimension of f_H and H are g and m/min respectively. From equation (3) and (11), L' can be expressed as follows:

$$L' = \frac{L}{p(l')^2 - P_{in}^2} \left\{ \left(P_{in} - \frac{4 f_H}{\pi d_1 d_2} \right)^2 - P_{in}^2 \right\} \quad \cdots (12)$$

Using (10) and (12), a blowable length can be calculated for the given pressure.

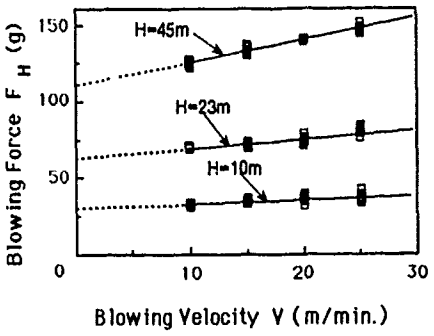

Fig.13 Blowing Force in Effective Length

4-3 Calculation and Verification of Blowable Condition

Fig.14 represents the calculated relationship between the vertical part length (H) and the total tube length (L) for the blowing velocity of more than 10m/min. Here the blowing pressures are 5.0, 7.0 and 9.0kg/cm², respectively. As the vertical part length becomes shorter, the blowable length increases. Fig.14 indicates this relation tends to saturate as the vertical part length becomes longer. Experimental results shown in Fig.14 (●, ▲, ■) are in agreement with calculations. As the results of above investigation, if two values are given among of L, H and P_{in}, another one can be calculated. In addition, the change in blowing velocity can be calculated. Already we have achieved a upto 80m vertical blowing in building wiring system.

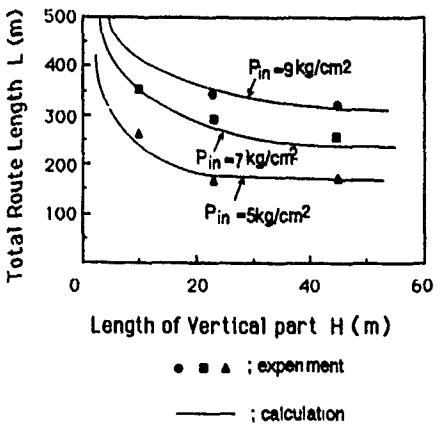

Fig.14 Blowable Hight and Length at Each Pressure

5. Conclusion

Equations to calculate the blowing force on fiber bundle was derivated by analyzing the air flow in the ABF tube theoretically. Using this equation, we derived the prediction method of the blowing velocity and the maximum blowable length for a horizontal route and a route that includes a vertical part at the tube inlet.

In the case of a horizontal route, calculation was derived by the equation of dynamic force balance at the tube inlet. The result has high accuracy within ±20% for the blowing velocity and the maximum blowable distance.

When a route includes a vertical part at the tube inlet, tension effect from the horizontal part to the vertical part must be considered. Therefore the blowable conditions can be calculated with three parameters of blowing pressure, tube length and vertical part length. Calculations and experiments are in good agreement.

As the results of this study, the prediction of blowing performance by the calculation has first become possible, which contributes the efficient and high accuracy route design method of ABF cabling system.

References

[1] S.A. Cassidy and M.H. Reeve, "A radically new approach to the installation of optical fiber using the viscous flow of air", Proc. IWCS, pp.250-253, November 1983.

Yoshiaki Terasawa

Sumitomo Electric
Industries, Ltd.

1, Taya-cho, Sakae-ku
Yokohama, Japan

Yoshiaki Terasawa was born in Hokkaido, Japan, on August 10, 1961. He received the B.S. and M.S. degree in applied physics from Hokkaido University in 1985 and 1987, respectively. He joined Sumitomo Electric Industries, Ltd., in April 1987 and engaged in research and development of optical fiber cable. Mr. Terasawa is a member of Communication R&D Development in Yokohama Research Laboratories.

Shigeru Tanaka

Sumitomo Electric
Industries, Ltd.

1, Taya-chi, Sakae-ku
Yokohama, Japan

Shigeru Tanaka was born in Tokyo, Japan, on December 2, 1951. He received the B.S. and M.S. degree from Tokyo University, Tokyo, Japan, in 1974 and 1976, respectively.

He joined Sumitomo Electric Industries, Ltd. in 1976, and has been engaged in the design and characterization of optical fibers and fiber cables. He is a Chief Research Associate of the Communication R&D Department.

Mr. Tanaka is a member of the Institute of Electronics and Communication Engineers of Japan.

Hiroaki Sano

Sumitomo Electric
Industries, Ltd.

1, Taya-cho, Sakae-ku
Yokohama, Japan

Hiroaki Sano was born in 1960 in Osaka, Japan, and received his M.E. degree in Polymer Science from Kyoto Univ. in 1984. He then joined Sumitomo Electric Industries, and has engaged in development of optical fiber manufacturing process and cables. Mr. Sano is a member of Communication R&D Dept. in Yokohama Research Laboratories.

DEVELOPMENT OF HARD CLAD PCF OPTICAL UNIT FOR AIR BLOWN FIBER SYSTEM

N. Suzuki H. Sano H. Nishimoto S. Yonechi

Sumitomo Electric Industries, Ltd

Yokohama, Japan

ABSTRACT

Air Blown Fiber System (ABF system) is a new system to install optical fiber which was proposed BTRL in 1983. Compared with the conventional system, the ABF system has many advantages, and it has been already put into practice to optical LAN using all-glass fiber.

Hard clad-PCF, on the other hand, has excellent characteristics in coupling efficiency with light source, because of its great NA (Numerical Aperture).

The authors have successfully developed HC-PCF unit for ABF system, to combine HC-PCF features and ABF systems ones. HC-PCF unit is covered with primary and secondary coatings. The primary coating is made of a material having small Young's modulus, which makes it possible to have HC-PCF, stable in transmission characteristics. In addition , with the HC-PCF unit, it is possible to install optical fiber for length of 500 m or more by single operation. The unit is also fully adapted in practice to short links such as optical LAN branch lines.

1.INTRODUCTION

More than 15 years have passed since the optical fiber was first put into practical use as a communication line. The optical fiber is essential for public communication line. Also in the sphere of LAN, the optical fiber attracts public attention, and is used for its backbone line, which forms the trunk of the network. In these years, high-speed, broad-band transmission of information, image transmission in particular, has been making a progress. Optical fibers have been used for communication of branch lines between work stations and local stations. In general, the branch lines have many lines, and have been frequently expanded and modified, as work stations are increased and displaced. It is, therefore, very important to realize an efficient and cost-saving system.

Air Blown Fiber System (ABF System) is a new optical fiber installation system BTRL proposed in 1983. The system construction is given in Fig. 1. In this system, a pipe cable incorporating plural pipes is installed in advance. When necessary,

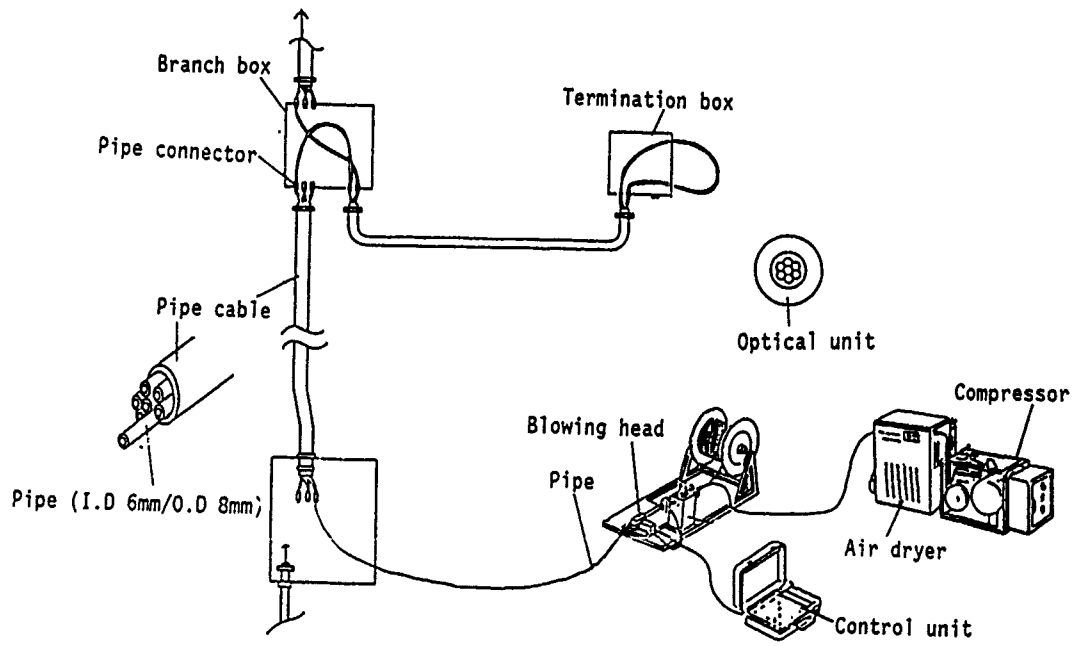

Fig.1 Construction of ABF system

compressed air is blown into an empty pipe. Then, an optical unit having plural optical fibers inside, is installed by means of compressed air flow. (This is called "blowing".)

In comparison with the conventional optical-fiber system, the ABF system has the characteristics mentioned below:

(1) Easy installation and removal of optical fibers with compressed air makes it possible to expand and modify optical fiber lines in accordance with urgent necessity.

(2) At the branching or connecting portions of pipe cables, the pipe cables are previously combined by connector. Then, the optical unit is blown with compressed air. This can reduce the number of optical fiber splices.

The ABF System permits efficient optical fiber laying. Optical units using all-glass fiber have been already put on the market, for example, graded index type and single-mode optical units.

When using optical fibers for branch lines, one of the important factors is that E/O and O/E converters are low-priced. In this respect, Hard Clad-PCF (HC-PCF) is judged to be important. HC-PCF has a high N.A. of nominal 0.4, and an excellent coupling efficiency with E/O converter. In addition, HC-PCF can be connected easily on the field, with crimp & cleave type connectors. To achieve an efficient and cost saving optical fiber network, in combination of the ABF system and HC-PCF, the authors have successfully developed HC-PCF unit for ABF system. This paper deals with the characteristics of the HC-PCF units.

2.CONSTRUCTION OF HC-PCF UNIT

2-1 HC-PCF

HC-PCF consists of all-glass core part, plstic clad part and jacket layer. The construction of HC-PCF is given in Fig. 2 and Table 1. The HC-PCF used this time has a core diameter of 200 μm, a clad diameter of 230 μm, and a theoretical NA of 0.4. The outside diameter of its jacket layer is approx. 0.5 mm.

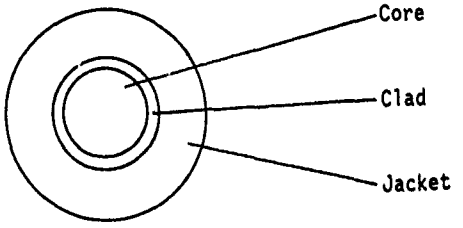

Fig.2 Structure of HC-PCF

Table.1 Structure of HC-PCF

Item	Structure
Core diameter	200 ± 5 μm
Clad diameter	$230\ ^{+\ 0}_{-\ 10}$ μm
Concentricity error	Not more than 6 μm
Jacket diameter	500 ± 50 μm
Theoretical NA	Nom. 0.4

2-2 HC-PCF Unit

The construction of HC-PCF unit is given in Fig. 3. In this figure, the conventional optical unit with all-glass fiber is shown for the purpose of comparison. As the blowing equipment to be used should be the same one as that used for the conventional optical unit, the outside diameter of the unit was 2 mm. The number of optical fiber was two, which is the essential number of optical communication. The fibers were covered with plastic primary coating. Out side the primary coating, the secondary coating was made with foamed polyethylene, as in the case of the conventional optical unit. Although the HC-PCF unit weighed as light as 2.3 g/m, it was about 15 % heavier than the all glass-fiber optical unit.

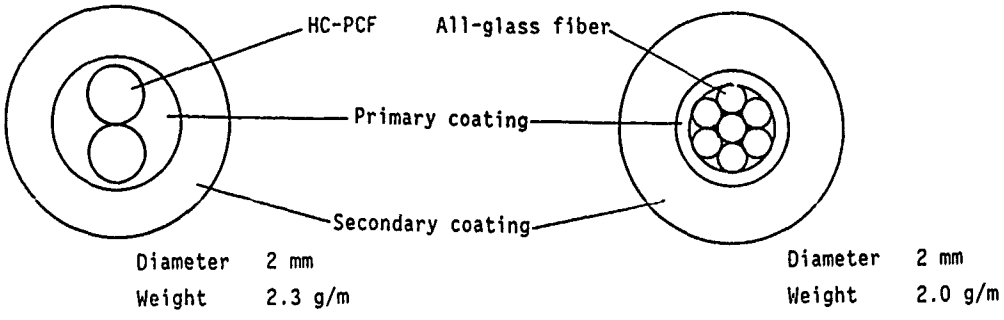

Fig.3 Structure of unit

3.TRANSMISSION CHARACTERISTICS OF HC-PCF UNT

The HC-PCF unit was evaluated with its primary coating materials A and B, of which physical characteristics are given in Table 2. As HC-PCF was used under overmode launching, its transmission loss is dependent on length. Two or more single-length HC-PCF units were evaluated.

Table.2 Propaties of primary coating material

	Material A	Material B
Young's modulus	40 kg/mm²	5 kg/mm²
Coefficient of linear expantion	$5*10^{-5}$ 1/°C	$5*10^{-5}$ 1/°C

3-1 Initial Transmission Characteristics

The transmission loss at 0.81 μm wavelength is given in Fig. 4. The unit length (m) is expressed on the X axis, and the transmission loss (dB) for the corresponding unit length, in the Y axis. The unit using the material A recorded a loss greater than that before unitization. The unit using the material B marked transmission loss as much as that before unitization. The material A has Young's modulus one digit larger than the material B. This may be attributable to a fact that the residual processing strain of the material gave excessive stress to HC-PCF. The temperature characteristics between -40°C-+70 °C were evaluated. The loss increase on the low temperature side is given in Fig. 5 and 6. Fig. 5 shows the temperature characteristics when using the material A for the primary coating, and Fig. 6, those when using the material B. The X axis indicates the unit length, and the Y axis, the loss increase (dB) for the initial value for the corresponding unit length. The unit using the material A shows an increase in loss, which is dependent on length of the unit. Because the Young's modulus of the primary coating is high, an excessive stress is applied to HC-PCF when the material contracts at a low temperature. Then, micro-bend is supposed to be produced on HC-PCF.

The unit using the material B, on the other hand, shows a slight increase of loss, but the increase of loss in not so much dependent on length of the unit. From this fact, the increase of loss at low temperature is in great part due to change of NA by variation of the refractive index of the clad part.

There is little influence by stress from the coating materials. That is, by using the material B for the primary coating, it is possible to perform unitization without reducing the transmission characteristics of HC-PCF. On the high-temperature side, it has been confirmed that any increase in loss is not produced, regardless of the material used.

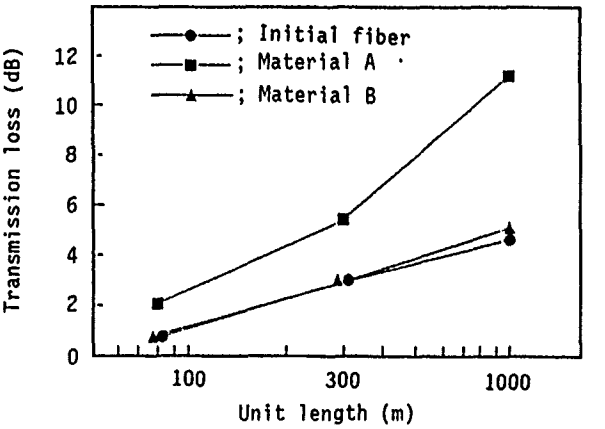

Fig.4 Transmission loss of HC-PCF unit

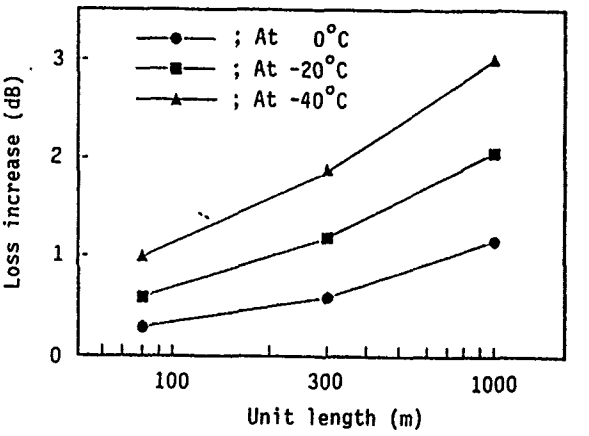

Fig.5 Temperature characteristics (Material A as primary coating)

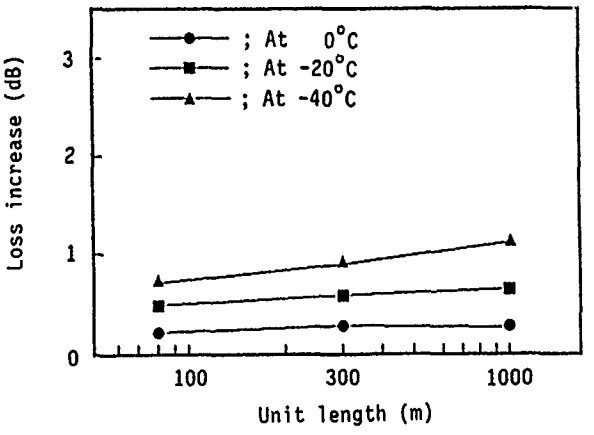

Fig.6 Temerature characteristics
(Material B as primary coating)

3-2 Long-term Reliability

The heat aging test was made at 70 °C for 1000 hours. The results of the test are given in Fig. 7. The units used for the test were 300 m- long. The unit using the material A showed a high increase of loss, although there is a tendency of loss recovery due to reduced residual processing strain of the material. The unit using the material B, on the other hand, keeps extremely stable transmission characteristics. Furthermore, the temperature characteristics of the unit, which using the material B, after heat aging test shows no particular change, compared with the initial characteristics. It has been known that the unit using the material B has long-term stable transmission characteristics.

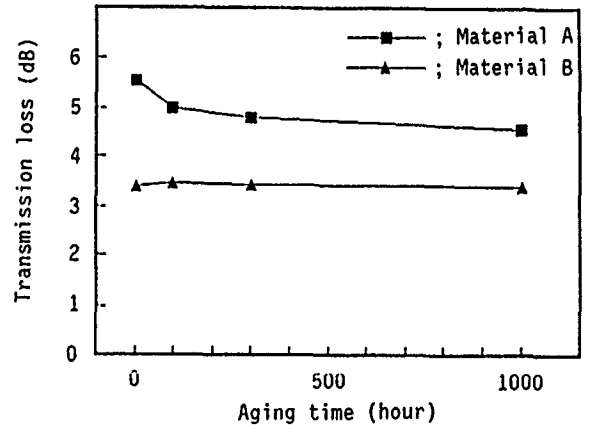

Fig.7 Result of heat aging test

4.BLOWING CHARACTERISTICS

Fig. 8 gives the results of the blowing characteristics of the HC-PCF unit, which were evaluated with the 500 m-long ABF pipe wound on a drum of which barrel diameter is 1 m. In this evaluation, the blowing equipment used was the same as that for the all-glass fiber unit. The X axis indicates the blowing length, and the Y axis indicates the blowing speed corresponding to the blowing length. The HC-PCF unit is slightly less efficient in terms of blowing, because of its weight heavier than that of the all-glass fiber unit. In ordinary in which air pressure is 8 kg/cm sq. or less, it is possible to perform 500 m blowing. In blowing under air pressure of 8 kg/cm sq., there is little change in blowing speed, as shown in Fig. 8. From this fact, it is judged that there is good possibility of 500 m or more consecutive blowing.

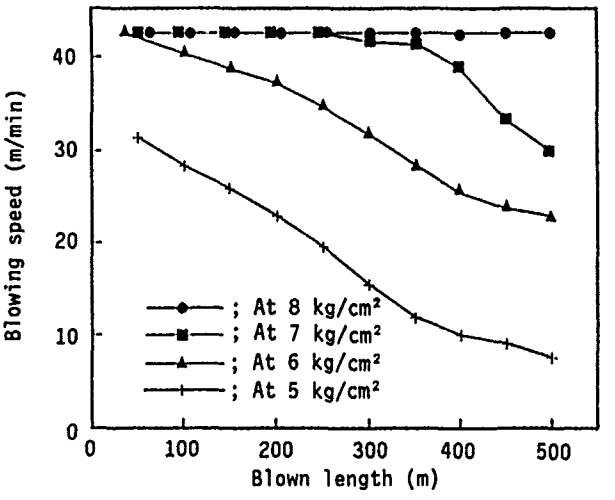

Fig.8 Blowing characteristics

5.EXAMPLES OF APPLICATIONS

Fig. 9 shows a example of the ABF system constructed for LAN in a building. In this example, all-glass GI fiber unit is used for the trunk backbone line, and the HC-PCF unit is used for the floor line. As a matter of course, the all-glass fiber unit can be used in the same pipe cable of the floor line. Connection between local stations of each floor and terminals can be made independently with single pipe cables. Another method of connection is to place a branch box for a pipe cable in the course of a route, and then from the branch box to connect with terminals by means of single pipe cable. In the latter case, in the ABF system, connection in the box can be made only by connecting with the pipe. The optical fiber can be made without splices. Moreover, the floor pipe cable can be combined together with metal cables for voice and/or data.

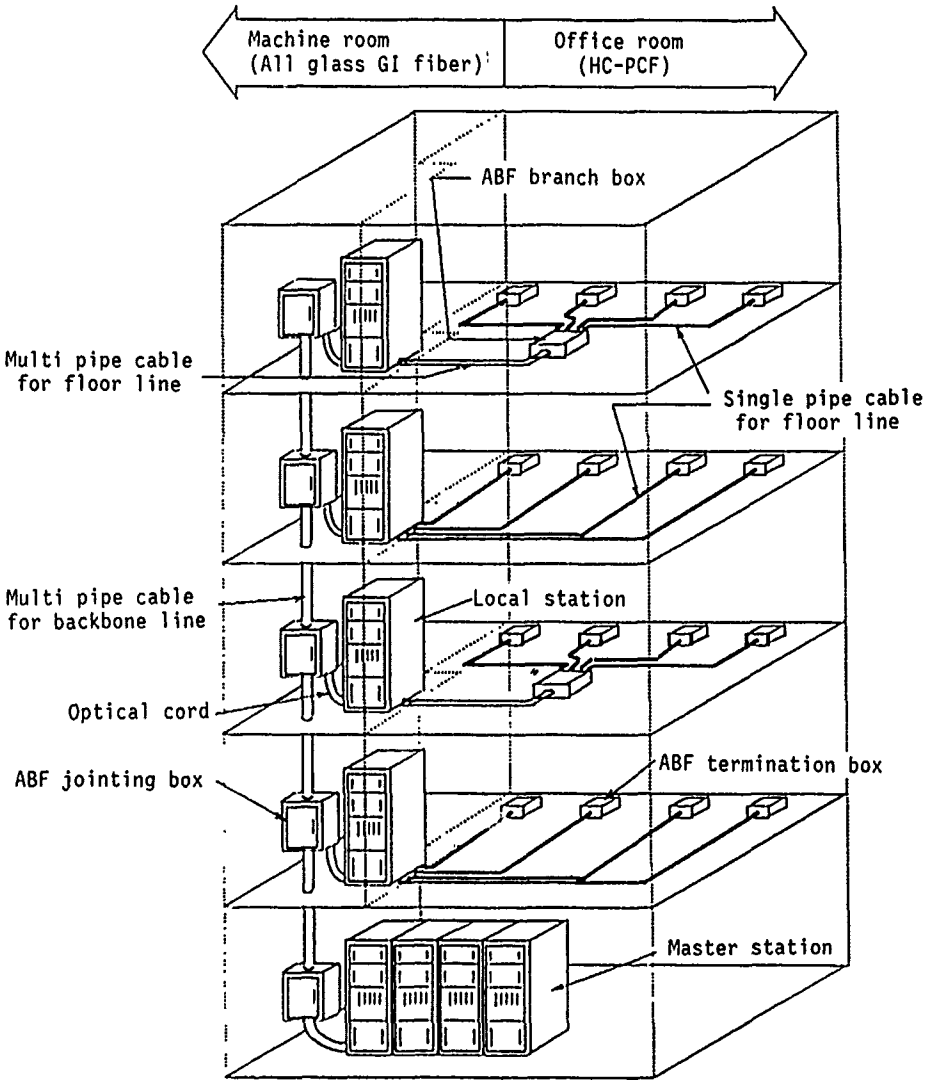

Fig.9 Example of HC-PCF unit application

6.CONCLUSION

We have developed the HC-PCF unit by combination of HC-PCF and ABF system, which have been attracting much attention in the sphere of optical LAN.

The HC-PCF unit permits low-cost and efficient optical fiber laying. By good selection of coating materials, it is possible to have the HC-PCF unit which has practically sufficient transmission characteristics, and can perform blowing of 500 m or more. In the future, there will be a steady increase in use of optical fiber in LAN branch lines. At the same time, demand for the ABF System, in particular HC-PCF, will be sure to increase.

REFERENCE

[1] S.A. Cassidy and M.H. Reeve, "A radically new approach to the installation of optical fibre using the viscous flow of air", IWCS '83, pp 250-253.

[2] H. Sano, K. Hayashi, Y. Terasawa, S. Tanaka and Y. Masuda, "Development of Optical fiber units for Air Blown Fiber (ABF) Cabling Systems", IWCS '89, pp 69-75.

Nobuyuki Suzuki

Sumitomo Electric Industries, Ltd.

1, Taya-cho, Sakae-ku, Yokohama, Japan

Nobuyuki Suzuki received his B.E. degree in engineering from University of Electro Communication in 1987 and joined Sumitomo Electric Industries, Ltd. He has been engaged in the development and design of optical fiber cables in the Fiber Optic Division.

Hiroaki Sano

Sumitomo Electric Industries, Ltd.

1, Taya-cho, Sakae-ku, Yokohama, Japan

Hiroaki Sano was born in 1960 in Osaka, Japan, and received his M.E. degree in Polymer Science from Kyoto Univ. in 1984. He then joined Sumitomo Electric Industries and has engaged in development of optical fiber manufacturing process and cables. Mr. Sano is a member of Communication R&D Dept. in Yokohama Research Laboratories.

Hiroaki Nishimoto

Sumitomo Electric Industries, Ltd.

1-1-3, Shimaya, Konohana-ku, Osaka, Japan

Hiroaki Nishimoto was born in Okayama, Japan on December 27, 1958. He received the B.S. and M.S. degrees in electrical engineering and computer science from the Okayama University in 1981 and 1983 respectively. Since joining the Sumitomo Electric Industries, Ltd., Osaka, Japan, in 1983, he has been engaged in the development work on the optical fibers and passive component for short distance data-comm. applications. Mr. Nishimoto is a member of the Institute of Electronics, Information and Communication Engineers of Japan.

Shin-ichi Yonechi

Sumitomo Electric Industries, Ltd.

1, Taya-cho, Sakae-ku, Yokohama, Japan

Shin-ichi Yonechi received his B.S. degree in mechanical engineering from Tohoku University in 1966. He then joined Sumitomo Electric Industries and has been engaged in development of fiber optic cables. He is now manager of Fiber Optics Cabling System Section and a member of the Institute of Electronics, Information and Communication Engineers of Japan.

A UNIQUE FIBER OPTIC DEPLOYMENT SCHEME ADDS RELIABILITY AND FLEXIBILITY TO COMPLEX FIBER OPTIC CABLE ROUTES

W. J. Beller, P. W. Hart, R. M. Keating

Pacific Bell, San Ramon, California

Abstract

The philosophy of being a high quality service provider has prompted Pacific Bell to develop, in cooperation with Raychem Corporation, a unique fiber optic deployment scheme, that is compatible with all fiber feeder architectures. The Fiber Distribution Point (FDP) is spliced to 24 fibers of a main feeder cable. All other fibers in the main feeder cable are uncut and continue on undisturbed to be used in other locations in the route. Deployment of the FDP facilitates administration of the fiber loop feeder network, reduces labor and hazard to main feeder facilities, allows flexibility of points of feed and the most appropriate sizing of feeder cables.

Introduction

Recent shifts in the way Pacific Bell provides service now require loop fiber to be constructed in a ring configuration where economically feasible, with fibers for service routed back to the CO in a direction opposite to, and in a different sheath than, fibers for protection of that service. Two types of rings are possible to construct:

The Diverse Fiber Loop

Utilizes completely different duct structures and manholes with separation of at least the width of a city street. (See Exhibit 1)

The Protected Fiber Loop

Utilizes the same duct structures and manholes, with separation within the structure of at least one vertical and one horizontal duct. (See Exhibit 2)

If neither of these two options for ring construction are possible due to lack of available conduit or reasonable economics, the minimum protection required is separation between the the individual buffer tubes within the same sheath, isolating the protection fibers in tubes separate from the primary service fibers. This non-ring construction is termed the Redundant Fiber Loop (Exhibit 3) and is the last choice for loop fiber construction. In this arrangement, the FDPs are spliced exactly the same as in ring architecture, but the protection fibers are routed to the end of the taper point before being spliced back onto fibers in different tubes but in the same sheath. In addition, this arrangement allows for easier administration and future completion of a ring when and if adequate conduit becomes available.

All lightwave systems currently being installed in Pacific Bell utilize a one-to-one service-to-protection arrangement. These plans provide for a self-healing design in the event the service fibers are physically damaged due to a cut of the cable sheath or individual fiber. Fiber Distribution Points (FDPs) can be used in exactly the same way as in non-ring construction, and in fact can now be administered and spliced more easily.

New Concepts

Ring architecture requires the Outside Plant engineer to understand a new concept. Route diversity in loop fiber optic systems is the new standard where economical. This concept, utilizing a ring configuration, requires using the same two fibers (transmit and receive) in the ring after being severed and spliced to the drop fibers, then routed back to the CO from the FDP in different cable sheaths and conduits. (See Exhibit 4)

Fiber Distribution Point (FDP) Description

The FDP is an integrated cable closure, fiber organizer and cable harness to provide remote access to feeder fibers. (See Exhibit 5) It is assembled in a factory environment, thoroughly tested and shipped to the field as a ready-to-deploy subsystem. The system incorporates the use of electrical heat-shrinkable sleeves and hot melt adhesives and is composed of five parts:

1. FOSC 100D base organizer trays and dome
2. FOSC 100B base, organizer trays and dome cable stub
3. Two, 50 ft, pre-installed 24 fiber cable stubs
4. Cable and dome seals
5. Accessory components and mounting bars

A 100 foot piece of 24 fiber cable has 10 feet of sheath and buffer tubes removed from the mid point. This is then looped and sealed through an

oval entry port in the FOSC 100B closure (distribution point) and the fiber organized in splice trays. There are six fibers per splice tray with the center of each fiber loop marked. Four small round cable entry ports in the FOSC 100B closure can handle one fiber service drop cable each with a diameter range of .2 to .6 inches. The two cable stub ends are prepared (stripped, moisture blocked and sealed) and placed in the FOSC 100D (main cable closure) through two round cable entry ports. The loose fibers are secured and stored in trays. The splice trays will accommodate most popular types of fiber connectors and are designed for low loss organization of fiber operating at 1550nm. Each closure is sealed and supplied with all necessary consumables.

The FDP provides access to feeder fibers in complements of 24. But as fibers are severed and spliced at each FDP in a ring configuration, a total of 48 fibers back to the central office becomes available. This enables the potential installation of 12 systems feeding from each FDP location, considering the requirement of four fibers per system; two for primary service and two for a completely redundant system.

The FDP contributes to higher splicing productivity in fiber optic cable construction by minimizing the amount of fiber splicing required at initial deployment. This results in real first-time cost savings that has measurably added to justification proposals for the construction of loop fiber feeder routes. The methods and practices developed by Pacific Bell for standard access to the feeder network require the use of the FDP interface (FOSC 100B closure), preserving the integrity of the main fiber optic feeder splice (FOSC 100D closure).

The FDP concept in a ring architecture scheme is uniquely adaptable to SONET-based systems using the add-drop multiplexer, as well as the self-healing aspects inherent to redundant ring architecture. Deployment during the present time frame in this arrangement positions the network to take full advantage of these future developments with no rearrangements required.

Installation

The installation begins with the routing of the main feeder cable into the oval port of the FOSC 100D closure. Use of this oval port enables looped cable entry, the insertion of uncut fiber buffer tubes into the closure so that only those fibers intended to be spliced to the 24 fiber stub cables need to be cut. The remaining uncut buffer tubes are accommodated within the closure, presenting no hazard to any service that may be working on fibers within those tubes at another location. This procedure enables mid-point entry on cables and the placement of long cable reels in an urban high-density environment while minimizing the placing and splicing time involved. The FDP is extremely lightweight and is easily moved in and out of manholes to facilitate splicing and testing. After splicing to the main feeder cable, drop cables can be installed into the FDP. Once the main feeder cable is spliced, no future access is allowed. This restriction limits the hazard for disturbing service to only those 24 fibers appearing in the FDP stub, providing ongoing reliability, flexibility and availability.

Conclusion

The FDP has been successfully deployed in major urban and suburban areas throughout the Pacific Bell region, specifically where future growth and multiple access is required or expected. Feedback from construction forces has been extremely positive. In the one year since deployment, the results of the FDP concept exceed original expectations of Pacific Bell. The system remains flexible to future needs, while not compromising the high standards of integrity and reliability required from a high quality service provider such as Pacific Bell.

W. J. Beller

Graduated from California State University at Long Beach in 1966 with a Bachelor of Science Degree in Mechanical Engineering. Has spent the last 20 years with Pacific Bell in various Outside Plant Construction and Engineering assignments.

Contact Address

Pacific Bell
2600 Camino Ramon
Room 2S100
San Ramon, CA 94583

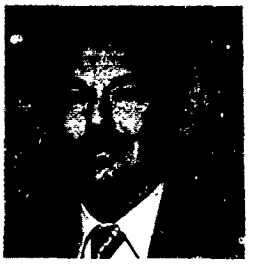

P. W. Hart

Has been employed with Pacific Bell for 27 years, holding various jobs in Outside Plant. Currently, Pat is in the Science & Technology Department responsible for specifications and standards for fiber cable and apparatus and has been involved with fiber technology for the past eight years.

Room 3S850

R. M. Keating

Started with Pacific Bell in 1968 and holds a Bachelor of Science Degree from the University of San Francisco. He has been working on various Outside Plant fiber projects since 1980 including the 1984 Summer Olympics in Los Angeles.

Room 1S200

EXHIBIT 1

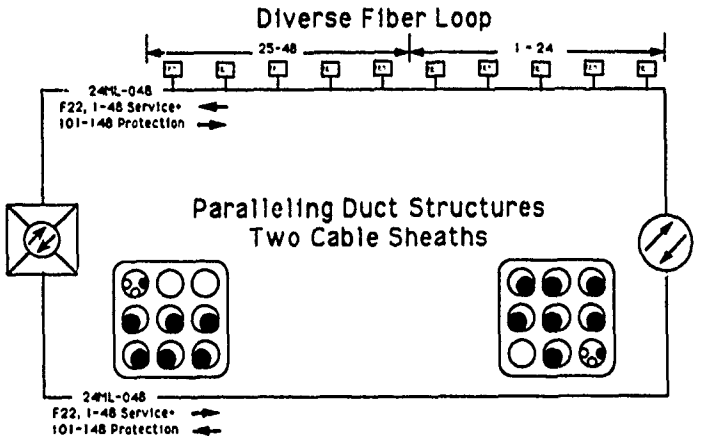

EXHIBIT 2

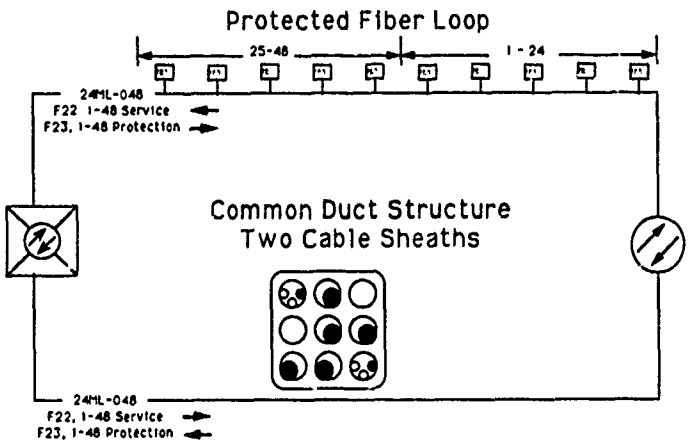

EXHIBIT 3

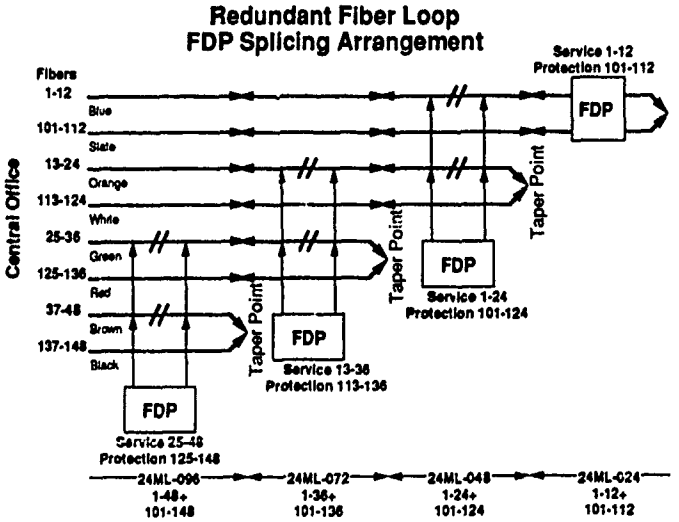

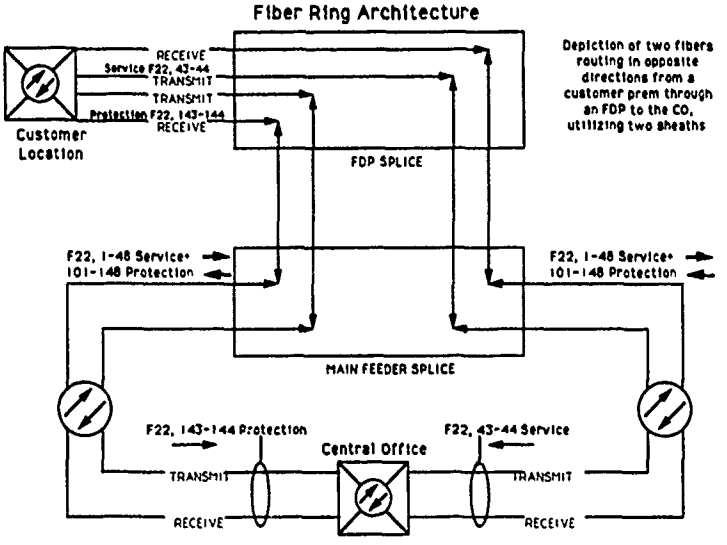

EXHIBIT 4

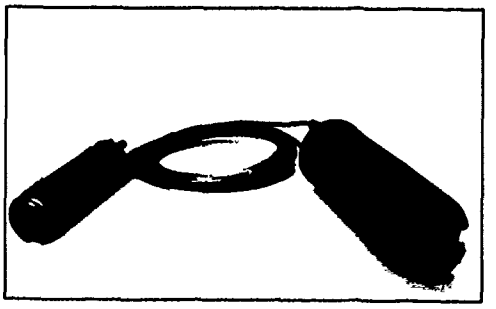

Bases,organizer trays, domes and cable.

Exhibit 5

THERMAL STABILITY TESTS FOR POLYOLEFIN INSULATIONS

T.N. Bowmer, R.J. Miner, I.M. Plitz, J.N. D'Amico and L.M. Hore
Bellcore
New Jersey 07701
U.S.A.

ABSTRACT

The thermal stability test methods and requirements used for selecting polyolefin (PIC) insulations need to be reevaluated in light of recent field failures. We review the advantages and disadvantages of pedestal and oven testing as well as detail the quantitative relationships between test lifetime, test temperature, stabilizer concentrations and field lifetimes. Samples with known field lifetimes are used to calibrate the laboratory tests and thereby determine the test criteria to ensure a 40 year minimum field life for PIC insulations. The results from interlaboratory round robins of pedestal and oven tests are also discussed.

INTRODUCTION

Interest in the thermal stability of polyolefin insulations has been intense[1-8] following the observations of cracks in foam-skin, high-density polyethylene insulations in aboveground closures in southwestern USA[1,2]. The test methods and requirements used for selecting polyolefin insulations need to be reevaluated in light of these field failures. The required accelerated aging test for PIC (Polyolefin Insulated Conductor) insulation must:

- simulate field conditions
- have the shortest possible duration
- show interlaboratory reproducibility.

High density polyethylene (HDPE) insulations are affected by many environmental factors but the two most important are temperature and physical stress[2,3,9-16]. High temperatures accelerate the rate of both oxidation of the polyolefin and stabilizer loss by extraction and evaporation. Physical stress accelerates craze formation and crack propagation. Since 1972, most buried cables have been filled with a oily hydrocarbon compound to make them water resistant. These filling compounds are known to extract stabilizer from the insulation[3,4-8,17]. It is important therefore that test procedures designed to screen cable insulations for long term applications take all these factors into account.

The stability of PIC insulations is now evaluated by an Oxidative Induction Time (OIT) test and laboratory pedestal tests[10,18]. The OIT test determines the time for oxidative degradation to begin at high temperatures (typically 200°C) in pure oxygen. This test is excellent both for screening materials and for quality control since relative changes in OIT values represent changes in stability and/or stabilizer concentrations. For example, a survey of OIT values was used to determine the percentage of PIC insulations in the field that are vulnerable to oxidation and cracking[2,19].

The current thermal stability performance test for PIC (Polyolefin Insulated Conductor) insulations is performed in heated pedestals at 110°C and 90°C for 45 and 365 days, respectively[18]. Insulated wires are coiled and heated in laboratory pedestals at these temperatures and the coils are examined for cracks after the prescribed times. In response to the most recent field failures, two changes were introduced into the test; (1) preconditioning PIC cable at 70°C and (2) using coiled samples in the test. The pedestal test was based on work performed in the 1970s[10,16] on solid PIC insulations from aircore cables. However, the appropriate test temperatures and times to simulate field lifetimes and conditions need to be reevaluated for the latest designs of PIC insulations and aboveground closures.

An alternative test method is to age insulated wires in forced-air ovens which should have improved temperature control and higher airflow rates compared to heated pedestals. The higher airflow rates should allow tests to be performed quicker and/or at lower temperatures. However, previous round robin testing of oven test protocols[20,21]

suffered from large variations in results between laboratories.

This paper will review the advantages and disadvantages of pedestal and oven testing as well as detail the quantitative correlations between test lifetime, test temperature, stabilizer concentrations, OIT values and field lifetimes. Samples with known field lifetimes are used to calibrate the laboratory tests and thereby determine the required test times to ensure at least a 40 year field life for PIC insulations. The results from interlaboratory round robins of pedestal and oven tests will also be discussed.

EXPERIMENTAL

PIC samples used in this study included foam-skin insulated wires from filled cables and solid insulated wires from both aircore and filled cables. These samples were standard products from three different cable vendors manufactured between 1987 and 1989. One vendor kindly supplied uncabled PIC wires; i.e., foam-skin and solid insulated wires that were never cabled or exposed to filling compounds. Various cable samples (4-12 years old) were excavated from buried field locations, adjacent to aboveground closures that contained cracked insulations or insulations with low OIT values[2,19].

Standard PC-6 (6x6x48 inch) pedestals from Kisco Company or Champion Metal Products were used. Accessories such as the terminal plates, plastic liners, grounding straps and support frames were removed before testing. Glas-Col Apparatus Company supplied heating mantles to fit closely over the top 12 (260 Watts) or 20 inches (500 Watts) of the pedestal. Temperatures between 60 and 110°C (±1°C) were maintained at the sample position using Glas-Col Model #PL612 proportional controllers. An I^2R model OTP-30A protection probe was used to ensure that power surges or controller problems did not expose the insulations to high temperatures (i.e., >3°C over the set temperature). For oven testing, Blue M model OV-510A-2 and model ESP-400C-5 forced-air ovens were used at 60-90°C (±1°C). Air flow rates were measured with a Alnor Compuflow meter model No. 8500D-II. Air exchanges per hour were determined by the method outlined in ASTM E 145 using a General Electric Type 1-50-A Watthour meter (Model AR2).

Preconditioning of cables entailed placing sealed cable sections in ovens at 70°C for 4 weeks. This preconditioning was supposed to simulate a cable exposed for a year or more to high temperatures in a cable reel yard[4-6].

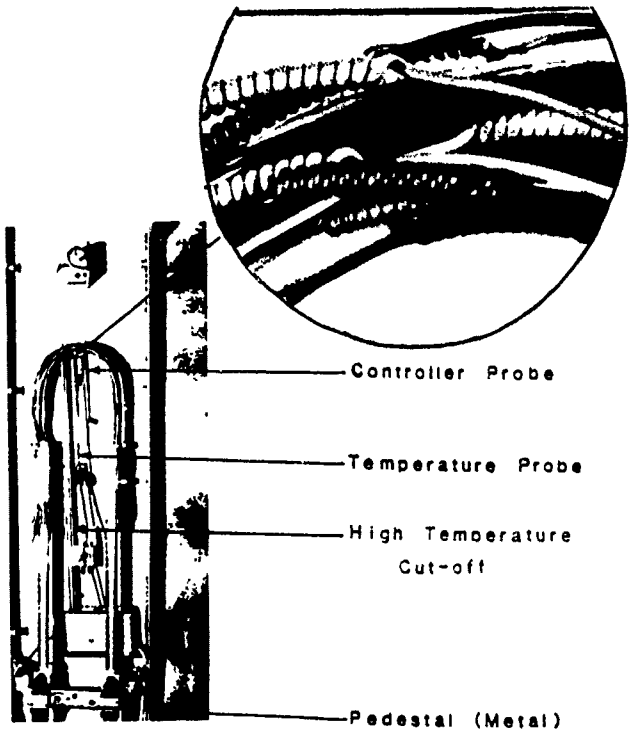

Fig. 1 Pedestal Test

For accelerated aging tests in pedestals and ovens, the insulations were removed from the cable sheaths, the filling compound wiped off with a dry cotton cloth, and the insulations coiled as outlined elsewhere[3,18]. Fig. 1 shows a typical arrangement of coiled insulated wires in a pedestal ready for testing. Typically, 20-50 insulated wires were selected with all colors represented equally. The coiled insulated wires were placed in heated pedestals or ovens at the specified temperatures. The samples were examined for cracks with a 5x magnifying glass at regular intervals of 1-4 weeks depending on the expected lifetime of the insulations. A plot of percentage of cracked insulations versus time was drawn for each accelerated test and the onset of cracking was defined as t_0.

Oxidative Induction Times (OIT) were measured in aluminum pans at 200°C on insulations stripped from the conductors as described previously[2,22]. The percent of the individual antioxidants, Irganox 1010

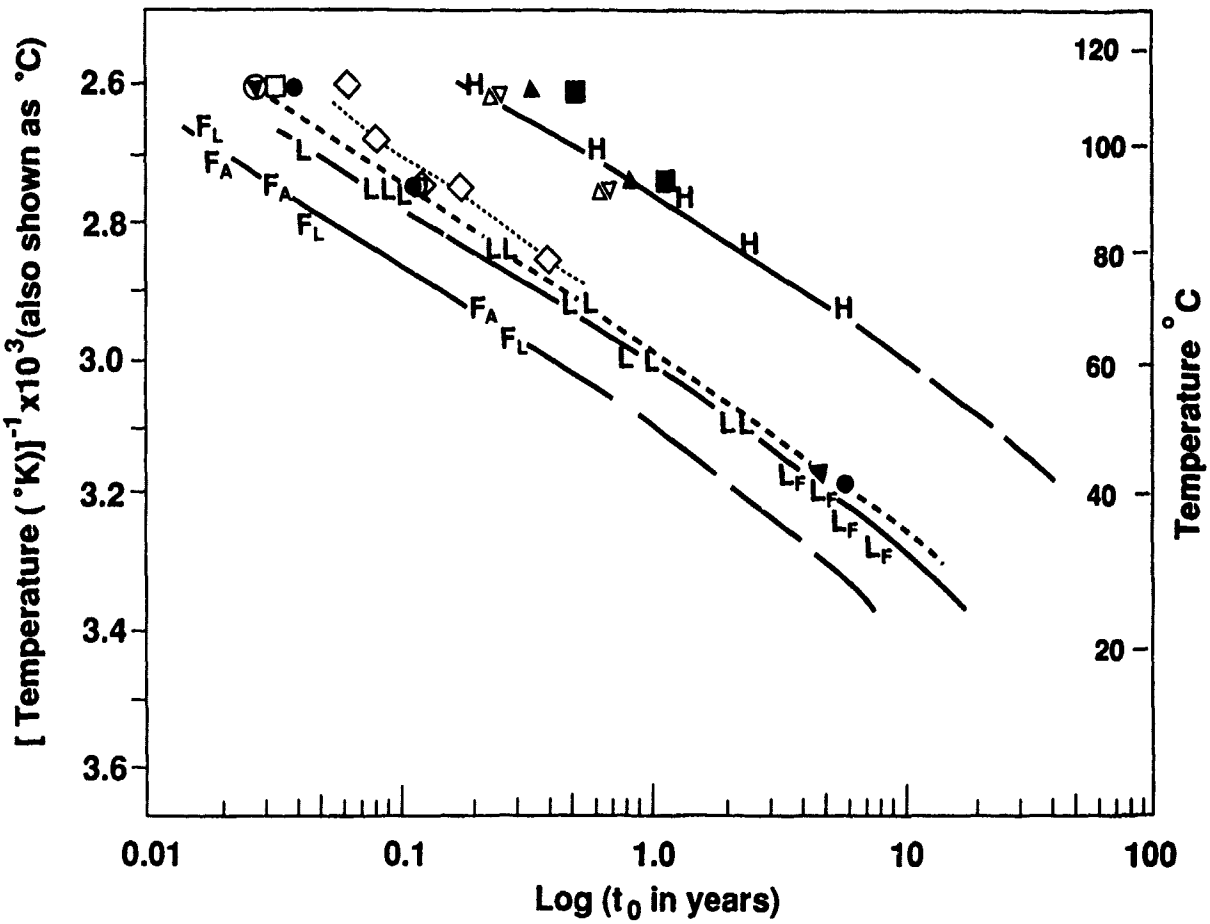

Fig. 2 Arrhenius plot for pedestal test results. Log (t_0 in years) versus [Temperature,°K]$^{-1}$ for "as received" foam skin HDPE insulations (■,▲), preconditioned foam-skin and solid HDPE insulations (Δ,∇,◊), field (L_F) and laboratory (L) results for LDPE insulations[2,10,16], aircore solid HDPE insulations (H), field excavated foam-skin HDPE insulations ("as excavated" - ●,▼ and preconditioned - ○,□) and field foam-skin HDPE insulations with OIT < 2 mins (F_A,F_L).

and Irganox 1024‡, in selected PIC insulations were determined by hot toluene extraction and liquid chromatography analysis of the extract[7,23,24].

RESULTS AND DISCUSSION

We shall discuss the pedestal, oven and OIT test results individually, examine some interlaboratory round robin studies and finally correlate test lifetime with field lifetimes and suggest test criteria to ensure at least a 40 year life for PIC insulations under field conditions.

‡ Ciba-Geigy stabilizers
Irganox 1010 = tetrakis{methylene (3,5-di-tert-butyl-4-hydroxy-hydrocinnamate)} methane
Irganox 1024 = N,N'-bis{3-(3',5'-di-tert-butyl-4-hydroxyphenyl) propanyl} hydrazine

Pedestal Test

Fig. 2 is the Arrhenius plot of log(t_0 in years) versus [test temperature(°K)]$^{-1}$ for representative data from our pedestal testing. The time-to-crack (t_0) values at 90°C were 2.5-3.0 times those at 110°C, independent of PIC sample tested. Included in Fig. 2 is test data from PIC insulations:

(a) manufactured in 1987-1989 (■,▲,Δ,∇,◊),
(b) excavated from the field (●,□,○,▼),
(c) with OIT < 2 mins that were gathered from field closures (F_A, F_L),

as well as published data[2,10,16] for low-density polyethylene (L,L_F) insulations and high-density polyethylene (H) insulations.

PIC insulations tested from "as received" cables (■, ▲ in Fig. 2) compared favorably with solid insulations from aircore cables tested in 1974[10,16] (---H--- in Fig. 2). If these insulations were preconditioned before pedestal testing then the time-to-crack values (t_0s) were 2.5±0.5 times lower because stabilizers were extracted from the insulations during this preconditioning. OIT values of insulations were typically reduced by 60-80% after preconditioning for 4 weeks at 70°C[3-6].

The PIC samples excavated from buried locations in the field were also pedestal tested (●,○,□,▼ in Fig. 2). For these field samples, preconditioning at 70°C for 4 weeks produced only a minor (20-30%) reduction in t_0 values. The combined field history of these PIC samples (time in storage, reel yards and buried underground) presumably produced a similar degree of stabilizer extraction as did the preconditioning treatment. The thermodynamic limit of stabilizer extraction was approached during the field life of the cable and any further preconditioning of the excavated field samples produced little further stabilizer extraction.

PIC insulations from these particular field samples were known to crack inside aboveground closures in Arizona after 4.5 and 5.5 years. In addition, 40°C is known to be the equivalent pedestal test temperature for PIC insulations exposed in Phoenix and Tucson, Arizona where these particular field samples were gathered[2,19]. Therefore field failure data could be added to Fig. 2 and this data confirmed that the same Arrhenius relationship applied for field aged,"as received", and preconditioned HDPE foam-skin insulations from filled cables, LDPE solid insulations from aircore cables and HDPE solid insulations from aircore cables. This series of parallel lines suggested that the temperature dependence was independent of stabilizer concentration and determined only by the oxidation mechanism for the polyethylene molecules. The stabilizer content and/or physical design (e.g., solid versus foam-skin) of a PIC insulation defined the specific t_0 value, but the temperature dependence was determined by the same oxidation mechanism in all the polyethylene insulations.

Sometimes, the t_0 values found from 110°C pedestal testing were longer than would be expected from lower temperature testing; e.g., note the diamond shaped points in Fig. 2. The enhanced lifetime at 110°C may arise from physical changes in the stabilizer or polymer. Irganox 1010 has a crystal melting transition at 110-120°C[25]. Crystallites of high density polyethylene also begin to melt at ~110°C. Such changes in crystallinity, morphology, shape, solubility and diffusion of the stabilizer in the polyethylene matrix may affect the loss rate, mobility and reactivity of the stabilizer. The polymeric matrix is also subject to temperature dependent changes in morphology, crystallinity, orientation and other physical effects that may contribute to the rate of stabilizer loss from the insulation. Such contributions to the degradation of PIC insulations are not clearly understood despite the numerous studies on small molecule diffusion in polyethylene[26].

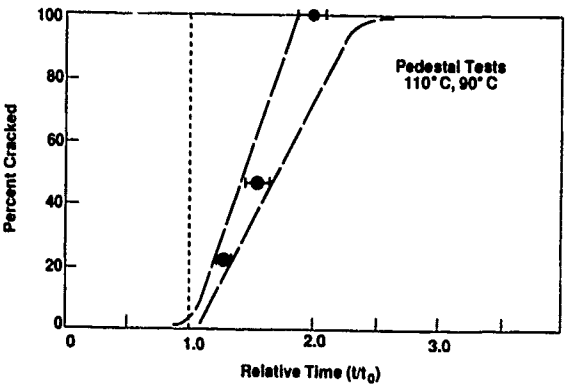

Fig. 3 Percent insulations cracked versus normalized time (t/t_0) for pedestal tests. Averages from 35 individual tests.

Despite the wide range of insulation sources, stabilizer percentages, test temperature and sample treatments, the development of cracked insulations showed a uniform dependence on time as illustrated in Fig. 3 where the percentage of cracked insulations is plotted against relative time (t/t_0). In the ideal case, all the insulations in a pedestal would crack at t_0. Differences in time-to-crack values were caused by (1) intrinsic variations during insulation/cable manufacture and (2) test variables. For example, cable manufacture variables such as extrusion temperatures and filling compound temperature, can lead to differences in stabilizer percentage and distribution within/between wires. Cable manufacturing variables typically produce a ~5% variation in OIT values along a single PIC insulation and a ~20% OIT variation between PIC insulations in the same cable[27].

Pedestal test variables such as physical stress on insulations and temperature variations across the sample bundle can result in significant variations in the time-to-crack value measured[3]. The temperature variation across the sample bundle can be large in the pedestal test. Steep temperature profiles were generated inside the laboratory heated pedestals. Heat efficiently flowed from the heated top section of the steel pedestal to the cold bottom section. In addition, the copper wires in the PIC samples and any metallic support structures can also extend down out of the heated zone and conduct heat out of the sample zone. Although the set temperature can be easily maintained at ±1°C, steep gradients of up to 5°C/inch can develop across the heated zone. It is therefore essential to keep the PIC sample coils in a uniform plane to minimize temperature variation across the sample bundle. We found that 30 sample coils can be easily placed within 1/2 inch (vertically) with the temperature range from top to bottom coil being within ±2°C. The temperature difference from top to bottom coil can be reduced to < ±1°C, if the 12 inch standard mantles are replaced with 20 inch long mantles.

From the Arrhenius plots (Fig. 2), the variation in the t_0 value for a given temperature change can be calculated. For example, a 1°C change in the 90°C pedestal test would result in a 6±1% change in the time-to-crack value found for the PIC sample. At 110°C, the analogous variation in time-to-crack values would be 5±1% for every 1°C change. For example, an insulation that cracked after 365 days at 90°C would be expected to crack after 400 days at 88°C.

As reported previously[3], crystals formed on the PIC insulations during the pedestal test, particularly after long test times (e.g., >80-100 days). There were two distinct crystals found on the insulations; cubic crystals (50-100 μm square) and long needle-like crystals (1-10mm long, 10-20 μm diam.). Using infrared spectroscopy, the cubic crystals were identified as melamine and the needle crystals as fiberglass. From 110°C tests using a sandblasted pedestal (i.e., no paint), melamine was concluded to be a thermal degradation product from the acrylic green paint on the pedestals. The PIC insulations provided an excellent seed site to initiate crystallization. Although melamine can act as a cation/free radical scavenger, no effect on t_0 was detected in PIC testing. Since the melamine was not absorbed into the insulation, no effect on the degradation mechanism was possible. The Fiberglass strands were physically abraded from the heating mantles and the smaller strands were distributed throughout the pedestal by air movement.

Forced-air Oven Test

Oven tests were performed concurrently with the pedestal tests using PIC samples from the same cables and reels. The normalized plot of percent cracked versus relative time (t/t_0) for the oven tests is shown in Fig. 4. Similar to the pedestal test, manufacturing and test variables both contribute to the scatter and shape of the percent cracked versus time profile. The major difference between the pedestal and oven tests was the relative size of the test variables. Whereas temperature variations were a major concern in the pedestal test, temperature variation inside the forced-air ovens was minimal (±0.5°C). The major oven test variable was airflow rate or air exchange rate. Generally, time-to-crack values for PIC samples inside ovens were shorter than in pedestals at the same temperature because the high air flow across the surface of the PIC insulations accelerated stabilizer loss by evaporation. Oven tests could also be performed at lower temperatures in reasonable times (< 1 year). However, airflow variations between ovens caused too much scatter in interlaboratory round robins[20,21] (see below).

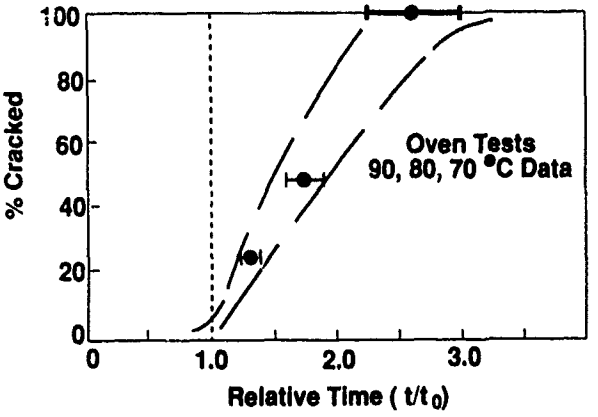

Fig. 4 Percent insulations cracked versus normalized time (t/t_0) for oven tests. Averages from 25 individual tests.

For a single oven, t_0 values were reproducible within ±5-10%. A consistent relationship was found between different test temperatures as shown in Fig. 5

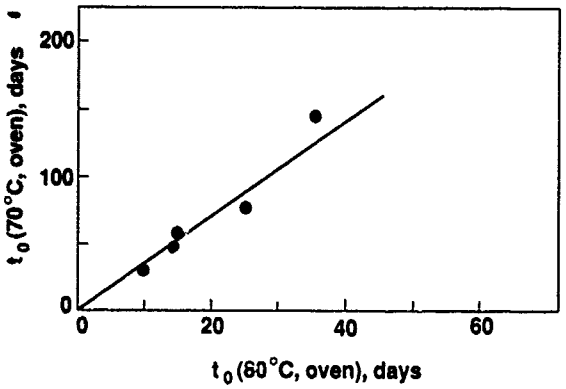

Fig. 5 Oven test results - t_0(70°C,oven) versus t_0(80°C,oven)

where the t_0 values found at 70°C and 80°C are compared for the model OV-500 model ovens However, there is insufficient data at present to define an Arrhenius relationship for the oven data. Long term, low temperature (>400 days, <70°C) oven tests are in progress to determine the temperature dependence for oven testing. In addition, the appropriate extrapolation to field conditions is unclear since both temperature and airflow effects were accelerated in the oven tests.

Table 1 compares oven flow characteristics and t_0 for our two different model ovens. The air speed inside model OV ovens was ~20% higher than in the model ESP ovens but the air exchanges per hour was higher in the model ESP ovens (600 cf. 200 exchanges per hour). The higher the air speed and air exchange/hour, the greater will be evaporation/loss of stabilizer and any volatile oxidation products. More stabilizer loss should lead to faster degradation and a lower t_0. However, the oven with the greater air exchange value had the greater t_0. A broader range of oven models and air exchange rates need to be tested before the variations in oven testing are quantitatively understood. However, the results for these two ovens suggested that removal of the volatile oxidation products was more important than stabilizer loss. Since such oxidation products can accelerate the degradation of polyolefins[28], their removal may increase the t_0 values for PIC insulations.

Table 1. Oven Characteristics

Parameter	Oven Model	
	OV-510A-2	ESP-400C-5
Volume (ft^3)	2.81	2.97
Air Exchanges/hour	200	600
Air Flow Rates (ft/min) inside oven at		
entry ports	1000±200	500±100
middle	120±20	100±20
exit ports	60±10	50±10
t_0 (days)	50±10	220±40

OIT (Oxidative Induction Time) Test

The OIT test[22] measures the oxidative stability by calorimetry at high temperatures, typically 200°C. The test is rapid (20-100 mins) compared to the pedestal or oven test, but the large extrapolation from 200°C to field temperatures of <40°C results in the absolute OIT value being an unreliable guide to field performance. For example, carbon black has a small OIT value at 200°C, but is an excellent thermal stabilizer at field conditions as evidenced by the long lifetime of black polyethylene cable sheaths in outside environments.

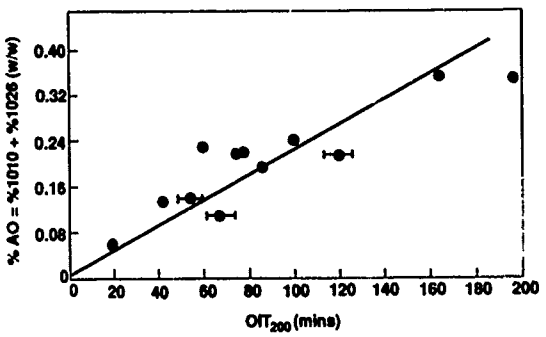

Fig. 6 OIT value versus total weight percent of stabilizer (%1010 + %1024)

The OIT value of a PIC insulation correlated linearly with the total weight percent of stabilizer (Irganox 1010 wt% + Irganox 1024 wt%) as shown in Fig. 6. Note that all the PIC insulations studied in this report contained the same two stabilizers at a similar 1010/1024 ratio of 0.5-1.0. Therefore the correlations

Table 2. Correlation Coefficients - Foam-skin, "as received" samples

PARAMETER		COMPOSITION (wt%)			LIFETIME				
		%1010	%1024	%AO	OIT (200°C)	FIELD	110°C ped.	90°C ped.	80°C oven
LIFETIME	t_0(80°C,oven)	0.9	0.95	0.96	0.93	0.98	0.7	0.9	
	t_0(90°C,ped.)	0.61	0.77	0.99	0.9	-	0.87		
	t_0(110°C,ped.)	0.45	0.54	0.61	0.9	0.9			
	FIELD	0.99	0.99	0.99	0.98				
	OIT (200°C)	0.78	0.91	0.91					
WT %	%AO (Total)	0.96	0.96						
	1024%	0.85							
	1010%								

between OIT values and test lifetimes described below may only apply to insulations stabilized with comparable quantities of Irganox 1010 and Irganox 1024. Extrapolations to other stabilizer systems may be invalid.

With this caveat in mind, the OIT value of an insulation correlated with pedestal test lifetimes, oven test lifetimes and field lifetimes of the PIC insulations. The linear correlation coefficients for cross comparisons between the various stability tests are listed in Table 2 for "as received", foam-skin HDPE insulations. An attempt to relate test lifetime to individual stabilizer concentrations was usually less successful than the OIT correlation. The OIT versus t_0 values for the 110°C pedestal test and the 80°C oven test are shown in Figs. 7 and 8 respectively. The 80°C oven results are shown for two different model ovens illustrating the large variations that can occur between ovens.

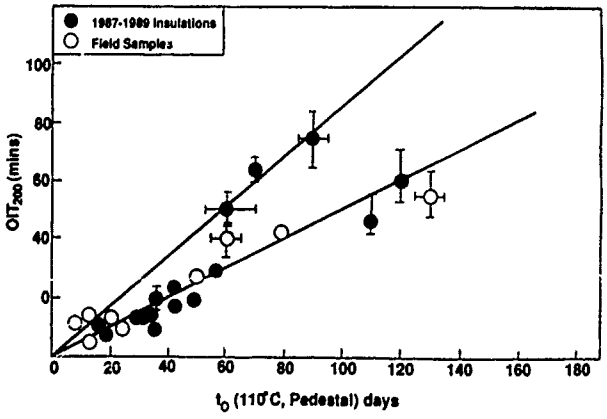

Fig. 7 OIT value versus t_0(110°C,pedestal)

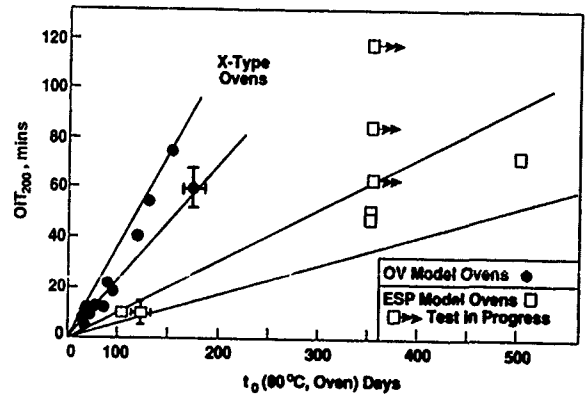

Fig. 8 OIT value versus t_0(80°C,oven)

Round Robins

Nine laboratories participated in round robins for the pedestal test and oven test sponsored by the TWCSTAC† committee. Cables were kindly supplied by Superior Cable with the copper conductors insulated with either foam-skin or solid high-density polyethylene (HDPE). Participating laboratories preconditioned their section of cable for four weeks at 70°C and performed the pedestal and oven tests as outlined elsewhere[18,5,6]. Not all laboratories were able to test all insulation designs under all test protocols. However, enough results were obtained for foam-skin insulated samples in oven tests at 80°C and in pedestal tests at 110°C and 90°C for analysis.

The percent of insulations cracked versus time (days) are shown in Figs. 9 and 10 for the foam-skin insulated samples tested in pedestals at 110°C and 90°C, respectively. At 110°C, results from four of the five participating laboratories agreed within experimental error and can be considered to follow a single curve. Cracks were first seen after 25±5 days with fifty percent of the insulations cracked after 32±2 days at 110°C. The samples tested at laboratory #3 survived twice as long as samples in any other laboratory.

The results from pedestal testing at 90°C (Fig. 10) showed larger scatter between laboratories than that found in the 110°C tests. Five of the seven participating laboratories reported that insulations cracked after 80±15 days with fifty percent of the insulations cracked after 105±10 days. Samples tested at laboratory #1 cracked after only 40-45 days, while insulations tested at laboratory #8 did not crack until 175 days.

Fig. 11 shows the results from the oven round robin tests performed at 80°C plotted in the same fashion as the results for the pedestal tests. The observed t_0 values were randomly scattered between 50 and 250 days. The same broad scatter was found for the time (days) for fifty percent of the insulations to be cracked (t_{50}); i.e., random scatter between 100 and 350+ days.

In general, the pedestal test results exhibited good correlation between laboratories. The scatter observed in t_0 and t_{50} values, particularly in the oven tests, was assumed to reflect inadequate definition in sample preparation, temperature control and/or experimental procedures. The significant variables in

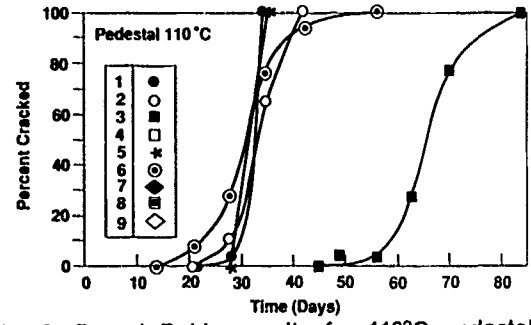

Fig. 9 Round Robin results for 110°C pedestal testing - Percent insulations cracked versus time

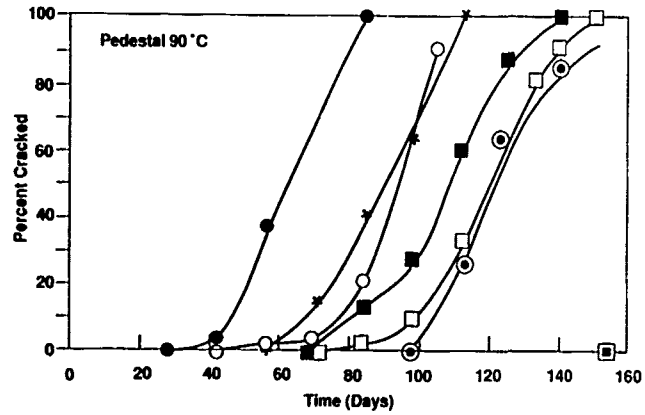

Fig. 10 Round Robin results for 90°C pedestal testing - Percent insulations cracked versus time

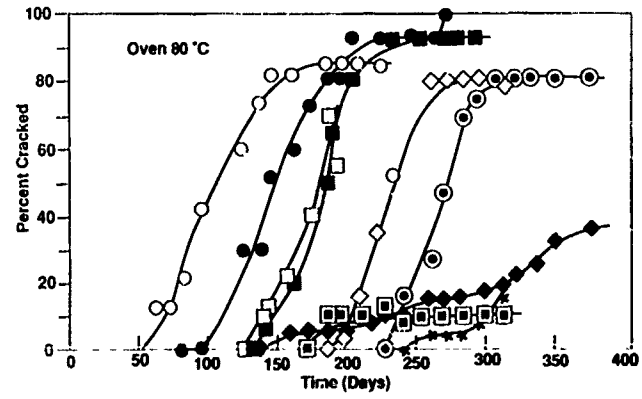

Fig. 11 Round Robin results for 80°C oven testing - Percent insulations cracked versus time

† TWCSTAC = Telecommunications Wire and Cable Standards Technical Advisory Committee

the pedestal test have been reviewed above and the steep temperature gradients inside the heated pedestals were assumed responsible for the anomalous results of Lab.#3 at 110°C and Lab.#8 at 90°C.

It is apparent, from the large scatter seen in the results shown in Fig. 11, that all the significant factors that effect oven aging have not been identified. Our oven results (see Fig. 8), as well as the 1977 robin test results[21] of an oven aging protocol for PIC insulations, showed similar broad scatter in time-to-crack values. Oven testing of insulations has been discussed by numerous authors[4-6,20,21] and variations in temperature control and airflow characteristics inside the ovens are assumed to be the critical variables in forced-air oven testing. The rapid air movement inside these ovens accelerated stabilizer loss and oxidation of the polyethylene. Typical airflow rates inside these ovens can range from 50 to 1000 ft/min with greater than 100 air exchanges per hour. ASTM Type IIB ovens were specified in this round robin and temperature control was expected to be better than ±1°C at the 80°C test temperature. Therefore, differences in airflow rates and/or air exchange rates were assumed responsible for the large scatter seen in Fig. 11.

Field Lifetime Correlations

Several field samples have been obtained to calibrate the accelerated tests (pedestal, oven, OIT, etc..). These samples were excavated from buried cables adjacent to aboveground pedestals where PIC insulations had been found to be cracked and/or have low OIT values (i.e., OIT < 2mins). Insulations from these buried cables were foam-skin high-density polyethylene insulations with OIT values from 8 to 60 minutes. Since these insulations were protected by cable sheaths in a cool environment, they are assumed to have similar oxidative stability as when installed. Most stabilizer extraction by the filling compound was expected to have occurred during reel yard storage and not during the buried lifetime of the cable. Therefore these PIC insulations were assigned a field lifetime equal to the time from their installation to the date when cracked insulations were found in pedestals.

These field samples ("as excavated" and preconditioned) were analyzed for stabilizers and subjected to OIT, pedestal and oven tests.

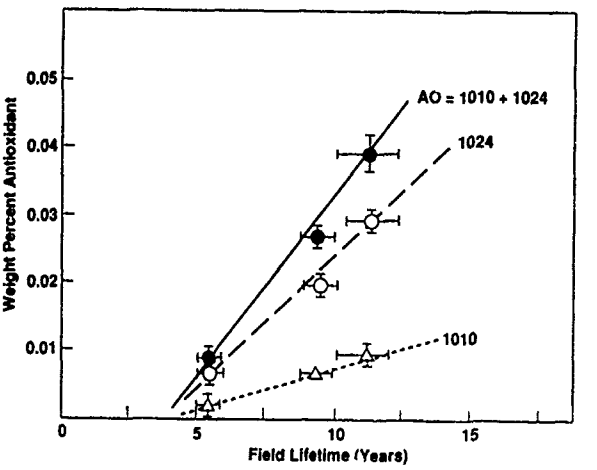

Fig. 12 Weight percent stabilizer versus Field Lifetime

Correlations between field lifetimes and test lifetimes as well as insulation composition were evaluated using linear least square analysis (LLSA). As shown in Table 2, the correlation coefficients for the LLSA fits were typically 0.9 or better except for the t_0(110°C ped.) values from preconditioned samples. Examples of the correlations are shown in Figs. 12-14 where wt% stabilizer, OIT value and t_0(110°C,pedestal) are plotted versus field lifetime. The required test lifetimes and insulation compositions to ensure a forty year field lifetime can be calculated by linear extrapolations from such plots.

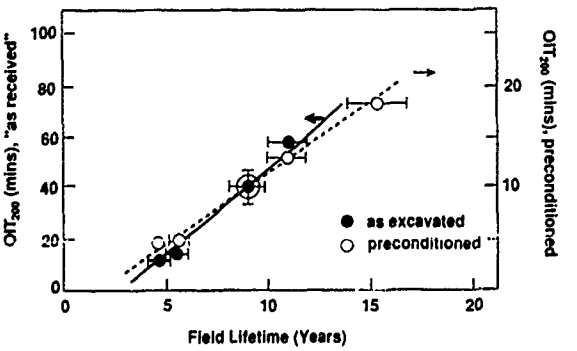

Fig. 13 OIT value versus field lifetime

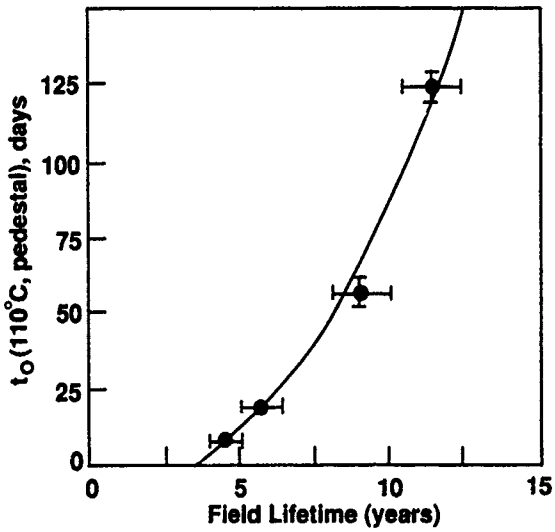

Fig. 14 t_0(110°C,pedestal) versus field lifetime

For a foam-skin HDPE PIC insulation to have a minimum lifetime of 40 years in an aboveground pedestal in the hot southwest of USA, these correlations implied that an insulation needs an OIT value of 270 mins as manufactured ("as received") and 48 mins after preconditioning. To achieve such OIT values, "as received" insulations should contain at least ~0.25% of Irganox 1010 and ~0.28 wt% of Irganox 1024. Table 3 lists the predicted test lifetimes for this insulation that will survive a minimum of 40 years in the field. Included in Table 3 are test lifetimes as extrapolated from the Arrhenius relationships .

The appropriate test conditions for ensuring a 40 year lifetime depends on the interpretation of preconditioning. Preconditioning at 70°C for 4 weeks did shorten the test time but was introduced primarily to (a) simulate storage in outside reel yards in hot climates and (b) ensure stabilizer retention at elevated field conditions. If preconditioning was viewed solely as a means to shorten test time, then the required t_0(90°C, pedestal) time should be ~350 days/2.5 = ~140 days for a preconditioned test sample. The factor of 2.5 was found earlier to be the average effect of preconditioning on test lifetime. However, if preconditioning accurately simulated field conditions, then the required t_0(90°C, pedestal) would be ~350 days for a preconditioned sample. Temperature measurements in reel yards[29] and t_0(90°C,pedestal) values of preconditioned field samples implied that the latter was true and preconditioning simulates field conditions.

A pedestal test on preconditioned PIC insulations at 90°C for 350 days or 110°C for 80 days simulates forty years in the worst field conditions expected in the USA. Such field conditions could be PIC insulations stored and used in hot climate like Arizona. Such a worst case scenario would include storage for ~1 year in a cable reel yard and then installation inside an aboveground metal closure in full sun exposure with the wire pair twisted together.

SUMMARY

We have reviewed the thermal stability tests for polyolefin insulations and shown that a combination of OIT tests and long term pedestal testing is the most reliable method for selecting insulations for outside plant applications. The pedestal test is reproducible and simulates field conditions. For a specific stabilizer

Table 3. Laboratory Test Times to simulate 40 years in field

Laboratory Tests	Laboratory Test Time predicted from		
	Linear extrapolations		Arrhenius Relationship
	as received	preconditioned	
t_0 (110°C,ped.)	500-600 days	90 days	80-100 days
t_0 (90°C,ped.)	1000-1200 days	200-250 days	350 days
OIT (200°C)	270 mins	48 mins	-

system, the OIT test is a short reliable test that can be used for quality control. Quantitative understanding of the effects of airflow on PIC insulations is required before the oven test can achieve interlaboratory reproducibility and be used as a product requirement test.

Insulations gathered from the field were used to calibrate the laboratory test methods and test criteria were established to ensure a 40 year minimum lifetime for insulations under field conditions.

ACKNOWLEDGEMENTS The authors wish to gratefully acknowledge the work of D. Baker, in particular, and many other scientists at AT&T, Canada Wire, Contel, Essex, General Cable, GTE, Northern Telecom and Superior Cable who participated in the TWCSTAC sponsored round robin studies. We thank the TWCSTAC committee and its chairperson, C. David Whitley, for permission to use the results in this study. P.C. Warren and E.P. Hjorth are thanked for their valuable comments and discussions on this manuscript.

REFERENCES

1. B. Havens, Outside Plant, 19 (Jan/Feb 1988)
2. T.N.Bowmer, Proceed. 37th Int. Wire & Cable Symp., p475 (1988)
3. T.N. Bowmer, E.P. Hjorth, R.J. Miner and O.S. Gebizlioglu, Proceed. 37th Int. Wire & Cable Symp. p490 (1988)
4. G.D.Brown, Procced. 36th Int. Wire Cable Symp.,p337 (1987)
5. L.E.Davis, Proceed. 36th Int. Wire Cable Symp., p475 (1987)
6. G.D.Brown and L.E.Davis, Proceed. 36th Int. Wire Cable Symp., p734 (1987)
7. K.D. Dye, V.J. Kuck, F.C. Schilling, M.G. Chan and L.D. Loan, Proceed. 38th Int. Wire & Cable Symp. p98 (1989)
8. L.P. Beltz, Procced. 38th Int. Wire & Cable Symp. p123 (1989)
9. J.Howard, Proceed. 21st Int. Wire & Cable Symp. p329 (1972)
10. H.Gilroy, Proceed. 23rd Int. Wire & Cable Symp. p42 (1974)
11. W.L. Hawkins, "Polymer Degradation and Stabilization", Springer-Verlag, Berlin (1984)
12. W.L. Hawkins, M.G. Chan and G.L. Link; Polym. Eng. Sci., **11(5)** ,377 (1971)
13. M.G. Chan, H.M. Gilroy, J. Johnson and W.M. Martin; Proceed. 27th Int. Wire & Cable Symp. p99 (1978)
14. B.L. Board and H.J. Ruddell, Proceed. 31st Int. Wire & Cable Symp. p300 (1982)
15. H.J. Ruddell, D.J. Adams, P. Latoszynski and B.T. de Boer, Proceed. 32nd Int. Wire & Cable Symp. p104 (1983)
16. L.D.Loan, Proceed. Golden Jubilee Conference on Polyethylenes 1933-83 (June 1983) London.
17. B.D.Gesner, J.W.Shea and F.R.Wight, Proceed. 22nd Wire Cable Symp. p7 (1973)
18. Bellcore Technical Requirements - TR-TSY-000421 - "Generic Requirements for Metallic Telecommunications Cable" Issue 2, Revision 1 (March 1989)
19. T.N. Bowmer, P.C. Warren and E.E. Hershkowitz; Plastics and Rubber Processing and Applications, in press (1990)
20. G.A.Schmidt, Proceed. 22nd Int. Wire Cable Symp., p11 (1973)
21. G.A.Schmidt, Proceed. 26th Int. Wire Cable Symp., p161 (1977)
22. ASTM D-3895, "Oxidative Induction Time of Polyolefins by Thermal Analysis" American Society for Testing and Materials, (Philadelphia) p335 (1986)
23. J. Fech and A. DeWitt, Proceed. 29th Int. Wire & Cable Symp. p327 (1980)
24. Ciba-Geigy Analytical Method No. C-219, "Determination of Irganox 1010 and Irganox 1024 in Polyethylene by Liquid Chromatography" Ciba-Geigy Corp. Ardsley N.Y. (1984)
25. Ciba-Geigy Corp., MSDS Document for Irganox 1010 (1986)
26. N.C. Billingham, "Oxidation Inhibition in Organic Materials" Vol. II (Eds. J. Pospisil & P.P. Klemchuk) p249 (1990)
27. L.M. Hore and E.E. Hershkowitz, Proceed. 39th Int. Wire & Cable Symp. in press (1990)
28. M. Blumberg, C.R. Boss and J.C.W. Chien; J. Appl. Polym. Sci., **9**, 3837 (1965)
29. T.N. Bowmer, R.J. Miner and R.C. Coker, Proceed. 39th Int. Wire & Cable. in press (1990)

Trevor Bowmer is a member of the Polymer Chemistry and Engineering Research Group in Bellcore. He received his Ph.D. in chemistry from the University of Queensland, Australia, where he studied radiation chemistry of polymers. Joining Bell laboratories in 1980, he investigated radiation cured systems and lithographic materials. In 1984, he came to his present position where his interests include degradation mechanisms and characterization of polymeric materials used in telecommunications applications.

Joe D'Amico has worked on engineering and material issues affecting all types of telecommunications and power cables in his 25 year career. He first worked with communications cable in Western Electric before joining General Cable Company in 1968 where as senior research physicist, he contibuted to the design and manufacture of all types of telecommunications wire, cable and optical fiber as well as electrical power cables. Since 1985, he has worked at Bellcore as a Quality Assurance Engineer and most recently as a member of Technical Staff in the Polymer Chemistry and Engineering Research District.

Russell J. Miner was a Member of the Technical Staff at Bellcore until his retirement in 1989. Before that, he was with Bell Telephone Laboratories from 1961 and worked in the Plastics Development and Applied Research Department. He studied the effects of soil burial, electron irradiation, outdoor aging, heat and fire on the plastics materials used by telecommunications companies.

Irene Plitz is a Member of Technical Staff in the Polymer Chemistry and Engineering Research District of Bellcore, Inc. She received her B.Sc. in Chemistry from Morgan State University in 1970 and then directly joined Bell Laboratories. Since transferring to Bellcore in 1984, her interests have centered on the chemical and structural analysis of organic materials.

Lal Hore is responsible for the preparation of Bellcore's Technical Requirements for Outside Plant Cables and the development of high speed transmission requirements for wire products. After receiving a M.Sc. (Applied Physics) from the University of Calcutta and a Dr. Tech. degree from the Technical University of Budapest in Electrical Engineering, he joined Bell Northern Research in 1970 to design and develop communications cables. In 1972, Lal moved to General Cable Company where he worked as a manager in the Communications Cable Section and then in the Applications Engineering Section until 1987 when he joined Bellcore.

SECONDARY PARAMETERS THAT CONTRIBUTE TO PIC CRACKING

K. DAWES, * T. A. HUNTER, * C. M. CHAN **

* Raychem Corp., P. O. Box 3000, Fuquay-Varina, NC 27526
** Raychem Corp., 300 Constitution Dr., Menlo Park, CA 94025

ABSTRACT

Several parameters that can dramatically enhance the degradation process of PE and thereby the cracking of the insulation have been identified. Certain parameters have been found which contribute significantly to impaired lifetime of the telephone wire insulation. The effect of humidity as shown by the reduction in oxidation induction time (O.I.T.) is described. This effect is only dominant on foam-skin insulation and to date no mechanistic explanation is in existence. The other area to be discussed is the effect of other secondary materials around a telephone splice. Notably the presence of polymeric materials that release volatile materials during the aging process. An example would be a poorly stabilized PVC which on decomposition can release hydrogen chloride. Hydrogen chloride will dramatically reduce the oxidative stability of PE and PP wire insulation whether it is solid or foam-skin. The importance of copper in catalyzing this reaction and a mechanism is discussed.

INTRODUCTION

Polyolefin insulated conductors (PIC) have become commonplace since the 1950's. However, over the last two decades PIC cable insulations have been a subject of concern[1] due to the fact that the lifetime expectancy of these insulations has not lived up to expectations in several geographical locations.

Several changes have occurred over the last two decades in the development of PIC cables including changing from low density polyethylene (LDPE) to high density polyethylene (HDPE) and several changes in the antioxidant package within the insulation.[2] The current incumbent insulation used in the U.S.A. is HDPE with an antioxidant package consisting of Irganox 1010 and together with a metal deactivator.[3] HDPE is used in both air core and water resistant PIC cables. The current water-resistant PIC cable used for buried applications was first introduced in 1976 and comprises of a foam-skin design, the cables are filled with a water resistant material such as petroleum jelly or Flexgel® [4] material.

A recent report [5] has concluded that the foam-skin PIC cables are susceptible to thermal oxidation and cracking after less than a decade in the field. The study was based on the measurement of the oxidation induction time (O.I.T.) for the PIC cables from pedestals in the South, Southwest and Mid West U.S.A. It found a relatively large percentage of insulations from HDPE foam-skin to have O.I.T. values of less than 2 minutes, especially in the Southwest. The study also clearly showed that the low O.I.T. or cracking problems are only prevalent at the access point, i.e. within the pedestals. Analysis of the PIC from a sample of buried cable showed that relatively high O.I.T. values are retained.

Many factors, such as temperature, stress, and UV are known to affect degradation [1,2] . We will discuss in this presentation our findings of an investigation to look at other factors that effect the depletion of stabilizers in PIC cables. In the study we have used the O.I.T. as a measurement of depletion of stabilizers. Although O.I.T. values are not recognized as reliable life predictors, accelerated aging tests have shown that if an insulation has a low O.I.T. it is more prone to cracking. [5]

EXPERIMENTAL

Oxidation Induction Times

Insulations were stripped from their copper conductor, and a sample (~ 9 mg) placed in an aluminum DSC pan. The pan was placed in a Dupont 910 thermal analyzer. After heating to 200°C in nitrogen the atmosphere is switched to oxygen. The time between introduction of oxygen and the onset of an exothermic reaction is the O.I.T. value in minutes.

RESULTS

Humidity

Samples of both solid and foam-skin PIC cables were evaluated using an accelerated test method at 60 and 90° C. Samples of the insulation were suspended in a sealed 8 oz. bottle (Figure 1), samples of water, inorganic salt solution or dessicant were placed in the bottom of the bottle to generate various relative humidities.

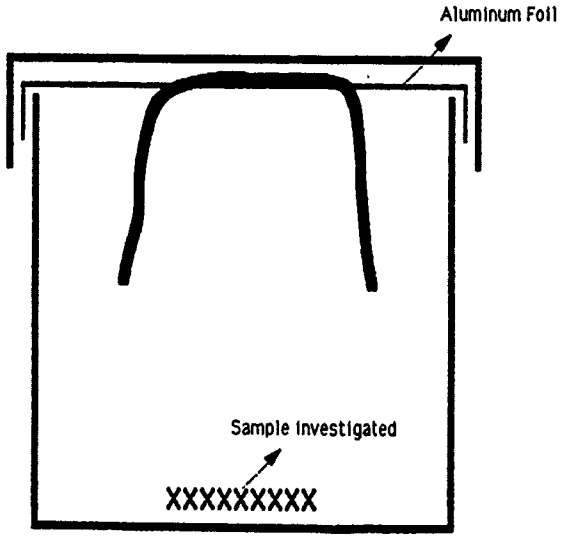

FIGURE 1
Sealed Bottle Experiment Set-up

The results show that there is virtually no effect of humidity on the O.I.T. of solid HDPE, (Table I). In the case of foam-skin HDPE the reduction in O.I.T., when compared to a dry sample, is dramatic even at the relatively low temperature of 60°C (Table II). After 6 weeks at 60°C, in approximately 90% relative humidity, the O.I.T. value for foam-skin PIC has dropped to 25% of its original value. At 90°C the effect is larger but is accompanied by the oxidative effect since the dry sample lost approximately 30% of its original value.

TABLE I

Effect of Humidity on Solid HDPE Insulation

Sample	O.I.T. after 8 weeks at 90°C (Min)
Control (Dry)	122
Humidity (Water)	125

Initial O.I.T. of sample 150 ± 7 minutes @ 200°C

TABLE II

Effect of Humidity on Foam-skin HDPE Insulation

Relative Humidity (%)	O.I.T. value after 6 weeks at 60°C (min)	O.I.T. value after 6 weeks at 90°C (min)
Dry	48	32
48	23	14
90	12	4

Initial O.I.T. 46 ± 5 minutes @ 200°C

Other experiments have been carried out to further show the effect of humidity. The results of the first experiment are shown in Figure 2. In this case a sample of cable that had been preaged and opened to give a splice situation was subjected to aging at 70°C and 95% relative humidity for up to 6 weeks, after which time period only 50% of the original O.I.T. remained. In the other sample the cable splice was used with a sealed closure PEDCAP GT®, in which dessicant was present. In the latter case 70% of the original O.I.T. is maintained. Neither samples were cleaned of filling compound.

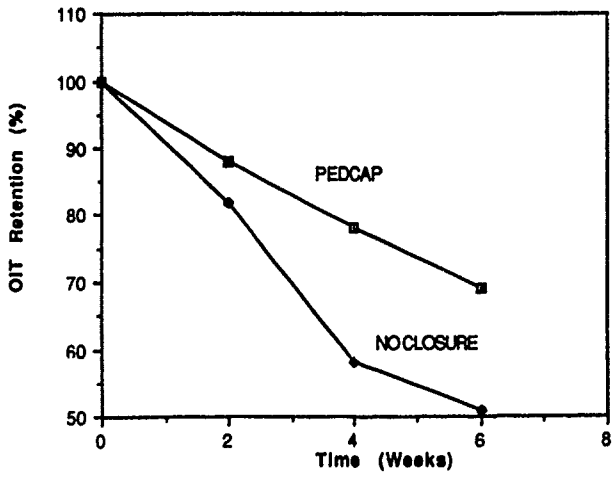

FIGURE 2

Plot of OIT Retention for Samples of Splices Aged at 70°C and 95% Relative Humidity

In a second experiment samples of splices made from a preaged cable (4 weeks at 60°C and 2 weeks at 80°, O.I.T. 21 ± 3 minutes white wire in green-white pair, blue binder) were placed in a test site in Arizona and covered with PEDCAP® heat shrinkable sealed closures inside a metal pedestal closure. One sample contained the normal addition of a dessicant bag, in a second sample the bag was removed and replaced with a moist sponge thereby generating a humid atmosphere within the closure. After 11 months of exposure in Arizona the closures were re-entered (the sponge was still moist) and the O.I.T. values for the control wire were measured. The closure containing the dessicant had maintained 77% of the original O.I.T. whereas the closure containing the wet sponge maintained only 33%. Interestingly, a sample which had no closure on the splice had maintained less than 5% of the original O.I.T. value.

Using the experimental set up shown in Figure 1 the effects of materials other than water have been evaluated. Samples of other materials were placed in the bottom of the sealed bottles and aged at 90°C, in no case was there any contact between the sample and the insulation under evaluation. A sample of an unstable grade of polyvinylchloride (PVC) when placed in the bottom of the bottle and aged for 6 weeks at 90°C showed a dramatic reduction in the O.I.T. of a sample of solid HDPE, the sample retained only 13% of its original O.I.T. whereas a sample with no unstable PVC retained 70% of its original O.I.T.

This discovery led us evaluate a range of different PVC materials relating to the outside plant applications and Table III shows the results of bottle experiments at 90°C on both solid and foam-skin. All these grades of PVC were taken from products commonly used in the outside plant.

The effect of some other materials are shown insulations in Table IV. Polyethylene shows little or no effect, whereas a silicone RTV system and a sample of a Neoprene foam shows significant reduction in O.I.T. The results shown in Table III and IV lead us to believe that acid outgassing was occurring, thereby leading to stabilizer depletion. The experiment above with the unstable grade of PVC in the sealed bottle was repeated but an acid scavenger was added, in this case the O.I.T. of the insulation under evaluation was identical to that of a control sample.

TABLE III

Seal Bottle Experiments with PVC Samples

Sample	Solid HDPE [1] O.I.T. (Min) After x weeks at 90°C			Foam-skin HDPE [2] O.I.T. (Min) After 2 weeks at 90°C
	8 Wks	16 Wks	26 Wks	
Control	124	107	111	9.9
PVC (1)	34	1	1	6.4
PVC (2)	24	1	1	2.6
PVC (3)	38	1	1	-
PVC (4)	90	60	1	-
PVC (5)	74	47	15	-
PVC (6)	114	97	100	-

1. Initial O.I.T. 150 ± 7 min.
2. Initial O.I.T. 14 ± 0.5 min.

TABLE IV

Sealed Bottle Experiments to Evaluate Solid HDPE Insulation [1] With Other Materials

Sample	O.I.T. After 5 Weeks at 90°C (Min)
Control	131
PE Insulation	120
Silicone RTV	40
Neoprene Foam	15

1. Initial O.I.T. 150 ± 7 min. @ 200°C

The results described so far were from experiments where there was no contact of the sample with the HDPE insulation sample and therefore we were dealing only with volatile materials which were outgassed from the sample being investigated. In the next series of experiments, the material under evaluation was in contact with HDPE insulation. The experiment was as follows: two sets of white solid HDPE insulations were prepared, one set was aged at 80°C and the other at 120°C in a sealed glass tube. The sets comprised of normal insulation (solid HDPE), insulation with the copper conductor removed and samples wrapped with a clear PVC tape. The results are shown in Table V and VI for temperature 120°C and 80°C, respectively. At 120°C there is a dramatic reduction in O.I.T. when either the PVC alone or PVC and copper are present, whereas at 80°C the rapid reduction of O.I.T. only occurred when both PVC and copper were present. At both temperatures, when both PVC and copper were present a yellow powder developed at the copper/insulation interface, the infrared spectrum of this is shown in comparison to Irganox 1010 in Figure 3. In addition, the copper concentration of the HDPE insulation after aging for 88 hours at 80°C with and without PVC tape was determined to be 322 and 22 ppm, respectively.

TABLE V

O.I.T. Values as a Function of Aging Time at 120°C

Aging Time (hrs)	Control	PVC Only	PVC + Conductor
0	128	-	-
90	127	5	1
268	116	4	1

TABLE VI

O.I.T. Values as a Function of Aging Time at 80°C

Aging Time (hrs)	Control	PVC Only	PVC + Conductor
0	128	-	-
90	115	108	2
268	104	95	1

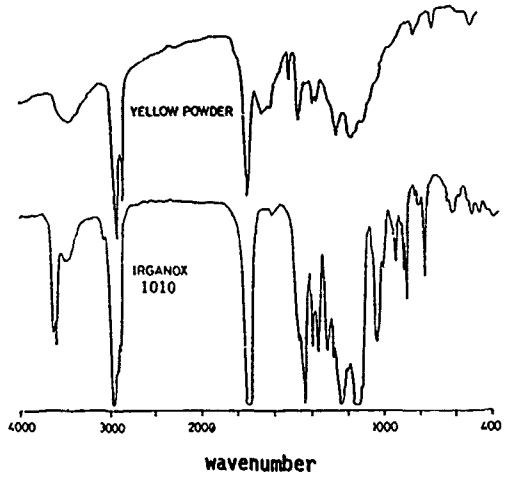

FIGURE 3

IR Spectra of Yellow Solid Detected at Copper/PE Interface

DISCUSSION

The results clearly show the effect of humidity on the oxidative stability of foam-skin PIC cables, in both laboratory and field studies. The reduction in stability only occurs for foam-skin PIC, whereas solid PIC shows no effect. Pusey and co-workers [6] have reported that the oxidative stability of solid PE insulation is in fact enhanced by the presence of moisture and they postulated that the enhancement is a consequence of a reduction in oxygen concentration. Their experiments were similar to the ones reported here since samples of insulation were hung over water in a sealed vessel.

The results, in the presence of humidity, for foam-skin PIC must be related to the loss of stability and thereby antioxidant depletion as shown by a dramatic reduction in O.I.T. The mechanism of this antioxidant depletion is not understood and no explanation can be given at this stage especially since it occurs very rapidly at relatively low temperatures and high relative humidity. The difference between the solid and foam-skin PIC with respect to humidity is presumably due to the cellular structure of the foam-skin design. The cellular structure will give rise to a substantially larger moisture vapor transmission rate when compared to a solid insulation construction. One could speculate on effects such as the leaching out of the antioxidants, (although attempts to detect stabilizers in the water residues proved negative) and possible hydrolysis of the stabilizers.

In this study we have used O.I.T. as a measure for the effect of humidity, Grune and Talarico have reported[7] on the effect of temperature and humidity of foam-skin HDPE using ultimate elongation (as the end-point) to build an Arrhenius model. They predicted only 1.4 years at 45°C and 98% relative humidity, the value for activation of energy was determined to be 2.81 kcal/mole. This value is substantially lower than that reported [8] (23.4 kcal/mole) for a study on the oxidation of HDPE by air oven aging at between 105 and 150°C.

The field studies in Arizona show the benefit of protecting a PIC cable splice with a sealed closure in which a dessicant is present to give a low humidity environment inside the closure. A recent technical memorandum [9] issued by Bellcore reports a substantial difference in the O.I.T. values of open splices versus a PEDCAP® airtight sealed splice in which a dessicant was present; the latter showing significantly higher O.I.T. values. The results may be explained by the action of a very humid environment since the samples that were analyzed came from a site in Mobile, Alabama, and had been in the field for 5 years.

The accelerated aging tests with other materials show that some materials in the vicinity or in contact with PIC cables can have a detrimental effect on the oxidative stability of the HDPE insulation. In this case the effect is seen on both solid and foam-skin insulation and is thereby different from the effect of humidity which is only prevalent on the foam-skin design.

The effect of the PVC in our experiments can be explained in terms of the stability of the PVC. PVC is known to dehydrohalogerate [10] during degradation, with a mechanism that is autocatalytic and generally proceeds at temperatures above the Tg of the composition. The more susceptible that PVC is to degradation then the more dehydrohalogenation that will occur. It is the product from dehydrohalogenation (hydrogen chloride) that penetrates the HDPE insulation and leads to stabilizer depletion. In fact, in a sealed bottle experiment using one drop of concentrated hydrochloric acid an O.I.T. value of 0.5 minutes was reached in 2 days at 90°C. The results in Table III show that care must be taken in using PVC as a generic material since many grades are very well stabilized and do not show a significant effect after 8 weeks at 90°C. A moisture curing silicone RTV also shows an effect in reducing O.I.T. and therefore the attack of acid gases is not limited to hydrogen chloride.

The experiments which were carried out with a poorly stabilized PVC tape in contact with HDPE insulation in the presence and absence of copper indicates that at low temperatures the hydrogen chloride attacks the copper. In the absence of copper, very little reaction is seen at 80°C whereas reaction readily occurs at 120°C. It appears that at 120°C there is a direct attack of hydrogen chloride on the HDPE. Kresta et al [11] have reported the attack of hydrogen chloride, generated from residual Ziegler-Natta catalysts, on antioxidants at very high temperatures for the case of polypropylene, (PP) the effect led to a reduction in stability of the PP after processing.

At the lower temperature of 80°C the hydrogen chloride appears to only attack the insulation in contact with copper. This implies that the acid gas is diffusing through the HDPE insulation and attacking at the copper/PE interface and causing the production of copper salts. Any chemical activity at the copper/PE interface will activate the antioxidants, especially the metal deactivator (Irganox 1024). Evidence of activity can be seen by the presence of the yellow solid at the interface. The infra-red analysis would suggest a complex material, the structure of which is closely related to some phenolic antioxidant as shown by the close similarity to Irganox 1010. Further evidence of the effect of copper can be seen from the order of magnitude increase in copper salt concentration in the insulation after aging at 80°C of solid HDPE in contact with PVC. The copper catalyzed oxidation process for PE insulation is well known [12, 13] and has been extensively studied.

The effect of these materials on the oxidative stability of PIC cable is difficult to assess in an outside plant environment where temperatures of less than 65°C are seen. Direct contact of an unstable PVC on a PIC insulation is probably a worst case situation, so this should be avoided. In the case of an unstable PVC grade or other materials used in the outside plant, care should be taken to evaluate the stability of the materials since acid gas generation will certainly lead to a reduction in oxidative stability of the insulation. We have detected hydrogen chloride from unstable tapes heated at 60°C for several weeks, and there are unpublished reports of corrosion in the outside plant being reported to be due to the presence of PVC materials. The effect is certainly not as dominant as the effect of humidity which can be stated to be a major contributing factor in the case of foam-skin PIC. Other effects on materials such

as UV irradiation have not been investigated but would be expected to contribute to the degradation of a range of materials such as PVC and lead to the generation of acid gases.

Accelerated aging [14, 15] is often used as a means to give some predictability of the lifetime of PIC cables in the field. Caution must certainly be used in these tests to ensure that no detrimental materials are in the vicinity of the samples under evaluation.

CONCLUSION

Several factors have been shown to contribute to the depletion of stabilization PIC cables as demonstrated by a reduction in the oxidation induction time. This reduction will certainly lead to an enhanced degradation process and could lead to premature failure of the cable in the form of embrittlement leading to cracking of the insulation. Humidity has been demonstrated to be a major factor in reducing oxidative stability although the mechanism of depletion is not understood. Other materials that release acid gases on decomposition during heat exposure also reduce the oxidative stability of PIC. A mechanism has been proposed which involved corrosive attack on the copper and then subsequent antioxidant depletion

ACKNOWLEDGMENTS

The authors wish to thank the following people for their contributions to this paper: Rick Powell and Rod Morton; and to Theresa Elliott for her help in preparing this manuscript.

REFERENCES

1. J. B. Howard, Proceedings of the 21st Int'l Wire & Cable Symp., 329 (1972)
2. H. M. Gilroy, Proceedings of the 23rd Int'l Wire & Cable Symp., 42 (1974)
3. M. G. Chan, Proceedings of the 23rd Int'l Wire & Cable Symp., 34 (1974)
4. D. M. Mitchell & R. Sabria, Proceedings of the 19th Int'l Wire & Cable Symp., 15, (1980)
5. T.N. Bowner, Proceedings of the 37th Int'l Wire & Cable Symp., 475, (1988)
6. B. B. Pusey, M. T. Chen, and W. L. Roberts, Proceedings of the 23rd Int'l Wire & Cable Symp., 209, (1971)
7. G. L. Grune and T. L. Talarico, Proceedings of the 34th Int'l Wire & Cable Symp., 187, (1985)
8. B. S. Bernstein and P. N. Lee, Proceedings of the 23rd Int'l Wire & Cable Symp., 202 (1974)
9. T. H. Bowner, Bellcore Technical Memorandum, TM-ARH-016639, (1990)
10. D. E. Winkler, J. Poly. Sci., 35, 3, (1959)
11. J. Kresta and J. Majer, J. Applied Poly. Sci., 13, 1859 (1969)
12. R. H. Hansen, C. A. Russell, T. DeBenedictis, W. M. Martin and J. V. Pascale, J. Polym. Sci. Part. A, 2 587 (1964)
13. L. Reich and S. Stivales "Autoxidation of Hydrocarbons and Polyolefins", 1969, Dekker, New York
14. L. E. Davies, Proceedings of the 37th Int'l Wire & Cable Symp., 484 (1988)
15. T. N. Bowner, E. P. Hjorth, R. J. Miner and O. S. Gebizlioglu, Proceedings of the 37th Int'l Wire & Cable Symp., 490 (1988)

Keith Dawes received First Class Honours B. S. Degree in Chemistry from University of Newcastle-upon-Tyne in 1966 and obtained his Ph.D from the University of Manchester in 1969. After post-doctoral fellowships at Columbia University and Oxford University, he worked at the Malaysian Rubber Producers Research Association. He joined Raychem Corporation in 1979 working in Corporate R&D at Swindon, England. He is now Development Manager for Raychem Telecommunications Division in North Carolina.

Chi-Ming Chan obtained his Ph.D in Chemical Engineering from California Institute of Technology. Currently, he is a Senior Staff Scientist in the Material Science and Characterization Department, Raychem Corporation. His current research interest includes surface analyses, surface structure and morphology studies, modification of polymer surface for adhesion and adhesion phenomena. He has published over twenty papers on this topic and has co-authored a book on Low Energy Electron Diffraction.

Thomas Hunter was employed for 5 years as a Product Development Engineer with the Telecommunications Division of Raychem Corporation, during which time he completed several research projects and received 4 U.S. patents. He received a B.S. Degree in Chemical Engineering at Lehigh University. After leaving Raychem to further his education, he performed plastics marketing research in a summer internship with Union Carbide. He is presently completing his Master of Business Administration in Marketing at Vanderbilt University and is expected to graduate in May 1991.

FIELD TEMPERATURES IN OUTSIDE PLANT

T.N. Bowmer and R.J. Miner
Bellcore
Red Bank, New Jersey 07701

&

R.C. Coker
U S WEST COMMUNICATIONS
Phoenix, Arizona 85012

ABSTRACT

Temperatures found in outside plant closures and reel yards have been measured as a function of time-of-day, plant design and local climate. The time-temperature profiles were explained in terms of local climate and heat flow characteristics of the various closure designs. The high temperatures found inside aboveground closures (140-150+°F) and in the reel yard (175°F) were particularly alarming since future networks will include widespread installation of remote switch electronics and optical fiber in these outside environments. Temperature profiles for both pedestals and cross-connect boxes were understood as a competition between solar heating and heat dissipation to the ground and air. Internal electronics and solar radiation were of equal importance in heating SLC cabinets to peak temperatures of 140+°F.

INTRODUCTION

Aboveground metallic and plastic closures are used to access buried plant and provide protection from the environment. The recent cracking of polyethylene insulations inside such closures[1] has highlighted the increased thermal degradation produced by solar heating of the closures. High temperature in outside plant is a major concern as modern switch technology expands out of the central office towards the home. For instance, integrated circuit packs are used in SLC (Subscriber Loop Carrier) cabinets and battery operated electronics located on the outside of houses are being contemplated. The electronics and batteries are well known to be sensitive to high temperatures, humidity and dust which are all present in the outside plant[2].

In 1971, temperatures inside B-type pedestals were reported to reach 125-130°F in hot climates like Phoenix, Arizona[3,4]. Since plant closure designs and practices have changed significantly since 1971, the temperatures reached inside such closures need to be reviewed. Previous studies on the solar heating of cabinets have not included field data from installed operating plant[5,6]. This memorandum reports temperatures measured in aboveground closures in New Jersey and Arizona during the summer. New Jersey represents a low risk area and Arizona represents a high risk area for thermally-initiated degradation processes. Temperatures were measured in pedestals, cross-connect cabinets and SLC cabinets as a function of time and position. In addition, temperatures of various cables (copper and fiber) stored in an outside reel yard are reported.

EXPERIMENTAL

Three standard PC 6/48 pedestals (6x6x48 inch), two typical cross-connect cabinets (6x4x2 feet) and two SLC remote switch cabinets (6x4x2 feet) were examined and the individual sites are listed in Table 1. These closures are representative of the aboveground closures currently used by most telecommunication companies in their outside plant.

AMEC Thermologgers Model TL-10 were used to measure and record temperatures at ten individual positions at each site. The unit operated for up to 2 days using 6V batteries recording the temperatures every 20-60 minutes. Chromel-Alumel solid wire thermocouples (24 AWG) were positioned inside and outside the closures. Outside locations included (a) in the air adjacent to the closure, (b) under bushes near to closure, (c) buried 1-2 inches in ground and (d) taped to the outside of the closure. Typical thermocouple locations at closure sites were

- taped to top of closure
- inside wire bundles or to splices (i.e., wireworks)
- in air at top, middle or bottom of closure
- with wire bundle inside sheathed cable at cable entry point
- taped to terminal plate in pedestals
- inside splice chambers in cabinets
- taped to cross-connect blocks in cabinets (top or bottom)

TABLE 1. SITE LOCATION

SITE	LOCATION	PLANT TYPE	COMMENTS
#1	Lincroft New Jersey	Pedestal PC 6/48	Pedestal faces west Wooded suburbia
#2	Via Villa, Phoenix Arizona	Pedestal PC 6/48	Pedestal faces south full sun exposure
#3	42nd/Dynamite, Phoenix,Arizona	Pedestal PC 6/48	Pedestal faces west Full sun exposure rural - open desert
#4	1022 N. Central, Phoenix, Az.	Cross-Connect Cabinet Type-40 cabinet set on concrete slab	Cabinet opens east-west Full sun exposure rural - open desert
#5	N. 52nd Phoenix, Az.	Cross-Connect Cabinet Type-80 cabinet SLC Cabinet Type-80D 6 fans	Cabinet opens north-south Cabinet opens north-south
#6	Desert Cove, Phoenix, Az.	SLC Cabinet Type-40 cabinet set on concrete slab 2 fans using outside air	Cabinet opens east-west Full sun exposure
#7	38th Ave., Phoenix, Az.	Reel Yard	Asphalt surface Open lot - full sun

- inside SLC electronics (i.e., air gaps between channel banks)
- inside fiber splice compartment in SLC cabinets

A two channel Fluke model 52 K/L thermometer was used for short term measurements (2-10 minutes) in the cable reel yard and reference measurements at closure sites. In addition, maximum temperatures were recorded using non-reversible temperature labels from Omega Engineering. The labels provided calibration checks for the other meters as well as long term data (more than one week) from the survey sites.

RESULTS AND DISCUSSIONS

Pedestals

Buried cables are typically placed ~30 inches deep and brought above ground for splicing, terminations and/or connections. These access points are protected inside metal pedestals that are typically 4-10 inches square and 24-48 inches high. The cable enters the bottom of the pedestal (18-24 inches below ground) and is brought up into the top half of the pedestal where the cable sheath is removed and the exposed insulated wires are spliced or terminated.

Figures 1-3 show the time-temperature profiles for the pedestal locations studied. Temperatures inside the pedestals can reach 25°F higher than the surrounding air because of solar heating of the metal pedestal. Temperature extremes and other characteristics of the time-temperature profiles are listed in Tables 2-3. Maximum temperatures of 125-130°F (~50°C) were reached inside pedestals when the outside air temperatures reached ~100°F. A 1971 study[3,4] of B-type pedestals reported similar maximum temperatures of 125-130°F for air temperatures of 100-105°F; i.e., a difference of 20-25°F.

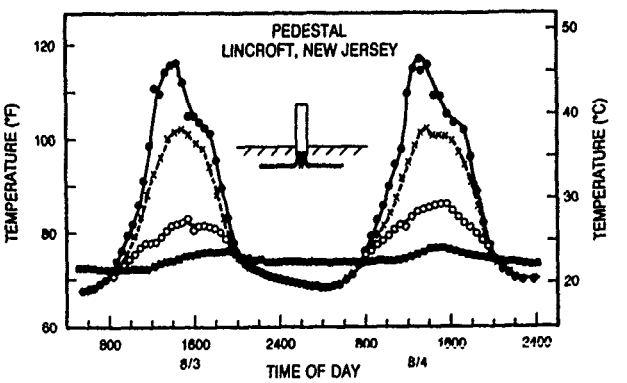

Fig. 1 Time-temperature profiles for site #1

- ● Top of pedestal - inside metal surface
- x Wireworks - middle of pedestal
- ■ Below ground level - bottom of pedestal
- o Outside air temperature

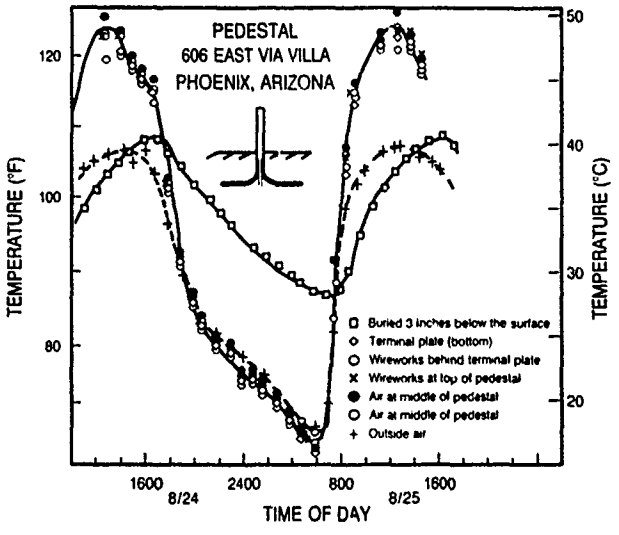

Fig. 2 Time-temperature profiles for site #2

Site #1 was a pedestal in suburban New Jersey with plentiful shade in the morning and late afternoon. The air temperature varied from ~70°F (4-6 am) to 90+°F (3-4 pm). The temperature of the inside top surface of the pedestal peaked at 120°F, the metal terminal plate at 105-110°F, and the wireworks at 100-105°F. The cable situated in the lower part of the pedestal is below ground level and therefore not affected by the solar radiation. In addition, the ground acted as an insulator and caused temperatures below ground level to be lower than air temperature during the heat of the day and ~5°F warmer at night. At night, the earth radiated the heat absorbed during the day into the bottom section of the pedestal.

Pedestals at sites #2 and #3 in Arizona were the same PC 6/48 design as used at site #1 in New Jersey. On the days we measured temperatures, the peak air temperatures in Phoenix, Arizona was 100-105°F compared to the 85-90°F in New Jersey. In addition, the ground temperature in Arizona was up to 25-30°F warmer than that measured in New Jersey. The observed differences in pedestal temperatures between sites #2,3 and #1 arose from the desert-like climate and flat, treeless terrain in the Phoenix area. While the time-temperature profile for site #1 was roughly gaussian, the profiles for the pedestals in Arizona were square-shaped with a rapid temperature increase at sunrise and a corresponding rapid

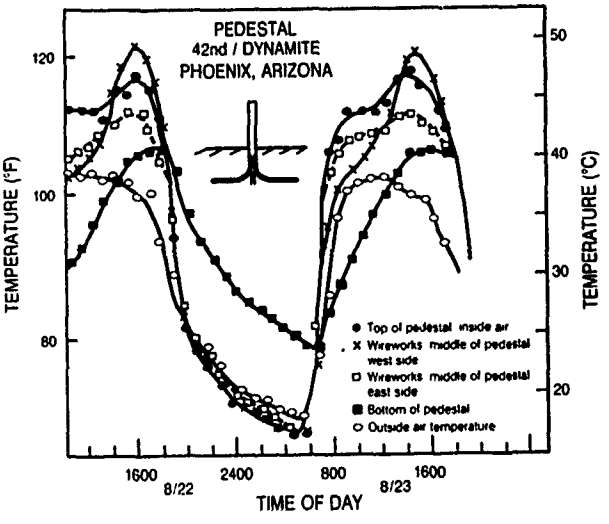

Fig. 3 Time-temperature profiles for site #3

TABLE 2. TEMPERATURE EXTREMES

SITE	T_{min} (°F) air	T_{min} (°F) wires	T_{max} (°F) air	T_{max} (°F) wires	$T_{wires} - T_{air}$ min °F	$T_{wires} - T_{air}$ max °F, (°C)
#1 Pedestal						
(a)	65	65	80-35	105	0	20-25, (10-12)
(b)			90-95	116	0	21-26, (10-12)
#2 Pedestal	64	64	105	125	0	18-20, (10)
#3 Pedestal	68	66	102	122	-3	18-20, (9-11)
#4 Cross-Connect Cabinet	62	66	108	115-120	0-1	10-15, (5-7)
#5 Cross Connect Cabinet	75	72	102	120-125	-3	18-23, (9-12)
SLC Cabinet	75	96	102	134-138	20-22	30-35, (15-18)
#6 SLC Cabinet						
(c)			105-110	155-160	--	45-50, (25-28)
(d)			102-104	150	--	45, (25)

TABLE 3. TIME-TEMPERATURE PROFILES

SITE	CHARACTERISTICS AT WIREWORKS			
	T_{max} (°F)	Time that wireworks were within 10°F of T_{max} (hours)	above 90°F (hours)	Width at half height (hours)
#1	105	3-4	8-9	9
#2	125	6	12	12
#3	122	6	12-13	12-13
#4	115-120	5-6	12	13
#5				
Cross-Box	120-125	6-7	11-12	11
SLC-Box	134-138	6	24	11-12

decrease at sunset. The pedestals in Arizona experienced higher absolute temperatures and remained at these maximum temperatures twice as long as the pedestal in New Jersey.

At site #2, the temperature was uniform in the top half of the pedestal; i.e., the same time-temperature profile was found for the air, the wireworks and the terminal plate, see Fig. 2. In contrast, temperatures in the pedestal at site #3 showed an asymmetry between the east and west sides of the pedestal (Fig. 3). The east side was warmer in the morning and the west side was warmer in the afternoon. The pedestals in Arizona are usually on flat ground with few trees and experience full sun exposure with minimal cloud cover. The different temperature profiles were assumed to arise from the orientation of the two pedestals; site #2 faced south and site #3 faced west. At site #2 the terminal plate conducted heat from the exposed side to the shaded side of the pedestal and rapidly brought the whole aboveground section of the pedestal into thermal equilibrium. Since the terminal plate at site #3 connected the north and south sides of the pedestal, thermal equilibrium within the pedestal was not reached and the temperature distribution inside the pedestal tracked the sun's position.

There are three general conclusions from the measurements in pedestals (sites #1-3):

- In full sun exposure, the maximum temperature difference between the air temperature and the wireworks inside a pedestal was ~20-25°F (10-15°C).
- The shape of the daily time-temperature profile was determined by the local geography. For example, the profile was square-shaped for open desert environments and gaussian for shady suburbia.
- The temperature profile inside the pedestal showed only minor variation presumably because of efficient thermal conduction through the metal terminal plate smoothed out any steep thermal gradients.

Cross-connect Cabinets

Cross-connect cabinets (also known as Feeder Distribution Interfaces, FDIs) are network distribution points and are typically 6x4x2 feet metal boxes containing as many as a thousand cross-connections and cable splices junctions. The cable splices are made inside a central chamber (6x4x1 ft) of the cabinet. Buried cables enter these chambers and splices are made and arranged in six compartments. The cross-connections are made through terminal blocks that are mounted on the outer 6x4 foot walls of this section. The cabinet at site #4 was mounted on a concrete slab at ground level (type 40 cabinet). The second cabinet (site #5) was raised 12-18 inches off the ground by two legs through which the cables entered (type 80 cabinet).

The time-temperature profiles for the two cross-connect boxes examined in Arizona are shown in Figs. 4 and 5. Similar to the pedestal at site #3, the time-temperature profiles for site #4 showed an asymmetry with the east side warmer in the morning and the west side warmer in the afternoon. The metal frames inside the cabinet at site #4 were oriented north-south and

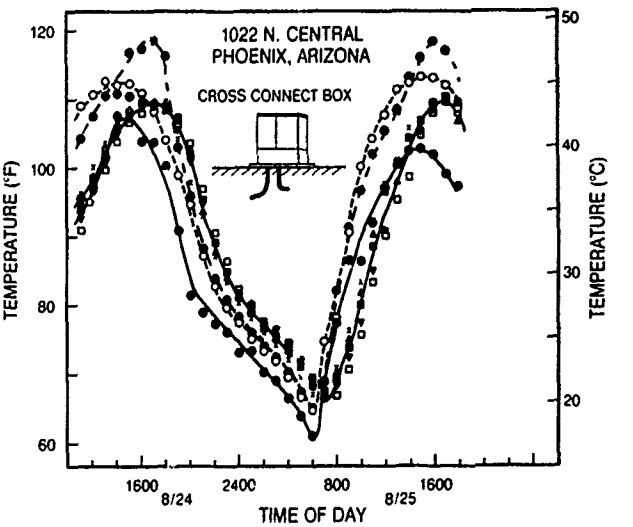

Fig. 4 Time-temperature profiles for site #4 cross-connect box

therefore heat conduction from east-to-west side was inefficient.

The temperature of the wireworks inside the splicing chamber was uniform and peaked at 5-10°F higher than the air temperature. The maximum temperature at the cable entry point at the bottom of the splice chamber was 105-108°F, only 2-5°F warmer than the outside air. There is a 2-4 hour delay between the peak temperature of the outside air (105-7°F) and the peak temperature of the wireworks in the splice chamber (110°F). This thermal lag is the characteristic time for the solar heating of the cabinet components including the outer steel doors, connection blocks, inner steel doors and copper wires. The more material between the plant and the sun, the longer the thermal lag was and the lower was the peak temperature. The thermal mass of the cabinet acted as a insulator for the components inside. The peak temperatures inside this cabinet were equal to the peak temperatures found in the pedestal at site #2 that was within 0.5 miles of this cabinet location. These similarities in peak temperatures and time-temperature profiles imply that pedestals and cross-connect cabinets are equivalent as absorbers of solar radiation.

The second cross connect cabinet (site #5) is oriented east-west, opens to the north or south, is set 12-18 inches off the ground and is not exposed to the windy conditions found at site #4. We measured temperatures at the top and bottom of the terminal blocks as well as in the wire duct at the middle of the blocks. The air temperatures varied from 102°F to 75°F. At the hottest part of the day, a linear temperature gradient was established with the top of the cabinet at ~125°F and the bottom at ~115°F. The hot air rose and concentrated at the top of the cabinet. At night the gradient disappeared and the temperature inside the cabinet cooled to 70-74°F.

The temperature differential between the wireworks and the outside air is a useful parameter for comparing different sites, see Table 2. The maximum differentials were 18-23°F for the type 80 cabinet at site #5 and 10-15°F for the type 40 cabinet at site #4. The heat absorbed into the site #4 cabinet was more efficiently dissipated into the ground and air than for the type 80 cabinet at site #5. All the pedestals and cross-connect cabinets examined in Arizona (sites #2-5) showed similar square shaped time-temperature profiles, similar values of peak temperatures and a maximum temperature increase

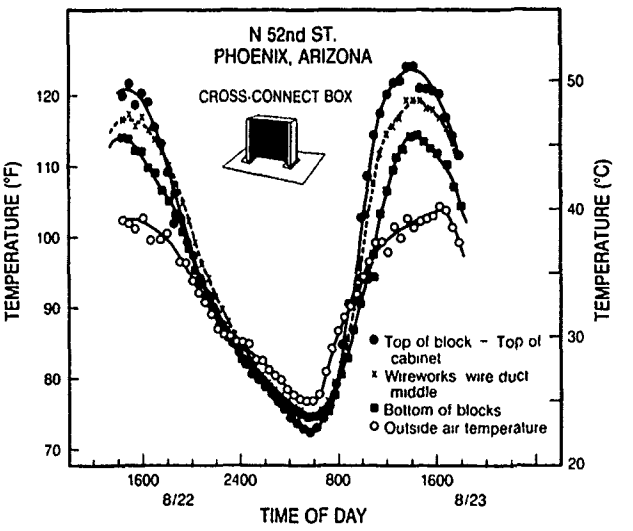

Fig. 5 Time-temperature profiles for site #5 cross-connect box

above the ambient air temperature of 15-20°F. Our results for both pedestals and cross-connect cabinets are simply understood by considering the closures as metal boxes heated by solar radiation with heat dissipation to the air and ground.

SLC Remote Terminal Cabinets

Subscriber Loop Carrier (SLC) cabinets are switching/distribution centers located far from the central office. A SLC cabinet has several compartments containing (1) AC and battery power supplies, (2) up to four individual switching systems with many electronic boards and channel packs, and (3) fiber and/or copper cables spliced into the switch. In respect to this temperature study, the major differences between SLC cabinets and cross-connect cabinets are:

- A SLC cabinet contains *heat-producing* electronic components and power sources (AC and batteries).
- SLC cabinets have fans to recirculate air and cool components; e.g., the cabinet at site #5 contained six fans that operated continuously.
- SLC cabinets have weather tight seals to prevent pollutants and dust particles from contaminating the electronic components. These seals also restrict air-exchange with the outside.
- The airflow within SLC cabinets is restricted by the high density of electronic components and the compartment walls.

The temperature measurements in the SLC cabinet at site #5 are summarized in Fig. 6 and Tables 2,3. The time-temperature profiles should be compared with the cross-connect cabinet results in Fig. 5 since both are type-80 cabinets and share the same site and climate. The absolute temperatures inside the SLC cabinet reached 135-140°F when the outside air temperature reached 102-104°F. At night the SLC cabinets operated at ~20°F above ambient air temperatures. In contrast, the temperatures inside pedestals and cross-connect cabinets equilibrated with the air temperature at night. The SLC cabinet was heated by solar heating from the outside and electronic heating from the internal circuit packs. Because the cross-connect cabinet and the SLC cabinet at site #5 had the same dimensions and shared the same local climate, the solar contribution (Δ_{solar}) should be the same for both cabinets. Since the heat generated by the SLC electronics ($\Delta_{internal}$) should be nearly constant with time, the temperature difference between the air and the wireworks at 6:00am should arise from the internal contribution only. Hence, the maximum temperature increase from solar heating of pedestals, cross-connect cabinets and SLC cabinets was 20±5°F, independent of geographic location and closure type. An additional temperature increase of up to 20°C was caused by the heat generated by the internal electronics inside the SLC cabinet.

The temperature was remarkably uniform across the SLC cabinet despite the high density of equipment and other restrictions to the air flow. The same temperature was found at the top of the cabinet, inside the SLC electronics in areas of both high and low air flows, at the modular splice in the cable entry port and inside the fiber splice box. The only exception to this uniform temperature was the one inch air gap at the bottom of the cabinet which was a consistent 5°F cooler than the rest of the cabinet.

These results are consistent with predictions made by McKay[5,6] who used test cabinets with resistors to simulate the heating load of the electronics. The temperatures measured for the SLC cabinet at site #5 matched his predictions for a SLC cabinet operating at moderate power (e.g., 500-700 watts) with ~5-6 fans operating continuously. If the fans failed in the SLC cabinet at site #5, cabinet temperatures are predicted to reach 200°F at the top of the cabinet and temperature gradients of >60-70°F would develop between the top and bottom of the cabinet. Future cabinet configurations may well include even higher densities of electronics and less air space inside the cabinets which will require efficient heat insulation and/or dissipation for such SLC cabinets.

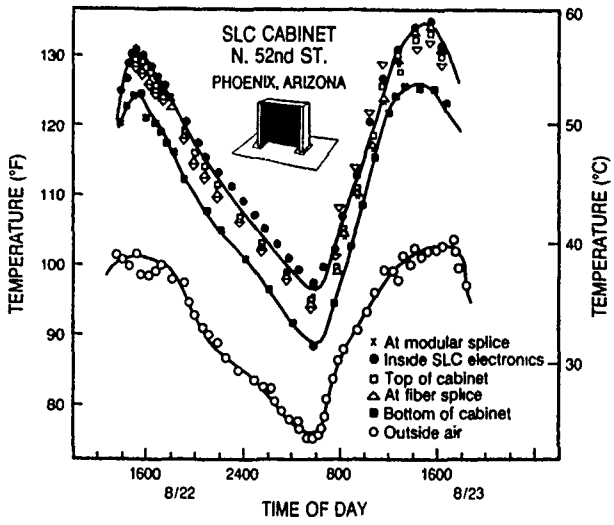

Fig. 6 Time-temperature profiles for site #6 SLC cabinet

The second SLC cabinet examined (site #6) was a modified type-40 cabinet with two fans arranged to draw outside air into the cabinet. Temperatures as high as 150-160°F were measured and gradients as much as 30°F were found across the cabinet. These temperatures and gradients are consistent with McKay's predictions[5,6] for a cabinet with only two fans.

Reel Yard

The final location was a typical cable reel yard where reels are stored in an open asphalt parking area. The temperatures of optical fiber, paper pulp and copper cables were measured, with and without thermal wraps, and at several places within the reels. The results are summarized in Table 4. The black cable sheath efficiently absorbed sunlight and reached 50-70°F above the ambient air temperature. The measured sheath temperature was sensitive to many factors including sun exposure, ambient air temperature, cable design, air currents and the presence of thermal wrap.

The maximum sheath temperature recorded was 175°F on a optical fiber cable of all dielectric design (i.e., no metal in cable). The sheath temperature of a copper cable of equivalent size and diameter was 150-155°F. The presence of the stainless steel and

Table 4. CABLE TEMPERATURES IN REEL YARD

SAMPLE CABLE (a)	TEMPERATURES (°F) AT SURFACE LAYER IN SUN	SHADE	1 LAYER DEEP	2 LAYERS DEEP	3-4 LAYERS DEEP	UNDER THERMAL WRAP
AIR	98-102	98-102	--	--	--	--
OPTICAL CABLES						
I	174-176	105-110	150	135	122	--
II	175	--	144	130	--	115-119
III	170	--	141	130	--	108-110
COPPER CABLES						
PIC[b]						
IV	159-160	108	143	126	--	110
V	150	114	135-140	--	--	110
PULP[b]						
VI	150	--	--	118	--	--
INNER DUCT						
VII (yellow)	140-143	--	--	--	--	--

(a) All cables were sheathed with black polyethylene and of approximately equal diameter (~1/2 inch). The optical fiber cables were all dielectric with no metallic sheaths. The copper cables contained stainless steel and aluminum sheaths as well as the copper conductors at their core.

(b) PIC = Cables containing Polyolefin Insulated Conductor
PULP = Cables containing Paper Pulp Insulated Conductors

aluminum sheaths in contact with the black polyethylene sheath was assumed to conduct heat away from the outer sheath and redistribute the heat throughout the copper cable. All dielectric fiber cables contain no metallic materials to conduct the heat away from the surface and therefore their cable sheaths were 20°F warmer than the copper cables. Further evidence for this mechanism of heat dissipation through the metallic components of a cable was found from measurements on a self-supporting cable where the cable sheath adjacent to the metal support strand was 5-8°F cooler than the sheath of the cable.

Shade is the most effective means to reduce the sheath temperature as evidenced by:

- Cable sheaths in the shade measured 104-106°F ≅ air temperature.
- Under thermal wrap, the temperature of the above optical fiber cable sheath decreased from 175°F to 110-120°F.
- The sheath temperature decreased as one moved deeper into the reel; e.g., temperatures of the fiber optic cable sheath decreased from 175°F at the outer strands to 122°F for strands in the fourth layer, see sample I in Table 4.

Thermal wrap reduced the temperature by not only shading the cable, but also reflecting the solar radiation. Since the black cable sheath absorbed the sunlight efficiently, a reflective cable sheath would be expected to reduce the sheath temperature significantly. This was confirmed by a surface temperature of 140-143°F found for a reel of inner duct (a yellow plastic tube) which compared favorably with the 170-175°F for the fiber cable and the 155°F for copper cable.

Since thermal wraps and reflective colors were so effective in reducing temperatures, then use of reflective coatings or closures in the outside plant should reduce thermal degradation of materials and equipment. Experiments with white reflective coatings[7] and poly(vinyl chloride) covers[8] have reduced peak temperatures inside some closures by up to 10°C which should result in a doubling of insulation life[9].

SUMMARY

Typical temperatures found in outside plant closures and reel yards have been measured as a function of time-of-day, plant design and local climate.

The time-temperature profiles were explained by combining local climate and ground conditions with heat flow characteristics of the various closure designs. Temperature profiles for both pedestals and cross-connect boxes could be understood as a competition between solar heating and heat dissipation to the ground and air. Internal electronic heating supplemented the external solar heating effect and produced 140+°F temperatures inside SLC cabinets.

The high temperatures found inside aboveground closures (140-150+°F) and in the reel storage yard (175°F) are particularly alarming since future networks will include widespread installation of remote switch electronics and optical fibers in these outside environments. Outside plant closures as well as the electronics, batteries, optical fiber cables and fiber coatings will all need to meet stringent performance tests to ensure efficient heat dissipation and long term thermal stability.

ACKNOWLEDGEMENTS

P.C. Warren and J. McKay are thanked for useful discussions and helpful comments on the manuscript.

REFERENCES

1. T.N. Bowmer, Proceed. 37th International Wire and Cable Symposium, 475 (1988)
2. B.T. Reagor, IEEE Trans. Comp. Hybrid Manuf. Tech., **CHMT-9(2)**, p209 (1986)
3. J. Howard, Proceed. 21st International Wire and Cable Symposium, 329 (1972)
4. H. Gilroy, Proceed. 23rd International Wire and Cable Symposium, 42 (1974)
5. J. McKay, Proceed. International Telecommunications Energy Conference *INTELEC* (Oct., 1989) Florence, Italy { TM-ARH-013463 & TM-ARH-013639 }
6. J. McKay, Proceed. International Telecommunications Energy Conference *INTELEC* (1988) "The Effect of Solar Radiation and Wind Speed on Air Temperature Rise in Outdoor Cabinets Containing Telephone Equipment"
7. E.A Capadona and D. LaPointe, Outside Plant, p 22 (July) 1988
8. R. Boast, private communication
9. L.D. Loan, Proceedings of the Golden Jubilee Conference on Polyethylenes 1933-83, (June 1983) London

Trevor N. Bowmer is a member of the Polymer Chemistry and Engineering Research Group in Bellcore. He received his Ph.D. in chemistry from the University of Queensland, Australia, where he studied radiation chemistry of polymers. Joining Bell laboratories in 1980, he investigated radiation cured systems and lithographic materials. In 1984, he came to his present position where his interests include degradation mechanisms and characterization of polymeric materials used in telecommunications applications.

Russell J. Miner was a Member of the Technical Staff at Bellcore until his retirement in 1989. Before that he was with Bell Telephone Laboratories from 1961 and worked in the Plastics Development and Applied Research Department. He studied the effects of soil burial, electron irradiation, outdoor aging, heat and fire on the plastics materials used by telecommunications companies.

Bob Coker worked with Outside Plant operations and materials for more than 30 years with Mountain Bell Telephone Company. From 1984 until his retirement in 1990, Bob was Assistant manager in Network Services in U S West Communications with interests covering the quality/reliability of all outside plant products and materials.

A NEW APPROACH TO TOTAL QUALITY ASSURANCE IN TELEPHONE CABLE PLANTS

E. ESPOSITO - G. MORE'

TELECO CAVI
Via Nazionale Adriatica, 2D - Roseto degli Abruzzi, Italy

ABSTRACT

This paper describes the approach of a telecommunication copper cable manufacturer to a Quality Assurance policy in order to satisfy the request of high quality products.

The standards, the quality control, the control procedures as well as the automatic test equipments are described.

The economic factors are also taken into account bearing in mind that every effort is directed to the aim of the optimization of every stage of production to guarantee the quality of the finished product.

1 INTRODUCTION

1.1 Quality Assurance Policy

In order to satisfy the request of high quality products, the manufacturer of telephone cables have put every effort to obtain the highest confidence on the characteristics of the finished product.

The necessity of controlling in a systematic and planned way the most significant industrial activities with the scope of meeting the product specification lead to the concept of "Quality Assurance".

It is now no more sufficient that the product pass the final acceptance test, but the organization of the production, in the whole, must assure that every step of the manufacture process is under strict control.

In a telephone cables manufacturing plant the items that need to be controlled in a definite and systematic way are: raw materials, manufacturing process, manufacturing equipments, measurement instruments.

1.2 Standards

The reference standards for Quality Assurance in Italy are the following:

UNI EN 29000
rules concerning the factory management with respect to Quality and Quality Assurance;

UNI EN 29001
critera for Quality Assurance in design, development, manufacturing, installation and service;

UNI EN 29002
criteria for Quality Assurance in manufacturing and installation;

UNI EN 29003
criteria for Quality Assurance in final tests and controls;

UNI EN 29004
criteria regarding the factory management with respect to Quality and factory Quality Systems.

Each manufacturer can apply all or part of the above standards depending on the choice of the relevant Quality System.

1.3 The Quality Handbook

The relationship between the different activities that affect the product quality are synthetically sketched in the "Quality Circle" (UNI EN 29004) in fig 1.

The idea shown by that representation is that a continuous line exists between manufacturer and customer aimed to the optimisation of the product from both technical and economic point of view.

The manufacturer delineates the different operative stages,together with the manufacturing, control and testing procedures in a document called "Quality Handbook", consisting of several items, of which some are outlined:

-Organization chart of the firm and the Quality Management, stating the exact responsibilities;
-Managing and technical procedures;
-Control of purchased materials;
-Operative procedures;
-In-process inspection and testing;
-Finished product testing;
-Measurement instruments calibration;
-Control of non conforming products;
-Correcting actions and checks.

The "Quality Handbook" is a private document of the Firm and undergoes periodical revisions and updatings in order to represent always the state of the art of the manufacturing process.

All the revisions and updatings are jotted down together whith the names of the individuals who are in charge of keeping the Handbook.

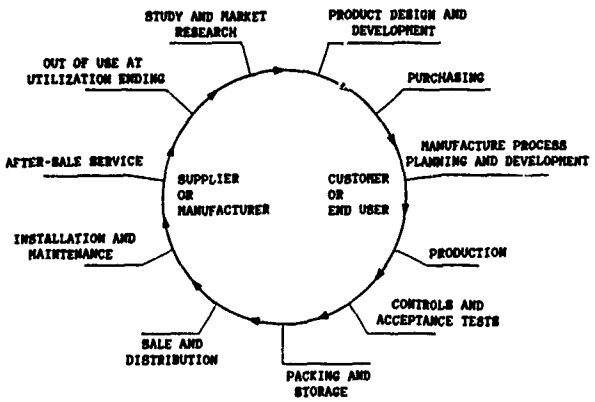

FIG. 1 Quality Circle

2 QUALITY CONTROL IN THE FACTORY

Like all the other products of the industrial engineering, the cables for telecommunications undergo a severe quality control.

This control starts as the raw materials enter the factory, continues through the different stages of manufacture and ends with the final acceptance test.

In table 1 a flow chart of the production cycle for telephone multipair copper cable meeting the SIP (*) spec. 1240 is sketched.

From this flow chart are evident the points where the Quality Assurance System are applied:
-Control on purchased materials;
-Control during the production;
-Control on finished products.

3 CONTROL ON PURCHASED MATERIALS

3.1 Definition of raw materials

The raw materials used for the manufacture of multipair telephone cables meeting SIP 1240 specifications have been defined together with their characteristics and acceptance limits during the design stage.

The definition of the material chemical and physical characteristics are of the outmost importance in order to:
-Define the specification of the material supplied;
-Plan the controls on the incoming material;
-Define the acceptance criteria.

3.2 Classification of the characterisics

Three different kind of tests are used for the classification of the characteristics of the materials, depending on their importance for the final product:
-Acceptance tests (A);
-Type tests (T);
-Extraordinary tests (E).

3.3 Characteristics criticity

The characteristics of the materials which undergo A and T tests are classified as function of the importance of the defects that could impair the performances of the finished cable as a consequense of the use of a material with characteristics outside the limits specified:
-Critical defects (C);
-Important defects (I);
-Secondary defects (S).

3.4 Sampling plan

The sampling plan is defined with reference to the kind of test and the criticity of the characteristic.

The basic element for the definition of a sampling plan is the choice of the Acceptable Quality Level (AQL).

The values of AQL can be taken from historical data,otherwise is a good rule to choose AQL = 1% .

The plan can be simple, double or multiple, while the severity degree can be reduced, normal or enhanced.

The control of a characteristic starts always with a normal severity degree,to pass to the reduced or enhanced control if particular conditions are to be verified (MIL STD 105/414). The rules to pass from a severity degree to another are shown in fig. 2.

Such plans are used to examine the characteristics subjected to Acceptance tests. For the characteristics subjected to Type tests suitable samplings can be made periodically during a three or six month period.

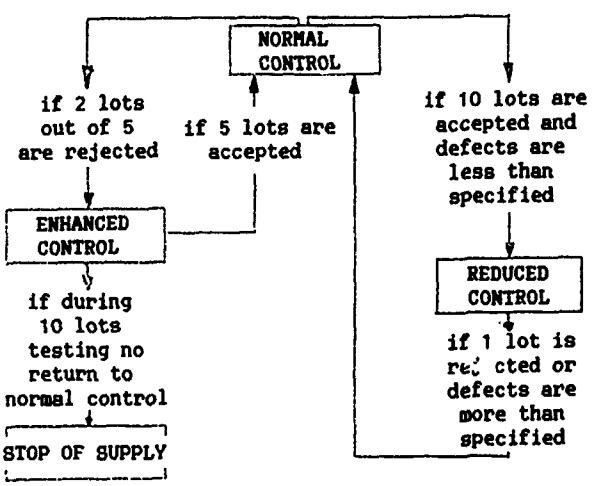

FIG. 2

3.5 Criteria for raw material acceptance

The acceptance of raw materials whose characteristics ara subjected to either Acceptance or Type tests depends on the sampling plans used (Appendix A) or on the limits in the control chart for single values.

3.6 Qualitative information on the material

All the test results are processed and an analysis is made in order to judge the quality of the material.

The criterion used to evaluate the quality of a measured characteristic is described.
The first indicator of the compatibility between the values of the examined characteristic and the limits of the specification is **Cp = Ts / Tn** used to compare the specification allowance
Ts = LSS - LSI with **Tn = 6 * S** (where S is the standard deviation). A characteristic meets the specification if Cp is equal or greater than 1.33.

The Cp value is not enough to define the agreement between material and specification and so another indicator is needed **Cpk = Cp * (1 - K)** whih **K = (Xm - Ms) / (Ts / 2)** where Xm and Ms are respectively the actual and the expected average values.Note that Cp is always equal or greater than Cpk.

A characteristic meets the specifications if both Cp and Cpk are equal or greater than 1.33.

A qualitative judgment on the material characteristic is summarized in fig. 3.

Cpk \ Cp	< 1	1 ÷ 1,32	⩾ 1,33
< 1	POOR	AT LIMIT	ACCEPTABLE
1 ÷ 1,32	---	GOOD	VERY GOOD
⩾ 1,33	---	---	EXCELLENT

FIG. 3

4 IN LINE CONTROLS

4.1 Manufacturing process

The in line controls guarantee the quality of the production, checking in the different stages of manufacture the parameters outlined in Tab. 2 . Tab. 2 shows the correlation between the variables in the process and the geometric, mechanical and electrical effects as well as the defects that can occour during the different stages of production.

For instance the check of the capacitance of an insulated conductor against an electrode immersed in water allows a monitoring of the material flux and the temoerature of the extrusion line.

Supposing that the insulated conductor is free of defects, the quality control measurements start with the first stage of stranding, i.e. the pair or the sub-unit (10 pairs) twisting.
If the pulling force during this stage is not properly adjusted, a pair asymmetry will result.
This kind of defect is detected by a measurement of the resistence unbalance between the two wires.

In the subsequent stage the pairs with different twisting pitches are combined together to form the 10 pairs sub-units and simultaneously the 100 pairs unit.
The ratios of the pair pitches within the sub-unit must be such that the capacitance unbalance K1 between adjacent pairs remain within acceptable limits.As a consequence the stranding process is checked by measuring K1. When the value of K1 is large, two possible errors have occurred:
-two pairs with the same pitch have been stranded in adjacent position as a result of the stranding machine loading error;
-a substantial difference between the pitches of all the pairs exists as a defect in the sub-unit construction.

The capacitance unbalance to ground (E1,E2) and to the sheath (E1a,E2a) can be large when the pulling force applied during the pair twisting is not regular or the insulated wires have a substantial diameter difference.

4.2 Controls on production lines

The lines for the production of multipair copper cables must be equipped with suitable instrumentation for the control of the process variables as well as the product characteristics. The following list oulines the instruments used in the different stages of manufacture.
-Insulation extrusion:
diameter, ovality, pulling force meters on copper wire;
diameter, eccentricity, capacitance meters and spark tester on the insulated wire.
-Pair twisting:
pitch control, wire pulling force meter, spark tester.
-Stranding:
pitch control, pair pulling force meter, spark tester.
-Sheath extrusion:
defect monitoring equipment, thickness and outer diameter meter, spark tester.

4.3 Line operator control

The operators on the different production lines have in charge suitable equipments to monitor the good operation of the lines and the conformity of the main product characteristics.
All the operators are trained on the instuments and on the specification limits of the characteristics under control.
All the measurement values are stored.

4.4 Quality control group operation

Between subseqent stages of manufacture, the semimanufactured products are checked following a preestablished scheme.
These tests guarantee the quality of the production and at the same time give informations on the trend of the characteristics, thus minimizing the line stops.

Another step toward quality and productivity improvement is the storage and the statistical processing of all the data resulting from the in-line tests.
The example in fig 4 shows the statistical distributions of the values of the conductor diameter measured on two different production lots resulting each by a different extrusion lines: TR1 and TR2.
All the values are within the specifid range with two different average values and little standard deviations. Thus every lot shows a good quality, but, if these two lots were used to manufacture the pairs of a sub-unit, the resulting distribution would have a different average value and a larger standard deviation (dotted line).

That decrease of the quality can be easily avoided by a proper use of the stored data.

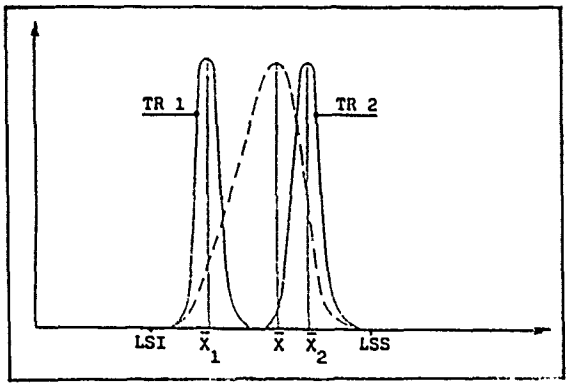

FIG. 4 Distribution of wire diameter for two different extrusion lines

5 FINAL ACCEPTANCE TEST

Another important aspect of quality control is the final acceptance test. At this stage the report of the tests made on the finished products demonstrates to the customer that the cables meet the expected quality.

A very important goal is to use time saving maesurement methodologies.
The final tests can be drastically reduced when the same typology of cable is manufactured in large lots for long periods of time. In this case statistical methods of maesurement can be applied. By means of suitable acceptance criteria and test procedure the confidense level of statistical investigation is about the same of total inspection.
The acceptance criteria can be expressed in terms of "factory quality factors" defined as follows:

Qs = (LSS - Xm) / S

Qi = (Xm - LSI) / S

where LSS and LSI are respectively the superior and inferior limits of the specified range, and Xm and S are respectively the average value and the standard deviation of the calculated distribution for every measured parameter.

In order to accept the production lot, the values of Qs and Qi must be greater than the value of the acceptance constant Ka.

The value of Ka is calculated from the tables as function of the LQA %, the type of the sampling plan (simple, double or multiple), the degree of severity of the plan (normal, reduced or enhanced) and the quantity of the lot.

The number of measurements to perform on the finished cable depends on the Qs and Qi values. For example, if the value of Q is greater than Ka, the measurements are performed on only "n" elements out of "m" cables.

On the other hand, if Q is smaller than Ka but still greater than the tolerance constant Kt, the measurements are performed on "n1" elements out of "m1" cables with "n1" and "m1" respectively greater than "n" and "m".

A value of Q smaller tha Kt means that the production lacks of uniformity and a statistical quality control becomes impossible. In this case the acceptance test follows the traditional routine.

During the final tests the quality control should attain Q values greater than Ka in order to reduce the number of measurements.

On the other hand too large Q values mean some drawbacks because of the increase of work load and rejected share at the intermediate stages of production. This is explained in fig. 5, where the Q values of a specific cable are shown as function of time.

In the beginning the values of Q were significantly greater than Ka. Following an attempt to widen the tolerance in the intermediate tests in order to reduce the percentage of rejection, the Q value dropped below Ka, thus increasing the work in the final tests.
Strict tolerances were reintroduced and the Q value raised above Ka as expected. A further attempt to widen the tolerance led to a drop of Q below Kt, so the conventional final acceptance tests had to be reintroduced.

This is is a good example on the feasibility of a trade off between tolerances and rejected products during the manufacture and the work load during the finished cable acceptance stage.

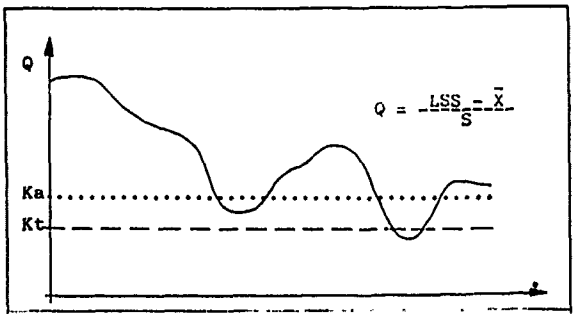

FIG. 5 Behaviour of Quality Factor vs. time

6 AUTOMATIC MEASUREMENT SYSTEMS

The capabilities of a measuring systems for cable characterization are briefly outlined.
- Computerized measurements: a comlete set of tests can be performed on the cable in automatic way. The resulting values must be processed with reference to the specifications, stored and tranferred to a central computer. It must be porrible to retrieve the data and to evaluate in detail all the tolerances and the statistics of the production.
- Ease of operation: the equipment should be as far as possible easy to operate and user friendly. The input of data should be minimized using code numbers that define all the sequences of measurement and evaluations.
- Reliability: the equipment needs to be moved inside the factory,so it must be transportable, rugged and all the circuitry and components must operate with a high degree of reliability under variable humidity and temperature conditions, with no need of a conditioned air environment.

- Flexibility: the equipment must be flexible both in hardware and in software so that the configuration can be changed at low cost in order to meet the customer requirements and be adaptable to a change of demand.

Examples of automatic measuring systems are shown in fig. 6 and 7.

The system in fig. 6 can be used for both high and low frequency measurements.

The system in fig. 7 performs the following measurements on a cable up to 200 pairs in a combined way: high voltage, insulation resistance, contact and continuity.
This latter system is of great importance for factory tests because, besides better reliability and time saving, improves the safety conditions of the operator and guarantees a total quality in the manufacture intermediate stages as well as in the final acceptance tests.

7 ECONOMIC FACTORS

The cost of quality control is strongly affected by the expenses for the number of proper qualified people taken on for testing.
Costs can be reduced not only reducing the number of operators, but also replacing high qualified operators with less skilled ones in the testing department.

The automation of test equipments helps in reducing the costs.
In fact every hand made measurement usually requires four operators: two people for connecting the cable to the test equipment, one to operate the system and one to record the measured values.
On the other hand only one people is needed to connect the cable and to operate an automatic system; furthermore this operator do not need a detailed knowledge of the cable measuring techniques.

Anyway the optimization of each production stage is the only way to improve the process efficiency and to reach the goal of an economic production.

8 CONCLUSIONS

In order to meet the severe requirement imposed by the Administrations on copper cables for telecommunications, as well as to guarantee high quality products at reasonable costs it is necessary to introduce in the factory the concept of "Quality Assurance".

The availability of automatic measuring systems to control the outcome of the production in the different stage of manufacture is a fundamental tool to obtain a total quality and, at the same time, to reach the goal of cost saving.

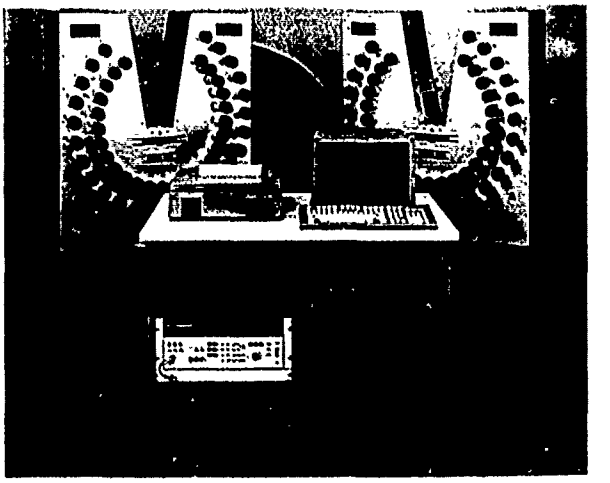

FIG. 6 : Computerized Automatic Cable Measuring System

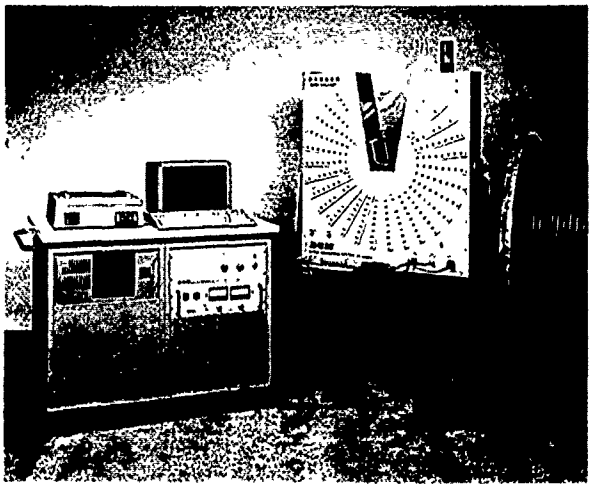

FIG. 7 : High Voltage and Insulation Resistance Measuring System

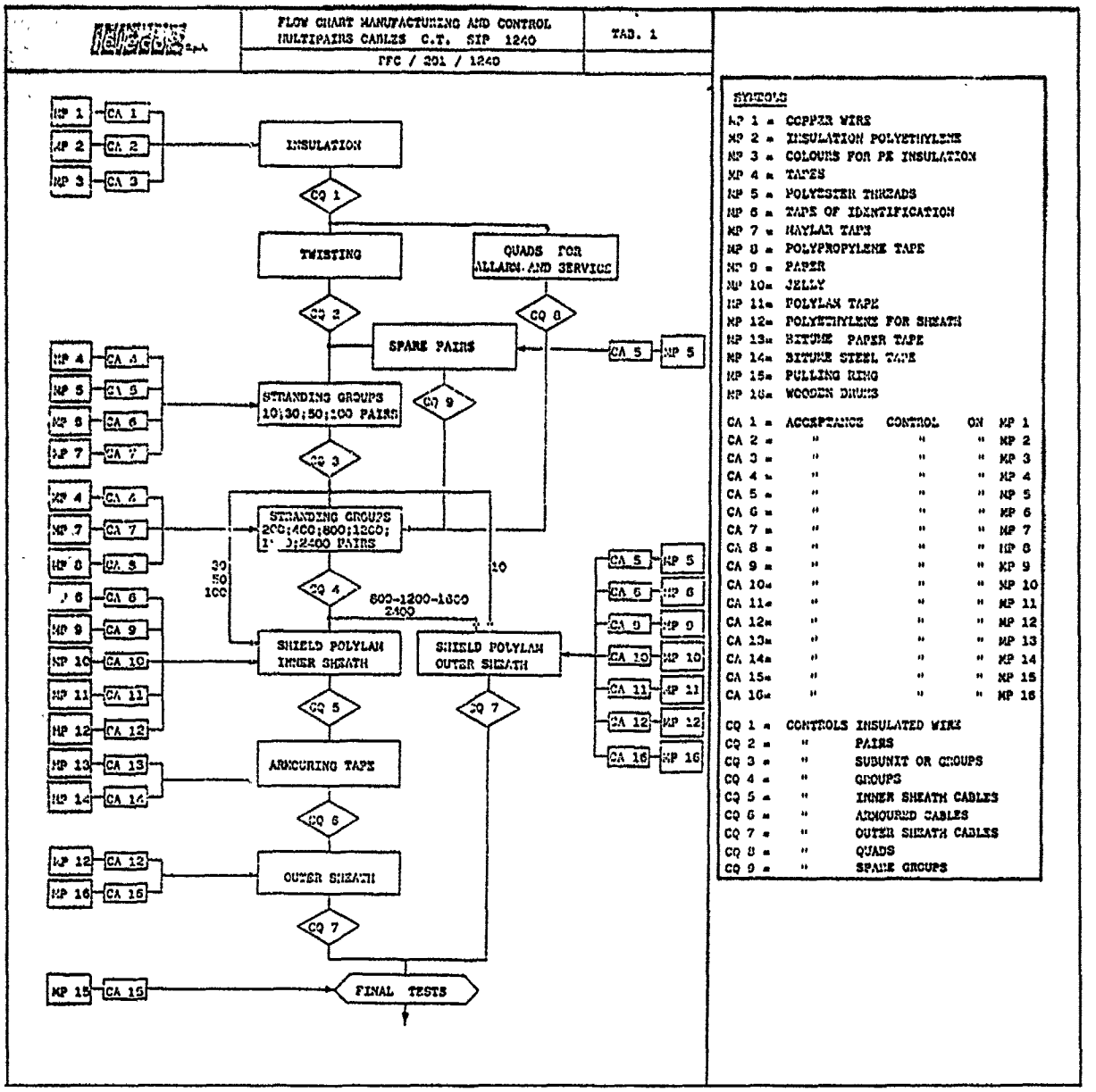
FLOW CHART MANUFACTURING AND CONTROL
MULTIPAIRS CABLES C.T. SIP 1240
FFC / 201 / 1240
TAB. 1
INSULATION
CQ 1
TWISTING
QUADS FOR ALLARM AND SERVICE
CQ 2
CQ 8
SPARE PAIRS
STRANDING GROUPS 10;30;50;100 PAIRS
CQ 9
CQ 3
STRANDING GROUPS 200;400;800;1200; 1600;2400 PAIRS
30
50
100
10
CQ 4
600-1200-1600 2400
SHIELD POLYLAM INNER SHEATH
SHIELD POLYLAM OUTER SHEATH
CQ 5
CQ 7
ARMOURING TAPE
CQ 6
OUTER SHEATH
CQ 7
FINAL TESTS
SYMBOLS
MP 1 = COPPER WIRE
MP 2 = INSULATION POLYETHYLENE
MP 3 = COLOURS FOR PE INSULATION
MP 4 = TAPES
MP 5 = POLYESTER THREADS
MP 6 = TAPE OF IDENTIFICATION
MP 7 = MAYLAR TAPE
MP 8 = POLYPROPYLENE TAPE
MP 9 = PAPER
MP 10= JELLY
MP 11= POLYLAM TAPE
MP 12= POLYETHYLENE FOR SHEATH
MP 13= BITUME PAPER TAPE
MP 14= BITUME STEEL TAPE
MP 15= PULLING RING
MP 16= WOODEN DRUMS
CA 1 = ACCEPTANCE CONTROL ON MP 1
CA 2 = " " " MP 2
CA 3 = " " " MP 3
CA 4 = " " " MP 4
CA 5 = " " " MP 5
CA 6 = " " " MP 6
CA 7 = " " " MP 7
CA 8 = " " " MP 8
CA 9 = " " " MP 9
CA 10= " " " MP 10
CA 11= " " " MP 11
CA 12= " " " MP 12
CA 13= " " " MP 13
CA 14= " " " MP 14
CA 15= " " " MP 15
CA 16= " " " MP 16
CQ 1 = CONTROLS INSULATED WIRE
CQ 2 = " PAIRS
CQ 3 = " SUBUNIT OR GROUPS
CQ 4 = " GROUPS
CQ 5 = " INNER SHEATH CABLES
CQ 6 = " ARMOURED CABLES
CQ 7 = " OUTER SHEATH CABLES
CQ 8 = " QUADS
CQ 9 = " SPARE GROUPS

telecom

TAB. 2

PROCESS	PROCESS VARIABLES	GEOMETRIC EFFECT	EFFECT R,L,G,C	ELECTRICAL EFFECT	MECHANICAL EFFECT	DEFECTIVE CABLE	RIGHT CABLE
EXTRUSION	**CONDUCTOR :** Impurities, circularity, irregularity, diameter. **INSULATION :** Temperture, diameter, eccentricity, colour, impurities, material, speed, cooling, defects, bubbles, dispersion, expansion.	dc di si	R G C	Ri ε ρ	Ac KRc Ai KRi Sf Rt	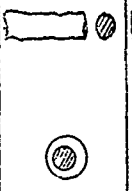	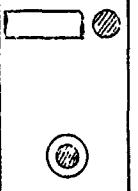
PAIR TWISTING	Tension, torsion, pitch, pitch symmetry, defects of insulation.	dc l S	R L G C	ρ Ra ,Rb ΔR Ri	Ac KRc Sf Rt	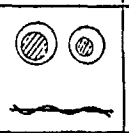	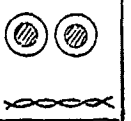
PAIR STRANDING (sub-unit/ unit)	Pitch swing, stability of unit/sub-unit, tension on pairs, material of binding wire, defecs of insulation.	l , dc S , Dc p	R L G C	ε K1 C1 E1,E2 Ri	Ac KRc F	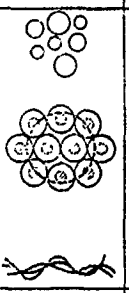	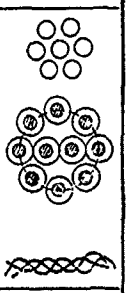
GROUP STRANDING	Stability of stranding pitch, materials of identification wire, wrapping and binding yarns, swing on group pairs.	l , p S Dc Sn L	L G C	ε K1 C1 E1,E2 Ri	Ac KRc F		
INNER SHEATH EXTRUSION	Material, temperature, defects conducibility, carbon black, dimensions, Al screen, filler, overlapping adhesion, PE/H5 adhesion, overlapping width.	S Dc Sn L s s_o	L G C	ε K1 C1 E1a,E2a E1,E2 Ri	Ag,KRg Ap,Apg Am,KRm	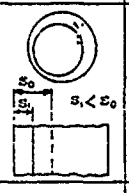	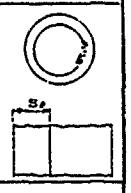
ARMOURING	Steel tape and paper tape materials, bitumen, tapes overlapping, defects.	Dc L Sn p	L G C	ε	Am KRm F		
OUTER SHEATH EXTRUSION	Material, temperature, defects conducibility, carbon black, dimensions.	Dc s	L G C	ε	Ag KRg		

dc = Conductor diameter
di = Insulation diameter
si = Insulation thickness
s = Sheath thickness
s = Overlapping width
l = Conductor distance
p = Pitch
L = Tapes width
Sn = Tapes thickness
Dc = Actual diameter on sheath

Ac = Conductor elongation
Ai = Insulation elongation
Ag = Sheath elongation
Am = Tape elongation
KRc = Conductor break. load
KRi = Insulation break. load
KRg = Sheath break. load
KRm = Tape break. load
Sf = Slippage
Rt = Shrinkage
F = Cable flexibility

Ap = Polylam adhesion
Apg = Polylam/PE adhesion
Ri = Insulation resistence
ρ = Conductor resistivity
ε = Dielectric constant
Ra,Rb = Conductor resistences
ΔR = Resistence unbalance
C1 = Mutual capacitance
K1 = Capacitance unbalance
E1,E2 = Pair to ground unbalances
E1a,b = Pair to pair unbalances

R = Electrical resistence
L = Inductance
G = Conductance
C = Capacitance

APPENDIX A

Example 1

Acceptance control by variables (unilateral)
Material: Polyethilene for sheaths
Characteristics: Density (critical)
Superior limit of spec range: LSS = 0.940 gr/cm3
Sampling plan: simple, normal severity
Varieble: unknown
Acceptable Quality Level: AQL = 1%
Number of controls: 4
Measured values: 0.936 0.935 0.933 0.938
Average value: Xm = 0.9355
Standard deviation: S = 0.0021
Quality factor: Qs = (LSS - Xm) / S = 2.143
Acceptance constant: K = 1.45
Control: Qs > K 2.143 > 1.45 conform.

Example 2

Acceptance control by variables (bilateral)
Material: Steel tape
Characteristics: Breaking load
Limits of spec. range: LSS=460 MPa LSI=320 MPa
Sampling plan: simple, normal severity
Variable: unknown
Quality acceptance level: QAL = 1.5%
Number of controls: 4
Measured values: 364 425 435 400
Average value: Xm = 406
Standard deviation: S = 39.17
Quality factor: Qs = (LSS - Xm) / S = 1.378
Qi = (Xm - LSI) / S = 2.195
Acceptance constant: K = 1.34
Constant for maximum standard deviation F=0.353
Maximum standard deviation.
MSD = (LSS - LSI) * F = 49.42
Controls:
Qs > K 1.378 > 1.34 conform
Qi > K 2.195 > 1.34 conform
S < MSD 39.17 < 49.42 conform
(The three conditions must apply at the same time)

REFERENCES

1) L. M. Chattler "A guide to electrical specification requirements for multipair telephone cables", WIRE ASIA 82, Singapore, Oct 1982

2) V. Reich "Quality assurance in telephone cable plants", Wire Industry, March 88

3) A. Iacobini "Il controllo statistico della qualità", Ed. Universitaria, Roma 1985

4) K. Ishikawa "Guide to quality control", Nov. 88

5) MIL 105/414 Standard

6) UNI EN 29000 Standard

Ernesto ESPOSITO was born in 1951 in Roseto degli Abruzzi (Italy)
He received the Doctorate in Telecommunication Engineering in 1976 from the University of Bologna.
From 1977 he is employed in Teleco Cavi where, after an experience in the design of optical and copper cables, is now in charge of the "Research and Development" and "Quality Control" Departments.

Gianfranco MORE' was born in Mosciano S.Angelo (Italy).
He received the Doctorate in Mechanical Engineering in 1988 from the University of Bologna.
From 1988 works in Teleco Cavi in the "Quality Control" Department.

"IMPLEMENTATION OF A HIGH PRODUCTIVITY PLANT, FOR PLASTIC INSULATED TELEPHONE CABLES"

A. MARSILIA , G. PATERNOSTRO

MANULI CAVI

FULGORCAVI

ABSTRACT

This paper deals with a new plant able to produce more than 2 million km of pair per year, that was installed in the same place of an existing manufacturing facility, without stopping the production and using part of the older machinery step by step as far as the new ones were installed and the market grew.
After briefly discussing cable design and results of prototypes, the machinery layout is described.
The key feature is the stranding facility, able to strand in one operation a group of 100 pairs,(divided in 10 subunits) starting from 200 single wires.
The testing facility and results are then outlined, and finally the future developments are discussed.

FOREWORD

Telephone cable with plastic insulated unit twins for underground distribution were introduced in the network of SIP (Italian telephone operating company) in the year 1988 and gradually replaced paper insulated, quad type lead sheathed cables that were used since many years.
By year 1990 all copper cables ordered by SIP for this network are the new ones.
Because of the change of insulation and from quads to twins new machines were needed and, in order to improve productivity all manufacturing activity, formerly in three different plants, was concentrated in one.
A new layout was designed and implemented, without stopping the production and using part of the older machinery.

CABLE DESIGN

Main cable design is with 10 pairs sub-units and 100 pair units (in one make-up and lower count design 50 pair units are used).
Even-count color code (up to 10) is used in each sub-unit.
Conventional stranding was with single twisters in separate operation, and 100 pair unit stranding with drum-twisting cabling machine.
The basic idea was then to gang-connect twinning and stranding in one operation.
The cable has very good high frequency performance, especially the cross-talk characteristics at 80 KHz and 1 MHz are suitable for supporting data transmission, narrow band ISDN and some 2 Mbit/s flows.
Of course, these characteristics were required also in one operation manufacturing.
No S-Z twinning or stranding was allowed by SIP (TELCO) specification, because of early attempts that showed poor high-frequency characteristics and bad cable shape.

GRO ? TWINNING

In order to achieve 100 pairs simultaneous twinning in 10 sub-units, 10 twisters grouped in 10 machines were needed. A simple and classical vertical design was choosed for the twister, with supply reels on the same axis inside the flier, rather than vertical stacked reels.
This provides equal paths for the wires of the pairs and simple and effective tension system.
Since 10 different twist-lengths were used in separate twinning, (in order to achieve good cross-talk characteristics), similar and suitable twist lengths that could be obtained with one single motor and gears were choosed, and tested on a prototype twister- This twister has continuonsly variable twist length by electronic drive.

The trial cable results were satisfactory, therefore the construction of the group twisters was approved.
Whilst waiting for the complete machine the first group twisters were delivered and a method of take-up was devised, by adopting the capstan and take-up of spiral wrapping machines, formerly used for paper insulation.
The operation of the machines at maximum rated speed (2000 twist per minute) has allowed considerable debugging.
The critical parts were the ball bearing and clutch (this part was then changed in other machines); some resonance effect was detected and removed.
The quality of the pairs was good and cross-talk characteristics of the cable satisfactory.

INSULATION

High speed (2200 m/min) lines with tandem drawing were needed.
Two european manufacturers were selected. Lines 1 and 2 are from manufacturer "A"- Lines 5 and 6 are from manufacturer "B" with copper drawing machine from manufacturer "C", which were available from previous separate drawing operation for paper insulated cables- Lines 3 and 4 were assembled with take-up from manufacturer "B" and the rest of the line from manufacturer "A", because take-ups from manufacturer "A" showed early problems in changeover at top speed, and the only practical solution was a new designed device; on the other hand extruders from manufacturer "B" have more faults on the insulation. For that matter, the best insulating material, was found to be medium density PE.
No important scrapes or abrasion on insulation was found in the following manufacturing stages, and compatibility with filling compounds is good as high density PE or better.
These insulation lines, like almost all modern machinery, have PLC computer control. During start-up and debugging some PLC has caused many inconveniences, but of course these feature are useful for reporting processing conditions and for integrated quality control.
The first three lines installed supplied at least 100.000 km pair per month, therefore 6 lines will allow a manufacturing capacity of 200.000 km pair per month, more than 2 million km pair per year.

UNIT STRANDING AND TWINNING

The basic idea was to gang-connect twinning and stranding together, in order to have one man operation for the whole time in which the machine is running.
In the first phase, the old rotating take-up strander was connected and syncronized with the 10 group twisters.
The maximum speed at which the line could run was 80 m/min ,rather good for a machine 16 years old, but unsatisfactory to achieve maximum productivity target, because two underestimated problems arose.
The first and plain one, was the diameter of the take-up reel (1250 mm) which allows a maximum length of 100 pair unit, about 2 km. Since the wire length on the twisters is more than 72 km, the sum of stop times for changing the take-up reel was more than one 8 hours shift.
The second problem, and tricky one, was the tension and stop devices of the binders in sub-units formig systems. Binders breaks occurred often during speed changes and sometimes were undetected by the stop devices, thus allowing sub-units without identification inside the cable, and causing many problems for detecting and repairing.
The solution was to change both the rotating take-up and the binders group (new oscillating plates were also fitted). The new strander has 1600 mm diameter take-up, thus allowing more than 6 km unit length, with a total stop time for reel change about 2 hours. Besides the new machine can run at 100 m/min, increasing therefore production and productivity.
The new binders have electronic tension control, and electronic stop system directly connected with the spinning head, so that tension can be carefully adjusted and changes with speed, whilst any eventual break will positively stop the line.
The additional total time for changing the binding tapes during a complete 72 km run was less than 1 hour and, by adjusting the length on the bobbins, stops could be made in the same time with reel changing.

Loading of insulated wire is the most time consuming operation. For the first phase, no automatic loading is provided, for the reason of simplicity and also because of the huge personnel problem arising from the change to plastic insulated cable, from older paper insulated cable.

At that time, the twisters groups were equipped with storage rails and manually operated loading device. The time for loading each reel with one man is about 3 minutes. Thus 10 hours are needed with one men only. By using a team of people (that can temporarily leave other work) a satisfactory arrangement is reached, loading the machine in 2-3 hours, attaining production targets. A robotized handling and loading system is already designed and installation will begin by end of 1990, this system will allow attaining also productivity targets.
Since a rigid system like the above outlined one can be vulnerable by mechanical or electrical failures, one additional group twister module is provided, in order to minimize the stop time for maintenance, and working for manufacturing spare pairs or sub-units for small size cable, during normal operation.
The complete line is controlled by a PLC and a controller reports on a display a written alarm condition like wire n°1 break, door not closed on machine n°2, etc. Otherwise an alarm lamp system would require at least 300 lamps for the same function.

TESTING FACILITY

All machines are fitted with in line controls, therefore major deviations are early detected and cared for, but transmission and electrical parameters should be measured on finished cables, according specifications, on statistical basis.
In order to reduce test time a computerized and fully automatic bridge was choosed, equipped with additional test frames. During measuring time (about 1 hour and half), the operator connects a second cable to the additional frames, thus saving about 1 hour in this operation.
We have found that, for about 130.000 km pair per month with an average pair count 400÷600 pairs the total measuring time (according specified percentage) is 18÷20 days on 3 shifts with one instrument.
Since the target is 200.000 km pair per month, a second instrument was ordered for delivery in the secon half of 1990.
The control of semi-finished products (E.G. 100 pair units), is performed at the process stage with a smaller bridge for low frequency characteristics, measuring 10 pairs on different sub-units on every 6 km length.
If a systematic defect is detected (E.G. due to improper twinning operation), it could be removed before starting the following work shift.
Continuity (opens), and defective contact (shorts), are other time consuming checks, to be carried out on finished cables on 100% of conductors.
For this task, automatic testers with pair sorting rotating heads were choosed. The pick-up speed is 11÷13 cores/second and the performance is complete check of 12 cables with 1200 pair count in 6 hours with 2 men. The productivity gain is at least 3 to 1 in man hour, compared with traditional ring-out technique.
Two set of each tester (continuity and defective contact) are used.

OTHER MACHINES

Conventional machinery like cable stranders, armouring lines, jacketing extruders and filling equipment were already available, or new ones were bought as complement and installed. In order to improve productivity, modifications were made with larger diameter pay-offs and larger size of rolls on tape applicators.

CONCLUSION - NEW DEVELOPMENTS

The main result is the possibility of manufacturing 100 pairs unit (base of almost all cables) starting with intermediate copper wire, with only 5 people per shift.
The main new developments is the handling and loading robot system, wich will be operational in 1991. Since the data of loaded reels are stored in the handling system computer, complete tracking and connection for quality management system is allowed.
Other development, already planned or in progress is the installation of additional machines for efficient production of smaller size cables.

ACKNOWLEDGEMENTS

The authors wish to acknowledge the advice of Dr. F. Montalti of S.I.P. on cable design and performance.

REFERENCES

(1) G. Paternostro "State of the art on telecommunication cables.Jelly Filled local telephone cables"
Paper of S.E.C.R.I. Symposium - SHANGHAI, 1986.

(2) F.W. Horn "Cable, inside and out"
Lee's ABC of telephone - CHICAGO, 1974.

(3) E. Esposito "Test and measurement parameters for telephone multipair copper cables"
I.W.C.S. Proc. ATLANTA, 1989.

Group of multiple pairing machines.

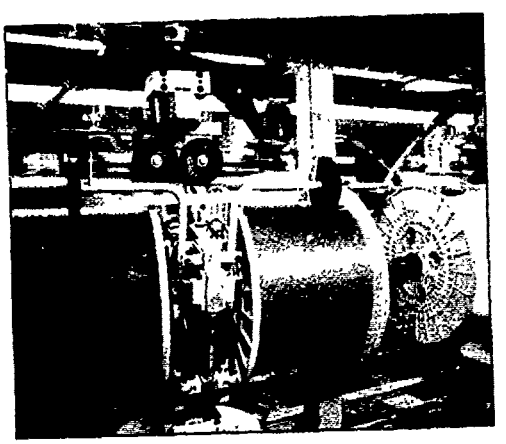

Detail of a multiple pairing machine.

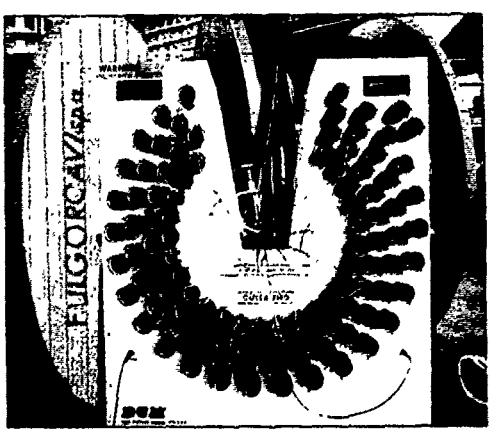

Automatic machine for measuring electrical and transmission parameters (including high frequency).

A.Marsilia
Manuli Cavi (Alcatel Cables Italy)
18 Via Crocefisso - 04100 Latina - Italy.

Antonio Marsilia was born in 1938 and received his Dott.Ing. degree in electronics engineering from Napoli univ.
He is corporate industrial and technical director of Manuli Cavi Group.
He is author of scientific and technical books and papers.

G.Paternostro
Fulgorcavi (Alcatel Cables Italy)
18 Via Crocefisso - 04100 Latina -Italy.

Giovanni Paternostro was born in 1946 and received his Dott.Ing.degree in electronics engineering from Roma univ.
He is manager for Telecomm Cables design and development of Manuli Cavi /Fulgorcavi Group.
He is author of technical papers and patents on cable process and measures.

INTRODUCTION OF A C.I.M. SYSTEM DEDICATED TO THE PRODUCTION OF POLYETHYLENE-INSULATED, COPPER-PAIR TELEPHONIC CABLES

B. Pugno A. Ragni

CEAT CAVI Industrie TORINO

Abstract

To operate with a CIM philosophy implies the ability to match technological and human resources within an organisation strongly predisposed towards overall company goals, as against specific operative objectives.

Such an approach must be considered within a much wider "Quality System" and requires a strong evolution of company culture.

The term "quality" does not only signify a better production and at lower cost, but above all it implies collaboration within the company and cooperation outside it.

It is in the light of this "Comaking" approach that a new CIM system for polyethylene-insulated, copper-pair metallic cables has been developed for the custom of SIP in the Ascoli Piceno plant.

The project is divided into several operational phases, amongst which the present phase is concerned with the control of each extrusion line and with its integration at department level.

The development plan foresees a horizontal broadening of the system, with a gradual extension to the whole production process and with vertical integration, this latter operation carried out in order to avoid mere "technological islands" and to obtain a full managerial supervision both of the qualitative and productive areas.

Nomenclature

SIP: Italian Telecommunic. Operating Company.
CCI: Ceat Cavi Industrie.
CIM: Computer Integrated Manufacturing.
JIT: Just in Time.
WIP: Work in Process.
ISDN: Integrated Services Digital Network.

Introduction

Following the massive development of telecommunication systems, there is a general trend within the industrialised world of instituting national networks through the introduction of ISDN systems. For this reason, while fully accepting the prediction of a strong growth in optical fibre cables for long and medium distances, it is just as evident that the distribution network shall still be predominantly based on copper-pair metallic cables, at least for the next ten years. In Italy, SIP has opted for the highest quality and reliability, able to sustain a transmission capacity of up to 2Mbit/s. Such a goal can be attained through the cooperation of client and supplier (Comaking). The requirement for this project follows from Sip's strong wish to modify radically the whole concept of industrial cable testing.

An industrial operation guaranteing quality means having to adapt the whole enterprise organisation to such "quality" production (Fig.1). It is thus absolutely vital to view such an undertaking not simply as a financial outlay, but as a positive advantage with beneficial returns, even in economics terms. Strategically, Quality signifies a lowering of the costs to be assigned to design, production and service. It may also be a means through which to increase the cable market value and to improve price policy.

By adopting the "quality warranty" concept over the entire productive and control cycle, the supplier will be required not only to analyse the conformity of the final product but also to certify the whole process.

There is a need to overtake the traditional system based on the control of the product at the end of the manufacturing process.

The quality of the product is the result of the quality of the manufacturing process.

The operational means to sustain a global quality philosophy have been identified to exist with in a system of automatic integration for the telephonic cables production units in Ascoli. Such a system has been designed by following the CIM philosophy.

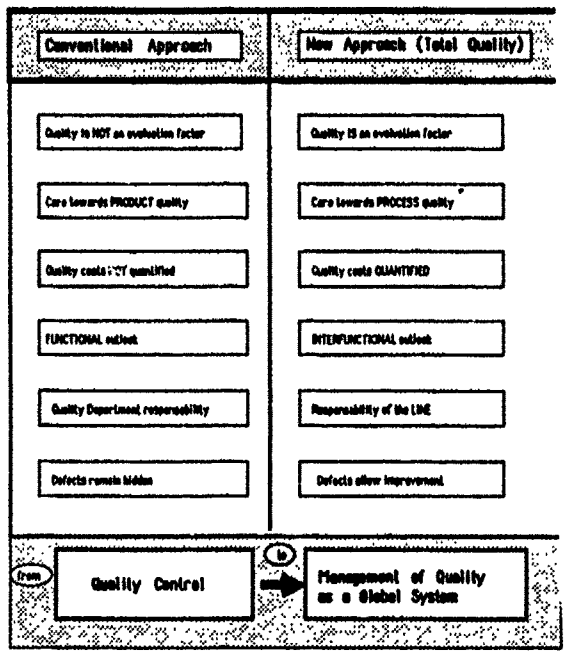

Fig. 1

CIM as Company Strategy

The ever-increasing demand for competivity in the world markets forces companies towards solutions aimed at compensating the general trends of product cost increases in parallel with working hours reductions. Already during the eighties, the search for efficiency has led to a massive introduction of computerised systems in the manufacturing field.

This event has actually led to swift improvements in production alone, though without any global benefit for the company.

In fact, the technological improvement of each manufacturing area cannot in itself be synonymous with efficiency for the whole productive cycle, as the latter is controlled by temporal and qualitative components (what, where and how to manufacture), these being all parameters which influence production costs. The concept of CIM (Computer Integrated Manufacturing) is based on the assumption that general enterprise benefits are not only obtained by investing in automation, but also by constructing a framework of organisational, architectural and methodological support around the automation itself.

After compiling and putting into practice all such preconcepts (doubtless an undertaking easier said than done), a whole series of goals may be deemed attainable:
-productivity increases
-reductions in scrap
-quality improvements
-an increase in flexibility
-reduction of resources lock-up
-optimum use of machinery
-shortening of delivery times

Obviously, such benefits vary in entity, mainly as functions of the costing structure of the sectors under review.

Benefits of CIM in the Cables Industry

The world market in cables has been estimated in 1988 as over 40 billion dollars. Future growth is predicted to be around 2-3% per year, excepted for telecommunication cables, where growth is estimated at a yearly rate of 7-8%.

The average manufacturing cost of cable can be divided into:
62% raw material
15% operator costs
15% machinery (including servicing, capital interest etc...)
5% buildings
3% interest on stock

It may be assumed that manufacturing costs amount to approximately 2/3 of sales volume.

According to a survey carried out on the major world cable manufacturers, savings varying between 6 and 22% were estimated (Figs. 2 & 3).

Such a wide spread of estimates clearly indicates that there are two different trends in the cable industry concerning the introduction of automation systems, one favourable, the other much less predisposed to it.

It is expected that the evolution of the cable market in the nineties will favour volume production in the telecommunication sectors, with the requirement for large-scale fusion in the manufacturing of such cables, while in the special cable area, requirements will instead lean more towards manufacturing flexibility, in order to produce small batches of a great variety of products.

Both these requirements may be satisfied the introduction of CIM systems.

The CIM system in CEAT CAVI Industrie

Firstly a CIM project must consider the relationships between responsible departments. In particular, the departments most directly involved in the project are the following: Commercial, Research and Development, Manufacturing, Logistics, Servicing, Quality, Stock Control, Organisation, Management, Planning, and Information Systems.

The key aspect to follow for a successful accomplishment of the project is the direct involvement of all the interested parties, with a full mandate from the Board of Management.

It is of paramount importance not to neglect the human component.

Thus, an investment in training is required, as is careful planning directed not only to the testing stage but also to the instruction stage.

Training also means involvement: to involve personnel in the analysis and definition phases is more important than simply to train the operator in the use of a system with which he will not feel at ease.

One of the most important factors is COMMUNICATION. This is the real bond, the "sticking material", akin to the "medium" which fluidifies the canvas dyes and enables painting to take place.

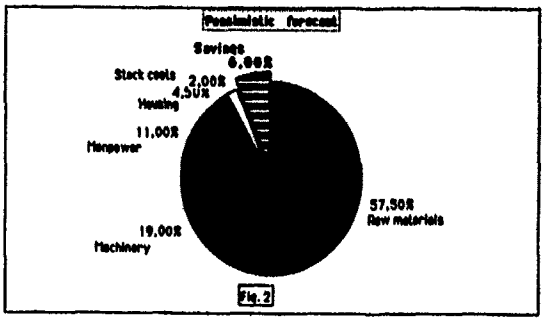

Fig. 2

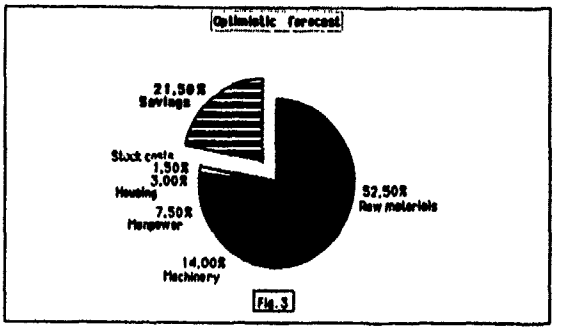

Fig. 3

The Communication factor must be followed carefully both in the definition phase and in the system realization.

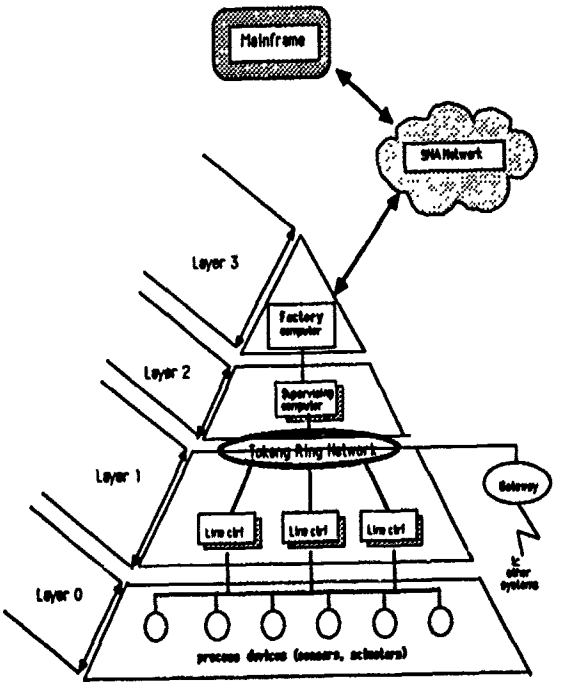

Fig. 4

In the first phase, communication is the means used to harmonise the requirements and requests of the various interested parties. It is strongly recommended that a proper analysis Methodology be followed, most of all to facilitate such a process. In the realisation phase, it is also fundamental to define a "system of communication" to support the varied elements which are part of a CIM system. However, the choice of Standards to conform with this trend is made arduous by the difficulty the market experiences in observing such parameters.

In order to make use of a common language, it is necessary to refer back to a model with schematic drawings of the concepts involved. For this, the pyramid model is generally accepted, having become a sort of "logo" for CIM systems. (Fig.4). In particular, within CCC the selected configuration is characterised by four levels:

-level 0: machinery
-level 1: production line/cell
-level 2: department
-level 4: plant

Level 0 (Machinery):
in this level belong all the "devices" strictly dedicated to operational activities, that is employed to guarantee the functionality of the machinery (sensors, actuators, PLC control, etc...)

Level 1 (Production line/cell):
by production cell one means an ensemble of machinery dedicated to the correct operation of a defined manufacturing function. The process is controlled and guided by a system of process management. Examples of production cells are wire drawing, insulating, armour etc.

Level 2 (Department):
corresponds to a group of several lines which cover the whole manufacturing cycle of a product. As an example, in the manufacturing of telephonic cables, the cycle is from the wire drawing stage to the final sheathing and cable testing.

Level 3 (Plant):
the plant level represents the point convergence of all the manufacturing departments. At this level a direct connection takes place with the managerial systems (Orders, Stock-taking, Total Quality, General Production Planning, Industrial Accountancy), and also with the Technical Systems (Material Bill and Technological Data).

Within the levels mentioned above, it is evident that the higher the level the greater the requirement for data processing. On the other hand, at low levels the main demand on the systems is to be capable of interacting in a synchronous manner with field activities and thus with data collection and transmission.

The Manufacturing Process.

The level of automation present on cable manufacturing machinery is still very limited at the present time. Some machines have installed an automation system for the loading, unloading and swapping of reels, for the purpouse of ensuring a continuous operation and to relieve the working load of the operators. However, nowadays other

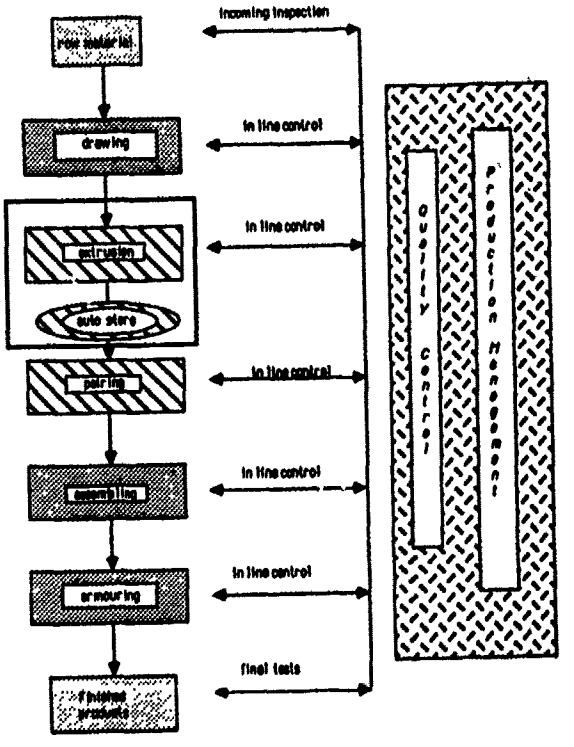

Fig. 5

machinery is available on the market, new machines which possess control devices designed to overview completely the setting of manufacturing parameters, as well as to manage the analysis and control of the activities relevant to manufacturing and quality.

From such a perspective, the Telephonic Department of the CCI plant at Ascoli Piceno may rightly be considered at the forefront of the technology, in as much as a sizeable funding plan has already been defined, in order to equip the plant with more advanced machinery to support sophisticated control systems.

The principal characteristics of the department are as follows:

- production capability of 1.8 x 10^9 m of copper-pairs/year
- a related labour force, including laboratory staff, of 180
- of copper-pair identification using seven main colours
- scrap of the order of 4.5%
- production period from beginning of manufacture to finished product 20 days.

The manufacturing process is represented in figure 5, where can be seen on a striped background the areas already equiped with advanced systems at levels 0 and 1. In the same figure, within the square border is visible the portion already connected to a level-2 supervision system.
The short-term plan is to extend the level-2 system to the whole striped area. In the medium term, plans are concerned with the completion of all level-2 functions and the integration of all supervision in a complete level-3 system. In the long term, it is foreseen to extend both the automation and the supervisory systems to the whole Department.

System Architecture

The system described is derived from the partnership between CCI and large swiss-finish producer of cable manufacturing machinery. In figure 4 the architecture of the system installed at Ascoli is shown schematically using a pyramidical model.

System components are the following:

-level-0 process and line controllers: on two extrusion lines and for the automatic store.

-local token-ring network

-level-2 area supervisor

As Yet, the area supervisor (PC 386 IBM compatible) is not connected to the superior level, from which it would receive the manufacturing plan. Thus, it presently allows the loading of "operational orders" both for each product type and as a function of a secondary parameter (typically the colour of the extruded component). Therefore, operational "suborders" are generated by the supervisor. Each order is associated to an execution priority and a current state. By activating the manufacturing process, the system selects automatically the available resources (lines) and unloads the operative sequence on the best-suited one.
The system is completely parameter-defined, and it is thus possible to obtain a balance between the functionality of specific resources, the requirement for basic semi-finished products and the need to minimise any production change.
Through the system, real-time monitoring is available for a dozen production/quality parameters related to the networked lines.
A series of reports are being produced at the present time, concerned with production and quality, aiming to synthesise data from all the lines connected to the system.

At extrusion line level, the controllers are based on programmable control and on industrial IBM compatible PC.

Principal characteristics are:
-process management through programmable control for the active elements of the manufacturing line;
-local managing of production and quality using industrial PC, with a ligh flexibility and adaptability;
-ease of use for the operator, able to communicate with the machine through a colour -touch-screen and understandable graphics.

Instead, the automatic store controller is based on a micro PDP from DEC, also equipped with multiple local functions.

At any rate, the global System also allows the netwcrking and thus the integration of disparate level-1 elements through gateways.

In its integrity, the system offers multiple advantages:

-optimisation of line efficiency and of product quality, independently from the ability and qualification of the operator;
-continuous line supervision;
-memorising of many product manufacturing specification, thus enabling changes in production considerably faster than at present;
-continuous control and recording of product quality, with complete documentation.

The development plan for the system foresees the extension to the whole manufacturing process, so as to:
-balance the best way possible the resources of each stage on the grounds of scheduling requirements
-increase the interchangeability of plant flexibility
-reduce/eliminate intermediate stocks
-associate quality and production data to each batch of completed products, and not only to each manufacturing stage (total trace ability)
-notify immediately process anomalies, in order to prevent scrap formation.

In fact, it is clear that only total management enables the desired objectives to be attained.

Bruno Pugno was born in Asti, Italy, in 1951. Graduated from Turin University in 1975, he has been experienced in data processing area as well as in manufacturing automation environment in different Companies. Since 1987 he has been Responsible for the Information Systems and Automation Dept. at CCI in Turin.

Attilio Ragni was born in Perugia, Italy, in 1952. A graduate of Turin Polytechnic (1976), he has gained experience in optical fibre technology, as well as in telecom cable design and process development. Since 1987 he has been responsible for telecom cable R & D at CCI in Turin.

ARAMID TAPES AS ANTI BALLISTIC PROTECTION OF AERIAL OPTICAL FIBRE CABLES

Sjaak J.B. Bensink, Willem W.J. Dekker

AKZO Fibres and Polymers, Arnhem, Holland

ABSTRACT

Aerial cables - particulary metal free Optical Fibre Cables - are sometimes damaged by hunters using the cables to adjust their guns or to shoot birds. This not only can lead to a decrease of signal transmission inside these cables, but even sometimes to a total loss of the cable installed. Even an Optical Fibre Cable with longitudinal aramid as strength member can be damaged by shotgun pellets. In order to reach good antiballistic properties, tighter constructions, like woven tape, are needed. As a result of an extensive testing program, we have found that 2 Twaron aramid tape layers, of 550 g/m^2 each, offer good antiballistic protection, under severe circumstances.

INTRODUCTION

Aerial Optical Fibre Cables generally contain dielectric materials only. The use of such materials instead of metals has been found to reduce installation and maintenance costs. In addition, the cable is less susceptible to corrosion and is lighter. However, recent observations revealed there are some negative side-effects to this choice of dielectric materials. In some countries, aerial cables appear to be used as a target by private hunters, adjusting the range of their guns or simply shooting birds. In the case of dielectric cables, this not only can lead to loss of optical transmission inside these cables, but sometimes also to total breakage of the installed cables. It will be clear that risks as referred to above, call for the development of shotproof cables.

TWARON ARAMID AS SHIELDING MEMBER

A well-known material used for anti-ballistic purposes (bullet proof vests, armored shields etc.) is Twaron aramid yarn in the form of woven fabrics. Therefore, we tested three different cable constructions based on a design containing such fabrics. With the development of the anti ballistic protection we have kept in mind that:

1.
The ballistic protection has to be an element adapted to the methods of processing and construction typical to the cable industry.

2.
Technical and economical aspects ask for a protection as thin as possible and having the lowest possible weight.

3.
The protection has to be considered as an independent element, with a function, different from that of the reinforcing elements, such as the central strength member and peripheral aramid yarns. A ballistic impact - even if the protection has been damaged - should not harm the long term tensile properties and modulus of the cable.

RESULTS

After extensive weaving, shooting, and processing trials, we have come to the following conclusions:

1.
A longitudinal aramid strength member is **not** suitable as an anti ballistic shield. Since the aramid yarns are partly damaged (see pict. 1), the long term properties of the cable are also harmed.

2.
For a good ballistic protection two layers of Twaron anti ballistic tape are required:

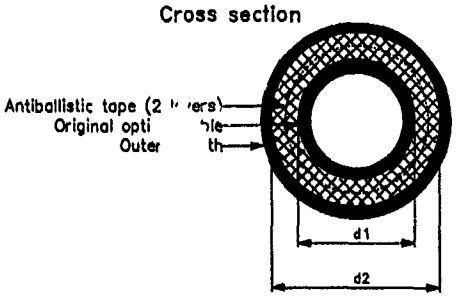

The two layers can be either cross wound or positioned parallel to the cable axis:

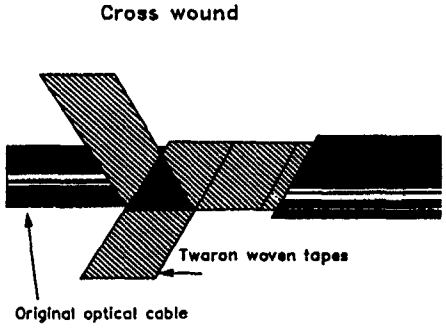

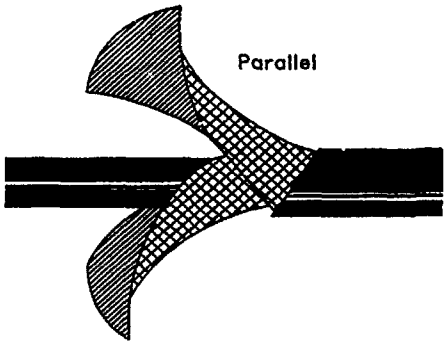

3.
The following tape construction gave a **good** ballistic protection: (see pict. 2).

Yarn : Twaron type 1040, 1260 dtex
Warp : 24 yarns/cm
Weft : 17 yarns/cm
Weave : Twill 2/1
Weight: 550 g/m^2 per tape
Layers: 2

Excellent ballistic protection (see pict. 3) was obtained using:

Yarn : Twaron type 1040, 1260 dtex
Warp : 28 yarns/cm
Weft : 18 yarns/cm
Weave : Twill 2/1
Weight: 630 g/m^2 per tape
Layers: 2

4.
The amount of aramid for a **good** ballistic protection is about 40 g/m for a cablediam. of 10 mm, and about 80 g/m for a diam. of 20 mm.

Picture 1 Only aramid as a longitudinal strength member.

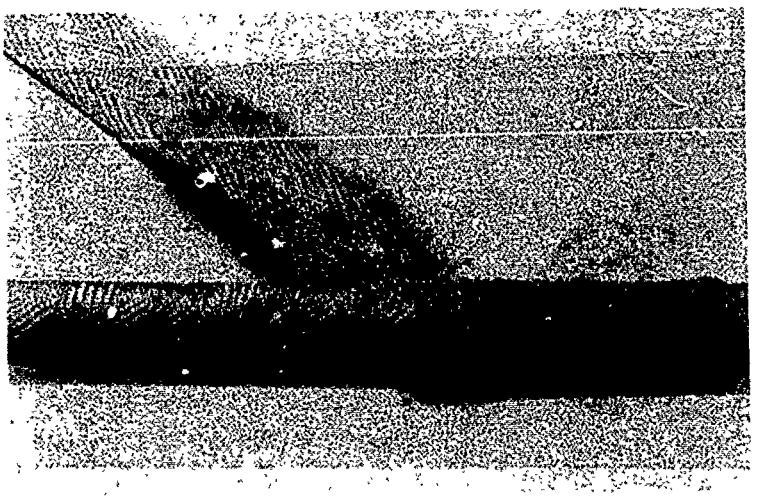

Picture 2 Two layers of tape of 550 g/m2.

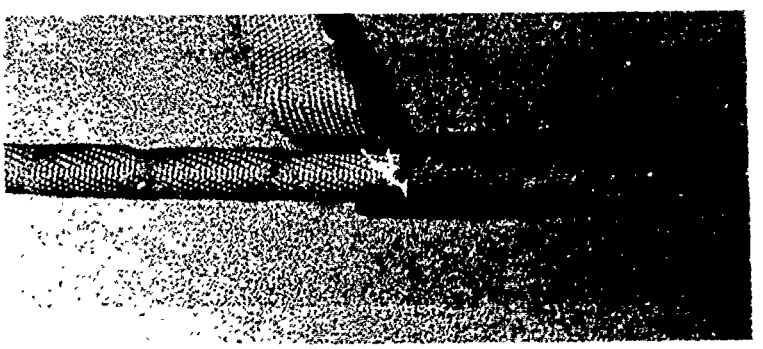

Picture 3 Two layers of tape of 630 g/m2.

CABLE SAMPLES

Three cable types were tested. Each of them contained 6 optical fibres in a loose tube design. Except for one, all samples contained one or more aramid yarn layers as longitudinal strength members (These members absorb linear, radial and flexural loads during production and installation, and in practical use). Cable type A contained no aramid reinforcement at all:

Cable type A

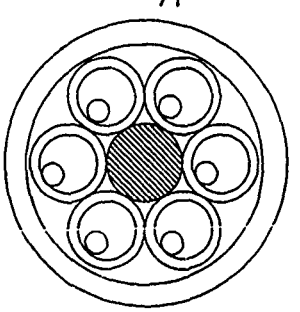

Cable type A was covered with 1-3 layers of Twaron woven tapes, spiraled around the cable by hand and subsequently covered and bound by a heat-shrinkable tube. Types B and C contained aramid yarns as a strength member (longitudinal to the cable axis), but were not covered with Twaron woven tapes as we wished to test their antiballistic behaviour without the ballistic tape.

Cable type B

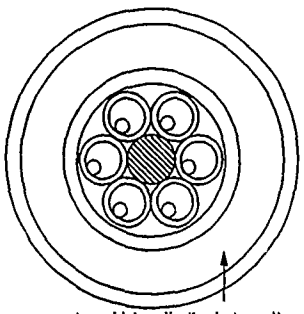

Cable type C

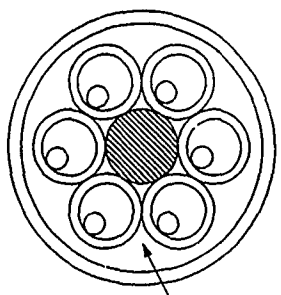

SHOT TYPE AND SIZES

On the basis of the common denominator of all recorded cases we chose 2 3/4" Remington 1 1/8 oz. cartridges, of 12 gauge, containing 6 or 8 size lead pellets or steel pellets in size 4 or 6. The number of pellets contained in these different shot sizes are approximately:

	Shot size	Pellets/charge	Recorded velocity
Shot type S	4	152	405 m/sec
[Steel]	6	253	402 m/sec
Shot type L	6	253	395 m/sec.
[Lead]	8	462	387 m/sec.

In practice, the choice of lead and steel is governed by regulations that vary per country. Compared to a lead pellet of equal size, the energy transferred from a steel pellet to a cable is basically higher. This is accounted for by the fact that all the energy of a steel pellet is absorbed by the cable. The energy of a lead pellet is partly absorbed by the pellet itself due to its deformation. Therefore, we decided to use both steel and lead pellets in different shot sizes.

DISTANCE BETWEEN CABLE AND SHOT-GUN

Normally the distance between hunter and prey will be such that the prey will not be scared off before being shot at. Nevertheless, for our tests we have chosen a distance of only 15 meters to ensure that enough pellets hit the cable.

TESTING OF THE CABLES

The shooting trials have been carried out at the government institute:

Staatliches Beschussambt
Mellrichstadt
Bundesrepublik Deutschland

The target area had a cross section measuring approximately 1.5 m. In this area, a cable loaded by 5 kg was suspended vertically:

Test unit for ballistic evaluation

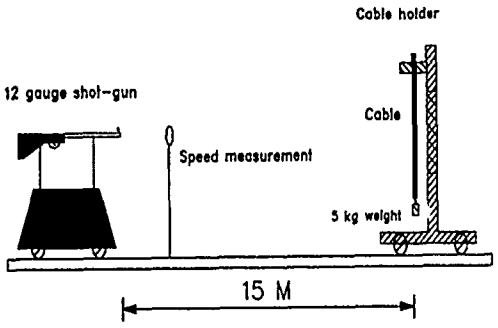

Every cable was tested with one shot size and type. The results were analyzed on the basis of photographs of the cable layers after the outer sheaths had been peeled off. From samples containing Twaron woven fabrics, we removed the heat shrunk tubing and one or more layers of fabric to examine the optical cable itself for any damage. The test results showed whether a cable containing optical fibre units had been damaged. Where no damage was observed, the aramid yarn and tape layers had been analyzed for penetration by the pellets. For every shot, the speed of the pellets was measured by means of two photodiodes.

COMMENTS

We ensured that each sample was hit by enough pellets in the protected area for us to be able to draw valid conclusions. Some of the cables were therefore shot at twice.

TEST RESULTS

CABLE TYPE A:

A cable without ballistic protection (and also without longitudinal aramid strength member) is damaged completely by any shot. (see pict. 4). Not only the outher sheath has been penetrated but all inner parts of the cable - loose tubes, optical fibres etc. - have also been severely affected.

Good ballistic protection is obtained by 2 layers of tape of 550 g/m^2. The pellets have penetrated the cable up to the inner sheath. The dents that were subsequently formed in the inner sheath sometimes showed minor cracks. The inner part of the cable, however, is free from damage (pict. 2).

Excellent ballistic protection was obtained using a tape of 630 g/m^2 in weight. The inner sheath nor the optical fibres were damaged at all (pict. 3).

CABLE TYPE B and C:

The longitudinal aramid strength member has a very limited antiballistic behaviour. Since the aramid yarns are partly damaged (see pict. 1), the long term properties of the cable are also harmed!

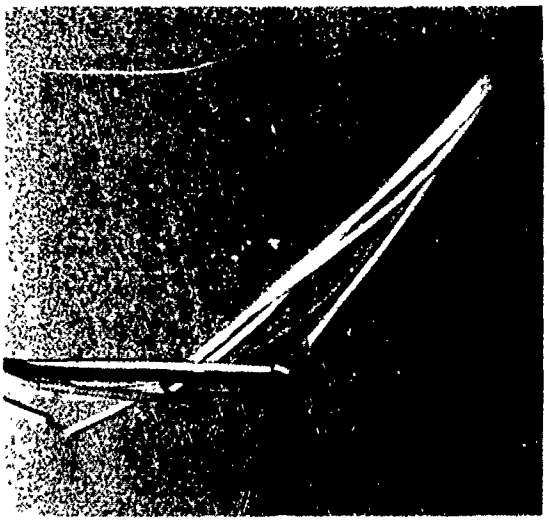

Picture 4 No ballistic protection.

DISCUSSION

This study has shown that a two layer Twaron aramid tape construction of 550 g/m^2 per tape offers a good antiballistic behaviour under severe circumstances (short shooting distance). In practice it may be possible that a lower tapeweight per m^2 may also have sufficient ballistic properties. Apart from this a reduction in tapeweight (without reduction of the antiballistic properties), may also be realized by using a 1/1 weave instead of the used 2/1. New experiments are being carried out to check this.

Sjaak J.B. Bensink
AKZO Fibers & Polymers
P.O. BOX 9300
6800 SB ARNHEM
HOLLAND

Sjaak J.B. Bensink was born i. 1960 and received his B.E. degree in Mechanical Engineering at the Technical Highschool Arnhem in 1985. From 1985 to 1990 he worked as a Processing Engineer at AKZO's Industrial Fibres Institute in Arnhem. Since June 1990 he is working as a End-use Development Engineer Optical Fibre Cables.

Willem W.J.Dekker
AKZO Fibers & Polymers
P.O. BOX 9300
6800 SB ARNHEM
HOLLAND

Willem W.J. Dekker received his Physics Degree at the Technical Highschool in 1981, and joined AKZO that same year. He performed Basic Research on Laser Induced Chemical Processes and later joined the AKZO Fibres & Polymers group. Since 1984 he worked with Twaron Aramid Fibres in Braided Packings and Optical Fibre Cables. He is currently working in production facilities for Conventional Synthetic Fibres.

Two-point bending apparatus, fracturing optical fibres at different speeds in one run; measurements in standard and vacuum environment

W. Griffioen, G. Segers and E. van Loenen

PTT Research, P.O. Box 421, 2260 AK Leidschendam, The Netherlands

Abstract

A two-point bending dynamic fatigue testing apparatus, in which in one run 5 sets of 10 fibres can be fractured at 5 different speeds, is described. Measurements are reported on standard and carbon-coated fibres at room conditions. The apparatus can also operate in vacuum as well as at low temperatures. Measured inert strains of 17% after 5 days in vacuum agree well with existing two-point bending results at liquid nitrogen temperatures. Fibre lifetime predictions are discussed.

Introduction

In many countries high investments have been made in optical fibre cables. In the future the investments are expected to increase rapidly, mainly due to installation of the 'last mile'. It is of great importance that the lifetimes of the optical fibre cables are sufficiently long. An important possible failure cause is fracture of the fibres due to stress induced crack growth [1]. This crack growth depends on environmental conditions and on stresses at the fibre surface, in most cases caused by bending of the fibre in the cable structure.

In many laboratories fatigue experiments, in which fibres are fractured, are carried out in order to get information about the corrosion process. Two lifetime models that relate results from laboratory experiments with lifetime at service conditions are commonly used In the 'Prooftest Compared Aging' (PCA) model, information from the manufacturer about failure and environmental condition during prooftest as well as information about the weak flaw statistics is necessary [2]. Estimated lifetimes hence strongly depend on knowledge about the production process. The 'Crack at Prooftest Level' (CPL) model does not need manufacturers information (except prooftest level), but requires knowledge of both corrosion-speed scale-factor B and corrosion-susceptibility n [3]. To obtain B and n separately, not only fatigue measurements, but also measurements of the inert strength, defined as the strength before crack growth can occur, must be carried out. Different techniques to measure inert strength, known from literature, result in CPL lifetime predictions varying five orders of magnitude [4,5,6].

Inert strengths can only be measured by means of dynamic fatigue experiments, since in static fatigue experiments no fracture occurs due to the absence of crack growth. A two-point bending dynamic fatigue apparatus is developed for our experiments. In one experimental run 5 sets of 10 fibres are fractured at 5 different speeds, in an environment which is the same for all fibres. Results are presented as a function of vacuum (removing "agressors", necessary for a crack to grow) exposure time Measurements at low temperatures are in preparation in our laboratory. Measured inert strengths are compared with results from literature using low-temperature bending and using low-humidity and high strain-rate pulling techniques [4,5,6]. Furthermore, measurements on standard and carbon-coated optical fibres at room conditions will be presented. Results are discussed using the PCA and CPL lifetime models.

Lifetime estimation

Optical fibres made from silica glass consist of ring structures of SiO-tetrahedrals. The mechanical bonds of these tetrahedrals should result in a strength (= maximum stress) of 20 GPa. The stress concentration at crack tips, characterized by the stress intensity factor $K_I = Y\sigma\sqrt{a}$, in which Y is a geometrical factor, a the crack depth and σ the applied stress, causes the fibre to fracture at lower stress levels [1]. Fracture occurs when K_I reaches the critical value of $8 \times 10^5 N/m^{3/2}$ [4]. For an elliptical crack Y is 1.24 [4]. Hence a unique relation between crack depth and strength exists.

In practice lower strengths are observed than would follow from the relation between crack depth and strength. Moreover the strength of optical fibres depends on time. This can be explained by crack growth due to a stress induced chemical reaction (dissociative chemisorption [7]) which breaks the bonds. The stress is largest at the crack tip. This means that it is not only of importance how corrosive the aggressor is, but also what its size is, in order to fit in the crack tip. Water and ammonia turn out to be most dangerous for stress induced corrosion of silica glass [7]. Corrosion of silica glass is usually described by a power law in which the crack growth da/dt is proportional to K_I^n, with n the corrosion susceptibility [1]. It can be derived that, for fracture at a level sufficiently below the inert strength σ_i, the following equation holds approximately.

$$\sigma_i^{n-2} = \frac{1}{B}\int_0^{t_f} \sigma^n(t)dt \qquad (1)$$

In this equation $1/B$, which is a function of n, is a scale factor for the speed of crack growth, and t_f is the time to fracture. For static stresses, $\sigma(t) = \sigma_s$, the time to fracture t_s follows.

$$t_s = B\sigma_i^{n-2}/\sigma_s^n \qquad (2)$$

For dynamic stresses which increase linearly with time, $\sigma(t) = \dot{\sigma} \cdot t$ the strength σ_d at fracture can be derived in a way similar to the derivation of equation 2.

$$\sigma_d = \left[\dot{\sigma}(n+1)B\sigma_i^{n-2}\right]^{\frac{1}{n+1}} \quad (3)$$

Using equation 2 and 3 it can be seen that only n and $B\sigma_i^{n-2}$ can be derived from laboratory measurements at different stress levels (or rates). B and σ_i cannot be found separately. In other words: it is not possible to distinguish between fast growing small cracks (low B, high σ_i) and slowly growing large cracks. Extrapolation from short time, high stress laboratory measurements to long time, low stress service conditions, using formula 2, is not possible because more than one kind of crack distribution exist. One crack distribution (intrinsic) is due to the cooling of the fibre when it is drawn from the preform and is uniformly distributed, also for short pieces [3]. Another crack distribution (extrinsic) can have many causes, such as dust particles from the fibre drawing furnace, which usually gives larger cracks than those from the intrinsic distribution. Depending upon the production technique the number of these weak flaws can vary from several per kilometer until 'almost complete elimination' [8]. The distribution measured for short lengths in laboratories will hence not be the same as that which causes failure in service.

During a prooftest the weakest flaws are eliminated. The prooftest level σ_p can also be used to estimate lifetimes of the fibres in service. In the 'Crack at Prooftest Level' (CPL) model, it is assumed that after prooftest always a crack exists, which corresponds to the prooftest level [3]. Using equation 2 the (minimum) time to failure t_{CPL} is found.

$$t_{CPL} = B\sigma_p^{n-2}/\sigma_s^n \quad (4)$$

In the CPL-model it is necessary to know the B-value. This value can be obtained from the value $B\sigma_i^{n-2}$, measured in the laboratory, if the inert strength distribution of the fibres before fracture is known. For the CPL-model thus additional inert strength measurements are necessary.

In another model, the 'Prooftest Compared Aging' (PCA) model, the aging at prooftest during time t_p is compared with aging in service [2]. Using statistical information, such as the failure rate F_p at prooftest and the distribution of weak flaws, characterized by the Weibul parameter m_{ex} (extrinsic), an estimation of the lifetime t_{PCA} at given failure rate F_s in service follows [2].

$$t_{PCA} = t_p \cdot \left(\frac{\sigma_p}{\sigma_s}\right)^n \cdot \left[\left\{1 + \frac{ln(1-F_s)}{ln(1-F_p)}\right\}^{\frac{n-2}{m_{ex}}} \cdot (l+C) - 1\right] \quad (5)$$

In this equation, which is derived for equal lengths for prooftest and service at which the failure rates are defined, C is equal to $B/(\sigma_p^2 t_p)$. In this model also the value of B must be known. The inventors of the PCA-model argue that C is always much smaller than 1 and can be neglected, eliminating the need to know the value of B [2]. A value of C much smaller than 1 is however not a sufficient condition for neglecting C in equation 3. This may only be done if also C is much smaller than $(\sigma_s^n t_s)/(\sigma_p^n t_p)$, or in other words: $t_s \gg t_{CPL}$. Fortunately, since a value C of zero always gives the smallest lifetime, the PCA-model can be used as a worst case model, without the need of knowing B. A disadvantage of the PCA-model is the dependency on manufacturers information. The Weibul parameter m_{ex}, which can only be obtained by measuring very long lengths of optical fibre depends strongly upon changes in the production process. The failure rate F_p at prooftest is not always supplied by the manufacturer. Furthermore the environmental condition during prooftest, assumed to be equal to that in service in the PCA-model, can differ significantly from the service environmental condition, even when specified equal. Immediately after drawing and coating of the fibre the surface of the quartz will be very dry. Since moisture from outside needs a certain time to reach the quartz surface through the primary coating, the time between drawing of the fibre and prooftesting is of importance too.

Inert strength

Inert strength is defined as the strength of the fibre before crack growth can occur, and is uniquely related to the depth of the largest crack of the tested piece. In order to measure inert strength it is necessary to reach the level of fracture in a time short compared with the time that a crack needs to grow. Once reaching the inert strength test conditions, the strengths should be independent of the speed at which the fracture level is reached, and this independence is hence a good criterion to recognize inert condition. When the environmental conditions, such as water, do not contribute significantly to the stress concentration near the crack tip, which is most likely, the environmental conditions at which the inert condition is reached is not of importance. Different inert strength measuring techniques should hence be comparable. The first known method is reducing the reaction speed of the aggressor by means of low temperatures, e.g. liquid nitrogen [5]. The second method is to remove the aggressor by using low humidity or vacuum [4]. The third method is high speed pulling [6].

Apparatus

In order to compare inert strength measurements at low humidities with those at low temperatures, a two-point bending technique [9] is developed which will operate under both environmental conditions. With this technique a fibre is placed between grooves in two parallel plates in a 'C-shape', the 'C' in a plane perpendicular to the plates. When the distance between the plates is reduced the curvature of the fibre, which is maximum just in the middle between the plates, increases until fracture occurs [9].

In figure 1 the experimental setup for the two-point bending dynamic fatigue measurements is shown. Five moving plates, each with ten fibre-fixing grooves, can move towards five grooved static plates. The fibres are placed between the plates in ten parallel 'C-shapes'. The moving plates are pushed by three driving-bars which are connected to a slide with special bearings, driven by an 'in vacuum' stepper motor [10]. Just before a set of plates touch, and after the fibres between those plates have fractured, the moving plate is disconnected from the three driving-bars by means of unlocking pins. With this construction it is possible to close the different plates at different times. The construction is such that turning over of the moving plates is avoided when fibres are breaking asymmetrically (at one side of the plate first).

With the apparatus described, it is possible to fracture five sets of ten fibres, each with five different speeds in a single experi-

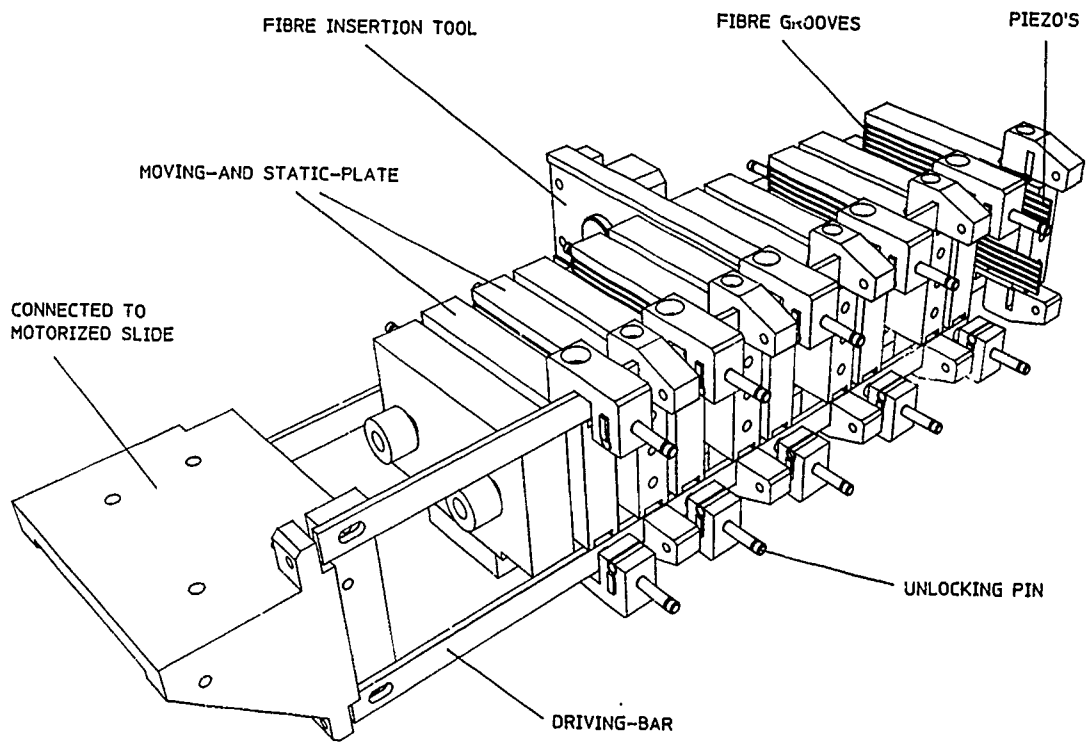

Figure 1: Two-point bending dynamic fatigue testing apparatus. Five moving plates, each with ten fibre fixing grooves, can move towards five grooved static plates. Using an unlocking pin mechanism the plates can close at different times, allowing different speeds at which the fibres between the plates fracture.

mental run. The fracturing of the fibres is detected by means of individual piezo's. A special tool is used in order to insert the fibres between the plates at a fixed position This is necessary to assure correct detection of fracturing fibres with the piezo's. The piezo's are connected to a control unit. After detecting the fracturing of all the fibres between a set of plates at a certain speed, this unit immediately changes the speed of the driving-bars to the next speed The apparatus is constructed in such a way that when a set of plates is closed, the distance between the next set of plates is 4 mm. This means that at the time that the fibres between the first set of plates have fractured at plate distance x and the speed of the driving-bars is changed, the distance between the next set of plates will be x + 4 mm. Since x is always less than 3 mm in our experiments, the crack growth of the fibres between a set of plates (with x + 4 = 7 mm) before the speed of the driving-bars is changed, can be neglected with respect to the crack growth at the next speed (until x = 3 mm), as can be understood by comparing the lifetimes using formula 2

In order to calibrate the apparatus several experiments, with all the moving plates at the same speed, have been carried out. The information is used to correct the values of the counter of the stepper motor at which the plates are closed A reproducibility of median values of the plate-distance of 5 μm is achieved. This is less than the 'natural' spreading of 10 μm (corresponding to a Weibul parameter m of the order 100 [9]) of the optical fibres. The individual fracturing of the fibres can be studied with the described apparatus. Fracturing neighbours are not found to influence eachother. 'Chain-fracturing at one side', which would occur when the plate turns over when fibres at one side of the plate fracture first, is also not observed.

Experimental results

In figure 2 a typical Weibul plot of (maximum) fracture strains ϵ_{max} [9], obtained with our equipment, is shown. The fibre A is a UV-acrylate coated monomode fibre which is taken from a 20°C and 75 % RH environment. A set of measurements with five different plate speeds, is carried out in only one hour, including the time to insert the fibres between the plates. Weibul parameters m ranging from 50 to 70 have been measured, which agree well with experiments performed in other laboratories [9].

In figure 3 the median fracture strains of the same fibre A are plotted as a function of the plate speed. From the slope a corrosion susceptibility n of 20 is deduced. Measurements on UV-acrylate coated fibre B (stored at unknown environmental condition) show somewhat higher strengths and a higher n-value of 30. In figure 3 also the results of measurements on two types of carbon coated fibres, C and D, are shown. Within the accuracy of the measurements an n-value of ∞ ($|n| > 200$) is found, which agrees well with dynamic pulling fatigue experiments on those fibres [11]. Bending experiments, performed in another laboratory [12], show however lower n-values for carbon coated fibres, ranging from 45 to 65. Our measurements show initial strength weakening (at low speeds) of the carbon coated fibres, which is also observed in dynamic pulling measurements [11]. The two-point bending strengths of these fibres are however larger than those measured with dynamic pulling experiments of the suppliers [13]. Surprisingly high bending strengths are also found in another laboratory [12]. It is possible that the deposition process of the carbon coating creates weak flaws, which are not measured

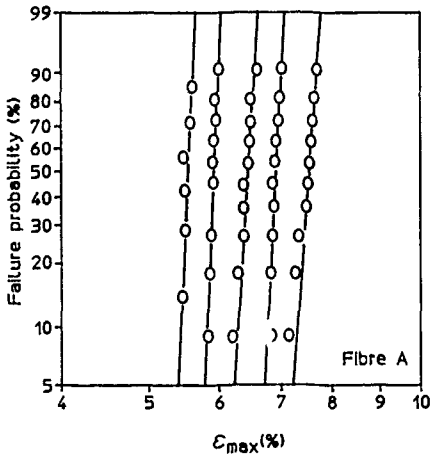

Figure 2: Weibul plot of fracture strains obtained with two-point bending dynamic fatigue measurements at different plate speeds on standard fibre A, taken from a 20°C and 75% RH environment.

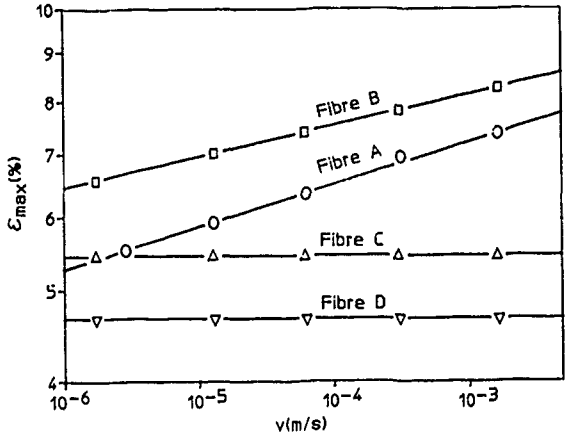

Figure 3: Median fracture strains obtained with two-point bending dynamic fatigue measurements on fibres taken from an 20°C and 75 % RH environment (except fibre B) as a function of plate speed. Fibres A and B are UV-acrylate coated fibres, while fibres C and D are additionally carbon coated.

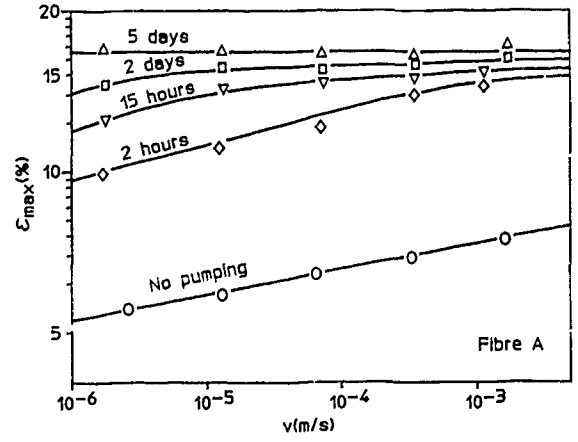

Figure 4: Median fracture strains obtained with two-point bending dynamic fatigue measurements on UV-acrylate coated fibre A as a function of plate speed, for different pumping times.

by the two-point bending technique, due to its short measuring length. More detailed investigation to the length dependence of the strength of carbon coated fibres is recommended. It should be mentioned that also carbon coated fibres with strengths comparable with those of standard coated fibres are produced [14].

In figure 4 the median fracture strains of standard fibre A, obtained with two-point bending, as a function of the speed at which the plates approach, are shown for different pumping times. A vacuum of $5 \cdot 10^{-5}$, 10^{-5}, $5 \cdot 10^{-6}$ and $3 \cdot 10^{-6}$ mbar is reached after pumping during 2 hours, 15 hours, 2 days and 5 days respectively. Before pumping, at every experiment the fibres are taken from a 20°C, 75 % PH environment. Only after pumping for five days the strengths saturate at a speed independent level of 17 %. This value is close to the value which is obtained by two-point bending in liquid nitrogen [5].

Reported inert strengths, measured with pulling at -40°C bone-dry-grade CO_2 environment [4] and with high speed pulling [6] are a factor of two lower than obtained by us. It is however not known during what time the fibres of the first mentioned reference were stored in the inert environment, which according to our measurements is very important. The reported high speed pulling inert strengths were not reached in the experiment, but were obtained from extrapolation of the deviations from the linear relation between log(strength) and log(speed) at the highest speeds [6]. It should be noted that in our two-point bending measurements maximum stress rates of 70 GPa/s are reached, differing only one order of magnitude from the value reached in the high speed pulling experiment [6], while the inert strength is far from reached in our experiment at standard condition. Differences in inert strengths may also be explained by a different behaviour in pulling and bending. It is suggested to perform high speed pulling measurements in a more inert environment and compare measurements with bending, using the same fibres.

Analysis

In figure 4 the fracture strains of fibre A are given as a function of the speed v at which the plates approach eachother. With two-point bending the stresses of the fibre do not increase linearly with time when v is constant. First there is a non linear relation between the stress σ and the strain ϵ of an optical fibre, $\sigma = E_0(1 + \frac{1}{2} \cdot \alpha\epsilon)\epsilon$, in which $E_0 = 72$ GPa is the Young's modulus at zero strain and $\alpha = 6$ is constant [15]. Then there is the relation between the (maximum) strain of a fibre, bent between plates, and the plate distance d_{plate} : $\epsilon = 1.198 \cdot d_{fibre}/d_{plate}$, in which d_{fibre} is the diameter of the (uncoated) fibre [9]. Using equation 1, neglecting higher order non linear elastic terms and assuming constant v from a plate distance sufficiently larger than that at fracture, a relation between fracture strain ϵ_d and plate speed v, similar with equation 3, is obtained.

$$\sigma_d = E_o(1 + \frac{1}{2} \cdot \alpha\epsilon_d)\epsilon_d = \left[\frac{v(n-1)B\sigma_i^{n-2}}{1.198 \cdot d_{fibre}E_o}\right]^{\frac{1}{n-1}} \qquad (6)$$

Solving the quadratic equation for ϵ_d, an expression for the slope S in figure 4, which is $d\log(\epsilon_d)/d\log(v) = v/\epsilon_d \cdot d\epsilon_d/dv$, is found.

$$S = \frac{1 + \frac{1}{2}\alpha\epsilon_d}{1 + \alpha\epsilon_d} \cdot \frac{1}{n-1} \qquad (7)$$

Using this equation, from figure 4 an n-value of 20 is found for fibre A without pumping. With equation 6 and figure 4 again, from which both $B\sigma_i^{n-2}$ and σ_i are obtained, a B-value of $1.3 \cdot 10^{-8} GPa^2 s$ is found when n is 20.

As an example to calculate the lifetime, the following additional information is used: $F_p = 2\%, F_s = 1\%$ (both for 1 km), $m_{ex} = 10$ (worst case known from literature), $t_p = 1s$ and $\sigma_p = 0.7$GPa. When σ_s is taken at one third of σ_p, the PCA model gives a lifetime of 118 years. In order to guarantee CPL lifetimes of 30 years, σ_s must be of the order of one seventh of σ_p.

Conclusions

A two-point bending dynamic fatigue apparatus, in which five sets of ten fibres can be fractured at five different speeds, is described. With this apparatus the corrosion susceptibility n of fibres can be measured in one short experimental run. Standard and carbon coated fibres are measured in 20°C and 75 % RH environment, resulting in n-values from 20 to ∞ ($|n| > 200$). The bending strengths of the carbon coated fibres are somewhat higher than their pulling strengths, known from literature. The described apparatus can also operate in vacuum and liquid nitrogen (experiments in preparation) environment. It took five days of pumping at room temperature to reach an inert strain of 17%, close to the liquid nitrogen value, known from literature. Using this information, a B-value of $1.3 \cdot 10^{-8}\ GPa^2 s$ is found when n is 20. Hence the CPL lifetime model, which doesn't contain uncertain production process parameters, results in a lower allowable service stress of 1/7th of prooftest, than the value of 1/3th of prooftest, obtained when the PCA lifetime model is used. Further research, studying the discrepancy with inert strengths obtained from high speed pulling measurements, is recommended.

References

1 A.G. Evans, S.M. Wiederhorn, "Proof testing of ceramic materials- an analytical basis for failure prediction", Int. J. Fract. 10 (1974) 379.

2 Y. Mitsunaga, Y. Katsuyama, Y. Ishida, "Reliability assurance for long-length optical fibre based on proof-testing", Electronics Letters, vol.7, no. 16 (1981) 567.

3 Th. Staub, P. Laeng, "Mechanische Eigenschaften und Dauerverhalten von Glasfaser für die optische Übertragungstechnik", Bull. SEV/VSE (1986)7, P.361.

4 D. Kalish, B.K. Tariyal, "Static and dynamic fatigue of a polymer-coated fused silica optical fiber", J. Am. Ceram. Soc. (USA) 61 (1981) 518.

5 W.J. Duncan, P.W. France, K.J. Beales, "Effect of service environment on prooftesting of optical fibres", Proc. 7th ECOC (1981) 4.5.

6 T. Svenson, "High strain-rate testing of optical fibres", Proc. 37th IWCS (1988) 217.

7 T.A. Michalske, B.C. Bunker, "The fracturing of glass", Scientific American, december (1987) 78.

8 S. Ito, H. Sato, F. Mizutani, K. Tsuneishi, H. Kanamori, "Fabrication of long length, high strength single mode fiber by VAD process", Proc. 12th ECOC (1986) 51.

9 M.J. Matthewson, C.R. Kurkjian, S.T. Gulati, "Strength measurements of optical fibers by bending", J. Am. Ceram. Soc. (USA) 69 (1986) 815.

10 In-Vacuum motion system (step-size 4.4 μm) from Princeton Research Instruments, Inc., Princeton, NJ (USA).

11 K.E. Lu, G.S. Glaesemann, G. Kar, "Hermetically coated optical fibers", Proc. 36th IWCS (1987) 241.

12 D.J. Stockton, "Current fibre strength issues for British Telecom", COST 218 temporary document 218TD(89)034, Birmingham (UK) 1989.

13 Private communications with suppliers.

14 N. Yoshizawa, Y. Miyazima, Y. Katsuyama, "A one-hundred-fiber submarine cable composed of hermetically coated fiber ribbons inserted into slots", Proc. 38th IWCS (1989) 603.

15 F.P. Mallinder, B.A. Proctor, "Elastic constants of fused silica as a function of large tensile strain", Phys. and Chem. of glasses, 5, no.4 (1964) 91.

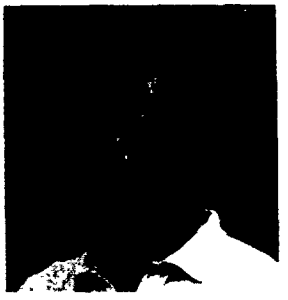

Willem Griffioen was born in Oegstgeest, the Netherlands, on October 8, 1955. He received the B.S. and M.S. degrees in physics and mathematics from Leiden University, Leiden, the Netherlands, in 1978 and 1980. He worked at Leiden University from 1980 to 1984, where he investigated macroscopic quantum properties of liquid and solid ^{3}He/^{4}He-mixtures at ultralow temperatures and in high magnetic fields. In 1984 he joined PTT Research, P.O. Box 421, 2260 AK Leidschendam, The Netherlands. His work includes research and development of fibre optic cables, installation techniques and reliability of optical fibres.

Gerrit Segers was born in Lisse, the Netherlands, on august 9, 1954. He completed his study with a B.S. degree in electronic engineering in 1975. After his military services he joined a company where he worked at the service department of nautical apparats. From 1980 to 1986 he worked at the Christiaan Huygens Laboratory at Noordwijk where he was involved in the electronic engineering of radar-systems. In 1987 he joined PTT Research, where he is involved in engineering in both analog and digital electronics.

Eddo van Loenen was born in Den Haag the Netherlands, on august 6, 1960. He completed his study with a B.S. degree in chemistry in 1984. He worked at Philips Research, Eindhoven, from December 1984 till October 1988. He investigated new methods to deposit thin metal alloy films on substrates used for phase change erasable optical recording. In 1988 he joined PTT Research. His work includes the development of instrumentation and methods used in the research of optical fibers and cables.

Quick-Access to Fracture Statistics at Ultra-Wide-Range Tensile Test of Optical Fibers.

Jan Björkman and Torbjörn Svensson
Swedish Telecom,
Technology Department,
Material Laboratory,
S-123 86 FARSTA Sweden

Abstract

A new instrument has been developed for tensile testing of comparatively long lengths of optical fibers. The instrument enables rapid evaluation of failure statistics from both tensile- and static loading of the fiber. An advantage of the new principle of testing is, that several failures occur at each shot, thus saving the time available for testing. This enables tensile testing at considerably lower strain-rates than the ones usually applied. It also simplifies static testing at any required level of strain.

An important feature of the instrument is the loading of fiber by controlled strain, which simplifies the evaluation of failure data since no adjustment of data due to varying fiber thickness or coating strength will be necessary. Also, the estimation of fiber failure in cables is usually based on strain in fiber, being an argument for measuring strain instead of stress on the fiber in a fatigue test.

The application of a new technique is presented along with a comparison with end-load tensile tests of commercial fibers.

Introduction

When characterising the fatigue of optical fibers by means of tensile tests, the strength should be studied within the widest range of stress rates attainable. This is important since fatigue mechanisms may change with time and load, making impossible a reliable extrapolation of tensile test data from ordinary strain rates. The strive should also be, to better simulate during a test the operating condition of fiber in cables.

For these reasons, a new instrument has been developed at the Material Laboratory. The instrument enables tensile testing of optical fibers at long-lasting load and very low rates of strain. It is called "expander", and its working principle is that of controlling the fiber's strain along the entire length of fiber, independent of the occurence of fiber fractures. The rate of strain can be chosen within a wide range. The accessible ratio between the highest and the lowest rate for the instrument is about 50,000 times, the lowest strain rate being about $5 \cdot 10^{-6}$ %/s corresponding to the stress rate $3.5 \cdot 10^{-6}$ GPa/s in typical singlemode fibers. The expander thus extends and completes the testing facilites at the Material Laboratory, which also include an instrument for high-speed tensile test of fiber.

The high-speed instrument covers a wide range of stress-rates, the span being about 1,000,000 times, but it was designed mainly to cover high strain-rates aiming at the inert strength of optical fibers, which is accessible only at the highest rates usually attained by the instrument, i.e. about $2 \cdot 10^{3}$ GPa/s. Tensile testing at such extremely high stress rates enables the evaluation of the fiber's B-value, which is used for lifetime estimation of optical fibers[1-3]

The expander was designed to further extend the lower limit of accessible strain-rates to complement the high-speed instrument, and also to enable mapping of failure events of statically loaded fibers.

Reference tests

In all, three types of acrylate coated singlemode fibers from the

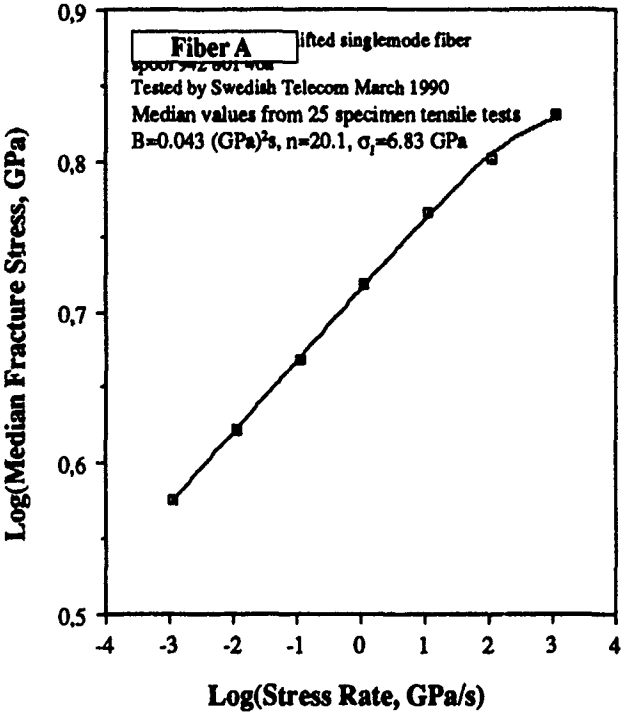

Figure 1. Rate dependence of fiber strength. Data from reference tensile test.

vendors A, B and C have been tested in the new instrument. Reference tests on fiber A were first made in the high-speed tensile test machine. Figure 1 shows the median fracture strength of fiber A for 25 specimens at each rate. Within the applied range of rates, approximately 0.001 GPa/s to more than 1,000 GPa/s, the mean fracture data (squares) fits well to a commonly used 3-parameter equation for fatigue of glass (curve) which is used for the characterization and lifetime estimation of optical fibers.

Then a number of tensile tests were performed in the expander at rates ranging from 0.35 MPa/s to about 170 MPa/s. On the basis of the reference test, the compatibility between the first well-known technique and the new expander technique could be studied. As can be seen in Figure 2 below, test data from the both techniques can be successfully transformed from strain to stress,

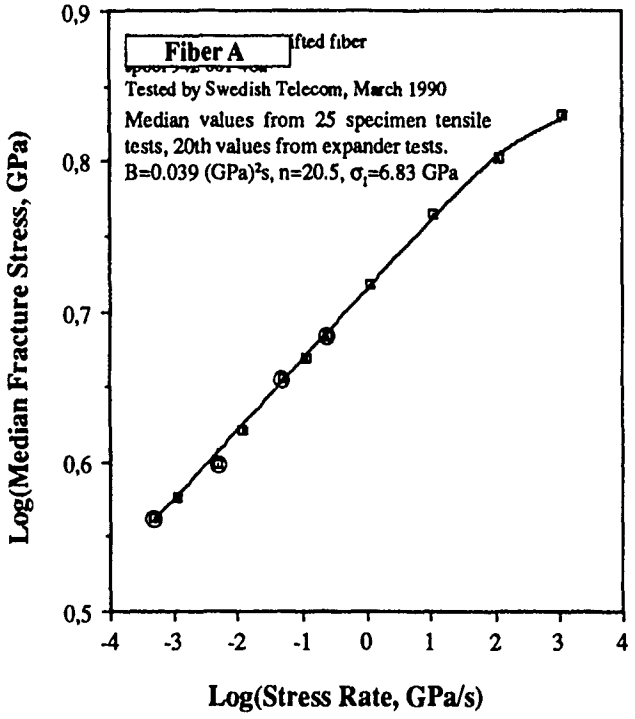

Figure 2. Comparison of data from the reference tensile test and the expander test.

so that they will coincide at similar loading rates, within the common three decades used. Data marked by circles are expander data from tests on 30 meter fiber samples. The remaining data represent the median values from separate measurements of 25 end-loaded specimens of 0.5 m length. To fully understand how to unify data from the two techniques, a thorough reading of the next chapters is recommended.

Fracture statistics from a single shot

Strength always varies along an opical fiber. Therefore, it will be necessary to measure the strength of a sufficiently large number of fiber specimens to certify an accurate measure of the average strength, which is used for the evaluation of the fiber's fatigue parameters, n and B. These parameters determine e.g. the shape of the curves shown in Figure 1 and 2, according to equation (6) in the chapter entitled **Two-stage fatigue**.

Usually, a number of 25 specimens will be sufficient when

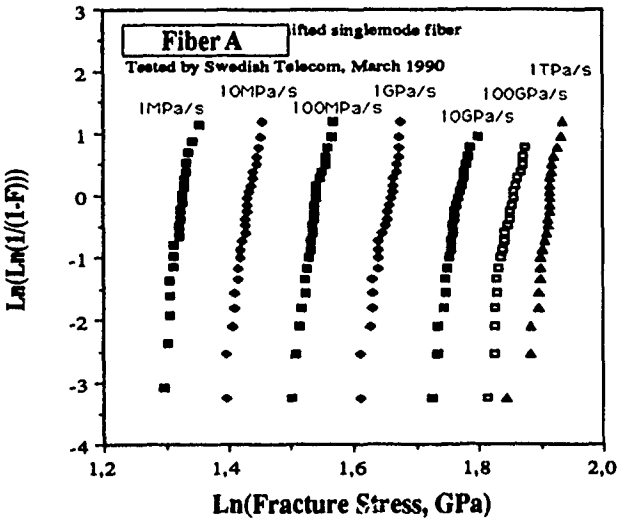

Figure 3. Weibull plot of tensile strength of 175 specimens at different stress rates.

testing high-strength optical fiber having a weibull modulus around 60, see Figure 3. In an expander test, on the other hand, a single long specimen is continuously loaded until a sufficient number of fractures have occured, see Figure 4 below. The useful number of failures is limited by the design of the expander and the length of

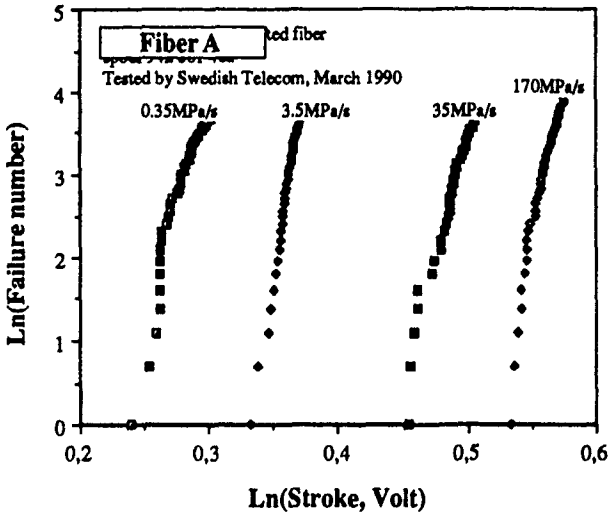

Figure 4. Weibull plot of scanned failures in four specimens at different strain rates.

the tested fiber. 30 to 60 scanned failures are readily obtained in a single shot. This implies that a considerable amount of time can be saved by using the expander.

The reference test has shown that the expander can deliver data with a rate dependence and weibull modulus which are comparable to those from ordinary end-load tests.

Additional tests presented in the chapter **Extended tests** below, have certified the function of the instrument also at extended low-rate testing. A quick access to very slow tensile tests, and static tests, will be important when studying low-stress and long-

time fatigue where a reliable characterization of optical fibers is strived for, and where exessive extrapolation of ordinary speed data may be detrimental due to competing fatigue mechanisms.

Calibration

The evaluation of raw data from the expander tests, and the subsequent comparison to data from ordinary tensile tests will be shown, before the results from the ultra-low-rate tests are presented. Due to the different principles of loading the specimen and sampling the failures, the entities to be measured will depend on the technique used.

In an ordinary tensile test the fracture load is measured and transformed to mechanical stress (GPa) in which case the cross sectional area of the fiber is known and assuming that the fiber's coating will not significantly contribute to the fracture load. In practise, the load supported by the coating may be 5% of the total load, and will hardly influence the evaluation of the essential fatigue parameters B and n.

In an expander test the data may be readily transformed to fiber strain by calibration. By knowing Young's modulus for the fiber glass the fracture strain can be substituted by tensile stress on the glass. Unfortunately, the ordinary/high speed tensile test data must also be adjusted (by some unknown value ≈5%) to level with the expander stress data. However, the rate-dependent strength of fiber glass at lower loading rates does not depend on the type of load used, stress or strain. This allows the convenient use of a simple factor to unify the expander- and tensile tests' raw data.

In Figure 2, such a factor (2.81 GPa/V) was used to adjust the expander test data to nominal stress data from tensile tests.

Scanning the failure sites

The breaking sequence of failure sites when loading a fiber depend on the applied technique.[4] In an ordinary/high speed tensile test separate specimens are loaded until they fracture. This implies that only the weakest site in a specimen will fail, leaving other parts, almost as weak, unaffected. According to the limited number of failures, the cumulative failure probability is usually written

$F_i=i/(N+1)$

where N is the total number of failed specimens and "i" is the ordinal number of the specimen, all specimens being assorted in an ascending order of fracture load.

In an expander test there is only one specimen. Theoretically, no potential failure site will escape the load, though other parts of the fiber have already failed. Thus all failure sites have the potential of being loaded until they fracture, making it possible to scan every failure site in an ascending order of strength. In principle, there is no limit for the number of possible failures, which implies that the cumulative failure probability instead must be defined as

$F_i=1-\exp(-i)$

according to equation (1) and (2) in the next chapter.

It has been shown, that the discrete F-data from an expander test of a fiber with random space distribution of truly weibull distributed failure sites, will be perfectly aligned to a straight line in a weibull diagram. The slope of a line fitted to F-data from an ordinary tensile test will also be the same, but for natural reasons the F-data in the latter case must deviate from the line in a step-like manner.[4]

In practice, essentially straight lines will be observed when logarithmed values of fracture load are plotted either versus the logarithm of "Ln(1/(1-F))" or versus the logarithm of "i". This is visible in Figure 3 and 4.

In order to compare data from the different techniques a common entity for the fracture load is needed. If the total length of loaded fiber and the number of failures are essentially the same when using the different techniques, the median value of the fracture loads is preferred. Median values have been applied in Figure 1 and 2, based on a total number of 25 and 39 fractures in the tensile- and expander tests, respectively.

If the total length of fiber and the number of failures depend significantly on the applied technique, one may assume that the failure sites are weibull distributed, and evaluate the fiber's site parameter, σ_0, which must refer to one and the same reference length of fiber. The experimentally determined value of the shape parameter m (the "weibull modulus") should not depend on the technique used, since such dependence would indicate the presence of an additional failure mode. When using test data from a **single** technique (expander- or ordinary tensile tests) in order to evaluate the relative rate dependence of strength (i.e. the fatigue parameter n) small attention must be paid to the problem of choosing an average entity. Median and mean values of strength, as well as the site parameter (when falling within the set of measured data) all may be used with similar results.

Weibull diagrams have been used here for convenience only, and the weibull distribution per se is not necessary for the evaluation of the essential fatigue parameters B and n dealt with in this paper. However, since the principle of applying a homogene load along a breaking fiber probably has been quite sparsely discussed in the past, the following chapter will show, how to relate the weibull parameters to this test technique.

Weibull parameters

By applying weibull statistics[5] on the failure of optical fibers, the cumulative failure probability F can be defined by the failure distribution Np according to the expression

$$F = 1-\exp(-N_pL) = 1-\exp\left(-\frac{L}{L_{ref}}\left(\frac{\sigma}{\sigma_0}\right)^m\right) \qquad ...(1)$$

with σ_0 refering to a given length L_{ref}, L being the total length. The value of the shape parameter m is proportional to the strength scatter, and the site parameter σ_0 corresponds to a hypothetic fiber strength at the value of F where $\ln(\ln(1/(1-F))) = 0$, i.e. where $F \approx 63\%$.

During a tensile test a certain number of failures will occur. Assuming a homogene load along the fiber, the failure distribution Np, up to and including the last failure, will be scanned completely, since no part of the fiber may escape the load. The distribution Np describes the number of failures per unit length, and it is a function of the fiber strength which depends on the time history of the applied load σ. In this case, the distribution can be written

$$N_p = i/L \qquad ...(2)$$

where i denotes the ordinal number of the fracture when increasing the load σ. By inserting equation (2) into equation (1) you will get

$$Fi = 1\text{-}Exp(\text{-}i) = 1\text{-}Exp(-\frac{L}{Lref}(\frac{\sigma_i}{\sigma_0})m) \qquad ...(3)$$

Equation (3) thus, is valid for the failure-independent loading of the entire length of fiber. F_i is the cumulative failure probability including failure no i, that is the probability that the fiber somewhere will fracture at a stress load smaller than, or equal to σ_i. To evaluate m och σ_0 the logarithmed values $Ln(Ln(1/(1-F_i)))$ are usually plotted versus $Ln(\sigma)$. Applying this on equation (3) yields

$$Ln(Ln(1/(1-Fi))) = Ln(i) = Ln(\frac{L}{Lref}(\frac{\sigma_i}{\sigma_0})m) \quad ...(4)$$

or $Ln(i) = Ln(L/Lref) - mLn(\sigma_0) + mLn(\sigma_i)$

A linear curve fit to data according to $y = A + Bx$ where $y = Ln(i)$ and $x = Ln(\sigma_i)$ then will yield

$$m = B \text{ and } \sigma_0 = Exp\{\frac{Ln(L/Lref)-A}{m}\} \qquad ...(5)$$

It is thus possible to evaluate the shape- and the site parameter with data from testing of fibers using the expander.

The expressions (4) and (5) are applicable also on data from tensile test of end-loaded fiber specimens, but the entity Ln(i) must then be substituted by $Ln(Ln(1/(1-F_i)))$ in which $F_i=i/(N+1)$.

As it was previously pointed out, the expander technique implies a considerable saving of time. However, further improvements still are accessible by applying an accelerated test procedure. This procedure will now be explained.

Accelerated testing

During very slow tensile testing of optical fibers much time can be saved by beginning the test at an elevated load. This is accomplished by rapidly increasing the load up to a certain level, where the tensile test will start. The procedure is simple, since all that is needed, is to reduce the tensile speed when reaching the proper load for continued tensile test at nominal rate. See Figure 5, where the specimen is rapidly preloaded to a level σ_s approaching that of the estimated fracture load at slow tensile testing, σ_d.

Sometimes a static load as high as 90% of the nominal dynamic strength σ_d may be applied. Shortly after the static load is applied, the load rate is adjusted to the requested value, and the tensile test is continued until the specimen fails at the level σ. By applying this procedure it will be possible to save 90% of all the time required to make the specimen failure at the nominal rate.

However, it is not obvious whether the captured data from applying an accelerated procedure are useful. If certain requirements on the duration and level of the load are not met, the value of the fracture stress after a preload may differ significantly from the value after constant-speed loading from zero load, i.e an ordinary test procedure. An excessive duration of the preloading time is not allowed, since the failure stress may then slightly decrease. Nor is it allowed to start on a level which is too close to the expected fracture stress at nominal loading rate, see Figure 6.

The allowable load and duration of the static preload can be calculated in order to save time required for testing. Doing so,

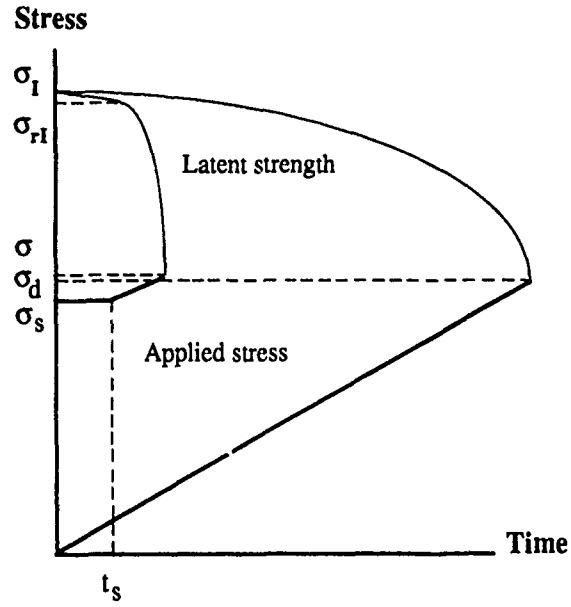

Figure 5. Current strength and applied stress at normal and accelerated tensile tests. Schematic.

significant savings were made at expander tests, which would havelasted for a week ore more. By reducing the time at test, the risk for disturbances was also reduced and the utilization of instruments improved.[6]

The limitations of the level and duration of the loading time will be briefly commented in the following.

Two-stage fatigue

Knowing the fatigue parameters, an accurate value of the dynamic (tensile) strengh σ_d of silica based high-strength singlemode fiber may be obtained by iteratively solving the equation

$$\sigma_d^{n-2} = \sigma_I^{n-2} - \frac{\sigma_d^{n+1}}{B(n+1)d\sigma/dt} \qquad ...(6)$$

which is obvious from the close fit of curves to high-stress-rate data in Figure 1, 7 and 8. The fatigue of a fiber with an inert, or initial, strength σ_I is determined by the applied load and the values of the parameters B and n. In the above expression the applied load is assumed to increase from zero load with a constant stress rate dσ/dt. This term, σ_d, is what is measured at the event of fracture when testing the fiber by conventional means at a nominal rate.

Initially applying a static load σ_s for a period t_s will reduce the inert strength σ_I due to static fatigue according to the equation

$$\sigma_{rI}^{n-2} = \sigma_I^{n-2} - \frac{\sigma_s^n t_s}{B} \qquad ...(7)$$

The term σ_{rI} is the residual inert strength of the fiber at the onset of the final, shortened tensile test. This term will be used in the readily derived expression below for the accelerated tensile strength σ of preloaded fiber, where σ is assumed to be measured at a constant stress rate which is applied after the static preload.[7]

$$\sigma^{n-2} = \sigma_{rI}^{n-2} + \frac{\sigma_s^{n+1}}{B(n+1)d\sigma/dt} - \frac{\sigma^{n+1}}{B(n+1)d\sigma/dt} \qquad ...(8)$$

By estimating the value of σ_d from Eq (6) and by using Eq (7) and (8) to calculate the value of σ, it is possible to study the influence of static preload on the measured strength at accelerated tensile testing. This is shown for a typical singlemode fiber in Figure 6, where the ratio σ/σ_d between accelerated strength and nominal tensile strength is plotted versus the ratio σ_s/σ_d between static prestress and nominal tensile strength. According to the figure, practically no influence on the failure strength due to the accele-

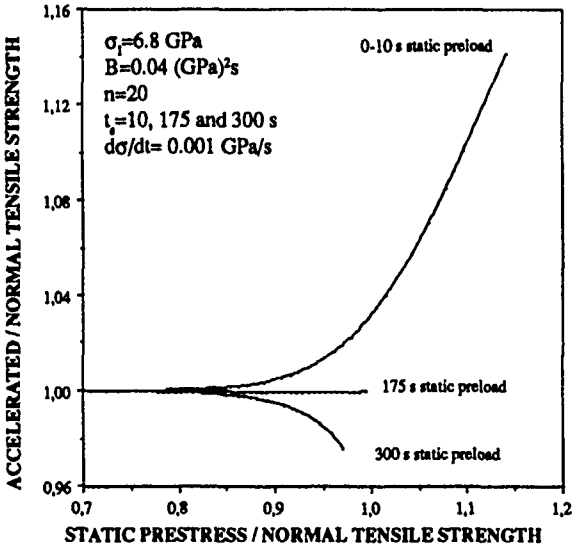

Figure 6. Tensile strength after varying level and duration of the static preload.

rated test procedure may be observed when the ratio between the static prestress and nominal strength is smaller than 0.8, i.e. the maximum ratio which was applied at the lowest rates tested by expander in this study.

Extended tests

Final tests were made on Fiber B and C, fully utilizing the expander's low-strain-rate ability, its lower limit being $5 \cdot 10^{-6}$ %/s or 3.5 kPa/s. The accelerated test technique was sucessfully applied within the range 3.5 kPa/s to 350 kPa/s, reducing the time of test with about seven days. A calculated value of 0.8 was applied as the maximal preloading ratio. Owing to the unexpected improvement of fiber strength below 350 kPa/s the real value turned out to be even smaller.

According to previous results[2,3] from several optical fibers tested, including the fibers A, B and C in this paper, the tensile strength σ_d within the range 1 MPa/s to 1 TPa/s may be accurately described by the equation (6)

$$\sigma_d^{n-2} = \sigma_I^{n-2} \cdot \frac{\sigma_d^{n+1}}{B(n+1)d\sigma/dt}$$

Typical values of fatigue parameters for acrylate coated fibers are σ_I = 6.6-7.1 GPa, B= 0.01-0.053 (GPa)²s and n= 18-25 when a standard test environment is employed, 50% RH at 23 °C.

However, an unexpected slowing of fiber fatigue at very low

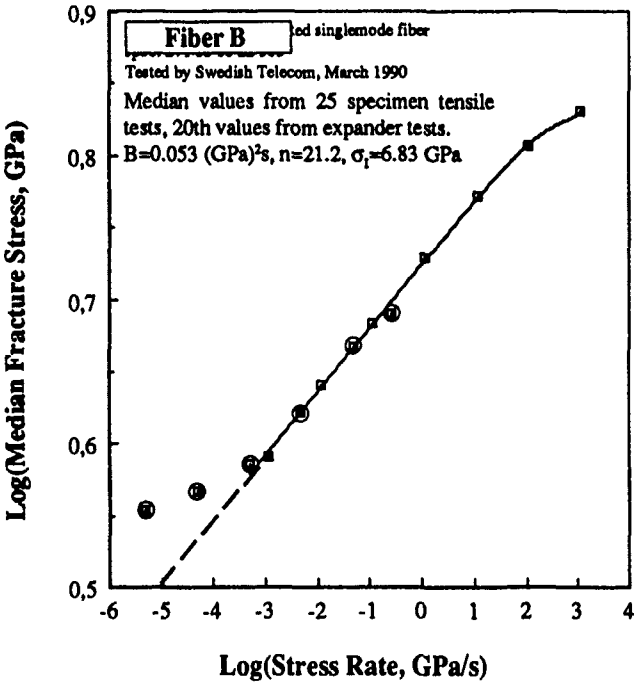

Figure 7. Extended test of fiber B.

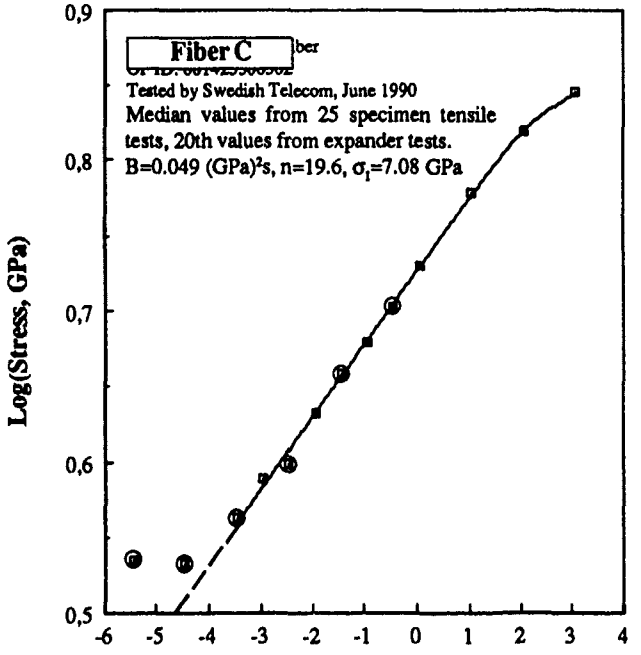

Figure 8. Extended test of fiber C.

strain rates, below 10^{-3} GPa/s, is observed in fiber B and C due to Figure 7 and 8. Careful attention has been paid to maintain proper test conditions, including preconditioning of the fiber in the (standard) test environment for more than a week. Probable errors caused by fiber slippage, transducer nonlinearity and drift are very small and have not influenced data significantly. A high repeat-

ability of the expander test data was also confirmed, the maximum deviation being about 1% between average strength data for all rates in a repeated test series on fiber C, including the lowest rates used. For all known reasons, the measurements made should be considered significant at all rates used, and truly reflecting the properties of fiber B and C. The unexpectedly high strength of the fibers B and C observed at extremely low strain rates may be caused by slow crack blunting or relaxation of tensile strain close to the fiber's surface. However, a deeper analysis of the physical reason is beyond the scope of this paper.

Summary

A technique for scanning all failure sites along a continuosly loaded fiber has been theoretically analysed and implemented by a new instrument. The function of the instrument has been certified by a series of tensile tests on optical fibers. The new instrument, the expander, enables evaluation of fatigue parameters of optical fibers at considerably lower strain rates than previously. Tensile tests using the expander have been performed at stressing rates from 175 MPa/s down to 3.5 kPa/s (which is about 300 times slower than ordinary tests). The expander may also be used for static tests with unlimited endurance.

Also, a general technique for time-saving tensile testing of optical fibers has been analysed. This accelerated-test technique is applicable to any tensile testing machine, and it is based on the beginning of tensile tests at a high load. Under certain conditions this procedure will have no significant influence on the measured fracture strength of optical fibers. The technique supports tensile testing at very low speed, and the time saved may be used for testing an increased number of specimens, thus improving the accuracy of evaluated fatigue parameters.

The first technique of scanning all failure sites requires a special instrument, but offers the necessary failure statistics in a single shot. Combining the expander testing technique and the accelerated test, enables vast time savings during low-rate testing of optical fibers, thereby supporting an improved characterization of fiber fatigue and a reliable estimation of fiber lifetime. ■

References

1. T. Svensson, "Dragprovning av optofiber vid hög hastighet", Tvt Rapport Plm 88 201 (1988).

2. T. Svensson, "High Strain-Rate Testing of Optical Fibers", Proc of the 37th International Wire and Cable Symposium, Reno, USA, nov 15-17 1988, p 217-24

3. T. Svensson, "Will a Reduced Bend Loss Sensitivity Affect the Lifetime of Optical Fiber?", Proc of the 38th International Wire and Cable Symposium, Atlanta, USA, nov 14-16 1989, p 705-09

4. T. Svensson, "Mekanisk provning av optofiber med expander", Tvt Rapport Plm 87 018 (1987).

5. W. Weibull, "A Statistical Distribution Function of Wide Applicability", J Appl Mechanics, vol 18 (1951) p 293-297

6. T. Svensson, "Expander - nytt instrument för långtidsprovning av optofiber", Tvt Rapport Plm 90 080 (1990).

7. T. Svensson, "Statisk förbelastning sparar tid vid dragprovning av optofiber", Tvt report Plm 90 082 (1990)

Jan Björkman graduated as chemical engineer at the Malmö Technical School. He has studied mathematics at the Stockholm University and polymer science at the Royal Institute of Technology, Stockholm. He joined Ericsson Cables in 1966 where he worked with polymer materials. In 1977 he joined Swedish Telecom where he is responsible for polymers.

Torbjörn Svensson joined Swedish Telecom in 1985 where he is engaged in quality assurance and techniques for testing fibers and cables. He is the inventor of a high-speed technique used for tensile test of optical fibers and also of the technique used for single-shot statistics of fiber strength which is presented in this paper.

DEVELOPMENT FOR GEOMETRY MEASURING METHOD OF OPTICAL FIBER

KUN IK JUN, YUNG IK LEE, BONG NAM PARK

Taihan Electric Wire Co., Ltd.
Seoul, KOREA

ABSTRACT

We developed a more accurate measuring apparatus for geometry of optical fiber by means of near field scanning method.
This measuring apparatus controlled effectively reflected light in a microscope itself, which has been a problem recently and we disposed of a weighted moving average method in order to improve measuring errors caused by crack of optical fiber cutting end-face or by outside dust sticked on cutting end-face.
And when the boundary of core and cladding is found out, we maintained repeatability less than 0.05 um on applying interpolation to compensate the interval between pixels.

1. INTRODUCTION

It is known several method as a measuring one of geometry for optical fiber, but the measuring apparatus of geometry for optical fiber by means of near field scanning method is widely used owing to short time for measuring and simplicity of its using.(1)
It is possible to measure simultaneously core diameter, cladding diameter, non-circularity, concentricity-error of multi mode fiber and single mode fiber by near field scanning method but there were some problems in this one and difficulty in case of high accuracy.

2. MEASURING EQUIPMENT

The scheme of a measuring apparatus is shown in Fig. 1.
This equipment was installed on the vibration isolated table in order to minimize the vibration and each light source was utilized to measure a core and cladding.
The microscope lens and IR Vidicon were arranged in a straight line and beam splitter were equipped in the middle to measure cladding by means of reflected light on optical fiber end-face.
The light is entered through large core fiber between beam splitter and light source and a pinhole for controlling an incident angle is installed in order to modulate the touching surface of light which is entered into beam splitter on the shooting side of light by large core fiber.
The side of beam splitter is open to verify adjustment of angle and avoid arising of unnecessary reflected light in microscope body and is intended to control the inside angle.
An optical fiber is layed in the face of microscope lens and controlled by a fine adjustment positioner.
The data of optical fiber end-face which is shown through a microscope is collected at regular intervals and calculated in a short time by micro computer.

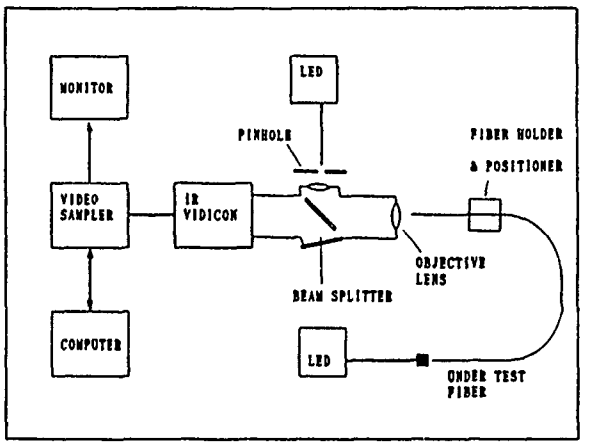

Fig. 1 Scheme of measuring apparatus.

The problem of measuring apparatus of near field scanning is that the base line of image reflected in IR vidicon by unnecessary reflected light from a microscope itself(2) arising is easily shifted, and cladding diameter and non-circularity is directly influenced, if any dust is adhered to an optical fiber end-face or any crack exists at cutting time.

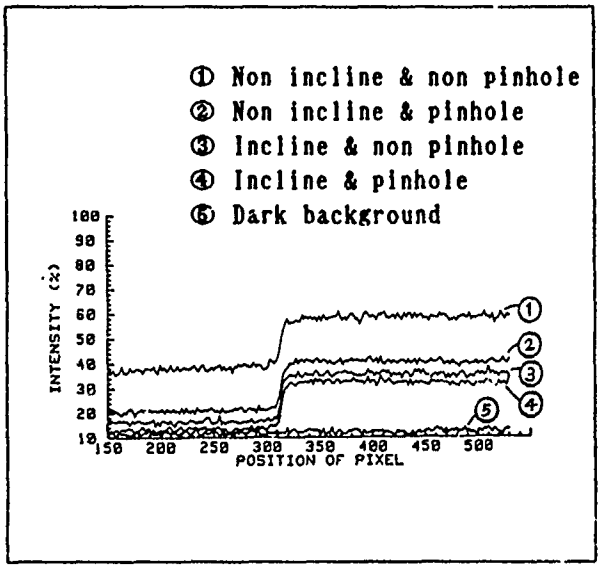

Fig. 2 Shift of base line depended on the structure of measuring apparatus.

2.1 SHIFT ON BASE LINE OF IMAGE

The base line of image is shifted mainly by the outside light of cladding and unnecessary reflected light by optical device.
Because the shift of base line operates to lower S/N ratio, it is necessary to minimize the shift of base line for accurate measuring.
The test results for suppression of reflected light is shown in Fig. 2.

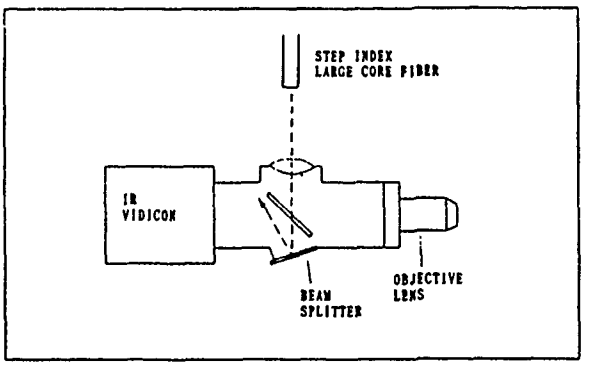

Fig. 3 Reflected light on the lateral face of microscope.

(1) The reflected light is not directly entered into IR vidicon by inclining the lateral microscope body.
The inside of microscope is considered not to reflect of light, but the reflected light arising weakly is planned to spread out in the space, not arriving at the side of beam splitter like Fig. 3 and the result like graph ③in Fig. 2 is obtained.

(2) The step index large core fiber is used to radiate incidence light used for measuring the cladding end-face of optical fiber, in equal density on all parts of end-face.
And pinhole is installed like Fig. 4 for controlling out lighting angle of large core fiber in order to avoid the reflected light by any light which exists in the edge of objective lens.

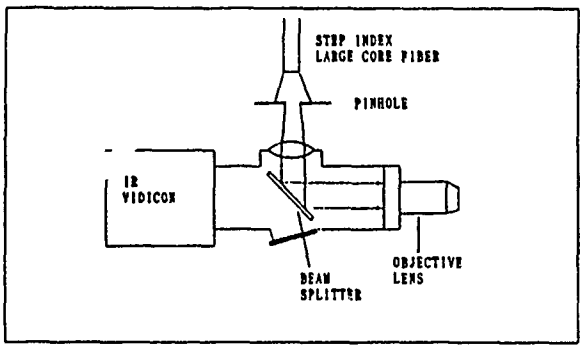

Fig.4 Suppresion of reflected light by means of incident angle limit.

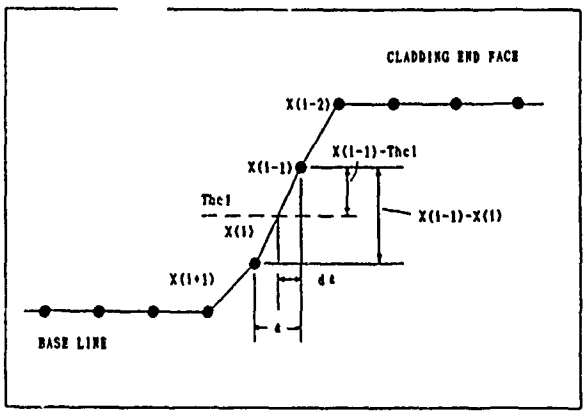

Fig.5 Appliance of interpolation on the boundary.

2.2 BOUNDARY DETERMINATION OF CORE AND CLADDING

It is possible to determine the boundary of core and cladding by means of k-factor established.
The data interval is determined by the magnification of microscope and vidicon since the resolution of IR vidicon is arranged as 1024 by 1024 pixel. Consequently, there is a regular interval between pixels and the position of pixel is not to the one of k-factor, and this is compensated by the interpolation.
If each sampling pixel is like Fig.5, the necessary length for this compensation is defined as;

$$d\ell = \frac{\{ X(i-1) - Thcl \} \times \ell}{X(i-1) - X(i)} \qquad (1)$$

X(i) : i-th sampling data
Thcl : Threshold level of cladding boundary
ℓ : interval between each pixel

2.3 DEFECT ON CLADDING BOUNDARY

Even though a cut diamond blade is used for cutting optical fiber, defect can be arisen at a touching part of the blade of a knife and dust is adhered on the cutting end-face.
So, this fact should make a measuring error.
It is necessary to compensate the defect part in a calculating algorithm in order to avoid these errors.
The data of this part can be eliminated because the data of part having a crack on cutting is much more small than the one of radius.
When non-circularity of core and cladding is calculated from a 60 radius data obtained at each end-face, the noise element contained in a measuring apparatus itself influences the data which we want to obtain.
So, the radius data is defined like Eg.2 by weighted moving average method as;

$$Dn = \{(D_{n-3} \times 1.49) + (D_{n-2} \times 8.23) + (D_{n-1} \times 23.51) + (Dn \times 33.28) + (D_{n+1} \times 23.51) + (D_{n+2} \times 8.23) + (D_{n+3} \times 1.49)\} / 99.74 \qquad (2)$$

The graph of cladding radius after and before using a weighted moving average method is shown Fig. 6.

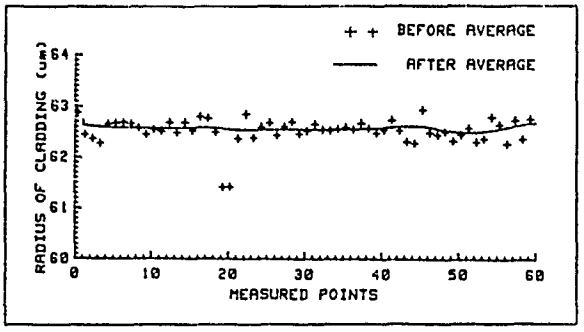

Fig. 6 Graph of cladding radius after and before using a weighted moving average method

2.4 MEASURING RESULT

Single mode fiber was repeatedly tested for testing repeatability of a measuring apparatus.
The standard deviation (1 sigma) of repeatedly measured data for each item is summarized like table 1.

Tested item	Unit	S.D (1σ)
Cladding diameter	um	0.0454
Cladding non-circularity	%	0.0223
Concentricity error	um	0.0301

Table. 1 Repeatability of single mode fiber

Repeatedly measured data in table 1 results from repeated test for same fiber re-cutted and maintains repeatability less than 0.05 um.

3. CONCLUSION

We developed a more accurate apparatus for measuring the geometry of optical fiber.
It is improved the mechanical of microscope to suppress the reflected light and data processing algorithm to compensate a measured data.
So we got a stable characteristics of all measuring test results which can be maintained less than 0.05um data deviation.

REFERENCE

(1) M. Nishimura, T. Ohshima, S. Suzuki : "Automatic Measurement of Geometry for Optical Fiber", Denshi Tsushin Kakkai Sougou Zenkoku Daikai, P975, 1982.

(2) W. J. Stewart : "Optical Fiber and Preform Profiling Technology", IEEE TRANSACTIONS ON MICROWAVE THEORY AND TECHNIQUES, VOL. MTT-30, NO. 10, P1439-1454, OCTOBER 1982.

KUN IK JUN
Taihan Electric Wire
Co.,Ltd.
785, Kwanyang-dong,
Anyang,Kyungki-do,
430-060, KOREA

Kun-ik Jun received from Myungji junior College in 1980 and joined Taihan Electric Wire Co.,Ltd. He has been engaged in measurement and inspection of optical fiber.
He is now a senior engineer of the Quality Assurance Department.

BONG NAM PARK
Taihan Electric Wire
Co.,Ltd.
996, Shihung-dong,
Guro-ku,Seoul,
152-030, KOREA

Bong-nam Park received the B.E degree from Yonsei University in 1979. He joined Taihan Electric Wire Co.,Ltd. When he has been engaged in R&D of optical fiber cables.
Now he is a General Manager of the Quality Assurance Department.

YUNG IK LEE
Taihan Electric Wire
Co.,Ltd.
785, Kwanyang-dong,
Anyang,Kyungki-do,
430-060, KOREA

Yung-ik Lee received his M.S degree from Yonsei University in 1981. He joined Taihan Electric Wire Co.,Ltd. When he has been engaged in physics. Now he is a Section Manager of the Quality Assurance Department.

THE COMPARATION OF TWO PROCESSING METHODS BETWEEN DUAL LAYER BUFFER TUBES

Wei-Shyan Chien, Teng-Chih Feng, Chia-Hsien Wu
Show-Zone Chuang, Tien-Jey Sheu, Rex Chou

Telecommunication Laboratories
Directorate General of Telecommunications
P.O.Box 71, Chung-Li, Taiwan, ROC

Abstract

The advantages of the dual layer tube are great, such as much better kink resistance, preventing the fiber from being "caught" and free from "score" and "snap" etc.

In this paper, two processing methods of dual layer buffer tube have been introduced and their physical and mechanical properties have been compared. It is clear that coextrusion for the inner and outer tubes is a better method.

1. Introduction

Although the dual layer buffer tube around the optical fiber has represented optimal protection for a long time, the the different two processing methods, coextrusion and two-step production, are less mentioned. For the dual layer buffer tubes made by the two methods, the outer and inner layers should have some comparable physical and mechanical properties to ensure the good capacity of processing and compatibility.

2. Materials

Polybutylene terephthalate (PBT) and polyamide 12 are used in the outer and inner layers of the buffer tube.

PBT polymers are semicrystalline thermoplastic resins with a very sharp melting point at 433℉ They exhibit good tensile strength, toughness, and low moisture absorption, resulting in excellent dimensional stability (see Table 1). The smooth, hard resin surface results in low static and dynamic coefficients of friction. With high flexural modulus property, PBT polymers are beneficially used in outer layer of buffer tubes.

Table 1 : Some Mechanical and Physical Properties of PBT Polymers[1,2,3]

Property	Unit	Value of property
Melting point	°F	433
Heat deflection temperature	°F	130 @ 264 psi
Tensile strength	psi	7.5～8.5*10³
Moisture absorption	%	< 0.4
Impact(notch)	ftlb/in²	0.7～1.0
Flexural modulus	psi	3.4～15*10⁵
Flexural strength	psi	12*10³
Dielectric strength	V/mil	400～500
Dielectric constant		3.1～3.8(1 kHz)
Volume resistivity	ohm-cm	10^{15}
Dissipation factor		0.002(1 kHz)

The polyamides, or nylon, were the first materials to be recognized as engineering thermoplastics, owing to their superior mechanical properties, especially when exposed to elevated temperatures or

solvents. All nylons absorb moisture to a greater or lesser extent (see figure 1). The different types of polyamides absorb moisture at different rates and retain various amounts of moisture depending on their chemical composition. The concentration of amide groups in a nylon polymer affects the water absorption of nylon most, since water associates with the amide groups in the amorphous areas [4]. The water absorption of polyamides then varies with the amide content of the polyamide, as shown in Table 2. Moisture affects most properties of the polyamides. For nylons 66 and 6 especially, the flexural modulus changes are appreciable and predictable as seen in the Figure 2. Compared with other nylons, the water absorption of polyamide 12 is lowest. Meanwhile, polyamide 12 has the same good mechanical and physical properties (see Table 3).

3. Processing methods

Two Different processing methods, coextrusion and two-step production, for producing dual layer buffer tubes are

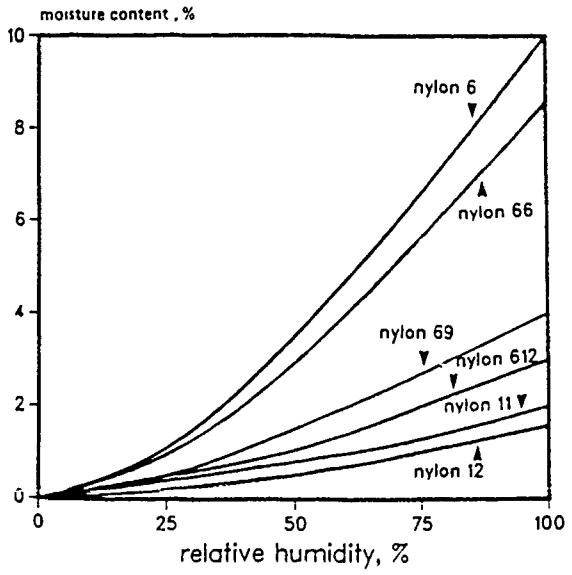

Figure 1 : Moisture absorption of various nylons as a function of environment

TABLE 2 : Moisture Absorption of Some Polyamides[5,6]

Polyamide	H_2O Absorption, 24hr (ASTM D570)	% Amide
Nylon 66	1.0～1.3	38
Nylon 6	1.3～1.9	38
Nylon 69	0.5	32
Nylon 612	0.4	28
Nylon 12	0.25～0.3	22

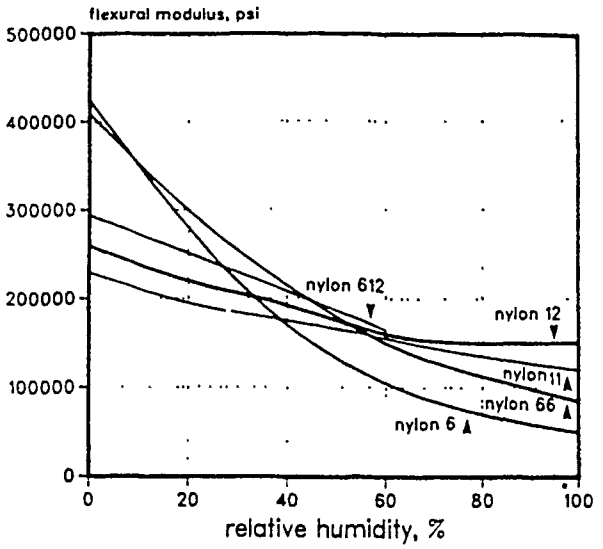

Figure 2 : Effect of moisture on flexural modulus

Table 3 : Some Mechanical and Physical Properties of Polyamide 12

Property	Unit	Value of property
Melting point	°C	179
Heat deflection temperatures	°C	145 @ 66 psi
Tensile strength	psi	8.5 ± 10^3
Break elongation	%	300
Moisture absorption	%	0.25～0.3
Impact(notch)	ftlb/in	2.0～5.5
Hardness	rockwell	105
Flexural modulus	kpsi	165

introduced as follows:

The outer and inner layers of buffer tubes can be manufactured simultaneously by coextrusion in one production step. A typical coextrusion line for manufacturing dual layer buffer tube is shown in Figure 3. The primary extruder is put in horizontal line, used for producing the inner layer and the secondary extruder is put in vertical line, used for producing the outer layer. PBT and polyamide 12 (for the outer and inner layers) were extruded simultaneously at a crosshead die through the two different extruders. The traditional process for manufacturing dual layer buffer tube is by a two-step production. In this process of two-step production, the inner buffer tube was extruded with polyamide 12 completely first, and then, put on the outer layer around the first inner tube with PBT from another extruder.

4. Processing considerations

PBT has a low melt viscosity at normal processing temperatures (450-500℉). It should be dried prior to molding (2 - 4 hours @ 250℉) to provide parts with the optimum performance. Temperatures above 520℉ should be avoided to minimize the the loss of desired properties.

Nylon 12 has a broad range of processing temperatures (400-500℉). Due to moisture absorption, it should be dried prior to molding in a clean air-circulating oven or in a specially designed dryer using desiccant. Excessive heat should be avoided during drying because of the danger of oxidation degradation. Safe temperatures are generally below 175℉.

5. Comparison between the two processes

There are some different encounters between the two processes:

(1) Coextrusion is more convenient and economical than the process of two-step production.

(2) By coextrusion, the inner tube can be free from water when cooled with water.

(3) From the process of two-step production, the inner tube must be rolled up in a rotary machine. When the first step is completed, it is paid off for producing the outer layer.

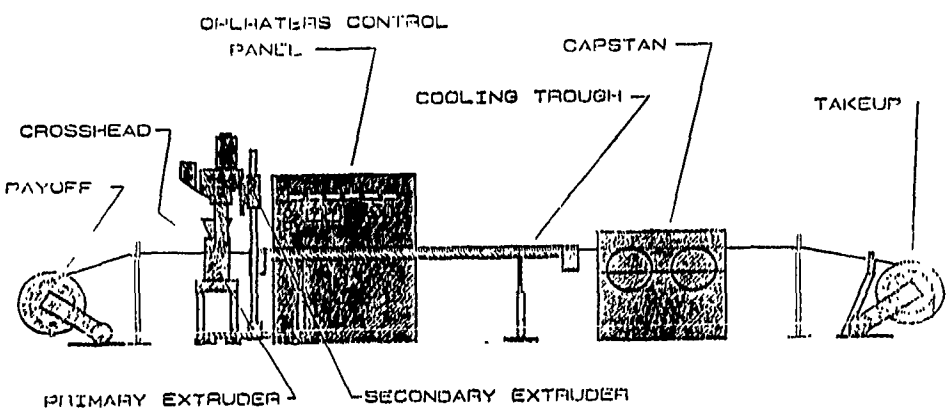

Figure 3 : A typical coextrusion line

6. Stripping strength

The method for measuring the stripping strength of the dual layer buffer tubes manufactured from the above two different processes is described as follows:

Sample preparation

The type and dimension of test specimens are shown in figure 4. Five specimens were used for each dual layer buffer tube.

Figure 4 : The type and dimension of test specimen for stripping strenyth

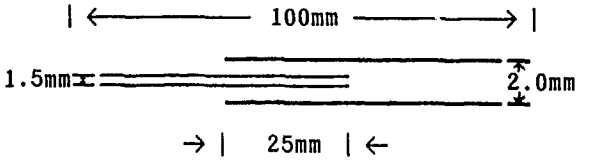

Characterization

The stripping strength of all samples were studied by using a Instron universal testing instrument Model 1122. The data was measured as follows:

(1) 9.8 kg (from coextrusion)

(2) 4.2 kg (from two-step production)

Obviously, the stripping strength of the dual layer buffer tubes made from coextrusion is the greater one.

7. Tensile strength and elogation

The method for measuring the tensile strength and elogation of the double buffer tubes is accordance with the specification of ASTM. The data was measured as follows:

A. Tensile strength

(1) 25.8 kg (from coextrusion)

(2) 23.5 kg (from two-step production)

B. Elogation

(1) 290 % (from coextrusion)

(2) 300 % (from two-step production)

Differences in tensile strength and elogation between the two kinds of dual layer buffer tubes manufactured by different processing methods is slight.

8. Discussion

(1) By the process of two-step production the inner buffer tube should be extruded completely first. The piping -hot inner tube must be immersed immediately in water for cooling. From the method of coextrusion, the inner tube can be free from water. It is very important for the higher moisture absorption polymers of polyamides to be free from water. Moisture absorption from the atmosphere begins immediately after molding and proceeds until the mosture in the piece is at equilibrium with the moisture in the environment.

(2) From the method of two-step production, the inner tube could have the higher possibility of being scored due to the first step, being rolled up and paid off.

(3) The advantages of the layer design from a mechanical strength and fiber protection standpoint is : A. Much better kink resistance while at the same time maintaining flexibility of the buffer tubes than is possible

with a single layer. B. The inner layer (Nylon 12) has a much smoother surface than polyester, thereby preventing the fiber from being "caught" on the inside surface of the tube either during manufacturing or during installation. C. Enables stripping of the buffer tubes so that the chance of damaging a fiber is negligible (score and snap). Single layer buffer tubes do not offer this type of stripping.

(4) Owing to the difference of processing methods, the stripping strength of the dual layer buffer tubes made from coextrusion is the greater one. The buffer tubes with a higher stripping strength could not see any strain of consequence during installation.

9. Conclusion

Two different processing methods are used for producing dual layer buffer tubes. The process of coextrusion is an economical and suitable method for manufacturing dual layer tubes in one production step.

10. References

(1) J.P.Bell and J.H.Dumbleton, J. Polym. Sci. Polym. Phys. Ed.,7, 1033 (1969).
(2) C. Zhou and S. B. Clough, Polym. Eng. Sci., 28, 65 (1988).
(3) F.Fontaine,J.Ledent,G.Groeninckx, and H.Reynaers, Polymer, 23, 185 (1982).
(4) Puffr, R., and Sebenda, J., J. Poly. Sci. Part C, 16:79 (1967).
(5) Vydyne Engineering Thermoplastic Resins, Composite Data Sheet, Monsanto Publication No. 6540A.
(6) Design with Plastics, Du Pont Publication E-32986.

Wei-Shyan Chien
Outside Plant Lab.
Telecommunication Labs.
P.O. Box 71
Chung-Li
Taiwan
R.O.C.

Wei-Shyan Chien received his M.S. degree in Chemistry from the University of Chung Yuan in 1983. He joined the Telecommunication Laboratories in 1983 and has been engaged in research and development of outside plant technology.

Teng-Chih Feng
Outside Plant Lab.
Telecommunication Labs.
P.O. Box 71
Chung-Li
Taiwan
R.O.C.

Teng-Chih Feng received his M.S. degree in Chemical Engineering from the South Dakota School of Mines and Technology in 1982. He joined the Telecommunication Laboratories in 1983. Mr. Feng is now a project manager of the Outside Plant Technology Lab.

Chia-Hsien Wu
Outside Plant Lab.
Telecommunication Labs.
P.O. Box 71
Chung-Li
Taiwan
R.O.C.

Chia-Hsien Wu received his M.S. degree in Applied Chemistry from the University of Chinese Culture in 1984. He joined the Telecommunication Laboratories in 1984 and has been engaged in research and development of outside plant technology.

Show-Zone Chuang
Outside Plant Lab.
Telecommunication Labs.
P.O. Box 71
Chung-Li
Taiwan
R.O.C.

Show-Zone Chuang received his M.S. degree in Chemical Engineering from the National Cheng-Kung University in 1983. He joined the Telecommunication Laboratories in 1983 and has been engaged in research and development of outside plant technology.

Tien-Jey Sheu
Outside Plant Lab.
Telecommunication Labs.
P.O. Box 71
Chung-Li
Taiwan
R.O.C.

Tien-Jey Sheu received his M.S. degree in Chemistry from the University of Chung Yuan in 1984. He joined the Telecommunication Laboratories in 1984 and has been engaged in research and development of outside plant technology.

Rex Chou
Outside Plant Lab.
Telecommunication Labs.
P.O. Box 71
Chung-Li
Taiwan
R.O.C.

Rex Chou was born in 1948 and graduated from the University of Chung Yuan in 1970 with a B.S. in Electronic Engineering. He joined the Telecommunication Laboratories in 1978, where he is a member of outside plant technology study group.

Long-Term Stability of Organic Materials in Optical Fiber Cable

By

Ting-Chung Chang,Yih-Chyuan Lin,Jing-Chung Lin,Chieh-Mei Hsiao

Telecommunication Laboratory ,Chung-Li,Taiwan,R.O.C.

Abstract

A newly established procedure which selects supported Pd/Al_2O_3 catalyst as hydrogen absorbent is adopted to evaluate hydrogen evolution from thermal degradation of organic cable materials such as fiber coating materials, water-proof filling compounds, jacket, sheath, central member, etc. in the range of 50 to 100°C. From the experimental result, a mathematical model has been developed to predict the hydrogen concentration generated by the organic cable materials. According to the Arrhenius plots of initial rates of hydrogen evolution, the activation energies of hydrogen evolution from organic cable materials were in the range from 6 to 16 kcal/mole variable with organic cable materials. Correlation between aging temperature and the time to reach maximum hydrogen amounts was obtained and the ambient temperature saturation time could be predicted from the high temperature accelerated aging test.

Introduction

It has been long recognized that hydrogen evolved from organic materials inside optical fiber cables will gradually contaminate the optical fibers(1,2,3,4,5,6,7). The cumulation of hydrogen within the cable eventually cause a significant loss of transmission due to the pronounced absorption by H_2 or/and -OH at near infrared region.(8,9,10) To understand whether materials are suitable for cables when the long term stability are the subject to consideration, evaluations of their hydrogen evolutions are essential. Previously, we have reported a newly developed method to analyze hydrogen evolution by using Pd/Al_2O_3 catalyst as hydrogen adsorbents.(11) Due to the high efficiency of H_2-adsorbing and -desorbing on the surface and bulk of Palladium, trace of hydrogen generated from cable materials can be quantified continuously without any escaping of hydrogen from sample containers during aging and sampling processes on GC analysis. The high sensitivity has allowed us to detect 1.4 -- 3.3 times more of hydrogens than those by headspace vials or glass tube methods.In addition,continuous monitoring of hydrogen generation offers the advantage of near-real-time measurement of samples at various aging temperatures with minimum sample perturbation. The significant difference of results between this method and conventual methods has promoted us to reexamine the hydrogen evolution phenomena of optical cable-used organic compounds. Especially, the aging-time-related hydrogen generations at various temperatures. A mathematical model to estimate the hydrogen evolution from organic cable materials has been established and activation energies of hydrogen evolutions from cable materials are obtained. The aging results are also coalesced to an accelerated test at elevated temperature to examine the feasibility of using established model to predict the aging related hydrogen evolution from cable-used organic materials since the long term stability is a major concern for the materials used in optical fibers.

Experimental

Method of hydrogen generation analysis

Figure 1 is the schematic diagram showing the apparatus used in the hydrogen evolution measurement for optical cable materials. The catalyst was

pretreated by flushing with a hydrogen/argon flow followed by the desorption procedure at 400°C. After the pretreatment, a pure argon was then switched into the sample compartment to carry the evolved hydrogen from aging sample to the catalyst for adsorption. At the end of aging, the temperature on the catalyst reactor was raised to 400°C at a rate of 10°/min. In the meantime, the time profiles of hydrogen desorption from the catalyst and the temperature of the reactor were measured simultaneously by a TCD-GC and a thermocouple respectively.

Materials

Jelly-filled and pressurized optical cables are used as obtained. Optical cables contained organic materials such as fiber coatings, water-proof filling compounds, wrapper materials are aged at 50°, 70°, and 100°C and analyzed using catalyst adsorption method.

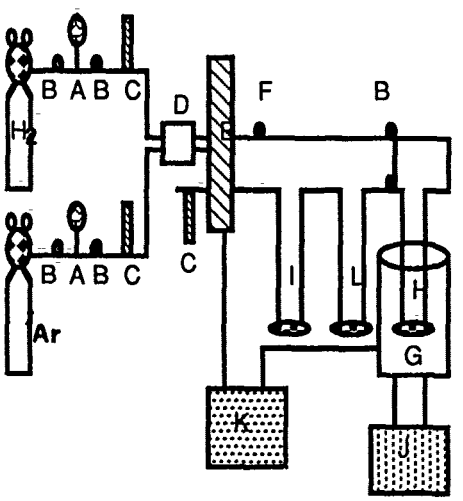

Figure 1: Schematic diagram of the hydrogen adsorption system.

A: pressure gauge E: T.C.D.
B: needle valve F: injecter
C: flow meter
D: mixing chamber G: furance
H: quartz reactor(contain sample)
I: quartz reactor (contain SiO_2)
J: temperature controller
K: recorder
L: quartz reactor(contain catalyst)

Results and discussion

Figure 2 to figure 4 show time-dependent cumulations of hydrogen evolved from optical cable materials aged at 50°, 70°, and 100°C. The weight of each sample used in the measurement was ca. 0.5 g. In these figures, the hydrogen generated progressively as the aging time continued. The generation eventually reached a saturation after certain time of ageing. For the same sample aged at different temperatures (50°, 70°, and 100°), the amounts of hydrogen generation at saturation points were found to be the same, yet the times to reach the saturation were different. This implies that the total hydrogens related to the degradation involved hydrogen evolutions are limited. Assuming hydrogens were generated through the thermal activation process, the total amounts of hydrogen (H, ul/g) evolved from optical cable materials can be modeled as following by using Arrhenius formula:

$$H\ (ul/g) = A*\exp(-E/RT)*t^x \quad ----(1)$$

Where A is a proportional constant, E is the activation energy for hydrogen generation, R is the gas constant equal to 1.987 cal/(mole k) , T is the aged temperature, t is the ageing time, and x is the time constant.

Fig.2 Temperature Dependence of H_2 Evolution from Acrylate

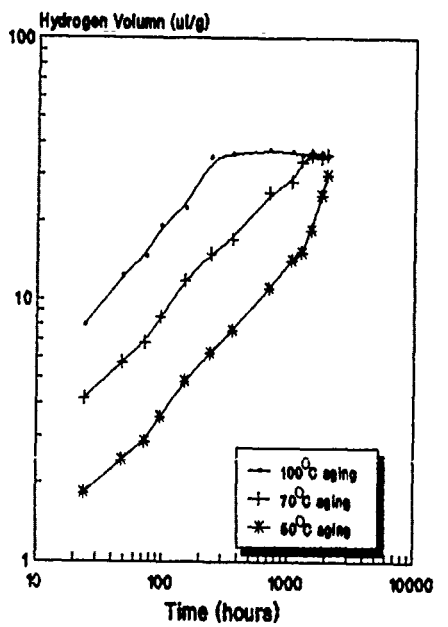

Fig.3 Temperature Dependence of H_2 Evolution from Silicone Coating

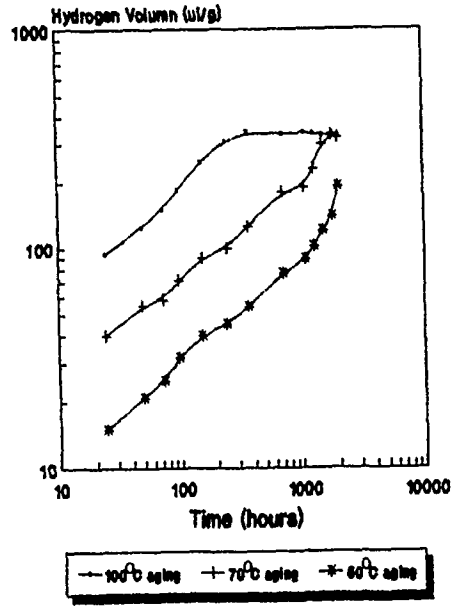

Fig.4 Temperature Dependence of H_2 Evolution from Polyisobutene

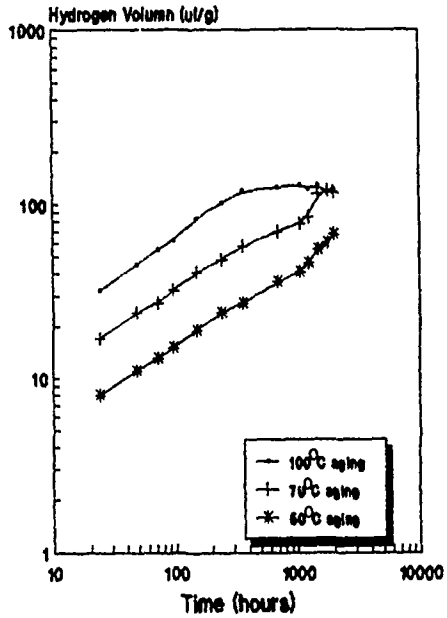

The hydrogen generations in Figure 2 to 4 also exhibit a monotonically increasing complied with the aging time. The hydrogen evolution curves at various aging temperatures can be fitted into straight lines with the same slope for the same sample at points before reaching the maximum evolution. The values of these slopes are 0.45 to 0.60 depending on which optical cable materials were tested. Figure 5 shows the Arrhenius plot on the initial rate of hydrogen evolution ($\ln(H/t^x)$ vs. $1/T$). Typically, the Thixotropic jelly A has a calculated activation energy for hydrogen evolution of 6.0 Kcal/mole. Table 1 summarized the results of time constants x and activation energies for optical cable materials.

Table 1 Activation Energy and Time Constant of Optical Fiber Cable Materials

Material	Activation Energy	Time Constant
Fiber A	12.4 kcal/mole	0.51
Fiber B	7.4 kcal/mole	0.46
Fiber C	16.0 kcal/mole	0.53
Mylar	13.0 kcal/mole	0.43
Kevlar	10.0 kcal/mole	0.45
Polyisobutene	8.0 kcal/mole	0.45
Thixotropic A[1]	6.0 kcal/mole	0.50
Thixotropic B[1]	6.0 kcal/mole	0.54
Thixotropic C[1]	12.0 kcal/mole	0.50
Silicone[2]	7.0 kcal/mole	0.49
Desolite[3]	15.0 kcal/mole	0.46
Acrylate[4]	12.0 kcal/mole	0.57

1: Buffer tube filling compound
2: Thermal curing primary coating material
3: Trade name (primary coating)
4: U.V. curing primary coating material

It is also important to know whether the accelerating aging at high temperatures (for example at 100°C) is meaningful in predicting the aging behavior by using above model for cable materials. The data were reexamined to compare to the calculating results according to equation 1. Taking the time where the hydrogen generation reaches the maximum, we can obtain following relations:

$$H_1 \max\ (ul/g) = A*\exp(-E/RT_1)*t_1^x$$

$$H_2 \max\ (ul/g) = A*\exp(-E/RT_2)*t_2^x$$

Since the same material has the same maximum of hydrogen generation at different temperatures, $H_1 \max$ (ul/g) is equal to $H_2 \max$ (ul/g), and

$$(t_2/t_1)^x = \exp[(E/R)((T_1-T_2)/T_1T_2)] \quad --(2)$$

Equation 2 shows the relation between aging temperatures and times to reach

the maximum of hydrogen generation. We can use this equation to predict the times to reach maximum hydrogen generation at ambient temperatures from a high temperature accelerated aging test. The errors between calculated results and actual experimental results are within 10%.

Fig.5 Arrhenius Plot of H_2Evolution Rate from Thixotropic A

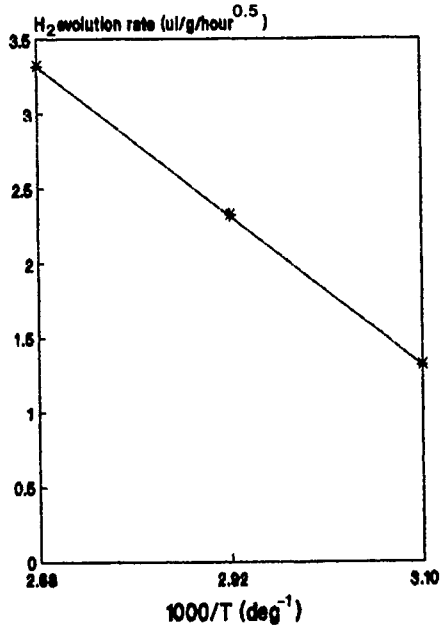

Conclusion

1. the hydrogen evolution from optical fiber cable materials can be precisely analyzed by using Pd/Al_2O_3 as hydrogen adsorbents, and the amounts of hydrogen generation can be expressed as:

$H\ (ul/g) = A*\exp(-E/RT)*t^x$

2. The time constant "x" is in the range of 0.45 to 0.60, and the activation energy for hydrogen generation from optical cable materials is in the range of 6 to 12 Kcal/mole.

3. The correlation between aging temperatures and the times to reach the maximum amounts of hydrogen evolution was established, and the maximum hydrogen generation can be predicted with precision by a simple accelerated aging test.

Reference

1. R.J.Stone,Opt.Letts.,p.297(1982)
2. Y.Mitsunage et al.,Eletron Letts., p.76(1984)
3. K.Noguchi et al., Electron Letts., p.246(1984)
4. S.R.Barnes et al.,Electron Letts., p.712(1985)
5. Abe.K.,Lowe.R.,IWCS Proceeding, p.424(1894)
6. D.L.Philen,et al. IWCS Proceeding, p.415(1984)
7. I.Plitz,Paul C.WArren,IWCS Proceeding p.616(1987)
8. Naoya Uchida, et al.J.Lightwave Technol.,p.1132(1986)
9. M.Fox,et al. Electron Letts.,p.916 (1983)
10. K.Noguchi,et al.J.Lightwave Technol., p.236(1985)
11. Ting-Chung Chang,et al. IWCS Proceeding,p.475(1989)

Mr. Ting-Chung Chang received his M.S. in Applied Chemistry in 1984 from Tsing Hua University and then directly joined Telecommunication Laboratories. He is now a research scientist and a member of outside plant Laboratory in T.L..

Yih-chyuan Lin received his B.S. degree in Chemistry in Taiwan and his Ph. D. degree in Photochemistry from Georgetown University. After working as a postdoctoral Fellow in the Institute of Materials Science at the University of connecticut, he joined Telecommunication Laboratories in 1989 and worked on the development of materials for telecommunication application.

Mr. Jin-Chung Lin received his M.S. in Polymer Science in 1983 from Tsing Hua University and then directly joined Telecommunication Laboratories. He is now a research scientist and a member of out-side plant Laboratory in T.L..

Ms. Chieh-Mei Hsiao received his M.S. in Chemical Engineering from Tsing Hua University.She joined Telecommunication laboratories in 1981 and presently worked as a research scientist in out-side plant laboratory of T.L..

STUDY, EVALUATION AND MANUFACTURING TESTS OF DIFFERENT PBT's FOR THE SECONDARY COATING OF OPTICAL FIBER

Susana CAMARA

ALCATEL STANDARD ELECTRICA, S.A.
Maliaño, Cantabria. Spain

ABSTRACT

The gradual development and expansion of the O.F. systems is branching out to different fields in the communication sector.

Owing to the enormous evolution of optical fibers, the necessity of specific materials meeting special requirements is greater every day. We can mention cables for different applications, for instance, cables exposed to very high levels of mechanical interferences or adverse environmental conditions.

Moreover the common objective is to achieve better productivity which involves a saving of costs in process and labor.

In this paper, we present different polybutylene terephthalates (PBT) with their performance, characteristics, processability and final conditions of the cable manufactured.

INTRODUCTION

For use in the telephone cable industry, we have chosen four different materials from the Plastic World Market that showed "a priori" great posibilities to be used as secondary coating of singlemode and multimode optical fiber cables.

The manufacturing of the cables studies was carried out in a specific extrusion line using loose tube technology and stranding over a central strength member.

The paper describes the properties of the raw materials, the processability and a comparative study of the manufactured loose tubes in the following tests: mechanical properties before and after thermal ageing, physical and chemical properties, compatibilities with filling compounds and transmission parameters.

We have manufactured a 16 optical fiber cable in eight loose tubes (two samples of each evaluated PBT) stranded over a pultruded fiber reinforced rod and sheathed with a polyethylene-aramid yarns-polyethylene jacket.

We also indicate the attenuation changes at 1300 and 1550 nm, obtained during a temperature cycle from -20ºC to 60ºC, as well as the ageing tests of this cable.

We consider the results obtained of the materials used, their performance and the final product achieved, in order to choose the suitable PBT for the different technical requirements of the cable.

The four PBT's will be called materials A, B, C and D throught this paper.

RAW MATERIALS PROPERTIES

First a comparative study was made of the four PBT's as raw materials, that is to say, their mechanical, thermal and physical properties were determined. In tables I, II and III below, the evaluations carried out, the results obtained and the international norms according to which each test was made, are shown.

Likewise, the compatibility of these polyesters, with two types of filling compounds, was studied. The two types used were polyisobutylene and paraffinic compounds which are the kind generally used as filling for O.F. cables. To carry out tnese experiments test pieces consisting of empty tubes of the four PBT's, 250 mm long, were subjected to an accelerated ageing immersed in the filling compound for 7 days at 70ºC. After this period of ageing the mechanical properties (tensile strength and elongation) and their variation were studied.

The results are shown in Table III below.

TABLE I

MECHANICAL PROPERTIES

PROPERTY	TEST METHOD	UNIT	VALUES OBTAINED A	B	C	D
Tensile strength at break	DIN 53455	N/mm^2	35	35	40	30
Elongation at break	DIN 53455	%	240	220	210	260
Modulus of elasticity (tensile test)	DIN 53457	N/mm^2	2450	2000	2400	2250
Modulus of elasticity (flexural test)	DIN 53457	N/mm^2	2500	2200	2200	2200
Stress at 3.5 % strain	DIN 53452	N/mm^2	65	60	70	75
Impact strength, 23ºC	DIN 53453	KJ/m^2	NO BREAK	NO BREAK	NO BREAK	NO BREAK
Notched impact strength, 23ºC	DIN 53453	KJ/m^2	3.4	NO BREAK	NO BREAK	3

TABLE II

PHYSICAL AND THERMAL PROPERTIES

PROPERTY	TEST METHOD	UNIT	VALUES OBTAINED A	B	C	D
Density, 23ºC	DIN 53479	g/cm^3	1.31	1.31	1.31	1.32
Melting flow index 250ºC/2.16 kg	DIN 53735	g/10 min	13	11	11	14
Coefficient of linear expansion, -30º to +70ºC	DIN 53752-A	$10^{-4}K^{-1}$	0.7	0.7	0.5	0.7
Vicat softening part	DIN 53460	ºC	185	180	175	180
Linear mould shrinkage (flow direction)	-	%	2.0	2.0	2.1	1.8
Oxygen index	ASTM D-2863	%	23	24	24	23

TABLE III

		TENSILE STRENGTH (N/mm^2)	ELONG. (%)	% VARIAT. T.S.	ELONG.
	Before ageing	35	240		
COMPOUND A	Filling compound 1			-9.8	+2.3
	Filling compound 2			-9.6	+8.3
	Before ageing	35	220		
COMPOUND B	Filling compound 1			- 9.5	+5.0
	Filling compound 2			-10.1	+7.9
	Before ageing	40	210		
COMPOUND C	Filling compound 1			-5.7	+5.9
	Filling compound 2			-7.8	+9.0
	Before ageing	30	260		
COMPOUND D	Filling compound 1			-3.7	+6.6
	Filling compound 2			-8.3	+9.0

EXTRUSION PROCESS

After the studies carried out in the laboratory, the four polyesters were extruded. Loose tubes were made using the extruder with a 30 mm screw, 4 heating zones and with a 1:2.75 compression ratio. (Figures 1 and 2).

FIGURE 1

FIGURE 2

As far as temperatures and extruder tools are concerned, we trial to find the ideal ones for each of the PBT's.

There were some variations in how each material was worked and in the results obtained.

A description of the way each material was worked and the results achieved are shown below.

MATERIAL A:

- Drying of pellets: in a drying oven:

  90ºC

  12 hours

- Loose tube dimensions:

  Inner diameter 1.2 mm

  Outer diameter 2.0 mm

- Temperature profile: Hopper to nozzle ºC

  200/221/230/235/245/250

  Die: 280ºC

  Melt: 280ºC

- Output: 90 m/min.

  Screw Speed: 55 rpm

- Filling compound: Injection pressing 2 bar

MATERIAL B:

- Drying of pellets: in a drying oven:

  100ºC

  24 hours

- Loose tube dimensions:

  Inner diameter 1.2 mm

  Outer diameter 2.0 mm

- Temperature profile: Hopper to nozzle ºC

  220/230/235/235/245/250

  Die: 280ºC

- Output: 90 m/min

  Screw Speed: 57 rpm

- Filling compound: Injection pressing 2 bar

MATERIAL C:

- Drying of pellets: in a drying oven:

  100ºC

  24 hours

- Loose tube dimensions:

  Inner diameter 1.2 mm

  Outer diameter 2.0 mm

- Temperature profile: Hopper to nozzle

  220/235/245/250/255/255

  Die: 285ºC

- Output: 90 m/min

  Screw Speed: 62 rpm

MATERIAL D:

- Drying of pellets: in a drying oven:

  120ºC

  4 hours

- Loose tube dimensions:

  Inner diameter 1.2 mm

  Outer diameter 2.0 mm

- Temperature profile: Hopper to nozzle

  240/240/240/240/240/250

  Die: 280ºC

- Output: 85 m/min.

  Screw Speed: 65 rpm

- Filling compound: Injection pressing 2.4 bar

The four polybutylenterephtalates have been worked with these small deviations in the processing conditions and in this way quite acceptable variations in physical measurements (diameter, oval) and attenuation values in the fibers have been achieved, although, obviously, we believe that the results of two of the types experimented with are a little better.

THERMIC CYCLES

This test allowed us to study the behaviour of the cable in temperatures ranging from -20ºC to +60ºC. The cable was put into a climatic device and tested using the following thermic cycles (Figure 3).

The attenuation at 1300 nm of each one of the fibers was tested at 20ºC. Then the temperature was raised to 60ºC, reached in 40 minutes. The climatic device was kept at 60ºC for 12 hours, enough time for the whole cable to reach this temperature. At the end of the 12 hours the fibers were measured again. After measuring the fibers, the temperature was lowered to -20ºC, reached in 90 minutes. The climatic device was left at -20ºC for 12 hours, at the end of which time the attenuation of the 16 fibers was measured again. Then the temperature of the climatic device was raised to 20ºC again. After the cable had been subjected to this temperature for 3 hours, the attenuation tests were carried out again.

The whole cycle was repeated a second time. There were no significative variations in fiber attenuation in any of the partial measurements nor at the end of the cycle.

FINAL PROPERTIES OF THE CABLE

Besides the properties, already shown, of all the materials which make up the cable and the results of the specific tests carried out, the following general properties of the cable can be added:

Attenuation at 1300 nm.	Ave.	0.36 dB/km
	Max.	0.38 dB/km
Attenuation at 1550 nm.	Ave.	0.24 dB/km
	Max.	0.25 dB/km

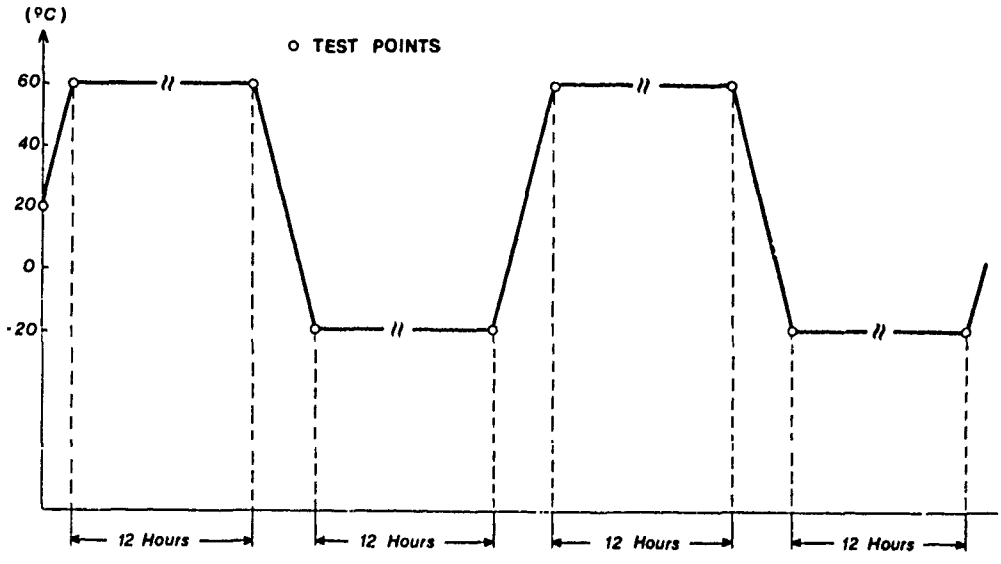

FIGURE 3: THERMIC CYCLES

CONCLUSIONS

The study made shows that the four PBT's, used as raw materials, possess similar and suitable characteristics for their use as secondary coating for loose tube type optical fibers. Any one of the materials could be considered, in principle, as ideal for said technology. Likewise, the ageing of the polyesters, using gel type filling compounds when tested, is satisfactory. None of them exceeded variations higher than 10% in the mechanical parametes studied. As far as their processability is concerned, it can be said that all of them are transformed suitably by extrusion, although it must be pointed out that the performance of two of the polyesters (namely A and B), is better. The results are also better when it is a question of dimensional stability (diameter and ovality) of the tubes manufactured.

In the temperature cycle tested the attenuation measurements are absolutely correct and acceptable.

REFERENCES

1. EVALUATION OF OPTICAL FIBER TERMINATING CABLES WITH FLAME-RETARDANT POLYURETHANE JACKETING. By S. Cámara. I.W.C.S. 1988.

2. ASTM Standards.

3. METAL-FREE SINGLE-MODE OPTICAL FIBER CABLE WITH HIGH MECHANICAL PROPERTIES. By C.G. CORTINES. I.W.C.S. 1988.

4. DIN International Norms.

SUSANA CAMARA received her Master Degree in Chemistry from Oviedo University in 1984, where she specialized in Organic Chemistry.

She joined ALCATEL STANDARD ELECTRICA in 1987 where she presently works in the R & D Materials Department.

MECHANICAL RELIABILITY CONSIDERATIONS FOR FUSION SPLICES IN OPTICAL FIBERS

H. H. Yuce
Bellcore
445 South Street
Morristown, NJ 07962

P. L. Key
Bellcore
331 Newman Springs Road
Red Bank, NJ 07701

T. Wei
GTE Laboratories Incorporated
40 Sylvan Road
Waltham, MA 02254

SUMMARY

We have measured the tensile strengths of fusion splices immediately after splicing without recoating or installing plastic protective sleeves. Splices prepared by three different operators were tested to evaluate operator effects. The strengths of all splices were very low, independent of the operator, with median strengths close to the normal prooftesting stress of 50 ksi. The deterioration in fiber strength was due to abrasion that occurred during the splicing operation. There was little further decrease in strength after aging the splices at 60 and 80°C both in deionized water and at 94%RH for periods of 1 day, 1 week, and 1 month.

We also prepared splices with plastic protective sleeves. The measured strengths of these splices were nearly equal to the original glass strength indicating that the sleeve carries most of the load in the splice. However, after aging sleeve-protected splices at 60 and 80°C in deionized water and at 94%RH, their strengths were reduced to values similar to those of unprotected splices.

INTRODUCTION

The mechanical reliability of optical fibers has been of major interest since their introduction into the telephone network. Initial work in this area has concentrated on the strength of long lengths of fiber. This was appropriate since the first applications of fiber optics for telecommunications have generally concentrated on long distance transmission. Optical cables for this application contain long lengths of fiber with relatively few splices, some of which are prefabricated in the factory with the remaining being made in the field. However, as use of fibers spreads throughout the telecommunications plant, shorter cables containing field splices are becoming more common. Whapham[1] estimates that five to eight splices per subscriber will be required for a branched distribution and loop network.

The preparation of either a mechanical or fusion splice involves several steps which may damage the glass surface. This includes removing the cable structure, stripping the coating, cleaning the stripped fiber, cleaving the fiber, splicing, fiber recoating, and installation of the splice supporting structure. Many of these steps expose the glass surface to mechanical damage and the degrading effects of the environment. In a recent paper[2], we examined the effects of the stripping and cleaning procedures on the mechanical properties of fiber. Others[3-6] have shown that it is possible, with specialized laboratory techniques, to produce fusion splices with strengths nearly equal to that of unspliced fiber. In this paper we examine the effects of normal fusion splicing techniques on the strength of fiber. As part of our study, we considered some of the variables in the fusion splicing process which can affect the strength of the splice. Specifically, we measured the tensile strength of fusion splices with and without plastic protective sleeves. Also, splices were prepared by three different persons to evaluate operator effects. We also tensile tested splices after aging in 60 and 80°C deionized water and 60 and 80°C 94%RH for periods of 1 day, 1 week, and 1 month. Finally, fibers from two different manufacturers were spliced and tested. In total nearly 4,000 fusion splices were made and tested for this study.

EXPERIMENTAL

The objective of this work was to characterize the degree of strength reduction introduced by fusion splicing. Commercially available optical fibers representative of current production capability were obtained from two vendors; the fibers are designated herein as Fibers A and B. The fibers were 125μm glass coated with a UV-cured urethane acrylate to an overall diameter of 250μm. We used the same nominal procedure to prepare all fiber ends for the fusion step. This included stripping the coating with a single commercially available stripping tool. The blades of the stripping tool were cleaned regularly. The stripped ends were wiped clean using lint-free lens paper dipped in ethyl alcohol, and the fiber ends were cleaved using a single blade type cleaver built into the fusion splicer. All splices were made using the same commercially available arc-fusion splicer to eliminate the splicing machine variable. Half of the splices made in this study had a heat-shrunk, plastic protective sleeve installed over the stripped and spliced area; the other half were prepared without the sleeve.

The tensile strength of the spliced samples was measured on a screw-driven universal tensile testing machine at a strain rate of 5% per minute in a test environment of 22°C and 45%RH. Samples were gripped on 10 cm diameter capstans covered with a soft elastomeric sleeve and were secured with masking tape. A gage length between capstans of 50 cm was used and 61 samples were tested for each condition. Splices were tested both in the as-spliced condition and after aging the splices in deionized water and high relative humidity (94%). In addition, samples of unspliced, as-received fiber and as-stripped, unspliced fiber were tested to serve as base-lines for our study. The variables considered in this work were:

Fiber vendor	A, B
Splice type	sleeved, unsleeved
Operator	1, 2, 3
Aging Conditions	Deionized water - 60, 80°C 94% RH - 60, 80°C
Aging time	1 day, 1 week, 1 month

RESULTS AND DISCUSSION

The strength of optical fibers normally can be fit to a Weibull distribution with a very steep slope characteristic of a narrow distribution of strengths. However, the splice strengths for both fibers showed a very broad distribution; results for Fiber A are shown in Figures 1-3. and a poor fit to a Weibull distribution in general. Therefore, we report our results in tabular form in terms of the median strength. The effect of fusion splicing on the tensile strength of fibers A and B is summarized in Tables 1 and 2 respectively. Several observations about fusion splicing are apparent. First, the stripping operation is the cause of the largest deterioration in strength; for example, from 776 ksi as-received to 111 ksi as-stripped for fiber A. The splicing operation produces only a small additional strength loss. Examination of the fractures indicated that failure always occurred in the stripped region away from the fusion zone. Thus, the low strength observed is the result of damage to the exposed glass surface during the stripping operation and during the fusion operation. The use of a heat-shrunk, plastic protective sleeve increases the measured strength of the splice significantly in the unaged condition. This indicates that the load is carried across the weak splice by the sleeve and that the measured strength is not a true indicator of the fiber strength.

Aging in deionized water or in high humidity has little effect on the strength of unsleeved splices. The flaws introduced into these fibers by the stripping and splicing operations are so large that they do not increase in size significantly in the corrosive aging environment. However, aging in either deionized water or high humidity causes large decreases in the strength of splices with a heat-shrunk plastic sleeve. The aging environment rapidly destroys the ability of the sleeve to carry load such that the measured strength of aged sleeved samples approaches the strength of unsleeved splices. As shown in Tables 1 and 2, the results with fibers A and B were similar.

The effect of operator variation is shown in Figure 4 and Table 3. In general, there was little difference in the strengths of splices made by different operators. It is tempting to attribute this to good training or to "operator-proof" equipment. Actually, it is probably due to neither. In the case of unsleeved splices, the strengths are uniformly low due to stripping. In the case of sleeved splices, the strengths are uniformly high because the loads are carried by the sleeves.

The results of this study, like that of our earlier one[1], show that the splicing operation, especially stripping of the coating, is very deleterious to the strength of fiber. It is suggested that improvements need to be made in the tooling used in splicing. In addition, it is important to design splice enclosures to minimize the stresses on the splice and to protect them from the service environment.

CONCLUSIONS

The strength of fusion splices can be significantly less than the strength of the unspliced fiber. The coating stripping operation is the primary cause for the low strength. Heat shrunk plastic sleeves provide an initial strengthening effect, but this is rapidly lost when the splices are exposed to moisture. Splices remain an area for improvement to assure the mechanical reliability of the optical fiber network.

REFERENCES

1. R. Whapham; "Fusion can bring fiber to the home"; **Telephony**; 217(20) 42,46 (1989).
2. T. Wei et al; "Degradation of Fiber Strength During Coating Stripping", Proceedings 38th International Wire and Cable Symposium, 199-203 (1989).

3. J. T. Krause, C. R. Kurkjian, and U. C. Paek; "Strength of Fusion Splices for Fibre Lightguides"; **Electronics Letters;** 17(6); 232-233 (1981).

4. J. T. Krause, C. R. Kurkjian, and U. C. Paek; "Tensile Strengths > 4 GPa for Lightguide Fusion Splices"; **Electronics Letters;** 17(21) 812-813 (1981).

5. Y. Negishi et al; "High-Strength Fiber Splice Applied for Submarine Optical Fiber Cable"; **J. Optical Communications;** 6(4) 122-126 (1985).

6. J. T. Krause; "Ultrahigh-Strength Fibre Splices by Modified H_2/O_2 Flame Fusion" **Electronics Letters** 22(20) 1075-1076 (1986).

Table 1 - Effect of Fusion Splicing on Fiber "A" Strength

Fiber Condition	Aging Condition	Median Strength, ksi	
		Unsleeved	Sleeved
Unstripped, unspliced	Unaged	776	-
Stripped, unspliced	Unaged	111	-
Stripped, spliced	Unaged	92	610
Stripped, spliced	1 day, 60°C,94%RH	71	410
Stripped, spliced	1 week, 60°C,94%RH	68	369
Stripped, spliced	1 month, 60°C,94%RH	62	180
Stripped, spliced	1 day, 80°C, 94%RH	70	191
Stripped, spliced	1 week, 80°C, 94%RH	64	92
Stripped, spliced	1 month, 80°C, 94%RH	92	77
Stripped, spliced	1 day, 60°C,deionized water	70	112
Stripped, spliced	1 week, 60°C,deionized water	62	96
Stripped, spliced	1 month, 60°C,deionized water	72	79
Stripped, spliced	1 day, 80°C, deionized water	68	85
Stripped, spliced	1 week, 80°C, deionized water	70	85
Stripped, spliced	1 month, 80°C, deionized water	77	91

Table 2 - Effect of Fusion Splicing on Fiber "B" Strength

Fiber Condition	Aging Condition	Median Strength, ksi	
		Unsleeved	Sleeved
Unstripped, unspliced	Unaged	694	-
Stripped, unspliced	Unaged	137	-
Stripped, spliced	Unaged	62	512
Stripped, spliced	1 day, 60°C,94%RH	60	367
Stripped, spliced	1 week, 60°C,94%RH	55	330
Stripped, spliced	1 month, 60°C,94%RH	62	161
Stripped, spliced	1 day, 80°C, 94%RH	56	171
Stripped, spliced	1 week, 80°C, 94%RH	68	83
Stripped, spliced	1 month, 80°C, 94%RH	67	69
Stripped, spliced	1 day, 60°C,deionized water	53	74
Stripped, spliced	1 week, 60°C,deionized water	48	42
Stripped, spliced	1 month, 60°C,deionized water	56	38
Stripped, spliced	1 day, 80°C, deionized water	54	55
Stripped, spliced	1 week, 80°C, deionized water	63	46
Stripped, spliced	1 month, 80°C, deionized water	69	44

Table 3 - Effect of Splicing Operator on Fiber Strength

Operator	Fiber	Median Strength, ksi	
		Unsleeved	Sleeved
1	A	92	610
2	A	104	612
3	A	91	634
1	B	62	512
2	B	112	515
3	B	97	508

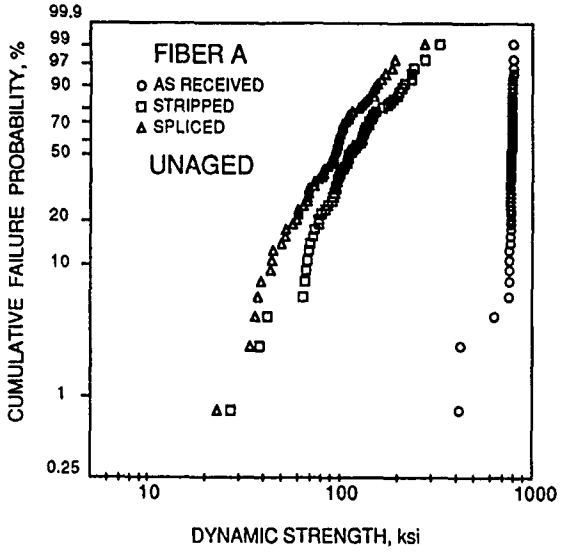

Figure 1 - Effect of Stripping and Splicing on Strength of Optical Fiber - Without Plastic Protective Sleeves

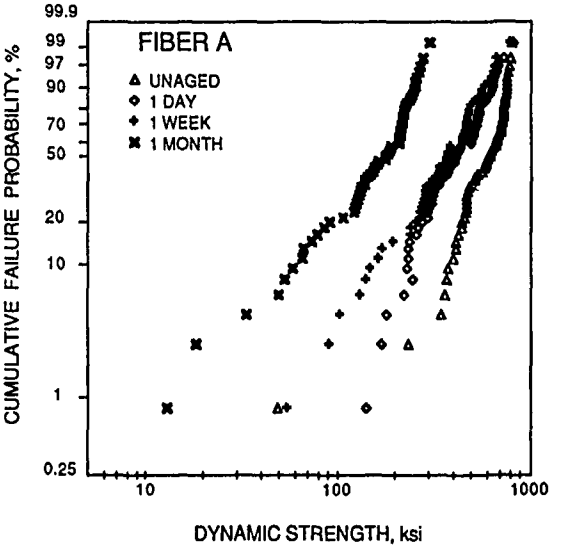

Figure 3 - Effect of Aging at 60 °C, 94% RH on Strength of Fusion Splices in Optical Fibers - With Plastic Protective Sleeves

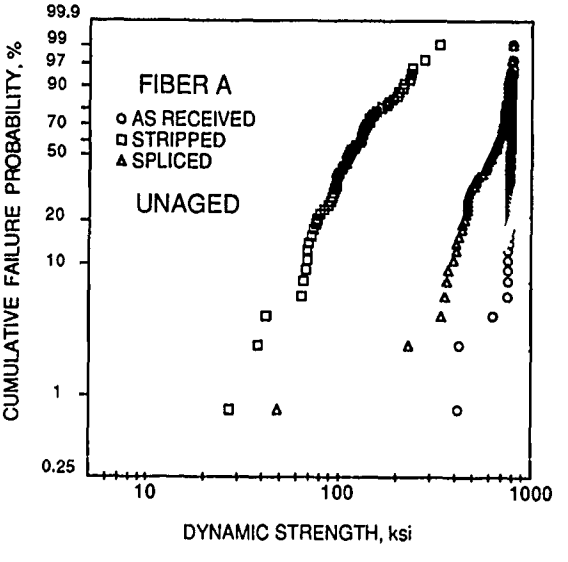

Figure 2 - Effect of Stripping and Splicing on Strength of Optical Fiber - With Plastic Protective Sleeves

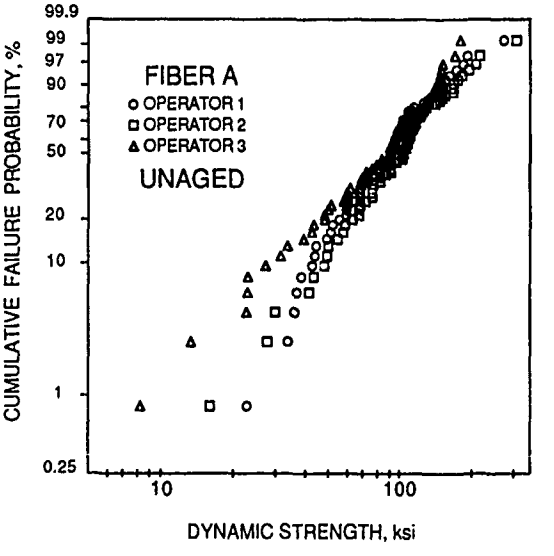

Figure 4 - Effect of Operator on Strength of Optical Fiber Fusion Splices - Without Plastic Protective Sleeves

Hakan Yuce is a Member of the Technical Staff in the Fiber Distribution and Reliability group at Bellcore in Morristown, New Jersey where he is involved in failure analyses and reliability studies of optical fibers. He received a B.S. in mechanical engineering from the Technical University of Istanbul, an M.S. from MIT, and a PhD from Stanford.

T. (Mike) Wei is a Research Supervisor in the Optical Fiber and Components Department of GTE Laboratories in Waltham, Massachusetts. After receiving a PhD in Physics from the University of Pennsylvania, Mr. Wei joined 3M company where he conducted research on fiber optics and polymer physics. In 1984, he joined GTE where he is responsible for fabrication, characterization, and reliability studies of optical fibers.

Leland Key is District Manager of the Metallurgical Science and Engineering Research group at Bellcore in Red Bank, New Jersey. After receiving a PhD in Materials Science from the University of California at Berkeley, Mr. Key joined Bell Labs where he conducted research on the mechanical behavior of materials. In 1983, he joined Bellcore where he is responsible for metals research.

MEASURING METHOD FOR ELONGATION/SHRINKAGE IN STRANDED OPTICAL FIBERS BY MEANS OF TRANSMISSION PULSE DELAY TECHNIQUE

FRANCISCO J. SAEZ DE LA MAZA

ALCATEL STANDARD ELECTRICA, S.A.
39600 MALIAÑO - CANTABRIA - SPAIN

ABSTRACT

The monitoring of the fiber elongation during cable pull tests is considered to be necessary for the evaluation of tensile strength in optical fiber cable designs.

This paper is a method to test and evaluate the elongation and/or shrinkage of fibers by the Transmitted Pulse Delay Technique, which we consider as an improvement on the traditional Phase Shift Technique.

The paper describes the test set, characteristics of the equipment used, and shows the results of several types of cables which have been tested, mainly aerial and special cables (OPGW cores) which we knew would be subject to very high levels of mechanical interference or adverse environmental conditions.

1.- GENERAL

This study has been used on optical fiber cables manufactured with loose tube technology and in all cases, a great deal more has been found out about fiber overlength inside the tube, free grades, helix lay lengths, etc.

All this data is of capital importance in the study of turnkey projects where not only cables are included, but also installation and maintenance are required.

The results achieved experimentally are in accordance with those theoretically calculated, and were fundamental to the design and manufacture of the prototypes tested. The direct measurements of fiber stress must be included in the optical cable qualification testing.

In order to optimize the design of optical fiber cables it is necessary to find out the resistance to elongation/shrinkage with the guarantee that any residual tension is transmitted to the fibers. This objective is essential in all types of optical fiber cables, but it is indispensable in those cables exposed to very high levels of mechanical interference or adverse environmental conditions because when it is a question of cables being installed with residual stress in the fibers, a shortening of their lifetime is to be expected.

That is why it is necessary to always keep the idea of 'no stress', well in mind when it comes to designing optical fiber cables. If this is not done we would face the risk of a decrease in the optical characteristics of such cables throughout their lifetime which, on the other hand, would be considerably shortened.

As this type of test gives us an idea of the state of the fiber inside the optical fiber cables we also believe it is necessary to include it in the qualification trials.

The method described below is based on the delay, in time, of the pulse produced by a laser, along the length of an optical fiber when said fiber is submitted to elongation by means of mechanic pulling.

2.- DESCRIPTION OF THE TEST

The essence of the test consists in measuring the differences in the length of time it takes a pulse to pass along a fiber in repose and the length of time it takes it to pass along the same fiber which has been subjected to a mechanic pull. The difference in the lengths of time, expressed in lengths, by means of a factor of speed, is the elongation of the fiber.

To carry this out we use a Network Analy-

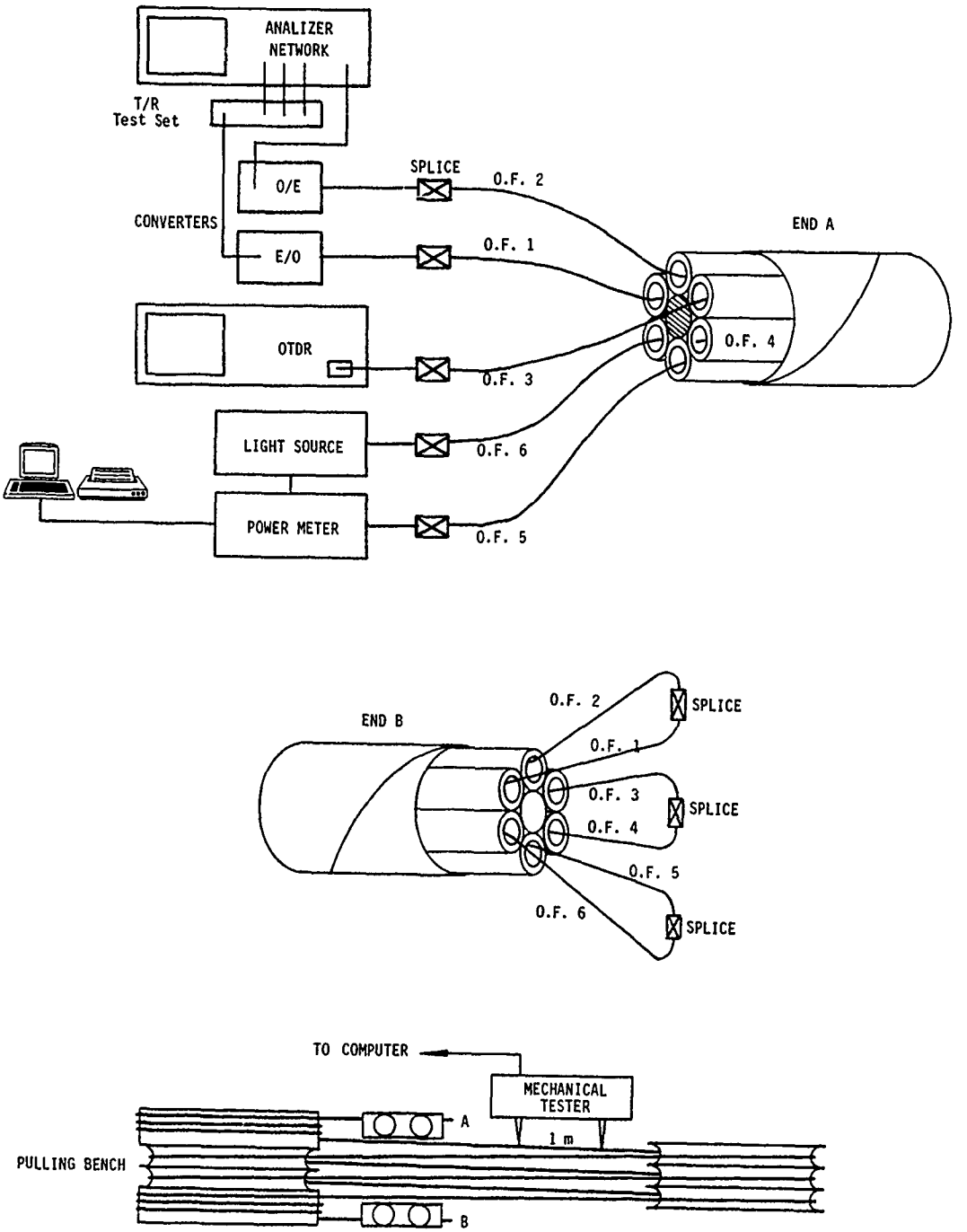

FIGURE 1: DIAGRAM OF THE SET UP OF THE EQUIPMENT AND PULLING BENCH

zer which is made to work at frequencies of between 100 Mhz and 2 Ghz, depending on the length of the fiber being tested:

$$L = \frac{Np - 1}{span} = \frac{Np - 1}{Fstop - Fstart}$$

where,

L = length of fiber under test, in meters.

Np = Number of points -Sampling-.

Fstop = Final frequency.

Fstart = Start frequency = 100 Mhz.

according to the length of fiber under test, L, the final Fstop is calculated.

The frequency range to be worked in is:

$$f = Fstop - Fstart = \frac{Np-1}{L} \cdot \frac{1}{n} \cdot c$$

where,

n = refractive index of fiber, and

c = speed of light.

Also, we use an Electro/Optical Converter which sends the signal produced by the Network Analyzer to the optical fiber, and an Optical/Electric Converter which converts this pulse into an electric signal, which in turn is processed by the Network Analyzer.

The Analyzer generates a pulse which goes into the fiber and, at that same instant, the time it takes to pass along the whole length of said fiber is registered.

Then the cable is subjected to a pull or shrinkage, so that the length of time it takes the pulse to pass along the fiber, increases or decreases according to the speed of the propagation of light inside the fiber.

3.- MEASURING METHOD

A diagram of the set up of the equipment and pulling bench used in the test is shown in Figure 1.

A cable of about 100 meters in length is subjected to mechanic pull by using a pulling bench which monitors by means of a computer, the tension, the elongation and the attenuation variations.

At the same time, and with the help of the above mentioned equipment, the elongation of the fiber inside the cable being tested, is monitored by means of the increase in the length of time it takes the pulse to pass through the fiber.

REFRACTIVE INDEX VARIATION

In order to determine the real value of the elongation to which the fibers are submitted, it is necessary to correct the value obtained in the test equipment. This is due to the changes which take place in the Refractive Index of the fiber under tension.

In tests carried out in our laboratories, using unstranded fibers, the following results, shown in Figure 2, were obtained.

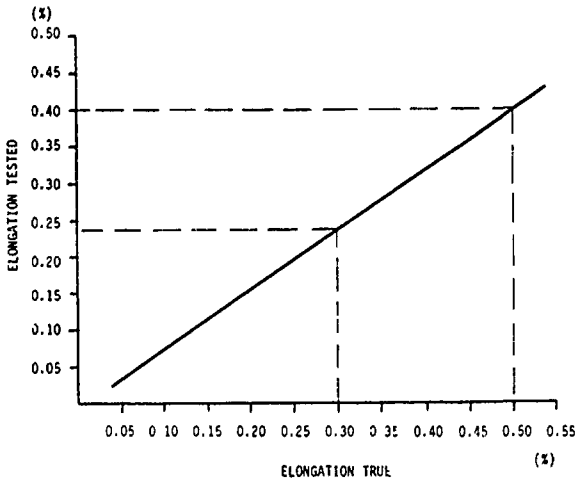

FIGURE 2: VARIATION OF THE ELONGATION TESTED AND REAL

An 0.8 slope is obtained:

Measured elongation = 0.8 Real Elongation.

Therefore real elongation is what the measuring equipment reads, divided by the factor 0.8.

This fact must be kept in mind when we want to find out the real elongation of the fiber. What we want to know is what the fiber's highest degree of liberty is without it suffering any elongation, in other words when the stranded core suffers a pull and, therefore, to elongation.

4.- CABLE TESTS

The equipment used can be seen in Figure 3 while an overall view of the pulling bench is shown in Figure 4.

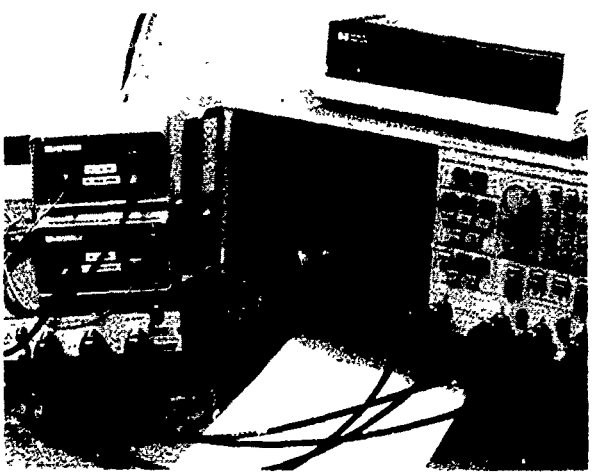

FIGURE 3: EQUIPMENT USED

EQUIPMENT USED

- Analyzer Network-T/R Test Set.
- E/O and O/E Converters.
- OTDR.
- Stabilized light source.
- Power meter.
- Computer.
- Splicer.

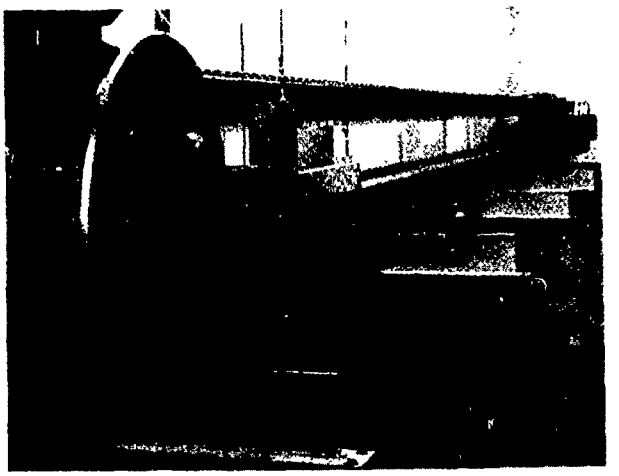

FIGURE 4: PULLING BENCH

OPTICAL CORES UNDER TEST

No. of optical fibers: 6

Type of fibers: Single mode

Max. attenuation at 1300 nm: 0.4 dB/km

Max. attenuation at 1550 nm: 0.25 dB/km.

Fiber coating: Loose tube

Material: Polyester

Inner Diameter: 1.1 mm

Outer Diameter: 1.8 mm

Filling Compound

Stranding: Central member: E-Glass

Outer Diameter: 2.1 mm

The six loose tubes, with a lay length of 65 mm, are stranded around the E-Glass.

The core is fully filled and then jacketed with a polyester glass tape applied helically.

These cores are later used as optical cores for OPGW cables.

THEORETICAL CALCULATION OF ELONGATION

The fibers were housed inside the loose tubes with an overlength of 1.5‰ which was monitored during extrusion and, later on was measured and checked with equipment specially designed for monitoring said parameter. This equipment is shown in Figure 5.

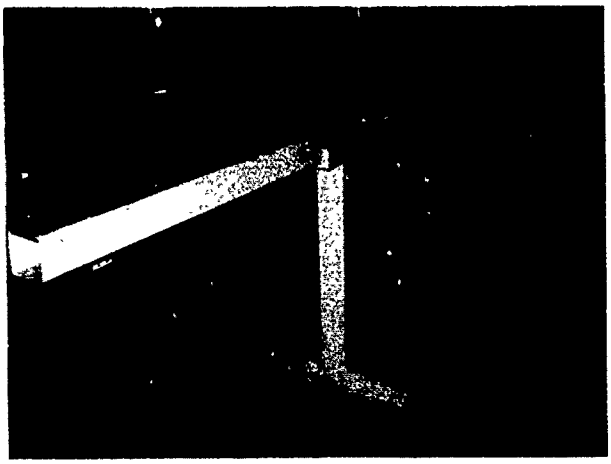

FIGURE 5: EQUIPMENT FOR MONITORING THE OVERLENGTH

In accordance with the loose tube and stranded optical cable design, the length of the fiber inside the loose tube is expressed thus:

$$l = \sqrt{P_o^2 + (2\pi r_o)^2}$$

where,

P_o = lay length, in this case = 65 mm.

r_o = helical radius, in this case, and when the overlength is zero, in other words, the fiber is situated in the center of the tube, it has a value or r_o = 1.95 mm.

Therefore, using the above mentioned data, the length of the fiber for an overlength of zero, is l = 66.1447 mm. When the overlength is of 1.5‰ the length of fiber is l_f = 66.2439 mm.

With these new overlength conditions, the result obtained is a fiber stranded with a new helixial radius:

$$r_f = \frac{\sqrt{l_f^2 - P_o^2}}{2\pi} = 2.03354$$

and the elongation to which the optical core can be subject, in accordance with the above mentioned data, is:

$$\Delta\,(\%) = 100\left[\sqrt{1 + \frac{4\pi^2}{P_o^2}(r_f^2 - r_o^2)} - 1\right]$$

therefore, the r_o is now the radius of the minimum helix to which the fiber can be brought when the core is subjected to a pull, in other words, when it touches the inner wall of the loose tube, with the consequent increase in the lay length: r_o = 1.525 mm.

With this new data we get a Δ = 0.845%, which is the maximum elongation to which the optical core can be subjected without the fiber being submitted to any stress; we will now contrast this value with the experimental data.

5.- RESULTS OF EXPERIMENTS

Distance between pulleys: 15 meters

Diameter of the pulleys: 600 mm

No. of turns: 3

Trial speed: 25 mm/minute

Cable length: approximately, 250 meters

Length being tested: 95 meters

Pulling range: Between 150-1800 N

The length of the fiber tested, according to measurements taken by the Analyzer Network, was 260.94 meters, as can be seen in Figure 6. The sample was, at that time, situated on the pulling bench and subjected to an initial force of 150 N. Then the different tensions were applied and monitored, as per Figure 7.

The dotted line corresponds to the elongation of the core, and the unbroken line to the variation of attenuation in the fibers. According to said Figure 7, the attenuation of the fiber begins to increase when the pull to which the core is subjected is approximately 1100 N and equivalent to an elongation of 0.7% of said core.

When this point is reached, the Analyzer

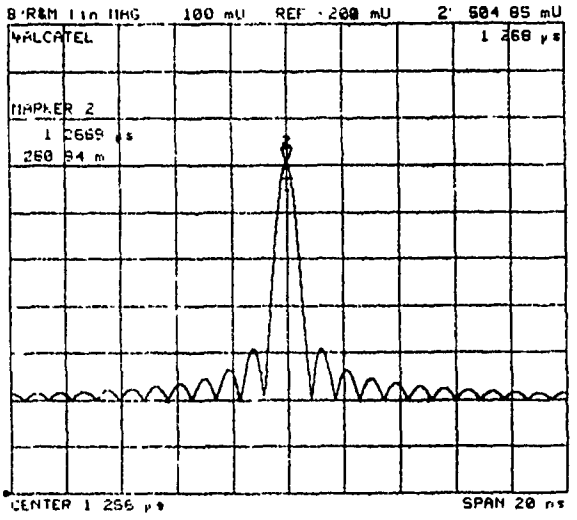

FIGURE 6: LENGTH OF THE FIBER TESTED

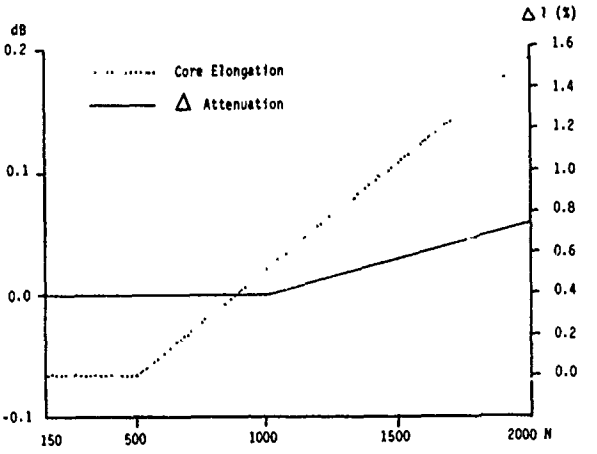

FIGURE 7: ELONGATION OF THE CORE AND VARIATION OF ATTENUATION

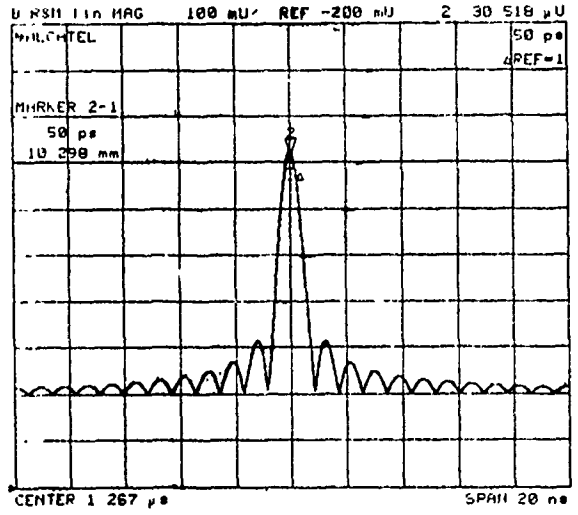

FIGURE 8: 0.01% FIBER ELONGATION

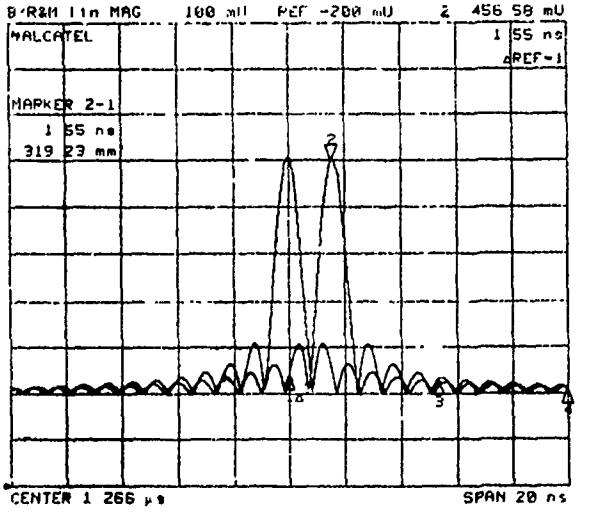

FIGURE 9: 0.32% FIBER ELONGATION

Network shows at the same time that the fiber is beginning to elongate. This can be seen in Figure 8, where the length is of 10.298 mm, equivalent to an elongation of 0.01%.

Continuing with the trial, and when degradation of the fiber is about to begin, taking a measurement at 1600 N of tension in the cable, the fiber is elongated by 0.32%, as can be seen in Figure 9. This means the real elongation is 0.32 : 0.8 = 0.397%.

6.- CONCLUSIONS

Using a pulling bench, an Analyzer Network, E/O and O/E Converters, it is possible to carry out the necessary elongation test to design optical fiber cables. The expected lifetime of the optical fiber inside a cable should not, therefore, be shortened even if it has undergone great strain, which might have demaged it, during cable installation. Even though the damage

done might not be noticed at the time.

We suggest that the fiber elongation measurement be included in the optical cable qualification tests, and what we are offering is a new practical method.

The trustworthiness of this method can be proved by comparing the results obtained with the theoretical calculation. In the first case a value of 0.7% for maximum elongation of the core was obtained, comparable to a theoretical degree of the fiber's freedom of movement of 0.845%.

REFERENCES

1. DIGITAL TRANSMISSION SYSTEM BY OPTICAL FIBERS LASHED TO THE GROUND WIRE OF HIGH TENSION LINES by C.G. Cortines, F.J. Saez. IWCS 1984.

2. DISEÑO Y FABRICACION DE CABLES DE FIBRA OPTICA by C.G. Cortines. II Jornadas de Comunicaciones Opticas. Madrid 1985

3. COMUNICACIONES POR FIBRA OPTICA EN EL SECTOR ENERGETICO. III Jornadas de la Calidad en la Industria Energética. Santander 1987.

4. METAL-FREE SINGLE-MODE OPTICAL FIBER CABLE WITH HIGH MECHANICAL PROPERTIES. C.G. Cortines. IWCS 1988.

5. STRENGTH OF OPTICAL FIBERS. RESIDUAL STRAIN LEVELS FOR FIBER. Optical Fibers, 1988.

6. NETWORK ANALYZER SYSTEM OPERATING AND PROGRAMM by Manual. H.P. 1988.

FRANCISCO J. SAEZ DE LA MAZA was born in 1947. He graduated as a B.S. in 1967 at Santander Technical University. He joined ITT Standard Electrica in 1971 and worked at Material Development Laboratory and participated in development of several telecommunication cable products mainly in the area of electric tests. In 1984 he passed to the Optical Fiber Development Group, and presently is with ALCATEL Standard Electrica the responsible for the Optical Fiber Laboratory of the Telecommunications Cable Division.

He also is the author of several papers and patents.

New Single Loose Tube Cable with Spiralling Fiber Channel in Finnish Field Trial

T. Räsänen and J. Ravela

Nokia Telecommunication Cables
P.O.Box 77, 01511 Vantaa, Finland

Abstract

Due to the need for simple and economic cable design and the increasing popularity of installing optical fiber cables by ploughing in the Nordic countries the new single loose tube cable with spiralling fiber channel and improved crush resistance has been developed and installed for commercial field trial.

The modified extrusion manufacturing process for the single loose tube has effected, potentially, low cost manufacturing of the cables. The developed cable types show excellent performance in the tested optical and mechanical characteristics.

The 1.55 um attenuation stability is in the range of 0.01 dB/km between -45°C...+55°C, and the crush strength in the range of 2000 kg/10 cm. The field trial ploughing of the 0.8 mm diam. wire armored cable into the road bank has demonstrated a cost effective way of installing direct burial cable connections.

1. Introduction

In the Nordic countries the use of ploughing for direct burial of optical fiber cables has become increasingly common in the last few years. The driving force for this trend has been the cost reduction of the installed direct burial cable connections. The present common optical fiber cable designs are, however, quite crush sensitive. Therefore in the ploughing installations special measures have been taken against the crushing force from rocks, freezing water etc. in the soil. Slitted PE-pipes have been used as protection around the cables. Also cables with the maximum crush resistance available in the range of 600 kg/10 cm have been used. Without long term experience on the installed cables it is very difficult to determine the required crush resistance for the various surroundings in the soil. However, improvement of the crush strength will enable more general use of ploughing installation in the Nordic environment.

To reduce the cable costs and to match the cable design for ploughing the new single loose tube cable with spiralling fiber channel and with improved crush strength characteristics has been developed. The pilot production batch of this cable was installed in a field trial in summer 1989.

This paper describes the new cable design and presents test results of the developed cable types and the commercial field trial.

2. Cable Design

When investigating the design for the new cable it was recognized that production of conventional cable, i.e. stranded loose tube and slotted core types is vulnerable and time consuming with many separate steps and relatively expensive, and therefore a more simple and production efficient cable design is required. However, the benefits of excess fiber length, and strain and contraction margins in loose stranded cables were regarded advantageous to give the mechanical reliability. From that basis an idea of a cable with more simple manufacturing and less use of different materials but still with the same or even better mechanical properties than conventional stranded cables was developed. The production efficiency of the single loose tube cables was evident. But also some of their disadvantages were recognized; difficulty in organizing the fibers for controlled strain and contraction margins and the need for special, complicated filling compound for the large size tubes. To avoid these disadvantages the idea of a single loose tube cable with spiralling channel to accommodate fibers or units of fibers was generated. A regular spiralling channel extending up to or over the center line of the tube element would force also the fibers/units to take a similar spiralling path randomly following the tube bore. This thinking lead to the cable design with combined tubing and "stranding" in one production step and with very crush resistant cable core.

To verify the matching of the fiber path with the spiralling channel and to search for optimum geometrical factors of the core element a series of tests was made. With a constant cross sectional geometry of the element (i.e. 6 mm o.d., 3 mm size bore with some non-concentricity) the spiral pitch and the excess length of the fibers were altered in experimentally manufactured cores with 6 single mode fibers. Corresponding theoretical bending radii and contraction margins were calculated and the attenuation increase at -45°C was checked. The results are shown in fig. 1 on the next page.

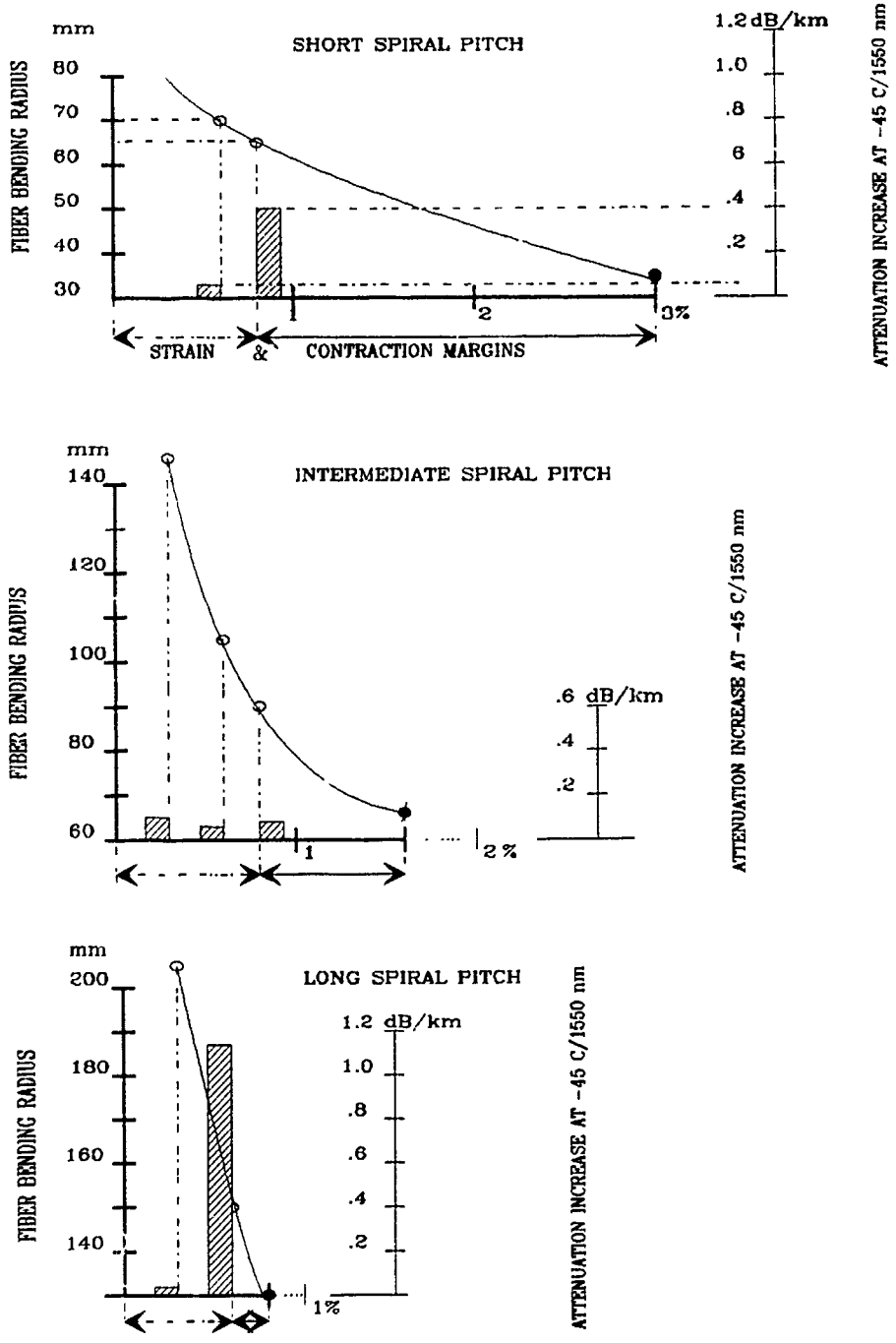

FIGURE 1: THE MUTUAL DEPENDENCE OF THE LOW TEMP. ATTENUATION, FIBER RADIUS, THE SPIRAL PITCH AND STRAIN & CONTRACTION MARGINS

It can be seen that in the samples with the longest spiral pitch (corresponding to almost a straight bore tube) there is a strong correlation between the fiber excess length and the attenuation increase due to the limited contraction margin. In the samples with the shortest spiral pitch there is also a remarkable correlation although contraction margin is large. In this case attenuation growth at -45°C is due to macrobending. With the intermediate spiral pitch no correlation exists between the fiber excess length and the attenuation increase. With these dimensions a strain margin in the range of 1 % can easily be reached without sacrificing the low temperature performance even in the bare unstabilized core element. The relatively large strain and contraction margins in the small size element are based on the possibility of the fibers to straighten down to the center axis of the element. After this test series core elements have been standardized to the sizes presented in fig. 2.

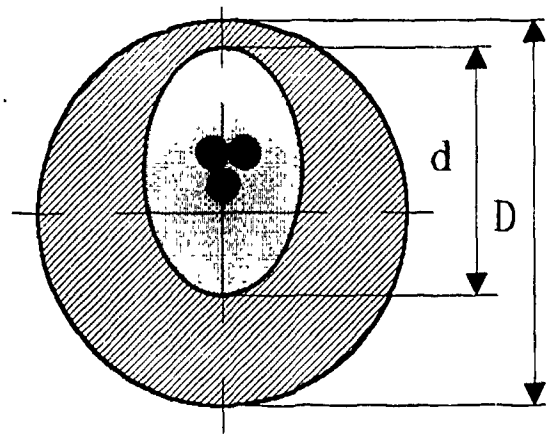

FIBRE COUNT	2-12	-18	-36
D	6	7	8
d	3.5	4.5	5

FIGURE 2: CORE ELEMENT DIMENSIONS (in mm)

The manufacturing process of the core element differs slightly from a normal secondary coating process. To create the spiralling channel a rotating extrusion tip is used. The fibers can be bundled into 6 fiber subunits on-line. The jelly is fed through the tip and the fiber excess length is created by a bias capstan using accurate tensile and temperature control.

In order to have an element rugged enough for further production steps and which could form an integral part of the cable various engineering plastics were studied. PBT was an easy choice because it was known from other applications and gave an even and regular shape also in the modified extrusion. Young's modulus in the range of 2000 N/mm^2 is sufficient to give good handling characteristics to the element in processing.

The coefficient of linear thermal expansion of approximately 0.7 x 10^{-4}/K is small enough to give good temperature stability of the fibers in the core. However, Young's modulus drops drastically above approximately +40°C and also post shrinkage is increased at elevated temperatures. As tube filling compound a normal thixotropic compound with good low temperature characteristics down to -45°C is used.

The first Spiral Space^R cables have been manufactured with thin 0.8 mm diam. steel wire armoring for direct burial, see fig.3. This armoring gives good attenuation stability between -45....+55°C and tensile strength up to the pulling force of about 2 km weight of the cable with no fiber strain.

To bring the weight and the costs further down Twin Rod Reinforced (TRR) cables were developed for direct burial and duct installations, see fig. 3. Two approximately 1.6 mm diam. rods of either steel or fiber reinforced plastics (FRP) are embedded symmetrically parallel to the core element in the cable jacket. The rods give reasonable attenuation stability and the pulling force of above 1 km weight of the cable.

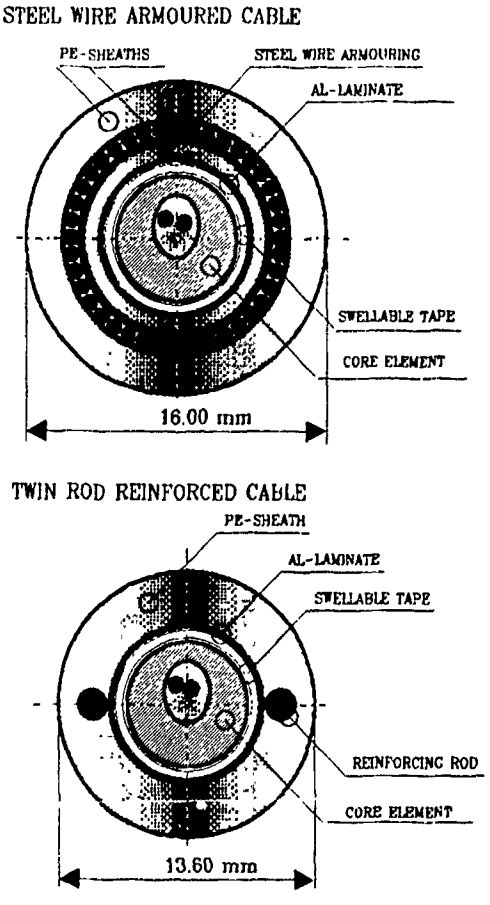

FIGURE 3. TWO CABLE DESIGNS

The core element as such is strong and stable enough to form an integral part of the cable in non-demanding applications such as indoors. Indoor cables can be manufactured just by adding a few synthetic fiber reinforcement yarns around the core and sheathing it with flame retardant material.

3. Cable characteristics

The 0.9 mm and 1.4 mm diam. wire armored and twin rod reinforced Spiral Space^R cables are being type tested for the Finnish Telephone Operating Companies' approval. Here are presented the major results so far of the type testing programme.

3.1 Test results for the core unit

The Young's modulus of a 6 mm o.d. core tube has been measured to be about E = 2200 N/mm^2 at room temperature and thermal expansion coefficient of the tube material to be 0.6...1.2 x 10^{-4}/K between -45....+55^{o}C.

To check the proper excess length of the fibers the tube has been tensile tested at +20^{o}C and the attenuation of the tube fibers has been checked at -45^{o}C. The measured excess lengths in the range of 0.5 % have been in the design range and tube contraction at -45^{o}C has generated practically no attenuation increase.

The post-shrinkage of the tubes has been checked after aging at +80^{o}C and has been found to be non-significant. The major part of the crush strength of the cables has been found to be due to the core element.

As all of the above demonstrates the Spiral Space^R unit itself possesses many cable-like characteristics and after some improvements could possibly be used as a cable as such (see section 6).

3.2 Test results for the cables

The attenuation stability for a 12-fiber 0.9 mm diam. wire armored and a non-metallic twin rod reinforced 4-fiber cable were tested with two cycles between -45....+55^{o}C. The 1.55 um attenuation increase at -45^{o}C was less than 0,01/0.02 dB/km for the 4- / 12-fiber cables. The attenuation stability of the 1.4 mm diam. wire armored cable should be even better due to the higher amount of steel in the cable. The tensile strength of the cables has been evaluated according to IEC-794-1-E1 and from short 7 m samples. Depending on the design, the quality of strength member steel varies: armoring steel wires have tensile strength of 400 ... 500 N/mm^2 and TRR cable steel approximately 1500 N/mm^2 with elastic strain regions of approximately 0.1 and 0.4 % respectively. The strain curves for the 7 m cable samples are presented in fig. 4.

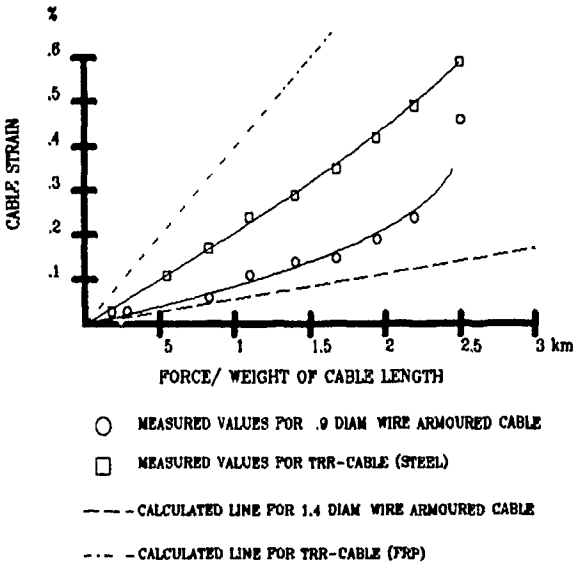

FIGURE 4: STRAIN CHARACTERISTICS OF THE TWO CABLE DESIGNS

From the curves it can be concluded that allowing 0.2 % strain in the 0.9/1.4 mm diam. wire armored and 0.4 % strain in the TRR cable, gives a maximum pulling force 2.1/3.1 and 1.8 times kilometer weight of the cables, respectively.

Crush resistance has been determined according to IEC-794-1-E3 and the results are in fig.5.

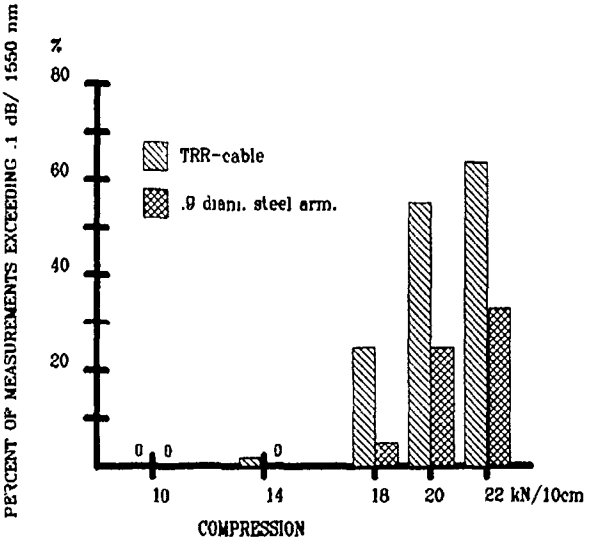

FIGURE 5: CRUSH RESISTANCE OF THE TWO CABLE DESIGNS

TOTAL NUMBER OF MEASUREMENTS/ CABLE DESIGN, N=60

Crush resistance of both designs is in order of magnitude better than in comparable conventional stranded loose tube and slotted core types /1/.

Impact resistance has been tested according to IEC 794-1-E4 and the test results are on the following table.

Table 1. Impact resistance of experimental cables (R is the radius of the hammer).

R (mm)	Impact resistance (Joule) Twin Rod Reinforced	0.9 mm diam. wire armored
10 mm	> 5 (≈7)	> 10 (≈14)
50 mm	> 5	> 10
300 mm	> 10	> 10

Impact resistance is limited by the appearance of cracks in the cable core (not broken fibers or attenuation increase). Due to this the of use somewhat softer core polymer would increase impact resistance but on the other hand would decrease crush strength.

Kink resistance, repeated bending and torsion of the cables have been tested according to IEC-794-1-E10, E6 and E7, respectively, with the following parameters:

Kink:
5 times down to 20 cm bending radius

Repeated bending:
1000 times (+/- 180°) with 20 cm bending radius

Torsion:
20 cycles (+/- 180°)

All the cables passed these tests.

4. The direct burial ploughing field trial

A 0.8 mm diam. wire armored 6-fiber Spiral Space^{R} cable was installed for field trial by the Oulu Telephone Company on 30 km route in summer 1989. The cable was ploughed to a 70 cm depth into the road bank with the speed of approximately 10 km per day using special ploughing apparatus, see fig. 6.

Fig. 6. The cable plow used in the field trial. Plough angle can hydraulically be adjusted according to the slope of the road bank.

No attenuation increase nor attenuation steps due to crush were found after installation although during the installation the cable was handled quite roughly from time to time.

The cable joints were placed inside buried enclosures with easy re-entry capability for possible reorganizations.

Due to the improved cable design enabling efficient ploughing, the installation costs (excluding jointing) proved to be equal, within a few percent, to the existing installation costs of erecting a pole line and hanging an aerial cable. The installation costs were about 30...50 % of those for normally dug direct burial line. This field trial has demonstrated a very cost effective way of building new direct burial optical fiber cable connections.

5. Future prospects

In order to make Spiral Space^{R} core element stronger and more stable, and so reduce or even replace the need of outside reinforcements, new materials are under development and evaluation. Especially self reinforcing plastics like liquid crystal polymers, their blends with engineering plastics, and composites seem to be quite promising. Together with rotating extrusion tools they are able to establish a spiralling orientation of filaments and create a tough but flexible rope-like structure.

Work on modification the design to adapt the fiber ribbons has been started.

6. Conclusion

The new, potentially low cost single loose tube cable design with spiralling fiber channel and optimized crush strength performance has been developed and installed in a commercial field trial. The test results on both the wire armored and, twin rod reinforced cables show excellent performance in all optical and mechanical characteristics. The crush resistance of approximately 2000 kg/10 cm is the highest known for a cable with a polymer cable core. The 1.55 um attenuation stability is in the range of 0.01 dB/km between -45....+55°C, depending on the fiber count in the fiber channel and the sheath construction. The field trial ploughing of 0.8 mm diam. wire armored Spiral Space® cable into the road bank has demonstrated a very cost effective way of direct burial installation at the cost level of the building of a new aerial cable line.

In the future the cost performance of the installed Spiral Space® cables may be further improved by the use of the very low cost twin rod reinforced cable design. Also reinforcing the polymer core with liquid crystal polymers or composite materials may enable the use of the polymer core as a cable as such.

Acknowledgements

The authors wish to thank the Oulu Telephone Company and especially Network division manager Seppo Sederholm for their fruitful co-operation during the field trial and manager Markku Pikkarainen together with his colleagues at the Finnish PTT for collaboration in the testing.

References

1. J. Kurki, L. Stormbom, L. Oksanen, T. Räsänen, E. Leino: Reliability and Environmental Performance of Cabled Single-mode Optical Fibres. Proc. 38th IWCS, pp. 380...389.

Timo Räsänen received the Dipl. Eng. degree in electronics in 1971 from the Helsinki University of Technology. Before joining Nokia Cables he was engaged in R&D of digital transmission technology in the Telecommunications Laboratory of the University and in Nokia Electronics. In Nokia Cables he has, since 1979, been responsible for the development of optical fiber cable technology, including transmission systems, and for technical support in the marketing of optical fiber cables and systems.

Jussi Ravela received the Engineer degree in 1973 from the Technical Institute of Helsinki in mechanical engineering. He worked as a design engineer in the Technical Department of Nokia Cables up to 1984, being engaged in designing cabling machinery and devices, e.g. for the fabrication of optical fibers and their further processing. Sirce then he has been working as a R&D engineer in the area of optical Fiber Cable Technology focusing on materials, cable designs and processing.

OPTICAL TALK SET AND OPTICAL CABLE IDENTIFIER USING POLARISED-WAVE-EXTERNAL-MODULATION METHOD

A.Fujisaki, H.Ogoshi, S.Sentsui, M.Kurokawa, M.Mizutani*, M.Miyazaki*

OPTO-TECHNOLOGY LABORATORY, THE FURUKAWA ELECTRIC CO.,LTD.
6, Yawatakaigan-dori, Ichihara Chiba 290 Japan
*TOKYO ELECTRIC POWER COMPANY
1-3, Uchisaiwai-cho, 1-Chome, Chiyoda Tokyo 100 Japan

Abstract

The polarization fluctuation in single mode optical fiber is caused by change of boundary conditions. Utilizing this phenomenon, external modulation can be possible. Polarized-wave-external-modulation (PWEM) using photoelastic effects, have been applied to optical fiber cable identifier and optical talk set that can be tapped on any part of a vacant optical fiber on the job site.

1. Introduction

The amount of installed optical fiber cables is increasing year after year with the advances and expansions of optical communications, and sometimes many optical fiber cables are installed in the same ducts or the same poles. This has necessitated the device to correctly identify the optical fiber cable that is required to be accessed for cable root change, transfer, branching or other work. For the identification of optical fiber cables containing no copper pair, nor steel-wire strength member, the identification method by a search coil that has been used for conventional metallic cables cannot be used. A new device for identifying objective optical fiber cable has been developed to solve this problem.

It is also necessary to have communication during optical fiber jointing work to find the quality of splices along the cable line. By now we use a vacant optical fiber for this purpose when the cable contains no not have a copper pair for order. Since the most of the talk set is connected to the end of the vacant fiber, no communication is possible for the work of the remaining stand-by fiber. To solve this problem we have developed an optical talk set that is tapped on any part of fiber without cutting the fiber.

The basic concept of these devices are derived from the study on polarization fluctuation in single mode optical fiber.

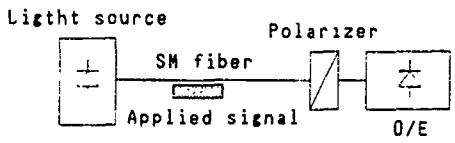

Fig.1 Principle of optical system

2. Principles

A light injected into the single-mode optical fiber is known to subject to polarization fluctuations with the change of environmental conditions of the installed optical fiber cable. Polarization fluctuations are attributed to partial double refraction of the optical fiber, which is caused by a fluctuating external stress or by other causes, such as optical fiber cable vibration overlapping in a longitudinal direction. [1] When a stress is intentionally applied halfway in optical fiber like Fig.1, the light intensity passing through a polarizer at the photodetection side varies in accordance with fluctuations of the plane of polarization that follow the applied signal.

Fig.2 shows the spectral distribution of polarization fluctuation by external forces, magnet fields and other factors observed in the past our experiment. The vertical axis in Fig.2 shows the fluctuation of light intensity at polarizer outputs Photoelastic effects caused by stress distortion in optical fiber and Faraday effect directory by magnetic field are causes of such. Taking

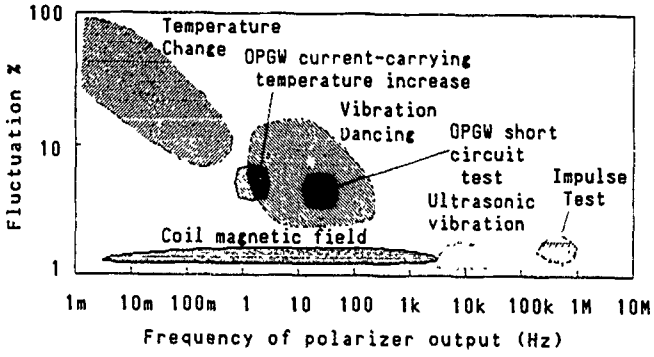

Fig.2 Spectral distribution of polarization fluctuation

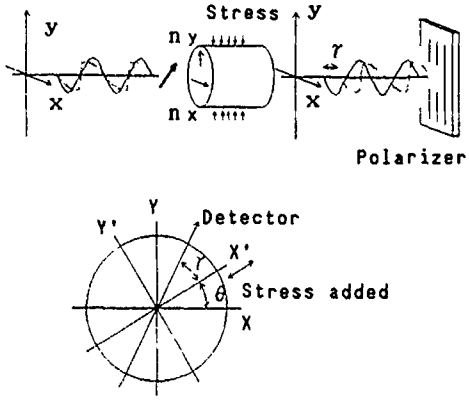

Fig.3 Explanation of signal input from the side of optical fiber

electromagnetic induction noise to peripheral equipments, device size and other factors into consideration, our devices used the photoelastic effects.

The principles of polarized-wave-external-modulation (PWEM) method by photoelastic effects are described below. Fig.3 shows a mechanism of signal input from the side of optical fiber , and a relation of coordinates. The electric vector E and light intensity P in the single mode optical fiber before applying a stress can be expressed by Equ.① .

$$\dot{E} = a e_x \cos\omega t + b e_y \cos(\omega t + \psi) \qquad ①$$

$$e_x = e_x' \cos\theta - e_x' \sin\theta \quad (a^2+b^2 = 1)$$
$$e_y = e_y' \sin\theta + e_y' \cos\theta \qquad ②$$

e_x' : unit vector of x'-direction
e_y' : unit vector of y'-direction

$$E^2 = a^2 + b^2$$

Change of coordinate (e_x, e_y) to (e_x', e_y'), E is expressed Equ.③ .

$$\begin{aligned}\dot{E} &= a(e_x'\cos\theta - e_x'\sin\theta)\cos\omega t \\ &\quad + b(e_y'\sin\theta + e_y'\cos\theta)\cos(\omega t+\psi) \\ &= e_x'\{a\cos\theta\cos\omega t \\ &\quad + b\sin\theta\cos(\omega t+\psi)\} \\ &\quad + e_y'\{-a\sin\theta\cos\omega t \\ &\quad + b\cos\theta\cos(\omega t+\psi)\}\end{aligned} \qquad ③$$

When stress is applied the orthogonal index of refraction n x and n y in the core of the optical fiber changes, and phase difference α (t) and β (t) occur in x and y direction.

Then electric vector E ' is expressed Equ.④ .

$$\begin{aligned}\dot{E}' &= e_x'\{a\cos\theta\cos(\omega t+\alpha) \\ &\quad + b\sin\theta\cos(\omega t+\alpha+\psi)\} \\ &\quad + e_y'\{-a\sin\theta\cos(\omega t+\beta) \\ &\quad + b\cos\theta\cos(\omega t+\beta+\psi)\}\end{aligned} \qquad ④$$

Electric field E_d of polarizer output light is expressed by Equ.⑤ , when polarization angles of the polarizer is γ to x' coordinate.

$$\begin{aligned}E_d &= D\{a\cos\theta\cos(\omega t+\alpha) \\ &\quad + b\sin\theta\cos(\omega t+\alpha+\psi)\}\cos\gamma \\ &\quad + D\{-a\sin\theta\cos(\omega t+\beta) \\ &\quad + b\cos\theta\cos(\omega t+\beta+\psi)\}\sin\gamma \\ &= D[\{a\cos\theta\cos\alpha \\ &\quad + b\sin\theta\cos(\alpha+\psi)\}\cos\gamma \\ &\quad + D\{-a\sin\theta\cos\beta \\ &\quad + b\cos\theta\cos(\beta+\psi)\}\sin\gamma]\cos\omega t \\ &= D[\{-a\cos\theta\sin\alpha \\ &\quad - b\sin\theta\sin(\alpha+\psi)\}\cos\gamma \\ &\quad + D\{a\sin\theta\sin\beta - b\cos\theta\sin(\beta \\ &\quad + \psi)\}\sin\gamma]\sin\omega t\end{aligned} \qquad ⑤$$

$$E_d = A\cos\omega t + B\sin\omega = E_o\sin(\omega t + z)$$

$$E_o^2 = A^2 + B^2 = P \qquad ⑥$$

$$\begin{aligned}P &= D^2/2[1+\{a^2+b^2\{\cos^2\theta\cos\gamma \\ &\quad - \sin\theta\sin\gamma\cos(\alpha-\beta) \\ &\quad + ab\{\sin2\theta\sin2\gamma\cos\psi \\ &\quad + \cos2\theta\sin2\gamma\cos\psi\cos(\alpha-\beta) \\ &\quad + \sin\psi\sin(\alpha-\beta)\}]\end{aligned} \qquad ⑦$$

When a=1,b=0 : linearly polarized light

$$P = D^2/2[1 - \cos 2\theta \cos\gamma - \sin\theta \sin \cos\{\alpha(t) - \beta(t)\}] \quad ⑧$$

When $a = 1/\sqrt{2}$, $b = 2$, $\psi = -\pi/2$
: elliptically polarized light

$$P = D^2/2[1 - \sin 2\gamma \sin\{\alpha(t) - \beta(t)\}] \quad ⑨$$

$$\sin\{\alpha(t) - \beta(t)\} = \kappa\, Vm \sin\omega mt$$

When the stress is applied through thickness vibration of piezoelectric element, phase difference varies according to the piezoelectric element drive voltage of $Vm\sin\omega mt$.
By this, the intensity-modulated light from polarizer output determined by the drive voltage of the piezoelectric element can be obtained as shown in Fig.4. [2]

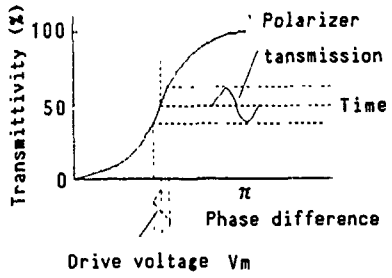

Fig.4 Piezo drive voltage vs. polarizer output

- Optical cable identifier -

For the optical cable identification, We use a mechanical vibration of signal to the optics system shown in Fig.1 to apply a stress to the optical fiber from outside of the cable. By this method, photoelastic effects occur, and the applied frequency can be confirmed also by the spectrum of polarizer output. Thus, by injecting a light into one fiber in the cable, which is to be identified beforehand, by applying mechanical vibration signal at the job site, and by detecting this signal at the photodetection side at office, the optical fiber cable identifier can be realized.

The circuits actually using other fibers are not affected during this identification. Furthermore adjoining optical fiber cables do not detect the signal neither.

-Optical talk set tapped on to an optical fiber-

Fig.5 shows the principles of the optical talk set which does not need cutting the optical fiber on the job site. A voice signal can be sent to photodetection side by contacting piezoelectric element driven by a voltage, which is FM-modulated by a voice signal. By this up-calling of job site to office can be realized. And by local detection method, office to the job site of down-call will be possible. Directly FM-modulated light by voice signal is injected from office side, and leak light by local detection is detected and demodulated on the job site.

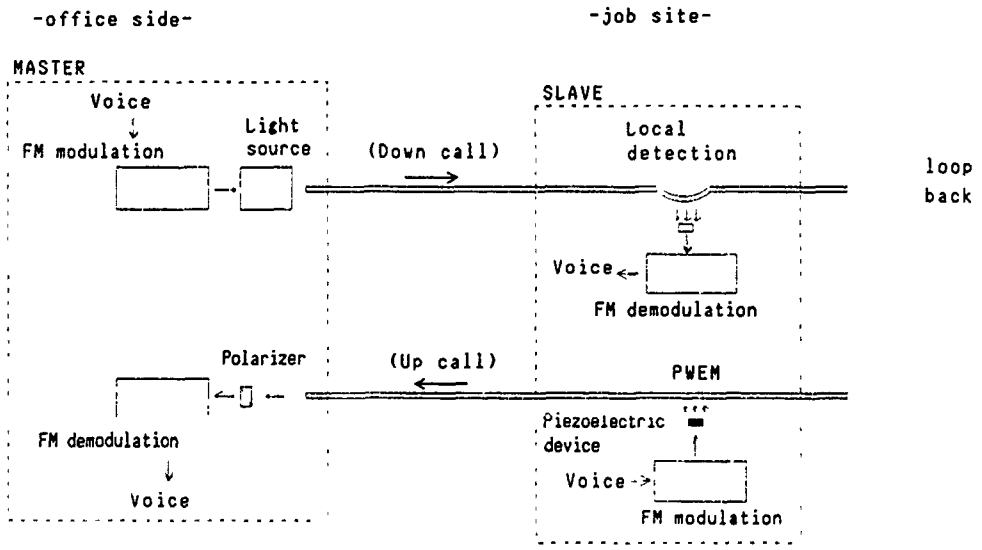

Fig.5 Principles of optical talk set

3. Feature of devices

- Optical cable identifier -

The optical cable identifier manufactured for a trial consists of the signal inputting tool to be used at the job site and the optical transmitter/receiver to be used in the office. The signal input tool holds the cable and apply mechanical vibration of approximately 350 Hz as a identification signal. The applied frequency is set to be higher than the frequency regions which are always caused by temperature change and dancing of installed cable. The optical transmitter/receiver consists of the light source, and of the photodetector and signal comparator. The light source injects linearly polarized light of a semiconductor laser diode operating in the 1.3 μm band to the optical fiber. The photodetector detects the light from the optical fiber in needed optical cable, which is looped back connected on the far end through the polarizer. The signal is demodulated it into a electric signal identified in signal comparator. Allowable looped optical fiber transmission losses of 25 dB could be confirmed with the trial fabrication. Fig.6 shows a spectrum of polarizer output.

- Optical talk set tapped on to optical fiber -

Fig.7 shows a spectrum of polarizer output and source signal. The S/N ratio of the demodulated signal is sufficient for speeches. The optical talk set without cutting optical fiber consists of the master unit used at M/IDF in the office side and of the slave unit used on the job sites.

(Master unit) The down-call circuit uses 1.55 μm as a light source, because it has a large amount of leak light by bending on the slave unit. For the up-call optical fiber for talk set is connected by looping back at the far end. The light which is directly FM-modulated by voice signal from the microphone of the master unit is also modulated by PWEM at the job site of slave unit, and inputs to the polarizer and demodulates signal from slave unit. The carrier frequency of both FM-modulated signal is 455 KHz for down-call by direct modulation and 1 MHz for up-call by PWEM.

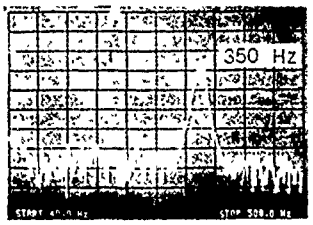

Fig.6 Spectrum of polarizer output in optical cable identifier

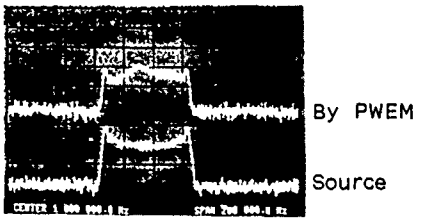

Fig.7 Spectrum of polarizer output in optical talk set

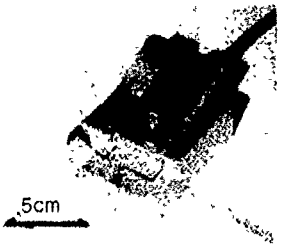

Fig.8 Tapping tool of talk set

(Slave unit) The Tapping tool that set ribbon fiber without cutting it consist of two parts. One is which bends the optical fiber and detects the leak light for the down-call reception and the other is the tool to press the optical fiber on the piezoelectric device for PWEM signal input. Insertion loss of local detection tool is less than 0.4 dB at 1.3 μm and of PWEM tool is 0 dB. Fig.8 shows a tapping tool of slave unit.

(Speech performance) Allowable transmission losses of looped optical fiber for up-call is more than 25 dB and allowable transmission loss between master and slave unit for down-call is more than 20 dB. No influence are caused to the live optical fiber even if the tools using piezoelectric device are applied to it by mistake.

4. Operation of the devices

Fig.9 shows the operation modes of the devices. In the optical cable identification process, one end of the vacant optical fiber of the workable cable is loop-back connected, and optical transmitter/receiver is connected to the optical fiber at the other end. Identification is performed by installing the signal inputting tool to the needed optical cable at the job site. Identification signal is received at the office side.

After optical cable identification, communication line will be set. Communication line by talk set is installed by loop-back connecting one end of vacant optical fiber in advance and connecting the other end to the master unit. On the job site, cable sheath is stripped off, and the closure is removed and the tapping tool of slave unit is set to the optical fiber.

Fig.10 shows a operating mode of optical talk set.

5. Conclusion

Polarized-wave-external-modulation method is studied. Device to support identification of optical fiber cable and optical talk set has been developed. At present, studies are made to enhance the handling and usage in commercial applications.

6. References

[1] Fujisaki et.al "A Study on Polarization Fluctuation on Single-Mode Optical Fiber" OEC'88 PP.140-141,1988.

[2] Amnon Yariv "INTRODUCTION TO OPTICAL ELECTRONICS" Holt, Rinehart and Winston,Inc U.S.A.

[3] Fujisaki et.al "Optical Cable Identification Device" IEE-J, CMN-90-2,1990.

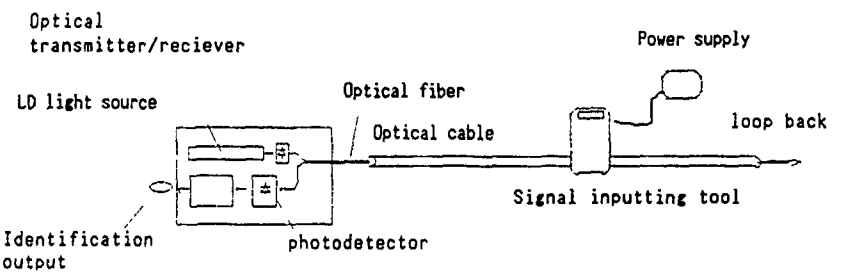

Fig.9 Operation of optical cable identifier

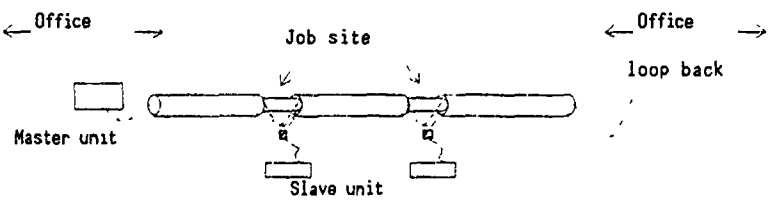

Fig.10 Operating mode of talk set

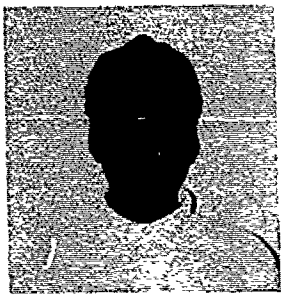

AKIRA FUJISAKI

The Furukawa Electric Co.,Ltd.

Mr. Fujisaki received B.S.degree in electrical engineering from Waseda University in 1987 and joined The Furukawa Electric Co.,Ltd.
He has been engaged in optical fiber transmission research section.

MICHITOYO KUROKAWA

The Furukawa Electric Co.,Ltd.

Mr. Kurokawa received B.E. degree in control engineering from Osaka University in 1970 and joined The Furukawa Electric Co.,Ltd. He has been engaged in development of telecommunication cables.
He is now manager of optical cable system development department.

HARUKI OGOSHI

The Furukawa Electric Co.,Ltd.

Mr. Ogoshi received M.E. degree in electrical engineering from Ibaragi University in 1980 and joined The Furukawa Electric Co.,Ltd. He has been engaged in optical cable system development department.

Morinobu Mizutani

Tokyo Electric Power Company

Mr. Mizutani graduated Koganei Industrial high school in 1970 and joined Tokyo Electric Power Company. He has been in development of construction technology of telecommunication systems and optical fiber cables. He is now assistant to the manager of electronics and telecommunication department.

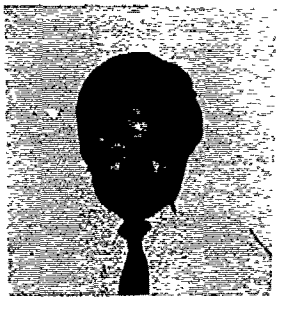

SHINTARO SENTSUI

The Furukawa Electric Co.,Ltd.

Mr. Sentsui received B.S. degree in physical engineering from Tokyo University in 1970 and joined The Furukawa Electric Co.,ltd. He has been engaged in research and development of superconduction coaxial line, characterization and measurement of optical fiber. He is now a manager of optical fiber transmission research section.

Mitsuo Miyazaki

Tokyo Electric Power Company

Mr. Miyazaki received M.E. degree from Electronic Communication University. He has been in charge of department on a telecommunication facility for power transmission control.

PREDICTING FIBER PROTRUSIONS FROM CONNECTORS WITH LINEAR PLATE THEORY

J. M. Anderson K. B. Bradley

AT&T Bell Laboratories, Norcross, Georgia 30071

ABSTRACT

Conventional connector designs appear unable to meet the performance requirements of systems operating at rates of 565 Mb/s and higher. Reflections generated at connections in these systems degrade laser stability and limit system performance. Physical-contact (PC) connectors utilize fiber protrusions to decrease reflections. One such connector, the single-mode ceramic-ferrule type, will exhibit consistently low insertion loss and return loss on the order of -40 dB if a protruding fiber configuration is used. This memorandum describes a method of predicting fiber protrusions for physical-contact connectors polished on compliant pads.

INTRODUCTION

The demand for single-mode fiber-optic systems operating at high data rates has spawned a need for the development of high performance connectors. Conventional connector designs appear unable to meet the performance requirements of systems operating at rates of 565 Mb/s and higher. Significant problems in systems operating at high rates result from Fresnel reflections since the reflected optical power can be diffused back into the laser cavity degrading laser stability. In a typical system operating at 565 Mb/s, a return loss of -30 dB is large enough to prevent optical power feedback from causing unstable operation of the laser.

Return losses of -30 dB and higher have been accomplished in several ways. In the "angle-butt" method, the connector ferrules are polished so that the ferrule end is not perpendicular to its longitudinal axis. This configuration has produced acceptable return loss when used in such connectors as the slant biconic. Return loss can also be increased with the use of index-matching gels applied at the interface between fiber ends. Another method, growing in popularity, is the convex physical-contact configuration in which the fibers contact each other under pressure. This results in lower insertion loss and reduced reflection; it also diminishes the chance of dust particles introducing an air gap between fiber ends. Of particular interest is the single-mode straight-tipped connector which exhibits consistently low insertion loss and return losses on the order of -40 dB when fiber protrusions of 1 to 2 μm are used. A 0.1° maximum variation in perpendicularity at the end of the single-mode ceramic capillary is such that protrusions as small as 0.5 μm consistently result in mated fiber ends meeting under pressure. Because of the growing demand for this type of high-performance connector, a simple method for predicting fiber protrusion obtained via various polishing techniques has been developed.

Figure 1 illustrates the method by which a connector with a ceramic ferrule is polished to obtain fiber protrusion. The connector is placed in a polishing fixture, and the fiber end is polished by sliding it over the polishing surface with a light downward pressure. It has been observed that fiber protrusions asymptotically approach a specific length following a large number of polishing strokes under constant pressure. When this routine is represented by a model based on linear plate theory, the asymptotic fiber protrusion may be predicted after specifying parameters such as average polishing force, lapping-film thickness, effective ferrule radius, and the compliance of the pad.

MODEL DESCRIPTION

The compliant polishing pad is modeled as a laterally loaded plate resting on an elastic foundation or subgrade as shown in Figure 2. For small numbers of polishing strokes, both the fiber and the ceramic ferrule carry loads to the polishing surface; however, as the polishing continues, the glass fiber is polished down such that the entire load is carried by the ceramic ferrule. This load is assumed to be distributed over a ring area because this is the only region of the ferrule that comes into contact with the polishing surface following a large number (approximately 50) of polishing strokes. Also, because the attrition of the glass fiber is much faster than the ceramic ferrule, the wear of ceramic can be neglected. Therefore, the asymptotic load on the compliant pad after 50 strokes may be taken as shown in Figure 3. The effect of the polishing fixture is neglected because most of the applied pressure is supported at the ferrule tip. Assuming that the local reaction of the foundation is proportional to the plate deflection w the reaction intensity is given by the expression kw. The constant k, expressed in pounds per square inch of deflection, is called the foundation modulus. The governing differential equation in cylindrical coordinates for a symmetrically bent plate resting on an elastic

foundation and experiencing a uniformly distributed load is[1]

$$\left[\frac{d^2}{dr^2}+\frac{1}{r}\frac{d}{dr}\right]\left[\frac{d^2w}{dr^2}+\frac{1}{r}\frac{dw}{dr}\right]=\frac{q-kw}{D}\ , \quad (1)$$

where r is measured radially from the center, q is the uniform pressure, and D is the flexural rigidity of the plate; i.e.,

$$D=\frac{Eh^3}{12(1-\nu^2)}\ , \quad (2)$$

in which E is Young's modulus, h is the plate thickness, and ν is Poisson's ratio. The solution to (1) is simplified by introducing the notation

$$\frac{k}{D}=\frac{1}{l^4}\ , \quad (3)$$

where l is in inches. Letting $x=r/l$, a dimensionless independent variable, the general solution to (1) is

$$w=q/k+C_1\,ber(x)+C_2\,bei(x)+C_3\,ker(x)+C_4\,kei(x)\ , \quad (4)$$

in which C_1, C_2, C_3, and C_4 are constants.[2] The functions *ber* and *bei* are the respective real and imaginary parts of a Bessel function of the first kind, and *ker* and *kei* are the respective real and imaginary parts of a Bessel function of the second kind.[3] Under linearizing assumptions, reactions and shear forces are proportional to loading. Thus, moments, slopes, and deflections are linear functions of the applied load. For this reason, superposition was used to determine the deflection of the complaint polishing pad under the loading shown in Figure 3. Figure 4 illustrates how superposition is used to evaluate the deflection of the pad using solutions which are readily available. For the situation shown in Figure 4, the total deflection of the plate is

$$w=w_1+w_2\ , \quad (5)$$

where w_1 is the deflection resulting from a uniform load distributed over a circular area of 20-mil radius and w_2 is the deflection due to an opposing uniform load acting over a circular area of 15-mil radius. The area over which the load is assumed to be distributed was determined by selecting the area which yielded theoretical protrusions in line with protrusions already documented. A typical deflection profile obtained using this method is shown in Figure 5. Only half of the profile is shown, but the entire profile is symmetric about the vertical axis. Knowing the deflection of the complaint pad during polishing, the amount of fiber protrusion is determined as shown in Figure 6. A computer program performs all the computations necessary to determine fiber protrusion.

EXPERIMENTAL PROCEDURE AND RESULTS

To check the accuracy of the model, six 5-mil diameter fiber ends, terminated in ceramic-ferrule type connectors, were polished. First, a dry, rough polish was performed on a polishing film which uses 5-μm aluminum oxide particles as the wear agent on a 2-mil layer of Mylar backed by a foam layer approximately 11-mils thick. This step was performed to remove excess epoxy from the ferrule end. Next, a wet, fine polish was performed using polishing paper which consisted of a 4-mil polyester layer under 1.5μm cerium oxide particles. This paper was placed on a polishing cloth, which served as the compliant subgrade. The compliance of the polishing cloth was determined experimentally. In the experiment, a 2 X 2 inch piece of the cloth was deflected by a 40-mil diameter pin. The deflections caused by incremental 1-pound loads were recorded and are shown in Figure 7. The average modulus of the polishing cloth was determined to be approximately 350,000 psi/in.

A special polishing tool was used which allowed for precise control of polishing loads. A schematic of the tool is shown in Figure 8. Touching only the outside ring when polishing, the weighted polishing tool automatically applied the desired polishing pressure to the ferrule end. Two connectors were polished for each of 0.402, 0.604 and 0.814-pound loads. Each connector was polished using 50 strokes as shown in Figure 8. The asymptotic fiber protrusions, measured using an interferometer, are shown in Figure 9. The predicted protrusions were obtained by setting the parameters in the computer model as follows: Young's modulus of the polising paper to 550,000 lb/in^2, Poisson's ratio to 0.5, and the thickness of the polishing film to 4 mils. It is clear from the plot that the model can predict fiber protrusions. Illustrating the power of the method as a tool for identifying polishing techniques and materials, the plot shown in Figure 10 is representative of how polishing-pad compliance and polishing pressure affect fiber protrusion.

The curvature of the fiber end is also a parameter which must be controlled to reduce reflections and protect the integrity of the protruding end. Assuming the fiber asymptotically takes the shape of the paper during polishing, the model can predict the curvature of the fiber end. The plot shown in Figure 11 illustrates the effects of polishing-pad compliance and polishing pressure on the curvature of the fiber end. The curvatures shown are the values obtained at the fiber center.

CONCLUSION

The work described supports the use of physical-contact (PC) connectors by demonstrating the feasibility of using linear plate theory as a tool to predict fiber protrusion. The ability to predict protrusions of optical fibers is important in identifying materials and techniques which produce interfaces optimizing the performance of connectors in single-mode fiber-optic systems operating at rates higher than 565 Mb/s.

ACKNOWLEDGEMENTS

The authors gratefully acknowledge the support and contributions of several members of AT&T Bell Laboratories.

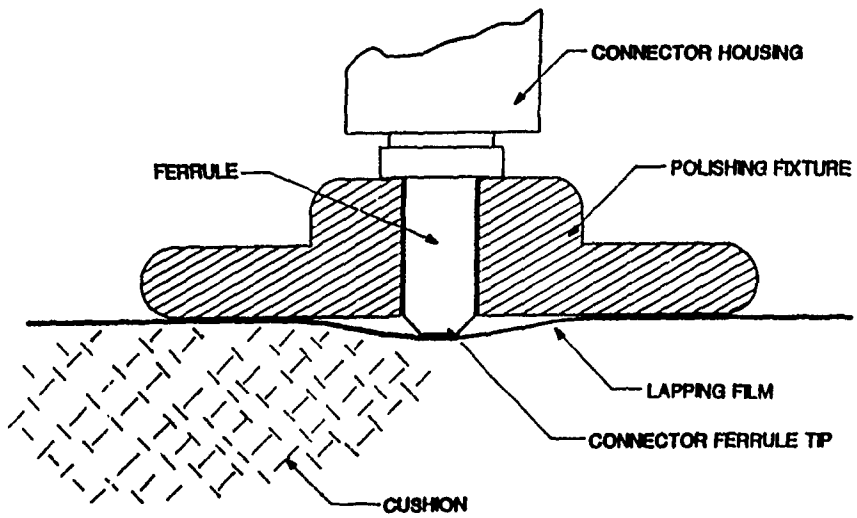

FIGURE 1. POLISHING TECHNIQUE USED TO OBTAIN FIBER PROTRUSION

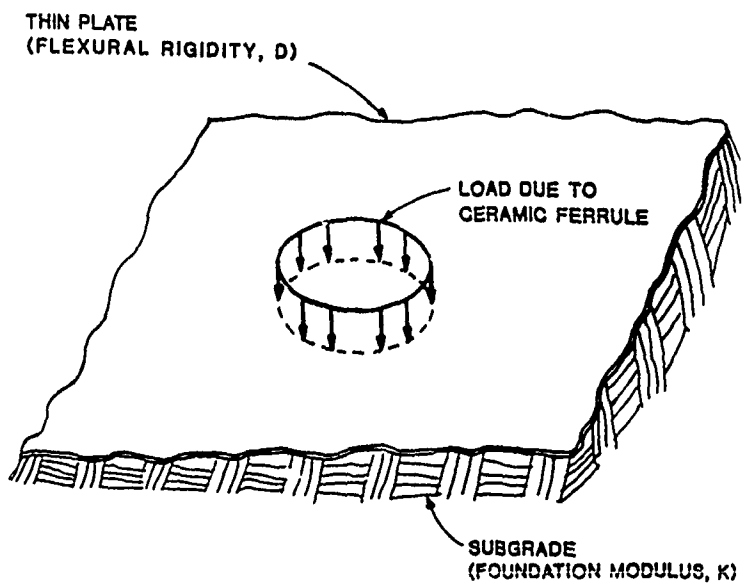

FIGURE 2. POLISHING OF A CERAMIC ST®CONNECTOR MODELED AS A LATERALLY LOADED PLATE ON AN ELASTIC FOUNDATION

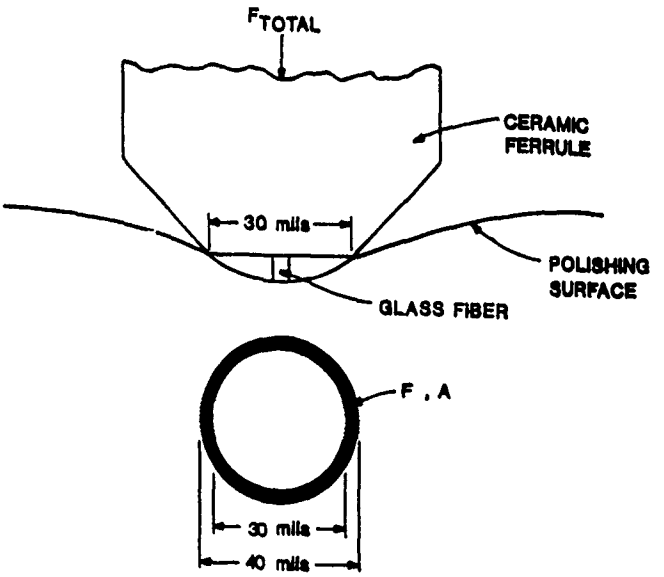

FIGURE 3. EFFECTIVE LOADING DURING POLISHING

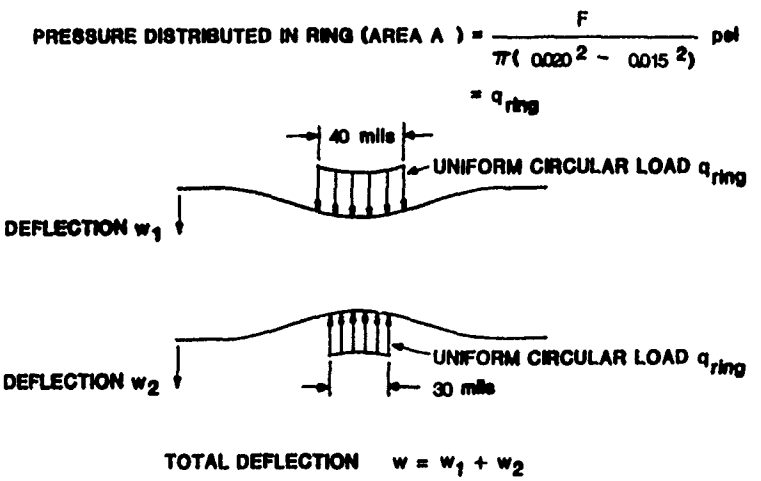

FIGURE 4. SUPERPOSITION USED TO MODEL POLISHING PRESSURE

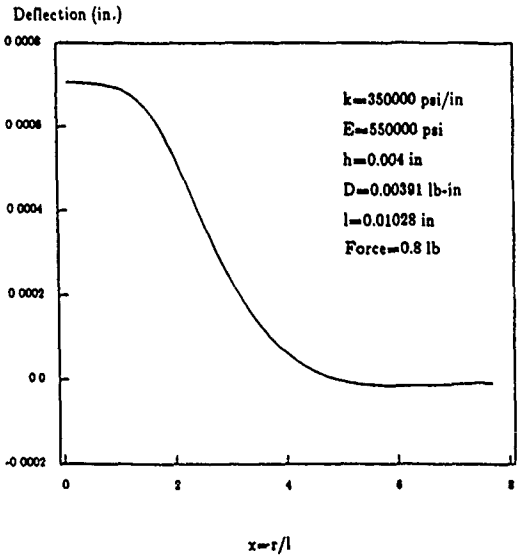

FIGURE 5. TYPICAL THEORETICAL DEFLECTION PROFILE

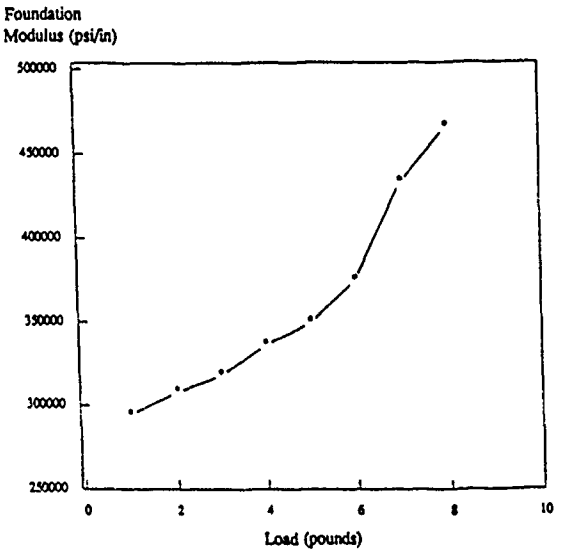

FIGURE 7. COMPLIANCE OF BUEHLER POLISHING CLOTH

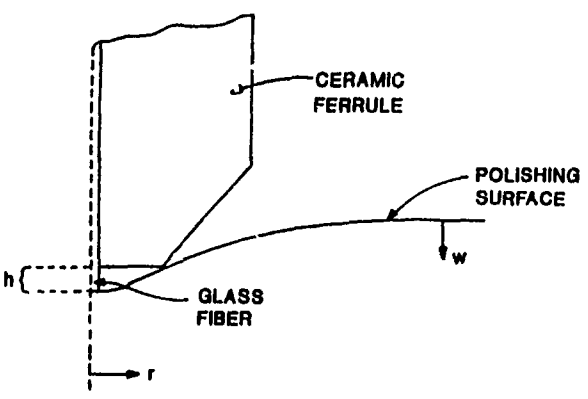

FIBER PROTRUSION = h

= w(@r = 0) − w(@r = 0.015 in.)

FIGURE 6. FIBER-PROTRUSION CALCULATION

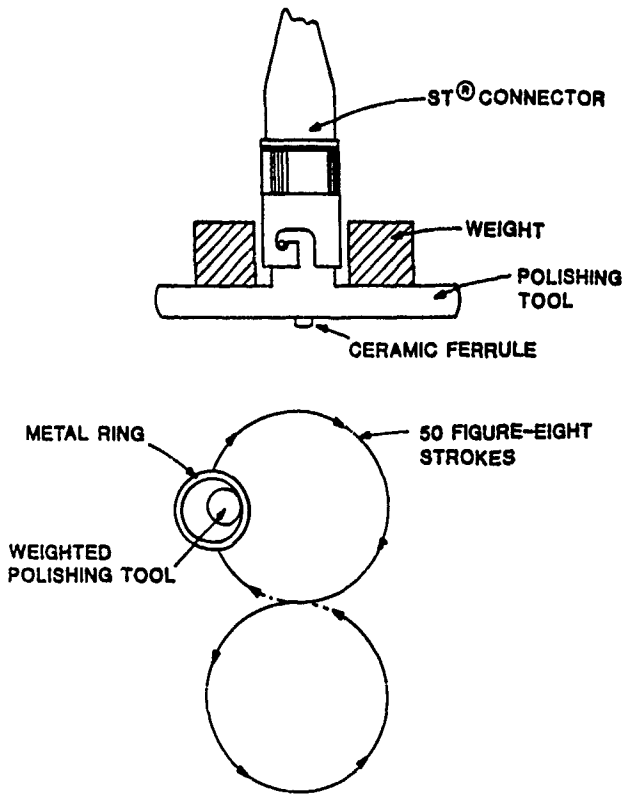

FIGURE 8. POLISHING TECHNIQUE USED IN EXPERIMEMT

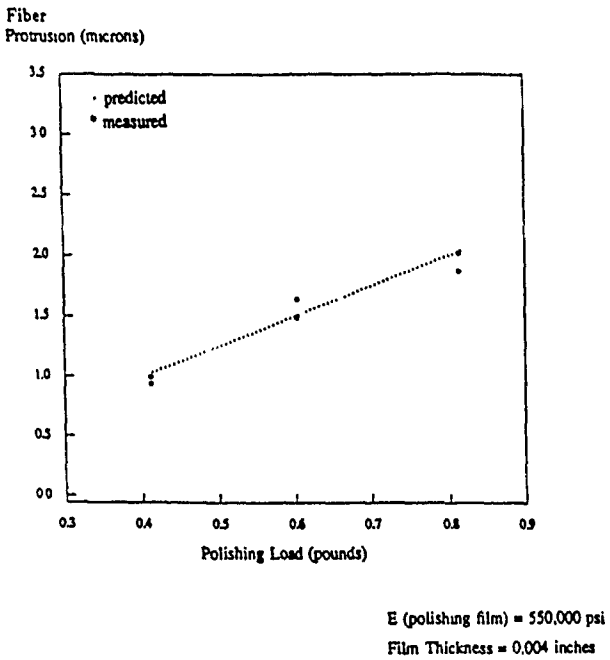

FIGURE 9 COMPARISON OF MEASURED AND PREDICTED FIBER PROTRUSIONS

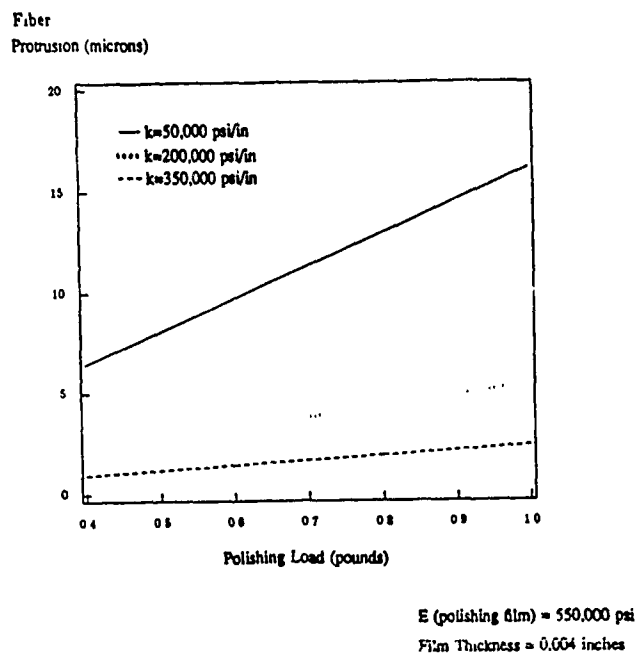

FIGURE 10. INFLUENCE OF POLISHING-PAD COMPLIANCE ON FIBER PROTRUSION

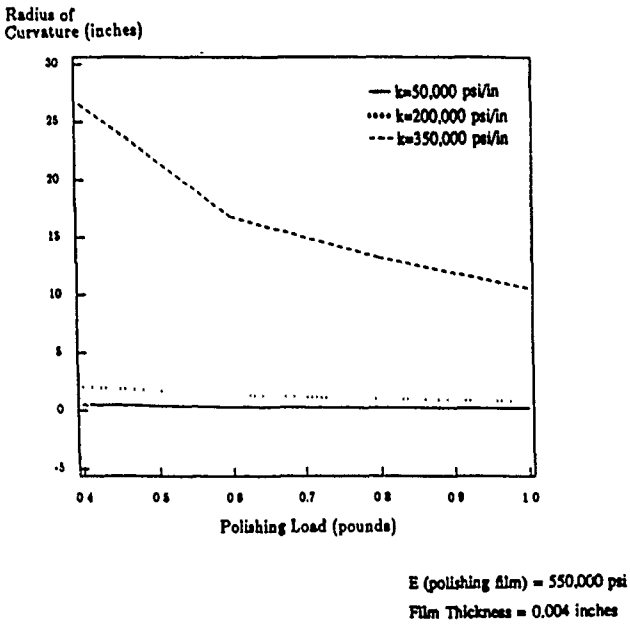

FIGURE 11. INFLUENCE OF POLISHING-PAD COMPLIANCE ON RADIUS OF CURVATURE OF FIBER END

REFERENCES

1. S. Timoshenko and S. Woinowsky-Krieger, "Theory of Plates and Sheels," McGraw Hill Book Company, 1959, pp. 259-267.

2. K. B. Bradley, W. W. King, and C. J Myers, "Predicting the Polished Shape of Ferrule Ends with Linear Plate Theory," Technical Memorandum, Case 40461-411 (March 8, 1988).

3. N. W. McLachlan, "Bessel Functions for Engineers," Oxford University Press, 1961, pp. 138-140.

Kelvin B. Bradley is a Member of Technical Staff in the Lightguide Apparatus Department at AT&T Bell Laboratories in Norcross, Georgia. He has design responsibility for the *ST*® Lightguide Connector product family. He joined AT&T Bell Laboratories in 1986 after obtaining a B.S. in Mechanical Engineering from Purdue University. He received a M.S. in Engineering Science and Mechanics from Georgia Institute of Technology in 1987.

Jerry Anderson received his Bachelor and Master's degree in Mechanical Engineering at Auburn University and his Ph.D. in Mechanics from Stanford University in 1968. He served on the faculty of Georgia Institute of Technology as Professor of Mechanics from 1968 to 1979 when he joined Bell Laboratories in Norcross, Georgia. He is presently supervisor of the Lightguide Connector Group which has responsibility for the design of AT&T's fiber optic connectors.

OPTICAL CABLE SUBMERSION SENSOR

Y.SATO, H.SAWANO, Y.KIKUCHI, H.SUZUKI, and N.SATO

Fujikura Ltd.

ABSTRACT

A maintenance system for optical transmission line is newly developed. It includes an optical fiber submersion sensor. The sensor fiber is stored in an optical cable all along the line with a water swellable yarn. When water immerse into the cable, a water swellable yarn expands its volume, and gives the sensor fiber lateral force to increase loss attenuation. Observing the loss change of the sensor fiber by, for example, OTDR, submersion points are able to search. In this work, we have newly designed a submersion sensor using a single mode optical fiber, and investigated its performances. Furthermore, to get the behavior of the water swellable yarn, we considered reliability of the whole sensor.

1.BACKGROUND

For maintenance of transmission lines, gas-pressurized maintenance system is generally applied. But recently, in case of optical transmission lines, another maintenance system is proposed. That requires water-blocking structure(1) for cables and new checking system for every part of the line. A distributed submersion sensor is one of the most promising systems for checking a state of the lines. As single-mode fibers are widely used now, it is particularly attractive to apply a single-mode fiber for the sensor fiber instead of a multi-mode fiber.

The distributed submersion sensor using a multi-mode optical fiber was already investigated.(2) But a sensor using single-mode fiber has advantages of low loss and easiness of controlling the loss increment of the fiber. And it is considered that single-mode fibers are applicable to the total maintenance system. In this work, we have chosen a single-mode fiber for the sensor instead of a multi-mode fiber to realize these schemes. Since the characteristics of bending differs between a single-mode and a multi-mode fiber, we investigated a mechanism of loss increment of a single-mode fiber. As a result, we have succeeded to develop a submersion sensor using a single mode-fiber.

The most important parts of newly developed maintenance system are submersion sensors and sensing systems. One powerful technique of submersion sensing is OTDR (Optical Time Domain Reflectmeter) loss analyzing technique automatically controlled by computers. We have made special efforts on developing the sensor fiber.

With further consideration about the characteristics of the submersion sensor, these criteria are required to single-mode fiber sensors.

1)Rapid responsibility.
2)Enough sensitivity for OTDR measurement.
3)Suitable value of saturated loss for OTDR measurement.
4)Stability of saturated loss.
5)No dependence on kinds of water immersed into the cable.

Using OTDR for monitoring the fiber loss, the loss increment of the fiber should be large enough to sense by OTDR and within the dynamic range of OTDR. So the value of loss increment should be in the range from about 0.5 dB to about 5 dB.

Some of the criteria disagree with the requirements to guarantee a cable characteristics such as stretching, bending, etc. So we made compromises on these occasion. Concerning about the fifth criterion, we developed new water swellable material by controlling composition of polymers so as to sense in any kinds of water.

2.PRINCIPLE

An optical fiber cable with submersion sensor consists of sensor fiber

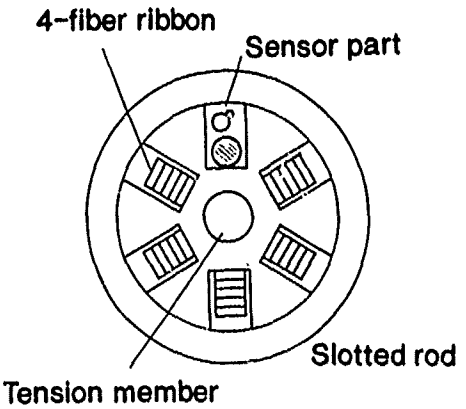

Fig.1 Cross secton of 100-fiber cable with optical submersion sensor.

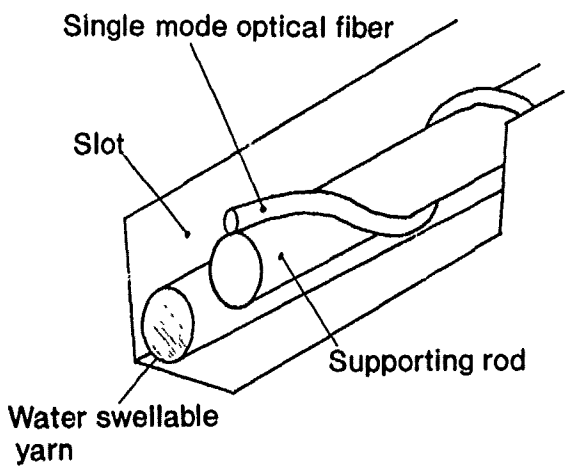

Fig.2 Details of the sensor part.

and water swellable yarn. Fig.1 shows schematic view of investigated cable. This structure is typical 100-fiber cable. Fig.2 shows details of the sensor part. When water immerse into the cable through the sheath, water swellable yarn expands, and give lateral force to the sensor fiber. These processes are shown in Fig.3. Several structures, for example, a fiber stranded on a water swellable yarn, or stranded with self shrinking yarn, etc. were investigated.

As well known, there are two loss increase mechanisms in single-mode fiber cables. One is macro-bend and the other is micro-bend. Macro-bend is called uniform-bend in other words.

Recently, fiber sensors, which originate in loss increase of the fiber caused by physical perturbation, come into practical use such as a pressure sensor. In this study, the cable structure was determined, as the main factor of loss increase is micro bendings.

Sensor structure shown in Fig.3(b) is one of the micro-bend sensor configurations and that is favorable for a single mode fiber from the view point of controllability and stability in sensor performance.

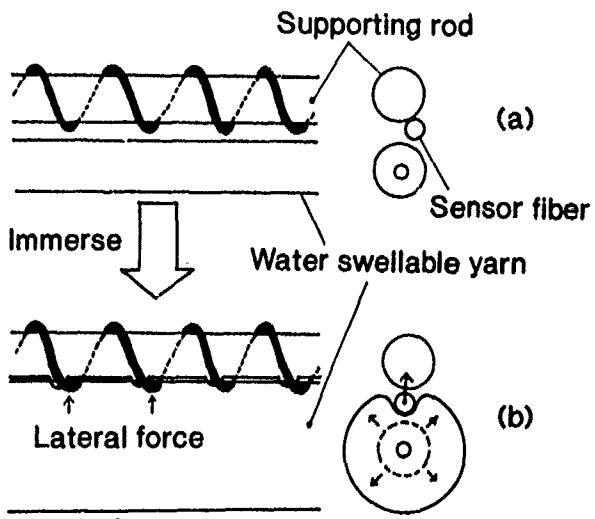

Fig.3 Princple of submersion sensing.

3.EXPERIMENTAL

At first, time response of the sensor was examined for pure water, salt solution, and seawater. Salt solution is NaCl and CaCl2 mixed solution imitated water in manholes. Fig.4 shows the block diagram of submersion sensing test. A cable sample with 5mm cut in the middle of the sheath submerged into a water bath at the temperature of 25°C, watching the attenuation change of the sensor fiber at the wavelength of 1.55μm.

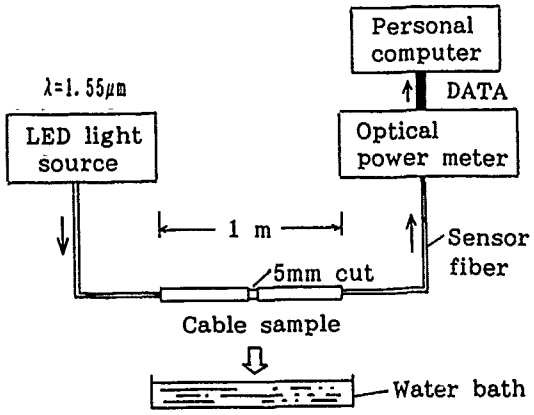

Fig.4 Block diagram of submersion sensing test.

4.RESULTS

The experimental results is shown in Fig.5. The added losses are up to 0.3-0.6 dB for each kind of water. These values are suitable enough for loss measurement by OTDR. And for the three waters the added losses all saturate in 3 or 4 hours from submersion and these are kept constant. The saturate value of the added loss are in the order of seawater, salt solution, and pure water. This order corresponds to the ionic strengt' of three kinds of water, because the expand rate of water swellable yarn differs for each water.

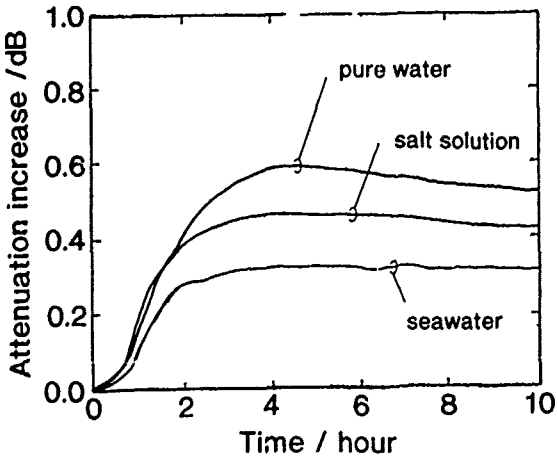

Fig.5 Time responce of the sensor.

5.CONCLUSION

From the experimental results, it is clear that;

1)The attenuation increase is up to about 0.3 dB in seawater, and up to 0.6 dB in pure water.
2)The attenuation increases are saturated in about 3 or 4 hours in every kind of water, and are kept constant.
3)The added loss of the sensor is in the order of seawater, salt solution, and pure water.

Finally it is proved that the sensor works well in various kinds of water, and shows good performance and reliability. Therefore, the proposed system is applicable to constitute for the conventional gas-pressurized maintenance system.

ACKNOWLEDGMENTS

The authors would like to express great appreciation for the useful advice and encouragement from Dr. K. Inada.

REFERENCE

1)Sawano et.al.,"Optical fiber cable with submersion sensor fiber", 36th IWCS, USA, 1987.
2)Kukita et.al,"A new nonmetallic and waterproof optical fiber cable with absorbent polymer ribbon", 36th IWCS, USA, 1987.

Yoshiyuki SATO

Fujikura Ltd.

1440 Mutsuzaki,
Sakura, Chiba, 285,
JAPAN

Mr.Sato was born in 1963. He joined Fujikura Ltd. after his graduation from Tohoku University with the M.E. degree in 1988 and has been engaged in research and development of optical cables. He is now an engineer of telecommunication cable section and a member of IEICE of Japan.

Hideo SUZUKI

Fujikura Ltd.

1440 Mutsuzaki,
Sakura, Chiba, 285,
JAPAN

Mr.Suzuki was born in 1948. He joined Fujikura Ltd. after his graduation from Gunma University with the B.E. degree in 1971 and has been engaged in materials, polymer processing, and development of optical cables. He is now the manager of telecomunication cable section and member of IEICE of Japan.

Hiroyuki SAWANO

Fujikura Ltd.

1440 Mutsuzaki,
Sakura, Chiba, 285,
JAPAN

Mr.Sawano was born in 1955. He joined Fujikura Ltd. after his graduation from Hokkaido University with the M.S. degree in 1983 and has been engaged in research and development of optical cables. He is now an engineer of telecommunication cable section and a member of IEICE of Japan.

Nobuyasu SATO

Fujikura Ltd.

1440 Mutsuzaki,
Sakura, Chiba, 285,
JAPAN

Mr.Sato was born in 1943. He joined Fujikura Ltd. after his graduation from Tohoku University with the B.E. degree in 1966 and has been engaged in research and development of transmission cables. He is now the general manager of transmission cable department and a member of IEICE of Japan.

Yoshio KIKUCHI

Fujikura Ltd.

1440 Mutsuzaki,
Sakura, Chiba, 285,
JAPAN

Mr.Kikuchi was born in 1955. He joined Fujikura Ltd. after his graduation from Tohoku University with the M.E. degree in 1980 and has been engaged in research and development of optical fibers and cables. He is now the chief of telecommunication cable section and a member of IEICE of Japan.

Optical Power Measuring System for Fiber Ribbon

Y.Unami M.Tanaka T.Yamada

Fujikura Ltd.
Chiba,Japan

ABSTRACT

A new optical power measuring system that can realize the high efficient measurement for fiber ribbons has been developed. The measurement of the optical powers from all cores of a fiber ribbon can be automatically completed within a minute with one time operation.

The system consists of LED light sources and an optical powermeter, and they have some excellent features.

A new original method, forward light feedback (FFB), has been developed in order to stabilize the light from the LED light source. The FFB method is the key technology that achieves the high stability and the high efficiency of this system. The optical powermeter identifies the optical power from each core of a fiber ribbon without synchronous signals.

This system can be applied up to 12 fiber ribbons at the wavelengths of 1.31 um, 1.55 um and 0.85 um, and can realize the measurement of more than 30 dB fiber loss at 1.31 um. It takes only between 23 and 44 seconds to complete measuring a 12 fiber ribbon.

1. Introduction

Recently optical fiber networks are rapidly expanding. At the same time, high fiber count cables such as 1000 fiber optical cables are required.[1] Optical fiber ribbons have been adopted in many high fiber count cables on account of their compact size and the advantage of mass splice[2]. The optical accessories, tools or equipments for fiber ribbons have been also developed. It is expected that a fiber ribbon is the main structure of optical fiber cables for future optical fiber networks.

It is indispensable to measure the transmission loss of optical fibers, the splicing loss or the insertion loss of optical components in fiber optics. Conventional optical power measuring methods are designed for single fibers, not suitable for fiber ribbons. Now increasing the demand of fiber ribbons, it is strongly desired that the new measuring method fitting to the structure of fiber ribbons appears.

This report describes a new optical power measuring system for fiber ribbons that has performed high stable and high efficient measurement.

2. Outline of the system

2.1 System configuration

The system consists of LED light sources and an optical powermeter. Fig.1 shows the system configuration for a 8 fiber ribbon as an example. The one end of a sample fiber ribbon is connected with the LED light sources. Usually the jumper fiber cable is used, which has single connector ends and a fiber ribbon end shown in Fig.1. Another end is connected to the optical head of the optical powermeter. The light from all cores of fiber ribbon is detected by one photo diode.

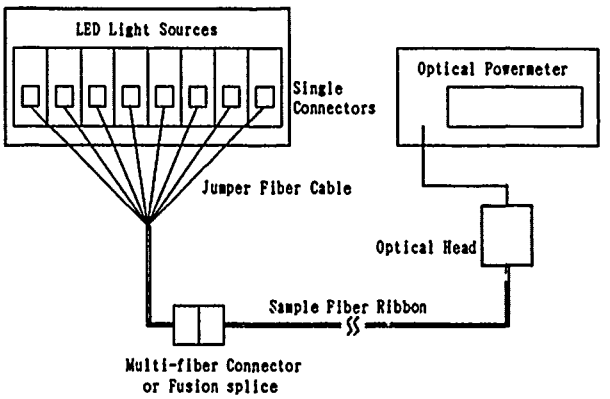

Fig.1 System Configuration

2.2 Description of operation

The LED light sources turn on and off according to the certain timing shown in Fig.2, therefore the optical powermeter detects the series of optical pulses. One cycle is composed of an all channels-on pulse and each channel-on pulse. They can be distinguished by measuring the pulse width. All channels-on pulses are the separator of the cycles and also the start/end trigger to the optical powermeter.

The optical powermeter searches an all channels-on pulse at first. After detecting the pulse, it starts to measure the

optical powers from channel 1 to channel 8 and stores the data in the internal SRAM. When the optical powermeter detects next all channels-on pulse, finishes the measurement.

In order to realize the operations described above, following abilities are required.

1) The light of the LED light source must be instantaneously stabilized with no warm up after switched on.

2) The optical powermeter is required quick response to the optical pulse.

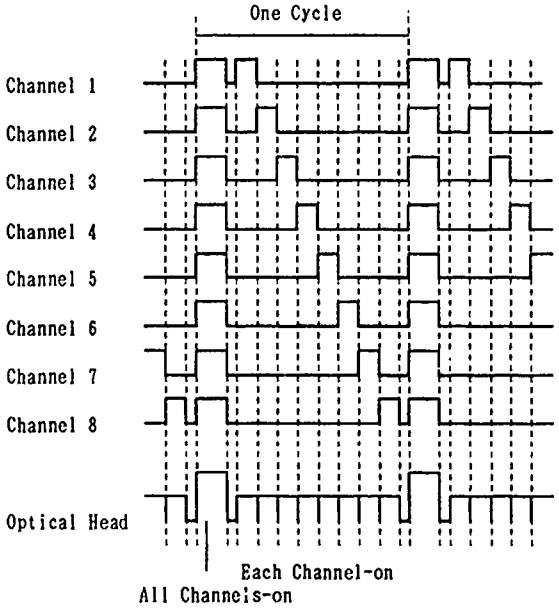

Fig. 2 Timing of Optical Pulses

3. Light source

3.1 Light emitting device

LED and LD are often used for many applications in fiber optics. LD is superior to LED from the viewpoint of its high fiber coupled power and narrow spectrum. But its optical power is easily fluctuated by the reflected power from the ends of the connectors or the other optical components. It is difficult to control and stabilize the spectrum of LD to the temperature change.[3][4] In addition the light of LD is polarized, so that it is not available in some applications. Therefore LD is not suitable for high stable measurements.

On the other hand, the light of LED is almost free from the influence of reflected power and it has no polarization. LED is adopted in this system to realize high stability and accuracy.

Surface emitting LED is used for GI fiber and edge emitting LED for SM fiber. The edge emitting LED has an advantage of high power coupling efficiency to SM fibers. The edge emitting LED module fitting to the usage of this system has been developed.

3.2 Stabilizing method for LED

In general, there are two well-known methods to stabilize the power of LED as follows:

1) Temperature compensation method

The LED drive current shall be changed according to the previous measured temperature characteristics of the LED.

2) Temperature control method

The temperature of the LED device shall be kept constant by a micro cooler, etc.

But these methods are not available to this system from the viewpoint of the instantaneous stability.

A new method to stabilize the light of an LED, forward light feedback (FFB) method, has been developed. The FFB method is the key technology to this system and has several excellent characteristics as follows:

1) Instantaneous stabilization with no warm up.

2) High stabilization to temperature change.

3) High stabilization to long time operation.

4) High repeatability to turning on and off.

The features are compared with the two conventional methods in table.1.

Method	Temperature Compensation	Temperature Control	FFB Method
Instnataneous Stability	Low	Low	High
Stability to Temperature	Low	High	High
Electrical Circuit	Small	Large	Small
Adjustment of Circuit	Complicated	Simple	Simple
Supply Current to Circuit	Small	Large	Small

Table. 1 Stabilizing Methods for LED

3.3 Principle of FFB method

Fig.3 shows the block diagram of the FFB method for SM fibers. The light from the LED is led to the optical wavelength band pass filter that limits the full width half max. (FWHM) less than 20 nm. The light is divided into the optical output and the monitor photo diode by high stable fused tapered SM fiber coupler. The current generated at the photo diode is fed back to the LED driver. This feedback loop realizes highly stabilized output power, because the part of the power coupled to the fiber is used as the feedback signal. Also the center wavelength and FWHM have very slight fluctuation even if the original spectrum of the LED has more fluctuation. Fig.4 shows the principle of the stabilization to temperature change for example. It can be easily understood that both the power and the spectrum are stabi-

lized at the same time.

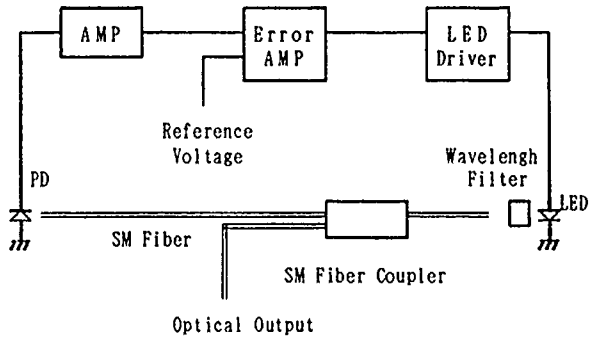

Fig. 3 Block Diagram of FFB Method

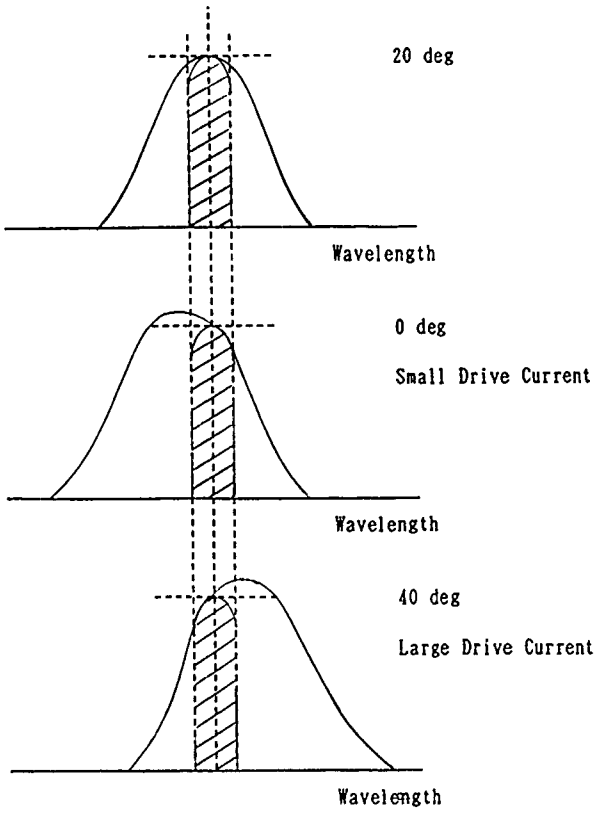

Fig. 4 Principle of FFB Method

3.4 Characteristics of FFB method

For example, the characteristics of 1.55 um LED light source for SM fibers are shown in Fig.5 to Fig.7. The power stability after switched on is shown in Fig.5, the power stability to temperature in Fig.6 and the response to the step control signal in Fig.7. Compared with the conventional temperature compensation method, the characteristics are much improved. Especially as shown in Fig.7, the power is stabilized within 20 ms after switched on, and this excellent feature is quite unique to FFB method.

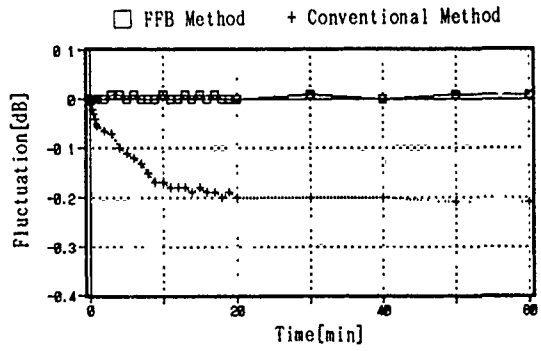

Fig. 5 Power Stability after Switched On

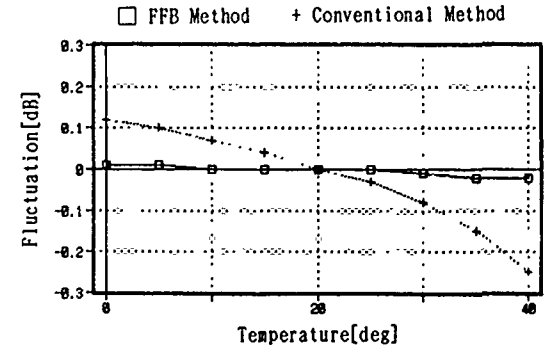

Fig. 6 Power Stability to Temperature

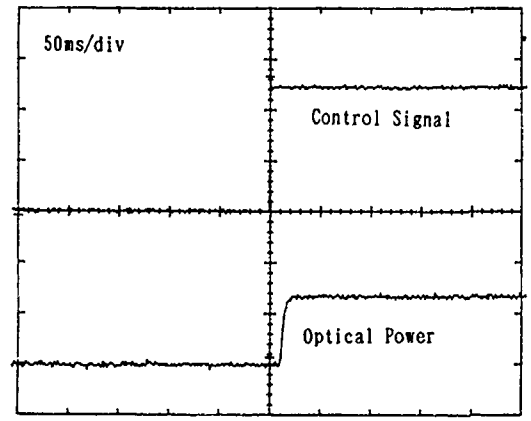

Fig. 7 Response

Table.2 shows the characteristics of the two types of LED light sources for SM fibers. The special terms in Table.2 are defined as follows:

1) Temperature stability is the maximum fluctuation of the power at the temperature from 0 to 40 deg.

2) Long term stability is the maximum fluctuation between the power just after switched on and that after 2 hours.

3) Short term stability is the maximum

fluctuation of the power for 1 minute after 10 minutes from switched on.
4) Repeatability is the maximum fluctuation of the power in 100 cycles of switched on for 10 seconds and switched off for 20 seconds.

Item	1.31um for SM	1.55um for SM
Fiber Coupled Power	-27.8 dBm	-28.7 dBm
Peak Power Wavelength	1311 nm	1553 nm
FWHM	18.6 nm	19.6 nm
Temperature Stability	0.03 dB	0.04 dB
Long Term Stability	0.02 dB	0.02 dB
Short Term Stability	0 dB	0.01 dB
Repeatability	0.01 dB	0.02 dB

Table.2 Characteristics of FFB LED Light Sources

4. Optical powermeter

4.1 General description

The optical powermeter consists of the main body and the optical head. A photo diode is used as a light detecting device in the optical head. In order to cover the wide measurement range and to keep the high resolution, the optical powermeter has several ranges. The ranges are controlled according to the detected power by the internal micro processor automatically. The optical powermeter is designed to detect modulated lights in order to reduce the influence of the dark current of the photo diode.

4.2 Improvement of response

The range control is one of causes of the slow response to optical powermeters. Especially, several range controls degrade the response extremely.
To improve the response and keep the stability, two different types of A/D converters are used in the optical powermeter shown in Fig.8. The high speed and low resolution type is used for range control, the high resolution type for measuring optical powers. This method realize the quick range control with maintaining the high accuracy.

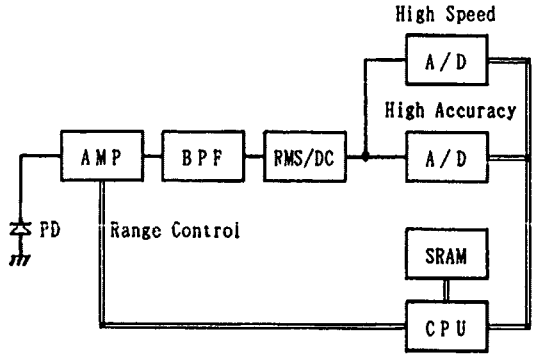

Fig.8 Block Diagram of Optical powermeter

4.3 Photo diode

A large diameter photo diode is adopted to detect the lights from all cores in line. The diameter of the photo diode is 5 mm to meet the present structure of fiber ribbons.
The spatial non-uniformity of the photo diode's sensitivity is important factor because it affects the repeatability of the system directly. In this system the value is only 0.03 dB.

4.4 Functions

The optical powermeter has following functions.
1) Auto offset function cancels the dark current of the photo diode and the offset of amplifiers.
2) The sensitivity of the photo diode dependent on the wavelength is compensated by setting the wavelength from the front panel.
3) The sensitivity of the photo diode dependent on the temperature is compensated automatically by micro processor.

4.5 Performance

The optical powermeter has following performances.
1) The resolution is 0.01 dB.
2) The measurement range is -10 to -60 dBm.
3) The applicable wavelength range is 750 to 1800 nm.
In addition, a large LCD is equipped in the main body, and it can display absolute, relative and reference values of maximum 12 fiber ribbon at the same time.

5. System performance

Fig.9 shows the outside view of the prototype of this system. The system can be applied up to 12 fiber ribbons at the wavelengths of 850 nm, 1310 nm and 1550 nm.
It is obvious by the principle that the system need only between 23 seconds and 44 seconds to complete the measurement of a 12 fiber ribbon. The measuring time is about 1/10 compared with the conventional ways of measuring each core one by one.
Using the light pulse modulated by 270 Hz , the dynamic range of 30 dB is realized. When a low power close to the minimum detectable power (-60 dBm) is measured, the system can average the data of the cycles maximum 8 times by setting the number of cycle from the front panel of the optical powermeter for improving the stability.
The total fluctuation of the prototype was only 0.05 dB at the temperature of 0 to 40 deg. Actually We tried to measure the loss of a 50 km SM 8 fiber ribbon at 1.31 um, the results were almost equal to conventional ways.

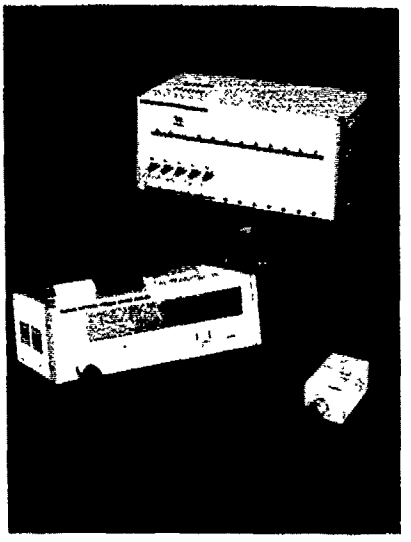

Fig. 9 Outside View

6. Conclusion

A new optical power measuring system suitable for fiber ribbons has been developed. It takes advantage of the structure of fiber ribbons and realizes the much reduction of the measuring time with maintaining the high accuracy.

In the system, two significant methods have been proposed as follows:

1) FFB method provides highly stabilized LED light sources.

2) The response of an optical powermeter is improved by two types of A/D converters.

It is expected that the system can provide the highly efficient measuring environment in many applications for fiber ribbons.

References

(1) H.Sawano et al.: One-Thousand-Fiber Optical Cables Composed of Eight Fiber Ribbons, 38th IWCS, 1989

(2) T.Onodera et al.: Development of Single-Mode 4 Fibers' Ribbon Splicer with the Accurate Splice Loss Estimation Function, IOOC, 21C2-4, 1989

(3) Yamada, M. and Y.Suematsu: A Condition of Single Longitudinal Mode Operation in Injection Lasers with Index-guiding Structure, IEE Journal of Quantum Electron., QE-15 8, p.743 (Aug.1979)

(4) Yamada, M., F.Iida, S.Kido, and R.Ishibashi: Longitudinal Mode Control by Temperature Compensation in Injection Lasers, Trans.of IECE of Japan, E-61, 11, p.896 (Nov.1978)

Yoshiharu Unami

Fujikura Ltd.

1440 Mutsuzaki, Sakura, Chiba, 285, Japan

Yoshiharu Unami was born in 1961. He joined Fujikura Ltd. after his graduation from Chiba University with the B.E. degree in 1982 and has been engaged in research and development of optical systems. He is now an engineer of optical communication system section and a member of IEICE of Japan.

Masao Tanaka

Fujikura Ltd.

1440 Mutsuzaki, Sakura, Chiba, 285, Japan

Masao Tanaka was born in 1950. He joined Fujikura Ltd. after his graduation from Osaka University with the B.E. degree in 1974 and has been engaged in research and development of optical systems. He is no' a member of technical staffs of optical system division and a member of IEICE of Japan.

Takeshi Yamada

Fujikura Ltd.

1440 Mutsuzaki, Sakura, Chiba, 285, Japan

Takeshi Yamada was born in 1950. He joined Fujikura Ltd. after his graduation from Waseda University with the B.E. degree in 1973 and has been engaged in research and development of optical systems. He is now a manager of optical communication system section and a member of IEICE of Japan.

LOW INSERTION LOSS FILTER-EMBEDDED OPTICAL FIBER RIBBON

H. Hosoya K. Asano M. Ohsawa H. Yokosuka

Opt-Electronics Laboratory Fujikura Ltd.
1440, Mutsuzaki, Sakura-shi, Chiba, 285, Japan

Abstract

A new and very small device consisting of an optical filter and a single-mode optical fiber ribbon has been developed. It had a very compact design and an extra low insertion loss for all fibers of the ribbon. A four-fiber ribbon was fixed on a V-grooved substrate. A four-fiber ribbon was split and fixed on a V-grooved substrate. The slit was formed diagonally against the fiber axes. The endfaces of the four fibers were polished to mirror surfaces. The optical loss caused by the slit width was about 0.3 dB which was good agreement with the theoretical value. An optical filter was inserted into the slit. It was confirmed that the desired wavelength selsctivities were achieved by the charateristics of the optical filter. The results are as follows : insertion losses were about 0.5 dB at 1.31 um for four fibers and more than 50 dB at 1.55 um. The filter-embedded optical fiber ribbon was proven to have such excellent features as low insertion loss, compact design and high optical reliability.

1. Introduction

With the recent rapid trend to practical application of optical fiber communication systems, optical parts possessing varying features have been finding use for higher performance and expanding applications of such systems. Particularly those which have wavelength selectivity been given an important role to play in many systems. Up to the present bulk type[1] optical parts consisting each of a combination of very small lens, prism, etc., have been developed and partly put into practical use. In addition, some types, which comprise various optical elements inserted into a joint section at which polished optical fibers are butt joined to each other with their optical axes aligned, have been proposed. With these parts, however, minimization of insertion loss, mass production and miniaturization are left as problems yet to be solved in the future.

Moreover, the recent trend to practical application of optical fiber cables using optical fiber ribbons has stimulated demand for an optical part that is well adapted to a multifiber optical ribbon. Though known to be able to contribute to attaining higher density and lower costs, the optical part for use with the multifiber ribbon has not been given much consideration because of the difficulty of aligning the optical axes of many optical elements with high precision .

We have developed an optical part called "Low-Insertion-Loss Filter-Embedded optical fiber ribbon". This optical part is fabricated by embedding a small optical filter in a single-mode fiber ribbon. In this paper, we describe the characteristics, construction and other features of this optical part.

2. Construction

The basic construction of this optical part is shown in Fig. 1 and the external view in Fig. 2. A four-fiber ribbon is fastened on a substrate having four V-grooves. A dielectric multilayer-film filter chip capable of selecting desired wavelengths is inserted and fastened in a slit formed in the ribbon.

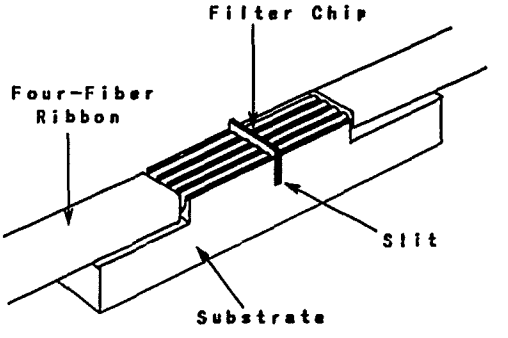

Fig. 1 Constraction of Filter-Embedded Optical Fiber Ribbon.

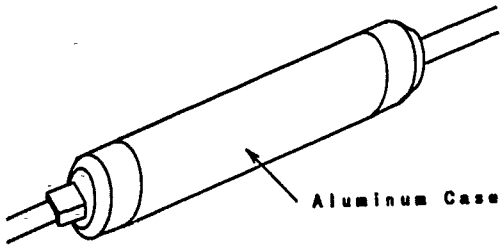

Fig. 2 External view of Filter-Embedded Optical Fiber Ribbon.

The Filter-Embedded Optical Fiber Ribbon is fabricated by the procedure shown in Fig. 3.

(1) Bond a four-fiber ribbon, stripped of its center sheath, with adhesive to a substrate having four V-grooves.

(2) Form a slit in the middle of the ribbon so as to extend to the substrate, using a fast-revolving thin ceramic blade. Then mirror finish the inner surface of the slit and the end faces of the four fibers with an abrasive-containing grinding fluid. The slit is about 45 um wide. With this fiber ribbon, it is unnecessary to align the optical axes of the fibers facing each other across the slit.

(3) Insert a filter chip into the formed very small slit and bond it with optical adhesive. The filter chip used was a 30 um thick chip thinned by lapping its substrate side.

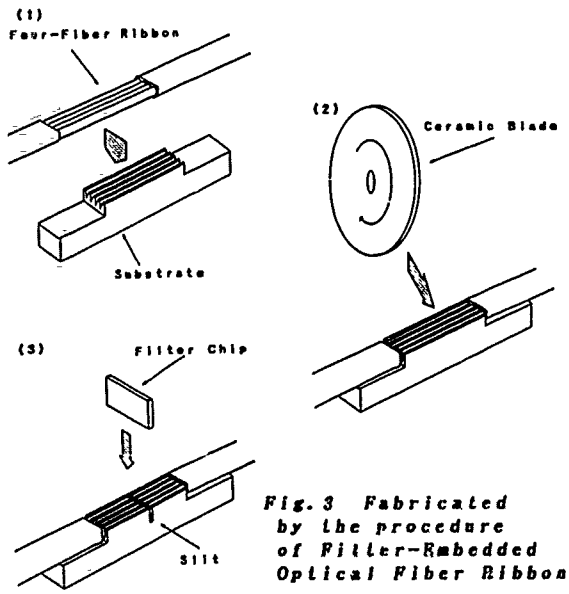

Fig. 3 Fabricated by the procedure of Filter-Embedded Optical Fiber Ribbon.

These components are packaged in an aluminum case and fixed therein with a filler-added resin. The optical part is of a very compact design with a diameter of 5 mm and a length of 35 mm.

Thus the optical part comprises only a small number of components and does not require aligning of optical axes, so it can be fabricated very easily.

3. Optical Characteristics

The filter used was a short-wavelength-pass filter which passes wavelengths around 1.31 um and cut offaround 1.55 um. An example of the optical characteristics of the filter embedded in the fiber ribbon is given in Table 1. An example of the loss spectrum for the passing band is given in Fig. 4 and that for the cut off band in Fig. 5. The cut off for the passing band was measured by a monochromator and that for the cut off band by a variable wavelength laser diode. The fiber ribbon used was a single-mode type of about 9.5 um in M.F.D. The filter was inserted with an angle of inclination of about 8° to the optical axes of the fibers to increase the return loss.

Table 1 Optical characteristics of Filter-Embedded Optical Fiber Ribbon.

	INSERTION LOSS at 1.31μm	INSERTION LOSS at 1.55μm	RETURN LOSS at 1.31μm	RETURN LOSS at 1.55μm	POLARI-ZATION at 1.31μm
#1	0.47dB	67dB	51dB	48dB	1.0%
#2	0.46dB	67dB	53dB	50dB	0.5%
#3	0.44dB	68dB	50dB	48dB	1.0%
#4	0.45dB	68dB	49dB	47dB	0.9%

The insertion loss at 1.31 um is considered attributable mainly to the sum of the insertion loss by the gap between the fibers and the transmission loss at the filter element. The theoretical values[2] of gap loss are shown in Fig. 6. With a slit width of 45 um, a loss of about 0.3 dB is expected. The loss of the filter element is about 0.15 dB at 1.31um. The sum of the two losses well agree with the data of Table 1. The four fibers in the ribbon exhibit nearly the same characteristics. The total insertion loss is very small because of the design which substantially eliminates optical axis misalignment.

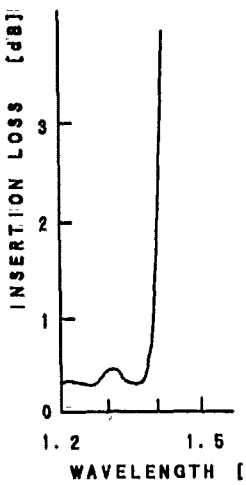

Fig. 4 Loss-Spectrum for the passing band of the Filter-Embedded Optical Fiber Ribbon.

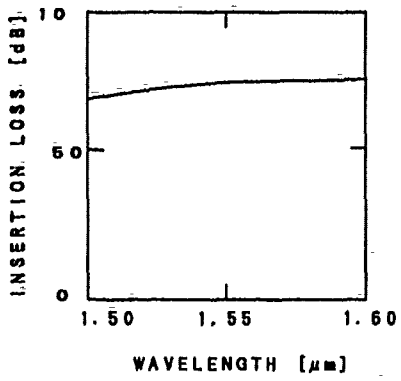

Fig. 5 Loss-Spectrum for the cut off band of the Filter-Embedded Optical Fiber Ribbon.

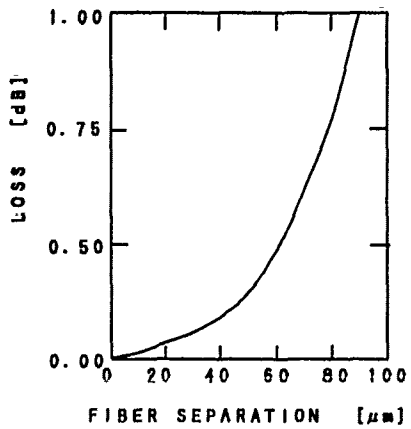

Fig. 6 The theoretical fiber separation loss.

The small irregularities of the loss-wavelength curve for the passing band are nearly the same with those of the loss spectrum of the filter element. This indicates that the characteristics of the filter element are represented as they are except for the gap loss.

The insertion loss at 1.55 um is virtually determined by the characteristics of the filter element. The data of Table 1 and Fig. 5 show that the characteristics of the filter element are not impaired at all.

The return loss basically is determined by the insertion angle of the filter element.

The polarization characteristic is as low as 2% or less, i.e., it is at a sufficient level for practical use.

Figs. 7 and 8 are insertion loss histograms for the passing band and for the cut off band, respectively, prepared based on the results of invesigating 125 filter-embedded optical fiber ribbon . As

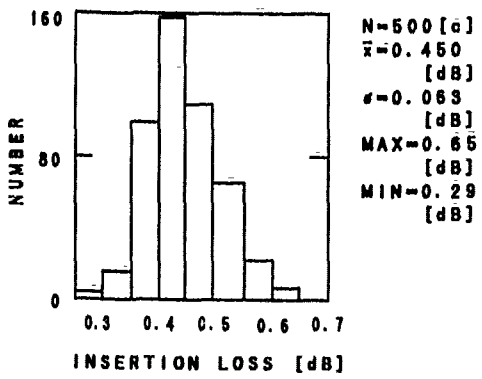

Fig. 7 Insertion loss histogram of Filter-Embedded Optical Fiber Ribbon at 1.31μm.

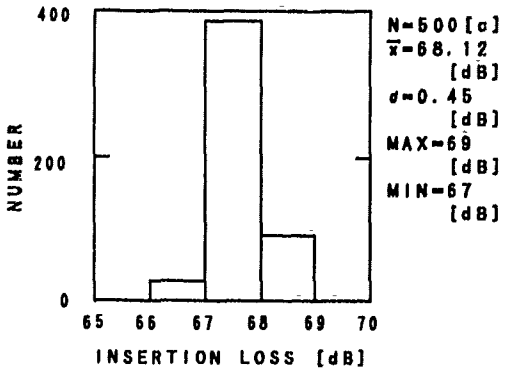

Fig. 8 Insertion loss histogram of Filter-Embedded Optical Fiber Ribbon at 1.55μm.

seen from these figures, the filter characteristics are very good with a maximum value of insertion loss of 0.65 dB or more for the passing band and 67 dB or more for the cut off band. Taking this into consideration with the small variations in the characteristics, it becomes evident that the part can be fabricated with very high stability.

4. Reliability Testing

Various reliability tests shown in Table 2 were performed. In the heat cycling test, the variation in insertion loss was found to be kept stable at a level of less than 0.1 dB (as shown in Fig. 9), and no residual loss was observed after 100 heat cycles.

Table 2 Reliability Test Conditions and Result of Filter-Embedded Optical Fiber Ribbon.

ITEM	TEST CONDITION	RESULT
TEMPERATURE CYCLING	-10 TO 60℃ 100 cyc.	<0.1dB
HUMIDITY	70℃ 90%RH 1000H	<0.1dB
HIGH TEMPERATURE	70℃ 100H	<0.1dB
LOW TEMPERATURE	-20℃ 100H	<0.1dB
VIBRATION	1.5mm 10~55Hz 3 DIRECTION	EXCELLENT
IMPACT	50G >11msec.	EXCELLENT

The filter used herein was a non-ion assist type dielectric multilayer film. This film presents a troublesome feature that the wavelength characteristic varies with the temperature change. However, the result of the high-temperature high-humidity test shows no variation in insertion loss even after the lapse of 1,000 hours as shown in Fig. 10. This indicates that the humidity control by packaging can produce a sufficient effect.

The results of the high- and low-temperature tests also show no variation in insertion loss. Moreover, any variation in insertion loss was not observed at all in the vibration and impact tests.

Thus the optical part developed by us was proved to be very good in environmental resistance, long-term reliability and mechanical properties.

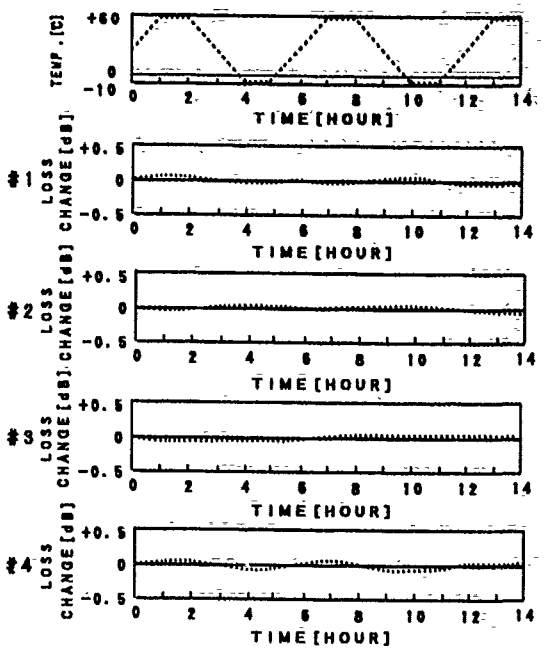

Fig. 9 Temperature Cycling Test Result for Filter-Embedded Optical Fiber Ribbon.

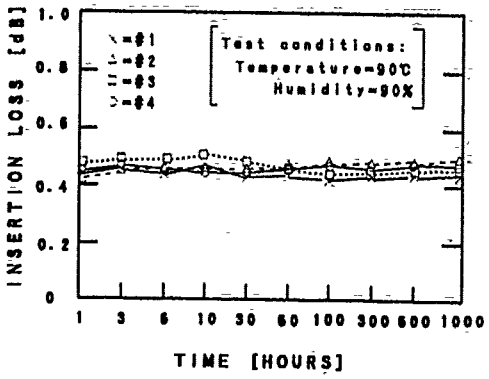

Fig. 10 The result of high-temperature high-humidity test of Filter-Embedded Optical Fiber Ribbon.

5. Conclusion

We deveroped an optical part by embedding a dielectric multilayer-film filter in a single-mode optical fiber ribbon and confirmed that it possesses the following features:

(1) Incorporation of optical element in multifiber optical ribbon.
(2) No need for optical axis alignment in production process.
(3) Small insertion loss.
(4) High reliability.
(5) Miniaturization with higher density.

These features owe much to the development of the fine slitting technique and the assembly technique. The process of manufacturing this optical part is, of course, higher-precision fine slitting technique in order to develop optical parts possessing varying features in the future.

References

1)G. Winzer, "Wavelength Multiplexing Components-A Review of Single-Mode Devices and Their Applications", J.Lightwave Technol., Vol.LT-2, pp369-378, 1984

2)D.Marcus, "Loss Analysis of Single-Mode Fiber Splices," B.S.T.J., Vol.56, No.5, pp703-718, 1977

Hideyuki Hosoya

Opt-Electronics Laboratory
FUJIKURA LTD.

1440,Mutsuzaki, Sakura-shi,Chiba,285 Japan

Hideyuki Hosoya was born in 1959. He received the M.Sc. degree in physics from Yamagata University in 1983. He joined Fujikura Ltd. in 1983 and has been engaged in research and development of telecommunication cables and accessories. He is a member of the Institute of Electronics, Information and Communication Engineers of Japan.

Kenichiro Asano

Opt-Electronics Laboratory
FUJIKURA LTD.

1440,Mutsuzaki, Sakura-shi,Chiba,285 Japan

Kenichiro Asano was born in 1966. He graduated in opt-electronics engineering from Tokyo Kougakuin College of Technology He jointed Fujikura Ltd. in 1989 and has been engaged in research and development of telecommunication cables and accessories.
He is a member of the Institute of Electronics,Information and Communication Engineers of Japan.

Makoto Ohsawa

Opt-Electronics Laboratory
FUJIKURA LTD.

1440,Mutsuzaki, Sakura-shi,Chiba,285 Japan

Makoto Ohsawa was born in 1960. He received the B.E. degree in 1983 from Sophia University. He jointed Fujikura Ltd. in 1983 and has been engaged in research and development in the telecommunication cables and accessories.
Mr.Ohsawa is a member of the Institute of Electronics, Information and Communication Engineers.

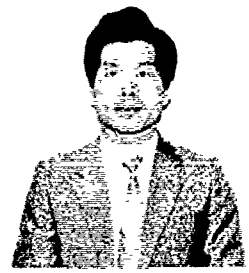

Hiroshi Yokosuka

Opt-Electronics Laboratory
FUJIKURA LTD.

1440,Mutsuzaki, Sakura-shi,Chiba,285 Japan

Hiroshi Yokosuka graduated in mechanical engineering from Tokyo Metropolitan Technical Junior College in 1967.
He has been engaged in development of telecommunication cables and accessories. He is now a Manager of the Fiber and Cable Accessory Department in Opt-Electronics Laboratory of Fujikura Ltd.
Mr. Yokosuka is a member of the Institute of Electronics, Information and Communication Engineers of Japan.

The Architecture and Technology of the Next Generation of All-Fiber Loop

John Tardy
James K. Wheeler

AT&T Bell Laboratories
Whippany, New Jersey 07981

ABSTRACT

As all-fiber loop systems evolve, Local Exchange Carriers (*LEC*s) expect the per-living-unit life cycle costs for providing standard telephony services on these systems to be in close parity with Digital Loop Carrier (*DLC*) systems using copper distribution. Architectures must allow *LEC*s to build an infrastructure today that can be used to provide tomorrow's services. In addition, *LEC*s expect flexible powering arrangements that meet their specific local conditions for terminal equipment. The design of the next generation of the all-fiber loop addresses each of these goals.

1. OVERVIEW

All-fiber loop systems that provide telephony services have been available since 1988[1] [2]. Many of these systems took on the high-level architecture shown in Figure 1. This architecture consists of the following components:

- An interface to the local switch either via Bellcore's *TR-TSY-000008* specification[3] (see Figure 1) or via a Digital-Loop-Carrier (*DLC*) Central Office Terminal (*COT*) (this terminal point is called the *Serivce Node*),
- A feeder line consisting of a lightwave MUltipleXer (*MUX*) operating over single-mode fibers,
- A *DLC* Remote Terminal (*RT*) (or *Access Node*),
- A distribution plant consisting of single-mode fibers with an Optical InterConnect (*OIC*) panel at the *RT* location,
- A Distant Terminal (*DT*) (or *Optical Network Unit*) located either on, or in close proximity to, the end-user's premises.

The active double-star architecture allows Local Exchange Carriers (*LEC*s) to build a fiber infrastructure that can support tomorrow's services such as Broadband *ISDN* and *CATV* transport. Because the double-star architecture is similar to the traditional metallic distribution architecture, a simple extension of outside-plant engineering procedures for metallic distribution to the all-fiber architecture is possible. Since 1988, *LEC*s have gained experience at more than 20 all-fiber loop sites and, as a result, have expressed several challenging objectives for the next generation of architecture and technology of the all-fiber loop:

- The Installed First Cost (*IFC*) of an all-fiber loop may exceed by up to forty percent that of a *DLC* system that uses metallic distribution to provide the same services. However, the life-cycle cost of an all-fiber loop must be near parity with that of the equivalent metallic system.
- End-user services, such as Plain Old Telephone Service (*POTS*), coin, Voice Frequency (*VF*) special services, *DDS*, and *ISDN*, that are available on metallic loops must be available on all-fiber loops.
- Operations, Administration, and Maintenance (*OA&M*) procedures for all-fiber loops must be improved over those of metallic systems. This objective is a step toward lowering the life-cycle cost of an all-fiber loop.
- Fiber loop systems must comply with Bellcore's *TR-TSY-000303* local switch interface specification[4].
- The use of standardized transport methods, such as Synchronous Optical NETwork (*SONET*)[5], in the feeder plant is required.
- The *RT* must have the capability, improved over that of the first-generation all-fiber loop systems, to manage bandwidth for the best match between the local switch and the *DT*s and for the most efficient use of feeder plant capacity.

- Flexible powering arrangements for the *DT* must be available.
- The architecture must provide for an upgrade to support transport of *CATV* signals.

The next-generation architecture described in this paper addresses these objectives while retaining the basic configuration shown in Figure 1.

2. CONFIGURATION

2.1 End-to-End Overview

The most economical topology for accessing many end-users spread over a large area is still the multilevel star network, and the next-generation all-fiber loop system retains the active double-star architecture shown on Figure 1. However, the components that make up the system are new developments, use the latest technology, and establish an infrastructure for future services. Integration of functions at the switch and the *RT* is a key advance in the new *DLC* system. We will be discussing the following network components: the switch interface, the *RT* and *DT*, and the connecting feeder and distribution optical links.

2.2 Switch Interface and the Feeder Plant

A major cost saver for new *DLC*s is the capability to connect directly to a digital switch via high-bandwidth digital interfaces, eliminating *COT*s with analog interfaces. Today, switches assemble the basic Pulse Code Modulation (*PCM*) streams into higher-rate signals consisting of 24 *DS0*s for transmission on the feeder plant at the *DS1* rate, 1.544 *Mbps*. Existing *DLC* specifications, *TR-008* and *TR-303*, are organized around this bit rate. Next-generation *DLC* systems will support these interfaces as well as special applications and service on a large number of *DS1* links.

SONET is the standard signal format for the *CO*-to-*RT* feeder facility, and the next-generation *DLC* system is designed to make the best of the format. The system will multiplex 28 *DS1* signals to the 51.84-*MHz* *STS-1 (OC-1)* rate, the base rate for *SONET*[5] [6], and will combine three such signals to form an *OC-3* signal at the 155.52-*MHz* rate, the standard for the next-generation *DLC* feeder facility. Thus, the bandwidth between the *CO* and *RT* is increased way beyond what a single *RT* needs for narrowband services. The connection between the *OC-3* interfaces is via single-mode fibers, with a maximum span of 30 *km* (18.6 miles) without repeaters. The optical feeder interface parameters conform to the *ANSI* T1.106 standard[7]. All critical elements of the feeder operate with 1+1 protection.

Concentration can be a major cost saver for our customers. The new feeder interfaces allow per-call concentration from 1:1 (no concentration) to 8:1, or higher. Therefore, *LEC* engineers can optimize the feeder configuration based on local traffic patterns, adding or removing feeder capacity as required. The standard 2:1 concentration ratio for *TR-008* Mode 2[3] is supported.

The standard feeder provides point-to-point (*CO*-to-*RT*) transport, but the new high-bandwidth interfaces provide opportunities for taper, hub and ring network applications. The output of the switch interface is routed to the *OC-3* multiplexer via the standard *DSX1* cross-connect panel. In case of an analog interface, a *TR-008*- or *TR-303*-compatible *DLC COT* can be inserted between the *DSX* panel and the switch.

2.3 The Next-Generation Digital Remote Terminal

The architecture of the new digital *RT* for fiber distribution, Figure 2, was designed to meet the needs of *DLC* applications in the 1992-1997 time frame. Considerable time and effort were spent trying to understand our customers' needs, some of which are listed in Section 1. Flexible configurations, to match divergent and changing requirements, are a must. We reduced cost by maximizing sharing and by integrating functions that are common to major applications.

The core of the *RT* supports functions that are not specific to the distribution format and medium. The standard feeder connection is an *integrated SONET OC-3 interface and multiplexer* which delivers the full payload of one *STS-1* signal to the *RT*. The remaining two *STS-1* payloads can serve other *RT*s at the same site via *STS-1E* connections, or they can be re-formed into a partial *OC-3* signal and serve *RT*s at other sites in an add/drop taper feeder or ring network. Alternatively, one of the two remaining *STS-1*s can serve up to 28 *DS1 pipes* to end-users requiring this service while the other remaining *STS-1* is re-formed into a partial *OC-3*. To make use of the bandwidth available from an *OC-3* interface, or to use external multiplexers and existing feeders, the feeder interface can be configured for *STS-1E* or up to 28 *DSX1 electrical feeder connections*.

The *RT* core can implement interfaces that range from a simple fixed-assignment between the feeder and distribution sides in *TR-008* Mode 1, to the full Time-Slot-Interchange (*TSI*) function in the *TR-303*

mode. In the latter configuration, any feeder channel can be connected to any distribution channel. These connections can be semi-permanent assignments or, in the case of concentration, per-call associations. All critical functions, such as system timing, *TSI*, multiplexing, etc. are fully protected. An integrated test head that is functionally a remote measurement unit eliminates the need for a *DC* test pair. This test head can perform the full range of channel and drop tests on almost any customer circuit. Intelligence native to the *RT* core allows tests to be performed autonomously (routine testing), under commands from a "dumb" terminal, or via links to network operations systems, including *LMOS* and *MLT*. Controllers keep track of configurations, provisioning, and inventory, keep performance records, and can provide alarms and fault sectionalization with higher resolution than previously possible. This information can all be accessed locally or remotely from *LEC OS* systems.

Note that in discussing the *RT* core, no mention was made of fiber or metallic distribution. The core functions are common to both, and support fiber *and/or* metallic distribution. *Metallic distribution* can be configured by providing shelves equipped with standard *DLC* channel units. *Fiber distribution* is achieved by providing digital and optical interfaces between the feeder-interface/core complex and the distribution links, which terminate in the distant terminals. The distribution system provides a *DS1* signal[8] (with its payload of up to 24 *DS0*s) to each *DT*.

Depending on its configuration and mode of operation, a single next-generation fiber *RT* can serve from 672 to 1000+ lines and occupies about the half the space of a system that uses older dual channel banks (which provide 192 lines per dual bank) to provide the same number of lines. New outside plant cabinets take advantage of the reduced size and fit into the landscape unobtrusively.

The full *TSI* capability provides a *bandwidth management function* that can be used to eliminate local switch terminations for services that do not use that switch. For fiber distribution the function gives flexibility in *bandwidth shedding or growth* situations by increasing the efficiency of the feeder plant. In the *TR-008* mode, if the initial configuration of a *DT* link is exhausted, a service order for an additional line can require a re-configuration of the *RT*, addition of *RT* and *DT* plant, or both. In the *TR-303* mode such requests can be usually satisfied by re-provisioning the channel assignments, unless of course the 24-*DS0* capacity of the distribution link is exhausted.

2.4 Distribution Plant

An optical interconnect at the *RT* site provides a flexible rearrangement and maintenance access point between the optical interfaces and the outside plant. Installation testing methods have been developed to guarantee the performance of single-mode fiber in the short wavelength transmission region[9]. Therefore, equipment costs in the next-generation system are reduced through the use of ultra-low-cost, short-wavelength compact-disc laser technology.

Optical-splitter technology is employed at the *RT* and the *DT* to combine both directions of transmission on a single fiber. The additional cost of splitters at both ends of the optical path is offset by the use of low-fiber-count media and closures, and by reduced installation costs. In addition, the use of a single fiber *lowers OA&M* (life-cycle) costs relative to multi-fiber loop systems.

Use of the short wavelength region leaves the long wavelength region accessible via wavelength-division-multiplexer technology. Therefore, the same distribution fiber may be used for the transport of *CATV* signals or Broadband *ISDN* without a significant impact on the design of the telephony equipment and with the benefits of single-fiber transmission outlined above.

2.5 Distant Terminal Functionality

The Distant Terminal (*DT*) consists of plug-in units housed in an outside plant closure mounted either outside the end-users' premises or on a curb a short distance from the end-users' premises. The entire payload capacity of the *DT DS1* signal can be used to provide up to 24 end-user circuits at the *DT*. As a result, the *DT* can serve up to sixteen living units in residential applications, depending on end-user line take, while previous all-fiber loop systems served a much smaller number of living units. The *IFC* per living unit decreases with an increasing number of living units due to the increased sharing of *DT* common equipment. In addition, use of the *DS1* rate on the *RT/DT* fiber reduces costs by permitting the use of components that are sold in high volumes.

The *DT* incorporates many complex functions (see Figure 3): an Optical Interface which terminates the fiber, a Controller which forms a transmission and control bus that is accessed by the Channel Units (*CU*s), a Ringing Generator (*RG*) which drives alerting circuits in end-user telephone sets, and a

flexible Power Interface (*PI*) which powers the electronics in the *DT*. Transmission and signaling characteristics are compliant with *TR-TSY-000057*[10].

End-user circuits can be provided by an assortment of plug-in *CU*s supported by the *DT*. This modular feature enables the *DT* to provide the same variety of services, simultaneously on different tip/ring pairs, that can be provided by a *DLC RT* using metallic distribution. These services include Plain Old Telephone Service (*POTS*); a variety of switched, non-locally-switched, and non-switched Voice Frequency (*VF*) special services; coin; *DDS*; and *ISDN*.

The Controller monitors the health of the circuitry in the *DT* as well as the health of the *DS1* link from the *RT*. When it detects trouble, the Controller notifies the *RT* via a data link. The *RT* will, in turn, report the trouble to the central office and maintenance center. The *DT* must support the evolution of trouble reporting toward pinpointing the type of trouble and the plug-in that is in trouble. Evolution toward the capability of remote inventory of plug-ins is also a feature of the *DT*.

In addition, the *DT* supports on-demand testing of the tip/ring pairs between the *DT* and the end-users' equipment (called "drop testing") as well as of the carrier-derived channel from the central office through to the analog side of the *DT CU* (called "channel testing"). These testing and monitoring features decrease the life-cycle cost of the all-fiber loop by giving maintenance-center personnel more accurate information with which to dispatch repair personnel and by bringing the maintenance procedures closer to being pro-active rather than reactive.

2.6 Distant Terminal Powering

A variety of methods to power the *DT* are provided by the flexible Power Interface (*PI*), shown in Figure 3. The methods are:

- Commercial 120-*VAC* connection at the *DT* location,
- Connection to a *DC* power source located at the opposite end of the drop pair (this method is called *back powering*),
- Connection to a centralized *DT* power plant that is shared among many *DT*s (called *network powering*).

Commercial *AC* power is obtained by placing a power meter on each curb-side *DT* or by sharing a power meter on one *DT* with other *DT*s. The number of *DT*s sharing the meter depends on *LEC* and local power utility practices. For a premises-mounted *DT*, *AC* power is obtained either by a connection to the premises *AC* wiring or by placing an adapter ring on the end-user's power meter. The advantage of the commercial-*AC* method is that the *LEC* does not have a power distribution system to maintain. However, installation costs are increased because electrical contractors must be hired to handle the 120-*VAC* connections.

Back powering is accomplished by using *DC* sources placed on several living units to power a common curbside *DT* or by using one *DC* source to power a premises-mounted *DT*. The advantage this method has over the commercial-*AC* method is that the power and voltage levels involved (–48 *V* is recommended) are within safe limits for *LEC* personnel to handle. Material and maintenance costs are increased because this method requires additional pairs in the drop cables to each living unit to carry power.

For network powering, one *DC* power plant can be located at the *RT* site to power the entire serving area, or several smaller power plants can be located within the serving area, each serving a small number of *DT*s. Because local practices may prohibit the installation of cabinets of any appreciable size (that is, larger than a *DT*) most *LEC*s will choose to locate one power plant at the *RT* site. To carry the power to the *DT*s, a metallic distribution network must be installed and maintained alongside the fiber network. If voltage and power levels are to be kept within safe limits for *LEC* personnel to handle (up to ±130 *VDC* with respect to ground limited to 100 *W* at the power plant output), the distribution network must either be made up of large-gauge cables or smaller-gauge cables with a few pairs connected in parallel. To prevent cable corrosion, many *LEC*s would source –130 *V* and ground as opposed to +130 *V* and –130 *V*. In addition, *LEC*s prefer to work with cables typically used for telephony transmission such as 19, 22, 24, or 26 *AWG* in 25-, 50-, or 100-pair cables. As a result of these limitations, a star, as opposed to a bus, distribution network must be installed using a separate output at the power plant for each *DT* and parallel pairs to connect to each *DT*. However, the advantage of network power is in the way it addresses backup power.

The *AC* and backpowering schemes place backup batteries in the *DT* structure (shown as a dashed box

in Figure 3) to provide a minimum of eight hours of operation of the *DT* during commercial power outages whereas the network power scheme improves battery maintenance operations by placing batteries in a centralized location. In addition, the network-power method makes feasible the use of a generator to provide power for *DT*s during long outages. Note that the use of generators is more practical when a single generator can be placed at an *RT* site to power the whole serving area as opposed to several generators dispersed throughout the serving area.

3. OBSERVATIONS

The *DLC* system with the capabilities described here will meet *LEC* expectations in the coming decade. Expectations are bound to change, most likely grow. The architecture of our new *DLC* system will support such growth at all the network nodes. The new *RT* already includes features described in *TR-303* as *future plans* for advanced terminals, such as *RT* intelligence, integrated test head, and other functions. The technology of all the all-fiber loop will advance in the future, and a key design rule is that such advances must be supported, not blocked. The built-in flexibility will eliminate the need for drastic changes in the system, allowing for graceful evolution for years to come.

REFERENCES

1. R. M. Huyler, D. E. McGowan, J. A. Stiles, and F. J. Horsey, "The Architecture and Technology for the All-Fiber Loop," *37th International Wire and Cable Symposium*, November 1988, pp. 129-133.

2. F. A. Huszarik, R. Mariani, R. Yakimovich, and J. Justice, " Installation and Testing of Multiservice Fiber Links in the Subscriber Loop: A Case Study," *37th International Wire and Cable Symposium*, November 1988, pp. 158-162.

3. *Digital Interface between the SLC® 96 Digital Loop Carrier System and a Local Digital Switch*, Technical Reference TR-TSY-000008, Issue 2, August 1987, Bell Communications Research, Inc.

4. *Integrated Digital Loop Carrier Generic Requirements, Objectives and Interface*, Technical Reference TR-TSY-000303, Bell Communications Research, Inc., Issue 1, September 1986, Revision 2, July 1989.

5. American National Standard for Telecommunications - *Digital Hierarchy - Optical Interface Rates and Formats Specifications*, ANSI T1.105-1988, Exchange Carriers Standards Association, Inc., 1988.

6. R. J. Boehm: Progress in Standardization of SONET, pp. 8-16, May 1990 IEEE LCS, IEEE, NY

7. American National Standard for Telecommunications - Optical Interface Specification: Single Mode, ANSI T1.106-1988, Exchange Carriers Standards Association, Inc., 1988

8. American National Standard for Telecommunications - *Carrier-to-Customer Installation — DS1 Metallic Interface*, ANSI T1.403-1989, Exchange Carriers Standards Association, Inc., 1989.

9. James J. Refi and Michael J. Swiderski, "System Requirements and Installation Testing for Fiber-to-the-Subscriber," *39th International Wire and Cable Symposium*, November, 1990.

10. *Functional Criteria for Digital Loop Carrier Systems*, Technical Reference TR-TSY-000057, Bell Communications Research, Inc., Issue 1, April 1987, Revision 1, November 1988.

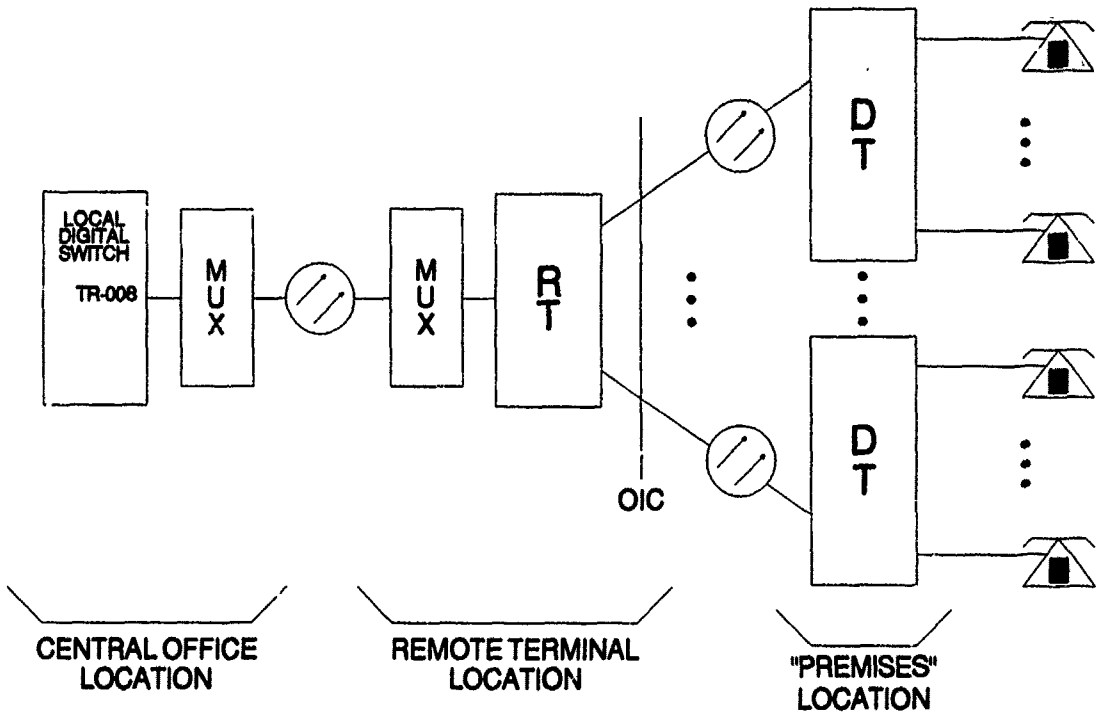

FIGURE 1. CURRENT-GENERATION ALL-FIBER LOOP

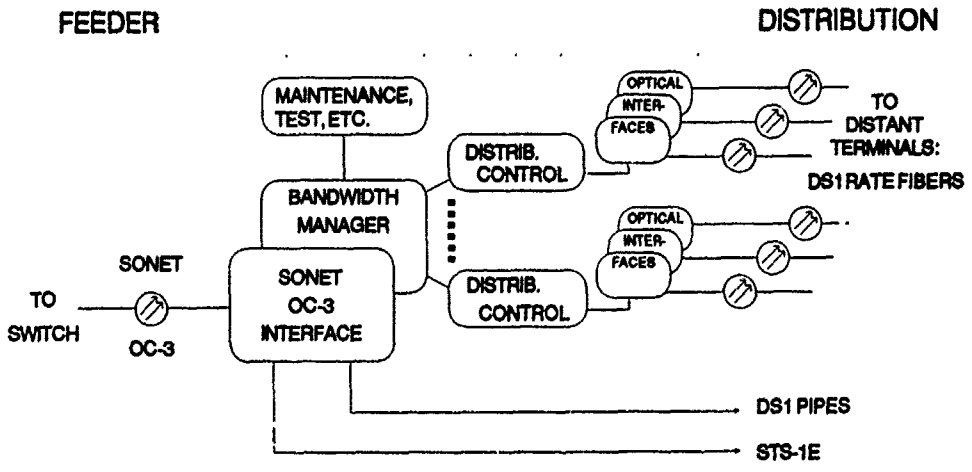

FIGURE 2. NEXT-GENERATION FIBER RT

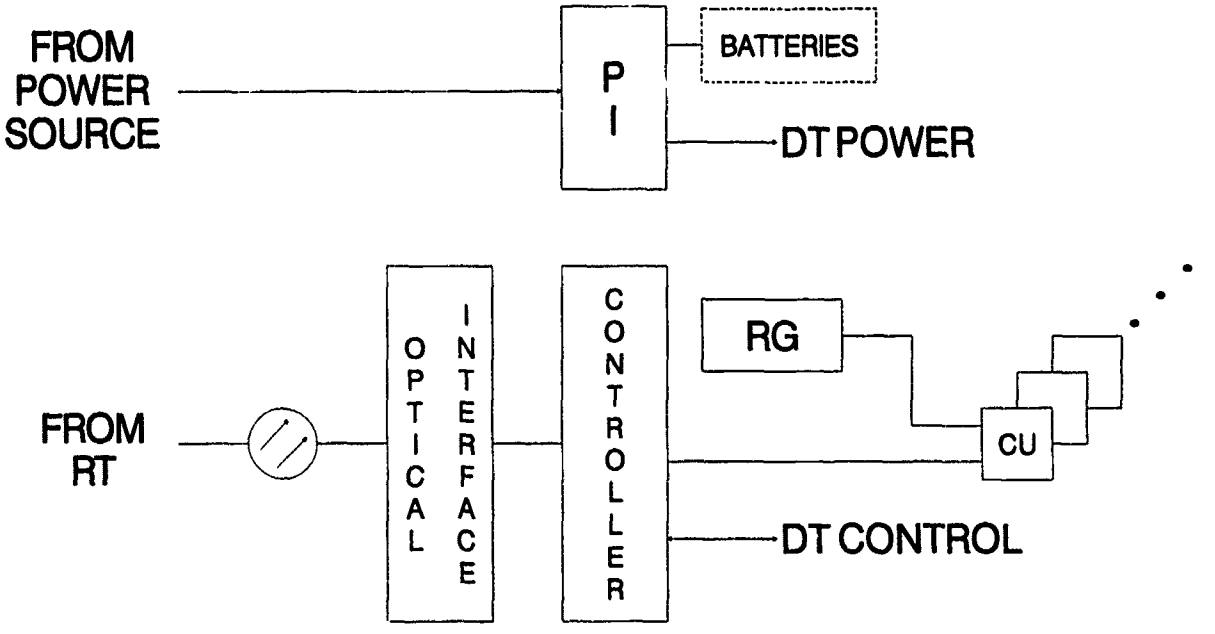

FIGURE 3. NEXT-GENERATION DT ARCHITECTURE

JOHN TARDY
AT&T Bell Laboratories
Whippany, NJ 07981

John Tardy is a Member of Technical Staff at AT&T Bell Laboratories and is a systems engineer in the Loop Systems Planning Department of the Fiber Access Systems Laboratory. His most recent prior experience was product development for AT&T's Energy Systems business, preceded by a long series of assignments in development and systems engineering of computer automated test and other C.I.M. facilities, hardware and software. He has the B.S. and M.S. degrees in Electrical Engineering with specialization on Automatic Control Systems. He is a senior member of IEEE with long involvement with IEEE standards, is a member of the NSPE. He has published a number of papers and holds several patents in the fields related to his assignments.

JAMES K. WHEELER
AT&T Bell Laboratories
Whippany, NJ 07981

James K. Wheeler is a Member of Technical Staff at AT&T Bell Laboratories. He has a BS degree in Physics from North Georgia College and BSEE and MEE degrees from The Georgia Institute of Technology. James is a systems engineer in the Fiber Access Systems Laboratory and has extensive experience in the development of digital loop carrier systems. He is currently working on the SLC® Series 5 Fiber-To-The-Home System.

SYSTEM FOR ACQUISITION, ANALYSIS AND STATISTICAL ELABORATION OF TRANSMISSIVE AND GEOMETRICAL MEASUREMENTS ON OPTICAL FIBRE CABLES

G. BUGA (*), M. FLORIS (*), F. ESPOSTO (**), F. NANNI (**)

(*) SOCIETA' CAVI PIRELLI, LIVORNO FERRARIS (ITALY)
(**) SIP D.G., ROMA (ITALY)

ABSTRACT

In a system of quality assurance for optical fibre transmission links, it is necessary to have complete traceability and ease of access to all the fibre characteristics measured during each stage of the manufacturing and installation process; this involves the collation of data from the fibre supplier, from finished cable measurements, and from acceptance tests after the cable has been installed. This paper describes a fully automatic computerised system for this application which has been established at Pirelli factory (1), for optical cables produced for SIP (2). The system correlates data obtained from the fibre supplier with measurement results from the appropriate finished cable and transfers them to a floppy disk which is sent to SIP. Subsequently the corresponding installation data are added to the disk, thus creating a single data base containing the complete history of a fibre link, the availability of which is also useful for monitoring and assessing variation of the link's performance in the future. This system will be gradually extended to all cable suppliers and installation companies working for SIP.

INTRODUCTION

A key point in any quality assurance system is product traceability with the complete availability of measurements throughout the manufacturing process.
Despite being extensively used since ten years ago, fibre optic transmission links do not have a computerised data base of their performance characteristics.
If this is important for traditional telecommunication links, then it is considered essential for fibre links in view of their strategic importance in transmitting very high numbers of telephone channels in the long distance trunk network.
For the cable manufacturer the availability and comparison of individual measurements at the various stages of the production process is indispensable for satisfactory production control in the short to medium term, while the availability of statistical elaboration is essential for medium to long term process control and for product quality control and improvement.
The data from the fibre supplier and the cable manufacturer are then integrated with the data obtained during the installation phase, thus providing the network operator with a complete history of the project (stored, for example, on a floppy disk), which facilitates future investigations of any faults or malfunctions and can provide a complete picture of the network at any moment.
This supposes of course that there is sufficient accuracy of alignment between the measuring instruments used in the various stages of characterisation of the fibres and cables.

(1) At Livorno Ferraris (Vercelli-Italy)
(2) principal Italian Telephone Operating Company

QUALITY CONTROL FOR OPTICAL CABLES (TRANSMISSION CHARACTERISTICS)

Control of the fibre transmission characteristics during cable production is carried out by the manufacturer according to the flow chart in fig. 1.
A data acquisition and elaboration system, called Apollo, operates within the cable factory, acquiring and correlating the results of measurements carried out on the fibres at various points in the process.
This system also carries out statistical elaborations, either periodically (e.g monthly) or on request, to give a precise picture of the situation in a very short time.
A second system, called Floppy, interfaces with the central mainframe computer, which contains the data necessary for the identification of the fibres in the cable, and carries out, for all of the fibres of the cables produced in a determined period, the correlation between the measurements of the fibre supplier (available from floppy disks provided with each fibre delivery) and those of the finished cable acquired from the Apollo system.
The correlated data are archived according to project on a floppy disk which is sent regularly (monthly) to the network operator and to which will be added the results of tests carried out by the cable installer (attenuation of the individual cable lengths, of the joints

and of the repeater section).
The data contained in the data base will then be used for statistical elaboration of the various parameters and made available to the appropriate regional headquarters.

THE APOLLO SYSTEM

The Apollo system manages all of the transmission and geometrical measurements carried out in the factory during the production process according to the scheme shown in fig. 2.
The actual measurements benches connected to the system are as follows:

Measurement	No. of instruments
Backscattering	6
Spectral attn., cut off wavelength	2
Geometrical characteristics	1
Chromatic dispersion	1

Each bench is served by a PC which controls the execution of the tests and then stores the results on a floppy disk, reducing manual intervention by the operator to a minimum.
The program then compares the results with the appropriate specified acceptance limits, thus avoiding any error due to the operator.
Every day, the data on the floppy disks are transferred to a computer which is completely dedicated to the management of the measurement results.
The use of a PC with a 40 Mbyte hard disk makes it possible to have on line data from the measurement of up to 20,000 fibres, which corresponds to about 4 months of actual cable production.
This permits statistical evaluations and comparisons based on the availability of a considerable quantity of data.
The main program is very easy to use as it is menu driven, its main function and services being as follows:

- centralised printing of test results, including backscattering (fig. 3) and spectral attenuation curves
- centralised printing of summaries of the individual results for each cable length, including elementary statistics (max, min, average) (fig.4)
- comparison of cable attenuation between partly finished and finished cables
- statistical comparison of attenuation between different wavelengths and temperatures
- statistical elaboration according to the type of measurements, either partial or periodic (e.g. monthly) (fig. 5)
- monthly trends of the principal characteristics (fig. 6)
- storage of the results on tape cartridge or high density floppy disk for definitive back-up (every 4 months).

This system structure, based on independent peripheral PCs, has been chosen because it does not limit the number of instruments that can be connected to it, provided that the PC dedicated to system management has sufficient memory for the data obtained from several months of production.
Furthermore the use of floppy disks for data storage and manual transfer to the central PC, instead of using a permanent LAN, permits extension of the system in a very simple manner and improves operational flexibility by freeing the equipment from fixed locations with limited radius of action.
This is important for example in backscatter testing where it is convenient to move the measurement bench around the whole of the testing department, often several hundred metres from the central PC.
Measurement automation, apart from guaranteeing reliability and objectivity, is fundamental in achieving appreciable reductions in testing time.
The Apollo system constitutes the basis for the creation of the program which automatically provides all the measurements relevant to the various phases of production and allows them to be compared to ensure that no degradation of the fibre characteristics has occured during each production phase, while at the same time carrying out statistical elaboration of the available measurements.

THE FLOPPY SYSTEM

The Floppy system automatically compiles a data base which, for all the cables tested in a determined period, contains the identification data of the cables, the identification code of each of the fibres, the measurement results from the finished cable and the test data provided by the fibre supplier.
Fig. 7 shows the flow chart describing the operation of the Floppy system.
On arrival of every fibre delivery, the technical data provided on floppy disks by the fibre supplier is systematically transfered to both the mainframe computer (for stores management of the fibres) and the PC dedicated to Floppy (archive of supplier's measurements).
At the start of the production of each cable, when the fibres are taken from the stores, the correspondence between the fibre's code number from the supplier and its position in the cable is recorded on the mainframe computer.
The Floppy program performs the following steps:

- searches in the mainframe computer for the cables tested in a chosen period
- retrieval of the code numbers of the fibres used in these cables
- retrieval of the data from the archive of supplier's measurements by means of the fibre code number
- retrieval of the measurements on the finished cable

- transfer of these three sets of data together with the cable identification data, which is also taken from the mainframe computer, to the floppy disk which will be supplied to the customer.

The complete history of the fibres used in the cable is therefore obtained completely automatically and forms the basis of a database of service to the end user.

A complete monthly elaboration, involving about 5,000 fibres, requires approximately 4 hours and each high density floppy disk can contain data for about 7,000 fibres.

Table 1 shows the data supplied to the customer (SIP) for each fibre in the cable.

Simple statistical elaborations are also carried out on the data provided in the database to allow direct comparison of the data of the cable manufacturer with those of the fibre supplier.

Table 2 shows the comparison between cable manufacturer and fibre supplier with regard to attenuation values, at 1300 nm and 1550 nm, obtained by backscattering technique.

CONCLUSION

The system described here has been in service since the beginning of the year for the fibre and cable part and will soon be completed with the installer's data.

Among the many advantages obtained, the following are of particular note:

- greater automation of factory measurements with consequent reductions in both measurement time and operator error
- magnetically stored archives
- ease of access and recovery of the measurements
- process control by means of automatic comparison of the measurements from different stages
- availability of statistical elaborations and evaluations, in real time, to permit design validation
- completely automatic traceability of measurements by project

This system could also be used to evaluate the quality and reliability of the suppliers (fibre and cable manufacturers, and installers) by comparing measurements from the various phases.

As a future prospect, accessability to the data could be extended to end users with the possibility of inserting data relevant to maintenance interventions and link modifications, thus providing real time monitoring and effective management of the network.

ACKNOWLEDGMENTS

The authors wish to thank the management of Società Cavi Pirelli and SIP for the authorisation to publish this paper.

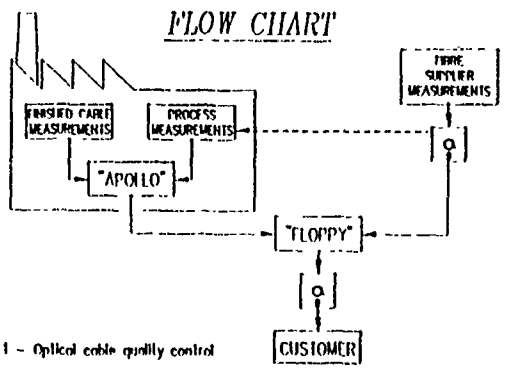

FIG 1 – Optical cable quality control

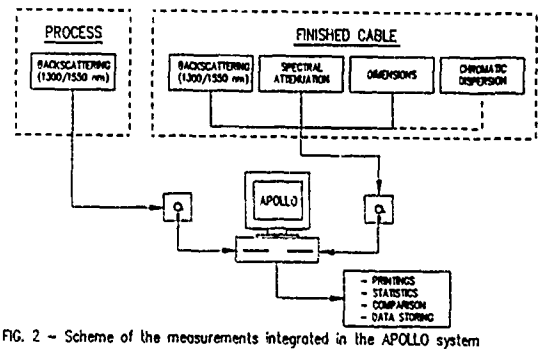

FIG. 2 – Scheme of the measurements integrated in the APOLLO system

SOCIETÀ CAVI PIRELLI s.p.a.
LIVORNO FERRARIS FACTORY
Via GORETTA ,1
13046 LIVORNO FERRARIS (VC), ITALY

QUALITY ASSURANCE Dep.

DATE 9/7/90
PAG. 1/25

Backscattering Attenuation

MANUF. N°: 73695 STAGE: FINITO BENCH: 010/025
LENGTH N° 2 WAVELENGTH: 1550 nm PULSE: 1000 ns
DRUM N°: 16/485242 TEMPERATURE: 20 °C
CABLE LENGTH: 2130 m

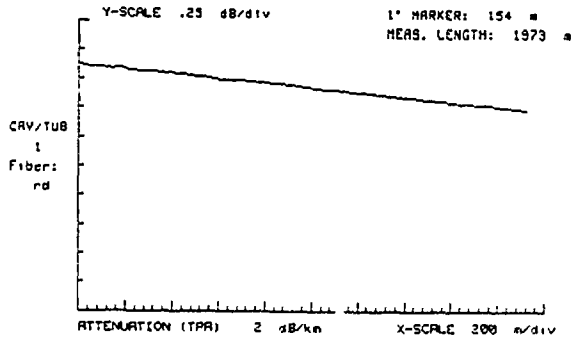

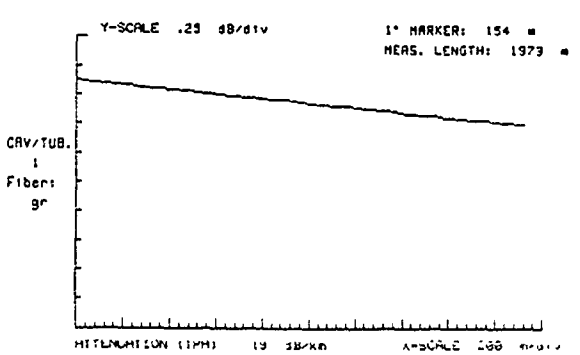

OPERATOR:4

FIG. 3

SOCIETÀ CAVI PIRELLI s.p.a.
LIVORNO FERRARIS FACTORY
Via GORETTA ,1
13046 LIVORNO FERRARIS (VC), ITALY

QUALITY ASSURANCE Dep.

DATE 9/7/90
PAG. 1/1

ATTENUATION MEASUREMENTS

CUSTOMER: S.I.P. ORDER: 894375 TEMPERAT.. 20 °C
MANUF. N°: 73695 LENGTH N°: 2 DRUM N°: 16/485242
SPEC.. 1233/89 ROUTE: MILANO-BOLOGNA
STAGE: FINITO SIZE: 50 FO (SM) / PM9E
WAVELENGTH: 1550 nm BENCH: 010/025 CABLE LEN.: 2130 m

	Color Fiber	Back.Att. (dB/km)	Cut-B.A. (dB/km)		Color Fiber	Back.Att. (dB/km)	Cut-B.A. (dB/km)
CAV/TUB 1	rd	0.20	0.00	CAV/TUB 4	rs	0.20	0.00
	gr	0.19	0.00		vd	0.20	0.00
	ye	0.19	0.00		gl	0.20	0.00
	br	0.19	0.00		ar	0.20	0.00
	bl	0.18	0.00		bl	0.19	0.00
	vl	0.19	0.00		vl	0.19	0.00
	rd-b	0.19	0.00		rs-a	0.20	0.00
	gr-b	0.19	0.00		vd-a	0.20	0.00
	ye-b	0.19	0.00		gl-a	0.19	0.00
	br-b	0.19	0.00		ar-a	0.20	0.00
CAV/TUB 2	rd	0.20	0.00	CAV/TUB 5	rs	0.20	0.00
	gr	0.19	0.00		vd	0.19	0.00
	ye	0.20	0.00		gl	0.20	0.00
	br	0.19	0.00		ar	0.21	0.00
	bl	0.19	0.00		bl	0.19	0.00
	vl	0.20	0.00		vl	0.20	0.00
	rd-b	0.20	0.00		rs-a	0.20	0.00
	gr-b	0.20	0.00		vd-a	0.22	0.00
	ye-b	0.20	0.00		gl-a	0.21	0.00
	br-b	0.20	0.00		ar-a	0.20	0.00
CAV/TUB 3	rd	0.19	0.00				
	gr	0.22	0.00				
	ye	0.19	0.00				
	br	0.20	0.00				
	bl	0.20	0.00				
	vl	0.20	0.00				
	rd-b	0.19	0.00				
	gr-b	0.19	0.00				
	ye-b	0.21	0.00				
	br-b	0.20	0.00				
STAT. PAR.	MAX:	0.22	0.00	DATA N° : 050			
	MIN:	0.18	0.00				
	AVG:	0.20	0.00				

NOTE:

OPERATOR: 4 SUPERVISOR: Q.A.D. MAN.: G.B. CUSTOMER:

FIG. 4

LIVORNO FERRARIS FACTORY
Via GORETTA ,1
13046 LIVORNO FERRARIS (VC), ITALY

DATE 10 Jul 1990

BACKSCATTERING ATTEN. (1550 NM)

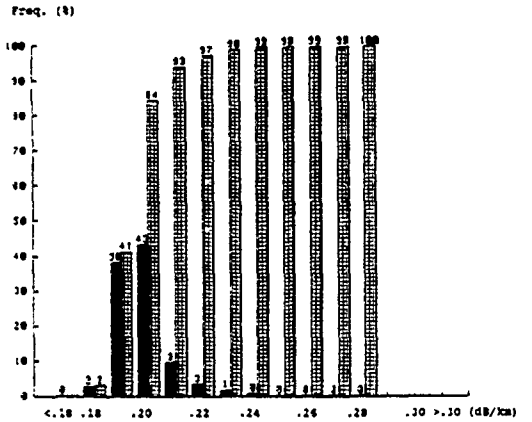

- DATA N°	= 1670		- N° CLASSI	= 13
- MAX	= .28	(dB/km)	- AMPIEZZA CLASSI	= .01 (dB/km)
- MIN	= .17	(dB/km)		
- AVG	= .198	(dB/km)		
- STANDARD DEV.	= .01	(dB/km)		

NOTE: HISTOGRAM ON 1 - 30 JUNE 1990

AUTHOR: APPROVED BY:

FIG. 5

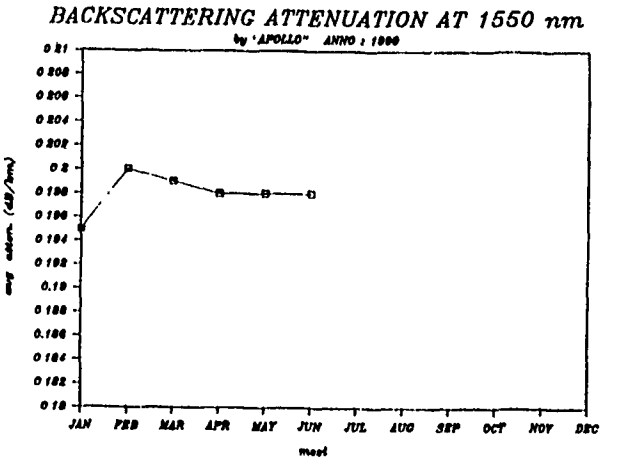

FIG. 6

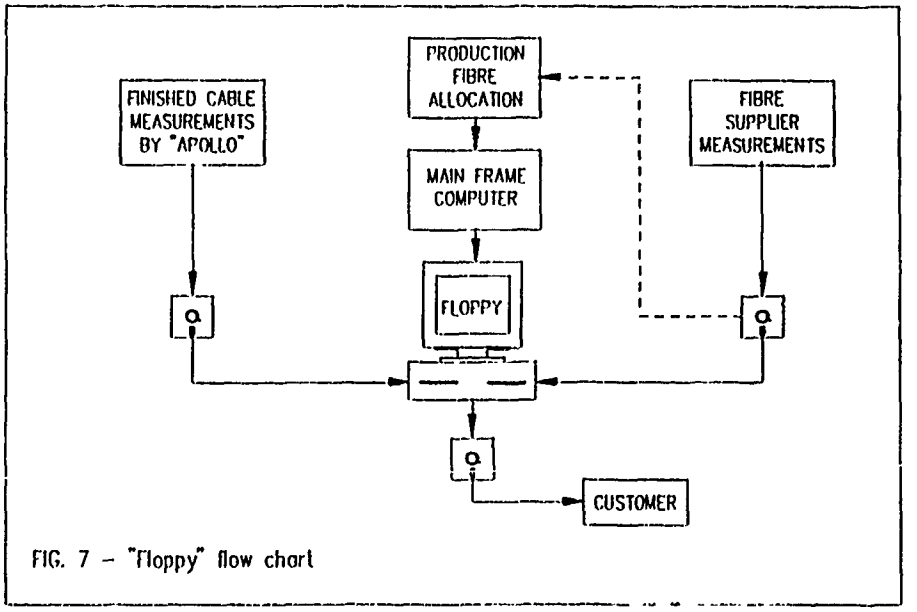

FIG. 7 – "Floppy" flow chart

TABLE 1

File FIBRE : record structure of one fibre.

- Cable measurement date
- Cable manufacturer
- SIP order
- Route identification
- Cable type
- Cable length (m)
- Drum number
- (1) Manufacturing number
- Slot identification
- Fibre position in the cable
- Backscattering attenuation at 1300 nm (dB/km)
- Backscattering attenuation at 1550 nm (dB/km)
- Backscattering linearity code

- Fibre identification number
- Fibre type
- Fibre supplier
- Invoiced length (m)
- Backscatter [illegible]ttenuation at 1300 nm (dB/km)
- Backscattering attenuation at 1550 nm (dB/km)
- Cut-off wavelength (nm)
- M.F.D. at 1300 nm (micron)
- M.F.D. at 1550 nm (micron)
- (2) Cladding diameter (micron)
- Cladding non-circularity (%)
- Mode field concentricity error (micron)
- Linearity of the backscattering curve (dB)
- Zero-dispersion wavelength (nm)
- Zero-dispersion slope (ps/nm^2/km)
- Max chromatic dispersion between 1285/1330 nm (ps/nm/km)
- Max chromatic dispersion between 1285/1330 nm (ps/nm/km)

Note :

(1) Data related to the cable (from cable manufacturer)

(2) Data related to the fibre (from fibre supplier)

TABLE 2

CABLE MANUFACTURER (CM) : Società Cavi Pirelli
PERIOD . 01 May 90 / 31 May 90
CABLE NUMBER . 237
FIBRE NUMBER . 7600
FIBRE SUPPLIER (FS) : F.O.S.

PARAMETER	DATA N°	MAX	MIN	AVG	STD.D.	MAX-MIN
Att.1300 (CM) (dB/Km) :	1235	0.41	0.30	0.340	0.014	0.11
Att.1550 (CM) (dB/Km) .	7600	0.27	0.12	0.198	0.011	0.11
Att.1300 (FS) (dB/Km) :	7600	0.41	0.32	0.348	0.011	0.09
Att.1550 (FS) (dB/Km) :	7500	0.25	0.17	0.192	0.007	0.08
Cut-off (FS) (nm) .	4622	1320	1163	1242	24	157
MFD 1300 (FS) (micron) .	4622	9.89	9.30	9.551	0.114	0.59
MFD 1550 (FS) (micron) :	4500	12.65	10.57	11.206	0.158	2.09
Cladd.D. (FS) (micron) :	4622	126.6	124.0	125.28	0.36	2.6
Cladd.non-circ.(FS) (%):	4621	1.8	0.1	0.55	0.22	1.7
Conc.err.(FS) (micron) :	4622	1.00	0.01	0.531	0.213	0.99
OTDR linearity(FS) (dB):	4505	0.020	0.005	0.0147	0.0033	0.015
Lambda 0 (FS) (nm)	2616	1323	1311	1317	2	12
Slope (FS) (ps/nm^2/Km):	2616	0.089	0.084	0.0875	0.0007	0.005
CD1285 (FS) (ps/nm/Km):	2500	-2.38	-3.40	-2.916	0.194	1.02
CD1525 (FS) (ps/nm/Km):	2500	18.21	16.92	17.595	0.214	1.29

LEGEND

Att.1300	= backscattering attenuation at 1300 nm
Att.1550	= backscattering attenuation at 1550 nm
Cut-off	= cut-off wavelength
MFD 1300	= mode field diameter at 1300 nm
MFD 1550	= mode field diameter at 1550 nm
Cladd.D.	= cladding diameter
Cladd.non-circ.	= cladding non-circularity
Conc.err.	= mode field concentricity error
OTDR linearity	= linearity of the backscattering curve
Lambda 0	= zero-dispersion wavelength
Slope	= zero-dispersion slope
CD1285	= max chromatic dispersion coefficient between 1285/1330 nm
CD1525	= max chromatic dispersion coefficient between 1525/1575 nm

Giancarlo Buga
Società Cavi Pirelli
Stabilimento di Livorno Ferraris
Via Goretta
13046 Livorno Ferraris
(Vercelli) - Italy

Mr. Buga was born at Rho (Milano), Italy in 1957 and received his doctorate in electronic engineering from the Polytechnic of Milan. During the doctorate he developed studies about coherent optical transmission at CSELT (Turin). He joined Società Cavi Pirelli where he has been engaged in optical cable design and development Dept.. Now he is the manager of the Testing and Quality Dept. of Livorno Ferraris Factory. He takes part in the work of international and national standardization bodies, such as CCITT, IEC, CEI, dealing with optical fibre cables and systems.

Marco Floris
Società Cavi Pirelli
Stabilimento di Livorno Ferraris
Via Goretta
13046 Livorno Ferraris
(Vercelli) - Italy

Mr. Floris was born at S. Vito dei N. (Brindisi) Italy in 1963 and received his doctorate in physics from the University of Lecce in 1986. During the doctorate he developed studies about non-linear physics. He joined Società Cavi Pirelli - Livorno Ferraris factory in 1987 where he has been involved in optical cable measurements and software development in the Quality Control Department.

Feliciano Esposto
SIP D.G. R/IT-CM
Via di Val Cannuta, 250
00166 Roma - Italy

Mr. Esposto was born at Acervia (Ancona), Italy in 1948. He received his doctorate in physics from the University of Torino in 1976.In 1969 he joined CSELT, where he did research on optics and optical communications, particularly holography and optical fiber characterization. Since 1980 he is with SIP, the Italian Telecommunication Operating Company, which like CSELT belongs to the STET group, where he has been involved in optical fiber transmission system design. At present he is the Manager of "Cables, Apparatus Design and Outside Plant" Division at SIP headquarters in Rome. Feliciano Esposto is co-author of many papers and lectures at Superior School "Guglielmo Reiss Romoli". (At present time, a photo of Mr. Esposto is not available)

Fabrizio Nanni
SIP D.G. R/IT-CM
Via di Val Cannuta, 250
00166 Roma - Italy

Mr. Nanni was born at Roma, Italy, in 1960. He received the title of doctor in Physiscs from the University of Rome La Sapienza.From 1986 he has collaborated with the laboratory of research on optical communications: Fondazione "U. Bordoni" in Rome working on Photoconductivity Ultrafast Phenomena, Semiconductor Lasers and Ultrafast Photodiodes characterization. In 1988 he joined SIP, the Italian Telecommunication Operating Company, where he has been engaged in the study and development of optical fibres, copper cables as well as optical cables specification and characterization both in laboratory and in field. Moreover his present responsibilities include CCITT Comm. XV, IEC 86A, ETSI-TMI and COST 218 activities. (At present time, a photo of Mr. Nanni is not available)

ELABORATION OF THE DATA OBTAINED FROM ELECTRICAL MEASUREMENTS CARRIED OUT ON DISTRIBUTION CABLES WITH POLYETHYLENE INSULATED PAIRS

G. BUGA (*), A. CHECCHIA (*), N. SCAFURO (*), G. CLERICO (*), F. MONTALTI (**), S. GAY (**)

(*) SOCIETA' CAVI PIRELLI, MILANO (ITALY) - (**) SIP D.G., ROMA ('ALY)

ABSTRACT

We have implemented an information system, running on a personal computer, that is capable of processing the data obtained from electrical measurements carried out on copper pair telecommunication cables and of producing a complete statistical evaluation of the production. The statistical coefficients obtained not only serve as quality indicators to the customer in accepting product checked on a sampling basis, but are also useful, within the factory, for assessing the best course of action to take either to correct the production process or to improve product quality.

We believe that this is an important step in the achievement of a factory working to a Total Quality Assurance standard.

INTRODUCTION

In a Quality Assurance system the management of data in an appropriate information system is of particular relevance.
The data itself may derive from various sectors of the company and may provide information regarding raw materials, production processes or finished products.
Within the company, the analysis of these data has implications not only for the production activity but also for other functions aimed at preventing problems, such as design and material procurement.
Data analysis is also important to the customer, who wants to be provided with adequate information regarding the quality of the supplied product.
The present paper describes a system which elaborates the data obtained from measurements carried out on copper pair telecommunications cables which have polyethylene insulation, with polyethylene/aluminium moisture barrier sheath, and may be filled or unfilled, and armoured or unarmoured, depending on requirements.

These cables form the most important part of the urban distribution network of SIP (*) together with optical cables which are more widely used in the urban junction network and the medium and long distance trunk network.
Among the many measurements (dimensional, mechanical, physical, electrical and transmissive) performed on the copper pair cables during the production process, those regarding the electrical and transmissive properties of the finished cable are particularly important [1].
This is because, only at the finished cable stage, it is possible to know the definitive value of many of the characteristics and thereby confirm the correctness of actions taken earlier in the production process.
This paper describes in detail the system, called ARGO, which has been developed for this purpose.

OBJECTIVES

To obtain:
1) Operational information for each cable length and for each production lot.
The former enables identification of non-conforming or otherwise unsatisfactory cable lengths and permits decision on immediate action.
The 'atter, generally on a weekly basis, allows the application of statistical criteria for each characteristic to decide the acceptance or rejection of each lot.
2) Monthly quality information that permits decisions on eventual remedial action or on product improvement.

DESCRIPTION OF THE ARGO SYSTEM

The system elaborates all the data obtained from the automatic measurement apparatus.
These include the basic electrical characteristics of the cables, both at low frequency (d.c. and voice frequency) and at high frequency, and comprise:

Ohmic resistance	d.c.
Capacitance	1000 Hz
Capacitance unbalance (pair to pair)	1000 Hz
Capacitance unbalance (pair to earth)	1000 Hz
Impedance	1 MHz
Attenuation	1 MHz

(*) principal Italian Telecommunication Operating Company

Far end crosstalk (ELFEXT) and near end crosstalk (NEXT) measured at 1 MHz according to the following combinations:

- Type A ELFEXT within each subunit
- Type B ELFEXT between adjacent subunits
- Type C NEXT within each subunit
- Type D NEXT between adjacent subunits
- Type E NEXT between non-adiacent subunits

All of the above characteristics are measured within unit (100 pairs) on large cables or on the entire cable when there are less than 100 pairs in the cable.
The measurements are carried out according to a statistical sampling plan based on a given percentage of lengths and units (1).
To ensure that meaningful information is obtained from the statistical elaboration, the cables are grouped together according to type of construction (i.e. filled or unfilled), conductor diameter (0.4 - 0.6 mm) and number of pairs.

Table 1. Example of grouping codes for cables with 0.4 mm conductors:

No.of pairs	2400 1600	1200 800	400 100	200 50 30	10
No.of unit layers	3	2	1	1	1
0.4 mm unfilled	G4S1	G4S2	G4S3	G4S4	G4S0
0.4 mm filled		G4T2	G4T3	G4T4	G4T0

The statistical analysis makes use of the method of variables [2] [3], both as a basis for product acceptance and for the periodic quality information.
For each of the above groupings, the typical population element is the individual pair and it is therefore possible to ensure that sample of sufficient size for statistical analysis is achievable with currently available automatic test equipment.
In practice, these equipments allow the complete examination, both at voice frequency (1000 Hz) and high frequency (1 MHz), of 100 pairs (10x10 pairs) in a relatively short time.
According to the sampling criteria employed it is therefore possible to generate a considerable amount of data obtained from measurements on the pairs of the various cable lengths.
By collecting together these data on the basis of cable grouping, a statistically large population is achieved and sampling uncertainties are thus minimised.
If production is well managed with regard to the QA plan then the target of achieving a product which conforms with the design and specifications is attained by a reasonably stable process, either from a knowledge of the process capability and therefore automatically controlled, or from planned measurements checks in each stage of the process (i.e. using control charts).
It is of course implicit that such techniques do not limit improvement of the product.
The analysis of the measurements carried out on the finished cables therefore indicates the level of conformity and the stability of the production process.
To achieve this goal it is sufficient that the analysis is carried out on relatively short production periods (i.e. weekly).
Furthermore, it is possible to judge the statistical conformity of each characteristic, by means of appropriate coefficients relating to the estimated out of limit percentages, to compare with the present Acceptable Quality Levels (AQL).

(1) It is not in fact possible to refer to the actual size of an inspection lot in continuous production. Sampling is also based on an appropriate choice of the units in the cable, the minimum criterion being at least one unit from each layer.

ORGANIZATION OF THE DATA ELABORATION

Elaboration occurs in correspondance with two important phases of the production; these are:
- Inspection of the delivery lots (e.g. weekly)
- Qualitative information (e.g. monthly) prepared by elaboration of all the data obtained from the weekly inspections.

Flow chart for date elaboration:

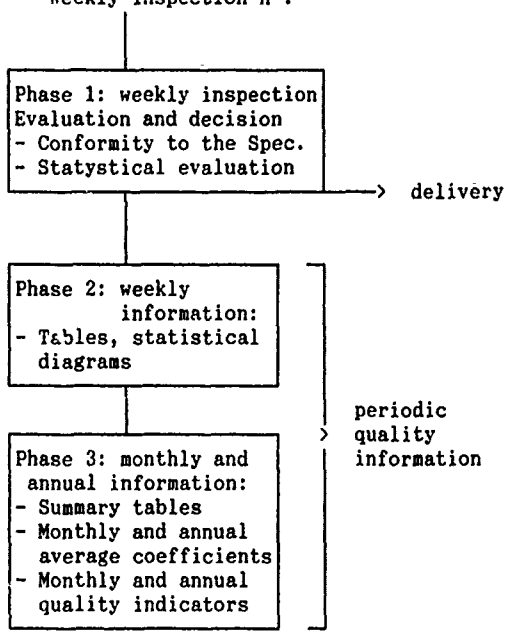

ELABORATION OF DATA FROM WEEKLY INSPECTION

Having grouped the cables according to the criteria of Table 1, each length measured by the automatic apparatus is checked for conformity to the specifications.

Data elaboration then proceeds as follows:
Electrical characteristics (other than crosstalk)
. Ohmic resistance (d.c.)
. Mutual capacitance (1000 Hz)
. Capacitance unbalance (1000 Hz)
. Attenuation (1 MHz)
. Impedance (1 MHz)
From the data collected for each cable length the distribution parameters minimum, maximum, mean and sample standard deviation are calculated.
Then, using all the accumulated data for all cable lengths of the same grouping, which have been measured during the week, the following parameters are obtained: minimum, maximum, 95th percentile, median, mean, standard deviation, sample size, number of data out of specification and their values, and the standardised variate Z as an evaluation of quality.
In the case of capacity unbalances, the above parameters for each length and for the week are calculated from the absolute values of the data,then, using the same data with correct sign, the parameters of mean, standard deviation and stardardised variate Z are also obtained.
Additionally for capacitance unbalances based on the absolute values of the data accumulated during the week, the qualitative coefficient Cpk is calculated [4]. This coefficient, which is defined in Appendix 1, evaluates the ability of a process to satisfy requirements and with what margin of safety, especially in the case of particularly numerous distributions.
The coefficient Cpk is calculated with reference to the specified limits for 95% of the values.
There is also the possibility to request statistical diagrams of the accumulated data: histograms, cumulative frequency and NPG. (1)
The standardised variate Z is calculated from the formula given in Appendix 1 and is compared to the corresponding acceptance value K which is determined from the specified AQL.
Typical values of K for various values of AQL are given in Appendix 1.
Note that the number of accumulated data for each characteric, measured on many lengths of the same lot, can easily reach many hundreds and often several thousands (see Appendix 2).
This means that the uncertainly in the calculation of Z and Cpk is reduced to the minimum and therefore the statistical evaluation is practically certain, both from the point of view of the producer (risk of rejecting a compliant lot) and of the customer (risk of accepting a non-compliant lot).

CROSSTALK CHARACTERISTICS: ELFEXT AND NEXT AT 1 MHz.

In this case the specified requirements for the five combinations are given for each measured group.

(1) NPG = Normal Probability Graph

The data are therefore examined group by group for conformity to the specifications and, for statistical characterisation, they are accumulated for each cable length when more units are measured (eg. 3 units for 2400 pair cable = 24x100 pairs).
Referring to one single cable length, in fig. 1 is reported the histogram of C NEXT, while in fig. 2 is plotted the NPG graph relative to the previous histogram.
Based on past experience, the size of the distributions obtained is sufficient for analysis.
The weekly inspection therefore reports two sets of statistical parameters; the first based on the data for each unit, and the second based on the accumulated data for all the cable length of the same grouping.
The reported parameters are: mean, minimum, maximum, 98th (or 99th) percentile, median, standard deviation, number of combinations measured, and number of measurements out of specification with details of their values.
To evaluate the production process it is necessary to examine distribution which are typically non-normal.
This involves calculation of the process coefficients Cpk (see Appendix 1) for each unit, for each cable length, and then for all the accumulated data from all the cable lengths measures.
By examining the coefficient Cpk from all the data it is possible to evaluate the stability and alignment of the process and its margin of safety with respect to the specified limits.

MONTHLY AND ANNUAL INFORMATION

From the data obtained from the weekly inspections during one month it is possible to prepare, for each cable grouping (see table 1), a monthly summary of the parameters which characterise the weekly distributions. Additionally, for each measured characteristic and distribution parameter, monthly values for process mean, process standard deviation and average statistical evaluation coefficients (see Appendix 1 for formulae) are given together with their ranges.

	Weekly	Monthly
Max and min values	x	x
95th percentiles (2)	x	x
98th percentiles (3)	x	x
Mean values (4)	x	x
Median values	x	x
Standard deviation (4)	x	x
Coefficients Z and Cpk (4)	x	x

2) Electrical characteristics other than crosstalk
3) Crosstalk characteristics
4) With calculation of the process average

A similar arrangement is used for the annual summary.
Customers that regularly receive the monthly information therefore have a complete knowledge of the quality achieved by the manufacturer, based on all the measured data.

Appendix 2 gives examples of the elaboration for various typical parameters of a cable grouping.

METHOD OF DATA ELABORATION

The results of all the electrical measurements performed by the automatic apparatus for each unit are stored in files.
These are then transfered, by means of high density 5'14" floppy disks, to the hard disk (capacity > 30 MB) of commercially available personal computer with a maths co-processor; from whence data elaboration is carried out automatically.
By means of a menu driven program, the operator has only to enter identification data for the units measured during the week and cross references lot number, works code, period, etc.
All the work of elaboration and presentation of the data in graphical form is carried out automatically without the presence of the operator.

STATISTICAL EVALUATION CRITERIA
Weekly inspection

For each characteristics, including capacitance unbalance with correct sign, the coefficient Z is calculated according to the formula given in Appendix 1 and is then compared with the acceptance value K, which has been calculated for the chosen AQL for the size of sample available.
If $Z \geq K$ then the lot is acceptable.
In some cases the calculation of Z is not reliable and it is necessary to resort to the coefficient Cpk, as defined in Appendix 1.

PERIODIC QUALITY INFORMATION

For each characteristic the condition for conformity to the specification is $Cpk \geq 1$ (where Cpk is calculated with the formula in Appendix 1). However, much company effort is expended on improvement and so many Cpk values are notably greater than 1.
In some cases the alternative criterion of Z greater than K, as above, is used.

CONCLUSIONS

The ARGO system has shown itself to be an important tool for data management not only for external use, where it provides complete quality information based on all performed measurements, but above all for internal use as an element of quality management and in supporting product improvement and corrective action when necessary.

The system has been in service for about one year and will gradually be improved in the light of experience, adding subsidiary service programs if necessary.

ACKNOWLEDGEMENTS

The authors wish to thank the Management of Società Cavi Pirelli and SIP for the permission to publish this paper.

BIBLIOGRAPHY

[1] Specification SIP CT 1240 - 1990
[2] A. Bowker, H.P. Goode - "Sampling Inspection by Variables" Mc.Graw-Hill New York
[3] ISO 3951 Sampling procedures and charts for inspection by variables for percent defective
[4] J. A. Clements - "Process Capability Calculations for Non-Normal Distributions" Quality Progress Sept. 89

Appendix 1

FORMULAS

standardized variate:

$$Z = \left| \frac{L_{MAX} - |\bar{x}_s|}{S_s} \right|$$

process capability:

for Cap. Unbalance:

$$C_{pk} = \frac{L_{95\%} - x_{50\%}}{x_{95\%} - x_{50\%}}$$

for Cross-Talk:

$$C_{pk} = \frac{\bar{x} - L_{98\%}}{\bar{x} - x_{98\%}}$$

process average value

$$\bar{\bar{x}} = \frac{\sum_{i=1}^{n} n_i \cdot \bar{x}_i}{N}$$

process standardized variate

$$Z_{proc} = \left| \frac{L_{MAX} - |\bar{\bar{x}}_s|}{S_{p_s}} \right|$$

process standard deviation

$$S_p = \sqrt{\frac{\sum_{i=1}^{n} (n_i - 1) \cdot S_i^2 + \sum_{i=1}^{n} n_i \cdot \bar{x}_i^2 - \frac{\left[\sum_{i=1}^{n} n_i \cdot \bar{x}_i\right]^2}{N}}{N - 1}}$$

L_{MAX}= spec. limit on max $L_{95\%}$= sp.l. on 95% $L_{98\%}$= sp.l. on 98%

$x_{50\%}$ = median value $x_{95\%}$ = value at 95% $x_{98\%}$ = value at 98%

$\bar{x}_s$ = average of values with sign ($\bar{x} = \bar{x}_s$ if values are all positive)

S_s = stand. dev. of values with sign ($S = S_s$ if values are all positive)

$\bar{\bar{x}}$ = process average value S_p = process stand. deviation

n = n° of samples N = total data n° n_i = data n° of i^{th} sample

$\bar{x}_i$ = average value of i^{th} sample S_i = stand.dev. of i^{th} sample

Acceptance coefficient K

for 1000 data:

AQL = 0.15 %	K = 2.9
AQL = 0.25 %	K = 2.75
AQL = 0.5 %	K = 2.5
AQL = 1 %	K = 2.27

Appendix 2

SOCIETA' CAVI PIRELLI S.p.A.

TEST DEPT. - LIVORNO FERRARIS DATE: 06/01/1990

OPERATOR: TEST DEPT. MANAGER:

MONTHLY SUMMARY OF ELECTRICAL MEASUREMENTS NORM. AT 20°C

CARRIED OUT BY DCM DEVICE MONTH OF MAY

CUSTOMER: SIP WEEKLY INSPECTION: TE90/14,TE90/15,TE90/17

SPECIFIC.:SIP 1240 DELIVERY N°:3 CABLE FAMILY: G4S1 WEEK N°:3

CABLE SIZES: n° 13 TE2400X2X0.4G/H5E

WEEKLY FILES: G4S1.4,G4S1.8,G4S1.10 FILE NUMBER: MAGG4S1.4

PAIR-PAIR CAP. UNBAL. (pF/500m) L95%=100pF/500m LMAX=150pF/500m

	1° week	2° week	3° week	month	
minimum	0.00	0.00	0.00	min	0.00
				max	0.00
average	8.05	7.76	7.94	min	7.76
				max	8.05
median	5.07	4.40	5.01		
95% value	28.21	26.91	27.95	min	26.91
				max	28.21
maximum	84.94	64.09	60.05	min	60.05
				max	84.94
CPK	4.10	4.25	4.14	min	4.10
				max	4.25
average (-)	1.04	0.54	0.56	min	0.54
				ave*	0.78
				max	1.04
S (-)	12.53	12.38	12.38	min	12.38
				ave*	12.45
				max	12.53
Z (-)	11.89	12.07	12.07	min	11.89
				ave*	11.98
				max	12.07
data N°	8100	5400	4050	17550	
data out of spec. N°	0	0	0	0	
% data out of spec.	0.00 %	0.00 %	0.00 %	0.00 %	

*:monthly process average value (-):referred to values with sign

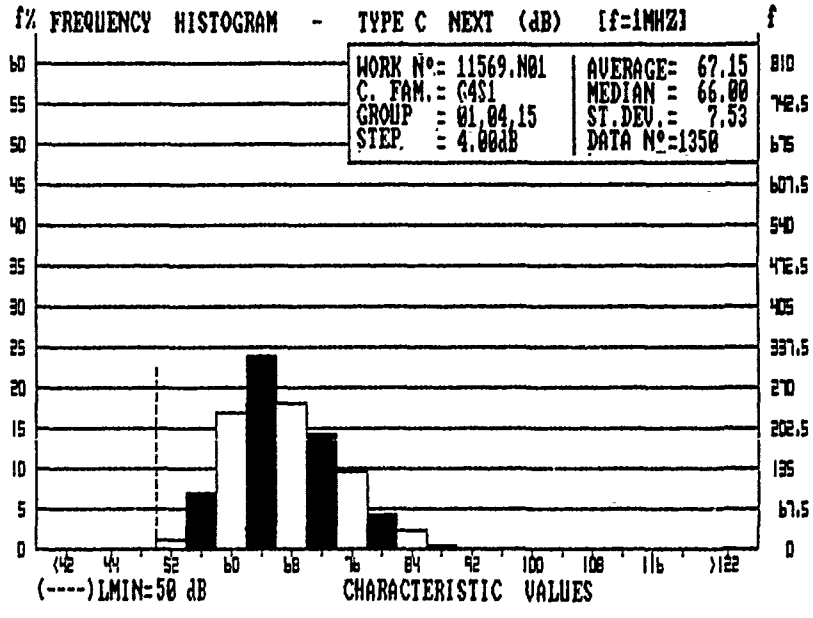

Fig. 1

C NEXT histogram
for one cable length
Size TE2400x2x0.4G/H5ENE

MONTHLY SUMMARY OF ELECTRICAL MEASUREMENTS NORM. AT 20°C
CARRIED OUT BY DCM DEVICE

MONTH OF MAY

CUSTOMER: SIP WEEKLY INSPECTION: TE90/14,TE90/15,TE90/17
SPECIFIC.:SIP 1240 DELIVERY N°:3 CABLE FAMILY: G4S1 WEEK N°:3
CABLE SIZES: n° 13 TE2400X2X0.4G/H5E
WEEKLY FILES: G4S1.4,G4S1.8,G4S1.10 FILE NUMBER: MAGG4S1.4

NEXT - CROSS-TALK COMB. C (dB/Km) LMIN=50dB/Km LMAX=63dB/Km

		1° week	2° week	3° week	month	range
minimum	min	48.0	48.5	46.7	46.7	4.6
	max	50.5	51.3	50.1	51.3	
98% value	min	51.6	51.3	52.1	51.3	3.0
	max	54.3	53.5	53.7	54.3	
average	min	64.3	64.2	64.0	64.0	2.2
	ave*				65.0	
	max	65.7	66.3	65.3	66.3	
maximum	min	86.5	89.6	86.4	86.4	37.3
	max	96.9	123.7	103.8	123.7	
CPK	min	1.12	1.10	1.17	1.10	0.29
	ave*				1.16	
	max	1.39	1.33	1.33	1.39	
S	min	6.73	6.72	6.59	6.59	1.31
	ave*				7.32	
	max	7.84	7.90	7.80	7.90	
unit N°		18	12	9	39	
cable length N°		6	4	3	13	
data N°		8100	5400	4050	17550	
d. out of spec. N°		16	13	10	39	
% d. out of spec.		0.20 %	0.24 %	0.25 %	0.22 %	

* : monthly process average value

MONTHLY SUMMARY OF ELECTRICAL MEASUREMENTS NORM. AT 20°C
CARRIED OUT BY DCM DEVICE

MONTH OF MAY

CUSTOMER: SIP WEEKLY INSPECTION: TE90/14,TE90/15,TE90/17
SPECIFIC.:SIP 1240 DELIVERY N°:3 CABLE FAMILY: G4S1 WEEK N°:3
CABLE SIZES: n° 13 TE2400X2X0.4G/H5E
WEEKLY FILES: G4S1.4,G4S1.8,G4S1.10 FILE NUMBER: MAGG4S1.4

MONTHLY SUMMARY OF NON-CROSS-TALK PARAMETERS

LA: aver.lim LMAX: upper lim of spec. L95%: lim. on 95%		RESIST. (Ω/Km) LA=144 LMAX=150	MUT.CAP (nF/Km) LA=50 LMAX=55	PG C.UNB. (pF/500m) L95%=700 LMAX=1200	PP C.UNB. (pF/500m) L95%=100 LMAX=150	IMPEDAN. (f=1MHz) (Ω) LMAX=140	ATTEN. (f=1MHz (dB/Km) LMAX=27
minimum	min	132.54	40.58	0.00	0.00	111.80	19.77
	max	134.82	41.06	0.00	0.00	118.00	20.71
average	min	136.58	42.41	105.15	7.76	119.78	20.76
	ave*	138.06	42.88			120.45	21.15
	max	138.62	43.23	161.46	8.05	122.06	21.51
95% value	min	139.93	43.53	289.06	26.91	124.40	21.26
	max	141.72	44.60	390.47	28.21	125.10	22.28
maximum	min	149.59	44.05	445.97	60.05	127.00	21.95
	max	149.88	45.50	697.46	84.94	130.20	23.12
CPK	min			2.24	4.10		
	max			2.98	4.25		
ave.(-)	min			-139.01	0.54		
	ave*			-64.81	0.78		
	max			-39.64	1.04		
S (-)	min	1.81	0.58	129.01	12.38	1.73	0.33
	ave*	2.12	0.79	169.49	12.45	2.70	0.47
	max	2.15	0.82	196.63	12.53	2.91	0.41
Z (-)	min	5.84	14.43	5.90	11.89	6.94	13.39
	ave*	5.63	15.28	7.46	11.98	7.24	12.38
	max	6.44	21.36	8.94	12.07	10.38	19.00
data N°		7800	3900	3900	17550	3900	3900
d.o. spec.N°		0	0	0	0	0	0
%d.out spec.		0.00 %	0.00 %	0.00 %	0.00%	0.00 %	0.00 %

*:monthly process average value (-):referred to values with sign

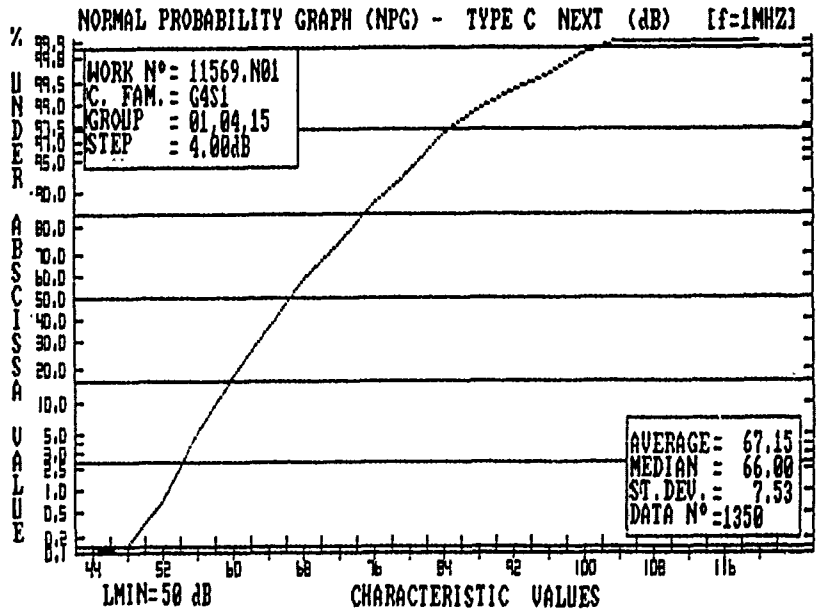

Fig. 2

C NEXT Normal Probability Graph for one cable length Size TE2400x2xO.4G/H5ENE

Giancarlo Buga
Società Cavi Pirelli
Stab. di Livorno Ferraris
Via Goretta
13046 Livorno Ferraris
(Vercelli) - Italy

Mr. Buga was born at Rho (Milano), Italy in 1957 and received his doctorate in electronic engineering from the Polytechnic of Milan. During the doctorate he developed studies about coherent optical transmission at CSELT (Turin). He joined Società Cavi Pirelli where he has been engaged in optical cable design and development Dept. Now he is the Manager of the Testing and Quality Dept. of Livorno Ferraris Factory. He takes part in the work of international and national standardization bodies, such as CCITT, IEC, CEI, dealing with optical fibre cables and systems.

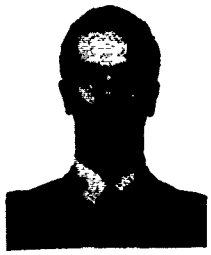

Andrea Checchia
Società Cavi Pirelli
GT/I-Q C. 2411
Viale Sarca, 202
20126 Milano - Italy

Mr. Checchia was born at Ancona, Italy in 1960. He received his electronic engineering degree from the University of Ancona in 1987. He was the holder of a scholarship, awarded by Fondazione G. Marconi of Pontecchio (Bologna, Italy), for studying optical fibre profile synthesis. He joined the Telecommunication Group of Società Cavi Pirelli S.p.A. in 1989 where, in the Quality Department, he has been involved in the development of software for quality control of conventional and optical fibre cables.

Nicola Scafuro
Società Cavi Pirelli
Stabilimento Alfacavi
S. P. 135 - Km. 4.500
84091 Battipaglia
(Salerno) - Italy

Mr. Scafuro was born in 1955 and received his M.S. in electronic engineering degree from University of Naples in 1980 He was involved in the research and development of phased array antennas up to 1985 and afterwards in the production and testing of optical fiber cables. He joined Società Cavi Pirelli in 1988 and he is currently the Quality Assurance Manager of Azienda Alfacavi TLC of the Pirelli Group.

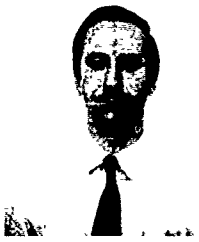

Giorgio Clerico
Società Cavi Pirelli
GT/I-P C. 2412
Viale Sarca, 202
20126 Milano - Italy

Mr. Clerico was born at Vische (Torino), Italy in 1949. He received his electrotecnic engineering degree from Polytecnic of Turin in 1973. He joined Società Cavi Pirelli in 1978 where was involved in Quality Control of Telecommunication cables; at present he is engaged in cable design Dept. and also takes part in the work of international and national standardization bodies, such as CCITT, CECC, IEC, dealing with optical fibre cables.

Francesco Montalti
SIP D.G. R/IT-CM
Via di Val Cannuta, 250
00166 Roma - Italy

Mr. Montalti was born at Firenze, Italy in 1953. He received the doctorate in Physics from the University of Rome in 1976. In 1979 he joined the Research Centre of Industrie Face Standard where he was engaged in research about optical fibres, integrated optics and optical transmission systems. In 1985 he joined SIP, the Italian Telecommunication Operating Company where he is currently responsible of the development of cable and apparatus for Telecommunication plants. He is involved in the activities of International Standardization Entities namely CCITT and IEC.

Stefano Gay
SIP D.G. R/IT-CQ
Via di Val Cannuta, 182
00166 Roma - Italy

Mr. Gay was born in Roma in 1949. He received his electronic engineering degree from the University of Roma in 1975. He specialized in telecommunications at Istituto Superiore PT in Roma and in quality and reliability engineering in Birmingham UK. His professional activities before joining SIP include: TELECOMMIT-Transmission apparatus sector; FATME (Ericsson Group) - Switching systems sector; PAGE EUROPE (Contel Group)-Product management in radio transmission equipment. Since joining the Transmission Network Engineering Division of SIP two years ago, he has been in charge of the Control and Technical Qualification of Manufacturers Service in the Quality Control Sector.

EVALUATION OF FUNGAL AND BACTERIAL GROWTH IN SIMULATED FIBER OPTIC CABLES CONTAINING WATERBLOCKING TAPES.

D.A. Ross McQueen and Lynne E. Windsor

KT Industries Ltd.
Winnipeg, Manitoba, Canada

ABSTRACT

Waterblocking tapes used in telecommunication cables usually consist of a pair of permeable substrates laminated together enclosing a superabsorbent polymer in powder form. The substrates may be constructed from paper or from man-made fibers. In most cases the tape is wrapped around the cable core beneath the jacket or shield. If water enters the cable the tape swells and blocks the movement of water along the cable. If bacteria or fungi multiply in the wetted waterblocking tape, elements or compounds detrimental to the cable may be produced. Using a device that simulates the interior of a telecommunication cable, measurements of the bacterial and fungal populations of waterblocking tapes were conducted. Different permeable substrates were tested as were several antimicrobial compounds.

INTRODUCTION

Exposure to hydrogen can cause a reduction in the transmission qualities of fiber optic cables (1). Microbial production of hydrogen is one source of this gas. The growth of both fungi and bacteria is of importance when considering the microbial production of hydrogen inside a cable. Many bacteria are synthesizers of hydrogen (5); and fungi are primary biodegraders that will provide a nutrient source for the hydrogen producing bacteria. Bacterial and fungal growth may occur when the interior of the cable is wetted following a cable break. The amount of growth inside the cable will depend on the nutrients inherently present in the cable components and also on the amount of nutrients in the water that has entered the cable.

In this paper a method is described that simulates conditions in the interior of a cable and allows an estimate of the amount of microbial growth that would occur if the cable shielding is disrupted and water is allowed to enter. Paper and spun bonded polyester (SBP) were compared for their ability to support bacterial and fungal growth. In addition, several antimicrobials were screened for their effectiveness in preventing fungal and bacterial growth.

MATERIALS AND METHODS

Construction of Simulated Cable

Figure 1 shows three sections of simulated cable. It was constructed of two main components: a piece of acetal rod (10 mm x 113 mm) and a piece of polycarbonate tubing (12 mm ID x 75 mm). The acetal rod simulated the core of the cable and the tubing simulated the jacket. A 57 mm x 70 mm piece of waterblocking tape was wrapped around the acetal rod which was then inserted into the polycarbonate tubing.

Source of Fungi

Cultures of Aspergillus niger, Aspergillus flavus and Penicillium funiculosum were kindly provided by Dr. S. W. Peterson of the USDA Northern Regional Research Centre.

Source of Bacteria

Citrobacter freundii was obtained from the American Type Culture Collection.

Media Preparation

Fungal cultures were propagated on Special Methods Agar which consists of 5.0 grams of pancreatic digest of casein, 2.5 grams of yeast extract, 1.0 gram of dextrose and 15 grams of agar per liter. The mineral salts media used to prepare fungal inoculum contained 40 mM ammonium nitrate, 8 mM monobasic potassium phosphate, 3 mM potassium chloride, and 1 mM magnesium sulfate (10). The mineral salts media used to prepare bacterial inoculum contained 12.4 mM ammonium nitrate, 5.1 mM potassium phosphate (monobasic), 4 mM potassium phosphate (dibasic), 2.8 mM magnesium sulphate, .08 mM sodium chloride, .007 mM iron sulfate, .007 mM zinc sulphate and .006 mM manganese sulphate (2). Nutrient agar was prepared by adding agar to a concentration of 1.5% to nutrient broth which consists of 3 grams of beef extract and 5 grams of peptone per liter.

Cultivation of Fungi

The fungi were grown on special methods agar at 28°C. After 5 to 6 days growth, 20 mls were taken from a 100 ml aliquot of sterile mineral

salts media and poured onto the plate to be harvested. The surface of the plate was then scraped with a sterile loop, and the resulting spore suspension was poured back into the flask containing the 100 mls of mineral salts media.

Cultivation of Bacteria

C. freundii was grown on nutrient agar at 34°C. After 1 to 2 days growth, 20 mls were taken from a 100 ml aliquot of sterile mineral salts media and poured onto the plate to be harvested. The surface of the plate was then scraped with a sterile loop, and the resulting suspension was poured back into the flask containing the 100 mls of mineral salts media.

Inoculation of the Simulated Cable

Inoculum was drawn up between the rod and tubing into the waterblocking tape to a distance approximately one-half way up the tube leaving an interface between the wet area and the dry area. The simulated cable was weighed before and after inoculation so that the amount of inoculum could be calculated. One gram of increased weight was assumed to be one milliliter of inoculum.

Evaporation from the top was prevented by wrapping adhesive tape around the junction of the rod and tube. Evaporation from the bottom was prevented by either incubating the tube with its bottom in mineral salts media or by wrapping the bottom with aluminum foil and masking tape. This created a situation similar to that which occurs when the jacket of a cable is disrupted; the waterblocking tape becomes saturated with water and there is a limited evaporation surface from which the water can escape.

Determination of Fungal Growth

The presence or absence of fungal growth in the simulated cable was determined microscopically using a dissecting microscope after 7 days incubation. The presence of reproductive structures characteristic of the inoculated fungus were used as an indication that fungal growth had taken place.

Measuring Bacterial Presence

The dilution plate technique relied on consecutive dilutions to separate the bacteria to such a degree that when cultured on the appropriate media each bacterium produced a single colony that was readily observable (4).

Following 6 to 10 days of incubation 34°C the simulated cable to be analyzed was disassembled and the waterblocking tape was immersed in 100 mls of sterile distilled water (SDW). 1 ml of this dispersion was removed and placed into another 100 mls of SDW and mixed well. This step was repeated until a 1 ml sample contained a countable number of bacteria. The final step was to take 1 ml of the final dilution and disperse it into 25 mls of nutrient agar kept at 45°C. This was then poured into a sterile petri plate and allowed to solidify. After 24 hours incubation at 34°C a dissecting microscope was used to determine the number of colonies on the plate. The number of bacteria in the section of simulated cable was then determined by multiplying back through the dilution series.

RESULTS AND DISCUSSION

With reference to the Military Specification 810D (7), ASTM Specification G22 (2), and TAPPI Specification T487 pm-79 (10) a method was developed that allows the observation and quantification of microorganisms growing in an environment that closely approximates the interior of an actual cable. The device that allows this simulation is constructed of simple materials and is referred to as simulated cable. Using simulated cable, paper based and SBP based waterblocking tapes were compared for their ability to support fungal and bacterial growth under conditions that approximate those found inside an actual cable after water entry. Simulated cable was also used to screen several antimicrobials for their ability to control fungal and bacterial growth.

Fungal Growth

Simulated cable was inoculated with three diferent species of fungi. Aspergiller niger, Aspergillus flavus and Penicillium funiculosum are known for their ability to use cellulose as a carbon source (8,9,11). They were inoculated into simulated cable made with paper based or SBP based waterblocking tape. Observations were made after one week of incubation at 28°C.

Fungi that are provided with a suitable substrate will grow and form reproductive structures. These structures on the fungi used are colored and were easily detected through the outer transparent tube of the simulated cable. Growth by each of the fungal species was evident when paper was used. Figure 1(b) shows the typical appearance of fungal growth inside simulated cable made with paper based water blocking tape and inoculated with A. niger. Under low magnification the dark ring of growth was seen to be composed of mycelia and reproductive structures characteristic of this fungus. The same results were also seen with A. flavus and P. funiculosum with the dark band consisting of mycelia and reproductive structures characteristic of the inoculated fungus. Figure 1(a) was inoculated with sterile minimal salts media and acted as a negative control. No growth could be observed on the negative control macroscopically or with a dissecting microscope. Figure 1(c) had the anti-fungal agent 2-(4-thiazolyl)-benzimidazole incorporated into the superabsorbent powder and no growth was observed.

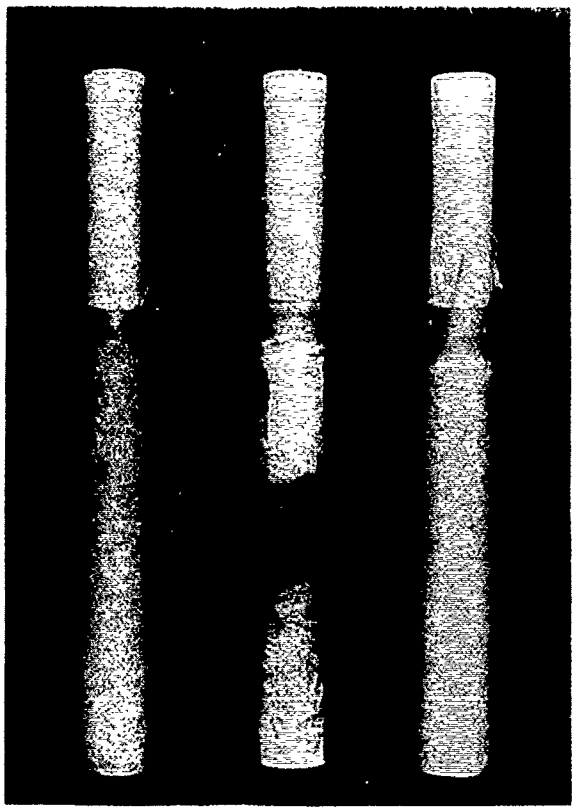

(a) (b) (c)

Figure 1

As expected growth was observed only on the moist side of the wet-dry interface. Fungi require moisture so growth would not occur in the non-wetted area. The limited growth on the wet side is probably related to the need of the fungus for air. For the fungus to survive in the top part of the wetted area there must be a supply of air pockets providing oxygen to the fungus. As the distance from the wet-dry interface increases fungal growth is restricted because there is less evaporation and thus fewer air pockets.

On SBP there was no evidence of growth by P. funiculosum or by A. flavus. Darkening of the SBP was observed in the simulated cable inoculated with A. niger. Figure 2(a) is a section of simulated cable constructed with SBP based waterblocking tape inoculated with sterile mineral salts media. Figure 2(b) is of a similar construction, but was inoculated with a spore suspension of A. niger. Although the faint color of the growth suggests that the degree of fungal growth was greatly reduced, the area of darkening reached the bottom of the tube suggesting that there were adequate air pockets extending from the wet-dry interface down to the bottom of the tube. The presence of air pockets down the length of the tube is best explained by the limited wicking ability of SBP.

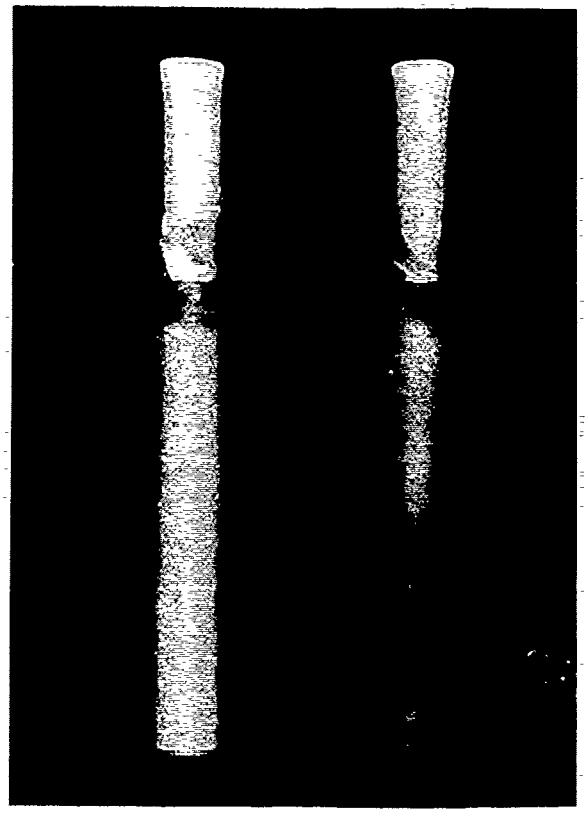

(a) (b)

Figure 2

Bacterial Growth

Because hydrogen is a by-product of bacterial metabolism and because bacterial metabolism is related to their growth rate, the numbers of bacteria present in the simulated cable can be used as an indicator of the potential for hydrogen production.

To compare the abilities of paper and SBP based waterblocking tapes to support bacterial growth, inoculum from two different sources were used. Simulated cable containing waterblocking tapes made with either paper or SBP were inoculated with C. freundii which is known for its ability to produce hydrogen (5) or with samples of ground water. The ground water contained a variety of unidentified bacterial species and thus provided an inoculum that would be closer to the bacterial population to which an actual cable would be exposed.

Bacterial presence was measured using the

dilution plate technique, which is commonly used in soil science to measure the bacterial populations in soil samples (4).

When the appropriate dilution of suspensions made from substrates incubated inside simulated cable was plated out, lens shaped bacterial colonies developed within 24 hours (Figure 3). The number of colonies on the plate was determined under low magnification. The number of bacteria in the section of simulated cable was then determined by multiplying back through the dilution series.

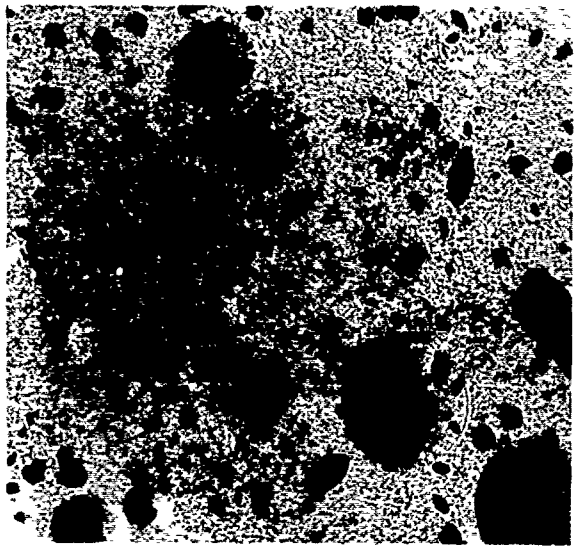

Figure 3 (x5)

This exercise was conducted twice for each inoculum type and in all cases the numbers of bacteria found in simulated cable containing paper based waterblocking tape and in simulated cable containing SBP waterblocking tapes were found to be similar (Table 1)

	PAPER	SBP
CITROBACTER		
1st Replication	2.44×10^8	4.17×10^8
2nd Replication	8.20×10^7	5.8×10^7
GROUND WATER		
1st Replication	3.2×10^7	7.1×10^7
2nd Replication	5.9×10^7	4.2×10^7

Table 1

The significance of the differences between the treatments should be considered with an understanding of bacterial population dynamics in mind. Bacterial populations double at regular intervals. They reproduce by the fission of the individual into two equal parts, and on average they double at the same rate. If the numbers in a population growing under stable conditions are monitored over time, there will be a set period over which they will double. A population of Escherichia coli (a common human colon bacteria), for example, will double every 20 minutes when growing under ideal conditions. Had there been significant differences between the environments in the simulated cable made with the two different substrates then a difference of several doublings would have been expected over the 6 to 10 days that the tubes were incubated.

Larger numbers of bacteria were expected in the simulated cable containing paper. Cellulose is usually considered a biologically utilizable substrate while SBP is not. The almost equal numbers of bacteria growing on both substrates suggests that paper is as inert as polyester under the conditions found within the simulated cable. The reason for this apparent contradiction can be found in the biology of cellulose degradation.

Cellulose is a polymer of glucose. The bonds joining the glucose monomers are extremely durable making the cellulose resistant to biological breakdown. All biological degradation of cellulose occurs through the activities of the enzyme cellulase. Only specialized forms of bacteria and fungi are capable of synthesizing this enzyme. For there to be significant growth of non-cellulase producing bacteria on a cellulose based substrate they must live in concert with an organism that produces cellulase. Long term experiments may demonstrate that the number of bacteria growing in simulated cable containing paper based waterblocking tapes may increase over time as populations of cellulytic microorganisms increase. The process of cellulose decomposition, however, is likely to be very slow because of conditions that occur in the interior of the simulated cable if it remains saturated.

The environmental factors that have the greatest effect on the rate of cellulose decomposition are moisture levels and oxygen availability (3). Observations of fungi growing inside simulated cable suggest that there is only a limited area on the wet side of the wet dry interface where there is enough oxygen to support aerobic growth. If there are similar conditions inside an actual cable, then most of the wetted area will be anaerobic. Anaerobic decomposition of cellulose is inefficient and under these conditions a lengthy period of time would likely be required before sufficient glucose is present to support enough hydrogen production to affect the quality of the fiber optic transmission.

Control of Fungal and Bacterial Growth

For long term protection of the cable, where deemed advisable, antimicrobials may be incorporated into waterblocking tapes to control the growth of fungi and bacteria. It was found that fungal growth could be controlled by both 2-(4-thiazolyl)-benzimidazole and copper-8-quinolinolate. Following inoculation in simulated cable with either A. niger, A. flavus or

P. funiculosum, no fungal growth could be detected in paper based waterblocking tapes containing either of these antimicrobials after one months incubation.

Two antimicrobials were tested for their effectiveness in controlling bacterial growth in simulated cable made with paper based waterblocking tape. After four days of incubation there was a reduction in bacterial numbers (3×10^4 with antimicrobial versus 1.6×10^7 without antimicrobial) when 1, 2 Dibromo-2, 4-dicyanobutane was used. However, copper-8-quinolinolate showed no effective control of bacterial numbers (2.1×10^7 with antimicrobial and 4.1×10^7 without antimicrobial).

CONCLUSIONS

The results presented here suggest that the composition of substrates of waterblocking tapes may not be an important determinant in the cellulytic activity of fungi or in the production of hydrogen by bacteria. Following inoculation of simulated cable containing paper substrates with several species of fungi, observations suggested that aerobic cellulose decomposition will occur in a small area at the wet-dry interface. Little or no decomposition will occur with paper substrates in the flooded area as long as it remains saturated, and little or none will occur in the dry area as long as it remains dry. In the case of non-wicking substrates such as SBP entrapped air pockets in the flooded portion may allow for a limited amount of fungal activity in that area.

The results also suggest that the number of bacteria is not affected by the composition of the substrates of the waterblocking tapes. Unless sufficient nutrients enter the cable with the water, hydrogen producing bacteria will be dependent on the activities of cellulytic microorganisms to degrade the cellulose to a useable nutrient. Efficient cellulose degradation will occur in a very limited area with paper substrates.

Tests of antimicrobials using the simulated cable suggest that fungal and bacterial growth can be controlled with the addition of antimicrobial agents to the waterblocking tape.

ACKNOWLEDGEMENTS

The assistance of Dr. David Punter and Dr. Jim Reid of the Department of Botany at the University of Manitoba in the taking of the photomicrographs of bacterial colonies is gratefully acknowledged.

REFERENCES

1. Anderson, W., Johnson, A. and DeVito, A. 1989. Field Measurements of Hydrogen Gas of Installed Submarine Single-Mode Fiber Cables. IWCS Proceedings 1989, p675.

2. ASTM Designation G22 - 76 (1985): Determining the Resistance of Plastics to Bacteria.

3. Atlas, R.M. and Bartha, R. 1987. Microbial Ecology. Benjamin/Cummings Publishing Company.

4. Collins, C.H. and Lyne, P.M. 1984. Microbiological Methods. Butterworths, Toronto and Boston.

5. DeVos, P., Stevens, P. and De Ley, J. 1983. Hydrogen Gas Production from Formate and Glucose by Different Members of the Enterobacteriaceae. Biotechnology Letters 5:69-74.

6. Gray, T.G. and Gest, H. 1965. Biological Formation of Hydrogen. Science 148:186-191.

7. Military Specification MIL-STD-810D; Method 508.3.

8. Skinner, C.E., Emmons, C.E. and Tsuchiya, H.M. Henrici's Molds, Yeasts and Actinomycetes. 2nd ed. John Wiley and Sons, Inc. New York.

9. Smith, J.E. and Berry, D.R. 1975. The filamentous fungi. Volume 1 Industrial Mycology. Published by Edward Arnold.

10. Technical Association of the Pulp and Paper Industry (TAPPI) Specification T487 pm-79 (1979): Fungal Resistance of Paper and Paperboard.

11. Thom, C. and Church, M.B. 1926. The Aspergilli. Published by The Williams and Wilkins Company, Baltimore.

Ross McQueen received a M.Sc. in Botany from the University of Manitoba and a Ph.D. in Plant Pathology from the University of Minnesota. He joined KT Industries in 1989 and has been engaged in product development.

Lynne Windsor is president of Fourwin Associates Limited, a Winnipeg based research and development consulting company engaged in product design and production methods. He has been involved with KT Industries in this capacity since 1976.

NOVEL PASSIVE COMPONENTS FOR THE LOCAL LOOP

C FAY, A R HEWINS, R JOHNSON, S J TURPIN, T D WAINE

BICC CABLES LTD
Communications and Electronics Division
Helsby
Cheshire
WA6 ODJ
England

R A FREEMAN, P L J FROST

BRITISH TELECOM RESEARCH LABORATORIES
Martlesham Heath
Ipswich
IP5 7RE
England

ABSTRACT

Local optical networks have been in development for a number of years; a key area requiring further development is the outside plant passive components particularly for wide scale deployment of fibre.

New components were designed to meet the usual requirement for the local network but with added features required for three topologies: Fibre-to-the-home (FTTH), Fibre-to-the-kerb (FTTK) and distributed star.

The various passive components were designed by British Telecommunications plc and BICC plc, and installed by BT plc in an extensive field trial in Bishop's Stortford, Hertfordshire, UK.

This paper covers the key components which were designed, together with the testing regime employed for each. Also covered are the topologies used and the installation practices undertaken. One of the prime reasons for the trial was to discover how easily regional installation personnel could adapt to fibre in the Local Loop.

INTRODUCTION

The design of the passive components was initiated by British Telecom's desire to field trial singlemode FTTH systems. The two systems chosen were TPON (Telephony on a Passive Optical Network) and BIDS (Broadband Integrated Distributed Star).

TPON exists in three basic forms; house, street and business. House TPON employs fibre from the exchange to the home and utilises bidirectional operation over a single fibre through passive optical splitters. Street TPON employs fibre from the exchange to a street multiplexer via passive optical splitters, with a copper drop to the customer.

Business TPON is essentially the same as House TPON, providing fibre from the exchange to the business, but is geared to business needs by the provision of additional lines.

BIDS employs fibre to the home but the fibre is first routed through a street cabinet containing an opto-electronic interface unit known as the Broadband Access Point. This distributes the appropriate services (telephony and broadband) to the customers.

In order to successfully install the new networks it was necessary to design a range of novel passive component housings for outside plant use. It was in some way fortunate that no plant existed which could easily be modified, as this enabled design to start as a completely new concept.

The basic plant requirements for the networks included exchange optical distribution shelves, street side cabinet mounted flexibility points, manhole housed distribution points and external wall mounted customer joints.

TPON

The requirement of the TPON network is that the optical split must be a minimum of 32 way. This was accomplished using a 4-way split at the flexibility point (cabinet) and an 8-way split at the distribution point. The passive splitters are sealed modules requiring no internal access on site. A schematic of the TPON network is shown in Figure 1.

The system is based on duplex transmission (ie, one fibre per customer). Due to the split nature of the system only one exchange fibre is required for each 32 way split system, therefore a minimum of ten fibres are required from exchange to flexibility cabinet which houses ten 4-way passive splitters.

Each of the splitters feeds four distribution points, each of which contains an 8-way passive splitter. One of the eight legs is reserved for testing and the other seven are for customer connections. The total number of customers fed by each system is therefore 28. There is also a broadband overlay (BPON - Broadband on a Passive Optical Network) which for power budget reasons is input into the system at the 16 way split level. This is achieved by running two extra fibres per splitter to the flexibility cabinet and accessing the 4-way splitter at the 2-way split position. This effectively gives a 3dB addition to the power budget for broadband. The TPON trial was a combination of blown fibre and conventional cables.

BIDS

The BIDS network uses a split system but all splitting is performed electronically via a street sited Broadband Access Point (BAP). See Figure 2.

The BIDS network requires a minimum of six fibres; two for telephony (transmit and receive) and four for broadband. At the BAP the signals are multiplexed onto the outgoing fibres as either telephony or as a combination of telephony and broadband. From the BAP onwards there are dedicated fibres to the customers; and, as with TPON, there is only one fibre per customer. The BIDS trial was wholly blown fibre.

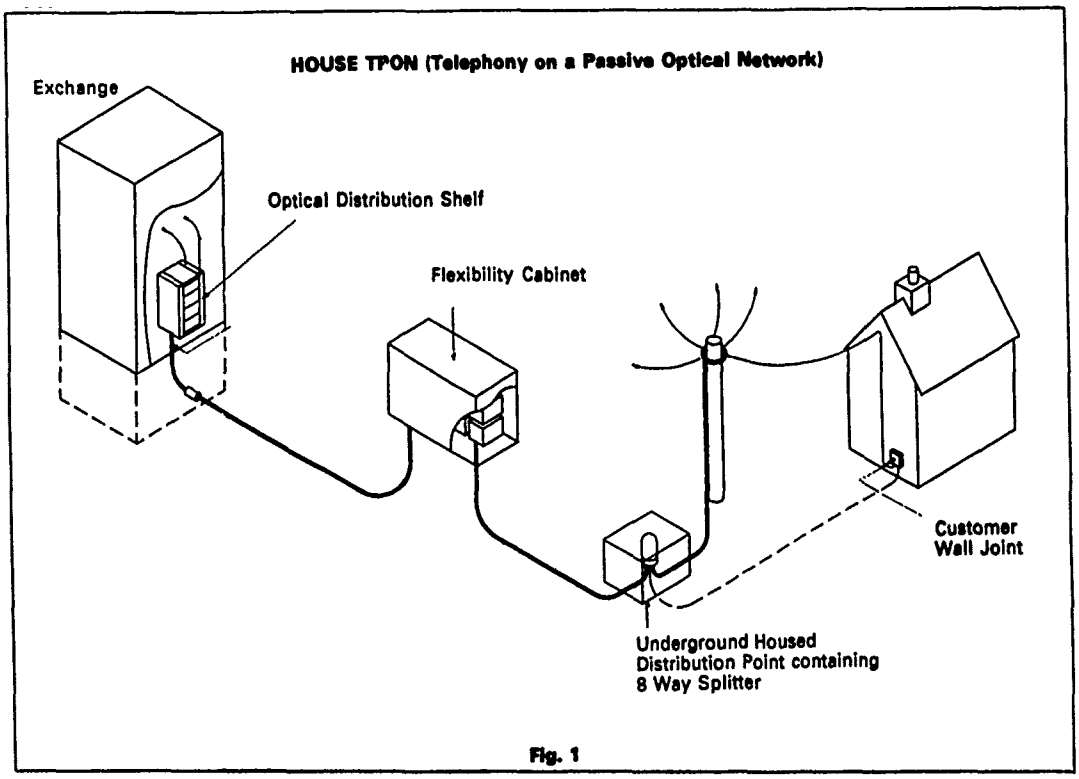
HOUSE TPON (Telephony on a Passive Optical Network)
Exchange
Optical Distribution Shelf
Flexibility Cabinet
Customer Wall Joint
Underground Housed Distribution Point containing 8 Way Splitter

Fig. 1

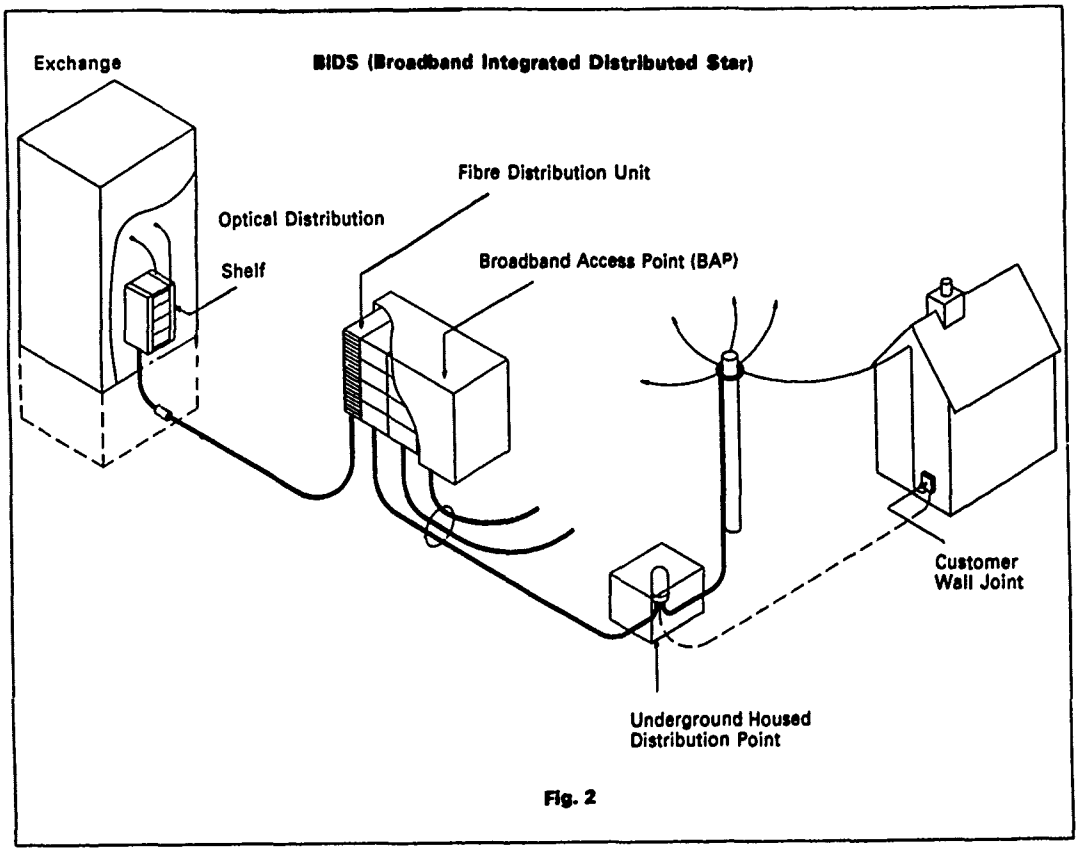
Exchange
BIDS (Broadband Integrated Distributed Star)
Fibre Distribution Unit
Optical Distribution Shelf
Broadband Access Point (BAP)
Customer Wall Joint
Underground Housed Distribution Point

Fig. 2

PASSIVE COMPONENTS

Optical Distribution Shelf (BIDS & TPON)

The distribution shelf used was designed for incorporation into a BT standard TEP 1E rack. It was necessary for it to handle both conventional tubed fibre and also blown fibre. Each fibre could either be spliced through directly to a pigtail or connector fitted for patching purposes. Because of the requirement for clip-on power monitoring (for TPON) it was important that the fibres could be accessed easily and safely without harm to adjacent fibres. For this reason a single fibre cassette system was used which housed both the fibre splice and, where appropriate, a connector. The shelf was also designed to slide out from the rack for access. See Figure 3.

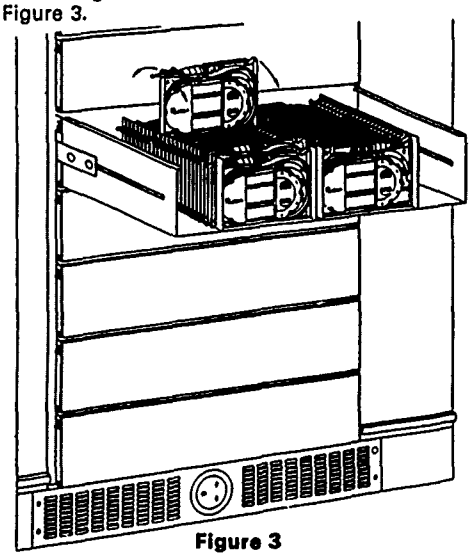

Figure 3

Only basic approvals testing was necessary for the distribution shelf since its operation was its most important feature. However the shelf was given two tests both of which were optically live.

1. MECHANICAL ENDURANCE

   300 extensions of the shelf.
   (Change in optical path loss -0dB)

2. RAPID CHANGE OF TEMPERATURE

   +5°C to +40°C.
   (Change in optical path loss <0.1dB)

Flexibility Cabinet (TPON)

The flexibility cabinet housing is a standard BT roadside cross-connection cabinet. This was chosen in order to make the field trial as close to present day copper technology as possible. The requirements for the cabinet were that it must have the facility for housing ten 4-way splitters and associated splices. In order to maintain a modular system it was decided from an early stage that each of the 4-way splitters would be housed in its own joint box, giving good environmental and mechanical protection. The main criteria behind the joint design was the ease with which the optical splitter could be housed and subsequently spliced to the incoming and outgoing fibres. There was also a requirement for clip-on detection.

To achieve these requirements it was decided to place upon the splitter a physical size and fibre configuration that it would enable it to fit correctly into the organiser. It was also decided that fibres would enter the splice trays through one position so that a 'page' style format could be used for the splice trays. This necessitated a new design of splice tray. The final tray design was arrived at using the following criteria.

(i) Fibres enter through the same position
(ii) Maximum size of 170mm x 80mm x 6.5mm
(iii) One splice per side of tray
(iv) No glueing of input tubes
(v) Clip-on power monitoring possible
(vi) Any fibre lengths accommodated.

Figure 4 shows a photograph of the splice tray.

Figure 4

The flexibility point organiser had to be designed such that it could be accessed easily even when fitted closely side by side. This was achieved by fixing the organiser onto a hinge so that it could swing forward to be worked on. Figure 5 and 6 show the closed and open positions respectively.

The flexibility point underwent a number of approvals tests as below:

(i)	Vibration -	10Hz, 0.7mm amplitude Duration 8 hours (Change in optical path loss <0.1dB)
(ii)	Dry Heat -	55°C Duration 96 hours (Change in optical path loss <0.2dB)
(iii)	Damp Heat -	40°C 93% RH Duration 96 hours (Change in optical path loss <0.1dB)

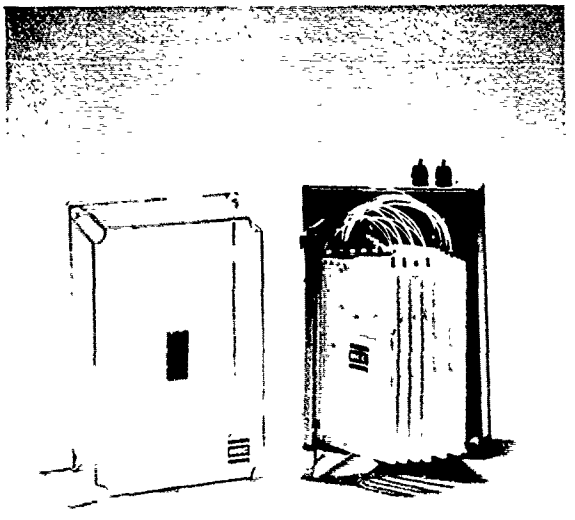

Figure 5

Distribution Point (TPON)

In order to maintain some uniformity of design amongst the various products the same splitter fittings and cassettes were used for the distribution point. Unlike the flexibility point the distribution point is designed for use in manholes and footway boxes.

It is also designed to accept up to seven customer drop cables, all of which may be installed at different times. The latter point dictated that the closure must be a ready access type suitable for many openings, while still maintaining environmental integrity. Figure 7 shows a picture of the DP.

The testing regime for the distribution point was considered to be probably the most critical since these items were to be sited below ground, potentially immersed in water and subjected to heavy traffic vibration.

The tests undertaken were as follows:

(i)	Impact	1kg
(ii)	Cable Retention	1kn
(iii)	Head of Water	1 metre
(iv)	Change of Temperature	-20°C to +50°C for 150 hours
	(Change in optical path loss <0.2dB)	
(v)	Vibration	10Hz, 0.7mm amplitude for 5 days
	(Change in optical path loss <0.1dB)	

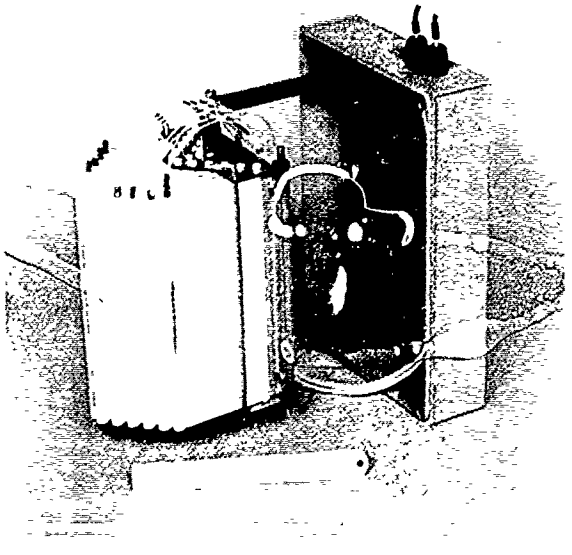

Figure 6

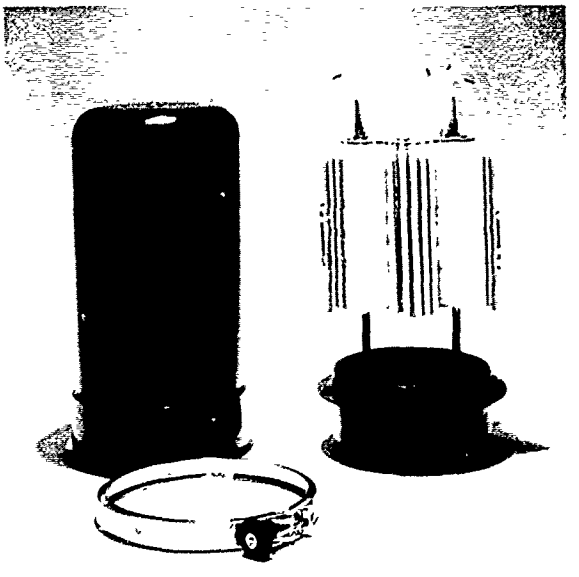

Figure 7

Test Access Connector (TPON)

The DP, as mentioned above contains an 8-way splitter which has one leg on both input and output sides reserved for test access. For this purpose a test access connector was developed. One feature of the connector was that it should have a very high return loss in both the mated and unmated states. The connector was based on the established ST[1] style, with the ferrule end face polished at an angle to provide the high return loss.

Figure 8 shows the connector dimensions and angle of polish.

The basic testing regime for the test access connector was the following:

(i) Insertion loss (150 measurements @ 1550nm 0.73 ± 0.36dB)

(ii) Return loss (20 measurements @ 1300nm 52 ± 2dB)

(iii) High temperature endurance
65°C for 500 hours
(Insertion loss <1.5dB after test)

(iv) Tensile 5N force
(Insertion loss <1.5dB after test)

(v) Rapid change of temperature
+70°C to -10°C
(Insertion loss <1.5dB after test)

(vi) Mechanical endurance
500 matings
(Insertion loss <1.5dB after test)

(vii) Vibration
10-500Hz at 1 octave/min
(Insertion loss <1.5dB after test)

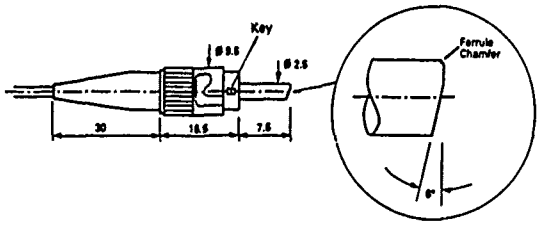

Figure 8

[1] ST is a trademark of AT&T Technologies

Customer Wall Joint (TPON & BIDS)

The final item on the passive network is the customer wall joint which is the lead-in to the customers' premises. It provides two main functions; acting as an interface between external and internal cable types, and providing a clip-on detection position external to the customer premises. As with other external fittings to buildings the design had to be such that it was as unobtrusive as possible. The final design (see Figure 9) was a compromise between size and function.

The overall size is 240mm x 160mm x 90mm.

The testing criteria for the CWJ had to take into account the fact that it is externally exposed to the weather and potentially physically vulnerable due to its positioning. The mechanical performance was tested as follows:

(i)Impact DIN 53453 0.5kg steel ball 50mm ø from 1 metre

(ii)Moisture Sealing to IP-5 (Dust was not considered an important factor)

The environmental performance factors were:

(i)Cold -25°C for 96 hours

(Change in optical path loss <0.2dB)

(ii)Dry Heat 40°C for 96 hours

(Change in optical path loss <0.2dB)

(iii) Temperature Change -25°C to +40°C for 36 hours

(Change in optical path loss <0.2dB)

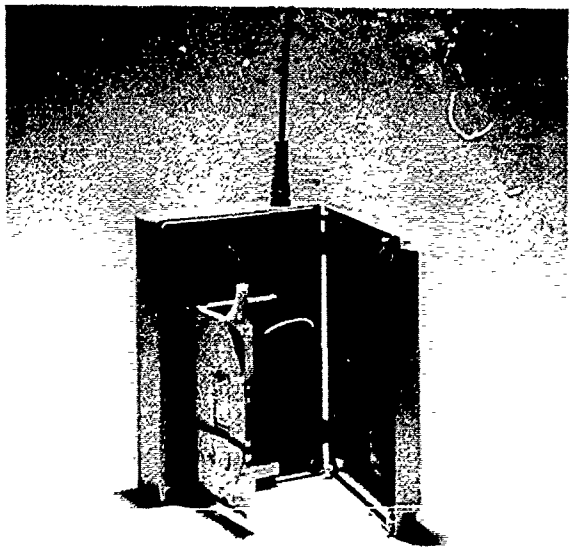

Figure 9

BIDS - Components

The components used for the TPON network were used for the BIDS network wherever possible. For example the distribution shelf, and customer wall joint were unchanged. The distribution point uses the same basic building blocks as the TPON DP but does not contain a passive splitter. The BIDS DP is purely for through splicing to upto 14 customers.

The only major item designed for BIDS was in connection with the Broadband Access Point (BAP) shown in Figure 2. The BAP contained the street sited opto-electronics and fibre handling unit. The fibre handling requirement was particularly onerous in terms of fibre numbers and space available. The dimensional constraints were 1.2m x 145mm x 310mm. In this space 224 fibres were to be arranged in groups of 7 (blown units of 7 fibres were used) and excess fibre stored. This was achieved using a sliding drawer system of storage in which each seven fibre unit was allocated to each drawer. See Figure 10. The whole unit was manufactured from aluminium to maintain compatibility with the rest of the metalwork in the BAP. The testing of the BAP fibre distribution unit was:

Temperature Change 10°C to +70°C
for 10 hours
(Change in optical path loss <0.1dB)

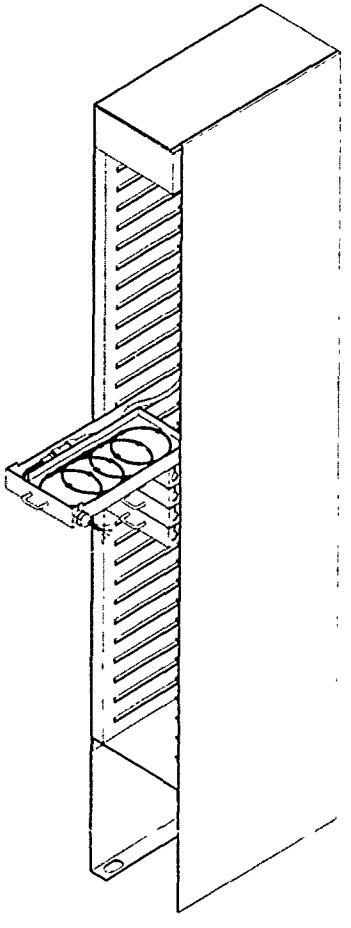

Figure 10

CONCLUSION

There have been predictions for some time concerning fibre-to-the-home and its attendant increased services. With this will come a volume increase and a quickening of pace in the development of both infra-structure and services. This trial has shown that the concept is in fact now a reality.

Products now exist which can be supplied to those wishing to take advantage of the technology using standard installation techniques which require only minimal skill and training.

ACKNLOWLEDGEMENTS

The authors would like to thank the Directors of BT plc and BICC plc for their permission to publish this paper.

Christopher Fay joined BICC in 1981 after gaining a BSc in Physics from Liverpool University. He spent his first four years as a Components Development Engineer designing passive components for optical cable installations, followed by two years in the Cable Systems Department before returning to the Passive Components Department in 1987 as the Group Leader.

Andrew Hewins joined BICC in 1985 after gaining a BSc in Mechanical Engineering from Salford University. He has worked as a cable systems engineer in the Defence Sector of BICC Cables examining potential markets and opportunities. Since 1989 he has worked as a Senior Engineer in the Passive Components Group designing components for optical cable installation.

Robert Johnson received his BSc in Applied Physics from the South Bank Polytechnic in 1977. Since 1983 he has been involved with the design and development of fibre optic passive components. He joined BICC in 1988 as Group Leader - Interconnect. He is a member of the Institute of Physics.

Stephen Turpin is a Senior Engineer in the Passive Components Group at BICC Cables Ltd, C&E Division. He has 19 years experience with the design and development of fibre optic components. Since joining BICC in 1988 he has been involved in the development of passive components relating to all areas of optical cable installation.

David Waine joined BICC in 1979 as an apprentice Electrical Engineer. In 1983 he moved to the Passive Components Department as a technician assisting with the design and development of components for optical cable installations. In 1987 he became an Engineer in the Passive Components Department. In 1990 he moved to the position of Product Manager - Passive Components.

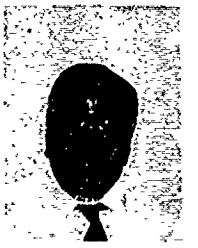

Robert Freeman joined British Telecom in 1964 as an apprentice. In 1975 he joined the Submarine Systems Division of British Telecom Research Laboratories concerned initially with the development of under sea cable grapnels, later moving to the development of optical fibre fusion machines and cable jointing methods and equipment. In 1988 he became project leader on a number of external optical plant developments including responsibility for local loop optical field trial developments. Currently he is employed as a Head of Group within the Services Division at BTRL. He holds a number of patents and has published papers on blown fibre.

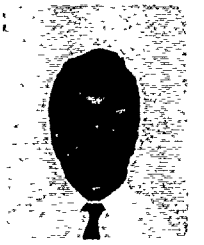

Peter Frost joined British Telecom Research Laboratories in 1973 as a trainee technician apprentice. In 1984 he joined an optical measurements group concerned with the characterisation and selection of both single and multimode connectors of use in BT. In 1988, he became responsible for the design of internal and external optical plant components for use in British Telecom's local loop field trail. He holds a number of patents associated with optical plant and is now working on future component designs.

VARIATIONS OF OXIDATIVE INDUCTION TIMES OF POLYOLEFIN INSULATED CONDUCTORS

E. E. Hershkowitz
L. M. Hore

Bellcore
445 South St.
Morristown, NJ 07960-1910

Abstract

Oxidative Induction Time (OIT) represents a rapid method for the examination of levels of stabilization in polyethylene insulations. This can be interpreted as an indication of the suitability of the product to withstand the rigors imposed by field service conditions. One serious question on the use of this test arises from the fact that only a few milligrams of insulation is used for the test. How representative is this sample and what credence can be given to an OIT value?

We have examined wire insulations from several sources, uncabled, cabled and reeled, for variations in OIT. Longitudinal and sectional measurements were made. While process conditions, chemical systems and raw materials will produce different absolute results, the small variations presented seem to validate the use of the OIT as a representative measure.

1. Introduction

The stability of foam skin conductor insulations, and hence all polyethylene insulations, used in telecommunications cable has been the subject of much discussion.[1-5] The results of these discussions have led to improvements in the stability testing for finished cable. The pedestal test has been revised and much work is going on to review oven aging and other accelerated methods. Still, these represent long duration testing with weeks of conditioning of specimens and then weeks of exposure at elevated temperatures. The real time limits of actual production requires a rapid test which can serve as both the in process and final shipment "go/no go" gauge. In this area the OIT test, with a typical time of under two hours is extremely attractive.

Insulation materials are subject to oxidation as soon as they are made due to the presence of heat and oxygen. All stages of manufacture serve to further deplete the initial reservoir of stabilizer in the formulation. The filling and jacketing of a cable involve elevated temperatures. All of the thousands of conductor feet in a cable are then judged on a three milligram sample of insulation. In order to understand what variations could be expected in manufacture we undertook to examine a number of cases.

2. Experiments

Materials

Two samples of insulated conductors, one foam skin and one solid insulation, were obtained in sufficient length so that a 25 foot section could be selected and the OIT measured every six inches. Production cables using a 65° C and an 80° C filling compound were examined prior to and after aging at 70° C for four weeks. The cable samples were examined along the length as well as in section. The white conductors were selected for testing to conform with previous work, as yet unpublished, done at Bellcore. In the case of the cables they were taken from standard manufacture product awaiting shipment. No special attempt was made to acquire special samples and all were of recent manufacture -less than six months- prior to testing with the bulk of the storage time spent in laboratory conditions.

Methods

The cables were cut from reels received at the Bellcore laboratories in Chester, NJ. Care was taken to select samples away from an end which had been exposed to the air for any length of time greater than one day. In the samples used for pre-aging prior to testing an additional amount was left on each end so that the cap could be placed and later cut off with a length of cable. In all of the discussions in this paper we will refer to the dimensions of the final sample and disregard the material trimmed off to avoid "cut end effects".

The OIT analysis was performed using the method referenced in Bellcore's TR-TSY-000421, Issue 2, using a DuPont TA 2100 system equipped with a Differential Scanning Calorimeter (DSC), an auto-sampler and an automatic gas selection valve. This allowed the samples to be analyzed in a continuous manner and prevent any effects which may have resulted from delays imposed by a 40 hour five day week.

3. Results

A single conductor of 26 ga. foam skin insulation was obtained from the manufacturer prior to cabling. This conductor was examined in the as received condition by

taking samples every six (6) inches over a twenty-five foot length. The results are shown in Figure 1. In this and all following figures the results are shown as a scatter with the mean and 1σ shown as horizontal lines.

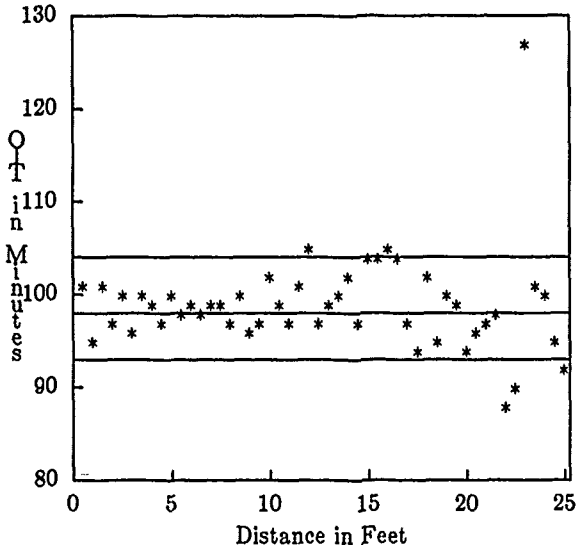

Figure 1. OIT values for a foam skin insulated conductor prior to cabling. $\bar{X}$=98, σ=5 minutes.

Figure 2 gives the distribution of OIT values for a similar experiment using a solid 26 ga. conductor, also prior to cabling.

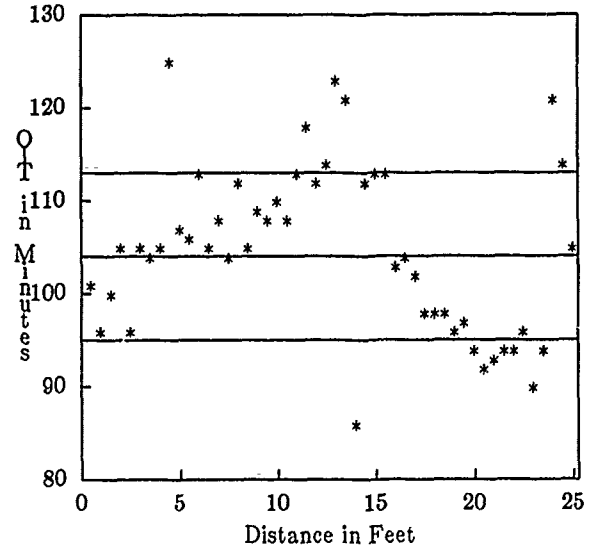

Figure 2. OIT values for a solid insulated conductor prior to cabling. $\bar{X}$=103, σ=9 minutes.

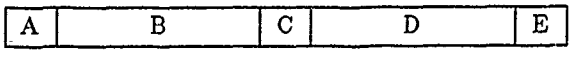

Figure 3. Sections of the 2.3 meter test cable. A, C, & E are each 10 cm. B & D are each 1 meter.

The next tests were done on white conductors taken from a 26 ga., foam skin, 100 pair cable filled with 65° C Extended ThermoPlastic Rubber (ETPR) filling compound. A section of cable was removed from a reel and sectioned for test (See Fig. 3). An initial section 10 cm. long was set aside as Section A. The next one meter section (B) was held for other testing. A second 10 cm. section (C) was cut for this study. The next one meter section (D) was cut and placed in an oven to age at 70° C for 28 days. Another 10 cm. section (E) was removed and added to the unaged part of this test. In all the twenty white wires in a total length of 2.3 meters of this cable provided eighty (80) data points for an unaged cable and an additional twenty (20) points after aging. This presents a view of forty-six (46) meters of conductor.

Figures 4,5 and 6 present the data from sections A, C and E respectively and are presented as cross-sectional views of the cable.

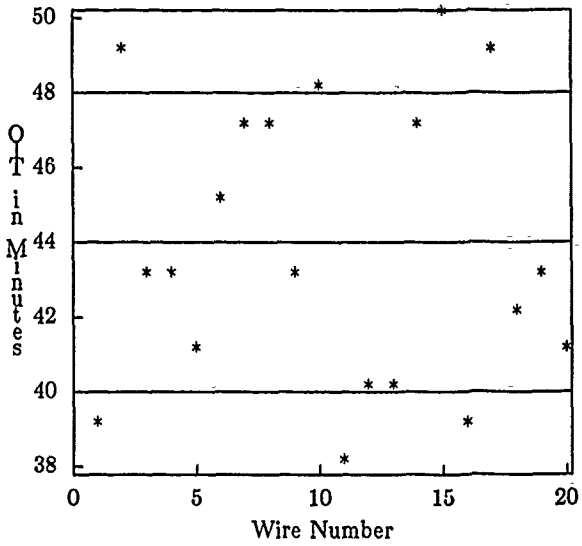

Figure 4. Section A, the first 10 cm. of the test cable. $\bar{X}$=44, σ=4 minutes.

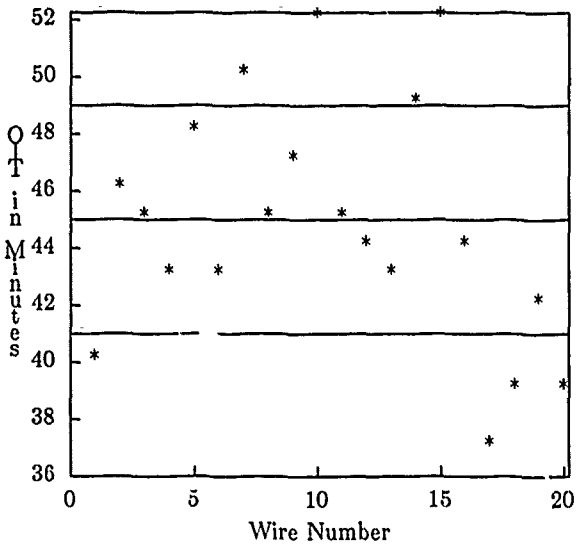

Figure 5. Section C, the center 10 cm. of the test cable. $\bar{X}$=45, σ=4 minutes.

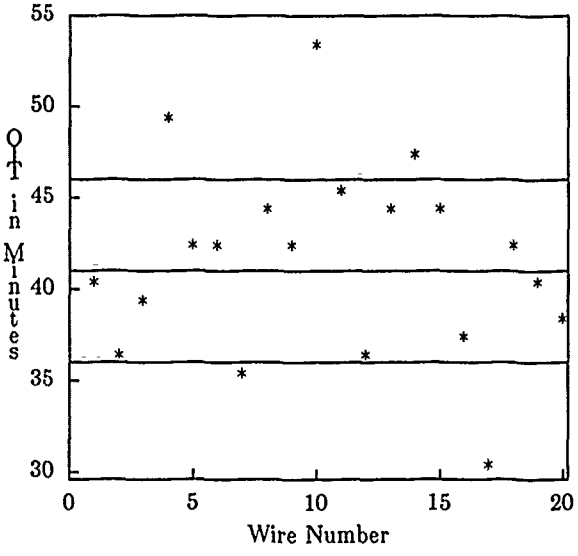

Figure 6. Section E, the last 10 cm. section of the test cable. $\bar{X}$=41, σ=5 minutes.

In order to present the composite view of a cable, Figure 6 combines all sixty readings of the unaged conductors over a span of 2.3 meters for an examination of 46 conductor-meters.

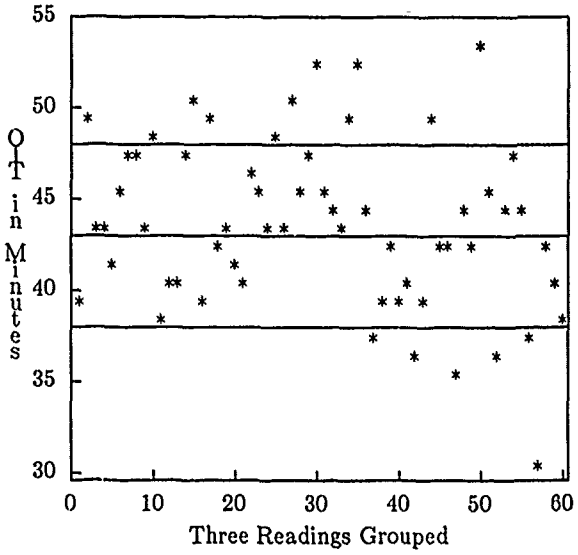

Figure 7. Combined values obtained from sections A, C and E. $\bar{X}$=43, σ=5 minutes.

After aging for 28 days at 70° C the twenty white conductors in section D were tested. The results are shown in Figure 7.

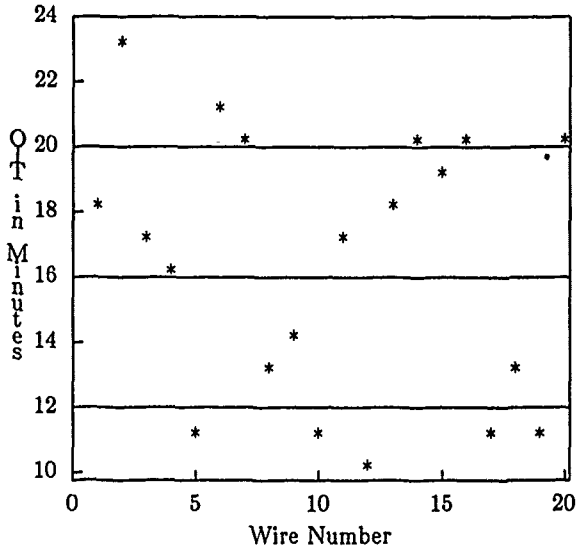

Figure 8. OIT values for section D, conductors aged for 28 days at 70° C. $\bar{X}$=16, σ=4 minutes.

After the completion of the previously described testing, we turned toward the questions raised by the introduction of 80° C ETPR filling compounds and solid polyethylene insulations. A production length of a 24 ga., 600 pair, solid PE conductor insulation cable was chosen. This provided 120 white conductors which were aged in the cable for 28 days at 70° C. A 30 cm. section was then removed from the center of a two meter length and the insulations at either end were tested for OIT values. Figure 8 presents the results in aggregate (240 values).

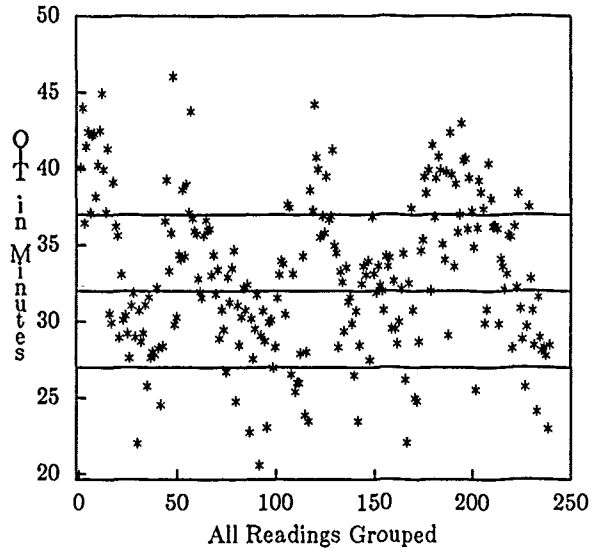

Figure 9. OIT values for 120 white conductors from a 24 ga., 600 pair, solid insulation, 80° C filled cable. $\bar{X}$=32, σ=5 minutes.

4. Discussion

The initial intent of this investigation was to determine the variation in OIT value along a conductor and within a cable. This was done to determine the validity of estimation of cable quality by the use of the OIT value. While this work does not represent an exhaustive study of all cables from all manufacturing locations we feel that the samples which were used represent the standard materials available in commerce and that these are representative of the industry. Two other factors must be considered in viewing these analyses. Each laboratory must determine the repeatability of their own measurements and maintain an internal calibration. The preparation of samples must be done in a consistent manner.

Based on the considerations given above it is our conclusion that variation in OIT measurements obtained from a product either in production or after manufacture correlate well with other manufacturing variables. While absolute value comparisons between various labs may have to await further refinements in the actual OIT test used, it seems clear that a trend can be established.

5. Acknowledgments

The authors wish to thank O. Mandel and A. Stephenson for their laboratory analysis work and E. P. Hjorth for his assistance.

6. References

1. T. N. Bowmer, Proceed., 37th Int. Wire & Cable Symposium, p. 475 (1988)
2. L. E. Davis, Proceed., 37th Int. Wire & Cable Symposium, p. 484 (1988)
3. T. N. Bowmer, E. P. Hjorth, R. J. Miner, and O. S. Gebizlioglu, Proceed., 37th Int. Wire & Cable Symposium, p. 490 (1988)
4. L. E. Davis, Proceed., 36th Int. Wire & Cable Symposium, p. 475 (1987)
5. G. D. Brown, L. E. Davis, Proceed., 36th Int. Wire & Cable Symposium, p. 475 (1987)

Lal Hore is responsible for the preparation of Bellcore's Technical Requirements for Outside Plant Cables and the development of high speed transmission requirements for wire products. After receiving a M.Sc. (Applied Physics) from the University of Calcutta and a Dr. Tech. degree from the Technical University of Budapest in Electrical Engineering, he joined Bell Northern Research in 1970 to design and develop communications cables. In 1972, Lal moved to General Cable Company where he worked as a manager in the Communications Cable Section and then in the Applications Engineering Section until 1987 when he joined Bellcore.

NEW TECHNOLOGY FOR A SINGLE MODE MECHANICAL SPLICE

Steve Lischynsky, Helmut Lukas, Robin McIntyre, Grant Pacey

BELL-NORTHERN RESEARCH Ltd. (BNR)
Ottawa, Ont. Canada

ABSTRACT

The wider deployment of fiber to new network applications will result in increased emphasis on cost, less availability of skilled craft people and less convenient installation environments. In response to these concerns a new molded mechanical splice has been developed which offers the economies of mass production, superior performance and reduced skill requirements through the elimination of polishing and adhesives.

Superior optical performance and fiber retention have been realized by fully exploiting the properties of a plastic material resulting in an efficient design with minimal number of parts and complexity.

Testing indicates that the environmental sensitivity of insertion loss over the temperature range of -40°C to +80°C is less than 0.1dB and that the splice exceeds the handling durability imposed by the minimum skilled craftsperson.

INTRODUCTION

Most fiber splicing products currently in use were designed primarily for trunking applications. With the increased use of fiber for telecommunication feeder and distribution, as well as in CATV and LAN networks, a new set of factors must be taken into account. These applications are typified by larger amounts of fiber, more concern for cost, less skilled craft and a less convenient installation environment.

Recognizing these new aspects, a new generation mechanical splice has been developed to meet the needs for wider fiber deployment. Main features include: a cost effective design, superior performance and reduced skill requirements through minimizing the number of installation steps, eliminating the need for assembly of parts in the field and the need for polishing or adhesives.

Through full utilization of material properties an efficient design with few parts and minimal complexity has been achieved. By developing an extensive understanding of the interplay of the design, the splice material properties and the fiber itself, techniques have been found to minimize transverse offset of the fiber cores due to cladding diameter differences, eliminate adhesives through direct clamping of the fibers and to minimize fabrication costs by using highly repetitive precision molding.

This paper will review the design and development of the new splice. Specifically, it will examine the changing requirements for splicing as the wider deployment of fiber occurs, discuss the new technology employed, describe the design and review the results of laboratory testing conducted to verify the technology.

BACKROUND

As fiber migrates from trunking to feeder and access applications a number of factors affecting splice design take on heightened emphasis. Firstly, the amount of fiber and cables will increase significantly making splicing cost a more important factor. It also implies that all craftspersons rather than a select few, will have to splice fiber and be outfitted with splicing tools. In addition, these networks are generally less secure than trunking applications, making repairs more frequent and necessitating that they be done under more adverse and less convenient conditions. Currently a large percentage of splicing is being done in vans because of the associated equipment; however, there will be far more midspan splices with lateral cables in these new applications. By eliminating the need to splice in vans and the associated slack cable, congestion in the already overcrowded manholes can be eliminated. All of these issues imply that splices designed for these applications need to show an increased emphasis on cost effectiveness, ease of installation and superior optical performance.

Based on the analysis of these factors a set of key requirements were defined as follows:

- Designed for mass production and automation
- Low insertion loss ≤ 0.1dB
- High return loss ≥ 40dB
- Rapid installation time ≤ 1min. (excluding fiber prep.)
- Rugged yet compact design
- Minimum fiber retention of 500g strength
- Stable long term performance

DESIGN FEATURES

A cost effective, high performance splice has been developed that allows fiber joining with minimal effort and skill. Cost effectiveness is achieved with a design that has no loose parts to be assembled in the field, that is designed for automatic assembly and employs high volume precision production methods. Installation takes approximately 1min. excluding conventional fiber preparation and uses no adhesives or polishing. Only a few simple installation steps are required to achieve blind splice losses better than 0.1dB and reflections better than -40dB. A functionally simple and rugged installation tool has been designed to complement the splice features.

An illustration of the splice is shown in fig. 1.

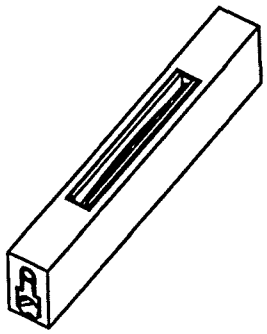

Fig. 1 Molded splice configuration.

A side view cross-section of the splice is shown in fig. 2. It consists of four plastic molded parts including: the outer body structure, a fiber clamp containing a precision 60° vee-groove and two identical jacket buffer adapters which are used to accommodate fibers with different jackets. Clamping force to the vee-groove element is provided by a spring. A highly stable index matching gel is applied to the vee-groove area at the time of factory assembly to achieve low insertion loss and reflection.

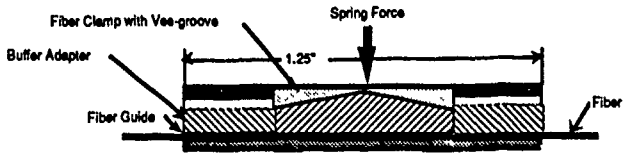

Fig. 2 Side view of molded splice showing fibers in place under vee-groove clamp.

The fibers are aligned by clamping their cladding surfaces between the vee-groove and the inner surface or anvil portion of the body. A carefully chosen balance between spring force and material properties has been selected through extensive research such that the fibers cause plastic deformation of the clamping surfaces so as to conform to the individual diameters as is shown in fig. 3.

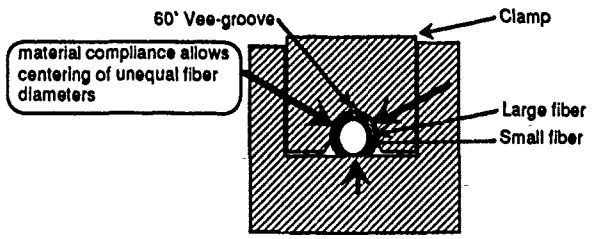

Fig. 3 Cross section of fiber clamp showing how conformance of vee-groove results in collinear alignment of fibers with different cladding diameters.

The plastic vee-groove has a number of important advantages over the conventional rigid or non compliant vee-groove approach for alignment. Firstly, the equilateral triangle formed by the 60° vee-groove and the anvil results in a system of equally balanced forces about the fibers. This causes equal deformation at each bearing surface of the vee such that each fiber's theoretical center is coincident with the centroid of the vee-groove. As a result the fiber centers are self-aligned in a collinear fashion so as to eliminate offsets due to differences in cladding diameter. Secondly, the plastic deformation minimizes the stress level applied to the fiber by distributing the clamping force over a larger area of the cladding surface. Finally, the fibers are clamped adequately in spite of the differences in cladding diameter which occur with typical production variations.

A spring holds the vee-groove alignment clamp closed to align the fibers. The installation tool opens the clamp for fiber insertion and also provides the ability to facilitate rotation of the fibers relative to each other for tuning purposes if desired.

The buffer adapters are fitted at each end of the splice body to accommodate different fiber jacket diameters and to provide bending strain relief to the bare fiber as it enters the vee-groove clamp. The adapters are factory fitted and colour coded and can handle the standard jacket diameters of 900μm and 250μm or a mixture of both.

DESIGN CONSIDERATONS

In order to design a plastic based mechanical splice a number of important design considerations were taken into account. This was particularly important for the material selection where the key requirements were established as:

- low enough compressive yield strength to deform to the fiber diameter variations under moderate force, yet sufficiently high to maintain holding pressure on the relatively small surface area of the fiber.
- high creep strength so as to maintain the fiber retention over time under long term exposure to varying environmental conditions
- good molding characteristics i.e.;
  - low shrinkage to allow maintenance of high dimensional tolerance including mold loss,
  - insensitivity to minor variations in process parameters,
  - good surface finish.
- chemical compatibility with the index matching gel
- high long term stability under the wide range of conditions typically found in the outside plant and in-building environments
- high toughness to prevent shaving by the cleaved fibers during insertion

Having established a number of candidate materials, testing was conducted to study their stability characteristics with respect to time and temperature. Thermal cycling testing to study loss sensitivity was carried out between -40°C and +80°C. Fig. 4 illustrates the typical characteristics observed. As can be seen, the exhibited variation is well within acceptable limits and is comparable to that seen with more exotic all-glass splice designs.

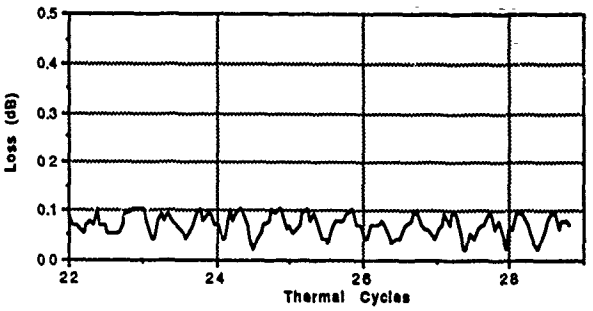

Fig. 4 Graph of insertion loss sensitivity during temperature cycling between -40°C and +80°C.

Long term material creep resistance studies were conducted to investigate fiber retention/alignment with respect to stress relaxation. Although there was initially some concern regarding the plastic creep, this characteristic proved to be an asset in practise since the fiber retention strength actually increased with time. This is an additional benefit derived from the balanced compressive stresses which are inherent in this design.

SPLICE INSTALLATION AND TOOL

The splice is installed by use of a simple plastic tool which is illustrated in fig. 5.

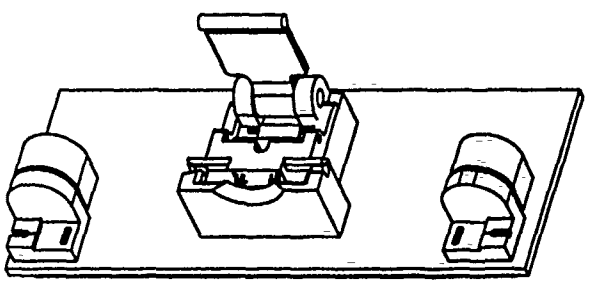

Fig. 5 Illustration of splice installation tool.

For installation the splice is placed into a receptacle provided in the tool and the operating lever is rotated forward so as to open the vee-groove clamp to accept the bare fiber. Each fiber is stripped, cleaved and cleaned using conventional techniques. Lay-in type of guides are provided in the tool to guide the fibers easily into the entry ports of the splice. Fiber strain relief clamps are provided at each end of the tool to retain the fibers prior to closing the vee-groove clamp. Precise centering of the fiber interface within the splice is not critical, however, guages have been molded into

the tool so that the craftsperson can check that the correct length of bare fiber has been provided.

The fibers are secured by rotating the operating lever of the tool back to release the vee-groove clamp. An ejection mechanism is also activated by this operation to facilitate removal of the splice.

Tuning to minimize fiber core eccentricity mismatch can be conducted if desired by reopening the fiber vee-groove clamp to facilitate fiber rotation. The unique self-locking design of the deformable 60° vee-groove is such that the fibers remain wedged in position after release of the clamp. Simple rotation is enough to break the locking action so that one of the fibers can be rotated relative to the other.

DESIGN VERIFICATION RESULTS

Extensive design verification testing has been completed to ensure the validity of the design. Fig. 6(a) and 6(b) show graphs of insertion loss for fibers of both similar and mismatched diameters. Fig. 6(c) shows measured results of reflection. An insertion loss of 0.04dB was obtained for fibers with similar diameters and eccentricities of 0.3 μm or less. A slightly higher loss of 0.07dB was obtained for mixed splicing of fibers with diameters at each end of the production specification (i.e.; 123μm and 127μm) with eccentricities similar to those in the like diameter tests. These results were obtained without tuning during splicing. The impact of the diameter mismatch has been significantly reduced due to the self-centering action of the conformal vee-groove. Furthermore, the design is very forgiving in that there is significant margin to tolerate fibers with diameters beyond the tolerance limit of the specification.

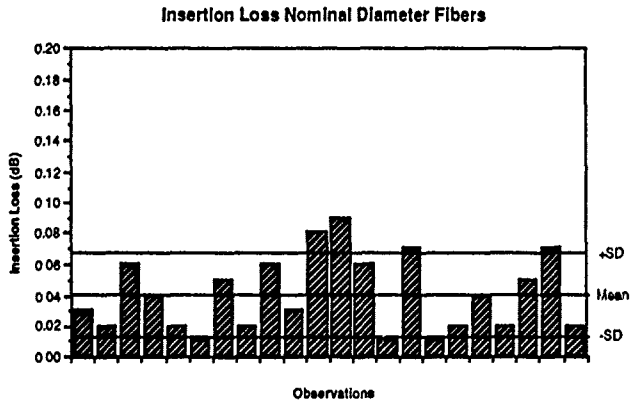

Fig. 6(a) Insertion loss for fibers of like diameter and typical eccentricity (22 samples).

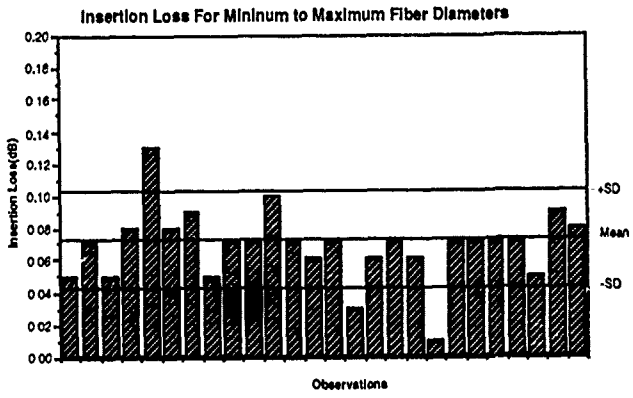

Fig. 6(b) Insertion loss for fibers of unlike diameter and typical eccentricity (26 samples).

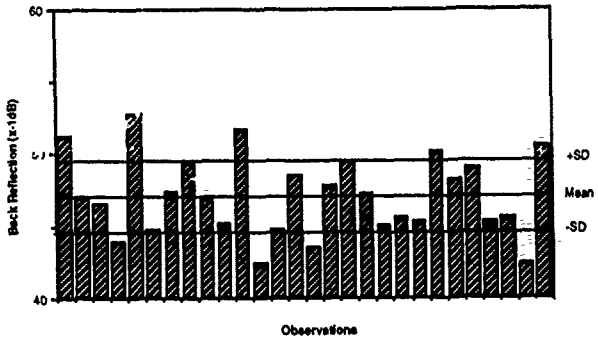

Fig. 6(c) Return losses for 28 samples.

The results of fiber retention testing are indicated in fig. 7. A mean of 1290g with 100% of the samples greater than 500g was achieved, easily meeting the Bellcore standard of 454g for fiber retention and robustness.

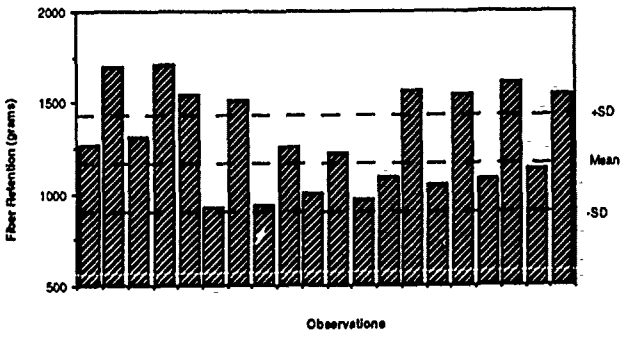

Fig. 7 Fiber retention for 20 samples.

Table 1 shows the results of key tests conducted to verify the reliability of the splice for long term performance.

	CHANGE DURING	CHANGE AFTER
THERMAL CYCLE (-40°C to +80°C)		
Loss	≤0.1dB	0.04dB Avg. Increase
Retention	———	10% Avg Increase
HEAT AGE (12 weeks @ +80°C)		
Loss	≤0.03dB	0.05dB Avg. Increase
Retention	———	15% Avg. Increase

Table 1. Loss and fiber retention results for long term reliability tests.

CONCLUSION

A new plastic mechanical splice has been designed to meet the needs associated with the wider deployment of fiber in telco, CATV and LAN applications. The splice is made of a precision molded plastic material which facilitates mass production and gives superior optical performance. It is easily installed in the field using a simple fixture and uses no adhesives or polishing. Extensive verification testing has been conducted and the splice has been shown to meet the requirements for long term reliability in outside plant and in-building applications.

AUTHORS

Helmut Lukas completed his toolmaker's training in West Germany. A mechanical designer with many years of experience, he has been involved with numerous telecommunication product developments, including copper connector blocks, splice closures, coaxial cable splicing, and a special project involving the development of a hydraulic prosthetic arm. For the past sixteen years, Helmut has been involved with the development of optical fiber connection technology including fusion and mechanical splicing and connectors.

Steve Lischynsky received a B.A.Sc. in Mechanical Engineering in 1971 from the University of Manitoba, Canada. Since joining Bell-Northern Research in 1980, he has been involved with the development of electronic and fiber optic connection technology. Previously he has worked for ITT as a project engineer where he was responsible for designing military connectors.

Robin McIntyre received her BSc. from the University of Waterloo in Chemistry, 1985. Since joining BNR in 1986, she has been involved in materials application engineering of high performance polymers, adhesives and optical gels for fiber optic interconnection technology and telecommunication applications.

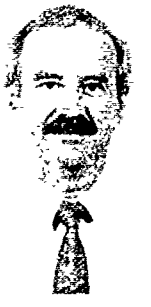

Grant Pacey graduated as a mechanical technologist from the Northern College of Applied Arts and Technology (Kirkland Lake, Ontario) in 1969. He completed his B.A.Sc in Mechanical Engineering at Queen's University (Kingston, Ontario) in 1972 and his MBA at the University of Ottawa, Ontario in 1981. He joined BNR in 1973 and initially worked in the design of terminal equipment, electronic packaging and in mechanical development and evaluation. During the past fourteen years he has been involved in the development of technology for fiber interconnection and outside plant fiber hardware system studies. Grant is currently manager of the Optical Connection Systems Development Department at BNR.

NEW CONCEPT IN FIBER MANAGEMENT HARDWARE

George Debortoli, Laurence Beaulieu, Brian Osborne, Lorne Brown
Bell-Northern Research (BNR) Ltd.
Ottawa, Ontario, Canada

Abstract

The need for physical fiber management is increasing as fiber systems migrate from trunking to feeder plant and ultimately to the distribution plant. With this migration, the number of fibers entering a central office or remote facility increases by several orders of magnitude. There is a need for fiber cross connect or interconnect hardware that occupies a minimum of space, provides easy access to individual fibers, and allows for flexible rearrangement without becoming an administrative nightmare. Bell-Northern Research has developed a unique system for managing fiber that terminates and self-administers a large number of fibers in a variety of applications.

Introduction

The investigation of requirements for managing fiber in the fiber centers of tomorrow's networks led to the development of the Fiber Management System. The Fiber Management System addresses a variety of applications including telecommunications, data communications, and private networks. The system is designed for central office administration of fiber between equipment and outside plant, and equipment to equipment. The flexibility of the design allows the system to be used in huts or CEVs, and as an interconnect or cross connect. It is also applicable in customer premises for the termination and administration of fiber backbones and LANs.

Network Requirements

Bell-Northern Research identified six major requirements for managing the all-fiber central office of the future:

1. slack management
2. spare fiber management
3. equipment interconnection
4. connection rearrangement
5. centralized administration
6. test access

Slack Management

Today's number one requirement in the use of fiber networks is to effectively manage cable slack. The root cause of cable slack is the inability to readily install connectors in the field. To minimize installation costs, many network providers are using cables that are preconnectorized at both ends. Engineering the exact length of these cables is difficult, resulting in a cable that is usually too long. To prevent cable entanglement problems, the slack must be effectively managed.

Spare Fiber Management

Because of the different economic periods used for cable provisioning and equipment provisioning, there is a need for spare fiber management. Typically, outside plant cable is provisioned for a much longer period of time than the equipment. The spare fibers resulting from these different provisioning periods require orderly termination and identification in order to provide service on demand.

Equipment Interconnection

To avoid service disruptions, eliminate delays, and reduce costs, there is a requirement for quick interconnection to the outside plant. This requires the orderly termination of both the outside plant and equipment cables in the central office. Once the fibers are terminated, they can be quickly interconnected with a simple patch cord.

Connection Rearrangement

Interconnections need to be rearranged to accommodate fiber network evolution and growth. As systems evolve and grow, they can require rearrangement of equipment interconnections with minimal downtime. Rearrangement must not disrupt existing cables and services. Quick rearrangement of connections is also required for restoration due to physical cable failures.

Centralized Administration

Fiber interconnections require administration from a central location, rather than being scattered throughout the central office. Centralized cable appearances allow cable and equipment to be administered separately. Centralization simplifies records and network management, and the interconnection of leased fibers.

Test Access

There is a need to access and test fiber prior to equipment connection. By terminating the ends of all fibers on connectors, in one location in the central office, the task of locating individual fibers for testing is simplified. Testing can take place without interfering with other central office activities.

Fiber Management Requirements

Bell-Northern Research translated the network requirements into the following basic requirements for a fiber management system:

1. high termination density
2. termination and splicing integration
3. single-sided front access
4. multiple applications
5. patch cord and cable management
6. future technology compatibility

High Termination Density

Future networks with large fiber counts require high termination density. Since connector density affects the number of bays required, a high bay density decreases overall patch cord length and the need for interbay patch cords. A high termination density saves floor space, providing more placement options for the system, thereby reducing facility costs.

Termination and Splicing Integration

To achieve high density, termination and splicing integration is required. This simplifies installation, lowers costs, and places the splice with the connector. Connector splice and fiber slack can all be contained and protected within a single unit.

Single-Sided Front Access

Single-sided front access is required for small and large central offices, huts, CEVs and customer premise applications. Single-sided front access simplifies planning, installation, and operation.

Multiple Applications

A fiber management system must address a variety of applications including interconnect and cross connect. This minimizes the cost of inventory, training, and engineering, and simplifies standardization. The system must accept various connector types for both single-mode and multimode fiber.

Patch Cord and Cable Management

Controlled routing and separation of cables and patch cords is required. Controlled routing ensures proper bend radius and prevents entanglement. Separation of cables and patch cords provides easy identification and access.

Future Technology Compatibility

A fiber management system must be reconfigureable to meet changing technologies, without changing the overall concept of fiber management. The system must be capable of accommodating connectors, WDMs, splitters, and attenuators, as they evolve.

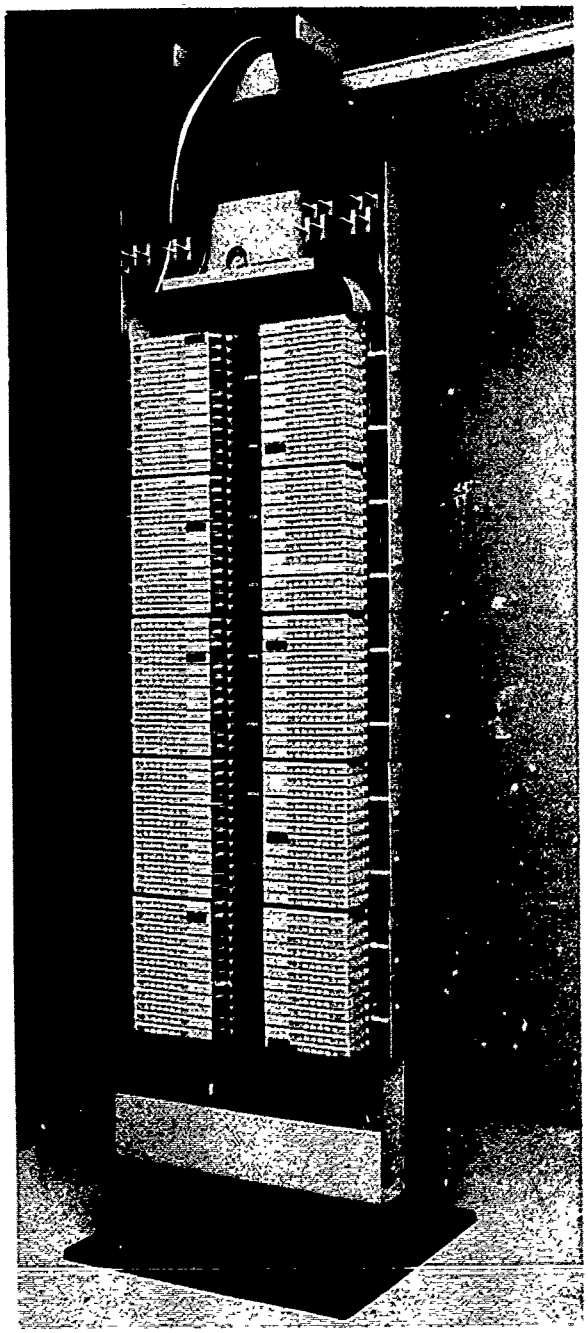

Figure 1 Fiber Management System fully equipped and configured for cross connect

System Solution

Bell-Northern Research in conjunction with Northern Telecom designed the Fiber Management System, to meet these network and fiber management requirements in a variety of applications.

The Fiber Management System consists of a frame, cable panels, shelves, and connector blocks, as shown in Figure 1.

.e and Shelves

The Fiber Management System frame and shelves are uniquely arranged in two columns, to separate cables from patch cords. Outside plant is terminated on one column and equipment is terminated on the other. Cables run in channels along the outer edges of the frame, and patch cords are contained within the center of the frame. To make an interconnection, patch cords are placed vertically in the center channel between the two columns.

The single-sided frame is 7 feet high and meets NEBS standards for a 23-inch wide frame.

The frame can be configured for either cross connect or interconnect by changing the cable panel at the top of the frame. The frame shown in Figure 1 is configured for cross connect.

The cable panel is used for routing cable to and from the frame, and provides strain relief and bonding.

The transition shelf at the bottom of the frame protects and provides space for interbay patch cords.

The frame has the capacity for 5 shelves each containing 24 connector blocks. Each shelf has cable guides and guides for controlling the bend radius of the patch cords.

The Fiber Management System has the capacity to terminate up to 960 fibers on *ST-type connectors. There are 480 fibers terminated on one column and 480 on the other.

Multiple frames can be used in a lineup to accommodate large offices.

Connector Blocks

The Fiber Management System connector blocks integrate the connectors, splices, and slack fiber into one assembly, as shown in Figure 2. This integration provides the high port density and visual relationship of the connector and splice for circuit tracing and testing.

The splice pack holder inside a connector block holds and protects up to eight fiber splices. Storage is provided for incoming fibers and connector pigtails, while maintaining bend radius control.

The connector sleeve couplers are mounted in individual, snap-in, plastic adaptors. These adaptors can be customized to accommodate a variety of connector types.

* ST is a trademark of American Telephone and Telegraph.

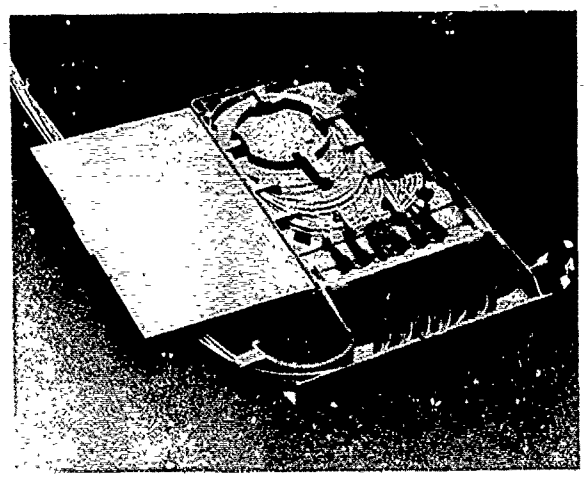

Figure 2 Top view of a connector block with the protective cover open

A drop handle at the front of the connector block provides protection to the patch cord connectors. Guides in the drop handle provide bend radius control for the individual patch cords. A guide is also provided to control bend radius where the patch cords exit the connector block. There is space at the front of the drop handle for fiber identification labels. These can be color coded for identifying outside plant appearances and various equipment types.

Figure 3 shows a bottom view of a connector block fiber guard and storage area. Under the fiber guard, which snaps open, a storage compartment allows two turns of tubed fiber to be wrapped around a spool. The two turns that remain in the block during operation provide sufficient slack for the connector block to be extended for patch cord attachment and maintenance.

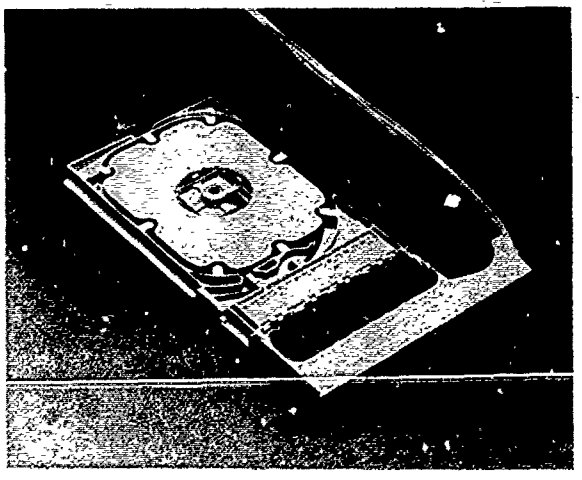

Figure 3 Bottom view of a connector block and fiber guard

The blocks are mounted in the shelf on guides. Figure 4 shows a connector block extended with the drop handle down and a connector being accessed. Clearly shown is the protection provided to the connectors by the drop handle, and the ample space provided for designation.

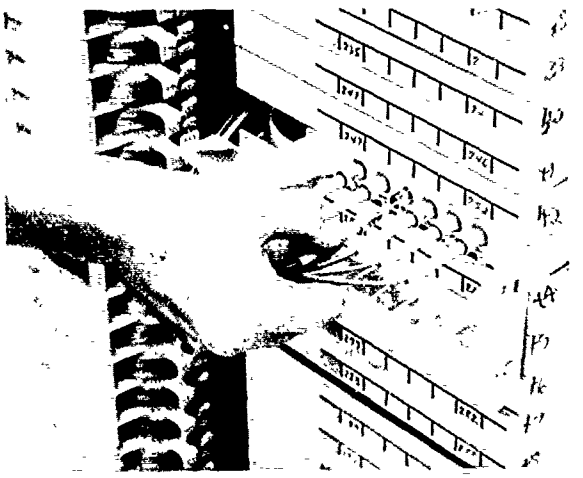

Figure 4 An extended connector block with the drop handle down

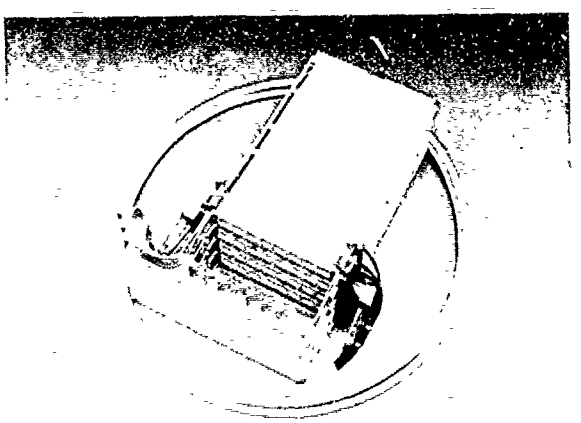

Figure 5 A factory stubbed connector block and cable

For most telco applications, six connectors are used in each connector block. To simplify installation, groups of four blocks can be factory stubbed with a 24–fiber inbuilding cable, as shown in Figure 5.

The stubbed assembly, partially inserted in the shelf, as shown in Figure 6, is temporarily supported for shipping and handling, by molded plastic brackets. Once inserted in the shelf, these brackets are removed and the stubbed cable routed up the side of the frame to the cable vault for splicing to the outside plant.

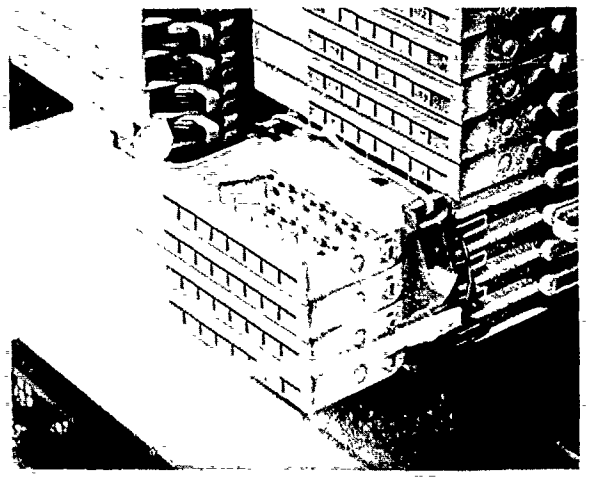

Figure 6 Installation of a stubbed connector block

Testing

The Fiber Management System has undergone extensive testing and evaluation at BNR with operating craftsmen. The absolute insertion loss through the system, when configured as a cross connect, averages less than 0.9 dB (2 connectors and 2 splices). Therefore, the Fiber Management System does not contribute to the overall loss. When the blocks are partially withdrawn from a shelf for accessing the connectors, and returned to the closed position, the average change in insertion loss is 0.05 dB with the maximum change under 0.3 dB. In the normal operation of placing, tracing, and removing patch cords, tensile loads of 3 pounds or less could be applied to a cord. To demonstrate the superior patch cord guidance through the system, loads up to 10 pounds were applied, and the loss did not increase by more than 0.5 dB. When the loads were removed, the loss returned to its original value.

Summary

Future fiber networks require solutions that do not apply today. At the present rate of fiber evolution, there is an obvious need for effective fiber management.

The Fiber Management System is designed to address this evolution by providing high density in a single-sided frame that effectively manages the cables and patch cords in many applications. The connector blocks can be easily adapted to meet a variety of needs. Extensive testing and evaluation have proven the effectiveness of this system.

George Debortoli graduated from the Eastern Ontario Institute of Technology, in mechanical engineering. Since joining BNR in 1964, he has been involved in the design and development of numerous telecommunications products, including transmission systems packaging, outside plant hardware and connection systems, and central office protection and termination hardware. George is currently responsible for the design of optical connection systems within the Outside Plant and Business Systems Connection Development group at BNR.

Laurence Beaulieu graduated from the University of Manitoba with a B.Sc. in mechanical engineering in 1978 and an M.B.A. in 1983. Laurence has worked in the Outside Plant and Business Systems Connection Development group since joining BNR in 1983. He has been involved in the design and development of systems and products for both copper and fiber based telco networks and customer premise networks. He is currently project leader for Fiber Hardware Systems Planning and Engineering in the central office and outside plant networks.

Brian Osborne graduated as a mechanical engineering technologist from the Eastern Ontario Institute of Technology in 1962. He joined BNR in 1966 and for the past 24 years has been involved in the design and development of outside plant hardware and cross-connection systems. Brian is currently the manager of Outside Plant and Business Systems Connection Development at BNR.

Lorne Brown graduated from the University of Alberta with a B.Sc. in mechanical engineering in 1987. He has been in the Outside Plant and Business Systems Connection Development group since joining BNR in 1987. Lorne has been involved in the research and development of copper and fiber connection systems. He is currently involved in the evaluation and testing of optical connection systems at BNR.

Acknowledgements

The authors wish to thank W. Eisele, J. Desjardins, R. Kurita, H. Lukas, and B. Carty for their assistance on this project and the preparation of this paper.

HIGH RETURN LOSS AND LOW INSERTION LOSS MULTIFIBER CONNECTOR WITH POLYMERIC FILM

Y. Tamaki H. Yokosuka H. Hosoya M. Hayashi

Opt-Electronics Laboratory Fujikura Ltd.
1440, Mutsuzaki, Sakura-shi, Chiba, 285, Japan

Abstract

The multifiber connector is usually used with refractive index matching gel between the mating interface to get high return loss and low insertion loss. But it is not easy to put the gel on the ferrule end face in the manhole and it is sometimes difficult to get stable connection when it is disjoined and rejoined often. This paper describes a newly developed a multi-fiber connector with high return loss and low insertion loss by applying polymeric film on the mating face.

1. Introduction

Since fiber optic cable have been introduced into telecommunication subscriber networks, the number of the fibers in a cable has increased every year. A 1000-fiber cable which is composed of 4-fiber or 8-fiber ribbons, has been developed and introduced into the networks in Japan. In order to splice or measure the large fiber count cable, a fiber ribbon connector is widely used both in the field and the building. In general, the fiber ribbon is spliced by the ribbon connector using refractive index matching gel to optimize return loss and insertion loss performance. The index matching gel is sometimes inconvenient to repeat disjoining and rejoining, and to be used where air is not clean or where it has wide temperature change.

The 8-fiber ribbon connector with the film has demonstrated excellent optical properties in various reliability tests. The return loss during a 30,000 times repeatability test of one to more than 100 8-fiber connectors, is larger than 30dB and mean value is 38dB. The insertion loss of the connector in the test is 0.25dB. The insertion loss of variation during the -10 to 60 °C temperature and high humidity test of 90%RH at 70 °C, was less than 0.1dB. Furthermore it was proved that the connector can be used with both 1.3 and 1.5μm wavelength, with same high return loss and low insertion loss performance.

2. Anti-reflection Film

Several types of anti-reflection films have been reported. The film for optical connectors should satisfy the following conditions.

1). Has an low attenuation loss within the applicable wavelength range.
2). Has a refractive index which is equal to that of optical fibers.
3). Can be formed in the film thickness 20 micron or less.
4). Has an appropriate elasticity.
5). Does not adversely affect the plug end face when being connected.

The materials which satisfy the above conditions may be in the form of film or liquid before they are processed. We selected and studied materials in film form as their thickness can be easily controlled, they are easily attached on a plug end face at low temperature and can be attached in a short time.

The properties of the selected material are shown in Table 1.

Table 1 PROPERTIES OF THE POLYMERIC FILME

ITEM	DATA
REFRACTIVE INDEX	1.48 ~ 1.50
YOUNG MODULUS	0.1kg/mm^2
TRANSMISSIVITY	99 %

3. Sample Structure

As the sample optical connector, we used an 8-fiber optical connector which is widely used for connecting single-mode ribbon fibers.(1) The connector is composed of a plastic ferrule, a rubber boot, two alignment pins and a plate spring. The ferrule comprises a pair of holes in which the alignment pins are inserted, and 8-micro-holes which are precisely positioned in order to receive ribbon fibers therein. The ferrule is made of thermosetting plastic and molded by precision transfer molding process.

The optical fibers used are standard single mode fibers of 1.3 μm wavelength. Figure 1 shows the structure of a connector.

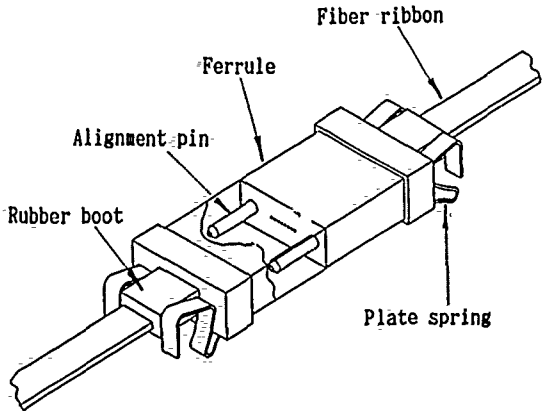

Fig.1 FIBER-RIBBON CONNECTOR

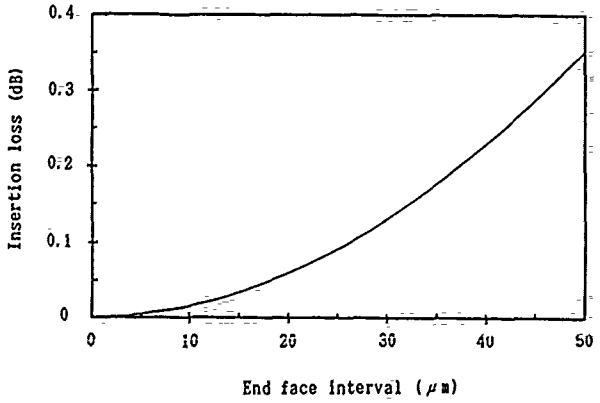

Fig.2 INSERTION LOSS vs ENDFACE INTERVAL

The anti-reflection film was first fixed on a polish-finished plastic connector end face, and then cut into prescribed dimensions for attachment. We determined the film thickness to be less than 20 μm in consideration of the relation between the end face interval and the insertion loss as shown in Fig. 2.

Figure. 3 indicates the plug structure with the anti-reflection film which attaches on an end face.

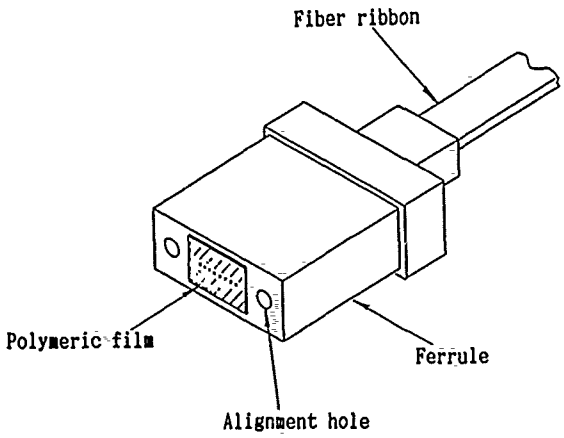

Fig.3 PLUG STRUCTURE

4. Result

The pressure on the connector end face applied by the clip was set at 1.0 kg for evaluation to simulate conditions of a normal operation.

The anti-reflection film was attached only on the end face of a master plug for evaluation. The identical samples were prepared in two ways for comparison ; one by connecting with conventional refractive index matching gel and the other by connecting with the anti-reflection film. The insertion loss of the both samples were then measured by means of a 1.3 μm LED light source. Fig. 4 shows the result of the measurement of insertion loss.

The mean insertion loss was respectively 0.2 dB and 0.24 dB for the connection with the index matching gel and with the anti-reflection film. The result shows that the anti-reflection film does not deteriorate the insertion loss which is comparable to the index matching gel.

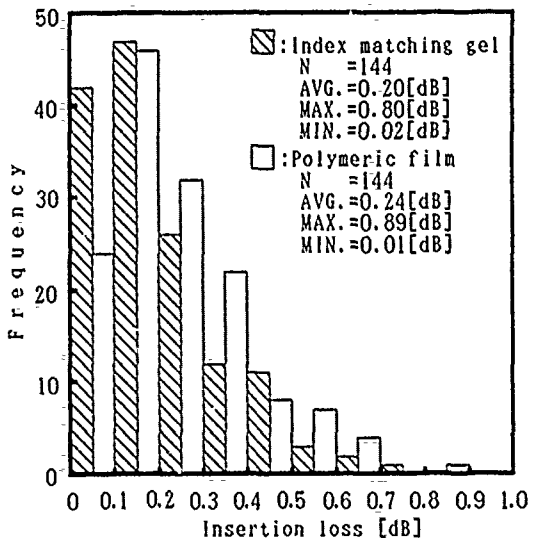

Fig.4 INSERTION LOSS

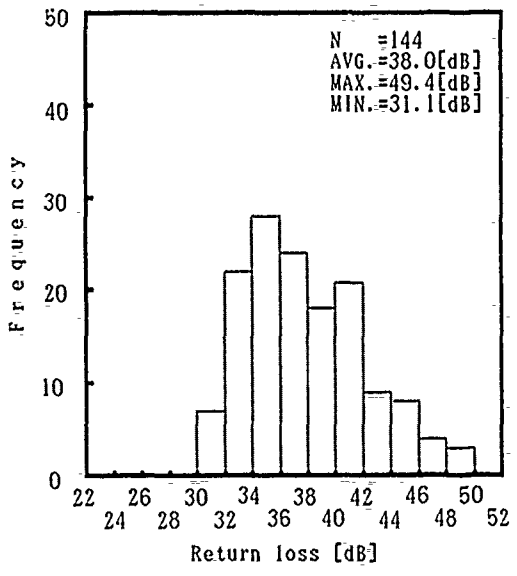

Fig.5 RETURN LOSS

The return loss was measured by a optical return loss measuring set (measured wavelength : 1.3 μm). Fig. 5 shows the result of measurement of return loss. The film sample showed excellent result at 30 dB or higher with the average at 38.0 dB. The loss variation at the temperature cycle test from -10°C to +60°C and the high-temperature and high-humidity test at 70°C and 90%RH remained favorably as low as at 0.1 dB or lower.

No abnormalities such as peeling off was observed after 20 cycles of the temperature cycle test and after 100 hours of the high-temperature, high-humidity test.

The samples were subjected to repeated attachment/detachment tests for 30,000 times while the insertion and return losses were continuously measured in order to test the mechanical durability of the film. Fig. 6 shows the result of the test. The film samples showed extremely stable properties throughout the tests. No irregularity was observed in the state of the film after the evaluation tests.

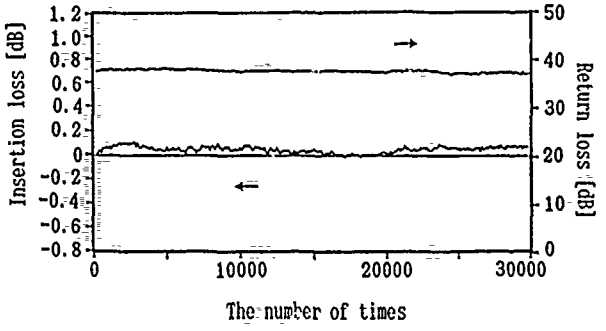

Fig.6 REPEATABILITY TEST

5. Conclusion

We performed a study on the anti-reflection film which can be attached on the connection interfaces of optical connectors and which can be repeatedly attached/detached without any optical degradations. We realized a thin film which achieved low insertion loss and high return loss comparable to the index matching gel. We manufactured on trial basis an 8-fiber optical connector with the proposed thin film, and the connector demonstrated excellent properties with 30 dB or higher return losses and on average 0.24 dB insertion losses. It was confirmed that the anti-reflection film was applicable to multi-fiber ribbon connectors.

References

(1) S. Nagasawa et al., "MECHANICALLY TRANSFERABLE MULTIFIBER CONNECTORS" IOOC '89, paper 21c2-1,1989

Yasuhiro Tamaki

Opt-Electronics
Laboratory
FUJIKURA LTD.

1440,Mutsuzaki,
Sakura-shi,Chiba,285
Japan

Yasuhiro Tamaki was born in 1955. He received the B.E. degree in mechanical engineering in 1977 from Saitama University.

He joined Fujikura Ltd. in 1982 and has been engaged in research and development of telecomunication cables and accessories.

Mr. Tamaki is member of the Institute of Electronics and Communication Engineers of Japan.

Hideyuki Hosoya

Opt-Electronics
Laboratory
FUJIKURA LTD.

1440,Mutsuzaki,
Sakura-shi,Chiba,285
Japan

Hideyuki Hosoya was born in 1959. He received the M.Sc. degree in physics from Yamagata University in 1983. He joined Fujikura Ltd. in 1983 and has been egaged in research and development of telecomunication cables and accessories. He is a member of the Institute of Electronics, information and communication Engineers of Japan.

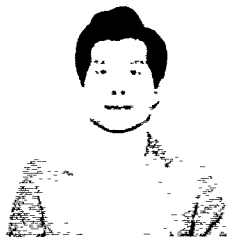

Hiroshi Yokosuka

Opt-Electronics
Laboratory
FUJIKURA LTD.

1440,Mutsuzaki,
Sakura-shi,Chiba,285
Japan

Hiroshi Yokosuka graduated in mechanical engineering from Tokyo Metropolitan Technical Junior College in 1967.

He has been engaged in development of telecommunication cables and accessories. He is now a Manager of the Fiber and Cable Accessory Department in Opt-Electronics Laboratory of Fujikura Ltd.

Mr. Yokosuka is a member of the Institute of Electronics and Communication Engineers of Japan.

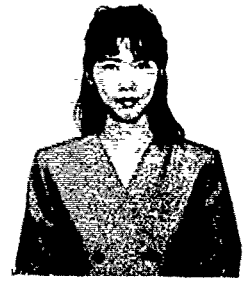

Mariko Hayashi

Opt-Electronics
Laboratory
FUJIKURA LTD.

1440,Mutsuzaki,
Sakura-shi,Chiba,285
Japan

Mariko Hayashi was born in 1965. She received the B.E. degree in industrial chemistry in 1988 from Nihon University.

She joined Fujikura Ltd.in 1988 and has been engaged in research and development of telecomunication cables and acesories.

Miss Hayashi is a member of the Institute of Electronics and Communication Engineers of Japan.

FIELD EVALUATION RESULT OF HERMETICALLY COATED OPTICAL FIBER CABLES FOR PRACTICAL APPLICATION

Yutaka KATSUYAMA, Nobuyuki YOSHIZAWA, and Takamasa YASHIRO

NTT Transmission Systems Laboratories,
Tokai-Mura, Naka-Gun, Ibaraki-Ken, 319-11 JAPAN

ABSTRACT

A field test was carried out for evaluating total performance of hermetically coated fibers (HCFs). Three cables containing a large volume of HCFs and non-hermetically coated fibers (NHCFs) were manufactured and installed in duct and aerial routes. The characteristics of the 2 types of fibers were examined and compared. The field test result clarified that the cable installation and splicing were satisfactory in the field, although the hermetic coating might prevent fiber core monitoring and local detection. The total performance of HCFs was found to be excellent; the long-term reliability is much better, and the construction is comparable to the NHCFs. In conclusion it is possible to put the HCFs into practical use and HCF is promising to construct maintenance-free optical network.

I. Introduction

Hermetically coated optical fibers are expected to provide highly reliable optical networks, because of their high resistance to both static fatigue and optical loss increase due to hydrogen diffusion [1],[2],[3]. Many approaches to improving the resistance were tried, and amorphous carbon coating was found to be promising.

A large n-value (fatigue resistance parameter) of hermetically coated fibers has already been attained, while maintaining the resistance to hydrogen-induced optical loss. However, initial strength of hermetically coated fiber was about 20 % lower than that of non-hermetic fibers [2],[3]. We proposed high-strength hermetically coated fibers with small roughness of carbon coating [4]. This provided the hermetically coated fibers whose initial strength was as large as the non-hermetic fibers, getting rid of the big problem of the conventional hermetically coated fibers. Our next approach is to clarify the performance of large volume of the hermetically coated fibers in the field. Efficient splicing and local monitoring should also be examined

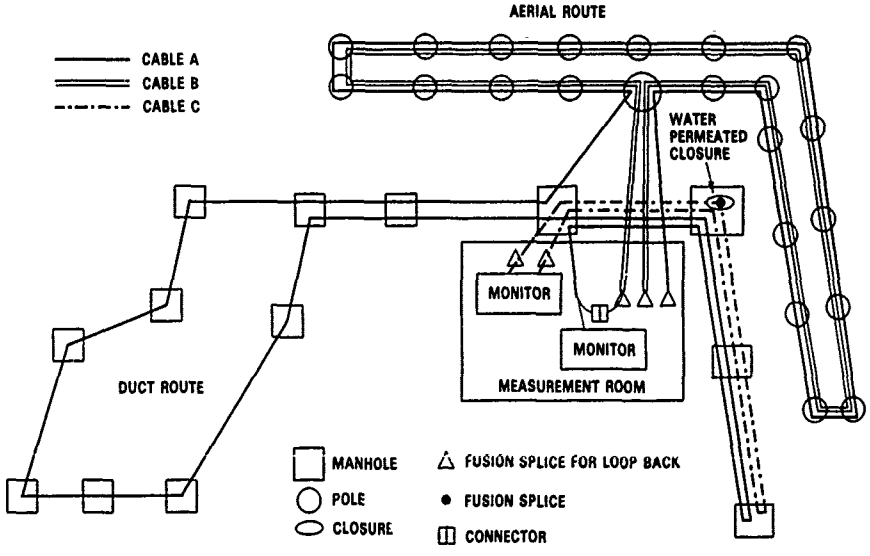

Fig.1 FIELD TRIAL ROUTE

before the practical application. Thus, we carried out a field trial.

In this paper, the total performance of long cables containing the hermetically coated fibers is presented, which was examined and obtained in the field trial.

II. Outline of Field Trial of Hermetically Coated Optical Fiber Cables

(1). Field Trial Configuration

Figure 1 shows field trial routes. Three optical cables A, B and C were installed in duct and aerial routes. The cable A line was constructed by connecting both the duct and aerial routes, the cable B line by just the aerial route, and the cable C line by just the duct route. The main parameters of the 3 cables are listed in Table 1.

Table 1 Optical Cables for the Field Trial.

Item			cable A	cable B	cable C
Cable Length (km)			2.76	2.86	0.53
Outer Dia.(mm)			17.5	16	17
Strength Member			Steel	Steel	Kevlar®
Fiber Number	Total		128	120	100
	DS SM	HC	24	22	25
		NHC	72	66	25
	N SM	HC	24	8	25
		NHC	8	24	25

The ends of cables A and B were terminated inside a measurement room, and the fibers were spliced to obtain 4 dispersion-shifted single-mode (DS SM) fiber links (130 km each; 1.55 μm use), and 4 normal single-mode (N SM) fiber links (45 km each; 1.3 μm use), including both hermetically coated (HC) fibers and non-hermetically coated (NHC) fibers. Additional links were constructed by cable C in the same way as for cables A and B. In a manhole of the cable C line, the fibers in cable C were cut and re-spliced, followed by protected with a closure, as shown in Fig. 1. Water was permeated intentionally into the closure to evaluate the optical loss stability of the cable C links.

The optical loss of the cables and the splice loss were measured to obtain the statistical data. Total length of the cables was 6.15 km. Total lengths of the installed hermetic and non-hermetic fibers were about 250 and 500 km, respectively.

(2). Mechanical Characteristics of the Field Trial Cables

The cross-section of cable B is shown in Fig. 2 as a typical example of the 3 cables. The optical fibers were drawn and coated with carbon layer in CVD process, followed by UV-curable resin coating (0.25mm dia.). The installed cables were 4-fiber-ribbon/slotted-rod type designed for water-blocking performance [5]. Five ribbons are accommodated in a slot. Cables A and B contain an interstitial pair for monitoring.

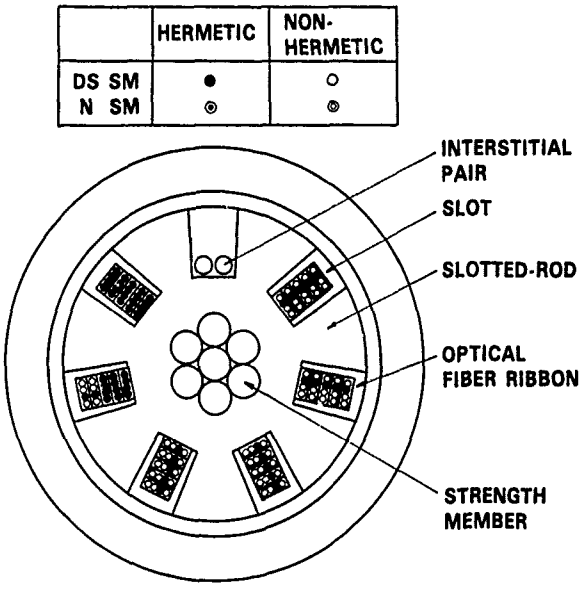

Fig. 2 CROSS-SECTION OF CABLE B

Table 2 Tensile strength measurement conditions.

Item	Condition
Gauge Length (mm)	300
Strain Rate (%/min.)	20

The strength distributions of the fibers in the cable were evaluated. A 30-m long piece was cut from an end of cable A, and the optical fibers were extracted from the cable piece. Twenty pieces of measurement samples were obtained from each fiber, and the tensile strength of each sample was measured under the condition listed in Table 2. Thus, 20 strength values were obtained, giving a median strength of the fiber. The same measurement was repeated for 50 hermetically coated fibers and 48 non-hermetically coated fibers. The histogram of the median strength distribution is shown in Fig. 3. The average values of

the median strengths were almost identical each other for both hermetically coated and non-hermetical. · coated fibers.

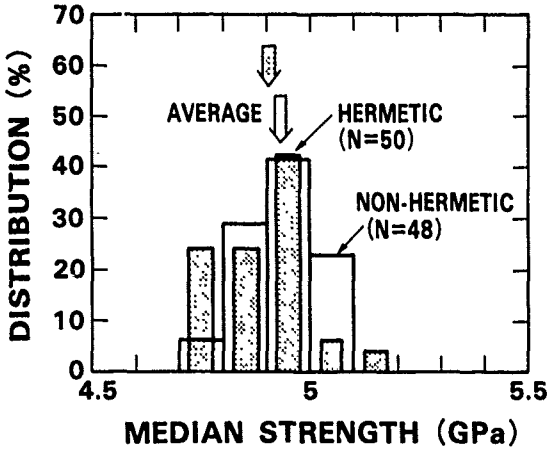

Fig. 3 STRENGTH DISTRIBUTION

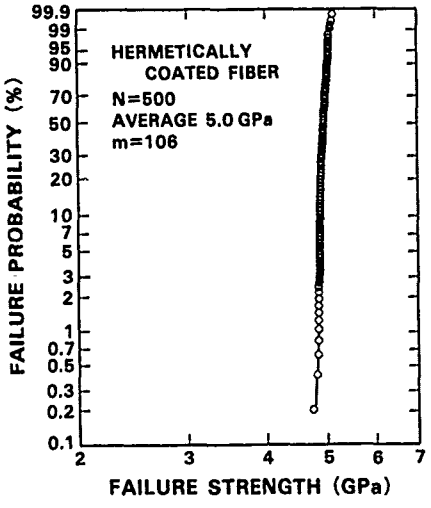

Fig. 4 WEIBULL PLOTS OF STRENGTH

Figure 4 shows the strength distribution plotted in a Weibull probability chart. Five hundred strength values were plotted in Fig. 4 for the hermetic fibers, including both DS SM and N SM fibers. It is found that the distribution can be represented by one straight line, and no weak portion was observed. This clarified that the hermetically coated fibers have uniform strength distribution even in different fibers obtained from the cable end.

The fatigue parameter n was measured for the hermetically coated fiber. The strain rate dependence of median strength, given by 10 measurements at each strain rate for one fiber, allowed to determine n-value. Figure 5 shows the histogram of n-value obtained for 25 fibers. The measured n-value of the hermetically coated fibers was larger than 200, which is 10 times as large as that of non-hermetically coated fibers. The average n-value was 340.

Figure 6 shows the strain rate dependence of the tensile strength σ_d measured for the 25 fibers. It is clear that the strength is almost independent of strain rate, indicating very high n-value.

III. Field Evaluation Results

(1). Optical Loss Changes due to Installation

The optical cables A, B and C were installed, and the optical losses were measured before and after the

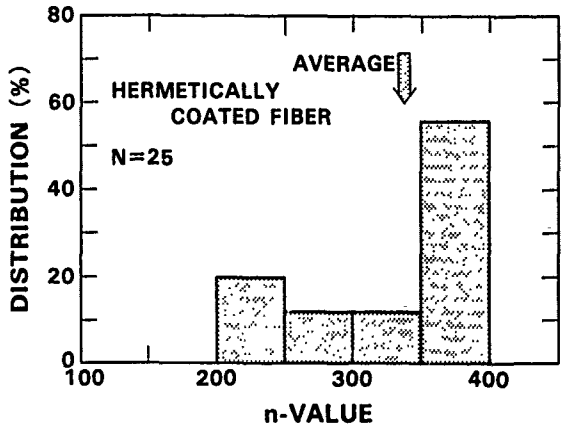

Fig. 5 MEASURED n-VALUE FOR HC FIBER

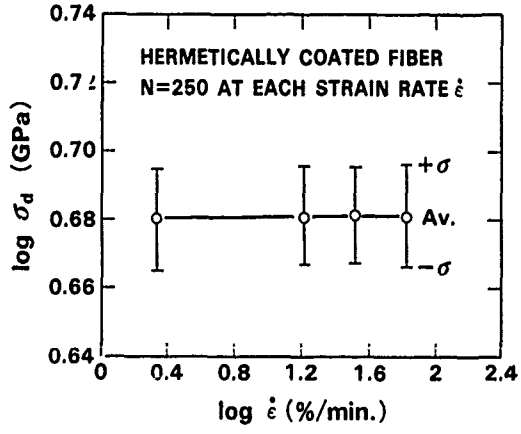

Fig.6 DYNAMIC FATIGUE TEST

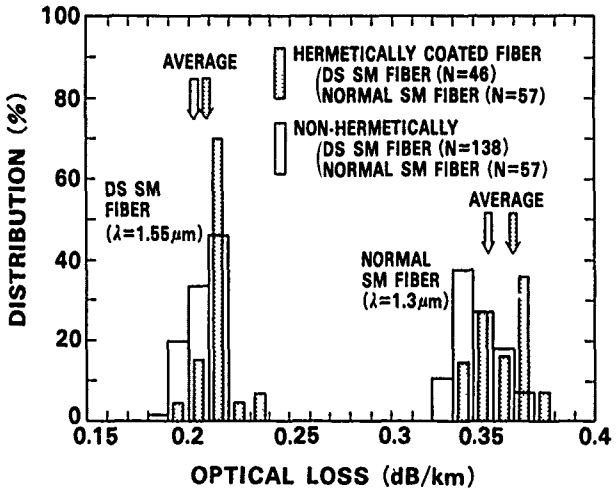

FIG.7 OPTICAL LOSS OF THE CABLES

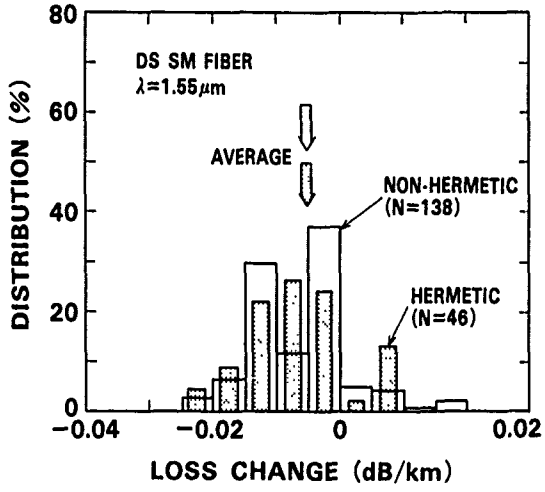

Fig.8 (b) OPTICAL LOSS CHANGE DUE TO INSTALLATION

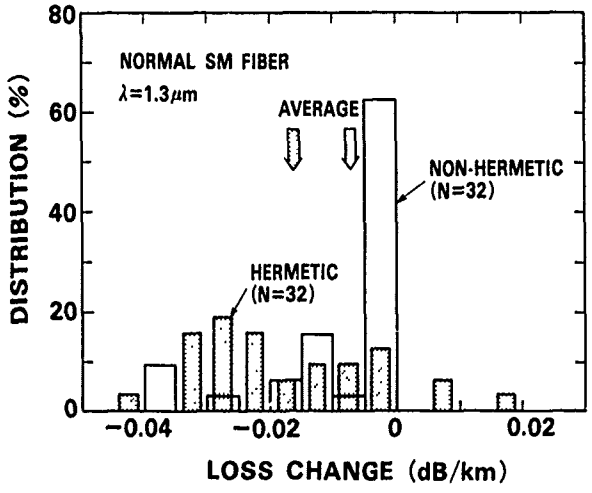

Fig.8 (a) OPTICAL LOSS CHANGE DUE TO INSTALLATION

installation. The installation was conducted by the ordinary pulling method. Figure 7 shows the measured optical loss of the cables before installation. It is found that the optical losses are almost identical. However, the average optical losses of hermetic fibers are about 3 % larger than those of non-hermetic fibers both at 1.3 and 1.55 μm. This may be because the drawing conditions for the hermetic fibers are different from those for non-hermetic fibers, caused by the CVD process for the carbon coating.

Figures 8 (a) and (b) show the optical loss changes of cables A and B due to installation. The optical losses of the installed cables were measured with OTDR, and the difference between the values before and after the installation was plotted in Fig. 8. The average changes are within 0.02 dB/km, and no significant differences are found between hermetic and non-hermetic fibers.

(2). Splice Experiment and Local Detection for Fiber Identification

After the cable installations, 484 splices were carried out with the existing fusion splicers. The hermetic fibers can be spliced successfully with the cleaning discharge method [6], which enables to remove the carbon layer simply and effectively. Figures 9 and 10 show the single-splice loss and mass-splice loss distributions for DS SM and N SM fibers, respectively. The splice losses were also measured with OTDR by launching optical power at the both ends successively, obtaining 2 values at each splice point, and averaging the value to determine the splice loss. It is found that the splice losses for hermetic fibers are identical to those for non-hermetic fibers. The average splice losses were 0.043 and 0.051 dB (N SM fiber), and 0.050 and 0.046 dB (DS SM fiber) for hermetic fibers and non-hermetic fibers, respectively, which verify the low-loss splices of the hermetic fibers.

Figure 11 shows measured mass-splice loss as a parameter of the environments (indoor or in the manhole). No significant difference was found between the splice losses obtained indoor and in manhole. It is also found that the standard deviation σ of the splice loss is small for the hermetic fibers rather than non-hermetic fibers. This suggests that no significant problem existed in the mass-fusion splice of the hermetic fibers, though the cleaning discharge was necessary.

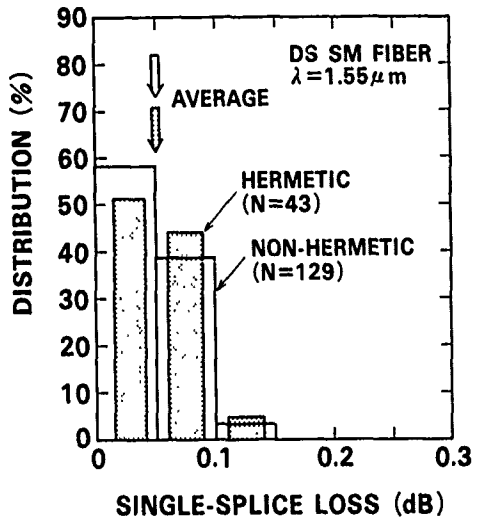

Fig. 9 SINGLE-SPLICE EXPERIMENT

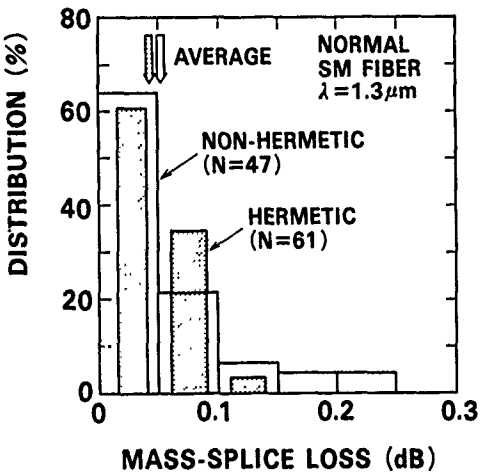

Fig.10 MASS-SPLICE EXPERIMENT

In the splice, fiber number identification was made by the local detector, which allowed to detect optical power by bending the fiber. The relative received power was measured with changing optical loss, which is equivalent to the fiber length from optical launching point. The result is shown in Fig. 12. The received power for the hermetic fibers is 5.5 dB smaller than that for non-hermetic fibers. Nevertheless a dynamic range of 20 dB was obtained for the hermetic fibers in the field.

(3). Optical Loss of the Links

After the installations and splices were completed, eight optical links were obtained. The links were constructed so as to have four types of combination by selecting hermetically coated (HC) or non-

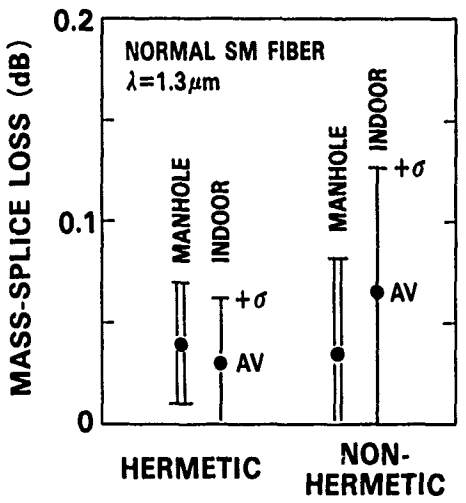

Fig.11 MASS-SPLICE EXPERIMENT

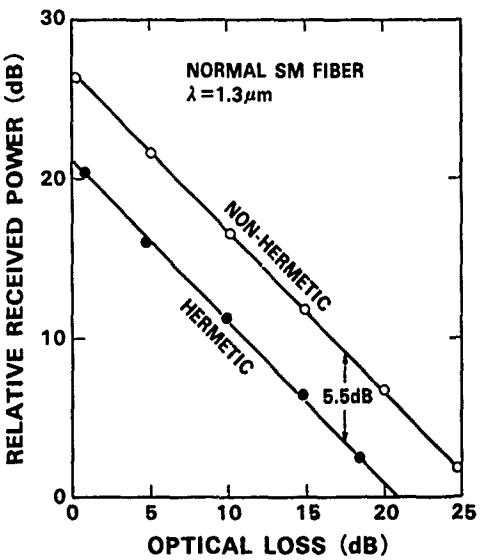

Fig.12 RECEIVED POWER IN LOCAL DETECTION

hermetically coated (NHC) fibers, and dispersion-shifted single-mode (DS SM) or normal single-mode (N SM) fibers. The optical losses are summarized in Table 3. The optical loss of the hermetic fibers was about 5 % larger than that of non-hermetic fibers, resulting mainly from the fiber loss.

The spectral loss was measured for the links with a monochrometer. Typical example of measured spectral loss of the hermetic link is shown in Fig. 13, including the splice losses. The loss was also measured with OTDR at 1.3 μm, and this coincided

Table 3 Measured Optical Loss

Link	Fiber	Joining		Optical Loss (dB/km)
	Length (km)	Number/ Link	Average Loss (dB/point)	
HC/DS	129.1	Splice 45 Conn-ector 1	0.065	0.24
NHC/DS1			0.066	0.23
NHC/DS2			0.072	0.23
NHC/DS3			0.050	0.23
HC/N	44.9	Splice 16	0.069	0.38
NHC/N1			0.054	0.36
NHC/N2			0.044	0.36
NHC/N3			0.040	0.35

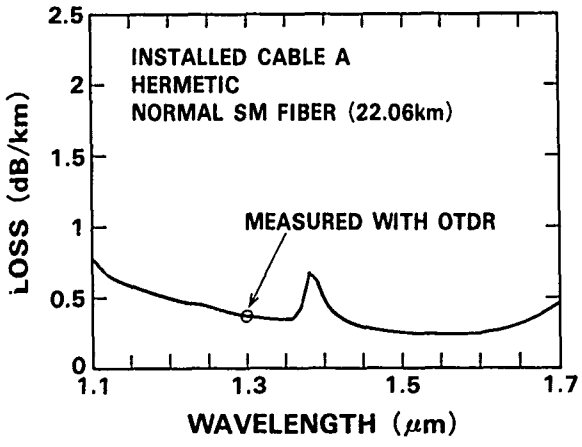

Fig.13 OPTICAL LOSS

with that measured with the monochrometer. Lower-loss regions than 0.5 dB/km are obtained around 1.3 μm and 1.55μm, as shown in Fig 13.

(4). Optical Loss Stability

Water was permeated intentionally into the closure in the cable C line, as shown in Fig.1, and the optical losses of the links were measured 7, 21, 49, and 80 days after the permeation. No significant loss increase was observed for the data obtained within 49 days. The optical loss of the non-hermetic fiber link was about several tenths larger than initial value at 1.39 μm after 80 days. However, the loss of the hermetic link was stable even after 80 days. The long-term stability of the optical loss will continue to be evaluated for all the links of cables A and B, as well as cable C

IV. Conclusion

A field test was carried out for evaluating total performance of hermetic fibers. Three cables containing a large volume of hermetic and non-hermetic fibers were manufactured, installed and examined. The hermetically coated fiber cables were found to have much higher fatigue resistance and much higher stability of optical loss than conventional fiber cables, and equivalent transmission characteristics and splice efficiency in the field. It concludes that this technology can be introduced into practical networks, resulting in the construction of highly-reliable optical network.

Acknowledgment

The authors would like to express their thanks to K. Ishihara and S. Shimada for their encouragements and guidance.

References

[1]. R. Hiskes et. al. ,"High performance hermetic optical fibers", Tech. Digest of Optical Fiber Communication Conference, 1984, Paper WI6-1.

[2]. R. G. Huff, F. V. DiMarcello, and A. C. Hart, Jr., "Amorphous carbon hermetically coated optical fibers", Tech. Digest of Optical Fiber Communication Conference, 1988, Paper TUG-2.

[3]. K. E. Lu, M. T. Lee, D. R. Powers, and G. S. Glaesemann, "Hermetically coated optical fibers", Tech. Digest of Optical Fiber Communication Conference, 1988, Paper PD1-1.

[4]. N. Yoshizawa, and Y. Katsuyama, "High-strength carbon-coated optical fiber", Electron. Lett., vol.25, p.1429-1431, 1989.

[5]. S. Kukita, T. Nakai, A. Hayashi, and H. Koga, "A new nonmetallic and waterproof optical fiber cable with absorbent polymer ribbon", IWCS, p.357-371, 1987.

[6]. N. Yoshizawa, Y. Miyajima, and Y. Katsuyama, "A one-hundred-fiber submarine cable composed of hermetically coated fiber ribbons inserted into slots", IWCS, p.603-610, 1989.

AUTHORS

Yutaka
KATSUYAMA

NTT Transmission
Systems Labs.

He was born in Kyoto, Japan, in 1949. He received the B.S., M.S., and Ph.D. degrees in mechanical engineering, all from Kyoto University, Kyoto, Japan, in 1971, 1973 and 1981, respectively. He joined NTT Electrical Communications Labs., Ibaraki, Japan, where he has been engaged in the research and developmental work on design and characterization of optical fiber cables. Dr. Katsuyama is a senior member of the IEEE, and a member of Optical Society of America and Institute of Electronics, Information and Communication Engineers of Japan.

Takamasa
YASHIRO

NTT Transmission
Systems Labs.

He was born in Tokyo, Japan, in 1941. He received the B.S. and M.S. degrees in chemical engineering, all from Keio University, Tokyo, Japan in 1966 and 1968, respectively. He joined NTT Electrical Communications Labs., Ibaraki, Japan, where he has been engaged in the research on plastic materials for electrical insulation and optical fiber jacketing. Mr. Yashiro is a member of the Institute of Electronics, Information and Communication Engineers of Japan.

Nobuyuki
YOSHIZAWA

NTT Transmission
Systems Labs.

He was born in Tokyo, Japan, in 1954. He received the B.S., M.S., and Ph.D. degrees in mechanical engineering, all from Waseda University, Tokyo, Japan, in 1977, 1979 and 1986, respectively. He joined NTT Electrical Communications Labs., Ibaraki, Japan, where he has been engaged in the research and design of submarine optical fiber cables. Dr. Yoshizawa is a member of the IEEE, and the Institute of Electronics, Information and Communication Engineers of Japan.

Polymer Optical Fiber Cables for both Automotive and Customer Premises Application

Wolfgang Eickhoff, Helmut G. Haag, Dragan Stankovic and Peter E.Zamzow

AEG KABEL Aktiengesellschaft

Mönchengladbach, Federal Republic of Germany

Abstract

Two applications of Polymer Optical Fiber Cables are described, i.e. automotive and inhouse systems. Requirements, system designs and components are described. Characteristics of the Polymer Optical Cables developed for these applications are presented in detail.

1. Introduction

The most important characteristics of Polymer Optical Fibers (POF) are

- low attenuation
- high bandwidth
- light weight
- high flexibility
- simple mounting and interconnection techniques
- immunity against electromagnetic interference
- elimination of electromagnetic radiation
- galvanic separation
- utilisation of low cost components (LED, connector) possible in POF-systems

The field of application is broad. Here, a few practical applications shall be discussed

- automotive LAN's
- intelligent home.

The POF system and cable require concepts that are specifically suited for the different applications.

2. Automotive Application

2.1 Task Description

The number of electrical and electronical functions in the automobile is steadily increasing. The conventional cabling of these systems by point-to-point interconnections is becoming increasingly unhandy and leads to spatial constrains and unwanted weight. Thus it has to be worked on novel cabling concepts which exhibit more flexibility (reduction of number of types) and lower weight. Therefore a separation of power supply and data transmission is necessary. The data transmission system then shall have the form of a Local Area Network (LAN) as it is known e.g. for computer interconnections. Advantages of such a system are a reduced harness, improved exchange of data for better functions and ease of diagnosis /1,2/.
Optical fibers can advantageously be utilised as transmission medium to eliminate problems of electromagnetic interference from sources internal and external of the automobile (e.g. radio transmitters) /3,4,5/.

2.2 System Design Considerations

When considering possible network topologies for automotive application, those containing an active central station should be avoided for reliability reasons. Two network topologies will be discussed in the following, namely the bus with passive taps and the passive star.
The bus with passive taps is common in electrical systems; the required line length is low; the absence of active stations (in the sense of repeaters) increase the reliability; on the other hand, an interruption of the line e.g. by an accident may lead to a severe distortion of functionality.

The passive star contains a central station, which is, however, being a purely passive component, tolerable from the standpoint of reliability. The required line length is higher than in the case of a bus structure; on the other hand, an interruption of a line disconnects only one station which means high reliability.

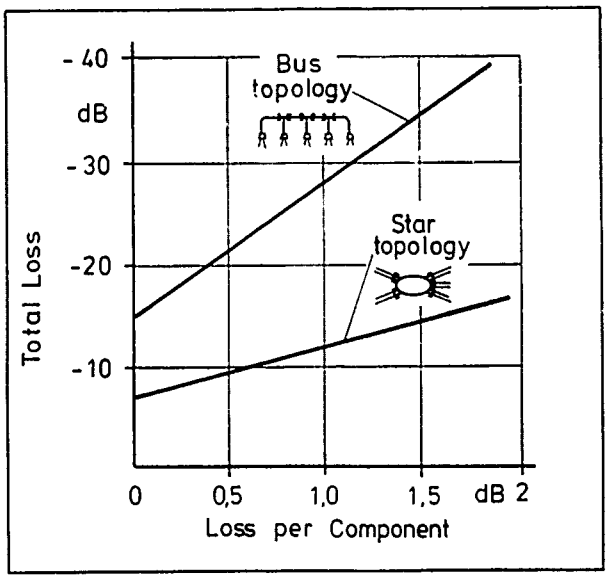

Fig.1 Design consideration for network topology

Besides the above considerations, the power budget is the most important criterion for the choice of the network topology.In Fig. 1 the maximum loss between two stations is shown in dependence of the loss of the components, i.e. connector or coupler. Fiber attenuation is not included in this diagram. It is easily seen that the star network exhibits a much better power budget than the bus network; this difference increases with the number of stations. Thus the star network is the most common network in fiber optic systems and was also adopted for our system.

2.3 Star Couplers

Two kinds of star couplers will be described in the following, namely the transmission star coupler and the multireflection star coupler.

When utilizing POFs, the transmission star coupler usually consists of a mixing rod with fibers connected to both ends (Fig. 2). A light signal coupled into the mixing rod from any of the fibers at one side is guided in the mixing rod and distributed equally over the remote side. Therefore any of the fibers coupled to that side receive an equal part of the signal. When connecting one fiber of each side of the mixing rod to every station, each station can communicate with each other. The fibers coupled to the mixing rod are densely packed to avoid losses. The advantage of this type of star coupler is its relatively low loss, the disadvantages are the use of two fibers per station and the relatively large size of the coupler due to minimum bend radii of the fibers.

The multireflection star coupler (Fig. 2) is built up similarly, only that the fibers are not densely packed and the surface between the fiber ends is reflecting. In this case a light signal emerging from any fiber is distributed to all fibers at both ends of the mixing rod. This allows the utilization of only one fiber per station, provided that a 3 dB-coupler is implemented in each station. The advantage of this type of coupler is its small size, the disadvantage is the higher system loss.
Thus the transmission star coupler should be used in trucks, where space does not pose a problem but line lengths are greater, whereas the multireflection star coupler should be used in passenger cars.

2.4 Light source, Receiver and Power Budget

LED Characteristics

As a light source we use a GaAlAs-Double-Heterostructure LED with an emission wavelength of about 650 nm. The LED is mounted in an hermetically sealed metal housing (Fig. 3) in order to achieve an operation temperature range of -40°C to +125°C which is necessary for application in automobiles. For high coupling efficiency to the POF the chip is mounted in a reflector (produced by an embossing technique) that is located in close proximity to the glass window of the housing cap. The power coupled into the POF (diam. 1 mm, NA = 0.54) is shown in Fig. 3 in dependence of temperature. These devices show no degradation over 6000 hrs when operated at 150°C and 50 mA cw.

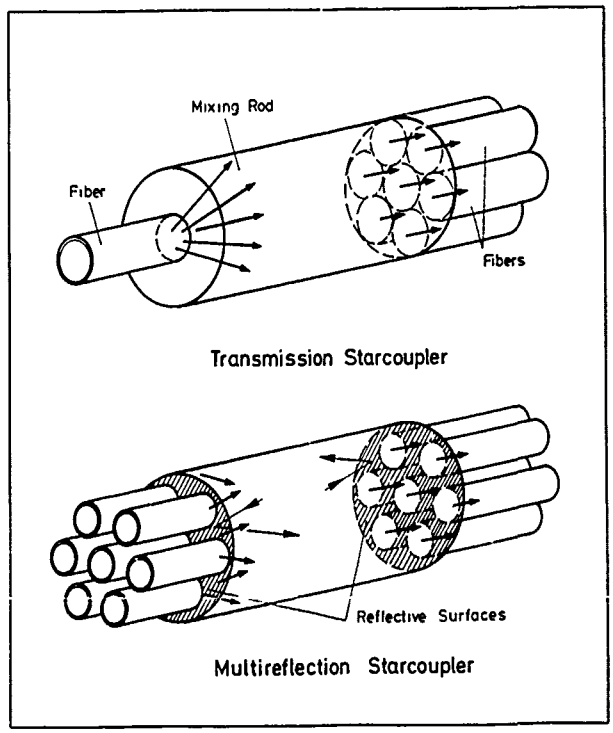

Fig. 2 Two types of star couplers

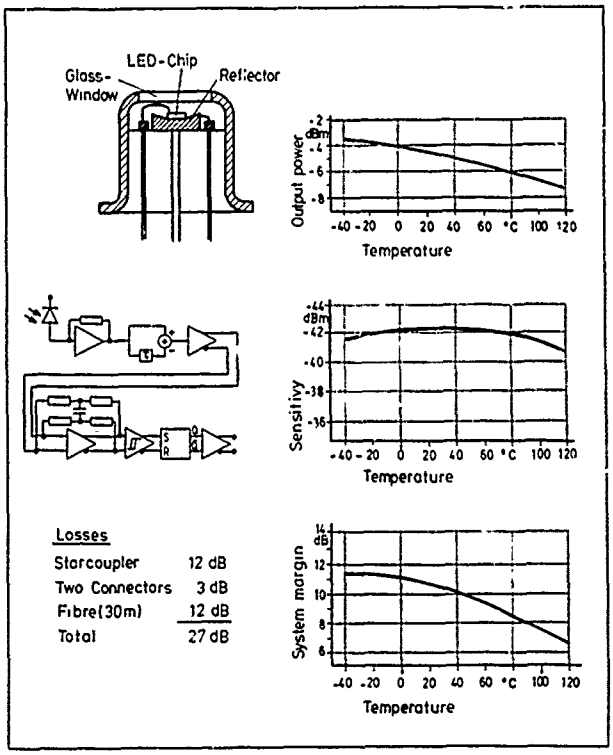

Fig. 3 Light source, receiver circuit and power budget for automotive POF systems

Receiver circuit

Another important component of an optical system is the receiver circuit. The design goals of our receiver were

- sensitivity of - 42 dBm
- operating temperature range -40°C to 125°C
- baudrate DC - 2 Mbit/s
- bit-to-bit dynamic range 20 dB

The block diagram of the receiver gate array is shown in Fig. 3. It was produced in silicon bipolar technology. Fig. 3 shows also that the design goals have been met.

Power Budget

The power budget of the whole system is also given in Fig. 3. There are three sources of loss, namely the starcoupler, the connectors (there are only two optical connectors between any two stations) and the fiber. The system was designed for a line length of 15 m, thus the maximum length between two stations is 30 m. As the operating temperature range of the fiber should be - 40°C to + 125°C, a relatively high loss of 0.4 dB/m has to be accepted. Taking into account the output power of the LED and the sensivity of the receiver as given above, one arrives at the system margin depicted on the lower part of Fig. 3. It shows that the system can be safely operated in the whole temperature range of - 40°C to + 125°C.

2.5 Polymer Optical Fiber Cables

The most important requirements for POF cables in automotive application are

- extreme temperature range - 40°C to 125°C
- small size
- high mechanical stability
- immunity against typical automotive chemicals.

These aspects lead to a requirement profile for the cables and harnesses. The next step is the definition of specifications including test procedures.
The mobile LAN may require two types of POF cables

- pure data transmission cables
- mixed data/energy transmission cables

Therefore the following POF cable types have been realized (Fig. 4)

- cable with 1 POF
- cable with 2 POF
- round hybrid cable (2 POF, 3 copper wires)
- flat hybrid cable (2 POF, 3 copper wires)

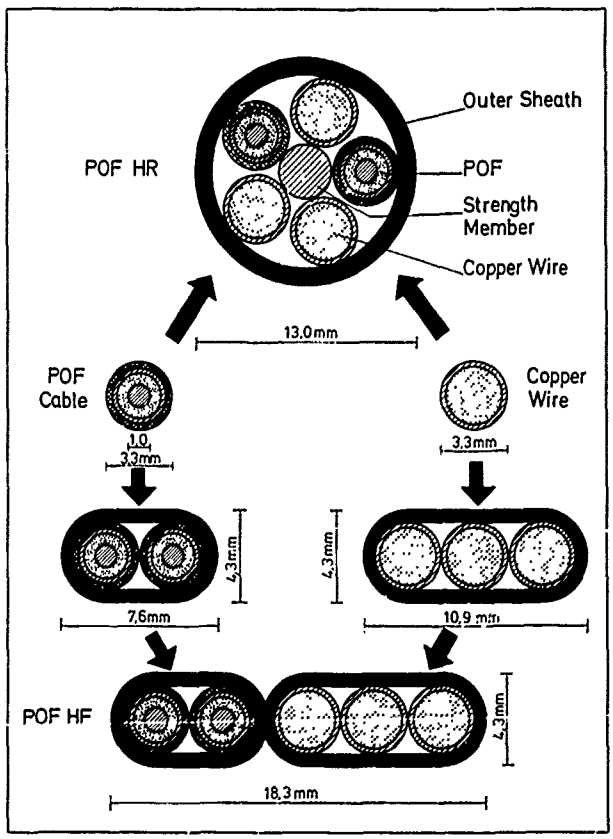

Fig. 4 Family of POF-cables with and without copper wires

The test procedures can be classified in three groups. The measurements of mechanical characteristics simulate the handling of the harness during car manufacturing and the stress during utilisation (e.g. door open, door closed). Testing the optical transmission characteristics e.g. under mechanical and temperature stress allows a judgement on functional ability. Long term tests finally judge the aspect of degradation of the cables.
The test methods and the results for the different cable types are shown in Fig. 5.

2.6 Economical Aspects

The above described developments and achieved results show that all components for an optical transmission system based on star couplers are available for practical application tests. The technical advantage is obviously. The optical system offers larger bandwidths, this means higher comfort in application, is immune again electromagnetic interference, this means no from outside induced distortion. Moreover the system is in total much smaller and lighter than the conventional copper harness. In the case of service, a star coupler system with central supervision possibilities facilitates and therefore reduces cost in trouble shooting and repair.

But as all those advantages cannot be judged quantitatively, the only way to the market is the price. Even if the connectors, transmitter, and receiver for POF are much cheaper than for silica fibers, those systems cannot reach the existing prices for copper cable harnesses. The price for those POF systems with the price of today almost reach 1000 DM were the copper system costs a 100 DM. The necessary price reduction could perhaps arise from larger quantities in other areas of application, for example "Inhouse application".

3. Inhouse Application

3.1 Task Description

The need for transmission of information in office buildings and private homes for communication and for controlling of appliances has become increasingly important during the last years.

No single wire-based media is able to support the whole range of application in the home while at the same time satisfying the additional user requirements in the areas of cost, ease of installation, etc.

The recent developments in Polymer Optical Fiber technology offers the possiblity for achieving all these user requirements in the home, except those demanding wireless operation (infra-red remote control, etc.).

Due to the high bandwidth, POF is able to transmit digital data from a very low bit rate up to several MBit/s. Also it is able to transmit audio and video signals (CD-Player, CATV, etc).

3.2 System design considerations

The topology of a home system determines the requirements for the logical and physical connections of the equipment to the network. In this chapter three network topologies to create a home system network are described and compared.

Ring Networks

Figure 6a shows a ring configuration. This type of network is the most commonly used in local area networks. Essentially, it consists of a number of simple point-to-point links with regeneration at each node, thus it is not necessary to have taps in the system. Due to the unidirectionality of the regenerators the information flows in a single direction around the ring.

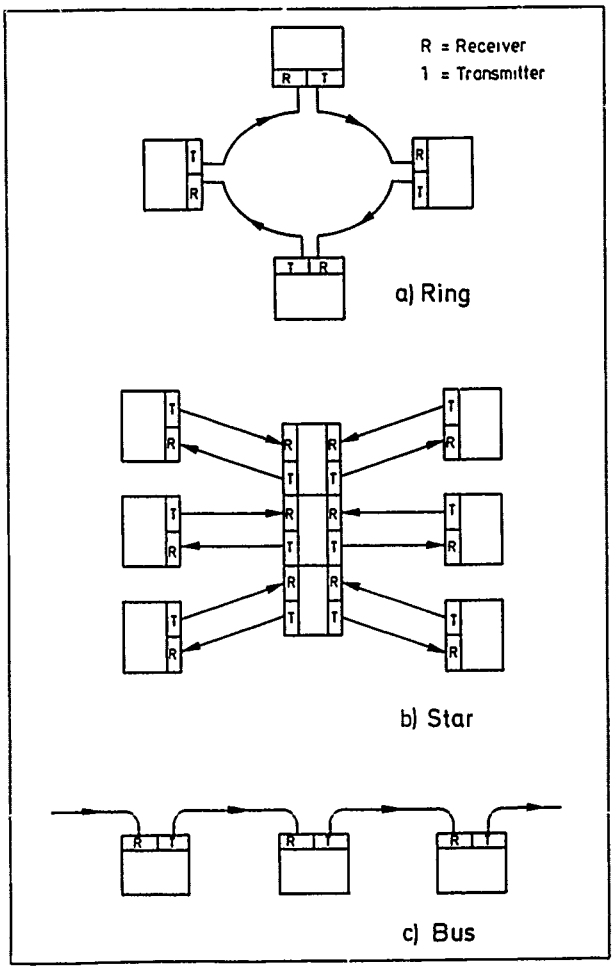

Fig. 6 Network topologies

Performance	Method	Measurement	POF C1	POF C2	POF HF	POF HR
optical attenuation 1) Automotive Application 2) Costumer Premisses Application	cut-back-method (10m/2m)	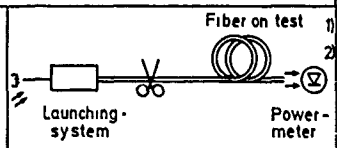	1) <400dB/km 2) <200dB/km	<400dB/km <200dB/km	<400dB/km	<400dB/km
increase in optical attenuation during bending	test mandrel radius r, length of the sample l = 10m; test duration 1h;		<0.05dB r = 30mm	<0.05dB r = 30mm	<0.05dB r = 40mm	<0.05dB r = 30mm
increase in optical attenuation during temperature cycling	climatic chamber (Tmax, Tmin); length of the sample l = 10 m; temperature cycle: -40°C <T<110 °C	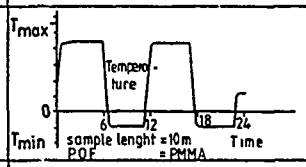	<0.05dB/m	<0.05dB/m	<0.05dB/m	<0.05dB/m
increase in optical attenuation during tensile performance	continuous increase of the tensile load, length of the sample l = 25m	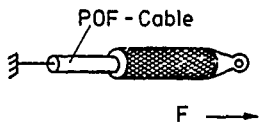	<0.02dB/m Fmax = 150 N	<0.02dB/m Fmax = 400 N	<0.02dB/m Fmax = 1000 N	<0.01dB/m Fmax = 1000 N
increase in optical attenuation during crush test	continuous increase of compressive load length of the sample l = 10m	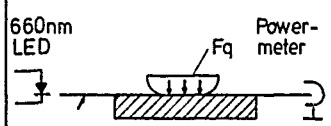	<0.05dB Fmax = 50 N/cm	<0.05dB Fmax = 150N/cm	<0.05dB Fmax = 150N/cm	<0.05dB Fmax = 200N/cm
twist test	torsion cycles until sample damaged torsion angle ±90°C; cycle duration 2-30sec	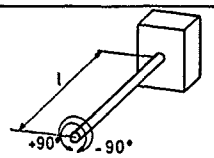	> 30000 T = 1s l = 30mm	> 30000 T = 2s l = 50mm	>10000 T = 2s l = 50mm	>20000 T = 2s l = 50mm
repeated bending	torsion cycles until sample damaged mandrel radius. 15mm - 30mm, bending frequency 5 - 60min.	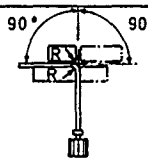	> 10000 T= 1s r = 20mm	>10000 T= 1s r = 20mm	10000 T=1s r=20mm	10000 T= 1s r = 20mm
low temperature cable bending	torsion cycles until sample damaged test temperature -40° C temperature ageing: 105°C/2days	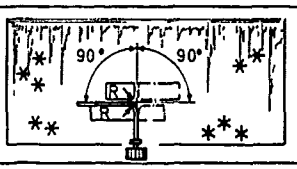	> 3000	> 3000	> 3000	> 3000
cable tensile strength	tensile strength / strain of the sample	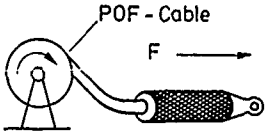	150N 2%	400N 2%	1000N 2%	1000N 2%

Fig. 5 Test Procedures and Results

This is a relatively inexpensive approach, however, unless some optical bypasses are included in each node, it is necessary to have all the nodes active all the time.
Information fed into the network passes through all the nodes therefore a number of transmission channels must be provided between all nodes (which in turn leads to a very high bandwidth if for example upto 30 TV channels are needed), these may be provided either by wavelength division multiplexing, time division multiplexing, or space division multiplexing. All these methods have a large cost associated with them. Moreover the ability of POF for those operational usage is limited.

Star Networks

Figure 6 b shows a star configuration. In contrast to the ring network this type has a separate link for every node on the system. This therefore implies that such a system requires considerably more fiber and has associated installation problems. The advantage of such a system is in terms of reliability and availability of service to the connected devices, however a star centre failure can be a major problem which may require the use of high-reliability design techniques and uninterruptible power supplies.

If the splitting at the star centre is done at the electrical interface feeding into multiple LEDs there is no requirement for expensive optical splitters, in addition the interface to the connected devices are simpler and cheap as only point to point links are needed.

Bus Networks

Figure 6 c shows a bus configuration, this is a broadcast medium such that a signal transmitted by any one device is made available to all others. The simplest method of implementation is to allow one transmitting device to send to all others through a distributor coupler.

In such a topology it is difficult to expand the network unless the distributor is oversized at the beginning (i..e. having spare ports), alternatively an additional coupler could be added in series with the previous one, however, the power budget has to be well sized.

Because the optical power is evenly split by the distributors it often becomes very low in level and necessitates the use of amplifiers or repeaters. In addition light power is lost at the connection points which must use some form of power splitting by optical means.

Conclusion

In our opinion the most appropriate topology for a fiber optic home network would be an active star topology with point to point links. In such a network the links are simple point-to-point and there is no need for expensive components such as splitters etc. (if the splitting is done at the electrical interface). One possible inhouse system is shown in Fig. 7.

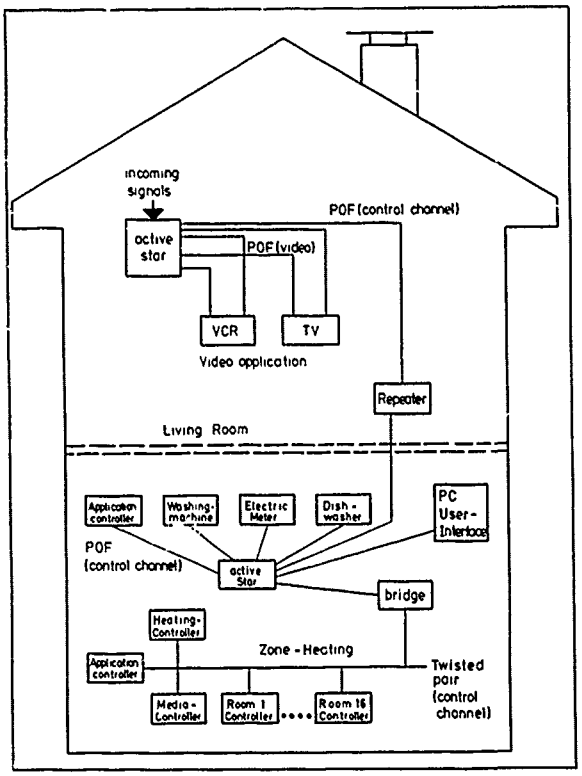

Fig. 7 POF in customer premises applications

This chapter has described some basic considerations for optical fiber networks. In order to proceed further it is necessary to develop a specification for the requirements of an optical fiber network and then to look at various system design options for its implementation. This will lead to a better understanding of the topology issues. Below is a start for such a specification based on the distribution of audio/video systems, this needs to be discussed and added to:

- Size: 100 - 200 meters
- DIY (Do It Yourself)
- Connections for 22 units, 40 outlets
- Up to 30 TV channels of 8 MHz
- VHF/UHF coverage (40-860 MHz)
- Single connector type for all units
- Control channel available to all units
- Low cost (<60 US $/point-to-point link)
- Acceptable picture quality (S/N 50-70dB)
- For control channel BER better than 10^{-9}

Performance	Measurement	Result
optical attenuation (10 m / 2 m)	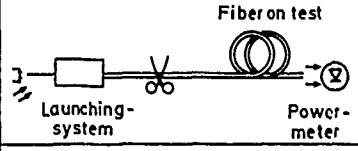	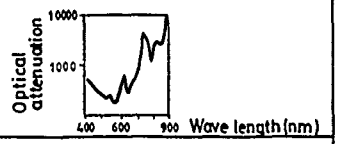
increase in optical attenuation during bending	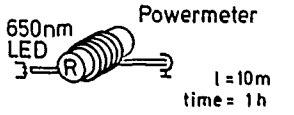	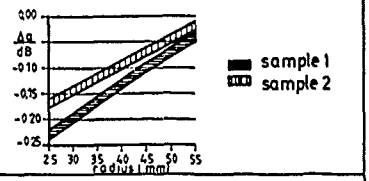
increase in optical attenuation during temperature cycling	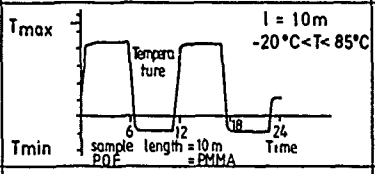	
increase in optical attenuation during tensile performance	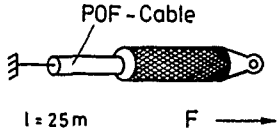	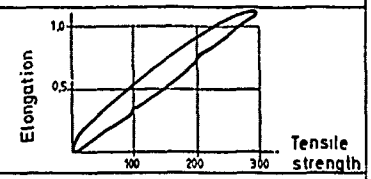
increase in optical attenuation during crush test	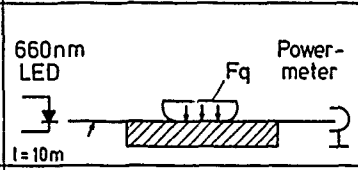	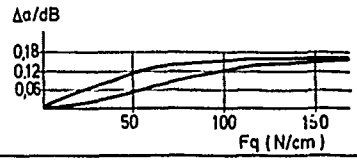
twist test	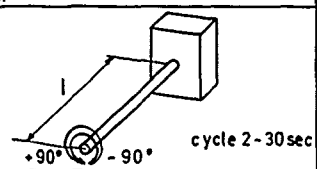	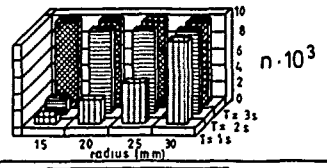
repeated bending	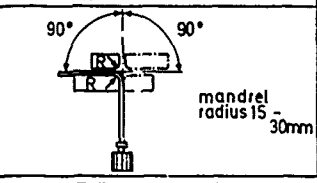	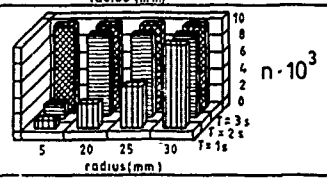
low temperature cable bending	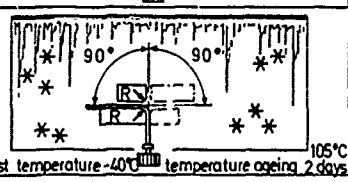	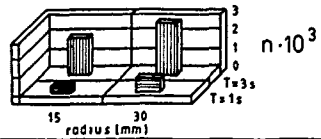
cable tensile strength	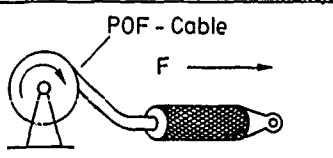	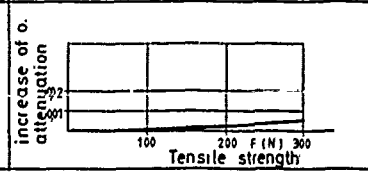

Fig. 8 Tests and Results for POF-Cable Type C2

3.3 Polymer Optical Fiber Cables

The most important requirements for POF cables in inhouse application are

- low attenuation
- small size
- long lifetime
- free of halogen
- Do-It-Yourself potential

In contrast to mobile applications the requirements concerning mechanical stability and broad temperature range are less stringent. This leads to the selection of different materials as compared to cables for automotive applications. The test procedures and the results are shown in Figs. 8.

3.4 Economical aspects

On the way to less energy consumption together with increase in service comfort, steering problems arise in the household area-private and commercial. Up to now no acceptable concept based on copper wires are available. This means that a POF system could offer new possibilities. Any price comparison is difficult, sometimes impossible.
Here the price of the POF system will be compared to the cost reduction by energy savings, and an extra fee will be paid for more comfort. A 10 % energy saving over 5 years gives for a normal 4 person household a possible invest - including installation by DIY - in the range of 1000 DM. This means that here the break even point for the price will be higher but a lot of design features must be considered.

4. Future Trends

Optical fiber cables were first introduced to the market in the second half of the 1960s. In these early days their application was limited to simple displays and lightguides because of their high transmission losses and the lack of suitable opto-electronical devices.

But leaded by Japan, the POF underwent a rapid development in the recent years. With the reduction of the transmission loss down to 150 dB/km POF became very attractive for the application in optical communication systems.
There are mainly three fields in which present-day research concentrates for further improvement of POF characteristics

- attenuation
- bandwidth
- high temperature stability

In automotive application the main concern is the limited temperature range of standard POF. However, modified production techniques or new materials /6/ have extended the usable range from 85 °C to almost 125°C which is sufficient for most applications. For inhouse applications one would like to have POF with lower attenuation. Very promising work is reported on new fluorinated materials /7/ which could bring down attenuation by an order of magnitude. Very recently, the first production of a graded index POF was reported /8/, that also exhibits low attenuation. These results may open wide new markets for POF systems.

5. References

/1/ R. K. Jurgen, "Coming form Detroit: networks on wheels", IEEE Spectrum (6/1986),p. 53 - 59

/2/ T. Naegele, "The next big auto market: the multiplexed data bus", Electronics (8/1986), p. 81 - 82

/3/ Y. Himono et.al., "Optical Link for Automotive Multiplex Wiring", SAE Techn. paper 840494

/4/ N. Yumoto et.al. "Optical Data Link for Multiplex Wiring, SAE Techn. paper 830320

/5/ W. Eickhoff, "Fiber Optic Transmission Systems for Automotive Data Busses", ISATA 1989

/6/ A. Tanaka, E. Takahashi and N. Wakatsuki, "New polycarbonate core plastic optical fiber for high-temperature use" Proc. OFC'86, paper TUG4

/7/ P. Herbrechtsmeier, "Polymere Lichtwellenleiter - Neue Einsatzgebiete für Hochleistungs- kunststoffe in der Kommunikationstechnik", Symposium Materialforschung 1988, p. 199

/8/ Y. Koike, E. Nihei, and Y. Ohtsuka, "Low-loss, high-bandwidth GI plastic optical fiber", 16th ECOC (1990), paper WeB3.3

Wolfgang Eickhoff
AEG KABEL AG
Telecommunication Development
Mönchengladbach, West Germany

Wolfgang Eickhoff (41) was born in Telgte, West Germany. He received the Diplom degree in physics from the University of MUnster in 1973. In 1982 he received the Dr. rer. nat. degree from the University of Hamburg.
From 1973 to 1978 he was a member of the AEG Telefunken Research Institute in Ulm, West Germany, working on characterization of optical fibers. In 1979 he became a Member of the Max-Planck-Institute for Solid State Research in Stuttgart and in 1980 he became Assistant Professor at the Technical University in Hamburg working on single-mode fiber characterization and sensors. Since 1986 he has been Manager, Development Optical Components at AEG KABEL.

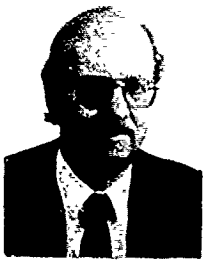

Helmut G. Haag
AEG KABEL AG
Sales Division for Telecommunications
Mönchengladbach, West Germany

Helmut G. Haag (42) is Manager of Sales Division for Telecommunications. After reaching his Dipl.-Physiker-degree from the University of Stuttgart he joined AEG KABEL in 1975 for the development of coaxial cables. Later he has been also responsible for the development of optical fiber cables. From 1980 to 1983 he built up the production plant for these cables. In autumn 1983 he took over the Technical Sales Division and in Jan. 1990 the total Sales Division.

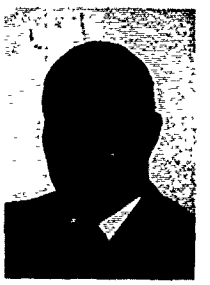

Dragan Stankovic
AEG KABEL AG
Telecommunication Development
Mönchengladbach, West Germany

Dragan Stankovic (32) is a member of the Development Group for optical fiber cables. He reached his Dipl.-Ing.-Degree from the University of Aachen and joined AEG KABEL in 1987. Since then he works on optical cables with POF.

Peter E. Zamzow (Speaker)
AEG KABEL AG
Telecommunication Development
Mönchengladbach, West Germany

Peter E. Zamzow (50) is director of the Telecommunication Development Division. After finishing his postgraduate studies in telecommunications in Munich and Graz as Dipl.-Ing. he joined AEG KABEL in 1970. He has been engaged in development and production of telecommunication cables. In 1980 he became head of the fiber optic division at AEG KABEL and in 1982 he was nominated as a senior engineer. Since 1985 he has covered his present position.

FEASIBILITY STUDY OF COMPACT HIGH-Tc SUPERCONDUCTING POWER CABLES

S.TANAKA N.ICHIYANAGI Z.IWATA M.NAKADE*

THE FURUKAWA ELECTRIC Co., LTD. CHIBA, JAPAN
*TOKYO ELECTRIC POWER Co., INC. TOKYO, JAPAN

ABSTRACT

The use of compact high-Tc superconducting power cable holds great promise in the densely packed underground spaces of large cities. One important parameter in the design of high-Tc superconducting power cables is the AC loss associated with AC applications. We determined the magnetization curves by the AC magnetization method to quantitatively evaluate the AC loss in high-Tc superconducting bulk and wire samples. In the region of small applied maximum fields, the AC loss increased in proportion to the third power of the applied maximum field as indicated by the Bean model. Using a new approach based on the Bean model, we developed a conceptual design for a compact high-Tc superconducting power cable that could be installed in existing cable ducts (150 mm in diameter). It was found that the use of such cables permits a reduction of transmission costs compared to conventional cables.

1. INTRODUCTION

If high-Tc superconducting power cables can be put to practical use, their refrigeration and heat-insulation structures will be remarkably simpler and more compact than those of metal superconducting power cables. In addition, the required costs can be cut, and the economical break-even power transmission capacity can probably be reduced to below a few GW.[1]

Spurred by these possibilities, various laboratories have tried to develop conceptual designs for high-Tc superconducting power cables. These cables have been designed by considering only the surface current with a minimum AC loss on the assumption that the value of lower critical field (Hc_1) is around 1000 G, which is about the same as for Nb, Nb_3Sn, and other metal superconductors.[2,3] However, recent reports have revealed that high-Tc superconductors have lower critical fields of less than 100 G,[4] which is one order of magnitude smaller than those of metal superconductors. If a cable is designed with the surface-current technique based on this finding, the cable will have a substantially large outside diameter of 1 m or more.[5,6]

To solve this problem, a method for designing compact high-Tc superconducting power cables using the Bean model was developed.

Given the present-day situation surrounding electric power systems, the demand for electric power is expected to grow steadily particularly in large cities. This will increasingly require expansion of underground power transmission cables.

If compact large-capacity cables can be fitted into existing cable ducts and tunnels without new construction, transmission costs can be reduced to a large extent.

Based on this premise, this paper aims to establish a future model system, assuming that the demand for electric power is double the demand served by the present underground transmission cable systems in large cities. To apply to this model system, a conceptual design for compact high-Tc superconducting power cables (66 KV 1000 MVA/cct and 600 MVA/cct) were implemented using the Bean model and their required critical current density (Jc) was determined. Hysteresis curves were measured for yttrium based and bismuth based silver-sheathed wires by the AC magnetization method and the validity of the Bean model was studied.

2. APPLICATION PATTERN FOR HIGH-Tc SUPERCONDUCTING CABLE

2.1 Concept of Application Pattern

If demand for electric power will continue to increase by 2.5% a year in the future, the power transmission system 30 year hence will have to have double its present capacity. However, if underground cables are constructed, difficulties will be encountered in finding additional underground space for new cable ducts and tunnels to meet this demand.

If a high-Tc superconductor can be used for cable materials, its refrigeration and heat-insulation will be simpler than those required for conventional metal superconducting cables which are cooled with liquid helium. In addition, the greater dielectric strength of liquid nitrogen than that of liquid helium will reduce the insulation thickness of the cable.

Therefore, it is feasible to make a cable with a small outside diameter in spite of large capacity. This means that present-day cables could be replaced by large-power superconducting ones using existing ducts and cable tunnels. In short, the high-Tc superconducting cable is expected to promise cost reduction for underground cable construction and efficient utilization of underground space for urban development.

2.2 Future Model System

The model of the present-day power system, which forms the basis for the present study, is shown in Fig. 1 (a).

Based on this system, a model of the future system is shown in Fig. 1 (b) and (c). Normal-conductor

cable systems with internal cooling have an outside diameter of about 150 mm or more and require new construction of more cable tunnels and ducts below substations B_1 and B_2 to meet double the present-day power demand.

On the other hand, if a high-Tc superconducting cable with double the power transmission capacity of present-day cable systems could be fitted into existing cable ducts and cable tunnels, construction costs would be reduced significantly.

Furthermore, a high-Tc superconducting cable has a greatly reduced power loss compared to conventional cables and can carry very large current so that low-voltage power transmission becomes possible. This would permit uniform voltage distribution at low levels (e.g., 66 kV), which would achieve significant cost reduction by eliminating primary substations.

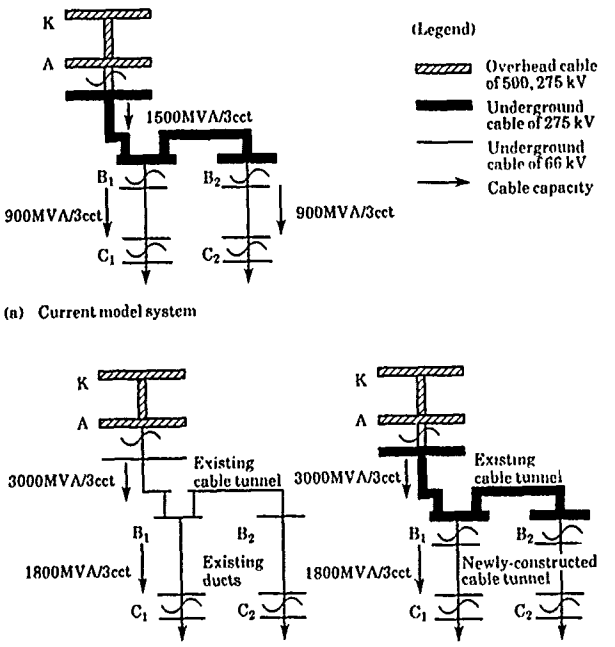

Fig. 1. Model Systems

3. DESIGN OF COMPACT HIGH-TC SUPERCONDUCTING CABLE BY USING BEAN MODEL

3.1 Surface Current Density and Conductor Diameter

In conventional superconducting cable designs, the surface current density concept has been used. Surface current density is expressed as the amperage of current flowing in the unit width of the circumference of a cylindrical conductor. For a superconducting cable cooled with liquid helium, the surface current density was designed so that the magnetic self field at the conductor surface did not exceed the superconductor lower critical field Hc_1. When the field applied to the conductor is equal to the lower critical field, the surface current density is given by Eq. (1).

$$Is\ (A/cm) = \frac{5}{2\sqrt{2}n}\ Hcl\ (Oe) \qquad (1)$$

As a result, the superconducting tape is in a perfect Meissner state and the AC loss in it negligibly small. This was justified by the necessity to minimize heat generation from the conductor.

In a cable design based on surface current, the minimum conductor diameter D is derived from the power transmission current I, as shown in Eq. (2).

$$D = \frac{I}{n \cdot Is} \qquad (2)$$

At equal power transmission currents, the greater the surface current density, the smaller the conductor diameter can be made. However, as is clear from Eq. (1), the surface current density is restricted by a physical value that is inherent to the superconductor called the lower critical field.

Table 1 shows the critical temperatures and fields for the main superconductors. High-Tc superconductors have exceptionally high upper critical fields Hc_2, and are promising for use in magnets and other high-field applications. However, although the values of Hc_1 vary from one high-Tc superconductor to another,[7,8] they are significantly smaller than those of metal superconductors.

Table 2 shows the surface-current values for various superconductors and the minimum conductor diameters required for a power transmission current of 10000 A. For metal superconductors, the minimum conductor diameter is less than 10 cm. Moreover, for high-Tc superconductors, the minimum conductor diameter is up to 1 m, which prohibits fabrication in cable form. For this reason, the conductor diameter must be reduced by conducting the current both on the conductor surface and in it. In other words, high-Tc superconducting wire should be used in the region of Hc_1 to Hc_2. However, if this is done, conductor losses due to the penetration of field will occur. Consequently, quantitative evaluation of AC losses in high-Tc superconducting wire is a new technical challenge.

Table 1. Critical Temperature and Field for Main Superconductors

	Superconductors	T_c(K)	Hcl (Oe)	H_{c2} (T)	$\frac{H_{c2}\,//}{H_{c2}\perp}$
Metal	N_b	9.1	800 - 1000	0.19	1
	$N_b\ T_i$	9.8	700 - 900	15	1
	$N_{b3}\ S_n$	18.2	600 - 700	29	1
Oxide	$Y\ B_{a2}\ Cu_3\ O_{7-x}$	93	52 - 120	150*	- 10
	$B_{i2}\ S_{r2}\ C\ \ C_{u3}\ O_x$	110	6 200	220*	- 30
	$Tl_2\ B_{a2}\ C_{a2}\ C_{u3}\ O_x$	125	- 150	220*	- 40

* Estimated values

Table 2. Surface Current and Minimum Conductor Diameter (for 10000 A)

Superconductor	Surface current (A/cm)	Minimum conductor diameter (cm)
N_b	450 to 563	5.7 to 7.1
$N_{b3}\ S_n$	338 to 394	8.1 to 9.4
$Y\ B_{a2}\ C_{u3}\ O_x$	29 to 67	47.5 to 109 8

3.2 AC Loss Evaluation using Bean Model

Conventional methods for measuring AC loss with sufficient accuracy and sensitivity involve either measuring magnetization in the wire by applying static or quasi-static fields to it (e.g., by means of a SQUID susceptometer), or measuring the voltage developed in the wire when a known AC current is applied. With the former method, however, the eddy current generated in the stabilized metal portion of the wire cannot be measured, and the effect of flux creep tends to cause the results of measurement to vary substantially with the application of different field frequencies. With the latter method, because the critical current density of samples is still low, the self-field generated is substantially smaller than the field applied to the wire during cable operation.

To solve these problems, we measured the AC loss actually developed when the high-Tc superconducting wire was exposed to an AC field of the commercial frequency (50 Hz). More specifically, the AC field was applied to short samples of high-Tc superconducting wire, and the AC loss was determined from the area surrounded by the resulting

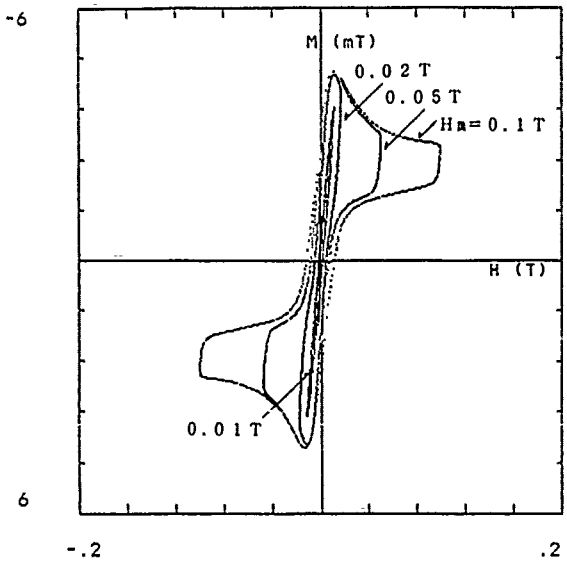

Fig. 2. Magnetization Curves for Y-based Superconducting Bulk (77 K)

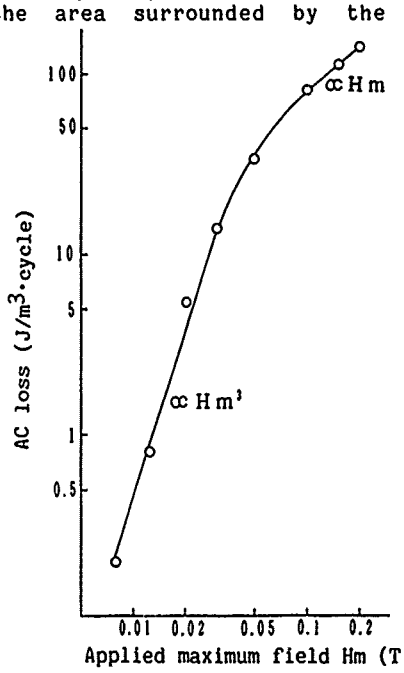

Fig. 4. AC Loss in Y-based Silver-Sheathed Tape

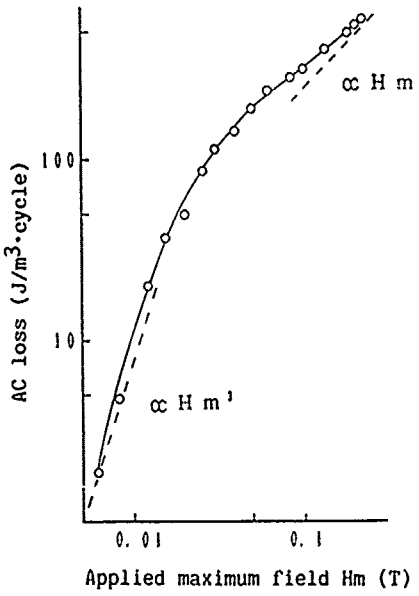

Fig. 3. AC Loss in Y-based Superconducting Bulk (77 K)

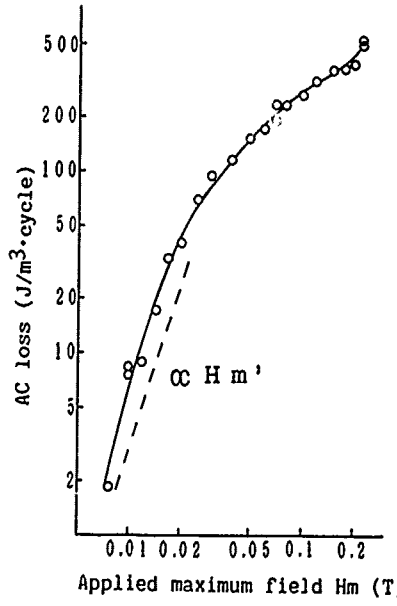

Fig. 5. AC Loss in Bi-based Silver-Sheathed Tape (77 K)

magnetization curves[9] (this method is hereinafter referred to as the AC magnetization method) to perform quantitative evaluation of the AC loss.

Fig. 2 shows the magnetization curves for a $YBa_2Cu_3O_{7-x}$ sintered bulk sample (5 mm wide × 2mm thick × 25 mm long). The surface field Hp obtained when the field reaches the center of the superconductor (i.e., when the absolute value of magnetization reaches its maximum) is approximately 0.012 T. Fig. 3 shows the AC loss vs. the applied maximum field for the sample.

Figs. 4 and 5 show the AC loss vs. the applied maximum field for silver-sheathed tapes of $YBa_2Cu_3O_{7-x}$ (5 mm wide × 0.2 mm thick × 30 mm long) and $Bi_2Sr_2CaCu_2O_x$ (3 mm wide × 0.17 mm thick × 30 mm long), respectively. The value of Hp for the two samples was approximately 0.020 T and 0.017 T, respectively.

The critical density of Bi-base Ag sheathed tape by 4 probe method was 8×10^3 A/cm^2.

As is clear from Figs. 3, 4, and 5, the AC loss is proportional to the third power of the applied maximum field Hm in the range below Hp. The AC loss also shows a tendency toward approximating a straight line proportional to the first power of Hm in the range of Hp ≪ Hm. These characteristics agree well with the field dependency of the AC loss determined by the Bean model.

The silver-sheathed wire incurs eddy current loss in addition to the hysteresis loss induced in the superconductor. The AC losses determined by the AC magnetization method shown in Figs 4 and 5 include the eddy current loss. However, the finding that the AC loss curves for the silver-sheathed tape in Fig. 5 have a similar shape to that of the bulk sample in Fig. 3 suggests that the eddy current loss is much smaller than the hysteresis loss as in the case of metal superconductors, under operating conditions with magnetic fields of 0.2 T and a frequency of 50 Hz.

As a result of the above AC loss measurements, we decided to adopt the assumption that the AC losses developed in superconducting wires could be ignored as insignificant except for the hysteresis loss, and that the hysteresis loss could be roughly evaluated by the Bean model.

The Bean model[10] is one of the models providing the field and current density distribution in a superconductor required for calculation of the hysteresis loss. Fig. 6 shows the field and current density distribution based on the Bean model.

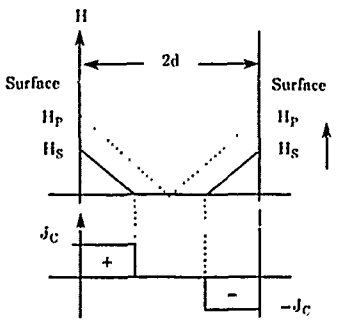

Fig. 6. Field and Current Density Distribution Based on Bean Model (when superconducting infinite plate placed in external field)

According to the Bean model, the hysteresis loss Wh (J/m^3·cycle) for a sheet superconductor is given by Eq. (7):

$$Hm \leqq Hp \quad Wh = \frac{2\mu_0}{3} \cdot \frac{Hm^3}{Jc \cdot d} \qquad (7)$$

The critical current density estimated by this formura and Fig. 3-Fig. 5 is one to two order higher than those by 4 probe method, which is supposed to be due to the fact that shield current is much larger than transport current.

Further, according to the Bean model, the hysteresis loss for a cylindrical superconducting conductor is given by Eq. (8):

$$Wc = \frac{4\sqrt{2}\mu_0}{3} \cdot \frac{I^3}{Jc \cdot Pe^2} \cdot f \qquad (8)$$

where Pe is the perimeter of the conductor and fis the frequency.

3.3 Conceptual Design Method of High-Tc Superconducting Cable

Fig. 7 shows the conceptual design flow chart for a high-Tc superconducting cable. First, the rated capacity, rated voltage, critical current density, and diameter of the small coolant pipes inside conductor are input as parameters to determine the individual cable sizes. After the cable size has been determined, the conductor loss, dielectric loss, and penetration heat are calculated. In this paper, the conductor loss is calculated on the basis of the Bean model using Eq. (8). In this equation,

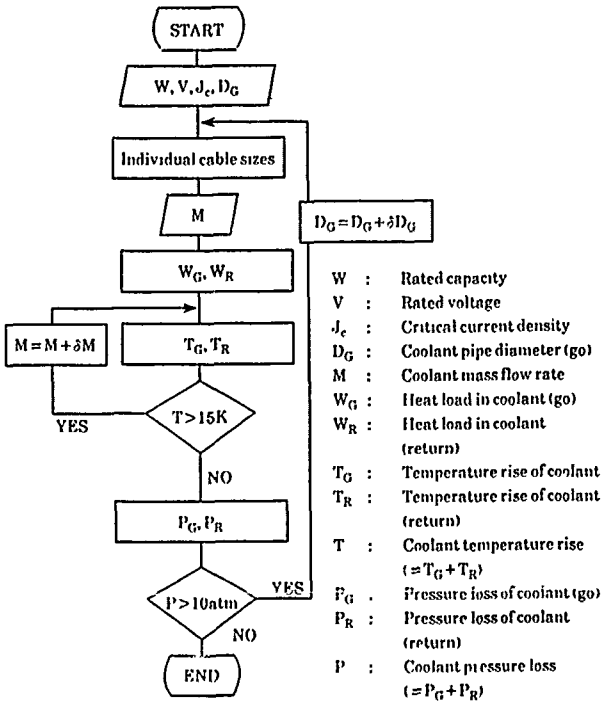

Fig. 7. Conceptual Design Flow Chart for High-Tc Superconducting Power Cable

the value of Jc was set to the transport current density, assuming that the transport current density would equal the shield current density because of future improvements in wire fabrication techniques. The mass flow rate M of the coolant required to remove the heat mentioned above depends on the cooling distance, quantity of heat to be removed, specific heat of the coolant, and coolant temperature rise T. This paper assumes that the critical temperature of the high-Tc superconducting cable will be around 90K and that the cable will operate at 65K to 80K. Based on this assumption, the value of M was increased until T fell below 15K, and then the pressure loss required for the coolant to circulate was determined. The heat transfer between the "go" and "return" flows was ignored as safety calculation because it reduced the temperature difference between them and restricted the temperature rise at outlet. In addition, since the coolant pressure was assumed to be 10 to 20 atm during cable operation, the diameter of coolant pipe and heat-insulation tube was increased so that the pressure loss was reduced to less than 10 atm over the entire cooled length of 2.5 km for both feeding and returning. The channel for returning coolant was designed so that the pressure loss in it was almost equal to that in the coolant pipe.

3.4 Conceptual Design of Compact High-Tc Superconducting Power Cable and Required Jc

Fig. 8 shows the structure of the high-Tc superconducting power cable.[11] To reduce the cable size, the cable was composed of three cable cores enclosed in a heat-insulating tube as shown in Fig. 8 (a). A former in each cable core formed an cooling channel for liquid nitrogen and high-Tc superconducting tapes were wound around its outer layer to conduct electric current. To make the cable flexible, the superconducting layer was sandwiched between a stabilizing copper layer and a reinforcing stainless-steel layer in the form of a tape as shown in Fig. 8 (b). Superconducting layer side of copper layer should be coated by silver for the chemical stability. Liquid nitrogen impregnated semi-synthetic paper with a high dielectric strength was used as insulation.[12] The outer layer of each core had an external high-Tc superconducting conductor to shield against magnetic flux induced by the transmission current.

The heat-insulation tube enclosed the three cable cores and a coolant return channel and consisted of stainless-steel corrugated pipes and heat-insulation material (superinsulation, etc.).

The results are shown in Table 3. The pressure loss P reaches 367 atm/2.5 Km at Jc = 1 × 10^5A/cm^2. The pressure loss decreases to 10.9 atm/2.5 Km at Jc= 1 × 10^6A/cm^2 because the conductor loss (hysteresis loss) is reduced by a factor of 10, which adequately meets the required value. In this case, the conductor loss is 3.02 W/m. The total of dielectric loss and heat penetration is 1.27 W/m and friction loss is negligibly small. It is believed that Jc = 1 × 10^6A/cm^2 (with flux density of 0.21 T at conductor surface) is sufficient to design a 1000 MVA 66 kV high-Tc superconducting power cable with 130-mm diameter. Conceptual design for 600MVA cable showed that the required value of Jc is 2 × 10^5 A/cm^2 (0.13T).

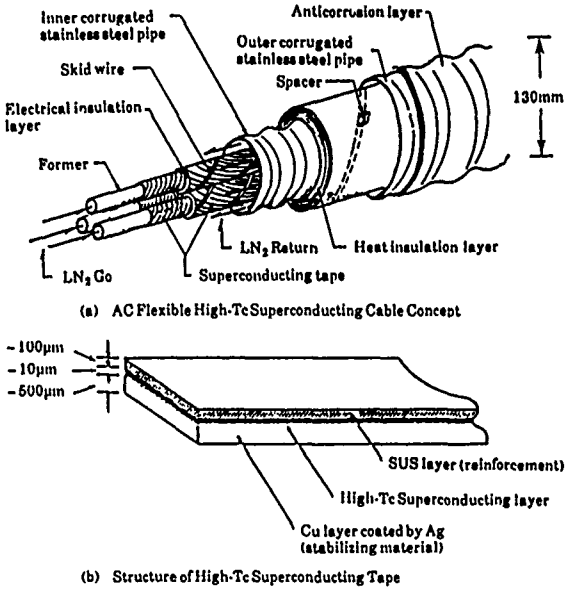

Fig. 8. Structure of High-Tc Superconducting Cable

Table 3. Conceptual Design of 66kV 1000MVA High-Tc Superconducting Cable

Inner diameter of former	mm	19.4		
Conductor outside diameter	mm	24.1		
Shield conductor inside diameter	mm	35.9		
Core outside diameter	mm	38.1		
Heat-insulation tube inside diameter	mm	87.7		
Heat-insulation tube outside diameter	mm	130.0		
Critical-current density	A/cm^2	10^5	10^6	10^7
Conductor loss	W/m	30.2	3.0	0.3
Dielectric loss	W/m	0.5	0.5	0.5
Thermal penetration	W/m	0.7	0.7	0.7
Coolant temperature rise	K	15.0	15.0	15.0
Coolant pressure loss	atm	367.3	10.9	1.9

4. COST CONSIDERATIONS

Transmission costs were studied for the model systems shown in Fig. 1 (b) and (c). Cost considerations included construction costs, capitalized costs of transmission and refrigeration losses, all calculated by the levelized annual cost method. The basic requirements for cost calculation are shown in Table 4.

The high-Tc superconducting cable between B and C permits use of existing ducts, and eliminates the cost of cable tunnel construction and therefore reduces costs by as much as 58%, compared to normal-conductor cables. Because of this, although the normal-conductor cable is better over the other sections, the high-Tc superconductor cable generates a 15% cost reduction over the entire cable system. In addition, with high-Tc superconducting cable, the need for primary substations is eliminated by the

uniform voltage, so that the total cost of substations is reduced by 28%.

The result is shown in Table 5. Assuming that the high-Tc superconducting wire costs as much as Nb_3Sn, the high-Tc superconducting cable system achieves a 21% overall cost reduction compared to the normal-conductor cable system.

Table 4. Basic Requirements for Cost Calculation

Item		Requirements
Basic formula		Power transmission cost [¥/yr] = Construction cost [¥] x α + cost of power loss + refrigerator operating cost [¥/yr] where α = { 0.126 (for cable) / 0.142 (for transformer)
Cable	High-Tc superconducting cable cost	Calculations are made on the assumption that the superconducting wire material costs as much as Nb_3Sn. The cost of the refrigeration system is also included in the calculation.
	Internally-cooled cable cost	Proven values are used on the assumption that the internally-cooled cable cost is equal to that of OF cables.
	Cost of cable duct and tunnel	The proven value mean for three years is used.
Transformer	High Tc superconducting transformer cost	Calculations are made on the assumption that the superconducting wire material costs as much as Nb_3Sn. The cost of the refrigeration system is also included in the calculation.
	Transformer cost (normal conductor)	Proven values are used.
	Cost of Substation construction	Determined on basis of proven values for three years. The switching station construction cost is calculated on the assumption that it is about 70% of that of a substation.

Table 5. Cost Evaluation for Model Systems (Absolute values derived on the assumption that total transmission cost of normal-conductor cable system = 100)

	High-Tc superconducting cable system	Normal conductor cable system
Cable system	45	53
Substation	34	47
Total	79	100

5. SUMMARY

A conceptual design of a compact high-Tc superconducting cable was developed using the Bean model. Based on the results, various requirements for accommodating superconducting cable in existing ducts (150-mm diameter) for present-day power systems were clarified. The costs were evaluated and the applicability was studied. The following findings were obtained.

(1) Based on a present-day cable model system, a future model system was established on the assumption that demand for electric power will double compared to today's levels. Comparative studies were made using superconducting and normal-conductor cables.

A large-capacity high-Tc superconducting cable can be substituted for conventional cables in existing cable ducts and tunnels. In addition, it promises advantages of cost reduction and efficient utilization of increasingly crowded underground space.

(2) The magnetization curves for the Y-based and Bi-based silver-sheathed tapes were measured by the AC magnetization method to determine the AC loss. The AC loss was proportional to the third power of the applied maximum field Hm in the range below Hp, whereas it showed a tendency toward approximating a straight line proportional to the first power of Hm in the range of Hp $\ll$ Hm. These characteristics agree well with the field dependency of the AC loss determined by the Bean model. The results of these AC loss measurements suggest that the Bean model provides a useful means for approximate evaluation of the AC loss in superconducting wire employed in high-Tc superconducting power cables.

(3) Using the Bean model, we developed a conceptual design for a high-Tc superconducting cable by which the pressure loss of liquid nitrogen coolant is below 10 atm and the cable outside diameter is minimized. This design confirms that the optimal cable system voltage is 66 kV so that the cable can fit into the existing 150-mm ducts. Furthermore, conceptual designs for high-Tc superconducting cables of 1000 MVA and 600 MVA (with 130-mm cable overall outside diameter) showed that the required value of Jc is $1 \times 10^6 A/cm^2$ (0.21 T) and $2 \times 10^5 A/cm^2$ (0.13 T), respectively.

(4) Assuming that the cost of high-Tc superconducting wire is about the same as Nb_3Sn, the high-Tc superconducting power cable system effects a 21% cost reduction over a normal conductor cable system.

ACKNOWLEDGMENT

The authors wish to thank Mr. M. Nakamura (Tokyo Electric Power Co., Inc.), Mr. Y. Furuto (The Furukawa Electric Co., Ltd.) for their useful advice and discussions.

REFERENCES

[1] T. Hara, K. Okaniwa, N. Ichiyanagi, S. Tanaka, "FEASIBILITY STUDY OF COMPACT HIGH-TC SUPER-CONDUCTING CABLES", *1990 Winter Meeting of IEEE* 075-2PWRD 1990.

[2] T. Hoshino, N. Higuch, I. Ishii, S. Fuchino, "Study of 1-3GVA Superconducting Cables Made of Nb_3Sn and High-Tc Superconductors", *IEE of Japan Trans B*, Vol. 108, No. 9, pp. 431-438 1988

[3] K. Nakame, H. Suzuki, "Study of Superconducting Cables Applied for Electrical Systems", *1988 General Annual Meeting of IEE of Japan* 1988

[4] *NIKKEI SUPERCONDUCTORS* Japan Oct. No. 17. 1988

[5] T. Hara, K. Okaniwa, N. Ichiyanagi, S. Tanaka, F. Fnokubo, Y. Furuto, *1989 General Annual Meeting of IEE of Japan*, No. 845 1989

[6] N. Ichiyanagi, F. Enokubo, Y. Furuto, *International Symposium on New Developments in Applied Superconductivity*, Suita, Osaka, Japan pp. 343-347 Oct. 1988
[7] N. Murayama, et al. *Japan Journal of Applied Physics* Vol. 27 No. 9 L1629-1630 Sep. 1988
[8] A. P. Malozemoff, et al., "Remanent moment of high-temperature superconductors: Implications for flux-pinning and glassy models, *Phys. Rev. B* Vol. 38 No. 10 Oct. 1988
[9] M.P.Maley, J.D.Thompson, L.R.Newkirk, "ac losses in Nb3Ge composite tape conductors", *CRYOGENICS*, p.675-678 Nov. 1981.
[10] C. P. Bean, *Phys. Rev. Letters 8*, p250 1962
[11] E. B. Forsyth, R. A. Thomas, "Performance summary of the Brookhaven superconducting power transmission system" *Cryogenics* Vol. 26 Nov. pp599-614 1986
[12] T. Fukuda, et al., "Development of VHV OPPL Insulated Oil-filled Cable", *THE FURUKAWA REVIEW* No. 6 1988

Satoru Tanaka was born in Yamaguchi,Japan on July 18,1960. He received the B.S. degree in electronics engineering from Osaka University, Japan in 1987. He joined the Furukawa Electric Co., Ltd. in 1987. He works in the reseach and development of superconducting power system.

Mr. Tanaka is a member of the Institute of Electrical Engineering of Japan.

Naotaka Ichiyanagi was born in Kyoto, Japan on April 29,1947. He received the B.S. degree and M.S. degree in applied physics from the Tokyo Institute of Technology, Japan in 1971 and in 1973 respectively. He studied in the physics department, graduate school of Mcgill University, Canada from 1973 to 1974. He joined the Furukawa Electric Co., Ltd., in 1975. He works in the research and development of large power transmission cables.

Mr. Ichiyanagi is a member of the Institute of Electrical Engineering of Japan.

Zensuke Iwata was born in Tokyo, Japan, on October 5, 1944. He received the B.S. degree in electrical engineering from the University of Tokyo, Tokyo,Japan, in 1968. In 1986 he joined the Furukawa Electric Co., Ltd., Japan. He has been in charge of the research and development of high-voltage power transmission cables and their accessories. He is general manager of power cable R&D department.

Mr.Iwata received the Prizes of Progress from the IEE of Japan for the contribution to the research of cryogenic cable in 1976, and for the development of internal conductor cooling bulk power transmission system in 1989 respectively.

Mr.Iwata is a member of the Institute of Electrical Engineers of Japan,a member of the Cryogenic Association of Japan, a member of the IEEE and a member of the CIGRE WG21-09,13.

Masahiko Nakade was born in Ishikawa,Japan on April 24, 1961. He received the B.S. degree and M.S.degree from Tokyo Institute of Technology, Japan in 1985 and in 1987 respectively. He joined Tokyo Electric Power Co., Inc. in 1987. He works in the research and developement of superconductivity for electrical power systems.

Mr. Nakade is a member of the Cryogenic Association of Japan.

Trailing Cables With Optical Fibers And Special Tests

Peter Delage, Rudolf Buchwald and Georg Hög

AEG KABEL Aktiengesellschaft
Mönchengladbach, Federal Republic of Germany

1. Abstract

Trailing cables are for example used for conveying systems. To design and produce a trailing cable with optical fibers (OFTC) one has to consider a variety of technical boundaries but this type of cable is nowadays according to the latest state of art. This contribution deals with the construction and relevant tests and their results for OFTC designed for rated voltages from 1 kV to 35 kV.

The mentioned advantages are utilized in mobile equipment, which get their energy and control signals by trailing cables.

The optical fiber (OF) used is a single mode fiber with a mode field diameter of 9 µm or a graded index fiber with a core diameter of 50 µm or 62,5 µm. The paper describes the possible constructions for the OF element with graded index fibers used for the various applications of the OFTC.

Further the relevant mechanical and thermal tests and their results for the various constructions are described.

2. Introduction

The modern optical fiber technology has gotten more and more interest in the last years for cables used for power utilities. The advantage of optical fiber cables are not only the bandwidth in comparison with copper cables, but also the insencitiviness to magnetic interference.

These advantages can be used for mobile applications, where the equipment gets their power as well as control signals over a trailing cable. The main operational area for trailing cables is the conveyer and hoisting technique.

Two examples are shown in the Fig. 1 and 2. The constructive solution of trailing cables with integrated optical fibers is not easy, because such cables are submitted permanently to mechanical stresses like bending and torsion. This fact must be taken into consideration by designing the power cable.

At this the suitable choice for the material is decisive for the functioning of the cable. The following paper describes such constructions, the relevant tests and the results for cables with nominal voltages from 1 kV to 35 kV.

Fig. 1/2: OFTC, Used with Dredger and in Surface Mining

The constructions of the cable is similar to commercial trailing cables, where in the interstices of the insulated power wires the optical fiber element is integrated. (1) (2)

In the paper special tests are described which take under consideration the optical fibers. These tests and their results confirm the serviceability of optical fibers used in such power cables. No negative interaction between power conductors and optical fiber cables occurs.

3. Cable Design

3.1 Optical Fiber (OF) - Element

For the transmission of control and video signals from a conveyer to a central computer an optical fiber element is integrated in a trailing cable.

This optical fiber element must be sufficient to the requirements of a trailing cable. The separation of the telecommunication part from the power core must be possible without difficulties, so that both parts can be used as independant cables. To guarantee this, the construction of the optical fiber element must be accomodated especially the mechanical stress of the cable.

For the production of the cable with a vulcanized rubber outer sheath a temperature of about 200°C and a pressure of 20 bar over 15 minutes to the optical fiber element is to be considered.

The optical fiber element has to be examined as outdoor cable from the distribution point of power and telecommunication part to the termination. To fulfil these conditions the following basic constructions of optical fibre elements were realized.

Type 1

- Optical fibers with UV-coating
- Central loose buffer with FRP armoring
- Rubber jacket

Type 2

- Optical fibers with UV-Coating
- Stranded tight buffered fibers around a central FRP element
- ETFE tube
- Rubber jacket

Type 3

Like type 2, but optical fibers with silicon coating.
The various constructions are shown in detail in Figure 3. These elements are technical equivalent, but type 3 is especially suitable for higher temperature usage.

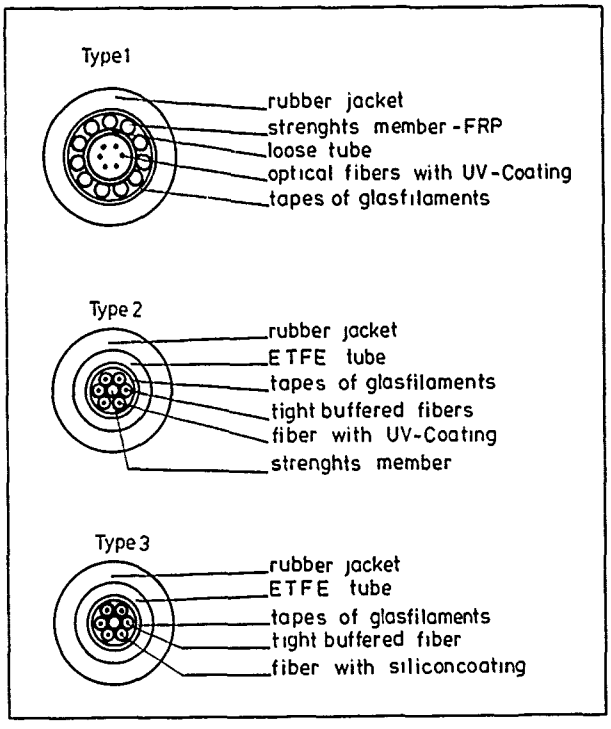

Fig. 3: Basic Elements for OFTC

The typical datas for the used graded index fibers are shown in the following table:

Core diameter	:	50 µm
Reference surface diameter	:	125 µm
Coating diameter	:	250 µm
Attenuation at 850 nm	:	≤ 2,7 dB/km
Attenuation at 1300 nm	:	≤ 0,7 dB/km
Bandwidth at 850 nm	:	≥ 600 MHz * km
Bandwidth at 1300 nm	:	≥ 1000 MHz * km

3.2 Trailing Cable

Figure 4 shows the principal construction of the optical fiber trailing cable (OFTC).

The power element consists of a special conductor made for high flexible use. A high-grade rubber insulation guarantees good mechanical and electrical properties. The power conductors are stranded with a short pitch length (340 mm); in the interstices two protective conductors and the optical fiber element are laid in. Over the

filling inner jacket a torsion protection made out of plastic threads is laid into the outer rubber jacket which guarantees good mechanical and thermal properties. The outer diameter of the complete cable is about 75 mm.

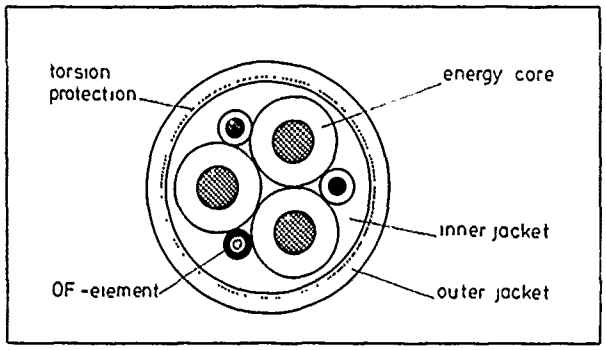

Fig. 4: OFTC (3x240 mm^2) with Optical Fiber Element (OF)

4. Tests and results

4.1 Optical Fiber Elements

The described OF-elements were tested according IEC as follows:

° Tension	IEC 794-1-E1
° Crush	IEC 794-1-E3
° Impact	IEC 794-1-E4
° Repeated bending	IEC 794-1-E6
° Torsion	IEC 794-1-E7
° Kink	IEC 794-1-E10
° Temperature cycling	IEC 794-1-F1

The test methods are described in the appendix. The following test parameters were chosen:

° Tension
Sample length: 100 m
Speed : 10 mm/min
Measurement datas: elongation, fiber attenuation at 1300 nm

° Crush
Sample length: 100 m
Measurement datas: pressure, fiber attenuation at 1300 nm

° Impact
Energy: 3 Nm
Number of impacts: ≥ 400
Measurement datas: material behaviour, fiber attenuation at 1300 nm

° Repeated bending
Bending radii: 30 mm, 60 mm, 120 mm
Measurement datas: material behaviour, number of cycles, fiber attenuation at 1300 nm

° Torsion
Angle: ± 180°
Sample length: 2 m
Load: 50 N
Measurement datas: material behavoiur, number of cycles

° Kink
Angle: 360°
Measurement datas: material behaviour, bending rate, fiber attenuation at 1300 nm

° Temperature cycling
Sample length: ≥ 1000 m
Temperature: - 25°C to 90°C
Measurement datas: temperature, fiber attenuation at 1300 nm

The test method for the optical fiber attenuation is shown in the appendix (insert-loss-measurement)

4.2 Results on OF-Element

° Tension

This test shows for the various OF-Elements very different results. The construction witha central tube and FRP armouring (type 1) shows only an increase of A = 0.1 dB/100 m up to a load of 5 KN. For type 2 and type 3 the stranding of the buffers ??? around a central strength nubmer is the determining factor, so that the maximum pulling force is limited to 500 N, what is based on the low cross section of the FRP-element (100 mm diamter). Type 3 is a little bit better than type 2, because the Silicon coated fiber is more insensitive against mechanical stress than the UV-coated fiber. The results are shown in the diagramme of figure 5.

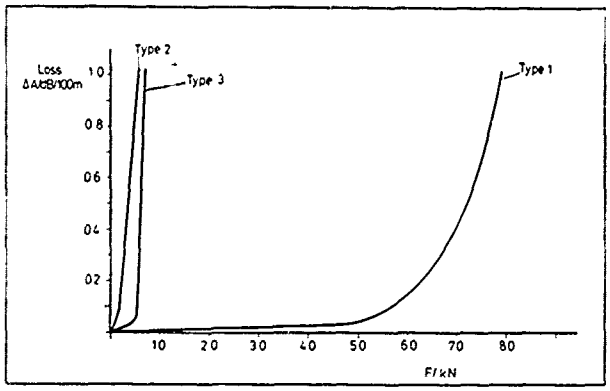

Fig. 5: Tension Test on OF-Element

° Impact

With an energy of 3 Nm for type 2 after a total number of 95 impacts a fiber breakage occurs. By changing the coating to a silicon material this behavoiur is improved up to 200 impacts with 3 Nm, until also a fiber breakage is noticed. Only for

type 1 by use of a FRP-armouring no fiber breakage happens by number of impacts greater than 400; no change of attenuation is measured. Figure 6 shows the results.

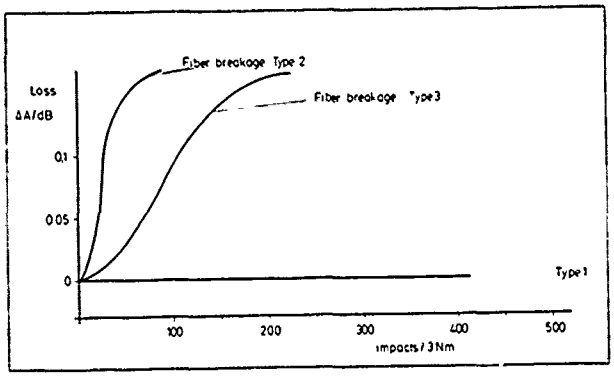

Fig. 6: Impact Test on OF-Element

- **Crush**

All constructions show an increase of attenuation by a load greater than 2000 N (figure 7). For type 1 this increase is much higher than for the other types, but in comparison to these types reversible. It is shown in the figure that all constructions are suitable for lateral forces lower than 1500 N.

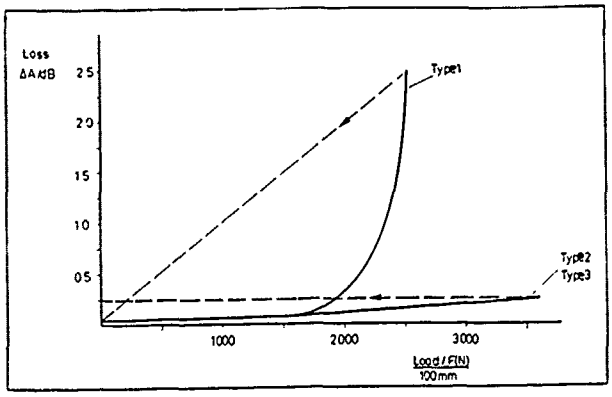

Fig. 7: Crush Test on Of-Element

- **Repeated bending**

This test is for all constructions uncritical. In no case a fiber breakage or a change in attenuation is measured by more than 100.000 cycles around a radius of 60 mm and an angle of ± 90°C.

- **Torsion**

Also in this test by 500.000 cycles and an angle of ± 180° the three constructions no change of attenuation or fiber breakage occurs.

- **Kink**

Up to radii R ≥ 30 mm no change of attenuation is measured. Figure 8 shows that for all constructions an increase of attenuation is measured only for radii lower than 15 mm. In this case the behavoiur of the constructions are similar.

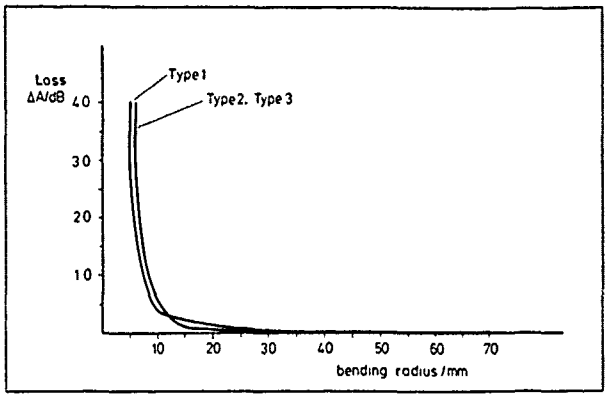

Fig. 8: Kink Test on OF-Element

- **Temperature cycling**

All constructions were tested in two cycles between - 25°C and 90°C. The change of attenuation was increased at 1300 nm. Figure 9 shows clear, that all OF-types are equivalent. The maximum increase of attenuation is lower that 0,1 dB/km at λ = 1300 nm for all elements. At room temperature the increase is reversible.

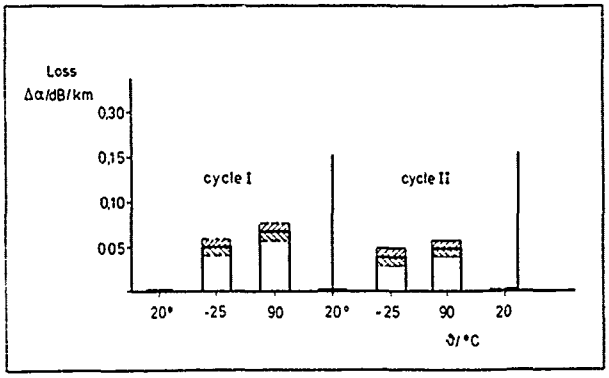

Fig. 9: Temperature Cycling on OF-Element

On basis of the described tests and their results for the trailing cable only the type 1 element was examined. To improve the mechanical behaviour in deviation from figure 3 a thin hytrel sheath was extruded over the FRP armouring. Figure 10 shows the element in detail.

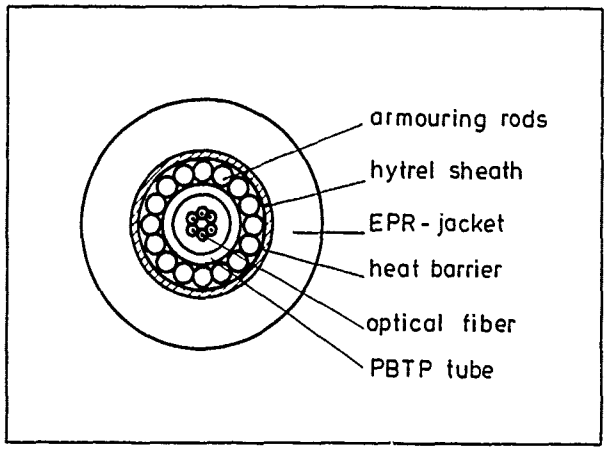

Fig. 10: Tested OF-Element in the Trailing Cable (OF)

4.3 Tests On Trailing Cable With Optical fiber Element (OFTC)

On the completed cable tension, torsion and a bending test up to a temperature of 90°C were made.

- **Tension**

For the tension test the stress on the OFTC was increased to 30 N/mm² (Figure 11). The optical attenuation was measured during this test at λ = 1300 nm.

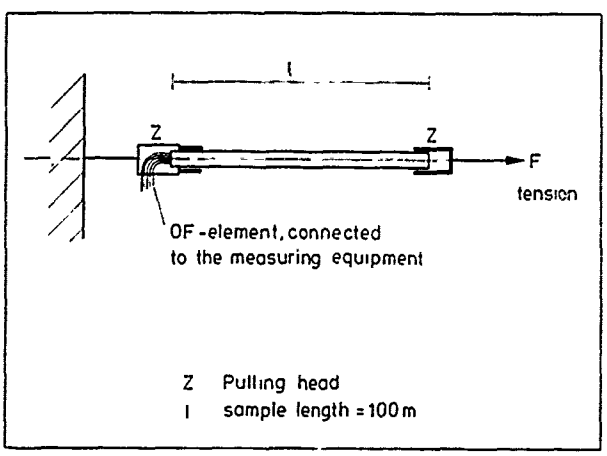

Fig. 11: Tension Test on OFTC

- **Torsion Test at ambient and maximum conductor temperature**

The OFTC was torded 10000 times with an angel of ± 60°C and the optical attenuation was measured with the IR-method during the test. To perform this test at conductor temperature 90°C the ends of the sample were connected in series. An induced current of 690 A heated the cable to the wanted temperature (Figure 12).

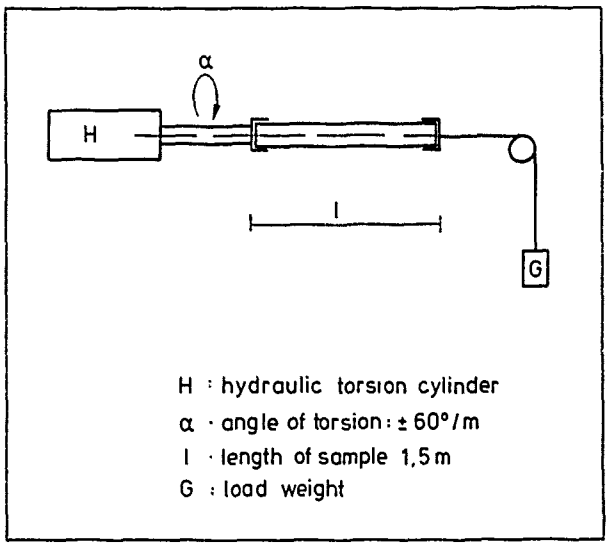

Fig. 12: Torsion Test on TC

- **Bending test at ambient and maximum conductor temperature**

The sample was spooled 20 times up and down at different bending diameters. Bending diameters: 12x, 10x, 8x, 6x D. For this test with conductor temperature 90°C the cable was heated by an induced current of 690 A. After every winding cycle the cable was heated to 90°C again (Figure 13).

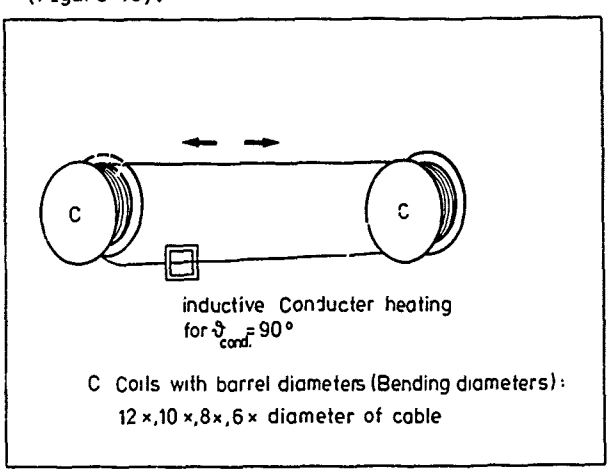

Fig. 13: Bending Test on TG

4.4 Results

The above mentioned tests showed that the OFTC withstood all the mechanical and thermal tests without faults.

The stresses that will occur in practice are accordingly uncritically for the OFTC.
For great importance is the applicability demonstrated at different temperatures, because in

most of the known publications tests were done at ambient temperature. The test results are shown in the figures 14 to 16.

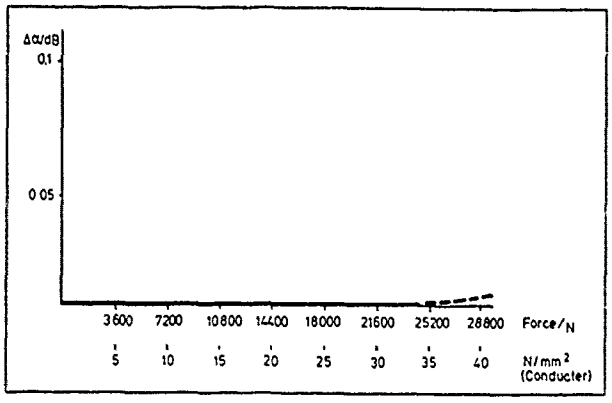

Fig. 14: Tension Test on OFTC

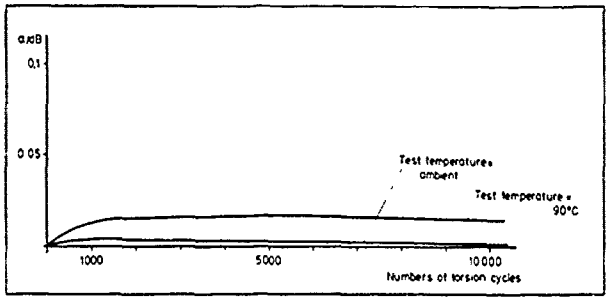

Fig. 15: Torsion Test on OFTC

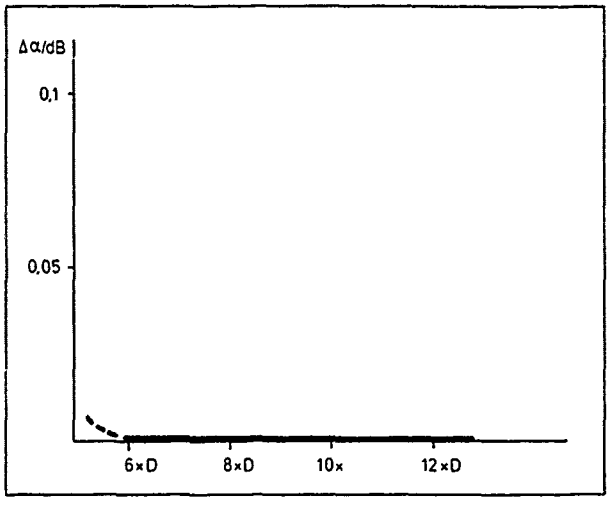

Fig. 16: Bending Test on OFTC

5. Outlook

This publication shows that the use of OF is without problems in combination with trailing cables, even if these cables are loaded with high mechanical and thermal stresses.The performed investigations were at first limited to the OF-element with graded index fibers, where the investigations were performed on different OF-elements.

Because of the mechanical tests the construction with central unit core and (FRP) - armouring seems to be the best. The decribed tests on the OFTC are limited for this element. For futurous constructions the application of other OF-elements in a trailing cable will be tested. Additionally the application of singlemode fibers in OF-elements will be tested too.

6. Appendix

IEC test methods on optical fiber element

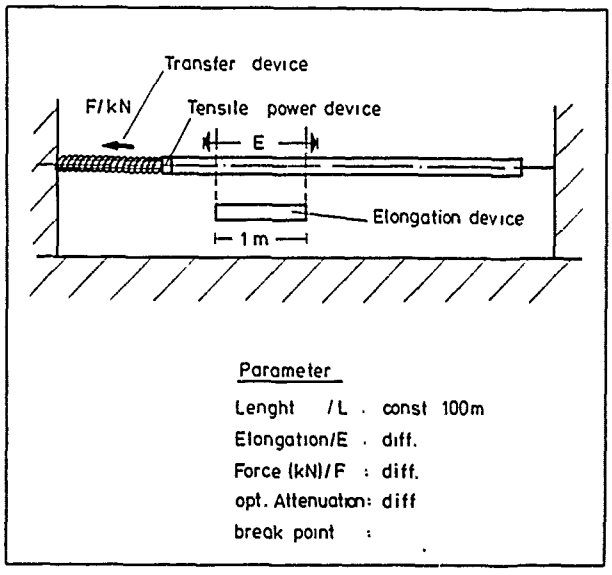

Tension: IEC 794-1-E1

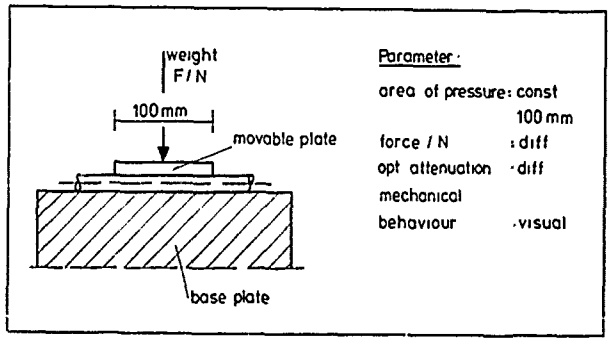

Crush: IEC 794-1-E3

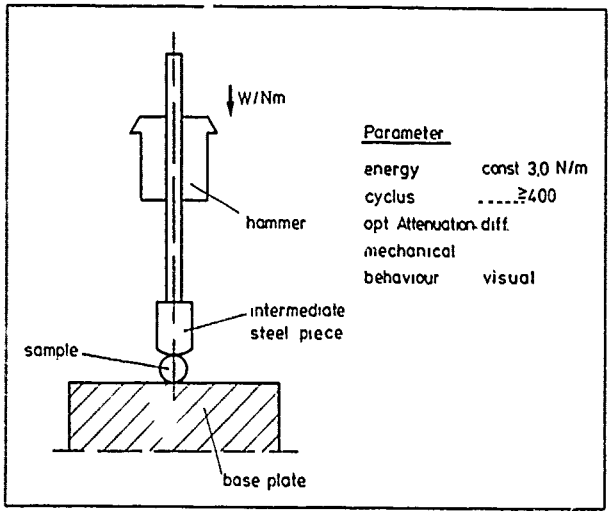

Impact: IEC 794-1-E4

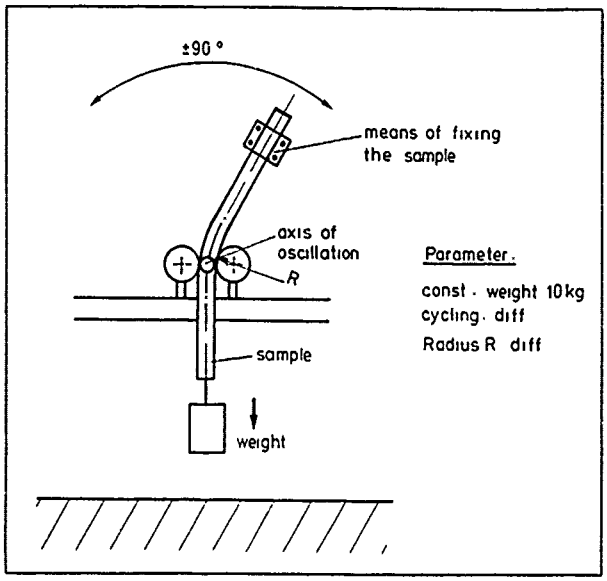

Repeated Bending: IEC 794-1-E6

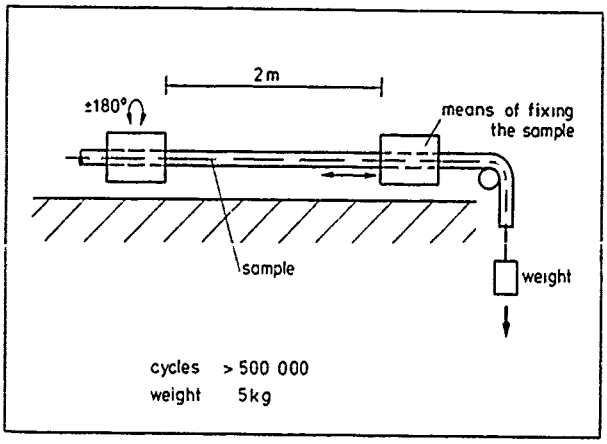

Torsion: IEC-794-E7

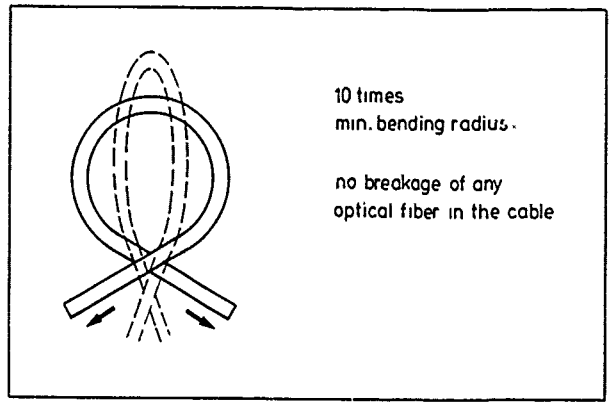

Kink: IEC 794-1-E10

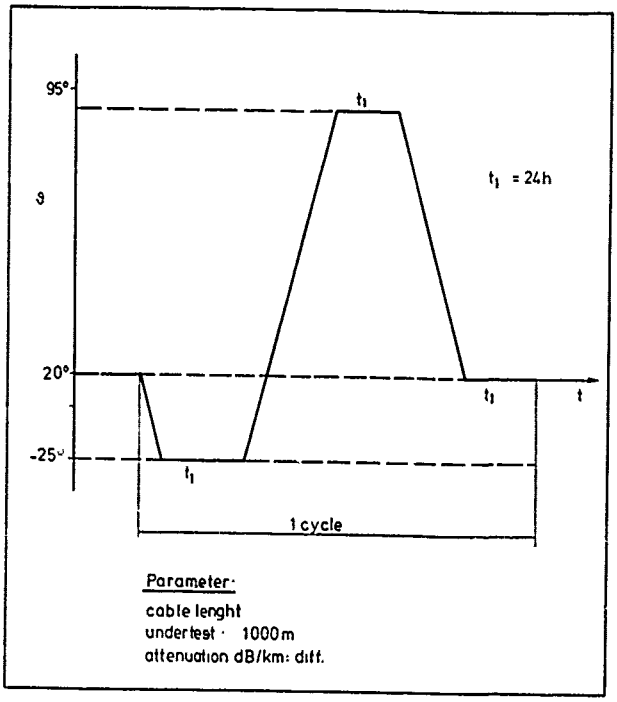

Temperature Cycling: IEC 794-1-F1

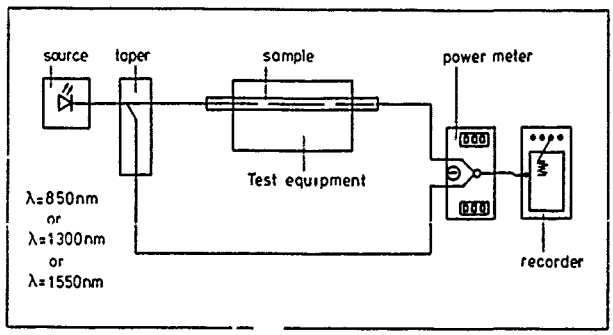

Optical Measurement . ...od for the Measurement of the Attenuation

7. Literature

(1) Araki et al., A new heat resistant optical fiber with special coating

(2) Bernd Harjes, Energie- und Datenüber' agung mit Lichtwellenleitern

Peter Delage
AEG KABEL AG
Mönchengladbach, West Germany

Peter Delage (33) is head of the Development Group for Special Optical Cables. After getting his Dipl.-Ing.-Degree he joined AEG KABEL in 1983 in the Development Group for Optical Fibre Cables. Since 1986 he covers his present position.

Rudof Buchwald
AEG KABEL AG
Mönchengladbach, West Germany

Rudolf Buchwald (39) is head of the Development Group for Flexible Power Cables. After getting hid Dipl.-Physics-degree he joined AEG KABEL in 1980 in the high voltage laboratory. Since 1986 he was a groupleader in the quality control for power cables. In 1989 he took his present position.

Georg Hög
AEG KABEL AG
Mönchengladbach, West Germany

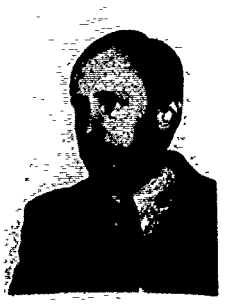

Georg Hög (40) is head of the Development Group for Optical Fibre Cables. He reached his Dipl.-Ing.-Degree from the University of Aachen and joined AEG KABEL in 1977. After being engaged in the development of symmetrical telecommunications cables he got the responsibility for this group in 1980. since 1985 he covers his present position.

EVALUATION OF FIBER OPTIC SYSTEM COMPONENTS FOR USE IN SPACECRAFT ENVIRONMENTS

Grant M. de Goede, Wen-Chi Chen, Allan R. Jackson

TRW, S&TG, Redondo Beach CA

Abstract

An evaluation was conducted on the performance of 1.3µm fiber optic system components in conditions which would indicate their viability for for use in spacecraft applications. The replacement of copper based cabling with fiber optics has occurred rapidly in ground based systems, but their use in commercial or military space is extremely rare or non-existent.

The commercially procured system components evaluated in this study would be applicable for use in medium to low data rate (150 Mbaud/s or less) digital onboard communication systems. The evaluation shows good promise for the early use of fiber optic systems which require low to medium link lengths between terminating stations, such as ring based local area networks.

Introduction

This paper presents test program data and evaluation of the capability of selected fiber optic components to perform in space environments. The emphasis is on commercially available components that would be required for a 1.3µm medium speed digital network such as an FDDI local area network.

The applicability of a component or system for space missions usually revolves around the accurate prediction and bounding of performance based on the range of temperature, shock, vibration and radiation that the part may experience during storage, launch and mission lifetime. Adequate characterization of a device's performance at military or commercial standardized environmental limits must be performed to insure that accurate reliability and worst case analysis can be done.

In the case of fiber optic local area network components numerous publications exist which examine device performance. In the early 1980s most of these studies involved .8µm wavelength fiber optic devices and systems. More recently attention has shifted to 1.3µm wavelength systems which offer technical advantages as well as the existence of a rapidly accepted local area network standard, namely FDDI.

System Components and Interconnects

The four main components which comprise the optoelectronic portion of a medium speed (125Mbaud) 1.3µm digital network are the light emitting diode (LED), PIN photodiode, connectors and optical cable. The main performance criterion for such a fiber optic system is the insertion loss or link budget between transmitting and receiving stations. An often overlooked but highly important portion of this insertion loss is the interface between the active devices and the optical cable or between two runs of optical cable.

The selection of the system components to be tested was based on a extensive study of commercially available components whose characteristics match those of the targeted medium speed space platform local area network. The choice of fiber was limited to multimode fiber with widely accepted core/cladding diameters and an inherent resistance to radiation induced attenuation. LED and PIN photodiode devices were limited to non-pigtailed TO-18 or TO-46 windowed packages which were compatible with standard connector/device receptacle mounts. While somewhat lower in coupling efficiency than pigtailed devices The use of this type of interconnect offers the advantages of cost and modularity. It should be noted that the availability and standardization of the FDDI connector was unclear at the time of these tests.

Test Mechanism

The selected components were subject to a series of tests and measurements including thermal vacuum test, thermal cycling test, vibration test and total gamma dose radiation test. Initial insertion loss measurements were performed in accordance with EIA-455-34. Thereafter coupling loss changes observed during and after testing were recorded.

The thermal cycling tests were carried out in accordance with EIA-RS-455 and FOTP-3. A total of 100 cycles from -65°C to 150°C were run for cable assemblies and 50 cycles for the LED and PIN photodiode connector assemblies.

Thermal vacuum testing used the same cycle conditions as the thermal cycling tests at a pressure of 1×10^{-5} Torr for 50 cycles minimum.

Vibration testing was set up per MIL-C-83522 Para. 4.7.11.4 and MIL-STD-202. Test conditions consisted of sinusoidal vibration from a frequency range of 10 to 2000Hz with a 20G peak level. For detailed procedures see EIA-RS-455 and FOTP-11.

Shock testing was performed per MIL-STD-202, method 213B. Conditions consisted of a 300G peak value half sine waveform of 3ms normal duration. For detailed procedures see EIA-RS-455-14.

Radiation testing was carried out in accordance with MIL-STD-883, method 1019. A cobalt 60 source with an exposure rate of 8400 Rads(Si)/minute was used.

Optical Fiber Characteristics

The two major fiber types which are used in medium speed LED based LAN applications are pure silica core step index fibers and doped silica core graded index fibers. A pure silica core along with either a polymer based (plastic) cladding or a Flourine (F) or Boron(B) doped silica cladding is the basis of the multimode step index fiber. A graded index fiber consists of a Germanium (Ge) doped silica core which can be codoped with F or Phosphorous and a cladding of pure or doped silica. A primary protective "buffer" coating of silicone (acrylate) is standard on both step and graded index fibers. Figure 1 is a sketch of a typical optical fiber's construction.

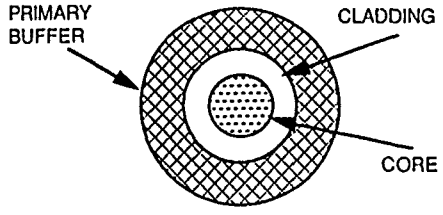

Figure 1. Optical Fiber Construction

The attenuation and bandwidth of a fiber type are the most critical performance factors to consider. In a space environment temperature and radiation will produce the greatest variation in a fibers attenuation.

For temperature, the most significant loss mechanism affecting optical cables is due to microbending losses at low temperatures. These losses can vary widely depending on the type of cable construction, "loose" tube or tight secondary jacket. Generally loose tube construction is likely to show smaller low temperature losses than tight buffered construction. However in both cases the buffer coating thickness and softness can be adjusted to reduce low temperature loss.[1] Primary buffer coated silica clad fibers without cabling show no significant change in attenuation due to temperature. However, uncabled plastic clad silica core fibers have exhibited extremely large losses(-20dB @ 70°C for a 50m length) at low temperatures.[2]

The study of radiation effects on optical fiber has proved to be a very complex task with conflicting results and theories often being put forth. However, for applications in a natural space environment permanent induced loss measurements provide useful worst case data even if a complete theoretical understanding of loss mechanisms, annealing and radiation hardening is currently unavailable. In general the induced loss due to ionizing radiation is higher at low temperatures and short times following exposure and partial annealing can be optically or thermally achieved.[3] Pure silica core fibers have exhibited induced losses of ≤10dB/Km for total doses of up to 10^7 rads(Si) at room temperature.[4] For relatively low total doses, graded Index multimode fibers with GeO_2 doped silica cores have been repeatedly shown to have lower radiation induced losses than GeO_2 cores which are also co-doped with P.[5]

Optical Fiber Testing

A step index fiber optic cable manufactured by Raychem (RC) and graded index fiber (with only a primary buffer) from AT&T (ATT) were chosen for testing. Their respective characteristics are listed in Table 1.

Manufacturer	Raychem	AT&T
Part Number	LSC	n/a
Core/Clad Dia. (μm)	100/140	62.5/125
Index Profile	Step	Graded
Numerical Aperture	0.22	0.23
Attenuation (dB/Km)	12	0.75-1.5
Bandwidth (MHz-Km)	20	150-600
Buffer Coating	Silicone	Polymid
Inner Jacket	ETFE	n/a
Strength Member	Kevlar	n/a
Second Jacket	ETFE	n/a

Table 1. Optical Fiber Specifications

The AT&T 62.5 μm core graded index fibers were terminated with SMA type Amphenol 906-110-5005 connectors or with Canon SZ20 type 3899 connectors. The AT&T fiber had a polymid primary buffer coating but no further jacketing. The Raychem cable, consisting of pure silica core step index fiber with tight jacket coating and Kevlar strength members, was terminated with either SSMA 01-01-001, SMA 906-500-5002, or Canon SZ20 connectors. Fiber assemblies were tested in the configurations shown in Figure 2.

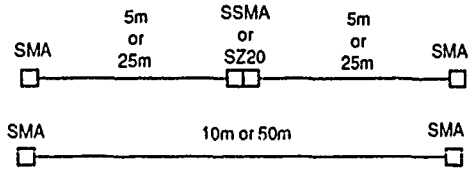

Figure 2. Optical Fiber Assembly Types

Thermal cycling, thermal vacuum, vibration, shock and radiation tests were performed on the fiber assemblies. The general fiber test measurement setup is shown in Figure 3.

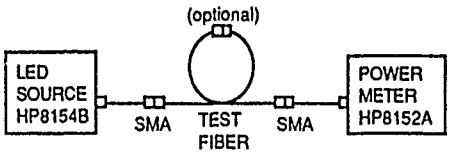

Figure 3. Optical Fiber Test Setup

The thermal cycling test results displayed in Table 2 show the average induced loss within each thermal cycle for various fiber assemblies. A positive value indicates a loss from the 25°C measurement and a negative value indicates a gain. The maximum induced loss for any cycle is also listed in parantheses. Raychem cables with an SSMA interconnect at the assembly center displayed the largest induced loss at low temperature. The other Raychem assembly and the two AT&T assemblies show little variation in their high and low temperature induced losses.

Table 3 displays the average induced loss within each thermal vacuum cycle. The Raychem fiber assemblies with SSMA interconnects show smaller average induced losses than were exhibited in the thermal cycling results. The 50m Raychem assembly with a midpoint SZ20 interconnect showed surprisingly large loss at high temperature.

Fiber Test Assembly	Average Induced Loss (dB)	
	25°C to 150°C	25°C to -65°C
RC 10m SMA/SMA	+0.3 (+0.7 max)	+0.2 (+0.3 max)
RC 10m SMA/SSMA/SMA	-0.1 (+0.6 max)	+0.9 (+1.8 max)
ATT 10m SMA/SMA	-0.01 (-1.4 max)	-0.1 (-1.2 max)
ATT 10m SMA/SMA	-0.5 (-1.1 max)	-0.2 (-0.7 max)

Table 2. Thermal Cycling Average Induced Loss

Fiber Test Assembly	Average Induced Loss (dB)	
	25°C to 150°C	25°C to -65°C
RC 10m SMA/SZ20/SMA	+0.3 (+1.5 max)	+1.4 (+2.6 max)
RC 10m SMA/SSMA/SMA	+0.2 (+1.2 max)	+0.3 (+1.0 max)
RC 50m SMA/SSMA/SMA	+1.4 (+1.9 max)	+0.1 (+0.8 max)
ATT 10m SMA/SZ20/SMA	-0.1 (-0.2 max)	+0.2 (+0.9 max)
ATT 10m SMA/SMA	+0.2 (+1.3 max)	+0.4 (+1.1 max)
ATT 50m SMA/SMA	-0.2 (-0.7 max)	+0.3 (+0.8 max)

Table 3. Thermal Vacuum Cycling Average Induced Loss

Vibration testing evaluated four cable assemblies, both SMA and SSMA connectorized samples. Test data showed less than .1dB attenuation change and no damage to the optical fiber assemblies. Shock testing similarly showed less than .1dB attenuation change and no damage to the optical fiber assemblies.

Radiation testing consisted of total gamma ray dose testing on a 50m AT&T fiber and a 10m Raychem optical cable. After a total dose of 3.2×10^7 rad(Si) the AT&T fiber had an induced loss of 3.77dB or an equivalent loss of .075dB/m. The Raychem fiber exhibited an induced loss of .68dB after a total dose 44×10^7 rad(Si) which is equivalent to .068 dB/m.

LED Characteristics

As with .8μm wavelength AlGaAs LEDs the two basic types of 1.3μm InGaAsP LED structures are the surface emitter and the edge emitter. Edge emitting LEDs are often touted as outperforming surface emitters in fiber optic communication systems due to their higher fiber coupled power and

coupled power modulation products.[8] However, in a space based short repeater distance, medium speed application these performance differences are not as crucial. Other characteristics that gain importance in such an application are device operating lifetime, coupled power sensitivity to fiber alignment, wavelength temperature dependence and output power sensitivity to both temperature and radiation.

The failure rate of surface emitters has been determined to be less than .3%/decade at 70°C (-1dB power output).[9] Edge emitters operating lifetimes have been determined to be equivalent or slightly lower.

The tighter optical beam divergence of edge emitters would likely make them more susceptible to variations in fiber coupled power to due shifts in LED/fiber alignment.

It is well known that increasing temperature shifts the LED's center wavelength of emission to longer wavelengths (coefficients for commercial devices ranging from .3nm/°C to .7nm/°C).[10]

Based on a survey of manufacturers specifications a surface emitter's output power is generally less sensitive to temperature variation than an edge emitter's output.[11] For increasing temperature a general value for surface emitting LEDs is .7%/°C while edge emitters exhibit a sensitivity of 1.1%/°C at best. However, these values were based on testing that did not extend into the temperature extremes that are represented by the thermal cycling tests described above. Specifying the output power sensitivity in these terms presents problems when extended over a large range i.e. for a 100°C temperature increase a edge emitter with a sensitivity of 1.1%/°C would have no optical output power. Other authors have identified an exponential equations for both surface and edge emitters which describe the output power and temperature relationship.[12,13] It should be noted that some edge emitters, depending on specific structure, tend to exhibit a threshold current lasing characteristic at low temperatures.

Previous gamma ray irradiation tests performed on InGaAsP LED's showed no significant degradation of optical output power for total doses of up to 10^7 rads(Si).[14]
However, it is unknown if these devices were under forward bias during irradiation. Other studies on AlGaAs LEDs have shown that forward biasing devices during irradiation
likewise results in small decreases in optical power at similar total doses.[15]

LED Testing

The devices chosen for test were a Lytel (LE-0399) TO-18 packaged surface emitter and a Stantel (LH40A-24) TO-46 packaged edge emitter. Manufacturers specifications are given in Table 4.

Manufacturer	Lytel	Stantel
Part Number	LE-0399	LH40-24
Power Out (I_f=100mA)		
(fiber launch, µW)		
62.5/125 µm	30	
50/125 µm		45
100/140 µm		100
Rise/Fall Time (ns)	4	5
Spectral Width (nm)	140	80
Forward voltage (V)	2 max.	2 max.
Forward current (mA)	150 max.	200 max.
Oper. Temp. (°C)	0 to +70	-20 to +70

Table 4. LED Specifications

The LEDs were soldered into the connector compatible device receptacle (either an Amphenol 905-138-5001 SMA device mount or a 202345 SSMA Raychem device mount) and then mounted on the test circuit board schematically shown in Figure 4. The LED TO packages were secured in the receptacles with the use of epoxy. The availability of commercially integrated device/connector components has only recently improved.

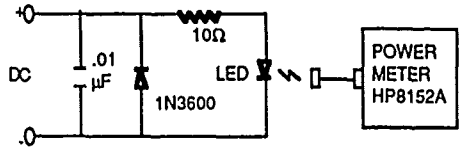

Figure 4. LED Thermal Cycle Test Circuit

Thermal cycling and total dose radiation tests were performed on the LED devices. In the thermal cycling test cases a 10m length of optical cable was connected to the LED receptacle with the appropriate SMA or SSMA connector. The opposite end of the 10m cable exited the test chamber to provide output power measurement access. A 50 mA drive current was used to model the dissipation characteristics of an LED operating under a 50% duty cycle and 100mA of "on" current. Only D.C. output power measurements were performed. For the radiation test cases the devices were exposed solely(not fitted in a device mount) and total optical power emitted from the device window was measured.

Table 5 displays the average power variation within each cycle for the three devices. It is notable that the Lytel LED with SSMA/Raychem fiber connection exhibited greater variation in power than the other Lytel test device. The edge emitting Stantel device as expected produced the

largest variation at high temperature. The loss of power at high temperatures was much less severe than predicted by both the equations given in (12) and (13). The LEDs were not under forward bias during the room temperature gamma ray irradiation testing. The results of this testing is shown in Table 6.

Device (Setup)	Average Power Variation Within Cycle (dB)	
	25°C to 150°C	25°C to -65°C
Lytel(SMA/AT&T)	-2.86	+1.38
Lytel(SSMA/Raychem)	-3.98	+2.39
Stantel(SMA/Raychem)	-4.5	+0.8

Table 5. LED Thermal Cycling Results

	Output Power Deviation From Prerad (dB)				
	Lytel-a	Lytel-b	Stantel-a	Stantel-b	Stantel-c
Total Dose (rad(Si))					
100K	+.03	+.02	+.26	+.34	+.22
1M	-.23	-.14	+.14	+.22	+.03
26M	-.02	-.02	+.09	+.16	+.04

Table 6. LED Output Power Radiation Effects

PIN Photodiode Characteristics

InGaAs PIN photodiodes are typically used in medium speed 1.3μm fiber optic receiver applications. The structure of these PIN photodiodes can be mesa or planar and operate with either front or back illumination. The spectral response of the InGaAs material provides a relatively high value of responsivity (.6 to .8 A/W) in the 1.3μm wavelength region.

Other important PIN photodiode characteristics, for the application being considered, are response speed, reliability and dark current. A PIN photodiodes response speed (rise/fall time) is also directly related to the devices photosensitive window area. A larger area results in greater device capacitance which results in a slower response speed. Currently available commercial InGaAs photodiodes (125 μm photosensitive diameter or less) with TO style packaging are specified with rise/fall times ranging form .3ns to 2.0ns.

Accelerated life testing of planar InGaAs photodiodes has been extensively performed with the thermal activation energy for these devices ranging between .85eV and 1.5eV.[18,19] These figures lead to failure rates for 70°C operation ranging from a high of .0036% failures/decade to a low of .000022% failures/decade. It should be noted that failures in these studies is achieved when a ten fold increase of dark current from the original value is obtained . It is often cited that the planar structure has been shown to be more reliable and immune to environmental conditions than a mesa structured device due to the ease of passivation with SiN.[20,21,22]

A PIN photodiode's dark current (or reverse leakage current) is the intrinsic current produced even when no optical power is incident upon it. The dark current is very dependent on the both device temperature (positive correlation) and the area of the photosensitive surface (positive correlation).

A survey of manufacturer's specifications shows that most commercial InGaAs photodiodes (125μm photosensitive diameter or less) exhibit a dark current of between 1 and 10 nA at 25°C. The relationship of dark current to temperature has been described by others as (Eq. 1) $I_d \approx e^{-E_g/nKT}$ for operation over 20°C to 100°C. E_g is the bandgap energy, K is Boltzmanns constant, T is the temperature in Kelvin and n is between 1 and 2.[23,12] The large dark current at high temperatures drastically increases the shot noise contribution of the photodiode at the receiver and along with the increasing thermal noise (based on the load resistor) can dramatically affect receiver sensitivity.

With the exception of leakage current, InGaAs photodiodes have shown no degradation of optical and electrical characteristics for a total dose of up to 10^8rads(Si).[14] The dark current exhibited increases up to a factor of six from pre-irradiation values.

Transient radiation within the PIN photodiodes operating environment creates radiation induced current which is similar to dark current. For dose rates of up to at least $1x10^4$rads(Si)/s

this radiation induced current will be insignificant compared to the nominal dark current of an InGaAs PIN photodiode (125 μm diameter).

PIN Photodiode Testing

The planar PIN photodiode samples tested were a Lytel TO-18 packaged device and a Telcom TO-18 packaged device. As with the LEDs the photodiodes were placed in SMA device receptacles and then mounted on the test circuit board schematically shown in Figure 5.

Unfortunately only two photodiode test samples were available for thermal cycle testing. The devices were connected to an optical light source in the same fashion that the LEDs were connected to a output power meter. A -5V bias was continually supplied to the devices during the thermal cycling. Both the dark current and the current produced with a 1.3μm optical source at a stable intensity were measured. Throughout the temperature cycling tests the dark current and optical response currents were very consistent at a given individual temperature. Table 7 displays the average currents measured for the three temperatures.

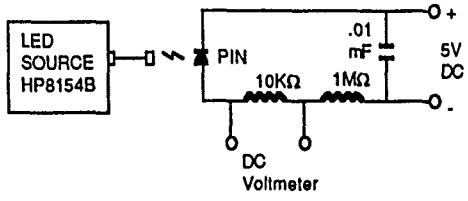

Figure 5. PIN Photodiode Test Circuit

	Telcom AT&T 10m		Lytel Raychem 10m	
Temp. (°C)	Dark(nA)	Illum(nA)	Dark(nA)	Illum(nA)
-65	0.6	1530	0.6	2270
+25	35	1992	0.4	4230
+125	997	2624	552	4226

Table 7. PIN Photodiode Temperature Cycling Results

The large dark current seen at room temperature for the Telcom device is outside the manufacturers specification but the trends exhibited by both devices are notable. An extreme increase in dark current at high temperatures is seen in both devices.

The devices both exhibit a significant current decrease for incident optical power measurements at -65°C. These low temperature current losses are partially attributed to the fiber power losses seen in the fiber thermal cycling tests but low temperature photodiode characteristics may also be contributing.

Link Budget Analysis

A link budget for a 1300nm spaceborne ring network fiber optic node to node connection can be calculated using the information presented. The link budget in Table 8 is for a link consisting of a surface emitting SMA connectorized LED, AT&T 62.5μm core fiber (tight buffer jacket loss estimated) and a SMA bulkhead interconnect. Similar positive link margins can be calculated for the other components evaluated. The minimum loss case assumes the largest LED fiber power launch and no channel loss.

LED Fiber Power Launch (average 50% duty cycle)	-18.2dBm (15μW)	
LED Delta (-65 to +150°C)	-2.9dB	
	+1.4dB	
LED Lifetime Delta	-1.0 dB	
Bulkhead Connector	-1.0 dB	(est.)
Connector Delta (-65 to 150°C)	-0.5 dB	(est.)
Fiber (30m)	-0.1 dB	
Fiber Delta (-65 to 150°C)	-2.0 dB	(est.)
Fiber Delta ($1x10^7$rad(Si))	-2.3 dB	
Fiber Output Power (min)	-27.8 dBm	
(max)	-16.8 dBm	

Table 8. Sample Link Budget Calculations

Commercially available FDDI receivers are specified with a worst case -31dBm sensitivity (average power output from a 62.5μm fiber) for $2.5x10^{-10}$ BER at 125Mbaud.[28] However, these receivers are typically only specified for operation up to 70°C. As temperature increases higher the shot noise contribution of the PIN photodiode's rapidly increasing dark current will overtake the thermal noise, due to the receiver's front end load resistance, as the dominant noise source in the receiver. This will drastically reduce the receiver's sensitivity. Thus, it may be necessary to provide control of high temperatures in the electronics bay housing the fiber optic receiver.

Star coupled fiber optic networks represent an alternative to the ring approach used in FDDI. However, the introduction of an optical star coupler would add a large signal loss between stations(10dB for an 8x8 star coupler). This is severe and any realistic positive link margin for a star network in a space application would seem unattainable. In summary Table 8 shows that ample link margin exists for a spaceborne 1.3μm ring network using currently available components.

Besides the establishment of a viable link margin for a spaceborne network other issues require further investigation. At the component level these include effects of the space environment on LED and photodiode bandwidth and the electronic transmitter and receiver circuitry. System issues include network fault tolerance and most importantly an analysis of the benifits and detriments in the areas of power, weight, complexity, noise immunity and throughput that fiber optics provide for a particular application.

REFERENCES

1. B. Wiltshire, M. H. Reeve, "A review of the environmental factors affecting optical cable design," *J. Lightwave Tech.*, Vol. 6, No. 2, pp. 179-184, Feb. 1988.

2. A. R. Johnston, L.A. Bergman, "Application of fiber optics in spacecraft," *SPIE*, Vol. 224, pp. 74-84, 1980.

3. E. J. Friebele *et al.*, "Radiation effects and defect centres in fiber optic materials," *Proc. Opto '86* (Paris, France), Vol. 4, No. 8, pp. 436-9, Aug. 1986.

4. T. Kakuta *et al.*, "Radiation resistance characteristics of optical fibers," *J. Lightwave Tech.*, Vol. 4, No. 8, pp. 1139-1143, Aug.1986.

5. A. Iino, J.tamura, "Radiation resistivity in silica optical fibers," *J. Lightwave Tech.*, Vol. 6, No. 2, pp. 145-9, Feb.1988.

6. R. Greenwell, "Fibers that stand up to radiation hazards," *Photonics Spectra*, pp. 129-139, Apr. 1987.

7. R. H. West, "A local view of radiation effects in fiber optics," *J. Lightwave Tech.*, Vol. 6, No. 2, pp.155-164, Feb. 1988.

8. M. Ettenberg *et al.*, "On the reliability of 1.3μm InGaAsP/InP edge emitting LEDs for optical fiber communication," *J. Lightwave Tech.*, Vol. 2, No. 6, pp. 1016-1023, Dec. 1984.

9. M. Fukuda, "Laser and LED reliability update," *J. Lightwave Tech.*, Vol. 6, No. 10, pp. 1488-1495, Oct. 1988.

10. D. M. Fye, "Low current 1.3μm edge emitting LED for single mode fiber subscriber loop applications," *J. Lightwave Tech.*, Vol. 4, No. 10, pp.1546-1551, Oct. 1986.

11. A. Jackson *et al.*, "Formal PM&P report," *TRW IOC*, Dec. 1987.

12. D. Gloge *et al.*, "High speed digital lightwave communications using LEDs and PIN photodiodes at 1.3μm," *Bell System Tech. J.*, Vol. 59, No. 8, pp. 1365-1373, Oct. 1980.

13. H. Temkin *et al.*, "InGaAsP LEDs for 1.3μm optical transmission," *Bell System Tech. J.*, pp. 8-24, Jan. 1983.

14. B. Leskovar, "Radiation effects on optical transmission systems," *Trans. on Nuclear Science*, Vol. 36, No. 1, pp. 543-551, Feb. 1989.

15. J. J. Wiczer, C. E. Barnes, "Optoelectronic data link designed for applications in a radiation environment," *Trans. on Nuclear Science*, Vol. 32, No. 6, pp. 4046-4049, Dec. 1985.

16. J. M. Senior, "Optical Fiber Communications," London: *Prentice Hall*, 1985, ch. 7.

17. R.H. Saul, "Recent advances in the performance and reliability of InGaAsP LEDs for lightwave communication systems," *Trans. on Electron Devices*, Vol. 30, No. 4, pp. 285-295, Apr. 1983.

18. S. R. Forrest *et al.*, "Reliability of vapor-grown planar $In_{0.53}Ga_{0.47}As$/InP PIN photodiodes with very high failure activation energy," *Electron Device Letts.*, Vol. 9, No. 5, pp. 217-9, May 1986.

19. H. Ishihara *et al.*, "High temperature aging tests on planar structure InGaAs/InP PIN photodiodes with Ti/Pt and Ti/Au contact," *Electronics Letters*, Vol. 21, No. 10, pp. 447-8, May 9, 1985.

20. J. C. Campbell *et al.*, "Planar InGaAs PIN photodiodes with a semi-insulating InP cap layer," *Electronics Letters*, Vol. 21, No. 10, pp. 447-8, May 9, 1985.

21. Snodgrass, Klinman, "Lightwave receiver for the undersea lightwave system," *J. Lightwave Tech.*, Vol. 2, No. 6, pp. 969-973, Dec. 1984.

22. S. Miura, "Planar imbedded InP/GaInAs PIN photodiode for very high speed operation," *J. Lightwave Tech.*, Vol. 5, No. 10, pp. 1371, Oct. 1987.

23. G. H. Olsen, "Low leakage high efficiency reliable VPE InGaAS 1.0-1.7μm photodiodes," *Electron Device Letts.*, Vol. 2, No. 9, pp. 217-9, Sep. 1981.

24. O.K. Kim,"A low dark current planar InGaAs PIN photodiode with a quaternary InGaAsP cap layer," *J. Quantum Electronics.*, Vol. 21, No. 2, pp. 138-143, Feb. 1985.

25. K. W. Mitchell, "Optimizing photodetectors for digital communication in radiation environments," *Trans. Nuclear Science*, Vol. 25, No. 6, pp. 1545-9, Dec. 1978.

26. K. W. Mitchell, "Optimizing photodetectors for radiation environments," *Trans. Nuclear Science*, Vol. 24, No. 6, pp. 2294-7, Dec. 1977.

27. J. J. Wiczer *et al.*, "Transient effects of ionizing radiation in photodiodes," *Trans. Nuclear Science*, Vol. 28, No. 6, pp. 4397-4401, Dec. 1981.

28. "DLX2000 transceiver specification", British Telecom & DuPont Technologies, Jul. 1989.

29. W. H. Hardwick, A. H. Kalma, "Effects of low dose rate radiation on optoelectronic components and the consequences upon fiber optic data link performance", *Trans. Nuclear Science*, Vol. 26, No. 6, Dec. 1979.

30. G. A. Taylor, J. C. Thacker, "Space application of fiber optics systems," *SPIE*, Vol. 296, Fiber optics in adverse environments, 1981.

Copper & Optical Fibre Transmission Network of Italy, Current & Future Requirements

F. Esposto, F. Montalti, F. Nanni.

SIP-Direzione Generale, Rome Italy

ABSTRACT

The rapid evolution toward digital technologies will provide a varied and powerful types of technical communication facilities.
All types of information are handled, transferred, processed and stored by uniform digital techniques. This requires the availability of high capacity digital transmission media.
For this reason SIP, Italian Telecommunication Operating Company is strongly involved in a development programme of optical fibres for the junction and trunk network, and at the same time is improving the performance of the subscriber network with the introduction of a new family of multipair copper cables.
Bearing in mind that the key for the successful introduction of the fibre in the subscriber loop is the availability of POTS services with fibre at competive costs compared with the copper ones, several experiment with innovative technologies are in a development stage.

INTRODUCTION

SIP is responsible in Italy for the provision of TLC services at national level. To face the growing and more and more diversified needs of the market with adequate network infrastructures and service offering, SIP is currently engaged in a complex restructuring and modernization process at technological, structural and operative level.
The growth of investments is a significant measure of the SIP effort in developping and modernizing the telecommunication network. By the launching in 1988 of an accelerated development plan (named "Europe Plan"), the SIP investments passed from about 5000 billion lire in 1987 to 5900 and about 7800 billion lire in 1988 and 1989 respectively; the total investments in 1990 is 9000 billion lire and in the period 1991-1994 is foreseen about 40000 billion lire.

STRATEGIC GUIDELINES

The strategic guidelines for the development of the TLC network and services can be summarized by the following key issues:

Development of the basic telephone service

A first-priority target is to assure a subscriber and traffic growth rate of the network coherent with the maximum potential demand, in order to line up Italy to the most developped countries in Europe. The subscriber lines will grow from the present 22 millions to more than 25 millions in 1993 at an average annual growth rate of 4.9%. The annual growth rate of the traffic is expected to be higher (6% in average) passing in the same period from 24 to more than 30 billion calls per year.

Improvement of the quality of service

The objective of an outstanding quality of the network and the offered services is essential. From the network strategy point of view, the key factors to improve the quality of the service are the modernization of the network infrastructures, the deployment of the most advanced technologies, the development of integrated operation support systems allowing for a centralized real-time management of network traffic and facilities.

Digitalization of the network

The digitalization of transmission and switching facilities is essential to pave the way for the introduction of new services, the improvement of the quality standards and the consequent incentivation of the traffic growth.

Development of specialized data networks

The continuing high growth rate and data transmission market, near to 20% per year, entails the upgrading and the development of the public data networks, namely RFD (circuit-switched network for voice and data), Itapac (packed-switched network), and CDN for the provision of digital leased lines.

Introduction of new technologies

Among the newer technologies allowing for enhanced service offering, an important role is played by ISDN; the pilot Network will be open in 1991 in 10 major metropolitan areas collecting initially 3000 subscribers; the widespread offering will start in 1993 with the massive diffusion of ISDN functionalities in the basic digital network and the foreseen interconnection to the other European networks.
The laying of optical fibre cables, beside rapidly increasing in the trunk transmission network, will be gradually extended to the subscriber loop plant; the initial target is to provide early availability of high bit rate capacity and wideband services to major business customers in large metropolitan areas.

Evolution of the network management systems

The automation of operation procedures and the introduction of more advanced network management systems that SIP has already introduced, made easier and more efficient in a digital network environment, is a driving force to improve the quality of service and to increase the operation efficiency (costs reduction of operation and maintenance).

EVOLUTION OF THE DIGITAL NETWORK

The first introduction of digital switching into the Italian network
began in 1980 at transit level and in 1984 at local level. Now the industrial reconversion cycle is completed and from 1989 only digital switching is supplied.
At the end of 1989 the total subscriber digital lines installed, add up to about 5.8 million, i.e. 25% of the total 23.9 million lines; the percentage of digital subscriber lines will reach the 55% at 1993.

Sensibly greater is the digitalization rate in the transit switching side, where from the present 50% we will reach the 85% of digital trunks at 1993.
In the trunk transmission network, presently consisting of 55 million km-circuits, the first PCM transmission systems were introduced in the early '60ies at progressively increasing bit rate from 2 Mbit/s to 8 and 34 Mbit/s, on both copper cables and radio links; more recently higher capacity systems at 140 and 565 Mbit/s has been introduced, mainly on fibre optical cables. Since 1986 no copper cable is installed, with the exception of the loop plant.
Depending on the technical availability and the economic application areas of PCM systems, together with the digital switching development trend at the different hierarchical levels, the penetration of digital systems in transmission network is rather different on the short distances with respect to the medium and long distances. In the period 1989 to 1993 the percentage of digital km-circuits is increasing from 35% to 60% in the local network, from 77% to 100% in the SIP trunk network.
The extension of the fibre optical network is presently equal to 5600 Km-cable and will grow to 27500 km-cable in 1992. At this end, beside the large deployment of optical cables at metropolitan and regional level, a nationwide optical network will be available, having a capacity and a meshing degree sufficient to guarantee multirouting and protection rerouting against severe congestions or catastrophic failures.

STRUCTURE OF THE CABLE NETWORK

Junction and trunk network

The experience acquired during the last three years (1987-1989) of field applications allowed to confirm the excellent performance of the optical cables and systems in operative traffic conditions.
Starting from middle '86, as soon as the single mode fibre became reliable and convenient from the economical point of view, after the necessary field trials, this technology was gradually introduced in the network with the installation of cables for 38.000 Km of fibre in 1987, 97.000 in 1988 and approximately 180.000 Km in 1989.
Taking into account the cable performances and the traffic need a medium/high count fiber cable

has been developed both for underground and aerial installation.
The fibre used is single mode optimized at 1300 nm with matched cladding index design. In Table 1 the optical characteristics of such fibre are reported. The cable for trunk and junction network application has a loose slotted core structure with number of fibres ranging from 10 to 60. In order to reduce the size of the cable the fibres are stranded together in bundles of ten for the underground cable (Fig. 1) and in bundles of five for the aerial cable.
The cable is jelly filled with PU and PE inner and outer sheaths with a double layer of aramidic yarns as pulling element.
In the underground cable an heat welded stainless steel corrugated tape 0.15 mm thick, acts as humidity barrier and rodents protection.
In Table 2 the mechanical characteristics of the optical cables above described, are reported.
The cables are presently equipped with 34 Mbit/s, 140 Mbit/s and 565 Mbit/s transmission systems. The 565 Mbit/s system at 1550 nm operational wavelenght is already installed (by June 1989); the high performances and the excellent results obtained (typical repeter span = 80 km) with such transmission system are a reason to continue its application in the long distance network plants.
The total quantity of fibre installed by the end of 1990 adds up to about 625.000 km.
This value includes both Subscriber, Junction and Trunk network (Fig. 2).
At the end of 1990, among the systems at 565 Mbit/s already installed and those which are being installed, the resulting extension is:

- 565 Mbit/s (1300 nm) systems:
  25.000 km/system

- 565 Mbit/s (1550 nm) systems:
  6000 km/system

The next step takes into consideration systems at higher bit-rate. Currently SIP is considering the opportunity to introduce in the network the 2.4 Gbit/s system, bearing 16 bit streams at 139,264 Kbit/s, for which the repeater span will remain similar to the present 565 Mbit/s (so the allowed attenuation between the point S and R is likely to be equal to 24 dB).

Subscriber Network

Starting from the end of 1988 a new generation of multipair copper cable (fully colour coated structure, following IEC 708/1 standard) has been introduced in the subscriber network, in order to meet the requirements of the 2 Mbit/s transmission lines that link the digital loop carriers (30 channels multiplexers) to the digital local switches.
The design of the new multipair copper cable has been studied to improve high frequency characteristics.
The copper wire ($\varnothing$ = 0.4 mm) is Polyethylene insulated and twisted in pairs. The pairs are combined together to form the 10 and then 100 pairs units.
The cable ranges from 10 to 2400 pairs, can be jelly filled and has Polyethylene/Aluminium inner and Polyethylene outer sheaths. Both armoured (steel tape) and unarmoured solutions are used.
In order to guarantee the final product quality and performances of such cables a quality assurance programme is under development in cooperation with the manufacturer industries.
The multipair copper cables have been extensively used in Italy during 1989 for distribution network: 6 Million km/pair.
The future overall program foresee for 1990 and 1991 years, approximately 15 Million km/pair.
Furthermore it is remarkable the introduction, in near future, of 400 channels multiplexers.
The possibility to use optical cables for business subscribers network is rapidly growing. Nowadays there are more than 30.000 km/fiber in the subscriber network.
The problems to be solved in these applications are several. Field demonstrations of fibre based broadband networks have generally been successfull from a technical point of view, but the link cost for POTS services is still high and this is the main drawback to a widespread diffusion.
As a consequence the key for the successful introduction of the fibres into the subscriber loop is a drastic reduction of the cost of the involved technologies, that can be obtained for example with mass production of the components, large scale integration of the optical and electronic devices, system optimization, improvement of manufacturing process.

In this scenary a very interesting solution is offered by the ribbon technology already used with good results by other companies. SIP is seriously considering ribbon technology for distribution network with the goal of giving to residential subscriber POTS services on fibre at a competitive price if compared with the copper ones. In this way the network will be ready for the implementation of new services.

With these targets, and in order to make experience with this new technology some experimental plants are under development and will be completed at the end of 1990.

In this case each ribbon contains 4 fibres; the cable has a semiloose slotted rod (5 slots) with 5 ribbon inserted into each slot to form a 100 optical fiber unit (Fig. 3).

The maximum fibre count up to now manufactured in Italy is 400, but major potentiality cables can be designed.

The cable is jelly filled with PU and PE inner and outer sheaths with a double layer of aramidic yarns as pulling element.

An heat welded stainless steel corrugated tape is used. The cable design and the fibre used (single mode type) is studied to guarantee the mechanical, environmental as well as optical performance both 1300 nm and 1550 nm wavelengths.

CONCLUSIONS

The dramatic evolution of the Italian cable network will continue in order to support the change from analog to digital technology with the goal of properly satisfying the market pressure and giving new services and better quality to the subscribers.

The SIP's network is continuosly evolving toward new technologies and solutions that show high quality to support both the various telecommunications services expected and the raising of random-demand of new services from subscribers.

Both a new generation of multipair copper cables for subscriber network and optical fibre cables for trunk and junction network are extensively used with excellent results and better quality; moreover a new generation of optical fibre ribbon cables for local loop have been designed to be on time with the world technical evolution and to be ready for the implementation of new services, mostly for broadband applications, developping the "Fiber to the Home" project.

Feliciano Esposto
SIP-D.G. R/IT-CM
Via di Val Cannuta, 250
00166 Roma-Italy

F. Esposto was born at Arcevia (Ancona), Italy in 1948. He received his doctorate in physics from the University of Torino in 1976. In 1969 he joined CSELT, where he did research on optics and optical communications, particularly holography and optical fibre characterization. Since 1980 he is with SIP, the Italian Telecommunication Operating Company, wich like CSELT belongs to the STET group, where he has been involved in optical fibre cables design and characterization. At present he is the Manager of "Cables, Apparatus Design and Outside Plant" Division at SIP Headquarters in Rome. Feliciano Esposto is co-author of many papers and lecturers at Superior School "Guglielmo Reiss Romoli"

Francesco Montalti
SIP-D.G., R/IT-CM
Via di Val Cannuta, 250
00166 Roma-Italy

F. Montalti was born at Firenze, Italy in 1953. He received the doctorate in Physics from the University of Rome in 1976. In 1979 he joined the Research Centre of Industrie Face Standard where he has engaged in research about optical fibres, integrated optics and optical transmission systems. In 1985 he joined SIP, the Italian Telecommunication Operating Company, where he is currently responsible of the development of cable and apparatus for Telecommunication plants. He is involved in the activities of International Standardization Entities namely CCITT and IEC.

Fabrizio Nanni
SIP-D.G., R/IT-CM
Via di Val Cannuta, 250
00166 Roma-Italy

F. Nanni was born at Roma, Italy, in 1960. He received the title of doctor in Physics from the University of Roma "La Sapienza". From 1986 he has collaborated with the laboratory of research on optical communication Fondazione "U. Bordoni" in Rome working on Photoconductivity Ultrafast Phenomena, Semiconductor Lasers and Ultrafast Photodiodes characterization. In 1988 he joined SIP, the Italian Telecommunication Operating Company, where he has been engaged in the study and development of optical fibres, copper cables as well as optical cables specification and characterizationboth in laboratory and in field. Moreover his present responsabilities include CCITT Comm XV, IEC 86A, ETSI-TM1 and COST 218 activities.

SINGLE MODE FIBRES
OPTICAL CHARACTERISTICS

	STANDARD	REDUCED MODE FIELD		DISPERSION SHIFTED
	1300 nm	1300 nm	1550 nm	1550 nm
CORE DIAMETER (μm)	10	9.5	10.5	8.1
CLADDING DIAMETER (μm)	125	125	125	125
PRIMARY COATING DIAMETER (μm)	250	250	250	250
ATTENUATION (dB/km)	0.3 - 0.5	0.31 - 0.45	=< 0.25	0.20 - 0.28
CHROMATIC DISPERSION (ps/nm*km)	=< 3.1	=< 3.1	=< 18	=< 3.0
CUT-OFF WAVELENGTH	1100 - 1290	1150 - 1290	1150 - 1290	1120 - 1320

TABLE 1

MECHANICAL CHARACTERISTICS OF CABLES

NUMBER OF FIBRES	10 - 30	40 - 50	60	100
OUTER DIAMETER (mm)	18	19	19.5	22
WEIGHT (kg/km)	<280	<320	<350	<450
MAX PULLING STRENGTH (KN)	2.5	3	3	4
PERCUSSION RESISTANCE (J)	>20	>20	>20	>20
CRUSHING RESISTANCE (KN)	>15	>15	>15	>15
MINIMUM BEND RADIUS (mm)	250	250	250	300

TABLE 2

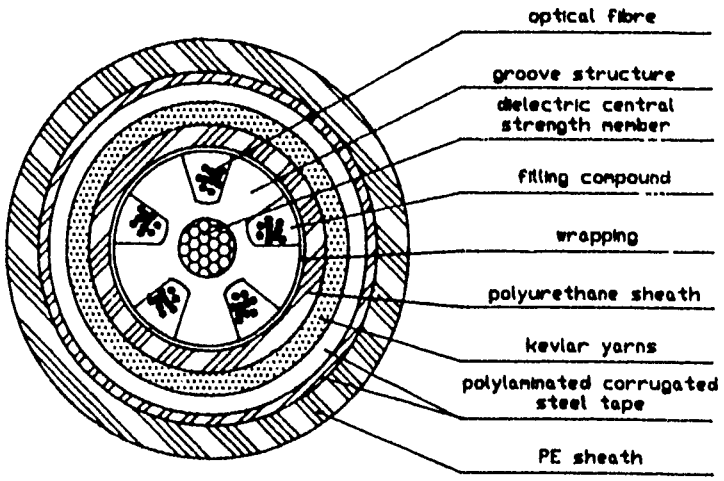

FIG.1

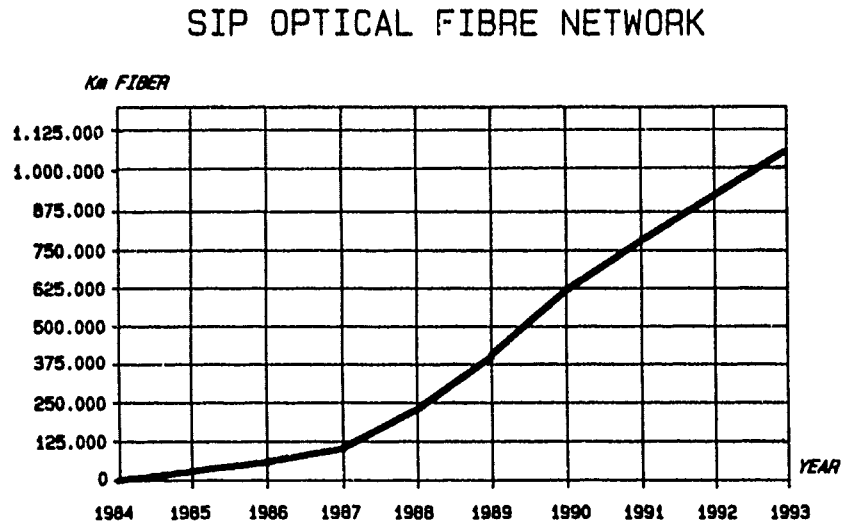

FIG.2

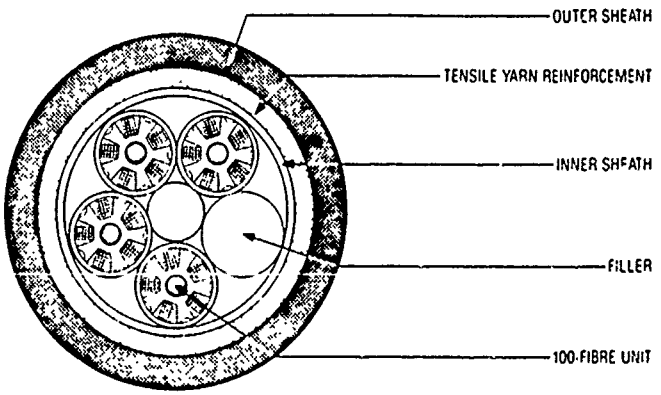

Figure 3 -400-fibre slotted core ribbon cable

EVOLUTION OF FRANCE TELECOM'S TRANSMISSION AND DISTRIBUTION NETWORKS

Jean LE MEZEC

Centre National d'Etudes des Télécommunications
France Telecom, Lannion, France

Abstract

Some of the main features which characterize the France Telecom's network will be first reviewed : they include a high digitalisation of the network, the introduction of an extensive videotex service known as MINITEL, availability of ISDN at every point of the national territory, the development of videocommunication networks. The evolution trends in each part of the network will then be analysed : trunk network, local transmission, subscriber loops.

France Telecom's network has undergone a profound evolution over the past twenty years, an evolution which will become even more pronounced during the next ten years. When assessing the evolution of the architecture of the network, the services it offers and the mode of transfer of signals, it is important to take a long term view ;it is even more crucial when analysing the evolution of the infrastructure radio towers, cables and associated equipment. This infrastructure, which represents a considerable amount of investment evolves to keep pace with the demand of services and the technological improvement ; the pace, of course, will be dramatically accelerated when a new technological breakthrough is made in the relevant field. The successive breakthroughs in optical techniques, in microelectronics and in signal processing were, - and will be in the future, - accelerating factors in the evolution of the network.

A similar long term evolution of the telecommunication network is taking place in all developped countries.A similar observation can be made in all major technical domains. Some sociologists call this effect "the autonomy of technique", [1] a worldwide phenomena, independant, in its long term aspects, of the first decisions taken in each country. As an example, we observe that all countries have adopted digital techniques for switching and transmission, whatever were the first choices. Similarly, all countries are turning to optical fibers, as the main transmission medium.

However, each country differs from the others in the short term, as a result of local factors, such as national regulations (are you, for instance, allowed to transmit TV channels right to the home, or not) or geographical factors (large or small cities, distances, mountains for instance). Moreover, in order to understand the short term trends, one must examine historic factors which determine the present state of the telecommunication network in each country, including strategic decisions taken by the country in question. For France, such decisions concerned digitalisation, videotex and videocommunication.

Accordingly, let us begin by describing the dominant features which characterize the France Telecom network before examining the major trends governing the long term evolution in each part of the network.

The highly digitalised France Telecom network.

The France Telecom network is mainly devoted to telephone appliances and, at a smaller extent, to data communication, including videotex. For a French population of 56 million, we have, in 1990, approximately 27 subscriber lines. Almost every home is connected to the telephone network, some subscribers have two or more telephone lines, and a large number of business users have their own PABX connected to the main network.

The mean feature of this basic telephone network, - used also for data transmission, - is its high degree of digitalisation. Let us quote the following figures, valid by the end of 1988 and improved on over the last two years, which represent the percentage digitalisation of different parts of our telephone network :

- 63 % of the local exchanges ;
- 68 % of the trunk exchanges ;
- 93 % of local transmission ;
- 69 % of trunk transmission.

In order to understand the relevance of these figures, it would be necessary to give a thorough description of the local telephone network. Some indications will be given later in this paper, but, for the time being, let us say that these figures are a result of the early technical decision taken around 1970, in favor of digital switching and transmission techniques at a time where other countries opted for spatial electronic switching. As a consequence, every French subscriber, - residential or professionnal, - can be connected upon request by a digital link to the national digital network.

This possibility explains the early commercial opening and rapid extension of ISDN in France, - our so-called NUMERIS system : commercial opening for the basic rate of 144 kbit/s in december 1987 and for the primary rate of 2 Mbit/s in september 1989 ; national coverage in 1990. This rapid growth is possible as a result of many factors : high level of digitalisation of the network ; digital connexity through the whole territory since 1986 ; synchronisation of the whole network (for the 2 Mbit/s channels) since 1987 ; implementation of CCITT nr. 7 common channel signalling system, started in 1987 and to be completed in 1990 ; use of CSN system (digital subscriber access unit), one at least in every local exchange in 1990. Let us recall that this digital connexity is not obtained by an overlay network, but by the use of the main network itself.

Even before the extension of ISDN, a variety of data communication services are offered through the telephone switched network : they are generally at a rather low bit rate (1,2 kbit/s to 9.6 kbit/s or even 64 kbit/s ; however TRANSMIC services offer 2 Mbit/s channels.

The TRANSPAC system is a fast packet switched network, which is said to be the first in the world with more than 60,000 direct access points and a traffic of 2000 billions characters per month. It is used to fulfil professional uses and to connect big service providers to our videotex network, the so-called MINITEL service.

The later, which is fully operational has an exceptional extension : by the end of 1988, there were in service 4,2 million MINITEL terminals, to be compared with the figure of 27 million telephone subscribers. The majority of offices have a MINITEL terminal, as well as a great number of homes, connected through their copper pair telephone line.

A new activity for France Telecom :providing videocommunication networks.

According to French law, France Telecom is authorized to provide cable TV directly to the home and we are now engaged in extensive cabling for video services.

In 1982, when the French government decided to promote a national TV cabling plan, France Telecom had a monopole on cable communication, including TV distribution. Since then, new regulations have been established (1987,1990) and this field is now open to competition. For its share, F.T. has a contract with 52 large cities for TV cabling, which involve the installtion of the equipment necessary for cabling 4.500.000 homes in 1992. At first all these homes will not be connected to the network : the terminal connection will be made only upon request, but the required equipment will be available at the distribution center.

As everybody knows, two techniques are in competition : coaxial cables and optical fibers. Techno-economical parameters, industrial problems, the possibility of introducing services other than conventionnal TV distribution are some of the factors to be considered in the difficult choice between these two techniques. Additionnal local factors can be determinative. As a result, 700.000 TV distribution lines are planned to be made of optical fibres. The rest will rely on coaxial terminations to the subscriber's home. But in any case, both kind of networks will use optical fibers for the transmission of signals between the head-end and the distribution centers.

During the last thirteen years, a large amount of experience in the field of optical videocommunication techniques has been gained in France, both in F.T. (including CNET) and in industry. The Biarritz experiment, launched in the late 70'S is well-known and we shall not go over it in detail in this paper. This experiment concerned 1500 subscribers, who benefited from both distributive services (mainly TV distribution) and interactive services (including picturephone services), in a star switched network. This network is still in operation but it has not been designed to be generalised to other cities. However, important

conclusions have been drawn from this experiment, leading to a more cost-effective system, centered on TV distribution, enriched by some interactive systems as broadband information retrieval.

For technico-economical reasons, multimode fibers are used in the commercial systems. The choice of multimode fibers allow the use of LED's, cheaper than lasers, as light sources. As a consequence, a limited bandwidth is available and the basic service relies on the distribution of one TV channel (optionnally two) to each subscriber : so, the later selects one (or two) TV channels among 15 (or 30) available at the distribution center, by using a narrow-band return channel. On the other hand, systems with coaxial termination bring to the home a multiplex of 15 or 30 TV channels and the selection is made by .ie subscriber on his receiving equipment. However, the coaxial systems use a tree architecture which is not adapted to interactive services. On the contrary, the star architecture of the optical fiber systems permits the connection of the subscriber to be linked to the telephone and ISDN network. These optical videocommunication networks will offer large scale experimental fields for new services such as pay-per-view TV or improved videotex services. They may represent another step in the evolution of the network, where broadband distribution and narrowband interactive services are carried out on the same physical line, without integration of signals.[2]

However, it appears that single-mode fibers will be essential for the broadband local network of the future as they are, from now on, for the trunk networks

Building a new optical SDH trunk network

As we have seen before, digitalization of the network was not the main reason for building a new optical trunk network. Owing to the high quality of our relatively young coaxial cable network, togother with digital radio links, a high degree of digitilisation of the trunk network has been obtained. However, we have at least three reasons for building, new optical trunk network which is now under construction.[3]

The first reason is the need for higher and higher transmission capacities which can be obtained only by the use of optical fibers. Satisfactory operation of the used 140 Mbit/s transmission systems was achieved without great difficulty. The rate of 4 x 140 Mbit/s which is becoming our standard rate originally caused some problems, which have been solved : soldering between coaxial sections, high values of reflection coefficients were the more important of these difficulties. However the rate of 16 x 140 Mbit/s which will be needed on large parts of the trunk network cannot be obtained on coaxial lines. This is a sufficient reason for installing optical fibers.

A second reason is the possibility of improving the quality of the network with optical fibers. In terms of transmission quality, the existing coaxial network fulfils the requirements specified by CCITT, as shown by long term quality tests on the network. However, it is clear that an order of magnitude, at least, can be gained with optical fiber systems. Another important factor is the small influence of lightning on optical cables and systems : to suppress completely this effect on our cables, we have decided to use all-dielectric optical cables, without any metal part.

A third reason is the possibility of taking advantage of the large bandwidth of optical fibers to transmit additionnal bits for operation and maintenance. This is obtained by the Synchronous Digital Hierarchy (SDH) systems. The new trunk network under construction will use STM 4 (622 Mbit/s) and STM 16 (2,488 Mbit/s) systems, according to this hierarchy.

These reasons led F.T. to define a "target" optical trunk network, designed to optimize investment, quality, safety, operation and maintenance. The target network's architecture is based on an interconnection network linking the trunk network nodes (trunk exchange sites, international gateway exchanges) and on sector networks which link medium-size cities to these nodes.

The building of this optical network began in 1987 and a large part of it is installed : by the end of 1990, optical connections will enable Paris to be linked to neighbouring countries, to submarine cable terminals and to international satellite stations. To complete the program, an average length of about 2000 km per year will be installed up to the year 1998.

Such a program involves civil engineering and cable engineering. To minimize civil engineering costs and to allow for planned extensions, two or three cable ducts are laid simultaneously, only one of which is in use at present. Cable pulling and jointing is then undertaken according to demand.

The length of cable pulling sections, which is also the distance between successive jointing, is 2400 meters in more than 90 % of cases and we hope to increase this length to 4800 meters. Proceed to larger pulling sections seems to be unrealistic, for practical reasons. We use for jointing only soldering techniques in order to have a small reflection coefficient. From our experience, distributed feedback laser emitters in nigh bit rate systems operating with small attenuation fibers must be used with care to avoide reflections along the line, which reduce the performance of the transmission link.

Two types of cable structures are used :
- the slotted core structure for which France was a worldwide leader producing the first practical realizations as early as 1977 [4] : a 10 - slot single unit slotted - core structure, with up to three fibers per slot and a total fiber number up to 30 is used as trunk cables ;
- the loose tube structure whereby one or more fibers are protected by a loose-fitting plastic tube : this variety of trunk cables uses six fibers per tube and a varying number of tubes, giving a maximum total capacity of 36 fibers.

In the two cases, the cables are completely free from metal components, including the central and outside strength members. For instance, the central strength member is usually a Fiber Reinforced Plasticrod. The maximum outer diameter of the cables is 14 mm.

Two wavelengths are used : 1300 and 1550 nm. For 4 x 140 Mbit/s systems, the regeneration span is 42 km at 1300 nm and will be increased to about 80 km at 1550 nm. One objective is to have some stability in the interconnexion network mapping with fixed position of the nodes, the necessary evolution of this network being obtained by adding new links between these nodes.

This high capacity trunk network, built year after year, will be the skeleton of the F.T. network of the nineties and beyond.

Local transmission

By local transmission, we mean this part of the transmission network which is intermediate between the trunk network and the distribution network. In France, local telephone areas are organized around local telephone switches with routing capability (CAA : Centre à Autonomie d'Acheminement). The subscribers are connected either directly to such a switching center, or the a local switch which is itself connected to a CAA, or even to a distant unit which is itself connected to a CAA or to a local switch. In medium or large cities, there can exist many CAAs. The local transmission network is made by transmission links between these switching centers. In each local area, there is at least a CAA (or there will be soon, as the network is an evoluting structure that we built year after year) which is connected to the trunk network.[3]

We have quoted before the percentage of digitilisation of the local transmission network in France : more than 93 % in 1990. Although its remains some coaxial cables and some local radio links, it is the part of the telecommunication network where the percentage on optical fibers is the highest. In fact, France Telecom decided to implement optical transmission in urban networks, first in Paris, and, more generally, in local telephone areas, using multimode fibers without waiting for single mode fiber equipment to become available. This decision was based on two main reasons :

- The proven technical advantage of optical fibers : compactness, light weight, wide-bandwidth, long-haul capability elimination of the remote power feeds and operation auxiliaries required in metal-cable digital transmission systems. In some cities like Paris, the possibility to extend the transmission capacity between switching exchanges, by replacing coaxial cables by optical fiber cables pulled in the same ducts was determinative from the point of view of costs and nuisances ;

- The economic advantages of the optical solution over copper-wire technique. The advantage is particularly significant at 34 Mbit/s, a rate well-suited to implement inter-exchange links .

The first test links where built in 1980 (Tuileries - Philippe Auguste in Paris) and in 1982, France Telecom began to place volume orders for 850 nm laser-diode systems. Such systems represent the majority of the system in service (about 4500 equipments).

In 1984, France Telecom decided to favor less expensive 1300 nm systems based on light emitting diodes (LEDs) and having a range comparable to the 850 nm laser-diode systems. There is more than one thousand 1300 nm LED systems in operation.

The same multimode fibers are used for the two systems as they are specified in the 850 nm and 1300 nm windows. This gives to France Telecom local transmission network a high flexibility to adapt the network according to the needs. Moreover laser diode systems at 1300 nm are available for long haul links up to 20 kms : more than a thousand of such systems are also in service.

However single-mode fibers and systems, first developped for subm arine links and trunk network applications, are now avalaible. So, it was decided in 1988 to discontinue the use of multimode fibers except for maintenance operations. This decision was motivated by the considerable superiority of single-mode fibers over multimode fibers :

- very low attenuation (less than 0,4 dB/km on the average, measured in the field) ;
- very wide bandwidth (several GHz/km) allowing very high bit rates : 140 Mbit/s or more can be used for these local applications, which is difficult or even impossible with multimode fibers.

As a consequence, a new optical local transmission network is the process of being built. In a few number of years the old multimode fiber network will become obsolete and we have to find the best management for this important investment, made in the years 80.

In this respect it may be interesting to pay some attention to the transport network feeding the distribution points of our videcommunication networks. They are, as a general rule, made of optical fibre cables, multimode first, single-mode now. This network is, from a fonctionnal point of view, separated from the local transmission telephone network. However in some cities, like Marseille, the need of building new high capacity transmission links for the transport part of the videocommunication network induced important civil engineering works. As a consequence, these works gave the opportunity to build a new optimized telephone local network, thus share the costs between the two networks : it is a first step towards integration of the networks, at the level of the cable ducts or at the level of the cables themselves, on way to save up money.

To this exception, the videocommunication network and the telephone network remain physically separated, specially in the subscriber loop.

The subscriber loop

Let us have a look at the existing subscriber loops which are made of copper pair cables. These loops constitute a subscriber network which is made of three parts :

- a transport section, from the switching center to a secondary repartition frame ;
- the distribution section, from this repartition frame to distribution points feeding 8 to 14 homes ;
- the branching section between the distribution point and the subscriber premises.

The topology of the subscriber cable network is of the tree type : the cables contain 224 to 2700 copper pairs as they come out of the primary repartition frame in the switching exchange and are then divided in smaller cables in duct chambers, up to the secondary frame and then to the distribution points where the structure become of the star type. So, each subscriber has his own copper pair and the topology of the overall subscriber line network is of the star type, a topology which is well adapted to any interactive service : we have adopted the same topology on our optical fiber videocommunication network to favour a future offer of interactive services, beyond the simple distribution of TV channels, a facility which is difficult to obtain with tree-type coaxial TV networks..

The use of secondary repartition frames is an important factor bringing flexibility to the network, which helps to adapt the investment to the subscriber demand. To complete this description, the following statistics demonstrate the average length of the three parts of this network :

- transport : 2000 meters (1000 m in Paris)
- distribution section : 600 meters (same in Paris)
- branching section : 150 meters (50 m in Paris)

The local subscriber network of France Telecom is relatively new : it has been installed, for the main part, in the seventies. The telephone equipment in homes is such that it leads to the creation of few new lines, apart from the building of new houses. However a systematic maintenance policy is applied, in order to improve the network reliability and to reduce maintenance costs. As a consequence of this policy, together with the ceration of new lines, the subscriber cable network is updated and up-graded to a rate of 8 % per year.

The aging of cables is not important, as the cable technique has been improved, specially the properties of the dielectrics used in cable design. Many tests have been carried out in the laboratory and on the network itself. The conclusion is that the life time of the existing subscriber network could be more than 15 years before aging effects become important. This result has to be compared with the previously quoted 8 % updating and upgrading rate : : consequently, with the present day policy, we could have a completely renewed subscriber network before aging effects appear.

These subscriber loops are usually used to transmit analog signals for telephone or Minitel service. It has been proved that the copper pairs used can generally transmit ISDN digital signals at the basic rate of 144 kbit/s. So the development of ISDN services is not, by itself, a factor which requires the replacement of copper pairs by optical fibers. It has been shown that many of the copper lines can support the primary ISDN rate of 2 Mbit/s, which is requested by some large business subscribers. However, as a general rule, we prefer to lay, in such cases, optical fiber cables which deliver a better digital transmission quality.

Nevertheless, the number of subscribers requesting such a high transmission rate, either for ISDN or for data communication, is to small to induce a rapid switching from existing copper pair distribution networks to optical fiber networks. Valuable exceptions are some business districts with a number of large firm headquarters : the new quarter of La Defense in Paris is one of them and we are laying in this district a fair number of fibers for private subscriber use, including leased lines and connection of PABXS to the main network.

In order to make more cost effective the introduction of optical fibers for professional users we have designed new systems which are now under development.

One of them is a ping pong transmission system, called SAMOS 'Synchronous Alternating Microprogrammed Optical System) which needs one single fiber and one single wavelength to establish a bidirectionnal digital link between two terminal stations separated by a distance up to 10 km [5]. The laboratory model was limited to 5 Mbit/s total flow : it works with a LED as light source. Higher bit rates are possible with lasers and faster microelectronics. Such a system can be used to address some professional needs with a flexible system, including PABX connection to the network, plus data communication, telecopy and fast videotex service.

Another way of reducing the cost is to share the more expensive components between many users. Passive couplers can divide the signal transmitted on one transmission line between 2, 4, 8 or more subscribers depending of the power budget. A fiber-sharing network is surtable for an optical fiber replica of TDMA (Time Domain Multiple Access) commonly used in satellite systems, each subscriber being allocated a time slot. Such a system has been designed at CNET under the name of MOLENE (Multiplexeur Optique pour Ligne Numerique Etoilée). This solution is fitted for low or medium bit rate services, e. g. telephone service, 144 kbit/s or 2 Mbit/s services. The MOLENE experimental model can provide 144 kbit/s ISDN connections to 12 subscribers. It works with LEDs [6]. A new version, adapted for the transmission of 2 Mbit/s channels, is under development.

Beyond these limited application, it appears that a massive introduction of optical fibers in the subscriber network relies on the emergence of moving picture communication, which needs really a broadband communication network.

The challenge of the nineties : single-mode fiber broadband subscriber loops

In France, as in other countries, we consider that the introduction of single-mode optical fibers in order to build the large bandwidth subscriber network of the future is a major challenge for the laboratories, the manufacturers and the telecommunications operators. To face with this challenge, we are doing our own research and test work and we are participating to the EEC cooperative projects, known under the names COST, ESPRIT, RACE and EUREKA.

We gained, at CNET, a first experience in the application of single mode fibers to video-communication networks with our TREGOR experiment (named after the TREGOR country, surrounding Lannion, the city where our research center is located). Reducing the cost of cable pulling and jointing, designing cost-effective equipment, measuring the transmission performance in the field for this application where some of our purposes [2].

Beyond the results of this first experiment, we need additionnal cost reductions before deciding a massive introduction of single mode fibers in the subscriber network.

So we have installed a field test-bed, inside and near Lannion : this experimental optical distribution designed for flexibility and cost-effectiveness, will be used to test different modulation systems, analog or digital, to transmit up to homes, speech, video, data, separetely or combined in a broadband ISDN.

The reduction of the cost per user is obtain first by engineering rules facilitating the re-use of existing ducts and chambers, thus

reducing the amount of civil engineering works, second by sharing the fiber between many users, as we did for our MOLENE system. This design has also the consequence of sharing between many users another expensive device : the laser emitter module. The network architecture is then of a tree-star type, with passive distribution points. Such a network offers a large flexibility : for instance a fiber can go straight through the distribution points by suppressing the passive optical divider or coupler and, thus, be used for connecting a large business user. From the operator's point of view, additionnal flexibility is added by the systematic use of secondary distribution frames, a technique used in telephone copper pair subscriber networks, which helps to make progressive investments, according to the needs.

We shall not discuss the different modulation schemes we are studying for the transmission and distribution systems, which may be analog (in some cases for video) or digital. Let us just recall that CCITT made the choice and is specifying for the target B - ISDN network,[7] the asynchronous transfer mode (ATM) of wideband digital signals ; this technique which was first demonstrated at CNET [8] combines the simplicity of circuit switching and the flexibility of packet switching, and has also significant advantages in transmission systems [9]..

Addressing to cable specialists, I should prefer to stress the point that cost reduction is also a matter of technology. This assertion is true for all kind of components which represent an important share in the network cost. Fiber and cable technology has an important role to play for reducing production costs as well as cable engineering. CNET laboratories, together with an industrial support are working along two directions in that field.

The first one is MCL (Multipulling and Cabling in line) a technique which combines the simultaneous pulling of six to eight fibers, and cabling these fibers in line, in a bundle or in a ribbon. Demonstration machines exist : they allow to pull six fibers simultaneously and to produce a six fiber ribbon at a speed of 100 m/mn ; commercial machines could be promptly avalaible. However, we are aware that their adoption in a manufacturing process involves major investments and major changes inside the organisation of fiber and cable industry. [10]

Another way along which we are working is the so-called POID (Plasma Inside and Outside Deposition), a new technique for producing preforms. In this technique, the core of the fiber (i.e. the small part of material inside which the light ray is transmitted) and the claddding (more than 95 % of the material constituting the fiber) are produced separately. We are waiting, from this research work, a further reduction of production cost and a longer fiber pulling length : large diameter preforms (up to 10 cm) can be grown by this method in a greatly reduced time. From our economic studies, such a process could bring a reduction of the fiber production cost by a factor of three.

It is clear that technologists have to bring their own contribution together with network designers and signal processing specialists, to ensure the emergence of the future single mode broadband subscriber networks.

Conclusion

Having described some of those specific features of the France Telecom's present network, we have analysed the evolution trends in the different parts of the network. We are in the process of building the optical synchronous trunk network of the year 2000 with an average annual rate of optical cable installation of 2000 km. The local transmission network, still largely relying on digital multimode links is being progressively converted to a higher capacity single mode network, sometime combined, in some large cities, with the videocommunication transport network. However, the local subscribers loop network, where optical fiber are being introduced at a small rate for business uses, is presenting the main challenge : the definition and construction of the broadband network of the future. It is a challenge in which fiber and cable specialists have a major role to play.

BIBLIOGRAPHY

1. Le système technicien, Jacques Ellul, Calmann-levy, ed, Paris, 1977.

2. Update on subscriber systems in France, D. Chapelain, OFC88, New-Orleans (USA), 1988.

3. Optical Fibers. Special issue of "COMMUTATION ET. TRANSMISSION", 1989.

4. G. Le Noane, M. de Vecchis - Further developments on compartemented fiber optic cable structure and associated splicing technique. IOOC. Tokyo June 1977.

5. Experimental data link using single mode fibers and ping-pong transmission, A. Jaillard and al. , EFOC/LAN 89. Amsterdam (Netherlands, 1989.

6. Transmission of narrow band services on a passive optical bus. J. Abiven. EFOC-LAN. Munich (FRG). June 1990.

7. CCITT Recommendation I 121 : Broadband Aspects of ISDN

8. Asynchronous time-division techniques : an experimental packet network integrating videocommunication.
A. Thomas, J-P Coudreuse, M. Servel, ISS84, Firenze (Italy), 1984.

9. Proposal for an ATM transmission system in the loop, G. du Chaffaut (proposal to CCITT - SG. XVIII, Geneva, 30 juin 1989 and private communication).

10. Evolution of passive components for videocom-munication networks, G. Le Noane, EFOC/LAN 88. Amsterdam (Netherlands), 1988.

ACKNOWLEDGMENTS

This review paper is based on the work of many colleagues from CNET laboratories in Lannion. I am pleased to acknowledge J-P COUDREUSE for his early work on ATM and for the PRELUDE experiment, D. CHAPELAIN and A. MADANI for their contributions to videocommunication networks, G. DU CHAFFAUT for ATM transmission in local networks and the proposed evolution of these networks, A. JAILLARD for the SAMOS system, J. ABIVEN for the MOLENE system, M. LE GALL for evolution of the trunk and local transmission network, G. LE NOANE for fiber and cable technology. I thank Mrs A.M. LE BERRE and M. DESERT for typing and preparing the manuscript, Miss Karen DELAMORE for reading and improving it.

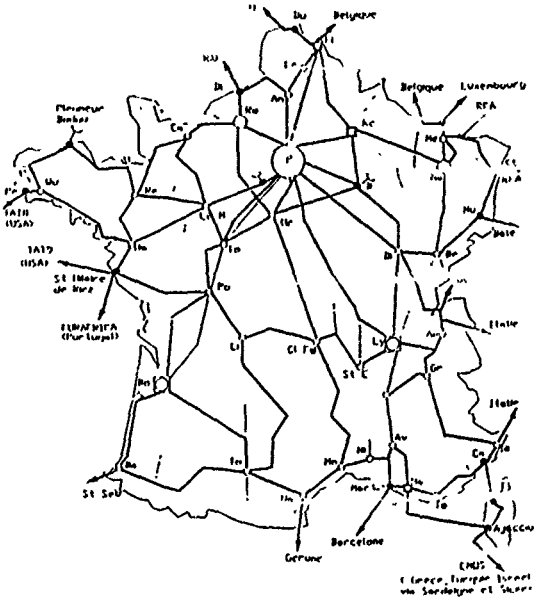

The French target trunk network, as seen in 1990

THE TRANSMISSION INFRASTRUCTURE IN BELGIUM

Susan Mirbach

RTT Belgian Telecom USA

1. Introduction

For many decades, the development of telecommunications has been determined by the evolution and extension of basic telephone service. Of all the services which are offered to the RTT's users (telephony, data transmission, videoconferencing, etc.), basic telephone service represents more than 90% of total traffic.

The RTT's existing transmission infrastructure, therefore, was essentially conceived for offering telephone service of a good quality at a competitive price. For a long time, the transmission techniques used were entirely analog. It was not until the mid 1970's that digital techniques began to be implemented.

The diagram in figure 1 shows the organizational hierarchy of the public service in Belgium (see figure 1); more than 550 local central offices, 40 regional central offices, 5 transit centers, and 4 international switching centers. The branches of this diagram constitute the transmission network infrastructure.

As you can imagine, all of the others services offered to the RTT's clientele such as data transmission, videoconferencing, and even leased lines, use this transmission infrastructure that was originally and primarily implemented for telephony.

The Belgian transmission network is hierarchical. It is composed of a local network, a regional or junction network, a trunk network, and an international network.

This presentation describes both the current status and the future evolution of the Belgian RTT's transmission network.

2. Local Networks

The local network ensures the connection of the subscriber's equipment terminal (telephone, PABX...) to the central office or local exchange. This network is structured in a star configuration: each subscriber line (in most cases a pair of symmetric copper wires in an underground cable) directly connects the terminal equipment to its calling number position at the central office.

2.1 Organization

The organization of the local network consists of two levels: the feeding cables go from the central office to street terminals; the distribution terminals go from the terminals to the subscribers(see figure 2).

As the cables leave the central office, they fan out in many directions (5 or 6). These cables are covered with steel ribbons under which is a layer of lead. They contain copper conductors insulated with paper. They have a capacity of between 200 and 2000 pairs. They are generally several kilometers long. These cables, unlike in many other countries, are not pressurized.

The number of pairs in these feeding cables is selected so that cable layings are spaced in 8-10 year periods. This corresponds to the optimal time interval, from an economic point of view, between two successive cabling efforts. A short distance from the central office, these cables are used for direct connections to subscribers. When used for greater distances, they terminate at a distribution terminal.

The distribution feeding terminals mark the border between the network and distribution network. There are approximately 20,000 distribution terminals in Belgium. Once put in service, they contain approximately 200 pairs of wire for power and 400 pairs of distribution. This permits about 100 subscribers to be operational.

From the distribution terminal, the distribution cables spread out toward the subscribers. These cables are chosen in order to last more than 20 years before the laying of new cables, especially given the low cost of cable in comparison to the costs of digging up the sidewalks, repaving, etc... 80 percent of residences already have local access constructed.

The distribution cables were standardized to contain betwen 14 and 200 pairs of wire. Insulated in polyethylene, they are filled with petroleum jelly in order to provide longitudinal watertightness. The splicing is accomplished with the help of heat shrink sleeves. This is a reliable system that is easy to apply.

Note that in 1992 this method of heat shrink splicing will be applied to feeding cables as well. In fact, at the end of 1991, the first feeding cables in plastic insulation will be delivered. Soon after this, lead cables with paper insulation will no longer be ordered.

The local access cable which is filled with polyurethane and is for traditional residences and contains between 2 and 6 pairs, is connected directly to the distribution cable and terminates at an intermediary deistribution device. In buildings, apartments, or offices, larger cables are used.

For distribution, paper insulated cables are used essentially for conductor diameter of .8 and 1mm. These are used when the subscriber connection is located far from the central office. The conductor diameter must be enlarged in such a way to be able to meet transmission standards. These cables can be connected to plastic cables with the aid of the heat shrink sleeves just mentioned.

Distribution via aerial lines is disappearing. These types of lines are now only installed for high distance connections in rural areas.

2.2 Subscriber systems

Other than the voice telephone service, the local network can also handle 64 kbit/s and higher for services such as data transmission, teletex, videotext, etc...A 2 Mbit/s service can be offered by installing regenerators. The current network supports a narrowband ISDN service. A commercial ISDN pilot is currently in progress with a few hundred subscribers.

For Bandwidths of 2,8,34, or 140 Mbit/s. a fiber optic infrastructure is essential. The 1990's will certainly see the development of fiber optic links between certain categories of subscribers (banks, manufacturers, zonings...) and the local central office.

It is worth mentioning that in the medium term, (1992), the RTT intends to establish a local broadband integrated pilot network (RTT contract with BBA signed in October 1987). Such a network would be used to satisfy the needs of business users. In the future, it could replace the existing RTT networks and the teledistribution network in Belgium. These networks are currently under study by the RTT and would be fiber optic based. In this context, the RTT plans to offer its customers the following services:

-Two-way telecommunications services such as the ISDN services at 64 kbps to provide : telephony, switched circuits for data transmission up to 64 kbps, packet-switching(teletex, interactive videotex...)

-2 Mbit/s service and the videophone;

- One way teledistribution services: TV distribution and distribution of audio programs.

3. Zonal/Junction Network

The junction or regional network consists of transmission links that connect each local central office to its respective regional central office. Thus, the zonal network has a starlike configuration around each of its forty zonal central offices. The reliability of this network is ensured by redundant links between each local central office and its respective zonal office. Note that in certain zones there are direct connections between central offices within the same zone. The average distance of junction or zonal links is 8 km; the maximum distance is 40 km. Traditionally these links have consisted of metallic cables. Since 1982, fiber optic cables have been used (see figure 3).

3.1 Metallic Cables

These cables are all "armoured" in lead, paper, and copper; they are constructed as follows:

The copper wires, insulated in paper, can have a diameter between .5 and 1mm.

The wire pairs are twisted two by two in star quads, the quads unroll in concentric layers to form the heart of the cable, a layer of lead around the core assures the water-tight quality, an armor of steel sheathing protects the cables from mechanical problems, the cables can hold between fifty and 2,000 pairs of wire.

The total length of these metallic cables that have already been laid amounts to 12,000 km. The number of "km pairs" of wires that these cables contain is 2,200,000 km pairs. There are approximately 360,000 pairs currently installed.

Until the end of the 1970's, the transmission technique used on these cables was purely analog: the voice channel is transmitted on two wires in the audiofrequency band (300-3400 Hz) on a symmetrical pair that is in general loaded. Most often the inductance of the loading coil and the distance between coils were, respectively, 129 mH, and 1.330 m for a pair whose wire diameter was about .8 mm.

Beginning in 1971, for economic reasons, the RTT began to use digital transmission at 2 Mbit/s on the metallic pair cables. This system allowed for 30 voice channels or 30 circuits to be transmitted at 64 kbit/s. These cables could not contain many 2 Mbit/s systems because of crosstalk problems.

Technical reasons for digitizing the zonal network were added to the economic reasons. The two key technical reasons were the decision to introduce digital central offices and the development of new services.

This is why, beginning in 1978, the RTT decided to lay cables that were specially conceived for the transmission of digital signals at 2 Mbit/s. These cables differentiate themselves from their predecessors by a screen of copper that separates the two transmission directions in order to avoid near-end crosstalk. This allows for an increased number of 2 Mbit/s systems.

Nevertheless, since the beginning of the 1980's, the metallic cables have been replaced by fiber optic cables as the medium of choice.

3.2 Fiber Optic Cables

The RTT has been ordering fiber optic cables since 1982. The initial cables were with multimode fiber optics(CCITT TEC G 651) which were the first to be commercially available. The working wavelength was 1300 nm.

Multimode fiber presents the inconvenience of a bandwidth limited to signal transmission of 140 Mbit/s at a maximum (1992 circuits at 64 kbit/s). This is why the RTT decided to severely restrict the number of fibers in the cables. Given the telephony requirements, many links had only two fibers each.

Beginning in 1988, the RTT resolutely shifted towards singlemode fiber optic (CCITT REC G 652) used at 1300 nm. These fibers can transmit signals at a very high rate (2.5 Gbit/s : 16 X 140 Mbit/s).

Since the singlemode fiber optics can be considered the infrastructure of the future, significant future requirements are anticipated. These fibers are needed to prepare and provide for emerging large bandwidth services.

The capacity for significant transmission potential will presumably allow for longer intervals between cable laying efforts. The interval would go from ten years for the metallic cables to twenty years or more for the fiber optics.

Beginning in 1991, the new synchronous digital hierarchy (SDH) will instigate a change in the topology of the junction (or regional) network.

Until today, the junction network has been developed in a tree-like topology: cables serviced remote buildings from a switching or transit center and the pairs of fibers that they contain have been used in the context of a star-shaped topology. The reliability of this type of network topolgy requires that it be backed up and redundant in capacity as well as in length.

From now on, the new cables will tend to be laid in a ring topology that ensures simultaneously the reliability and flexibility of the network, especially if the new capabilities of the synchronous hierarchy are leveraged. The total length of the required cables declines compared to the "double tree" system.

Note that the optical regional cables are technically identical to the cables used in the trunk network. This offers the economic advantage of being able to include the junction links in the long-distance cables.

Summary of the Current Situation (see figure 5):

a) Regional links

-length of multimode fiber cables : 1,000km;
-Km multimode fibers : 3,960km;
-length of monomode fiber cables : 500 km;
-Km monomode fibers : 1,700 km.

b) Regional links in Trunk cables
-Km-multimode fibers :960 km-fibers

c) Number of local offices served by fiber optic cables: 254 out of 552, of which 4 already have two optical link routes each.

Evolution

In 1997, 95% of the central offices will be interconnected by fiber optics.

4. The Trunk Network

The trunk network consists of the collection of transmission routes that link together central offices on the regional, transit, and international level. The reliablity of this network is insured by a meshed topology such that every regional center is connected to the network by at least two distinct lines.

These links carry a number of circuits at 64 kbit/s corresponding to approximately 50% of their maximum capacity. As a result, in the event that one of the lines is out, the alternate cable can accomodate the additional traffic.

The trunk network, as it is operated today, consists of the superimposition of three combinations of separate links of which two use analog techniques and one uses digital techniques at various bit rates.

4.1 The first combination, completed in 1965, is composed of links on cables with 24 symmetrical pairs, functioning in the frequency band of 12-552 kHz; each link consists of two cables (one per transmission direction in order to reduce the problems caused by crosstalk) of which the capacity is between 24 and 120 voice channels frequency multiplexed, thus 2,880 voice channels (see figure 6). The total length of these channels is 2,965 km.

4.2 The second combination, completed in 1979, is composed esentially of two links supported by cables with 12 coaxial pairs 1.2/4.4 mm and functioning in the frequency band of 300-12,000 kHz; every link has a capacity of 6 systems at 2,700 voice channels (see figure 7). The total length of these cables of 12 coaxial pairs is 1,250 km.

In addition, there are a few cable links with six

coaxial pairs at 3.7/13.5. These are used in the frequency band 4,000 - 60,000 kHz; every link has a capacity of three systems at 10,800 multiplexed voice channels which is 32,400 voice channels. The total length of these cables with six coaxial pairs is 350 km.

4.3 At the end of the 1970's, the RTT decided to install a combination of digital links at bit rates of 140 Mbit/s (1920 circuits at 64 kbit/s) linking the 40 regional central offices together. The reasons for this decision were not only economic but technical as well. The most important of these technical reasons was the establishment of digital regional central offices and the introduction of new services.

This network consists essentially of links on cables with 30 coaxial pairs at 1.2/4.4 mm (610 km); links on digital microwave and on multimode fiber optic cables (at an index gradient of 1300 nm) were also installed (see figure 8).

The RTT also converted some analog links to 12 MHz on cable to 12 coaxial pairs 1.2/4.4 mm in digital links at 140 Mbit/s, as well as links at 60 MHz into 565 Mbit/s.

Since 1988, the RTT has begun construction of a new digital trunk network exclusively based on the utilization of singlemode fiber optic cables (wavelength: 1,300 nm or 1,550 nm).

The RTT investment program is such that in 1996, virtually all of the major regional central offices of importance will be accessed by singlemode fiber optic cables.

For these links, the RTT utilizes cables deploying from 12 to 20 or 30 fibers depending on the traffic projected for these routes.

On average from now until the year 2000, the RTT will order approximately 200 km of cable per year for the trunk links, or about 4,500 km of fiber.

The appendix contains a study of the evolution of this trunk or regional network based on singlemode fiber optics through the 2002.

5. International Network

The international network, as it is operated today, consists of three types of links that permit access to the majority of countries in the world:
-links with neighboring countries
-satellite links
-combination of shares, ie. right of coownership, irrevocable rights of use (IRU), in foreign terrestrial and undersea links.

5.1 Links with neighboring countries

(see figure 9)
Note that there are still some analog links at high frequencies in service with neighboring countries. These links will be progressively phased out from now until 2000 and replaced by digital links.

5.2 Satellite Links

The earthstation at Lessive presently serves the Atlantic region within the Intelsat V system by means of two type A antennas that were put in service in 1972 and 1983 respectively.

Thanks to a third antenna, put in service in 1984 and operating within the Eutelsat system, the earth staion of Lessive serves many European countries (Scandinavia, Spain, Portugal, Italy, etc.)

Finally there is an earthstaion in Liedekerke, which is used for digital transmission within the IBS system.

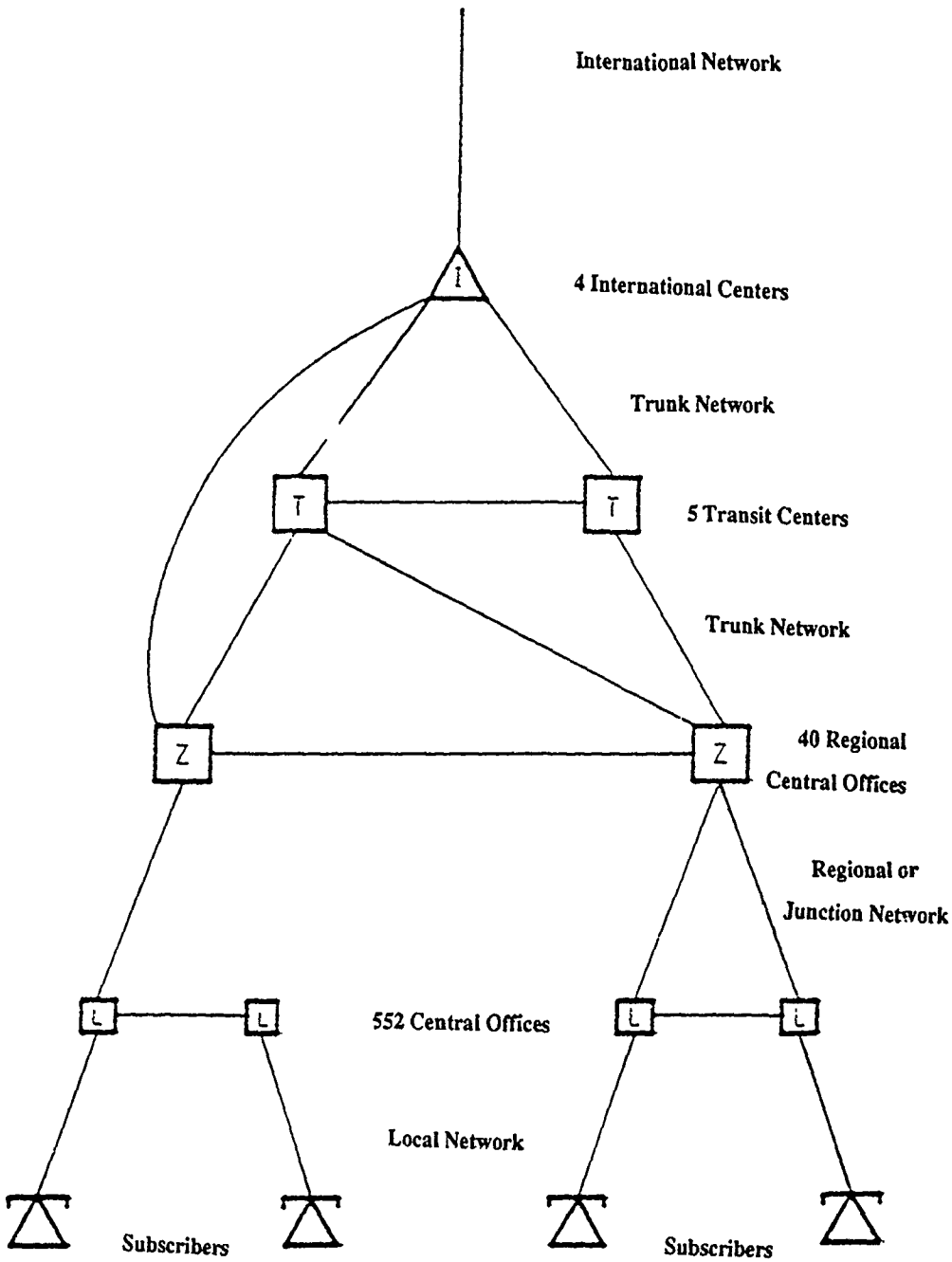

FIG. #1 TRANSMISSION NETWORK

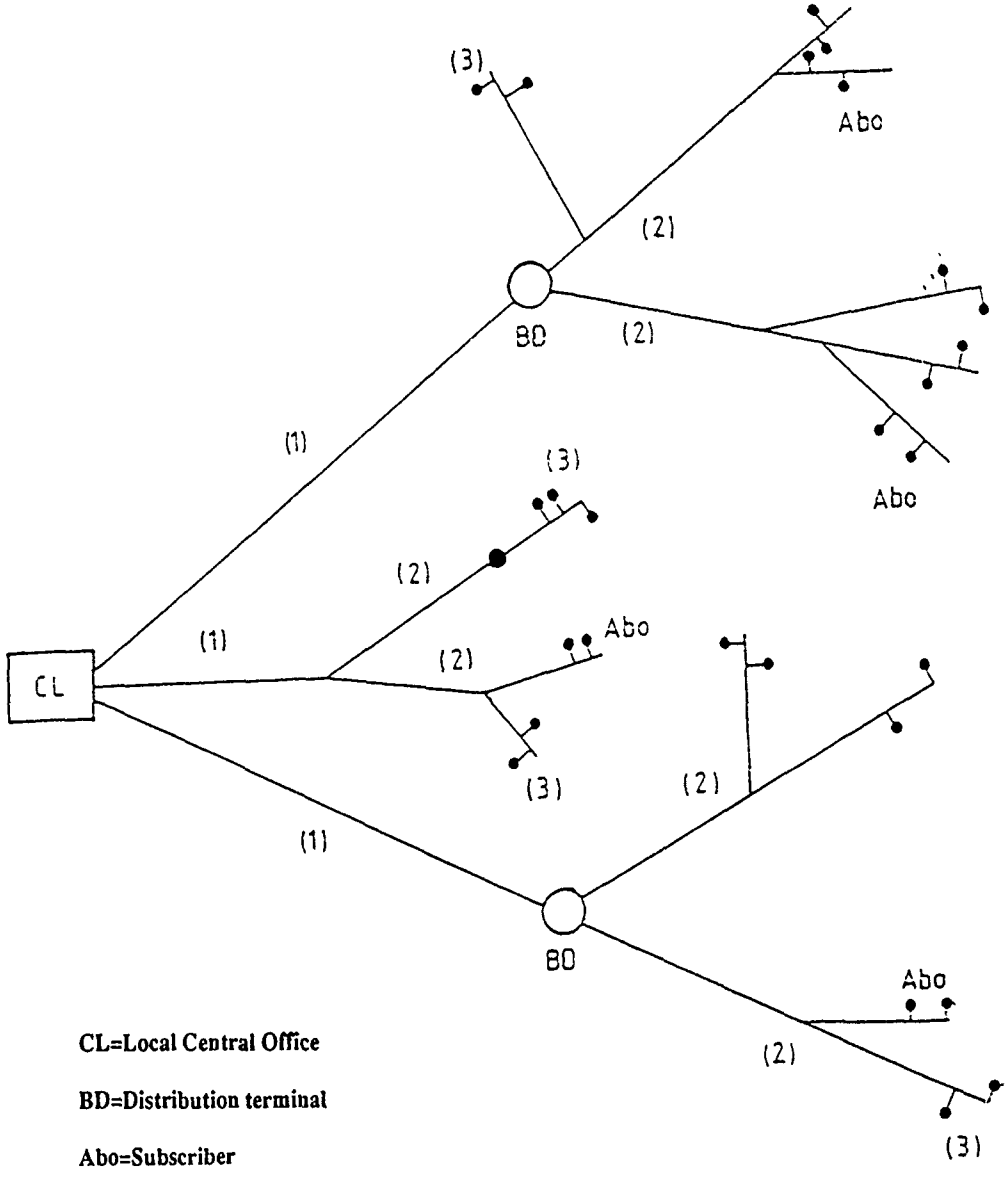

CL=Local Central Office

BD=Distribution terminal

Abo=Subscriber

(1)=Feeding Cable

(2)=Distribution Cable

(3)=Local Loop

FIGURE #2 ORGANIZATION OF THE LOCAL NETWORK

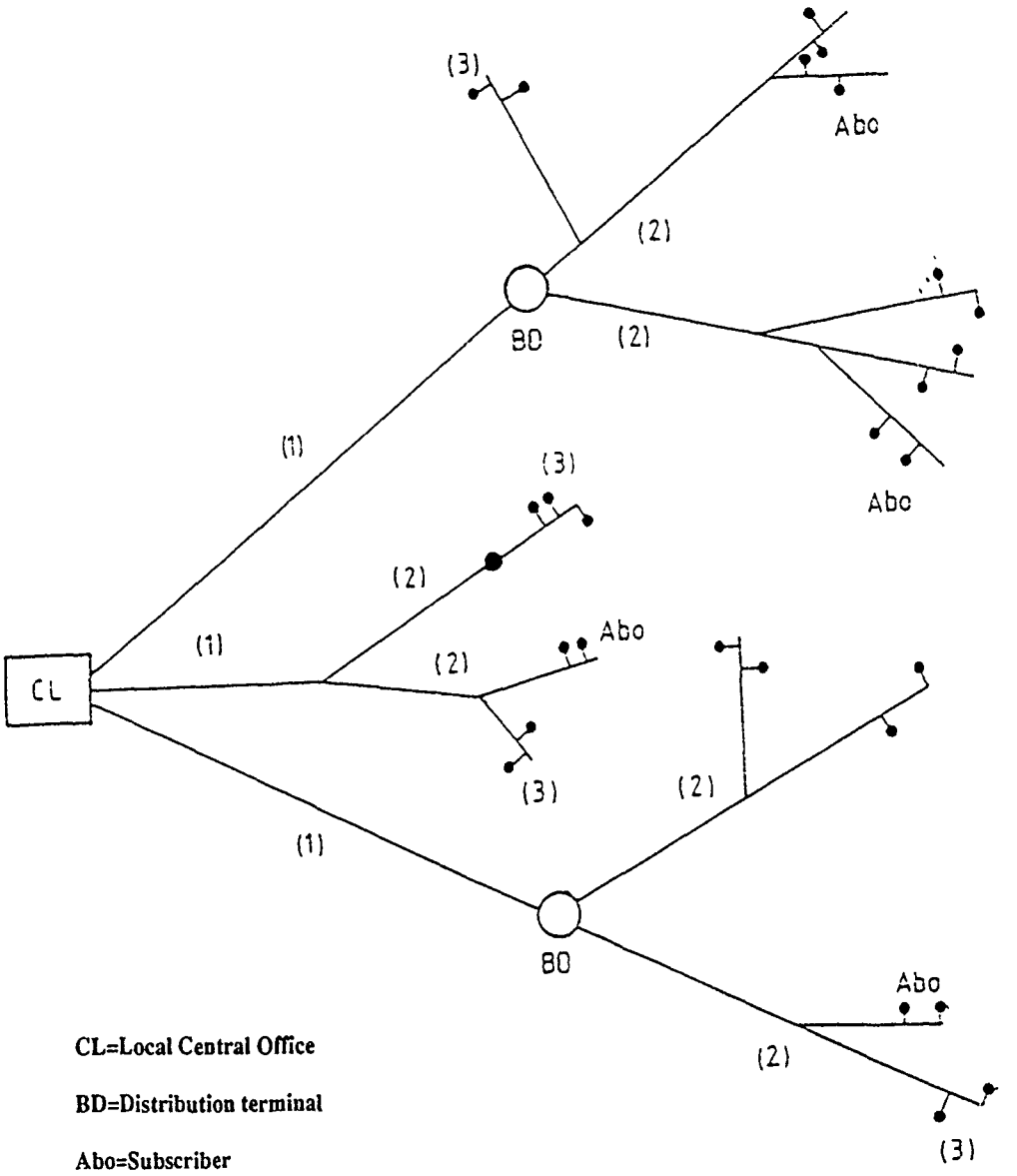

CL=Local Central Office

BD=Distribution terminal

Abo=Subscriber

(1)=Feeding Cable

(2)=Distribution Cable

(3)=Local Loop

FIGURE #2 ORGANIZATION OF THE LOCAL NETWORK

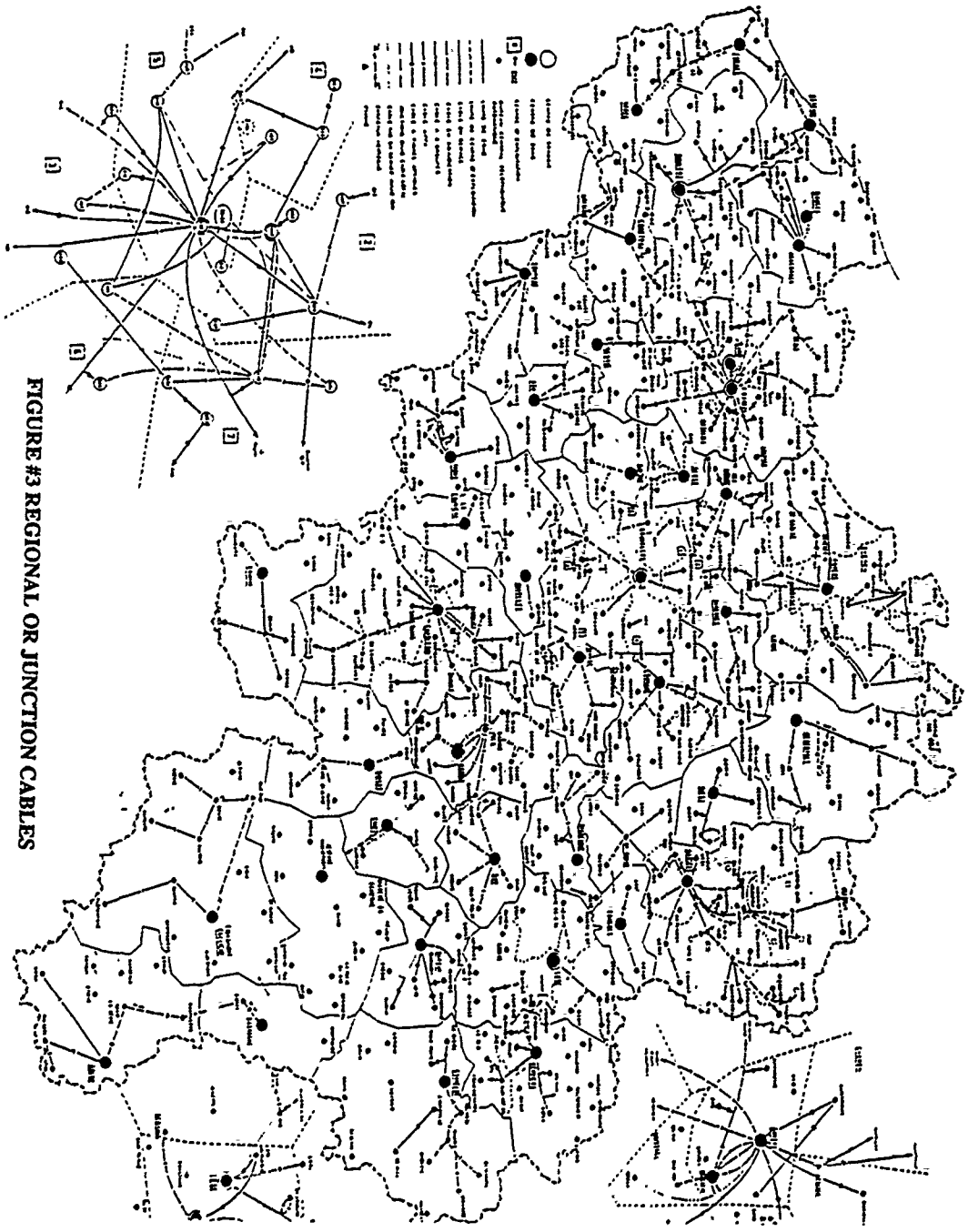

FIGURE #3 REGIONAL OR JUNCTION CABLES

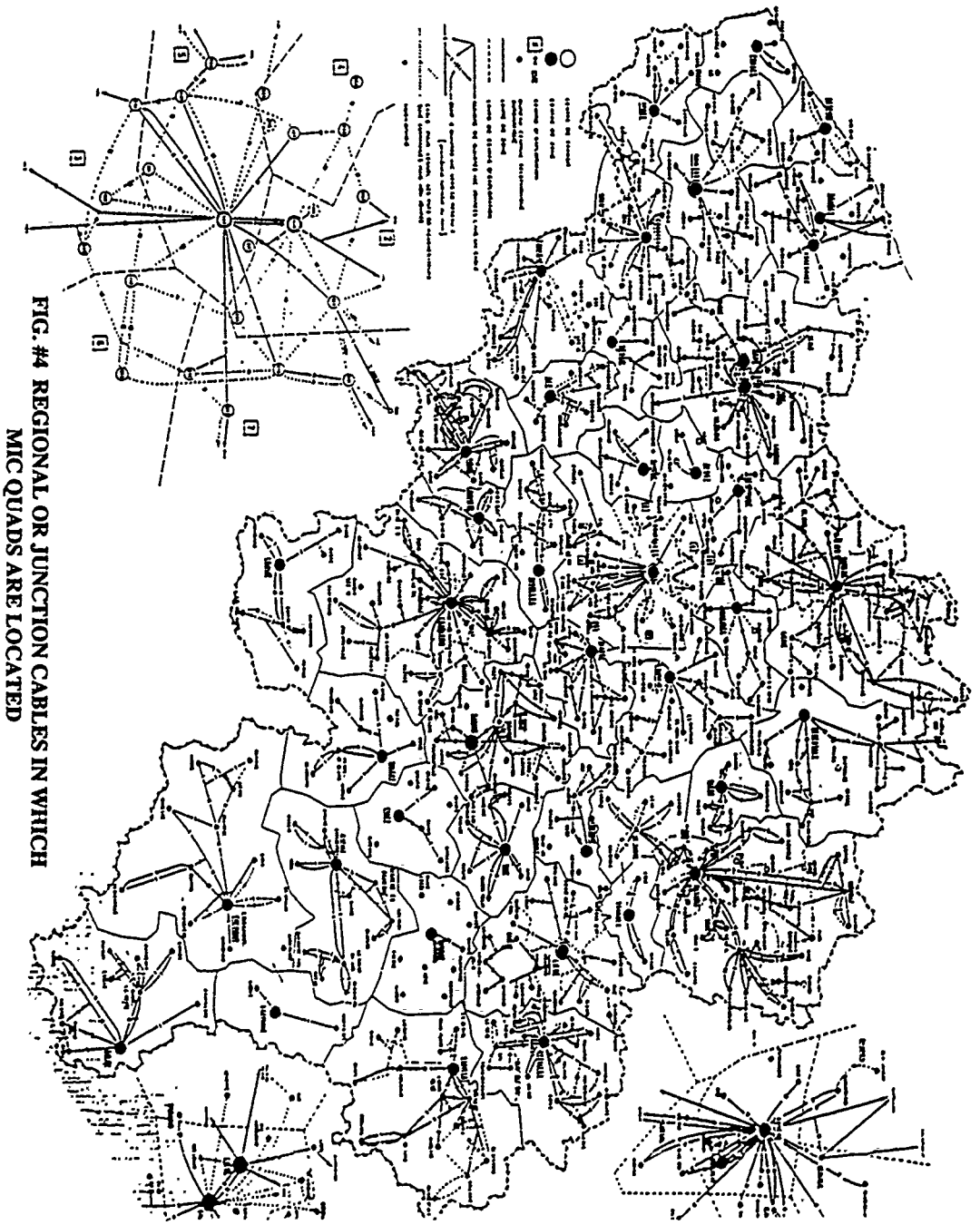

FIG. #4 REGIONAL OR JUNCTION CABLES IN WHICH MIC QUADS ARE LOCATED

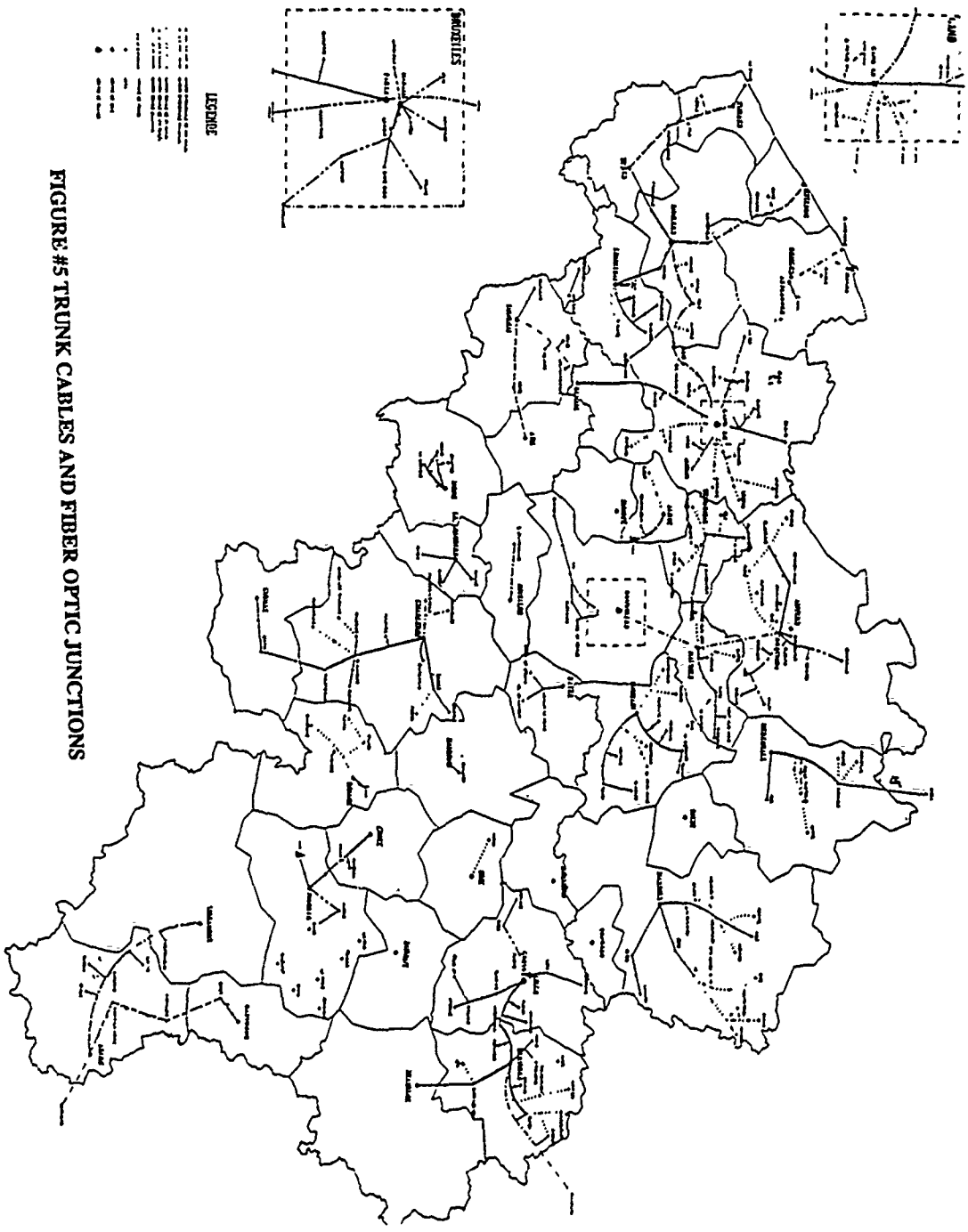

FIGURE #5 TRUNK CABLES AND FIBER OPTIC JUNCTIONS

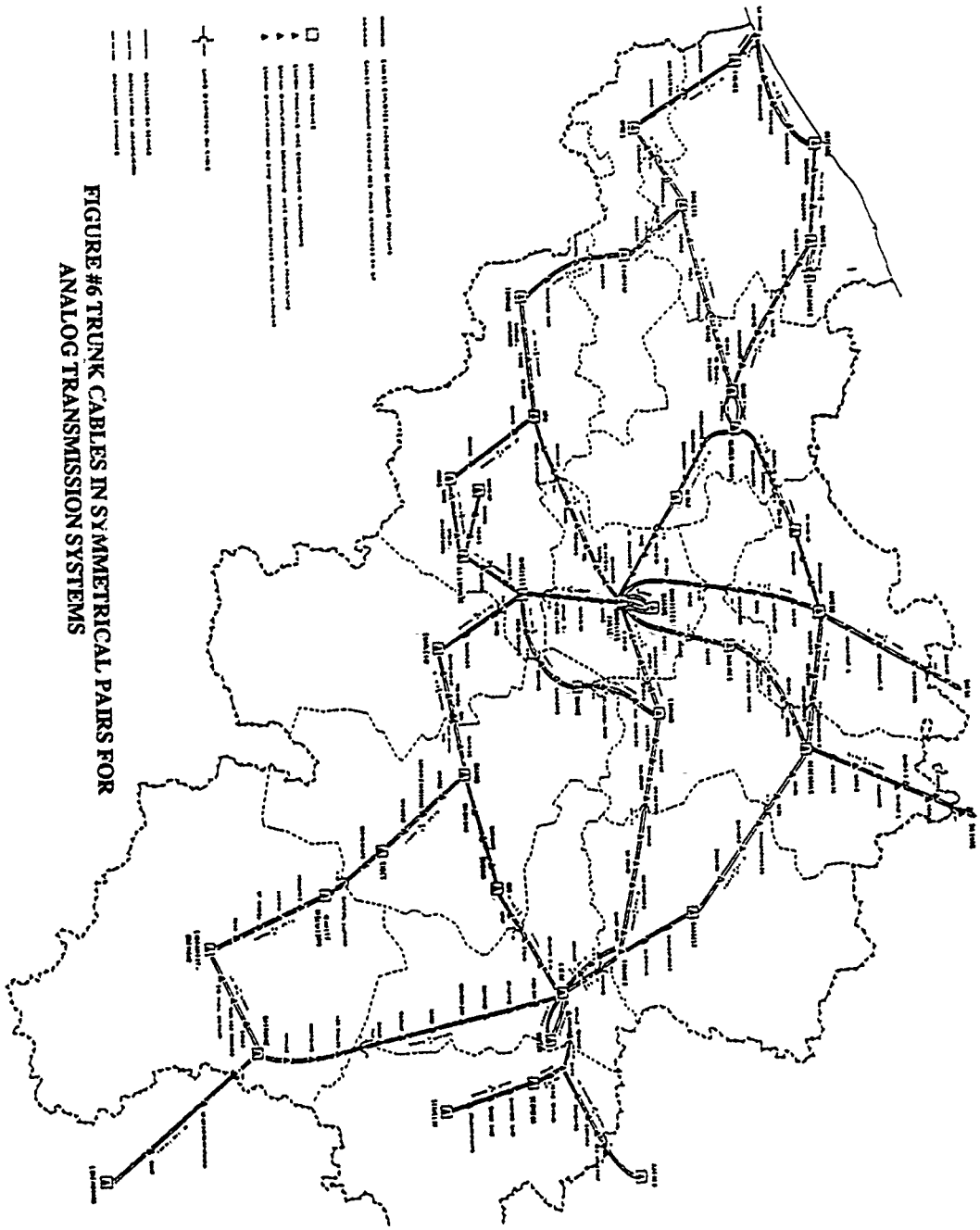

FIGURE #6 TRUNK CABLES IN SYMMETRICAL PAIRS FOR ANALOG TRANSMISSION SYSTEMS

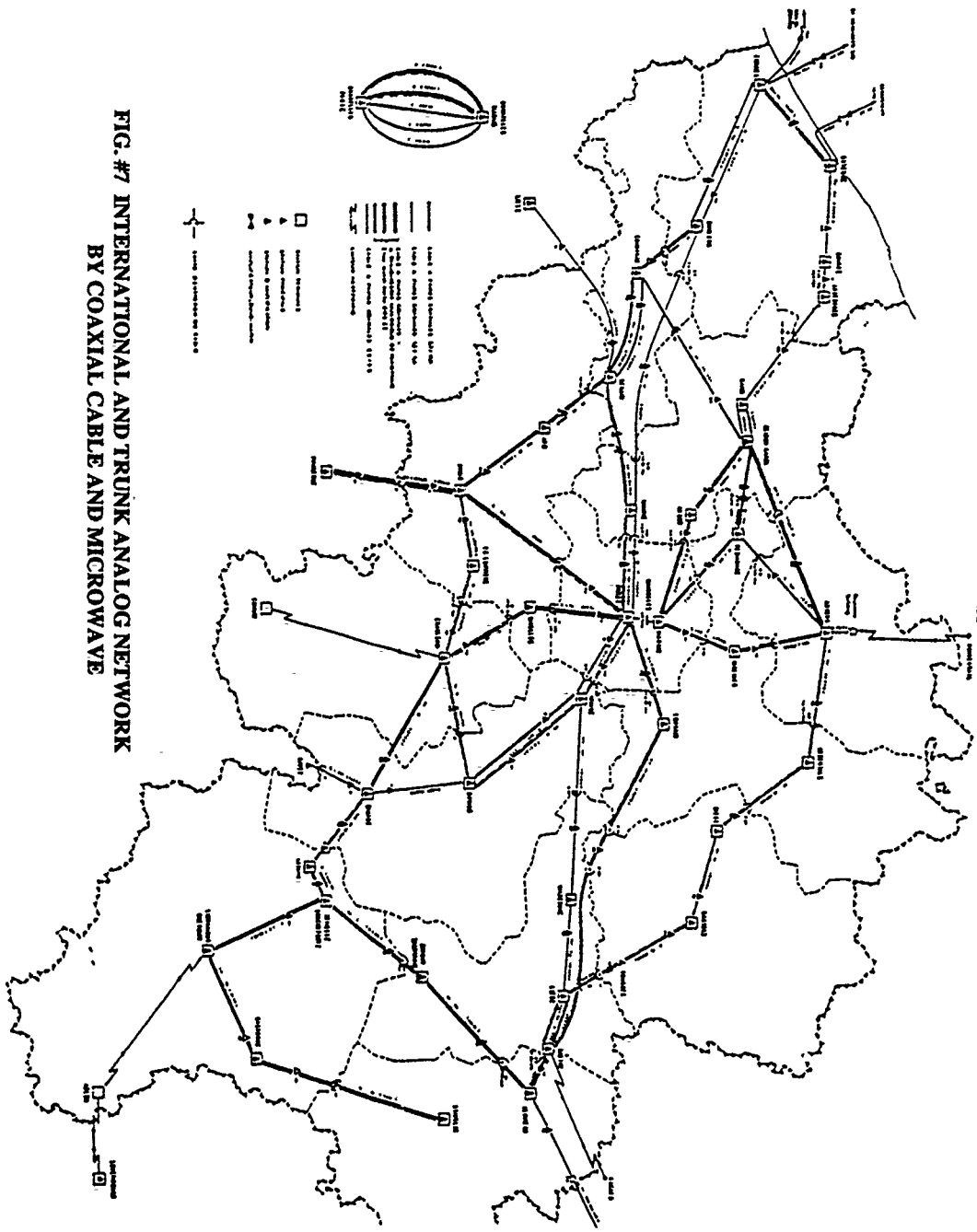

FIG. #7 INTERNATIONAL AND TRUNK ANALOG NETWORK BY COAXIAL CABLE AND MICROWAVE

FIGURE #9 LINKS WITH NEIGHBORING COUNTRIES

Country	Existing Digital Links	Future Digital Links
U.K.	UK-Belgium No. 5 6 monomode fiber optics	UK-Belgium No. 6 12 monomode fiber optics
	6X 140 Mbit/s (underwater links)	SDH-4/1992 (underwater links)
Netherlands	Antwerp-Roosedaal Micr. 10x140 Mbit/s	Liege-Maastricht 12 monomode fiber optics
	Herentals-Breda 12 multimode fiber optics 6 X 140 Mbit/s	5/91
Germany	Liege-Aachen Microwave 10x140 Mbit/s	-----
	Verulers-Simmerath 8 fiber optic monomode	
Luxembourg	Bastogne-Neidhauser Microwave 6x34 Mbit/s	-----
	Arion-Luxembourg 8 fiber optic monomode	
France	Courtrou-Lille Micr. 10x140 Mbit/s	Tournai-Lille 12 monomode fiber optics
	Mons-mauberge Coax. 4 X 140 Mbit/s	5/91 ; additional monomode fiber optic link/1994
Spain	-----	Via UK as an extension of the UK-Spain No. 5 and TAT-10 in 1990

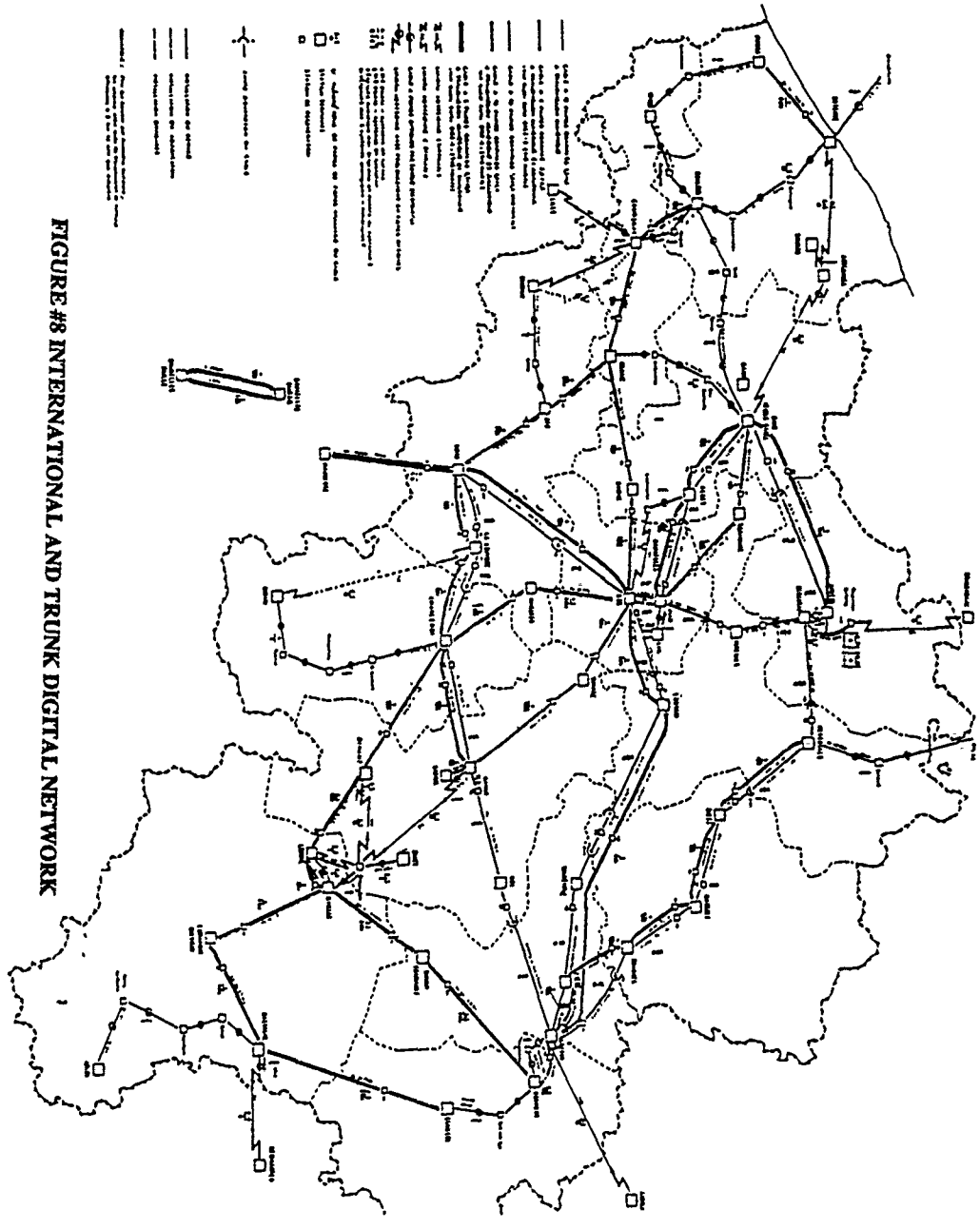

FIGURE #8 INTERNATIONAL AND TRUNK DIGITAL NETWORK

APPENDIX: EVOLUTION OF THE FIBER OPTIC NETWORK

1. Conditions and Requirements for the Design of the Optic Fiber Trunk Network.

The trunk network volutionary scenario is planned on the basis of a suitable model for the evolution of the demand on (digital) transmission capacity as a function of time. About 80% of this capacity is presently used for analog and digital telephone traffic. Though other services (digital TV, small -and broadband data) may develop to a higher relative significance in the next decades, they are not believed to become predominant before the end of the century.

As a consequence, the structure and dimensioning of the transmission network are essentially based on forecasts for switched telephony supplemented by needs from other smallband services. These are expressed as a list of 'bundles', each bundle representing a number of circuits required between two fixed terminal stations (located at the switching centres).

The set of 'bundles' represents the entire known demand of all services, except cable TV.

-Bi-routing.

Each bundle is 'bi-routed', i.e. its capacity is split into two halves routed through the network along two physically distinct routes (see figure - A1). Each pair of routes has neither common arcs (e.g. cable links) nor common nodes (transmission-centers). This approach guarantees that in case of a single arc failure (most common is a complete cable break) 50% of the capacity of each of the concerned bundles is preserved, irrespective of any restoration effort.

In the absence of saturated links, optimum bi-routing is defined by the shortest mesh between the end points of the bundle. Currently bi-routing is done at the demand level (mostly 2 Mbit/s), before multiplexing.

-Cascade multiplexing.

The routed bundles (2 Mbit/s) are multiplexed to the next higher hierarchical level (8Mbit/s), etc. up to the line level (typically 140 Mbit/s). In the trunk network, all intermediate hierarchical levels (8, 34 Mbit/s) are physically accessible on distribution frames for maximum flexibility:

4X 2 Mbit/s → 8 Mbit/s
4 X 8 Mbit/s → 34 Mbit/s
4 X 34 Mbit/s → 140 Mbit/s

The overall multiplexing scheme and the interconnection scheme on each distribution frame are optimized in order to minimize the overall investment of multiplex equipment, line equipment and cable capacity. The constraint is that the pre-calculated routes on the 2 Mbit/s level should be strictly obeyed.

-Spare capacity.

The network arcs are augmented by spare capacity, calculated by a heuristic programme. This spare capacity, spread over the entire physical network, should as a minimum allow to protect the network against any individual total cable fault (see - figure A2).

This type of network protection is implemented at the 140 Mbit/s level, which is considered to be a good compromise between ease of operation, cost and protection efficiency. In the planning model, bundles subject to arc failure are re-routed between their terminal points. This is a most suitable approach for automatic restoration using cross-connects in the network nodes. Unlike the basic routing mechanism (see above) re-routed bundles are allowed to be spread over an unrestricted number of individual routes ('flow' routing at the 140 Mbit/s level). This makes maximum use of the available space in the network. There are no

dedicated spares (using e.g. 1+1 or N+1 protection schemes). While the spare capacity strictly guarentees protection against single (but complete) cable breaks only, the restoration and dimensioning technique allow for a high degree of protection in multiple failure conditions.

-Investment scenarios.
The investment scenarios are determined by a collection of optimization software modules (routing, multiplexing, spare calculation) combined in an iterative cycle. Figure A3 gives a simplified description of the procedure used.

2. Impact of New Technologies: SDH, High Bitrate Systems, Digital TV, ATM, ...

-SDH (Synchronous Digital Hierarchy) and High Bitrate Systems.
The Synchronous Digital Hierarchy, presently in an advanced standardization phase, offers substantial improvement in manageability, performance monitoring and flexibility, compared to the existing Plesiochronous Hierarchy (PDH). SDH equipments will be available on the market in the early 90's, and will soon replace PHD products for all extensions to the network. Their introduction may have a major effect on the fibre cable investment shedule.

The SDH multiplex structure differs from the existing PDH; in particular, the reduction in hierarchical multiplex steps will have an impact on the eventual line capacity.

The transition phase between 100% PHD and 100% SDH will exist for a considerable time (10 years?) and generates additional requirements, if one is committed to fulfill the safety requirements (routing, restoration) as described in par. 1. This is because PHD routes can be protected by boch PHD and SHD, but SHD routes can only be protected within the SHD network itself. As a consequence, the implementation schedule fo single modefiber links will have to be accelerated and carefully planned.

-High bitrate systems.
The introduction of high bitrate systems (e.g. STM -16 in the SDH hierarchy equivalent to 16 X 140 Mbit/s) will largely compensate the growth of capacity needs above the requirements satisfied by the first generation systems (STM-4 or 565Mbit/s). At the beginning of the next century, a further generacon of more powerful systems (coherent optical systems) will substantially upgrade the capacity of the single mode fibre cables.

-Digital TV.
Digital TV transmission (long distance) in Europe is now on its way to be standardized at the H2i rate (32 Mbit/s). This means that one STM-16 system (two fibers) can carry up to two 64 TV channels simultaneously (each way). A single pair of fibers in each cable can easily deal with any realistic demand for many years.

-Broadband Services: ATM, HDTV, Video, LAN interconnection.
For the time being, it is still very uncertian how the demand for these services will evolve. Due to the present poor level of standardization, and the uncertain appeal to the general public, we assume that the volume of these broadband services in the trunk network will remain substantially smaller than the basic services for at least a decade. A small margin on the fiber count will suffice. In the longer term, when the volume of these services may become important, the use of high bitrate systems will provide the required capacity.

3. Evolution of the Belgian Digital Trunk Network (1991-2002), without considering SDH.
Figures A4 through A9 show the projected provision of new digital links. All of these links are implemented as single mode fiber cables. This results in a homogeneous meshed single mode fiber network by 2002. The need for new links is dictated by traffic expansion only, and does not take into account specific requirements resulting from SDH deployment.

Table 1 shows the capacity requirements expressed in 565 Mbit/s (or STM-4) systems, as well as the number of fibers derived from these requirements, covering 10 years expansion (7% traffic growth/ year) beyond the year of installation. Four more fibers are included for additional TV and early broadband services. Further expansion of broadband services is possible through the use of high bandwidth systems.

4.Impact of SDH Introduction.
The RTT has undertaken a study on introduction scenarios of SDH in the Belgian trunk network. The first results will be available at the end of the year.

The study first considers the network configuration for the target year 2002, resulting from earlier work which did not consider the effects of SDH. We can presume, however, that investments on new cable links will be restricted to single mode cables. The network available in 2002 therefore consists of the structure displayed in figure A10, supplemented by the residual portion of the present PDH network. The single mode portion of the network can be equipped with SDH systems when and where required.

When subsequently considering the demand for each year (scanning the years backwards from 2002 through 1991) routing of the bundles is distributed between the single mode (SDH) and the PDH part of the network in such a way that:

-investments on new cables are postponed as much as possible;
-the safety considerations contained in par.1 are strictly obeyed.

As explained above, this will result in a considerable amount of earlier investments in both cables and (SDH) equipment, compared to the pre-SDH case. However, because of the fact that by 2002 the single mode network has matured to a fully meshed structure, serving nearly all nodes, even without considering SDH, the total volume of cable and fibre investments will not change considerably.

The evolution towards SDH will also have an impact on inter-station cabling. SDH nodes will be more compact (virtually no connectorized distribution frames) and all transmission interfaces become optical. The existing copper cabling will be gradually replaced with a much smaller volume of optical cords. The total fiber length deployed will be negligible compared to the inter-station network.

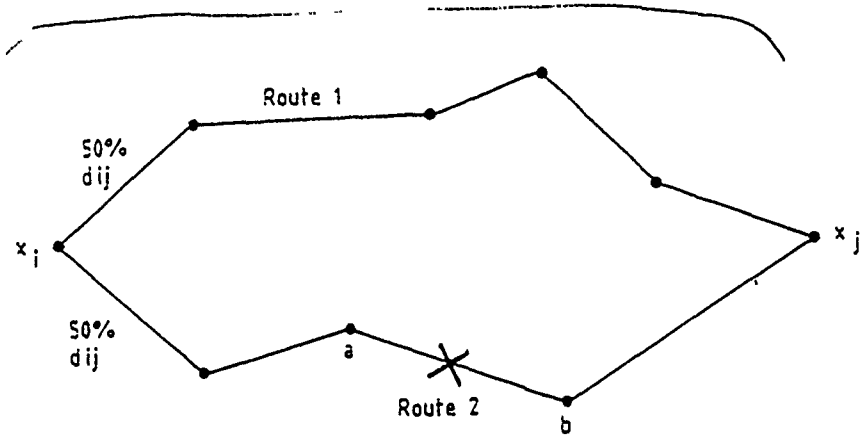

Fig. A1 dij : Demand to route between xi and xj

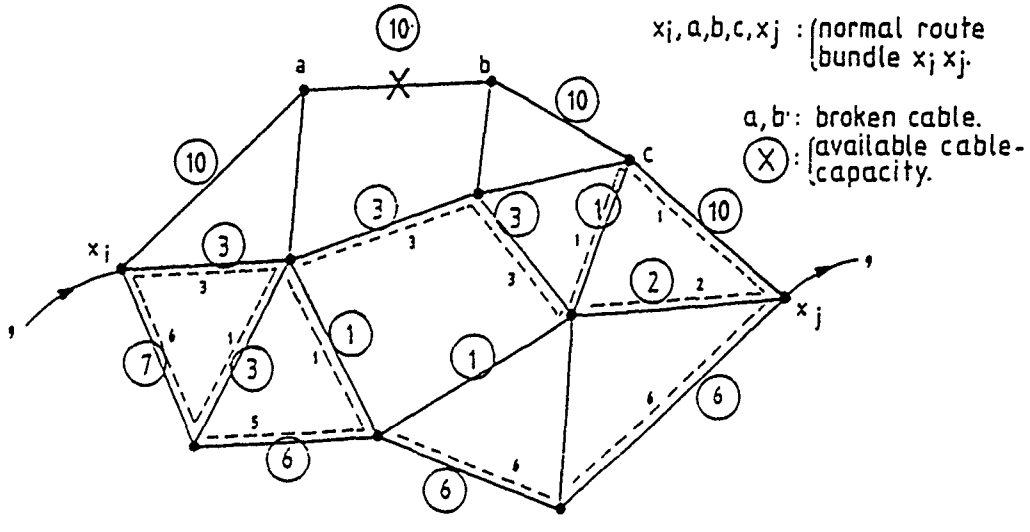

Fig A2 The rerouting of a bundle between xi and xj with a capacity of 9 results in a flowpattern.

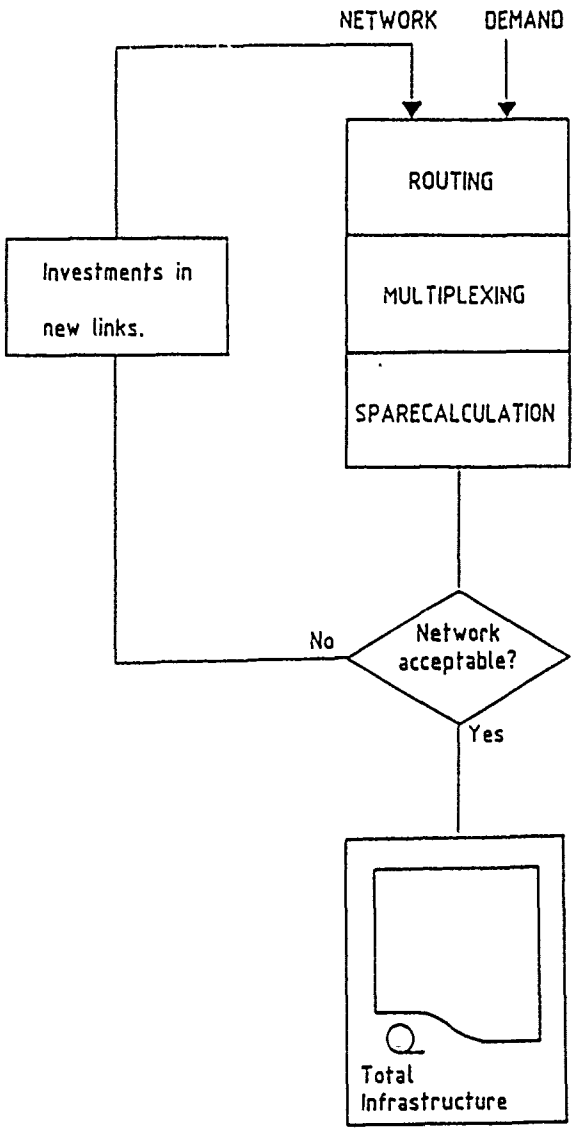
NETWORK
DEMAND
ROUTING
MULTIPLEXING
SPARECALCULATION
Investments in
new links.
No
Network
acceptable?
Yes
Total
Infrastructure

Fig A3

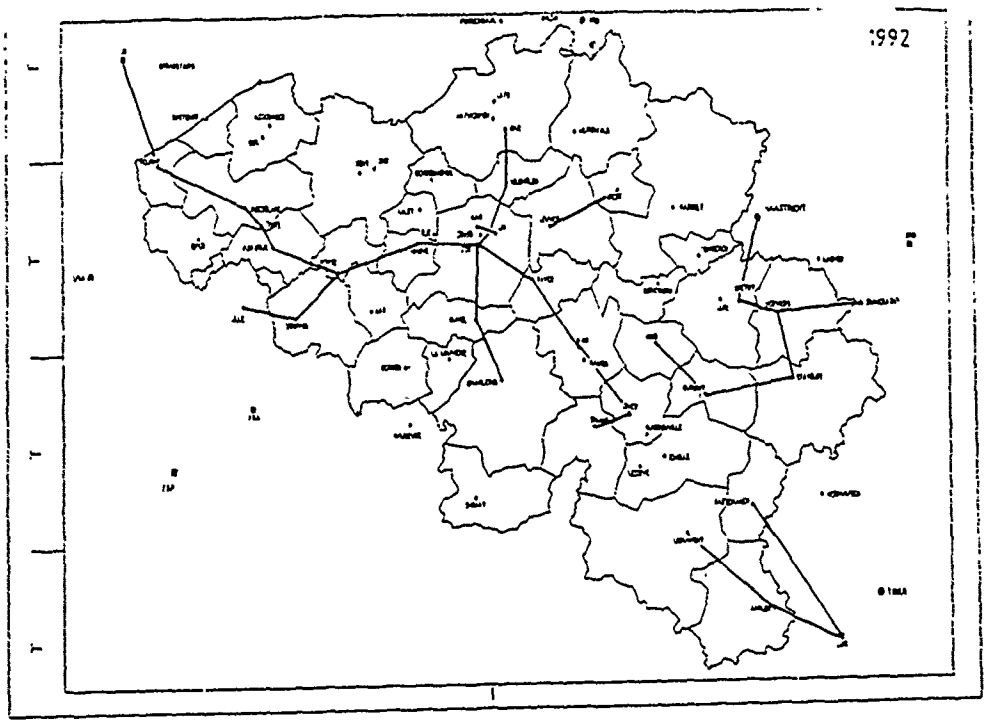

Fig A4 : Monomode network topology 1992.

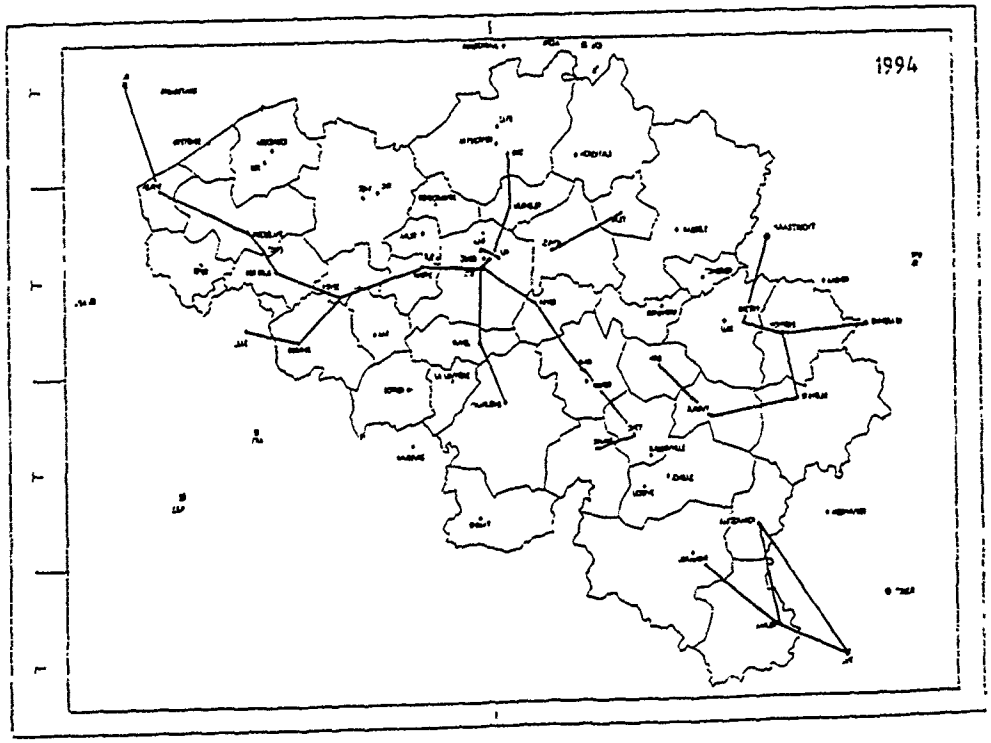

Fig A5 Monomode network topology 1994.

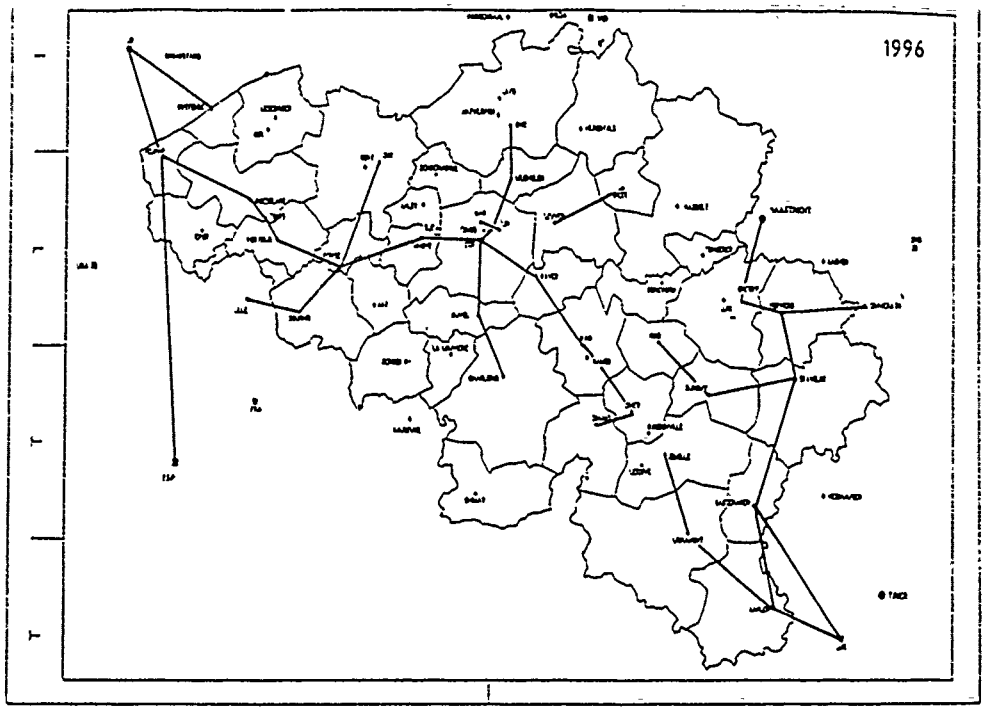

Fig A6 : Monomode network topology 1996.

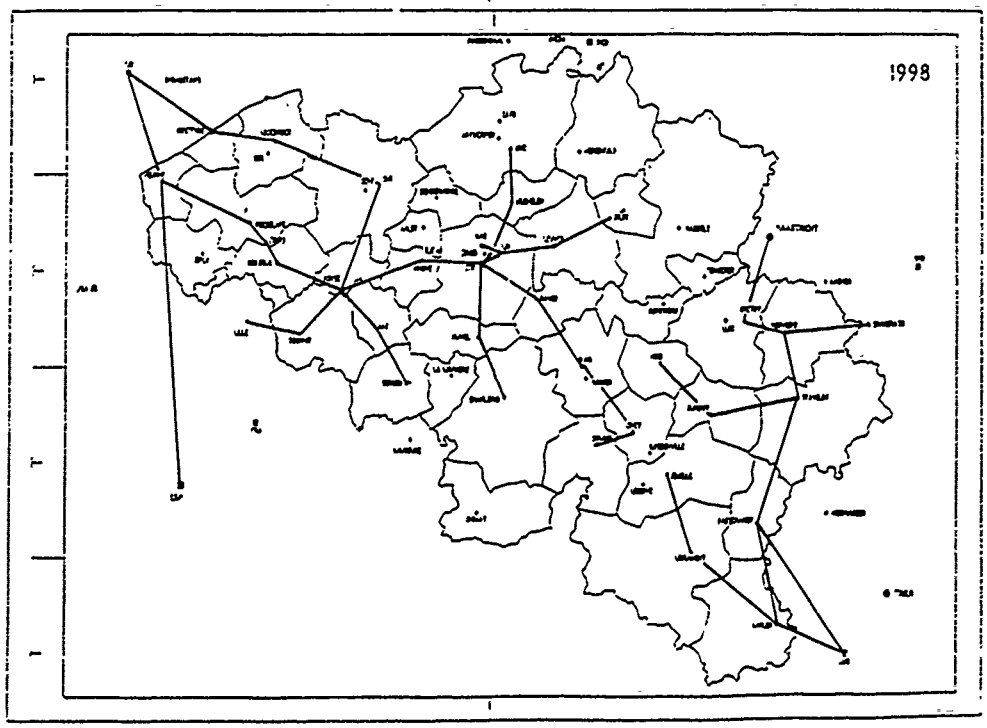

Fig A7 : Monomode network topology 1998.

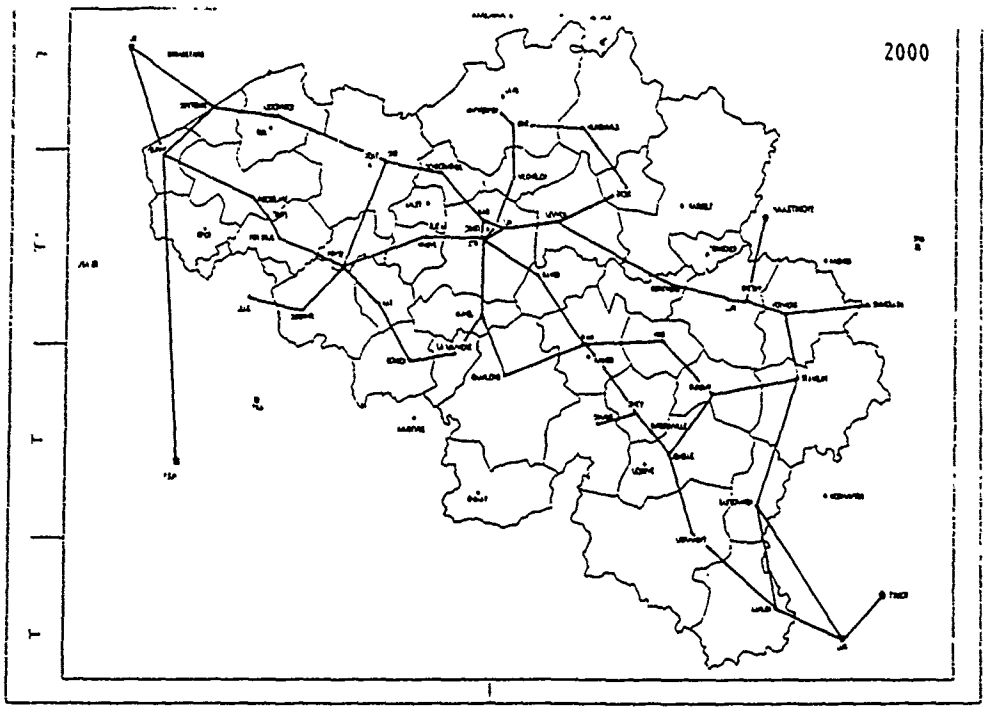

Fig A8 : Monomode network topology 2000.

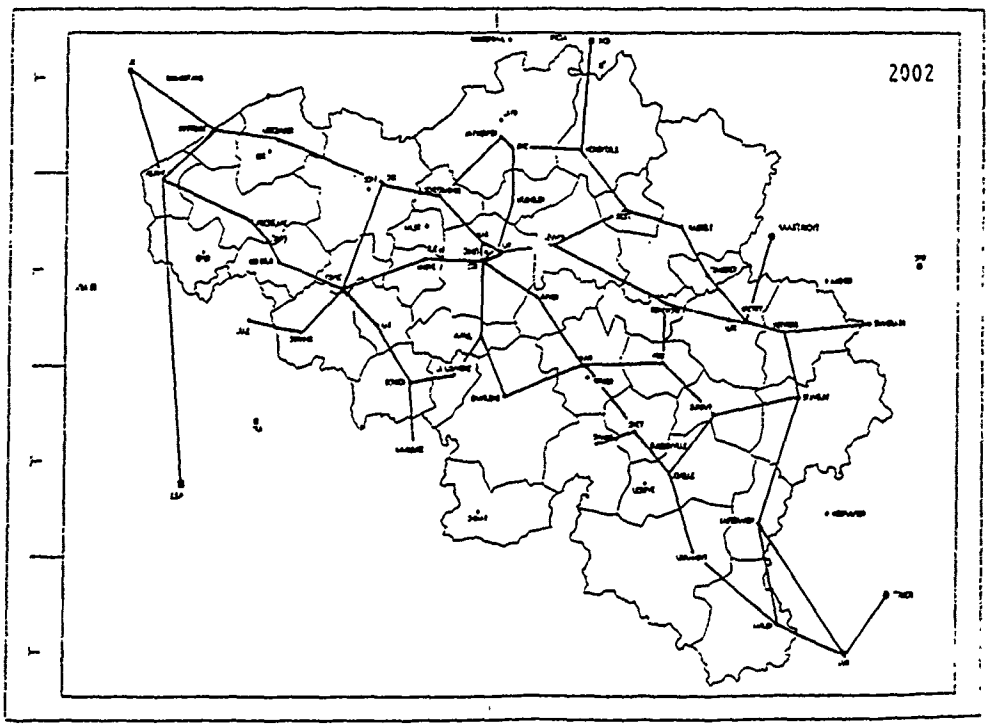

Fig A9 : Monomode network topology 2002.

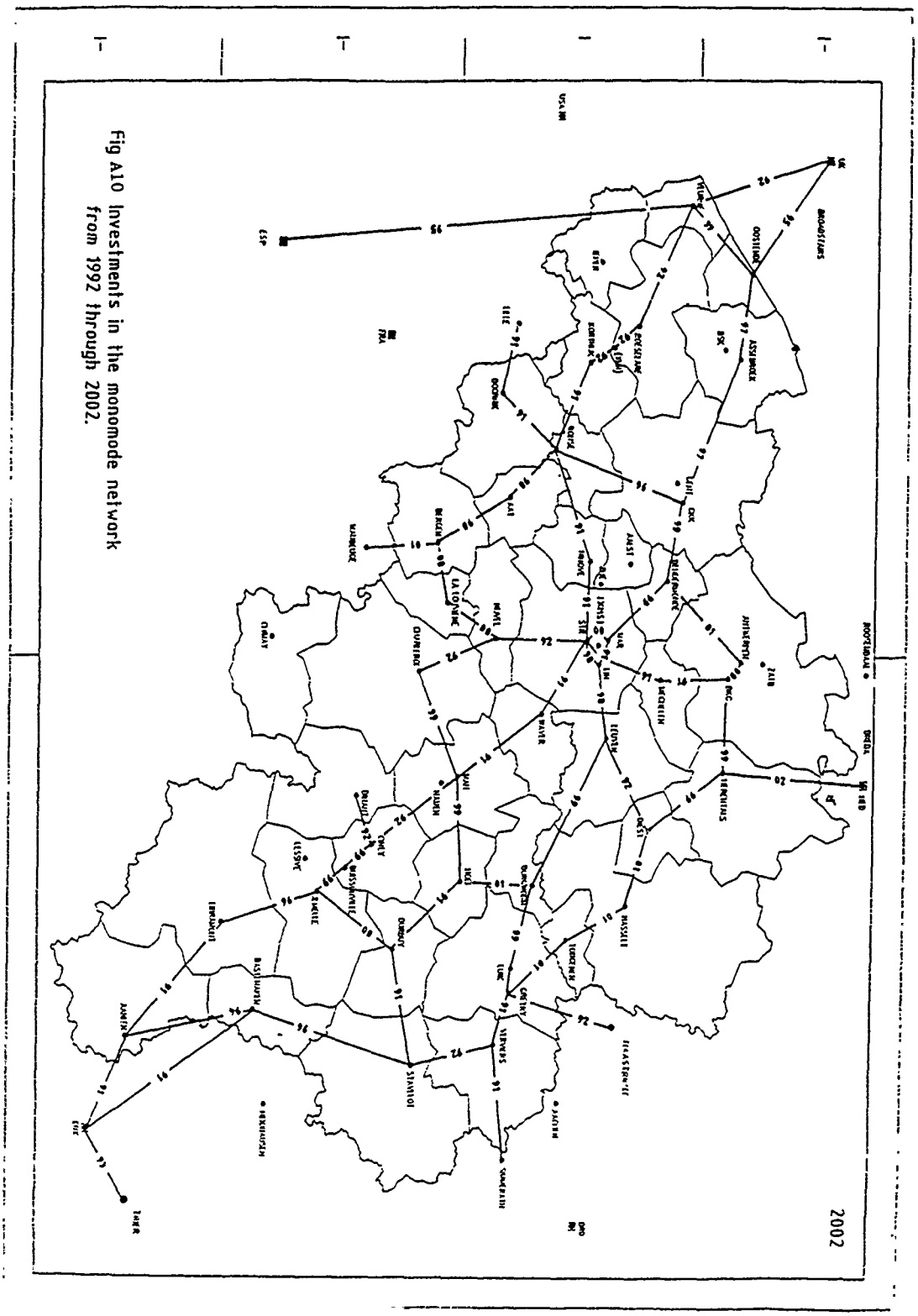

Fig A10 Investments in the monomode network from 1992 through 2002.

Table 1

NEW SINGLE MODE FIBRE CABLES 1991 - 2002

First Use	Cable	Length	Cap	Fibres
1991	Arlon - Libramont	41 km	2	8
1991	Arlon - Luxembourg	25 km	2	8
1991	Bastogne - Luxembourg	50 km	1	Radio
1991	Durbuy - Huy	25 km	4	12
1991	Durbuy - Stavelot	31 km	3	10
1991	Grétry (Liège) - Verviers	20 km	4	12
1991	Kortrijk - Ronse	26 km	4	12
1991	Linthout (Brussels) - Marais (Brussels)	3 km	6	16
1991	Namur - Wavre	33 km	5	14
1991	Ninove - Ronse	31 km	6	16
1991	Ninove - Stro (Brussels)	24 km	6	16
1991	Ronse - Tournai	22 km.	4	12
1991	Tournai - Lille (France)	30 km	5	14
1991	Verviers - Simmerath	40 km	3	10
1991	Stro (Brussels) - Wavre	23 km	5	14
1992	Charleroi - Nivelles	22 km	3	10
1992	Ciney - Dinant	14 km	1	6
1992	Diest - Leuven	27 km	6	16
992	Grétry (Liège) - Maastricht	40 km	2	8
1992	Kortrijk - Roeselare	17 km	5	14
1992	Roeselare - Veurne	35 km	3	10
1992	Stavelot - Verviers	23 km	4	12
1992	Nivelles - Stro (Brussels)	28 km	4	12

1992	Veurne - St.-Margaret's Bay (UK)	100 km	4	12
1994	Arlon - Bastogne	36 km	2	Radio
1995	Oostende - UK	120 km	3	10
1996	Bastogne - Stavelot	46 km	3	10
1996	Gent - Ronse	35 km	5	14
1996	Jemelle - Libramont	29 km	3	10
1997	Assebroek (Brugge) - Gent	38 km	4	12
1997	Assebroek (Brugge) - Oostende	23 km	4	12
1998	Ath - Mons	23 km	4	12
1998	Ath - Ronse	18 km	4	12
1998	Leuven - Linthout (Brussels)	24 km	9	22
1998	Linthout (Brussels) - Stro (Brussels)	3 km	8	20
1999	Berchem (Antwerpen) - Herentals	30 km	8	20
1999	Buissonville - Ciney	12 km	1	6
1999	Buissonville - Jemelle	8 km	1	6
1999	Charleroi - Namur	30 km	5	14
1999	Dendermonde - Marais (Brussels)	27 km	6	16
1999	Diest - Herentals	26 km	7	18
1999	Dendermonde - Gent	26 km	6	16
1999	Huy - Namur	27 km	8	20
1999	Leuven - Waremme	44 km	9	22
1999	Liège - Waremme	24 km	9	22
1999	Oostende - Veurne	25 km	3	10
2000	Antwerpen - Berchem	3 km	7	18
2000	La Louvière - Mons	17 km	7	18

2000	La Louvière - Nivelles	17 km	5	14
2000	Durbuy - Jemelle	27 km	3	10
2000	Marais (Brussels) - Stro (Brussels)	2 km	12	28
2001	Diest - Hasselt	21 km	6	16
2001	Grétry (Liège) - Tongeren	17 km	6	16
2001	Hasselt - Tongeren	19 km	6	16
2001	Huy - Waremme	20 km	8	20
2001	Mons - France	30 km	6	16
2002	Herentals - Nederland	50 km	5	14

SUSAN MIRBACH

Susan G. Mirbach is President of RTT-Belgian Telecom USA, the American operations of the RTT, Belgium's telecommunications authority. As such, she is responsible for all American operations, including setting up the carrier's customer service, sales and marketing efforts. In addition, she will oversee the future direction of the group.

Mirbach is also Vice President of Mirbach & Co. Inc., the Connecticut-based consulting firm within which RTT-Belgian Telecom USA operates.

Mirbach has extensive experience in the international telecommunications industry. She formerly was Director of Marketing and Major Accounts for France Telecom, Inc., the U.S. arm of France's national telecommunications organization. In her four years there, she managed the carrier's marketing efforts, and provided account management to many of its largest international clients. Prior to joining France Telecom, Mirbach was a Faculty Research Associate at INSEAD, the European Institute of Business Administration, Fontainbleau, France. Before that, she was a Consultant in the Business and Strategic Planning and the Energy Regulatory Groups of Coopers & Lybrand, Washington D.C.

Mirbach holds an M.B.A. in International Business from INSEAD, and has a B.A. with Honors in International Relations from Stanford University. She has also recieved a Certificate in Telecom Analysis from New York University.

EVOLUTION OF BRITISH TELECOM'S TRANSMISSION NETWORK

Dr S. Hornung and Dr T. R. Rowbotham

British Telecom Research Laboratories

Abstract

The business of telecommunications is experiencing both rapid growth and advancement of technology. To meet this challenge British Telecom is carrying out a major modernisation programme of its network involving a wholesale move to digital technology for both transmission and switching. Already all long lines traffic in the Public Switched Network (PSTN) is digitally switched, and by the year 2000 the overwhelming majority of core transmission will be carried by singlemode optical fibre. This will bring fibre to within 2km of the customer. This last gap can be bridged by optical fibre serving the business customer, however, the major challenge remains the modernisation of the access network serving the domestic customer. Both the Core and Access networks will be profoundly affected by the emerging concept of personal mobility.

Introduction

British Telecom (BT) is the major provider of telecommunications services in the United Kingdom. Its network is the fifth largest in the world at 24.5m lines, and growing at 4.5% per annum. Approximately 80m calls are handled per day and this figure is increasing at 10% per annum.
In 1989 BT had a turnover of over £11,000m.
In this paper we will examine BT's network as it stands and what major changes are envisaged over the next decade.

British Telecom's network today

BT's inland network is comprised of two sectors, the Core carrying long lines traffic, and Access for local distribution. The Core could also be further broken down into:

Long lines network: which carries the majority of long distance traffic between major switch units.

Inter office network: which carries traffic between the major switches and local exchanges serving a range of differing size communities.

Local network: provides the connection to the customers premises.

1981 saw the introduction of BT's major modernisation plan, which impacts the physical network in several important ways:

1. Large scale introduction of digital SPC switching technology (System X), and digital connection to customers. The old electromechanical switching units are being replaced at 10 per week. By the year 2000 all of BT's customers will have a digital SPC connection. The current figure is 30%.

2. Rapid introduction of single-mode optical fibre carrying digital traffic for long distance transmission. Long distance "Long lines" routes have been followed by intermediate "Inter office" network and a start has been made in the local access network.

3. The number of exchanges operated by BT is being reduced. The 360 long distance exchanges have been replaced by 53 Digital Main Switching Units. The 6200 Local exchanges will reduce to 1500.

Core Network

Long lines and Inter office network today:

The Long lines part of BT's network carries traffic between major switch units. Three transmission media are utilised, coaxial copper, line-of-sight radio and optical fibre transmission systems. The predominant medium carrier was soon identified to be fibre, because of the rapidly increasing traffic density. As of 1984 all new Long lines systems were based on singlemode optical fibre. To date 307,000km of fibre have been installed and carries 65% of all Long lines traffic (Copper co-axial 20%, radio 15%). The 53 Digital main switching units are now switching 89% of Long lines traffic.
It is envisaged that as traffic increases further, and more fibre is installed, optical transmission will become even more predominant. Signalling used in the Long lines network (and being introduced elsewhere) is the CCITT No. 7 common-channel, which has the benefits of fast call set-up time as well as making available advanced customer services of the "follow-me" type. This provides the basis for interconnection between

fixed and mobile networks, with the prospect of full personal mobility to come. The Inter office network modernisation is also proceeding with a total of 368,000km of singlemode fibre installed to date, carrying 56% of Inter office traffic. Of the remainder 39% consists of co-axial copper carrying digital transmission and 5% copper carrying analogue transmission. All analogue systems will have disappeared from the public switched network by 1994.

Future:

Present trends suggest that in the future the telecommunications network will need to cater for far more services than telephony alone. Data traffic is growing visibly, and demand is perceived for wideband services. Long lines traffic has grown some 60% between 1988 and 1990. A similar rise is anticipated by 1992 for both Long lines and Inter office.
In contrast providing additional capacity in line transmission plant is at present a slow, cumbersome and expensive business, involving the installation of new cable and duct, electronic regenerators and switches which currently only handle a fixed digital format.
In the near future a more flexible managed network can be realised by the introduction of the Synchronous Digital Hierarchy (1). This will provide drop and insert capability, higher order multiplexing, and higher ordre automatic crossconnecting. Such a network could offer the customer high quality transmission, rapid response to the customers demands and the ability to support a wide range of services, and BT is active in defining SDH standards.
A more long-term solution may lie in the better utilisation of the singlemode fibre already installed in the ground, which has capacity far beyond that which is used at present.
Newly-developed optical amplifiers could form low noise transparent repeaters capable of amplifying many optical signals simultaneously, while High-density Wavelength Division Multiplexed or coherent optical transmission could make many wavelength channels available for transmission. (2) By careful design of the network, more capacity could be added later at short notice by adding more terminals to an existing passive fibre network, in which optical wavelength would be used as a flexible means of determining the destination for transmissions in an "optical ether". The optical repeaters would amplify the additional signals regardless of their content, thus providing transparency to both bit-rate and format. The resultant low component count would also result in high reliability and a decrease in depreciation costs.

Access Network

Access Network today:

Modernisation of BT's core network has been rapid, and though increasing demands will ensure that the process continues, clearly the major challenge for the next decade and beyond will be the modernisation of the access (local) network. The use of optical fibre in the Inter-office network brings the fibre to within 2km of the customers premises. The last 2km however currently contains some 36m copper pairs.
The copper access network represents a large investment and today is BT's main revenue generating means. It was installed, however, over a long period of time and much of it is now aged. Incomplete records and poor joint performance result in a significant maintenance committment. As the copper network also has limited bandwidth capacity, there is now considerable interest in replacing much of it with optical fibre, and thereby benefiting from improved reliability as well as an increase in available bandwidth. However the large scale introduction of fibre into the local loop is a complex long-term issue, ultimately dependant on the most cost-effective means of providing the customer with the service required.
Most immediate reliability problems in the copper network are being overcome by replacing highly fault prone sections with new copper, particularly in areas where no fibre is anticipated within 5-10 years time.

Flexible access networks:

British Telecom is planning the introduction of single-mode optical fibre into its local loop in a number of stages; beginning with fibre for service provision to large and medium businesses, followed by small businesses and so on leading to the long-term goal of comprehensive fibre network, ultimately reaching even the single-line customer. The spearhead is the deployment of fibre in single star configurations using dedicated fibres between the central office and major business customers. To date 61,000km of fibre has been installed, which represents some 6% of BT connections Optimistic projection increases this figure to only 50% by the year 2000.
The key elements of these fibre access systems are summarised as:-

* Primary multiplexers located at customers premises along with appropriate higher order multiplexers and optoelectronics.

* Dedicated single-mode optical fibre cable network.

* Software to monitor and control the hardware and to interface with existing operations systems.

Several options exist for the progression of single-mode fibre systems to smaller customer sites. It is probable that single star fibre access systems will become economic for smaller numbers of circuits to business customers as component volumes increase and fibre handling techniques mature. However, alternative fibre architectures are more likely to find economic application for thw small business and domestic customer (3).

Access network in the future:

It is not currently economic to provide a dedicated fibre to the small business and domestic customer, based on existing service requirements. The introduction and proliferation of wide-band services both in the domestic and in the business sector will clearly change the situation, however growth in such services is at present uncertain.
One promising method of reducing the cost is by sharing some of the equipment amongst several customers. BT is primarily focusing its attention on two such networks.

Broadband Integrated Distributed Star (BIDS):

This is a classical double star (4). It is primariliy aimed at the domestic market and delivers telephony and cable TV on optical fibre to the customers' premises. This technology therefore represents an entry stategy for fibre in the local loop based on the provision of wide-band services at the same time as telephony. This will allow the initial higher cost to be offset by higher charges accrued by the delivery of entertainment services.
It is worth noting that BT's license is, however, due to be reviewed in 1990 with the possibility of further changes to come.

Telephony on Passive Optical Networks (TPON):

This is a relatively recent approach to network design which has lately been receiving much attention (5). Passive optical splitters are used to share a broadcast signal to typically 32-128 customers (remote terminals), and to combine signals in the return direction. TDM protocol is used in the broadcast direction and TDMA in the return direction.
Exchange equipment and a significant fraction of the optical plant are shared. The remote terminal can be located in the customers premises in the case of a domestic customer ("house TPON"), though further sharing can be achieved by siting the remote terminal in the street and serving a group of customers via a final copper drop ("street TPON"). Small business customers can be served by a remote unit delivering several lines ("business TPON"). In addition to the economic factors TPON offers flexible service provision, extra lines can be allocated by programming the exchange equipment, thus allowing BT to quickly respond to growing demand. Current cost projections indicate that the latter two versions will be cost effective when delivering POTS or ISDN telephony (6). TPON is therefore an entry strategy based on existing narrow-band services. The fibre will however be in place and capable of carrying additional services at marginal cost. These wide-band services can be multiplexed on the fibre network using WDM (or other) techniques (7). It is envisaged that different services could be provided by exploiting the spectral bandwidth of the fibre and using wavelength division multiplexing techniques. The customers will access different services as required. As well as telephony both broadcast and switch wide-band services can be provided.

Local access field trials:

The two network technologies described above offer radically different solutions to larger-scale fibre entry in the local loop. BT has decided to hold trials of both technologies with the following objectives (8).

1. To demonstrate the technical feasibility of using optical fibres in the local loop for single-line telephony customers.

2. To allow comparison of active and passive architectures with regard to cost, technical performance, ease of operation and customer response.

3. To give experience in practical operational aspects of the optical loop network, including installation, customer churn, reliability, maintenance and network control.

4. To provide experience to allow projection of procurement and operational cost with greater confidence than at present.

5. To give BT first-hand knowledge to allow full participation in the world debate on topologies, technologies and standards for optical local networks.

The location has been selected to be Bishops Stortford, a town of some 12,000 houses. Several suitable housing sites have been identified radiating outward from the telephone exchange in various directions. Within these estates there is the required mixture of modern and older property with local feed either being overhead or directly buried underground. There is very little duct all the way to the customers premises.
The BIDS networks will serve up to 112 customers. The TPON network will be trialled in all three forms, house, street and business, serving up to 298 customers. The first customer will be connected in the third quarter of 1990, and the trial ends in 1992 when the special license provided by the UK government expires.

Personal mobility:

The concept of personal mobility is rapidly gaining credibility as technology and market potential evolve (9). Some elements are already in place in the form of a fast growing cellular network, and the recently launched telepoint network.
Current costs are high although they may be expected to reduce as personal mobility becomes widely used.
Ultimately this technology can be expected to form a comprehensive mobile periphery to a fixed network, which will undoubtedly look very different to today's fixed network. The Long lines

network will need to cope with a great increase in traffic and clearly will need to be able to keep track of callers in order to make connections. The access network, on the other hand will need to connect the many short range radio mobility stations with small cells being required to serve urban areas. Such mobility stations will need spacing of order 100m and could be supported by passive optical networks (PONs) (amongst others) similar to those being trialled in Bishops Stortford.

Conclusions

British Telecom is in the midst of a massive modernisation programme of its network. The two major physical changes involve a wholesale move to digital technolgy and to all singlemode optical fibre transmission media. By the year 2000 this will be the case for the trunk and junction part of the network, and will bring fibre to within 2km of the customers premises. Current technology is also capable of serving large business customers with dedicated fibre links. The major remaining challenge will be the access part of the network.
Development work and field trials are testing several technical solutions which have the potential to bring the fibre to the small business or to within 100m of domestic customers. The last "gap" may be bridged by new high revenue earning services, and in any case could be served via radio promoting personal mobility as the primary way of accessing the telephone network. All indications are that traffic and new services will continue to grow rapidly and BT's network will need to stay ahead of the demand and satisfy its customers in a flexible and responsive manner.

Acknowledgements

The authors would like to thank colleagues at British Telecom Research Laboratories for helpful discussions and the Director, Network Technology, Britich Telecom Research and Technology for permission to publish this work.

References

1. Hawker I, Whitt S and Bennett G: "The Future British Telecom Core Transmission Network" 2nd IEE National Conference on Telecommunications York, England, 2-5 April 1989.

2. Brain M C: "Coherent Optical Networks" British Telecom Journal Vol. 7 No. 1, January 1989.

3. Hornung S, Wood R, Keeble P J: "Single-mode Optical Fibre Networks to the Home" ICC '90, Atlanta, USA.

4. Ritchie W K: "The Switched-Star Cable TV Network" BT Technology Journal Vol. 2 No. 4, 1984.

5. Stern J R et al: "Passive Optical Local Networks for Telephony Applications and Beyond" Electronic Letters November 1987 Vol. 23 No. 24.

6. Jensen J D, Weeks W I: "Fibre to the Pedestal. ...Then What?" ICC '90 Atlanta, USA.

7. Oakley K A et al: "Passive Fibre Local Loop for Telephony with Broadband Upgrade" Conference Proceedings "International Switching Symposium Loops and Services" 1988, 179-183.

8. Rowbotham T R: "Plans for a British Trial of Fibre to the Home" IEE Conference on Telecommunications, April 1989.

9. Groves I S: "Personal Mobile Communications - A Vision of the Future" BT Technology Journal Vol. 8 No. 1, January 1990.

Dr Stephen Hornung
British Telecom Research Laboratories, Martlesham Heath, Ipswich, Suffolk IP5 7RE.

Stephen Hornung graduated from the University of Exeter in 1975. In 1980, he received the D Phil degree from the University of Oxford for work in low-temperature physics.

Since 1979, he has worked for British Telecom Research Laboratories on optical fibre communications, specialising in measurements on optical fibres. He is currently head of group concerned with te development of optical components and test equipment.

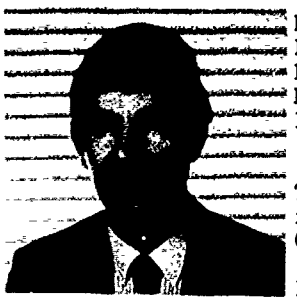

Dr Tom Rowbotham
British Telecom Research Laboratories, Martlesham Heath, Ipswich, Suffolk IP5 7RE.

Tom Rowbotham obtained in succession a BSc from Queens University Belfast (1964), MSc in Microwave Physics from University of Surrey (1968), and a PhD in Modelling of Transient Phenomena from University of Nottingham (1978). In 1986 he was appointed to a Special Professorship at Nottingham University.

He started his career with British Telecom in 1964 on satellite earth stations. In 1966 he became

Group Leader at Castleton Research Laboratories, South Wales developing Microwave Integrated Circuits. In 1974 he became Head of the Digital Tranmission Research Section at Martlesham Heath, moving in 1979 to Washington DC as Section Chief in charge of Communications R&D for the International Telecommunications Satellite Organisation (INTELSAT). In 1982 he became Head of the Optical Transmission Research Division, Martlesham Heath, and in 1987 he was appointed General Manager Network Systems covering switching, radio and optical transmission research in British Telecom Research Laboratories.

With effect from 1 April 1989 Dr Rowbotham became Director Network Technology at British Telecom Research Laboratories in charge of all Network related activities, with three departments, Network Systems, Network Management and Materials and Component Research (approx 2,000 staff).

THE COPPER AND OPTICAL FIBRE NETWORKS OF THE DEUTSCHE BUNDESPOST TELEKOM; CURRENT AND FUTURE REQUIREMENTS FOR COPPER/OPTICAL FIBRE CABLES

Dieter Freudensprung, Horst Middel

Deutsche Bundespost Telekom, FTZ Darmstadt, Germany

Abstract

The first part gives an overview of the copper cable and the optical fibre cable network of the Deutsche Bundespost Telekom (DBPT). The cable construction, statistical values and the demand for the next years are given.
Part two describes the future trend for copper cables and the activities of the Deutsche Bundespost Telekom for the introduction of the optical fibre cables and systems in the local loop. The status of the different pilot projects with the Raynet Corporation and several German telecommunications equipment manufacturers is given.

Introduction

Until about 1980 the cable-network of the Deutsche Bundespost Telekom has consisted of copper cables only. This has basically applied up to now to the local loop while, in the junction and trunk networks, the optical fibre cables have set out for their triumphal march. The Deutsche Bundespost Telekom has undertaken or is planning some field trials for the use of optical fibre systems in the local loop. Before discussing these activities, we will make some remarks on the existing network.

Present situation of the cable networks

1 The copper cables local network

The backbone of the narrowband service is the telephone service with presently about 30 million subscriber main stations in 3748 local networks and 6657 subscriber line areas. Related to main stations, other narrowband services such as telex have only a share of < 3 per cent. The subscriber line network is, therefore, tailored to for the telephone service.

The subscriber line network is a star network consisting of symmetrical copper cables and pairs which are 0.4, 0.6, 0.8 mm in diameter. The subscriber line area is divided into the main and distribution cable area. Main cables are provided section by section in keeping with the demand. Main cables are unfilled, PE insulated cables with a laminated PE sheath. Cables with pairs of 0.4 mm in diameter have a solid PE insulation. Cables with pairs of 0.6 and 0.8 mm in diameter have a cellular PE insulation. The cable construction does not make a difference between buried cables and duct cables. The same cable construction is, therefore, used for directly buried cables or cables pulled in ducts.

The pulling of cables in ducts restricts the maximum pair number to 2000 pairs of 0.4 mm diameter or to 1200 pairs of 0.6 mm. The smallest element is, as in the case of the formerly used paper insulated cables, a quad. Main cables are pressurized with a maximum pressure of 0.5 bar. The air flow through the

cable is monitored at the exchange for the purpose of fault signalling.

Because of the fact that costs of laying a cable are high as compared to cable costs, it is more economical, in the case of distribution cables, to choose - from the very start - a cable size meeting the final demand. The construction of distribution cables is similar to that of main cables, but they are filled and not pressurized.

Cables with pairs of 0.4 mm diameter have, like main cables, a solid PE insulation. Cables with pairs of 0.6 and 0.8 mm diameter have a foam skin PE insulation.

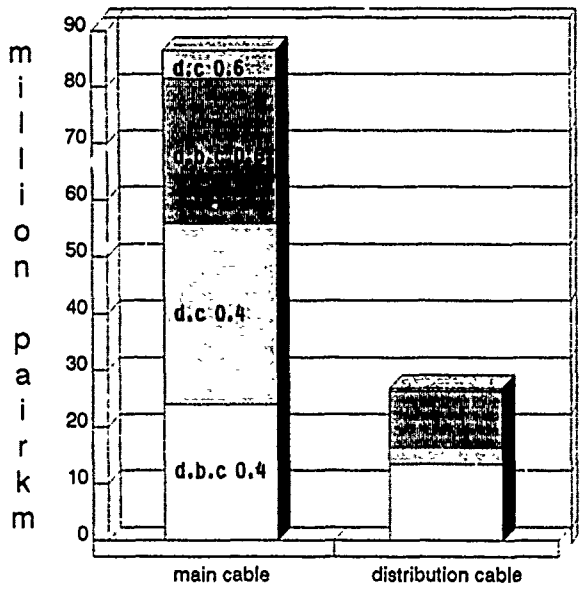

Figure 1: Main- and distribution cables of Deutsche Bundespost Telekom
Example: direct burried cables (d.b.c) 0.4 mm and ≥ 0.6 mm in diameter and duct cables (d.c) 0.4 mm and ≥ 0.6 mm in diameter

Figure 1 classifies the main and distribution cables according to the different diameters (0.4 mm and ≥ 0.6 mm) of the conductors and different kinds of cable laying (directly buried or in ducts). The sum of main and distribution cables contains a particularly large share (about 64 per cent) of pairs which are 0.4 mm in diameter. In Figure 1 no distinction is made between cables with plastic insulated pairs and a plastic sheath and paper insulated pairs with a lead sheath. The proportion of paper insulated cables in the local loop is about 25 per cent, but this share is decreasing year by year.

Aerial cables are of minor importance in the local loop of the Deutsche Bundespost Telekom. In principle, the aerial cables used have a maximum of 10 pairs. For many years, we have employed self-supporting cables with glass yarn in the sheath. Years ago we used what is termed "Figure 8 cables" some of which are still in the network. The small importance of the aerial cables in the local loop of the Deutsche Bundespost Telekom is shown in Figure 2. This figure indicates the pairkm of buried, duct and aerial cables.

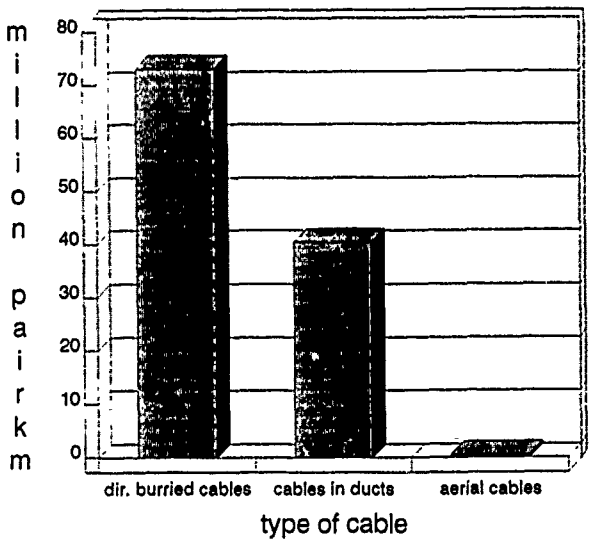

Figure 2: Direct burried cables, cables in ducts and aerial cables of Deutsche Bundespost Telekom

Assuming the latest forecasts, the state of network completion is 85 per cent for main cables and 94 per cent for distribution cables. Requests for a new telephone main station can be fulfilled in almost every case. The increase in main stations in 1989 was about 1 million. Only about 0.03 million new

subscribers have to wait more than 4 weeks because of lack of lines.

In spite of the large increase in the number of subscribers, the investment in the local loop for copper cables has been decreasing for many years. This trend is illustrated in Figures 3 and 4. Figure 3 shows the demand, split up for
- extension and
- replacement

of main cables.

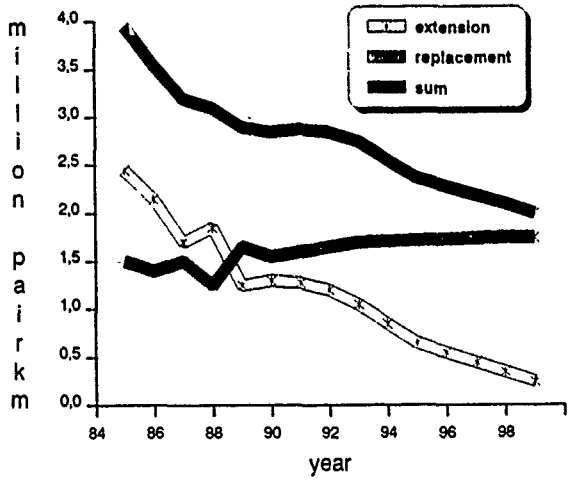

Figure 3: Material investments of Deutsche Bundespost Telekom
Example: main cables

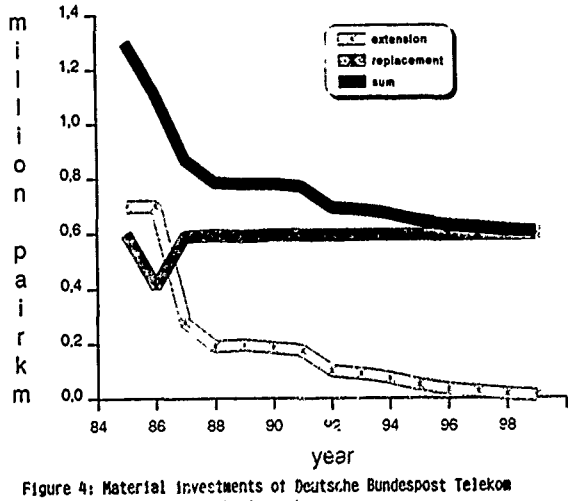

Figure 4: Material investments of Deutsche Bundespost Telekom
Example: distribution cables

Figure 4 indicates the corresponding values of the distribution cables. The large share of replacement is very important. All in all, the investment activities will decrease from the present figure of about 3.9 million pairkm to approximetely 2.7 million pairkm within 10 years.

1.2 The copper cable trunk network

For the extension of the trunk network we used only copper cables with symmetrical and coaxial pairs up to 1980. Since the introduction of optical fibre cables, the importance of copper cables has decreased in the trunk network. The supply of copper cables
- 9.5 million pairkm and
- 0.35 million coaxpairkm

is stagnating. The material investments for replacement and very small extension is now below 0.5 per cent of the supply and will decrease to less than 0.1 per cent. Copper-trunk cables are therefore no more of economic importance.

3 The Cable TV network

In the early eighties, the Deutsche Bundespost Telekom decided to install a large-scale coaxial-broadband network for CATV in the whole country.In this network with longitudinal welded outer conductors, the coaxial cables transmit in the frequence range up to 450 MHz a maximum of 35 TV signals plus 30 FM and 16 digital stereophonic sound signals. Because of the simultaneous offer of all programmes at the network subscriber interfaces, the network structure is a tree structure. In the CATV network a distinction is made between 4 levels. A and B basic links contain active elements. C basic links are connected to repeater points of level A and B without, however, containing any active elements. The links to the D level are passive couplers. D basic links terminate at the subscriber interfaces. The CATV subscriber line areas should be as congruent as possible with telephone subscriber line areas.

The number of households ready for connection was about 14.5 million in

the middle of this year and about 6.8 million homes were actually connected. This is equivalent to a provision rate of 55 per cent (ratio of homes ready for connection to total number of accommodation units) and a broadband service of about 47 per cent (ratio of connected accommodation units ready for connection).

With respect to the completion of the CATV network, it must be borne in mind that there are certain profitability constraints. The average investment per accomodation unit ought not to exceed DM 700,-. This strategy is shown in Figure 5. After a large increase until 1990, the investments will decrease in the future.

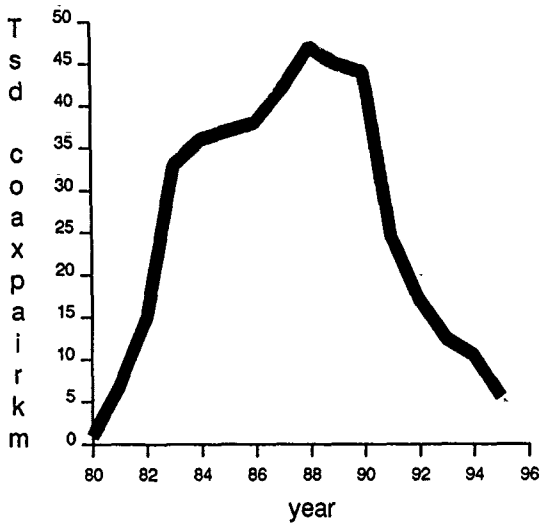

Figure 5: Material investments of Deutsche Bundespost Telekom
Example: CATV-cables

4 The optical fibre local network

Up to now, the Deutsche Bundespost Telekom has not conceived a strategy for the completition of the local network using optical fibre cables for small and/or broadband services. In 1986/87, however, the Deutsche Bundespost Telekom started to lay optical fibre cables in those parts of the 29 biggest local areas, where demand -e.g. centre of business- is expected. Optical fibre cables were also used in the junction network. Figure 6 shows the increase of optical fibre cables in the local network. The curve stops in 1990, the year when the planned completion, of the network for future services will come to an end. A total of about 250,000 fibrekm will be installed.

- 100,000 fibrekm of junction cables
- 75,000 fibrekm of junction cables for the general digitization
- 75,000 fibrekm in the local loop for new services

This prototype optical fibre network will be used, in part, in the prototype digital broadband network, which offers the possibility of direct distance dialling. The network is being developed for 1500 subscribers.

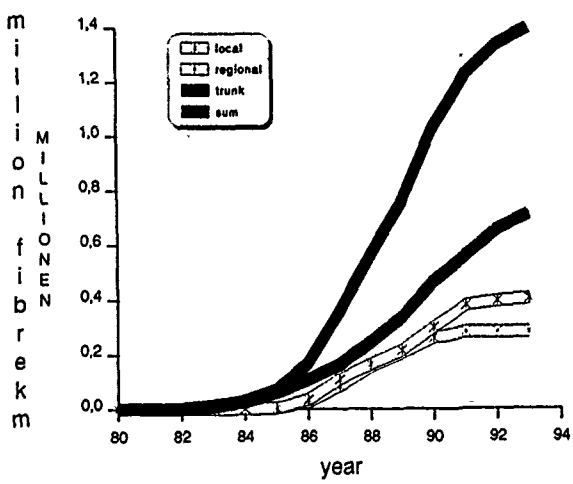

Figure 6: Optical fibres in the network of Deutsche Bundespost Telekom

5 The optical fibre trunk network

Since about 1985 only optical fibre cables have been installed in the trunk network. The optical fibre cables are single-mode optical fibre cables in bundle construction having a laminated PE sheath. The 1300 nm wavelength region is used for transmission.

The investment made for optical fibre cables in the trunk network will also decrease in the next years, because of

- large reserves were installed in the completion of the network for future services and
- the demand for future services has not existed up to now.

Moreover, the repeater spacing in the network was chosen such that, at present, it is possible to transmit 565 Mbit/s and, as soon as the systems available, even 2.4 Gbit/s.

This will quadruple the capacity of the existing network, without laying a single cable. Furthermore, the 1550 nm wavelength region is open for transmission.

Figure 6 shows the decreasing demand for optical fibre cables in the trunk network (trunk and regional).

Developments

1 Copper cables/ network

With the introduction of plastic insulated copper cables in the local network about 20 years ago, a transmission medium was introduced, which
- is very sophisticated
- has a long life.

We do not expect fundamental changes anymore. The introduction of the narrowband ISDN did not lead to new copper cables, either, because we can use the existing network for ISDN as well. In other words, the installed network with its existing cables fulfills both the requirements of analogue systems and the narrowband ISDN.

Bearing in mind that ISDN can transmit two channels with one pair, the copper network still contains substantial reserves.

As we expect, in the local loop, the changeover to an optical fibre network, we try to minimize the investment by the use of multiplex transmission systems (such as cable systems incorporating a few channels only).

To sum up, the development of copper cables is, in principle, coming to an end. Our efforts are, therefore, only aimed at maintaining the quality of the network and at buying the required cables as cheap as possible. After precise technical terms of delivery were defined in recent years, which allow both a European and worldwide tender of cable purchases, this goal was achieved.

For the sake of completeness, it is necessary to mention one new cable type of minor importance. We have developed a new ISDN-indoor cable instead of the commonly used PVC insulated indoor cable with a PVC sheath.

This new indoor cable has PE insulated pairs and a halogen-free sheath. Because of this, the capacity was reduced from 70 nF/km to 35 nF/km and the bus length between the Network Terminator (NT) and the telephone set was increased from about 150 m to approximately 230 m.

The development of copper trunk cables has been discontinued, because they are pushed aside by optical fibre cables. In the case of CATV cables, we await -as shown later on- the replacement of conventional cables in the near future or somewhat later.

2 Optical fibre cables/ networks

The successful use of optical fibre cables in the trunk network is limited in the local loop by economic constraints. One reason is the missing demand for broadband services and the other the lack of economic solutions and techniques. As we are of the opinion that, in the long run, optical fibre will be used in the local loop as well, we are looking for a flexible strategy. Regardless of the development and introduction of broadband services, we intend to use optical fibre systems for supplying the customers with conventional telecommunications services in order to achieve a significant cost reduction caused by the advantages expected from large quantities.

Left open is the option of extending these systems to broadband services. From this point of view
- optical fibre systems cannot be economically employed, at present, in the local loop

- the lackup demand for broadband services does not allow the completion of the local area with optical fibres
- pilot projects of technical and economical solutions for conventional services for the purpose of achieving a cost reduction by the use of large quantities
- possible extension to broadband services

The Deutsche Bundespost Telekom has decided to undertake several pilot projects. These pilot projects are known by the name of OPAL, which in this context, does not refer to a gem. It is a abbreviation for "OPTICAL ACCESS LINE".

2.1 Pilot projects with Raynet Corporation

The contract with the Raynet Corporation which was concluded in 1988 defines 3 levels:

OPAL 1
Level 1 is foreseen in the local loop 49 of the local area of Cologne. OPAL 1 is an optical fibre system for 192 analogue telephone sets and 96 network user interfaces for CATV. Project level 1 was officially initialized on Mai 31, 1990.

OPAL 2
Project level 2 is foreseen in local loop 23 in the local area of Frankfurt/Main. OPAL 2 is an optical fibre system for analogue and digital transmission. In the latter case it is intended especially for ISDN basic and 2 Mbit/s accesses and 2 Mbit/s fixed connections. Operation is planned to start in September 1991.

The 3rd level is an extension of level 2 to broadband communications services. Clear-cut concepts are still lacking.

2.2 Pilot projects for CATV in rural areas

Looking at the cost limit of DM 700,- DM per accommodation unit, the completion of the CATV network limits in rural areas on economical boundaries. But in these areas there are more than 50 per cent of all communities. To connect these also these communities to the CATV network, the Deutsche Bundespost Telekom is looking for economical solutions. It seems that optical fibre systems are one possibility.

OPAL 3
Raynet has been ordered this year to set up a pilot project system for CATV in a rural area. This is intended to verify the CATV system of OPAL 1 for a rural area and to verify the economics. The area will be the community "Lippetal" with about 4,500 accommodation units. The pilot project is still in the planning stage. The start of operation is foreseen in the middle of 1992.

OPAL 7
In fall 1989 we made a tender "Economical use of optical fibre systems for conventional telecommunication services in the local loop". One concept was a system for a "CATV network in rural areas". OPAL 7 is a pilot project developed by Bosch for these areas.

2.3 Other pilot projects in the local loop

As a response to the tender "Economical use of optical fibre systems for conventional telecommunication services", several proposals were made. Three of them are expected to become pilot projects. The latest date for the start of operation for all three projects is the last quarter of 1991. The services are: conventional telecommunication services, fixed connections and CATV.

OPAL 4
The local area of Leipzig is foreseen for OPAL 4. Siemens AG will install their system for a maximum of 400 main stations.

OPAL 5
In the "Media Park" of Cologne the company SEL (Alcatel) intends to install their system with 3x180 = 540 64 kBit/s channels.

OPAL 6
The companies AEG-ANT-PKI have created a cooperative group called

FAST to install their system in the local area of Nuremberg. It is a pilot project for about 200 main stations. The optical fibre cable is a ribbon cable.

Summary
Since the telephone network of the Deutsche Bundespost Telekom is almost 100 per cent equipped with copper cables and, in the last few years, only optical fibre cables have been used for completing the trunk network, a large number of pilot projects are undertaken to introduce fibre systems in local networks in order to pave the way for a future offer of telecommunication services at reasonable cost.

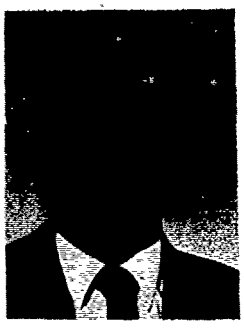

Dieter Freudensprung
Deutsche Bundespost Telekom
Fernmeldetechnisches Zentralamt
Am Kavalleriesand 3
D-6100 Darmstadt
Germany

Dieter Freudensprung studied at the Technical University of Aachen, received the diploma communications engineering in 1969 and joined the Deutsche Bundespost Telekom. Since 1971 he has been employed at the Telecommunication Engineering Center (FTZ) in Darmstadt. He was Head of several sections in the Outside Plant Division and has been Head of the Cable System Section since 1985.

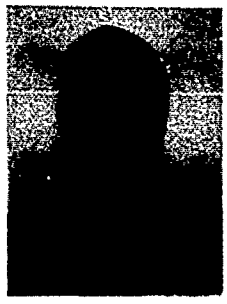

Horst Middel
Deutsche Bundespost Telekom
Fernmeldetechnisches Zentralamt
Am Kavalleriesand 3
D-6100 Darmstadt
Germany

Horst Middel received his diploma in telecommunication engineering in 1966 and joined the Deutsche Bundespost Telekom. Since 1974 he has been located in the Telecommunication Engineering Center (FTZ) in Darmstadt. He was engaged in cable technique of copper and optical fibre cables and is now responsible for cable measurements.

TRANSMISSION SECURITY: CROSSTALK TESTING OF FIBER OPTIC CABLES

Jeffery A. Fandl and Michael J. Ring

AT&T Network Systems, Norcross, Georgia

ABSTRACT

Many United States government agencies (Department of Defense and Department of Energy), who are users of fiber optic transmission systems, are as concerned about the optical security of the fiber in its various designs and cable configurations, as they are about the fiber's optical loss and bandwidth. Although the design of the fiber optic cable should prevent optical energy from one fiber being coupled into another fiber, these agencies are requiring that the fiber optic cables be qualified for their optical security by measuring the crosstalk of the cables. In order to satisfy their needs, a program has been established to measure crosstalk on samples of fibers in various cable designs. This paper will describe the AT&T Network Systems program to qualify the security of various fiber optic cables. These cables are the single mode and multimode versions of outside plant and inside plant cables, in loose fiber, buffered fiber, and ribbon configurations. The paper will document the crosstalk measurements for these cables, and discuss the test methods and test equipment. In addition, the subject of crosstalk and receiver sensitivity will be addressed.

INTRODUCTION

Crosstalk in fiber optics is defined as the measurable leakage of optical energy from one optical conductor to another. For a fiber optic cable, crosstalk is a parameter which quantifies how well one fiber is isolated from another.

The presence of crosstalk in a fiber optic cable can degrade the security of the fiber optic transmission. For the optical transmission to be secure, there should be no measurable crosstalk. For systems where secure communications (RED) are made over one or more fibers in a cable, while nonsecure communications (BLACK) are made over other fibers in the same cable, there should be no crosstalk between fibers.

The design of the fiber optic cable normally restricts any light path between fibers. The materials which surround the core of the fiber, such as the cladding glass, the single and dual coatings, and the buffer materials and strength members (if applicable), should isolate each fiber in a cable. The physical placement of the fibers in the cable also provides isolation. The measurement of crosstalk will determine the degree to which these factors prevent light from travelling between 2 fibers in a cable.

The connectors which are assembled onto the ends of a fiber optic cable, or splices which are used to join 2 cables, may contribute to the crosstalk, but the design of these components, and their physical placement in a system, also normally restrict crosstalk.

The Electronics Industries Association (EIA) and the Telecommunications Industry Association (TIA) have published a fiber optic test procedure for the measurement of crosstalk, FOTP-42, "Optical Crosstalk in Fiber Optic Components." This test procedure describes the approved method for measuring and calculating crosstalk, including the test equipment and test sample. The procedure itself is very simple to perform, but the accuracy of the measurement is limited by the dynamic range of the test equipment. The challenge of the crosstalk test is to be able to measure fiber optic noise at the lowest possible level.

DEFINITIONS

The following are definitions for terms used in this paper.

Source Fiber: The fiber which is connected to the optical source (LASER or LED).

Test Fiber: The fiber which is connected to the optical detectors.

Far End: The end of the test fiber farthest from the source.

Near End: The end of the test fiber nearest to the source.

P_r: The input power to the source fiber, measured at the output end.

P_f: The far end output power from the test fiber.

P_b: The near end output power from the test fiber.

CT_f: The inherent far end crosstalk, defined as -10 log (P_f/P_r) (for power in watts), or as $P_r - P_f$ (for power in dBm).

CT_b: The inherent near end crosstalk, defined as -10 log (P_b/P_r) (for power in watts), or as $P_r - P_b$ (for power in dBm).

dBm: Optical power in decibels referenced to one milliwatt.

HISTORY

The subject of optical crosstalk has been addressed previously, both experimentally and theoretically. Crosstalk measurements were made by Buckler and Miller in 1976 and 1977 for multimode ribbon cable, using the cross-coupling measurement technique.[1] This technique relies on an observer being able to distinguish between two adjacent surfaces that differ in luminance by only 1 percent. One fiber is energized using a visible He-Ne laser, while adjacent fibers are observed with an eye loupe. Filter material is inserted into the laser beam path, until the observer determines that the luminance of the energized fiber and the adjacent fiber are equivalent. The results of this experiment, which was performed on 2 different cable samples, showed a worst case far end optical crosstalk of 55 dB.

More recent crosstalk measurements have been made by Gossage, using optical sources and detection equipment.[2] These measurements, made at Sandia National Laboratories in 1988 for ribbon and loose tube cables, followed the EIA procedure FOTP-42. The purpose of this experiment was to measure ribbon to ribbon and tube to tube crosstalk. A worst case far end crosstalk of 58 dB was measured for the ribbon cable, using an 850 nm source, and a worst case far end crosstalk of 65 dB was measured for the loose tube cable, also at 850 nm.

Crosstalk has also been studied theoretically. Mathematical formulas for the crosstalk phenomenon have been published. Cherin and Murphy modeled crosstalk in the early 1970's, and studied the effect of cladding thickness, numerical aperture, length, kappa (a parameter indicating the power distribution among the modes of a fiber), and wavelength on far end crosstalk.[3] Their computer models showed that increasing the cladding thickness of the fiber improved the crosstalk isolation.

Snyder and McIntyre developed crosstalk formulas for 2 parallel, identical fibers, for a hexagonal array of fibers, for lossy fibers, and for fibers of unequal diameter.[4] They concluded that fibers must be nearly identical, and be touching, to be able to couple light from an energized fiber to an adjacent fiber.

TEST PROCEDURE

The industry standard for the measurement of optical crosstalk is EIA/TIA standard FOTP-42.[5] This procedure is used to determine the magnitude of the crosstalk between 2 fibers in a cable sample. The procedure may also be used to measure the crosstalk from optical connectors and splices. Figure 1 is a block diagram representation of the crosstalk measurement procedure for fiber optic cables. In this diagram, the symbol X represents the input connector of the source and detector.

The procedure states that the optical source shall be noncoherent, operating at the same wavelength as the system for which the cable is intended. The source and the launch optics shall overfill the source fiber of the cable sample. The detector shall be capable of capturing the entire output of the test fiber. The source shall be of an intensity that is at least 40 dB above the noise floor of the detection system.

The cable sample to be measured for optical crosstalk shall be between 18 and 22 meters (59.0 to 72.2 feet). The sample is to be suspended during the test so that microbending is prevented. Optical connectors may be assembled onto the ends of the fibers to facilitate connection to the source and detector.

The procedure described in FOTP-42 was followed for the crosstalk measurements documented in this paper. However, in order to better answer questions about the security of fiber optic transmission, other measurements were made using variations of the procedure. These variations will be described, and the test data will be documented.

TEST EQUIPMENT

The following table (Table I) describes the test equipment used to measure optical crosstalk.

TABLE I. TEST EQUIPMENT

Detection Equipment

power meter	Anritsu ML9001A
detector	Anritsu MA9612A
display resolution	.01 dBm
detector element	InGaAs photodiode
detector input	biconic connector
wavelength range	.75 μm to 1.7 μm
dynamic range	+3 dBm to -100 dBm
	(2 mw to 0.1 pw)
linearity (overall)	± .45 dB

Sources (LASER)

Source #	1	2
manufacturer	Photodyne	Anritsu
model number	1710-1300	MG97B
wavelength (nm)	1300	1300
operation	CW	modulated
		(300 MHz)
FWHM (nm)	2	3
connector	biconic/ST®	biconic

Sources (LED)

Source #	3	4	5
manufacturer	Photodyne	Photodyne	Photodyne
model number	1700-1300	1700-1550	1700-850
wavelength (nm)	1300	1550	850
operation	CW	CW	CW
FWHM (nm)	120	185	50
connector	biconic/ST	biconic	biconic

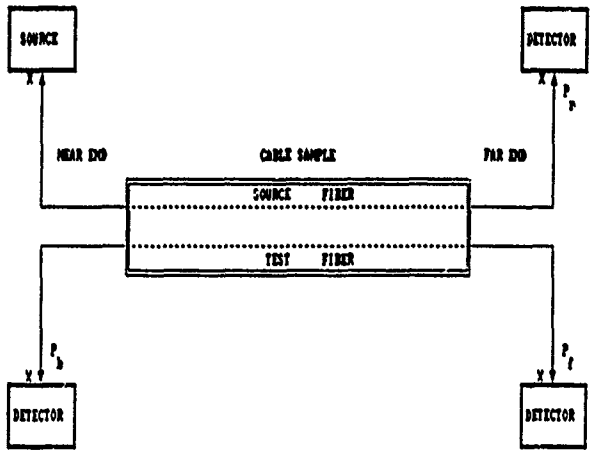

Figure 1. Test Procedure

The noise level of the test equipment was measured by darkening the detector, and reading the power meter every 2.5 seconds for 2 hours. The average power level over this time, which is the noise level of the test equipment, was .041 pw (-103.9 dBm). The maximum power level recorded was .101 pw (-100.0 dBm). This experiment was repeated twice, darkening the detector the first time by covering the input of the detector, and the second time by inserting one end of an interconnection cable with biconic connectors into the detector. For this second method, the other end of the interconnection cable was covered with a protective cap to darken the fiber.

TEST PARAMETERS

The following table (Table II) summarizes all of the test parameters for this project.

TABLE II. TEST PARAMETERS

Test Parameter #	Source	Exception to FOTP-42
1	1300 nm LED (#3)	none
2	1300 nm LASER (#1)	CW coherent source
3	1300 nm LASER (#2)	modulated coherent source
4	1550 nm LED (#4)	none
5	850 nm LED (#5)	none
6	1300 nm LED (#3)	fiber microbending
7	1300 nm LASER (#1)	CW coherent source
		fiber microbending
8	1300 nm LED (#3)	cable microbending
9	1300 nm LASER (#1)	CW coherent source
		cable microbending
10	1300 nm LED (#3)	restricted launch
		(mode strip)

Both LASER and LED optical sources were chosen for the measurements, instead of only the noncoherent LED source called for in FOTP-42, since both types of sources are used in fiber optic transmissions systems. For the same reason a modulated LASER source (at 300 MHz) was selected as a test parameter. It was also decided to study the effect of microbending on crosstalk, since in a real fiber optic installation, microbending of a cable or fibers may occur.

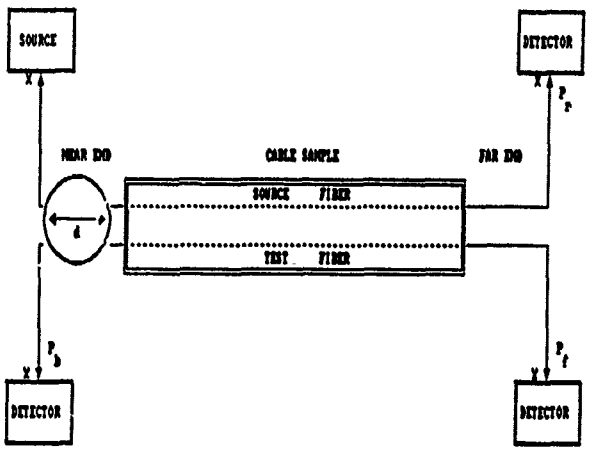

Figure 2. Test Procedure

The effect of microbending on crosstalk had been studied by Nishimura and others in the mid 1980's.[6] Their experiments showed that crosstalk does not increase before microbending loss increases rapidly. They also measured crosstalk on different lengths of fiber optic cables, and concluded that length dependence on crosstalk is very small.

Figure 2 is a block diagram representation of the crosstalk measurement procedure, showing how microbending was achieved. The cable samples were coiled to the minimum recommended bending radius for each sample, and the fibers in a cable sample were wrapped around mandrels of varying diameters at the near end of the cable. The source power and crosstalk powers were monitored during the microbending experiment. In this diagram, the symbol *d* represents the diameter of the cable coils and the mandrels.

CABLES TESTED

The following table (Table III) lists the cable designs for which optical crosstalk was measured. Included is the table number in this paper where the test data may be found.

TABLE III. CABLES

Cable Design	Cable Type	Fiber Type	Table #
outside plant	AccuRibbon®	single mode	IV
outside plant	ribbon	multimode	V
outside plant	Lightpack®	single mode	VI
inside plant	building cable	single mode	VII
inside plant	building cable	multimode	VIII
specialty	tactical	multimode	IX
specialty	shipboard	multimode	X
specialty	FDDI	multimode	XI
interconnect	duplex	multimode	XII

The ribbon designs consist of twelve parallel fibers, on approximately .01 inch centers, which for the AccuRibbon cable are held in place by a UV-curable matrix material, and for the multimode cable are sandwiched between clear pressure sensitive adhesive tapes. For the Lightpack design, up to twelve fibers are in a loose bundle, held together with spirally wrapped color-coded yarn binders.

The fibers in the building cable designs and the interconnect cable are buffered with color-coded PVC. For the tactical cable, the shipboard cable, and the FDDI cable, the fibers are buffered with a Hytrel® material. In addition, strands of Kevlar® surround the buffer materials for these cable designs.

RESULTS

The crosstalk measurements data, for the cable samples shown in Table III, is documented in the following tables. All of the source power values (P_r) are typical values for each cable sample. All of the crosstalk values, either in dBm or in dB, are worst case values for each cable sample.

For the inside plant, specialty, and interconnect cable samples, all of the combinations of fiber to fiber crosstalk were measured. For the Lightpack cable sample, 18 of the 84 fibers were selected for measuring, 12 from one bundle and 6 from an adjacent bundle, and all combinations of the 18 fibers were tested. For the ribbon cables, fiber to fiber crosstalk was measured within a ribbon, for adjacent fibers up to 2 fibers away from the source fiber. Ribbon to ribbon crosstalk was also measured, for 2 adjacent ribbons.

TABLE IV. DATA FOR ACCURIBBON CABLE

cable sample	144 fiber AccuRibbon cable (4GSX-144 BXD)
fiber type	8.3/125 μm single mode, depressed cladding
sample length	20.0 meters
connectors	biconic

crosstalk test: fiber to fiber, within same ribbon (12 fibers)

test parameters	P_r	P_f	P_b	CT_f	CT_b
	(dBm)	(dBm)	(dBm)	(dB)	(dB)
1300 nm LED	-35.5	< -100	< -100	> 64.5	> 64.5
1300 nm LASER (CW)	-3.1	< -100	< -100	> 96.9	> 96.9
1300 nm LASER (mod)	-18.2	< -100	< -100	> 81.8	> 81.8
1550 nm LED	-35.4	< -100	< -100	> 64.6	> 64.6
fiber microbending -					
.2" dia. mandrel					
1300 nm LED	-35.4	< -100	< -100	> 64.6	> 64.6
1300 nm LASER (CW)	-3.2	-82.7	-84.5	79.5	81.3
cable microbending -					
7" rad. loop					
1300 nm LED	-35.7	< -100	< -100	> 64.3	> 64.3
1300 nm LASER (CW)	-3.1	< -100	< -100	> 96.9	> 96.9

crosstalk test: ribbon to ribbon (24 fibers)

test parameters	P_r	P_f	P_b	CT_f	CT_b
	(dBm)	(dBm)	(dBm)	(dB)	(dB)
1300 nm LED	-35.3	< -100	< -100	> 64.7	> 64.7
1300 nm LASER (CW)	-3.2	< -100	< -100	> 96.8	> 96.8
1300 nm LASER (mod)	-18.2	< -100	< -100	> 81.8	> 81.8
fiber microbending -					
.2" dia. mandrel					
1300 nm LED	-35.3	< -100	< -100	> 64.7	> 64.7
1300 nm LASER (CW)	-3.2	< -100	< -100	> 96.8	> 96.8
cable microbending -					
7" rad. loop					
1300 nm LED	-35.4	< -100	< -100	> 64.6	> 64.6
1300 nm LASER (CW)	-3.1	< -100	< -100	> 96.9	> 96.9

TABLE V. DATA FOR RIBBON CABLE

cable sample	108 fiber ribbon cable (3BFX-108)
fiber type	62.5/125 μm multimode, graded index
sample length	21.7 meters
connectors	biconic

crosstalk test: fiber to fiber, within same ribbon (12 fibers)

test parameters	P_r	P_f	P_b	CT_f	CT_b
	(dBm)	(dBm)	(dBm)	(dB)	(dB)
1300 nm LED	-15.3	< -100	< -100	> 84.7	> 84.7
1300 nm LASER (CW)	-3.1	< -100	< -100	> 96.9	> 96.9
1300 nm LASER (mod)	-3.1	< -100	< -100	> 96.9	> 96.9
850 nm LED	-8.9	< -100	< -100	> 91.1	> 91.1
fiber microbending -					
.9" dia. mandrel					
1300 nm LED	-15.5	-89.7	-91.1	74.2	75.6
1300 nm LASER (CW)	-3.2	-85.1	-87.3	81.9	84.2
cable microbending -					
5" rad. loop					
1300 nm LED	-15.5	< -100	< -100	> 84.5	> 84.5
1300 nm LASER (CW)	-3.2	< -100	< -100	> 96.8	> 96.8

crosstalk test: ribbon to ribbon (24 fibers)

test parameters	P_r	P_f	P_b	CT_f	CT_b
	(dBm)	(dBm)	(dBm)	(dB)	(dB)
1300 nm LED	-15.3	< -100	< -100	> 84.7	> 84.7
1300 nm LASER (CW)	-3.1	< -100	< -100	> 96.9	> 96.9
1300 nm LASER (mod)	-3.1	< -100	< -100	> 96.9	> 96.9
fiber microbending -					
.25" dia. mandrel					
1300 nm LED	-16.1	< -100	< -100	> 83.9	> 83.9
1300 nm LASER (CW)	-3.4	< -100	< -100	> 96.6	> 96.6
cable microbending -					
5" rad. loop					
1300 nm LED	-16.1	< -100	< -100	> 83.9	> 83.9
1300 nm LASER (CW)	-3.4	< -100	< -100	> 96.6	> 96.6

TABLE VI. DATA FOR LIGHTPACK CABLE

cable sample	84 fiber Lightpack cable (4DHX-084)
fiber type	8.3/125 μm single mode, depressed cladding
sample length	21.4 meters
connectors	biconic

crosstalk test: fiber to fiber (18 fibers)

test parameters	P_r	P_f	P_b	CT_f	CT_b
	(dBm)	(dBm)	(dBm)	(dB)	(dB)
1300 nm LED	-34.8	< -100	< -100	> 65.2	> 65.2
1300 nm LASER (CW)	-18.2	< -100	< -100	> 81.8	> 81.8
1300 nm LASER (mod)	-18.2	< -100	< -100	> 81.8	> 81.8
fiber microbending -					
.25" dia. mandrel					
1300 nm LED	-35.0	< -100	< -100	> 65.0	> 65.0
1300 nm LASER (CW)	-18.3	< -100	< -100	> 81.7	> 81.7
cable microbending -					
5" rad. loop					
1300 nm LED	-35.0	< -100	< -100	> 65.0	> 65.0
1300 nm LASER (CW)	-18.3	< -100	< -100	> 81.7	> 81.7

TABLE VII. DATA FOR LIGHTGUIDE BUILDING CABLE

cable sample	4 fiber Lightguide building cable (LGBC-004A-SRX)
fiber type	8.3/125 μm single mode, depressed cladding, buffered
sample length	19.7 meters
connectors	biconic

crosstalk test: fiber to fiber (4 fibers)

test parameters	P_r	P_f	P_b	CT_f	CT_b
	(dBm)	(dBm)	(dBm)	(dB)	(dB)
1300 nm LED	-38.0	< -100	< -100	> 62.0	> 62.0
1300 nm LASER (CW)	-0.7	< -100	< -100	> 92.3	> 92.3
1550 nm LED	-35.3	< -100	< -100	> 64.7	> 64.7
fiber microbending -					
.1" dia. mandrel					
1300 nm LED	-38.0	< -100	< -100	> 62.0	> 62.0
1300 nm LASER (CW)	-0.7	< -100	< -100	> 92.3	> 92.3
cable microbending -					
1.5" rad. loop					
1300 nm LED	-38.0	< -100	< -100	> 62.0	> 62.0
1300 nm LASER (CW)	-0.7	< -100	< -100	> 92.3	> 92.3

TABLE VIII. DATA FOR LIGHTGUIDE BUILDING CABLE

cable sample	12 fiber Lightguide building cable (LGBC-012A-LRX)
fiber type	62.5/125 μm multimode, graded index, buffered
sample length	20.2 meters
connectors	biconic

crosstalk test: fiber to fiber (12 fibers)

test parameters	P_r	P_f	P_b	CT_f	CT_b
	(dBm)	(dBm)	(dBm)	(dB)	(dB)
1300 nm LED	-15.9	< -100	< -100	> 84.1	> 84.1
1300 nm LASER (CW)	-0.9	< -100	< -100	> 93.1	> 93.1
fiber microbending -					
.15" dia. mandrel					
1300 nm LED	-15.9	-98.5	-97.9	82.6	82.0
1300 nm LASER (CW)	-0.9	-96.7	-96.1	89.8	89.2
cable microbending -					
1.5" rad. loop					
1300 nm LED	-15.9	< -100	< -100	> 84.1	> 84.1
1300 nm LASER (CW)	-0.9	< -100	< -100	> 93.1	> 93.1

TABLE IX. DATA FOR TACTICAL CABLE

cable sample	2 fiber tactical cable (LTC-2MH-X)
fiber type	50/125 μm multimode, graded index, buffered
	radiation hardened
sample length	19.3 meters
connectors	biconic

crosstalk test: fiber to fiber (2 fibers)

test parameters	P_r	P_f	P_b	CT_f	CT_b
	(dBm)	(dBm)	(dBm)	(dB)	(dB)
1300 nm LED	-18.5	< -100	< -100	> 81.5	> 81.5
1300 nm LASER (CW)	-2.0	< -100	< -100	> 98.0	> 98.0
cable microbending -					
2.5" rad. loop					
1300 nm LED	-18.5	< -100	< -100	> 81.5	> 81.5
1300 nm LASER (CW)	-2.1	< -100	< -100	> 97.9	> 97.9

TABLE X. DATA FOR SHIPBOARD CABLE

cable sample	4 fiber shipboard cable (LSC-004LHT-A-X)
fiber type	62.5/125 μm multimode, graded index, buffered
	radiation hardened
sample length	21.8 meters
connectors	ST

crosstalk test: fiber to fiber (4 fibers)

test parameters	P_r	P_f	P_b	CT_f	CT_b
	(dBm)	(dBm)	(dBm)	(dB)	(dB)
1300 nm LED	-15.6	< -100	< -100	> 84.4	> 84.4
1300 nm LASER (CW)	-1.7	< -100	< -100	> 98.3	> 98.3
1550 nm LED	-14.7	< -100	< -100	> 85.3	> 85.3
fiber microbending -					
.5" dia. mandrel					
1300 nm LED	-15.6	< -100	< -100	> 84.4	> 84.4
1300 nm LASER (CW)	-1.7	< -100	< -100	> 98.3	> 98.3
cable microbending -					
3" rad. loop					
1300 nm LED	-15.6	< -100	< -100	> 84.4	> 84.4
1300 nm LASER (CW)	-1.7	< -100	< -100	> 98.3	> 98.3
restricted launch					
.7" dia. mode strip					
1300 nm LED	-23.2	< -100	< -100	> 76.8	> 76.8

CROSSTALK IN FANOUTS

For the multimode (62.5/125 μm) ribbon cable sample (see Table V), there was no measurable crosstalk present for the ribbons terminated with biconic connectors. However, since ribbon cables may be terminated with array splices (positive silicon chips), it was decided to measure fiber to fiber crosstalk for this ribbon configuration.

A ribbon in the cable sample was selected and connectorized on both ends with the array splice. Two multimode fanouts and two 1009C connectors (negative silicon chips) were utilized to connect this ribbon to the test equipment. When the measurements were made, measurable crosstalk *was* present. The power level of this crosstalk was low, -82 dBm worst case, and the crosstalk was present for both LASER and LED sources.

Since measurable crosstalk was not present for the ribbon terminated with biconics, it was assumed that the crosstalk present in the ribbon with arrays was due to either the array splice or the multimode fanout. To test the effect of the array splice on crosstalk, two 62.5/125 μm, ribbon samples were terminated on one end with an array splice, and terminated on the other end with biconics. The ends with the arrays were joined with 1009C connectors, while the ends with the biconics were connected to the test equipment. For this configuration there was *no* measurable crosstalk, although it was seen that measurable crosstalk (worst case power level -92 dBm) was present if the arrays were not assembled properly with the 1009C, either misaligned, or with insufficient index matching material. This experiment was repeated a second time with 2 different ribbon samples, with the same results.

TABLE XI. DATA FOR FDDI CABLE

cable sample	2 fiber FDDI cable (CA8023)
fiber type	62.5/125 μm multimode, graded index, buffered
sample length	10.1 meters
connectors	ST

crosstalk test: fiber to fiber (12 fibers)

test parameters	P_r	P_f	P_b	CT_f	CT_b
	(dBm)	(dBm)	(dBm)	(dB)	(dB)
1300 nm LED	-19.8	< -100	< -100	> 80.2	> 80.2
1300 nm LASER (CW)	-0.5	< -100	< -100	> 93.5	> 93.5
fiber microbending -					
.1" dia. mandrel					
1300 nm LED	-19.8	< -100	< -100	> 80.2	> 80.2
1300 nm LASER (CW)	-0.5	-98.4	< -100	92.9	> 93.5
cable microbending -					
2" rad. loop					
1300 nm LED	-19.8	< -100	< -100	> 80.2	> 80.2
1300 nm LASER (CW)	-0.5	< -100	< -100	> 93.5	> 93.5

TABLE XII. DATA FOR INTERCONNECTION CABLE

cable sample	2 fiber interconnection cable (1861A)
fiber type	62.5/125 μm multimode, graded index, buffered
sample length	21.3 meters
connectors	biconic

crosstalk test: fiber to fiber (2 fibers)

test parameters	P_r	P_f	P_b	CT_f	CT_b
	(dBm)	(dBm)	(dBm)	(dB)	(dB)
1300 nm LED	-19.0	< -100	< -100	> 81.0	> 81.0
1300 nm LASER (CW)	-7.3	< -100	< -100	> 92.7	> 92.7
850 nm LED	-8.9	< -100	< -100	> 91.1	> 91.1
fiber microbending -					
.25" dia. mandrel					
1300 nm LED	-19.0	< -100	< -100	> 81.0	> 81.0
1300 nm LASER (CW)	-7.3	< -100	< -100	> 92.7	> 92.7
cable microbending -					
.5" rad. loop					
1300 nm LED	-19.0	< -100	< -100	> 81.0	> 81.0
1300 nm LASER (CW)	-7.3	< -100	< -100	> 92.7	> 92.7

The effect of the fanout on crosstalk was tested by joining the array ends of two fanouts (62.5/125 μm) with the 1009C connector, and connecting the other ends of the fanouts to the test equipment. This product configuration *yielded* measurable crosstalk, with worst case power levels of -93 dBm with a LASER source, and -76 dBm with a LED source. Further analysis, using a visible He-Ne LASER, showed that the crosstalk probably was occurring at the transition point of the fanout, which is the point where the 12 fibers in the ribbon configuration are separated into individual fibers. At this point the fibers, unbuffered, are in close physical proximity, and are held in place by an epoxy. Apparently the stress on the fibers by the epoxy causes microbending which allows light from one fiber to channel to another fiber.

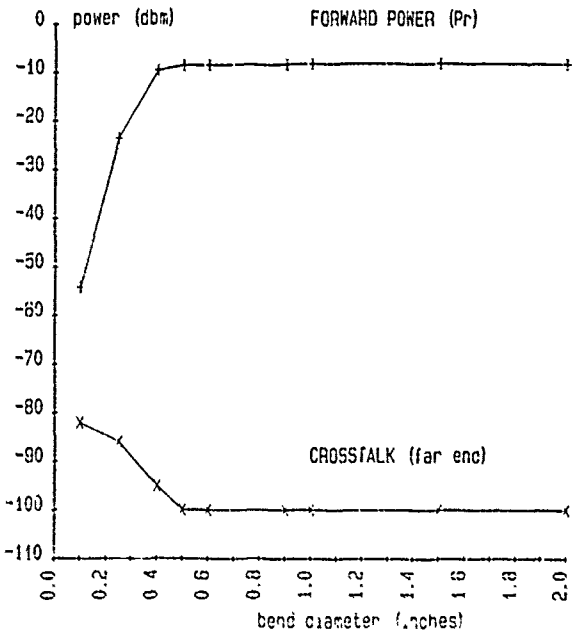

Figure 3. Single Mode Ribbon, LASER Source

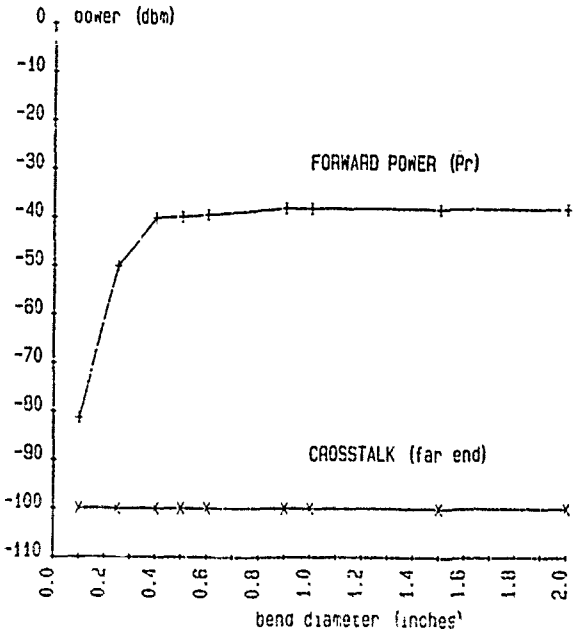

Figure 4. Single Mode Ribbon, LED Source

This test was repeated for the 50/125 μm, multimode fanout, and for the 8.3/125 μm, single mode fanout. The multimode version *had* measurable crosstalk, with worst case power levels of -97 dBm (LASER), and -85 dBm (LED). Measurable crosstalk *was not* present in the single mode fanout. This finding agrees with the work of Marcuse, Gloge, and Marcatili, who stated that crosstalk can be reduced by surrounding the fiber core with thicker claddings.[7] The core of a single mode fiber is surrounded by significantly more cladding glass than the multimode fiber.

The presence of crosstalk in ribbons terminated with array splices was also reported by Buckler and Miller,[8] and by Gossage[9]. These measurements were made for multimode (50/125 μm) ribbons only. Although it has been shown that misalignment of the array splices can be a cause of crosstalk, the more likely reason is microbending in the construction of the multimode fanout products.

DETECTABILITY OF CROSSTALK

As shown in Tables IV through XII of this paper, measurable crosstalk was detected for single mode and multimode cable samples when the fibers in the cables were bent around mandrels, whose diameter exceeded recommended bend diameters. This fiber bending induced microbending loss, which was channeled into adjacent fibers, both buffered and not buffered. Measurable crosstalk was also detected in multimode fanout products, also as a result of microbending loss.

Even though the crosstalk did exist under the conditions described above, it does not necessarily mean that the security of the fiber optic transmission would be degraded. The power levels of the crosstalk were at very low levels, -82 dBm for microbending of multimode fiber, and -76 dBm for multimode fanouts. To determine if crosstalk at these levels would compromise security, two areas were investigated: 1) the relationship between crosstalk (due to microbending) and forward loss; and 2) the detectability of crosstalk by optical receivers and photon counters.

An experiment was performed for single mode (8.3/125 μm) and multimode (62.5/125 μm) ribbon cable samples. The near end of a ribbon for each cable sample was tightly wrapped for one turn around 9 different sized mandrels, ranging in diameter from .1" to 2 inches. For each mandrel, the source power in dBm, measured at the far end of the cable sample, and the far end crosstalk power, also in dBm, were recorded. This was done for both LASER and LED sources. The data for this experiment is plotted in Figures 3 through 6.

In all cases, with the exception of the multimode ribbon sample with the LASER source, the forward loss of the source power increased before the far end crosstalk was detected. For the multimode ribbon sample, the source power was not attenuated by the fiber bending, while far end crosstalk was detected at a bend diameter of .9". The worst case crosstalk for this sample of -73.5 dBm occurred at the .1" diameter bend. Except for this one case, these results agree with the findings of Nishimura.[10] Crosstalk due to microbending of the fiber or the cable should be detectable by monitoring the forward loss of the source power.

To determine at what power level optical crosstalk can be detected and interpreted as information, thereby compromising security, the following analysis was made.

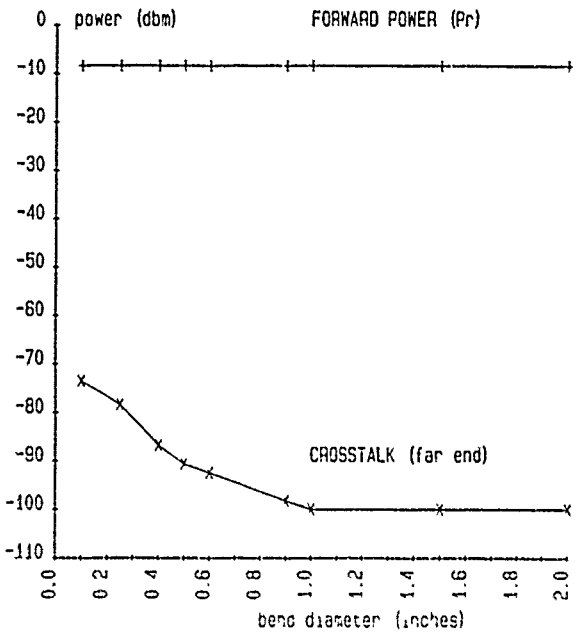

Figure 5. Multimode Ribbon, LASER Source

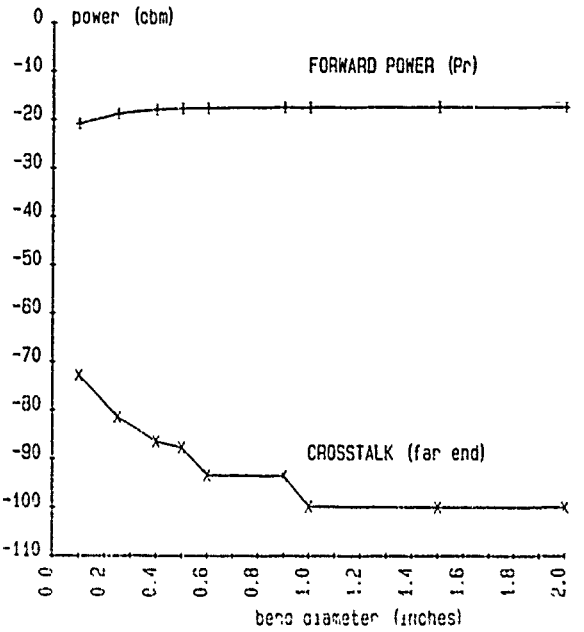

Figure 6. Multimode Ribbon, LED Source

For an optical receiver to convert light energy to electrical energy at some bit error rate, each optical bit must consist of a minimum number of photons. Table XIII lists the photon requirements for some detection techniques for a bit error rate of 10^{-9}.[11]

TABLE XIII. PHOTON REQUIREMENTS

Detection Method	Photons/Bit	Notes
direct detection		
(APD receiver)		
	10	quantum limit
	400	state of the art
	2000	typical receiver
coherent detection		
(homodyne receiver)		
phase-shift-keyed (PSK)	9	quantum limit
coherent detection		
(heterodyne receiver)		
phase-shift-keyed (PSK)	18	quantum limit
amplitude-shift-keyed (ASK)	36	quantum limit
frequency-shift-keyed (FSK)	36	quantum limit

To find the relationship between optical power and photons, the following calculations are made.[12] First, find the amount of energy (in Joules) per photon.

$E = hc/\lambda n$ where E = photon energy (Joules)
h = Planck's constant (6.63×10^{-34} Joule-sec)
c = speed of light (vacuum) (2.998×10^{8} meters/sec)
λ = wavelength (1.3 μm)
n = index of refraction (1.0003 for air)

Therefore, $E = 1.52847 \times 10^{-19}$ Joules/photon.

Next, calculate the number of photons detected per second for a given power level.

$M = P/E$ where M = number of photons per second of detection
P = power level (watts)

Using this equation, the number of photons detected per second was calculated for a constant source for different power levels The results are shown in Table XIV.

TABLE XIV. POWER LEVELS AND PHOTON COUNT

power (pw)	power (dBm)	photons/sec
100	-70	654,249,000
10	-80	65,424,900
1	-90	6,542,490
.1	-100	654,249
.01	-110	65,425

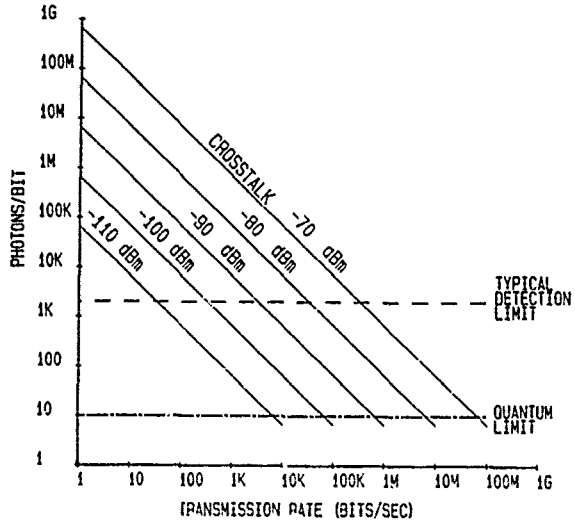

Figure 7. Detectability of Crosstalk

Finally, to find the number of photons per bit, divide the number of photons per second by the transmission rate.

$R = M/B$ where R = number of photons per bit
B = transmission rate (bits/sec)

Figure 7 is a plot showing the relationship between crosstalk power, transmission rates, number of photons, and receiver sensitivities. Also plotted are the fundamental quantum limit for APD receivers (10 photons/bit), and the typical limit for receivers (2000 photons/bit), which takes into account environmental variables.

As can be seen in the above figure, the ability of optical crosstalk to be detected and interpreted as information, is dependent on the speed of the transmission. The crosstalk levels measured for the cable samples documented in this paper, should only present security problems for very slow transmission rates.

Using the equations and the variables defined above, the minimum power levels for crosstalk to be intelligible at different transmission rates, can be calculated using the following relationships.

$$P \text{ (in watts)} = RBE$$

$$P \text{ (in dBm)} = 10 \log (RBE/.001)$$

These calculations, shown in Table XV, have been made for several transmission rates, and for both the fundamental quantum limit and the typical limit for detection. For reference, the slowest transmission rate is DS1, which is 1.5 Mb/s. Two other "slow" rates are DS3, 45 Mb/s, and the rate for FDDI, 100 Mb/s.

TABLE XV. POWER LEVELS AND TRANSMISSION RATES

detection limit (photons/bit)	transmission rate (Mb/s)	min power (watts)	min power (dBm)
10	1.5	2.4 pw	-86.27
	45	68.4 pw	-71.65
	90	137.1 pw	-68.62
	417	637.2 pw	-61.96
	1700	2.6 nw	-55.85
2000	1.5	471.9 pw	-63.26
	45	1.4 nw	-48.62
	90	27.5 nw	-45.60
	417	127.5 nw	-38.95
	1700	519.7 nw	-32.85

The above calculations show that an optical crosstalk power level of less than -100 dBm does not meet the fundamental quantum limit for detection, and also would not be detectable by state of the art detection equipment (APD receivers, photon counters, lock-in amplifiers, etc.), even at the slowest DS1 transmission rate. For all of the cable samples documented in this paper, all crosstalk power measurements were less than -100 dBm, except for microbending conditions. Even for these conditions, where measurable (greater than -100 dBm) crosstalk was encountered, the crosstalk level would not be detectable as information by today's typical receivers.

CONCLUSION

Optical crosstalk has been measured for 9 single mode and multimode fiber optic cable designs. The measurement procedure followed was EIA standard FOTP-42. Variations of the procedure were made, however, in order to more thoroughly qualify the cable designs for transmission security. Optical sources used included LED's (850 nm, 1300 nm, 1550 nm) and LASER's (1300 nm, CW and modulated). Detection equipment was sensitive to -100 dBm. Fiber to fiber measurements were made for all cable samples, and for ribbon cable designs, ribbon to ribbon measurements were made.

The following is a summary of the findings for this project.

- For all of the cable designs, there was no measurable crosstalk recorded at the -100 dBm power level, for both LED and LASER sources, for physical configurations which avoided microbending.

- For physical configurations where the cable samples were coiled to the recommended minimum bending radius, there was no measurable crosstalk.

- Measurable crosstalk was recorded when the fibers in some of the cable samples were wound for one turn around mandrels less than 1 inch in diameter, even for buffered fibers. However, for ribbon cable designs, there was no ribbon to ribbon crosstalk recorded.

- Crosstalk is present in multimode fanout products. There was no measurable crosstalk recorded for the single mode fanout.

• Array splices may contribute crosstalk if assembled improperly.

• Further experimentation showed the relationship of forward loss due to microbending, and crosstalk. The loss of forward power should be detected before significant crosstalk is present.

• An analysis of crosstalk and receiver sensitivity was made, which showed that a crosstalk power level of -100 dBm does not meet the fundamental quantum limit for detection, and is not sufficient to be sensed as information by state of the art detection equipment. For power levels greater than -100 dBm, which were detected for fiber microbending, the crosstalk level would not be detectable as information by today's typical receivers, and only would be detectable by state of the art equipment at the slowest transmission rates.

The crosstalk measurement program, which has been documented in this paper, has shown that secure and nonsecure data may be transmitted safely over different fibers within the same fiber optic cable. The cables listed in this paper will provide a secure means for fiber optic transmission.

Future work for the crosstalk measurement program will include the testing of various fiber optic splices and connectors.

ACKNOWLEDGEMENTS

The authors gratefully acknowledge the support of Larry Sherrets, who suggested the project and obtained the cable samples; Dwight Blanton, who connectorized the cable samples; and Chris Scholly, who reviewed the paper and offered support.

REFERENCES

1. Michael J. Buckler and Calvin M. Miller, "Optical Crosstalk Evaluation for Two End-to-End Lightguide System Installations," Bell System Technical Journal, Vol. 57, No. 6, July-August 1978, pp. 1759-1769.
2. Steven A. Gossage, "Partioning Optical Fiber Cable to Support Red and Black Communications," Sandia Report SAND88-3047, February 1989.
3. A. H. Cherin and E. J. Murphy, "Quasi-Ray Analysis of Crosstalk Between Multimode Optical Fibers," Bell System Technical Journal, Vol. 54, No. 1, January 1975, pp. 17-45.
4. Allan W. Snyder and Peter McIntyre, "Crosstalk Between Light Pipes," Journal of the Optical Society of America, Vol. 66, No. 9, September 1976, pp. 877-882.
5. FOTP-42, "Optical Crosstalk in Fiber Optic Components," EIA/TIA Standard, November, 1989.
6. A. Nishimura, et al., "Characterization of Crosstalk of Two-Core Single-Mode Bunch Fiber," European Conference on Optical Communication Proceedings, 1986, pp. 195-198.
7. Stewart E. Miller and Alan G. Chynoweth, (eds), Optical Fiber Telecommunications, Academic Press, Inc., New York, 1979, p. 67.
8. Buckler and Miller, op. cit., p. 1768.
9. Gossage, op. cit., p. 44.
10. Nishimura, op. cit., p. 196.
11. Tingye Li, "Advances in Lightwave Systems Research", AT&T Technical Journal, Vol. 66, Iss. 1, January- February 1987, pp. 5-18.
12. "Conversion of Optical Power to a Quantity of Photons per Second", Anritsu Application Engineering Note, MISC OPT-14, May, 1990.

Jeffery A. Fandl is a Senior Development Engineer with AT&T Network Systems in Norcross, Georgia, where he is responsible for testing of Lightguide Apparatus products. Mr. Fandl joined AT&T in 1979, after receiving his BS in Electrical Engineering from Georgia Institute of Technology. In 1984 he received his MS in Electrical Engineering, also from Georgia Tech. He is a member of the Optical Society of America.

Michael J. Ring is a Senior Development Engineer with AT&T Network Systems in Norcross, Georgia. He received his BS in Electrical Engineering from Rose-Hulman Institute of Technology in 1970, and his MS in Industrial Operations from Purdue University in 1974. He has been with AT&T since 1970, and is currently responsible for testing of Lightguide Apparatus products.

LIGHTNING PROTECTION OF BURIED OPTICAL CABLES

B.J. SYMMONS - STC*
G.W. REID - LTT**

*STC CABLE, NEWPORT, GWENT,UK.
**CULHAM LABORATORY, ABINGDON,UK.

ABSTRACT

Details are given of simulated lightning strikes to a range of STC designed optical fibre cables using a CCITT proposed recommendation for a Sand-Box test in which peak current levels from 50KA to 200KA were used. The paper discusses the nature of the test parameters used particularly with respect to the length and direction of the arc. Also, comparison is made with standard aircraft testing techniques for lightning damage susceptibility especially in relation to the test waveforms used. Considerable research has been done on this aspect for aircraft safety. The forces produced by buried arcs in the deformation of brass tubes was investigated as a reference method and is discussed in some detail.

CABLE TESTS

The susceptibility to damage of various cable constructions from lightning strikes has been extensively reported at this Symposium in previous years.

Notwithstanding this, we report briefly herein on tests conducted on a range of optical fibre cables, including all dielectric versions, manufactured by STC. The Culham Lightning Test and Technology Laboratory (LTT) provided the test facilities.

The simulated strikes at nominally 50KA, 120KA and 200KA impulse current levels to each cable, produced the same general damage features as reported by others, however in many instances, gross impairment of sheath integrity was evident without giving rise to loss of optical transmission.

Details of the cables tested are given in table 1. In these tests the metallic sheaths and copper conductors, where appropriate, were shorted together at each end of the cable and connected to the earth return of the pulse generator. The test parameters used are given in table 2 and the resulting damage to the cables is described briefly in table 3.

TEST REGIME AND FACILITY

The tests were performed generally to the Specification proposed by the CCITT for Recommendation K25.
A non-conducting rigid box of approximately 0.6 meters cube was used to contain the wet sand with the cables under test buried centrally in the box. The ends of the cable protruded through the sides of the container where they were connected to the capacitor bank return conductors as shown in figure 1. This assembly produces a symmetrical arrangement of return conductors around the electrode, simulating more closely the magnetic forces produced by free space conditions. The electrode shown in figure 2 was spaced from 25 - 50mm from the cable under test and a small hole was made in the outer insulation of the cables to ensure breakdown occurred at the centre of the cable opposite the arc electrode.

In the case of the cables having no metallic components the arc was made to a 25mm diameter aluminium rod placed behind the cable as shown in figure 3.

A circuit of the test facility is shown in figure 4. This was designed to generate lightning test waveforms for the aircraft industry as described in reference 1. It is capable of providing ringing or uni-directional clamped waveforms up to 200-300KA peak current. The capacitor banks and switches can be seen in the background of figure 1.

For these tests ringing waveforms were used for the low level shots and a mixture of ringing and clamped waveform for the high level shots.

The circuit parameters were adjusted to the requirements of the waveform described in the proposed CCITT recommendation.

DIAGNOSTICS

The current pulse was measured using a calibrated Rogowski coil whose output was electronically integrated to give the pulse current waveform. The signals were recorded using a digitizing recorder capable of sampling at ten million sample per second. This allows very rapid measurement of the waveforms produced and also the calculation of frequencies of the ringing waveforms. It will be noted the action integral ($\int i^2 dt$) is also obtained and this is discussed later in the paper. Typical test waveforms are shown in figures 5.

COMMENTS ON TEST METHODS USED

Test Waveforms

The type of test waveform internationally agreed for damage testing to aircraft is shown in figure 6 (reference 1) and the important test parameters used are peak current, action integral and charge transfer. For metal burn-through it has been shown that the low level long duration component "C" of this waveform causes the most damage (reference 2). This component is not considered in the CCITT proposals which only specifies time to peak and half value and the frequency of the damped oscillating waveform.

Action Integral

Aircraft testing has shown that the actual waveform shape to induce mechanical deformation is not too critical, the important factor being the action integral representing the energy transfer into a fixed resistance. This would probably be a more useful parameter to specify for cable tests. We have therefore included these values in the table of results.

Relating this information to the proposed CCITT recommendation a number of observations can be made. The original basis for the specification recommendation is not given but it is assumed it was derived as a fairly simple and convenient test which could reproduce the sort of conditions a lightning strike to a buried cable would encounter and which could be readily reproduced. As in all lightning simulation testing it is not economical or practical to produce the very large (MV) pulses with the associated high levels of energy contained in real lightning strikes.

There are unfortunately a considerable number of factors other than the action integral which could affect the degree of damage to the cables, a number of which have been considered by Fischer, Bow, Busch and Schrom in reference 3.

These include:

1. Size of the test box.
2. Effect of Water.
3. Type of Sand.
4. Use of Soil.
5. Shot to shot variations with nominally the same test parameters.
6. Earthing arrangements.

We have not investigated any of these effects further but find the conclusion which Fischer et al reached very reasonable, that is, the effect of the medium on the forces produced by the arc is likely to be considerable. In our experience these forces are primarily radial (as discussed later) and effectively confining them is likely to produce more axial force. Earthing outside the box is obviously desirable to facilitate the reproduction of consistent current waveforms. We would, however, have some reservations as described later, on the size of test box used. It was surprising to observe the large movement of the medium over some considerable distance from the arc; this was especially true at higher levels of current.

It is considered that the presence of water is not essential for producing the forces and damage (these occur for arcs in air), but it no doubt increases the effect of the breakdown process and produces a more compact medium to generate greater forces.

FORCES PRODUCED BY LIGHTNING TYPE ARCS

The information on this topic is rather limited because of the difficulties of measurement. It is often thought this is primarily due to the rapid heating of the medium. More recent investigation by P. Graneau (reference 4), suggests this is not the case and considers the shock-wave could be driven by ponderomotive forces of the Ampere-Neumann electrodynamics.

Work carried out at LTT has mainly dealt with forces in air by investigating the breaking forces on SRBP tubes enclosing arcs. These tests established the main forces to be radial shock waves and the

failure of the tubes was not greatly affected whether the ends were open or closed.

Tests have therefore been made in sand to investigate how the forces would vary with different directions of arcs through the sand, i.e. vertically and horizontally, and with varying lengths of arc between the electrode and the object of attachment, in this case the buried cable. Arc current levels were also varied to establish if the forces appeared to be predominantly dependent on the action integral.

In order to establish a reference with a minimum number of variables it was more convenient to represent the cable with a metal tube. The degree of indentation would then represent the degree of the force applied and consistent results achieved.

After preliminary tests to a number of different tubes of varying thickness and material it was found that a brass tube 19mm outside dia. and 1.6mm thick to be the most suitable. The specification for this tube was 70/30 Arsenical Brass, as drawn with a specification BS2817 Pt2/CZ 126-M. The tube was insulated with a 3mm thick rubber jacket.

Preliminary tests also showed how the effect of insulation and size of hole resulting from the arc attachment could affect the results.

BREAKDOWN OF SAND

The sand could be broken down without too much difficulty over considerable arc lengths.

The test facility as shown in figure 4 can readily supply pulses of voltage up to 120KV, and depending on the impedance of the test specimen, 100-200KA peak currents. For this test a 25KA peak current pulse was obtained with a charge voltage of 65KV and length of arc through the sand of 260mm which was nearing the limit of the present size of test box. The channel is obviously fairly resistive compared with the normal arc tests performed in air.

TEST PARAMETERS

The present series of tests to the brass tube, operated between 20 and 100 KA which involved charging voltages between 20 and 120KV. Discharge lengths between the electrode and tube were varied from 50 - 200mm and discharges were made both vertically through the sand and horizontally in the sand.

A summary of the results obtained from these tests are given in tables 4 and 5 and the results are plotted in figures 7 and 8.

DISCUSSION OF TESTS

At this stage the results have to be of a qualitative nature but it may be possible to interpret the tube indentation in a more quantitative manner at a later date. Difficulties do however exist because of the very fast impulsive nature of the forces. In these cases the damage effects can be dependent on the intensity and time profile of the forces and the nature of the object upon which they operate.

The mechanics of replacing the sand and re-aligning the tube after each shot limits the number of results that can readily be obtained. For the tests carried out we have used the extent of tube indentation (figure 9) as a measure of the forces upon it and have assumed the force from the arc will be dependent on the action integral of the current waveform. For this type of test there could be quite a spread of results for one operating condition and to investigate this would require an extensive series of shots.

The series of three shots at different action integrals for the 100mm horizontal arc length, (figure 7), support the implication that the forces are linearly dependent on the action integral.

The results of the vertical arc through the sand shown in figure 8 shows a reduction in tube indentation by a factor of 2.7 going from a 50mm to 100mm arc length. Increasing the length from 100 to 200mm only produced a change of about 5%. Comparing the indentation with a 100mm horizontal arc length to vertical arc (figure 8), shows that on average the forces are 80% greater for the totally enclosed horizontal arc.

The horizontal arc tests do not give such a clear pattern as those for the vertical arc. The set of three results obtained at the 100mm arc length gives a reasonably linear fit between the action integral of the pulse and the tube indentation. The results indicate arcs

longer than 100mm do not greatly affect the results.

NATURE AND EFFECTS OF ARCS THROUGH THE SAND

A number of photographs of the sand were taken during the pulse and after, to investigate the effect of the arc in the sand. Figure 10 shows a vertical arc in the sand with the electrode near the surface during a pulse. A substantial hole and disturbance of the sand is shown and this can be 200 - 300mm in diameter at the surface and would appear to be conical down to the tube. Where the electrode was placed close to the tube, i.e. 50mm, a large cavity was produced in the sand but did not break through the surface.

The result of the horizontal arc through the sand is shown in figure 11. These pictures were obtained by inserting a thin metal plate into the sand along the expected arc path after the shot and scraping the sand away from one side. The metal plate was now removed and the exposed half cavity is shown. Unfortunately, it is not clear from the photographs how much sand has fallen back into the bottom of the cavity after the shot.

In the case of the vertical arc considerable amounts of sand are ejected from the surface and a very substantial lid has to be held on to the top of the container.

In the case of the horizontal arc a large plate was placed over the top of the sand and held down with a weight. At the higher arc current of 70KA this weight could be lifted several centimetres into the air.

Initial tests with a long 210mm horizontal arc which brought the electrode close to the edge of the container, and a peak current of 85KA, completely shattered the wall. This gives some indication of the magnitude of the forces involved.

CONCLUSIONS

1. The indentation produced in the brass tube appears to be directly related to the action integral.

2. The force produced by a vertical arc 100mm long is lower than that from a horizontal buried arc by some 80%.

3. For the vertical arc, forces decreased by a factor of about 2.5 when going from a 50mm arc to one near the surface with an arc length of 150mm to 200mm. This distance effect needs to be investigated with much deeper sand.

4. The distance effects with the buried arcs look less pronounced generally.

5. The sand, though well packed down showed considerable movement over a large volume. It is not clear if this is due to current flow over this volume, or that the shock waves produced by a narrow current channel are causing this effect. Large cavities were produced in the sand.

REVIEW OF INFORMATION OF ARC IN SOILS

The amount of information available of lightning currents being carried by soil especially at the level of 50 to 100KA seems to be limited. Reports describing the effects produced are scarce and this type of information could be very useful in assessing whether the right type of simulations are being made for these tests.

Strikes to buried cables should only exist with soil or other media of fairly high resistivity as the current will dissipate across the surface and very little damage will be caused except at the point of arc attachment.

Kalyagin (reference 5), describes lightning track furrows covering distances of several tens of meters and in perma frost zones a furrow of 75m long was discovered. Transverse dimensions of the furrows are from 300 to 1500mm with depths of the order of 700mm.

"Closer to the cable the furrow is smaller and terminates by an explosion funnel above the cable or ground wire, sometimes such a track comes from the surface down to the cable in the form of burned-through channel with a diameter of 30-40mm which terminate beside the cable."

This relates reasonably well to the experimental data obtained in our tests although the distance of the furrows up to 75m long seems remarkably large and suggests very high voltages can be involved.

SUMMARY AND CONCLUSIONS

All the cables which were tested in sand exhibited to a greater or lesser degree the characteristic bending in the vicinity of the arc attachment point - even at the lower levels of impulse current. The cables tested in air did not exhibit this bending, and it is concluded that the extent of any deformation would largely be a function of the physical properties of the surrounding medium. Examination of the cables revealed that only with gross impairment of the sheath integrity was there loss of optical transmission.

From the tests and work carried out by the Cable Products Division of STC it is concluded that buried, all dielectric cables could be recommended for use in high Keraunic areas where peak lightning currents in the region of 120KA are experienced. Double armoured cables could also be recommended where rodent damage could also be experienced.

We consider that the physical parameters of the test at the high levels of current, viz. 200KA, do not reproduce the conditions which would be experienced by cables buried, say, to a depth of one metre. Lightning currents of this magnitude represent less than 0.1% of all strikes and special measures, such as encasing cables in steel tubing, may be the only satisfactory solution in these extreme cases.

It is considered that the pulse energy content of the test waveform could be usefully described if an action integral was specified.

The attempts to simulate more closely an actual lightning event by the use of a vertical arc which vents to atmosphere, showed that less damage could be experienced by the cable. This aspect needs to be investigated further with the test cables buried deeper in the medium. It was shown that lengths of arc greater than about 100mm did not greatly affect the extent of damage caused. It is our recommendation therefore, that any re-issue of the test specification requires that an arc length of not less than 100mm be used so as to give less variable results.

Very little information is available from the literature as to the nature of an arc in soil and useful future work could be to attempt high speed photography and to quantify such events.

ACKNOWLEDGEMENTS

The Authors would like to thank the Directors of STC plc and the Culham Laboratories for permission to publish the information contained in the paper. Thanks are also due to Dr. P.G. Hale and Mr. A.T. Summers for their valuable comments, and to Mr. R. Butler for his untiring work during the test programme.

REFERENCES

1. PHILLPOTT J. "Recommended Practice for Lightning Simulation and Testing Techniques for Aircraft". - MIL-STD-1757A. (Also Culham Laboratory Report CLM R163 1977).

2. LITTLE PF, HANSON AW, and DOBBING JA. "Arcs on Metal Sheet in Simulated Lightning Discharges", 1977, IEEE International Symposium on EMC, Seattle, pp 375-380.

3. FISCHER D, BOW KE, BUSCH WF and SCHROM EC. "Progress towards the development of Lightning Tests for Telecommunication Cables" IWCS proc. 1986.

4. GRANEAU P, "The cause of Thunder". J.Phy D: Appl. Phys.22 (1989). pp 1083 - 1094.

5. KALYAGIN AM "An analysis of the Damage to the Underground Communication Cables by Direct Lightning Strokes". Telecomm. and Radio Eng. Part 1 (USA) 1985 VOL. 39, pp 33 - 38.

CABLE NO.	CONSTRUCTIONAL DETAILS
1	POLY COATED STEEL STRENGTH MEMBER. 5 FILLERS, 2 x 0.9mm POLY INS. QUADS, 1 x 8 FIBRE LOOSE TUBE WATER BLOCKED CORE PAPER TAPED APL & POLY INNER SHEATH CORRUGATED STEEL AND POLY OVERALL TO 22.4mm
2	AS CABLE 1 BUT ADDITIONALLY WIRE ARMOURED AND HIGH DENSITY POLY SHEATHED TO 31.4mm
3	POLY COATED GRP STRENGTH MEMBER 5 FILLERS, 3 x 8 FIBRE LOOSE TUBES WATER BLOCKED CORE PAPER TAPED POLY INNER SHEATH CORRUGATED STEEL AND POLY OVERALL TO 24.2mm
4	POLY COATED GRP STRENGTH MEMBER 7 FILLERS, 1 x 8 FIBRE LOOSE TUBE WATER BLOCKED, PAPER TAPED AND POLY SHEATHED TO 15.6mm
5	GRP CENTRE, KEVLAR REINFORCED & H.D POLY COATED POLY BEDDING FOR 4 SECONDARY COATED FIBRES AND 8 NYLON FILLERS POLYPROPYLENE TAPE WHIPPING MPP SHEATH WITH NYLON 12 OVERSHEATH TO 8.1mm
6	POLY COATED STEEL STRENGTH MEMBER 5 FILLERS, 2 x 8 FIBRE LOOSE TUBES, 1 x 0.63mm COPPER QUAD WATER BLOCKED, PAPER TAPED APL AND POLY SHEATHED TO 16mm
7	POLY COATED STEEL STRENGTH MEMBER 6 x 2 FIBRE LOOSE TUBES WATER BLOCKED, PAPER TAPED APL AND POLY INNER SHEATH CORRUGATED STEEL AND POLY OVERALL TO 16.8mm
8	AS CABLE 7 BUT STEEL WIRE ARMOUR REPLACES THE CORRUGATED STEEL
9	FIG 8 AERIAL CABLE GRP CENTRE 2 FILLERS, 2 x 8 FIBRE LOOSE TUBES WATER BLOCKED, MYLAR TAPED, POLY INNER SHEATH CORRUGATED STEEL AND POLY OVERALL STEEL WIRE CATENARY
10	FIBRESPAN - ALL DIELECTRIC LONG SPAN AERIAL CABLE
11	SUBMARINE CABLE (6mm rt) POLY SHEATH

Table 1.
Constuctional Details
of the cables tested.

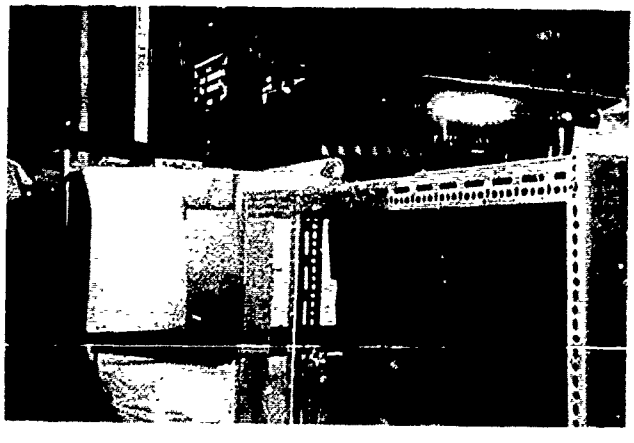

Figure 1.
The Test Facility

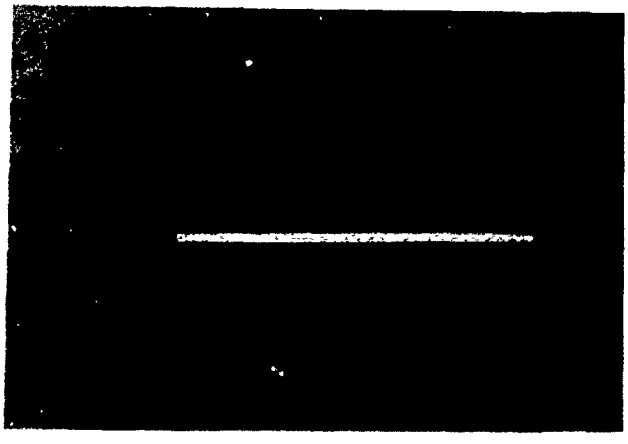

Figure 2.
Horizontal Arc Length

Cable No.	Arc Length (mm)	Peak Current (KA)	Rise Time (μS)	Time to ½ Peak (μS)	Frequency (KHz)	$\int i^2 dt$ $\times 10^6 A^2 S$
1	32	59	9 8	54	23 5	0 07
	30	127	9 6	60	-	0 42
	30	200	9 8	83	-	2.06
2	35	119	9 8	68	24.7	0 37
	30	199	9 2	67	-	1 80
3	34	52	9 6	54	24	0 051
	34	118	9 0	68	24 5	0 37
	33	203	9.4	52	-	1.3
4	55	42	13	40	42	0 03
	52	117	11	55	24	0 30
	56	201	10 2	40	-	0 98
5	55	54	11.6	53	24	0 055
	55	110	9.4	55	-	0 28
	56	197	10 6	36	-	0 85
6	33	56	11.2	56	27	0 069
	35	122	9 8	60	24	0 33
	33	204	11 0	30	-	0 64
7	36	52	11.2	54	24	0 052
	38	126	9 8	68	27	0 39
	36	205	10 4	40	-	0 79
8	35	47	10 2	50	25	0 04
	35	119	9 0	65	-	0 56
	33	191	9 8	66	-	1 5
9 (in air)	40	64	9 8	60	24	0 093
	40	139	9 6	65	-	0 7
	40	205	10 4	64	-	1 4
10 (in air)	52	224	8 8	112		2 67
10 (in sand)	36	208	9 6	50		1 47
11	40	55	11.2	57	24	0 06
	41	110	11.4	65	24	0 34
	38	206	10.4	46	-	1 16

Tests to Cable No.3 with Component 'C'

FAST BANK					SLOW BANK	
Arc Length (mm)	Peak Current (KA)	Rise Time (μS)	Time to ½ Peak (μS)	$\int i^2 dt$ $\times 10^6 A^2 S$	Peak Current (KA)	Q_c
55	-	-	-	-	1.75	130
55	112	10	56	0 25	1.7	126
58	201	9.4	32	0 74	2 2	186

Table 2.
The Test Parameters

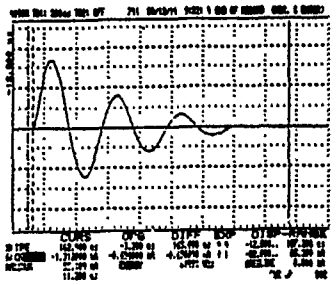

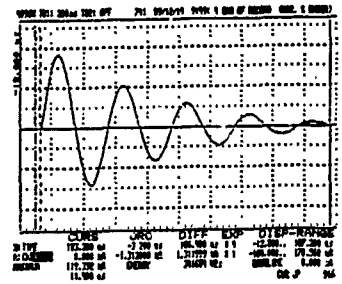

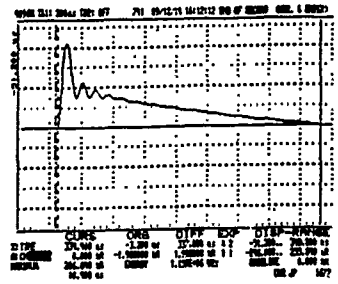

Figure 5.
Typical Test
Waveforms

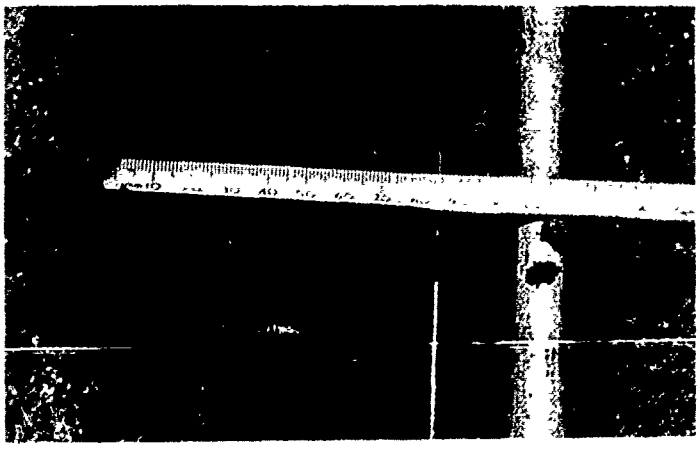

Figure 3.
Arc to an all
Dielectric Cable

	Peak Current (Nominal)	Observations
Single Armour (Cables 1,3,7 & 8)	50 and 120KA	Slight bending of the cables at attachment point. More aggravated bending at 120KA. Fibres and coppers where included were continuous.
	200KA	Outer sheath and steel armouring burnt away with severe cable bending. All fibres in Cable 1 and 6 fibres (3 tubes) in Cable 7 discontinuous. Coppers in Cable 1 remained continuous. Tests on Cable 3 involving the Component 'C' caused severe cable damage with loss of fibres.
Double Armour (Cables 2 & 11)	50,120 & 200KA	Very slight external damage at 50 and 120KA. Fibres in both cables intact and coppers in Cable 2 intact. At 200KA the outer sheath split on Cable 2 to expose the wire armour. One copper wire was discontinuous. All fibres in both cables were intact.
Non-Metallic (Cables 4 & 5)	50 & 120KA	Very slight external damage to both cables. All fibres intact.
	200KA	Extensive sheath damage by burning on Cable 4, core was exposed over 30mm but all fibres remained intact. Cable 5 had its sheath and core completely burnt away leaving the exposed GRP centre. All fibres discontinuous.
Non-Armoured (Cable 6)	50,120 & 200KA	Progressively more aggravated cable bending with increased impulse current. Fibres and coppers remained intact.
Aerial (Cables 9 & 10)	50,120 & 200KA (in air)	Very little damage. All fibres (and coppers in cable 10) remained intact.

Table 3. Damage to Cables

Results of Horizontal Arc Tests to Brass Tube

Spacing of Electrode to Rod (mm)	Peak Current (KA)	Action Integral $\int i^2dt$ ($A^2s \times 10^6$)	Depth of Indentation (mm)
50	36	2.7	0.9
100	19	0.7	0.6
100	44	3.8	1.45
100	82	13	9.9
150	40	3.6	0.5
150	74	13	10.1
300	48	4	2.8
300	71	9.9	5.4

Table 4.

Results of Vertical Arc Tests to Brass Tube

Spacing of Electrode to Rod (mm)	Peak Current (KA)	Action Integral $\int i^2dt$ ($A^2s \times 10^6$)	Depth of Indentation (mm)
50	41	4	0.6
50	66	7.4	7.8
100	24	1.1	0.1
100	49	7.0	1.8
100	73	15	7.1
150	54	6	2.3
150	70.5	10	3.4
300	69	0.3	3.4

Table 5.

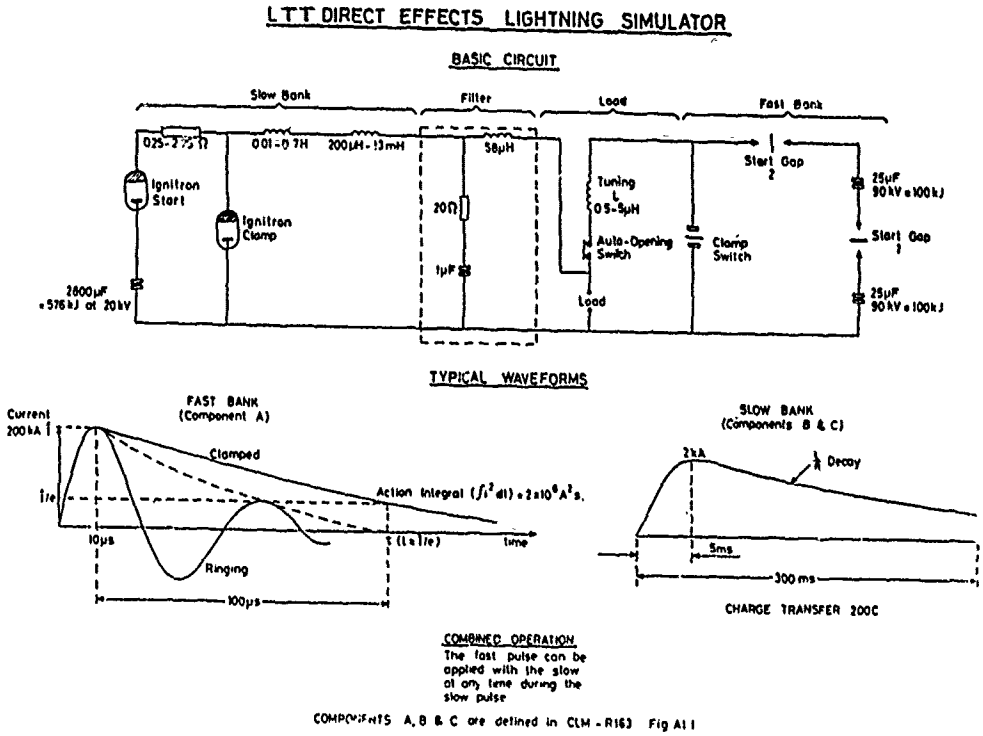

Figure 4.
Circuit of the
Test Facility

Component	Parameter	Value	Tolerance
high current component A	peak current	200kA	± 10%
	action integral	2 10^6 A^2s	± 10%
	pulse length	< 500us	
	rise time	< 25us	
intermediate current component B	average amplitude	2kA	± 10%
	charge transfer	10C	± 10%
continuing current component C	amplitude	200-800A	
	charge transfer	200C	± 20%
restrike (group 1 effects) component D	peak amplitude	100kA	± 10%
	action integral	0.25 10^6 A^2s	± 10%
	pulse length	< 500us	

Table Parameters for return current test waveform

Figure 6.
Waveform for Testing
to Aircraft

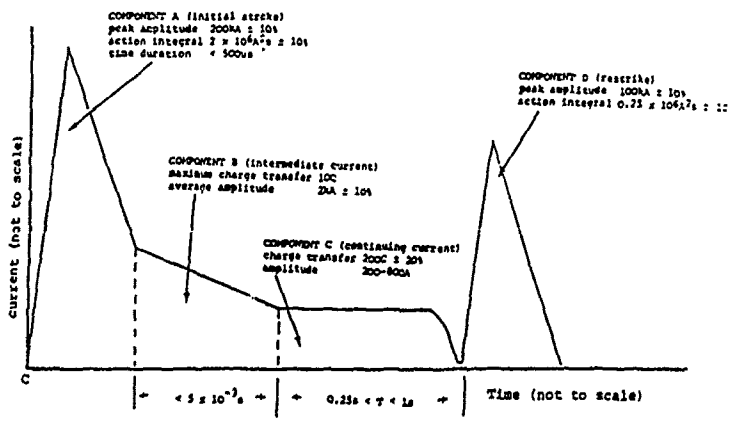

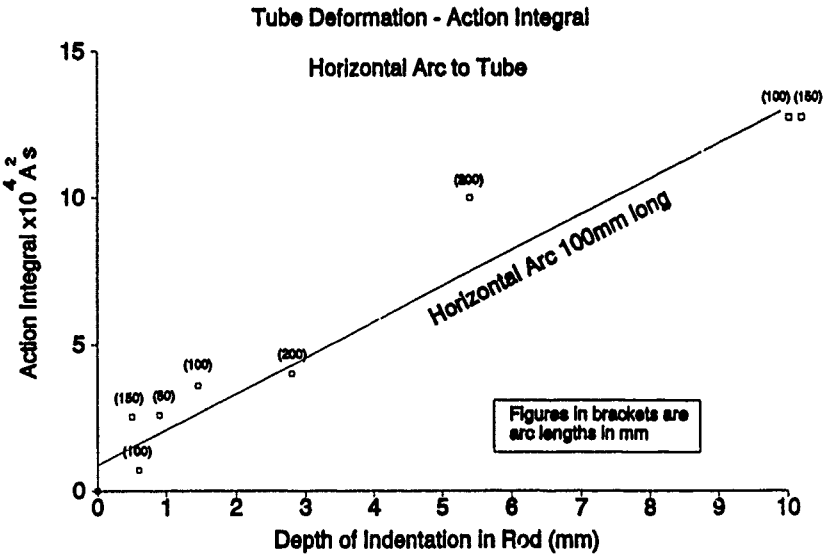

Figure 7.
Tube Deformation -
Horizontal Arc.

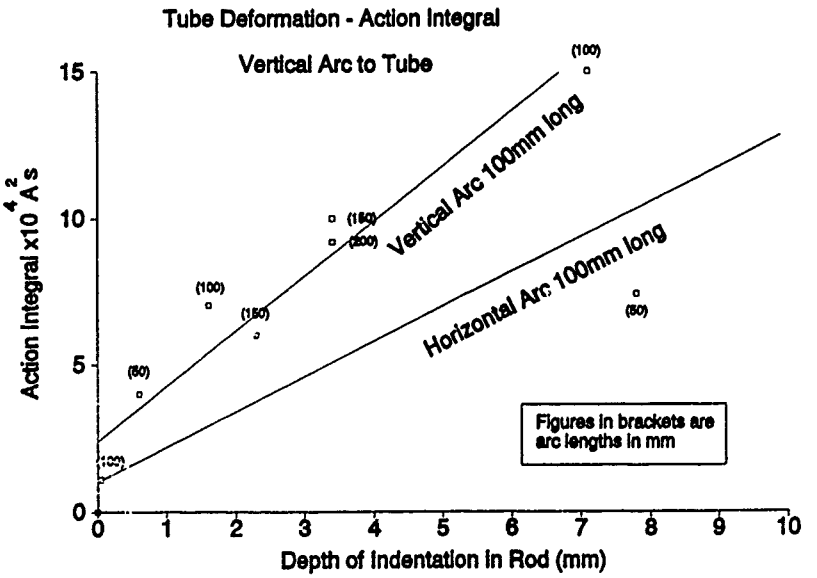

Figure 8.
Tube Deformation -
Vertical Arc.

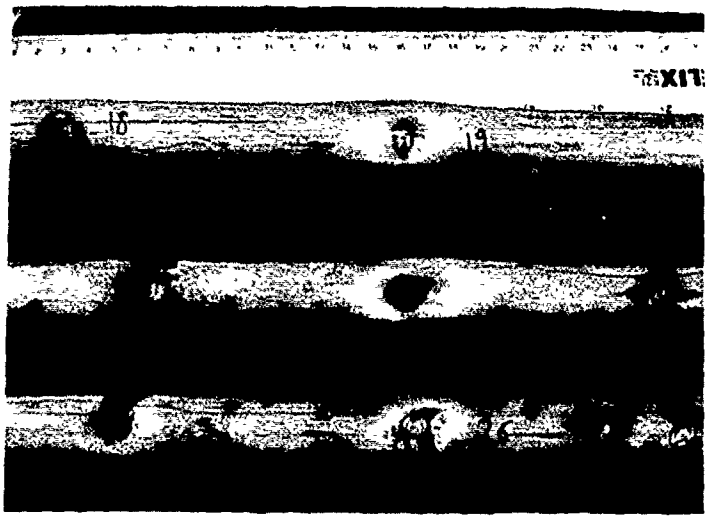

Figure 9.
Indentation of Brass Tube

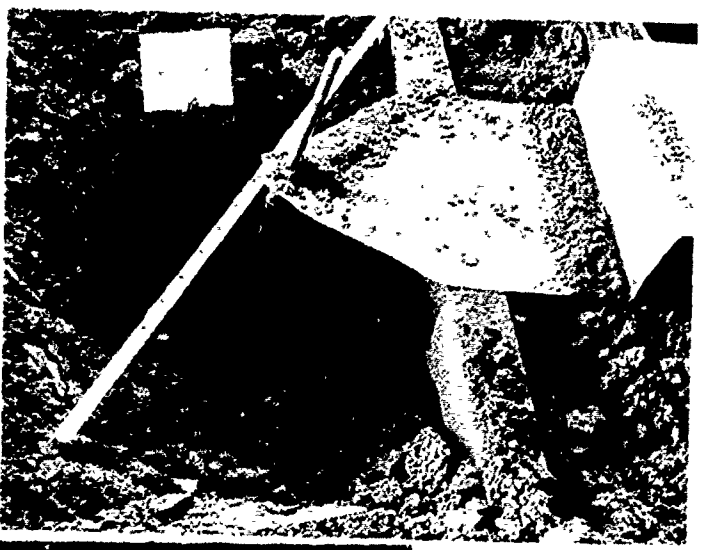

Figure 10.
Vertical Arc.

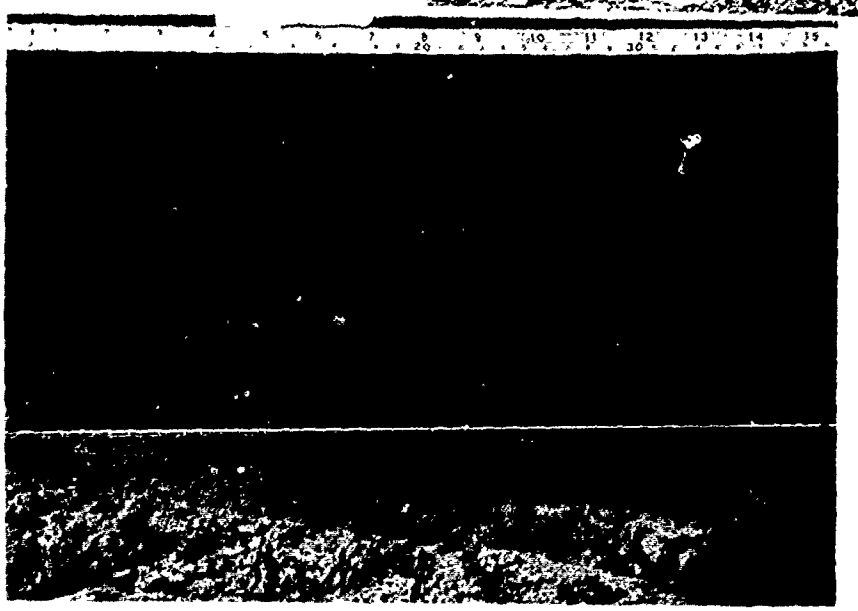

Figure 11.
Cavity formed by
Horizontal Arc.

Barrie J. Symmons,
STC CABLE,
Cable Products Division,
Wednesbury Street,
Newport,
Gwent.
NP9 OWS.

Mr. Symmons is a Principal Engineer with the Cable Products Division of STC Cable and is responsible for all aspects of cable system design. He is a graduate of the Open University, obtaining his B.A. degree in Pure and Applied Mathematics and is a Licentiate member of the Institute of Mathematics and its applications.

Gerry W. Reed,
Lightning Test and Technology,
Culham Laboratory,
Abingdon,
OXFORDSHIRE.
0X14 3DB.

Mr. Reid is an Electrical Engineer with the Lightning Test and Technology Unit at the Culham Laboratory. He is currently concerned with lightning strikes to aircraft and aircraft components especially carbon fibre composites. Prior to this work he spent 25 years with the UKAEA on a number of nuclear fusion experiments. Mr. Reid is a graduate of London University B.Sc. (Eng.) and a member of the Institute of Electrical Engineers.

AN IMPROVED CHARACTERISTIC IMPEDANCE MEASUREMENT TECHNIQUE

H. W. Friesen

AT&T Bell Laboratories
Norcross, Georgia 30071

Abstract

A number of characteristic impedance measurement techniques are being considered today by standards organizations for use in the LAN frequency range. The merits of the various methods depend on such things as the cable under measurement having a dielectric constant that does not vary with frequency, the cable pairs being electrically smooth and the adequacy of the data gathering and processing procedure. The first of several methods considered in this paper is based on delay and low frequency capacitance. This method finds favor in applications where capacitance is constant with frequency. A second method uses open and short circuit measurements on electrically short lengths. Its shortcoming is that a number of short lengths must be measured when structural variations are considerable. The third method is based on open and short circuit measurements made on electrically long cable lengths. Here more extensive data processing techniques are required to remove the effects of structural variations from the measurements. This third method is favored over the second because it allows reliable results to be obtained from a single electrically long sample length.

I. Introduction

Standards body working groups such as the EIA TR-41.8.1 committee are developing requirements for cable pair parameters such as the attenuation constant, characteristic impedance and near end crosstalk in the local area network (LAN) frequency range which today extends from 1 to 16 MHz. While the attenuation and crosstalk are readily measured over a range of frequencies by means of a network analyzer, obtaining the characteristic impedance, Z_0, is more challenging when cable pairs are not electrically smooth, i.e. free of reflections. A number of characteristic impedance measurement techniques are available for obtaining this parameter for metallic media. Several of these are based on open circuit and short circuit measurements.

Problems are encountered with the various methods. Measurements of a single electrically short length may not be representative of the longer lengths used in an application of the cable design. On the other hand, measurements made on electrically long lengths of twisted pair cables typically exhibit some degree of electrical roughness in the LAN frequency range due to structural variations. The structural variation of the cable pair is of interest, but a technique for separating this information from the characteristic impedance of the pair is required. Drawing a distinction between these two quantities when the measurements consist of open and short circuit values can require a considerable amount of effort.

The purpose of this document is first of all to consider the merits of several methods of arriving at the characteristic impedance. Second, it is to advance an improved data processing method for evaluating data obtained by fairly traditional measurement techniques. This is accomplished by making use of present day network analyzer and personal computer data measurement and processing capability.

II. Delay and Low Frequency Capacitance Method

2.1 Equations for Delay and Capacitance Method

The delay and low frequency capacitance method for obtaining the characteristic impedance (Z_0) has been in use for some time.[1] This method is very reliable for those media where the effective dielectric constant of the entire dielectric region and hence the pair capacitance is invariant with frequency. This method includes a broad category of cables such as all the polyethylene and polypropylene insulated outside plant cables and numerous indoor designs which use materials whose dielectric constant does not vary with frequency. It is based on a very reliable through-the-cable measurement (two port) of the insertion loss and phase. It involves only the one sample of cable required for the insertion loss and phase measurement.

$$\beta = \omega\sqrt{LC} \tag{1}$$

$$|Z_0| = \sqrt{\frac{L}{C}} \tag{2}$$

The method can be stated in terms of the approximate expressions in the high frequency range where the reactive primary cable parameters are controlling. We have Equation 1 for the phase constant β and Equation 2 for the magnitude of the characteristic impedance, Z_0, where $\omega = 2\pi f$ is the radian

frequency and L and C are the primary parameters of inductance and capacitance respectively. Dividing Equation 1 by the radian frequency yields the equation for phase delay τ given by Equation 3. The characteristic impedance equation can be restated in terms of the phase delay divided by capacitance as shown by Equation 4.

$$\tau = \sqrt{LC} \tag{3}$$

$$|Z_0| = \frac{\tau}{C} \tag{4}$$

Equations 2 and 4 represent the magnitude of the characteristic impedance without addressing the angle of this parameter. The above equations must be replaced with their complex counterparts at lower frequencies where the a.c. resistance of the pair is significant compared to the inductive reactance or when dielectric loss is considerable.

2.2 Delay and Capacitance Results

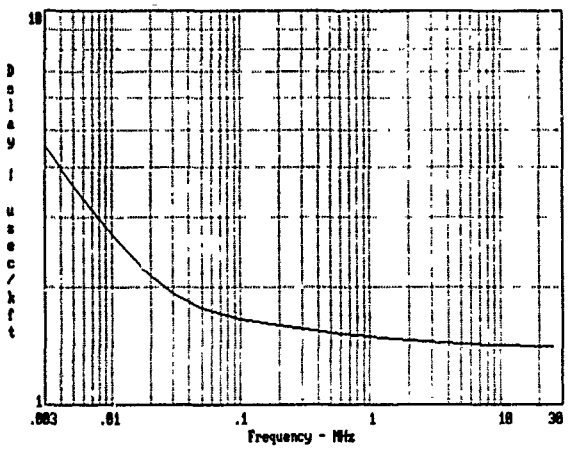

Fig. 1 Delay versus Frequency for a Typical Cable Pair

Figure 1 shows delay as a function of frequency for a broad range of frequencies extending from the voice region to beyond the twisted pair LAN range which today extends to the 16 MHz region. The abscissa and ordinate scales are logarithmic to more clearly show the asymptotic behavior. The delay decreases with the inverse square root of frequency rate in the low frequency region (below 20 kHz) where pair resistance and capacitance are controlling. In the high frequency region it asymptotically approaches a constant as the internal inductance decreases in accordance with the decreasing skin depth leaving only the constant space inductance. Figure 2 shows the magnitude of the characteristic impedance as a function of frequency for the same frequency range. In the high frequency region this response has the same asymptotic behavior as the delay curve.

This cable pair has a capacitance of 13.9 nano-Farads/kft which is constant over the whole frequency range being considered here. Applying Equation 4 to the delay values shown in Figure 1 does indeed result in the characteristic impedance values plotted in Figure 2 for the frequencies above 100 kHz where pair resistance is small compared to inductive reactance. The impedance trace obtained by this method is extremely smooth since it comes from the two port delay measurement (a relatively smooth function of frequency) and the low frequency capacitance.

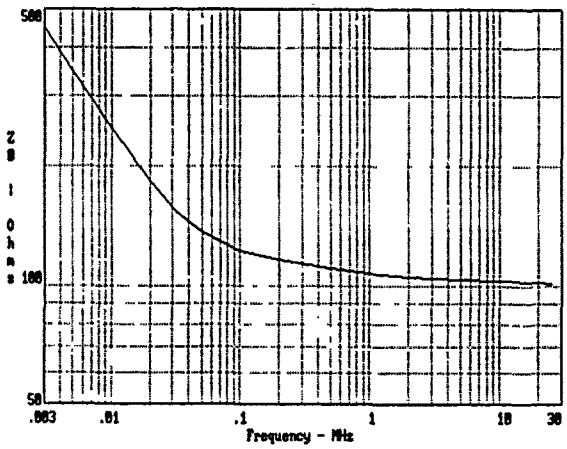

Fig. 2 Z_0 Magnitude versus Frequency for Pair Shown in Figure 1

For cables where the capacitance changes with frequency this method yields a somewhat erroneous result. Since it is based in part on the easy to measure low (voice) frequency capacitance, any change in capacitance with frequency, if not accounted for, will cause a corresponding error in the Z_0 value. In PVC insulated pairs the capacitance can decrease by approximately 10% as frequency changes from 1 kHz to 10 MHz. Assuming a constant capacitance in this case results in a Z_0 value 10% too small.

One might consider measuring capacitance at higher frequencies. There are a number of difficulties with this. Measuring at or near resonance points is not desirable in that it yields inaccurate results. Transmission effects which at 1 kHz are minimal, are significant at high frequencies and not as readily accounted for. Many capacitance measurement devices are limited as to high frequency capability. Measuring the capacitance of twisted pairs involves either measuring the individual three direct-to-mate and direct-to-ground components constituting a pair or measuring the pair directly in a balanced drive mode. All of this is more difficult at LAN frequencies. The difficulties with obtaining pair capacitance at high frequencies encourage one to consider single ended (one port) impedance measurements.

III. Open and Short Circuit Measurements on Short Lengths

3.1 Equations for Open and Short Circuit Measurements Method

A long used method of characterizing metallic media involves measuring the open and short circuit input impedances for cable lengths that are electrically short (under a quarter wavelength). Equations 5 and 6 define the relationships between the

$$Z_{sc} = Z_0 \tanh \gamma l \qquad (5)$$

$$Z_{oc} = Z_0 \coth \gamma l \qquad (6)$$

measured values and the desired secondary transmission parameters consisting of the propagation constant γ and the characteristic impedance Z_0.

$$Z_0 = \sqrt{Z_{sc} Z_{oc}} \qquad (7)$$

From Equations 5 and 6 we see the characteristic impedance can be calculated from the open and short circuit measurements by means of Equation 7. While Equations 1-4 dealt only in real quantities, in these equations both the impedances and the propagation constant consist of complex (vector) quantities having both real and imaginary components.

Making measurements below the quarter wavelength frequency implies that lengths up to 500 feet can be accommodated for frequencies up to 300 kHz. This cable pair characterization technique has been widely used in the telephone cable industry in the past when twisted pair cables were measured up through the analog carrier frequency range which went as high as 150 kHz.

When impedance measurements are desired at LAN frequencies, much shorter lengths must be measured if the less than a quarter of a wavelength guideline is to be followed. One proposal has focused on measuring open and short values on 3 meter lengths (approximately 10 feet) for frequencies up to 16 MHz. This approach is feasible when impedance bridges are used. Present day network analyzers feature S-Parameter capability to facilitate impedance measurements. The characteristic impedance (actually an input impedance) is calculated from the measured s_{11} parameter by means of

$$Z_0 = Z_c \frac{(1 + s_{11})}{(1 - s_{11})} \qquad (8)$$

Equation 8 where Z_c is the impedance at which the system is calibrated. For balanced pairs a transformer facilitates making balanced impedance measurements. Calibration is done with a known resistor connected to the balanced side of the transformer.

This arrangement offers excellent capability when the impedance being measured is within a decade or two of the nominal instrument value. Decreased accuracy results when measurement of the very high and very low open circuit and short circuit impedances respectively are attempted.

3.2 The Two-Termination Impedance Measurement Method

A variation of the open and short circuit impedance method is a so called two-termination method. In this case the measurements are made with known values of terminating impedance (actually good quality resistors). First, an input impedance measurement is made with the short sample terminated in a perhaps 25% lower than nominal impedance (75 Ohm resistor for 100 Ohm pair). A second measurement is made with the sample terminated with a 25% greater than nominal impedance. Equation 9 is an expression useful for computing the characteristic impedance. It states Z_0 in terms of the two terminating resistors (high and low) and two measured impedances R_h, R_l, Z_h and Z_l respectively. It can be seen that this equation reduces to Equation 7 if the low resistance value is assumed to be zero and the high resistance value infinite.

$$Z_0 = \sqrt{\frac{R_l Z_l (R_h - Z_h) - R_h Z_h (R_l - Z_l)}{(R_h - Z_h) - (R_l - Z_l)}} \qquad (9)$$

This measurement technique provides a way of dealing with the problems associated with measuring very small and very large impedance values encountered in short lengths when a network analyzer with S-parameter capability is employed.

3.3 Short Length Impedance Measurement Experiment

Evaluating the performance of a longer piece of cable by measuring a single short sample raises concern about what constitutes adequate sampling when structural variation is considerable. It is generally known that the electrical smoothness of a particular type of media is dependent upon the type of structure and the manufacturing and handling processes employed up through installation. For example, experience indicates that coaxial structures are smoother than twisted pair structures. Individually foil shielded twisted pairs are generally smoother than multipair structures because their geometry is controlled to a greater extent. Applying a twist to a group of pairs when forming them into a cable, which is known as stranding, results in a smoother product than bunching the pairs without stranding.

An experiment was carried out to determine how much impedance variation one encounters when short length measurements are made on numerous segments of a small pair count non-stranded cable, which is thought to be a worst case situation. A 500 ft. length of unshielded four pair cable was cut up into 50 ten foot pieces. The two-termination measurements were performed on all four pairs of each ten foot

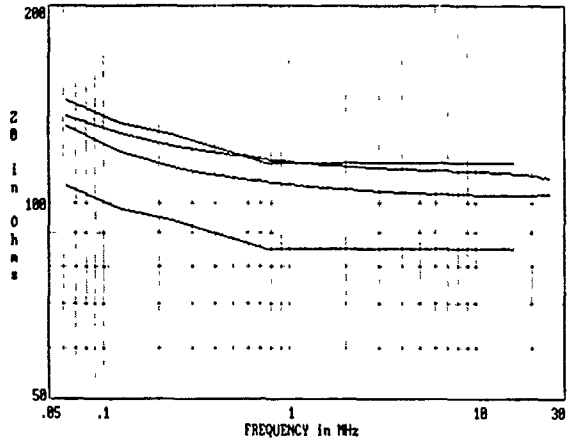

Fig. 3 Z_0 Measurements on Two 10 Ft. Samples

piece using a network analyzer with S-parameter capability. Care was taken during the course of the measurements to keep the cable pair fan-out region as short as possible, typically about 3 inches.

The smooth curves shown in Figure 3 are the results obtained for two adjacent ten foot segments. Shown here are the impedance results for one of the four pairs computed from the two-termination data. The frequency range extends from 62.5 kHz to 25 MHz. Also shown here are the connected straight line segment upper and lower proposed impedance limits as specified by the current horizontal media requirements draft of the TR-41.8.1 committee (hereafter TR-41.8.1). Both of the impedance plots are smooth. But they indicate that the characteristic impedance for the two adjacent ten foot pieces differ by about 9 Ohms. One sample indicates very acceptable values only slightly above the middle of the permitted range. The other sample indicates that this pair fails the upper limit for TR-41.8.1 in the 0.6 to 1 MHz frequency range.

Results for all 50 of the ten foot samples are shown in Figure

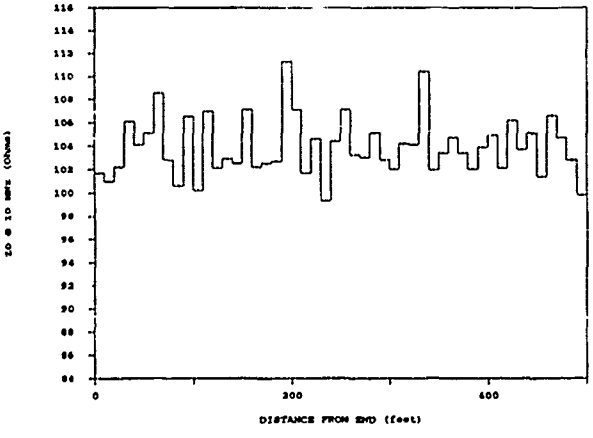

Fig. 4 Impedance Variation with Length Found in Cable Cutting Experiment

4. Here the 10 MHz impedance values are plotted versus distance from one end. The 10 MHz values from the traces from the previous figure appear at the 190 and 200 foot positions. It can be seen that the impedance values vary from a low of 99 Ohms to a high of 111 Ohms. Most of the segment by segment variation appears to be random. The last 150 feet indicates somewhat more periodic variation. The results for two of the other pairs in the four pair cable were similar. The remaining pair had only about half as much variation.

Figure 5 shows a histogram consisting of the fifty 10 MHz impedance values shown in Figure 4. This histogram shows that all but 9 of the values for this pair fall in the 102 to 107 Ohm range and that the extremes vary from 99 to 111 Ohms as indicated earlier. Constructing the histogram with 1 MHz impedance values would shift it to the right by about 5 Ohms. One or two pairs would be above the upper 115 Ohm impedance limit shown in Figure 3.

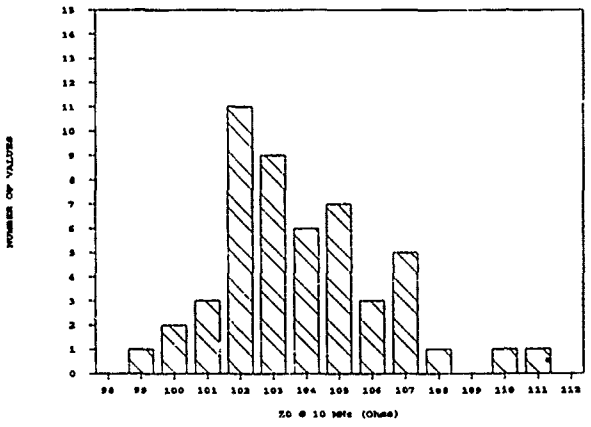

Fig. 5 Histogram of 10 Ft. Length Impedance Values at 10 MHz

The main conclusion from this experiment is that a single short sample impedance measurement can not be relied upon for determining what the characteristic impedance of a product really is. Several samples must be measured to determine a reliable average value of characteristic impedance for building wiring lengths ranging from perhaps 50 to 350 feet in the horizontal runs to work stations and longer runs between closets or in riser shafts. Structural variation such as that encountered here may be of concern but it needs to be quantified separately from the nominal characteristic impedance.

3.4 Difficulties Encountered with Short Length Measurements

Experience with S-Parameter measurements on short lengths has indicated possible measurement sensitivity problems in addition to the need for multiple samples. Figure 3 shows that the two curves do not have a constant separation over the entire

frequency range. They approach each other in the low frequency region. The shape of the lower of the two curves is consistent with the TR-41.8.1 limit while the other one is not. The upper curve is exhibiting a downward drift with respect to the lower curve as frequency decreases. In some measurement runs severe examples of this type of anomaly have been encountered to the point where the response crosses the upper or lower limit line. Recalibrating the network analyzer and repeating the run has typically cleared up the problem. This problem is basically a measurement accuracy issue. Using resistor values farther apart than the 75 and 125 Ohm values used to date might be beneficial.

The high end downward trend versus frequency of the upper curve in Figure 3, on the other hand, is probably not a measurement error. About 4/10 of a wavelength is being measured at 25 MHz. Some structural effects are evident in the one ten foot sample. This points to the need of going to even shorter samples when information for higher than 16 MHz frequencies is desired. End effects are another problem area. The considerably higher impedance for the two fanned out portions of a ten foot sample will have a considerable effect on the results obtained when convenient 1 foot fanouts are used. Shorter fanout regions can make pair identification difficult in a large multipair cable and are generally inconvenient.

IV. Z_0 Measurements on Electrically Long Lengths

4.1 Use of Input Impedance as a Z_0 Estimate

Under certain conditions open and short circuit input impedance measurements made on electrically long cable lengths can readily be used to obtain a characteristic impedance value. Equation 7 implies no length or frequency restriction. Actually, what is obtained is an input impedance to the two port device. The characteristic impedance can be assumed equal to the input impedance when the pair is electrically smooth.

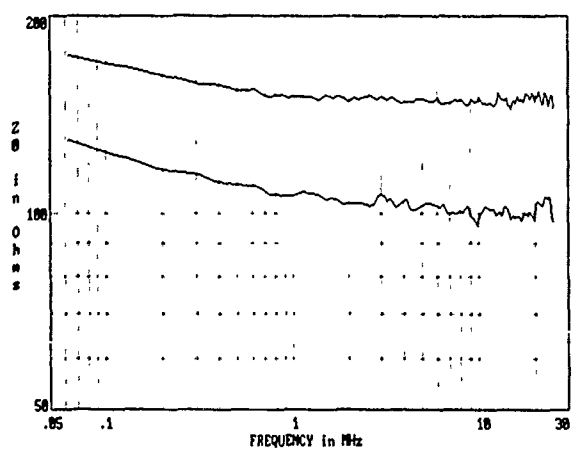

Fig. 6 Z_0 for 150 Ohm and 100 Ohm LAN Pairs Obtained from Open and Short Circuit Data

The input impedance computed from open and short impedance measurements is specified as the method for obtaining characteristic impedance values for the IBM Types I, II and III and later LAN cable designs.[2] This method has also been used for other cable designs. Figure 6 shows the input impedance obtained for two considerably different LAN cable pairs. The upper trace is for a 500 foot length of Type II cable which has a nominal 150 Ohm characteristic impedance. The lower trace is for a 500 foot length of 100 Ohm unshielded twisted pair (UTP) designed for LAN application where unshielded media is specified. For these two examples the Z_0 estimate resulting from the input impedance method exhibits only a small amount of roughness.

There is no problem with the pair characteristic impedance being obscured by the structural effects in Figure 6. These 150 Ohm and 100 Ohm pairs readily pass the nominal +/- 10% and +/- 15% limits respectively expected of them. The Type I and II foil shielded data pairs are relatively smooth at least in part because of the geometrical control achieved when foil is applied directly over two insulated wires. The UTP design considered in Figure 6 is smooth because of such features as the use of short twist lengths and stranding in addition to good control of insulation diameter. This degree of electrical smoothness, while not absolutely essential for good transmission, results in very small reflection losses and contributes to low jitter.

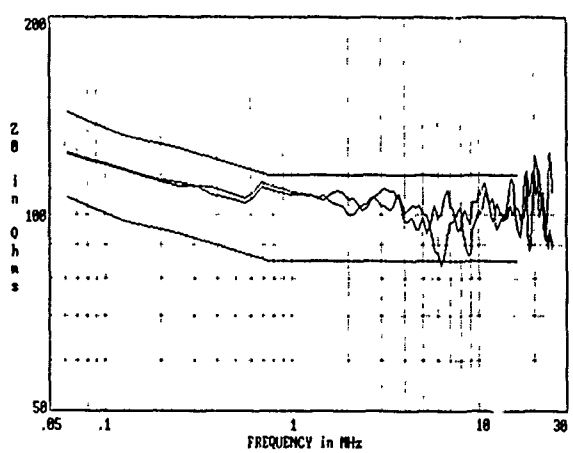

Fig. 7 Input Impedance Data from Two Ends of Cable Plotted against Upper and Lower Limits

Applying the input impedance measurement technique to the cable design considered in Section III, a non-stranded unshielded design similar to Type III cable, results in much rougher traces such as those shown in Figure 7. These results are from measurements that were made on one of the pairs in the 500 ft. sample of cable prior to cutting it up for the investigation discussed in the previous section. The single port input impedance measurements were made from both ends. Both sets of results are plotted here along with the proposed TR-41.8.1 limits. The difference between the two traces is due to structural effects appearing different when viewed from opposite ends of the cable. With the results plotted on a log-

log basis it can be seen that this pair is fairly well behaved up to several MHz. The scan from one direction does have a minimum value at about 6.3 MHz which falls below the TR-41.8.1 lower limit indicating that the pair fails if the input impedance traces are interpreted as characteristic impedance.

It can be seen that the responses shown in Figure 7 are for the most part centered around the desired 100 Ohms for frequencies above 2 MHz. This pair although not as smooth as the higher quality pairs shown in Figure 6 is basically at the right average impedance level and capable of good transmission performance. Rejecting this pair, based on input impedance being taken for a Z_0 estimate does not seem desirable. Such an approach allows a few sample points in the frequency domain (6.3 MHz region in this case) to be the basis for rejecting a reasonably good cable pair. This is somewhat analogous to allowing one ten foot segment in a distance domain plot such as that shown in Figure 4 to indicate failure for the same pair. What is really desired in either case is to allow the characteristic impedance to be represented by an average of the many measurements made either in the frequency or distance domain. A structural return loss or a two port excessive loss peak specification should form the basis for placing a limit on impedance and transmission irregularities.

4.2 Fitting Data with an Impedance Like Function

What is needed in the case of long length measurements is a way of extracting the characteristic impedance estimate from the possibly rough input impedance trace. One approach to dealing with frequency domain data such as that shown in Figure 7 is to fit an appropriate impedance like function to the data. Such a frequency function is one consisting of a constant and an inverse square root of frequency component as indicated by Equation 10. The basis for the $f^{-1/2}$ term comes from the internal conductor inductance which is a part of the total pair inductance. The skin effect phenomena results in the wire resistance increasing and the internal inductance decreasing as $f^{1/2}$.

$$|Z_0| = C_1 + \frac{C_2}{\sqrt{f}} \qquad (10)$$

Shown in Figure 8 is a least squares fit to one of the two scans of Figure 7 by the function represented by Equation 10. This example shows a very nice fit at low frequencies and intuitively good accommodation of the data at high frequencies. The C_1 and C_2 coefficients for this example are approximately 98 and 7 Ohms respectively where frequency is in MHz.

Appropriate weighting is desirable when fitting a function to the frequency domain data. The data presented here was obtained from a network analyzer. It consists of 401 equally spaced points on a linear frequency scale. To obtain the fitted result shown in Figure 8 a logarithmic weighting technique was used. A data point at 0.1 MHz was given a weighting of 10

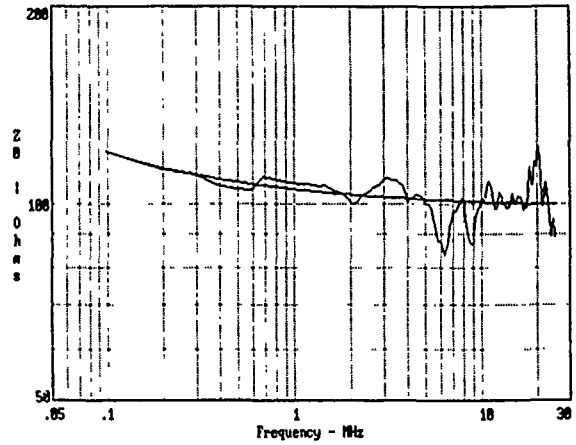

Fig. 8 Impedance Scan Least Squares Fitted with Function of Frequency Given by Equation 10

relative to a 1 MHz value and a 10 MHz value received a weighting of 0.1 relative to the 1 MHz value. Simply using a weight of one for each data point when data points are equally spaced on the frequency scale often results in poor fits at the low frequency end. What is desired intuitively is to place more emphasis on the data where it is less oscillatory thereby forcing a closer fit to those points. This weighting system is analogous to assuming one has uniformly spaced data on the log(f) scale. Another approach is to acquire data from the network analyzer on a log frequency basis where this feature is available using the same weighting for all values.

4.3 Using an Average of Several Impedance Scans

A better impedance estimate for an individual pair can be obtained by computing the average of data acquired from both ends. The average of two independent scans such as those shown in Figure 7 can be least squares fitted with the frequency function of Equation 10. The average fitted result generally falls half way in between the results obtained by

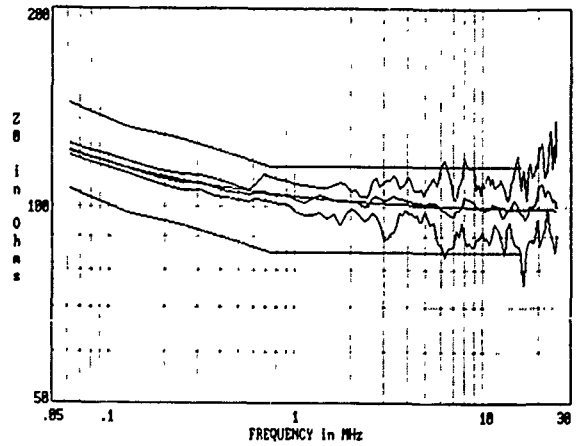

Fig. 9 Impedance Average of Four Pairs Fitted Frequency Function along with Impedance Extremes

fitting the individual scans.

Further averaging can be employed with regard to obtaining an average characteristic impedance for all pairs in a cable. The results obtained from averaging two scans each from several pairs are generally much smoother than results obtained from the two scans for an individual pair. Figure 9 shows the average for a four pair cable (8 scans) fitted with Equation 10. Also shown are the impedance maxima and minima computed from the eight scans at each frequency. The average of the several scans is smooth and relatively reliable, compared to the individual traces shown in Figure 7. The maxima and minima traces show that whereas variation across the four pairs is only a few percent at low frequencies, at the high frequencies it exceeds the 100 Ohm +/- 15% limits by a considerable amount for this relatively rough cable example. The fitted functions for the individual pairs while not shown here only varied by about 5% to 10% from the lowest impedance pair to the highest impedance pair, for this type of cable and readily stayed within the 100 Ohm +/- 15% limits expected of this design.

4.4 Smoothing Frequency Domain Data

Another technique that can be used in the frequency domain is that of smoothing or filtering the data in a digital manner. One form of filtering is to simply compute at each frequency a smoothed estimate of the magnitude of the characteristic

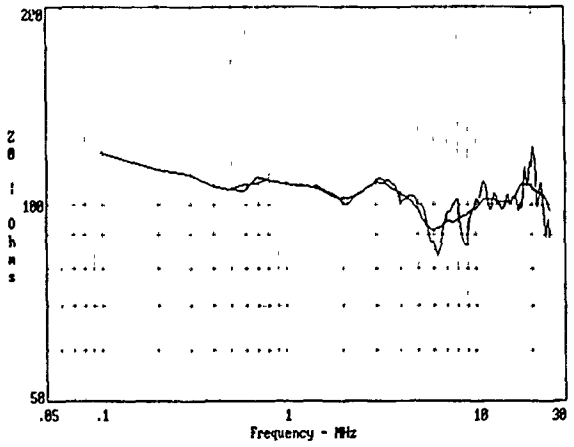

Fig. 10 Frequency Domain Filtering of Frequency Domain Data using a 1/2 Octave Wide Average

impedance based on an average of the values at and surrounding the particular point in frequency. This form of filtering does not have the physical basis as does filtering in the time domain but yields reasonably smooth looking results. Figure 10 shows results for the data plotted in Figure 8 where the width of the smoothing interval extends from $.5^{1/4}$ of the center frequency to $2^{1/4}$ times the center frequency and is 1/2 octave wide. The response in Figure 10 is much smoother than the unfiltered data but preserves the broad features. Increasing the width of the smoothing interval to an octave results in a smoother response in this case but there are situations where pairs exhibit broad high or low regions more than an octave wide.

4.5 Transformation to the Time Domain and Digital Filtering

Not all pairs are as well behaved as the one shown in Figure 7. Generally the input impedance data exhibits increasing oscillation with increase in frequency. When longer lengths of similar product are measured the resulting oscillations are more severe. Function fitting has uncertainties associated with it when the data is poorly behaved or when the function is inadequate as in the case of stranded conductors.

Frequently moderately strong peaks (+ or -) are encountered in the frequency domain data. They are evidence of periodic structural effects along the length of the pair. These effects are ones that can readily be filtered out if the data such as that shown in Figure 7 is transformed into the time (distance) domain. Also, filtering in the time domain has a stronger physical basis than smoothing in the frequency domain. In the frequency domain when doing smoothing, what one does with the real and imaginary components is not as clear. In the time domain only a real response exists for a causal system such as this one.

Further refinement of the long length characteristic impedance data processing technique discussed in the previous section, involves computing the impulse response for the frequency domain data. Digital filtering is carried out in the time or distance domain. This procedure is somewhat analogous to filtering the results from the cable cutting experiment discussed in Section 3.3 and shown in Figure 4. Any periodic tendencies in the structure show up as strong positive or negative peaks in the frequency domain but are readily smoothed away in the time domain. The filtered response is converted back to the frequency domain with the result being a frequency domain impedance trace that is much smoother especially at high frequencies than what was started with.

Converting to the time domain is based on the Fourier Integral

$$F(\omega) = \int_{-\infty}^{\infty} f(t)\, e^{-j\omega t}\, dt \qquad (11)$$

and the inverse Fourier Integral stated by Equations 11 and 12 respectively.

$$f(t) = \frac{1}{2\pi}\int_{-\infty}^{\infty} F(\omega)\, e^{j\omega t}\, d\omega \qquad (12)$$

The Fast Fourier Transform (FFT) and its inverse are the digital data processing counterparts of Equations 11 and 12. They can be used to do the necessary computations with reasonable amounts of processing time. The FFT algorithms

complete with program listings can be found in books on digital signal processing.[3]

The time domain signal obtained by means of the frequency domain to time domain transformation is dependent upon what sort of generator signal is assumed. For our purposes an impulse response of the reflection coefficient (actually s_{11} parameter) is suitable. This is analogous to the real time arrangement where a short pulse is applied to a pair via a transformer and a tap from the connecting line is fed to the high impedance input of an oscilloscope.

The computation procedure picks up with the rough frequency domain impedance estimate obtained from the open and short circuit measurements that were considered in Section 4.1. A reflection coefficient s_{11} is computed via Equation 13 which is

$$s_{11} = \frac{Z_0 - Z_c}{Z_0 + Z_c} \qquad (13)$$

the inverse of Equation 8. s_{11} becomes the $F(\omega)$ of Equation 12 which is transformed into an impulse response f(t). The Fast Fourier Transform algorithm in its simplest form works with an array size which is a power of 2. An adequate frequency domain representation extending to 25 MHz can be had with 256 frequency values where the frequency increment is 97.7 kHz. The input values are interpolated from the 401 network analyzer data points. The reflection coefficient is a complex quantity. Even symmetry applies to the real component and odd symmetry to the imaginary component. The computed time response is a real response starting at t=0 and extending over the round trip time of the cable pair but decaying with time due to the attenuation of the pair.

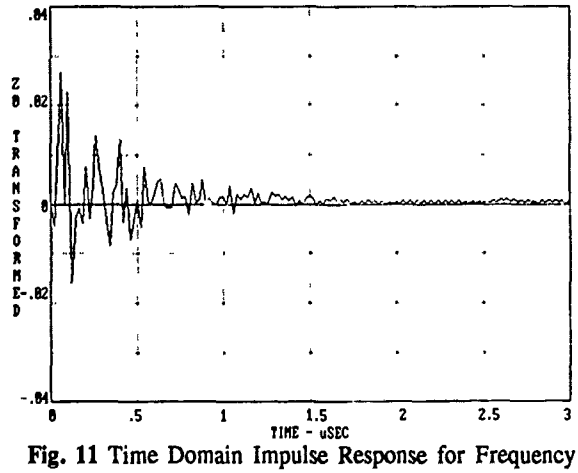

Fig. 11 Time Domain Impulse Response for Frequency Domain Impedance Plotted in Figure 8

Figure 11 shows a time domain impulse response for the data plotted as impedance in Figure 8. It shows the same structure as would be seen if a pulse response were observed at the transmitting end with an oscilloscope. The time scale extends from 0 to 3 micro-seconds which is the approximate round trip time of the 500 ft. cable pair being considered here. This response has the typical property of attenuating rapidly with frequency and in this example has greatly reduced amplitude after .5 micro-seconds. A perfectly smooth cable pair would yield a slowly decaying response (not exactly exponential) with no oscillation.

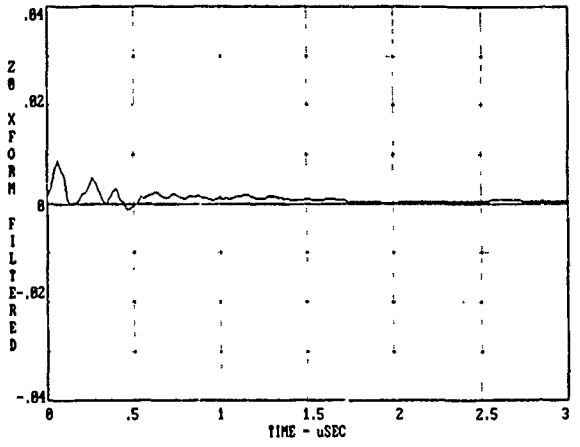

Fig. 12 Filtered Time Domain Response Obtained by Using a Digital Low Pass Filter

$$x_i = K x_{i-1} + (1-K) x_i \qquad (14)$$

Figure 12 shows the resultant time domain response after digital filtering. The data of Figure 11 has been passed through a digital low pass filter twice. This digital low pass filter is of the form represented by Equation 14. It indicates that the current array element x_i is to be replaced with some constant K where $0<K<1$, times the previous array element x_{i-1} (output) plus (1-K) times the current element (input). This digital filter has a frequency response similar to an analog low pass filter with a K close to unity resulting in a low cutoff frequency and K=0 resulting in no filtering.

The result of the filter scans is that much of the rapidly varying structure is removed. Low frequency content is preserved while high frequency content is attenuated. The filter factor K = 0.6 was used here with a sample interval of .02 micro-seconds. Since $K^2 = .36$ the time constant of a single stage of the filter must be about two sample intervals. In this example only a moderately strong filtering effect was used so as to better demonstrate the workings of the filter. In actual application a somewhat stronger filtering effect would be chosen. It could even be adjusted dynamically based on where strong frequency domain effects set in.

A Fast Fourier Transform analogous to Equation 11 was used to compute the frequency domain impedance results (transform back to the frequency domain). Figure 13 shows the frequency domain results after the transforming and filtering operation along with the prior trace. The filter has had almost no effect for frequencies below 2 MHz leaving the reliable portion of the impedance estimate unshifted. It has removed much of the

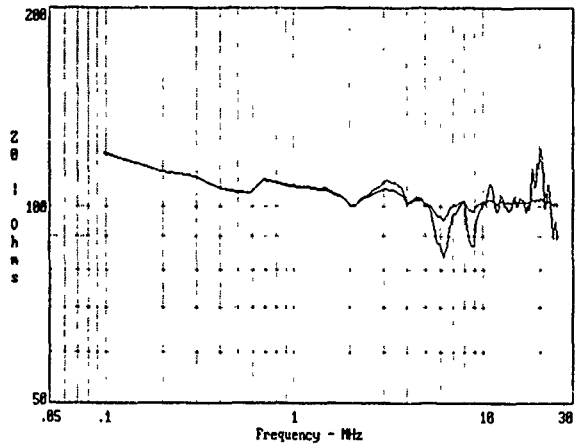

Fig. 13 Frequency Domain Impedance Calculated from Filtered Time Domain Results Shown in Fig. 12

structure for frequencies beyond about 6 MHz. It has left us with a much cleaner rendition of the desired characteristic impedance information with the amplitude of the strong peaks being reduced substantially. Whereas the frequency domain smoothing shown in Figure 10 simply established an average at any given point in frequency, this method actually removes almost all of the undesired structure leaving us with a result more like a smooth impedance response. A slightly stronger filter coefficient would effect further smoothing completely removeing the negative going peaks at 6 and 9 MHz.

The processed impedance result shown in Figure 13 fits well within the TR-41.8.1 limits shown in Figure 7. The least squares fit of Equation 10 if carried out on this representation would yield similar results to those obtained earlier but with much less brute force function fitting. This is especially true when one considers extending this measurement technique to longer pair lengths and/or higher frequencies.

Many different data sets have been processed with the transform and filtering method as well as the frequency domain approaches discussed in Sections 4.2 and 4.3. Generally the frequency domain methods are effective but this method represents a further refinement. The final results (fitted coefficients) obtained for pairs where the scans from the two ends are considerably different will be more alike when the transform and filtering technique is used. Results obtained via all the data processing techniques pertaining to long length impedance measurements have been compared to results obtained by the delay and capacitance method for cables where capacitance is invariant with frequency. The two methods agree very well, generally to within an Ohm.

VI. Conclusion

Of the several methods for obtaining the characteristic impedance of a cable pair the first method which involves the delay and low frequency capacitance involves the least effort. It is based on a through-the-cable measurement simultaneous with measuring the propagation constant. The low frequency capacitance value is readily obtained by means of a capacitance bridge. This method is to be recommended for dielectric cross-sections where capacitance can be assumed invariant with frequency. This covers a broad category of transmission media.

The short length and the long length one port measurement techniques both yield information from which valid characteristic impedance values can be calculated if enough representative data is obtained. The short length approach requires measurements on more than one length (maybe more than two) to obtain a meaningful average. The long length method requires meaningful processing of many data points obtained from a single long length. Both involve considerable effort. For the short length method the effort is manual with much sample gathering and preparation effort. The latter method uses a computer to do the work. Most of us would probably prefer to let a computer do the work.

In the long length approach data from a single long sample is adequate but data processing is required to separate the characteristic impedance information from the structural return loss information. The data processing features the use of frequency domain function fitting or smoothing or both. Further refinement involves the FFT and digital filtering in the time domain ending with frequency domain function fitting to obtain a characteristic impedance result for a range of frequencies where the smoothness of the final result is comparable to the two port result obtained from delay and low frequency capacitance.

A by-product of the long length method is that information pertaining to the smoothness of the pair is available. The structural return loss can be calculated from the input impedance data. While this document focuses on characteristic impedance, smoothness information is of interest in the case of many designs and should not be overlooked. This information is not available when the delay capacitance method is used.

References

1. Kreutzberg, J. and Nantz, T. D., "Precision Insertion Loss Measurements and Data Analysis on Multipair Cable," 24th International Wire and Cable Symposium, November, 1975, pp 175-179.

2. Hobgood, R. Benton, "Measurement of the Characteristic Impedance of Balanced Twisted Pairs using Scattering Parameters", International Wire & Cable Symposium Proceedings, 1983, pp 271-276.

3. Oppenheim, A. V. and Shafer, R. W., *Digital Signal Processing*, Prentice Hall, Inc., Englewood Cliffs, New Jersey, 1975.

HAROLD W. FRIESEN
AT&T Bell Laboratories
Norcross, GA

Harold W. Friesen is a Distinguished Member of Technical Staff at AT&T Bell Laboratories. He has been a part of the Transmission Media Laboratory since 1963. He received a BSEE degree from the University of Colorado in 1963 and a MEE degree from New York University in 1965. Hal has been involved in cable design, the development of fabrication methods and cable measurement techniques. He holds four patents in this area. He is a member of the IEEE.

OUTSIDE PLANT TESTING OF FIBERS IN THE SUBSCRIBER LOOP

T. Wei
GTE Laboratories Incorporated, Waltham, MA 02254

F. Fleming, M.A. Morrison, and C.R. Weckesser
GTE Telephone Operations, Cerritos, CA 90701

ABSTRACT

As more and more fibers are being deployed in the subscriber loop, testing and data handling issues have to be adequately addressed because of the increasing complexity associated with different fiber placing configurations under vastly different field conditions. In this study outside plant testing requirements in trunk and subscriber loop constructions were compared, and various optical testing instruments and procedures were evaluated for their functionality and relevance in the fiber loop. Data storage and handling techniques were also investigated for their effectiveness and efficiency. In most cases new procedures specific to optical testing in a fiber loop were then established. In summary, this study demonstrated that testing during outside plant construction, when it is done properly and efficiently, will allow advanced services to be successfully brought to the subscribers in a fiber loop network.

INTRODUCTION

With the introduction of optical fiber to the subscriber loop, both outside plant (OSP) construction and testing undergo considerable changes to accommodate a greater diversity of network configurations and cable structures, which could include designs with large fiber count cables.[1] It is also apparent that OSP optical testing for a fiber loop network has to be flexible and properly designed so it can be accomplished more efficiently and reliably.

During OSP construction of a fiber loop network, different crews may be involved in cable placing, fiber splicing, and terminal installation. In contrast to a fiber trunk network, a single testing method alone will not adequately address the different conditions encountered in a fiber loop network. This means that cable splicers and terminal installers have to be properly equipped to test fiber cables in diverse installations – from the central office (C.O.) to the remote terminal (RT), then to the customer's distant terminal (DT), as shown in Figure 1. Therefore, new test procedures need to be developed for short haul applications and a greater variety of optical test equipment should be made available accordingly.

OSP CONSTRUCTION AND TESTING

There are at least three phases in constructing a fiber plant: cable placing, fiber splicing, and acceptance testing. In considering testing requirements for a fiber network, the contrast in the OSP construction between a trunk network and a local loop network should be noted.

For a trunk network, the distance between two C.O.'s is usually of tens of kilometers. Each piece of the fiber cable, up to several kilometers in length, typically contains less than a hundred fibers. After placing cables, a single splicing method (for example, either standard mechanical or fusion splicing techniques) is frequently used to join the ends of individual fibers at an interval of a few kilometers. Because of unidirectional transmission in each fiber and a large end-to-end loss budget of 15-35 dB for a trunk installation, it may suffice to have a single end-to-end loss measurement for final acceptance testing. OSP testing could therefore consist principally of the total loss measurement at 1300 nm using either an optical power meter or an optical time domain reflectometer (OTDR).

On the other hand, in a fiber loop network the construction practices are more complicated. One of the reasons is that the network is comprised of several different cable structures and fiber counts. Moreover, the splice locations are very diverse and include customer's premises, curb side, controlled environmental vault, and C.O. Consequently, a single splicing method may not adequately address the needs at different locations. In some cases, the incorporation of new multiple fiber splicing methods would reduce labor costs and installation time.[2] In addition, the terminal installation and

possibly additional acceptance testing are also parts of the construction work for a subscriber loop.

Because of the diversity and complexity associated with constructing a fiber local loop, a plurality of tests may be required during different phases of the construction. Furthermore, due to a much smaller end-to-end loss budget (~ 5 dB), there is less margin in the insertion loss for each splice or connector. As a result, individual connections may need to be tested to achieve the optimal performance. In some applications, duplex transmission at 1300/1550 nm or 1300/850 nm in a single fiber may demand loss measurements at more than one wavelengths. Lastly since optical reflection may severely degrade the performance for certain broadband or AM video transmission systems, the optical return loss (ORL) becomes an important parameter to be tested in the OSP.

We evaluated the functionality and suitability of many different commercial instruments for OSP testing. This process also considered how to manage large amounts of data in the local loop network through mechanization. One of the objectives of this evaluation was then to develop testing procedures to ensure that the fiber network could be built with high reliability.

EVALUATION OF TEST EQUIPMENT

Instruments being examined in this study included OTDRs, optical power meters, ORL test sets, fault finders, visible fault locators, fiber identifiers and a high power microscope. Depending on the task on hand, cable splicers and terminal installers selected several items from the equipment list for testing. With the introduction of many sophisticated test instruments, both splicers and installers have to learn the fundamentals and operations of advanced test equipment. Consequently, proper training and follow-up also became essential parts of this study.

Based on the above considerations, we evaluated test instruments for their functionality, performance, degree of automation, user friendliness and compactness. For certain tests, memory or data storage capabilities save testing time and assure that accurate readings are recorded. All stored test results may later be down-loaded into a mainframe or a personal computer and displayed in a spread sheet format.

Table 1 provides a summary of test instruments and their functionalities. For each item on the list, a brief description and some special features are discussed separately.

Table 1.
List of Optical Test Equipment for a Fiber Loop

Test Instrument	Functionality
OTDR	End-to-end loss, insertion loss, fault locating
Optical Power Meter	End-to-end loss, insertion loss, continuity check
ORL Test Set	System ORL, component ORL
Fault Finder	Fault locating and identification, continuity check
Visible Fault Locator	Fault locating
Fiber Identifier	Continuity check, traffic check
Microscope	Fiber end inspection, connector finish check

OTDR

OTDRs have been used extensively in constructing a trunk network, providing an effective means of measuring overall and component losses, and locating faults. For loop applications, because of the shorter fiber run and a higher concentration of splices/connectors at two ends of the run, test requirements for an OTDR underwent major changes. For example, high resolution, short dead zone, masking function and data storage capacity are some of the useful features which can be found in newly developed OTDRs. Figure 2 illustrates the contrast between OTDR traces taken from a trunk fiber and a loop fiber.

Optical Power Meter

Optical power meters have been traditionally used in measuring the end-to-end loss. Because of the smaller loss budget and potential duplex transmission in a fiber loop, some new features including dual wavelength operation (at 1300/1550 nm) and automatic zeroing become very useful. The operation of some optical power meters may require separate sources. In most cases, memory or storage capabilities of loss values save time and assure that accurate readings will be recorded. An RS-232 interface option will also be advantageous in the loop since it allows all modes and parameters to be controlled externally, and all stored values to be down-loaded into a computer for future reference or analysis.

Since either OTDR or power meter will likely be used in the final acceptance testing, convenience in storing and retrieving test results for possible restoration work is an important consideration of OSP testing. Due to the large amount of fibers

being placed in a fiber loop network, management of these fibers is crucial and should be mechanized.

ORL Test Set

The ability to test ORL on individual connectors or the whole span will be a requirement for many high bit-rate and AM transmission systems because of the high sensitivity of some laser sources to optical reflection. Due to the variability in ORL performance of connectors, ORL testing should be included in most OSP testing. This feature could be incorporated into an OTDR or an optical power meter. Some stand-alone ORL instruments have recently become available.

Fault Finder

A fault finder is a portable, low cost instrument which provides digital read-outs. It can detect and identify both reflective and non-reflective faults, and can give a read-out of the distance to the fault or the end of cable. This unit would be useful for testing in the local loop – for example, it can be used during restoration work. It will supplement an OTDR when equipping the crew with more sophisticated instruments may not be practical in an emergency. Besides the loss reading, a unit which provides an ORL reading will be more attractive.

Visual Fault Locator

A visual fault locator can send a visible light into a piece of fiber so fiber breaks or high loss faults can be visually observed. Examples of such faults include poorly polished connectors, splices with high losses, and microbending losses in a splice tray or other areas.

Optical Fiber Identifier

This instrument commonly used in a trunk network will be useful in the local loop as well. An example of its applications is to identify fibers in a working cable for new construction or restoration. During restoration, the splicer would have to ensure that a live fiber is not being worked on. A source would be required on a non-working fiber.

Microscope

A high magnification, easy-to-operate microscope would be of considerable value when inspecting the finish of field-installed connectors.

Based on our understanding of the performance requirements for a fiber loop, we have evaluated test equipment, data management and staff training issues for OSP testing. With the accumulated knowledge of OSP test results and system performance, OSP testing will continue to evolve so fibers can be brought to the subscribers more reliably and economically.

CONCLUSION

In conclusion, the optical testing requirements in the local loop are more diverse than those in the trunk network. Many testing techniques and instruments have been evaluated. With the progressive evolution of fiber in the local loop and the introduction of more fiber optic components (such as splitters, couplers, isolators and attenuators), OSP testing will become more complex. We will continue our evaluation following the evolution of the loop network and the development of new test instruments.

REFERENCES

1. Special issue on *Subscriber Loop Technology*, J. Lightwave Technology, 7, No. 11 (1989).

2. F. Fleming and T. Wei, "Splices by the dozen," Telephony 218, No. 16, 166 (1990).

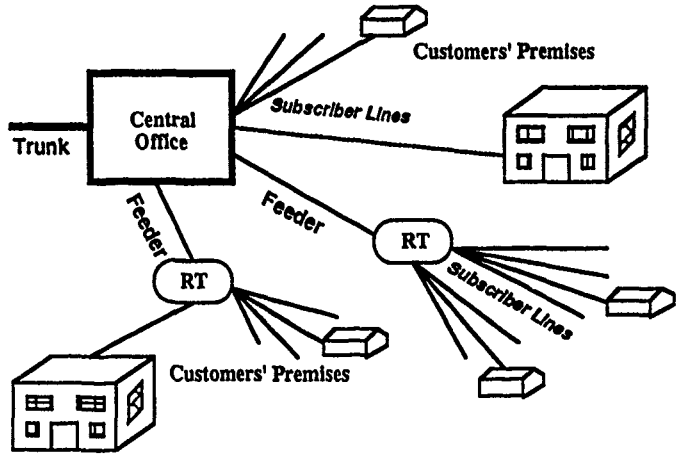

Figure 1. Optical fiber network

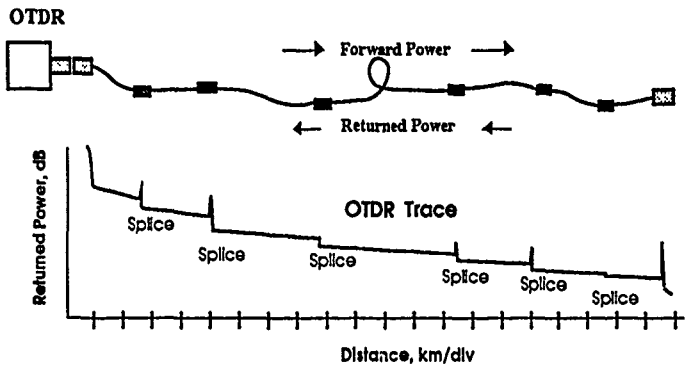

(A) Schematic of OTDR trace between two COs in a trunk fiber

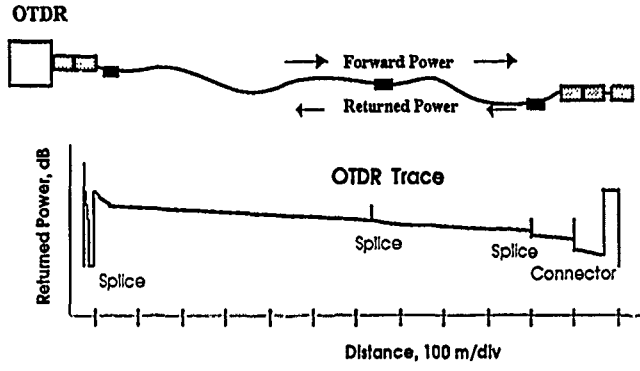

(B) Schematic of OTDR trace between CO and DT in a loop fiber

Figure 2. Schematic of OTDR traces: (A) trunk fiber and (B) loop fiber.

T. (Mike) Wei is Research Supervisor – Optical Fiber Research, GTE Laboratories, Waltham, Massachusetts. After receiving a Ph.D. in physics from the University of Pennsylvania, Mr. Wei joined 3M Company in 1978 where he conducted research in fiber optics. In 1984, he joined GTE where he is responsible for fabrication, characterization, and reliability studies of optical fiber and components.

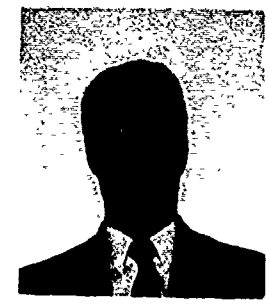

Mike Morrison is Service Manager – Advanced Operations Testing, GTE Telephone Operations, Cerritos, CA. He received a B.S. from the California State Polytechnic University and an MBA from the University of La Verne, CA. At GTE, Mr. Morrison is responsible for managing the service operations of the test bed facility.

Fred Fleming is Senior Analyst – OSP Construction, GTE Telephone Operations, Cerritos, CA. After four years in the military, he attended Suffolk University, MA, before joined New England Telephone as an OSP engineer. In 1977, Mr. Fleming joined GTE where he is responsible for the OSP construction.

Craig Weckesser is Engineering Manager – Advanced Operations Testing, GTE Telephone Operations, Cerritos, CA. He received a B.S. in electrical engineering from the University of Iowa. Mr. Weckesser joined GTE in 1973, where he is responsible for managing the engineering and installation of the test bed facility.

Design and Evaluation of Automatic Optical Fiber Operation Support System

Hidetoshi TAKASUGI*, Nobuo TOMITA*, Takuya UENOYA*
Ikuo NAKAMURA** and Yutaka YOKOO**

*NTT Network Systems Development Center
Chiyoda-ku, Tokyo, 100, Japan
**NTT Operations Systems Development Center
Kawasaki-ku, Kawasaki-shi, Kanagawa, 210, Japan

1 Abstract

The design and performance evaluation of an Automatic Optical Fiber Operation Support System is described. This system has been developed to carry out several tests on optical fiber cable networks automatically by remote control without interrupting services. The system functions are evaluated in a system which is specifically assembled so a trial. OTDR measurement is successfully achieved for an operational optical fiber line without increasing the error rate of transmitted signals. Also, the dynamic range of the OTDR measurements approximately 10dB. Cable or transmission equipment faults are clearly and separately distinguished.

2 Introduction

In order to satisfy customer demands for various services, fiber optics transmission systems have played a vital part in subscriber lines. Recently NTT has started to introduce the Central Terminal / Remote Terminal (CT/RT) system which provides basic plain old telephone services and ISDN services[1] and also introduced single-mode optical cables with multiple fibers into subscriber loops[2]. Although optical cable installation is rapidly increasing as an infrastructure of subscriber networks, an effective operation system has not yet been introduced for optical fiber lines. Therefore, we are facing to increasing problems related to the operation and maintenance of fiber lines. They are as follows :

(1) There has been an increase in the time required for the testing and maintenance of optical fiber cables due to manual operation.

(2) Currently, distinguishing between faults in fiber lines and those in transmission equipment is undertaken manually. This is very difficult to accomplish quickly and therefore makes the system less reliable for customers.

3) As subscriber loops line have become more extensive, and the number of optical fibers in a cable has increased, the administrative paperwork required for handling fiber plant information has become so great that its limit has almost been reached.

For better optical fiber network reliability and more effective fiber operation, the optical fiber subscriber network itself should have an operation system that can monitor the fiber line in service. In this paper, we describe the design of an Automatic Optical Fiber Operation Support System (called AURORA) and evaluate the system performance. This system is designed to measure optical fiber characteristics automatically without interrupting services. To evaluate the performance of the system, we checked the dynamic range of an optical time domain reflectometer (OTDR) measurement, the influence of the testing light on transmission quality and the capability of the fault distinction device. The configuration of each component and assessments of optical characteristics are also mentioned here.

3. System Design and Function

3.1 Basic Configuration

Figure 1 shows a schematic overview of the system. It consists of a test controller, a fiber selector, an optical branch module, a filter-

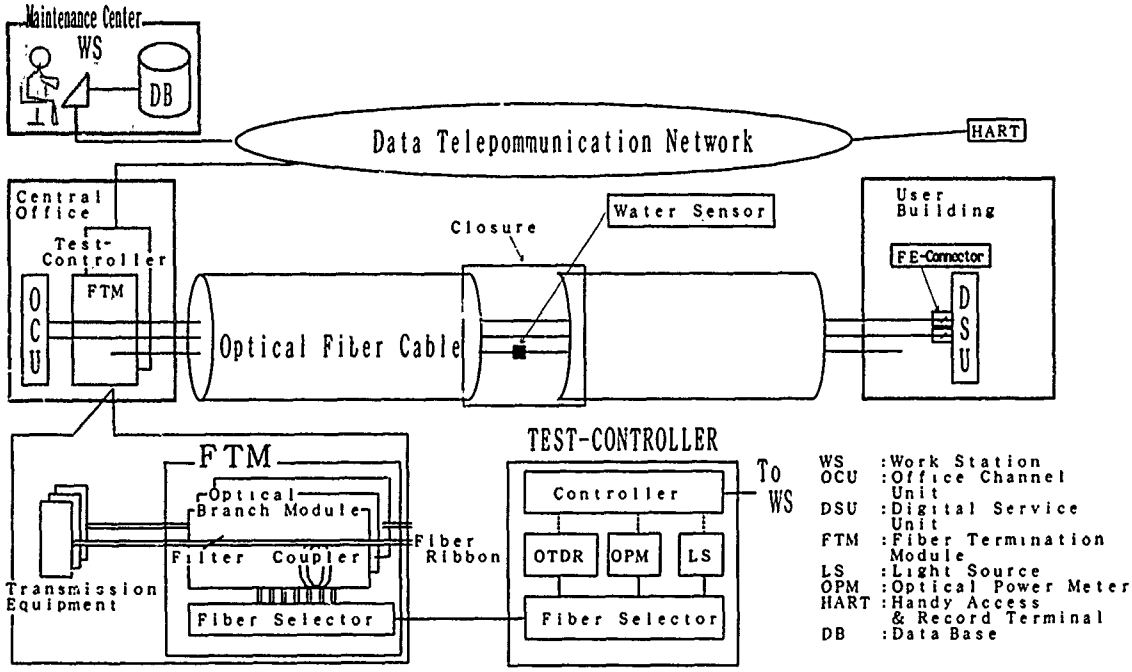

Fig.1 Schematic overview of the AURORA

embedded (FE)connector, a water sensor module, and a work station(WS). The WS, which is composed of a personal computer and a data base, commands the test controller and administers fiber information. The test controller, which is shown in Fig.2, is composed of a personal computer, a data base, an OTDR, light sources for optical loss measurement and fiber identification, an optical power meter and a fiber selector. The computer controls several testing devices through GP-IB commands, and processes the test data before storing then in the data base. In addition, this controller can be commanded by a Handy Access and Record Terminal(HART) which is carried by a field engineer.

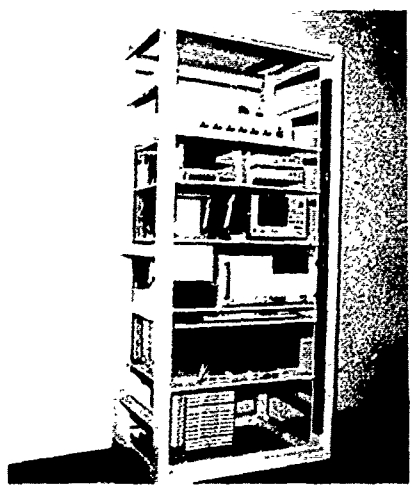

Fig.2 Photograph of Test-Controller

3.2 Components

(1)Optical Branch Module

Figure 3(a) and 3(b) show an optical branch module which is composed of optical couplers, filters and an accommodation box. Test lights are injected into an in-service fiber line through this coupler. The splitting ratio of the coupler between the communication and test passes was set at about 8 to 2, taking into consideration the dynamic range of the measurement capability, and the loss estimation of the communication line. Furthermore, for the transmission and test wavelength to be arbitrarily set within the bandwidth, the ratio is set flat at the wavelength band of 1.25μm to 1.65μm. The optical characteristics of the optical branch module are summarized in Table 1. The average optical losses for the communication pass and test pass are 2.28dB and 7.96dB, respectively.

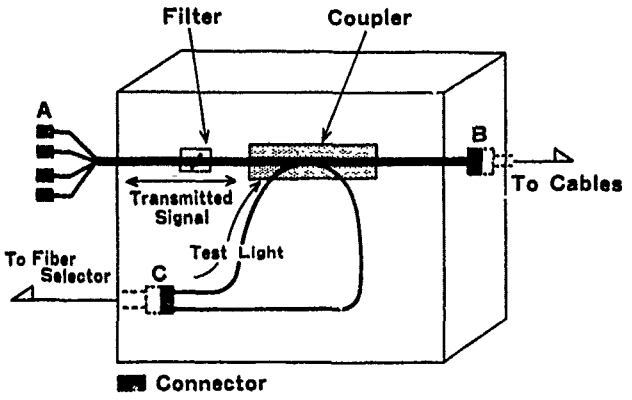

Fig.3(a) Structure of Optical Branch Module

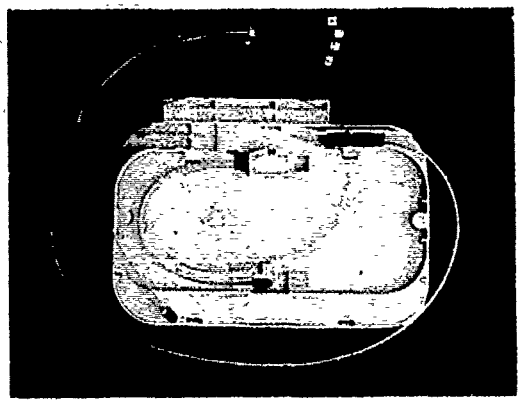

Fig.3(b) Photograph of Optical Branch Module

Table 1 Optical Characteristics of Optical Branch Module

Optical Loss	Average (dB)	Standard Deviation	Maximum (dB)	Minimum (dB)
communication ports at 1.31 μm	2.28	0.43	3.19	1.39
Test ports at 1.31 μm	7.96	0.50	9.15	6.81
communication ports at 1.55 μm	---	---	---	51.32

Communication pass : A - B in Fig.3(a) , Test pass : C - B in Fig.3(a)
Sampling Number : 118

(2)FE connector

Figure 4 shows the structure of the FE connector. An optical wavelength separation filter is inserted in the connector. The filter was designed to allow a 1.3μm wavelength transmitting signal to pass and to block and reflect a 1.55μm wavelength test light. For the FE connector to be used to detect the faults, it is necessary to

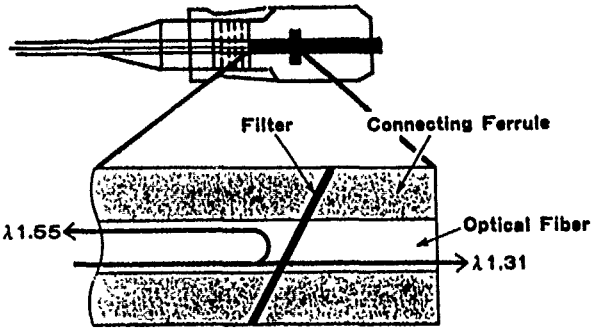

Fig.4 Structure of FE Connector

Table 2 Optical Characteristics of FE Connector

Wavelength (μm)	Reflection attenuation(dB)		Insertion loss(dB)	
	Required	Measured(n=5)	Required	Measured(n=6)
1.31	>22	x=26.5, min=24.9	<0.6	x=0.45, max=0.49
1.55	<10.5	x=8.75, max=9.92	>54	x=56.2, min=55.2

control the volume of test light back-reflection from the filter. Initially, the peak reflection distance and intensity from the FE connector are measured by using an OTDR and stored in data base. When trouble occurs in an outside section, the system measures the values of the FE connector again and compares them with the initial ones. If the comparison reveals differences between the initial and measured values, this indicates that a line fault has occurred. If not, it indicates transmission equipment trouble. The minimum attenuation of Fresnel reflection is about 14.3dB when a fiber is cut as a mirror. Therefore the volume of back-reflection attenuation at the FE connector should be below 10.5dB for the test wavelength, taking into consideration the margin of 3.8dB for changes in the OTDR and fiber selector characteristics. Optical characteristics of the FE connector are summarized in Table 2.

(3) Fiber selector

Two types of fiber selector have been designed. One type is an Mechanically Transferable (MT) connector[3]. The other is an Single fiber Coupling (SC) connector[4]. The MT-type, which is set into a Fiber Termination Module(FTM), selects

a test fiber ribbon with an MT connector, and the SC-type, which is set into the Test-Controller, selects a test fiber in a test fiber ribbon. The schematic structure of the MT-type fiber selector is shown in Fig. 5. It is composed of fiber ribbon cord with MT connector ferrules which are set onto a plane in a 10 x 25 matrix and an access head with an MT connector ferrule. MT connector ferrules in the matrix have two guide-holes and that in the access head has guide-pins to facilitate the alignment of the fiber ribbons. This selector can accommodate a terminated cable of up to 1,000 fibers at the matrix. The optical and mechanical characteristics of the fiber selector are shown in Table 3. The average connecting loss of the selector was 0.34dB with a maximum of 0.75dB. The loss fluctuation of the selector was examined in a repeated switching test (up to 10,000 times) as shown in Fig.6. It is found that the loss fluctuation is less than ±0.2dB and that the selector remains stable after repeated switching.

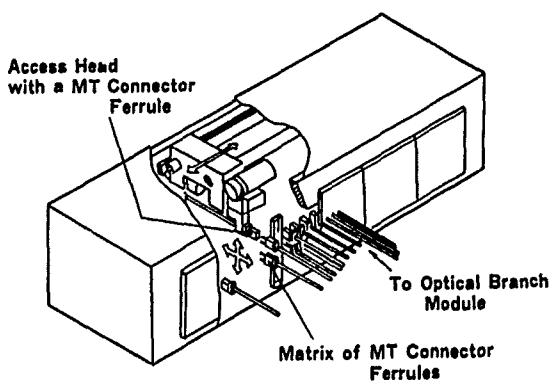

Fig.5 Structure of MT-type Fiber Selector

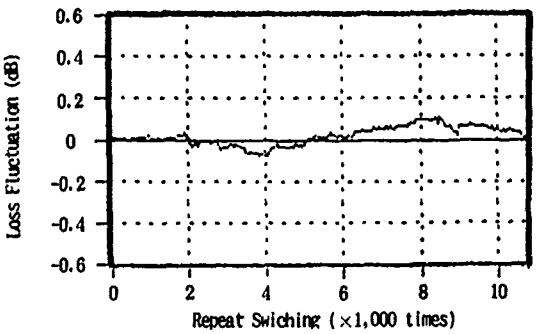

Fig.6 Fluctuation of Connecting Loss for Repeat Switching

(4)Water sensor module

The water sensor module[5] is set on a monitoring fiber inside a mechanical closure. When water leaks into the closure, absorbent material expands and bends the monitoring fibers giving them additional optical loss. The bending loss was designed to be over 2dB in order to make the loss increase clear. Then water can be detected by monitoring the bending loss by using the OTDR.

3.3 System dynamic range

In the OTDR test, the system dynamic range can be calculated[6] from :

$$D = (D_o - X_1 - X_2) \quad (dB) \qquad (1)$$

where, Do is the dynamic range of the OTDR which is defined here as a one-way loss conversion value at the peak noise level of the OTDR signal. In the OTDR, D_o is 24.7dB at a pulse width of 1μsec. and a wavelength of 1.31μm. X_1 is coupling loss which is estimated at 11.2dB including losses in both the fiber selector and the optical branch module. X_2 is the margin of measuring resolution which corresponds to the margin of the S/N ratio. When the resolution R is assumed to be half the noise width of the optical loss waveform from the OTDR, X_2 is given by :

$$X_2 = -5\mathrm{Log} (10^{R/5} - 1) \quad (dB) \qquad (2)$$

Table 3 Characteristics of Fiber Selector

Item	MT-type		SC-type	
	Targets	Results	Targets	Results
Connecting loss	≦ 0.95dB	Ave. 0.34dB Max 0.75dB	≦ 0.45dB	Ave. 0.11dB Max 0.28dB
Loss Fluctuation	≦±0.2dB	≦±0.2dB	≦±0.15dB	≦±0.15dB
Reflection Attenuation	≧28dB	Ave. 34dB Min 30dB	≧30dB	Ave. 36.2dB Min 35.3dB
Switching Speed	Ave. 10sec Max 15sec	Ave. 10sec Max 15sec	Ave. 10sec Max 15sec	Ave. 6sec Max 9sec

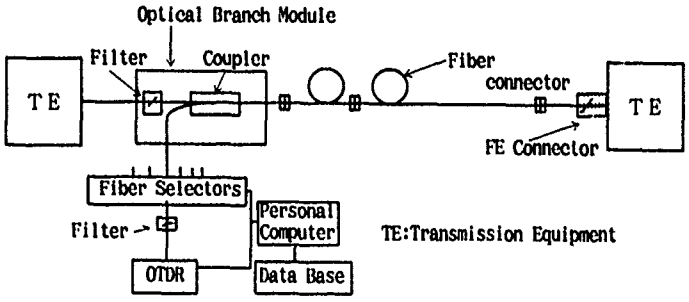

Fig.7 Experimental Configuration for System Evaluations

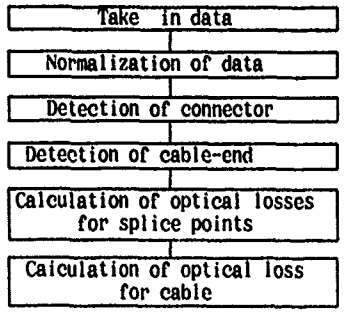

Fig.8 Flow of Automatic Process for OTDR Waveform

Therefore, in the system, the dynamic range of the OTDR test is calculated to be 10.6dB where R is 0.5dB.

4. System Evaluation

4.1 Automatic Processing of OTDR Waveform

The system's automatic processing and its dynamic range of optical loss measurement using OTDR were evaluated using the experimental configuration shown in Fig. 7. The OTDR measurement was carried out at a wavelength of 1.31μm, a pulse width of 1μsec. and for an averaging time of 120sec. The automatic process was driven as shown in Fig.8. Figure 9 shows the results of the evaluation. The dotted line represents the optical loss waveform in the fiber line measured with OTDR. The solid line represents an automatically processed result. It is clear that the solid line agrees well with the dotted line. Figure 10 compares manually processed data and the automatically processed data from the dotted line in Fig. 9. These results indicate that the automatic measurement of the OTDR function has a dynamic range of 10dB, when the permitted error is under 0.5dB. Furthermore, the dynamic range corresponds well with the results discussed in 3.3.

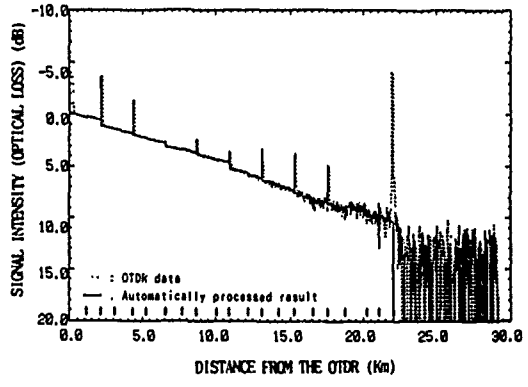

Fig.9 Waveform of OTDR Measurement and Automatic Process Result for OTDR Data

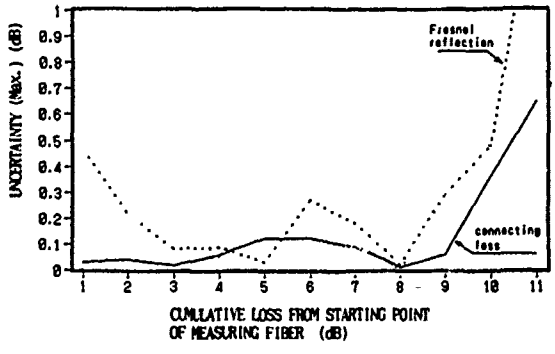

Fig.10 Differences Between Manually and Automatically Processed Results of Cable Connection Points

4.2 Influence of test light on service

In order to evaluate the influence of the OTDR test light on transmission quality, signal error rates were examined using the experimental configuration shown in Fig. 7.

Transmission units of F100M and CT/RT were employed in the examination. Line rates of the units are 100Mb/sec. and 6.3Mb/sec.

Figure 11 shows the error rate results. Transmitting signals were measured using pseudo-random pattern. Squares and circles in the figure indicate the error rates when the OTDR test light was on and off, respectively. From this figure, it is found that both error rates are the same, and this indicates that there is no reduction in transmission quality due to the test light.

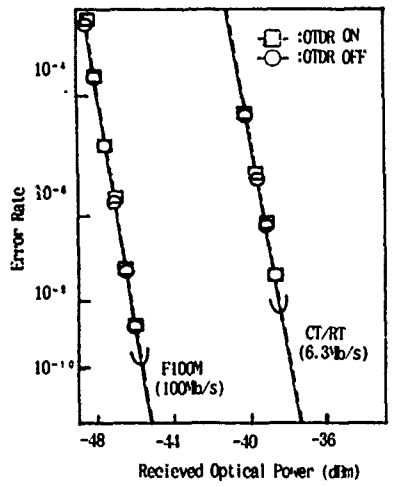

Fig.11 Comparison of Error Rates When OTDR is Off and On

4.3 Faults Distinction

The back-reflection of the FE connector was measured for a fiber broken by bending and for the disconnection of the MT connector, using the experimental setup shown in Fig. 7. Measurement conditions for the OTDR were a pulse width of 20nsec. and a sampling distance of 1.0m, in order to increase distinction accuracy. The measured OTDR waveform is shown in Fig. 12, where, a FE connector was used which had the maximum back-reflection attenuation for 1.55μm shown in Table 2. From Fig. 12 it can been seen that abnormal states are the noise level for a fiber broken by bending and 2.3dB smaller than the normal state for the disconnection of the MT connector Therefore, it is found that faults between fiber lines and transmission equipments can be satisfactorily distinguished by the difference between normal and abnormal optical characteristics of the FE connector.

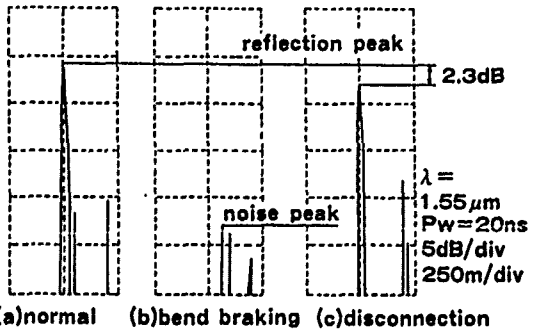

Fig.12 OTDR waveform of Fault Distinction Experiments

5. Conclusion

In order to promote the effective operation and maintenance of optical fiber lines, the AURORA and related components were designed and their performance evaluated. The trial system achieved the following results :

Characteristics of each component achieved to the levels of target. The fiber selector remained stable after repeated switching. The system dynamic range for the OTDR test function was 10dB, when the permitted error of measurement value was under 0.5dB.

Faults between in a fiber line or in a transmission equipment were clearly distinguished.

Therefore, the big reduction of the construction and maintenance time of optical subscriber line is expected by the AURORA. Furthermore, preventive line maintenance which assists the estimation of line degradation and need for cable renewal has the potential to be realized by periodic tests while usual service continues.

Acknowledgments

The authors are grateful to Mr. I. Sakakibara, general manager, Mr. M. Miyama and Mr. F. Takaesu, executive engineers in the fiber optics local network systems project group, for helpful advice.

References

(1) S.Takashima, "Introduction of Fiber Optic Subscriber Networks", JTR,vol.30 No4,1988.

(2) M.Kawase et al.,"Subscriber Single-Mode Optical Fiber Midspan Access", J. lightwave Techol. vol7. Noll pp.1675-1681,1989.

(3) S.Nagasawa et al.,"Mechanically Transferable single-mode Multifiber Connectors", 21c2-1, IOOC'89, pp.48-49,1989.

(4) E.Sugita et al.,"SC-Type Single Mode Optical Fiber Connectors", J.Lightwave Technol.vol7. Noll, pp.1689-1696,1989.

(5) S.Tomita et al.,"Water-Sensor with Optical Fiber", J.Lightwave Technol.,to be published

(6) N.Tomita, et al.,"Automatic Remote Optical Fiber Line Test and Administration System Design", in 1990 Spl.Nat.Conf. Rec.Common. IECE, Japan, NO.B-888.

Hidetoshi Takasugi

NTT Network Systems
Development Center

Tokyo,Japan

Hidetoshi Takasugi received his B.E.and M.E. degrees in materials science from Tsukuba University in 1985 and 1987. He joined NTT in 1987. He is Staff Engineer of Fiber Optics Local Network Systems Project Group in NTT Network Systems Development Center.

He is a member of the Institute of Electronics, Information and Communication Engineers of Japan.

Takuya Uenoya

NTT Network Systems
Development Center

Tokyo, Japan

Takuya Uenoya received his B.E. and M.E. degrees in electrical engineering from Waseda University in 1971 and 1973. He joined NTT in 1973. Since 1989 he has been General Manager of the Telecommunications Cable Systems and Outside Plant Project Group, Where has Developed metallic and optical fiber cable systems.

He is a member of the Institute of Electronics, Information and Communication Engineers of Japan.

Nobuo Tomita

NTT Network Systems
Development Center

Tokai, Ibaraki, Japan

Nobuo Tomita received the B.E. and M.E. degrees in electronics engineering from Kumamoto University in 1972 and 1974, and the Ph.D degree in information engineering from kyusyu University in 1988. He joined NTT Ibaraki Electrical Communications Lab. in 1974, and was engaged in research on broad-band and digital subscriber loops and development of construction components of optical subscriber loops. Since 1987, He is engaged in development of operation and maintenance systems for optical fiber lines. He is Executive Engineer of Fiber Optics Local Network Systems Project Group in NTT Network Systems Development Center.

Dr. Tomita is a member of IEEE and the Institute of Electronics, Information and Communication Engineers of Japan.

Ikuo Nakamura

NTT Operations Systems
Development Center

Kawasaki, Kanagawa,
Japan

Ikuo Nakamura received his B.E. degree in electrical engineering from Hokkaido University in 1976. He joined NTT in 1976. Since 1990 he has been Project Manager of Line/Loop systems operations Project Group, where has developed operations Systems for Optical fiber networks.

He is a member of the Institute of Electronics, Information and Communication Engineers of Japan.

Yutaka Yokoo

NTT Operations Systems
Development Center

Kawasaki, Kanagawa,
Japan

Yutaka Yokoo received his B.E. degree in electrical engineering from Shinshu University. He joined NTT in 1979 and was engaged in development of optical fiber cables for subscriber loops. Since 1990 he has been Senior Engineer of Line/Loop Systems Operations Project Group.

He is a member of the Institute of Electronics, Information and Communication Engineers of Japan.

Strictly BEND COUPLER BASED ATTENUATION MEASUREMENT TECHNIQUE FOR LOCAL APPLICATIONS

W. Lieber

SIEMENS AG,
Munich, West Germany

G. Boscher

RXS GmbH,
Hagen, West Germany

Abstract

A new technique for measuring attenuation is presented. The technique is based on the local injection and detection principle which requires no longer access to the fiber end face. The proposed method is independent of coupling conditions and can be applied for the measurement of splice loss, optical fiber attenuation, insertion loss of passive optical components (e.g. couplers) etc.. Due to the fact that the technique is in accordance with the Power-Through Method it takes intrinsic and extrinsic loss mechanisms into account.
A portable field measurement instrument employing the new concept has been developed. The system is described in detail and practical measurement results are shown to illustrate the high accuracy of the technique and its versatility in use with various fiber types, coatings, and colours.

Introduction

The optical attenuation of passive optical components, for example of a splice, a coupler, or a fiber, represents an important measuring quantity. Two techniques are currently used for measuring the optical attenuation in the field: the Optical Time-Domain Reflectometry (OTDR) and the Transmitted Light Measuring Method (Power-Through Method). However, the major disadvantage of both methods is that access to at least one fiber end is an absolute necessity. Therefore both methods do not allow for strictly local attenuation measurements. Nevertheless, a measurement technique, which requires no longer access to the fiber end face has long been overdue. Especially in Passive Optical Networks (PON) for Fiber to the Home (FttH) or Fiber to the Curb (FttC), where the integration of couplers leads to ambiguous OTDR-measurement results, is considerable demand for a local attenuation measurement system.

Therefore this paper investigates a new method for measuring attenuation, which is strictly based on the local injection and detection technique.

Measurement method

Local injection and detection systems (LID) allow the loss measurement of single-mode fiber splices using the "air gap method" by monitoring the transmitted power while aligning and fusing the fiber ends. However, this method is strictly limited to automatic fusion splicing techniques /1,2,3/. It can not be applied neither for measuring losses of fusion splices that have already been produced nor for measuring the attenuation of any other passive optical component, such as mechanical splices or couplers.

It is well known that a conventional light injection and detection system using macrobending mechanisms does not allow for unique attenuation measurements due to the uncertainty of the pertinent coupling efficiencies. Our new system, however, overcomes this problem by utilizing a bidirectional transmission and receiving system. The basic system for measuring the loss of any optical object (splice, fiber, coupler etc.), is outlined in Fig. 1. In a clip-on manner, light is launched on both sides of the object. The signals then propagate crosswise through the object to be measured and are detected on the opposite side. The receiver provides power ratio measurements by simultaneous detection of the signals of both the adjacent and opposite

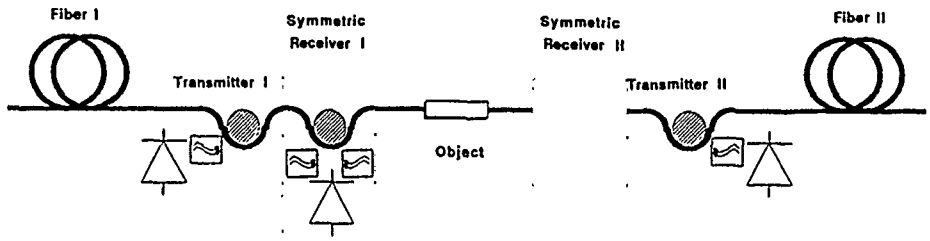

Fig. 1: Basic system for strictly bend coupler based optical loss measurements. The actual system consists of two transmitters and of at least one symmetric receiver.

transmitters. On each side of the object the power ratios are determined. This can be done by using one receiver on each side or more practically by measuring the two power ratios subsequently with the same receiver.

The basic fundamentals for calculating the loss are shown in Fig. 2. Assuming a non perfectly symmetric receiver, the coupling efficiencies for light propagating from the right and from the left are defined as CE_1 (dB) and CE_2 (dB). Let P_1 (dBm) and P_2(dBm) be the launched power from the left and right transmitter respectively, the receiver measures

$$P_{L1}\ (dBm) = P_1\ (dBm) - CE_1\ (dB) \qquad (1)$$

from the left and

$$P_{L2}\ (dBm) = P_2\ (dBm) - a_s\ (dB) - CE_2\ (dB) \qquad (2)$$

from the right. Here a_s denotes the loss of the sample under measurement in dB. Using the same receiver on the opposite side of the sample yields

$$P_{R1}\ (dBm) = P_1\ (dBm) - a_s\ (dB) - CE_1\ (dB) \qquad (3)$$

and

$$P_{R2}\ (dBm) = P_2\ (dBm) - CE_2\ (dB) \qquad (4).$$

Hence it follows

$$a_s\ (dB) = 0.5\ [P_{L1}\ (dBm) - P_{L2}\ (dBm) + P_{R2}\ (dBm) - P_{R1}\ (dBm)] \qquad (5).$$

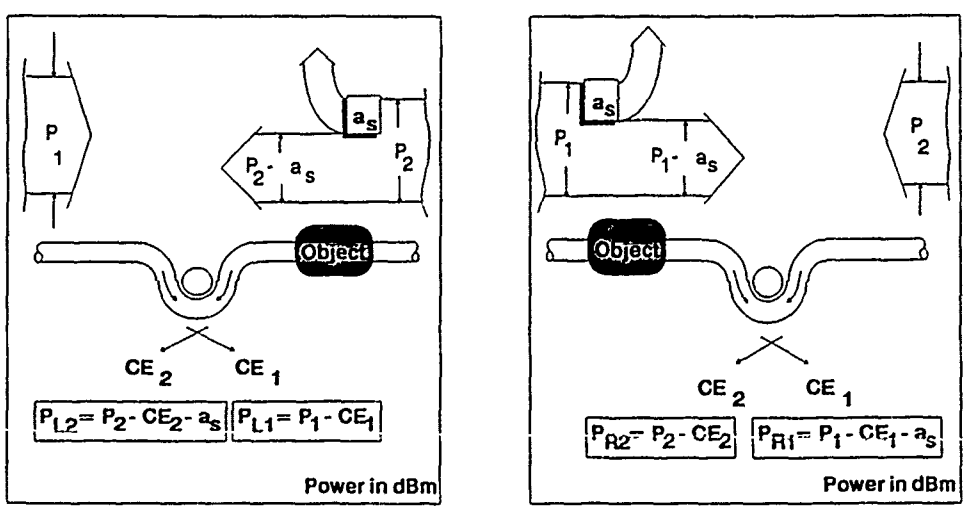

Fig. 2: Measurement of the power ratio at the left and at the right side of the object, respectively

As can be concluded the independence of the coupling efficiencies is obtained by a highly accurate measurement of the power ratio instead of an uncertain singular power measurement. With the power ratios from both sides, the measured attenuation is obtained directly in a unique manner without any additional assumptions.

Results

With the new test set various measurements were carried out for fusion and mechanical splices, fibers, and several passive optical components. Strictly single mode measurements are obtained using 1.3 um LEDs. To verify the independence of the coupling efficiencies a splice between a dark coloured dispersion-shifted and an uncoloured non-shifted fiber was made. Fig. 3 shows the frequency distribution of the measured splice loss. For 50 measurements an average splice loss of 0.28 dB and a standard deviation below 0.02 dB was obtained. The results are in excellent agreement with the two-way OTDR-measurement. Within 0.01 dB no systematic error was evident.

To demonstrate the variety of applications the attenuation of optical fibers and the insertion loss of optical couplers were measured. The accuracy was always found to be the same as indicated in Fig. 3. Further results will be shown during the presentation.

Conclusions

A nondestructive attenuation measurement method for applications where no access to fiber end face is available has been described and verified experimentally. The bidirectional receiving and transmitting technique provides complete independence of the coupling conditions. No systematic errors could be found. The results are always in excellent agreement with OTDR and Cut-Back measurement results.
The equipment can be used in a variety of applications. Nevertheless, first of all it is ideally suited to measure both splice loss in the field after the splice is done, as well as splitting ratios of couplers installed in a system. However, the instrument is also designed to provide attenuation measurements in production and lab environments.

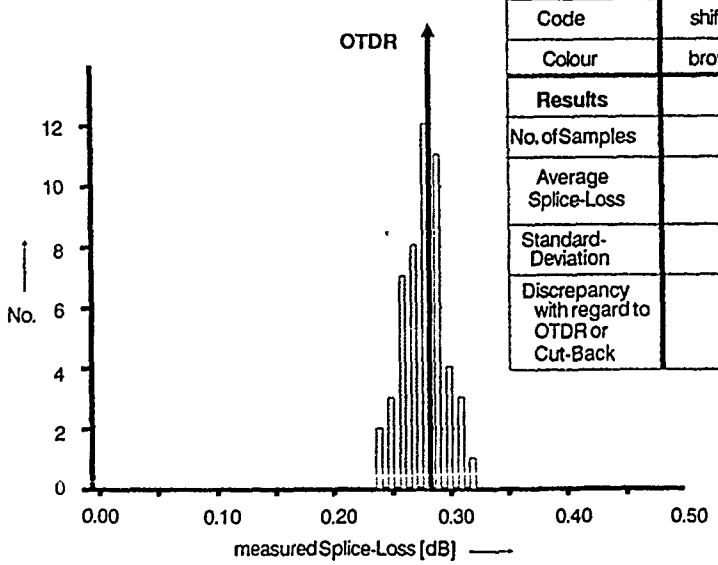

Samples	not identical	
Code	shifted	non-shifted
Colour	brown	uncoloured
Results		
No. of Samples	50	
Average Splice-Loss	0.28 dB	
Standard-Deviation	0.018 dB	
Discrepancy with regard to OTDR or Cut-Back	< 0.01 dB	

Fig. 3: Frequency distribution of the measured splice loss at 1.3 µm between a brown coloured dispersion-shifted fiber and an uncoloured non-shifted fiber.

References

/1/ T. Eder, W. Lieber, M. Heier, "Evaluation of fiber end face tilts during automatic fusion splicing of single-mode fibers" Proceedings of the thirty-seventh International Wire and Cable Symposium, November , 1988, Reno, pp. 407 - 411

/2/ Y. Kato, S. Seikai, T. Tanifuji, "Arc-fusion splicing of single-mode fibers: an apparatus with an automatic core-axis alignment mechanism and its field trial results", Journal of Lightwave Technology, Vol. LT-2, No. 4, August 1984, pp. 442 - 447

/3/ Y. Kato, T. Tanifuji, M. Tokuda, N. Uchida, "New optical monitoring method for arc-fusion splice of single-mode fibers and high precision estimation of splice loss", Electronics Letters, Vol. 18, No. 22, Oct. 1982, pp. 972 -973

Winfried Lieber received his diploma degree and Ph. D degree in electrical engineering from the University of Kaiserslautern, West Germany, in 1983 and 1987, respectively. He was engaged in optical fiber measurement techniques and in propagation problems in dispersion-optimized fibers. His work was concerned with group delay time measurements, cutoff phenomena and optical time domain reflectometry. In 1987 Winfried Lieber joined Siemens AG, Munich, West Germany. From 1987 to 1989 he was responsible for the development of fusion splicing equipment. Since the beginning of 1990 he has been concerned with passive optical components for "Fiber to the Home" activities.

Georg Boscher received his diploma degree in physics from the University of Munich, West Germany in 1967. He joined Siemens AG and worked in several departments. In 1970 he became responsible for development and testing accessories in the Telecommunication Cables Division. Since 1985 he has been working as a deputy director and head of the export sales and marketing department of RXS Schrumpftechnik-Garnituren GmbH, a fully-owned subsidiary of Siemens AG. RXS manufactures and markets accessories for the telecommunication and power industries.

WIRE AND CABLE MATERIAL SELECTION CRITERIA FOR THE 90's . . .

Guerry L. Grune

IBM Corporation, P.O. Box 12195, Research Triangle Park, NC 27709

The Evolution and Testing Methods for Flame Retardancy, Smoke Generation and Toxicity as it Relates to International Cabling Systems

I. INTRODUCTION

Public concern for overall fire safety in offices, high-rise hotels and commercial/industrial buildings has increased markedly due to highly publicized fires. In many cases, these fires have cast public scrutiny toward the wiring systems which allegedly have been the cause of the fires, and/or the propagation of fire between floors and horizontally across offices.

Inherently, today's office building will have a network of vertical and horizontal shafts and plenum areas which act as a medium for flame propagation from floor to floor and department to department. In conjunction with this concern, wire and cable usage and footage installed in buildings have dramatically increased with the advent of computerization. A wide range of twisted pair, coaxial, power and fiber optic cables are installed for a myriad of uses from computer terminals to telephones, from lighting to emergency alarms. These systems crisscross today's commercial office buildings and frequently, as new systems are put in, the older cables are often left in the ceiling and walls. Correspondingly, the potential fire hazard associated with cabling systems requires scrutiny.

II. THE EVOLUTION OF FIRE RETARDANT CABLING STANDARDS

In 1975, the National Fire Protection Association recognized a potential fire hazard in the plenum chambers of buildings and adopted, via the National Electrical Code, a standard for fire retardant and smoke suppressed wire and cable products. Since 1975, a hierarchy of flame retardancy has been incorporated in the National Electrical Code. These standards focused on the issues of flame spread and smoke generation based upon the premise that materials used on cables should be inherently flame retardant and should not propagate or foster the spread of fire within a building.

Historically the selection of cables for buildings have involved two fundamental criteria:

1. Mechanical Properties
   ie. Tensile strength, Flex Modulus, etc.

2. Electrical Properties
   ie. Volts/mil., Dielectric Constant, etc.

The advent of the aforementioned standards brought the issue of flame propagation and in the case of the U.L. 910 plenum test smoke generation to the forefront and placed a third criteria in the lap of the cable design engineer.

As we are all aware, materials selection is a series of trade-offs and every commonly used material has a unique combination of desirable characteristics and practical limitations. For example, polyethylene met these mechanical and electrical criteria very well in most wire and cable applications but its poor performance with respect to ignitability and flame propagation have fostered the use of more flame retardant materials such as polyvinylchloride and fluoropolymers.

During the 1980's, the U.S. continued to focus on the enforcement of the National Electrical Code specifications for flame retardant and smoke suppressed cabling materials. The test for flame retardancy from most severe to least severe are as follows:

* U.L. 910 Steiner Tunnel Test/CSA FT-6; Horizontal flame spread and smoke density measured

* U.L. 1666 Riser Test; Vertical flame spread

* U.L. 1581 Test/CSA FT-4 Vertical tray

* VW-1 Bunson Burner Flame Test Applied to single vertical wire

Recently the Canadian Standards Association adopted relatively similar standards with CSA FT-4 (similar to U.L. 1581) and FT-6 (same as U.L. 910).

III. THE INTERNATIONAL DEBATE. . . HALOGEN MATERIALS VERSUS NON-HALOGEN MATERIALS

The use of halogen containing materials; polyvinyl chloride, fluorocarbons, or polyolefins compounded with chlorine or bromine are the predominate cable materials used based upon their inherent flame retardancy and efficiency in meeting the flame and smoke requirements as developed by the National Fire Protection Association and Underwriters Laboratories.

Materials Selection And Flame Retardancy

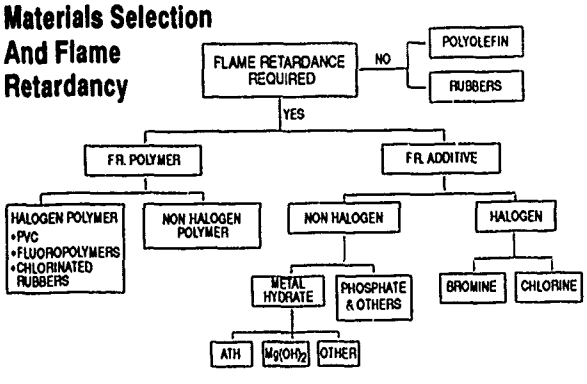

This chart provides a guide to generic materials selection based on flame retardancy.

From a more global sense, the harmonization of specifications for North America are distinctly different standards in contrast to the evolving European standard cables used in office buildings. The trend in North America toward optimizing the flame retardant characteristics of cables has not been the case in Europe. The Europeans have been focusing on "zero halogen" cabling systems and are fostering this trend in their specifications. In brief, their cable specifications place less stringent standards on the ignitability and propagation of flame to attain the objective of zero halogen or "LSHF" Limited Smoke/Halogen Free.

From a global sense, we must determine what is in the best public interest and the criteria by which halogen free cables are judged safer.

Certainly, as we move toward harmonization of standards and cabling systems in a world market, a set of criteria must be developed that assesses fire hazards for the civilian public.

IV. DEVELOPING STANDARDS FOR A TOTAL FIRE HAZARD ASSESSMENT

The conclusion reached by the Committee on Fire Toxicology[13] in their paper "Fire & Smoke - Understanding the Hazards" points us toward a total fire hazard approach to materials selection. Some conclusions from the text include;

"Carbon monoxide is well accepted as a factor in 50% to 80% of all fire fatalities"

"Other compounds such as hydrogen cyanide and its contribution to toxic hazard is uncertain."

Finally, "Fire hazard assessment to estimate the ability to escape a given fire is currently the best approach to measuring the fire hazard associated with materials."

These conclusions point squarely toward the development of material standards which have a total fire hazard assessment approach and that is:

- Flame Spread Ignitability & Propagation
- Visible Smoke Density & Generation
- Toxic Potency

It is noteworthy that toxic potency is an issue associated with office buildings, public facilities (auditoriums) and industrial plants. The issue of corrositivity and its measurement relates more to the

survivability of electronic equipment such as in military installations, naval ships and equipment.

In this context, an overall material selection criteria can be developed based on reviewing the currently accepted test methods for flame, smoke, toxicity and corrositivity.

V. FLAME RETARDANCY - IGNITABILITY & PROPAGATION

Assessing global standards for a total fire hazard assessment, the predominant and accepted test methods for North America (U.S./Canada) and Europe are noted as follows:

Fire Hazard Test Methods

Fire Hazard CRITERIA	NORTH AMERICA	EUROPE
Ignitability	Oxygen Index (ASTM D-2863)	IEC 332-3 Appendix A
Propagation	Vertical Tray UL 1581	IEC 332-3
Smoke	NBS Chamber (ASTM E-662)	3 Meter Cube (IEC 20(CO)178)
Toxicity	New York State (Univ. of Pittsburg)	ISO Guide TR 9122
Corrosivity	ASTM Copper Mirror Test	IEC 754-1

In the case of the North American market, a hierarchy exists for cables beyond "General Purpose" with the riser and plenum cable tests being far more severe.

Wire And Cable Flame Propogation Tests

CABLE APPLICATION	QUALIFICATION TEST	FLAME ENERGY
Plenum	UL 910 (Steiner) CSA FT-6	300,000 BTU/Hr
Riser	UL 1666	527,000 BTU/Hr
General Purpose	UL 1581 Vertical Tray IEEE 383 CSA FT-4 IEC 332-3	70,000 BTU/Hr

The general purpose test could be viewed as a test method, that with minor differences, would have a general global acceptance.

Global Differences In General Purpose Flame Test Method

PARAMETER	IEEE 383 (UL 1581)	FT-4	IEC 332-3
Burner Angle From Horizontal	0°	20°	0°
Cable Spacing	1/2 Cable Diameter	1/2 Cable Diameter	Based on Volume
Enclosure Size	Not Specified	Not Specified	1x2x4 Meter
Propagation	2.4 m 96"	1.5 m 59"	2.5 m 98"
Smoke Generation (UL Proposal)	< .1 Peak Meters Squared Per Second < 25 Meters Squared Over 20 Minute Test	None	None

VI. SMOKE GENERATION

Smoke, the visible bi-product of fire, can obscure the exit path as well as disorient people in a fire. There are several test methodologies for smoke measurement which include the frequently referenced ASTM 662/NFPA 258 and BS 6401 or NBS Smoke Density Chamber Test.

Internationally, the IEC 20(CO)178, often referred to as the London underground or three meter cube test, is similar to that of the NBS test. There are several other available test methods which aid in the development of our fire hazard assessment. These test methods will help provide a relative comparison of materials used for wire and cable.

In the U.S., the National Electrical Code has included a provision for Limited Smoke or "LS" cables. Currently, Underwriters Laboratory is working on a test method and standard; the proposed U.L. 1685 standard fire test for Limited Smoke cable will set smoke standards for cables burned in the General Purpose U.L. 1581 test. This is a definitive step toward a broader view in assessing the fire hazard.

It should be noted that these test methodologies along with the U.L. 1685 proposal provide definitive results in assessing a materials' smoke characteristics. Historically, the combustion of PVC created a dense and dark smoke. Based on the evolving plenum standards and the prospects of smoke standards for general purpose and riser cable, a new generation of reduced smoke compounds from flexible PVC producers is now available.

Smoke Properties Of PVC Samples Tested By ASTM E662 NBS Smoke Chamber

PVC MATERIAL TYPE	FLAMING (Dmc)	SMOLDERING (Dmc)
General Purpose Jacket Grade Type CM, CL-2	740	280
Reduced Smoke Grade General Purpose Jacket Grade Type CM, CL-2	280 △ = 164%	170 △ = 53%
Riser Cable Jacket Grade Type CMR, CL-2R	670	240
Reduced Smoke Grade Riser Cable Jacket Grade Type CMR, CL-2R	200 △ = 235%	190 △ = 26%
Plenum Grade Smokeguard Jacket Type CMP, CL-2P	<200	<170

The test data was performed by an independent laboratory for Gary Chemical Corp.

VII. TOXICITY

Toxicity is usually measured by lethality on test animals. It is a quantitative measurement usually expressed as an LC-50 value - or the lethal concentration for a 50% animal mortality. Unlike corrosivity measurements in a fire hazard assessment, it provides a comparison of materials as they could effect the survivability of humans in a fire situation. The variety of materials used by the wire and cable industry to meet the needs of the evolving standards discussed above, if exposed to a fire, would create some combination of toxic gases.

For the last two decades, many toxic potency test methods have been developed. The most predominant are noted in references 14 through 17. The debate over test methods for the ranking of materials and the actual fire scenario will most likely continue for decades.

Nevertheless, the University of Pittsburgh protocol, adopted by the State of New York for its uniform fire prevention and building code, Article 15, Part 1120, created a data bank unlike any other previous studies on the toxic potency of materials used in wire and cable.[2]

*Toxicity Test Results**

Major Materials Categories
Single Material Type

Material Class	LC_{50}, Grams
Fluoropolymers	8.9
Polyolefin	9.9
PVC	17.6
Hydrocarbon Rubber	18.4
Chlorinated Rubber	22.7

University of Pittsburg Test Protocol

There continues to be much debate about the test but it demonstrates that extremely toxic materials (LC 50 less than one gram) are rare and the dominant generic materials used in wire and cable fell in a range of 8.9 to 22.7 grams. In addition, the chlorinated materials faired better

than the non-halogenated polyolefins and the fluorocarbons.

Integration of this data base of wire and cable materials, with that used in office building and industrial plants, would enable a better assessment of materials selection in an overall fire hazard assessment.

The harmonization of toxicity test methods will be more controversial in the development of a global standard. Most European standards focus solely on halogen content using the IEC 754-1 requirement of 0% HCL halogen content and no bioassay testing. Correspondingly, the European test methods measure the % of acid gases, pH levels or changes in conductivity of a solution.

Relative to the central theme of this paper, it has been a dominant trend in Europe to standardize toward zero halogen materials. Some of this effort is attributed to a London subway fire which occured in the 1970's. The British Naval Engineering Standard 713 was a follow-on to this idea, spurred by the shipboard fires which occurred during the Falklands Islands war with Argentina in 1982. The British and European influences have found their way into international standards organizations, including the IEC Publication 332-2,[10] which addresses the testing of gases evolved during combustion of electrical cables.

VIII. CORROSIVITY

Corrosivity is an issue which is beginning to receive more attention from both the suppliers and users of international cables. Most of the problem is associated with that of the corrosive nature of the off-gases associated with equipment failure especially in critical military hardware that requires the ability to survive during potential fires in military action. Again, this involves halogens such as chlorine, bromine and fluorine, which have been shown to be corrosive, not only to metal surfaces, but also to human tissue. Many tests exist which can help determine and rank the corrosivity of these same off-gases; one of which includes the "copper mirror test" listed in ASTM B 284. This test involves the corrosion of a thin copper film which has been vacuum sputtered onto a flat glass surface. The rate of removal of the copper from this surface is based on the corrosive nature of the gases to which the surface is exposed. Correlation of this type of corrosivity with that of human tissue, however, is still in its infancy.

IX. ZERO HALOGEN VERSUS AN OVERALL FIRE HAZARD ASSESSMENT

Einhorn[9] points out that various products are evolved during combustion of plastics, and suggests that the research of the toxicological aspects of pyrolysis and combustion during fire exposure has lagged so far behind other aspects concerning flammability characteristics of materials that a fair assessment of the toxic hazard cannot be adequately described. Unfortunately, this is still as valid a summation of the evaluation of toxic potency for cabling materials today, as it was in 1975.

In the past 15 years, however political and legal actions in the U.S., Great Britain, Canada and throughout the European continent to alleviate the public's fear of burning plastics have become more dominant than the research efforts to determine the perceived risks.

This emocionalism, which drives specifications to solely assess halogen content may obscure the benefits of chlorine or bromine as it relates to a total fire hazard assessment for cables.

"Zero halogen" may be less of a solution than that of lowering halogen content to gain the optimal insulation or jacketing materials for electrical, mechanical, or fire hazard assessment parameters.

Continued emotionalism on the issue of toxicity and halogen content will cause further confusion and force the cable installer, architect, contractor, and distributor to be used as a pawn in the hands of material suppliers.

In the near term, some guidelines for the building architect and contractor are needed which utilize the most accepted test methodologies for fire hazard assessment and place them in a framework to quantitatively evaluate cabling systems. A formal fire hazard analysis is one that integrates all factors; ignitability, propagation, smoke, toxicity and corrositivity. The better product is the one that has the lower level fire hazard quotient.

The proposed fire hazard assessment quotient is a compilation of these five characteristics with Level 1 assigned to a cable having exceptional performance and Level 2 for that exhibiting minimum acceptable performance. In this framework, a cable must meet at least the minimum acceptable standards in each category to qualify as a low fire hazard cable, "LFHC". The "low net" or "low fire hazard cable" "LFHC" would be the summation of these performance levels divided by five. The lowest net cable being 1 or Level 1 and the minimum acceptable performance 2 or Level 2.

X. SUMMARY AND RECOMMENDATIONS

It is clear that international cabling system standards have evolved considerably during the last 15 years and continue to progress at a faster rate with the beginning of the new European Economic Community in 1992 as a partial reason for this acceleration. It is also clear that for at least the communications cabling market, current plenum U.S. and zero halogen European requirements are incompatible.

An important consideration is to reduce the number of types of cables which must be manufactured for global marketing corporations. Optimally, a cable that met the plenum U.L. 910 test and was zero or low in halogen content would be the best cable in this overall fire hazard assessment quotient and would be desired by cable engineers, building architects and cable installers worldwide. These cable developments, which incorporate good mechanical and electrical properties as well as achieving a better fire hazard assessment, are evolving. For example, Ontario Hydro specification L-891SM-77 includes a low halogen specification optimizing cable properties along with lowering halogen content by measuring acid gas concentration ($\geq$ 14%). Cables such as this low halogen cable are a positive step toward meeting a better overall fire hazard assessment with organic compounds.

This author believes that to achieve cost efficient cables with essentially no perceived fire hazards plus good electrical and mechanical properties, the cabling industry must use a radically different approach in the selection of materials and processes.

In the longer range, organic materials may give way to inorganic polymers and materials the development of which has progressed tremendously since the onset of the space race decades of the 50's and 60's. It is believed that to fully meet the strigent requirements covered in the topics of this paper, any organic system will be insufficient.

Inorganic based polymers have been extruded and reports published[11]. The list includes such exotic sounding names as polyphosphazenes and polybenzamidizoles, - both of which are currently being produced in this country. In an earlier report[12], some other possible jacketing materials for consideration by future minded cable manufacturers were described. Again, the cost/performance equation will balance this trend toward inorganic polymers, but for the short term the truly international cable manufacturer must consider all of the issues to optimize cable design in the framework of an overall fire hazard assessment.

REFERENCES

1. Levin, Fowell, Paabo, Stolte, Maker and Birky., Further Development of a Test Method for the Assessment of the Acute Inhalation Toxicity of Combustion Products, U.S. Dept. of Commerce, NBS, Washington, DC pp. 1-143, June 1982.

2. Anderson and Kopf, Registration Categories of the National Electrical Manufacturers Association for Compliance with the New York State Uniform Fire Prevention and Building Code, Arthur D. Little, Inc., Reference 60050, NEMA December, 1987.

3. Weeks, M., Flammability, Odor, and Offgassing Requirements and Test Procedures for Materials in Environments that Support Combustion, NASA Doc. No. NHB8060.1B Chpts. 1-4, September 1981.

4. Einhorn and Grunnet, The Physiological and Toxicological Aspects of Degradation Products During the Combustion of PVC Polymers, in Flammability of Solid Polymer Cable Dielectrics, EPRI Publication TPS 77-738, Palo Alto, CA, November 1979, pp.3.1.3-48.

5. Glew, Sansone, Gingue, Reduced Smoke and Applicable Compounds, Gary Chemical Literature, November, 1989.

6. Touval, I., Antimony Oxide: Synergism in Flame-Retardants, Plastics Compounding, Sept./Oct., 1982, Reprinted in M&T Chemicals Report - Rahway, NJ.

7. Are Plastics Unsafe? Plastics Technology, pp. 177-185, May, 1982.

8. Raje, R.R., Sciarra, J.J. and Greenberg, L., Schwarts, A. and M., The Acute Inhalation Toxicity in Rats from Pyrolysis Products of Polymeric Materials, J. Combustion Toxicology, 8, pp.45-51, February 1981.

9. Einhorn, I.N., Physiological and Toxicology Aspects of Smoke Produced During Combustion of Polymeric Materials, Environmental Health Perspectives, 11, pp. 163-189, 1975.

10. IEC Publication 332-3, Tests on Electrical Cables Under Fire Conditions, Part 1: Determination of the Amount of Halogen Acid Gas Evolved During the Combustion of Polymeric Materials Taken from Cables, pp.1-16, 1982.

11. Books, J.T., Indyke, D.M., and Muenchinger, W.O., Arylozyphosphazene Elastomers - New Flame Retardant Insulation Materials, International Wire and Cable Symposium Proceedings, pp. 1-4, 1984.

12. Grune, G.L., Materials Requirements for Multimedia Communications Cable, International Wire and Cable Symposium Proceedings, pp. 225-267, 1983.

13. Committee on Fire Toxicology National Academy of Sciences, Fire and Smoke - Understand the Hazard, 12-29, 63-77.

14. Levin, B.C., Fowell, A.J., Birky M.M., Paabo, M., Stolte, A. and Malek, D., Further Development of a Test Method for Assessment of Acute Inhalation Toxicity of Combustion Products, NBSIR 82-2532, 1982.

15. Alarie, Y. and Anderson, R.C., Toxicologic and Acute Lethal Hazard Evaluation of Thermal Decomposition Products of Synthetic and Natural Polymers J. Tox. & Appl. Pharmacol. 51, 341, 1979.

16. Alexeeff, G.V. and Packham, S.C., Use of a Radiant Furnace Fire Model to Evaluate Acute Toxicity of Smoke, J. Fire Sci, 2, 306, 1984.

17. Kimerle, G., Aspects & Methodology for the Evaluation of Toxicological Parameters During Fire Exposure, J. Combust Toxicol. 1, 4, 1974.

G.L. Grune
IBM Corp.
Future Lan Cabling Systems, Dept. H51A
Research Triangle Park, NC 27709

Guerry L. Grune obtained his B.S.M.E. from Duke University, 1978 (graduation with distinction) with a double major (A.B.) in Chemistry the same year. After working for Fiber Industries Incorporated, a subsidiary of Celanses and ICI of Great Britain, from 1978-1980 in the heavy denier polyester filament and liquid crystal high modulus organic fiber groups, he returned to graduate school at the University of Massachusetts. There he obtained his M.S.Ch.E. (1982) from the Departments of Chemical Engineering and Polymer Science and Engineering working under Dr. Robert W. Lenz in the area of thermotropic liquid crystals. Upon finishing his M.S. degree requirements in May 1982, he joined IBM-RTP. In addition to working with the IBM Local Area Network Community, other responsibilities have included corrosive gas testing of components and assisting in the growth of IBM fiber optic compatible products. Currently, he is completing his doctorate in Chemical Engineering at North Carolina State University.

ACKNOWLEDGEMENTS

The author wishes to acknowledge Mr. Charles A. Glew of Gary Chemical Corp. for his contributions to this paper and his ability to make us enthusiastic enough to complete this assignment. The efforts of Tina Sundstrom should also be noted for her assistance in preparing the text of this presentation. In addition, the following IBM colleagues are thanked for their support: Mr. Ray A. Solomon, Mr. John Baltz, Mr. Lee Haas, Mr. Chuck Wright, Mr. Jerry Zeiner, Dr. Inder Wadehra, Mr. Sam Corbett and Mr. Bob Love.

Fire Hazard Assessment Quotient

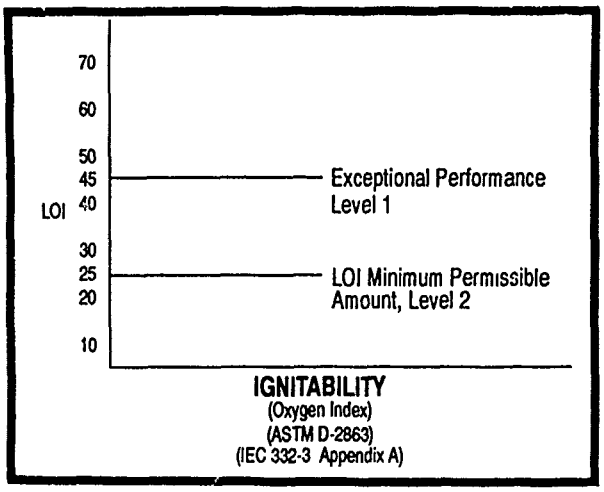

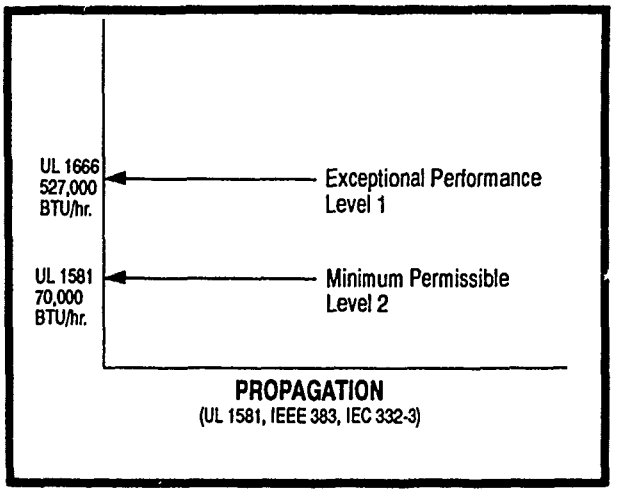

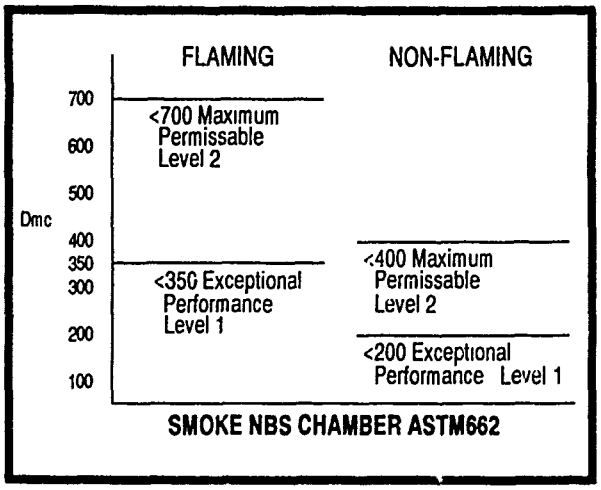

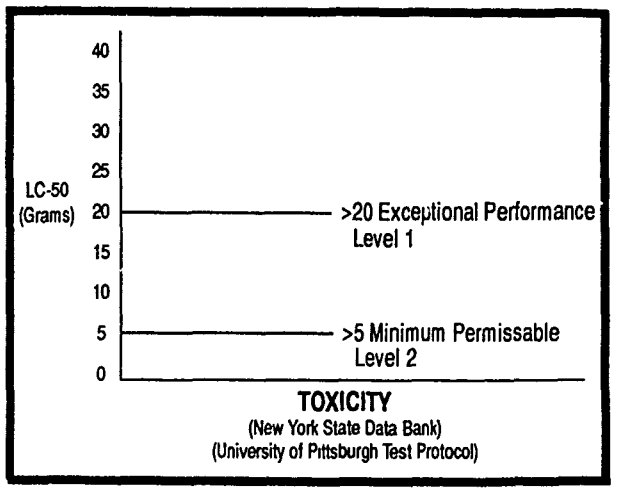

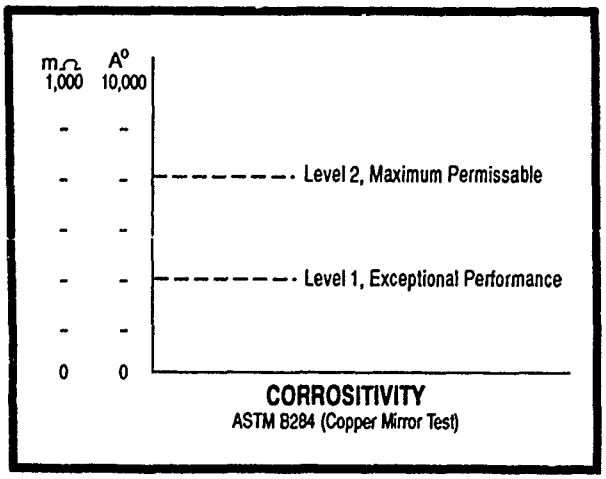

Sum of Levels / 5 =
Fire Hazard Assessment Quotient

Level 1 - Exceptional Performance

Level 2 - Minimum Permissible Performance

FLAMMABILITY TESTING OF NEW VINYL COMPOUNDS WITH LOW FLAMMABILITY AND LOW SMOKE RELEASE IN CABLES

A.W. Coaker, M.M. Hirschler, S. Shakir, C.L. Shoemaker

The B.F. Goodrich Co., Technical Center, P.O. Box 122, Avon Lake, Ohio 44012

ABSTRACT

A set of new vinyl compounds was prepared anticipating the publication of new requirements for limited smoke (.../LS) cables, to provide formulation guidelines. Commercial cables were used as controls and bulletinized compounds were made into TW and THHN tray cables. A new facility built by BFGoodrich to determine full scale fire performance of cables in vertical tray tests (on CSA FT-4) and the cone RHR test apparatus were used on 16 cables. The CSA FT-4 test was used also for measuring continuously heat release, smoke release and mass loss. Some cables had previously been tested at UL. Results in the two facilities showed excellent agreement for clear passes and clear failures. However, a cable rated borderline pass at UL failed in the BFGoodrich facility. Data from the cone correlated so well with cable tray results that the latter could be predicted from the former with reasonable accuracy. The final conclusion was that cables made with bulletinized vinyl compounds or with the other materials tested emitted higher levels of heat and smoke than cables made with the new experimental compounds.

INTRODUCTION

The flammability of cables is often measured in full scale vertical cable tray fire tests. These tests give an indication of real fire performance of cables, in specified scenarios.

It has been well established now that rate of heat release is the most important fire property, because it is a measure of the fire intensity [1,2]. Furthermore, it has been established that fire test results from the cone calorimeter rate of heat release instrument run over a suitable range of incident heat flux correlate well with those from full scale fire tests [3-5].

Most standard cable tray tests, including the one used in this work, tend to measure only the extent of flame spread due to the cables themselves, plus the length of charring of the cables. If cable tray fire tests are run, other fire properties can also be measured, of greater interest for fire hazard assessment [6-11]. The additional properties measured here are heat and smoke release.

A number of vertical cable tray tests had been run at a contract laboratory (Underwriters' Laboratories) in 1989, using three test protocols: CSA FT-4, UL 1581 and ICEA 529-T20. All the same cables had also been tested in the cone calorimeter [12].

A program of work was thus designed with four objectives:

(a) Build a new facility to run vertical cable tray fire tests.
(b) Investigate the full scale fire performance of some advanced vinyl compounds, when made into real cables, and compare them with that of traditional vinyl materials.
(c) Compare the results with several of the same cables previous results obtained using nominally the same test in a different facility.
(d) Test the same cables in the cone calorimeter.

EXPERIMENTAL

Procedures

The test methods used were:

Small scale: Cone calorimeter rate of heat release instrument (exposed area: ca. 0.01 m^2) [13].

Measurements made: The parameters reported from the cone calorimeter tests are: peak rate of heat release (Pk RHR, in kW/m^2), the time to sustained combustion, or time to ignition (TTI, in s), the total heat released (THR, in MJ/m^2), the smoke factor (SmkFct, in MW/m^2), the peak rate of smoke release (Pk RSR, in 1/s), the total smoke released (TSR, non-dimensional), the mass loss rate parameter (MLRP, in g/m^2s^2) and the ratio of time to ignition to peak rate of heat release (TTI/Pk RHR, in s m^2/kW). Some of these variables may not be generally known and they will, thus, all be explained briefly.

Rate of Heat Release: The rate of heat release (RHR) is a measure of the instantaneous amount of heat being released per nominal sample surface area. For each experiment, the maximum RHR value is the most significant one and is recorded here. The RHR values are calculated from the differences between the values of oxygen concentration measured and the background oxygen in the atmosphere.

Total Heat Released: The total heat released in each experiment (THR) per unit nominal sample surface area is determined by integrating the RHR data as a function of time.

Smoke Factor: The smoke factor is a smoke/fire hazard variable used to estimate the potential amount of smoke that a product would generate under full scale fire conditions. It is a realistic approach for such an estimate which takes into account both the potential for smoke obscuration for full sample destruction and the potential to cause other products to burn and release smoke in a real fire. It does so by incorporating the burning rate (as the peak rate of heat release)[14,15]. This takes into account the fact that those products made from materials with low peak RHR will not readily burn up totally in a fire, and will tend to cause less smoke to be generated from the ignition of other products. It is calculated as the product of the ignition of other products. It is calculated as the product of the total smoke released and the peak rate of heat release. The single value presented here is that at 5 minutes. The total smoke released is calculated as the time integral of the rate of smoke release.

Time to Ignition: The time to ignition is the time, expressed in s, until the entire surface of the sample burns with a sustained luminous flame.

Mass loss rate parameter: The MLRP [9,16] is the ratio of (a) the average mass loss rate between the times when the sample loses 10 and 90% of the total mass lost during the test and (b) the time to ignition. It gives an indication of the amount of "smoke" generated in a given amount of time and, thus, of the toxic hazard.

Time to ignition/Peak Rate of Heat Release: This parameter is proportional to the time to flashover, i.e. it may be the best individual indicator of overall fire hazard [17,19].

Full Scale [20,21]: CSA FT-4 cable tray test (70,000 BTU/h: 20.50 kW) [22]

In the full scale tests, measurements taken included: flame height (in cm), heat release (by oxygen consumption [23,24]), smoke release (determined with a laser in the exhaust duct) and mass loss (using a load cell).

Official failure criteria for cable tray tests are based on char length: if the entire cable tray length (UL 1581) or a length over 1.50 m (CSA FT-4) has charred the cable fails.

All cables were tested in the cone calorimeter and the vertical cable tray.

Materials

A total of 16 cables were used, including ten experimental power cables, all based on vinyl compounds, four commercial cables and two experimental communications cables. There were two types for the experimental power cables: THHN and TW. The THHN construction incorporates, of course, a nylon film, as required by the listed construction specifications, extruded over the vinyl insulation, beneath the vinyl jacket. These cables were all made with 9 #12 AWG conductors. The experimental power cables were, in general, made with compounds that contained significant levels of fire retardants, the only exception being those compounds designated "1" (1I, 1J), which contained none or very low levels.

Dimensional requirements for the THHN cables were that the vinyl primary insulation be at least 0.38 mm (0.015") thick on the average, and no thinner than 0.33 mm (0.013") at any point. The extruded nylon film was required to be no thinner than 0.10 mm (0.004") at any point. The primary vinyl insulation in the TW cables was required to be at least 0.76 mm (0.030") thick, on the average, and no thinner than 0.69 mm (0.027")at any point [25]. For either cable construction the overall outside vinyl jacket was required to be at least 1.52 mm (0.060") thick, on the average, and no thinner than 1.2 mm (0.048") at any point [26].

Experimental Vinyl Power Cables:

1I THHN TC/1J THHN TC
3I THHN TC/3J THHN TC
3I THHN TC/1J THHN TC
3I THHN TC/4J THHN TC

1I TW TC/1J TW TC
3I TW TC/3J TW TC
3I TW TC/1J TW TC
1I TW TC/3J TW TC
3I TW TC/2J TW TC
524 TC/3J TW TC

Other Cables:

Commercial:

Plenum:	Western Electric Omaha NEC-800-3D
Tray:	XLP/CU Black Jacket 14 pr #6 Super Flex
Other:	Yellow Ultragard Type SOO 90 deg C Super Trex 14/4, Essex THHN 600 V, 4 AWG, Single conductor

Experimental Communications:
IBM Type I
IBM Type II

RESULTS AND DISCUSSION

The main results of the CSA FT-4 full scale vertical cable tray tests carried out at Underwriters' Laboratories (UL) are shown in Tables 1-3. Tables 4 and 5 present the results of the tests run in the new facility at BFGoodrich. The majority of the cables

Table 1. Main Results of UL cable Tray Tests				
Cable	Flame height [cm]	Char length [cm]	Peak HCl [ppm]	Pass/Fail
1I 1J THHN	> 250	265	> 2332	Fail
1I 1J TW	175	133	547	Pass
1I 1J TW	150	132	587	Pass
3I 2J TW	50	60	204	Pass
3I 4J THHN	100	79	578	Pass

Table 2. Further Results of Cable Tray Tests				
Cable	Mass loss [g]	Mass comb. [g]	% Comb. loss [%]	Pass/Fail
1I 1J THHN	3870	4795	81	Fail
1I 1J TW	1455	6415	23	Pass
1I 1J TW	1350	6350	21	Pass
3I 2J TW	780	6775	12	Pass
3I 4J THHN	960	6370	15	Pass

Footnote on abbreviations: Mass comb.: mass of combustible present;
% Comb. loss: percentage of combustible mass lost.

Table 3. Heat and Smoke Results from UL Cable Tray Tests										
Cable	Total heat release [MJ/m^2]				Total smoke release [m^2]				Pk RHR [kW/m^2]	Pk RSR [m^2/s]
	5min	10min	15min	20min	5min	10min	15min	20min		
1I 1J THHN	44.4	105.8	117.3	126.3	121	398	407	411	403.2	1.90
1I 1J TW	12.9	34.7	45.0	53.3	124	264	293	295	81.8	0.68
1I 1J TW	14.1	34.6	46.4	55.1	137	244	274	275	77.1	0.71
3I 2J TW	10.1	21.5	30.3	38.9	100	170	180	183	42.8	0.44
3I 4J THHN	8.7	22.1	33.3	41.9	32	143	194	199	55.1	0.53
BLANK	6.3	12.8	19.3	25.8	0.6	1.8	2.4	3.8	24.7	0.003

tested passed the cable tray tests. This includes cables coated with standard fire-retarded vinyl compounds and those coated with advanced compounds.

Moreover, it was also interesting that the peak amount of HCl released depended on whether the cable passed or failed the test, rather than on the chlorine content of the cable coating materials. The cables that passed released only relatively small amounts of HCl, although they were all based on vinyl compounds. The average peak amount of HCl released by the cables passing the CSA FT-4 tests was 479 ppm. On the other hand, the failing cables reached peak HCl levels exceeding 2330 ppm.

The other standard results shown in Table 1, char lengths and peak flame heights, are of limited importance in yielding information of use for fire hazard assessment. Table 2 has data on mass of cables and mass loss. This is interesting because the fraction of combustible mass lost is under 50% for the cables that passed and over 50% for those that failed.

Table 3 shows some fundamental fire properties: information on heat and smoke released. It is clear from these data that the cables failing the test release more heat and more smoke than those passing the test. Furthermore, the rate at which the heat and smoke is released is also significantly higher for failing cables. Moreover, the peak rate of heat release also indicates which cables passed the test marginally. This was the case with the 1I 1J TW cable.

Table 4. Main Cable Tray Test Results for BFGoodrich Tests								
Cable	Pk RHR [kW]	Time [min]	Pk RSR [m^2/s]	Time [min]	Mass Loss [g]	Comb. Loss [%]	Flame Ht.** [cm]	Pass/ Fail
Essex THHN	387.9	4.60	0.913	5.2	2221	66.79	275	Fail
1I 1J THHN	383.7	5.75	1.602	6.2	3743	75.96	300	Fail
Ultragard SOO	370.2	9.00	1.547	6.9	3942	62.29	275	Fail
3I 1J THHN	355.7	5.60	1.518	5.2	3502	71.35	275	Fail
1I 1J TW	131.2	12.90	0.970	11.6	*	*	275	Fail
1I 1J TW	129.9	15.55	1.050	4.7	3615	56.51	275	Fail
1I 1J TW	123.5	10.80	1.107	5.0	3285	52.63	300	Fail
XLPE CU	101.5	7.95	1.848	6.6	1380	23.60	175	Pass
XLPE CU	92.9	7.25	1.729	6.0	1773	30.30	205	Pass
3I 1J TW	65.5	7.45	0.885	4.6	985	15.32	160	Pass
3I 4J THHN	52.9	12.75	0.580	10.3	769	12.52	110	Pass
3I 3J THHN	48.2	8.15	0.545	6.5	709	13.39	125	Pass
1I 3J TW	46.9	8.35	0.501	7.2	817	13.59	110	Pass
3I 3J THHN	45.8	7.30	0.523	6.9	651	12.56	120	Pass
1I 3J TW	44.9	8.80	0.477	6.5	864	13.07	125	Pass
3I 2J TW	44.3	6.70	0.770	6.7	760	11.19	105	Pass
3I 3J TW	38.7	6.90	0.516	6.2	746	9.62	100	Pass
524 3J TW	36.3	11.80	0.384	6.9	759	9.78	85	Pass
3I 3J TW	34.0	8.00	0.500	4.7	798	10.85	105	Pass
IBM TYPE II	33.7	4.35	0.398	4.1	505	11.90	85	Pass
IBM TYPE I	32.1	5.60	0.225	2.8	342	10.49	85	Pass
Plenum	31.0	1.75	0.037	1.8	340	10.05	80	Pass
Blank	20.5	3.10	0.012	12.8	--	--	65	--

* the load cell was malfunctioning in this test.
** measured from the bottom edge of the tray

The earlier work also indicated that the peak rate of heat release measured in the cone calorimeter was a significantly good indicator of pass/fail criterion. Moreover, there was good correlation between the peak RHR in the cone and in the cable tray test (Table 6).

The ratios between the total heat and total smoke released and percent combustible mass lost by failing and passing cables in the test was:

	Failing/passing
THR	4.7
TSR	2.8
% Mass Loss	4.6

This indicates that there is, generally, a clear distinction, although sometimes there may be borderline cases.

The smoke and the HCl results would appear to give an important message: the amount of smoke or HCl released in a fire is heavily dependent on the severity of the fire, or on the fire performance of the product tested. It is worth restating thus once more a fact often misunderstood. The level of smoke released is a primary function of the amount of material burnt, and depends only somewhat on the smoke-producing characteristics of the material or product itself. Thus, less smoke and gas is released in a full scale fire if the material burns less readily, and is only partly consumed.

The peak concentrations of carbon monoxide and carbon dioxide were also much higher for the cables that failed the tests than for those that passed, reflecting the larger amount of material burnt. However, the CO/CO_2 ratios were virtually the same for all tests: high at levels above 0.13. This is of particular interest

Table 5. Additional Cable Tray Test Results from the BFGoodrich Tests

Cable	Total heat release [MJ]				Total smoke release [m^2]			
	5 min	10 min	15 min	20 min	5 min	10 min	15 min	20 min
Essex THHN	39	60	61	61	86	160	165	168.6
1I 1J THHN	27	82	85	86	125	402	413	415.9
Ultragard SOO	8	76	110	120	105	403	455	459.5
3I 1J THHN	43	89	98	125	176	396	413	435.8
1I 1J TW	5	26	50	68	131	346	541	616.9
1I 1J TW	5	24	49	70	163	382	569	639.2
1I 1J TW	5	25	52	80	150	379	549	609.0
XLPE CU	2	16	25	31	40	281	343	404.5
XLPE CU	1	13	23	35	34	223	307	402.4
3I 1J TW	6	15	16	17	150	277	283	287.9
3I 4J THHN	2	5	12	16	17	58	149	181.4
3I 3J THHN	2	7	9	11	55	155	164	169.3
1I 3J TW	2	6	9	10	56	158	185	195.4
3I 3J THHN	1	7	8	11	32	134	142	144.0
1I 3J TW	2	8	10	12	51	157	189	197.4
3I 2J TW	1	5	5	8	114	219	227	237.2
3I 3J TW	2	6	7	9	61	151	164	172.4
524 3J TW	2	5	8	10	51	129	168	181.5
3I 3J TW	1	4	6	8	58	144	158	167.7
IBM TYPE II	2	4	5	6	42	69	74	79.1
IBM TYPE I	2	4	5	8	34	47	51	56.2
Plenum	1	3	4	5	4	6	8	10.2
Blank	7	13	19	26	0.026	0.039	0.068	0.091

The THR data has had the blank heat value (caused by the burner itself) subtracted.
The TSR values are as measured, because the blank TSR is negligible.

Table 6. Correlation Between the Cone Calorimeter and the Cable Tray Test

Property	Flux	Corr. Coeff R^2/Adj R^2	Slope	Intercept	CV [%]	p
THR @ 15	20	0.98/0.97	0.99±0.08	12.4± 3.3	17	0.001
THR @ 15	40	0.43/0.24	0.46±0.31	- 11.5± 34.2	89	0.232
Pk RHR	20	0.91/0.88	4.21±0.76	-334.3± 83.0	49	0.011
PK RHR	40	0.65/0.53	1.76±0.75	-223.3±148.1	97	0.100
Pk RSR	20	0.68/0.57	0.26±0.10	- 1.2± 0.8	46	0.088
Pk RSR	40	0.19/0.00	0.05±0.06	0.1± 1.0	72	0.457
TSR @ 15	20	0.86/0.81	0.10±0.02	94.6± 45.3	15	0.025
SmkFct	20	0.93/0.91	1.53±0.24	182.4± 18.7	10	0.008
TSR @ 15	40	0.75/0.67	0.05±0.02	- 26.5±104.1	19	0.057
SmkFct	40	0.71/0.62	0.32±0.12	234.1± 53.3	21	0.071

in view of the fact that these were very intense fires, where low CO/CO_2 ratios might have been expected. The instantaneous CO/CO_2 ratios were also of the same order, until the cables stopped burning and no more carbon oxides were emitted from them.

Tables 4 and 5, organized in decreasing peak RHR order, show that the cables can be subdivided into three categories:

(i) Cables that are clear failures
(ii) Cables that are borderline in passing or failing the test
(iii) Cables performing better than needed to pass the test

Category (i) consists of 4 cables: two commercial ones (Essex THHN and Ultragard SOO) and two experimental (1I 1J THHN and 3I 1J THHN, both with a non fire retarded jacket and nylon).

Category (ii) consists of two cables: one commercial (XLP/CU) and one experimental (1I 1J TW).

All the category (i) and category (ii) cables are not only high in heat release but also high in smoke release.

Category (iii) consists of all other cables.

Thus, it would be useful to subdivide these category (iii) cables into two or three classes depending on the amount and rate of smoke generated. This is particularly important in view of the requirement in the National Electrical Code for a category of "limited smoke," as yet undefined. Class (a) could be used for those cables that have total smoke released values of over 240 m^2 but under 400 m^2 which separates typical class (ii) from class (iii) cables, and peak RSR values of over 0.85 m^2/s. Class (b) could be for those cables with TSR between 200 and 240 m^2 and peak RSR between 0.70 and 0.85 m^2/s and class (c) would be those cables with TSR < 200 m^2 and peak RSR < 0.70 m^2/s. The choice of the criteria for the top class is based on the fact that tightly specified communications cables (which require much better fire performance than power cables normally) seem to give TSR values of up to 168 m^2 and peak RSR values of up to 0.40 m^2/s.

Under these criteria, cable 3I 1J TW is class (ii)(a), cable 3I 2J TW is class (iii)(b) and the others are class (iii)(c). This indicates that a number of the experimental cables have good enough fire performance that they clearly emit low amounts of heat and of smoke.

Figures 1 and 2 show indications of the rate of heat release and rate of smoke release, respectively, for an example of a cable from each class in the tray test. The trends are clearly the same as was observed in the earlier series of tests: passing cables and failing cables are normally clearly distinguished.

Figures 3-6 show comparisons, for the four main properties measured, RHR, THR, RSR and TSR, between the tests carried out at UL and at BFGoodrich on the same cables.

It is interesting to notice that the results for the tests that were clear passes and clear fails were very similar for both laboratories. The only case that showed a distinct difference was that of 1I 1J TW, which is a borderline product. This shows that the new facility is very close to reproducing the results of the tests in the established (UL) facility.

The cable that failed the test at BFGoodrich and passed at UL is an example of the inconsistencies of fire tests, due to very small differences in test construc-

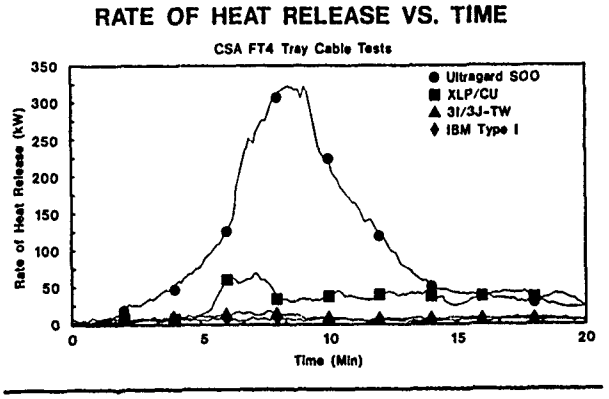

Fig. 1. Rate of Heat Release vs. Time: CSA FT-4 Cable Tray Tests.

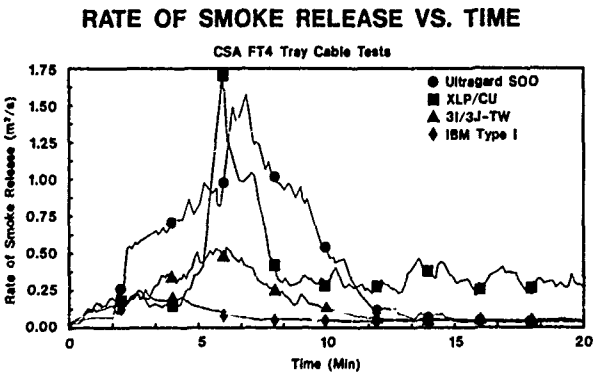

Fig. 2. Rate of Smoke Release vs. Time: CSA FT-4 Cable Tray Tests.

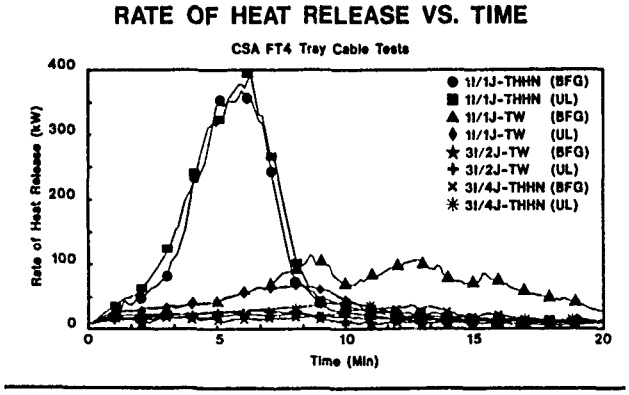

Fig. 3. Rate of Heat Release vs. Time: Comparison between BFG and UL results.

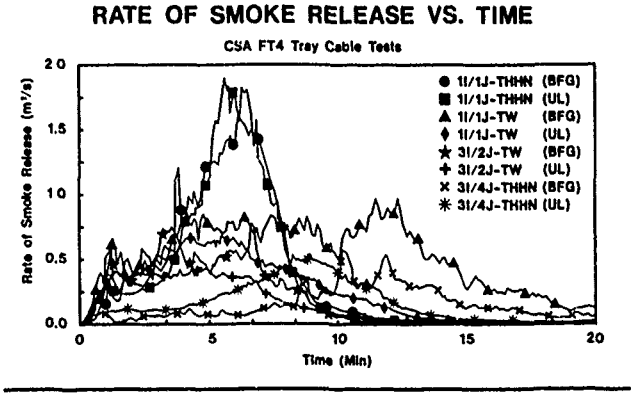

Fig 5. Rate of Smoke Released vs Time: Comparison between BFG and UL Results.

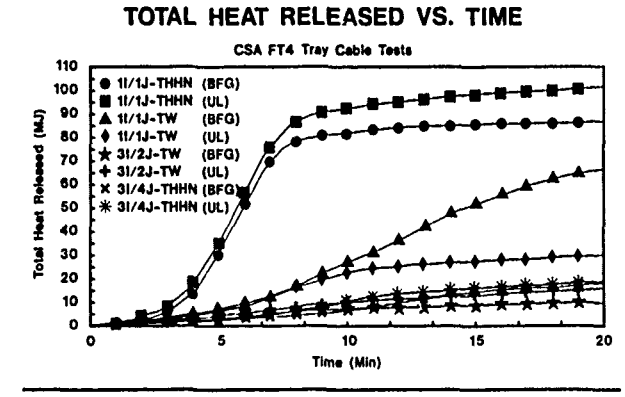

Fig. 4. Total Heat Released vs. Time: Comparison between BFG and UL Results.

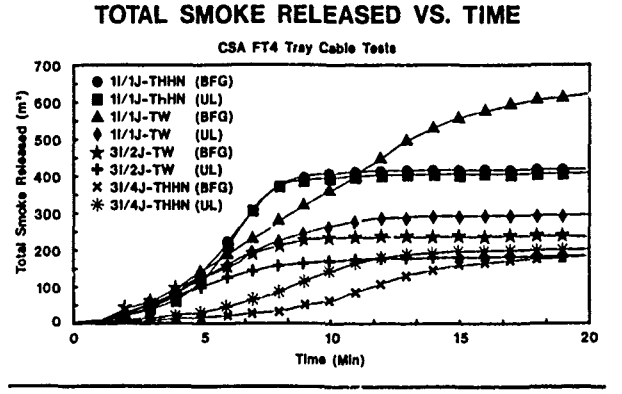

Fig. 6. Total Smoke Released vs Time: Comparison between BFG and UL results.

tion. The cable released slightly more heat at the BFGoodrich facility, partially through reradiation from the walls and ceilings and it, thus, continued burning to the top of the tray, while it stopped burning before the end at UL.

Figures 7-10 show that the old equations used for carrying out linear correlations between the cone and the cable tray test tend to give reasonably good correlations with the new test results too. The two exceptions appear to be the 1I 1J TW and the XLP/CU, viz. the class (ii) cables.

All the cables were also tested in the horizontal mode, in the cone calorimeter, at 20 and 40 kW/m^2 incident flux (Table 7). The cone calorimeter (heat and smoke) data are very consistent with the cable tray data, with the possible exception of the data for the two class (ii) cables. All the class (i) cables give the highest RHR and THR values at 20 kW/m^2, followed by the class (ii) cables. However, at 40 kW/m^2 one of the class (ii) cables (XLP/CU) is indistinguishable from the class (i) cables while the 1I 1J TW cable is significantly better, although the latter failed one of the tray tests and the former passed!

In terms of the most indicative fire index, TTI/Pk RHR, several cables stand out at 40 kW/m^2: the communications cables, 3I 3J THHN, 1I 3J TW, 3I 3J TW and 524 3J TW, all of which are (iii)(c) cables.

This suggests, clearly, that the cone calorimeter is capable of giving a good "a priori" indication of whether a cable will pass or fail the cable tray tests

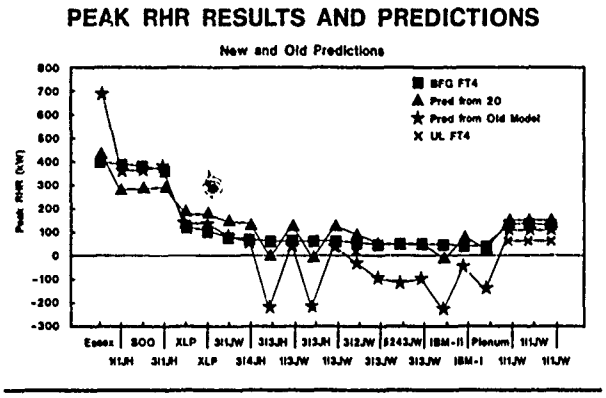

Fig. 7. Peak RHR results and predictions.

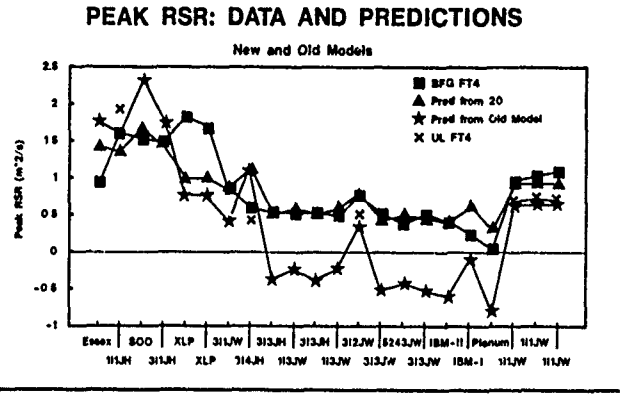

Fig. 9. Peak RSR data and predictions.

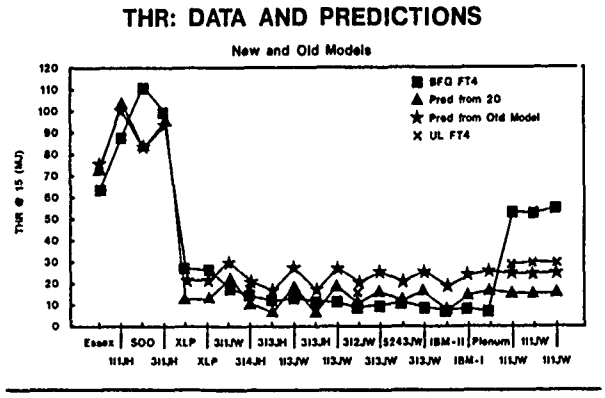

Fig. 8. THR data and predictions.

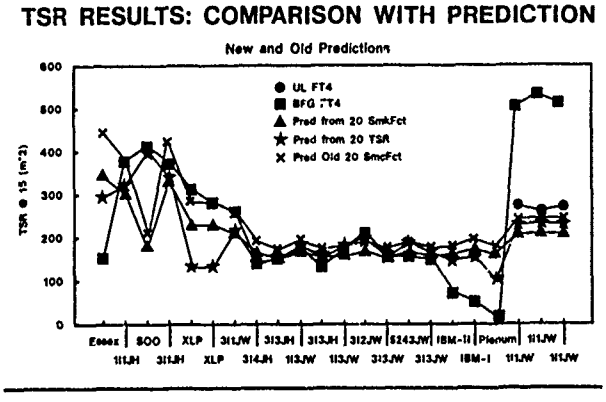

Fig. 10. TSR results: Comparison with predictions.

studied (CSA FT-4, UL 1581 or ICEA 529 T-20). It appears, for example, that if the peak RHR is significantly over 100 kW/m^2, at an incident flux of 20 kW/m^2, the cable will fail a cable tray test. When the cone calorimeter test is carried out at higher incident fluxes the peak RHR cut off point is higher: it appears to be near 200 kW/m^2 at 40 kW/m^2. However, borderline cases, i.e. class (ii) cables are still a problem.

New linear correlations have also been made, using the data obtained in the new series of tests, and the predicted cable tray results, also shown in Figures 7-10, are indicative of the reasonable degree of agreement found between the two full scale test facilities. This is a very important finding, because it has long been thought that exact replication of every minute detail of a full scale facility is essential to be able to replicate the data. Although the facility used at BFGoodrich is very similar, in most respects, to the one at UL, it differs in a few details. However, the results of the tests are clearly comparable.

It is of interest to recall that the compounds used in the experimental cables were also tested in the cone and Ohio State University (OSU) calorimeters [12]. The jacket compound test results were found to be very useful indicators of full scale cable tray test results. Moreover, cone and OSU test results were found to correlate well with each other [12,27], indicating that both are excellent techniques for predicting full scale fire performance of products, in a manner relevant to fire hazard assessment.

Table 7. Main Results from the Cone Calorimeter on Cables								
Cable	Pk RHR [kW/m²]	THR@15 [MJ/m²]	TTI [s]	SmkFct [MW/m²]	TSR@15	Pk RSR [1/s]	MLRP [g/(sm)²]	TTI/Pk RHR [s m²/kW]
20 kW/m²								
Essex THHN	241	60	201	199	2611	11.6	1.2	0.8
1I 1J THHN	162	87	96	155	2950	10.8	2.7	0.6
Ultragard SOO	163	68	318	29	3891	13.9	0.6	2.0
3I 1J THHN	167	80	81	186	3127	11.6	2.9	0.5
1I 1J TW	102	9	199	50	1702	7.1	0.8	2.0
XLPE/CU	108	7	958	83	601	7.6	0.3	8.9
3I 1J TW	96	15	114	63	1607	6.2	1.6	1.2
3I 4J THHN	90	5	950	15	702	9.0	0.1	10.6
3I 3J THHN	20	1	620	2	832	3.0	0.2	31.0
1I 3J TW	86	12	780	18	1172	3.6	0.3	9.1
3I 2J TW	69	5	551	15	1396	6.0	0.3	8.0
3I 3J TW	52	10	576	6	901	2.4		11.1
524 3J TW	48	6	252	11	1235	2.8	0.7	5.3
IBM TYPE II	19	3	6909	4	723	2.1	0.04	363.6
IBM TYPE I	66	8	483	16	796	4.2	0.2	7.3
PLENUM	41	10	142	3	138	1.3	0.9	3.5
40 kW/m²								
ESSEX THHN	318	64	32	846	3454	16.0	6.6	0.1
1I 1J THHN	285	154	21	754	8119	20.3	23.2	0.1
Ultragard SOO	283	134	36	518	5747	21.3	7.2	0.1
3I 1J THHN	269	136	24	707	6981	20.0	16.9	0.1
1I 1J TW	195	122	27	394	6033	16.3	10.5	0.1
XLPE CU	278	83	32	159	2925	14	8.4	0.1
3I 1J TW	205	114	30	407	5298	15.4	9.7	0.1
3I 4J THHN	89	18	69	76	3804	7.2	4.2	0.8
3I 3J THHN	158	54	41	239	5767	11.9	7.7	0.3
1I 3J TW	156	37	44	164	2518	8.1	7.0	0.3
3I 2J TW	176	97	30	388	5702	20.0	12.4	0.2
3I 3J TW	131	28	54	149	2366	7.8	10.4	0.4
524 3J TW	132	29	51	142	2737	7.8	6.9	0.4
IBM TYPE II	81	20	206	61	1551	7.2	1.1	2.5
IBM TYPE I	81	17	41	115	1528	12.8	3.2	0.5
PLENUM	84	25	75	33	503	4.9	2.0	0.9

CONCLUSIONS

A facility was built to carry out full scale vertical cable tray fire tests. The results of a series of fire tests carried out in this facility look very similar to those carried out in an established facility. This facility can be used to develop materials for /LS cables.

Vinyl wire and cable compounds have been developed which offer improved fire performance over that of traditional materials. These materials have been made into cables which perform well in small scale testing and pass full scale fire tests measuring rate of heat release. The better materials give off very little heat or smoke. These test results will form the basis for the development of new vinyl materials for use in /LS cables.

The cables tested that did not burn extensively, in the full scale tests, released very little smoke. The earlier work on UL-1581, CSA FT-4, and ICEA 529-T20 tests showed that those cables which did not burn beyond the failure points released an order of magnitude less of combustion gases, notably HCl, than the cables which failed.

Cone calorimeter test results on the cables tested could be correlated well with full scale test results, both in terms of heat and smoke release. This was particularly true for the cone calorimeter, at 20 kW/m^2 incident flux. These results could be, roughly, used to predict the results of full scale tests.

REFERENCES

1. Thomas, P.H., Int. Conf "FIRE: Control the Heat - Reduce the Hazard", Fire Research Station, October 24-25, 1988, London, paper 1.
2. Babrauskas, V., Int. Conf. "FIRE: Control the Heat -Reduce the Hazard", Fire Research Station, October 24-25, 1988, Londor., paper 4.
3. Babrauskas, V., J. Fire Sci. 2, 5 (1984).
4. Babrauskas, V. and Krasny, J., in "Fire Safety. Science and Engineering, ASTM STP 882" (Ed. T.Z. Harmathy), p. 268, Am. Soc. Test. Mats, Philadelphia, 1985.
5. Mulholland, G.W., Henzel, V. and Babrauskas, V., in Proc. 2nd. Int. Fire Safety Science Symp., (Ed. T. Wakamats, et al.), Hemisphere, Washington, D.C., p. 347, 1989.
6. Babrauskas, V., Fire Mats 8, 81 (1984).
7. Babrauskas, V., "Bench-Scale Methods for Prediction of Full-Scale Fire Behavior of Furnishings and Wall Linings", Soc. Fire Prot. Eng., Technology Report 84-10, Boston 1984.
8. Fowell, A.J., Fire Technol. 21(3), 199-212 (1985).
9. Hirschler, M.M., J. Fire Sciences 5, 289 (1987).
10. Tewarson, A., in Handbook Society Fire Prevention Engineers (Ed. P. di Nenno), Chapter 1/13, p. 1-179, NFPA, 1988.
11. Hirschler, M.M., 31st. IUPAC Microsymp. on Macromolecules Poly(Vinyl Chloride)", Prague, July 18-21, 1988, Makromol. Chem., Macromol. Symp. 29, 133-53 (1989).
12. Coaker, A.W., Hirschler, M.M. and Shoemaker, C.L., Fire Safety J., (in the press).
13. Babrauskas, V., "Development of the Cone Calorimeter. A Bench-Scale Heat Release Rate Apparatus Based on Oxygen Consumption", Nat. Bur. Stands, NBSIR 82-2611 (1982).
14. Babrauskas, V., J. Fire Flammability 12, 51 (1981).
15. Hirschler, M.M. and Smith G.F., in "Fire Safety Progress in Regulations, Technology and New Products", Fire Retardant Chemicals Assoc. Fall Conf., Monterey (CA), 1987, p. 133.
16. Babrauskas, V., Int. Conf. "FIRE: Control the Heat -Reduce the Hazard", Fire Research Station, October 24-25, 1988, London, paper 8.
17. Wickstrom, U. and Goransson, U., J. Testing Evaluation, 15(6), 346, 1987.
18. Hirschler, M.M., Int. Conf. Fire in Buildings (Interscience), Toronto, Canada, Sept. 25-26, 1989, Technomic, Lancaster, PA, p. 57.
19. Hirschler, M.M. and Poletti, R.A., J. Coated Fabrics, 19, 94 (1989).
20. Ebert, T.R., "Preliminary Modified Vertical Tray Flame Tests," E41877, 89NK14704, Underwriters' Laboratories, Inc., Northbrook, IL August 30, 1989.
21. UL letter for release of publication of results, Underwriters' Laboratories, Inc., Northbrook, IL, 1989.
22. Canadian Standards Association, C22.2 No. 0.3-M1985 (updated August 1988), Section 4.11.4, Vertical Flame Test: Cables in Cable Trays.
23. Parker, W.J., "Calculations of the Heat Release Rate by Oxygen Consumption for Various Applications," NBSIR 81-2407, February 1982.
24. Huggett, C., Fire Mats 4, 61 (1980).

25. UL 83, Thermoplastic Insulated Wires and Cables, 9th Ed., September 1983 (periodically updated), Tables 15.3, 15.5, Underwriters' Laboratories, Inc., Northbrook, IL.

26. UL 1277, Electrical Power and Control Tray Cables with Optional Optical Fiber Members, 1st Ed., January 1986 (updated October 1988), Table 10.24, Underwriters' Laboratories, Inc., Northbrook, IL.

27. Hirschler, M.M., Int. Conf. "FIRE: Control the Heat - Reduce the Hazard", Fire Research Station, October 24-25, 1988, London, paper 9.

DR. A. WILLIAM COAKER

Bill Coaker graduated from the University of the Witwatersrand in Johannesburg, South Africa, with a Ph.D. in chemical engineering. He worked for Masonite (Africa) Ltd. and the South African Council for Scientific and Industrial Research prior to emigrating to the United States in 1953. His work experience in the United States includes Director of Manufacturing Services at Tenneco Chemicals in New Jersey; Market Manager, Plasticizers for Monsanto in St. Louis; Senior R&D Group Leader, Plasticizers in St. Louis; R&D Group Leader, Vinyl Technology in Monsanto's Plastics Division in Springfield, Massachusetts, in addition to running a consulting business prior to joining BFGoodrich as R&D Associate in 1983. He is currently a Senior R&D Associate in the Geon Vinyl Division. Bill is Editor of the Vinyl Division Newsletter for the Society of Plastics Engineers, and is a member of SPE, ACS, and AICHE. He has authored several publications in the field of vinyl plastics and holds several patents.

DR. MARCELO M. HIRSCHLER

Dr. Marcelo M. Hirschler was born in Buenos Aires (Argentina and went to the University of Buenos Aires, where he obtained both a first degree and a Ph.D., in Physical Chemistry. He carried out research and teaching at the University of Buenos Aires, at Sussex University (in Brighton, UK, 1975-1977) and at City University (in London, UK, 1977-1984). He joined the BFGoodrich Co. in 1984 and is Manager of the Fire Sciences Department in the Geon Vinyl Division. His principal activities are in research and development, mainly in the fire testing, fire hazard and combustion toxicology areas. He is a member of ASTM (committees E5 (fire standards) and D9 (electrical materials), NFPA, of CSA, of the Combustion Institute, of the British Standards Institution and of the International Association of Fire Safety Science. He chairs ASTM Subcommittee E.05.15, on Fire Hazard Assessment of Interior Furnishings and Contents, and several task groups. He is on the Editorial Board of several scientific fire journals (Fire Safety Journal, Journal of Fire Sciences, Fire & Flammability Bulletin). He is also active across industry since he chairs the Technical Fire Subcommittees of the Coordinating Committee for Fire Safety (Society of the Plastics Industry) and of the Vinyl Institute. He has published over 150 scientific papers and one book, "The Combustion of Organic Polymers" (co-authored with Charles F. Cullis). Awards include the ASTM E.05 Certificate of Appreciation (June 1989) and the UK Interflam Trophy (1988).

DR. SALEEM SHAKIR

Dr. Saleem Shakir was born in Karachi, Pakistan, and attended N.E.D. University of Engineering and Technology, where he obtained his B.S. in Mechanical Engineering. He obtained his M.S. and Ph.D. in Mechanical Engineering from Michigan State University, U.S.A., in 1987. His areas of interest and research included heat transfer and combustion. He carried out research and teaching at Michigan State University prior to joining B.F.Goodrich in 1988. He is now an Advanced Research Engineer in the Fire Sciences Department, Geon Vinyl Division. His principal activities are in research and flammability aspects of product development. He is also responsible for carrying out small scale and large scale testing. He is a member of ASTM (where he serves on different task groups) and of NFPA.

DR. CRAIG L. SHOEMAKER

Craig L. Shoemaker received his B.S. degree in Chemical Engineering from Ohio University in 1982. He received his M.S. degree in Chemical Engineering at Ohio University in 1984, where he worked on melt transformation coextrusion. He received his Ph.D. in Chemical Engineering from the Ohio State University in 1988, where he worked on three dimensional computer image analysis of fiber orientations. From 1988 to the present, he has been working at the BFGoodrich Company Avon Lake Technical Center in the Geon Vinyl Division as an Advanced R&D Engineer. He is a member of SPE and has co-authored several papers in areas of image analysis and vinyl plastics.

IMPROVED PROCESSABILITY IN REDUCED EMISSION WIRE & CABLE MATERIALS FOR THE TELECOMMUNICATION INDUSTRY

S. Ramachandran, J. Jow, M. J. Keogh, P. J. Nesgood

Union Carbide Chemicals and Plastics Company Inc.
Somerset, New Jersey, USA

ABSTRACT

There is increasing focus worldwide for Telecommunication and Computer industry wire and cable materials that produce less combustion emission products, especially corrosive gases, during a fire. Thus far, such fire performance, along with acceptable physical, mechanical and electrical properties have been achievable in non-halogen, polyolefin based materials. However, current compounding technology for these materials usually suffers from inferior processing performance. Cable manufacturers have had to contend with lower line rates, narrow operating conditions and often are required to use specially designed equipment. In this paper, new Reduced Emission materials are outlined. These materials maintain the excellent balance of physical, mechanical, electrical and combustion emission products performance. More significantly, they also exhibit superior processing latitudes, resulting in better line rates and wider processing windows with less stringent equipment requirements.

INTRODUCTION

Electrical systems can be considered the "life-line" in modern society, providing heat, light, control and communication. Over the past several years, there have been widespread concerns regarding the potential damages from combustion products produced during a fire, especially from polymeric materials used in electrical systems. Events such as the 1975 and 1987 New York City Telephone Company fires[1,2], the Nippon Telephone and Telegraph fire in 1984 and the recent Hinsdale, Illinois central office fire in 1988[3], have heightened the public's interest because the fires were so disruptive and costly. There is widespread agreement that smoke from fires is more of a concern than heat and that corrosive combustion products are of concern to sensitive telecommunications and computer systems during a fire.

Nippon Telephone and Telegraph specified "non-halogen" wire and cables in their facilities soon after the fire damage in 1984[4], even though the technology in such materials was not as advanced as it is today. The worldwide trend seems to be in the direction of materials generating reduced combustion emission products, especially in areas such as Communications, Computers, Mass Transit[5] and Military[6].

The wire and cable industry has had a long record of manufacturing products that address the safety of the end user. In general, advances in technology have been closely monitored and improvements have been made. Concerns such as above have led to the development of non-halogen materials that tend to minimize combustion emission products.

NON-HALOGEN PRODUCTS

Conventional wire and cable products in the telecommunication and computer industry use materials containing halogens. Part of their fire resistance stems from the very fact that these materials give off halogen acid products that tend to retard the flame propagation. Even when there is no flame, or in the so called "smoldering" mode, depending on the heat level, these materials pyrolyze, producing halogen acid products. Some of these issues have been well documented [7,8,9].

In contrast, systems typically termed "non-halogens", rely on the polymers being made fire resistant by the addition of inert inorganic filler materials. The most common materials employing this technology are the polyolefin-based wire and cable products. Early efforts to produce such fire resistant polyolefin products had suffered from poor mechanical and processing characteristics. These deficiencies were the direct result of high filler loadings necessary to achieve the level of flame resistance required.

Hence, the target has been to develop products that are highly flame resistant and yet possess acceptable physical and mechanical properties. The most important challenge was to develop such products with superior processing (extrusion) characteristics, while maintaining the excellent combustion products performance. When all is said and done, perhaps one of the most critical characteristic of any product is the ease of processability for the end-use. If extrusion can be accomplished without recourse to specialized equipment, so much the better.

NEW REDUCED EMISSION PRODUCTS

In this paper, we will present results from the latest technology of developing polyethylene wire and cable products. These developments have centered on a "systems" approach, combining new technology in resins, fillers and additives to synergistically overcome the earlier deficiencies. This approach has produced products meeting or exceeding current performance criteria for telecommunication applications, while maintaining the improved combustion emissions quality of such systems. At the same time, these products exhibit the necessary ease of processing to be readily acceptable by the industry at large. Several products in this family are now available under the UNIGARD RE™.

Properties of New Reduced Emission Materials

Physical, Mechanical and Electrical Properties

Tables 1, 2 and 3 present data on typical mechanical and physical properties of these new materials. These data, covering a range of both wire insulation coatings and cable jacketing compounds, typify the superior balance of properties now achievable. Such excellent electrical and mechanical properties over a wide range of flame resistant levels (measured by the oxygen index value), illustrate that earlier deficiencies in such highly filled, flame resistant compounds have been overcome. These products also possess good low temperature properties.

Combustion Properties

Improvements of these compounds over conventional halogenated materials in terms of combustion properties, were tested using the following well known techniques:

1. UL-1581 vertical tray flame test modified for smoke measurements
2. ASTM E-662 Smoke Density
3. Acid Gas measurements by the U. S. Navy method[6]
4. Acid Gas measurements by the CSA method[10].

For comparison, typical commercial CMR cables of both PVC and Low Smoke PVC were tested. These were compared to the candidate non-halogen cable, made with insulation I_B and jacket J_D. Since material differences were evaluated in terms of smoke and combustion gas products, both the small scale and the vertical tray cable flame tests were conducted to demonstrate relationships.

Flame Propagation

Figure 1 illustrates that all three cables, namely, PVC, LSPVC and the non-halogen cable pass the UL-1581 vertical tray flame tests rather comfortably.

Smoke Obscuration

Figure 2 illustrates the difference in smoke opacity (1-Transmittance) of the PVC, LSPVC and non-halogen cables, measured during the vertical tray flame test. It is evident that while the LSPVC cable generated significantly less smoke than PVC cable, the smoke from non-halogen cable was undetectable.

Figure 3 demonstrates the same observation, albeit in the smaller scale NBS Smoke Chamber. Here, the three jacket materials, PVC, LSPVC and non-halogen, J_C, were tested under the flaming mode. In the static system of the NBS Chamber, small level of smoke from the non-halogen material was detected. However, this was significantly less than the LSPVC and PVC jackets. This difference between the Smoke levels measured in the UL-1581 test vs. the NBS Smoke Chamber can be attributed to the high-exhaust velocity, and dilution effect, in the vertical tray cable test. NBS Smoke Chamber measures, in a way, the worst case.

Acid Gas Generation

This test measures the level of acid gas generated by burning a small quantity of the material (jacket), absorbing the gaseous by-products of combustion in water and estimating the equivalent HCl level. There is considerable discussion in the scientific community as to the applicabilty of this test as an indicator of the corrosive combustion by-products from burning polymers. That not withstanding, there are several agencies around the world who use either this or a similar test in specifying and selecting products, especially for Telecommunication applications. Both the U. S. Navy as well as the Naval Engineering Standards (U.K) require these tests. Canadian Standards Association has a slightly modified version of the same test. Similar tests are also specified in Europe[11].

For comparison purposes, the regular PVC, low smoke PVC, and the non-halogen polyolefin (PO) jacket (J_D) were tested, according to the U. S. Navy method as well as the CSA method. Results are given in Fig 4. It is evident that the non-halogen PO jacket generates significantly less acid gas than the other two halogenated products.

PROCESSABILITY OF NON-HALOGEN MATERIALS

As mentioned before, earlier developments in non-halogen technology were centered on component optimization. While this indeed provided good mechanical and physical properties, not to speak of the expected

decrease in reactive combustion gas products, they did have one nagging problem for the person trying to extrude these on a commercial scale., viz. high filler loadings resulting in high melt viscosity, requiring specialized tooling, high power draw and an extremely slow line rates. All of these factors were counterproductive to the regular and increased use of these products.

Specifically, difficulties arose from the nature of these compounds and the rheological properties of these materials. These earlier materials tend to use ATH as the flame retardant filler. One significant problem was the release of gases (water vapor from decomposition of the fillers) at temperatures exceeding 180°C (356°F), and the high melt viscosities encountered below this temperature. It became necessary to custom design equipment to mitigate problems to some extent and achieve some improvements in the commercial extrusion rates. Obviously, this led to a very narrow "operating window".

With the "systems" approach in designing compounds that was outlined earlier, we now have materials that have overcome the processing barriers and enjoy a fairly wide operating window in terms of conditions. An extrusion process is typically considered to be a function of several parameters including polymer properties, design parameters and operating conditions.

By taking all these parameters into account, new non-halogen wire and cable materials have been designed. These highly filled compounds, can be processed using conventional extruders and metering screws, with parameters indicated in Tables 4 and 5.

Note that the temperature latitude is much broader than the 180°C max. dictated by the outgassing of conventional non-halogen, ATH based PO compounds.

During extrusion, the ability to withstand higher melt temperatures without outgassing enables the lowering of melt viscosity. This in turn allows the operator to increase screw speed and achieve higher output rates. In the case of the new Reduced Emission compounds, this is accomplished without resorting to specialized screw or tooling design. Both aspects, namely, no special equipment and higher line rates, are big advantages to the commercial cabler.

To illustrate this processing advantage, let us look at some typical processing data profiles. For comparison, we have used the most commonly available non-halogen jacket compound, namely Megolon S-300. This thermoplastic product has to be typically extruded using a very low compression screw specifically designed to minimize temperature excursions which results in outgassing and rougher cable surfaces. We have extruded both the Megolon S-300 and our typical non-halogen jacket Jc (DEFB-1638 BK), on a 2.5 inch (6.35 cm), 24:1, Davis Standard extruder, with a low compression screw (CR 1.5:1) having a metering depth of 0.110 inches. The extruder had a maximum RPM of 125 and 50 HP rating. The results are shown in Figs. 5 and 6.

Output vs. Screw Speed

In the first comparison, both Megolon and Jacket J_C were extruded at a barrel temperature setting of around 165°C (329°F), as recommended for Megolon, even though for the new Jacket Jc, a temperature profile around 200 - 220°C (392 - 428°F) would be recommended. In this run, the output rate (lbs/hr), was monitored as a function of screw speed (RPM). Fig. 5 illustrates that as the screw speed is increased, output for jacket Jc significantly increases over that of Megolon. Even more important, at RPMs exceeding 20, we could not effectively extrude Megolon due to the outgassing problem. Hence the Megolon line is discontinued beyond 25 RPM. This was a direct result of the high shear rate developed at higher speeds and the consequent increase of melt temperature well beyond the allowable maximum of 180°C (356°F), even though the extruder was set at 165°C. At screw speeds exceeding 25 RPM, outgassing occurred, with a very rough cable surface. On the other hand, with the new Reduced Emission compound, J_C, screw speeds of 75 RPM was easily achieved.

Melt Temperature vs. Screw Speed

Fig. 6 demonstrates the problem outline above as to the temperature excursions with Megolon at screw speeds exceeding 25 RPM's. Here, melt temperatures exceed the limit of 180°C (356°F), causing outgassing and a very rough cable jacket surface due to porosity. In contrast, the new Reduced Emission non-halogen jacketing compound, Jc, has a significantly higher melt temperature tolerance, as indicated. While both Megolon and jacket material Jc have increasing melt temperatures at higher RPMs, as indicated above, compound Jc does not outgas even at temperatures of 220°C (428°F). This affords not only a smoother surface for the cable, but the operator now has a much wider temperature latitude and a higher line rate, as outlined above.

Rheological Properties

The rheological properties of the two jacket compounds, Megolon vs. jacket Jc, were compared with a capillary rheometer study using the Goetfert Rheometer. Results from this test are provided in Fig. 7. It is once again evident that at a given temperature, jacket material Jc has much lower melt viscosity at varying shear rates, especially at rates corresponding to those encountered in large commercial extruders. Increasing shear rates result in a corresponding increase in polymer melt temperatures. While

this is detrimental to materials such as Megolon, where temperatures exceeding 180°C cause excessive porosity, the new compounds overcome this problem because of compounding technology.

APPLICATIONS

Currently, these new Reduced Emission polyolefin based compounds are marketed under UNIGARD RE™. These products are being evaluated for several mass transit, telecommunications, fiber optic insulation and jacketing as well as certain computer data processing applications. The main attraction of these compounds stems from their balance of properties as well as their ease of processing. Further details will be provided in future publications.

CONCLUSIONS

Based on the work outlined in this paper, it is clear that the compounding technology for developing non-halogen polyolefin based wire and cable compounds for the Telecommunication and Computer industries has advanced significantly. Unlike the past compounding difficulties of achieving flame resistance and physical, electrical and mechanical properties **ONLY** at a concomitantly diminished processing latitudes, current technology has vastly improved the options for cable manufacturers. It has been demonstrated that good mechanical, electrical and physical properties along with excellent combustion products performance are achieved, while maintaining processabilty. Significantly, these new developments have underscored the most important aspects for the person on the extruder line, namely, achieving good line rates, without specialized equipment and with a wider window of processing conditions.

ACKNOWLEDGEMENTS

The authors would like to express their appreciation to A. Adamczyk, H. G. Apgar, G. D. Brown, P. J. Dellatore, D. Folk, D. L. McDaniel, G. A. Schmidt, A. Soto, C. E. Rogers, D. R. Weaver and J. J. Yenchick for helping to develop these compounds as well as doing all the necessary test work.

REFERENCES

1. Lathrop, J. K., "Telephone Exchange Fire, New York, N. Y,", Fire Journal, July 1975.

2. Taylor, KT., "Temporarily Disconnected," Fire Journal, May/June 1989.

3. Isner, M.S., "Telephone Switching Station Creates Widespread Emergency," NFPA Investigation Report, Fire Journal, May/June 1990.

4. Nishizawa, H., "Recent Development of Non-Halogen Flame Retardant Materials in Japan," Proceedings, FRCA, March 1987.

5. Massachusetts Bay Transportation Authority, Specification P-120C, October 1978.

6. U. S. Navy Military Specification MIL-C-24640 and MIL-C-24643, September 28, 1984.

7. Keogh, M. J., "Reduced Emission Plenum Cable Telephone Jacket Compound," Proceedings, IWCS, 1987.

8. Keogh, M. J., "The Halogen Versus Non-Halogen Flame Retardance Question in Wire and Cable Applications," Proceedings, FRCA, March 1988.

9. Keogh, M. J., "Polyolefin Cable Materials with Reduced Smoke Toxicity and Smoke Corrosivity," Proceedings, International Conference on Fire Safety, Volume 13, 1988.

10. Canadian Standards Association, "Test to Determine Acid Gas Evolution,", C22.2 No.0.3-M1985, Section 4.31, February 1989.

11. IEC Standard Publication 754-1, 1982.

Table 1.

Reduced Emission Insulation Materials

Mechanical Property Profile

PROPERTY	I_A	I_B	I_C	I_D
Oxygen Index	25	28	36	44
Tensile Strength, PSI	2200	1900	1500	1600
Elongation, %	700	500	500	120
Secant Modulus, PSI	30,000	37,000	12,500	21,000
Cold Bend, ° C, (14 AWG)	- 50	- 40	- 40	- 20

Table 2.

Reduced Emission Insulation Materials

Electrical Property Profile

PROPERTY	I_A	I_B	I_C	I_D
Dielectric Constant, 1 MH_z	2.80	3.14	3.51	4.60
Dissipation Factor, 1 MH_z	0.008	0.001	0.016	0.012
Volume Resistivity Ohm-cm x 10^{-15}	2.0	1.3	0.26	0.15

Table 3

Reduced Emission Jacket Materials

Mechanical Property Profile

PROPERTY	JA	JB	JC	JD
Oxygen Index	28	36	40	44
Density	1.42	1.52	1.50	1.65
Tensile Strength, PSI	1700	1200	1700	1600
Elongation, %	500	450	175	130
Low Temperature Brittleness, ° C	- 12	+ 5	- 20	- 14

Table 4.

Typical Extruder Profile:Insulation

EXTRUDER TYPE

Screw L/D	:	15:1 to 24:1
Screw Type	:	Single flight, metering screw
Metering Depth	:	Shallow rather than deep
Screw Compression	:	2:1 to 3:1
Screen Pack	:	20/40/20 Mesh

TEMPERATURE PROFILE

Feed Zone	:	188°C (370°F)
Transition Zone	:	199°C (390°F)
Metering Zone	:	204°C (400°F)
Die	:	204°C (400°F)
Melt Temperature	:	199°C (390°F)
Conductor Preheat		120°C to 135°C (248 to 275°F)

Table 5.

Typical Extruder Profile:Jacket Material

EXTRUDER TYPE

Screw L/D	:	15:1 to 20:1
Screw Type	:	Single Flight Metering Screw
Metering Depth	:	Shallow rather than Deep
Screw Compression	:	2:1 to 3:1
Screen Pack	:	20/40/20 Mesh

TEMPERATURE PROFILE

Feed Zone	:	190°C (375°F)
Transition Zone	:	200°C (390°F)
Metering Zone	:	210°C (410°F)
Die	:	200°C (390°F)
Melt Temperature	:	200-220°C (390 to 428°F)

Fig. 1. FLAME PROPAGATION HEIGHT VS. TIME

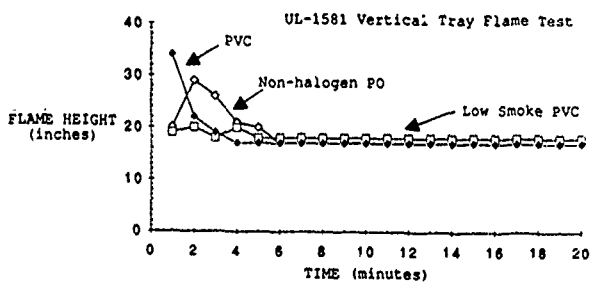

Fig. 2. SMOKE OPACITY VS. TIME

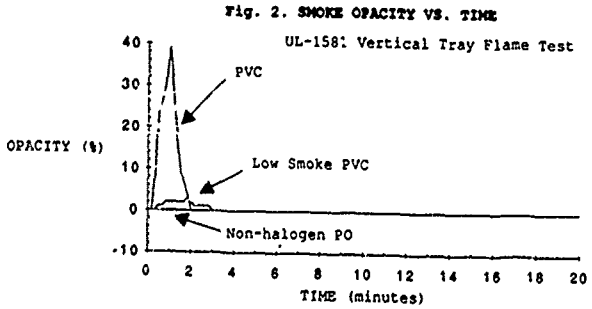

Fig. 3. SPECIFIC OPTICAL DENSITY (SOD) VS. TIME

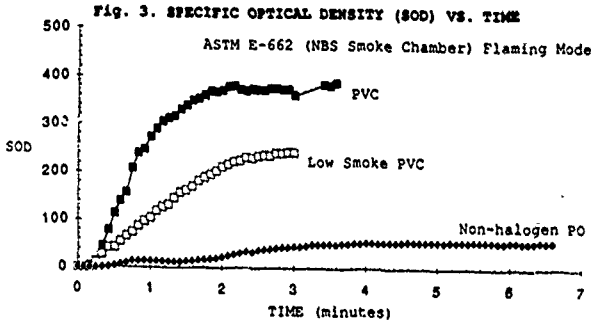

Fig. 4. ACID GAS OF VARIOUS CABLE JACKETS

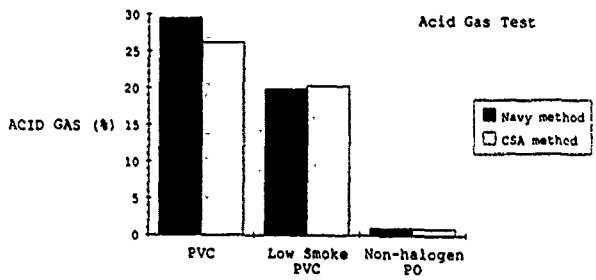

Fig. 5. OUTPUT RATE VS. SCREW SPEED

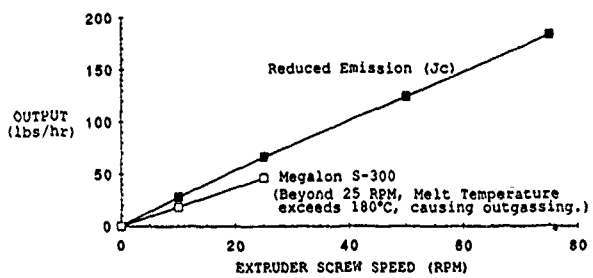

Fig. 6. MELT TEMPERATURE VS. SCREW SPEED

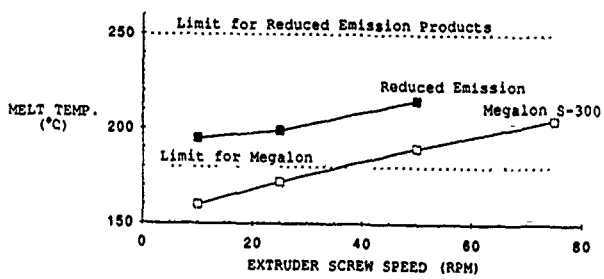

Fig. 7. VISCOSITY VS. SHEAR RATE

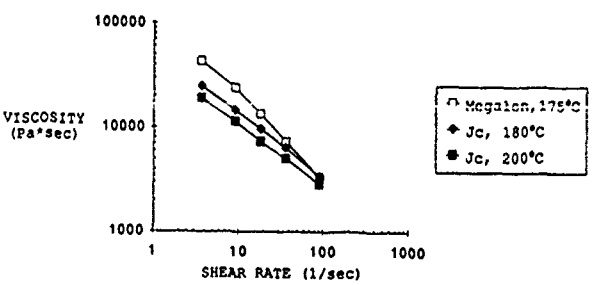

S. Ramachandran is a Development Scientist in the Polyolefins Division of Union Carbide Chemicals and Plastics Company Inc. Ram joined Union Carbide in 1973 as Research Engineer in the Metals Division and has held various positions in product and process development in several areas. His current responsibilities include new flame retardant wire and cable products' development. Ram received his B.Sc (Chemistry), B. Engg. (Metallurgy) from Indian Institute of Science in 1971 and M.S. (Mineral Sciences) from Columbia University in 1974 He also holda a M.B.A from SUNY, Buffalo, NY. Ram is a member of Society of Plastics Engineers, Wire Association International and American Society of Metals.

Jinder Jow is a Senior Engineer of Specialty Polyolefins Department at Union Carbide Chemicals and Plastics Company Inc. He holds a B.S. degree from National Taiwan University and M.S. and Ph.D. degrees from Michigan State University, all in Chemical Engineering.

Michael J. Keogh is a Research Associate in the Polyolefins Specialties Division of Union Carbide Chemicals and Plastics Company Inc. He received a B.S. in Chemistry from Manhattan College and a Ph.D. in Organic Chemistry from Purdue University. He has been involved in research and product development for wire and cable application for sixteen years. He holds over forty U.S. patents in this and related areas.

Patrick Nesgood is a Project Scientist with the Flame Retardant Materials R&D group of Union Carbide Chemicals and Plastics Company Inc. in Somerset, NJ. Mr. Nesgood has been involved for ten years in the compounding and extrusion of a wide variety of polymer compounds. He is presently involved in the development of extrusion technology for highly filled fire retardant wire and cable insulations and jacketing.

Mr. Nesgood received his B.S.M.E. from Fairleigh Dickinson University and did graduate work in Polymer Engineering at Rutgers University.

UPDATE ON SMOKE CORROSIVITY

Marcelo M. Hirschler

The Vinyl Institute
Wayne, NJ 07470

ABSTRACT

Smoke corrosivity used to be associated only with acid, mainly halogenated, gas emission. It was shown recently that all smoke is corrosive, even if it is not acid. Acid gas emission from burning materials does not correlate with smoke corrosive potential. Moreover, halogen free smoke can be more corrosive to metal surfaces than halogenated smoke. Corrosion effects are reduced by applying treatments soon after a fire. Many factors govern corrosion, e.g. smoke amount and composition, humidity and temperature. Smoke composition is a function of how the material is combusted. In particular as the fire air fuel ratio decreases, combustion is less complete and smoke corrosivity increases greatly. Thus, tests for regulation based on the corrosive potential of smoke need to address many parameters, and a set of 10 criteria have been developed for such tests. The effect of temperature on corrosion means that good fire properties (mainly low heat release) are essential to contain fire atmosphere corrosiveness, by keeping fires cooler and decreasing their propagation rate. The best way to manage smoke corrosivity is to avoid fires.

HISTORY OF SMOKE CORROSIVITY

Corrosion is a widespread phenomenon, which affects nearly every aspect of modern life. Everyday examples of such corrosion are too extensive to mention[1]. The costs incurred because of the need to replace equipment ruined by corrosion is so high that extensive research and testing is being carried out to identify causes and mechanisms as well as methods to alleviate the problem[2-5]. An example of corrosion, and the focus of this paper, is the corrosion following a fire in the electronics and telecommunications industries.

Although corrosion due to exposure to combustion products as a result of accidental fires in buildings has been noticed for a long time (and in fact an International Symposium on the issue was held in Stockholm in 1969[6]) not much work has been done until very recently to investigate it. Most corrosion work has focussed on other types of problems and has, thus, involved either long-term exposures to low concentrations of gases or liquids[7-9] or short-term exposures to solutions of individual corrosive chemicals[10]. Such work has only minimal relevance to accidental fires. New life was injected into this area with the International Smoke Corrosivity Conference of 1987[11].

Corrosive effects of smoke on electrical or electronic circuitry can be classified into three processes, viz. metal loss, bridging of conductor circuits and formation of non-conducting surfaces on contacts. The formation of deposits can be deleterious by causing a loss of electrical conductivity and, thus, making an electrical contact unusable, or by rendering a mechanical part, such as a ball bearing, ineffective because of it not being able to turn adequately.

In the past when smoke corrosivity has been considered, it has been thought that acid gases are the only entities responsible for corrosion and, thus, corrosive potential of the smoke from combustible materials, has been based simply on studies of material ranking based on acid gas emission following combustion. The tests used to determine such material rankings have normally involved burning samples in a hot tube furnace, under an air flow, capturing the water soluble effluents and titrating the solutions for its acid gas content (HCl, HBr, HF), for its acidity or for its conductivity. In some cases it was even decided that no test at all was needed by assuming that smoke corrosivity was directly proportional to the chemical composition of materials: i.e. that halogen content was a synonym for corrosive potential.

.... FIRST MODERN APPROACH TO SMOKE CORROSIVITY PERFORMANCE TESTING

Modern approaches to smoke corrosivity performance testing can be traced to the development of a test for the French telecommunications industry (CNET test, [12]). It marked a fundamental change in the thinking process and led to the understanding that smoke corrosivity could also occur with materials containing no halogens. This test is based on measuring the resistance of a copper printed circuit exposed to smoke. Furthermore, this test proposes consideration of a matrix of fire properties including smoke corrosivity, the others being the limiting oxygen index (ASTM D2863) and the ignitability (ASTM D1929).

In the CNET test a small sample of a material (600

mg) is mixed with some polyethylene (100 mg) and placed inside a 20 L chamber, which has been conditioned to a very high relative humidity and a slightly elevated temperature. The target is a copper printed circuit board, with a total area of ca. 5.6 cm^2 and a copper thickness of 170,000 Angstroms. Combustion is carried out by a rapid application of an intense flux, which elevates the sample temperature to ca. 800°C in a very short time. Water soluble combustion products are condensed onto the target, which is water cooled to a temperature appreciably lower than that of the bulk of the chamber. It should be mentioned that the original version of this test did not envision measurements on the sample after its exposure to the fire products. Table 1 describes all the materials mentioned in the present paper (W&C: abbreviation for wire and cable compound). Table 2 presents results for a variety of materials on the CNET test; it shows significant corrosion resulting from the smoke of halogen-free materials.

The ASTM E.05.21.70 Task Group on smoke corrosivity, established in the mid 1980's, set forth, early on in its deliberations, a set of 10 criteria that any smoke corrosivity performance test should ideally meet (Table 3[13]).

The reasoning behind the 10 criteria is as follows:

1. Performance has to be measured rather than to assume a correlation between performance and another property, e.g. acidity.
2. Smoke corrosivity results from a fire and this has to be modelled as well as possible to get realistic conditions.
3. Exposure should involve products in as close as possible to their end-use condition. Furthermore, a product should not be penalized by being exposed to a different fire depending on its other properties or composition.
4. The combustion module should be able to represent various fire conditions and not a single one (e.g. smoldering, flaming, flashover).
5. The target should represent the type of products at risk in the scenario of interest (e.g. circuit boards, computers, switchgear).
6. The target may need to be made of different materials, because the relative corrosivity of smokes may vary when compared, e.g. for zinc versus copper or versus platinum. Furthermore, different aspects of corrosion may be of interest (increased resistance versus bridging).
7. In a real fire post-exposure cleaning takes place only after a considerable time, because of the need of fire fighters to complete their work and a number of other legal and commercial considerations.
8. Smoke, and some of its components in particular, decays when moving along the fire path so that its corrosivity is very different depending on the location of the target with respect to the fire. Moreover, targets are usually at the same temperature as their immediate environment.
9. It is desirable to achieve a rapid throughput of testing, so that the equipment can be reused rapidly.
10. It is desirable to design a test that yields all required results without unnecessary sophistication.

It is important to judge the CNET test against the criteria set out in Table 3. This test is thus a milestone because it clearly satisfies criterion 1, which is the most important one. By satisfying this criterion a test measures actual corrosive performance rather than the "susceptibility of water to being corroded". The CNET test fails, however, to satisfy many of the other criteria.

Figure 1 compares CNET test results for some materials with those of two acid gas tests: HTF (hot tube furnace as used by the Canadian Standards Association[14]) and the faster "coil" test[15-16]. It is interesting to note that the two acid gas tests give virtually identical results and that the CNET test parallels them. This is in contradiction with the observation that smoke corrosivity does not necessarily parallel acid gas emission. The result is a consequence of three undesirable aspects of an otherwise good test: forced condensation, which eliminates the effect of non water-soluble products, lack of post-exposure and an unrealistically intense fire module.

There are four other important problems associated with the CNET test. Firstly, there is a very long time required to clean and condition (to the desired humidity) the chamber (a process which often requires several hours). Secondly, the small chamber volume does not allow finished products of any significant size to be tested. Thirdly, the good fire performance of a tested material does not yield any advantages in the test itself, because of the forced combustion in the presence of polyethylene. Fourthly, test results can be difficult to interpret because the copper "lines" in the circuit board are so close that there often is a combination of resistance increase due to metal loss and resistance decrease due to bridging.

OTHER PERFORMANCE TESTS PROPOSED

The use of static or dynamic test apparatuses was an issue of debate in the late 1980's, and it is still not fully resolved. Some of the advantages and disadvantages of each one have recently been discussed[13].

After reviewing the difficulties with the CNET test method, the ASTM task group then proceeded to attempt to develop a test using the combustion model believed to be the most adequate one: the cone calorimeter[17]. This

involved attempting to use lower air flow rates and a large (5 L) removable syringe, with a transfer tube and isokinetic sampling of the smoke in the cone exhaust duct. Although the concept seemed to offer many advantages, unfortunately, the practical end of the work was unsuccessful, probably because the strong air flows and the dynamic nature of the test resulted in atmospheres too dilute to cause significant corrosion.

Recently, researchers at Underwriters' Laboratories have decided to revisit the concept of smoke corrosivity testing using the cone calorimeter, but they have modified the sampling technique, in order to obtain higher concentrations of corrosive species[18].

A proposal has been made to use the tubular apparatus associated with the German smoke toxicity test (DIN 32436), either in its normal dynamic mode or by accumulating the smoke in a chamber. No work has, as yet, been done with this idea, which seems unlikely to reach closure.

Future test development has, thus, became centered on static chambers, and three candidate apparatuses have been under consideration since then: the plastic exposure chamber (ca.200 L) used in the NBS cup furnace toxicity test, associated with a radiant combustion chamber, the NBS smoke density chamber used in the ASTM E662 test (ca. 500 L), potentially associated with an external combustion chamber, and the CNET chamber (ca. 20 L).

FUNDAMENTAL WORK ON SMOKE CORROSIVITY STUDY OF EFFECTS OF COMBUSTIBLES

One of the first fundamental projects investigated the effects of fuel composition, exposure conditions and post-exposure on smoke corrosivity of actual metallic samples[1]. It used a wide range of combustible materials, which span the range of materials that could typically be found in modern environments. The exposure conditions attempted to simulate the wide range of conditions that can be found within an area affected by an accidental fire. The corrosion targets were materials likely to be present in a fire and susceptible to corrosive attack. A few anti-corrosion treatments were also evaluated for their effectiveness.

Experimental

The metal specimens were (a) a series of steel coupons 10 x 10 cm (4 x 4") and (b) copper mirrors 2.5 cm x 0.6 cm (1 x 0.25").

The steel coupons were cut from 12 gauge sheets of hot rolled 0.4 - 0.5% carbon steel and ground on the exposure side to a smooth 6 micron finish with a surface grinder. Immediately before exposure, the coupons were scrubbed with soap and water, rinsed with water, acetone, hexane, acetone again, alcohol and air dried, then weighed to the nearest 0.1 mg. The approximate weight of the clean metal coupons was 200 g. The copper mirrors were obtained from Evaporated Metal Films Corp., and used as received from the supplier. The thickness of the copper (ca. 500 A) corresponds to a 10% transmission of normal incident light of wavelength 5000 A.

Smokes were initially generated from eight different combustibles. In order to get information on background level, "smoke" was also generated in the absence of combustible material. Details of the materials have been presented in Table 1.

The composition of the PVC compounds used in this specific work is:

PVC WR compound

PVC resin	100 phr
Diisodecyl phthalate	65 phr
Tribasic lead sulphate	5 phr
Calcium carbonate	40 phr
Stearic acid	0.25 phr

PVC LH compound

Chlorine content	25.5 wt%
Plasticizer	14.8 wt%
Calcium carbonate	33.8 wt%
Other non-volatiles	0.4 wt%

Exposure of metals

The metals were exposed for 1 hour inside an NBS Smoke Density Chamber, fully lined with Teflon^{R} sheeting, so as to minimize HCl decay on the walls. The steel coupons were laid on the chamber floor and the copper mirrors were held in a plastic holder. In each experiment 15 g of combustible were burnt inside a quartz combustor, external to the chamber and identical to that used in the NBS cup furnace smoke toxicity test[19]. The targets were five steel coupons and two copper mirrors. The temperature of the furnace was set at 600°C in all experiments.

In every experiment, 6.1 g of water were injected into the center of the chamber, at a rate of 0.61 g/min. The water was fed by a Gilson Minipuls II peristaltic pump, with calibrated speed control display, to a coiled stainless steel tube, heated to ca. 150°C and vaporised.

In half the experiments, designated ROOM, the chamber air temperature was near ambient. During the other half of the experiments, designated WARM, a ceramic plate (12.8 x 22.5 cm; 5 x 9"), with embedded resistance coils capable of dissipating 2 kW of power, was placed inside the smoke chamber, to raise the chamber air temperature to 100-110°C.

Metal Treatment

Each of the five steel coupons was treated differently,

to simulate different scenarios from a real fire situation. This included pre-treatments (before exposure) and post-treatments (after exposure).

Pre-treatments:

OILY: Before exposure, one steel coupon was lightly coated with a general purpose machine lubricating oil with no corrosion inhibitors.

ICE: In the ROOM experiments one steel coupon was laid on an ice filled plastic bag to enhance condensation of water vapor onto the metal.

HOT: In the WARM experiments one steel coupon was put on top of the ceramic heater unit, to simulate exposure to real fire temperatures. The temperature of that surface was approximately 550°C.

Pre-treatments:

Three coupons received no pretreatment but rather diverse post-treatments, simulating potential post-fire anti-corrosion treatments.

TSP: One metal coupon was cleaned, a day after exposure, by removing the excess dirt, soot and debris and then agitating it for 2-3 min while soaking in a dilute aqueous solution of trisodium phosphate (22.1 g/l). The coupon was then rinsed with clean water and dried with air.

WD40: Another coupon was treated, again one day after exposure, by coating with WD40. After removing the excess dirt, soot and debris, WD40 cleaning oil was sprayed onto the metal surface and drained off.

Untreated: One coupon received no pre- or post-treatment.

A summary diagram of the exposures and treatments follows.

Chamber Temperature	ROOM	WARM
Conditions of Steel Coupons		
1	Untreated	Untreated
2	ICE	HOT
3	OILY	OILY
4	TSP	TSP
5	WD40	WD40

Time for corrosion after exposure

After they were exposed to smoke, all metallic targets were kept in a controlled environment chamber (25°C and 75% relative humidity, RH). The next day, two steel coupons were post-treated, as described, and returned to the controlled environment. After a total of 28 days, all targets were taken out of the chamber and cleaned.

Measurements

The steel coupons were stripped of corrosion by mechanical means and the metal loss determined by weight difference. The hydrocarbon products were dissolved off the copper mirrors with methanol and the copper salts then dissolved in water. Finally, the metallic copper remaining on the mirror was dissolved into concentrated hydrochloric acid and the copper ion content of the acid solution determined by atomic absorption spectrometry. These results were used to calculate, by difference, the mass of copper lost. The concentrations of a variety of combustion gases were measured inside the exposure chamber, including HCl, CO, CO_2 and NO_x. Details of these latter measurements will not be given here.

Acid gas emission measurements

The amount of acid gas emitted was measured for all the samples by the coil test method, described earlier [15, 16]. For the purposes of this report, results are reported in terms of proton concentration in 50 cm^3 of solution.

Corrosion of Steel Coupons

The results showed that all the combustibles caused loss of metal, as did even the simple presence of warm humidity. It thus became important to subdivide the analysis of results so as to look at individual effects.

The various conditions and treatments for the steel coupons used simulated different realistic scenarios. Thus, the coupons on the hot plate simulate products in contact with temperatures close to those prevalent in a real fire. The untreated coupons exposed at the chamber temperature, on the other hand simulate products present in compartments other than the fire room which are not cleaned after the fire exposure. Those coupons exposed on ice represent the unrealistic effect of enhanced condensation on a target, which will preferentially show the effect of water-soluble gases. The post-treatments, with TSP or WD40 at one day, after thorough cleaning of the combustion debris, represent alternative approaches to a fast recovery of the exposed products. In order to magnify the corrosive effect of smoke, all these coupons were cleaned before exposure and exposed without the protective benefit of the grease or oil usually present in real scenarios. The pre-treatment with oil was intended to simulate this effect.

Effects of Temperature Only: Untreated Coupons

The steel coupon in the warm chamber on the hot plate produced the highest overall level of corrosion of all conditions investigated (Figure 2). The amount of metal

lost was fairly constant (0.76 - 0.32 g), regardless of the material burned and there was no relationship between the type of combustion products and the amount of metal lost. In particular, the amount of metal lost for the HCl releasers, showed no correlation with the acid gas emission (Figure 3). Moreover, the smoke from these materials as a group is no more corrosive than the smoke from the group of halogen free materials (Figure 4) and the most corrosive smoke was due to nylon. The unrealistic conditions of the coupons on ice were the only ones where HCl emission correlated with corrosion level (Figure 3). At the end of the exposure, these steel coupons were always extensively covered with condensed water droplets, a condition never found on any of the coupons not on ice. Clearly, this condensed moisture promoted HCl condensation of HCl. Condensed water itself is also corrosive, as demonstrated by the results of the blank experiments. For the steel coupons at room temperature, but not on ice, corrosion does not correlate with HCl emission (Figure 3). The overall corrosiveness of the scenario with the steel coupons in the warm environment is almost identical to that of the previous scenario, but the distribution of effects among materials is very different. Under these conditions, the most corrosive smoke is again that of nylon, which is obviously very corrosive at higher temperatures.

Table 4 shows the acid gas emission measured for the smoke of these (and some other) materials. Four materials contained chlorine and were, thus, those yielding the most acid smoke, in the order indicated by their chemical composition: NPR, PVC WR PVC LH and HYP. The smokes of materials containing nitrogen are clearly alkaline. Particularly interesting is the fact that nylon smoke is alkaline, suggesting that ammonia is one of its principal components. The smoke from the nylon material contained very little NO_x, as measured in the exposure chamber. The high corrosivity of nylon smoke, and its dependence on the ambient temperature is an unusual issue which has also been the subject of further research.

Effects of Pre-Treatment or Post-Treatment

All simple anti corrosion treatments used were effective (Figure 2) in, reducing the metal loss to about half the amount for untreated samples.

Corrosion of Copper Mirrors

All the copper mirrors became open circuits (infinite resistance) at the end of the post exposure period. The corrosiveness of the smoke towards copper mirrors was thus determined by yield of soluble copper ions. It was again found that the most corrosive warm smoke among these materials belonged to nylon. The measurements showed a total lack of correlation with the pH of the smoke, particularly in the warm chamber.

The ratios of CO/CO_2 usually give an indication of combustion completeness. Moreover, they may be an indicator of the presence of incomplete combustion products, which could then be responsible for the corrosion not attributable to acid gas species. Table 5 presents these ratios. The carbon oxide ratios suggest that, while combustion is not complete, oxygen is not totally depleted. Corrosion results of this work should be compared with those from work under more oxygen rich and more oxygen poor conditions, as a subject worthy of further investigation.

Table 6 has the theoretical HCl smoke chamber concentration and the experimental peak and average values. The enormous disparity between the sets of values illustrates the phenomenon of HCl decay, even in a chamber lined with plastic to minimize such decay.

Conclusions From This Specific Work

All the steel coupons and copper mirrors experienced a significant amount of corrosion, whatever the material burnt. The highest degree of corrosion was observed on those steel coupons exposed to smoke while sitting on the heating element. The corrosion suffered by these coupons was due primarily to the heat, and possibly accelerated by water vapor. The amount of corrosion resulting when no material was burnt was of the same order than that found when burning any of the materials. This indicates the critical role of heat, in this as in all fire performance, making it worth recalling that heat release rate is the principal fire property[22, 23].

This suggests that the smoke itself did not play as important a role in causing corrosion than the high levels of heat and water vapor, typical of any fire.

Under some specific scenarios, the type of material burnt can indeed strongly influence smoke corrosivity. In particular, in the case of chlorine-containing polymeric systems, which can release HCl, their smoke is most corrosive towards steel coupons under those conditions which favor the condensation of water vapor.

In tests where, as opposed to real fires, conditions in the exposure chamber can cause excess condensation of water vapor, this has a tremendous influence on the relative values of smoke corrosivity of different smokes. However, it is clear that the level of smoke corrosivity in full scale fires depends on several factors: the fire scenario, the combustible material and the metal target involved.

It is particularly interesting to compare the corrosive tendency of the smoke of all the materials when analysed in a variety of ways, as reflected by Figure 5. This shows (a) the acidity of the smokes ($[H^+]$, in mol/dm^3), as measured by the coil test and their corrosivity in three ways: in terms of steel as (a) average of all experiments and (b) average of the warm chamber experiments only and (c) in terms of copper, as average of the warm chamber experiments, as measured by copper weight loss. While the ranking of acidity simply reflects the amount of HCl

emitted,, the three direct measures of corrosivity show that smokes of all materials are reasonably close in their corrosivity towards metal samples.

STUDY OF EFFECTS OF TARGETS (COPPER)

In the same apparatus described earlier (the NBS smoke chamber) a subsequent study was made, by using only copper targets, to investigate the type of measurement most useful for investigation of corrosion of copper. The targets initially used were two: the copper mirrors described before and copper atmospheric corrosion probes, based on a Wheatstone bridge principle, where one of the arms of the bridge remains unexposed to smoke but is exposed to the effects of temperature. The latter target is commercially manufactured (Rohrback P610 TF50 C11000) and has a copper thickness of 2500 A. The additional current required to reequilibrate the circuit is measured and converted into equivalent metal loss (in A), with a corrosometer (Rohrback CK3). The metal loss of the copper mirrors was determined in two ways: increase in resistance (at 1 h, end of exposure, and after 1, 3, 7, 14, 21 and 28 days) and copper dissolution (by atomic absorption, as described earlier). The metals were all exposed in the WARM environment, with no pre or post treatment. For comparison purposes, two of the materials used in the earlier work were reused: NYL (using exposure times of 10 and 60 min) and PVC LH, together with 5 new ones.

Figure 6 shows the results found, by all three methods of measurement. It also contains, for comparison purposes, the copper mass loss data of the earlier series of experiments (labelled old), which compares reasonably well with the new results. As a comment, for interpreting the graph, the maximum resistance normally measurable is 2 x 10^7 x, the log of which is 7.3.

The first obvious result is that, again, there is no correlation whatsoever between smoke corrosivity and the degree of acidity emitted, and that halogen-free smokes can corrode substantially. It is clear that there is a rough degree of correlation between the various targets, but that they do not correlate exactly. The copper mirror resistance results at 28 days and the copper mass loss show reasonable agreement. The Rohrback probes at 1 day agree reasonably well with the copper mirror resistance results at 1 day.

Copper mirrors (averages of two mirrors in each case) show serious reproducibility problems, partially because of uneven distribution of deposits on them and partially because of excessive sensitivity (thickness only 500 A). However, comparison of the mass loss measurement results with the earlier ones, with differences well within experimental error, indicates that these targets are of interest and should remain under some consideration. An investigation was made too of different ways in which to measure the copper mirror resistance: at a fixed distance between electrodes or at a variable distance, looking for the lowest resistance to be found. The results were inconclusive. Other probes have also been investigated: larger copper mirrors, copper wires and exposed circuit boards, but none have been shown to be effective. An issue of great interest in terms of these small copper mirrors is their ready availability and low price (< $1 each).

The Rohrback probes are much less sensitive and thus do not go off scale so easily. Moreover, measurements can be made either continuously or at any time after or during exposure. Furthermore, temperature effects will be minimized by the resistance reference copper.

Figures 7 and 8 show the logarithm of the increase in resistance of Cu mirrors and the thickness of copper lost in the Rohrback probes. These figures show one of the effects of keeping the targets post exposure, since there are several cases of crossover between materials when smoke corrosivity is measured at different times after exposure, both for the Rohrback probes and for the copper mirror resistances.

Figure 9 compares the mass loss of copper, and the pH of the smoke, for samples of very different chemical composition: containing Cl, Br, F, N, S and no heteroatom (other than oxygen). Three of the samples contain more than one type of heteroatom. It is obvious that there is no correlation between the chemical composition, or indeed the pH of smoke, and smoke corrosivity.

LARGE SCALE TESTS

A series of full scale smoke corrosivity tests were carried out at the University of Edinburgh, by A. Macmillan and D. Drysdale[20] using a variety of combustible materials and copper mirror (resistance) for measurements.

The chamber was 13.5 m^3 in volume and the combustibles were all allowed to burn on their own, in the presence of 100 g of Douglas fir wood. The combustibles used were ABS, NORYL, NYL, PP, PVC CIM, PVC LF and PVC WR. The effect of the wood alone was also investigated. Two additional parameters were investigated: the effect of oxygen availability in the vicinity of the burning process and the effect of chamber temperature.

In order to investigate the effect of oxygen the samples were burned at floor level at the center of the chamber, either unconfined (free burn), within a fire box (internal volume 0.41 m^3) lined with low density ceramic fibreboard with one side (41 cm x 41 cm) open (confined burn) or with the opening reduced to a slit 10 cm wide by 41 cm high (closed burn). Copper mirrors were located within the chamber at a height of 1.5 m from the floor. Measurements were made after the exposure (1 h) and after post exposure periods of 1, 2 and 3 days (at room temperature and 75 % RH).

The effect of temperature was investigated for a single fuel, viz. nylon, and it was done by raising the

temperature to various levels, viz. ca. 60, 80 and 110 °C.

The results confirmed, once again, that all smokes caused some degree of smoke corrosion. This can be seen in Figure 10 showing closed burn values measured after 3 days post exposure. In particular, Figure 11 gives details of results found for two halogen free materials, DFIR and NORYL, for all three exposures. The figure also shows that increased oxygen availability decreases the corrosion efficiency. This is a general trend for all materials, as indicated by averaging the resistance measurements of all 8 materials under each condition (Figure 12). It is very clear that corrosion is enhanced by restricting the oxygen access, in other words making combustion less efficient.

Figure 13 shows the effect of temperature on the smoke corrosivity of NYL: the resistance after exposure (1 h) increases by ca. 8 orders of magnitude when the temperature of the targets reaches 110 °C, indicating that temperature places a crucial role in smoke corrosivity.

FUTURE DIRECTIONS FOR SMOKE CORROSIVITY

The ASTM Task Group investigating smoke corrosivity is now concentrating its attention on a so called NIBS apparatus. It involves the chamber used for exposure in the NBS cup furnace toxicity test (ca. 200 L) and an external radiant combustor.

There has been some experience investigating the effect of burning conditions on test results in this apparatus, and it has been shown that several factors can have significant effects both on the absolute yields of individual carbon oxides, and on their relative yields. These include the mass of sample loaded, the length of irradiation time, the irradiation level and the oxygen concentration during combustion. It was found that the CO yields (or CO/CO_2 ratios) tend to be very low (compared to those found in real fires) unless the amount of smoke generated is sufficient to "flood" the chamber. This work (by M. Hirschler and G. Smith, of BFGoodrich) will be reported on fully elsewhere[21] and is mentioned here only in order to indicate it as an issue.

The targets proposed for use by the ASTM Task Group are the same Rohrback probes discussed here, probably at copper thicknesses of 2,500 A and 50,000 A. The latter would allow the use of larger samples, at the expense, perhaps, of losing some degree of accuracy.

The use of this static chamber appears, thus, to solve many problems discussed before. It suffers, however, from the inevitable problem of finding out whether there is a way of generating smoke in a manner truly relevant to the full scale fire scenario to be investigated.

CONCLUSIONS

The results of this work prove once again that a fire environment is corrosive, whatever the fuel involved. This is a consequence of the action of heat, condensed water vapor and oxygen, present in all fires.

There is no correlation between acid gas emissions from combustible materials and the corrosivity of their smoke.

The effects of humidity, temperature, oxygen availability and type of target investigated can be much more important than the fuel used. In other words, the fire scenario is crucial to understand the level of corrosion that will result.

Corrosion inhibiting treatments applied soon after the fire decrease the amount of corrosion.

Many parameters need to be addressed when devising tests designed to regulate materials based on smoke corrosivity. In particular, the large influence of temperature on corrosivity emphasises again that materials with good fire properties (typically low rate and amount of heat released) will be invaluable in containing the corrosiveness of fire atmospheres, by keeping the fire cooler and decreasing its propagation rate.

It has already been shown that rate of heat release is the crucial fire property in any fire[22]: it is clear now that smoke corrosivity is no exception.

REFERENCES

1. M.M. Hirschler and G.F. Smith, Fire Safety J., 15 57-93 (1989).
2. F.H. Haynie, J.W. Spence and J.B. Upham, in "Atmospheric Factors Affecting the Corrosion of Engineering Metals", ASTM STP 646, American Society for Testing and Materials, Philadelphia, PA, 1978, p. 30.
3. G. Reinhard and C. Irnmscher, Werkstoffe u. Korrosion, 34, 365 (1983).
4. V. Kucera, in "Materials Degradation Caused by Acid Rain", A.C.S. Symposium Series, ed. M.J. Comstock, American Chemical Society, Washington, DC, 1986, p. 104.
5. D.R. Flinn, S.D. Cramer, J.P. Carter, D.M. Hurwitz and P.J. Linstrom, in "Materials Degradation Caused by Acid Rain", A.C.S. Symposium Series, ed. M.J. Comstock, American Chemical Society, Washington, DC, 1986, p. 119.
6. "SKYDD 69 (Protection 69): Plastics - Fire - Corrosion", Proc. Intl. Symp. and 15th Nordic Fire Protection Day, Stockholm, April 23, 1969, Swedish Fire Protection Assoc., Stockholm, (October 1969).
7. M. McKenzie and P.R. Vassie, Brit. Corr. J., 20(3), 117 (1985).

8. R.B. Commizzoli, R.P. Frankenthal, P.C. Milner and J.D. Sinclair, Science 234, 340 (1986).
9. J.W. Spence, F.H. Haynie, E.O. Edney and D.C. Stiles, in "Materials Degradation Caused by Acid Rain", A.C.S. Symposium Series, ed. M.J. Comstock, American Chemical Society, Washington, DC, 1986, p. 194.
10. "Corrosive Effects of Combustion Products", international conference sponsored by ASTM, IEC, and ISO, London, UK, (Oct. 1987).
11. Test on gases evolved during combustion of electric cables. Part 1: Determination of the amount of halogen acid gas evolved during the combustion polymeric materials taken from cables. International Electrotechnical Commission (CEI), IEC Standard 754-1 (1982).
12. Fire Performance: Determination of the Corrosiveness of Effluents (158 CNET/LAB/SER/ENV). National Centre for Telecommunications Studies (CNET), France (1983).
13. J.D. Ryan, V. Babrauskas, T.J. O'Neill and M.M. Hirschler, in ASTM STP 1082, ed. H.K. Hasegawa, American Society for Testing and Materials, Philadelphia, PA, 1990, p. 75-88.
14. Test to determine acid gas evolution, CSA Standard C22.2 No 0.3-M1985, February 1989, page 94, Canadian Standards Association, Rexdale, ONT., Canada.
15. G.F. Smith, J. Vinyl Technol., 9(1) 18 (1987).
16. L.A. Chandler, M.M. Hirschler and G.F. Smith, Europ. Polymer J., 23, 51 (1987).
17. V. Babrauskas, Development of the Cone Calorimeter A Bench Scale Heat Release Rate Apparatus Based on Oxygen Consumption, Fire and Materials. 8, 81-95 (1984).
18. P. Gandhi, private communication, 1990.
19. B.C. Levin, A.J. Fowell, M.M. Birky, M. Paabo, A. Stolte and D. Malek, "Further Development of a Test Method for the Assessment of the Acute Inhalation Toxicity of Combustion Products", Nat. Bur. Stands. NBSIR 82-2532 (1982).
20. D.D. Drysdale and A.J.R. MacMillan, "The Corrosivity of Fire Gases", Report to the Vinyl Institute, Fire Safety J., in the press, 1990.
21. M.M. Hirschler and G.F. Smith, in the press.
22. P.H. Thomas, How heat release influences fire hazard, pp. 1-1 to 1-6 in "Fire: Control the Heat...Reduce the Hazard", QMC Fire & Materials Centre, London (1988).
23. V. Babrauskas, Effective Measurement Techniques for Heat, Smoke, and Toxic Gases, pp. 4.1 to 4.10 in "Fire:

Table 1. Materials Used in Experiments Described

A. First NBS Smoke Chamber Work

DFIR	Douglas fir wood
NPR	commercial polychloroprene (Neoprene W)
NYL	commercial nylon (Du Pont Zytel HSL 103)
PE	polyethylene non-halogen fire retarded commercial W&C (Union Carbide DEQD-1388, black)
PS	commercial polystyrene (Dow Styron 6069)
PVC LH	low halogen (experimental) flexible poly(vinyl chloride) W&C, described previously[16]
PVC WR	standard (non-commercial) flexible poly(vinyl chloride) W&C
WOOL	unbleached unwoven wool fibres (sample used for smoke toxicity testing[19])
NONE	no combustible material

B. Follow-up Work in NBS Smoke Chamber

ABS	Fire retarded acrylonitrile butadiene styrene (Borg Warner Cycolac KJT)
F CB	Fluorinated cable jacket compound
HYP	Chlorosulphonated polyethylene compound (Hypalon)
MEL	flexible polyurethane foam fire retarded with melamine (BASF Rest Easy)
PU FM	ordinary commercial non fire retarded flexible polyurethane foam

C. CNET Tests

CPE	Chlorinated polyethylene
CSP	Chlorosulphonated polyethylene commercial W&C
PR/ATH	Commercial ethylene propylene rubber W&C fire retarded with alumina
EVA/ATH	Commercial ethyl vinyl acetate W&C fire retarded with alumina
HYP LS	Smoke suppressed commercial chlorosulphonated polyethylene compound
LDPE	Low density polyethylene commercial W&C
POLEF/ATH	Commercial polyolefin W&C fire retarded with alumina
PTFE	Polytetrafluoroethylene commercial W&C
PVC FR	Conventional fire retarded commercial PVC W&C
PVC FRLA	Fire retarded low acid emission commercial PVC W&C
PVC LS	Smoke suppressed commercial PVC W&C
PVC RES	Pure PVC polymer
PVC STD	Conventional non fire retarded commercial PVC W&C
PVDF	Polyvinylidene fluoride
XLEVA/ATH	Commercial crosslinked ethylene vinylacetate W&C fire retarded with alumina

D. Large Scale Tests

NORYL	Polystyrene/polyphenylene oxide commercial compound (GE Noryl N190)
PP FR	Fire retarded polypropylene compound
PVC CIM	Rigid commercial PVC custom injection moulding compound
PVC LF	PVC experimental flexible fire retarded and smoke suppressed W&C

Table 2

CNET Test Results

	COR (%)
Halogenated materials	
HYP LS	1.8
Pure PVC + PE (@ 5 % Cl)	4.2
PVC LH	4.5
CSP	5.6
HYP	7.7
Pure PVC + PE (@ 10 % Cl)	7.7
PVC FRLA	8.8
CPE	10.9
PVC LS	11.7
PVDF	12.9
PTFE	14.1
PVC STD	14.2
Pure PVC + PE (@ 25 % Cl)	21.9
PVC RES	30.0
Halogen-free materials	
EPR/ATH	0
Polyethylene pure	0
PS	0.2
NYL	0.6
EVA/ATH	0.6
Diallyl phthalate	0.8
XL EVA/ATH	0.9
POLEF/ATH	1.1
Polyester	1.2
LDPE	3.5
Polysulphone	8.8

Table 3

Criteria for a Smoke Corrosivity Test

1. The test should measure corrosive performance.
2. The combustion module should be representative of energies and growth rates of real fires.
3. All products should be treated in the same way, irrespective of chemical composition or fire performance.
4. The test apparatus should allow the burning conditions to be varied.
5. The conditions in the exposure module should reflect those during real fires.
6. The exposure target should be capable of being varied.
7. The protocol should allow a reasonable period between the end of the exposure and the measurement time.
8. The protocol should consider transport of the combustion products, their decay before reaching the target and their deposition on the target surface.
9. Test protocol should allow rapid throughput of experiments.
10. Test should be as inexpensive as possible.

Table 4

Acid Gas Emission by the Coil Test (M)

NPR	1.21×10^{-2}
PVC WR	8.20×10^{-3}
PVC LH	2.32×10^{-3}
HYP	1.33×10^{-3}
ABS	5.01×10^{-4}
F CB	3.98×10^{-4}
DFIR	4.98×10^{-5}
XLPE	4.83×10^{-5}
PU FM	3.16×10^{-5}
PS	1.04×10^{-6}
NONE	1.00×10^{-7}
WOOL	4.22×10^{-8}
MEL	1.02×10^{-8}
NYL	9.60×10^{-9}

Table 5

Average Ratios of CO/CO_2 Yields

	ROOM	WARM
PVC WR	0.28	0.19
PVC LH	0.11	0.16
NPR	0.30	0.41
WOOL	0.16	0.21
DFIR	0.08	0.05
PE	0.03	0.03
PS	0.06	0.02
NYL	0.02	0.02

Table 6

HCl concentrations (ppm) in Warm Chamber

	Theoretical	Exp. Maximum	Exp. Average
NPR:	7,250	4,000	876
PVC WR:	3,610	1,850	305
PVC LH:	900	370	88

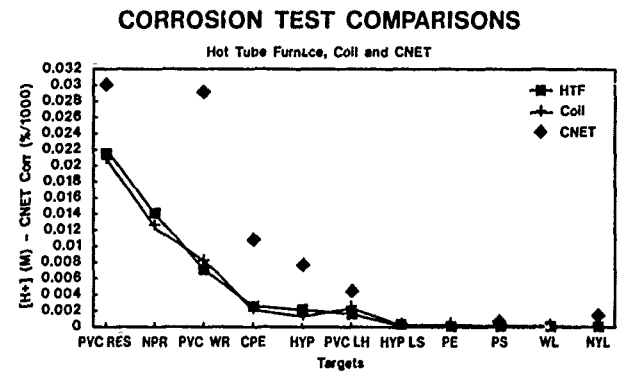

Fig. 1. Corrosion test comparisons - Hot Tube Furnace, Coil Test and CNET.

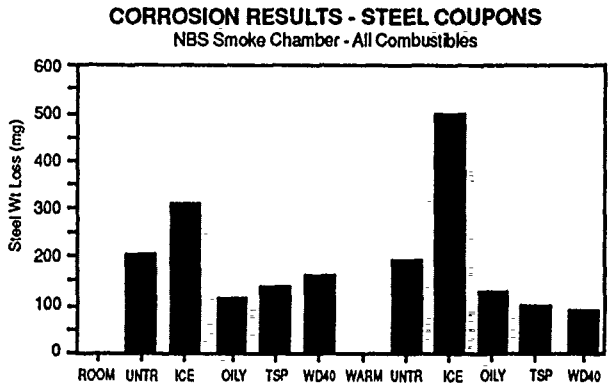

Fig. 2. Corrosion results - Steel Coupons.

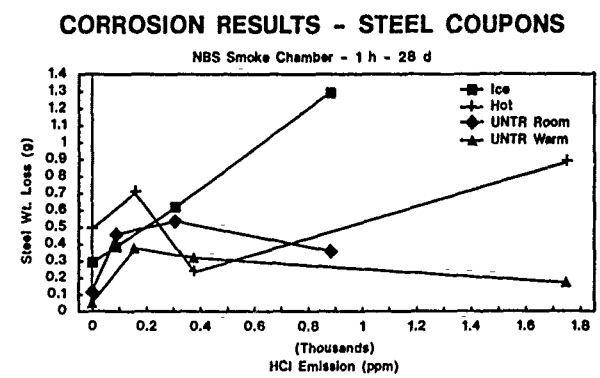

Fig. 3. Corrosion results - Steel Coupons weight loss vs. HCl emission.

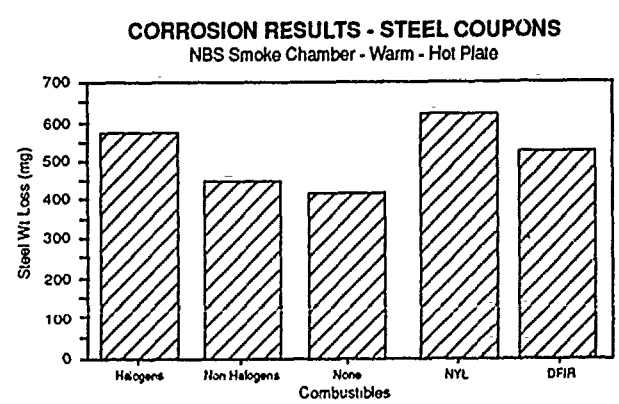

Fig. 4. Corrosion results - Steel Coupons weight loss from the smoke of various metals.

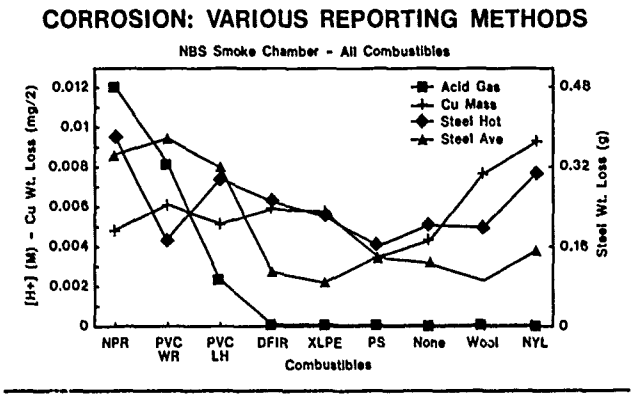

Fig. 5. Corrosive tendency of the smoke of materials as analyzed by various methods.

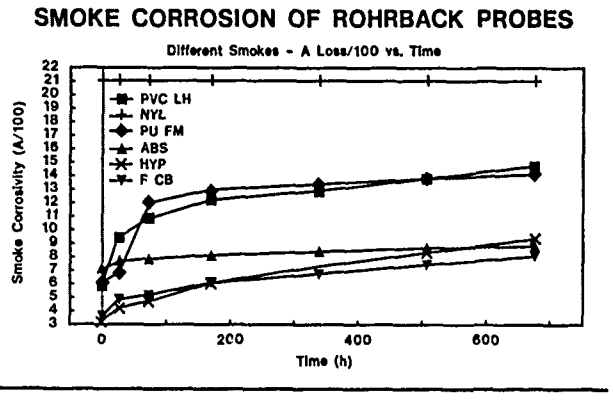

Fig. 8. Smoke corrosion of Rohrback probes.

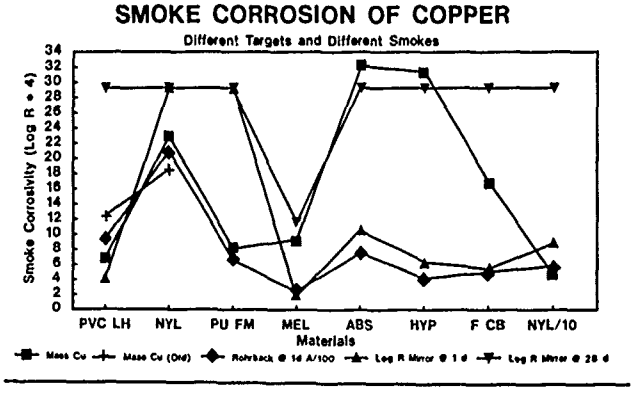

Fig. 6. Smoke corrosion of copper.

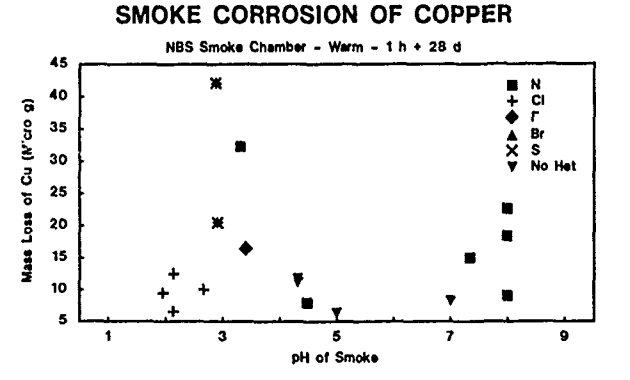

Fig. 9. Smoke corrosion of copper - mass loss of copper vs. pH of smoke.

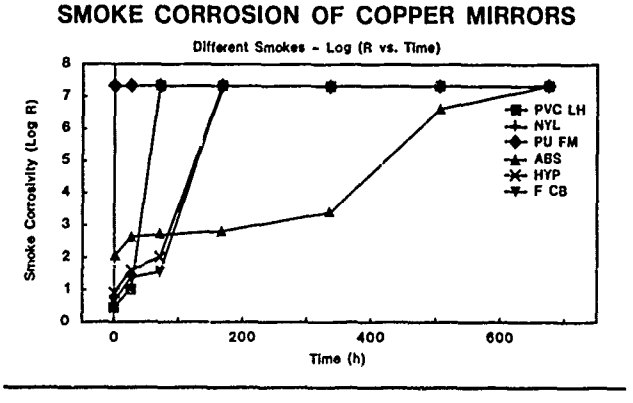

Fig. 7. Smoke corrosion of copper mirrors.

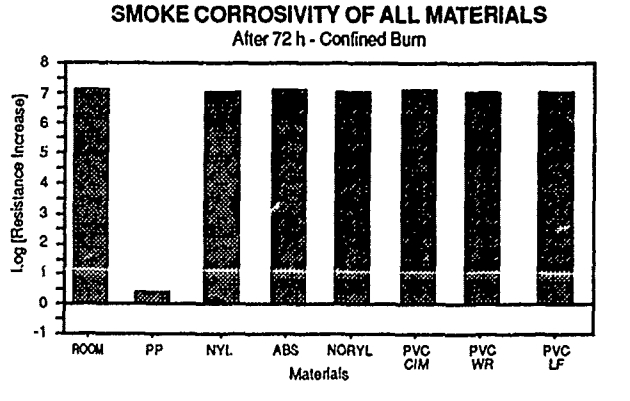

Fig. 10. Smoke corrosivity of all materials.

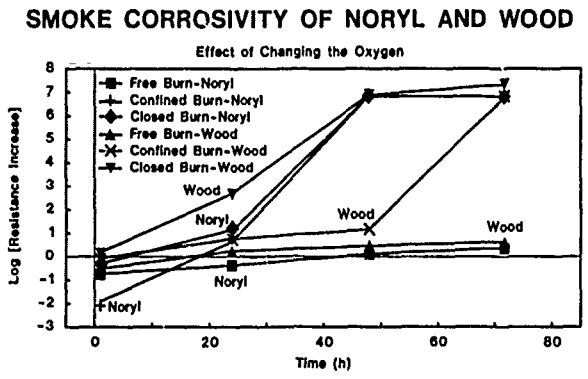

Fig. 11. Smoke corrosivity of Noryl and Wood - effect of changing the oxygen level.

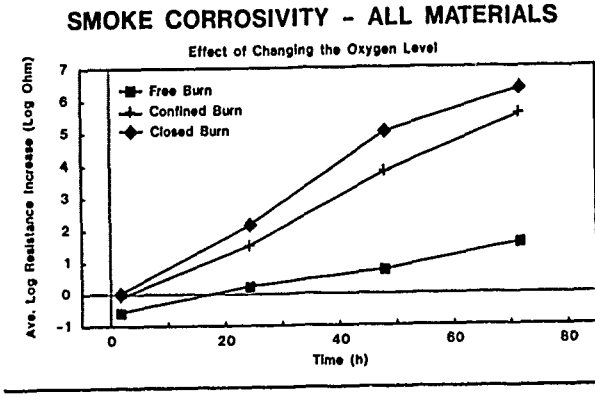

Fig. 12. Smoke corrosivity of all materials - effect of changing the oxygen level.

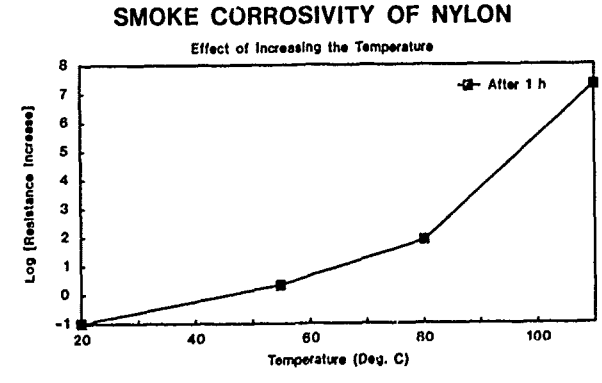

Fig. 13. Smoke corrosivity of Nylon - effect of increasing the temperature.

Dr. Marcelo M. Hirschler

Dr. Marcelo M. Hirschler was born in Buenos Aires (Argentina) and went to the University of Buenos Aires, where he obtained both a first degree and a Ph.D., in Physical Chemistry. He carried out research and teaching at the University of Buenos Aires, at Sussex University (in Brighton, UK, 1975-1977) and at City University (in London, UK, 1977-1984). He joined the BFGoodrich Co. in 1984 and is Manager of the Fire Sciences Department in the Geon Vinyl Division. His principal activities are in research and development, mainly in the fire testing, fire hazard and combustion toxicology areas. He is a member of ASTM (committees E5 (fire standards) and D9 (electrical materials), of NFPA, of CSA, of the Combustion Institute, of the British Standards Institution and of the International Association of Fire Safety Science. He chairs ASTM Subcommittee E.05.15, on Fire Hazard Assessment of Interior Furnishings and Contents, and several Task Groups. He is on the Editorial Board of several scientific fire journals (Fire Safety Journal, Journal of Fire Sciences, Fire & Flammability Bulletin). He is also active across industry since he chairs the Technical Fire Subcommittees of the Coordinating Committee for Fire Safety (Society of the Plastics Industry) and of the Vinyl Institute. He has published over 150 scientific papers and one book, "The Combustion of Organic Polymers" (co-authored with Charles F. Cullis). Awards include the ASTM E.05 Certificate of Appreciation (June 1989) and the UK Interflam Trophy (1988).

SECOND-GENERATION THERMOPLASTIC, ZERO-HALOGEN, LOW-SMOKE, FIRE-RETARDANT INSULATION COMPOUND

Michael Taylor, Peter Richardson, Joe Preston & Jack Taylor

Lindsay & Williams Ltd, Manchester, UK

Abstract

The development of a Low-Smoke, Halogen-Free, Fire-Retardant Thermoplastic, cable insulation material, known as D31 is described. Results are presented to show that the electrical, physical and ageing characteristics are similar to those of a typical PVC insulation material.

Comparisons are drawn with PVC insulation material and results presented to confirm that the flammability properties of the compound are far superior to those of a PVC insulation material, D31 generating only low levels of smoke, toxic fumes and acidic gases, whilst being significantly more difficult to ignite.

The thermo-mechanical properties of D31, coupled with its excellent breakdown voltage, would render the material suitable for the insulation of Power cables, whilst the low di-electric constant would allow its use in communication cable applications.

Introduction

The use of halogenated polymers and compounds, and their associated processing technology, has found application in cable manufacture for many years. Polymers such as Poly Vinyl Chloride (PVC), Poly Chloroprene (PCP) and Chlorosulphonated Polyethylene (CSP), have been compounded for various properties, to meet specifications for insulation and jacketing of cables. However, compounds based on these polymers are reported to possess inherent drawbacks when involved in a fire situation.[1,2,3,4,23,24] These can be summarised into three main areas:

1. Large volumes of dense black smoke are emitted.
2. Highly corrosive acid gases are released.
3. The materials can propagate a fire along a cable run.
4. Burning drops of molten material can fall away from the cable.

In response to these problems, certain low-smoke, halogen-free, fire-retardant thermoplastic compounds have gained acceptance as replacements for PVC in a wide range of cable jacketing applications, but in general the di-electric properties of these materials are comparable only to non-flame-retarded PVC compounds, and they have not found use as insulation materials.

However, in the instance of a fire where a Low-Smoke, Halogen-Free, Fire-Retardant jacketed cable is installed, it is desirable that the insulation material be also Low-Smoke, Halogen-Free and Fire-Retardant, in order to minimise the contribution of the insulation to the conflagration, and in order to have the ends of the insulation fire-retardant where the sheath is removed for termination. In view of this, we have developed an insulation compound which matches the mechanical and electrical properties of a typical PVC insulation material, but is halogen-free, fire-retardant, and generates only low quantities of smoke on pyrolysis.

Existing Halogen-Free compound technology was employed to develop the insulation compound, the improvements over Halogen-Free jacketing compounds being targeted towards better electrical properties and improved processability, up to the requirements of a typical UK PVC insulation material, known as a type TI2[5] material. In addition, the properties were targeted towards meeting an existing Halogen-Free insulation specification, namely a type HJ2[6] material. The requirements for these materials are outlined in Figure 1.

Initial Evaluations

A variety of compound formulations with various polymers, fillers and process aids were screened for the important mechanical, electrical and flammability properties. The general conclusions from these experiments are presented in Figure 2.

From the formulations considered, formulation 201 had the best overall performance for the parameters considered, and it was subsequently renamed "D31" for large scale manufacture and trials.

The results of these trials and subsequent laboratory testing are presented in the remainder of this paper.

PROPERTY	BS6746:1984 (1) TI2 REQUIREMENT	DIN VDE0207 PT23 (2) HJ2 REQUIREMENT
MIN TENSILE STRENGTH	10 MPa	5 MPa
MIN ELONGATION AT BREAK	150%	125%
LOW TEMPERATURE BEND (-15°C)	NO CRACKS	---
LOW TEMPERATURE ELONGATION (-15°C)	20%	---
LOW TEMPERATURE IMPACT (-15°C)	NO CRACKS	---
AFTER AGEING AT 80°C/90°C	(7 DAYS 80°C)	(14 DAYS 90°C)
MIN TENSILE STRENGTH	10 MPa	5 MPa
MAX ALTERATION	20%	-30%
MIN ELONGATION AT BREAK	150%	100%
MAX ALTERATION	20%	±30%
PRESSURE TEST AT 70°C/80°C	(70°C)	(80°C)
MAX INDENTATION	50%	50%
MAX SHRINKAGE, 1HR, 100°C	---	4%
HEAT SHOCK, 1HR, 150°C	NO CRACKS	---
CORROSIVITY OF FIRE GASES		
MIN pH	---	3.5
MAX CONDUCTIVITY	---	10 μScm^{-1}
'E' VALUE 70°C	0.037	---
VOLUME RESISTIVITY 20°C	---	MIN 10^{12} Ωcm
VOLUME RESISTIVITY 70°C	---	MIN 10^{12} Ωcm

Figure 1 Requirements for a typical PVC insulation material (1) and a halogen-free insulation material (2)

BASE POLYMER TYPE	A	B	C	D	E
FORMULATION NUMBER	184	116	204	201	179
TENSILE STRENGTH	*	*	**	***	*
ELONGATION AT BREAK	***	***	*	***	***
VOLUME RESISTIVITY	***	***	***	***	***
SURFACE RESISTIVITY	***	***	***	***	***
DIELECTRIC CONSTANT	**	*	*	***	*
OXYGEN INDEX	***	**	***	**	**
MOONEY VISCOSITY	**	**	**	***	***

Figure 2 General conclusions from screening programme. * = poor, ** = moderate, *** = good.

Mechanical Properties

The Mechanical Properties of D31 are presented in Figures 3-6, along with the requirements for a typical PVC insulation material[5] and a halogen-free insulation material.[6]

Figures 3, 4 and 5 show that D31 has adequate properties before and after thermal ageing, to meet the requirements for typical PVC and typical Halogen-Free insulation materials. In addition, the data presented in Figure 6 shows D31 to have a reasonable resistance to commonly encountered oils.

PROPERTY	D31 RESULTS	TI2[5] MIN REQUIREMENT	HJ2[6] MIN REQUIREMENT
Tensile Strength	10.5 MPa (1522 psi)	10 MPa (1450 psi)	5 MPa (725 psi)
Elongation at Break	740%	150%	125%
Hardness	94 Shore A	---	---
Tear Strength	11 Nmm^{-1} (62.7 lbf/in)	---	---

Figure 3 Mechanical properties of D31 compared with various specifications.

PROPERTY	D31 RESULT	ALTERATION	TI2[5] MIN REQUIREMENT	TI2[5] MAX ALTERATION
After Ageing 7 days at 80°C (176°F)				
Tensile Strength	10.5 MPa (1522 psi)	0%	10 MPa (1450 psi)	± 20%
Elongation at Break	654%	- 12%	150%	± 20%

Figure 4 Thermal ageing behaviour of D31

PROPERTY	D31 RESULT	ALTERATION	HJ2[6] MIN REQUIREMENT	MAX ALTERATION
After Ageing 14 days at 90°C (194°F)				
Tensile Strength	10.6 MPa (1537 psi)	+ 1%	5 MPa (725 psi)	- 30%
Elongation at Break	665%	- 10%	100%	± 30%

Figure 5 Thermal ageing behaviour of D31

PROPERTY	RESULT	ALTERATION
ASTM 1 oil		
Tensile Strength	8.8 MPa (1276 psi)	- 15%
Elongation at Break	650%	- 11%
ASTM 3 oil		
Tensile Strength	8.8 MPa (1276 psi)	- 15%
Elongation at Break	700%	- 6%
ASTM 5 oil		
Tensile Strength	7 MPa (1015 psi)	- 33%
Elongation at Break	640%	- 14%

Figure 6 Tensile properties of D31 after immersion in common oils 7 days at 25°C (77°F)

Electrical Properties

The results of the electrical tests presented in Figures 7 and 8 demonstrate that D31 easily surpasses the requirements for a zero-halogen insulation material.[6] More interestingly however, D31 is also able to satisfy the requirements for a type TI2 general purpose PVC insulation material.[5]

The di-electric properties are comparible to a typical PVC insulation material, and sufficient to render D31 suitable for communication cable. In addition, the breakdown voltage of D31, coupled with its excellent thermomechanical properties (as will be seen later) would allow D31 to find application in power cable insulation.

The 'K' value of D31 after immersion in water has been measured over a period of 672 hours (28 days), and Figure 9 shows the insulation resistance constant ('K' value) to fall steadily up to around 400 hours, after which it would appear to be beginning to reach equilibrium. This pattern of behaviour is similar to that reported for a zero-halogen jacketing material.[14] Notibly, the 'K' value is still well above the specified minimum for a TI2 PVC insulation material, (i.e. 0.037 MΩKm) after 28 days immersion in water.

PROPERTY		RESULT	TI2[5] MIN REQUIREMENT
Volume Resistivity	(20°C/68°F)	7.5 x 10^{14} Ωcm	10^{10} Ωcm
	(70°C/158°F)	5.4 x 10^{13} Ωcm	10^{10} Ωcm
			TI2[5] MIN REQUIREMENT
'K' Value	(20°C/68°F)	235 MΩKm	
	(70°C/158°F)	168 MΩKm	0.037 MΩKm

Figure 7 Electrical properties of D31 versus various specifications

PROPERTY	RESULT
Surface Resistivity (20°C/68°F)	1.4 x 10^{15} Ω
Dielectric Constant (23°C/73°F)	3.6
Dielectric Loss (Tan Δ) (23°C/73°F)	9 x 10^{-4}
Breakdown Voltage (23°C/73°F)	17.9 KV/mm

Figure 8 Miscellaneous electrical properties of D31

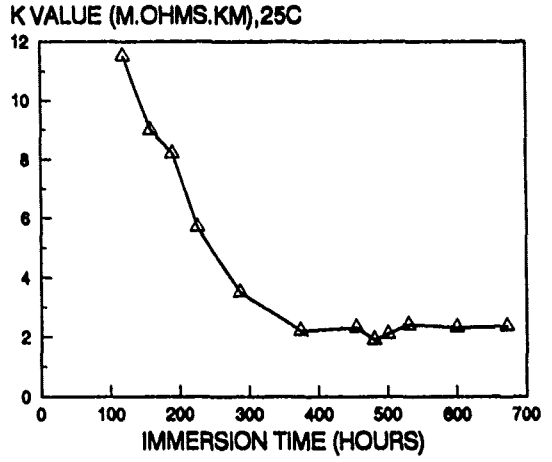

Figure 9 Insulation resistance constant versus time of immersion in water

Thermo-Mechanical Properties

The compound was characterised in terms of its physical behaviour over a range of temperatures by Dynamic Mechanical Thermal Analysis (DMTA). This technique measures the deformation of a material in response to vibrational forces. A Dynamic Mechanical Thermal Analyser was used to determine the changes in Storage Modulus (E'), and Loss Tangent (Tan Δ) which measures the energy dissipated per cycle compared to the energy stored by the compound. Any changes in the heat dissipation/storage behaviour, over a range of temperatures, would indicate a relaxation in the polymer system (e.g. Glass Transition, Tg). The method used has been widely reported[7,8,9] and the results for D31 are presented graphically in Figure 10.

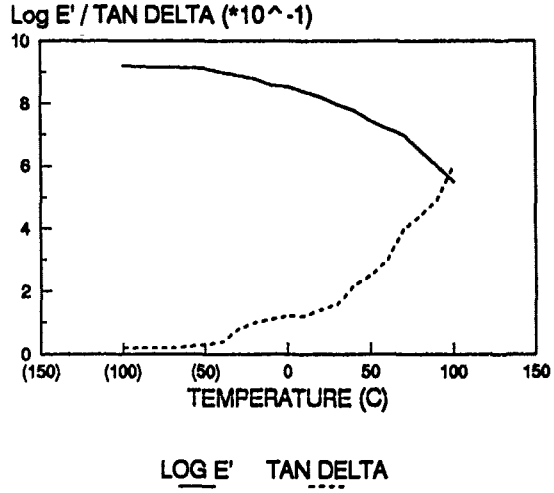

Figure 10 Dynamic mechanical thermal analysis of D31.

Two transitions are indicated for D31 namely the Glass Transition Temperature (Tg) at -30°C and the Crystalline Melting point (Tm) at around 100°C. Thus D31 would be expected to maintain its flexibility at temperatures down to -30°C (-22°F) and to begin to soften at between 90 and 100°C (194-212°F). This shows the product is suitable for telecommunication and power cable applications.

The Hot Pressure Performance of D31, shown in Figure 11 confirms the predictions of the DMTA, D31 easily meeting the requirements of a typical PVC[5] insulation material, and also a zero-halogen[6] insulation material, (Figure 12).

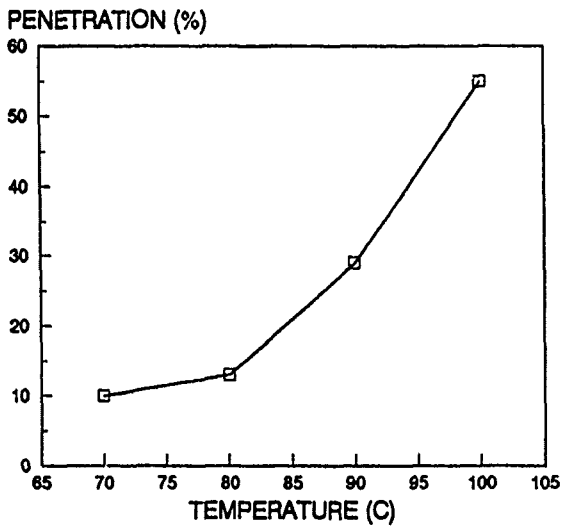

Figure 11 Hot pressure performance of D31

PROPERTY		PENETRATION	TI2[5] REQUIREMENT	HJ2[6] REQUIREMENT
Hot Pressure	70°C (158°F)	10%	50% max	
Hot Pressure	80°C (176°F)	13%		50% max

Figure 12 Hot pressure performance of D31

The results of other miscellaneous thermo-mechanical tests, presented in Figure 13, confirm that D31 complies with the requirements of both a PVC and a zero-halogen insulation material. Notably the elongation at break properties are excellent at sub-zero temperatures down to -15°C (5°F), and these would be expected to be maintained down to -30°C (-22°F), as predicted by DMTA.

TEST	RESULT	TI2[5] REQUIREMENT	HJ2[6] REQUIREMENT
Low Temperature Bend -15°C (5°F)	No cracks	No cracks	
Low Temperature Impact -15°C (5°F)	No cracks	No cracks	
Low Temperature Elongation -15°C (5°F)	500%	20% min	
Mass Loss, 7 days, 80°C (176°F)	0.5 mg/cm^2	2.0 mg/cm^2 max	
Shrinkage, 1 hour, 100°C (212°F)	2.6%	---	4% max
Heat Shock, 1 hour, 150°C (302°F)	No cracks	No cracks	

Figure 13 Miscellaneous thermo-mechanical properties of D31.

Flammability Properties

The flammability properties of D31 have been assessed by a series of experiments including smoke and toxicity tests, vertical burning, acid gas emission tests and oxygen index testing. In addition, results have been obtained from cone calorimetry.

Toxicity

In the event of a fire the emission of toxic fumes from halogenated insulation and jacketing materials can be hazardous, particularly in areas where large numbers of people are gathered, e.g. Hotels, Conference Halls, Underground Railway Stations,[10,11,12] and the potential for a cable and other items/materials (e.g. floor coverings, wall coverings etc) to generate toxic fumes is a particular concern in this scenario. Thus there is a need to minimise the contribution of a cable to this hazard.

The measurement of the toxicity of a material is a difficult area, and one which is the subject of intense debate. There are, however, several different specified methods for assessing toxicity, one of these methods being the NES 713[13] test which is specified for a number of military applications in the Naval Standards of Great Britian and the United States of America, and also in CNET (French Standards).

The NES 713 Toxicity Index is derived from the measured concentrations of those gases specified in the standard.[13] and which are commonly emitted in fires. The summation of these concentrations, in relation to fatal exposure levels to man, in thirty minutes forms the index. The British and United States Navy Specifications allow a maximum value of 5 for the Toxicity Index. Figure 14 shows that D31 is well within this specification. This low figure is complimentary to the similar

figures obtained from Halogen-Free jacketing materials such as Megolon S300,[14] and Megolon S1/S2[23] which has passed the test for the Airbus Industry Specification 1000.001, Issue 4. Thus allowing the cable designer to design low toxic hazard cables. The results also confirm the halogen-free nature of the product.

GAS	PPM	INDICES
CO_2	6250	1.2
CO	10	0.1
HCHO	0	0
HF	0	0
HCL	0	0
HBr	0	0
HCN	0	0
NOx	9	1.5
CH_2CHCN	0	0
NH_3	0	0
H_2S	0	0
SO_2	0	0
$COCl_2$	0	0
C_6H_5OH	0	0
		Index = 2.8

Figure 14 Toxicity factors for D31

Smoke Testing

The smoke-generation behaviour was assessed to NES 711,[15] and the results are presented in Figures 15 and 16. D31 is shown to be far superior to a typical PVC insulation material, when tested with the same apparatus under the same conditions.

The PVC insulation material generates smoke at an earlier part of the test than D31, and the rate of smoke generatio - PVC is much higher than that for D31. D3i ars to have reached its maximum smoke formation at 5 minutes, whereas the PVC material is still generating large quantities of smoke at the point where the test was terminated. The amount of smoke generated by D31 is shown to be far less than that for the PVC material, indeed, the values for smoke indices of these two material, presented in Figure 15 show that D31 easily meets the requirements of NES 518[22] which specifies a maximum smoke index of 20. However, the PVC insulation material generates an index well above this specified maximum. These results are in line with earlier reported results,[1,23,24] where non-halogenated compounds give a very low level of smoke whilst PVC compounds generate high levels of dense black smoke.

COMPOUND	SMOKE INDEX
D31	10.6
TI2 PVC[5]	189.1

Figure 15 Smoke indices from NES 711

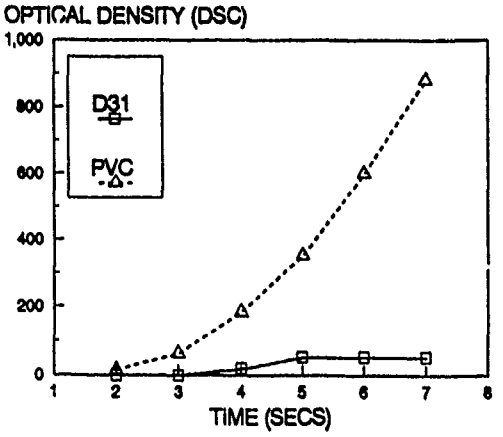

Figure 16 NBS smoke tests results for D31 and PVC (TI2[5]), (NES 711)

Vertical Burning

In order to assess the ignitability of D31 the UL94[16] Vertical Burn Test was employed and the stages of the test are shown in Figure 17-22. In comparison with a typical PVC insulation material, D31 is slow in igniting, whilst the PVC sample ignites almost instantly on application of the flame. D31 produces very little smoke and does not produce burning drips of material, whilst the PVC sample emits large quantities of dense black smoke, and molten material drips from the burning sample.

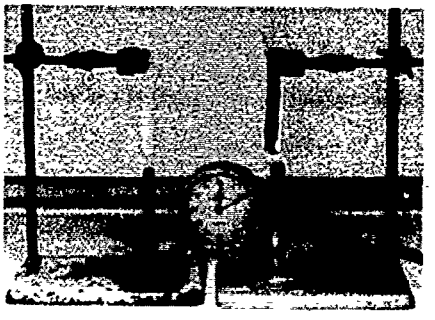

Figure 17 UL94, 10 seconds, D31 v PVC (LHS) (RHS)

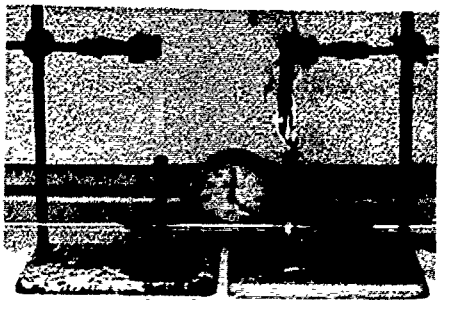

Figure 18 UL94, 20 seconds, D31 v PVC (LHS) (RHS)

Figure 19 UL94, 30 seconds, D31 v PVC (LHS) (RHS)

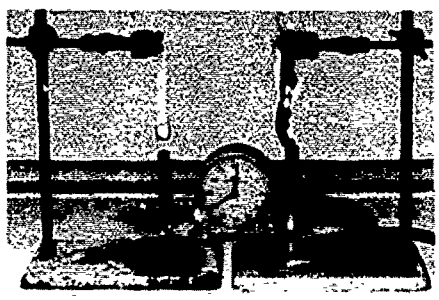

Figure 20 UL94, 40 seconds, D31 v PVC (LHS) (RHS)

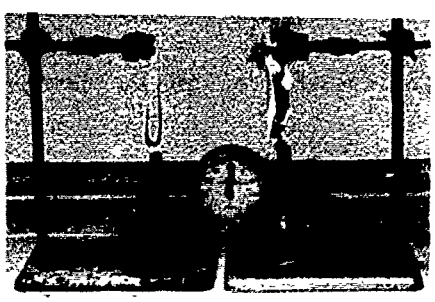

Figure 21 UL94, 60 seconds, D31 v PVC (LHS) (RHS)

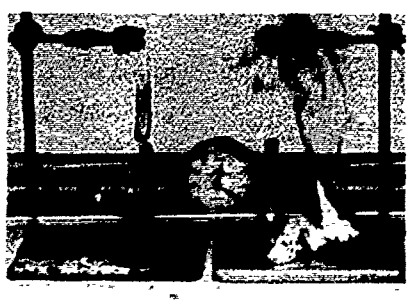

Figure 22 UL94, 120 seconds, D31 v PVC (LHS) (RHS)

Cone Calorimetry

The rate of heat release, smoke generation, ignitability, mass loss, carbon monoxide and carbon dioxide generation for burning materials, were measured for D31 and a typical PVC insulation compound using the cone calorimeter shown in Figures 23 and 24.

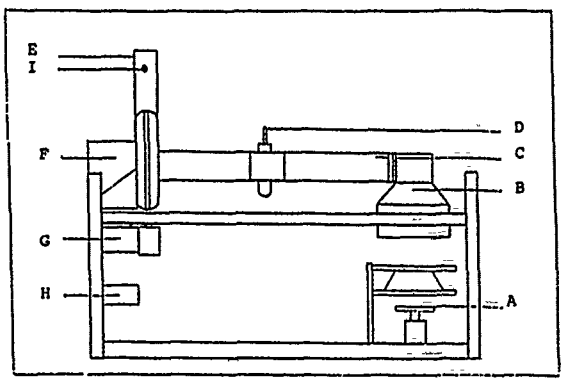

Figure 23 Schematic diagram showing the principle parts of the cone calorimeter.[20]

A - sample	F - blower
B - hood	G - blower motor
C - duct	H - motor speed control
D - gas sampler	
E - pressure ports	I - thermocouple

The results presented in Figures 25-28 show clearly that D31 is more difficult to ignite than a typical PVC insulation compound, has a lower rate of heat release and produces considerably less smoke and carbon monoxide. Additionally, D31 has a lower rate of mass loss, i.e. has considerably less volatiles than a typical PVC insulation compound.

The smoke emission of both compounds is again shown to be vastly different. The cone calorimeter measures a parameter related to the amount of smoke produced per mass of sample burned. It is expressed as the volume of smoke (m^3) of density (calculated by natural logs) of unit per 1 metre thickness (m^3 OD/kg = m^2/kg).[17] The results

show a similar ratio of smoke generation parameters for a typical PVC insulation material and D31, i.e. 828/52 and 882/59 for the cone calorimeter and NES 711 respectively, i.e. PVC generates 15 times the quantity of smoke generated by halogen-free D31.

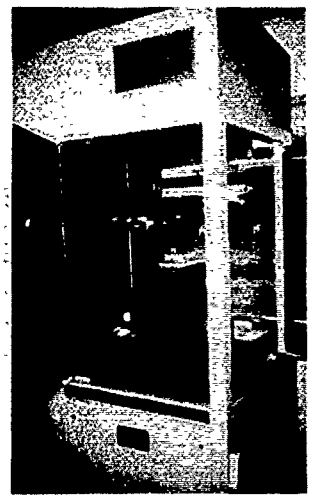

Figure 24 The cone calorimeter

TEST PARAMETER	UNITS	180 SECS*		300 SECS*	
		D31	TI2[5] MATERIAL	D31	TI2[5] MATERIAL
Ignition Time	Secs	132	63	132	63
Rate of Heat Release**	KW/m^2	80	128	80	118
Effective Ht of Combn	MJ/kg	20	12	22	13
Smoke Ext Area	m^2/kg	52	765	59	828
Carbon Monoxide	kg/kg	0.002	0.061	0.002	0.061
Carbon Dioxide	kg/kg	0.99	0.81	1.09	0.88

Figure 25 Summary of cone calorimeter results for D31 and PVC to ASTM E1354.[21]

* 180 and 300 seconds are nominal test times to draw a comparison with

** heat flux 30 KW/m^2

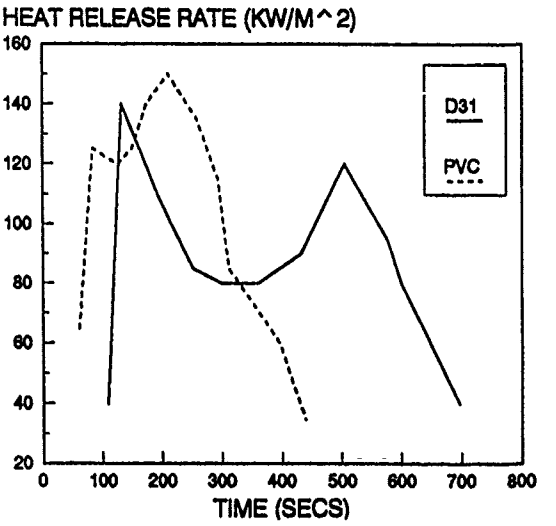

Figure 26 D31 and PVC (TI2)[5] heat release rate

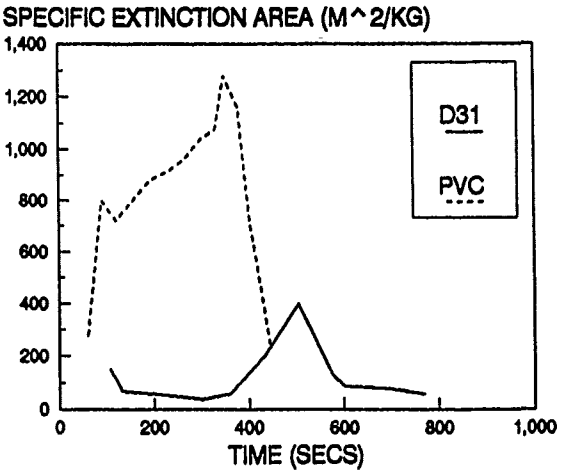

Figure 27 D31 and PVC (TI2)[5] specific extinction area

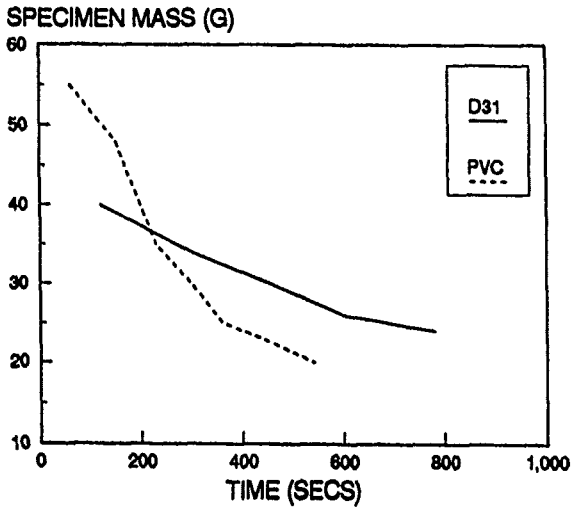

Figure 28 D31 and PVC (TI2)[5] mass loss

Acid Gas Emission

The evolution of acid gases from D31 and a typical PVC insulation material were assessed using commonly reported methods[18,19,23,24] which involve the combustion of a small sample in a current of air, the gases evolved being collected in wash bottles for analysis either by chemical methods,[18] or by the measurement of pH and conductivity.[19]

The results presented in Figure 29 show that D31 is far superior to PVC, emitting no halogen gases, and evolving only very small amounts of other acidic gases on combustion. PVC, however, is known to evolve large quantities of highly acidic hydrochloric acid on combustion, and this is confirmed by the low pH of the water solution, and its high value of conductivity. Furthermore, the chemical analysis[18] confirms that D31 is halogen- free and liberates no halogen-containing gases.

PROPERTY	RESULT		UNITS
	D31	TI2[5] MATERIAL	
Acid Gas Emission[18]	0	200	mgHCl/g
pH of Gases[19]	6.3	2.1	
Conductivity[19]	1.3	4500	µS/cm
Corrosivity	none	high	

Figure 29 Acid gas emission results

Small Scale Flame Tests

The results of small scale laboratory tests on D31 are presented in Figure 30. Again D31 is shown to be superior to a typical PVC insulation compound, having a higher oxygen index and a longer time to ignition.

TEST	RESULT	
	D31	TI2[5] MATERIAL
Oxygen Index[21]	27	24
UL94 Rating[16]	Pass (3 mm)	Fail (3 mm)

Figure 30 Small scale fire test results

Processing

Compound D31 is a highly-filled polyolefinic copolymer based compound and can therefore be processed on conventional thermoplastic extrusion equipment. As demonstrated by Figure 31, the viscosity of the melt, whilst higher than for typical PVC insulation material, is nevertheless considerably lower than that for previously reported[14] halogen-free jacketing materials.

The lower melt-viscosity should enable easier processing on equipment optimised for highly-filled polyolefins, and initial results would indicate this to be the case.

Considerable work, however, remains to be carried out in this area. Of particular interest is the determination of the minimum radial thickness (which appears to be 0.2 mm) which can be achieved by highly-filled polyolefins, and optimisation of die-designs for these materials. Work carried out in this area will be the subject of a future paper. In the meantime, preliminary results reveal that good line speeds can be obtained under similar processing conditions to typical PVC insulation compounds, thus leading to economic production speeds.

MATERIAL	ML (1+4 @ 125°C)	ML (1+4 @ 140°C)
D31	40	38
Type TI2[5] PVC	40	30
Megolon S300[25]	60	50

Figure 31 Mooney viscosity values for various cable materials

Conclusions

The aim of this work has been to develop an insulation material with the low smoke, low acid

gas and low toxic gas characteristics normally associated with zero-halogen jacketing materials combined with the physical and electrical properties of a typical PVC insulation material.

To this end, D31 has been shown to posses flammability properties comparible to zero-halogen jacketing materials, and being far superior to typical PVC insulation material,[5] whilst easily meeting the requirements of a zero-halogen low smoke insulation material.[6]

The electrical properties have been demonstrated to constitute a considerable improvement over those reported for zero-halogen jacketing materials, being comparible to typical PVC insulation materials,[5] and easily matching those required for zero-halogen insulation materials.[6]

The excellent thermo-mechanical properties of D31 make it suitable for use in communicaiton and power cable insulation, whilst the low temperature properties remain excellent down to -15°C, and would be expected to remain so down to -30°C. The smoke generation of D31 is minimal and significantly lower than that of PVC insulation materials. Indeed, in all the flammability assessments carried out to date, D31 gives far better performance than the typical PVC insulation compound, producing low levels of toxic and acidic fumes, and being more difficult to ignite. Significantly, D31 meets the requirements of the British Naval Engineering Standard NES 518[22] for toxic gas emission.

The processing behaviour is currently the subject of a detailed study program. It is expected that similar screw design technology previously reported for halogen-free jackets,[14] would need to be employed to give rise to similar output rates to typical PVC insulation materials.

It is the view of the Authors therefore, that D31 provides the cable designer and user with a viable halogen-free insulation material to replace PVC insulation materials in a number of power and communication cable designs. It is anticipated that this material will find application in areas where the generation of smoke, acidic gases and/or toxic fumes in the case of a fire would present particular problems. These include areas where large numbers of people gather, e.g. Hotels, Railway Stations, Airports, Hospitals; or where high value capital plant is involved such as Nuclear Power Stations, Telephone Exchanges, Computer Suites, etc. Additionally, there may be some applications in Military Cable Installations.

Acknowledgement

The Authors would like to express their thanks to Mr W Butler (Permanoid Ltd, UK), Mr P Barlow (Delta Crompton Ltd, UK) and Dr D Parmar (Kromberg and Schubert GmbHu Co) for their useful discussions during the preparation of this paper, and Miss S J Morrissey for her valuable help in the typing and formatting of this paper.

References

1. Mayer H.A., "Halogen-Free Fire-Retardant Cables", Wire Industry, July 1985.

2. Clarke A.J., Taylor J.A., "Halogen-Free, Low Smoke, Fire-Retardant Compounds and Cables", Polymers in a Marine Environment, 1989.

3. Taylor W.I., Scott K.A.C., PRI Fire Performance and Testing of Plastics, PRI, 1985.

4. "PVC in Fires", British Plastics Federation, London, 1987.

5. BS6746: 1984, "PVC Insulation and Sheath of Electric Cables".

6. DIN VDE 0207. Part 23: 1986, "Insulation and Sheathing Compounds for Cables and Flexible Cords; Halogen-Free Insulating Compounds".

7. Lee D.K., PhD Thesis, University of Manchester, 1988.

8. Okpe O., PhD Thesis, University of Manchester, 1988.

9. Wetton R.E., Polymer Testing, 4, 117, 1984.

10. Weardon T., Electronics Times, p12, 8 Jan 1987.

11. Philbrick S.E., BSI News, p11, May 1987.

12. Kynaston A., Electrical Equipment, p5, Nov 1984.

13. NES 713, Issue 2, "Determination of the Toxicity Index of the Products of Combustion from Small Specimens of Materials".

14. Artingstall A., Pyle A.J., Taylor J.A., "Recent Advances in Thermoplastic Zero-Halogen, Low-Smoke, Fire-Retardant Cable Compound Technology", 36th IWCS, Virginia, November 1987.

15. NES 711, Issue 2, "Determination of the Smoke Index of the Products of Combustion from Small Specimens of Materials".

16. UL94, "Tests for Flammability of Plastics Materials for Parts in Devices and Appliances", - "Vertical Burning Test for Classifying Materials".

17. Rapra Report, "Cone Calorimetry of D31 and PVC", project number K1125, 9 July 1990.

18. BS6425, part 1: 1983, "Gases Evolved during Combustion of Electric Cables".

19. DIN VDE 0472, part 813: 1986.

20. Diagram courtesy of RAPRA, UK.

21. ASTM E1354 "Proposed Method for Heat and Visible Smoke Release Rates for Materials and Products using an Oxygen Consumption Calorimeter".

22. NES 518, Issue 2, "Requirements for Limited Fire Hazard Sheathing for Electric Cables".

23. Mayer H.A., Hög G., "New Generation of Non-Halogenated, Flame-Retardant Compounds and Cables", 29th IWCS, 1980.

24. Dageforde H.G., Mayer H.A., "Flame-Retardant, Halogen-Free, Thermoplastic Telecom Indoor Wiring", 31st IWCS, 1982.

25. Lindsay & Williams Ltd Technical Data Sheets, Megolon Compounds.

Michael Taylor gained his BSc (Hons) in Polymer Science and Technology at the University of Manchester Institute Of Science and Technology in 1989. He had previously worked as a QC Technician at Armstrong World Industries, and as a Rubber Technologist at Pirelli Tyres UK. Michael joined Lindsay and Williams Ltd in July 1989 as a Development Technologist, and since then has been engaged in the design, testing and production of the Megolon range of Low-Smoke, Halogen-Free, Fire-Retardant Compounds.

Peter Richardson studied both Pure Chemistry and Polymer Science and Technology at the University of Aston in Birmingham. After working for Goodyear Tyre and Rubber and TBA Industrial Products in the Development Departments, he joined Rotunda Ltd in 1977. He progressed from Development Technologist to Technical Manager and subseuqently Production Manager.

When Rotunda and Lindsay & Williams amalgamated in 1987, Peter was appointed Factory Manager responsible for all production and technical matters at Lindsay and Williams. In 1989 he was appointed Technical Director of the Lindsay and Williams group, responsible for the development and quality control functions.

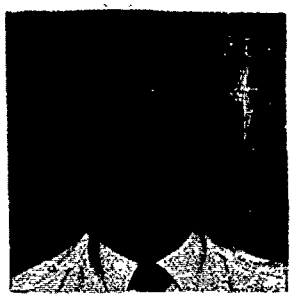

Joe Preston joined Lindsay and Williams Ltd in 1970 as a Laboratory Assistant following 2½ years experience in the Plastics Industry. He studied chemistry at the North Trafford College of Technology. In 1977 he became responsible for the Quality Control function at Lindsay & Williams. He transferred his efforts in 1982 to Development, working on specialised cable tapes, and in more recent years, the Megolon range of Low-Smoke, Halogen-Free, Fire-Retardant Compounds.

Jack Taylor began his working life as a Laboratory Technician examining fibre-reinforced polymers. He gained his BSc (Hons) and PhD degrees in chemistry at the University of Salford, subsequently joining Akzo Chemie UK where he worked on the synthesis of novel halogenated flame-retardants and evaluation of PVC stabiliser systems. Dr Taylor was Product Manager for the Megolon range of halogen-free, fire-retardant cable compounds until 1988 when he was appointed Sales Manager for all of Lindsay and Williams' cable products, which in addition to the Megolon range include semi-conductive cable tapes, insulating cable tapes and range of self-amalgamating tapes and puttys.

A STUDY ON FIRE-RETARDANT OPTICAL CABLE

S. Shimizu*, K. Nakata **, S. Ikegami**, K. Omae* and S. Sentsui*

* The Furukawa Electric Co.,Ltd. 6, Yawatakaigandori, Ichihara, Chiba, 290, Japan
** Kyowa Electric Wire Co., Ltd. 2-5, Kusune-kitamachi, Neyagawa-city, Osaka, 572, Japan

ABSTRACT

Fire-retardant optical cable must be employed for fire-protection systems. However, plastic coatings of optical fibers burn or decomposed under a fire so that optical fiber would be broken easily.

In this study, the cable design with new insulation paper and polyethylene containing magnesium hydroxide was proposed and tested for fire-retardant cable. Heating curve specified in JIS A1304 was applied for the test, in which the temperature reached 840°C in 30 minutes.

The temperature of the cable center was below 420°C in 30 minutes, then optical fibers didn't break and its loss didn't increase. So optical fibers enclosed in the cable were found to be providing high mechanical reliabilities even during a fire.

1. INTRODUCTION

Fire-retardant communication cables installed in fire-protection systems are required to maintain a communication function for a certain period of time in early times of a fire.

In testing fire-retardant cables, the cables are heated in accordance with a heating curve specified in the Japanese Industrial Standard (JIS) A1304. The temperature inside the heating furnace reaches 840°C in 30 minutes. Although the specification for the fire-retardant optical cable has not been established in Japan, it is thought that the optical fibers must not break and loss increases must be less than a few dB during the test. Conventional types of optical cables often cause break of optical fibers when they are subjected to fire retardant tests. The following factors are considered technical difficulties for fire-retardant optical cables :

1) The plastic coating of optical fiber decomposes and vanishes due to heat. Then the optical fiber strength cannot be maintained and the optical fiber easily breakes if a small strain is applied.
2) The optical fiber is applied a tensile stress due to the difference of the linear expansion coefficient between the cable and the optical fiber in it. For example, assuming the cable linear expansion coefficient to be 1.5×10^{-5}, which equals that of steel wires used as strength members in the cable, an elongation of 1.2% occurs if heated to 840 °C.
3) Because plastics used in constructing the cable melt and deform and gas generation due to thermal decomposition of them causes small gas explosions, mechanical strains are applied to the optical fiber.

Considering above mentioned factors, a fire-retardant optical cable design to suppress the temperature increase inside the cable core that uses optical fibers inserted in a metal pipe by insulating by paper and by absorbing heat by endothermic reaction by magnesium hydroxide have been studied.

2. CABLE DESIGN

2.1 MECHANICAL PROTECTION OF OPTICAL FIBER

The cable core was obtained by inserting optical fibers into stainless tubes and by stranding them. The provided protection against thermal deformation of the cable composition materials and against direct stresses by thermally decomposed gases for the optical fibers. A excess length of approx. 0.1% of optical fibers could be put to offset part of the thermal expansion distortion of the cable.

The cable itself was covered with a corrugated steel tube to protect it against external mechanical stresses. And the corrugated tube shielded air to suppress burning of the cable inner composite materials

2.2 HEAT INSULATION

The thermal conductivity of paper is small compared with those of typical metals and ceramics as shown in table 1. Paper was less expensive, and by wrapping it, the cable could have a flexibility to bend. From these reasons, paper could be promising as a heat insulator of cables. Nevertheless, paper was almost never used in fire-retardant cables because of its low heat resistance. In this study, the heat insulating performances of paper normally used, flame-retardant paper and high-density paper was investigated. The

	Thermal Conductivity at 300 K (W/m/deg)
Paper	0.18
Polyethylene	0.22
SiO_2 (Glass)	1.38
Al_2O_3	36
Stainless Steel	14 ~ 17
Iron	80
Aluminum	237
Copper	99

Table 1 Comparison of Thermal Conductivities of typical Materials

flame-retardant paper was made by impregnating organic flame retardant materials in it.

2.3 HEAT ABSORPTION

Taking the endothermic reaction beginning at a relatively low temperature, low cost and ability to be processed into consideration, polyethylene containing magnesium hydroxide was used as the endothermic material. The material has been used as flame-retardant polyethylene. The endothermic reaction of magnesium hydroxide becomes remarkable at approx. 350°C or higher.

3. TESTING METHOD

3.1 CABLE CONSTRUCTION

The cable core was obtained by stranding six stainless steel tubes of 1.2 mm in outer diameter and 0.8 mm in inner diameter around a galvanized steel wire of 1.2 mm in diameter. Using stainless tubes inserted with optical fibers, optical fiber cable could be fabricated.

Three types of cable samples using this cable core were fabricated and tested. (See figure 1)

#1~#4 : Inner polyethylene was covered around the cable core and paper was (or was not) wrapped on them.

#5~#6 : Paper was wrapped around the cable core and inner polyethylene was covered on them.

#7 : Paper was additionally wrapped on #6.

All the three cable types were covered with corrugated steel tube. In the cases of #1 to #6, the corrugated steel tubes were covered with polyethylene containing phosphorus.

Table 2 shows the characteristics of these samples fabricated by varying the kind of paper and the amount of magnesium hydroxide in inner polyethylene.

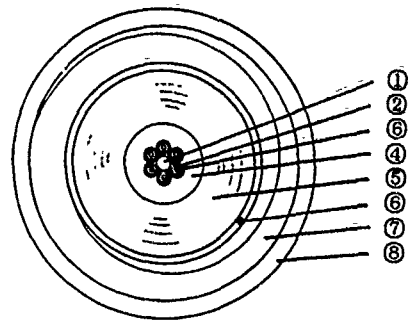

(a) Sample #1~#4

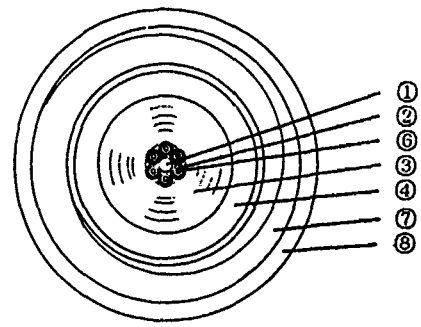

(b) Sample #5~#6

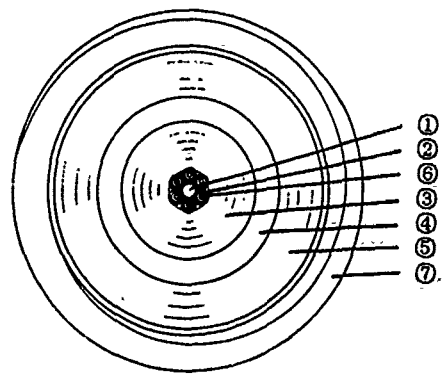

(c) Sample #7

① Galvanized Steel Wire
② Stainless Steel Tube
③ Inner Paper
④ Inner Polyethylene Sheath
⑤ Outer Paper
⑥ Thermocouple
⑦ Steel Corrugated Tube
⑧ Polyethylene Sheath containing phosphorus

Figure 1 Cross-sectional Structures of Tested Cables

Thermocouples were inserted in the stainless steel tubes of all samples to measure temperatures in center of the cables. A thermocouple was fixed on paper or inner polyethylene when the Sample #1 to #4 were tested.

When the Sample #7 was tested, each of optical fibers was fixed on the stainless steel tube on the edge of the sample to measure loss increase during the test.

3.2 TEST APPARATUS

The test apparatus is shown in figure 2. A cable of 1.3m in length was fixed horizontally on a vertical pearlite board.

3.3 HEATING CONDITIONS

The samples were heated 30 minutes in accordance with the temperature curve specified in the Japanese Industrial Standard (JIS) A 1304.

4. TEST RESULTS

4.1 MEASUREMENT RESULTS

Figure 3 shows the results of measuring temperature inside the cables. In the case of Sample #1, the temperature rapidly increased 8 minutes after starting the test and reached 700'C in 15 minutes. It took longer for the sample #2 and #3 than the Sample #1 to reach 100 and 400 'C ; 8 to 9 and 16.5 to 19 minutes after, respectively. The temperature increase speed decreased for 2 to 3 minutes at approx. 400'C.

The Sample #4 did not use paper, but has a cross-section of inner polyethylene 3.5 times those of the Sample #2 and #3. The temperature in the cable center reached 400'C in 15 minutes, but the temperature increase stopped in approx. 5.5 minutes.

In the cases of the Sample #5 and #6, the temperature in the cable center rapidly increased approx. 10 minutes after starting, but increased slower than the

Cable Sample No.	Inner Paper			Inner Polyethylene				Outer Paper		
	Material	Density (g/cm^3)	Diameter (mm)	Material	Diameter (mm)	$Mg(OH)_2$ Content (wt.%)	Content (g/cm)*	Material	Density (g/cm^3)	Diameter (mm)
#1	-	-	-	Conv.	3.6/ 7	0	0	Conv.	0.56	17
#2	-	-	-	F.R.	3.6/ 7	64	0.28	F.R.	0.69	17
#3	-	-	-	F.R.	3.6/ 7	64	0.28	H.D.	1.07	17
#4	-	-	-	F.R.	3.6/ 12	64	0.98	**	-	(14)
#5	H.D. and F.R.	1.19	3.6/ 12	F.R.	12 / 18	80	2.1	-	-	
#6	H.D.	1.07	3.6/ 12	F.R.	12 / 18	80	2.1	-	-	
#7	H.D.	1.07	3.6/ 12	F.R.	12 / 18	80	2.1	H.D.	1.07	28

Conv. : Conventional
F.R. : Flame-retardant
H.D. : High-density
* Weight per Cable-length
** Plastic Tape

Table 2 Characteristics of Samples

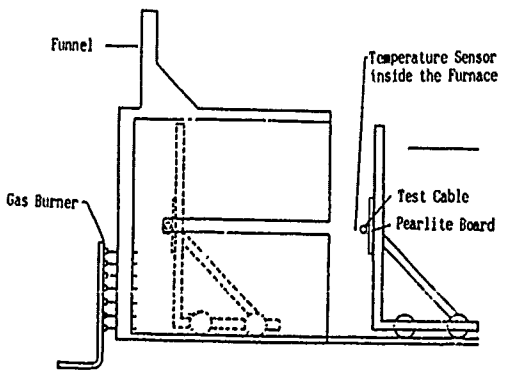

Figure 2 Apparatus of fire-retardant Test

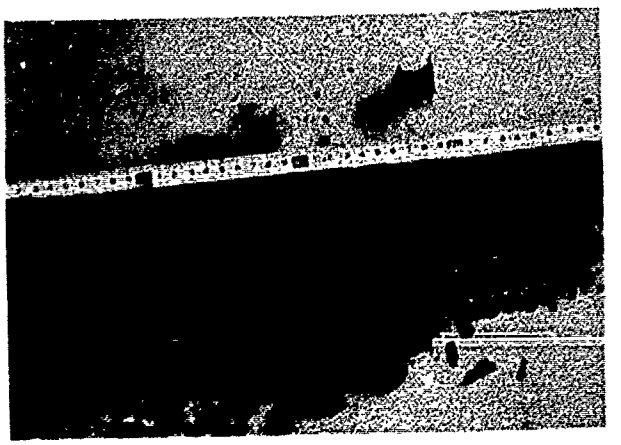

Photo 1 Sample #7 after the Fire-retardant Test

Sample #2 and #3, reaching 400°C in approx. 20 minutes. The temperature increase speed decreased 2 minutes at approx. 400°C, but increased rapidly thereafter. There were no differences in the temperature increase profiles of the two.

The temperature increase during the test temporarily decreased in the Samples #2 to #6, but the temperature reached approx. 700°C in 30 minutes afterward. The temperature of the Sample #7 reached 420°C in 30 minutes. Neither optical fiber break nor loss increases were observed during the first 30 minutes. Photo 1 shows the Sample #7 after the test. All the heated paper were carbonized and magnesium hydroxide was dehydrated and calcined. The optical fiber coating was thermally decomposed and vanished.

4.2 HEAT INSULATION EFFECTS

In the region of 400°C or lower where magnesium hydroxide endothermic reaction effects were none to compare paper effects, the temperature increases were slower with the Sample #2 and #3 than with the Sample #1 even if the effects of water evaporation latent heat were substructed, indicating that flame-retardant and high-density paper exelled in heat insulation. Comparing the Samples #2 and #3, the high-density paper exelled in heat insulation than the flame-retardant paper. Comparing the samples #1 and #2, heat insulation property improved by making conventional paper flame-retardant. However, comparing the Samples #5 and #6, it did not improve even if high-density paper was made flame retardant.

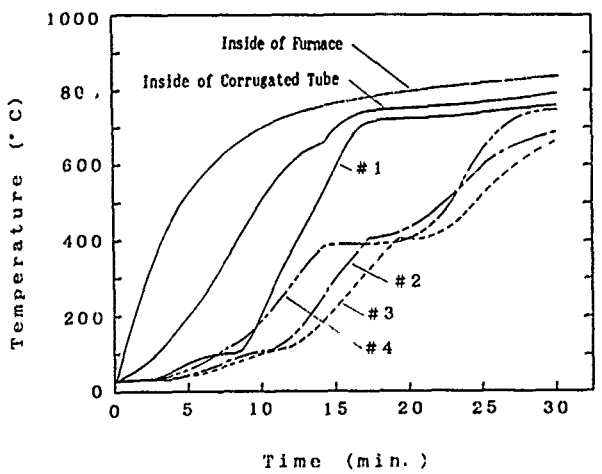

(a) Sample #1~#4

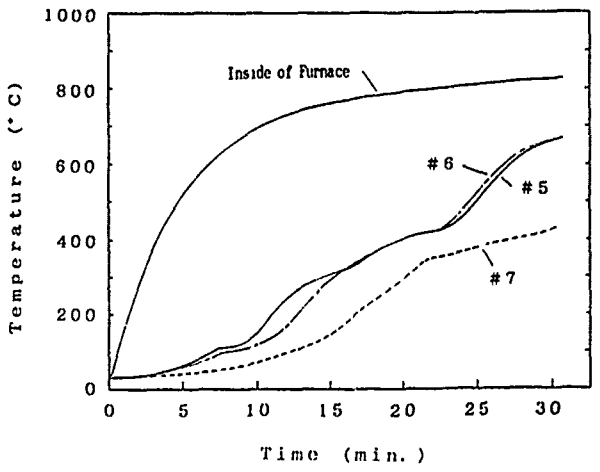

(b) Sample #5~#7

Figure 3 Variations of Cable Temperature

	#1	#2	#3	#4	#5	#6	#7
by water at approx. 100°C	2.9	2.1	1.3	0	2.1	2.1	1.6
by $Mg(OH)_2$ at approx. 400°C	0	2.4	2.6	5.4	3.4	3.1	>8.7

Unit : min.

Table 3 Duration of Endothermic Reaction (by measurement at Cable Center)

4.3 ENDOTHERMIC EFFECTS

The temperature increase speed decreased in the cable center at approx. 100 and 400°C.

At approx. 100°C, it could be observed with the samples other than the Sample #4. So it was thought that it was caused by paper, due to heat absorption by evaporation of approx. 10wt.% water contained in the paper.

The slow temperature increase speed at approx. 400°C could be observed with the samples other than the Sample #1. It was comfirmed by differential scanning calorific analysis (DSC) of inner polyethylene that it was caused by heat absorption due to the decomposition of magnesium hydroxide.

Table 3 shows sustained durations of endothermic reactions. These reactions can be expressed as follows:

H_2O (l) → H_2O (g) $\Delta H = 41$ (kJ/mol/deg)

$Mg(OH)_2$ → $MgO + H_2O$ $\Delta H = 81$ (kJ/mol/deg)

	Thermal Conductivity (W/m/deg)
Paper	0.10
Polyethylene	0.22
Stainless Steel	16

Table 4 Thermal Conductivities used in the Calculation

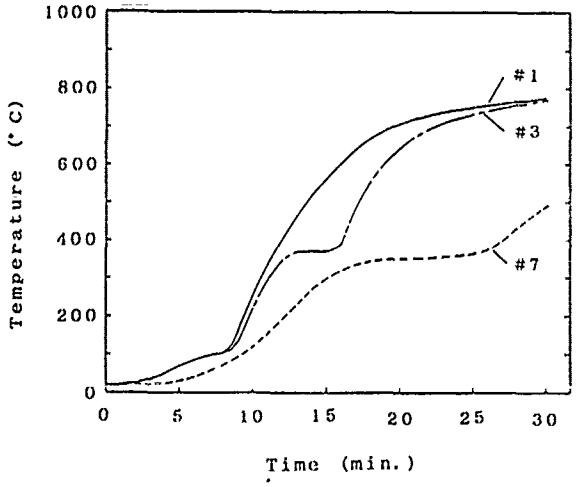

Figure 4 Calculated Temperature of Cable Center

5. NUMERICAL ANALYSIS

5.1 ANALYSIS METHOD

The temperature fluctuations inside the cable simply could be analyzed by the equation of unsteady-state heat conduction and by endothermic reaction speed. They were analyzed by the cylindrical coodinates one-dimensional finite element method. However, strictly speaking, state variations of various materials (paper carbonization, melting and thermal decomposition of polyethylene, and variations caused to magnesium oxide due to dehydration reaction of magnesium hydroxide) and variations of property values (specific heat, thermal conductivity and density) caused by temperature fluctuations have to be taken into consideration. So the analysis was complex. For these reasons, it was more useful in design to obtain the constants needed in calculations that could well explain the experimental results.

Table 4 shows the thermal conductivities used in the calculations. The following calculation formula was used for endothermic reactions.

$$\dot{Q} = a \cdot \exp(b/T)$$

$\dot{Q}$: Endothermic rate per unit weight. (Watt/g)
T : Absolute temperature (K)
a,b : Constant

	H_2O	$Mg(OH)_2$
a (Watt/g)	1.38×10^{-36}	2.56×10^{-11}
b (K)	31200	18000

5.2 ANALYSIS RESULTS

Figure 4 shows the calculation results of the temperature inside the cable. The calculation results show values higher than those obtained in measurements.

	#1	#3	#4	#6	#7
by water at approx. 100°C	2	3	0	0.8	5
by $Mg(OH)_2$ at approx. 400°C	0	3.0	7.1	13	13

Unit : min.

Table 5 Duration of Endothermic Reaction (by calculation)

However, all the test results can be expressed uniformly. It shows that a numerical analysis was possible to design cables of different constructions containing paper and polyethylene.

The results of the numerical analysis showed the following :

1) The temperature difference between the outer and inner surfaces of the inner polyethylene was only several centidegrees in its thermal conductivity, showing heat insulation effects could be expected nearly at all.
2) The paper thermal conductivity must be estimated lower than those mentioned in the literatures.
3) If a water content of paper was assumed to be 10 wt.%, the endothermic reaction at approx. 100°C well agreed with the measured value.
4) If the endothermic reaction sustained duration of magnesium hydroxide was assumed as the time from the temperature increase speed on the external surfaces of the inner polyethylene becoming slow at approx. 400°C to its inner surface temperature starting to rapidly increase, the durations with the samples were shown in Table 5. It showed that the sustained durations lengthen larger the amount of magnesium hydroxide contained in unit lengths of the samples.
5) When paper (or a heat insulator) was wrapped inside of polyethylene containing magnesium hydroxide, because the temperature inside the paper increased as time passed even if the temperature around paper was maintained constant by the heat absorbing material, eventually reaching the same temperature, the heat insulation effects of paper were small.

   By suppressing the heat inflow speed by wrapping paper on the exteriors of the cable, the effects of the endothermic materials can be lengthened.

6. CONCLUSIONS

The above results lead to the following conclusions.

1) The heat insulation effecs of paper are as follows.
   High-density paper ≧ flame-retardant paper
   > conventional paper
2) The effects of the water contained in paper on suppressing temperature increases cannot be ignored.
3) The endothermic reaction effects of magnesium hydroxide occur in approx. 400°C. The temperature increase suppression duration varies with the amount of the heat absorption in unit length of the cable.
4) The quantity of heat flowing in can be suppressed to lengthen the suppression effects of heat absorber by wrapping paper on rather the outer surface than the inside of a heat absorber,

In this study, the cable design with new insulation paper and polyethylene containing magnesium hydroxide was proposed and tested for fire-retardant cable. The temperature of the cable center was below 420°C in 30 minutes, then optical fibers didn't break and its loss didn't increase. So optical fibers enclosed in the cable could be providing high mechanical reliabilities even during a fire.

REFERENCE

1) M. Niijima, K. Komiyama and S. Sentsui
   Development of the Optical Fiber Cable installed in the Sewer Pipe Network.
   IWCS 1989, Session 13

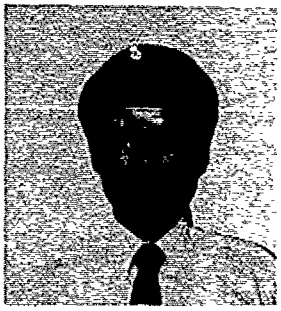

Shigeo Shimizu

The Furukawa Electric Co., Ltd.

6,Yawatakaigandori, Ichihara,Chiba,290,Japan

Mr. Shimizu was born in 1957. He received B.S. degree in nuclear engineering from Nagoya University in 1980 and joined The Furukawa Electric Co., Ltd. He has been engaged in development of optical fibers and cables.

He is a member of The Institute of Electronics, Information and Communication Engineers of Japan.

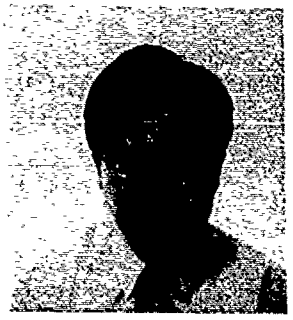

Kazuya Omae

The Furukawa Electric Co., Ltd.

5-1-9, Higashiyawata, Hiratsuka, Kanagawa, 254, Japan

Mr. Omae was born in Kyoto city, Japan, on June 17, 1951. He received B.S. degree in electronics from Kyoto University in 1974 and joined The Furukawa Electric Co., Ltd. He has been engaged in development of optical fiber cable and system.

He is a member of The Institute of Electronics, Information and Communication Engineers of Japan.

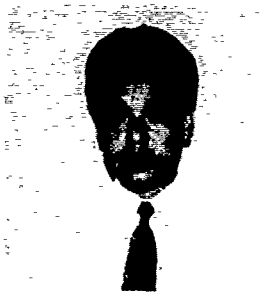

Katsumi Nakata

Kyowa Electric Wire Co., Ltd.

2-5, Kusune-kitamachi, Neyagawa-city, Osaka, 572, Japan

Mr. Nakata was born in Osaka prefecture, Japan,on Dec. 22, 1957. He received B.S. degree in chemistry from Himeji Institute of Technology, Himeji, Japan, in 1980 and joined Kyowa Electric Wire Co., Ltd. Since 1984, he has been engaged in design of optical-fiber cables.

He is a member of The Institute of Electronics, Information and Communication Engineers of Japan.

Shintaro Sentsui

The Furukawa Electric Co., Ltd.

6,Yawatakaigandori, Ichihara,Chiba,290,Japan

Mr. Sentsui received B.S. degree in physical engineering from Tokyo University in 1970 and joined The Furukawa Electric Co., Ltd. He has been engaged in research and development of superconduction coaxial line, and characterization and measurement of optical fiber.

He is now a manager of optical fiber transmission research section.

Seiji Ikegami

Kyowa Electric Wire Co., Ltd.

2-5, Kusune-kitamachi, Neyagawa-city, Osaka, 572, Japan

Mr. Ikegami was born in Kyoto prefecture, Japan,on Sep. 21, 1946. He received B.S. degree in chemistry from Kyoto Institute of Technology, Kyoto, Japan, in 1969 and joined Kyowa Electric Wire Co., Ltd. Since 1974, he has been engaged in design of cables.

He is a member of The Institute of Electronics, Information and Communication Engineers of Japan.

DEGREE OF CURE OF UV-CURED OPTICAL FIBER COATING DETERMINED BY THERMAL ANALYSIS AND PHOTOCALORIMETRY

Sam Huy, Minoru Chiba, Tomonori Hoshino,
Osamu Shimizu and Misao Hanai

Showa Electric Wire & Cable Co., Ltd.
Sagamihara, Kanagawa, Japan 229

The purpose of this study is to establish an easy evaluation technique which determines, with high reproducibility and reliability, the degree of cure of UV-cured resin coated on optical fibers. We carried out thermogravimetry/differential thermal analysis (TG-DTA) for such evaluation, and studied relations between the quantity of UV irradiation and the thermal decomposition behavior of polymer on a UV-curable resin (urethane acrylate). A characteristic thermal decomposition peak was observed in relation with the quantity of UV irradiation in the temperature range of 220 to 450°C. It was confirmed that the method can be applicable to evaluation of the degree of cure of UV-cured resin coated on optical fibers. It was also confirmed that the degree of cure of UV-cured resin coated on optical fibers can evaluated by photocalorimetry from the ratio of residual exothermic heat of photopolymerization emitted when the optical fiber coating is re-irradiated with UV to the heat of photopolymerization of individual UV-curable resins.

1. Introduction

Ultraviolet-curable resins (which are referred to, hereinafter, as UV resins) are being used as coating materials for optical fibers because of their quick-curing character, and the use of such resins is increasing year after year as the optical fiber market expands.

The properties of UV resins depend much on the degree of cure, and it is necessary to control the degree of cure to obtain UV resin coated optical fibers consistent in quality. It is therefore important to establish a method for evaluating the degree of cure of UV resins coated on optical fibers for determination of operating conditions of drawing and coating processes and for quality control during production.

The degree of cure of UV resins in sheet form can be known rather easily by measuring their gel fraction, Young's modulus or viscoelasticity. For UV resins coated on optical fibers, however, no effective method has been established mostly because of difficulty of sampling which caused poor accuracy and reproducibility of measurement.

The purpose of this study is to establish simple and convenient methods for evaluating the degree of cure of UV resins coated on optical fibers at high reproducibility and reliability, which are applicable even to multi-layered coating. Methods studied here are the thermogravimetry/differential thermal analysis (TG-DTA) which observes the thermal decomposition behavior and the photocalorimetric analysis which measures exothermic heat associated with photopolymerization.

Relations between the degree of polymerization or molecular weight and the thermal decomposition behavior have been studied much in the field of high polymers [1], and differences in thermal decomposition behavior by the degree of polymerization have been reported on methacrylic and acrylic polymers which are similar to UV resins [2]. It is judged therefore that it would be possible to distinguish differences in the degree of cure or molecular weight associated with irradiation also in UV resins. The photocalorimetry, on the other hand, is studied recently as an effective method for checking the curability in the fields of photosensitive resins and photoinitiators [3].

The two methods mentioned above were examined and turned out to be effective as methods for evaluation of the degree of cure of UV resins coated on optical fibers as reported below.

2. Experimental

2.1 Specimens

Three urethane acrylate UV resins, two (A and C) for primary and one (B) for buffer, available on the market were used. Optical fibers coated with UV resins (which are referred to, hereinafter, as coated fibers) listed in Table 1 were drawn by dual coating and UV irradiation, where the amount of UV irradiation was changed by adjusting the number of UV lamps and the drawing speed.

Each coated fiber was made to be 125, 200 and 240 μm in outer diameters of the fiber, primary layer and buffer layer, respectively.

Such coated fibers were cut into lengths of 1 to 2 mm to use them as specimens for TG-DTA and phtotocalorimetric measurements. In preliminary studies, cured sheet samples of 100 μm of UV resins A, B and C were cut into pieces of about 1 mm square for measurements. Uncured liquid resins were also used in preliminary studies on photocalorimetry.

2.2 Apparatus and Conditions of Measurement

A TG-DTA 200 analyzer of MAC Science was used for TG-DTA analysis. Measurements were made in the atmosphere of dry high-purity air flowing at 100 cc/min while the temperature was raised from room temperature to 800°C at a rate of 20°C/min. The amount of specimen was about 4 mg as determined from preliminary studies on accuracy and reproducibility of measurement. The value of DTG (Differential

Thermogravimetry) was determined using the software program included in the analyzer.

Photocalorimetric measurements were made using the combination of a DSC3100 analyzer and a UV9300 irradiator of MAC Science. The basic principles of the measuring system are shown in Fig. 1. The light from the extra-high pressure mercury lamp is made to be a uniform parallel light by the optical system for irradiation. The heat from the light source is blocked by a heat-cutting filter. An interference filter, an ND filter and an electronically controlled shutter are used to control the wavelength of irradiating light, the amount of irradiation and the time of irradiation, respectively.

For a liquid sample, a specimen of about 1 mg was coated thinly and uniformly on a flat aluminum pan so that the irradiating light reached the bottom of the specimen.

For a sample of coated fiber, pieces of specimens were arranged flat orderly. As for the standard sample, the same empty aluminum pan as those used for specimens was used. In order to minimize cure inhibition caused by oxygen, 365-nm ultraviolet light of 1 mW/cm² was irradiated for measurement in the atmosphere of nitrogen flowing at 50 cc/min. The temperature was maintained constant at 30°C.

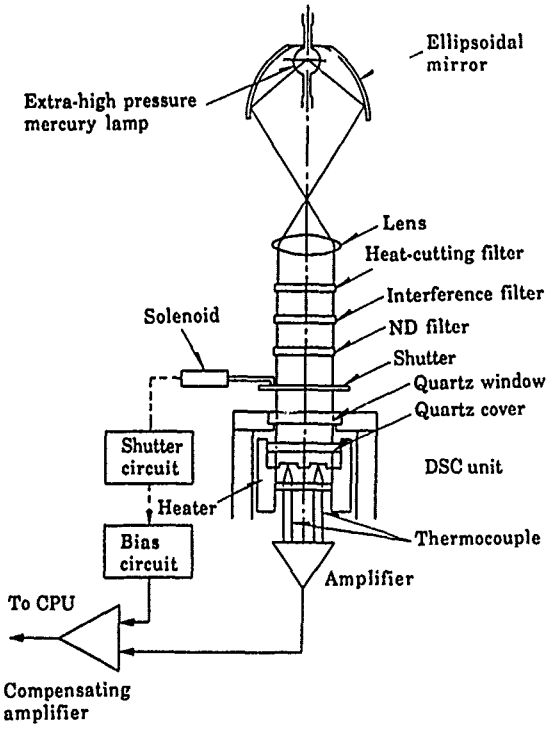

Fig. 1 Principles of photocalorimetry

3. Study of the TG-DTA Analysis

3.1 Basic Studies

The possibility of using the TG-DTA analysis as a method for evaluating the degree of cure of UV resins was studied. Thermal decomposition behaviors common to and different among UV resins were elucidated, and thermal decomposition behaviors of UV resins different in the degree of cure were examined.

3.1.1 Amount of Irradiation and Thermal Decomposition Behaviors of UV Resins

Gel fraction and Young's modulus measured on UV resin 'A' indicate that they are saturated at irradiations above 500 mJ/cm² (Fig. 2). Such trends were the same also for UV resins 'B' and 'C'. TG-DTA measurements were made therefore on UV resin 'A' preparing sheets irradiated to 100, 500 and 1000 mJ/cm². Results are shown in Fig. 3 (a, b, c). Effects of irradiation are visible on peaks occurring between 300 and 400°C. For the sample of low irradiation (100 mJ/cm²), the reduction in weight and the rate of reduction in weight are greater than those of samples of higher irradiation coming from low molecular weight components and unreacted acrylic group. When samples irradiated to 500 and 1000 mJ/cm² are compared, a difference is visible in the size of peaks occurring around 380°C although little difference was recognizable in conventional measurements of gel fraction and Young's modulus.

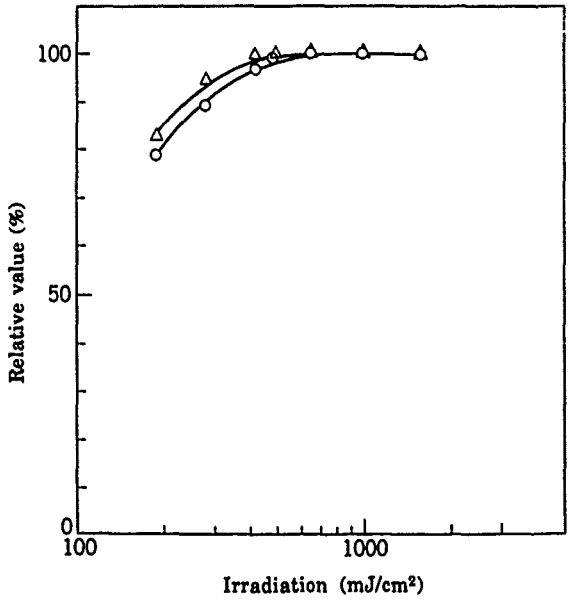

Fig. 2 Changes in gel fraction and Young's modulus by irradiation in UV resin 'A'
o : Young's modulus, Δ : Gel fraction

The TG-DTA measurements were made also on UV resins 'B' and 'C' to examine their thermal decomposition behaviors at different irradiations. As resins were irradiated more, the decomposition peak at 450°C grew in resin 'B' and the decomposition peak at 420°C grew and got sharper in resin 'C'. As for temperatures of decomposition peaks of respective resins, that of resin 'B' for buffer occurs at a temperature higher than those of resins 'A' and 'C' for primary. It is estimated that such difference in the temperature of decomposition peak comes from the ratio and kinds of soft and hard segments which form the molecular structure of each resin [4, 5, 6].

As discussed above, it is clear that the change in the degree of cure by irradiation is properly known for any of UV resins 'A', 'B' and 'C' from information of their thermal decomposition behaviors (DTG-DTA). In addition, the difference in the amount of irradiation not detectable from gel fraction or Young's modulus is detectable from DTG-DTA.

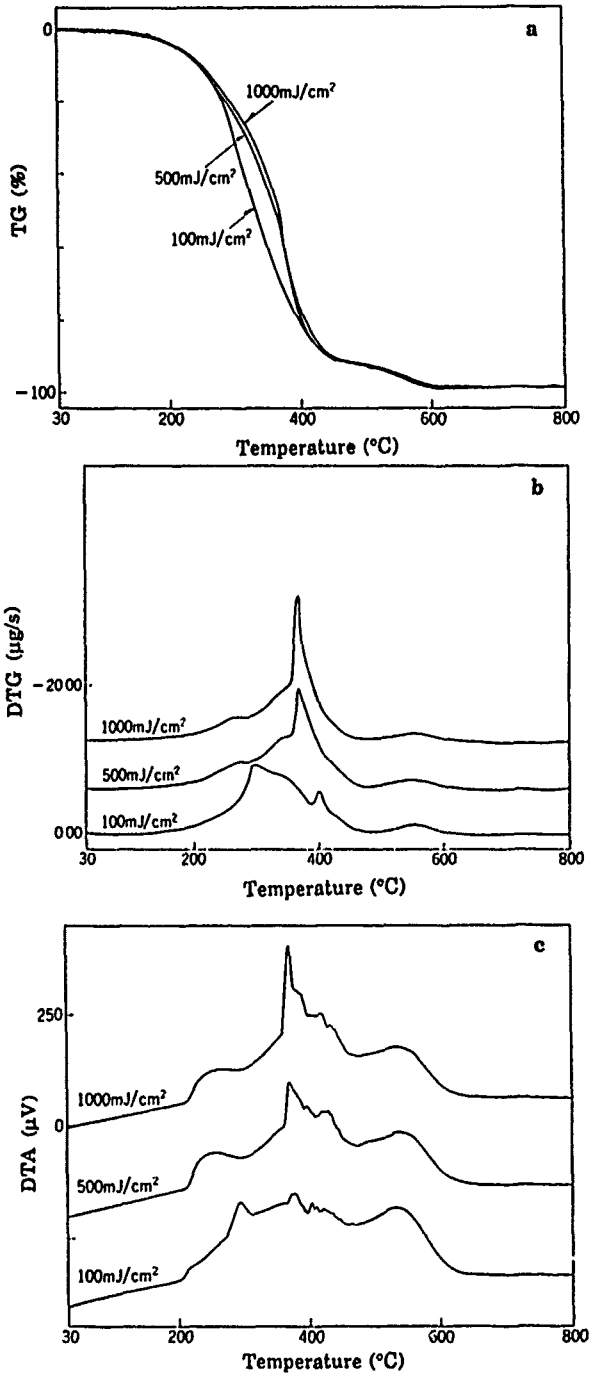

Fig. 3 Irradiation and thermal decomposition behaviors of resin 'A'
a: TG, b: DTG, c: DTA

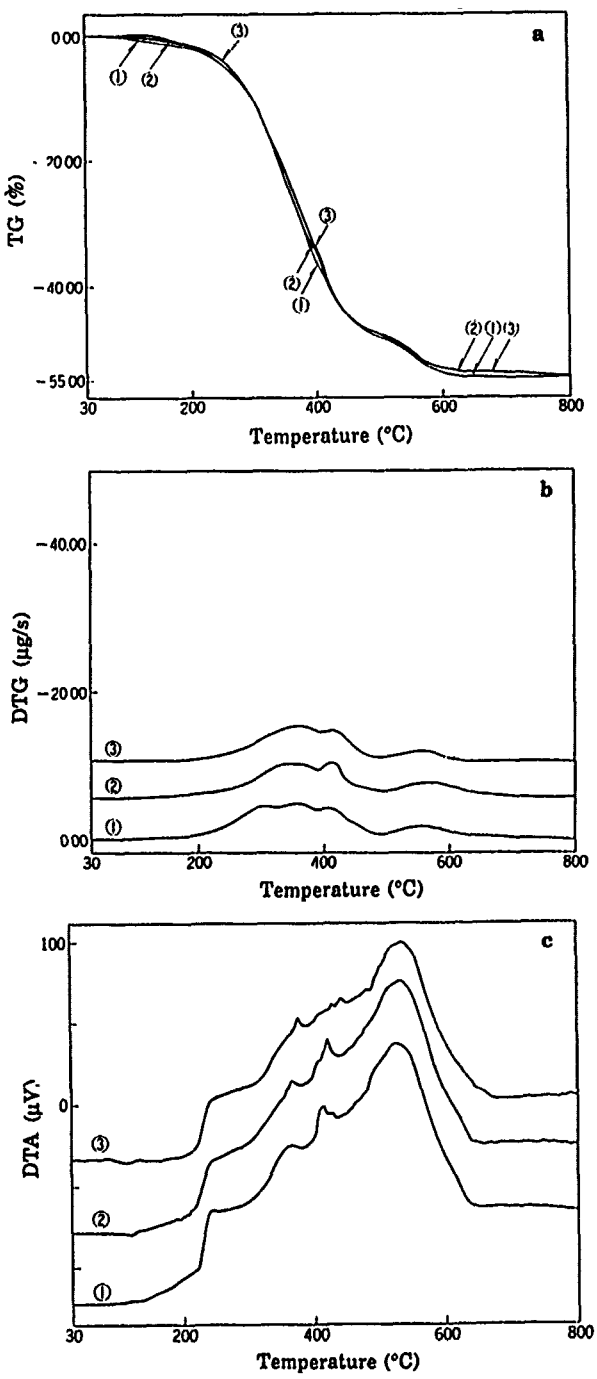

Fig. 4 Thermal analysis of 'A/B'-coated fibers for different relative irradiation
Relative irradiation: ① : 0.5, ② : 1.0, ③ : 1.5
a: TG, b: DTG, c: DTA

3.2 Evaluation of Degree of Cure of Coated Fibers

Based on the data that the degree of cure of UV resins is detectable by DTG-DTA measurements, such measurements were carried out on coated fibers of Table 1 Results are shown in Fig. 4. The reduction in weight (TG) tends to be constant at about 55% at temperatures 600°C and higher (Fig. 4a). The reduction corresponds to the loss of resins, or the weight of coated fibers subtracted by that of fibers (silica glass). Changes in TG by irradiation of 'A/B'-coated fibers are not as much as those observed on respective resins of sheet form. In DTG (Fig. 4b), however, the peak occurring at 250°C gets to be lower and those at

Table 1 UV coated fiber samples

Sample No.	Primary layer UV resin	Buffer layer UV resin	Relative irradiation
①	A	B	0.5
②	A	B	1.0
③	A	B	1.5
④	C	B	0.5
⑤	C	B	1.0
⑥	C	B	1.5

(Fiber OD: 125 μm, Primary OD: 200 μm. Buffer OD: 240 μm)

380 and 410°C get to be higher as the relative irradiation increases. Similar trends are seen also in DTA (Fig. 4c). It is estimated that the peak at 380°C which changes associated with the relative irradiation is much related with the internal primary layer of resin 'A'. It may be ascribable to the fact that the level of cure is lower in the internal layer under a low irradiation for the method of dual coating where the primary and buffer layers are irradiated at a time.

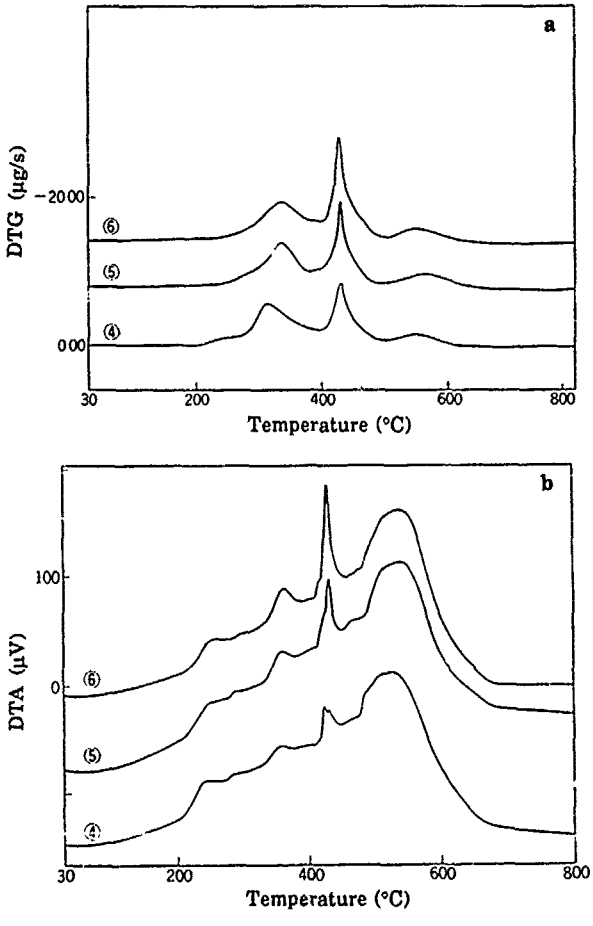

Fig. 5 Thermal analysis of 'C/B'-coated fibers for different relative irradiation
Relative irradiation: ④ : 0.5, ⑤ : 1.0, ⑥ : 1.5
a: DTG, b: DTA

Changes in DTG and DTA of 'C/B'-coated fibers by relative irradiation are shown in Figs. 5a and 5b. Changes are more marked than those in 'A/B'-coated fibers. The peak in DTA at 230°C gets smaller and those at 350 and 420°C get larger as the relative irradiation increases. Changes are especially marked in the peak at 420°C.

As discussed above, it is possible, by DTG and DTA, to evaluate changes in the degree of cure associated with irradiation on double-coated fibers where optical fibers are coated with two layers of resins of primary and buffer layers. It is also possible to estimate the state of cure of respective layers of double-coated fibers by conducting the TG-DTA analysis of individual resins in advance.

4. Evaluation of Curing by Photocalorimetry

The photocalorimetry, in principle, is a method which measures exothermic heat associated with photopolymerization. This method is usable to study curing of UV resins or exothermic heat associated with curing and, especially, the reactivity of photoinitiators. The purpose of this study is to examine whether it is possible to determine the component remained unreacted in cured resins by measuring the residual exothermic heat which is generated by re-irradiation.

Fig. 6 shows the exothermic change and the time of irradiation measured on uncured UV resins 'A', 'B' and 'C'. The exothermic change begins as soon as irradiation begins indicating the start of photopolymerization. The exothermic heat reaches its maximum within 5 s, but it takes about 50 s before the exothermic heat returns to the base line, i.e., before the reaction ended. The heat of reaction associated with photopolymerization and the time of exothermic heat to reach its maximum obtained from Fig. 6 are given in Table 2 for respective resins. The heat of reaction is the greatest in resin 'B' followed by resins 'C' and 'A' in that order. Resin 'B' for buffer emits more heat than resins 'A' and 'C' for primary. Such differences in exothermic heat are explained by kinds of photoinitiators and contents of multifunctional acrylates which depend on resins.

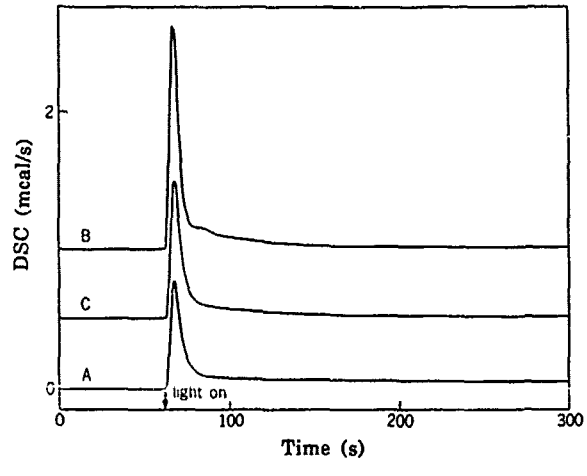

Fig. 6 Change in DSC of resins 'A', 'B' and 'C' (liquid) under irradiation

Table 2 Heat of photopolymerization and reaction time of UV resins

UV resin	Heat (cal/g)	Time to reach maximum (s)
A	30.1	4.1
B	45.4	4.0
C	32.8	3.8

Results of measurements on 'A/B'- and 'C/B'-coated fibers are shown in Figs. 7 and 8, respectively. The results are showing residual exothermic peaks due to re-irradiation indicating unreacted or uncured portions were remaining in cured coatings. The residual exothermic peaks by re-irradiation were especially large in samples ① and ④ which were irradiated at low doses. It is possible, in addition, to obtain the residual rate, X (%), of unreacted component by the formula given below by measuring residual exothermic heat of re-irradiation (Ws) of coated fiber samples:

$$X = \frac{Ws}{\alpha Wp + (1-\alpha)Wb} \times 100 \quad \cdots\cdots (1)$$

where,

Wp = exothermic heat of primary UV resin (cal/g),

Wb = exothermic heat of buffer UV resin (cal/g), and

α = weight ratio of the primary layer to the whole coating (which is about 0.6 for specimens used in this study).

Values of Ws and X obtained for coated fiber samples are summarized in Table 3. In comparing 'A/B'- and 'C/B'-coated fibers in Table 3, the rate of unreacted component is greater in 'A/B'- than in 'C/B'-coated fibers although the buffer layer and the relative irradiation were the same for both. This indicates that the 'C/B'-coated fibers are more suited to high-speed drawing of optical fiber than the 'A/B'-coated fibers.

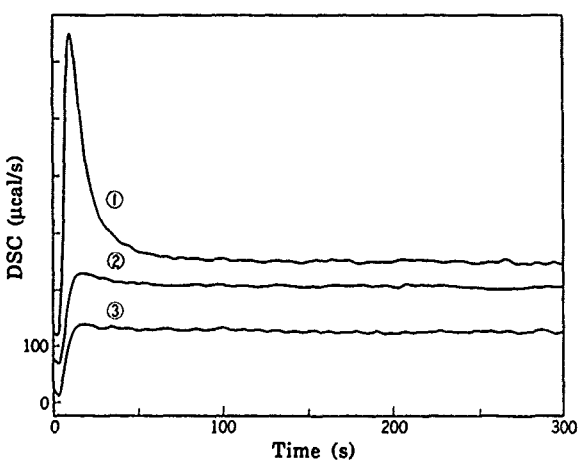

Fig. 7 Change in DSC of 'A/B'-coated fibers by relative irradiation

It is possible by the photocalorimetry to determine the state of cure of the whole coating but it is difficult to estimate the state of cure individually for primary and buffer layers. It has become clear, however, that the method of photocalorimetry can be used as a method for quantitatively estimating the state of cure of coated fibers meeting the purpose of this study.

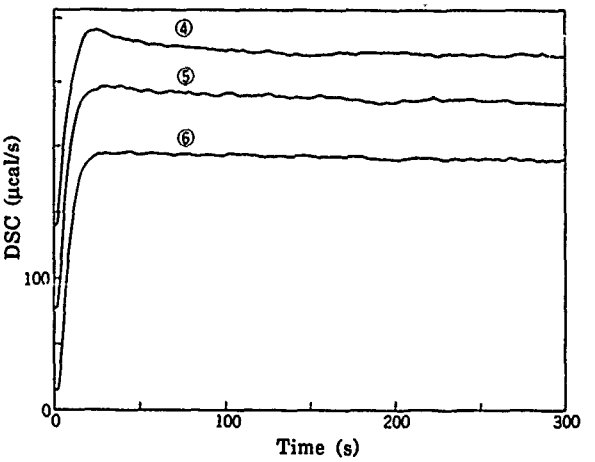

Fig. 8 Change in DSC of 'C/B'-coated fibers by relative irradiation

Table 3 Relative irradiation and state of cure of coated fibers

Sample No.	Coated resins	Relative irradiation	Residual exothermic heat, Ws (cal/g)	Rate of unreacted component, X (%)
①	A/B	0.5	11.9	33
②	A/B	1.0	2.9	7
③	A/B	1.5	0.4	1
④	C/B	0.5	1.9	5
⑤	C/B	1.0	0.8	2
⑥	C/B	1.5	0.2	0.5

5. Conclusion

Methods for evaluating the degree of cure of UV resins coated on optical fibers were examined. Methods examined here included the TG-DTA method which observes thermal decomposition behaviors of UV resins and the photocalorimetry for determining the rate of unreacted component remaining in UV-cured coating.

By the TG-DTA method, it was possible to see differences in the state of cure even in high irradiation ranges where Young's modulus is saturated. Double-coated optical fibers were used as samples as they were. TG-DTA decomposition peaks markedly changed in the range of 220 to 450°C according to the state of cure of respective resins, and it was possible to estimate the state of cure of respective layers.

The study on photocalorimetry indicated that the method is usable to determine the degree of cure of coated fibers. It will therefore be possible to use these methods for selecting UV resins suitable for high-speed drawing of optical fibers.

The TG-TDA method and the method of photocalorimetry are recommended as methods of high reproducibility and reliability for evaluating the degree of cure of UV resins coated on optical fibers.

It has also been confirmed that these methods are applicable not only to acrylic UV resins but also to other UV resins.

References

(1) N. Grassie, edit.: Polymer Degradation and Stabilization, Cambridge Univ. Press (1985).

(2) A. Inaba, T. Kashiwagi and J. E. Brown: Effects of Initial Molecular weight on Thermal Degradation of Poly (methyl methacrylate), Poly. Deg. and Steb., 21, p.1 (1988).

(3) W. Kunze and B. Stapp: Photocalorimetric Method and Applications, CRCA'88, Oct., p. 319 (1988).

(4) Techinical Review of SWCC, Vol. 39, No. 2, p. 207 (1989).

(5) N. Grassie: Trans. Faraday Soc., 49, p. 184 (1953).

(6) J. K. Haken and L. Tan: Mechanism of Thermal Degradation of Poly (Alkyl Acrylate)s Using Pyrolysis Gas Chromatography Mass Spectrometry, J. Polym. Sci., A-1, 26, p. 1315 (1988).

Biographies

Sam Huy was born in Phnom Penn, Cambodia, in 1952. In 1972, he came to Japan as Mombusho fellowship scholar. He received his Doctorate Degree in Polymeric Materials from Tokyo Institute of Technology in 1983, where he studied photopolymerization of diolefinic compounds. In the same year, he joined Toshiba Silicone Co. and worked on the development of low-H_2 RTV silicones and UV-curable silicones for optical fiber coating. Since 1988, he has been employed as chief engineer by Showa Electric Wire & Cable Co., where he presently works on the thermal stability of organic UV-curable resins and the determination of the degree of cure of optical fiber coated with UV-curable resins.

Minoru Chiba was born in Iwate Prefecture, Japan, in 1957. He graduated from Chuo University in 1981. In the same year, he worked for Nippon Rever K.K. He joined Showa Electric Wire & Cable Co., Ltd. in 1984. He has worked in material research division of electronic research & development department, where he is a chief engineer and is engaged in the research for UV-curable resins and other materials of optical fiber cables.

Tomonori Hoshino was born in Fukuoka, Japan, in 1959. He received B.E. and M.E. degrees in Material Science and Engineering from Nagasaki University in 1982 and 1984, respectively. He worked for Sasaki Glass Co., Ltd., Tokyo, Japan, from 1984 to 1987. He worked in research and development on glass ceramics. He joined Showa Electric Wire & Cable Co., Ltd. in 1987. He has been engaged in research on optical fiber.

Osamu Shimizu joined Showa Electric Wire & Cable Co., Ltd in 1972 upon graduation from Yokohama National University in the same year and has been engaged in research and development of plastic materials for communication and optical fiber cables. He was a chief engineer of material research division during this study. He is now a manager of engineering section of equipment wire and harness division.

Misao Hanai was born in Tokyo, Japan, in 1934. He received the B.Sc. degree in chemistry from Tokyo Metropolitan University in 1959. In 1960, he joined the Research Laboratory of Showa Electric Wire & Cable Co., Ltd., Kawasaki, Japan, and has been a general manager of Electric Research & Development department since 1989. He has worked in the research and development of equipment for non-wire and cable as well as electronic applications.

The Evaluation of Curing Behavior of UV Curable Coatings on Optical Fiber

Tohru Ohtaka, Tsuyoshi Watanabe, Yuji Naito, Katsutoshi Igarashi

Japan Synthetic Rubber Co.,Ltd. Tokyo Research Laboratory
3-5-1 Higashi-Yurigaoka Asaoku Kawasaki 215 Japan

Abstract

In recent years, as the line speeds of drawing fiber has been increasing, faster-curing coatings are required.

In the process of optimizing these new coatings, it has become important to analyze the kinetic curing characteristics of these materials.

Also, information on the curing behavior of coatings is important for cable manufacturers.

The purpose of this study is to examine the curing behavior of optical fiber coatings using a newly developed thermal analyzer.

Introduction

Ultraviolet curable coatings for protecting optical fibers are widely used throughout the world. These coatings enable fiber manufacturers to produce high performance optical fibers at rapid line speeds with easy handling.

Over the years, the manufacturers have been required to increase the line speed of drawing fiber, currently achieving rates as high as 12 m/sec[1]. In these situations, faster curing coatings are required.

In the process of optimizing these new coatings, it has become important to analyze the kinetic curing characteristics of these coatings. Furthermore, in the process of designing curing systems suitable for these coatings, information on the curing behavior of the coatings,(for example, induction time, reaction rate constant and photochemical after-effect) is important.

This paper reports a new technique for measuring the heat of photo-polymerization and new information on the curing behavior of optical fiber coatings.

Instrument

A new thermal analyzer shown in Figure 1, was developed for this study[2]. This analyzer consists of a UV lamp, a shutter, a heat sensor, and an analyzing recorder.

The main feature of this analyzer is to have the coating sample in contact with the sensor surface during irradiation. This intimate contact results in an extremely short response time to the thermal changes occurring in the sample.

The sensor shown in Figure 2 is made of tungsten in the shape of a helical filament. The filament is submerged in the coating under examination.

The heat generated during the polymerization process causes a change in the electrical resistance of the tungsten filament. This change in resistance is transformed to a voltage change by the bridge circuit. The voltage change is stored in one channel on the analyzing recorder.

Temperature changes are calculated from the voltage change using a conversion factor calculated from the bridge circuit conversion factor and the thermo-resistance constant of the tungsten filament (3450 ppm/℃).

A standard UV curing lamp used by the manufacturers of optical fiber was employed for this study.

Two type of shutters are mounted on this instrument : One is a mechanical shutter used for exact control of UV irradiation time, the other is a rotary disk shutter which is used for control of intermittent UV irradiation.

An optical fiber is used to transmit light from the sample-sensor chamber to the optical power meter. The light intensity change during experimentation is transformed to voltage change with the optical power meter. The voltage change due to light intensity change is stored in the other channel on the analyzing recorder. The power meter detects the precise moment when the ir-

radiation starts and also measure the light intensity.

Experiment

Samples

Three samples were prepared for this study. Sample A, a newly developed UV curable primary coating, containing the followings : polyether urethaneacrylate, monofunctional acrylate monomer and photoinitiator. Concentration of the reactive acrylate double bonds in sample A is 1.76 mmol/g.

Sample B is a newly developed secondary coating. Sample C is a standard UV curable secondary coating. Both secondary coatings consist of the following : polyether urethaneacrylate, monofunctional monomer, polyfunctional acrylate monomer and photoinitiator.

Concentration of the reactive double bonds in sample B and sample C is 3.35 mmol/g and 3.82 mmol/g, respectively.

Test Conditions

The samples were irradiated with UV light in a nitrogen atmosphere at room temperature. Irradiation time was varied between 200 msec and 4000 msec by changing the shutter speed. UV intensity was varied between 10 mW/cm^2 and 300 mW/cm^2 by changing the input power to UV lamp and by use of a metal mesh filter inserted between the UV lamp and the shutter. Value of UV intensity were checked with commercial UV power meter.

Results and Discussion

The heat of polymerization

Figure 3 shows a typical temperature transient curve measured by this instrument. The upper line in the figure shows the temperature transient of a sample at first UV irradiation. The base line shows the temperature transient of a fully cured sample which generates no heat of polymerization.

The lower trapezoidal line shows the light intensity transient at first UV irradiation.

The temperature difference between the upper line and the base line corresponds to the heat of polymerization.

Experimental values of the heat of polymerization are obtained from the following equation :

$$dHm = dTm \times Cp \qquad [I]$$

where dHm (cal/g) is the experimental value of the heat of polymerization, dTm (℃) is the temperature difference between the base line and the exotherm trace, and Cp (cal/g℃) is the specific heat of the sample.

Theoretically the heat of polymerization is calculated from the following equation :

$$dHc = Cd \times dHd \qquad [II]$$

where dHc (cal/g) is the calculated value of the heat of polymerization, Cd (mmol/g) is the concentration of double bonds in the sample and dHd (18.6 kcal/mol) is the heat of polymerization for acrylic double bond per 1 mol.

A comparison between the experimental values and calculated values of sample A and B are shown in Table 1. Close agreement between the experimental value and the calculated value is obtained.

Reaction rate constant and induction time

Conversion of polymerization is generally given by the following equation assuming that photopolymerization proceeds by a first order reaction :

$$P(t) = 1 - e^{-k(t-to)} \qquad [III]$$

where P(t) is conversion of polymerization at time t, k is the reaction rate constant of polymerization, t is the irradiation time and to is the induction time. In this experiment, conversion of polymerization is given by :

$$P(t) = dT(t)/dT(\infty) \qquad [IV]$$

where dT(t) and $dT(\infty)$ are the difference in temperature between the base line and exotherm trace at time t and at infinite time respectively.

Reaction rate constant and induction time can be calculated from the three determined temperature value using the following equations :

$$dT(\infty) = \frac{dT(t_1)dT(t_3)-dT(t_2)^2}{dT(t_1)-2dT(t_2)+dT(t_3)} \qquad [V]$$

$$k = \frac{1}{dt} \ln\left\{\frac{dT(\infty)-dT(t_1)}{dT(\infty)-dT(t_2)}\right\} \qquad [VI]$$

$$to = t_1 + \frac{1}{k} \ln\left\{\frac{dT(\infty) - dT(t_1)}{dT(\infty)}\right\} \quad [VII]$$

$$dt = t_2 - t_1 = t_3 - t_2 \quad [VIII]$$

The temperature transient curves for the two secondary coatings are shown in Figure 4. In the figure, reaction rate constant and induction time are shown.

From the results, it is clear that newly developed secondary coating (sample B) shows a k value about 1.5 times as high as the standard coating (sample C) and shows an induction time about 0.5 times as short as the standard coating.

Intensity dependence

Induction time and reaction rate constant dependence on UV intensity were investigated by measuring the heat of polymerization under several different UV intensities.

Figure 5 shows the relationship between the induction time and UV intensity. Assuming the UV intensity during fiber drawing is typically 2000 mW/cm^2, the estimated induction time of a standard coating is 4.5 msec. The induction time for a newly developed secondary coating exposed to the same UV intensity is estimated to be 1.5 msec.

The results show that a standard UV curable coating needs at least 3 msec more UV irradiation than the newly developed UV curable coating before polymerization takes place.

For instance, fiber drawing speed at 600 m/min, the time of 3 msec corresponds to one eighth of total transit time of 25 cm length lamp system.

Figure 6 shows the relationship between the reaction rate constant and UV intensity. The slope of the line in the Figure is 0.9. This value shows that the reaction rate constant is in proportion to the 0.9th power of the UV intensity.

It is said that when termination reaction is occurring between two propagation radicals in polymerization, that is to say bimolecular termination, the slope becomes 0.5[3].

When the termination reaction occurs at one propagation radical, that is to say unimolecular termination, the slope becomes 1.0.

Consequently the experimental value suggests that unimolecular termination is predominant in the termination reaction of the polymerization. This result means that polymerization reaction of this coating is strongly affected by polymerization inhibitor.

Photochemical after-effect

Figure 7 shows the temperature transient curve of the sample C under intermittent UV irradiation. The photochemical after-effect is observed to continue for more than 100 msec at 100mW/cm^2. And induction time is observed again in the second irradiation.

Results of this experiment (Irradiation time : 170 msec, darkness : 340 msec) at several UV intensities shown in Table 2.

As increasing UV intensity, the period of photochemical after-effect increases. This result suggests that the polymerization reaction continues over a longer period after UV irradiation in the curing system.

Conclusion

In conclusion, a new thermal analyzer, having a very short response time, has been developed to measure the heat of polymerization during UV curing. This analyzer provided the following useful information on the curing behavior of optical fiber coatings :

1) The induction time of a standard and a newly developed secondary coating, is estimated to be 4.5 and 1.5 msec respectively at 2000mW/cm^2 UV intensity.

2) From the relationship between reaction rate constant and UV intensity, it is implied that unimolecular termination is predominant in the termination reaction of the optical fiber coatings studied.

3) The photochemical postcure-effect continues for more than 100 msec at 100mW/cm^2 UV intensity.

Reference

1. U.C.Peak and C.M.Schroeder, Electron.Lett. 20,304 (1984)
2. T.Ohtaka et al., in Technical Digest, OFC'89 (1989) WQ9
3. Bagdasaryan "The theory of Radical Polymerization" CCCP 1959

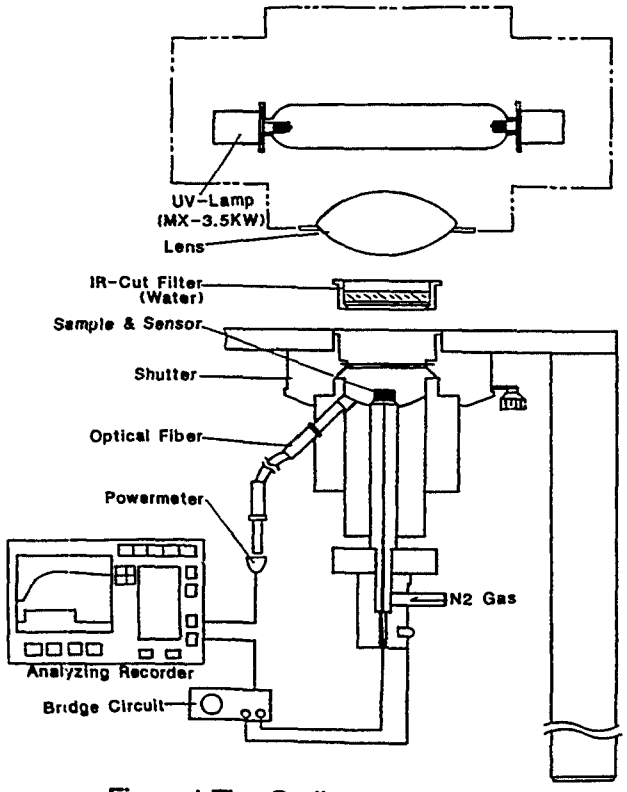

Figure.1 The Outline of Instrument

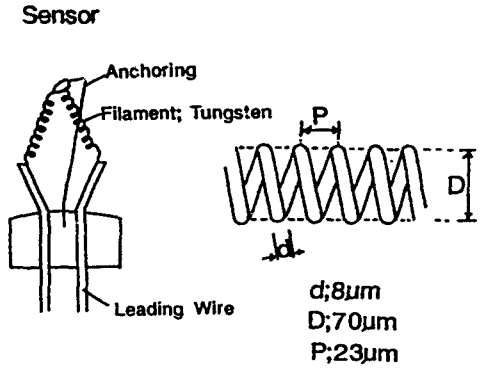

Figure.2 The Sensor

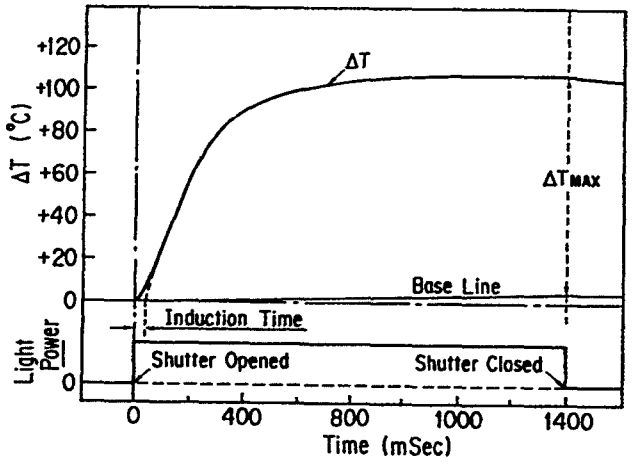

Figure.3 An Example of Polymerization Heat

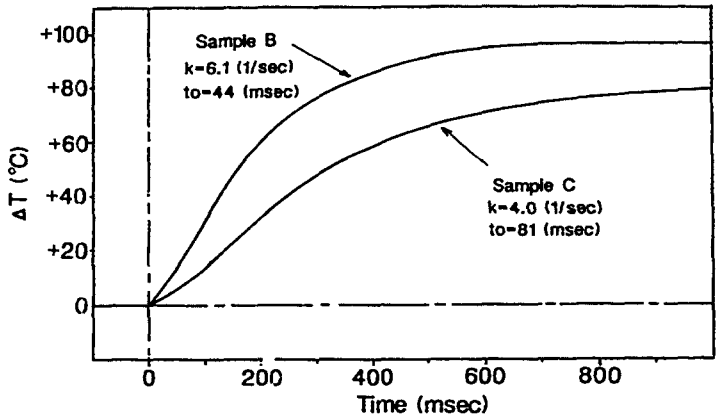

Figure.4 Temperature Transient Curve of 2 Coatings

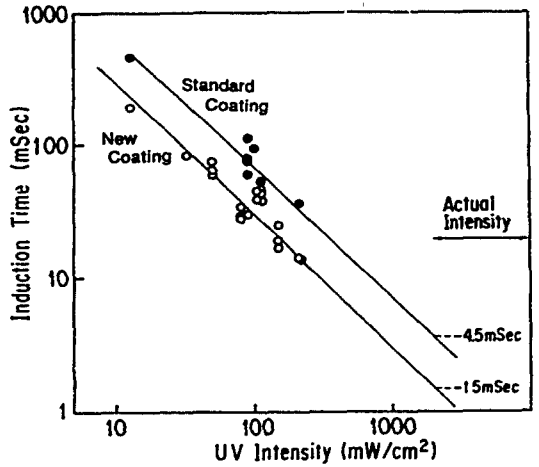

Figure.5 Induction Time vs UV Intensity

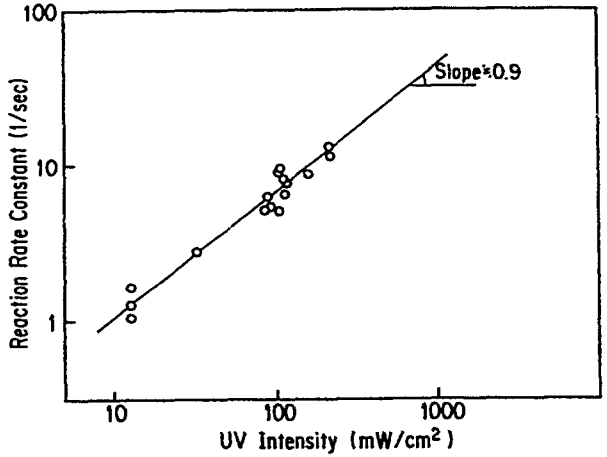

Figure.6 Reaction Rate Constant vs UV Intensity

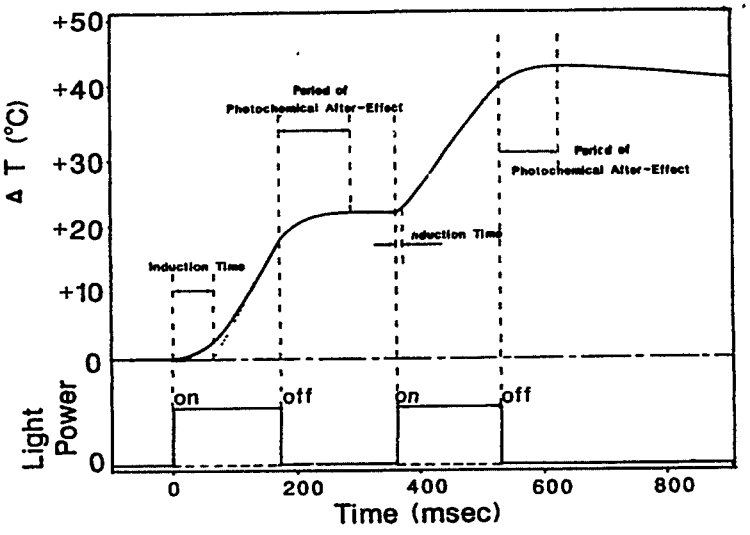

Figure.7 Photopolymerization under Intermittent UV Irradiation

Table 1. The Heat of Polymerization

Samples	Maximum Value of ΔT (℃)	The Heat of Polymerization Experimental Value (cal/g)	Calculated Value (cal/g)
A Primary Coating	54	30	33
B Secondary Coating	102	57	62

Specific Heat ; Sample A ; 0.55 cal/g·℃
Sample B ; 0.56 cal/g·℃

Table 2. Photochemical After-effect

UV Intensity (mW/cm2)	Photochemical After-effect (msec)		Induction Time (msec)	
	1 st Irradiation	2 nd Irradiation	1 st Irradiation	2 nd Irradiation
140	180	92	49	16
100	110	82	60	22
40	94	120	93	70

Tohru Ohtaka

Japan Synthetic
Rubber Co.,Ltd
Tokyo Research
Laboratory

3-5-1 Higashi-
Yurigaoka Asao-Ku
Kawasaki 215
Japan

Tohru Ohtaka received his B.S. degree in Synthetic Chemistry from Tokyo Institute of Technology in 1974 and joined Japan Synthetic rubber Co.,Ltd. He is a research associate of radiation curable material development division.

Tsuyoshi Watanabe

Japan Synthetic
Rubber Co.,Ltd
Tokyo Research
Laboratory

3-5-1 Higashi-
Yurigaoka Asao-Ku
Kawasaki 215
Japan

Tsuyoshi Watanabe received his M.S. degree in polymer chemistry from Kyoto University in 1985 and joined Japan Synthetic Rubber Co.,Ltd. He worked on application research of instrumental analysis to polymer. He is now a member of radiation curable material development division.

Yuji Naito

Japan Synthetic
Rubber Co.,Ltd
Tokyo Research
Laboratory

3-5-1 Higashi-
Yurigaoka Asao-Ku
Kawasaki 215
Japan

Yuji Naito graduated in Chemical Engineering Course from Sagamidai Technical High School in 1971 and joined Japan Synthetic Rubber Co.,Ltd. He has been engaged in research and development of plastics and rubber. He is now chief scientist of radiation curable material development division.

Katsutoshi Igarashi

Japan Synthetic
Rubber Co.,Ltd
Tokyo Research
Laboratory

3-5-1 Higashi-
Yurigaoka Asao-Ku
Kawasaki 215
Japan

Katsutoshi Igarashi received the B.S. degree in chemical engineering from Hokkaido University in 1969 and joined Japan Synthetic Rubber Co.,Ltd. He is currently a general manager of radiation curable material development division.

WATER SENSITIVITY AND ITS RELATIONSHIP TO STABILITY IN OPTICAL FIBER COATINGS

David M. Szum, Chander P. Chawla, Timothy E. Bishop, Kevin P. Murray, John M. Zimmerman

DeSoto, Inc., 1700 S. Mt. Prospect Road, Des Plaines, IL 60018
(708) 391-9000

ABSTRACT

Water sensitivity is an important concern for optical fiber manufacturers. Absorbed water has been shown to have a corrosive effect on glass and to increase optical attenuation of the glass fiber by causing dimensional changes. Water sensitivity has also been postulated to have an effect on the hydrolytic stability of the coating. Hydrolytic stability reflects the ability of water inside the coating matrix to hydrolyze the polymer backbone, thus decreasing cross-link density and causing degradation of the coating. Therefore, a thorough study of water sensitivity was performed to help understand the relationship of water absorption to cured coating stability. After establishing a ranking of water absorption, a correlation between this property and hydrolytic stability was sought. The test results lead us to conclude that water absorption has little correlation with coating hydrolytic stability. Instead, chemical structure of the coating composition has a profound influence on the hydrolytic stability.

INTRODUCTION

The use of acrylate photopolymers as protective coatings for silica glass fibers is well established in long-haul telecommunications. These materials offer performance advantages over other technologies in processing speed, low added attenuation over temperature and humidity extremes, mechanical protection of the glass, and controlled strippability for fiber splicing.

As this technology is advancing into other areas, i.e. LAN, submarine, sensor, OPGW, and other applications, reliability of the coatings and lifetime prediction under adverse environments have increased in importance. In "Fiber to the Home" design, the cost for a buried drop-line to each residential subscriber is estimated to be between $100 - $200[1]. Coating requirements for these demanding applications have been reviewed by Kar[2].

Major areas of study in the field of environmental degradation of the organic polymer include: thermal and thermo-oxidative aging[3,4] and stabilization using antioxidants[5,6], chemical effects due to short-term exposure to cleaning solvents, fuels and insecticides[7] and effects of moisture on both silica glass and polymer.

Silica glass fiber is well-known to degrade in moist environments due to stress induced corrosion of surface defects produced as an artifact of the drawing process.[8-11] The effects of temperature[12] and pH[13] on static fatigue have also been studied. Recent review papers by Kurkjian[14] and DiMarcello[15] highlight the present level of understanding the factors influencing fiber strength and fatigue as well as meaningful methods for measuring effects in short time spans.

In moist environments, the organic coating preserves fiber strength by serving as a barrier to water. However, equilibrium uptake is generally reached within a 6 to 24 hour period after immersion in 23°C water. The coating may also undergo temporary or permanent dimensional changes due to absorption or extraction that may also introduce stresses to the glass. Finally, the polymer may degrade via hydrolysis leading to diminishing of mechanical strength as cross-link density is lost.

Two methods are widely used to correlate the effects of water on fiber performance. One method, described below, is derivative of a test used in the plastics industry[16] while the other measures attenuation as a function of time stored within, and temperature of the immersion fluid[17]. It is significant that neither protocol differentiates between absorption phenomena and major mechanical changes in coating performance.

It has been postulated that there is a correlation between water absorption and hydrolytic stability in optical fiber coatings.[18] In this paper, an attempt is made to correlate absorption with hydrolytic stability. Changes in the mechanical behavior of the specimens were monitored by Dynamic Mechanical Analysis (DMA). Hydrolytic stability was assessed by examining the equilibrium modulus values of exposed and control sample made from the same film to minimize differences in preparation.

Dual coat construction, which includes a low modulus primary and a high modulus secondary coating, is a widely used fiber structure. For this preliminary study, only primary coatings were examined.

EXPERIMENTAL

The oligomers were prepared in a similar manner using reactants as obtained from the manufacturer without further purification. The molar ratio of diol, diisocyanate and hydroxyethyl acrylate were 1:2:2 in each case.

Coating Preparation

See Table I for the coating compositions that were tested.

The oligomers were weighed into eight-ounce lined steel cans. The remaining ingredients were added and the cans placed in a 65°C oven for one hour. The contents were then blended with an air mixer manufactured by Arrow Engineering Co., Inc. for fifteen minutes on a hot plate. Each solution was filtered through an extra-fine ADTEC filter cone into a new, cleaned, lined steel can and was centrifuged in an International IEC Centrifuge (Universal Model UV) at 1500 rpm for five minutes to remove the bubbles.

Film Preparation

Each coating was drawn down on a clean 9" x 12" glass plate using a Pacific Scientific Automatic Drawdown Apparatus and either a Gardner 3 mil or 10 mil bird bar film applicator. The films were cured under a 8 fm nitrogen blanket. The cure dose was 1.0 J/cm^2 as measured by an International Light Inc. IL370 Light Bug, which measures light in the 257-390 wavelength range. A Fusion "D" bulb on a Fusion Systems Model K523/2 Fusion Unit was used. Two films for each coating sample were obtained. The 10 mil films were used for maximum water absorption and both 10 mil and 3 mil films were used for aging.

Water Absorption

Each water absorption sample was cut into a set of three 1" x 1" samples. All these samples were dried in a 65°C oven for one hour and then cooled in a desiccator for ten minutes. Each sample square was weighed to the nearest ten-thousandths of a gram and then submerged in an eight-ounce jar of deionized water and weighed at intervals until a peak water absorption was obtained. The surface moisture was removed from each sample before weighing by patting dry with a Kim-Wipe tissue. This weight gain is recorded as a percentage of the initial dry weight of the sample and is reported in the discussion.

Dynamic Mechanical Analysis

Each aging sample plate was cut into 10-12 1/2" x 8" rectangular strips for Dynamic Mechanical Analysis (DMA) before and after aging. One strip from each coating was aged for 33 days at 95°C dry heat to eliminate the thermal aspect of the humidity test. The other samples were exposed to an atmosphere of 95°C, 95% relative humidity for various lengths of time. A Blue M Temperature /Humidity Chamber Model FR 251C 240V was used to provide the atmosphere.

Rheometric data was obtained from a Rheometrics Linear Rheometer by Rheometrics, Inc., Model RDSLA. Temperature sweeps were employed on all aged and unaged samples, starting and finishing at appropriate temperatures. The frequency was set at 1.0 radian/second. Data values of E′, E" and tan delta were printed and plotted at two degree intervals.

Before starting a sweep, the sample was preheated to 80°C for a minimum of five minutes in the dry nitrogen atmosphere (1% RH) of the rheometer's environmental chamber to remove water that may be present and act as a plasticizer.

RESULTS AND DISCUSSION

The water absorption data for the primary coating is presented in Table II. The values reported here are for the maximum absorption which may occur before 24 hours. Coatings 1 (polyether oligomer based) and 3 (polyester oligomer based) have high water absorption values (>2), whereas Coatings 2 (polyether-oligomer based) and 4 (polyester-oligomer based) have low water absorption values (<1). It will be seen later on that low H_2O absorption does not necessarily result in high hydrolytic stability. The initial dynamic mechanical analysis (DMA) curves for these four coatings are shown in Figures 1 through 4. All of these coatings have low equilibrium moduli (in the range of 2·1 to 3·5 MPa) and low glass transition temperatures (tan δ peak), Tg. The equilibrium modulus (Eo) is related to cross-link density (x) through the following relationship[18]:

$$X = \frac{Eo}{6kT}$$

Where k is Boltzmann's constant with a value of 1.38×10^{-16} erg/K, t is temperature in K, and X is number of cross-links per cm^3.

It assumes that (i) Poisson Ratio = 0.5; (ii) chain ends are tied into the network; and (iii) the ratio of mean square distance between the cross-linking points to the mean square end to end distance of the cross-linked chains in space is 1·0.

The DMA curves for the aged films are presented in Figures 1A-1G, Figures 2A-2G, Figures 3A-3G, and Figures 4A-4F.

Initial DMA experiments were conducted for longer periods of time (144 hours or greater) on 3 mil thick film specimens. Due to handling problems with the degraded samples, subsequent studies (<144 hours) utilized 10 mil thick specimens. A study of 3 and 10 mil samples aged for 144 hours showed no significant differences in their aging behavior.

The DMA curves were measured after a minimum of eight hours of aging and a maximum of 624 hours of aging. The moduli and tan δ values are summarrized in Tables III to VI. An examination of the samples aged at 95°C dry heat for 33 days showed no significant change in the Eo values compared to the unaged control samples for all four coatings.

First, let us consider the high water absorption Coatings 1 and 3. Data from Figures 1A-1G and Table III shows that there is very little change in dynamic mechanical properties for Coating 1 (polyether based) upon aging up to 624 hours. The Eo values remain practically constant for the entire aging period indicating no hydrolytic degradation of the coating. In contrast, Coating 3 (polyester based) exhibits (Figures 3A-3G and Table V) a steady decrease in Eo (up to ~84% for 624 hours). The decrease in Eo values is due to hydrolytic degradation (chain cleavage) of the coating. So, despite the fact that the two coatings have very similar water absorption values, they still have very different hydrolytic stabilities based on their chemical compositions. Ether linkages -C-O-C- are more stable to hydrolytic degradation than the ester linkages RCOOR.

The results of aging for low H_2O absorption Coating 2 (polyether based) and 4 (polyester based) are presented in Figures 2A-2G, Table IV and Figures 4A-4F, Table VI, respectively.

The polyether-based Coating 2 shows very small changes in Eo and tan δ values. In comparison, polyester-based Coating 4 exhibits a large decrease (~82%) in equilibrium modulus. This decrease is again due to hydrolytic degradation of the polyester-based coating.

The results of this study have shown that the hydrolytic stability of a coating is not solely dependent on the extent of H_2O absorption. Instead, it is dependent on the chemical composition of the coating. This point is clearly illustrated in Figure 5, which is a plot of cross-link density versus the hydrolysis time. This plot was constructed from the data presented in Tables VII to X. It can be seen from Figure 5 that, for both high (#1) and low (#2) water absorption polyether-based coatings, there is essentially no change in cross-link density indicating absence of degradation. The high (#3) and low (#4) water absorption polyester-based coatings, on the other hand, show a very sharp decrease in cross-link density as a function of hydrolysis time. The decrease, as explained earlier, is due to hydrolysis of the susceptible polyester linkage.

The cross-link density vs. time plots for coatings 3 and 4 (Figure 5) show a steady decrease in crosslink density for the first 72 hours. A linear regression of the data for this time period gives slopes of -8.78×10^{17} and -7.93×10^{17} cross-links per cm^3 per hour for coatings 3 and 4 respectively. The correlation coefficients were -0.98 and -0.95, which implies a linear decrease of number of cross-links as a function of time. The slopes represent the loss of number of cross-links per cm^3 per hour and can be considered to be pseudo hydrolysis rate constants. For both high and low water absorption polyester coating systems, the hydrolysis pseudo rate constants are very similar to each other for the first 72 hours. Both high and low water absorption polyether coating systems show a substantially lower pseudo hydrolysis rate constant (almost zero).

CONCLUSION

The above data indicate that there is little, if any, correlation between water absorption and hydrolytic stability in optical fiber coatings. There is, however, good correlation between chemical composition and hydrolytic stability in these coatings. Coatings using polyether-based oligomers are shown to be much more hydrolytically stable than those using unblocked polyester-based oligomers, regardless of water absorption values.

We are currently conducting similar studies on other chemical backbones, such as polycaprolactones, polycarbonates and polyolefins in order to compare their intrinsic hydrolytic stability to that of polyethers and polyesters.

ACKNOWLEDGEMENTS

The authors wish to acknowledge Dr. Robert Johnson, Carl Krautwurst, and Jennifer Chapman for invaluable aid in the preparation and testing of samples.

REFERENCES

1. P.W. Shumate, "Special Broadband Needs of the Outside Plant," Proceedings of Broadband '89 FOC/LAN, October 30, 1989.

2. G. Kar, "Progress in Optical Fiber Coatings," Proceedings of OFC'88, TU01, January 26, 1988.

3. D. Simoff, M. Chan, J. Chapin, and B. Overton, "Thermo-oxidative Aging of a Primary Lightguide Coating in Films and Dual-Coated Fibers," Proceedings of ANTEC '88, 586-589.

4. J. Flynn, "Lifetime Prediction for Polymeric Materials from Thermal Analytical Experiments," Proceedings of ANTEC '88, 930-932.

5. I.P. Heyward, M.G. Chan, and A.G. Ludwick, "Effect of Antioxidants on the Thermooxidative Stabilities of Ultraviolet Cured Coatings," ACS Symp. Ser. (Polym.Stab.Degrad.), 1985.

6. M.G. Chan, I.P. Heyward, D.A. Simoff, P.M. Pruitt, "The Stabilization of UV Curable Coatings for Optical Fibers," Fourth International Conference on Plastics in Telecommunications, September 1986, London, U.K.

7. H.H. Yuce, "Chemical Effects on Fiber Reliability," Optical Fiber Communications Conference Technical Digest, January, 1990, San Francisco, CA.

8. T.T. Wang, H.M. Zupko, "Long Term Mechanical Behavior of Optical Fibres Coated with a UV-Curable Epoxy Acrylate," J. Mater. Sci., 13, 2241-2248 (1978).

9. H.N. Vazirani, H. Schonhorn and T.T. Wang, "UV Cured Epoxy Acrylate Coatings on Optical Fibers I. Chemistry and Application," Optical Society of America, Topical Meeting on Optical Transmission, Williamsburg, VA February 22-24, 1977.

10. T.T. Wang, H.M. Zupko, H.N. Vazirani, and H. Schonhorn, "UV-Cured Epoxy Acrylate Coatings on Optical Fiber III. Effect of Environment on Long-Term Strength," J. Rad. Curing, 10, 22-24 (1977).

11. T.T. Wang, H.N. Vazirani, H. Schonhorn, and H.M. Zupko, "Effects of Water and Moisture on Strengths of Optical Glass (Silica) Fibers Coated with UV-Cured Epoxy Acrylate," J. Appl. Polym. Sci., 23, 887-892, (1979).

TABLE I

MODEL COATING FORMULATIONS

Components	Coating Number 1 Weight%	2 Weight%	3 Weight%	4 Weight%
Polyether Urethane Oligomer	58	58	--	--
Polyester Urethane Oligomer	--	--	58	58
Phenoxy Ethyl Acrylate[a]	28	28	28	28
Vinyl-Pyrolidone[b]	10	--	10	--
Iso Bornyl Acrylate[c]	--	10	--	10
2-Bentyl-2-Dimethyl-amino-1-(4-morpholino-phenyl)-Butan-1-One[d]	3	3	3	3
Bis(2,2,6,6,-Tetramethyl-4-piperidinyl) sebacate[d]	.5	.5	.5	.5
Ethylene Bis(oxyethylene) BIS(3-tert-butyl-4-hydroxy-5 methyl hydro cinnamate)[d]	.5	.5	.5	.5

a CPS Chemical Company, Inc.
b GAF Corporation
c Radcure Specialties, Inc.
d Ciba Geigy Corporation

TABLE II

WATER ABSORPTION DATA

Coating #	Maxiuum Water Absorption, %
1	2.27
2	0.77
3	2.46
4	0.91

TABLE III

DMA DATA FOR COATING 1

Coating 1	E'=1000 MPa (°C)	E'=100 MPa (°C)	Tan δ Peak (°C)	Eq Modulus (MPa)
Control 95°C, 95% RH	-60	3	18	3.50
8 Hours	-62	3	18	3.50
24	-59	3	20	3.50
48	-63	3	18	3.50
72	-66	4	19	3.40
144	-60	4	20	3.35
480	-61	6	23	3.00
624	-61	7	26	3.30
95°C, dry 792 Hours	-60	5	24	3.20

TABLE IV

DMA DATA FOR COATING 2

Coating 2	E'=1000 MPa (°C)	E'=100 MPa (°C)	Tan δ Peak (°C)	Eq Modulus (MPa)
Control 95°C, 95% RH	-54	-22	-10	2.50
8 Hours	-55	-24	-10	2.10
24	-55	-23	-9	2.10
48	-56	-24	-12	2.10
72	-56	-24	-12	2.00
144	-55	-23	-10	2.50
480	-53	-20	-7	2.20
624	-54	-20	-8	2.15
95°C, dry 792 Hours	-52	-16	-10	2.20

TABLE V

DMA DATA FOR COATING 3

Coating 3	E'=1000 MPa (°C)	E'=100 MPa (°C)	Tan δ Peak (°C)	Eq Modulus (MPa)
Control 95°C, 95% RH	-17	2	11	2.55
8 Hours	-16	3	12	2.05
24	-15	-1	11	1.70
48	-15	0	11	1.20
72	-16	-3	9	0.80
144	-20	-9	2	0.45
480	31	43	49	0.45
624	44	55	65	0.40
95°C, dry 792 Hours	-15	2	13	2.10

TABLE VI

DMA DATA FOR COATING 4

Coating 4	E'=1000 MPa (°C)	E'=100 MPa (°C)	Tan δ Peak (°C)	Eq.Modulus (MPa)
Control 95°C, 95% RH	-20	-5	12	3.00
8 Hours	-21	-6	4	1.40
24	-21	-6	5	1.05
48	-21	-8	4	0.70
72	-23	-9	3	0.40
144	-12	0	10	-0.40
480	38	39	45	-0.35
624	Too weak to measure			
95°C, dry 792 Hours	-19	-5	4	1.70

TABLE VII

CROSS-LINK DENSITY DATA FOR COATING 1

Hydrolysis Time, Hours	Temperature At Which X is Calculated, K	Cross-Link Density X x 10^{20}
0	323.16	1.31
8	323.16	1.31
24	323.16	1.31
48	323.16	1.31
72	323.16	1.35
144	323.16	1.25
480	323.16	1.12
624	323.16	1.20

TABLE VIII

CROSS-LINK DENSITY DATA FOR COATING 2

Hydrolysis Time, Hours	Temperature At Which X is Calculated, K	Cross-Link Density X x 10^{19}
0	303.16	9.96
8	303.16	8.37
24	303.16	8.37
48	303.16	8.37
72	303.16	7.97
144	303.16	9.96
480	303.16	8.76
624	303.16	8.57

TABLE IX

CROSS-LINK DENSITY DATA FOR COATING 3

Hydrolysis Time, Hours	Temperature At Which X is Calculated, K	Cross-Link Density X x 10^{19}
0	313.16	9.83
8	313.16	7.91
24	313.16	6.56
48	313.16	4.63
72	313.16	3.09
144	313.16	1.74
480	383.16	1.42
624	383.16	1.26

TABLE X

CROSS-LINK DENSITY DATA FOR COATING 4

Hydrolysis Time, Hours	Temperature At Which X is Calculated, K	Cross-Link Density X x 10^{19}
0	303.16	7.97
8	303.16	5.58
24	303.16	4.18
48	303.16	2.79
72	299.16	1.61
144	303.16	-1.59
480	353.16	-1.20
624	Too weak to measure	

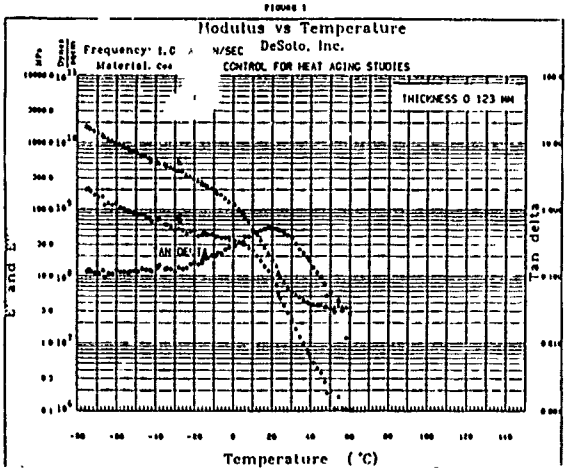
Modulus vs Temperature
Frequency: 1.0 RADIAN/SEC DeSoto, Inc.
CONTROL FOR HEAT AGING STUDIES
THICKNESS 0.123 MM
E' and E"
Tan delta
Temperature (°C)

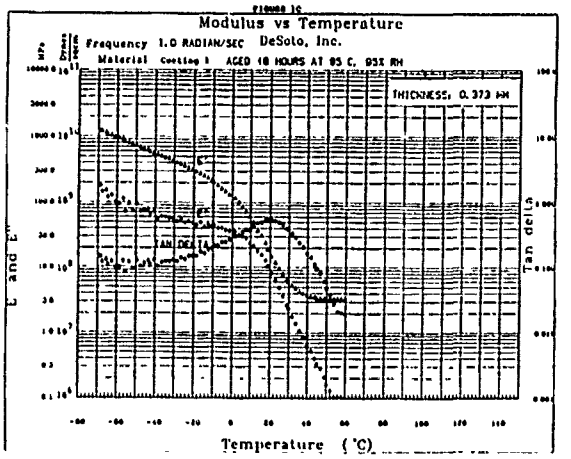
Modulus vs Temperature
Frequency 1.0 RADIAN/SEC DeSoto, Inc.
AGED 18 HOURS AT 95 C, 95% RH
THICKNESS: 0.373 MM
E' and E"
Tan delta
Temperature (°C)

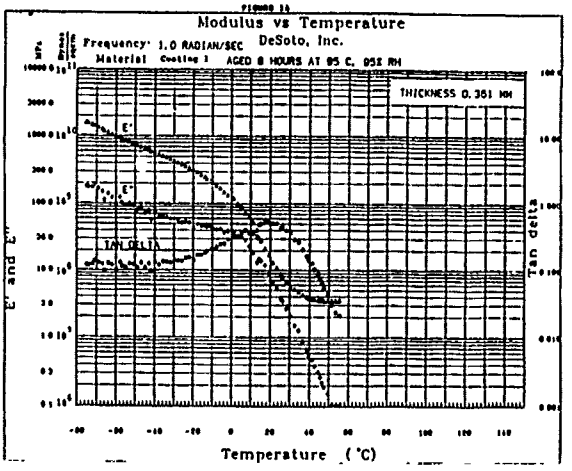
Modulus vs Temperature
Frequency: 1.0 RADIAN/SEC DeSoto, Inc.
AGED 8 HOURS AT 95 C, 95% RH
THICKNESS 0.361 MM
E' and E"
Tan delta
Temperature (°C)

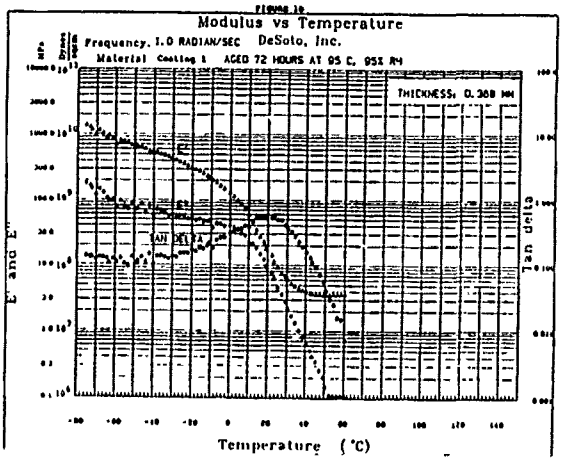
Modulus vs Temperature
Frequency. 1.0 RADIAN/SEC DeSoto, Inc.
AGED 72 HOURS AT 95 C, 95% RH
THICKNESS: 0.368 MM
E' and E"
Tan delta
Temperature (°C)

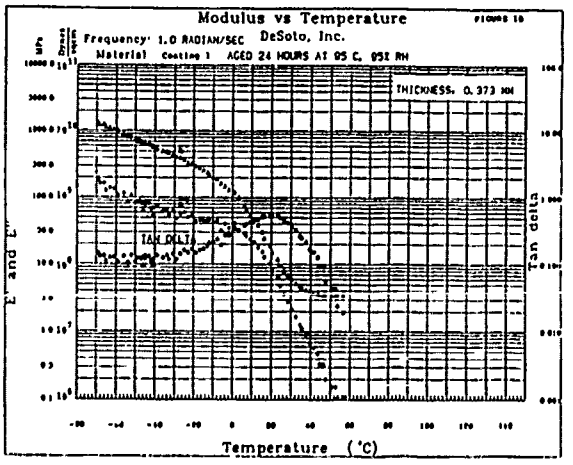
Modulus vs Temperature
Frequency: 1.0 RADIAN/SEC DeSoto, Inc.
AGED 24 HOURS AT 95 C, 95% RH
THICKNESS: 0.373 MM
E' and E"
Tan delta
Temperature (°C)

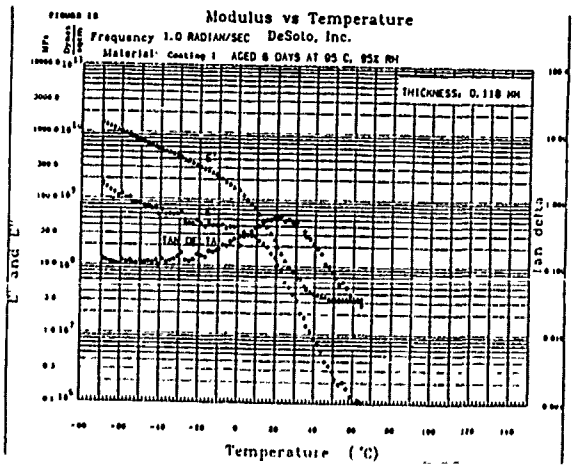
Modulus vs Temperature
Frequency 1.0 RADIAN/SEC DeSoto, Inc.
AGED 6 DAYS AT 95 C, 95% RH
THICKNESS: 0.118 MM
E' and E"
Tan delta
Temperature (°C)

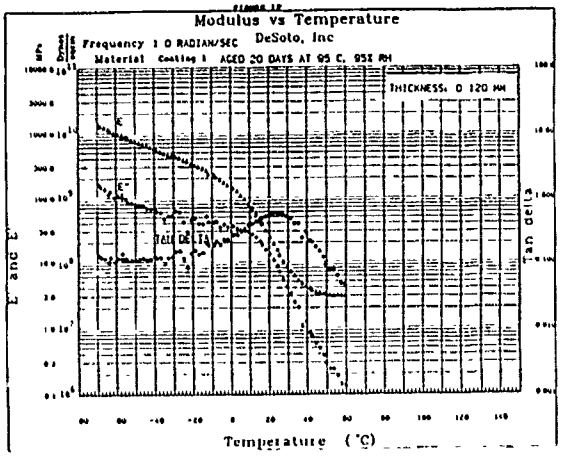
Modulus vs Temperature
Frequency 1.0 RADIAN/SEC DeSoto, Inc
Material Coating 1 AGED 20 DAYS AT 95 C, 95% RH
THICKNESS 0.120 MM
E'
E"
TAN DELTA
E' and E"
Tan delta
Temperature (°C)

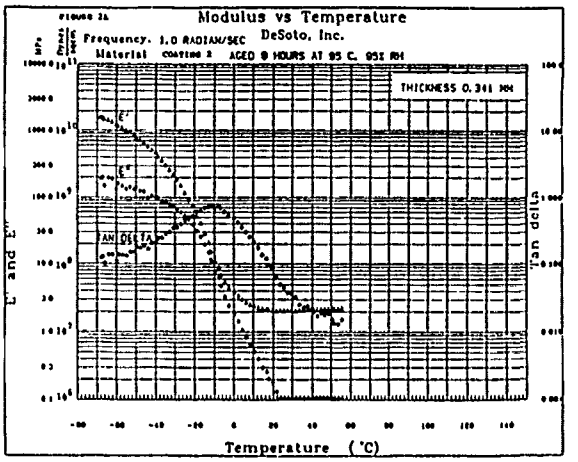
Modulus vs Temperature
Frequency 1.0 RADIAN/SEC DeSoto, Inc.
Material Coating 2 AGED 0 HOURS AT 95 C, 95% RH
THICKNESS 0.341 MM
E'
E"
TAN DELTA
E' and E"
Tan delta
Temperature (°C)

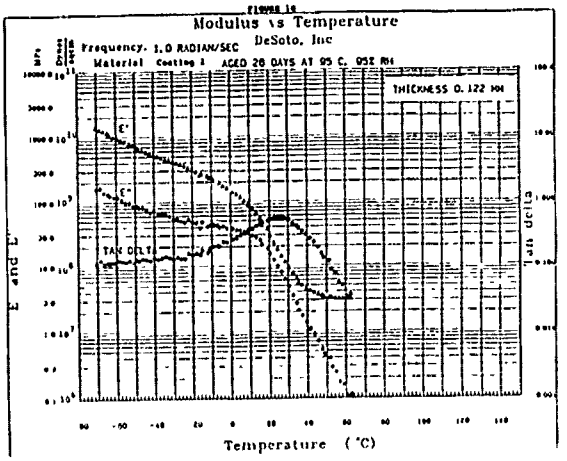
Modulus vs Temperature
Frequency 1.0 RADIAN/SEC DeSoto, Inc
Material Coating 1 AGED 28 DAYS AT 95 C, 95% RH
THICKNESS 0.122 MM
E'
E"
TAN DELTA
E' and E"
Tan delta
Temperature (°C)

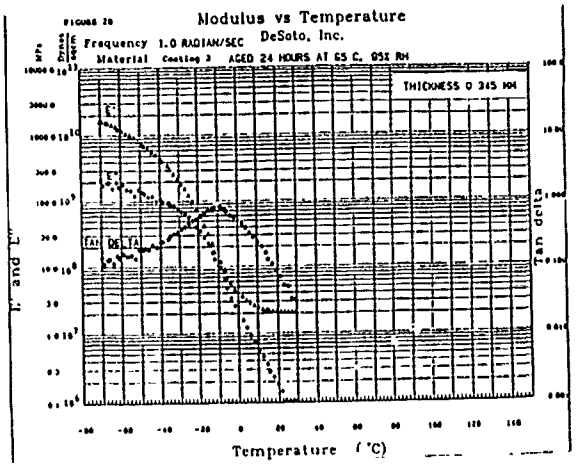
Modulus vs Temperature
Frequency 1.0 RADIAN/SEC DeSoto, Inc.
Material Coating 2 AGED 24 HOURS AT 65 C, 95% RH
THICKNESS 0.345 MM
E'
E"
TAN DELTA
E' and E"
Tan delta
Temperature (°C)

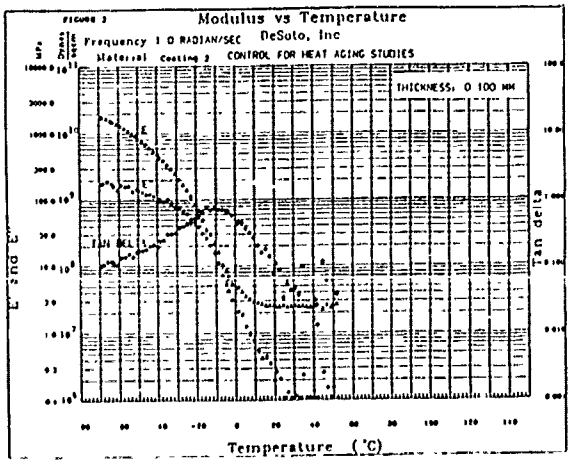
Modulus vs Temperature
Frequency 1.0 RADIAN/SEC DeSoto, Inc
Material Coating 2 CONTROL FOR HEAT AGING STUDIES
THICKNESS 0.100 MM
E'
E"
TAN DELTA
E' and E"
Tan delta
Temperature (°C)

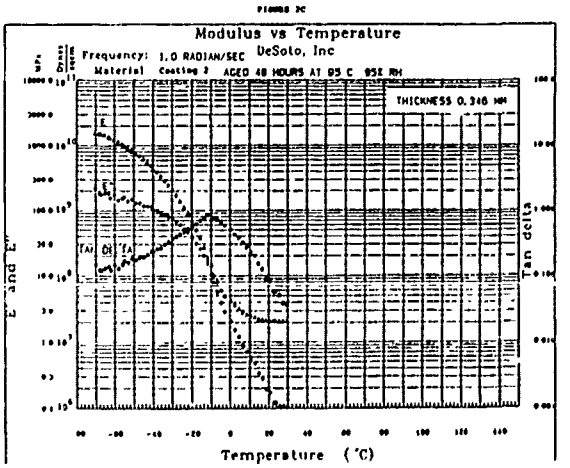
Modulus vs Temperature
Frequency 1.0 RADIAN/SEC DeSoto, Inc
Material Coating 2 AGED 48 HOURS AT 95 C 95% RH
THICKNESS 0.346 MM
E'
E"
TAN DELTA
E' and E"
Tan delta
Temperature (°C)

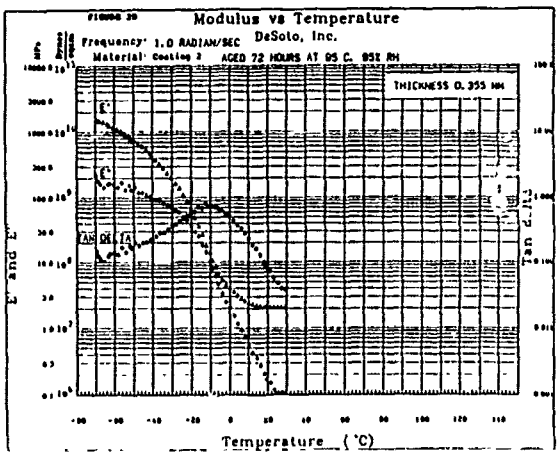
Modulus vs Temperature
Frequency 1.0 RADIAN/SEC DeSoto, Inc.
Material Coating 2 AGED 72 HOURS AT 95 C, 95% RH
THICKNESS 0.355 MM
E' and E"
Tan delta
TAN DELTA
Temperature (°C)

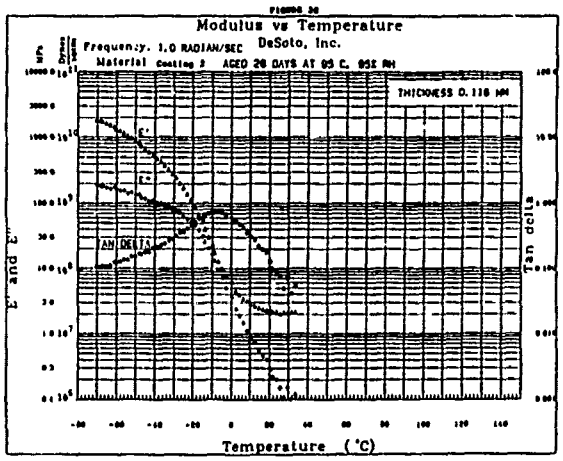
Modulus vs Temperature
Frequency 1.0 RADIAN/SEC DeSoto, Inc.
Material Coating 2 AGED 28 DAYS AT 95 C, 95% RH
THICKNESS 0.118 MM
E' and E"
Tan delta
TAN DELTA
Temperature (°C)

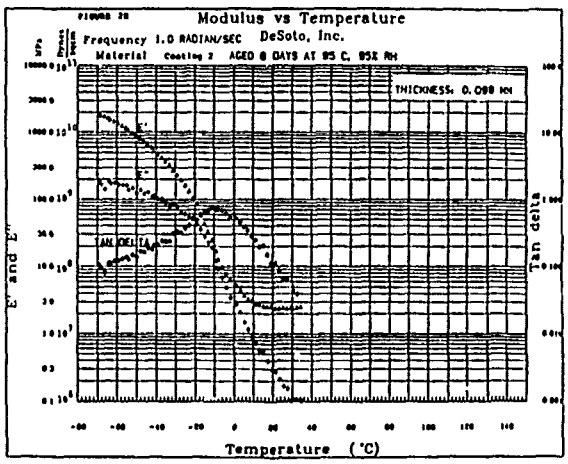
Modulus vs Temperature
Frequency 1.0 RADIAN/SEC DeSoto, Inc.
Material Coating 2 AGED 0 DAYS AT 95 C, 95% RH
THICKNESS 0.098 MM
E' and E"
Tan delta
TAN DELTA
Temperature (°C)

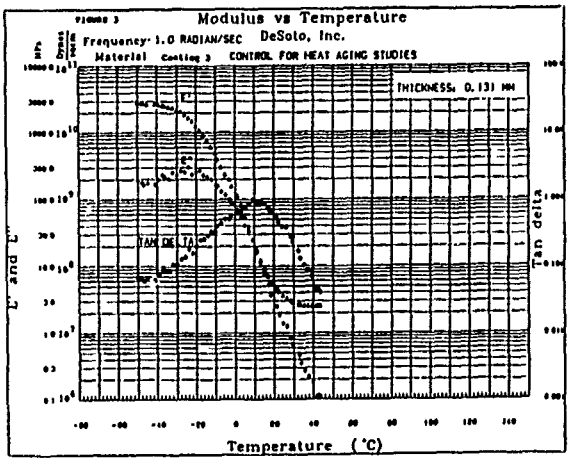
Modulus vs Temperature
Frequency 1.0 RADIAN/SEC DeSoto, Inc.
Material Coating 2 CONTROL FOR HEAT AGING STUDIES
THICKNESS 0.131 MM
E' and E"
Tan delta
TAN DELTA
Temperature (°C)

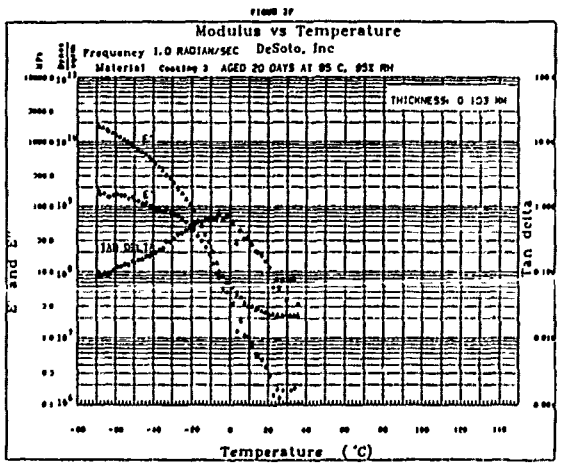
Modulus vs Temperature
Frequency 1.0 RADIAN/SEC DeSoto, Inc
Material Coating 2 AGED 20 DAYS AT 95 C, 95% RH
THICKNESS 0.103 MM
E' and E"
Tan delta
TAN DELTA
Temperature (°C)

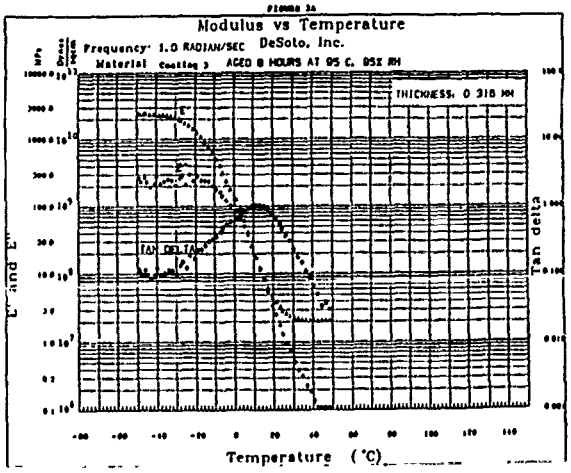
Modulus vs Temperature
Frequency 1.0 RADIAN/SEC DeSoto, Inc.
Material Coating 2 AGED 8 HOURS AT 95 C, 95% RH
THICKNESS 0.318 MM
E' and E"
Tan delta
TAN DELTA
Temperature (°C)

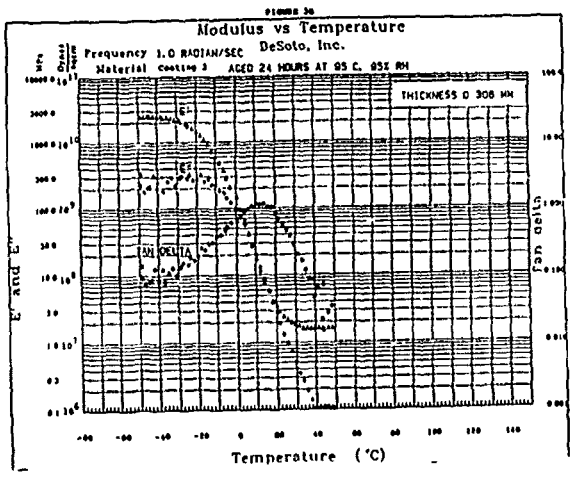
Modulus vs Temperature
Frequency 1.0 RADIAN/SEC DeSoto, Inc.
Material coating 3 AGED 24 HOURS AT 95 C. 95% RH
THICKNESS 0.308 MM
E' and E"
tan delta
Temperature (°C)

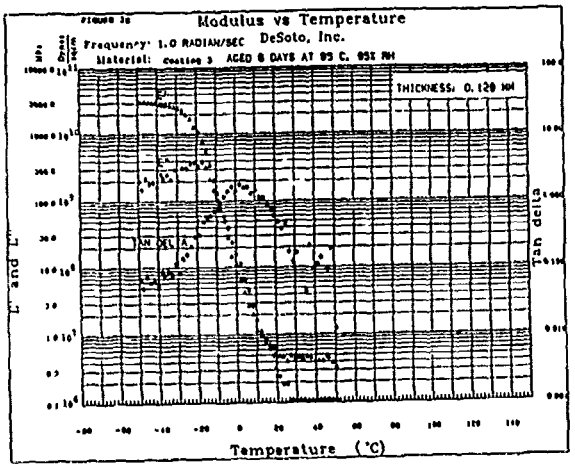
Modulus vs Temperature
Frequency 1.0 RADIAN/SEC DeSoto, Inc.
Material: coating 3 AGED 8 DAYS AT 95 C. 95% RH
THICKNESS: 0.120 MM
E' and E"
tan delta
Temperature (°C)

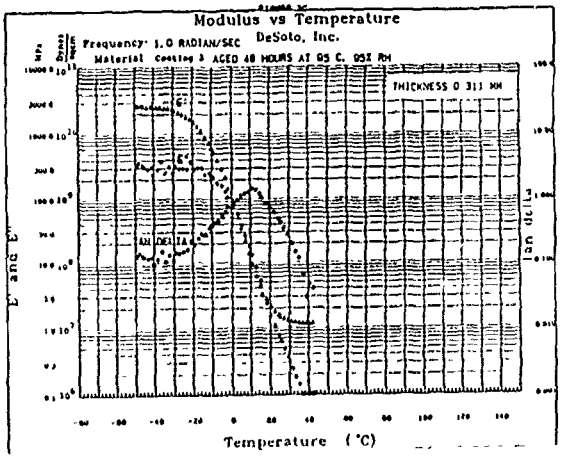
Modulus vs Temperature
Frequency 1.0 RADIAN/SEC DeSoto, Inc.
Material coating 3 AGED 48 HOURS AT 95 C. 95% RH
THICKNESS 0.311 MM
E' and E"
tan delta
Temperature (°C)

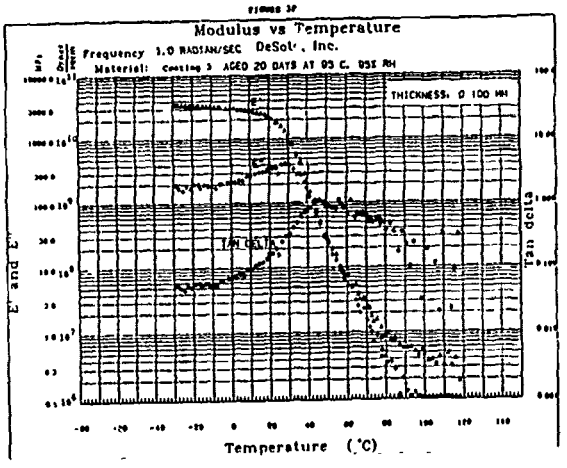
Modulus vs Temperature
Frequency 1.0 RADIAN/SEC DeSoto, Inc.
Material: coating 3 AGED 20 DAYS AT 95 C. 95% RH
THICKNESS: 0.100 MM
E' and E"
tan delta
Temperature (°C)

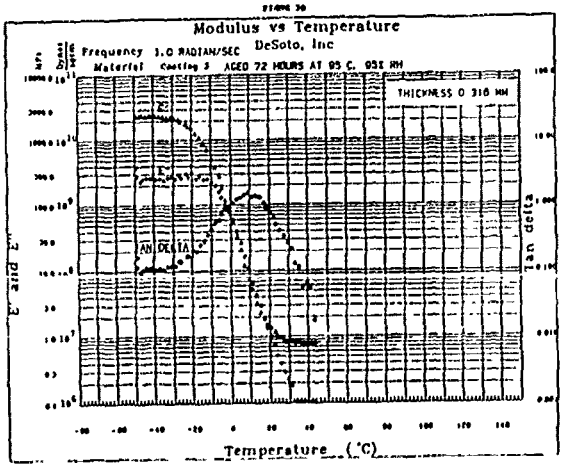
Modulus vs Temperature
Frequency 1.0 RADIAN/SEC DeSoto, Inc
Material coating 3 AGED 72 HOURS AT 95 C. 95% RH
THICKNESS 0.316 MM
E' and E"
tan delta
Temperature (°C)

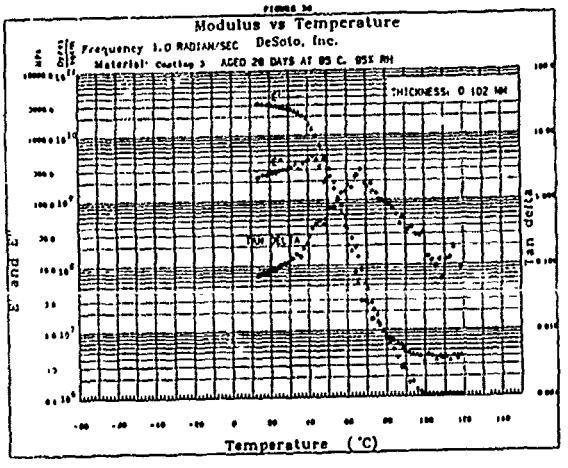
Modulus vs Temperature
Frequency 1.0 RADIAN/SEC DeSoto, Inc.
Material coating 3 AGED 28 DAYS AT 95 C. 95% RH
THICKNESS: 0.102 MM
E' and E"
tan delta
Temperature (°C)

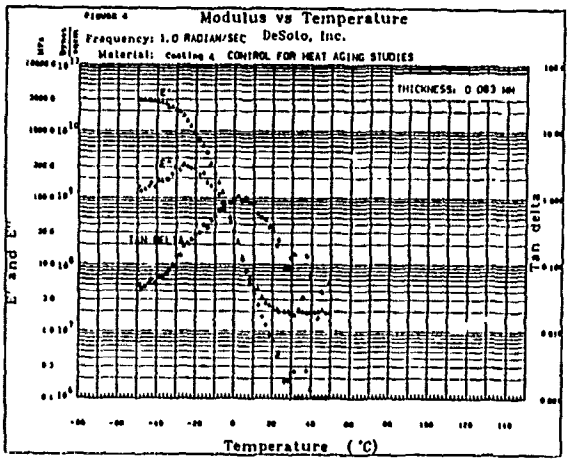
Modulus vs Temperature
Frequency: 1.0 RADIAN/SEC DeSoto, Inc.
Material: Coating 4 CONTROL FOR HEAT AGING STUDIES
THICKNESS: 0.083 MM
TAN DELTA
E' and E"
Tan delta
Temperature (°C)

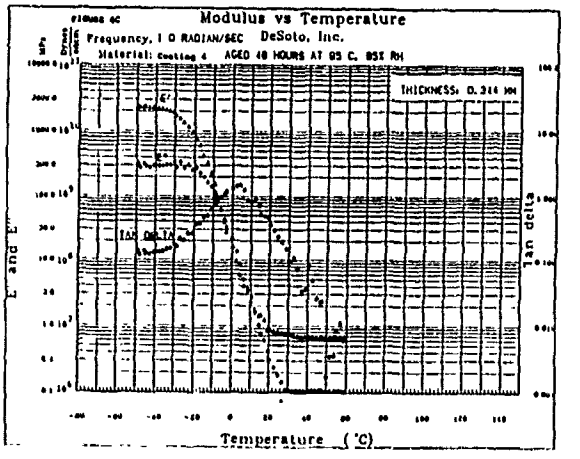
Modulus vs Temperature
Frequency: 1.0 RADIAN/SEC DeSoto, Inc.
Material: Coating 4 AGED 48 HOURS AT 95 C, 85% RH
THICKNESS: 0.314 MM
TAN DELTA
E' and E"
Tan delta
Temperature (°C)

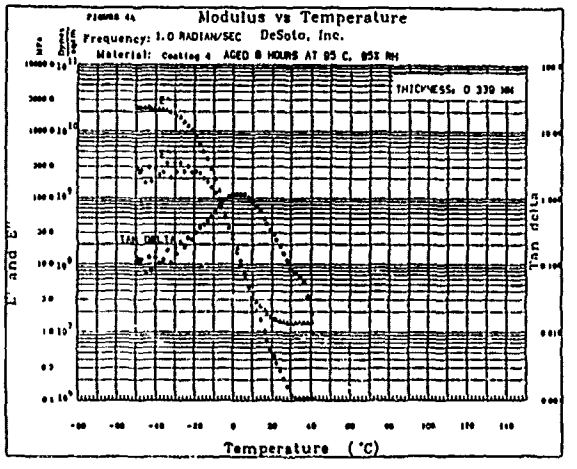
Modulus vs Temperature
Frequency: 1.0 RADIAN/SEC DeSoto, Inc.
Material: Coating 4 AGED 8 HOURS AT 95 C, 85% RH
THICKNESS: 0.330 MM
TAN DELTA
E' and E"
Tan delta
Temperature (°C)

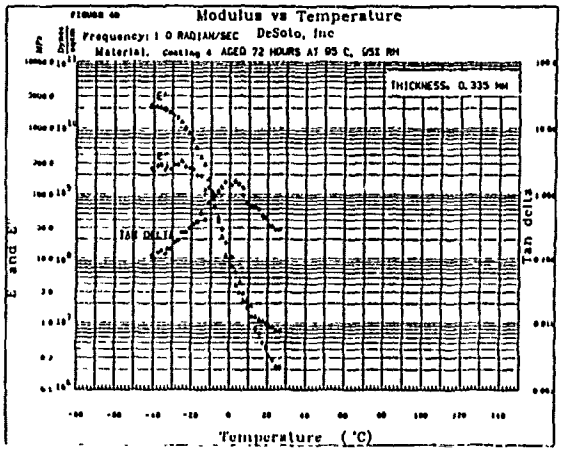
Modulus vs Temperature
Frequency: 1.0 RADIAN/SEC DeSoto, Inc
Material: Coating 4 AGED 72 HOURS AT 95 C, 85% RH
THICKNESS: 0.335 MM
TAN DELTA
E' and E"
Tan delta
Temperature (°C)

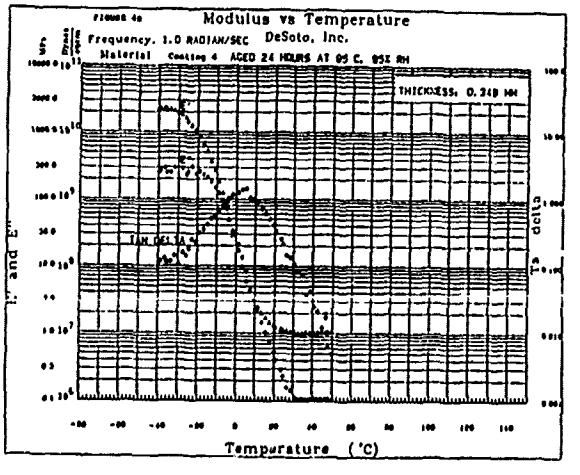
Modulus vs Temperature
Frequency: 1.0 RADIAN/SEC DeSoto, Inc.
Material: Coating 4 AGED 24 HOURS AT 95 C, 85% RH
THICKNESS: 0.249 MM
TAN DELTA
E' and E"
Tan delta
Temperature (°C)

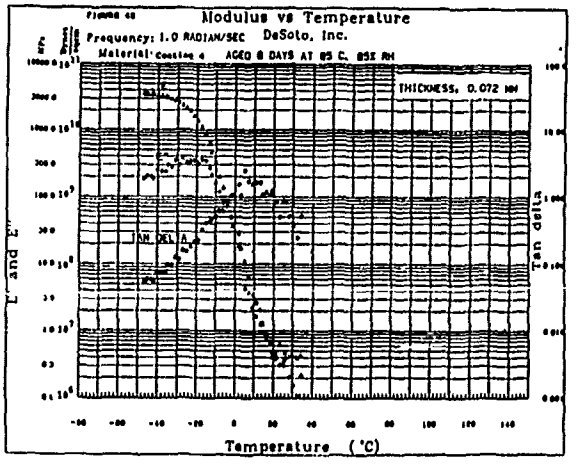
Modulus vs Temperature
Frequency: 1.0 RADIAN/SEC DeSoto, Inc.
Material: Coating 4 AGED 8 DAYS AT 95 C, 85% RH
THICKNESS: 0.072 MM
TAN DELTA
E' and E"
Tan delta
Temperature (°C)

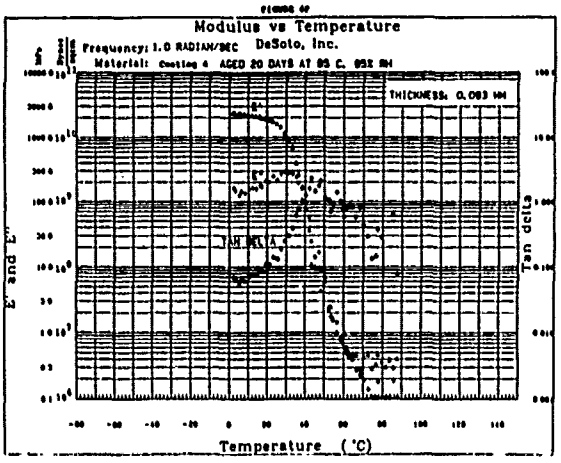

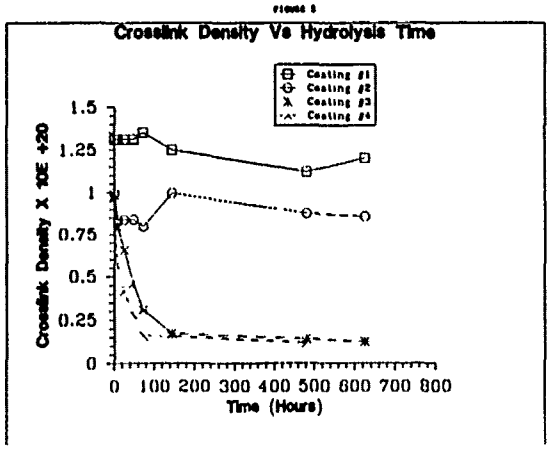

APPENDIX A

Synthesis of Polyether Urethane Acrylate

Isophorone diisocyanate (75.4 g), phenothiazine (0.1 g), and dibutyltin dilaurate (0.12 g) were charged to a 1 liter 4-necked round bottom glass flask equipped with a mechanical stirrer, dry air sparge, addition funnel, thermometer, reflux condenser, and a heating mantle. The mixture was stirred at 120 rpm, and 2-hydroxyethyl acrylate (33.2 g) was added from the addition funnel over a one-hour period. After three hours at 25°C, a 0.63 g sample was removed for % NCO analysis. The result from the analysis showed the intermediate product to have 15.00 % free isocyanate versus a theoretical value of 15.05 %. An additional amount of dibutyltin dilaurate (0.19 g) was then added to the flask, the stirring rate was increased to 200 rpm, and the contents were heated to 50°C. Polytetrahydrofuran 1000 from BASF Corp. (385.9 g, OH# = 56.0 mg KOH/g), preheated to 60°C, was added over a period of 45 minutes with the exotherm raising the temperature to 80°C. The contents were held at 80°C for one hour, and a final analysis showed the free isocyanate content to be less than 0.1 %. The theoretical structure for the oligomer is shown below.

Theoretical Structure of Polyether Urethane Acrylate:

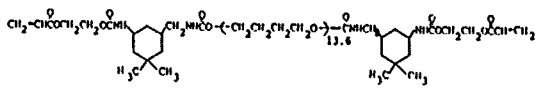

APPENDIX B

Synthesis of Polyester Urethane Acrylate

Isophorone diisocyanate (74.6 g), phenothiazine (0.1 g), and dibutyltin dilaurate (0.12 g) were charged to a 1 liter 4-necked round bottom glass flask equipped with a mechanical stirrer, dry air sparge, addition funnel, thermometer, reflux condenser, and a heating mantle. The mixture was stirred at 120 rpm, and 2-hydroxyethyl acrylate (33.2 g) was added from the addition funnel over a 47 minute period. After three hours at 25°C, a 0.34 g sample was removed for % NCO analysis. The result from the analysis showed the intermediate product to have 14.77 % free isocyanate versus a theoretical value of 14.87%. An additional amount of dibutyltin dilaurate (0.19 g) was then added to the flask, the stirring rate was increased to 200 rpm, and the contents were heated to 50°C. Millester 2-55 from Polyurethane Specialties Co. (399.3 g, OH# = 54.8 mg KOH/g), preheated to 80°C, was added over a period of 35 minutes with the exotherm raising the temperature to 82°C. The contents were held at 80°C for one hour, and a final analysis showed the free isocyanate content to be less than 0.1%. The theoretical structure for the oligomer is shown below.

Theoretical Structure of Polyester Urethane Acrylate:

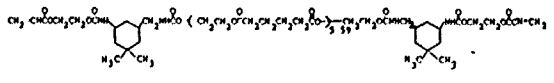

12. H.O. Chandan and D. Kalish, "Temperature Dependence of Static Fatigue of Optical Fibers Coated with a UV-Curable Polyurethane Acrylate," Presented at the 83rd Annual Meeting of the American Ceramic Society, Washington, D.C., May 6, 1981.

13. M.J. Matthewson and C. Kurkjian, "Environmental Effects on the Static Fatigue of Silica Optical Fiber," J. Am. Ceram. Soc., 71, (3) 177-183, (1988).

14. C.R. Kurkjian, J.T. Krause, and M.J. Matthewson, "Strength and Fatigue of Silica Optical Fibers," J. Lightwave Technol., 7, (9) 1360-1370.

15. F.V. DiMarcello, P.J. Lemaire and J.R. Simpson, "Fiber Measurements for Long Term Reliability: Strength, Hydrogen and Radiation," Technical Digest -- Symposium on Optical Fiber Measurement, NBS Special Publication #748, 69-78, (1988).

16. ASTM D-570-81 "Standard Test Method for Water Absorption of Plastics."

17. EIA Standard 455-75 "FOTP-75 Fluid Immersion Test for Optical Fiber Waveguides."

18. T. Chapin, "D-Lux 100 Series Optical Fiber Coatings," Lightguide Digest, Issue No. 3, 1989.

19. L.E. Nielsen in "Mechanical Properties of Polymers and Composites," Vol. 1, p.176, Marcel Dekker Inc., New York 1974.

David Szum received a M.S in Chemistry from the University of Illinois at Chicago. He is currently a research chemist for DeSoto, Inc. in the radiation cure unit. He has been engaged in research and development of coatings for fiber optical coatings. Dave joined DeSoto in January, 1989. DeSoto, Inc., 1700 S. Mt. Prospect Road, Des Plaines, IL 60018

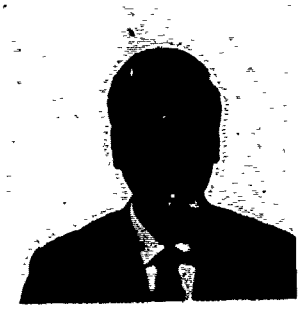

Chander P. Chawla received his Ph.D. in Polymer Science from the University of Southern Mississippi in May, 1990. He obtained a Master's degree in Chemistry from the University of Delhi, New Delhi, India in 1982 and a Master's degree in Polymer Science and Technology from Indian Institute of Technology, New Delhi, India in 1984. He has been working with DeSoto, Inc. as a Research Chemist in the area of fiber optics coating sicne October, 1989. DeSoto, Inc., 1700 S. Mt. Prospect Road, Des Plaines, IL 60018.

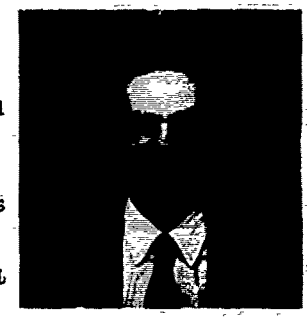

Timothy E. Bishop is a senior research chemist at DeSoto, Inc. He joined DeSoto in 1981 after receiving his B.S. in Chemistry from Illinois State University. He is engaged in developing UV curable coatings primarily for optical fiber. DeSoto, Inc., 1700 S. Mt. Prospect Road, Des Plaines, IL 60018.

Kevin P. Murray received a B.S. in Biology from Loyola University - Chicago in 1974 and an M.S. in Chemistry from Depaul University - Chicago in 1985. He has been involved in the field of radiation curing since 1982 and is currently the Technical Staff Leader of the Fiber Optic Materials group at Desoto, Inc. He has authored several publications in this area and holds nine U.S. patents. DeSoto, Inc., 1700 S. Mt. Prospect Road, Des Plaines, IL 60018.

John M. Zimmerman is a senior research chemist in the Radiation Curable Materials group at DeSoto, Inc. He joined DeSoto in 1983 after receiving his B.S./M.S. degrees at Illinois State University. Since 1984, he has been working on the development of oligomers for optical fiber coatings. DeSoto, Inc., 1700 S. Mt. Prospect Road, Des Plaines, IL 60018.

THE EFFECTS OF COATING CURE ON THE MECHANICAL CHARACTERISTICS OF OPTICAL FIBERS

H. H. Yuce*, I. M. Plitz**, R. A. Frantz* and M. Andrejco**

Bellcore

* 445 South Street, Morristown, NJ 07960

** 331 Newman Springs Road, Red Bank, NJ 07701

(201) 829-4945

ABSTRACT

The principal functions of an optical fiber coating are to preserve the strength and optical performance of the glass fiber by protecting it from adverse mechanical, thermal and chemical environments. The ability of the coating to protect the fiber against these stresses may depend upon attaining proper cure of the coating during manufacture. We have produced four fiber samples with coatings ranging from under-cured to over-cured, and have measured the mechanical characteristics - strength, fatigue, and strip force - of each. This paper describes the preparation of the fiber samples, measurement of their mechanical properties, and correlation of those measurements with the amount of coating cure. Our results show that the extent of cure affects both the strength and the fatigue characteristics of optical fibers.

1. INTRODUCTION

The growing use of optical fibers for telecommunications, particularly for services to end on the customer's premises, exposes the fibers to an ever-increasing array of environments. New and more severe conditions will challenge the protection afforded the glass fiber by its coating.

During manufacture, the fiber is drawn from a hot preform and is protected with a coating within a second, more or less, depending on the draw tower design and the draw speed [1]. The principal functions of the coating are to preserve the strength and performance of the glass fiber by protecting it from adverse mechanical, thermal and chemical environments. There are three potential coating systems available: ultraviolet (UV) cured acrylates [2], thermally-cured silicones [3], and hot melt thermoplastics [4]. The UV curable coatings are currently used for seventy-five percent of all silica glass optical fibers produced for telecommunications [5]. Therefore, this paper concentrates exclusively on these.

UV curing is a process which is ideally suited for optical fiber coatings. The process uses UV radiation to initiate chain reactions which can convert a fluid coating compound to a strong, solid material. Essentially complete curing takes place in only a fraction of a second. Coating systems for optical fibers generally consist of two layers of UV-cured acrylate. The inner layer is of a lower modulus than the outer and its function is to minimize microbending loses. The outer layer, on the other hand, provides mechanical and environmental protection.

It is well understood that the mechanical characteristics of the fiber will be affected by the properties of these polymeric protective coatings. The coatings may, for example, affect the strength distribution and fatigue behavior of fused silica fibers [6,7]. These effects have been identified as being caused by such coating properties as adhesion, water absorption, and water permeation. The protective properties of the coating are controlled by the extent of crosslinking in the polymer, which in turn is a function of the extent of cure attained as a result of the amount of UV curing radiation to which the coating is exposed. Under-cured coatings may be susceptible to chemical attack, thermal softening, and mechanical cut-through, each of which can expose the glass to environmental attack and premature failure. However, the specific relationship between the extent of cure and the mechanical properties of the fiber is not well understood. Hence, there is a growing industry concern about the potential problems that may arise from non-optimal curing.

We are therefore concerned with determining which coating properties may be most sensitive to the extent of cure and how this sensitivity may affect the mechanical properties of optical fibers. To investigate these effects, we have produced sample fibers in our laboratory with different UV curing doses applied to the coating. The fibers were drawn from a fire-polished fused silica rod to a diameter of 125 μm. They were immediately coated in-line with a single layer of a relatively high-modulus UV-curable

polyurethane acrylate coating to a nominal diameter of 250 µm. Using both the coating manufacturer's data (modulus as a function of dose) and our experience with our draw tower, we were able to establish draw speeds and UV curing lamp settings that provided four different degrees of cure, ranging from under-cured to over-cured. The production of these samples and the measurement of their various degrees of coating cure are described in the next section.

In this paper, we present the fiber strength, the fatigue characteristics, and the stripping force for each of the four sample fibers. Even though the glass was the same in all of these fibers, we observed significant differences in mechanical properties. We attribute these to the differences in coating cure.

2. SAMPLE PREPARATION

Curing is a function of the ultra-violet (UV) dose, which in turn is directly proportional to the intensity of the UV lamps and inversely proportional to the draw speed at which the coated fiber passes through the lamp assembly.

All fibers in this study were coated with *DeSoto 950-008*, a relatively high-modulus single-layer coating. We selected drawing conditions (see Table 1) which provided us with our first two fibers (designated herein as Fibers 1 and 2) with different degrees of cure. The UV curing of the coating was accomplished using a system from Canrad-Hanovia, Inc., in which two 12-inch long, 200 W/in medium pressure mercury vapor quartz lamps were operated at the power levels shown in Table 1. Our intent was that neither fiber should be obviously under-cured.

A sample of each fiber was subjected to overnight Soxhlet extraction in methyl ethyl ketone to determine the percent extractables. We followed the proposed standard procedure in the Telecommunication Industries Association draft Fiber Optic Test Procedure FOTP-10. A high amount of extractables indicates lower cross-linking and hence a lower extent of cure relative to a sample of the same coating with a lower percent extractables. We also recorded qualitative observations of the fibers, including color, odor, and surface feel. The observations and extractables data are included in Table 1. Although the data indicated a difference in the coating cure between these two fibers, it was also apparent that both were nominally fully cured or even over-cured. We needed to extend the range of our test fibers to include some that were relatively under-cured, although not to the extent that a fiber manufacturer might reject such product for shipment.

Because the lamps in the draw tower had been replaced since the first two fibers were drawn, we needed a way to approximate the draw tower doses so that we could have more control over the cure of additional fiber samples. We used UV-sensitive color-change labels (from UV Process Supply, Inc.), drawn through the draw tower at various speeds and lamp settings, to estimate the range of doses available. The labels are self-adhesive coated paper that were folded over a coated fiber (which was used only to carry the labels through the tower) and trimmed so that only a small flag projected from the fiber.

Several labels were also exposed at various speeds on a UV conveyor belt system (Fusion Systems Super Six UV Lamp System). An IL-390 Integrating Radiometer (a "Light Bug", from International Light,

Table 1 - Draw Conditions and Cure Measures for Sample Fibers

SAMPLE NUMBER	NOMINAL DRAW SPEED [m/min]	LAMP POWER [Watts]	PERCENT EXTRACTABLES [%]	QUALITATIVE OBSERVATIONS
1	23	3500	1.8	Yellow, Hard
2	38	3500	2.1	Nominal
3	50	3500	6.2	Nominal
4	50	2500	9.2	Acrylate Odor, Soft, Slightly Tacky

NOTE: Old UV lamps used when drawing fibers 1 and 2 were replaced with new lamps before drawing fibers 3 and 4.

Inc.) was passed through several times at these same settings to establish an average dose. The draw tower dose was estimated by comparing the labels from the draw tower to those exposed to a known dosage on the conveyor belt. Since the comparison was made visually, precise color matching was difficult. As a result, the dosage assigned to each label set from the draw tower may have an error as great as ± 10%.

Based on these dosage estimates, we drew two more fibers (designated herein as Fibers 3 and 4) using the draw tower conditions shown in Table 1. We again ran overnight Soxhlet extractions in methyl ethyl ketone on samples of these two fibers. Coupled with our qualitative observations, these results, shown in Table 1, indicated that we had achieved lower degrees of cure with these second two samples.

The mechanical properties of these four fibers were then measured and correlated against the differences in extent of cure.

3. EXPERIMENTAL PROCEDURES (MECHANICAL)

For our experiments we used two-kilometer lengths of optical fibers from each cure condition. As noted, each fiber had a nominal glass diameter of 125 μm coated with a UV-curable, urethane acrylate polymer coating to 250 μm diameter. The following mechanical tests were conducted in our laboratories.

Dynamic Tensile Strength - The tensile strengths of the fibers were measured with a screw-driven universal tensile testing machine in a laboratory ambient environment of 22° C and relative humidity of 50%. Samples were gripped on 5 cm (2 in) diameter capstans covered with a soft elastomeric sleeve. Masking tape was used to secure the ends of the fiber to the capstans. Tensile strength and dynamic fatigue resistance were determined by tensile testing at strain rates ranging from 25%/min to 0.025%/min. A total of 61 samples, each with a gage length of 50 cm (19.6 in), were tested at each strain rate.

Two-point Bending Strength - Fiber strength was also measured using a dynamic two-point bending method[8] [see Figure 1]. The test consists of bending a fiber sample in a 180° arc between two parallel plates which are driven together at a variable speed to maintain a constant stress rate. The fiber is bent to a continuously smaller radius until it eventually fractures, and by measuring jaw separation at the instant of fracture, the fiber strength can be determined. Two-point bending strength and two-point bending dynamic fatigue resistance were determined at stress rates ranging from 60 MPa/sec to 0.06 MPa/sec. A total of 21 samples were tested for each stress rate.

Stripping Test - The force required to strip the coating was measured using a commercial stripping tool mounted on a screw-driven universal tensile testing machine. Two gage lengths were used for the stripped section: 3 cm (1.2 in) and 1 cm (0.4 in). All tests were conducted at the rate of 50.8 cm/min (20 in/min).

4. EXPERIMENTAL RESULTS

The dynamic tensile test results for samples of Fiber 1 tested at four different strain rates are plotted on Weibull axes in Figure 2. Figure 3 similarly presents the results for Fibers 1-4 at the 2.5 %/min strain rate. Figure 4 shows the Weibull two-point strength distribution in deionized water for Fiber 1 while Figure 5 shows tensile dynamic fatigue results for the four fibers at the 6 MPa/s stress rate under ambient conditions. The summary of the strength testing both in tension and in two-point bending is given in Table 2. The strength data can be fit to a single Weibull distribution of the form:

$$P = 1 - \exp[-\sigma/\sigma_0]^m \qquad (1)$$

for all the fibers. In this equation, P is the cumulative probability of failure at a stress less than or equal to σ, and σ_0 and m are empirical distribution parameters. The values of the Weibull exponent m are listed on Figures 2-5.

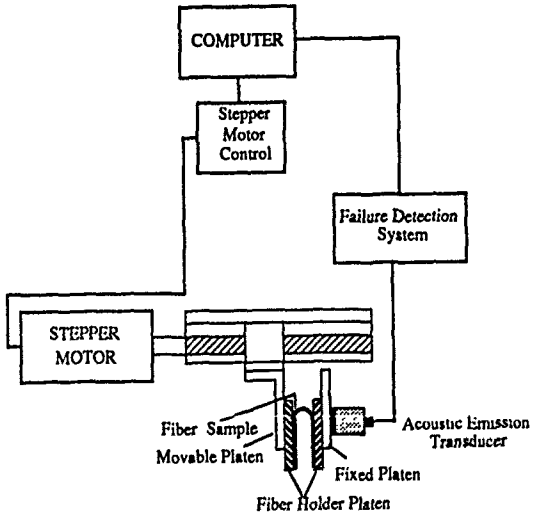

Figure 1 - Two-point bending testing unit

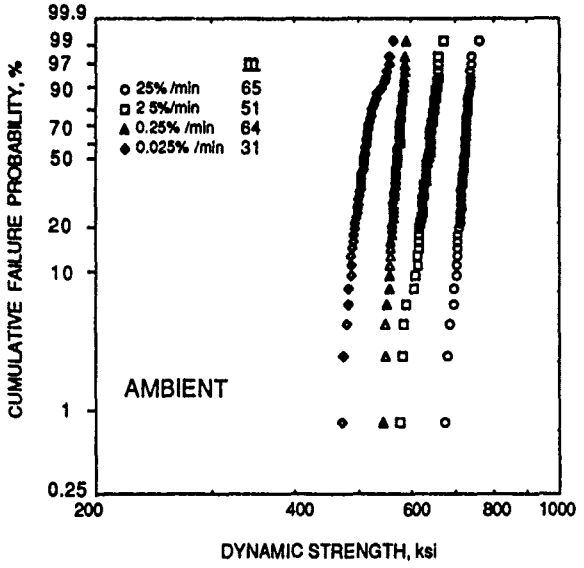

Figure 2 - Weibull tensile strength distributions for Fiber 1

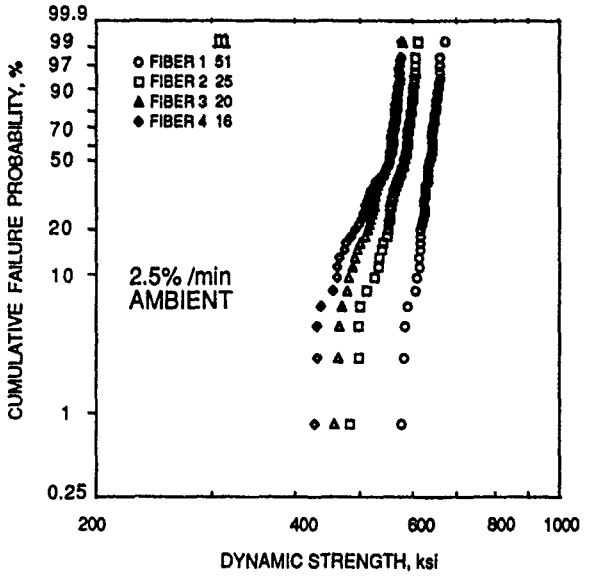

Figure 3 - Weibull tensile strength distributions at 2.5 %/min.

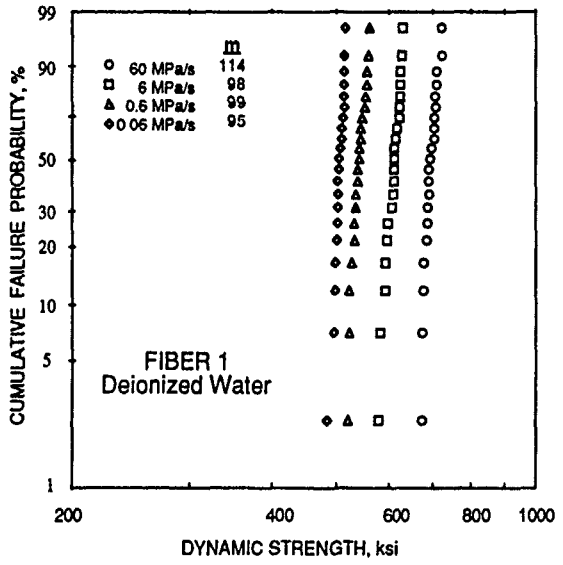

Figure 4 - Weibull two-point bending strength distributions for Fiber 1 at various stress rates.

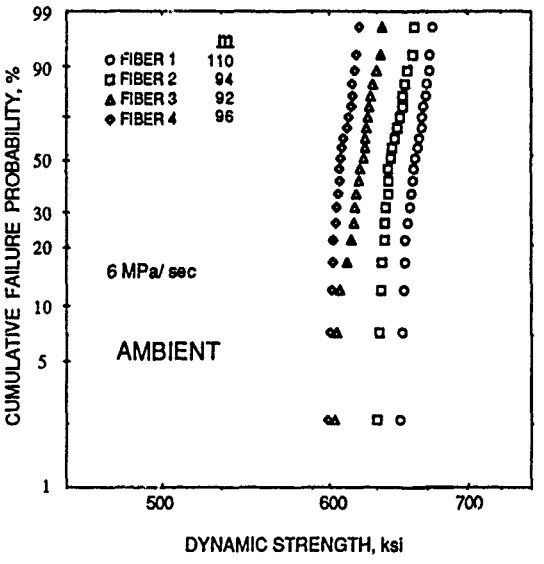

Figure 5 - Weibull two-point bending strength distributions for all fibers in ambient at a fixed stress rate.

In the presence of stress and certain chemical species such as water, the flaws existing in the glass can grow to a size to cause failure. Assuming that the growth rate of such flaws is proportional to a power function of the stress intensity, it can be shown that the dynamic breaking strength σ depends upon the applied strain rate, $\dot{\varepsilon}$:

$$\sigma = B\,\dot{\varepsilon}^{\,1/(n+1)} \qquad (2)$$

where **n** is the crack growth exponent associated with the power law dependence of the crack growth rate and ***B*** is an experimental parameter. The strength values of the data for Fiber 1 shown in Figure 2 are plotted as a function of strain rate in Figure 6, while the data from Figure 4 are plotted as

Table 2 - Summary of Dynamic Strength Testing

FIBER	TEST ENVIRONMENT	TESTING	MEDIAN [ksi]
1	Ambient	Tension	638
2	Ambient	Tension	585
3	Ambient	Tension	556
4	Ambient	Tension	545
1	Ambient	2- Pt. Bending	670
2	Ambient	2- Pt. Bending	642
3	Ambient	2- Pt. Bending	623
4	Ambient	2- Pt. Bending	608
1	Deionized Water	2- Pt. Bending	623
2	Deionized Water	2- Pt. Bending	603
4	Deionized Water	2- Pt. Bending	591
3	Deionized Water	2- Pt. Bending	585

Table 3 - Summary of Dynamic Fatigue Testing

FIBER	TEST ENVIRONMENT	TESTING	n
1	Ambient	Tension	24.6
2	Ambient	Tension	22.5
3	Ambient	Tension	19.6
4	Ambient	Tension	18.8
1	Ambient	2- Pt. Bending	23.3
2	Ambient	2- Pt. Bending	21.9
3	Ambient	2- Pt. Bending	19.2
4	Ambient	2- Pt. Bending	18.6
1	Deionized Water	2- Pt. Bending	22.8
2	Deionized Water	2- Pt. Bending	20.2
3	Deionized Water	2- Pt. Bending	18.3
4	Deionized Water	2- Pt. Bending	18.0

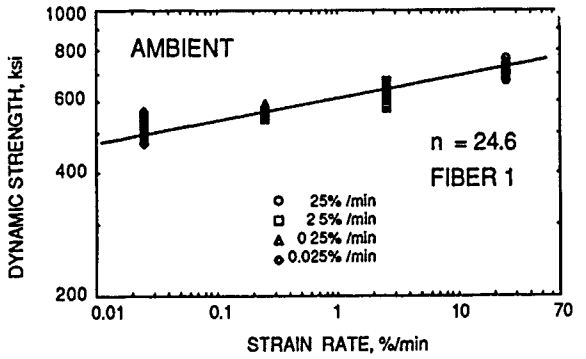

Figure 6 - Tensile dynamic fatigue for Fiber 1

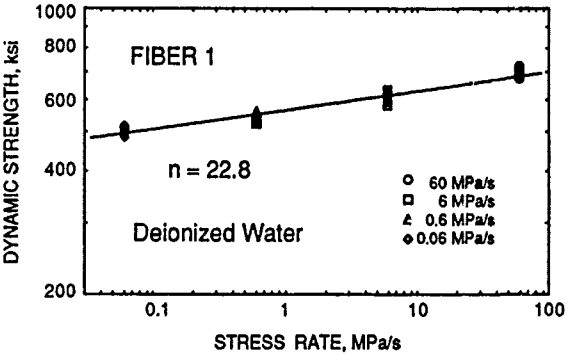

Figure 7 - Two-point bending dynamic fatigue for Fiber 1

a function of stress rate in Figure 7. Fitting the line predicted by equation 2 to these data yields the values of **n** listed on Figures 6 and 7. A summary of the fatigue testing both in tension and in two-point bending is given in Table 3.

The results of the coating stripping test for gage lengths of 3 cm and 1 cm are shown in Table 4.

5. DISCUSSION

The long term mechanical reliability of an optical fiber depends upon the initial distribution of flaws in the fiber and upon the rate of growth of these flaws in the presence of stress and chemical species from the environment. The coating outside a silica fiber acts as a barrier to the environment. It can also influence the chemical environment of the silica surface [9]. First, polymer coatings contain mobile ionic species and contaminants which can diffuse to the coating/glass interface. Second, while coatings are recognized as being fairly permeable, they do act to encapsulate the contaminants and moisture at the coating/glass interface. This encapsulation can lead to significant changes in the chemistry (for example, the pH) of the coating/glass interface which is the location of most strength-reducing flaws in fibers.

The median initial size of the flaws in a fiber is indicated by the median short term strength, with larger values of strength associated with smaller flaw sizes. Table 2 shows a summary of the strength tests for the four fibers ranked in order of decreasing strength both in tension (at a strain rate of 2.5% /min) and in two-point bending (at a stress rate of 6 MPa/s). The tension experiments were conducted in ambient, and the two-point bending experiments were conducted both in ambient and in deionized water. Table 2 shows that both tension and bending strengths under ambient conditions are ranked in the

Table 4 - Coating Stripping Force

FIBER	STRIPPING FORCE FOR 3 cm GAGE LENGTH [g]	STRIPPING FORCE FOR 1 cm GAGE LENGTH [g]
1	676±59	604±54
4	645±110	582±74
2	596±40	559±35
3	577±105	507±58

same order as the extent of cure shown in Table 1, with higher strengths associated with greater extents of cure. The median bending strength in deionized water showed a slight difference in ranking between Fiber 3 and Fiber 4. Figures 3 and 5 are representative Weibull plots comparing the four fibers under common testing conditions. Examination of ***m*** values calculated from these plots shows that the coating curing condition may affect the strength distribution as well. Figures 3 and 5 show the highest ***m*** value for Fiber 1. Part of the difference between Fiber 1 and Fiber 2 may be attributed to the increase in draw speed, which may be affecting the flaw size distribution. However, the only difference between Fibers 3 and 4 was the power of the curing lamps; the small difference in the strength distributions for these fibers can only be attributed to differences in the coating curing condition.

The effectiveness of the coating in protecting the fiber from the environment is indicated by the crack growth exponent **n**; large values of **n** are associated with slower crack growth and hence with a higher degree of protection. Table 3 summarizes the dynamic fatigue parameters for the four fibers. Once again the ranking of the fibers in decreasing order in terms of **n** shows agreement with the extent of cure; larger values of **n** are associated with greater extents of cure.

A summary of the coating stripping test is shown in Table 4. The results indicate that the extent of curing affects the strip force. With the exception of Fiber 4, stripping force paralleled the extent of cure. Fiber 4 showed an anomalously large stripping force. We observed that the stripped coating on Fiber 4 buckled rather than smoothly sliding off as a cylinder as with the other three coatings.

Tables 2-4 might suggest that a fiber manufacturer should maximize the extent of cure in order to maximize fiber strength. However, any attempt to define an optimal extent of cure must consider other coating properties. An over-cured coating may become brittle and subject to cracking, particularly if exposed to solvents. A high elastic modulus reduces the cushioning effect of the coating, increasing the susceptibility to microbending losses. Hydrogen generation has been observed to increase for coatings cured to very high levels [10]. High strip forces should be examined to insure that they do not cause problems with field stripping. These and other coating properties must be balanced in selecting the desired extent of cure.

6. CONCLUSIONS

The long term mechanical reliability of a glass fiber depends upon applied stress, fiber strength, the rate of growth of flaws in the glass, and the fracture toughness of the glass. In this study, the mechanical characteristics of optical fibers have been shown to have a dependence on the extent of cure of the fiber coating. While the actual UV curing dose applied to the fiber in the draw tower is difficult to measure, the relative extent of cure attained for a given coating material can be estimated from the weight loss during solvent extraction. In selecting an optimal cure for an optical fiber coating, consideration must be given, not only to the coating properties (modulus, solvent resistance, hydrogen generation), but also to the effect the coating cure has on the fiber's mechanical properties (strength, fatigue, strippability).

ACKNOWLEDGMENTS

The authors thank O. Gebizlioglu, P. L. Key, J. P. Varachi, Jr., and M. A. Saifi for their helpful criticism.

REFERENCES

1. B. J. Overton, and C. R. Taylor; *Polymer Engrg and Science*; **29**; No.17; 1165 (1989).
2. L. L. Blyler Jr.; *Org. Coatings Plast. chem.*; **42**; 247(1980).
3. E. M. Valles and C. W. Macosko, Macromol.; **12**; 521(1979).
4. T. J. Miller; *Org. Coatings Plast. chem.*; **40**; 217(1979).
5. G. Pasternack; *Proceedings of ANTEC '88*; 377.
6. T. Wei and B. J. Skutnik; *J. Non. Crys. Solids*; **102**; 100(1988).
7. H. H. Yuce, A. D. Hasse, P. L. Key and M. J. Andrejco; *Proc. of 37th Int. Wire and Cable Symposium*; 732(1988).
8. H. H. Yuce, M. E. Melczer, and P. L. Key; *Proc. Seventh Int. Conf. on Integrated Optics*; **2**; 44(1989)
9. J. T. Krause and C. J. Shute; *Adv. Ceram. Mater.*; **3**; 118(1988).
10. S. R. Schmid, DeSoto, Inc.; personal communication.

Hakan Yuce is a Member of the Technical Staff in the Fiber Distribution and Reliability Research District at Bellcore. He leads a research program dealing with optical fiber service life and potential mechanical failure scenarios that may occur in the outside plant environment. Mr. Yuce provides technical input and support to organizations responsible for generic requirements and responds to clients' immediate needs related to consultation on reliability and field failures. He also plays an active role in the standards arena under **EIA/TIA** working committees 6.6.7, fiber coatings and 6.6.8, fiber reliability. Hakan has a B.S. degree in Mechanical Engineering from Technical University of Istanbul [1977], an M.S.in Mechanical Engineering from M.I.T. [1982] and a Ph.D. degree in Mechanical Engineering and Material Science from Stanford University [1987].

Rolf A. Frantz is a Distinguished Member of Technical Staff in the Fiber Distribution and Reliability Research District at Bellcore. After receiving his Ph.D. from Brown University in 1972, he joined Bell Laboratories; his principal efforts were in the field of electrical insulating materials, an area in which he continued to work after transferring to Bellcore in 1984. Since 1988, the focus of his interest has been optical fiber coatings and their effects on long term fiber reliability.

Irene Plitz is a Member of Technical Staff in the Polymer Chemistry and Engineering Research District at Bellcore. She received her B.S. in Chemistry from Morgan State University in 1970 and then directly joined Bell Laboratories. Since transferring to Bellcore in 1984 her interest have centered on the chemical and structural analysis of organic and polymeric materials.

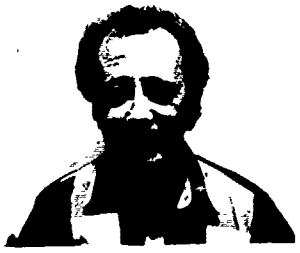

Matt Andrejco is a Member of the Technical Staff in the Fiber and Nonlinear Optical Materials group at Bellcore in Red Bank, New Jersey. He has an A.S. degree in Math and Physical Sciences from Mercer County College.

HIGH TEMPERATURE OPTICAL AND MECHANICAL PROPERTIES OF POLYIMIDE COATED FIBERS

DIPAK R. BISWAS AND DAVID K. ROLAND

SPECTRAN CORPORATION
50 HALL ROAD, STURBRIDGE, MA 01566

Abstract:

The use of polyimide coating on optical fiber has become increasingly important for high temperature applications. The standard telecommunication fibers with uv-cured epoxy acrylate coating, can, in general, withstand temperatures up to 100°C. Silicone and other polymeric coatings such as ladder siloxane polymer can withstand nearly 200°C. However, for temperatures in the range of 300°C, polyimide coating is strongly recommended. The purpose of this paper is to present the optical and mechanical properties of polyimide coated fibers tested at 300 to 350°C.

1. Introduction:

High temperature resistant coatings are in growing demand in the optical fiber industry. Applications of this coated fiber include automotive, aircraft, medical and others. Dielectric, metallic and polymeric coatings are considered for high temperature coatings. Dielectric coatings such as oxides, nitrides, and carbides are successfully applied on optical fibers. The coating thickness is generally less than 1 μm. For long lengths, dielectric coated fibers are further protected by an additional polymeric coating. Therefore, even though the dielectric coating can withstand fairly high temperatures, the application of dielectric/polymeric coated fiber will be limited to the temperature rating of polymer. In the case of metallic coatings, the coating thickness can be as high as 25-30 μm and an additional polymeric coating is not required for handling purposes. Different metal coatings such as low temperature melting indium, tin, aluminum and high temperature melting metals such as gold and copper are successfully applied on optical fibers. In the case of polymeric coatings, commonly used ultraviolet cured epoxy acrylate coatings can withstand up to 100°C whereas silicone [1] and ladder siloxane polymer [2] can withstand nearly 200°C. For temperatures greater than 200°C polyimide [3] is becoming an attractive candidate. This coating is capable of withstanding 300 to 400°C. It has excellent thermal stability, chemical resistance and good dielectric properties. The purpose of this paper is to present optical and mechanical properties of polyimide coated optical glass fibers at 300 to 350°C.

2. Experimental:

Multimode graded index optical fibers were used in this study. 100 μm core with a 140 μm clad glass fibers were coated with 15 μm thick polyimide coatings. Two different polyimide coatings were used; Polyimide A and Polyimide B. Change in attenuation was measured at 340 $\pm$ 5°C in air by using Electronic Industries Association Fiber Optic Test Procedure - 20 (EIA FOTP-20). Dynamic tensile strength of similar fiber was measured at room temperature and after exposure to 300°C for eight hours by using a Tensile

Testing Machine.

3. Results and Discussions:

Attenuation

Attenuation testing was carried out on polyimide coated fibers which were not protected by any cabling jackets or materials. This test was designed to subject the fibers to extremely adverse conditions. Approximately 300 to 900 m of loosely coiled polyimide coated fibers were placed in a high temperature chamber maintained at 340 ± 5°C. Change in attenuation was determined by monitoring the optical transmittance throughout the test. Delta attenuation results are shown in Figures 1 and 2.

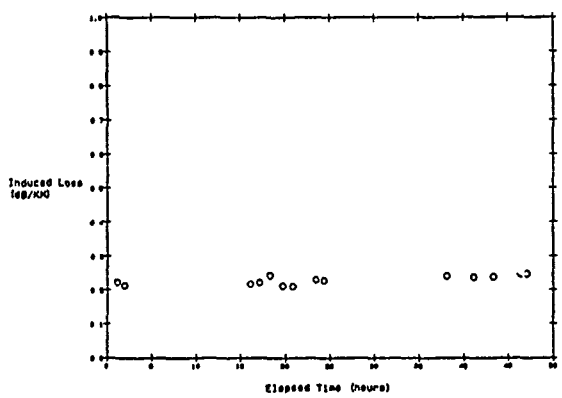

Figure 1.

Delta attenuation of Polyimide A coated fiber at 340 ± 5°C for 48 hours in air.

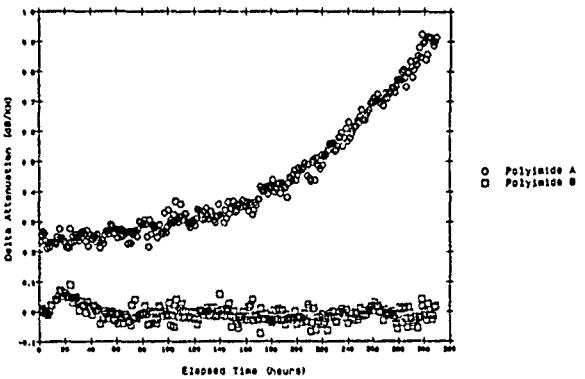

Figure 2.

Delta attenuation results of Polyimide A and Polyimide B coated fibers at 340 ± 5°C for 310 hours in air.

Change in attenuation of fibers with Polyimide A coating remained stable for the testing period of 48 hours. When the testing time at 340 ± 5°C was increased to 310 hours, Polyimide A coated fibers showed an increase in attenuation from 0.2 dB/Km to 0.9 dB/Km as shown in Figure 2. Polyimide B coated fibers during the same testing period of 310 hours at 340 ± 5°C showed no significant change in attenuation from the start of the experiment. Typical properties of this fiber at room temperature are shown in Table 1.

TABLE 1: Typical Properties of SG328 (100/140/170 μm) Fiber

Attenuation, dB/Km @ 850 r	3.5 - 5.0
Bandwidth, MHz.Km @ 850 nm	100-300
Numerical Aperture, (NA)	0.29 ± 0.02
Core Diameter, μm	100 ± 4
Clad Diameter, μm	140 ± 3
Polyimide Coating Diameter, μm	172 ± 2

Strength

Dynamic tensile strength of Polyimide A coated fibers was measured at room temperature by using a Tensile Testing Machine. A 0.7 m gauge length and 4%/minute strain rate were used for measuring the strength. The results are shown in Figure 3.

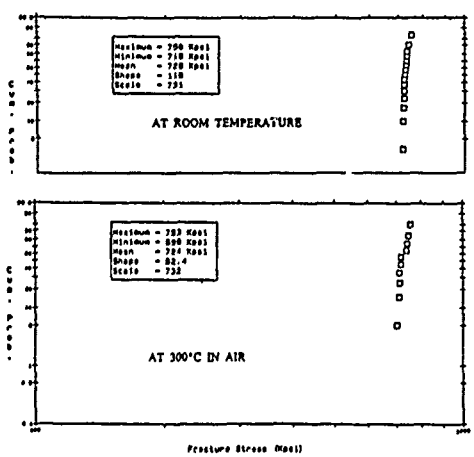

Figure 3. Typical Weibull plots at room temperature and at 300°C.

The strength of the fiber did not change after exposure to 300°C for eight hours. Scanning electron micrographs of Polyimide A and Polyimide B coated fibers which were exposed to 340°C for 310 hours are shown in Figure 4.

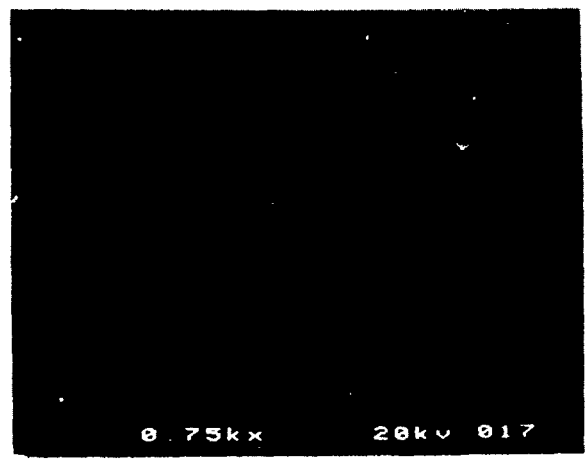

a

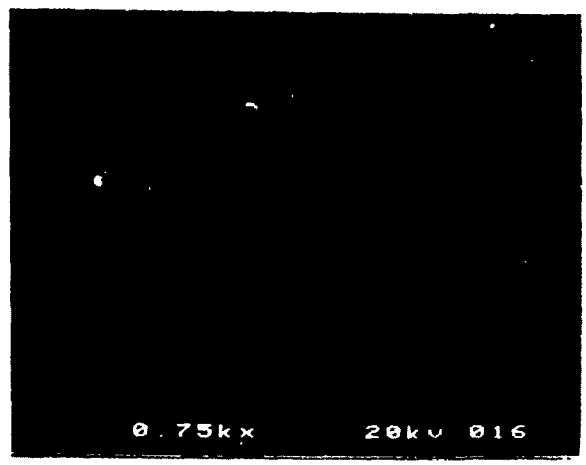

b

Figure 4.

Scanning electron micrographs of Polyimide A (a) and Polyimide B (b) coated fibers which were exposed to 340°C for 310 hours.

A slight change in surface morphology was noticed on Polyimide A coated fibers. There was no significant change in surface appearance on Polyimide B coated fibers.

4. Conclusions:

Based on the results of this study, it can be seen that polyimide coated fibers showed excellent optical and mechanical performance when exposed to 300°C in air. Polyimide A coated multimode graded index optical glass fiber showed an increase in delta attenuation at 340°C from 0.2 dB/Km to 0.9 dB/Km after 310 hours. But the attenuation of Polyimide B coated similar fibers remained unchanged at 340°C after 310 hours. The average strength of 720 Kpsi for Polyimide A coated fibers in air also remained unaffected when the fibers were exposed to 300°C for eight hours. If these polyimide coated fibers are further protected by high temperature cabling materials, they can be suitable for different high temperature applications for even longer periods of time.

References:

1. A. Wada et.al., OFC Tech. Digest, TUIS, 42 (1986).

2. S. Araki et.al., Proc of the 37th IWCS, 745 (1988).

3. D. Biswas, OFC Tech. Digest, THH3, 173 (1990).

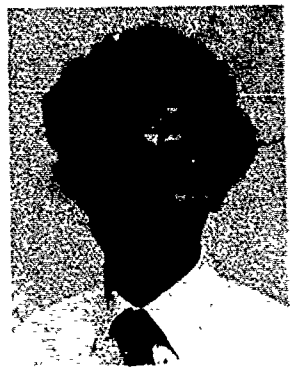

Dipak R. Biswas received his Ph.D. from the University of California, Berkeley in 1976. After working at Lawrence Berkeley Laboratory, University of Utah and Insititue of Gas Technology, he joined ITT Electro-Optical Products Division in 1981. At ITT and Alcatel Cable Systems he worked on optical fiber strength and coating developments for different commercial and military applications until 1988. Currently, as Director of Research and Development at SpecTran Corporation, he is working on strength and reliability of silica optical fibers, hermetic and high temperature coating development and sensor fibers.

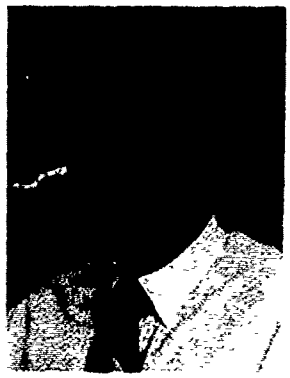

David K. Roland received his B.S. in Mathematics from Worcester State College. After working at Valtec Corporation as a member of Optical R&D Staff, he joined SpecTran Corporation in 1983 as an Engineer. He is involved in design and development of R&D as well as production optical fiber measurement equipments.

SINGLE-MODE OPTICAL FIBER INDEX OF REFRACTION DEPENDENCE ON PRODUCT PARAMETERS, TENSILE STRESS AND TEMPERATURE

D. H. Williams, J. J. Carr, and S. L. Saikkonen

Corning Incorporated, Product Engineering Laboratory
Corning, New York 14831

Abstract

This paper describes the results of a recent study to characterize effective index of refraction for commercially available unshifted matched-clad single mode optical fiber. Effective index of refraction was determined as functions of process range, tensile stress and temperature (over the specification range). Index of refraction was measured at the nominal operating wavelengths of 1300 and 1550 nanometers. Pulse time-of-flights, fiber lengths, applied tensile loads, elongations and temperatures were measured directly. This experiment provides effective index of refraction measurement accuracy to four decimal places.

Introduction

Material index of refraction (n) is defined as the ratio of the speed of light in a vacuum to the speed of light in a particular material. Material index is dependent on wavelength, composition and temperature of the propagation medium. Group index of refraction (N) is defined as the speed of light in a vacuum to the pulse speed of a group of wavelets from a light source, comprising a range of wavelengths, transmitted through a material medium. In a single-mode fiber the power is shared by the core and cladding which requires a power weighted average of the core and cladding group indices of refraction. Also, the wavelength of operation and the fiber index profile cause a waveguide related effect on the index. The combination of these two components makes up what is referred to as the effective group index of refraction (N_{eff}) for a single-mode fiber in operation, and is the parameter measured in this experiment.

Measurements of effective index of refraction in an optical fiber can be used to reveal several useful properties pertinent to the transmission medium. Current index of refraction values for long optical fiber lengths are obtained empirically, relying on winder length readings that generally limit accuracy to three decimal places. Also, index of refraction can be determined from transmitted time of flight of an optical pulse. The latter approach requires very accurate length measurements and is the approach used in this experiment.

This paper describes the experimental results of a study conducted to characterize effective index as a function of product parameters, tensile stress and temperature. One application for this information is when accurate length measurements of optical fibers are desired using an optical time domain reflectometer (OTDR). With index measurements to four decimal places, length can be measured to an accuracy of 1 meter in 10,000. The stress dependence on index of refraction can be used to provide a powerful diagnostic tool for cable stress analysis. This work advances index of refraction measurements to four decimal place accuracy and investigates the influence of stress and temperature across much greater ranges than previously known work.

Experimental Measurement Method

A Fresnel reflection millimeter resolution OTDR was used to measure the time of flight of an optical pulse launched into the near end of the fiber and returned to the same end. The effective index of refraction is calculated using equation (1):

$$N_{eff} = c/V_{eff}$$

$$V_{eff} = 2L/t$$

$$N_{eff} = ct/2L \qquad (1)$$

where $c = 3 \times 10^8$ m/s is the velocity of light in a vacuum.
L = fiber length
t = round trip time of flight

Experimental Procedure

Effective Index of Refraction versus Product Parameters

Selected fiber samples were representative of the typical manufacturing process range for delta and mode field diameter (MFD). Fiber lengths were deployed in a straight line and measured between fifty-meter benchmarks surveyed to within an accuracy of two millimeters. One end of the test fiber was coupled to a Fresnel reflection OTDR capable of 10 ps time of flight resolution. Each fiber was measured in an unstressed condition at room temperature (22°C), to characterize index of refraction as a function of product parameters.

Effective Index of Refraction versus Tensile Stress

Once fibers were characterized in their unstressed condition, each sample was deployed in a straight line for effective index versus stress measurements. For this phase of the experiment, the fiber sample ends were epoxied to grooved aluminum blocks and a straight tensile load was applied in about 0.2 pound (20 kpsi) increments up to 6 pounds (300 kpsi). Flight times, applied loads and elongations were recorded. Stresses were calculated using the applied loads over cross-sectional fiber areas and strains from elongations at each load, over original fiber length. Index was then determined from a time-of-flight measurement at any given stress.

Effective Index of Refraction versus Temperature

Index versus temperature measurements were performed with fifty-meter fiber samples loose coiled and placed in a temperature-controlled chamber. Initial measurements were performed at room temperature in their loose coiled configuration. The temperature chamber was cycled from -60 to +85 degrees Celsius in approximately 10 degree increments. Index of refraction was calculated from a time-of-flight measurement for each monitored temperature at equilibrium, and corrected for length changes due to thermal expansion or contraction from the room temperature length.

Experimental Results

Characterization of index of refraction over the selected sample range for delta and mode-field diameter showed index variations in the fourth decimal place. Over the full range of the product parameter tolerance the index variation was 0.0006. Also, the difference between effective index at 1300 nm and 1550nm was 0.0006 for each fiber measured. A graph, figure 1, of effective index versus MFD for the samples measured shows a near linear relationship.

Index versus tensile stress graphs show nearly linear relationships for both wavelengths as displayed in figures 2 and 3. The slope for each fiber measured was quite consistent at -0.000024/kpsi. Negative slope implies flight times, and therefore index, decreases with increasing tensile stress. Previous work on time-of-flight versus stress in a multimode optical fiber (Hartog, Conduit, and Payne)[1] resulted in a slope of -.000035/kpsi.

Figures 4 and 5 represent effective index versus temperature results. The effective index versus temperature slope was 0.000012/°C for each sample measured at either wavelength. Hartog, et al[1] also measured temperature dependence on index and obtained data which resulted in a slope of 0.000010/°C. Cohen and Fleming's work[2] reported a rate of change of 0.000010/°C also, which measured a depressed clad single-mode fiber (with a B_2O_3 doped silica core).

Conclusion

Effective index is dependent on product parameters, applied tensile stress and temperature. The average index at 1300 nm was 1.4675 and at 1550 nm was 1.4681. From the samples selected, which covered the range of product parameters the index variation was 0.0006 for both wavelengths and the index difference between the two wavelengths was 0.0006. An evaluation of the dependence of index on tensile stress and temperature reveals that the effects are nearly linear and the slopes were -0.000024/kpsi and 0.000012/°C, respectively.

References

1. Hartog, A.H., A.J. Conduit and D.N. Payne. 1979. Variation of Pulse Delay with Stress and Temperature in Jacketed and Unjacketed Optical Fibres. Optical and Quantum Electronics 11: 265-273.

2. Cohen, L.G. and J.W. Fleming. 1979. Effect of Temperature on Transmission in Lightguides. The Bell System Technical Journal 58: 945-951.

Biographies

Diane Williams is an Electro-Optical Equipment Engineer at Corning Incorporated's Product Engineering Laboratory in Corning, New York. She received her B.S. degree in Electrical Engineering from The University of Pennsylvania in 1986. In 1986, she joined Corning, and is presenlty responsible for single-mode measurements.

Jim Carr received his B.S. and M.A. degree in physics from the State University of New York in 1976 and 1979. He joined Corning Incorporated in 1985 and is presently a Sr. Mechanical and Environmental Engineer at the Product Engineering Labortory. His responsibilities include development, coordination, and evaluation of mechanical and environemntal reliability testing of optical fiber.

Stuart Saikkonen is currently the Supervisor of Product Reliability Engineering in Corning's Telecommuniation Products Division. He received his degree in Mechanical Engineering from Rochester Institute of Technology in 1981. His previous work in optical fibers includes the development of high-strength arc fusion splicing methods and other Optical Time Domain Reflectometry measurement techniques.

Figure 1

Effective Index vs MFD
(Unshifted Single-mode Fiber)
1295 nm

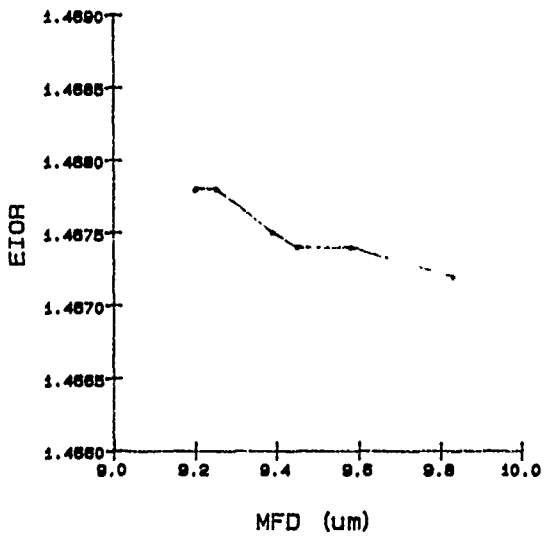

Figure 2

Effective Index vs Stress
(Unshifted Single-mode Fiber)
1295 nm

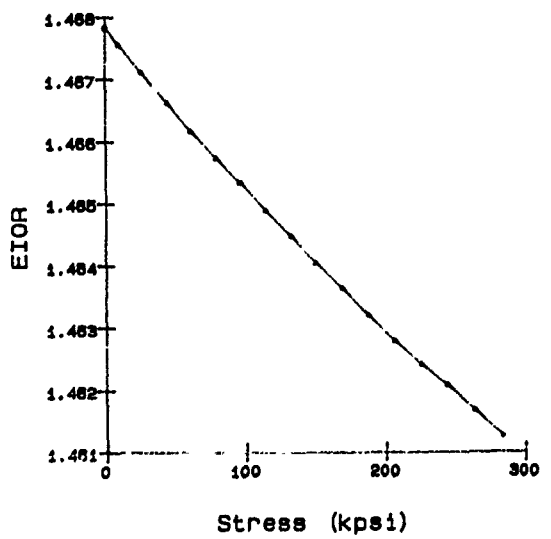

Figure 3

Effective Index vs Stress
(Unshifted Single-mode Fiber)
1532 nm

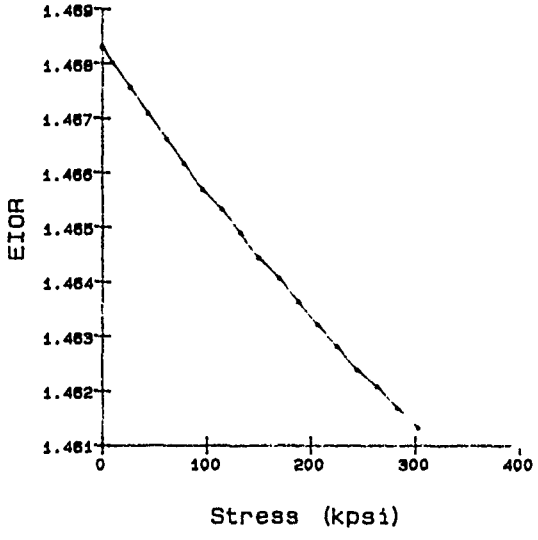

Figure 4

Effective Index vs Temperature
(Unshifted Single-mode Fiber)
1532 nm

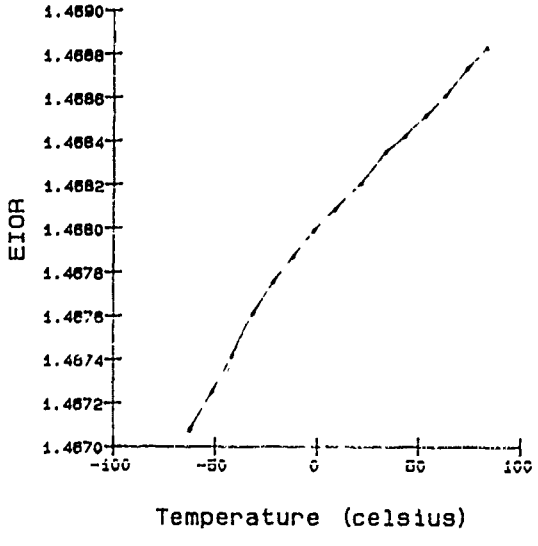

Figure 5

Effective Index vs Temperature
(Unshifted Single-mode Fiber)
1295 nm

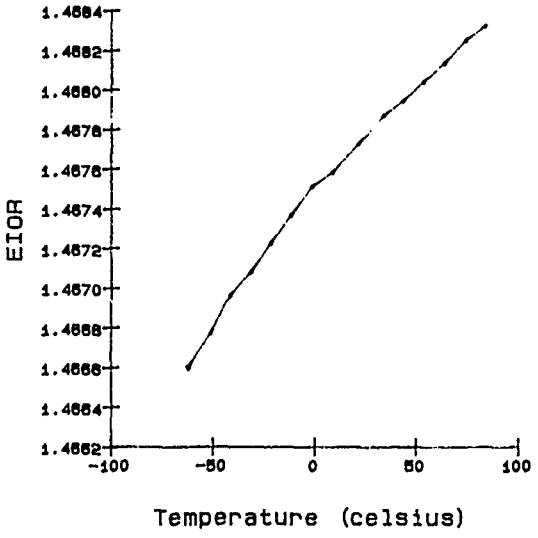

SYSTEM REQUIREMENTS AND INSTALLATION TESTING FOR FIBER-TO-THE-SUBSCRIBER

James J. Refi and Michael J. Swiderski

AT&T Bell Laboratories
Norcross, GA 30071

ABSTRACT

Fiber-to-the-subscriber systems generally impose maximum optical loss and total reflectance requirements on the outside plant fiber, splices and connectors, and these requirements depend on the particular vendor's transmission system and architecture. To insure that the system performance requirements are met, the outside plant should be tested during its construction phase and after completion. The completion tests are usually made at the system operating wavelength, although for multiwavelength systems the measurements may be made at a wavelength corresponding to the most demanding requirements.

In this paper, we describe the various techniques for measuring splice loss, end-to-end loss and reflectance, and explore the implications of making field measurements on emerging systems that use short wavelength transmission on conventional single-mode fiber.

INTRODUCTION

Since 1988, several architectures have been proposed and implemented in fiber-to-the-subscriber installations. These include the optical bus,[1] the passive double star (star-bus),[2][3] and the active double star.[4][5] Each has distinct requirements that vary depending on the manufacturer of the transmission equipment. Because of this diversity, and to enable a discussion of specific installation testing procedures and requirements, we focus exclusively on AT&T's Fiber-to-the-Home (FTTH) feature of SLC® Series 5 digital loop carrier.[4][6][7] This system uses an active double star architecture to currently provide up to four POTS channels per fiber with additional channels and services, such as video, in development.

A fiber-path extends from a remote terminal (RT) to a distant terminal (DT), which may be mounted on the side of a house (fiber all the way to the home) or to several DTs in a pedestal located on property lines (fiber to the curb). Operating bidirectionally over one single-mode fiber at an optical line rate of 1.544 Mb/s, the system can reach a carrier serving area (CSA) of up to 12,000 feet from the RT. The present version provides the POTS channels at a 1310 nm wavelength, while a future version will do the same at 780 nm.

Because one fiber runs between the RT and each DT, testing involves connecting to each fiber through optical connectors at the DT and at an interconnect cabinet in the RT. With this point-to-point topology, field testing methods and procedures are identical to those used in inter-office and loop feeder trunks.

Field tests on loop distribution fiber systems are frequently performed by construction technicians during and immediately after cable installation. The two types of field measurements most frequently performed are splice loss and end-to-end loss. Reflectance testing is not generally needed because there is a low failure probability when the route is constructed with quality components.

SPLICE LOSS TESTING

Installation times can be reduced by making "blind" splices and not checking their quality. However, construction crews are currently reluctant to enclose splices in a splice case that might be encapsulated and buried without at least first testing them for splice continuity, and preferably for splice loss. A variety of methods and equipment can be used.

Far-End Transmission and Detection

The simplest way to monitor the integrity of a splice is to connect a light source to one end of the first cable and detect the signal at the opposite end of the spliced cable as shown in Figure 1. Because it requires a minimum of three people (one at each end and a third at the splice location) and communication paths among them, this method for testing splices is not widely used in fiber-to-the subscriber installations.

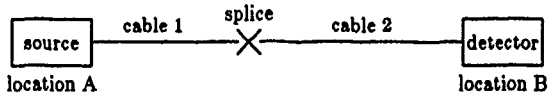

Figure 1. Far-end transmission and detection method for monitoring splice integrity.

Local Detection

The number of people needed to verify splice integrity can be reduced to two by using far-end transmission with local detection. With this method, light transmitted from location A is detected immediately after the splice rather than at location B as in Figure 1. The local detection might be accomplished by bending the fiber to cause some of its light to escape onto a photodiode. Fiber identifiers using this technique can be used to verify a splice's continuity by alternately clipping the identifier onto the fiber before and after the splice (Figure 2).

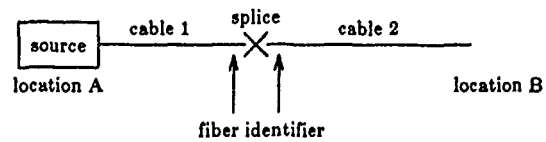

Figure 2. Local detection of transmitted power for monitoring splice continuity.

Alternatively, some of the light lost at a splice can be gathered and guided to a photodiode and used to measure splice loss,[8] and this method has been used in several loop installations.

• SLC is a registered trademark of AT&T.

Local Injection and Detection

Local Injection and Detection (LID) systems further simplify the splicing operation and reduce the number of people needed to make the test to one. Light injected into the fiber immediately before the splice is detected immediately after it. LIDs use the same detection principles already discussed together with macro- or microbending methods for injecting light sideways into the fiber. LIDs that use macrobends serve as "optimizers"—giving no indication of the splice's loss, but allowing the splice loss to be minimized. Microbend injectors couple enough light into the fiber so that the loss of certain splices can be measured.

Optical Time Domain Reflectometry

An Optical Time Domain Reflectometer (OTDR) measures the light reflected from discontinuities and continuously backscattered from the fiber itself. Changes in the backscattered signal between two points in a fiber show the loss between those points and this can be used to *estimate* the loss of the splice. The measurement is only an *estimate* because OTDRs introduce an error that depends on the similarity of the fibers on either side of the splice. Since the error may be either positive or negative, the measured splice loss may appear large when observed from one direction and low (perhaps even a "gainer") when viewed from the opposite direction. The only way to overcome this OTDR limitation is to measure the splice from both directions and average the two readings. Although OTDRs have enough dynamic range to measure all splices from both directions in loop distribution plant, bidirectional measurements are cumbersome to make. Consequently, splices are usually measured in only one direction and the measurement error taken into account when determining an acceptable OTDR splice loss reading.

In addition to the inherent error that depends on the fibers before and after a splice, an OTDR's receiver circuitry might introduce another error when used to measure the loss of a reflective joint. Sudden changes in optical power, such as when going from a small backscattered signal to an intense reflected power, temporarily saturate the receiver. Time is required for the receiver to recover during which the true signal backscattered from the second fiber is distorted. Unless an OTDR has a masking feature, this sudden change in signal power impairs its ability to measure the loss of reflective joints.

Another limitation, imposed by the pulse width of the OTDR, is it's ability to resolve closely spaced events. High resolution requires narrow pulses, but this leads to reduced pulse power which decreases measurement range. The resolution of most OTDRs designed for the local loop requires events to be at least 15 meters apart.

Direct Core Monitoring

Some fusion splicing machines use video imaging techniques for measuring parameters that affect splice loss.[9] By viewing the fibers vertically and horizontally with a video camera, parameters such as cladding and core offset; type, amplitude and length of core deformation; and variation in fiber outer diameters are analyzed to estimate splice loss. While producing good loss estimates of low loss splices, this method sometimes does not detect broken fibers or high loss splices.

END-TO-END LOSS TESTING

After installation of the fiber, splices and connectors, end-to-end loss tests are made on each fiber-path. The fiber is accessed through optical connectors at the DT and at the interconnect cabinet in the RT (Figure 3). The measured loss must be smaller than the maximum loss permitted by the operating system.

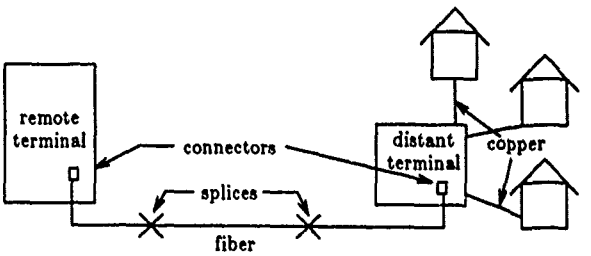

Figure 3. Measuring end-to-end loss between connectors in a point-to-point fiber-to-the-curb installation.

When measuring end-to-end loss, care must be taken to understand what components are included in the loss measurement. Depending on how it's measured, the loss may or may not include the end connectors. For example, one method for measuring the end-to-end loss of a single-mode installation consists of connecting a reference single-mode test jumper to the source and a multimode "photon bucket" fiber to the receiver to get a reference power reading, P_{ref} (Figure 4a). The installed test fiber-path is then inserted, and the test power P_{test} measured (Figure 4b). The measured loss L_{meas} equals $P_{ref} - P_{test}$. If the reference fiber is identical to the test fiber and the loss of the reference connection (L_r) the same as the test connection at the detector (L_{td}), then the measured loss includes the test fiber, splices and one connection (L_{to}). For a more accurate measurement, the loss should be measured in both the A to B and B to A directions and the readings averaged for each fiber-path.

Because a photon bucket fiber may not detect the presence of a defective connector at the receive end of the outside plant, a single-mode jumper is frequently used instead of the photon bucket jumper.

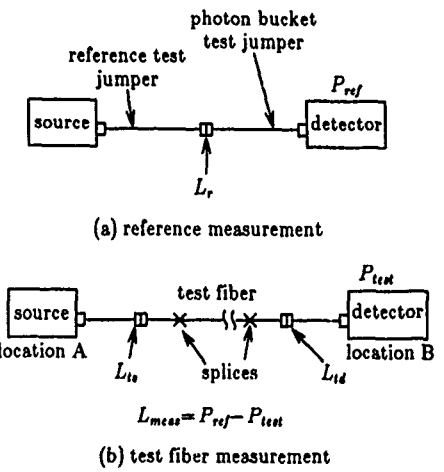

Figure 4. A method for measuring end-to-end loss.

The measured loss L_{meas} is called the *path loss*. For AT&T's current loop distribution system, the path loss must be less than 6.6 dB at 1310 nm in any environment, whether it's buried or underground (15° to 170°F), normal aerial (-10° to 170°F) or extended aerial (-40° to 170°F). This 6.6 dB value should be further reduced at the time of installation to include a margin for future repair splices. This will insure conformance to the 6.6 dB path loss requirement even after making future repair splices. Two repair splices should be budgeted for each type of splice used to build the plant.

In addition to simply insuring that the path loss is less than the 6.6 dB system requirement (minus an allowance for repair splices), the measured path loss can also be compared against a completion test target. This target is the maximum expected loss for the fiber length and number of splices and connectors in a particular route. It is tailored for each fiber path and computed from loss parameters for the fiber and each component in that path. For example, the completion test target for a 3.66 km buried route containing four passive splices and a connector on either end (the equivalent of one *connection*) might be: 3.66 km×0.5 dB/km + 4×0.25 dB/splice + 0.6 dB = 3.43 dB. Rather than use completion test targets, which typically vary for every fiber-path, field technicians are usually content with meeting the 6.6 dB system path loss requirement.

REFLECTANCE TESTING

When constructed with high quality components, there is a low probability that reflectances will cause system failure. So, routine reflectance testing is not justified. However, for those wanting to make such tests, two predominant methods. The "coupler method" (sometimes also called Optical Continuous Wave Reflectometry) measures the total reflectance from the fiber and all components. The second method is to use an OTDR to measure the reflectance from individual components. AT&T's system does not require maximum individual component reflectances, but rather a maximum cumulative reflectance from all the components including the fiber.

The Coupler Method

The coupler method uses an optical source, detector, and coupler to measure the total reflectance caused by crosstalk within the coupler, fiber backscatter, and component reflectances. Shown in Figure 5, this arrangement is first calibrated by holding the test connector against a mirror to reflect all the incident power back to the power meter. (Other techniques are discussed in EIA/TIA-455-107.) This power is then used as a reference for comparing other powers reflected when the test connector is connected to the test fiber-path. To obtain a valid measurement, the far end of the fiber-path should be properly terminated—preferably with the system optical interface line unit card.

Because attenuation increases with distance along the fiber-path, the measured total reflectance is more sensitive to reflectances near the input than to similar reflectances farther away. Clearly, the nearest connection is the one between the test jumper and the fiber-path under test. Consequently, a worn or damaged test connector may produce an erroneous reflectance measurement.

AT&T's bidirectional POTS transmission system can tolerate a total reflectance of -25 dB at 1310 nm. This level keeps the signal to interference ratio better than 6.5 dB, which equates to a 1 dB crosstalk power penalty for a PIN detector.[10] If the reflectance exceeds this level, an OTDR is used to identify the offending component(s).

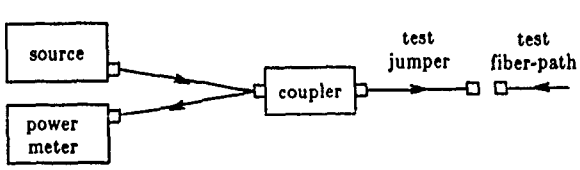

Figure 5. The coupler method for measuring total reflectance.

OTDR

Although OTDRs have the capability for measuring and locating component reflectances, they are not yet designed nor commonly used for this purpose.[11] When making such measurements, care must be taken to insure that the fiber's backscatter level before the reflectance is significantly higher than the OTDR's noise floor and that the reflectance peak is not clipped by the OTDR's receiver. Having established this precaution, the OTDR must still be calibrated. The calibration might be the Rayleigh backscatter computed for a particular fiber type and OTDR pulse, or a Fresnel reflectance of known magnitude.[12] Even after making such a calibration, individual component reflectances cannot always be measured directly because the measured reflectance is the sum of the component reflectance plus the fiber's backscatter, and these must be separated mathematically using the equation:[13]

$$CR = r + 10\log_{10}(10^{0.2m} - 1)$$

where:

CR = Component Reflectance in dB,
r = backscattering coefficient, and
m = OTDR reflectance measurement in dB which, because of the way OTDR losses are calibrated, is half the true reflectance height.

The r value depends on fiber type, measurement wavelength, and the OTDR pulse width used to measure the reflectance height. For the widely used depressed clad fiber, the r value at 1310 nm for a 1 μsec pulse is -49.2 dB. Therefore, if a reflectance is measured at 5 dB above backscatter (Figure 6), the component reflectance using the previous equation is -39.7 dB.

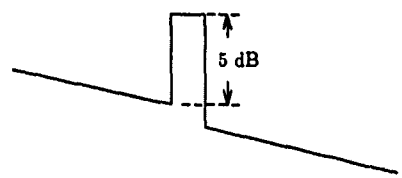

Figure 6. Measuring component reflectance with an OTDR.

SHORT WAVELENGTH OPERATION

When operated below its cutoff wavelength, a "single-mode" fiber behaves as a step-index multimode fiber carrying two or three modes. Interest in operating single-mode fibers at short wavelengths (780 to 850 nm) has arisen because of the widespread availability of inexpensive audio compact disc (CD) lasers, which can be purchased for less than $5 in large quantities.[14] Although more expensive when equipped with single-mode connectors or fiber pigtails, CD lasers offer the prospect for economy and volume production that may never be attained with long wavelength sources.

At low data rates over the short distances that characterize the local loop, the higher loss and reduced bandwidth (because of modal distortion[15][16] and chromatic dispersion) of single-mode fiber at short wavelengths is not a serious limitation. Some local loop systems have already been installed and are operating at short wavelengths.[6][17] The next generation SLC offering will likewise use short wavelength for POTS and 1310 nm for video.[18]

The potential economies of short wavelength transmission can be fully exploited if it does not entail extensive additional testing burdens on fiber manufacturers and installation technicians. This can be done by characterizing fiber, splices and connectors at short wavelengths and then using this information to establish 780 nm loss budgets so that the 1310 nm budget will be more restrictive. In this way, installations that meet the 1310 nm loss budget will, with high assurance, meet the 780 nm loss budget—thereby precluding the need for short wavelength field measurements.

Fiber Loss

At wavelengths longer than the fiber's cutoff wavelength, only the fundamental LP_{01} mode propagates. As wavelength decreases, the second order LP_{11} mode starts traveling and increases the launch power several dBs. At even shorter wavelengths, the third order mode group, comprised of the LP_{21} and LP_{02} modes, starts to propagate and increases the transmitted power by another couple of dBs.

The third mode group is loosely bound and may be present or absent depending on the length, curvature, and cutoff wavelength of the fiber. For example, third order mode power present on a short fiber length may not be present on a long fiber. This phenomenon introduces a transient loss (Figure 7) that causes the fiber to exhibit a nonlinear length scaling similar to what occurs in multimode fibers when excited with a non-steady state modal power distribution. The normalized loss in dB/km will therefore be unrealistically high because detectable third order power exits the short 2 meter cutback length but not the long length. To extinguish the third order mode power through the short strap, an appropriate mode suppression loop is used. Figure 7 shows how the presence of this loop causes the fiber loss to scale linearly with length—accomplishing the same objective as the mode filters used when measuring multimode fibers. Extensive single-mode fiber measurements using this loop shows an average 780 nm loss of 2.7 dB/km.

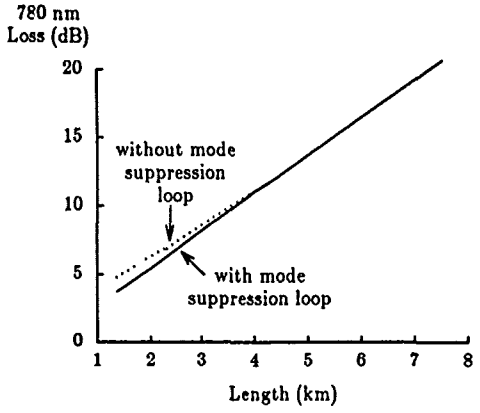

Figure 7. 780 nm loss versus length for a single-mode fiber having a 1310 nm cutoff wavelength.

Joint Loss

An optical joint (splice or connector) disrupts the modal power distribution in a fiber. Power in the first order mode may couple into second and third order modes, and power in the second order mode may couple into the first and third order modes. Because the third order power excited at a joint may or may not propagate to the end of a long fiber, this power cannot be expected to be present at the receiver. Consequently, short wavelength joint losses, like the fiber itself, should be characterized based on two mode propagation. Measurements on over 100 joints using mode suppression loops before and after the joint show that 780 nm joint losses are typically 32% higher than 1310 nm losses with a correlation coefficient of 0.92.

Component Reflectances

Although not substantially affected by the presence of two or three modes, reflectances at connectors and mechanical splices are several dBs larger at short wavelengths than at long. Possible explanations for this are that the index matching gel produces a greater mismatch to the fiber at short wavelengths or that short wavelengths more acutely discriminate the submicroscopic imperfections and changes in refractive index induced at the fiber junction. Short wavelength systems can be economically designed to tolerate these higher reflectances.

End-to-End Testing

If the end-to-end loss of an installed route is measured at 780 nm using the method outlined in Figure 4, but with a mode suppression loop in the reference test jumper, then the measured loss will be no greater than the completion test target computed using fiber and component loss values based on two mode propagation. This occurs because power coupled from the first and second order modes into the third order mode at joints could produce some third order power at the detector. Because this extra power was deliberately excluded from the joint characterizations, the short wavelength completion test target will be a conservative upper bound on the installed system's loss.

CONCLUSIONS

With point-to-point loop distribution fiber topologies such as those used in a star architecture, field testing methods and procedures are identical to those used in inter-office and loop feeder trunks. Splices can be tested as usual with the most popular methods being the OTDR and local detection techniques. When performed at the system operating wavelength, end-to-end loss tests reveal whether the system loss budget has been met.

The full economies of short wavelength transmission can be realized if it does not require extensive additional testing by the fiber manufacturer or the installation technicians. If the 1310 nm loss budget is more restrictive than the 780 nm requirement, then installations that meet the 1310 nm requirement will, with high confidence, meet the 780 nm loss budget—precluding the need for short wavelength field testing.

ACKNOWLEDGEMENTS

Dave Peckham and Chris Okafor developed the short wavelength fiber loss characterization methods, and Bob Fangmann established the end-to-end path loss budgets. Ray Nunn provided information on field practices based on actual installations.

REFERENCES

1. D. Wong and R. Narciso, "An Optical Bus Architecture in the Last Mile," *38th International Wire and Cable Symposium*, November 1989, pp. 136-140.

2. M. H. Reeve, "Line Plant Considerations for Passive Optical Networks for the Local Loop," *37th International Wire and Cable Symposium*, November 1988, pp. 134-140.

3. D. W. Faulkner, "Broadband Passive Optical Network Evolution," *Broadband (FOC/LAN) '89*, October 1989, pp. 165-167.

4. R. M. Huyler, D. E. McGowan, J. A. Stiles and F. J. Horsey, "The Architecture and Technology for the All-Fiber Loop," *37th International Wire and Cable Symposium*, November 1988, pp. 129-133.

5. F. A. Huszarik, R. Mariani, R Yakimovich and J. Justice, "Installation and Testing of Multiservice Fiber Links in the Subscriber Loop: A Case Study," *37th International Wire and Cable Symposium*, November 1988, pp. 158-162.

6. J. B. Haber, D. Kalish and J. J. Refi, "Single-Mode Media and Apparatus for Fiber-to-the-Home," *37th International Wire and Cable Symposium*, November 1988, pp. 163-171.

7. R. O. Tuckey and J. A. Stiles, "Field Experience With a Fiber-to-the-Home System," *15th European Conference on Optical Communication*, September 1989, pp. 190-193.

8. A. F. Judy, G. F. DeVeau and K. M. Yasinski, "Comparison of Single-Mode Splice Loss Measurement Methods," *36th International Wire and Cable Symposium*, November 1987, pp. 202-208.

9. O. Kawata, K. Hoshino, Y. Miyajima, M. Ohnishi and K. Ishihara, "A Splicing and Inspection Technique for Single-Mode Fibers Using Direct Core Monitoring," *IEEE Journal of Lightwave Technology*, Vol. LT-2, No. 1, April 1984.

10. P. P. Bohn and S. K. Das, "Return Loss Requirements for Optical Duplex Transmission," *IEEE Journal of Lightwave Technology*, Vol. LT-5, No. 2, February 1987.

11. F. P. Kapron, E. A. Thomas and J. W. Peters, "OTDR Measurements of Optical Return Loss," *Technical Digest - Symposium on Optical Fiber Measurements*, National Bureau of Standards, September 1988, pp. 35-38.

12. S. K. Das, A. F. Judy, G. M. Alameel, R. M. Jopson and T. F. Adda, "Reflectance Measurement in Lightwave Systems: A Comparison of Various Techniques," *Technical Digest - Symposium on Optical Fiber Measurements*, National Bureau of Standards, September 1988, pp. 25-30.

13. A. F. Judy and H. E. S. Neysmith, "Reflections from Polished Single Mode Fiber Ends," *Fiber and Integrated Optics*, Vol. 7, 1988, pp. 17-26.

14. P. Shumate as quoted in the article "Lightwave in the Loop," by H. Rausch, *Lightwave*, April 1988.

15. M. Stern, W. I. Way, V. Shah, M. B. Romeiser and W. C. Young, "800-nm Digital Transmission in 1300-nm Optimized Single-Mode Fiber," *Conference on Optical Fiber Communication/International Conference on Integrated Optics and Optical Fiber Communication*, Vol. 3, 1987, (Optical Society of America), paper MD2.

16. C. M. Ragdale and F. P. Kapron, "Measuring 825 nm Transmission on 1300 nm Single-Mode Fibers," *Technical Digest - Symposium on Optical Fiber Measurements*, National Bureau of Standards, September 1986.

17. A. Alexander, "Fiber Finds a Home at the Curb," *Telephony*, April 16, 1990, pp. 160-164.

James J. Refi
AT&T Bell Laboratories
2000 Northeast Expressway
Norcross, GA 30071

Jim Refi is a Distinguished Member of the Technical Staff in the Lightguide Systems and Applications Department at AT&T Bell Laboratories in Norcross, GA. Receiving the BSEE degree from Villanova University and the MSEE degree from Polytechnic University, Jim joined Bell Laboratories in 1966. Initially, he worked on land coaxial and multipair cables, and then switched to optical fiber in 1982. He has authored over fifteen papers and has a patent on a communication system using mode stripping.

Michael J. Swiderski
AT&T Bell Laboratories
2000 Northeast Expressway
Norcross, GA 30071

Michael J. Swiderski joined AT&T Bell Laboratories in 1968 and has been a Member of Technical Staff since 1982. He received his A.A. in Electronics Technology from Baltimore Junior College and served in the U.S. Army (Vietnam). He has been involved in Plated Memory Wire, Coaxial and Multipair Cable and Sheath Design, High Strength Fiber Optic Drawing, Lightguide Systems Design and Application, Fiber Restoration, and Lightguide Field Testing (Methods, Limits, Test Sets, Troubleshooting). He is currently a member of the Lightguide Systems Engineering Group.

IDENTIFICATION METHOD FOR OPTICAL FIBER TRANSMISSION OPERATION LINES WITH LOCAL-LIGHT INJECTION AND DETECTION COUPLING SYSTEM

Masatoshi SHIMIZU, Hideo KOBAYASHI, Ichiro WATANABE,
Terufumi MAKI and Takuya UENOYA

NTT Network Systems Development Center
Tokai-mura, Naka-gun, Ibaraki-ken, 319-11, Japan

Abstract

An identification method using a local-light injection and detection coupling system is developed. This method can identify a transmission fiber ribbon in a 6.3 Mb/s system without disturbing its operation. The relation of bending fiber radius to both local-light injection and detection coupling efficiencies is shown. This method can be used for distances of up to 21 km at a bending radius R=7 mm. Also, transfer splicing loss can be estimated using this coupling system.

1.Introduction

In subscriber optical cable re-routing or replacement, an optical fiber cable transfer splicing system that enables the rapid transfer splicing of existing operating fiber cables to newly-installed ones has been proposed[1][2]. In order to achieve transfer splicing at two construction points such as manholes, it is necessary to identify the working fiber efficiently and evaluate the success or failure of the transfer splicing by the use of local-light injection and detection. However, no identification method for transmission operation lines has been studied thoroughly.

This paper proposes an optical system for the identification of operational fibers with local-light injection and detection, and examines the identification performance.

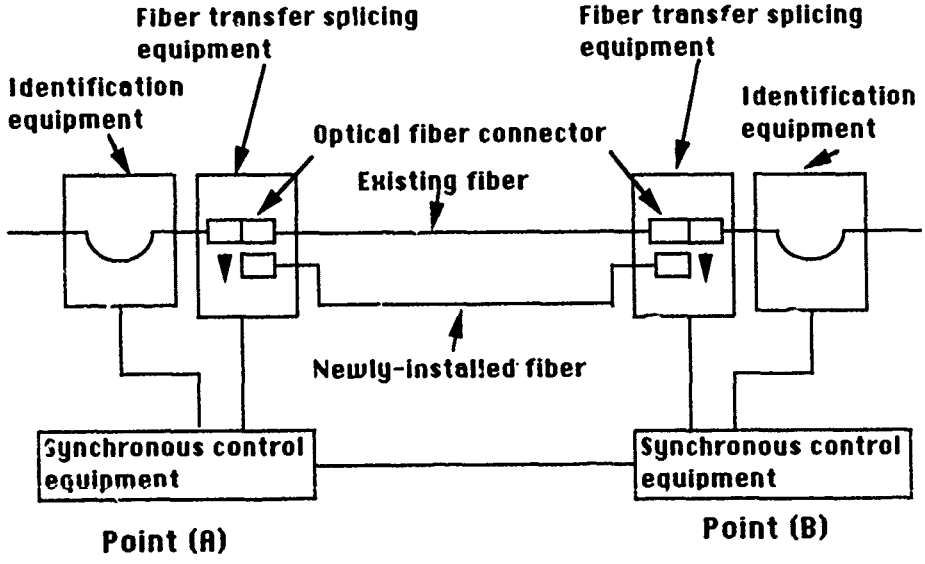

Fig.1 Optical fiber cable transfer splicing system configuration

2.Required Function of Optical Fiber Identification

2.1 System configuration

Figure 1 shows the optical fiber cable transfer splicing system configuration. This system is composed of optical fiber connectors, fiber transfer splicing equipment, synchronous control equipment and identification equipment. A Mechanically Transferrable (MT) optical fiber connector consists of a pair of plastic ferrules, two guide-pins and a clamp spring as shown in Fig. 2. The connectors are used to join 4- or 8-fiber ribbons containing 1.3 μm zero-dispersion fibers. Transfer splicing equipment is used for rapid transfer splicing from an existing optical fiber connector to a newly-installed one. Synchronous control equipment is used to control the two transfer splicing devices. Identification equipment is used to classify the transferred optical fiber ribbon. This equipment is explained below.

2.2 Required function

The identification system utilizes a local-light injection and detection coupling system. As shown in Fig.1, the identification light is injected into an existing fiber ribbon using a local injector at splicing point (A) and is detected using a local detector at splicing point (B) by bending the fiber ribbon.

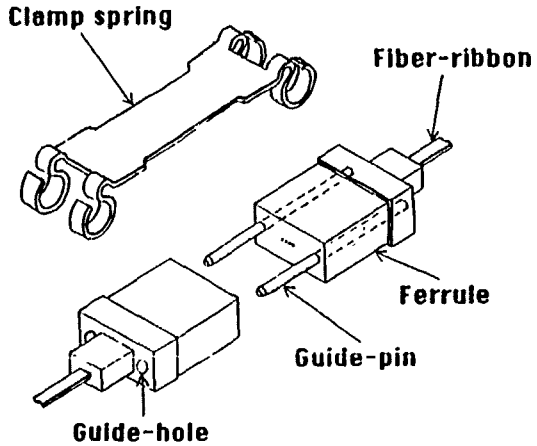

Fig.2 Mechanically Transferrable optical connector structure

Next, the method of identification flow between splicing points is shown in Fig. 3. The identification procedure is :(1) At splicing point (A), the fiber to be transfer spliced is selected from among the operating fibers. It is bent and an identification light is injected into it. (2) At splicing point (B), the fiber is confirmed by the identification light radiating from the bend and the identification light power (L1) is measured. (3) At splicing point (A), the newly installed fiber is selected and the identification light is injected into the fiber end face. (4) The same fiber is determined at splicing point (B). (5) Mechanically transferrable optical fiber connectors are mounted on a transfer splicing machine and rapid synchronous transfer splicing from the existing connectors to the new ones is accomplished. (6) After splicing, the identification light power level, (L2), is measured. (7) The success or failure of the transfer is evaluated from the difference between L1 and L2. From this identification flow, the required identification functions are the classification of transferred optical fiber ribbons, line number confirmation for 4- or 8-fiber ribbons and the evaluation of the success or failure of the transfer.

3.Design of Identification System

3.1 Local-light injection system

The fiber bending radius was studied, using the experimental set-up shown in Fig. 4, with regard to the local injection coupling efficiency η_{LI} at wavelengths of 1310 nm and 1550 nm. The local injection coupling efficiency η_{LI} is given by

$$\eta_{LI} = P_{LI2} - P_{LI1} \qquad (1)$$

Where P_{LI1} is the local injection optical power and P_{LI2} is the detected power from the fiber end face. The results are shown in Fig. 5. It can be seen that, as the bending radius is reduced or the optical wavelength is

increased, the local injection coupling efficiency η_{LI} increases.

3.2 Local-light detection system

Figure 6 shows the experimental set-up for measuring the local detection coupling efficiency η_{LD}. P_{LD1} is the detected optical power level from a bent fiber. P_{LD2} is the detected power level from a fiber end face. The local detection coupling efficiency η_{LD} is the value of the optical attenuator adjusted so that it becomes $P_{LD2}=P_{LD1}$. The results are shown in Fig. 7. As the bending radius is reduced or the optical wavelength is increased, the local detection coupling efficiency η_{LD} increases.

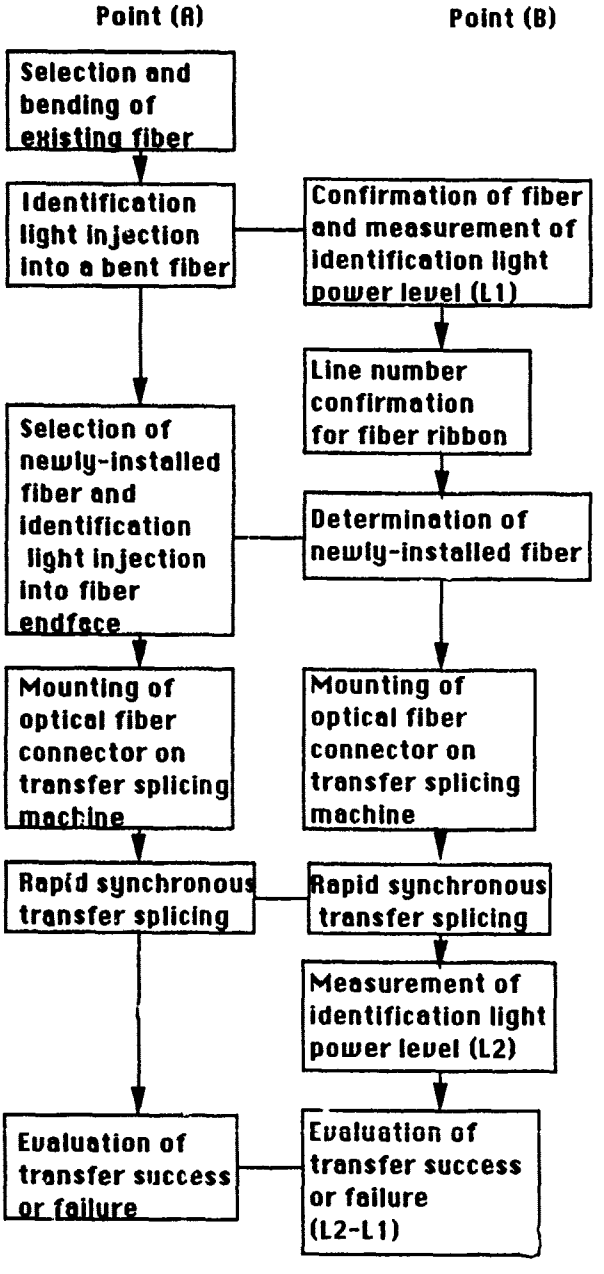

Fig.3 Method of identification

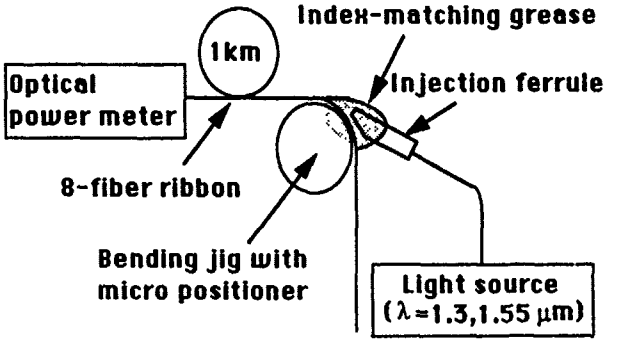

Fig.4 Set-up for measuring local injection coupling efficiency

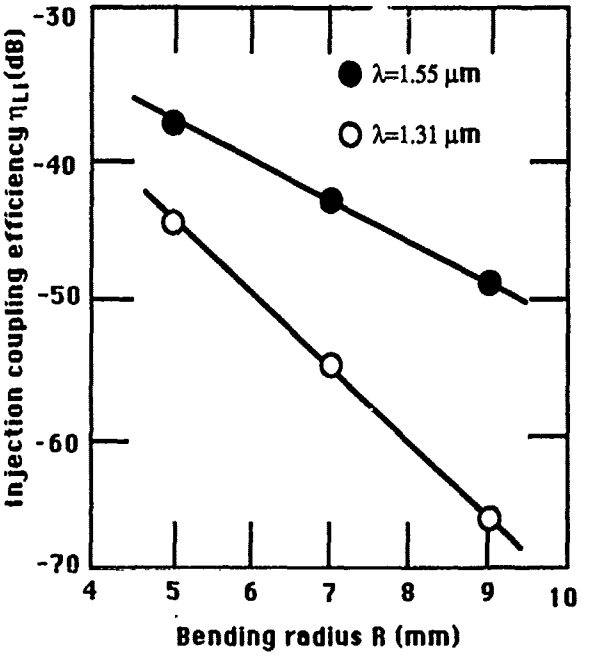

Fig.5 Dependence of local injection coupling efficiency on bending radius

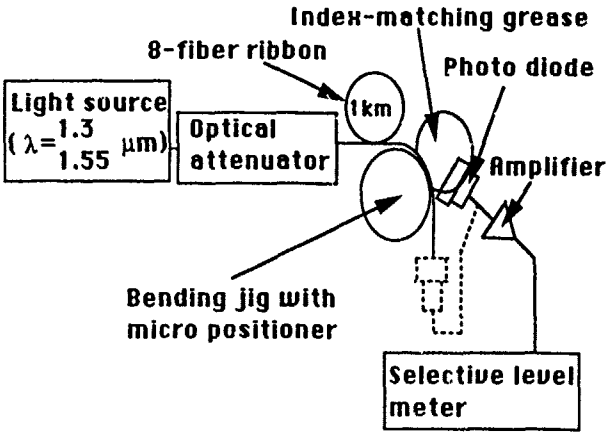

Fig.6 Set-up for measuring local detection coupling efficiency

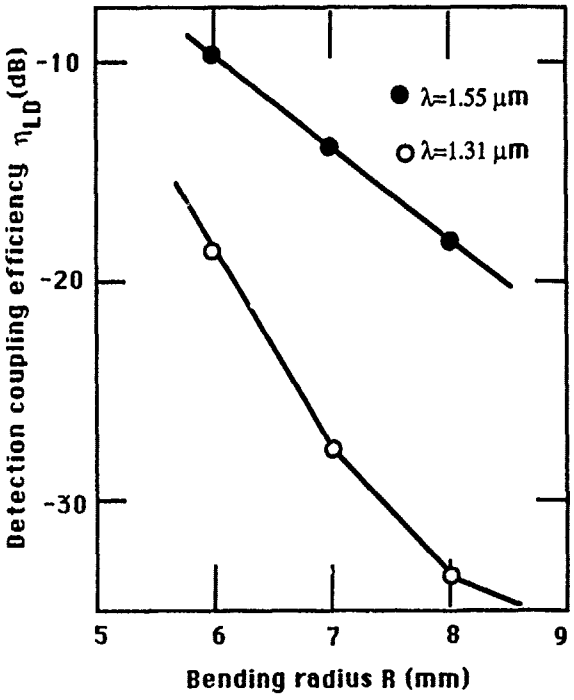

Fig.7 Dependence of local detection coupling efficiency on bending radius

3.3 D. of local-light injection and detection system

The relation of bending fiber radius with coupling efficiency between local-light injection and detection is shown in Fig. 8. It is found that the coupling efficiency is dependent on the fiber bending radius. For the identification system, the relation

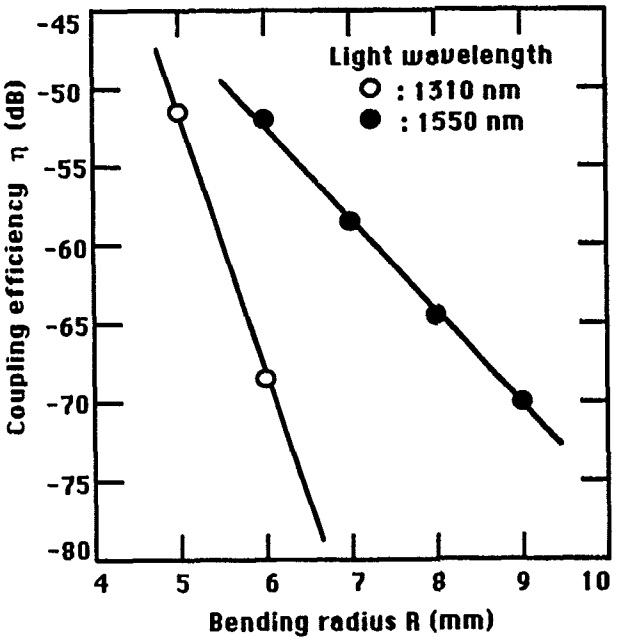

Fig. 8 Relation between bending radius and coupling efficiency

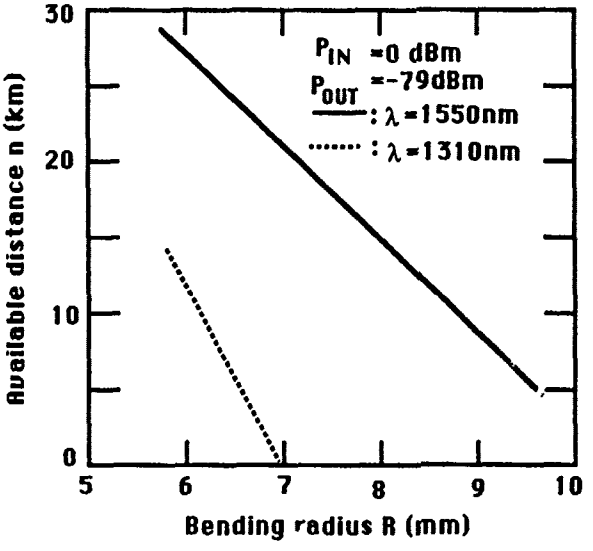

Fig.9 Calculated values of bending radius and available distance

between available distance n and coupling efficiency η is given by

$$\eta = \eta_{LI} + \eta_{LD} \quad (2)$$

$$P_{min} < P_{out} + \eta - n\,d \quad (3)$$

where P_{min} is the minimum received optical power, P_{out} is the light source output

power and d is the optical line loss. Based on equation (3) and Fig. 8, the relation between bending radius and available distance is estimated using the parameter values shown in Fig. 9. The available distance is 21km if the bending radius is 7mm and the identification light wavelength is 1550nm.

4. Line Number Confirmation

Figure 10 shows the local injection and detection identification characteristics. A 6.3Mb/s optical signal at 1310nm and a 1550 nm wavelength identification light modulated with 270Hz are transmitted. It is found that the identification light can be detected by this proposed method. Figure 11 shows experimental results on the effect of identification lights with wavelengths of 1310nm and 1550nm on a 6.3Mb/s transmission operation system at a wavelength of 1310nm. The difference between the operation signal power and the identification signal power necessary to maintain an error rate of below 10^{-9} was over 11dB at 1310nm and over 5dB at 1550nm.

For the purpose of line number confirmation for 4- or 8-fiber ribbons, a shutter covering half the fiber surface is placed between the photo-diode and the fiber ribbon in the local detector. The identification light is transferred into the top or bottom fiber and the line number is confirmed by the difference between detected optical power levels when the shutter is in place or removed.

5.Transfer Splicing Loss Evaluation

In order to evaluate the transfer splicing loss of an individual fiber in a fiber ribbon, it is necessary that the injection light is scanned across the width of fiber ribbon. The relation between the injection light source scanning time and local detection level is shown in Fig. 12. It is found that the identification light can be detected by the optical power radiated

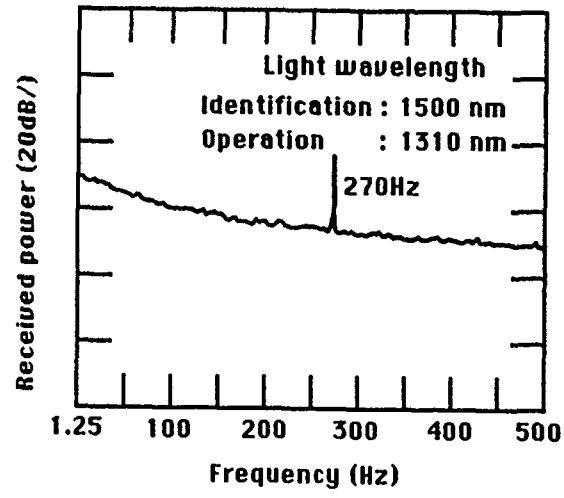

Fig.10 Local-light injection and detection identification characteristics for 6.3 Mb/s transmission operation system

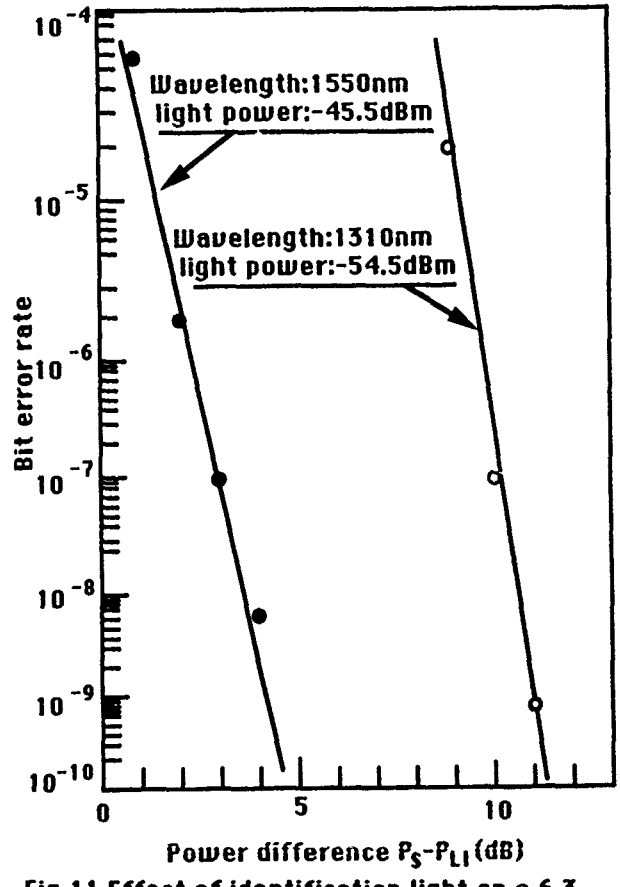

Fig.11 Effect of identification light on a 6.3 Mb/s transmission operation system (operation light power:P_S, identification light power:P_{LI})

from each fiber. A comparison between the end face injection-detection measurement and the local injection-detection measurement for the transfer splicing loss at two points is shown in Fig.13 . The deviation of loss difference for both measurement systems was 0.2dB. This confirms that transfer splicing loss can be measured with this system.

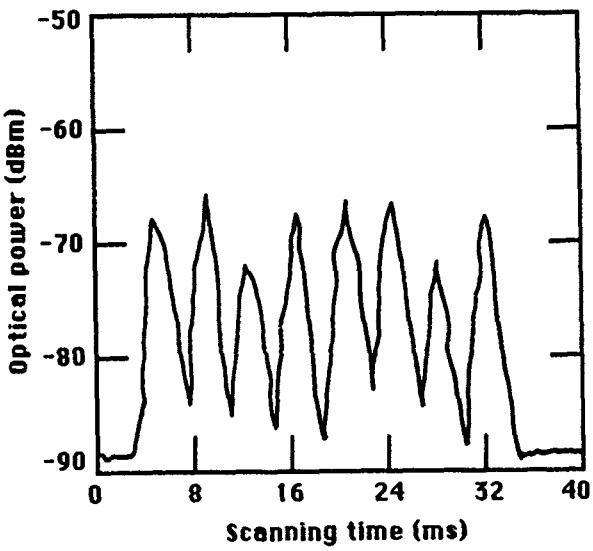

Fig.12 Relation between injection light scanning time and local detection power

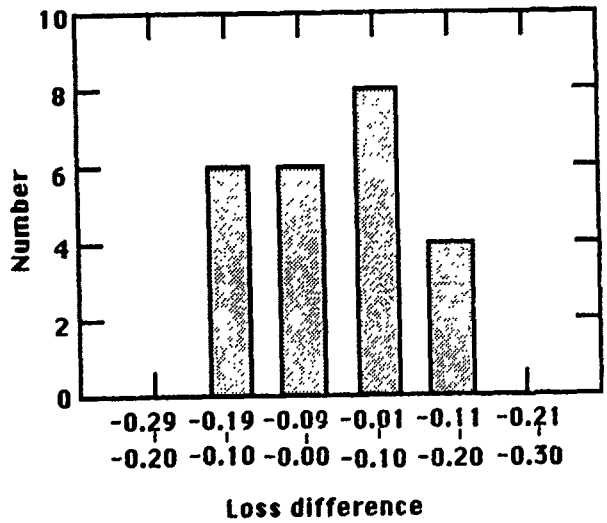

Fig.13 Deviation of loss difference between end face injection and detection and local-light injection and detection. Ave.=-0.006 dB, σ=0.091 dB, N=24.

6.Conclusion

An identification method for operational optical fiber lines with an optical fiber local-light injection and detection coupling system is proposed. It is confirmed that the identification light power does not disturb the 6.3Mb/s transmission operation system. The transfer splicing loss can be estimated using this system and this method can be used for distances of up to 21 km at a bending radius R=7 mm The identification performance is confirmed to be excellent.

Acknowledgement

The authors wish to thank S. Nagasawa, K. Hogari and F. Ashiya for their useful suggestions and discussions.

References

(1) I. WATANABE, M. SHIMIZU and H. KOBAYASHI: "Optical Fiber Cable Transfer Splicing System", IWCS, 1989, pp.191-197.

(2) H. KOBAYASHI, M. SHIMIZU, I. WATANABE, T. MAKI and T. UENOYA: "Optical Fiber Cable Transfer Splicing System for Fiber Ribbon Cables", ECOC, 1990, to be published.

Masatoshi Shimizu

NTT Network Systems
Development Center

Tokai, Ibaraki,
319-11, Japan

Masatoshi Shimizu received his B.E. and M.E. degrees in electrical engineering from Ibaraki University in 1981 and 1983, respectively.

He joined NTT in 1983. Since 1990 he has been a member of the Telecommunications Cable Systems & Outside Plant Project Group, where he has been engaged in the development of an optical fiber cable transfer splicing system. He is a member of IEICE of Japan.

Ichiro Watanabe

NTT Network Systems
Development Center

Tokai, Ibaraki,
319-11, Japan

Ichiro Watanabe received his B.E.degree in electrical engineering from Chiba University in 1983.

He joined NTT in 1983. Since 1990 he has been a member of the Telecommunications Cable Systems & Outside Plant Project Group, where he has been engaged in the development of an optical fiber cable transfer splicing system. He is a member of IEICE of Japan.

Hideo Kobayashi

NTT Network Systems
Development Center

Tokai, Ibaraki,
319-11, Japan

Hideo Kobayashi received his B.E.degree in mechanical engineering from Yamanashi University in 1968.

He joined NTT in 1968. Since 1990 he has been a member of the Telecommunications Cable Systems & Outside Plant Project Group, where he has been engaged in the development of an optical fiber cable transfer splicing system. He is a member of IEICE of Japan and the Japan Society of Mechanical Engineers.

Terufumi Maki

NTT Network Systems
Development Center

Chiyoda, Tokyo,
100, Japan

Terufumi Maki received his B.E.degree in mathematical engineering and information physics from Tokyo University in 1988.

He joined NTT in 1988. Since 1990 he has been a member of the Telecommunications Cable Systems & Outside Plant Project Group, where he has been engaged in the development of an optical fiber cable transfer splicing system. He is a member of IEICE of Japan.

Takuya Uenoya

NTT Network Systems
Development Center

Chiyoda, Tokyo,
100, Japan

Takuya Uenoya received his B.E. and M.E. degrees in electrical engineering from Waseda University in 1971 and 1973, respectively.

He joined NTT in 1973. Since 1989 he has been General Manager of the Telecommunications Cable Systems & Outside Plant Project Group, where has developed metallic cable and optical fiber cable. He is a member of IEICE of Japan.

A NEW SHEATH EVALUATION TECHNIQUE FOR SELF-SUPPORTING OPTICAL FIBRE CABLES ON OVERHEAD POWER LINES

L.A. Dissado*, M.J. Parry*, S.V. Wolfe*, A.T. Summers**, C.N Carter*

* STC Technology Ltd, Harlow, UK, ** STC Telecoms, Newport, UK.
* National Grid Research & Development Centre, Leatherhead, UK.

Abstract

Self-supporting aerial optical fibre cables, offer a cost effective solution for a digital telecommunications network on high voltage power transmission lines.

A new accelerated test method for evaluating the electrical degradation resistance of the sheathing materials for aerial cables is presented. The degradation mechanism and the environmental factors governing this degradation are discussed, together with the relationship between the acceleration factor and service performance.

Using details of the installation geometry and other service conditions, it is possible, using Weibull statistics, to make estimates of the sheath lifetime, and field trials have confirmed the validity of such estimates.

1. Introduction

Since the advent of optical fibres, the possibility of installing non-metallic, self-supporting aerial optical fibre cables on high voltage transmission lines has been investigated. In Europe, many such systems have been in successful operation for several years on a.c. power line routes up to 132 kV. These early cables were mostly polyethylene sheathed, and although some electrical degradation due to the electric field around the high voltage transmission line was anticipated, none was seen. As a result of the successful operation on 132 kV lines, installation on much higher voltage 'trunk' lines (400 kV) have recently been considered as a means of installing new digital telecommunications networks.

The cost of installing any new telecommunications network is very high especially across rugged terrains, with the highest proportion of the costs being for the installation. Self-supporting aerial cables, such as the Fibrespan system manufactured by STC offer a cost-effective solution for a digital telecommunications network. These cables can be installed easily along live transmission routes over spans of up to 1 km.

With a degradation resistant sheathing material the applications for aerial optical fibre cables expand enormously. In underdeveloped countries where an integrated power distribution network usually exists, but telecommunications networks tend to be poor, a single aerial cable could be easily installed on the existing power distribution network. This would give up to 12 optical fibre pairs, each capable of handling 7,000 simultaneous telephone calls at 565 Mbits/s. Elsewhere, electricity generating companies have the possibility of installing their own internal telephone/data transmission network. Extra capacity can be used for alarm circuits, closed circuit television surveillance of unmanned installations and future expansion or it can be leased to telephone or cable television companies.

STC has been working to replace polyethylene with new cable sheathing materials which are resistant to the effects of dry band arcing. This paper describes a new test method for assessing such materials for aerial optical fibre cables, which simulates the observed service degradation closely and quantifies the resistance to degradation by dry band arcing. This paper also describes how data generated from the tests may be used to quantify the reliability of a cable sheath for a system of known operational parameters.

2. The Mechanism of Dry Band Arcing

Any aerial optical cable installed on a high voltage transmission route will be capacitively coupled between the line and earth. As a consequence of this a voltage is induced onto the surface of the cable. In the dry, the high resistance ($\approx 1 \times 10^{12}$ Ω/m) of the cable does not allow a current to flow, so no electrical degradation occurs.

During periods of rainfall, the cable surface becomes uniformly wet and the resistance of the cable drops, ($\approx 1 \times 10^6$ Ω/m) and a current can therefore flow in the water film on the surface of the cable. When the rainfall stops, this current produces a Joule heating effect and begins to dry the cable out. In a new cable with a hydrophobic surface, droplets form which become polarised in the electric field, creating a field enhancement which leads to electrical discharges. As the cable becomes weathered by these electrical discharges and the local climatic conditions, the surface becomes more hydrophilic and the individual droplets of water become a continuous film. It is at this stage that the phenomenon known as dry band arcing[1-3] begins to become the dominant factor in the electrical degradation of the aerial cable sheath.

Joule heating in this continuous film of water begins to dry off the cable until a discrete dry band is formed. As this dry band has a resistance many orders of magnitude greater than anything else in the system, the total available voltage is dropped across the dry band resulting in an electrical discharge.

When the cable is totally wet it has a distributed resistance along its length, with the resistance to earth decreasing as the earthed clamp is approached. Hence the maximum current flowing in the system is immediately adjacent to the earthed clamp attaching the cable to the transmission tower (Fig.1). The maximum degradation is therefore expected at this point. This has been confirmed by cables that have failed in field trials where the electrical degradation always occurs very close to the earthed clamp.

The crucial period for dry band arcing is therefore during drying, although some limited discharging could occur during wetting. The area of sheath underneath the discharge is subjected to very high temperatures during arcing activity, and it is this high temperature which causes degradation to occur. In the case of polyethylene melting is followed by oxidation/ignition. A degradation resistant compound with enhanced high temperature performance will not exhibit a bulk melting behaviour and will consequently possess a lifetime in severe environments which is considerably in excess of a simple thermoplastic sheath material such as polyethylene.

A range of sheath materials incorporating mineral fillers has been developed for such applications[3], which are resistant to the intermittent high temperature excursions typical of dry band arcing. The long term behaviour of these materials can vary considerably depending on their detailed formulation, and therefore it is essential to match the suitability of any sheath material with a given application in question. The performance of degradation resistant materials has been compared using standard tests such as the comparative tracking index (CTI)[4] or the salt fog test[5]. However, it is noticeable that the observed degradation in comparative tests occurs fairly uniformly across the cable sample implying that the degradation mechanism in CTI and salt fog tests differs from that occurring in the field. Therefore while these tests can sometimes rank the materials qualitatively, it is essential to carry out a more rigorous quantitative evaluation of sheath material suitability if the cable is to be installed in systems rated above 132 kV, or in double circuit systems rated below 132 kV but with unfavourable phasing.

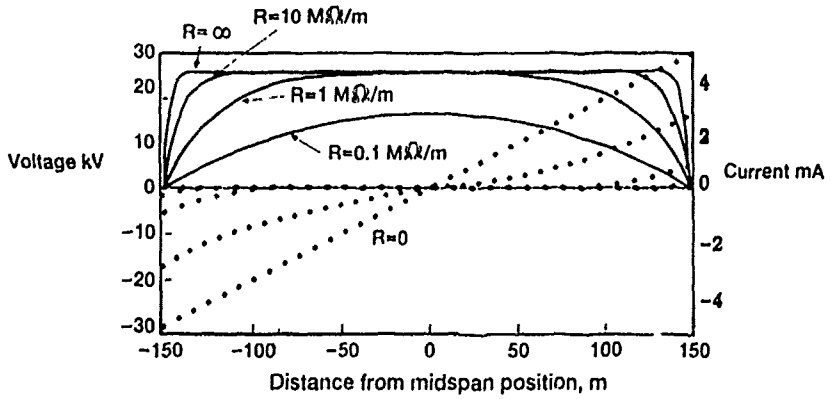

I–V characteristics for a 300 m span, 400 kV line

Figure 1

3. Development of a Sheath Degradation Test

In order to develop a test that accurately simulates the degradation mechanism seen under field conditions, it is necessary to establish the actual operating conditions and the local environment seen by the system. Dry band arcing is driven by the capacitive coupling of the optical cable to the field associated with the conductors of the HV line. The frequency of the arcing is a direct result of the frequency of discrete rain showers or other forms of precipitation, which can vary considerably depending on geographical location.

These are the two overriding factors governing the electrical degradation of an aerial optical cable sheath. The accelerated degradation test must therefore simulate these two factors as closely as possible.

3.1 Local Field Condition

It is possible to determine the capacitively coupled voltage in mid-span associated with high voltage conductors. Several software packages have been developed by National Grid Company (formerly the UK Central Electricity Generating Board) and others[1] which enable mid-spanvoltage contour maps to be generated. The magnitude of the voltage is governed by the tower dimensions and geometry and the line to earth voltage. The situation is complicated still further when double circuit lines are considered. The capacitively coupled voltage can vary dramatically with the relative conductor phasing of the two circuits.

If the normal nomenclature for the three phase angles of red, yellow, blue is used then favourable phasing would be: from top to bottom; left hand circuit, Red, Yellow, Blue; right hand circuit, Blue, Yellow, Red. Unfavourable phasing would be: left hand circuit, Red, Yellow, Blue; right hand circuit, Red, Yellow, Blue.

For a typical 132 kV double circuit system with unfavourable phasing (Fig. 2) the capacitively coupled voltage at the mid tower position is of the same order as that found on a 400 kV double circuit system with favourable phasing (Fig. 3). Figures 4 and 5 show the same 132 kV double circuit system with favourable phasing and during single circuit operation respectively.

These figures show the large variations possible on dual circuit systems due to phasing arrangements. They also show the importance of selecting the optimum clamping position of the aerial cable to minimise the capacitively coupled voltage.

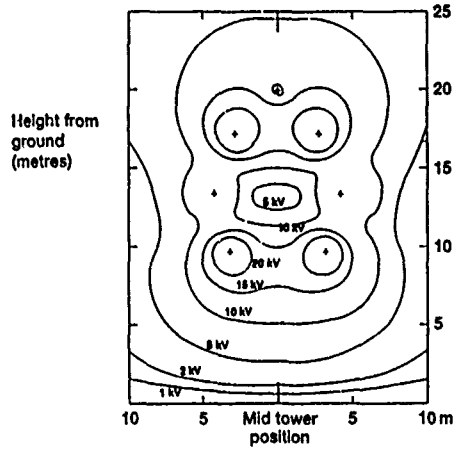

Dual cicuit 132 kV voltage contour map unfavourable phasing

Figure 2

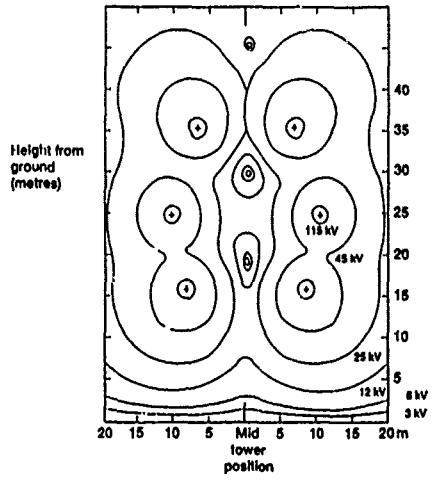

Dual circuit 400 kV voltage contour map favourable phasing

Figure 3

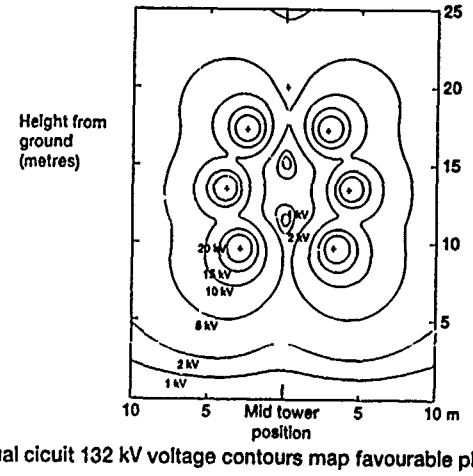

Dual cicuit 132 kV voltage contours map favourable phasing

Figure 4

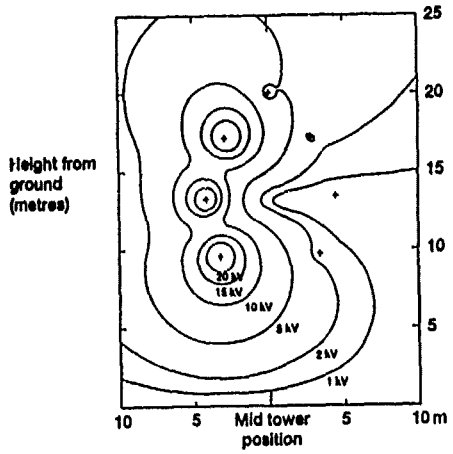

Dual circuit 132 kV voltage contour map (single circuit operation)

ure 5

The voltage contour maps shown in Figs 2-5 apply in mid-span, between two towers. However, distortion of the voltage contour lines will occur as the earthed tower is approached, and the electric field along the sheath begins to increase. The distance over which the capacitively coupled voltage drops to earth potential depends upon the surface resistivity of the aerial cable sheath. Figure 1 shows the critical distance as a function of surface resistivity for a wet cable[6]. In a dry cable, the sheath is highly insulating and the surface resistivity is extremely large. For a high resistivity sheath, this critical distance is between 1 and 10 m. The voltage/current relationship as the tower is approached is also shown as a function of surface resistivity of the cable. These parameters are of particular importance as all sheath degradation observed to date in field trials and in-service cables has occurred within extremely close proximity to the optical cable earthing position (Fig. 6).

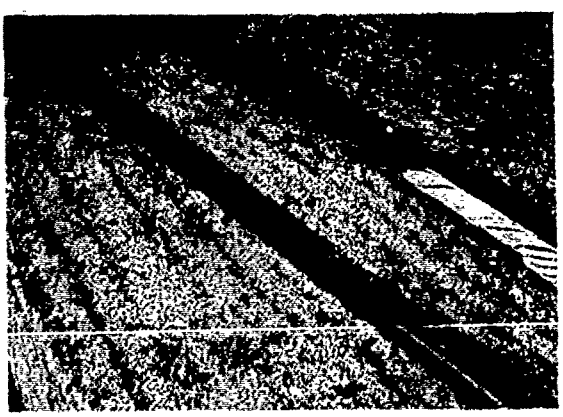

Field failure of polyethylene sheathed cable

Figure 6

It is therefore reasonable to assume that the worst-case situation is where all the mid-span voltage drops off over the 1 m of cable adjacent to the tower. In this case the local field close to the clamp would have the same numerical value as the mid-span voltage.

The mid-span voltage depends upon the proximity of the optical cable to the conductors. Consideration should be given to the fact that this distance is not fixed, and that the optical cable could approach the conductors more closely during high winds or in high ice loading conditions.

3.2 Frequency of Dry Band Arcing

Most dry band arcing occurs at the end of a period of rain, and therefore one period of arcing can be equated with one rain period. This is a convenient way of accelerating possible degradation in a laboratory situation, providing average local rainfall behaviour for the intended cable location is known. It should be emphasized that one long period of rain has the same severity as one short rainshower.

4. Laboratory Test

An accelerated electrical degradation test has therefore been devised based on the above considerations. It was not possible to capacitively couple the test samples to a high voltage test line and instead short lengths of cable (10-20 cm) were directly coupled between a high voltage transformer and earth, using simple annular electrodes. The test sample is therefore subjected to a constant electrical field (applied voltage/electrode spacing). The magnitude of this field is equivalent to the maximum field seen by a capacitively coupled cable, (i.e. the mid-span voltage being dropped across the last metre of cable). From the voltage contour plots the maximum field seen by a cable in service is of the order of 12-15 kV/m. To accelerate the electrical degradation, fields of 20-60 kV/m have been used for all of the laboratory tests.
Dry band arcing is induced by subjecting the cable samples to an intermittent water spray regime. Acceleration is achieved by increasing the number of drying cycles compared with the service climate seen by the cable. A typical accelerated spray regime comprises spray duration of two seconds at two minute intervals. The acceleration factor can be estimated from local climatic monitoring and would be approximately 1000 times for a typical UK service environment. Figure 7 shows a schematic diagram of the laboratory test facility.

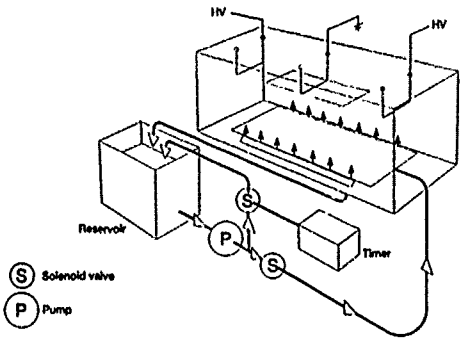

Schematic diagram of laboratory test chamber

Figure 7

Although capacitive coupling is not used in this test, the directly coupled test samples all exhibit degradation typical of that seen in service, but on an accelerated timescale.

A cable sample is judged to have failed when sheath degradation has proceeded to a stage where the central cable core is just exposed, but no significant degradation of the core itself has occurred (Fig. 8). For the results to have statistical significance, ten samples of each sheathing material are tested at each of the electrical fields used.

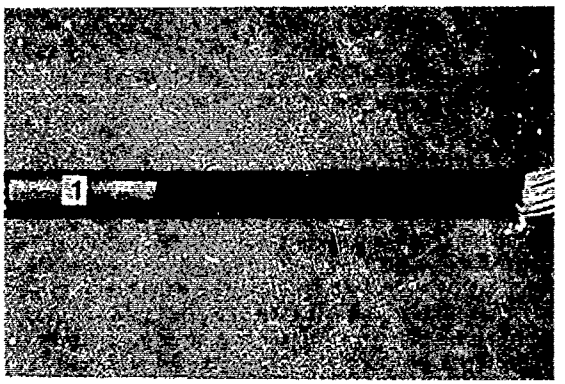

Laboratory sample tested to failure (filled sheath)

Figure 8

5. Data Analysis

Weibull statistics have been used to analyse sets of data from the accelerated tests under constant field conditions. A typical set of data for a sheath material is shown in Fig. 9. The failure time along the x axis refers to the accelerated test time. This can be expressed in real service life by multiplying by the acceleratic factor. The Weibull analysis yields the characteristic time to failure, τ_c (63% probability of failure), and the shape of the plot, β.

A series of plots at different fields such as that shown in Fig. 9 can be expressed in terms of a field/lifetime plot in real service time by plotting the field as a function of τ_c multiplied by the acceleration factor. One such plot for a sheath material is shown in Fig. 10. This actually represents the failure time for one termination, but, in order to assess service performance, the critical parameter is the time to first failure of N terminations or N/2 spans. This can be estimated providing the average field close to the clamp is known together with τ_c and β at that field. The median time to the first failure is obtained by equating the Weibull failure probability function:

$$P_f(t) = 1-\exp\left[-(t/\tau_c(E))^{\beta} \right]$$

where t is the time to failure
$\tau_c(E)$ is the characteristic time at a given field
β is the Weibull shape parameter

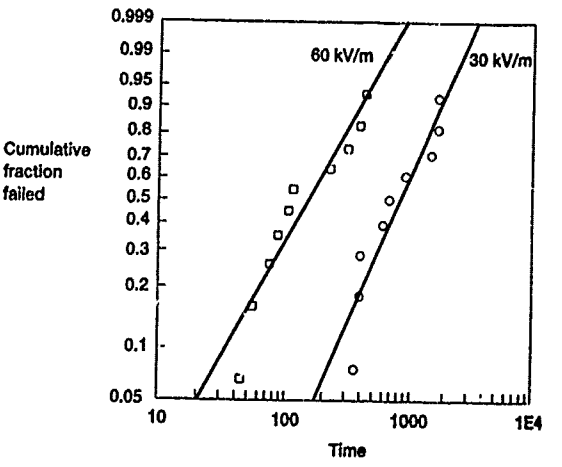

Combined Weibull plot for polyethylene

Figure 9

with the median ranking probability for the first failure and solving for the time. The time to second and subsequent failures can be estimated in a similar manner. Standard techniques also exist for determining the confidence limits on these calculations.

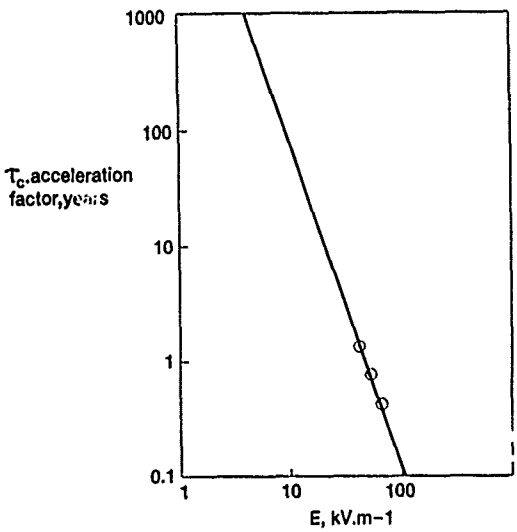

Lifetime – field plot for polyethylene

Figure 10

As an example, using the data in Figure 10, the estimated lifetime of polyethylene in a 50 span system is 36 years at 3 kV and 5 months at 15 kV.

Clearly the accuracy of such estimations depends not only on the accuracy and scatter of such laboratory test data, but also on the accuracy with which the system parameters can be obtained. The magnitude of the electrical field around the transmission tower can only be predicted from a mathematical model. Attempts have been made in the past to directly measure the electric field around transmission towers, but the low impedance of the measuring system (compared with that of air) has affected the field giving unreliable results. Data monitoring in present and future field trials will lead to other measurements of the electrical environment of the tower. The climatic conditions however can be accurately measured.

STC currently has a trial span on a 400 kV dual circuit line on the West coast of Scotland to confirm laboratory generated tests. A datalogger has been set up on this trial and is monitoring 14 environmental and electrical conditions on and around the cable. This line is reputed to be the most severe in the UK, both in terms of the electrical environment (small towers, unfavourable phasing) and the climatic conditions. At STL in Harlow, England, a precipitation detector has been set up to back-up the information from the field trial. This detector monitors the total number of rainfall/precipitation periods, which will be used to give a more accurate value for the acceleration factor for the UK.

An acceleration factor for any global location can therefore be determined from a knowledge of the local climatic conditions. Lifetimes can be estimated from this and by calculating the mid-span voltage of the transmission line in question from the contour plot programme.

6. Results

6.1 Polyethylene Model

The test method was initially used to determine the degradation resistance of polyethylene sheathed aerial cables. The objective of this work was to define a model for the observed degradation, using a material for which field data was available.

Electrical degradation measurements were carried out at three fields, 30, 40 and 60 kV/m. For polyethylene, the dry band arcing caused severe local melting of the sheath which eventually ignited causing failure of the sample. Weibull analysis of these results as described in the example in section 5 above was carried out, and the results compared with field data. An early polyethylene sheathed cable on a 400 kV transmision line (15 kV/m) failed after nine months in service. The time to first failure, predicted from the Weibull analysis at this field was 5 months. This close correlation between the predicted failure time and the field failure time increased the confidence in the test method and has led to the identification of alternative sheathing materials.

6.2 Alternative Sheathing Material

There are both mechanical and electrical requirements for aerial optical cable sheathing materials. Mechanical properties are important for installation considerations such as stringing tension. Retention of mechanical properties at high temperatures is also important especially in tropical and sub-tropical installations.

A number of different filled materials have been assessed at 60 kV/m. Figure 11 compares the degradation results of three filled materials with polyethylene. The filled materials all have a considerably higher value of τ_c than polyethylene, but the importance of the shape parameter β can also be seen by comparing materials A and C.

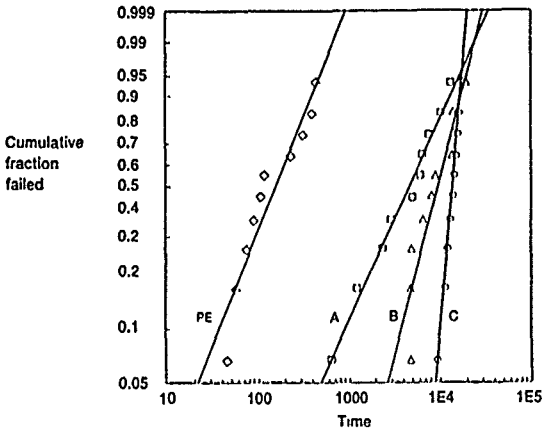

Comparison of sheath degradation rate of different materials

Figure 11

Material C has a much higher value of the shape parameter than material A, this increases the time to first failure considerably. The narrow distribution associated with material C also leads to smaller error bars around the distribution, thus leading to greater accuracy in the predicted lifetimes.

Material C also has the best mechanical properties, sheath grip and high temperature performance of the three materials investigated. This material is currently being used for the UK's first commercial installation aerial optical fibre cable.

6.3 Line Equipment

A similar approach has also been made in assessing the effects of line equipment on the electrical degradation resistance of aerial cable. The clamping system used to connect the aerial cable to the transmission towers (suspension clamp), consists of spiral steel wires, coated with a grit layer on the underside to assist the gripping of the sheath.

Electrical degradation tests at 60 kV/m were carried out using polyethylene sheathed aerial cable, but with the simple annular earth electrode replaced with half a suspension clamp. It was thought that the individual wires of the suspension clamp would give a stress enhancement to the electric field and lead to shorter degradation times. The actual results were considerably better than those obtained with the simple annular electrode. Figure 12 compares the electrical degradation distribution of polythylene sheathed aerial cable, with and without suspension clamps. This effect is now thought to be due to the clamp producing a graded field which reduces the rate of degradation.

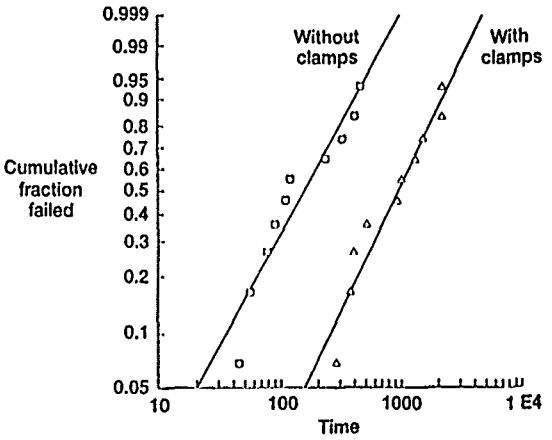

Comparison of Weibull distribution for PE with and without suspension clamps

Figure 12

7. Conclusions

A test technique and analytical procedure have been developed to enable a quantitative comparison of degradation resistance of aerial optical cable sheath materials and accessories to be made. An estimate of sheath lifetime can be made using details of the installation geometry and other service conditions, and the validity of the estimate has been confirmed by field trials. The technique is also used in assessing the optimum tower clamping position for an aerial cable in a specific service environment.

The testing and analytical procedure has been employed by STC in the development of the Fibrespan cable and its associated installation technology. This has enabled the Fibrespan system to be used with confidence in severe combined electrical and climatic conditions, confirming its suitability for an extremely large range of applications world-wide.

8. References

1. A.T.M. Grooten, E.J. Bresser, A.G.W.M. Berkers, 'Practical Experience with Metal-Free Self-Supporting Aerial Optical Fibre Cable in High Voltage Networks', IWCS, 1987.

2. S.M. Rowland, K. Craddock, C.N. Carter, I. Houghton, D. Delme-Jones, 'The Development of a Metal-Free, Self-Supporting Optical Cable for Use on Long Span High Voltage Overhead Power Lines', IWCS, 1987.

3. L.A. Dissado, M.J. Parry, S.V. Wolfe, 'Sheath Materials for Aerial Optical Cables', Fifth International Conference on Plastics in Telecommunications, London, September, 1989.

4. BS 5901:1980, 'Method of Test for Determining the Comparative and Proof Tracking Indices of Solid Insulating Materials Under Moist Conditions', (= IEC 112).

5. IEC 507, 1975, 'Artificial Pollution Tests on High-Voltage Insulation to be Used on A.C. Systems'.

6. C.N. Carter, 'Dry Band Electrical Activity on Optical Cables Separately Strung on Overhead Power Lines', IWCS, 1988.

9. Acknowledgements

The authors wish to thank the Directors of STC Technology, STC, Cable Products Division and the National Grid Company, Research and Development Centre, for permission to publish this paper.

Len A. Dissado
STC Technology Ltd
London Road
Harlow
Essex
CM17 9NA
UK

Len Dissado was born in St. Helens, England. He gained his PhD from University College, London University and was awarded a Research Fellowship at the Australian National University. After a period with the Atomic Energy Authority at Harwell, and a further period at ANU, he joined the Dielectrics Group at Chelsea College, London University, in 1977. He has been working as consultant with STC since 1980, specializing in the area of dielectrics and d.c. insulation.

Mark J. Parry
STC Technology Ltd
London Road
Harlow
Essex
CM17 9NA
UK

Mark Parry was born in London, England. He joined the Materials Science Laboratories of British Telecom in 1978 working on polymeric items used in the UK Telecommunications network. He received an MSc from the London School of Polymer Technology in 1988. After a short period working on thermoplastic natural rubber at the Malaysian Rubber Producers Research Association, he joined STC Technology in 1989, where he has worked on polymeric materials for use on both optical and copper cables.

Sue V. Wolfe
STC Technology Ltd
London Road
Harlow
Essex
CM17 9NA
UK

Sue Wolfe was born in London, England. She joined STC in 1970 to work on cable materials and cable development. She gained her BSc from Thames Polytechnic in 1976, and her PhD from Queen Mary College, University of London in 1982. After a period as Head of Department in the London School of Polymer Technology at the Polytechnic of North London she returned to STC Technology in 1989 where she has continued to work in optical fibre cables, particularly in the area of high voltage reliability.

Andy T. Summers
STC Telecommunications
Cable Products Division
Wednesbury Street
Newport
Gwent
NP9 0WS
UK

Andy Summers was born in Haverfordwest, Wales, in 1961. He graduated from Aston Universtiy in 1984 with a B.Sc in Electrical and Electronic Engineering. After this he joined STC as Measurements Engineer, to develop production and reference test methods for optical cable manufacture. In 1986 he became Quality Manager for the Optical Fibre and Cable Manufacturing Units, from where he became Technical Manager for optical cables, based at Newport.

Chris. N. Carter
National Grid Company
Research & Development Centre
Kelvin Avenue
Leatherhead
Surrey
KT22 7SG
UK

Chris Carter graduated from the University of London with a B.Sc Honours degree in Mathematics and Physics in 1963. He has since carried out research work for the CEGB on magnetohydrodynamic power generation, superconducting magnet design, ac loss measurements in superconductors, failure mechanisms in power cable stop joints and, since 1979 on the development of optical communications on power lines.

SIMULATED LIGHTNING TEST FOR OPTICAL FIBER CABLE

Roger C. Finn - Bell Northern Research (BNR) Ltd. - Ottawa, Ontario, Canada.

Bannu P. Hurtig - Bell Canada - Toronto, Ontario, Canada.

Robert J. Williams - Northern Telecom Canada Ltd. - Saskatoon, Sakatchewan, Canada

Abstract

Lightning can and does damage buried optical fiber cable. In the recent past, many researchers have attempted to optimize a simulated lightning test method as a means of characterizing the electrical parameters of the optical fiber cable. This paper presents the results of a test method developed to more accurately control the environment around the target cable sample. The current levels for the test ranged from 80 - 200 kA. The mechanical damage and the thermal damage to the cable sample were analyzed separately and led to the conclusion that the mechanical damage outweighs the thermal damage under most test conditions. The effects of the sand mesh size, moisture content level, and the distance of the discharge electrode from the target cable sample are reported in terms of how they affect the repeatability of the test method. Conclusions have also been drawn about the heat of fusion parameter for various shield materials, which could be useful in optimizing cable design.

Introduction

Laboratory experiments using simulated lightning surges and actual field experience indicate that lightning can damage buried optical fiber cables which contain metallics in the core or the sheath. The damage to the cable can range from a small pinhole in the outer polyethylene jacket to fiber attenuation increase or breakage. Based both on experimental and field data, it is hypothesized that the damage mechanisms are crushing, dielectric breakdown to near earth, thermal effects and arcing between metallic components of the cable.

At the time the research was undertaken, the existing method[1] for simulated lightning tests on optical fiber cable had yielded inconsistent results. The results being monitored were sheath damage and post surge fiber continuity. The existing method utilized a box with inside dimensions of 915 mm x 915 mm x 1220 mm into which the optical fiber cable sample was inserted. The box was filled with sand so as to bury the cable sample, then water was added to the sand until the sand was saturated. An electrode was inserted horizontally into the box such that its tip was about 25.4 mm from the target sample. The sample was then surged with a decaying envelope oscillatory current waveform with a time to half value of about 50-80 µs. The current waveform was monitored for each test and appeared to be very consistent. A typical waveform is shown in Figure 1. Table I provides the mathematical equation for such a surge and statistically compares theoretical values with those found experimentally.

The inconsistent results found from the tests were attributed to variations in the impedance of sand medium between the discharge electrode and the target. This would affect the transduction efficiency of the electrical energy into mechanical and thermal energies which cause damage to the cable. Possible contributions to the inconsistent results were:

(a) Sand regularity or grain size,
(b) Moisture content or moisture gradient,
(c) Impurities or ionic content of water,
(d) Electrode distance to target and
(e) Target sample orientation with respect to electrode.

To study the effects of each of these parameters, a new test method was devised and testing was done in three phases, these being exploratory, moisture level threshold determination and correlation between the "spherical" and the "sandbox" methods. This test method permits accurate control of the sand medium parameters.

TABLE I -Mathematical Model Of Current Waveform

$$I(t) = E * \left[\frac{C}{L}\right]^{0.5} * EXP\left[\frac{-R * t}{2 * L}\right] * SIN(wt)$$

$$w = 2\Pi f = \left[\frac{1}{L * C} - \frac{R^2}{4 * L^2}\right]^{.05}$$

$$t_1 = \frac{1}{f * 4}$$

$$I(t_1) = E * \left[\frac{C}{L}\right]^{0.5} * EXP\left[\frac{-R * t_1}{2 * L}\right]$$

$$Ln(0.5) = \frac{(t_1 - t_2) * R}{2 * L}$$

I(t) : instantaneous current (Amps) at time t (sec)
E : initial voltage on capacitor C (fds)
L : inductance of circuit L (H)
R : resistance of circuit (ohms)
f : frequency of oscillation
t_1 : time to first peak (sec)
t_2 : time to half value of envelope (sec)

TEST PARAMETER STATISTICS - LIMITS

Test Ckt.	Factor	C µfd	L µh	R Ω	f_1 kHz	t_2 µs	$I(t_1)/E$ Measure	$I(t_1)/E$ Calculate
A	Mean	10.28	12.21	0.261	14.3	83.0	0.764	0.761
	Std.Dev.		0.13	0.015	0.0	3.7	0.014	
B	Mean	10.28	9.54	0.256	16.2	67.7	0.843	0.844
	Std.Dev.		0.12	0.006	0.1	1.2	0.009	
C	Mean	8.22	9.90	0.258	17.8	67.7	0.738	0.759
	Std.Dev.		0.11	0.004	0.1	0.8	0.013	
D	Mean	12.85	7.93	0.198	15.9	71.8	1.034	1.046
	Std.Dev.		0.12	0.006	0.1	1.6	0.020	
E	Mean	12.85	6.02	0.175	18.2	61.9	1.158	1.196
	Std.Dev.		0.12	0.007	0.2	2.0	0.033	
F	Mean	12.85	8.04	0.331	16.1	49.5	0.879	0.918
	Std.Dev.		0.01	0.005	0.0	0.5	0.009	
G	Mean	12.85	4.96	0.116	20.0	72.4	1.353	1.391
	Std.Dev.		0.08	0.007	0.2	3.2	0.027	
Stand. Limit					16-30	50-80		

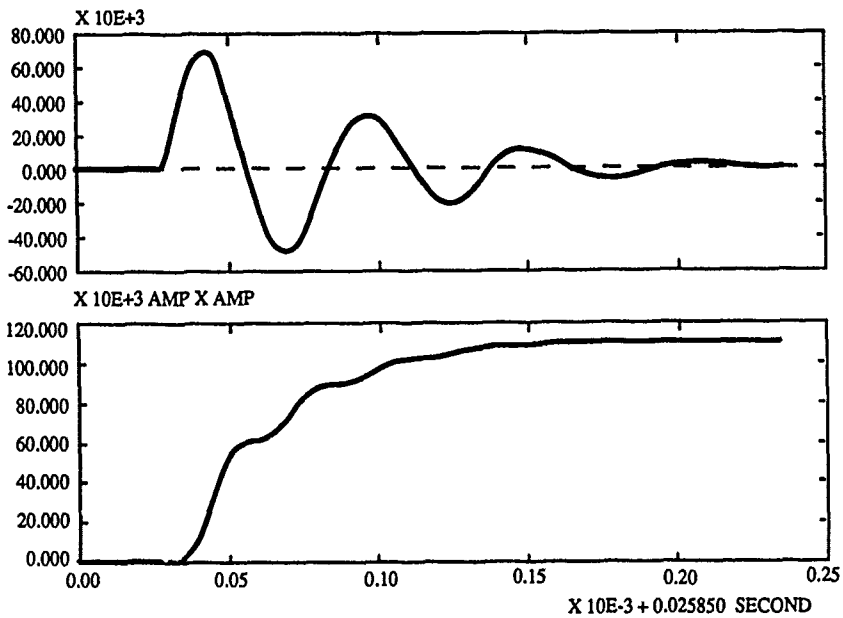

I = 64 kA Time To Half Value = 68.7 μs

Freq. = 18.4 kHz $I T^2 \triangleq 1.1 \times 10E+5 A.s^2$

Figure 1 - Typical Simulated Lightning Waveform Characteristics

Test Phase I - Exploratory

The objective in this phase of testing was to study the thermal impact of simulated lightning surges by controlling sand mesh size, water type and the surge electrode distance. A polyethylene spherical subassembly of 203 mm diameter, 3.2 mm wall thickness, was manufactured with holes in it to accommodate the target sample and the surge electrode. The spherical sub-assembly was mounted on a polyethylene cylinder (with a 6.4 mm wall) to facilitate its fastening and location in the sandbox. Due to concerns about explosion, the sphere was installed in the sandbox and the sandbox was filled with regular sand to buffer any explosion. The electrical circuit to create the simulated lightning and the connection of the target metallics to the return were as for the original sandbox method. Metallic tubes were used as surge samples instead of cables (refer to Figure 2). This was done to eliminate the variability associated with the physical configuration of optical cables.

Weight loss was selected as an accurate indicator of thermal damage. Tin, lead and aluminium tubes (outside diameter 20 mm) were tested. Due to the thinner wall thickness of the aluminium tubes, 1.6 mm, compared to 3.2 mm of tin and lead, the mass loss was only significant in the aluminium material. Aluminium targets were utilized exclusively for this phase of testing at surge currents of 140 kA to 160 kA.

Pure silica sand was utilized for all the tests conducted. The first variable to be tested was the sand mesh size. Dry sand was employed and the mass loss results for 35# and 125# mesh size are given in Table II and Figure 3. It should be noted that a reconstruction technique had to be used to determine the mass loss as distinct from target material loss due to mechanical damage or sharding. Marginally more thermal damage and more consistent results were found with the finer mesh 125# sand than with the 35# sand.

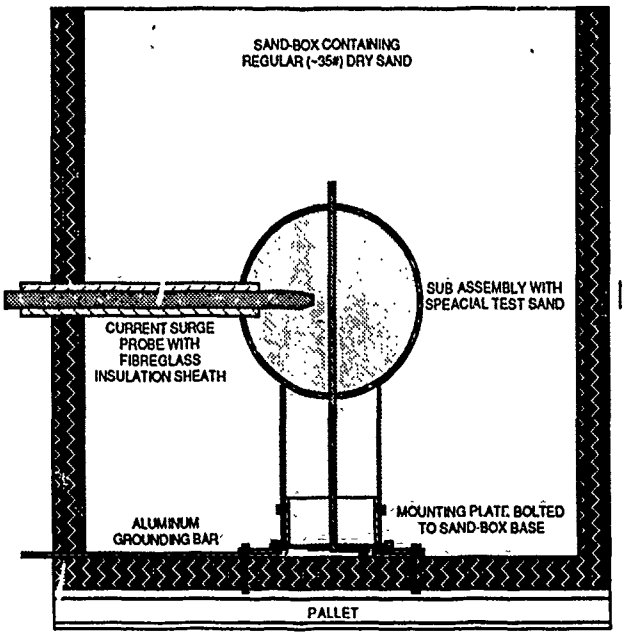

Figure 2 - Test Set-Up For Phase I Testing

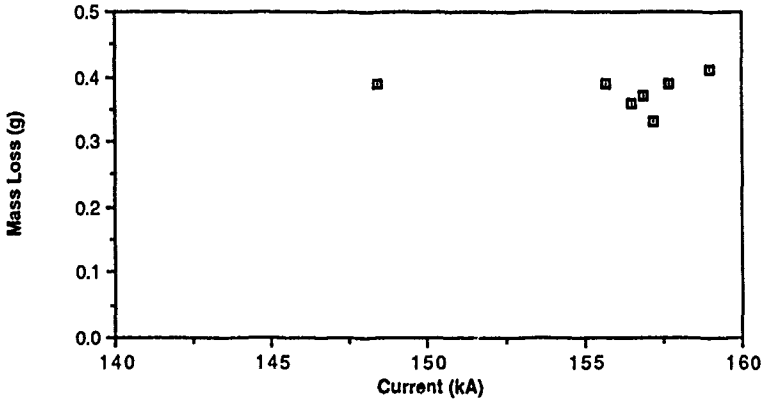

Figure 3a : Data For Dry Fine (125#) Sand

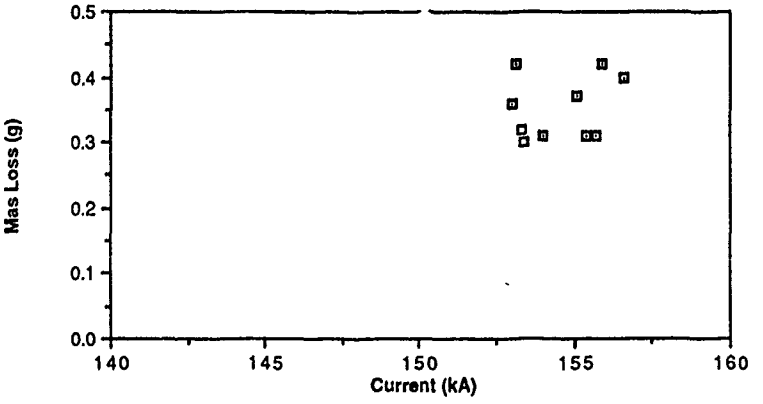

Figure 3b : Data For Dry Coarse (35#) Sand

Table II - Phase I Lightning Surge Testing Results

RECONSTRUCTED WEIGHT LOSSES FOR FINE SAND,
WITH NO WATER AND NO SALT, PROBE SET AT 2.54 cm.

Target #	ML(g)	ML_{avg}	I(kA)	I^2t(E+6) $(kA)^2.sec$	$T_{1/2}$(E-6) (sec)	V (kV)	F(kHz)
a	0.39	0.38	148.4	0.7899	98.76	118.8	19.07
b	0.39	0.38	155.7	0.8749	98.25	122.6	18.99
c	0.36	0.38	156.5	0.8594	94.75	118.3	19.11
d	0.37	0.38	156.9	0.8513	95.25	122.0	19.19
e	0.33	0.38	157.2	0.8677	94.75	123.1	19.19
f	0.39	0.38	157.7	0.8873	96.25	122.6	19.23
g	0.41	0.38	159.0	0.8793	97.27	123.0	19.23

RECONSTRUCTED WEIGHT LOSSES FOR COARSE SAND,
WITH NO WATER AND NO SALT, PROBE SET AT 2.54 cm.

Target #	ML(g)	ML_{avg}	I(kA)	I^2t(E+6) $(kA)^2.sec$	$T_{1/2}$(E-6) (sec)	V (kV)	F(kHz)
i	0.36	0.34	153.0	0.8431	95.75	122.2	19.11
ii	0.42	0.34	153.1	0.8098	88.75	122.5	19.11
iii	0.32	0.34	153.3	0.8252	93.75	123.2	19.19
iv	0.30	0.34	153.4	0.8322	95.75	122.9	19.19
v	0.31	0.34	154.0	0.8271	95.75	122.6	19.07
vi	0.37	0.34	155.1	0.8461	91.75	121.2	19.15
vii	0.31	0.34	155.4	0.8481	95.25	123.0	19.15
viii	0.31	0.34	155.7	0.8374	94.75	123.1	19.19
ix	0.42	0.34	155.9	0.8325	92.27	122.9	19.11
x	0.40	0.34	156.6	0.8378	93.75	121.9	19.19

Legend: ML: Mass Loss Of Target,
I: Current,
I^2t: Energy Of Surge,
$T_{1/2}$: Half-time Of Surge,
V: Voltage Reading Of Surge,
F: Frequency Of Arc.

With the addition of de-ionized water to the sand in the sphere at two distinct saturation levels, problems were encountered with repeatability. Mechanical damage was noted to overshadow the thermal counterparts and later reconstruction was not possible with 100% and 50% saturation levels. Erratic surge current path was noted in terms of split strike or strike along the sphere wall. Introducing an impurity of 5% NaCl with similar levels of saturation did not yield any significant differences.

The surge electrode distance was varied from 25.4 mm to 12.7 mm and resulted in inconsistent thermal damage at the reduced distance.

Test Phase II - Water Level Threshold Determination

The goal for the second testing phase included the threshold determination for the water content level in the sand at which sufficient thermal damage imparted to the target would be evident in a repeatable fashion. In addition, polymer coated Electrolytic Chrome Coated Steel (ECCS) sheathing material for optical cable, 0.152 mm thickness, was also employed as the target. The ECCS was longitudinally formed (uncorrugated) into 20 mm diameter tubes, to characterize the mass loss vs surge current as was done for the aluminium in the previous phase. Further aluminium targets with slightly thinner walls (0.889 mm) were also tested.

In order to minimize the previously encountered problems of erratic strikes, primarily under moist sand conditions, the polyethylene spheres were enlarged from 203 mm to 254 mm diameter. The target orientation was also altered from vertical to horizontal mount and the surge electrode was introduced from above. For practical reasons the sandbox was reduced in size to 460 mm x 460 mm x 370 mm inside dimensions. The test set-up is depicted in figure 4. Since 35# sand is more readily available than the 125#, this grade of sand was utilized for testing. The surge electrode was positioned 25.4 mm away from the target.

Testing was performed on sub-assemblies containing moisture levels of 100%, 50%, 33% and 25% saturation. It was noted with the 100% and 50% saturated samples, as with the samples tested in phase I, that mechanical damage appeared to be consistent, but that the thermal damage appeared insignificant and could not be determined. Moisture levels of 33% and 25% yielded what appeared to be consistent thermal and mechanical damage. Inspection of those samples indicated that minimal reconstruction of samples was necessary in both of these cases. Figures 5 to 9 depict the results obtained in this test phase. It is interesting to note that the sphere size used eliminated the need for the sand contained in the larger sandbox, since there was no sign of the spheres splitting or exploding even at the full saturation levels.

In the steel tube, the threshold surge current for mechanical damage was observed at approximately 40 kA. Thermal damage, monitored by mass loss, was observed to become significant at approximately the 65 kA level. The material was noted to undergo a steep incline in thermal damage from this current value through to the 120 kA range where a levelling effect was noted through to the 150 kA region. The test results are shown in figure 10.

A plot of the mass loss for the various test samples vs the level of soil saturation at current levels of 105 kA and 85 kA is shown in figure 11.

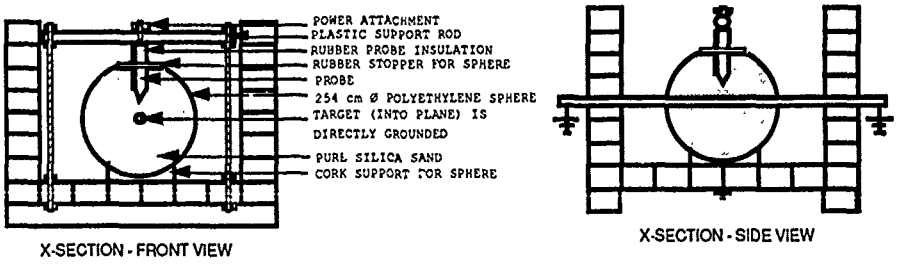

Figure 4 : Test Set-Up For Phase II Testing

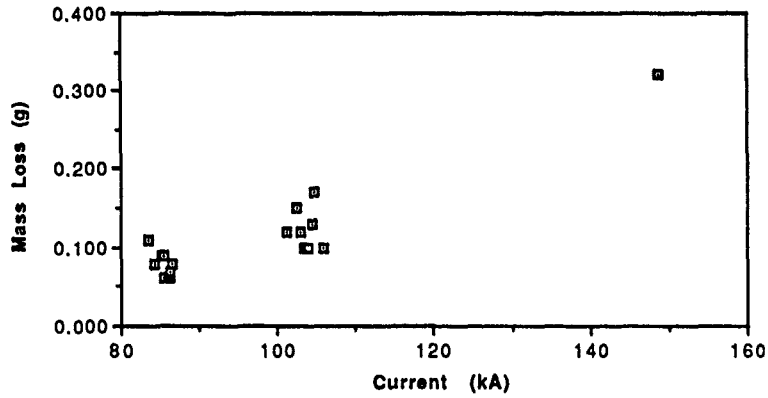

Figure 5 : Current vs. Mass Loss For Al. In Dry Sand

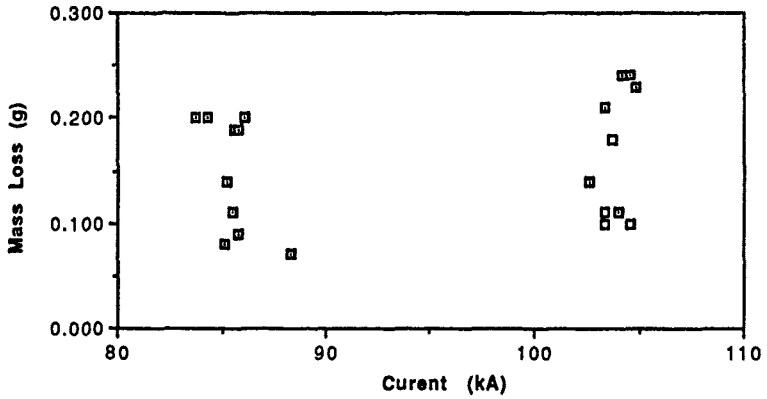

Figure 6 : Current vs. Mass Loss For Al. In 25% Sat. Sand

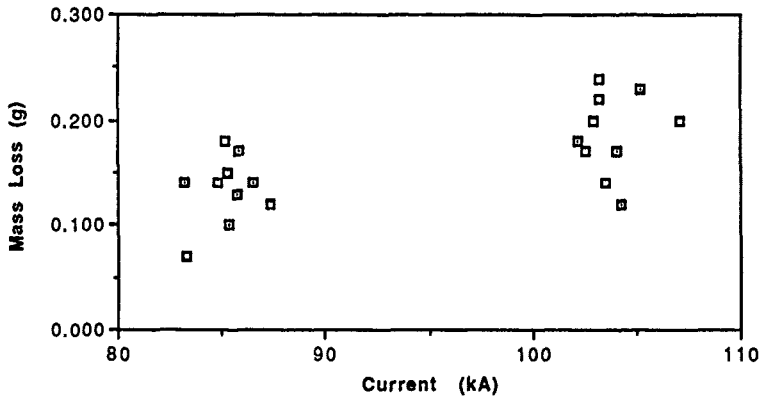

Figure 7 : Current vs. Mass Loss For Al. 33% In Sat. Sand

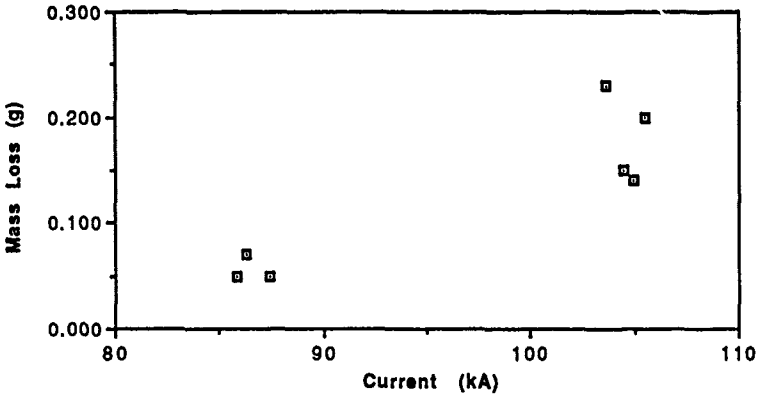

Figure 8 : Current vs. Mass Loss For Al. In 50% Sat. Sand

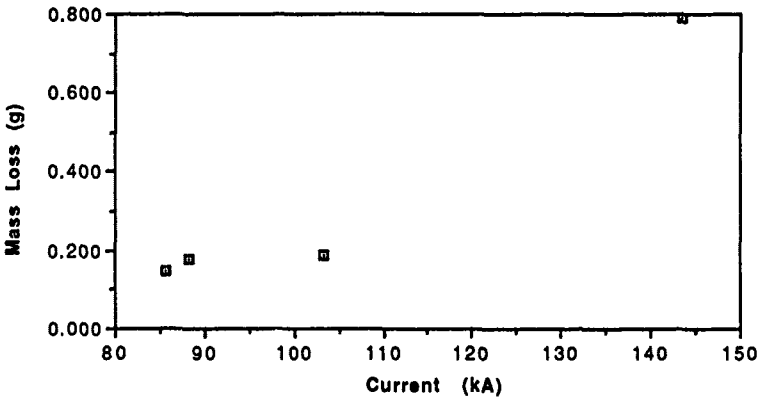

Figure 9 : Current vs. Mass Loss For Al. In Saturated Sand

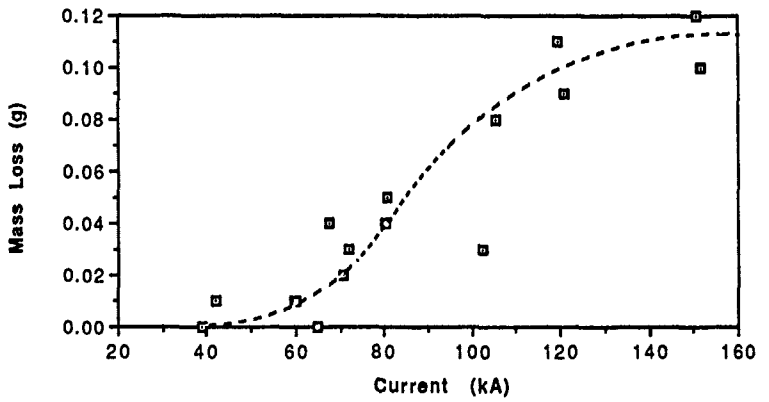

Figure 10 : Current vs. Mass Loss For Steel In Dry Sand

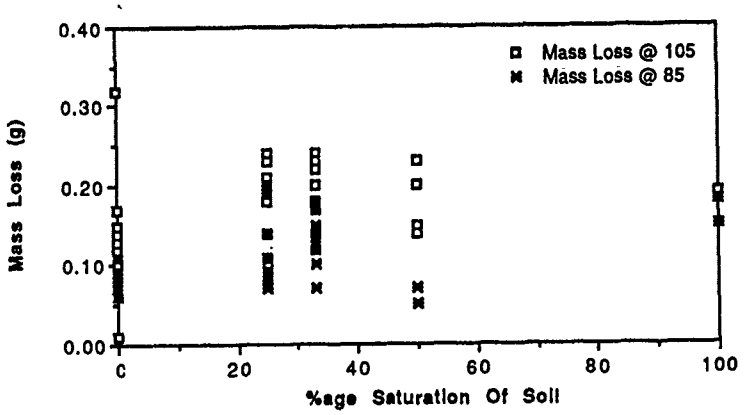

Figure 11 : Mass Loss vs. % Saturation At Discrete Currents

Test Phase III - Optical Fiber Cable Testing in Sphere and Sandbox

The intention of this phase was to determine whether a correlation existed between the proposed TIA test procedure on simulated lightning tests for optical fiber cable[2] and the sphere subassembly test method (see Figure 4), since the latter is easier to perform and more cost-effective. The comparison criteria were based on visual cable damage inspection and fibre continuity measurements. Aluminium targets were also tested. The sand moisture level was monitored and controlled to 65% saturation of the sand or 13% by weight (w/w).

Two sheath types over the same tube-in-slot core construction were tested. When viewed from the outside in, sheath design A consists of poly-steel-poly and sheath design B is the same with the addition of a rodent protective armour (poly-steel). A cross-sectional drawing is shown in Figure 12.

The relatively high surge current levels of 85, 125 and 165 kA were used, since lower current levels would not yield any significant damage to the optical cable under test[3]. Forty-eight samples, 24 from each sheath type and 24 aluminium samples were tested in both the sandbox and the sphere. The hole in the sphere had to be enlarged to accommodate the bond clamp assemblies on the cable samples.

The post surge optical continuity tests proved inconclusive since the cables tested did not exhibit any failures for either the sandbox or the sphere test procedures. For these two methods, visual inspection of the physical damage on all cable samples displayed similar trends or severity of damage within the individual sheath design and the surge current level categories. For the aluminium targets, the visual inspection showed comparable results from the two test methods. As expected from previous testing at high moisture levels, mechanical damage dominated resulting in insignificant mass losses due to thermal damage.

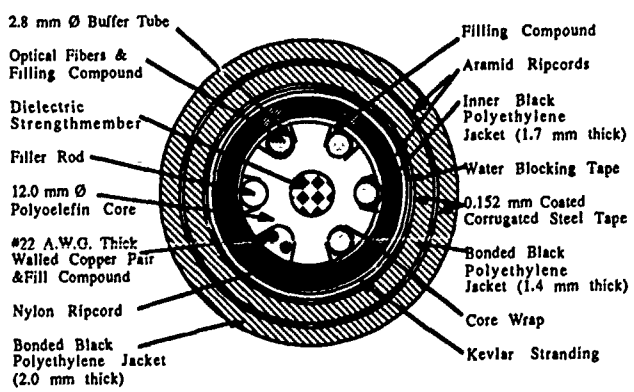

Figure 12 : Fiber Optic Cable Cross-Section

Discussion

Based on the test results on aluminium and steel materials, it is hypothesized that, for a given target material composition of known cross-sectional area, a critical current exists at which material fusion (and therefore mass loss) will occur[4]. The mass loss will increase thereafter to a finite plateau level at which the majority of the excess energy is translated into further physical damage to the target.

The critical current is unique for each target material's composition and is determined from the equation (1);

$$S = \frac{I_0}{A}\sqrt{T_{1/2}}$$

where S is the fusion factor of the metal, I_0 is the critical current, A is the target's cross-sectional area (within as yet undetermined limitations) and $T_{1/2}$ is the time to half value of the surge current. A plot of the current vs mass-loss for a particular material should, therefore, resemble the graph shown in figure 13. The plot of the fusion factor vs the temperature of fusion for some known materials, including aluminium and steel shielding material, is given in figure 14.

The steel shielding material was observed to have the onset of thermal damage at approximately 65 kA in dry sand. The plot obtained for mass-loss vs current for (figure 10) this material appeared to follow the hypothetical plot (figure 13). The temperature of fusion for this material is quoted as being 1206° C. The calculated fusion factor value corresponds with the one obtained by extrapolating the plot in figure 14.

The steel material, however, was observed to undergo significant mechanical damage at the lower current levels, i.e. prior to the onset of appreciable thermal damage. Mechanical damage was, furthermore, observed to increase markedly as current levels were increased. Thermal damage can be considered a minor contributor compared to the physical or mechanical damage resulting from the surge current impact on the targets tested.

Field experience indicates that the damage due to lightning is not restricted to only mechanical damage at the primary impact point, as was observed in the two test methods. In actual field conditions, thermal damage is observable at the primary lightning entry location on the cable as well as longitudinally for some distance on both sides of the impact point. This raises a concern that the present test methods do not adequately reflect the damaging mechanisms encountered in the field for buried plant.

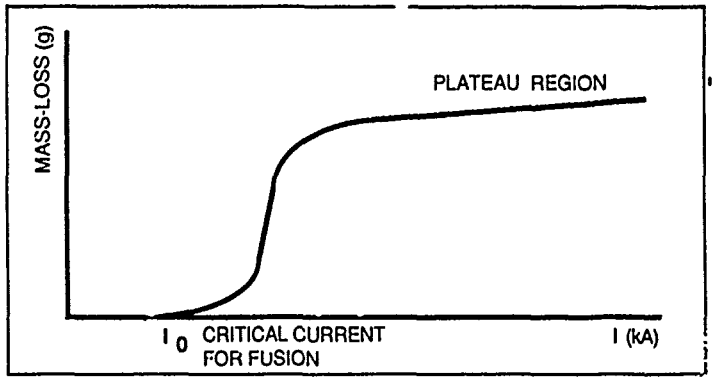

Figure 13 : Hypothetical Plot For Current vs. Mass Loss

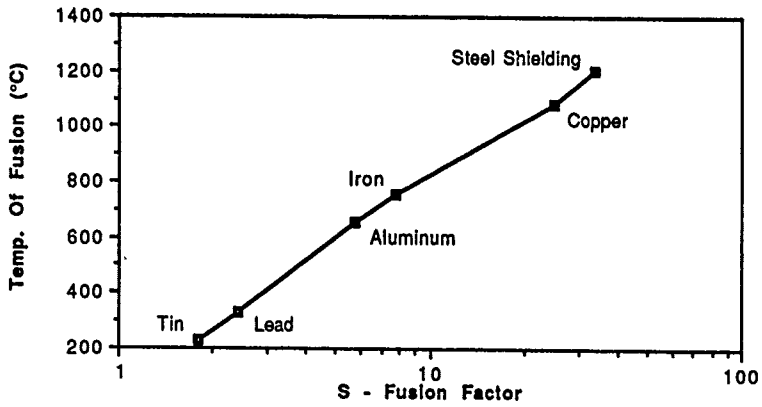

Figure 14 : Fusion Factor vs. Temperature Of Fusion

Conclusion

It has been demonstrated that the observed inconsistencies in the simulated lightning test method can be largely overcome by controlling the sand medium variables, e.g. sand mesh and moisture content. The sphere subassembly method facilitates easy and cost-effective control of these variables.

There is good correlation between the sandbox and the spherical subassembly methods for simulated lightning test for the optical fiber cable.

The dry sand medium yields the most consistent results and should be considered as a design tool for comparison purposes. However, for cable qualification, the real-life moist conditions must be reflected in the proposed EIA/TIA test procedure[2].

To assess installed cable reliability, a need exists within the industry to develop criteria to quantify physical damage imparted by simulated lightning strikes.

At moisture saturation levels of 33% and below, the thermal damage mechanisms played a significant role. Above this value the mechanical damage prevailed. Field data indicates that significant thermal damage occurs on the cable at the main strike location and the current propagation along the shield causes thermal damage to the cable symmetrically away from the primary strike zone.

The fusion factor directly relates to the current threshold for thermal damage in optical cable shielding materials. When designing cables material choices can be optimized with respect to the fusion factor to yield maximum lightning protection. This needs further development.

Authors

Roger C. Finn graduated with a M.Sc. (Polymer Chemistry) and a B.Sc. (Industrial Chemistry) from the University Of The Witwatersrand (Johannesburg, South Africa). He has been involved in materials engineering relating to telecommunications applications of fiber optic splicing, gels and cables, intertoll fiber optic cable protection, copper cable technology, polymer thick film inks, protection devices, polymers, adhesives, sealants, encapsulants, device packaging and molding since joining BNR's Materials Technology group in 1980. He holds several patents in these diciplines on the behalf of BNR and Northern Telecom Ltd.

Bannu P. Hurtig received a BASc in Electrical Engineering from the University of Waterloo and a MASc, also in Electrical Engineering from the University of Toronto. In 1985, she joined Bell Canada in the Electrical Protection Research group of Corporate Engineering. Her background includes development of protection standars for optical fiber cable in intertoll applications. Currently she is Supervising Engineer and her portfolio includes research on grounding topologies for digital switching and transmission systems.

Robert J. Williams received a diploma in Mecahnical Engineering from the Gwent College of Technology (Newport, Gwent, UK). He has been in the employ of Northern Telecom since 1976, initially in the R & D laboratories of the Communications Cable Division, where his activities involved environmental testing of cables and production of PVC formulations for wire and cable use. In 1980 he was transferred to the Optical Cable Division where he held managerial positions in the manufacture and development of optical cables. He is currently Marketing Product Manager for fiber access cables, including fiber in the loop activities. He hold numerous patents concerned with optical cables.

References

[1] Bell Communications Research, "Generic Requirements for Optical Fiber and Optical Fiber Cable", TR-TSY-000020, Issue 4, March 1989.

[2] TIA PN-2190, FOTP-181, "Lightning Damage Susceptibility Test for Fiber Optic Cables with Metallic Components", November 1989.

[3] Williams, R.J., Rowe, J.A., Hurtig, B.P., Plouffe, M., "Performance Characteristics of Enhanced Buffer Tube Cable", IWCS 1987.

[4] CCITT Publication, "The Protection of Telecommunication Lines and Equipment Against Lightning Discharges", 1974.

AUTHORS INDEX

International Wire & Cable Symposium

SPONSORED BY: IWCS
WITH PARTICIPATION BY:
U.S. ARMY COMMUNICATIONS-ELECTRONICS COMMAND
(CECOM)
FORT MONMOUTH, NEW JERSEY
18, 19, 20 and 21 November 1991
Adam's Mark Hotel, St. Louis, MO

Please provide a 300-500 word abstract (25 copies) of proposed technical paper on such subjects as design, application, materials, and manufacturing of communications and electronics wire and cable of interest to the commercial and military electronics industries. Such offers should be submitted no later than 15 March 1991 to the Headquarters, US Army Communications-Electronics Command, ATTN: AMSEL-RD-C3-TP, (Pat Hudak) Fort Monmouth, New Jersey 07703-5202.

TITLE: _____

AUTHORS: _____

COMPANY: _____

ADDRESS: _____

AUTHOR(S): _____

CONTACT FOR CORRESPONDENCE: _____

ADDRESS AND TELEPHONE: _____

_____

I. PAPER TITLE: _____

_____

II. BACKGROUND (Why was work undertaken?):

III. PRIMARY CONCLUSION OR RESULT:

IV. DESCRIBE THE NOVELTY AND HOW THIS WORK ADVANCES THEORY OR TECHNOLOGY:

V. 300-500 WORD COMPREHENSIVE SUMMARY, INCLUDING METHODOLOGY IN REACHING CONCLUSION OR RESULT:

Fold Here

Stamp

Commander
US Army Communications-Electronics Command
Attn: AMSEL-RD-C^3-TP (P. Hudak)
Fort Monmouth, NJ 07703-5202

Fold Here